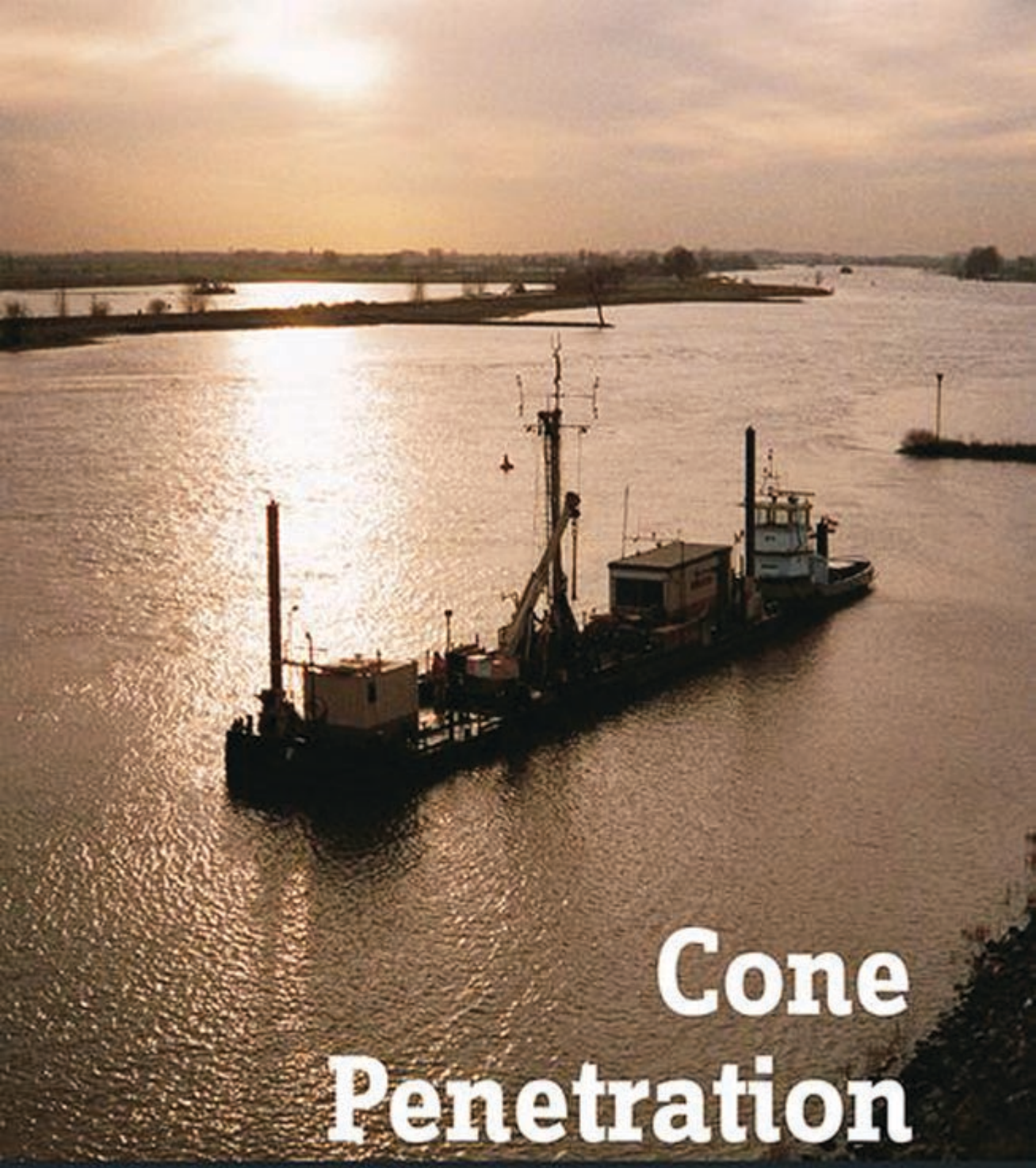

Cone Penetration Testing 2018

CRC Press
Taylor & Francis Group
A BALKEMA BOOK

Editors
Michael A. Hicks, Federico Pisanò & Joek Peuchen

CONE PENETRATION TESTING 2018

Taylor & Francis
Taylor & Francis Group
http://taylorandfrancis.com

PROCEEDINGS OF THE 4TH INTERNATIONAL SYMPOSIUM ON CONE PENETRATION TESTING (CPT'18), DELFT, THE NETHERLANDS, 21–22 JUNE 2018

Cone Penetration Testing 2018

Editors

Michael A. Hicks
Section of Geo-Engineering, Department of Geoscience and Engineering, Faculty of Civil Engineering and Geosciences, Delft University of Technology, Delft, The Netherlands

Federico Pisanò
Section of Geo-Engineering, Department of Geoscience and Engineering, Faculty of Civil Engineering and Geosciences, Delft University of Technology, Delft, The Netherlands

Joek Peuchen
Fugro, The Netherlands

CRC Press
Taylor & Francis Group
Boca Raton London New York Leiden

CRC Press is an imprint of the
Taylor & Francis Group, an **informa** business
A BALKEMA BOOK

Cover image courtesy of Fugro © 2018

CRC Press/Balkema is an imprint of the Taylor & Francis Group, an informa business

© 2018 Delft University of Technology, the Netherlands. All rights reserved. Published by Taylor & Francis Group plc.

Typeset by V Publishing Solutions Pvt Ltd., Chennai, India

All rights reserved. No part of this publication or the information contained herein may be reproduced, stored in a retrieval system, or transmitted in any form or by any means, electronic, mechanical, by photocopying, recording or otherwise, without written prior permission from Delft University of Technology, The Netherlands.

Although all care is taken to ensure integrity and the quality of this publication and the information herein, no responsibility is assumed by the publishers nor the editors and authors for any damage to the property or persons as a result of operation or use of this publication and/or the information contained herein.

The full papers of Cone Penetration Testing 2018 are available online via open access:
https://www.taylorfrancis.com/.

Published by: CRC Press/Balkema
Schipholweg 107C, 2316 XC Leiden, The Netherlands
e-mail: Pub.NL@taylorandfrancis.com
www.crcpress.com – www.taylorandfrancis.com

ISBN: 978-1-138-58449-5 (Hardback + USB)
ISBN: 978-0-429-50598-0 (eBook)

Cone Penetration Testing 2018 – Hicks, Pisanò & Peuchen (Eds)
© 2018 Delft University of Technology, The Netherlands, ISBN 978-1-138-58449-5

Table of contents

Preface xi

Committees xiii

Sponsors xv

Keynote papers

Penetrometer equipment and testing techniques for offshore design of foundations, anchors and pipelines 3
M.F. Randolph, S.A. Stanier, C.D. O'Loughlin, S.H. Chow, B. Bienen, J.P. Doherty, H. Mohr, R. Ragni, M.A. Schneider, D.J. White & J.A. Schneider

Inverse filtering procedure to correct cone penetration data for thin-layer and transition effects 25
R.W. Boulanger & J.T. DeJong

Use of CPT for the design of shallow and deep foundations on sand 45
K.G. Gavin

CPT'18 papers

Evaluating undrained rigidity index of clays from piezocone data 65
S.S. Agaiby & P.W. Mayne

On the use of CPT for the geotechnical characterization of a normally consolidated alluvial clay in Hull, UK 73
L. Allievi, T. Curran, R. Deakin & C. Tyldsley

New vibratory cone penetration device for in-situ measurement of cyclic softening 79
D. Al-Sammarraie, S. Kreiter, F.T. Stähler, M. Goodarzi & T. Mörz

Estimation of geotechnical parameters by CPTu and DMT data: A case study in Emilia Romagna (Italy) 85
S. Amoroso, P. Monaco, L. Minarelli, M. Stefani & D. Marchetti

Cone penetration testing on liquefiable layers identification and liquefaction potential evaluation 93
E. Anamali, L. Dhimitri, D. Ward & J.J.M. Powell

Dutch field tests validating the bearing capacity of Fundex piles 101
S. Van Baars, S. Rica, G.A. De Nijs, G.J.J. De Nijs & H.J. Riemens

Estimation of spatial variability properties of mine waste dump using CPTu results—case study 109
I. Bagińska, M. Kawa & W. Janecki

Strength parameters of deltaic soils determined with CPTU, DMT and FVT 117
L. Bałachowski, K. Międlarz & J. Konkol

Estimation of the static vertical subgrade reaction modulus k_s from CPT 123
N. Barounis & J. Philpot

Estimation of in-situ water content and void ratio using CPT for saturated sands 129
N. Barounis & J. Philpot

NMO-SCTT: A unique SCPT tomographic imaging algorithm 137
E. Baziw & G. Verbeek

Effect of piezocone penetration rate on the classification of Norwegian silt 143
A. Bihs, S. Nordal, M. Long, P. Paniagua & A. Gylland

Quantifying the effect of wave action on seabed surface sediment strength using a portable free fall penetrometer 151
C. Bilici, N. Stark, A. Albatal, H. Wadman & J.E. McNinch

Interpretation of seismic piezocone penetration test and advanced laboratory testing for a deep marine clay 157
M.D. Boone, P.K. Robertson, M.R. Lewis, D.E. Gerken & W.P. Duffy

CPT-based liquefaction assessment of CentrePort Wellington after the 2016 Kaikoura earthquake 165
J.D. Bray, M. Cubrinovski, C. de la Torre, E. Stocks & T. Krall

Use of CPTu for design, monitoring and quality assurance of DC/DR ground improvement projects 173
A. Brik & P.K. Robertson

Cost effective ground improvement solution for large scale infrastructure project 179
A. Brik & D. Tonks

Evaluation of existing CPTu-based correlations for the deformation properties of Finnish soft clays 185
B. Di Buò, J. Selänpää, T. Länsivaara & M. D'Ignazio

Ultimate capacity of the drilled shaft from CPTu test and static load test 193
M.A. Camacho, J. Mejia, C.B. Camacho, W. Heredia & L.M. Salinas

Interpreting properties of glacial till from CPT and its accuracy in determining soil behaviour type when applying it to pile driveability assessments 199
A. Cardoso, S. Raymackers, J. Davidson & S. Meissl

Variable rate of penetration and dissipation test results in a natural silty soil 205
R. Carroll & P. Paniagua

Rapid penetration of piezocones in sand 213
S.H. Chow, B. Bienen & M.F. Randolph

Applying Bayesian updating to CPT data analysis 221
S. Collico, N. Perez, M. Devincenzi & M. Arroyo

Geotechnical characterization of a very soft clay deposit in a stretch of road works 227
R.Q. Coutinho, H.T. Barbosa & A.D. Gusmão

Analysis of drainage conditions for intermediate soils from the piezocone tests 235
R.Q. Coutinho & F.C. Mellia

Behaviour of granitic residual soils assessed by SCPTu and other in-situ tests 241
N. Cruz, J. Cruz, C. Rodrigues, M. Cruz & S. Amoroso

Rate effect of piezocone testing in two soft clays 249
F.A.B. Danziger, G.M.F. Jannuzzi, A.V.S. Pinheiro, M.E.S. Andrade & T. Lunne

A modified CPT based installation torque prediction for large screw piles in sand 255
C. Davidson, T. Al-Baghdadi, M. Brown, A. Brennan, J. Knappett, C. Augarde, W. Coombs, L. Wang, D. Richards, A. Blake & J. Ball

Effects of clay fraction and roughness on tension capacity of displacement piles 263
L.V. Doan & B.M. Lehane

Shaft resistance of non-displacement piles in normally consolidated clay 269
L.V. Doan & B.M. Lehane

Effects of partial drainage on the assessment of the soil behaviour type using the CPT 275
L.V. Doan & B.M. Lehane

Analysis of CPTU data for the geotechnical characterization of intermediate sediments 281
M.F. García Martínez, L. Tonni, G. Gottardi & I. Rocchi

Detection of soil variability using CPTs 289
T. de Gast, P.J. Vardon & M.A. Hicks

MPM simulation of CPT and model calibration by inverse analysis 295
P. Ghasemi, M. Calvello, M. Martinelli, V. Galavi & S. Cuomo

Challenges in marine seismic cone penetration testing 303
P. Gibbs, R.B. Pedersen, L. Krogh, N. Christopher, B. Sampurno & S.W. Nielsen

Numerical simulation of cone penetration test in a small-volume calibration chamber: The effect of boundary conditions 309
M. Goodarzi, F.T. Stähler, S. Kreiter, M. Rouainia, M.O. Kluger & T. Mörz

Transition- and thin layer corrections for CPT based liquefaction analysis 317
J. de Greef & H.J. Lengkeek

Soil classification of NGTS sand site (Øysand, Norway) based on CPTU, DMT and laboratory results 323
A.S. Gundersen, S. Quinteros, J.S. L'Heureux & T. Lunne

Numerical study of anisotropic permeability effects on undrained CPTu penetration 329
L. Hauser, H.F. Schweiger, L. Monforte & M. Arroyo

Evaluating undrained shear strength for peat in Hokkaido from CPT 335
H. Hayashi & T. Yamanashi

Interpreting improved geotechnical properties from RCPTUs in KCl-treated quick clays 339
T.E. Helle, M. Long & S. Nordal

Some experiences using the piezocone in Mexico 347
E. Ibarra-Razo, R. Flores-Eslava, I. Rivera-Cruz & J.L. Rangel-Núñez

Evaluation of complex and/or short CPTu dissipation tests 351
E. Imre, T. Schanz, L. Bates & S. Fityus

New Russian standard CPT application for soil foundation control on permafrost 359
O.N. Isaev, R.F. Sharafutdinov, N.G. Volkov, M.A. Minkin, G.Y. Dmitriev & I.B. Ryzhkov

Thermophysical finite element analysis of thawing of frozen soil by means of HT-CPT cone penetrometer 365
O.N. Isaev, R.F. Sharafutdinov & D.S. Zakatov

Large deformation modelling of CPT probing in soft soil—pore water pressure analysis 371
J. Konkol & L. Bałachowski

The use of neural networks to develop CPT correlations for soils in northern Croatia 377
M.S. Kovacevic, K.G. Gavin, C. Reale & L. Libric

CPT in thinly inter-layered soils 383
D.A. de Lange, J. Terwindt & T.I. van der Linden

CPT based unit weight estimation extended to soft organic soils and peat 389
H.J. Lengkeek, J. de Greef & S. Joosten

Impact of sample quality on CPTU correlations in clay—example from the Rakkestad clay 395
J.S. L'Heureux, A.S. Gundersen, M. D'Ignazio, T. Smaavik, A. Kleven, M. Rømoen, K. Karlsrud, P. Paniagua & S. Hermann

Use of the free fall cone penetrometer (FF-CPTU) in offshore landslide hazard assessment 401
J.S. L'Heureux, M. Vanneste, A. Kopf & M. Long

Fibre optic cone penetrometer 407
P. Looijen, N. Parasie, D. Karabacak & J. Peuchen

Some considerations related to the interpretation of cone penetration tests in sulphide clays in eastern Sweden 411
A.B. Lundberg & E.A. Alderlieste

Effect of cone penetrometer type on CPTU results at a soft clay test site in Norway 417
T. Lunne, S. Strandvik, K. Kåsin, J.S. L'Heureux, E. Haugen, E. Uruci, A. Veldhuijzen, M. Carlson & M. Kassner

Evaluation of CPTU N_{kt} cone factor for undrained strength of clays 423
P.W. Mayne & J. Peuchen

Applying breakage mechanics theory to estimate bearing capacity from CPT in polar snow 431
A.B. McCallum

Empirical correlations to improve the use of mechanical CPT in the liquefaction potential evaluation and soil profile reconstruction 435
C. Meisina, S. Stacul & D.C. Lo Presti

Rigidity index (I_R) of soils of various origin from CPTU and SDMT tests 441
Z. Młynarek, J. Wierzbicki & K. Stefaniak

A state parameter-based cavity expansion analysis for interpretation of CPT data in sands 447
P.Q. Mo & H.S. Yu

Permeability estimates from CPTu: A numerical study 455
L. Monforte, M. Arroyo, A. Gens & C. Parolini

Pore pressure measurements using a portable free fall penetrometer 461
M.B. Mumtaz, N. Stark & S. Brizzolara

Influence of soil characteristics on cone and ball strength factors: Case studies 469
T.D. Nguyen & S.G. Chung

A method for predicting the undrained shear strength from piezocone dissipation test 477
E. Odebrecht, F.M.B. Mantaras & F. Schnaid

Realistic numerical simulations of cone penetration with advanced soil models 483
Z.Y. Orazalin & A.J. Whittle

Calibrating NTH method for ϕ' in clayey soils using centrifuge CPTu 491
Z. Ouyang & P.W. Mayne

CPT interpretation and correlations to SPT for near-shore marine Mediterranean soils 499
S. Papamichael & C. Vrettos

Characterization of a dense deep offshore sand with CPT and shear wave velocity profiling 505
J.G. Parra, A. Veracoechea & N. Vieira

Calibration of cone penetrometers in accredited laboratory 513
J. Peuchen, D. Kaltsas & G. Sinjorgo

Defining geotechnical parameters for surface-laid subsea pipe-soil interaction 519
J. Peuchen & Z. Westgate

Shallow depth characterisation and stress history assessment of an over-consolidated sand in Cuxhaven, Germany 525
V.S. Quinteros, T. Lunne, L. Krogh, R. Bøgelund-Pedersen & J. Brink Clausen

Assessment of pile bearing capacity and load-settlement behavior, based on Cone Loading Test (CLT) results 533
Ph. Reiffsteck, H. van de Graaf & C. Jacquard

CPT based settlement prediction of shallow footings on granular soils 539
J. Rindertsma, W.J. Karreman, S.P.J. Engels & K.G. Gavin

Analysis of acceleration and excess pore pressure data of laboratory impact penetrometer tests in remolded overconsolidated cohesive soils 545
R. Roskoden, A. Kopf, T. Mörz & S. Kreiter

CPT-based parameters of pile lengths in Russia 551
I.B. Ryzhkov & O.N. Isaev

Comparison of settlements obtained from zone load tests and those calculated from CPT and PMT results 557
A. Sbitnev, B. Quandalle & J.D. Redgers

Direct use of CPT data for numerical analysis of VHM loading of shallow foundations 563
J.A. Schneider, J.P. Doherty, M.F. Randolph & K. Krabbenhøft

Evaluation of existing CPTu-based correlations for the undrained shear strength of soft Finnish clays 571
J. Selänpää, B. Di Buò, M. Haikola, T. Länsivaara & M. D'Ignazio

Applications of RCPTU and SCPTU with other geophysical test methods in geotechnical practice 579
Z. Skutnik, M. Bajda & M. Lech

CPT in a tropical collapsible soil 585
C.S.M. Soares, F.A.B. Danziger, G.M.F. Jannuzzi, I.S.M. Martins & M.E.S. Andrade

Liquefaction resistance by static and vibratory cone penetration tests 591
F.T. Stähler, S. Kreiter, M. Goodarzi, D. Al-Sammarraie & T. Mörz

In situ characterisation of gas hydrate-bearing clayey sediments in the Gulf of Guinea 599
F. Taleb, S. Garziglia & N. Sultan

Gas effect on CPTu and dissipation test carried out on natural soft-soil of Barcelona Port 605
D. Tarragó & A. Gens

Comparison of cavity expansion and material point method for simulation of cone penetration in sand 611
F.S. Tehrani & V. Galavi

Soil behavior and pile design: Lesson learned from some prediction events—part 1: Aged and residual soils 617
G. Togliani

Soil behavior and pile design: Lesson learned from recent prediction events—part 2: Unusual NC soils 623
G. Togliani

A probabilistic approach to CPTU interpretation for regional-scale geotechnical modelling 629
L. Tonni, M.F. García Martínez, I. Rocchi, S. Zheng, Z.J. Cao, L. Martelli & L. Calabrese

CPTu-based soil behaviour type of low plasticity silts 635
L.A. Torres-Cruz & N. Vermeulen

Interpretation of soil stratigraphy and geotechnical parameters from CPTu at Bhola, Bangladesh 643
Z.A. Urmi & M.A. Ansary

Thermal Cone Penetration Test (T-CPT) 649
P.J. Vardon, D. Baltoukas & J. Peuchen

Development of numerical method for pile design to EC7 using CPT results 657
J.O. Vasconcelos, J. O'Donovan, P. Doherty & S. Donohue

Prehistoric landscape mapping along the Scheldt by camera- and conductivity CPT-E 663
J. Verhegge, Ph. Crombé & M. van den Wijngaert

Comparative analysis of liquefaction susceptibility assessment by CPTu and SPT tests 669
A. Viana da Fonseca, C. Ferreira, A.S. Saldanha, C. Ramos & C. Rodrigues

Application of CPT testing in permafrost 677
N.G. Volkov, I.S. Sokolov & R.A. Jewell

Comparison of mini CPT cone (2 cm^2) vs. normal CPT cone (10 cm^2 or 15 cm^2) data, 2 case studies 683
G.T. de Vries, C. Laban & E. Bliekendaal

The development of "Push-heat", a combined CPT-testing/thermal conductivity measurement system 689
G.T. de Vries & R. Usbeck

Free fall penetrometer tests in sand: Determining the equivalent static resistance 695
D.J. White, C.D. O'Loughlin, N. Stark & S.H. Chow

The variability of CPTU results on the AMU-Morasko soft clay test site 703
J. Wierzbicki, R. Radaszewski & M. Waliński

Shear strengths determined for soil stability analysis using the digital Icone Vane 709
M. Woollard, O. Storteboom, A.S. Damasco Penna & É.S.V. Makyama

Metal objects detected and standard parameters measured in a single CPT using the Icone with Magneto click-on module 715
M. Woollard, O. Storteboom, L. Gosnell & P. Baptie

Simulation of liquefaction and consequences of interbedded soil deposits using CPT data 723
F. Yi

Correlations among SCPTU parameters of Jiangsu normally consolidated silty clays 731
H. Zou, S. Liu, G. Cai & A.J. Puppala

Author index 739

Cone Penetration Testing 2018 – Hicks, Pisanò & Peuchen (Eds)
© 2018 Delft University of Technology, The Netherlands, ISBN 978-1-138-58449-5

Preface

The Technical Committee TC102 of the International Society for Soil Mechanics and Geotechnical Engineering (ISSMGE) and the Organising Committee of CPT'18 extend a warm welcome to all participants of the 4th International Symposium on Cone Penetration Testing (CPT'18). The symposium is being held at Delft University of Technology, in Delft, The Netherlands, 21–22 June 2018, and is the fourth in a series of successful symposia endorsed by TC102 of the ISSMGE, following on from: Linköping, Sweden, 1995; Huntington Beach, California, 2010; and Las Vegas, Nevada, 2014.

The Netherlands has a long history of pioneering research in geotechnical engineering, soil mechanics and testing of soils, motivated by the necessity for engineering constructions on reclaimed land and problematic deltaic soils. This included the first application of (electric, strain gauge) cone penetration testing by Fugro in 1964. Fugro then hosted the first symposium on cone penetration testing in 1972 in The Netherlands, with the proceedings of this "Sondeer Symposium 1972" comprising 6 papers in the Dutch language. One of the highlights of this 2018 symposium is a paper on a fibre optic cone penetrometer—a probable first. It is therefore with great pleasure that Delft University of Technology is hosting CPT'18.

The aim of the symposium is to provide a forum for exchange of ideas and discussion on topics related to the application of cone penetration testing in geotechnical engineering. In particular, the symposium will focus on the solution of geotechnical challenges using the cone penetration test (CPT), CPT add-on measurements and companion in-situ penetration tools (such as full flow and free fall penetrometers), with an emphasis on practical experience and application of research findings. As CPTs play a major role in geotechnical engineering, CPT'18 will bring together the world's experts who are working to improve the quality of cone penetration testing and reduce the difficulties involved. The symposium will be attended by academics, researchers, consultants, practitioners, hardware/software suppliers, certifiers and students. It will be a unique opportunity for meeting people and sharing high-level knowledge.

The peer-reviewed papers contained in the proceedings have been authored by academics, researchers and practitioners from many countries worldwide and cover numerous important aspects related to cone penetration testing in geotechnical engineering, ranging from the development of innovative theoretical and numerical methods of interpretation, to real field applications. The main topics are: interpretation of CPT results, application of the CPT, and equipment development.

A total of 189 abstracts were submitted and the authors of those abstracts that fell within the scope of the symposium were invited to submit full papers for peer review. A total of 122 papers were received and, of these, 104 papers were accepted for inclusion in the symposium proceedings (including 3 keynote papers). The editors would like to thank the Scientific Committee for their assistance in the review process. They would also like to thank the keynote lecturers, authors, participants and sponsors. The editors are grateful for the support of the chair and members of TC102.

On behalf of the Organising Committee, we welcome you to The Netherlands and hope that you find the symposium both enjoyable and inspiring.

Michael Hicks
Federico Pisanò
Joek Peuchen
April 2018

Taylor & Francis
Taylor & Francis Group
http://taylorandfrancis.com

Cone Penetration Testing 2018 – Hicks, Pisanò & Peuchen (Eds)
© 2018 Delft University of Technology, The Netherlands, ISBN 978-1-138-58449-5

Committees

ORGANISING COMMITTEE

Michael Hicks, *Delft University of Technology, The Netherlands (Chair)*
Federico Pisanò, *Delft University of Technology, The Netherlands (Co-Chair)*
Joek Peuchen, *Fugro, The Netherlands (Co-Chair)*
Matthijs Baurichter, *Delft University of Technology, The Netherlands*

SCIENTIFIC COMMITTEE

Shiaohuey Chow, *The University of Western Australia, Australia*
Jason DeJong, *University of California, Davis, USA*
David Frost, *Georgia Institute of Technology, USA*
Jürgen Grabe, *Hamburg University of Technology, Germany*
Michael Jefferies, *Golder Associates, UK*
Cristina Jommi, *Delft University of Technology, The Netherlands and Politecnico di Milano, Italy*
Mandy Korff, *Deltares and Delft University of Technology, The Netherlands*
Lone Krogh, *Ørsted Wind Power, Denmark*
Michael Long, *University College Dublin, Ireland*
Dirk Luger, *Deltares, The Netherlands*
Tom Lunne, *Norwegian Geotechnical Institute, Norway*
Diego Marchetti, *Studio Prof. Marchetti, Italy*
Paul Mayne, *Georgia Institute of Technology, USA*
Dominique Ngan-Tillard, *Delft University of Technology, The Netherlands*
Eric Parker, *RINA Consulting, Italy*
John Powell, *Geolabs Ltd., UK*
Nick Ramsey, *Fugro, Australia*
Peter Robertson, *Gregg Drilling and Testing, USA*
Rodrigo Salgado, *Purdue University, USA*
Nina Stark, *Virginia Tech, USA*
Nabil Sultan, *Ifremer, France*
Frits van Tol, *Deltares, The Netherlands*
Jędrzej Wierzbicki, *Adam Mickiewicz University in Poznań, Poland*
Cor Zwanenburg, *Deltares, The Netherlands*

Taylor & Francis
Taylor & Francis Group
http://taylorandfrancis.com

Cone Penetration Testing 2018 – Hicks, Pisanò & Peuchen (Eds)
© 2018 Delft University of Technology, The Netherlands, ISBN 978-1-138-58449-5

Sponsors

Symposium Organiser

TU Delft

Gold Sponsors

FUGRO

PAGANI® GEOTECHNICAL EQUIPMENT

Silver Sponsors

a.p. van den berg The CPT factory

Geomil equipment

GEOTECH SPECIALISTS IN GEOTECHNICAL FIELD EQUIPMENT

Bronze Sponsors

MARCHETTI DILATOMETER

LANKELMA GEOTECHNIEK ZUID SPECIALIST IN GEOTECHNICAL AND ENVIRONMENTAL SOIL INVESTIGATION

Datgel DATA SOLUTIONS Geotechnics • Geoenvironment • Laboratory

Deltares Enabling Delta Life

profound

Eijkelkamp GeoPoint SoilSolutions

Taylor & Francis
Taylor & Francis Group
http://taylorandfrancis.com

Keynote papers

Taylor & Francis
Taylor & Francis Group
http://taylorandfrancis.com

Cone Penetration Testing 2018 – Hicks, Pisanò & Peuchen (Eds)
© 2018 Delft University of Technology, The Netherlands, ISBN 978-1-138-58449-5

Penetrometer equipment and testing techniques for offshore design of foundations, anchors and pipelines

M.F. Randolph, S.A. Stanier, C.D. O'Loughlin, S.H. Chow, B. Bienen, J.P. Doherty, H. Mohr, R. Ragni & M.A. Schneider
University of Western Australia, Perth, Australia

D.J. White
University of Southampton, Southampton, UK

J.A. Schneider
USACE, St. Paul, MN, USA

ABSTRACT: This paper attempts to categorise geotechnical field site characterisation tools in a hierarchical manner, as appropriate for the progression from initial surveys to detailed geotechnical design of specific infrastructure. In general, the hierarchy reflects more the sophistication, and hence cost, of the field tools, although small-scale tools developed to explore box core samples are something of an exception, with the potential for high quality data at low cost. These ideas are explored in the context of modern developments in equipment and methods of deployment, and in the manner in which the data may be used efficiently in design.

1 INTRODUCTION

The current economic climate for offshore energy is requiring improved efficiency in the design of subsea infrastructure, a key starting point for which is optimising site investigation (SI) data and their application in design. Geotechnical design for deep water developments is dominated by subsea infrastructure such as subsea foundation units and in-field pipelines founded within the uppermost sediment layers. Even anchoring systems, particularly for mobile drilling systems, will generally lie within the top 10 to 20 m of the seabed. Hence the vast majority of deep water infrastructure is founded within sediments that are well within reach of relatively modest-sized robotic seabed tools or free-fall penetrometers. There is, however, a marked difference between testing requirements for pipeline design parameters, where the focus is generally the upper 0.5 m of the seabed, and those for subsea foundations and anchors.

For coastal and other shallow water developments, the challenge of acquiring in situ test data is reduced somewhat, although for applications like cable laying it may be sufficient just to identify sediment type. Economic pressures, particularly for wind and wave energy applications, will require optimisation of the spatial frequency of acquiring data in situ, and how the data are then applied in design to best advantage.

This paper discusses advances in site investigation approaches, with initial focus on novel approaches for near-surface characterisation and cost-effective free-fall penetrometry, which have particular relevance for deep water projects or for identifying surficial sediment types generally. The advances are considered in light of the need to balance cost and quality of data at different phases of a project. The paper also discusses the growth in 'direct' use of CPT data in design methods, such as for jack-up rig foundations. Potential differences between 'indirect' use of CPT data to derive simplified strength profiles, and more direct incorporation of what may appear relatively minor fluctuations in the cone resistance through the stratigraphy, are examined.

2 PHASES OF GEOTECHNICAL SITE CHARACTERISATION

2.1 *Exploratory phases*

For a new development, early investigation phases are focused on obtaining geophysical data in order to establish a broad geological model for the region. Historically, very limited (if any) geotechnical data

on the upper seabed sediments are obtained until later. This approach is influenced to a large degree by cost, since geophysical data may be gathered using relatively small vessels, with limited deck space for accommodating geotechnical investigation equipment.

Nowadays, however, lightweight (compact) tools, such as box core samplers, free-fall penetrometers and lightweight seabed frames equipped with small diameter coiled rod cone penetrometers are being incorporated increasingly in geophysical investigations. These provide early indications of the near-surface sediment properties, which are difficult to assess from standard seismic reflection tools (Peuchen & Westgate 2018).

In spite of inevitable disturbance of the soil recovered in a box core, reasonable quantitative estimates of intact and remoulded shear strength may be obtained from miniature penetrometer (T-bar or ball) tests conducted in the upper 0.3 m or so, depending on sample recovery (Low et al. 2008). As discussed in more detail later, additional parameters for pipeline design may be determined from torsional tests on novel types of penetrometer (White et al. 2017).

Free-fall penetrometers also offer cost-effective investigation of the near surface seabed. Even simple devices that just measure the deceleration (e.g. Stark et al. 2009, 2012) will allow approximate estimation of the strength of the upper sediments, providing useful guidance for pipeline route assessment. Modern lightweight free-fall piezocones offer much more quantitative assessment of the strength profiles through the upper material (Stegmann et al. 2006), provided the interpretation approach is appropriate (Chow et al. 2017).

2.2 *Main geotechnical SI phases*

In the main phases of geotechnical site investigation, larger vessels capable of handling larger and more sophisticated drilling and field testing equipment are used. Even here, though, the modern trend is for more compact, seabed-based robotic drilling and testing equipment, rather than conventional drill ships. In deep water, seabed-based systems are preferable in terms of cost (with compact equipment allowing smaller vessels) and datum stability since the systems are decoupled from wave-induced vessel motions.

Advances in robotic control have led to a number of commercial seabed-based robotic drilling, sampling and testing systems. The pioneer amongst these in terms of increased depth of water and soil depth investigated was the portable remotely operated drill (PROD), developed by Benthic Geotech (Figure 1). The equipment fits within standard shipping containers for transport.

Figure 1. Benthic Geotech's portable remotely operated drill (PROD).

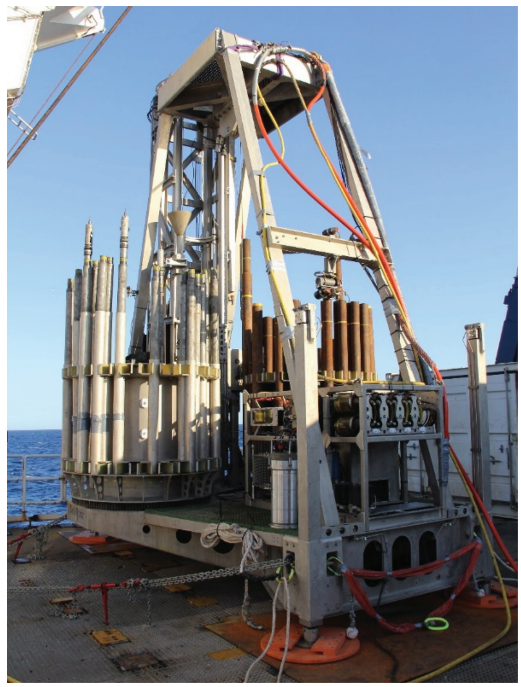

Figure 2. Fugro seafloor drill.

PROD and other systems, such as the Fugro Seafloor Drill (Figure 2), use an umbilical cable to power the seabed frame, although smaller systems can use remotely operated vehicles (ROVs) as a power source (Randolph 2016).

Seabed frames with advanced actuation offer the potential for more sophisticated penetration testing, for example by varying the rate of penetration in order to explore effects of strain rate and partial consolidation. This can yield measurements

that are more representative of conditions around the target infrastructure—which may involve significant changes in soil strength due to installation and in-service loading.

Full-flow penetrometers, such as the T-bar and piezoball with projected areas typically a factor of 10 greater than that of the shaft immediately behind the probe, provide potential for cyclic motion in order to remould the surrounding soil. They are often considered as applicable only for shallow uniform fine-grained sediments. However, experience in layered carbonate material has shown that they provide consistent data to CPTs in layered sediments, generally with T-bar and ball resistances showing slightly lower magnitudes of spikes in resistance (see Figure 3).

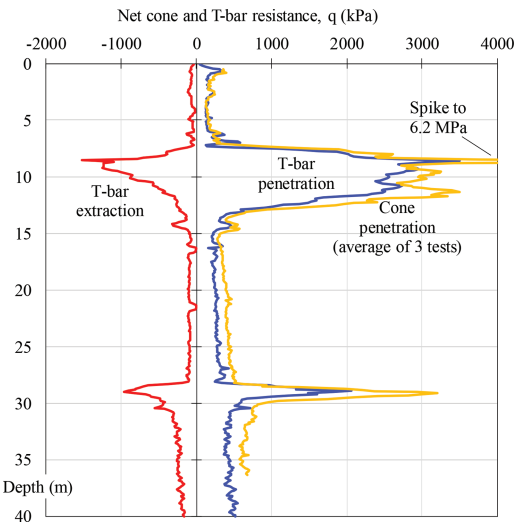

Figure 3. Comparison of in situ cone and T-bar penetration tests from Australian North-West Shelf.

The addition of pore pressure sensors on so-called 'piezoball' penetrometers, either as discrete button filters or continuous annular filters, enhances their potential as a stratification tool, and also allows field assessment of consolidation properties by means of dissipation tests (Mahmoodzadeh et al. 2015).

As illustration of this potential, Figure 4 shows the range of penetration resistance mobilised in a carbonate silt, relative to a standard rate penetration test. The data are from the RIGSS JIP (White et al. 2017) and span a factor of 20 between fully remoulded conditions and those after full consolidation.

The data from Figure 4 were obtained under laboratory conditions, in a centrifuge model test, although similar data may be acquired from in situ tests. In the carbonate silt, penetration under undrained conditions even at the very high rates associated with free-fall penetrometers, gives lower resistance than for drained conditions at a very slow penetration rate. In stronger soils, such as medium dense silica sand, undrained conditions will most likely provide the highest penetration resistance due to the dilative nature of such soils. The effect of sand density on the relative magnitudes of drained and undrained penetration resistances is well illustrated by the penetrometer data presented by Chow et al. (2018).

The very high resistances in sand mobilised under undrained conditions have been observed in field free-fall penetrometer tests, leading to rapid arrest of the penetrometer (Stark et al. 2012). Although this limits the depth that can be

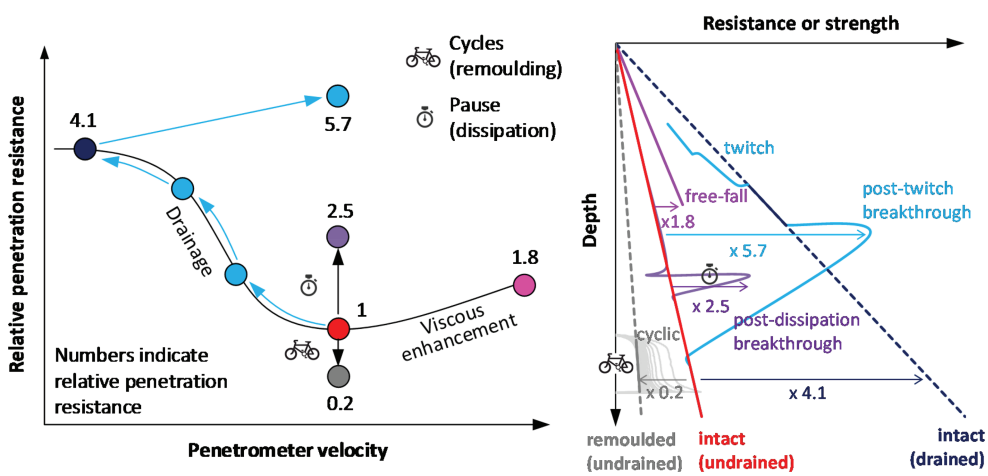

Figure 4. Penetration resistances mobilised in a carbonate silt through different penetrometer test procedures.

explored, the information of shallow sandy sediments with high (undrained) penetration resistance has value for design. With some additional inputs, for example knowledge of mineralogy and particle size of the sediments, the deduced penetration resistances may be interpreted in terms of relative density, in the same way as for static CPTs (White et al. 2018).

Prior to cavitation the undrained strength of sand may be estimated using the framework of Bolton (1986) or a state parameter approach (Been et al. 1991). After cavitation, although this is unlikely to occur in deep water, an upper limit to the penetration resistance may be estimated by considering the cavitation pressure as a 'back pressure' acting in conjunction with the geostatic effective stress state.

Improvements in control and testing procedures open the door to much more sophisticated seabed testing. Figure 5 shows schematically the range of shear strength data that may be acquired, relative to strengths relevant for design of different offshore infrastructure. The diagram reflects the variations in penetration resistance arising from different testing procedures, as discussed with respect to Figure 4. The horizontal spread reflects changes in strength due to consolidation (left side) or disturbance and remoulding (right side), while the vertical axis signifies changes in strength due to shear strain rate.

Modern robotic systems also have the control potential to allow seabed testing that targets stiffness measurement. For example, fatigue design of riser systems requires information on the vertical riser-soil stiffness, and how that varies with time and displacement amplitude of cyclic perturbations.

For a steel catenary riser, the relevant stiffness may vary by 1 or 2 orders of magnitude through the touchdown zone as the displacement amplitude of the riser changes. At a given amplitude, the stiffness will also tend to reduce in the short term as the soil responds to cyclic shearing, but to increase with time due to consolidation (Clukey et al. 2017, Yuan et al. 2017).

Future potential for field tests, either on the seabed or in recovered box core samples (Kelleher et al. 2010, Boscardin & DeGroot 2015), is discussed in the following section, drawing on recent experience on Australia's North-West Shelf and in the Caspian Sea.

3 NOVEL SHALLOW PENETROMETERS FOR PIPELINE DESIGN PARAMETERS

3.1 *Background—RIGSS JIP*

The Remote Intelligent Geotechnical Seabed Surveys Joint Industry Project (RIGSS JIP) was initiated by the University of Western Australia (UWA) and is reaching the end of the 3 year program of activities. A focus of the JIP has been the development of new and improved techniques for in-situ geotechnical investigation of the upper few metres of the seabed.

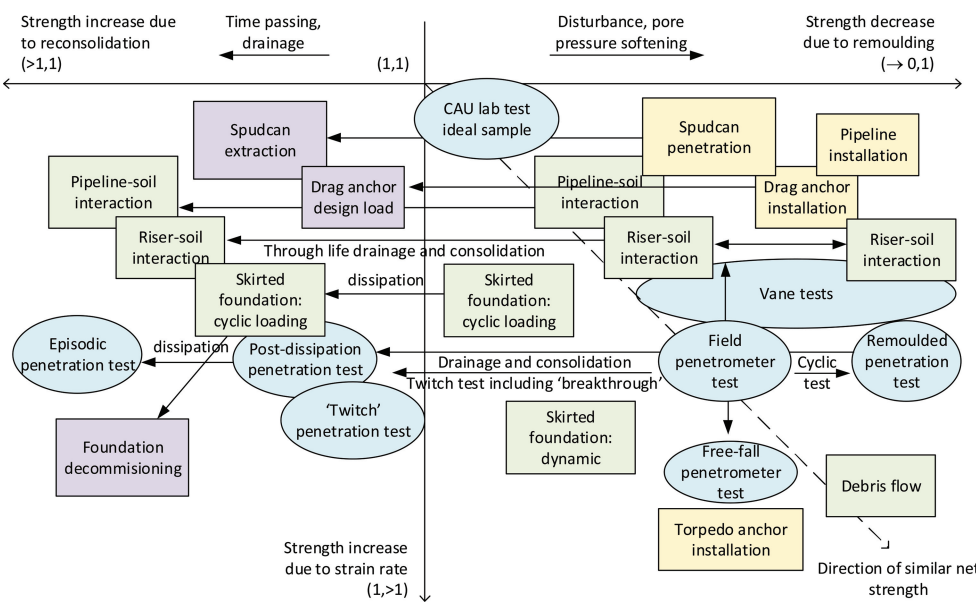

Figure 5. Map of different soil tests and design applications (extended from Randolph et al. 2007).

The RIGSS JIP has pursued three 'visions', which are illustrated in Figure 6:

1. The RIGSS SI: A remote SI platform with robotic control of intelligent tools gathering parameters targeted towards design.
2. Earlier geotechnical definition in projects: leading to reduced uncertainty and risk, and a reduced need to carry multiple options through design.
3. Direct geotechnical design: a design philosophy using in situ test data more directly to determine the response of pipelines, foundations, and other geotechnical systems

Together, these three ideas aim to allow more accurate forecasting of the behaviour of seabed infrastructure. New types of penetrometer can be shaped and manipulated in ways that more closely represent the infrastructure being designed. The resulting data provide the potential to eliminate or simplify the journey from measured resistance to a lab-based strength and back to a predicted resistance or capacity.

A particular focus of the RIGSS JIP has been on shallow surveys that cover extensive areas, such as for pipelines, where low-cost, remotely operated SI tools and smart testing techniques offer potential to improve efficiency and deliver more valuable data. Intelligent tools—such as the shallow penetrometers—give data that can be fed more directly into geotechnical design, reducing the timescale and uncertainty associated with the design outcome.

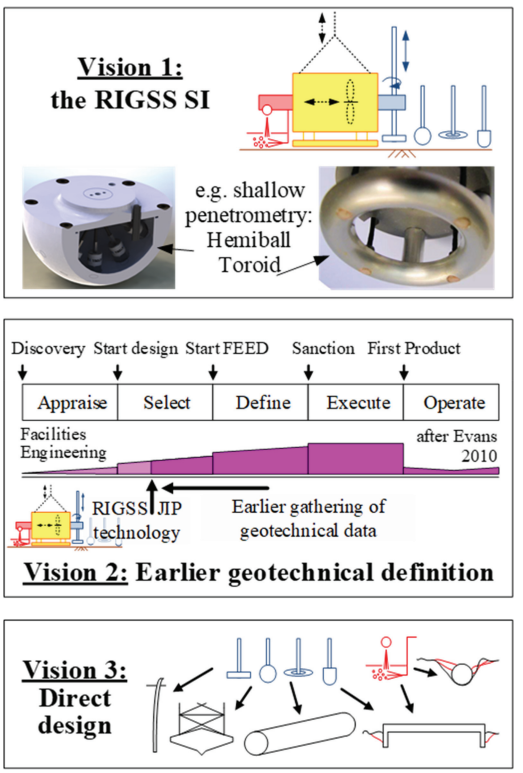

Figure 6. RIGSS JIP motivations (after White et al. 2017).

3.2 *Offshore box core testing*

Three types of 'shallow' penetrometers have been pursued within the RIGSS JIP. The toroidal and hemispherical ('hemiball') penetrometers were first described by Yan et al. (2011); more recently a ring-shaped variant on the toroid with a flat interface has been trialled. During a test, these devices are penetrated to a depth of less than a diameter (of toroidal bar, or hemiball) and are then subjected to one or more stages of rotation under maintained vertical load. Their shape and the interfacial sliding mode of failure resemble a pipeline, or other surface infrastructure such as mattresses or surface foundations.

Devices at box core scale have been developed and trialled in the UWA laboratory on reconstituted kaolin and carbonate silt samples. The system has also been taken offshore, for field trials on two surveys by the RIGSS JIP partners. The general design of the box core toroid penetrometer and the integrated data acquisition system are shown in Figure 7. The vertical force and torque on the penetrometer are monitored continuously, as are the pore pressures at multiple locations on the surface.

The soil-interface resistance is derived from the measurements, in terms of both total and effective

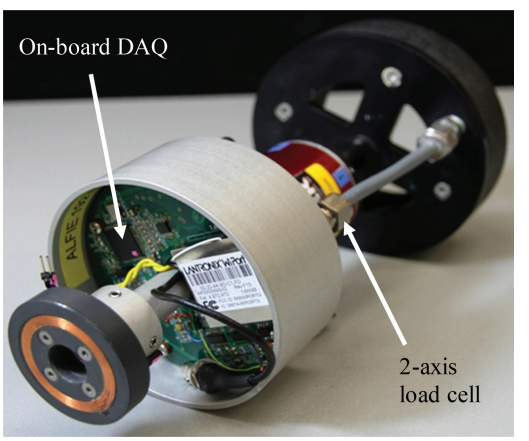

Figure 7. Toroid penetrometer with on-board DAQ and 2-axis load cell (vertical force and torque).

normal stresses. Dissipation stages allow the consolidation coefficient to be determined for fine-grained soils, while the timing of rotation stages may be varied to deduce both drained and undrained interface strengths.

Box-coring operations during one of the recent offshore trials are shown in Figure 8. By utilising multiple box core sleeves, sampling operations may be continued in parallel with shallow penetrometer testing within a previously recovered box core sample. Depending on the drainage properties of the samples, a full set of penetrometer tests in the box core might take 1–3 hours. If this aligns with the cycle time for the vessel transit between locations and box core recovery, then two sleeves can be alternated between sampling and testing.

The box core actuator system is shown during testing within a box core sleeve in Figure 9. Another approach is to take large diameter tube samples from the box cores, and perform tests off the sampling critical path using the arrangement shown in Figure 10.

The initial field trials provided valuable lessons to improve the procedures for deploying the tests and determining the best combination of tests to perform in a given soil type, to optimise the information gathered. The deck of a survey vessel is a challenging environment for performing precision testing, but vessel motions and changes in ambient temperature have had no detrimental effect on the

Figure 8. Typical box corer during sample recovery to deck.

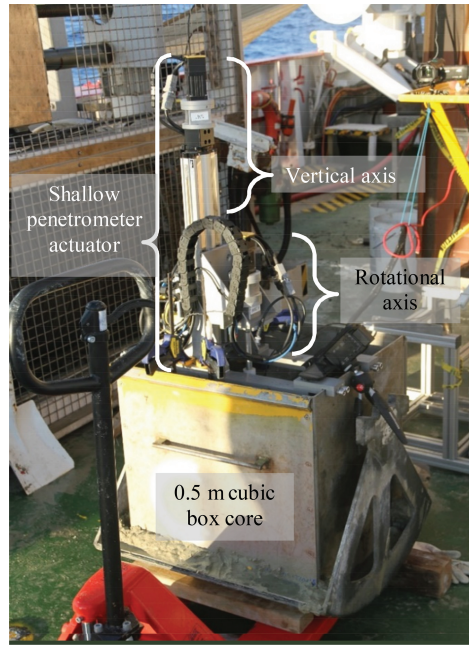

Figure 9. Shallow penetrometer system in 'box core' mode.

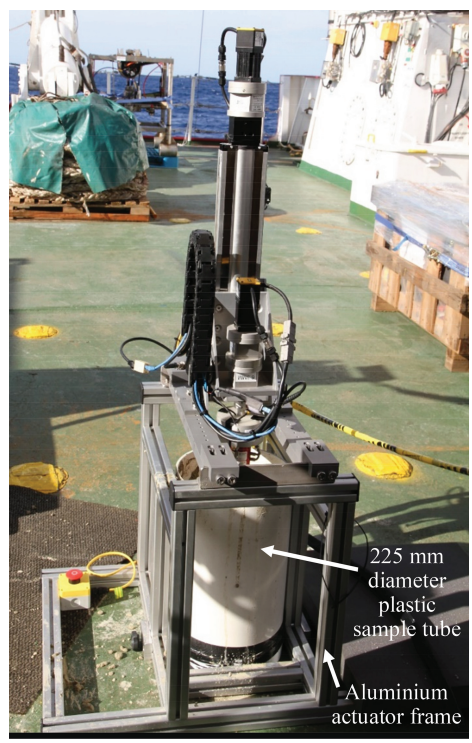

Figure 10. Shallow penetrometer system in 'tube sample' mode.

measurement quality emerging from the shallow penetrometer tests. To date, the testing equipment has required operation by a researcher familiar with the equipment and software controls. As the technology evolves, simpler systems will be created. We anticipate that shallow penetrometer testing could then be available on a basis similar to the existing Fugro DECKSCOUT and other box core penetrometer systems.

A typical set of results is used to illustrate the performance of the toroid penetrometer (Figure 7), operated in a box core sample of carbonate silt. The initial stage of a toroid test involves vertical penetration of the device to a depth of typically 20% of the diameter (Figure 11). The results are converted to a linear profile of undrained strength, s_u, using the bearing capacity model set out by Stanier & White (2015). In this approach, the bearing factor, N_c, is varied according to the depth and strength gradient, and a (small) adjustment is also made for soil buoyancy. An iterative process is required to reach s_u because N_c varies with s_u itself. The minimal noise in the measured data is equivalent to less than 0.1 kPa of strength (Figure 11).

After reaching the target depth, the vertical load on the penetrometer is maintained constant, while the excess pore pressure at the invert dissipates (Figure 12). The initial response—over the first five seconds of the dissipation—shows a rise in pore pressure, typical for dilatant soils. During the subsequent 10 minutes, the response follows closely the analytical model set out by Yan et al. (2017), based on numerical analysis. By matching the curves at the 50% dissipation point, a consolidation coefficient of 65 m^2/year is determined.

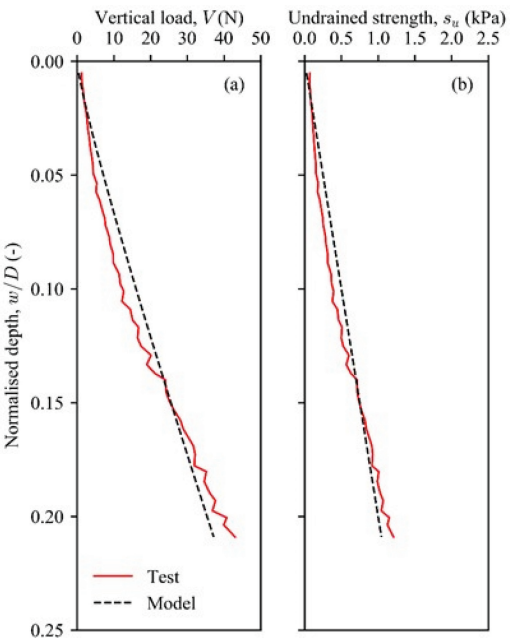

Figure 11. Fitting of measured toroid penetration response in carbonate silt with analytical model: (a) measured vertical load; and (b) interpreted profile of undrained shear strength, s_u.

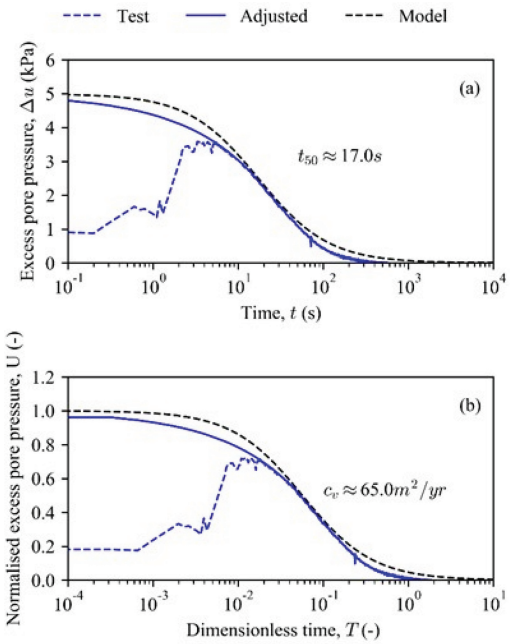

Figure 12. Toroid dissipation in carbonate silt: (a) measured response; and (b) interpreted coefficient of consolidation, c_v.

The next stage of the test involves rotation of the toroid (Figure 13). Initially a high rotation rate is used to mobilise the undrained interface strength, including any initial peak but continuing towards the stable or residual value used in pipeline design. The rotation rate is then reduced by a factor of 10. Rotation continues as the resistance rises towards the drained limit, controlled by the interface friction angle.

The measured torque and vertical force are converted to interface friction ratio by dividing the torque by the effective radius (at which the resultant of the circumferential resistance acts) and multiplying the vertical force by a 'wedging factor' (White & Randolph 2007) to give the total normal force on the interface. The resulting interface friction ratio can be fitted by undrained and drained limits (Figure 13), which are key inputs to pipeline design. The rate of transition provides another indication of the consolidation coefficient, which may differ from the initial dissipation stage.

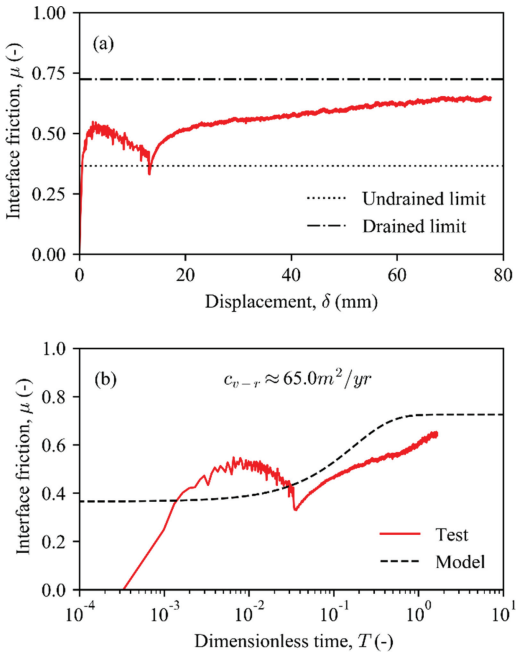

Figure 13. Toroid rotation in carbonate silt: evolution of interface friction, μ with (a) displacement; and (b) dimensionless time.

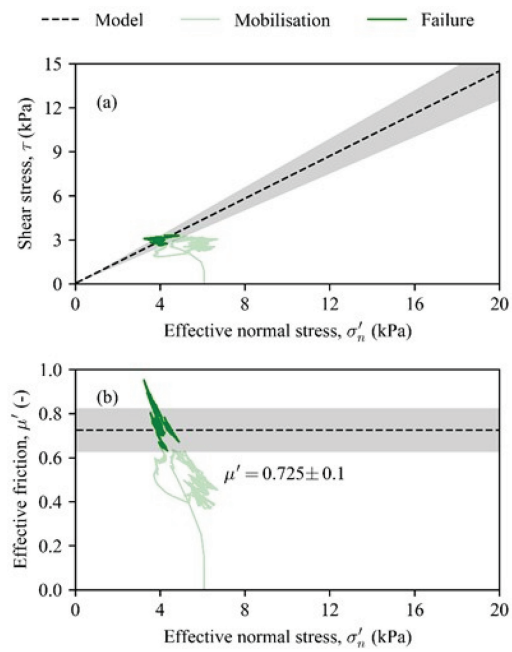

Figure 14. Toroid effective stress interpretation: (a) effective stress envelope; and (b) effective interface friction, μ'.

The undrained limit, if the soil has been normally consolidated under the penetrometer vertical load, is the 'c/p' or normally consolidated undrained strength ratio for the interface. The drained limit is $\tan(\delta_{res})$ where δ_{res} is the residual interface friction angle. This interpretation is aligned with conventions for pipeline design (White et al. 2017, DNVGL 2017).

The interface response can also be interpreted in effective stress terms using the pore pressure measurements (Figure 14). This provides useful confirmation of the drained friction, particularly if the tests are curtailed before pore pressure equilibrium is reached.

An additional type of test involves episodic rotations with intervening dissipations, which results in gradually increasing undrained resistance with each cycle (Yan et al. 2014, Boscardin & DeGroot 2015). The data may be interpreted within a consolidation framework, and used to support assessment of 'consolidation hardening' by which pipeline axial friction can rise through cycles of movement.

Overall, subject to a suitable box core sample being recoverable, a short series of shallow penetrometers tests (e.g. 2–3 tests performed over several hours), supplemented with conventional miniature T-bar (or ball) penetrometer tests, can provide all of the geotechnical strength and consolidation parameters required for pipeline design. We hope that these technologies will be taken forward by the RIGSS JIP partners over the coming years, allowing wider adoption in project practice.

4 FREE-FALL PENETROMETERS

4.1 *Introduction*

Free fall penetrometers (FFPs) may be divided into different classes, according to the sophistication of instrumentation (ranging from just accelerometers to fully instrumented with tip and shaft load cells and pore pressure sensors). Recent developments have included two-stage combined FFP systems where free-fall penetration is followed by static penetration. In addition, extended base FFPs have been explored for soft sediments, as discussed later. The discussion below describes different types of FFPs, and then summarises interpretation in fine-grained sediments.

4.2 *Probe geometry*

A variety off FFPs are shown in Figure 15. They vary in mass and geometry from the 52 mm diameter by 0.215 m long 0.7 kg expendable bottom penetrometer (XBP, Stoll & Akal 1999) to the

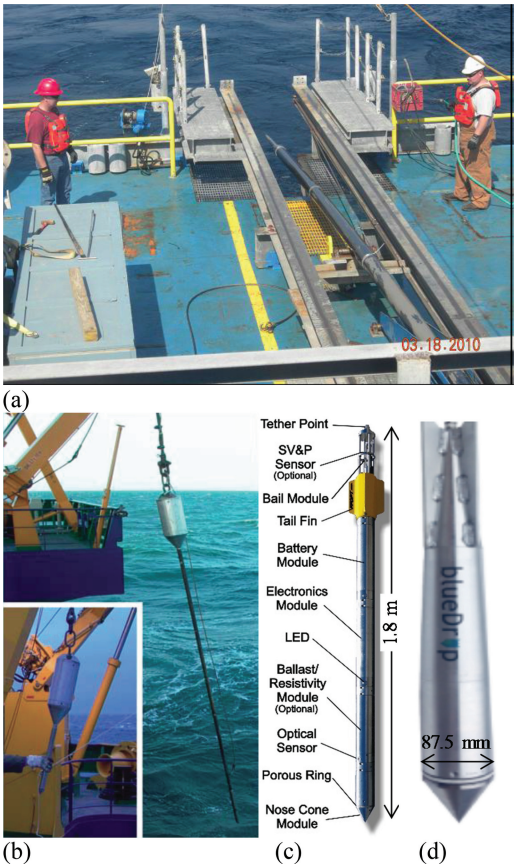

Figure 15. FFPs: (a) CPT Stinger (Young et al. 2011) (b) University of Bremen FFCPT shown in long and short (inset) modes (Stegman et al. 2006) (c) Brooke Ocean 'FFCPT-660' (Mosher et al. 2007) and (d) BlueDrop (Stark et al. 2014).

160 mm diameter (with a standard CPT tip) by 23 to 35 m long 3200 kg CPT-Stinger (Young et al. 2011). Penetration is generally proportional to mass (or momentum) per unit area (Peuchen et al. 2017), with the XBP generally penetrating less than 0.3 m, and the CPT-Stinger capable of reaching 20 m of dynamic penetration followed by another 15 m of static penetration.

A class of intermediate size probes capable of 4 to 6 m of penetration in soft clays, 1 to 2 m penetration in stiff clays and silts, and less than 0.5 m penetration in sands is seeing increased use for shallow investigations in soft materials. These penetrometers are relatively portable and can be used from survey size vessel with a high-speed winch for deployment and retrieval, with diameters of 100 to 200 mm, lengths of 1 to 6 m, and mass of 10 to 500 kg. They include:

- NAVFAC eXpendable Doppler Penetrometer (XDP) (Beard 1985, Orenberg et al. 1996, Thompson et al. 2002)
- Seabed Terminal Impact Naval Gauge (STING) (e.g. Mulhearn 2003)
- Brooke Ocean Free Fall CPT (FFCPT) (Furlong et al. 2006)
- Bremen Free Fall CPT (FFCPT) (Stegmann et al. 2006)
- NIMROD (Stark et al. 2009)
- LIRmeter (Stephan et al. 2011)
- BlueDrop (Stark et al. 2014)
- Graviprobe (Geirnaert et al. 2013)
- Instrumented Free-Fall Sphere (IFFS) (Morton et al. 2016a)
- SEADART1 (Peuchen et al. 2017)

4.3 *Sensors*

Historically FFPs were only equipped for acceleration or velocity measurements. With the need for higher quality measurements of the location of the seabed, soil strength, as well as inferences of soil type, additional sensors such as optical sensors, tip stress, sleeve friction, penetration pore pressure, and resistivity have been added to probes.

The most efficient means of FFP operation is whereby the instrumentation package has sufficient power and storage for a series of tests. In a continuous test mode, where the penetrometer is repeatedly deployed and retrieved, the instrumentation package should have storage and battery capabilities for about 12 hours of testing. After this the package can be removed from the penetrometer for battery recharging and data download, or alternatively the package could be replaced with a spare system, allowing testing to continue without delay.

Modern data acquisition systems allow for this mode of operation. For example, the UWA instrumentation package shown in Figure 16 is sufficiently compact to fit within the smallest FFPs, but allows for sampling rates of up to 500 kHz and at a practical sampling rate of 1.5 kHz for FFP tests, up to 225 hours of data storage and 20 hours of continued use before the batteries require recharging.

All FFPs measure acceleration along an axis aligned with the body of the FFP (although often sensors with different measurement ranges are included to optimise resolution). The UWA instrumentation package shown in Figure 16 is an inertial measurement unit (IMU), which measures acceleration along each axis of a Cartesian coordinate system and provides independent measurements of the rotations about each axis of the same coordinate system. Transforming the measurements from the body reference frame of the FFP (which will be changing during an FFP test if the

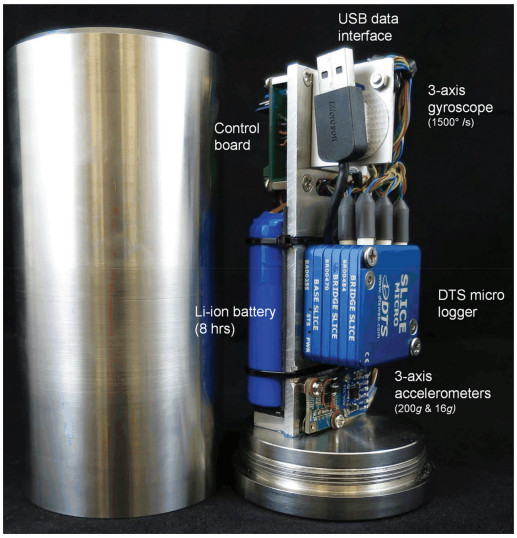

Figure 16. UWA inertial measurement unit (IMU).

FFP tilts by varying amounts) to a fixed reference frame avoids the difficulty in identifying the component of the acceleration signal that is due to FFP rotation from that due to changing acceleration (Blake et al. 2016).

O'Loughlin et al. (2014) showed that the corrections using this approach become appreciable at tilts in excess of 10°. Conical shaped penetrometers appear to tilt less than this threshold (Kopf et al. 2007), but for other penetrometers, particularly the free-fall sphere penetrometer (described later), the tilts are likely to be much higher, such that an IMU approach is required.

4.4 *Interpretation using acceleration data*

The ultimate objective of a FFP test in fine-grained material is to assess the undrained shear strength s_u. This may be derived from the tip resistance in the conventional way as for a static CPT, but with appropriate allowance for the high strain rates resulting from the high velocity penetration. Ideally, the FFP should measure the tip resistance directly. However, for FFPs that do not include a tip load cell, estimation of the tip resistance involves a number of steps and uncertainties.

The tip resistance may be derived from the penetrometer mass, m, times the measured acceleration, a = v(dv/dz) according to

$$q_{t,FFP} = \frac{W_b - mv(dv/dz) - Q_s - F_D - F_b}{A_{tip}} \quad (1)$$

where v is the FFP velocity, z the penetration, W_b the submerged weight of the FFP in water, Q_s the frictional resistance along the shaft, F_D the drag resistance (due to soil inertia), F_b the buoyancy force equal to the effective weight of the displaced soil and A_{tip} the cross-sectional area of the tip (True 1976, Rocker 1985, O'Loughlin et al. 2004, Chow et al. 2017).

The challenge with this approach is in correctly identifying and quantifying the magnitude of the various terms in Equation (1). A further complication is that, since the undrained shear strength (derived from the tip pressure $q_{t,FFP}$) contributes towards the shaft resistance, an iterative approach is needed in solving for the tip resistance. This may be avoided for extended base FFPs such as the free-fall sphere and STING, since the shaft resistance may be excluded from Equation (1). However, it may then be necessary to consider the additional soil mass that moves with the base (Morton et al. 2016b).

4.4.1 *Hydrodynamic and soil drag*

Soil drag resistance can dominate interpretation of strength in weak seabeds at shallow embedment, and accounting for this parameter is necessary for accurate strength assessments as well as in probe design. Soil drag is calculated in the same manner as for hydrodynamic drag, as

$$F_D = 0.5 C_d \rho_s A_{tip} v^2 \quad (2)$$

where ρ_s is the saturated density of the soil and C_D is the drag coefficient, the value of which depends on the penetrometer geometry. The density must be estimated (since samples are not taken) and there is uncertainty in the drag coefficient.

Consideration of the acceleration trace during the free-fall in water phase allows the fluid drag characteristics, and its variation with Reynolds number for a particular geometry, to be established (Morton et al. 2016a, O'Beirne et al. 2017). It is common to estimate the soil drag coefficient as the same as the fluid drag coefficient, which tends to vary from about 0.15 (increasing with L/D) for cylindrical penetrometers with hemispherical tips, to about 0.26 for spheres.

If the fluid and soil drag coefficient are assumed equal, the influence of the tether on drag characteristics should be considered. Depending on probe mass, geometry, fall height through water, and tether characteristics, tethered terminal velocities may be half or less than untethered velocities, as indicated by offshore data in Figure 17. Upon seabed impact the tether may tend to go slack, changing the drag resistance implied by the probe impact velocity.

4.4.2 *Shaft frictional resistance*

For probes that only measure acceleration or velocity, the friction along the side of the probe must be subtracted from the total resistance to

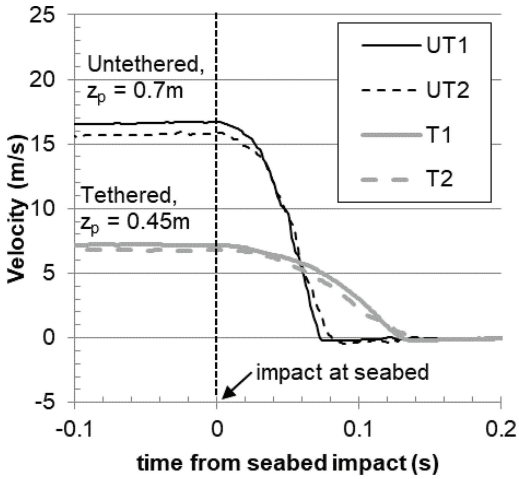

Figure 17. Influence of tethering on penetration of NAVFAC XDP drop through 30 m of water into a low plasticity clay with s_u of 10 to 20 kPa in the upper 0.75 m.

assess tip resistance. Shaft friction on the side can be estimated based on the undrained strength through an adhesion factor, α, which is commonly assumed to be the inverse of the soil sensitivity. The total shaft friction at any given penetration is:

$$Q_s = \sum \Delta A_{shaft} R_{f,shaft} \alpha s_u \tag{3}$$

The significant uncertainty in soil sensitivity (or α), and how that varies with depth, will propagate through to the accuracy of the estimated tip resistance. The shaft friction is also found to exhibit much higher rate effects than the tip resistance (as discussed later) and hence a higher rate parameter $R_{f,shaft}$ (Steiner et al. 2014, Chow et al. 2017). The uncertainty in both the soil sensitivity and $R_{f,shaft}$ is the most significant factor for accurate estimation of soil strength using the accelerometer measurement.

4.5 *Cone tip resistance and derivation of s_u*

Improved estimation of soil strength can be obtained by measuring the FFP tip resistance directly with a load cell. Interpretation is similar to that for a static CPT, with the additional need to deduct drag resistance and to discount the soil strength for strain rate effects, according to:

$$s_u = \frac{q_{c,FFP} - q_D + u_2(1-\alpha_{cone}) - \sigma_{v0}}{R_{f,tip} N_{kt}} = \frac{q_{net,d}}{R_{f,tip} N_{kt}} \sim \frac{q_{net,s}}{N_{kt}} \tag{4}$$

where $q_{c,FFP}$ is the measured tip resistance, u_2 the pore pressure measured or estimated at the cone shoulder, α_{cone} the unequal area ratio, σ_{vo} the overburden stress, q_D the drag resistance (equivalent to F_D/A_{tip} from Equation (1)), $R_{f,tip}$ the strain rate factor for tip resistance, N_{kt} the cone factor, $q_{net,d}$ the resulting dynamic net cone resistance and $q_{net,s}$ the static net cone resistance from a conventional CPT.

4.6 *Viscous rate effects*

The extremely high penetration velocity of an FFP (especially at shallow depth) leads to very high strain rates in the soil that will enhance the soil strength beyond nominally undrained values. The effect of strain rate may be modelled using either a semi-logarithmic (or inverse hyperbolic sine function) or power law (including the Herschel-Bulkley formulation). The simple power law of

$$R_{f,tip} = \left(\frac{\dot{\gamma}}{\dot{\gamma}_{ref}}\right)^{\beta} = \left(\frac{v/D}{(v/D)_{ref}}\right)^{\beta} \geq 1 \tag{5}$$

has generally been adopted as it is found to capture rate effects better than logarithmic functions over large ranges of strain rate (Biscontin & Pestana 2001). Here $\dot{\gamma}$ is the strain rate, $\dot{\gamma}_{ref}$ the reference strain rate associated with the reference value of undrained shear strength and β a strain rate parameter. The average strain rate may be linked directly to the normalised velocity, v/D. Due to the different rate effects observed for the tip and shaft resistance (see later, Figure 19) different strain rate parameters, β_{tip} and β_{shaft} are recommended for estimating $R_{f,shaft}$ and $R_{f,tip}$ in Equations (3) and (4) respectively.

The reference strain rate, and hence selection of v_{ref} and D_{ref}, should correspond to nominally undrained conditions, similar to those that would develop in a static cone penetrometer test. For instance selection of v_{ref} = 20 mm/s and D_{ref} = 35.7 mm would result in a strength that would be comparable to that measured by a 10 cm^2 cone penetrated at the usual 20 mm/s. For an FFP with diameter of 100 mm, travelling at velocity, v = 10 m/s, v/D = 100 s^{-1}, two orders of magnitude higher than in the static 10 cm^2 cone test. For this magnitude variation in strain rate, the strain rate parameter β_{tip} is typically in the range 0.03 to 0.09 for tip resistance (Lehane et al. 2009, O'Loughlin et al. 2013, 2016, Chow et al. 2017).

4.7 *Example interpretation from test data*

An example interpretation from centrifuge experiments in kaolin clay (Chow et al. 2017) is provided in Figure 18 to Figure 20. The interpretation based solely on acceleration measurements (but with

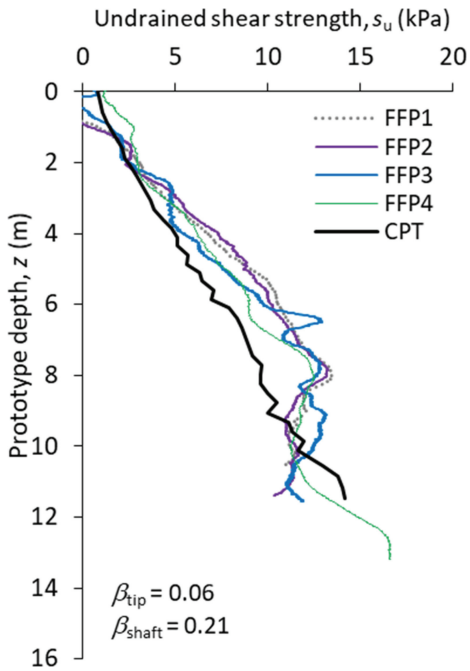

Figure 18. Estimated s_u profiles using the accelerometer method (after Chow et al. 2017).

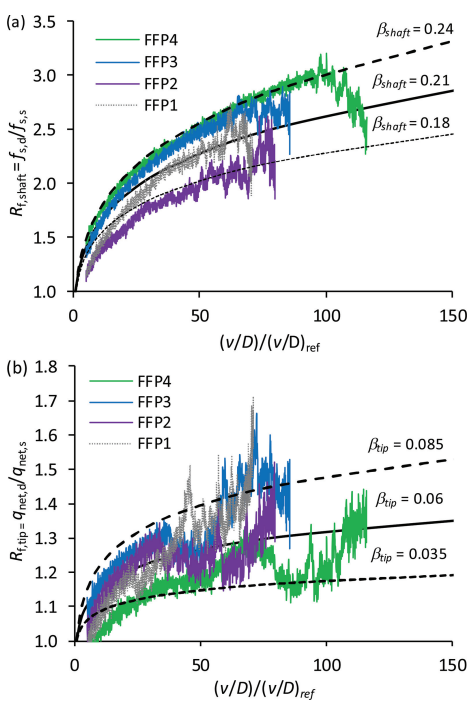

Figure 19. Back-fitted rate parameters for (a) shaft resistance and (b) net tip resistance (after Chow et al. 2017).

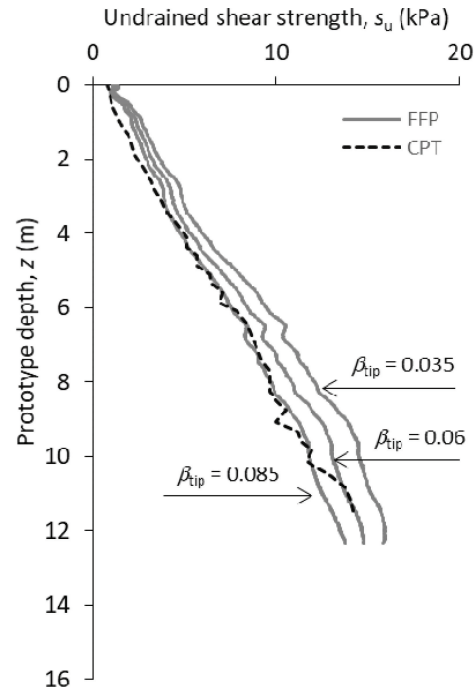

Figure 20. Deduced s_u profiles using tip load cell (after Chow et al. 2017).

no account taken of any 'tethering' effects since these are negligible for the centrifuge model test) underestimates the strength deduced from static CPTs by approximately 50%, even when separate strain rate parameters (β_{tip} and β_{shaft}) are applied, as established in direct measurements from the tip and shaft load cells of the FFP (see Figure 19). This large discrepancy is caused by the uncertainty in estimating the dynamic shaft resistance reliably (Chow et al. 2017).

Figure 20 shows (for the same Chow et al. 2017 centrifuge tests) that when the interpretation is based on the tip load cell and u_2 pore pressure measurements, s_u values determined from static CPTs and FFP tests are essentially indistinguishable. The interpretation on Figure 20 uses a median $\beta_{tip} = 0.06$, with variations in β_{tip} (reducing to $\beta_{tip} = 0.035$ and increasing to $\beta_{tip} = 0.085$) leading to changes in the FFP s_u interpretation that vary by less than ±10%. Interestingly, the u_2 excess pore pressure response was mainly negative in the FFP tests and positive in the static CPTs, although the measured (negative) u_2 without adjustment was needed in Equation (4) for correcting the unequal area effect in order to provide the agreement in Figure 20.

The negative u_2 measured during the dynamic penetration has been attributed to local effects due

to the cone geometry and position of the u_2 sensor (Chow et al. 2014). The phenomenon may be considered a result of Bernoulli effects, as illustrated by computational fluid dynamics analyses for free fall in water (Lucking et al. 2017, Mumtaz et al. 2018). Negative u_2 values following embedment were also found in large deformation finite element analyses for soils that show strain rate dependency of strength (Sabetamal et al. 2016). This requires further experimental validation, and is particularly important if FFPs are to be interpreted to provide Robertson-style soil behaviour types.

4.8 *Penetrometer shape*

Where accurate determination of s_u at shallow depths (e.g. < 1 m) is required, there may be benefits in employing 'extended base' FFPs. Examples include the plate-tipped STING (Mulhearn 2003, Fawaz et al. 2016; Chow & Airey 2014; see Figure 21a) and the free-fall sphere (Morton et al. 2016a, b; see Figure 21b). Due to the relatively large tip area of these FFPs, drag resistance becomes a significant and often dominating component of the soil resistance.

In addition to the better resolution in s_u permitted by the larger tip area, there is essentially no shaft resistance on an extended base FFP, so that the complex calculation of dynamic shaft resistance is avoided. This allows s_u to be determined indirectly from the acceleration measurements, meaning that this class of FFP does not require load cell measurements.

Example interpreted s_u profiles for the free-fall sphere are provided in Figure 22 for a lake-bed clay in Northern Ireland and a nearshore clay in the Firth of Clyde, off the West coast of Scotland. Significant penetrations were achieved, particularly in the very soft lake-bed clay, using impact velocities typically in the range 4 to 8 m/s.

Figure 21. Extended base FFPs: (a) STING (Fawaz et al. 2016), (b) free-fall sphere.

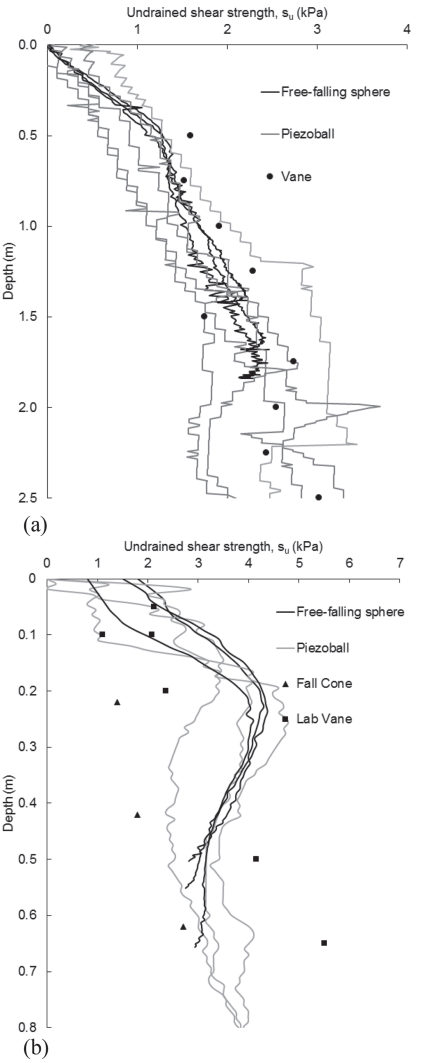

Figure 22. Comparison of undrained shear strength profiles derived from free-fall sphere acceleration data and push-in piezoball penetration resistance: (a) a lake site (Lough Erne, Northern Ireland) and (b) a nearshore site (Firth of Clyde, Scotland) (Morton et al. 2016a).

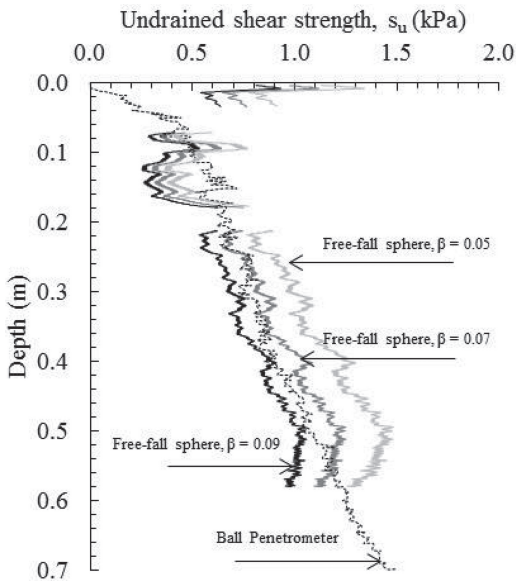

Figure 23. Sensitivity of interpreted s_u profiles to changes in the strain rate parameter (Morton et al. 2016b).

The free-fall sphere s_u profiles are seen to agree well with static piezoball tests on Figure 22, where the same piezoball factor was used (at each site) to calculate s_u from the static and FFP net resistance, and the same strain rate parameter, $\beta = 0.07$ and drag coefficient, $C_d = 0.26$ were used for both sites. Interpretation of the Clyde tests—static and free-fall—required adjustment of the bearing capacity factor at shallow depths, as discussed in the following section.

The sensitivity to uncertainty in β is demonstrated by Figure 23, which compares centrifuge s_u profiles from free-fall sphere tests with equivalent static profiles for a reconstituted carbonate clay from Laminaria (Timor Sea); β is varied by ± 0.02 from the base case $\beta = 0.07$ (used for both the centrifuge and field tests). The lower bound $\beta = 0.05$ corresponds with the largest departure from the base case profile established using $\beta = 0.07$, although by less than 20%. This uncertainty is comparable to the differences that are commonly linked to uncertainty between different laboratory strength tests (Bienen et al. 2010).

4.8.1 *Shallow embedment correction factors*

For large diameter penetrometers, it is necessary to modify the bearing capacity factor, N_{FFP}, for shallow embedment (e.g. Rocker 1985, Aubeny & Shi 2006, White et al. 2010, Morton et al. 2016a). The bearing capacity factor tends to increase from the shallow foundation factor at the seabed interface to the deep factor at depth. In soils with a constant strength, the deep factor is typically reached within approximately four diameters (depending on the normalised strength ratio $s_u/\gamma' D$). The shape of the transition to 'deep' conditions will be influenced by the strength gradient and unit weight of the soil (e.g. Stanier & White 2015).

4.9 *Summary comments on FFPs*

In spite of the cost-effectiveness of free-fall penetrometers (FFPs), compared with mobilising a seabed frame to conduct static penetrometer tests, the quality and usefulness of the data acquired need to be considered carefully within the context of the site investigation objectives. In the early stages of characterising the seabed, and particularly for spatially extensive surveys for pipeline routing, it may be sufficient to acquire data that merely distinguishes rock (or cemented) outcrops, from sandy deposits all the way down to fine-grained sediments of different strengths. Where soft sediments can be anticipated, quantitative strength data in the upper metre or so would be useful even at a preliminary SI stage.

Lightly instrumented FFPs are sufficient for primary categorisation of the seabed material. Penetration of the seabed will be minimal for cemented crusts, and unlikely to exceed a fraction of a metre in most types of coarse-grained (silty sands and coarser) material, regardless of the mineralogy or relative density (Stark et al. 2012). This may be sufficient during concept selection and pipeline routing studies. However, where anchors are anticipated, it may be difficult to distinguish between sandy sediments sufficiently thick for good drag anchor performance, and superficial sand layers overlying rock, resulting in much less certain anchor holding capacity.

As in other methods of site investigation, the guiding principle must be to ensure free-fall penetration (and ideally deduction of the tip resistance profile) to depths compatible with the design target. In fine-grained sediments, where quantitative assessment of the shear strength profile is important, the required accuracy needs to be considered in choosing the type of FFP.

The new generation of combined dynamic and static penetrometers, where calibration of dynamic effects can be achieved through overlapping zones of dynamic and static data (Young et al. 2011, Randolph 2016), are an excellent cost-effective approach for moderate-sized foundation or anchoring solutions. However, the deployment of such systems requires prior knowledge that the sediments are fine-grained and relatively low strength, excluding any sandy layers or other obstructions. Additionally, since calibration with

respect to rate factors etc. is sensitive to the soil type, the correction may not be valid over the full depth of dynamic penetration.

For assessing the shear strength of the upper 1 m or so of the seabed, smaller FFPs, either free-falling piezocones or extended base devices, are more cost effective than larger FFPs. Ideally one or two independent static CPTs should be included for calibration, balancing the operational efficiency of FFP testing with the improved confidence and accuracy from calibration against data from static penetrometer tests (Steiner et al. 2012). Overall, though, for free-falling cone penetrometers, direct measurement of tip resistance, albeit under dynamic conditions, is essential, given the uncertainties associated with drag resistance at shallow depths and estimating the rate-enhanced shaft resistance.

5 APPLICATION OF PENETROMETER DATA IN DESIGN

5.1 *Trends of indirect and direct penetrometer correlations*

Along with the development in geotechnical site investigation, which routinely includes in situ penetrometer testing, methods to use the acquired data more directly for foundation design have become widespread. The boundary between 'indirect' and 'direct' is not clear cut, but here the former is restricted to deriving simplified profiles of fundamental soil properties such as shear strength or the equivalent (friction angle or relative density) for free-draining sediments. By contrast, direct design approaches derive foundation design parameters from the CPT data, such as modern approaches for axial pile capacity in sand as detailed in Recommended Practice 2Geo of the American Petroleum Institute (API 2011).

For shallow foundations there are a range of approaches, from directly correlating the penetrometer resistance with the foundation capacity (e.g. Lee and Randolph 2011, Pucker et al. 2013, Bienen et al. 2015), using the cone tip resistance as input in numerical analysis (e.g. Schneider et al. 2018), to inferring the soil type from the penetrometer data and using the deduced strength in traditional bearing capacity predictions (e.g. Safinus 2015). The last approach might really be considered as 'indirect' except that the method to extract the layering and strength properties is fully automated.

As with any other engineering application, though, the prediction method cannot increase the quality or relevance of the input data. Hence, in order to obtain accurate predictions, sufficient high quality penetrometer data are required at the target location in combination with a sound correlation method. Furthermore, while computational power is ever increasing, the target application may still limit what is practicable for routine design (e.g. direct input of a CPT profile into large deformation numerical analysis to obtain a jack-up spudcan load-penetration curve).

Jack-up spudcans have been the focus of a number of proposed correlation methods recently, as a result of often sparse site investigation data available for a priori predictions and relatively high proportion of incidents and accidents (Osborne et al. 2006, Hunt 2008, Jack et al. 2013). The proposed approaches to using penetrometer data in design differ in the detailed treatment of soil behaviour, but also in the computational effort required.

Assigning soil layers in the geotechnical design process retains an element of subjectivity that is difficult to remove. Automatic identification of primary geotechnical layers from in situ penetrometer data, for example following Robertson's approach of categorising the soil behaviour type index ($I_{c,RW}$ – Robertson & Wride 1998, I_B – Robertson 2016) to assign strength values, feeds into a top-down calculation to arrive at the predicted spudcan penetration resistance profile (Safinus 2015). The method offers the advantage of capturing the evolution of the soil profile (and plug) with spudcan penetration, with an example provided in Figure 24. Limitations of the approach include the reliance on correlations of questionable accuracy to infer soil unit weight and strength parameters for carbonate sediments, in particular sands.

The cone tip resistance profile can also be used directly to obtain the spudcan load-penetration curve via a correlation factor. With the bearing capacity factor N_c of a deeply penetrated foundation of approximately 9.0 and recommended average value of N_{kt} of approximately 13.5, a correlation factor of 0.67 is arrived at for clay (Osborne et al. 2011). Similar direct correlation factors for spudcans penetrating into siliceous and uncemented carbonate sand are provided in Pucker et al. (2013) and Bienen et al. (2012), respectively. This direct correlation method has been benchmarked against field data from offshore wind installations on sand sites in the North Sea (Edwards et al. 2013), with similar performance to predictions based on ISO (2012, previously SNAME) – see Figure 25.

Layered soil profiles introduce the issue of scaling, as a large size object such as a spudcan will have an averaging effect, while a penetrometer will resolve finer detail of strength variation. In the guidelines originating from the InSafe JIP (Osborne et al. 2011) a strength averaging approach is adopted to account for the apparent size effect.

Two other aspects of scale are important. The first involves differences in drainage regime for the

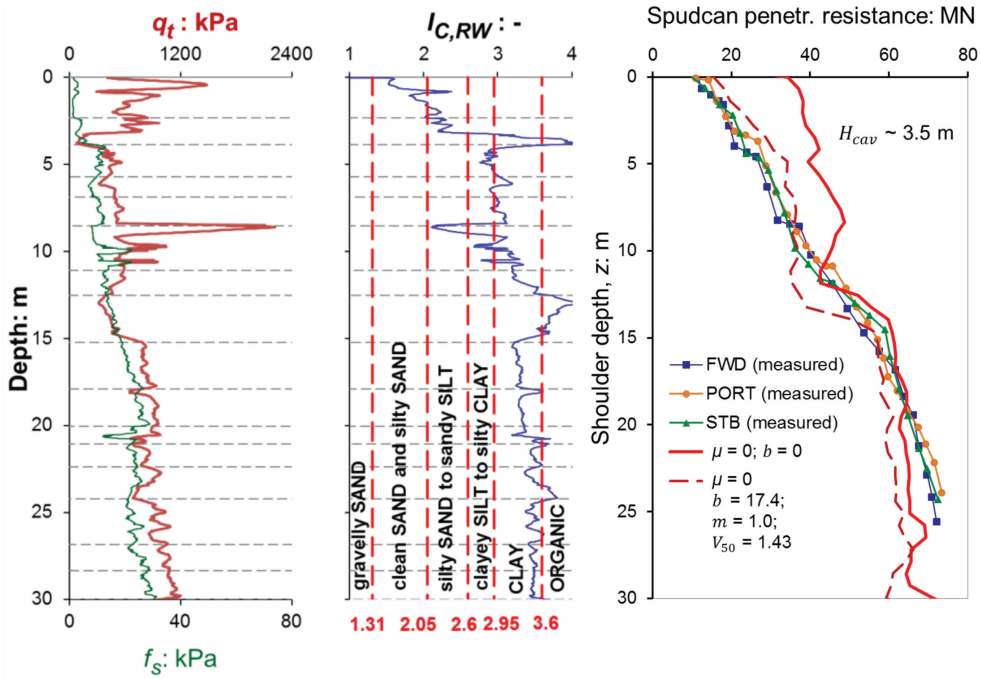

Figure 24. Spudcan load-penetration curve prediction (after Safinus 2015).

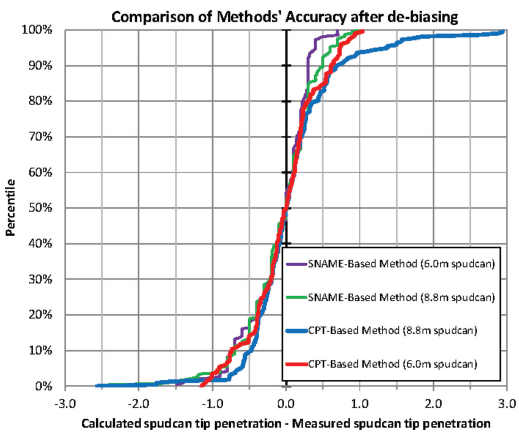

Figure 25. Comparison of the performance of direct CPT correlation and predictions based on ISO (2012).

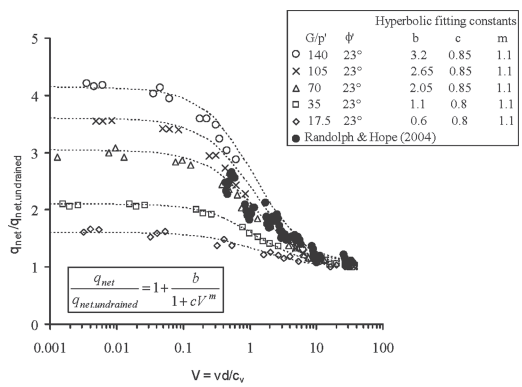

Figure 26. Normalised enhancement of penetration resistance with non-dimensional velocity.

penetrating object compared with a penetrometer. The second concerns the different modes of failure arising in strongly stratified profiles, i.e. with sand layers interleaved with layers of fine grained sediments.

The drainage regime may be close to fully undrained for a large diameter foundation such as a penetrating spudcan, even in sediments that are essentially free-draining during a penetrometer test. These differences in drainage characteristics lead to variations in the mobilised resistance, as illustrated in Figure 4 and Figure 5. The guidelines resulting from the InSafe JIP (Osborne et al. 2011) recommend modifying the factor of N_c/N_{kt} by the ratio between spudcan and penetrometer 'q_{net}' values arising from partial drainage, as illustrated in Figure 26. Values of q_{net} are estimated from the consolidation curves for normalised velocities

$V = vD/c_v$ using the spudcan and penetrometer diameters.

Erbrich (2005), Amodio et al. (2015) and Erbrich et al. (2015) provide detailed discussion of the effect of drainage on spudcan response, including additional consideration of cyclic degradation of the carbonate soils prevalent in areas of oil and gas developments offshore Australia (North West Shelf, Bass Strait).

With respect to the different penetration mechanisms that occur in stratified profiles, some methods (e.g. Safinus 2015) take specific account of effects such as squeezing of soft material overlying stronger material, punch-through for 'sand over clay' profiles, and allowance for a plug of stronger soil being trapped ahead of the penetrating spudcan. Simpler approaches are based on direct correlation to obtain an estimate of the spudcan load-penetration curve from the cone tip resistance, including consideration of the averaging distance. A method of this type is described by Bienen et al. (2015) for stratified 'sand over clay' profiles that may bear the risk of punch-through failure.

Jack-up spudcans are only one application example, of course, with other relevant applications affected by soil stratification including laterally loaded piles and anchor response. The example provided in Schneider et al. (2018) illustrates the merit of using in situ penetrometer data as input into numerical analysis to obtain foundation capacity in soil with layering. Another example, but for suction caisson capacity, is given below.

This section has illustrated a range of approaches to utilise penetrometer data in design. Penetrometer based methods need to be evaluated alongside more traditional design approaches, using data from actual foundation performance, in order to improve confidence in the methods and encourage further evolution. This also offers the opportunity of evidence-based selection of the most economical prediction method, balancing an appropriate level of sophistication relative to the available input data.

5.2 *Direct and indirect application of penetrometer data in numerical analysis*

Most foundation and anchor design is based on 'interpreted' penetrometer data, where simplified piecewise linear variations of shear strength are fitted to profiles of net penetrometer tip resistance using appropriate bearing (i.e. cone, T-bar, ball, etc.) factors. Schneider et al. (2018) discuss the potential errors that may arise from this approach, comparing results obtained using either an idealised strength profile, or the actual variation of (factored) net cone resistance.

Figure 27 shows the strength profile deduced from CPT data using a cone factor of $N_{kt} = 13.5$, from the second example (C6) considered in Schneider et al. (2018). The CPT profile is compared with the corresponding idealised s_u profile of $s_u = \max(1.9, 1.43z)$ kPa, where z is the depth in m. Corresponding ratios of the idealised and 'direct' (i.e. from the CPT profile) shear strengths are shown in Figure 28.

The idealised strength profile shown in Figure 27 might not be considered an appropriately 'conservative' idealisation for use in design. However, in practice such profiles are generally fitted (conservatively) through a number of CPT profiles, rather than being a strict lower bound to all profiles. The purpose here is to explore what potential over prediction of capacity might arise from the mismatch of the shear strength profiles in the upper few metres.

For the shallow foundation systems considered by Schneider et al. (2018), the vertical capacity of strip foundations of widths 5 to 20 m estimated using the CPT data directly were some 15% lower than those based on the idealised s_u profile. More significant differences were found for a foundation system compromising two linked skirted foundations, with skirt tips embedded 1.75 m, where the moment capacity using the CPT data was less than 50% of that from the idealised profile.

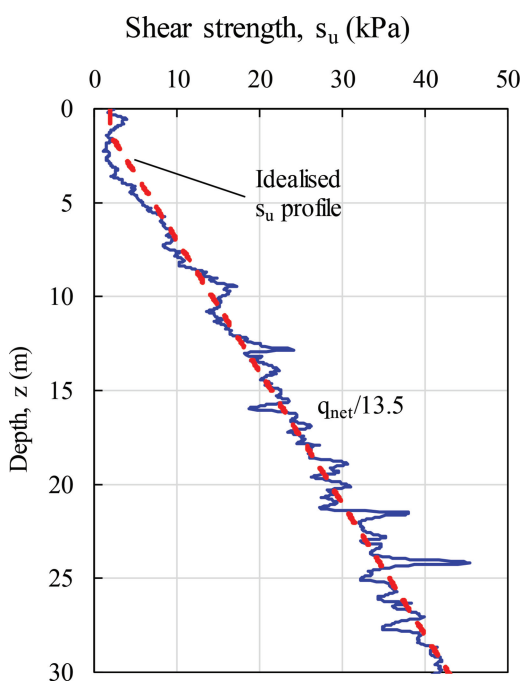

Figure 27. Strength profiles from Schneider et al. (2018).

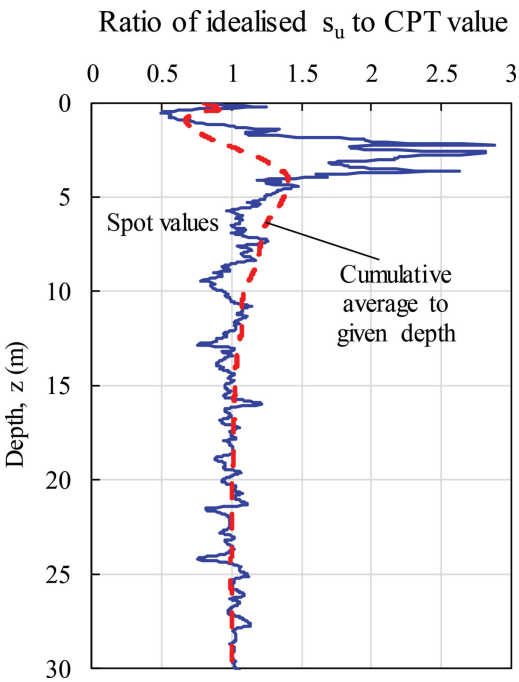

Figure 28. Ratios of spot values and cumulative averages for the idealised and 'direct' s_u profiles.

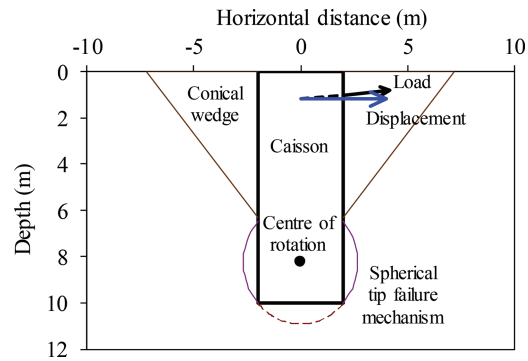

Figure 29. Suction anchor and upper bound failure mechanism.

Table 1. Strength and anchor capacities for different s_u profiles.

	CPT data	Idealised s_u	Ratio
Average s_u (0 to 10 m)	6.7 kPa	7.3 kPa	0.92
Anchor capacity (rotating)	828 kN	957 kN	0.86
Anchor capacity (translating)	3041 kN	3278 kN	0.93

Considering the profiles of cumulative average strength ratio shown in Figure 28, it might be expected that the capacity of a suction anchor would be relatively insensitive to the detailed stratigraphy observed from the CPT data, in particular the weak zone between 2 and 5 m depth. However, there are still significant differences.

Common applications for suction anchors for deep water developments include relatively small caissons for manifolds and pipeline end terminations. Typically, lateral loading for such caissons is applied near the seabed surface, leading to a rotational failure mode.

Figure 29 shows a 4 m diameter caisson embedded to a depth of 10 m, with loading applied at a depth of 1 m at an angle of 5 ° from the horizontal. The corresponding upper bound failure mechanism (Murff & Hamilton 1993) is as indicated, with a conical wedge failure extending to a depth of about 6 m, below which there is a rotating spherical failure.

Upper bound capacities evaluated using either the factored CPT data directly or the linearised s_u profile shown in Figure 27 are 828 kN and 957 kN respectively. The nearly 15% difference may be attributed partly to the approximately 9% difference in the cumulative average shear strength for the two profiles between 0 and 10 m. However, the weaker upper soil layer leads to further difference in capacity for a caisson with loading applied near the ground surface. By contrast, capacities for a purely horizontally translating caisson differ by just the difference in average shear strength over the relevant depth range. These results are summarised in Table 1.

It is possible to obtain similar capacities by judicious choice of the idealised s_u profile (for example, a crustal shear strength of 2.1 kPa, below which the shear strength is given by $s_u = -4.2 + 2z$ kPa). However, offshore design tends to follow a phased approach, with a geotechnical interpretive report providing simplified strength profiles for a range of possible foundation or anchoring systems, and detailed design undertaken in a subsequent engineering phase. The potential for significant overestimation of capacities due to subtle limitations in the idealised strength profiles is evident.

6 SUMMARY

This paper has considered a number of issues pertaining to penetrometer testing and interpretation with respect to offshore geotechnical design. The important trends are for improved cost-effectiveness, timely acquisition of quantitative strength (or

other design) data, and increased sophistication in testing and control procedures.

In keeping with these trends, the paper has included extended discussion of free-fall penetrometers and the techniques required to obtain equivalent 'static' strength or resistance parameters. Similarly, the potential for integrating box core sampling and deck-based penetrometer testing in early phases of (geophysical focused) site investigation has been discussed. The manner of the box-core tests, with close control of load and displacement on different axes of motion, is extendable to seabed-based testing, consistent with the underlying objective of 'bringing the laboratory to the seabed'.

A final consideration has been the manner in which penetrometer data should be utilised in design calculations. Important issues here are (a) to make appropriate allowances for the differences in scale between penetrometers, seabed layering and the design target; and (b) the increasing potential to incorporate the full detail of CPT data in design calculations.

ACKNOWLEDGEMENTS

This work forms part of the activities of the Centre for Offshore Foundation Systems at UWA, currently supported as a node of the Australian Research Council Centre of Excellence for Geotechnical Science and Engineering. The authors are grateful for support from the RIGSS JIP sponsors: Fugro, Shell, Total and Woodside Energy. In addition, Mark Randolph acknowledges support through the Fugro Chair in Geotechnics and David White acknowledges support through the Shell Chair in Offshore Engineering.

REFERENCES

Amodio, A., Erbrich, C.T., Murugavel, V. & Moyle, I. 2015. Re-visiting Yolla—managing jack-up storm stability: geotechnical assessment. *Proc. 15th Int. Conf. The Jack-Up Platform Design, Construction & Operation*, London.

API 2011. *RP 2GEO—Geotechnical and foundation design considerations.* American Petroleum Institute, Washington.

Aubeny, C.P. & Shi, H. 2006. Interpretation of impact penetration measurements in soft clays. *J. Geotech. & Geoenv. Eng.*, ASCE, 132(6): 770–777.

Beard, R.M., 1985. Expendable Doppler penetrometer for deep ocean sediment measurements. *ASTM Special Technical Publication*, 883: 101–124.

Been, K., Jefferies, M.G., & Hachey, J. 1991. The critical state of sands. *Géotechnique*, 41(3): 365–381.

Bienen, B., Cassidy, M.J., Randolph, M.F. & Teh, K.L. 2010. Characterisation of undrained shear strength using statistical methods. *Proc. 2nd Int. Symp. Frontiers in Offshore Geotech. ISFOG2010*, Taylor & Francis, London: 661–666.

Bienen, B., Pucker, T. & Henke, S. 2012. Cone penetrometer based spudcan penetration prediction in uncemented carbonate sand. *Proc. Offshore Technology Conf.*, Houston, Paper OTC 23002.

Bienen, B., Qiu, G. & Pucker, T. 2015. CPT correlation developed from numerical analysis to predict jack-up foundation penetration into sand overlying clay. *Ocean Engineering*, 108: 216–226.

Biscontin, G. & Pestana, J.M. 2001. Influence of peripheral velocity on vane shear strength of an artificial clay. *Geotechnical Testing Journal*, 24(4): 423–429.

Blake, A., O'Loughlin, C.D., Morton, J., O'Beirne, C., Gaudin, C. & White, D.J. 2016. In-situ measurement of the dynamic penetration of free-fall projectiles in soft soils using a low cost inertial measurement unit. *Geotechnical Testing Journal*, 39(2): 235–251.

Bolton, M.D., 1986. The strength and dilatancy of sands. *Géotechnique*, 36(1): 65–78.

Boscardin, A.G. & DeGroot, D.J. 2015. Evaluation of a toroid for model pipeline testing of very soft offshore box core samples. *Proc. 3rd Int. Symp. Frontiers in Offshore Geotech. ISFOG2015*, Taylor & Francis, London: 363–368.

Chow, S.H. & Airey, D.W. 2014. Free-falling penetrometers: a laboratory investigation in clay. *J. Geotech. & Geoenv. Eng.*, ASCE, 140(1): 201–214.

Chow, S.H., Bienen, B. & Randolph, M.F. 2018. Rapid penetration of piezocones in sand. *Proc. Int. Symp. Cone Penetration Testing, CPT'18*, Delft.

Chow, S.H., O'Loughlin, C.D. & Randolph, M.F. 2014. Soil strength estimation and pore pressure dissipation for free-fall piezocone in soft clay. *Géotechnique*, 64(10): 817–827.

Chow, S.H., O'Loughlin, C.D., White, D.J. & Randolph, M.F. 2017. An extended interpretation of the free-fall piezocone test in clay. *Géotechnique*, *67*(12): 1090–1103.

Clukey, E.C., Aubeny, C., Zakeri, A., Randolph, M.F., Sharma, P.P., White, D.J., Sancio, R. & Cerkovnik, M. 2017. A perspective on the state of knowledge regarding soil-pipe interaction for SCR fatigue assessments. *Proc. Offshore Technology Conf.*, Houston, Paper OTC 27564.

DNVGL 2017. *Pipe-soil interaction for submarine pipelines. Recommended Practice F-114,* DNVGL, Oslo.

Edwards, D., Bienen, B., Pucker, T. & Henke, S. 2013. Evaluation of the performance of a CPT-based correlation to predict spudcan penetrations using field data. *Proc. 14th Int. Conf. The Jack-Up Platform—Design, Design, Construction & Operation*, London.

Erbrich, C.T. 2005. Australian frontiers—spudcans on the edge. *Proc. Int. Symp. on Frontiers in Offshore Geotechnics, ISFOG*, Perth: 49–74.

Erbrich, C.T., Amodio, A., Krisdani, H., Lam S.Y., Xu, X. & Tho, K.K. 2015. Re-visiting Yolla—new insights on spudcan penetration. *Proc. 15th Int. Conf. The Jack-Up Platform Design, Construction & Operation*, London.

Fawaz, A., Teoh, A., Airey, D.W. & Hubble, T. 2016. Soil strength in the Murray River determined from a free falling penetrometer. Proc. *5th Int. Conf. on Geo-*

tech. & Geophysical Site Characterisation, ISC'5 Gold Coast: 1217–1222.

Furlong, A., Osler, J.C., Christian, H., Cunningham, D. & Pecknold, S. 2006. The moving vessel profiler (MVP) - a rapid environmental assessment tool for the collection of water column profiles and sediment classification. *Proc. Undersea Defence Technology Pacific Conf.*, San Diego: 1–13.

Geirnaert, K., Staelens, P., Deprez, S., Noordijk, A. & Van Hassent, A. 2013. Innovative free fall sediment profiler for preparing and evaluating dredging works and determining the nautical depth. *WODCON XX*: 1–11.

Hunt, R., 2008. Achieving operational excellence for jack-up rig deployments—how shall we get there? *Proc. 2nd Jack-Up Asia Conf. and Exhibition*, Singapore.

ISO, 2012. *Petroleum and natural gas industries—site-specific assessment of mobile offshore units—part 1: Jack-ups, 19905–1,* Int. Organization for Standardization, Geneva.

Jack, R.L., Hoyle, M.J.R., Smith, N.P. & Hunt, R.J. 2013. Jack-up accident statistics—a further update. *Proc. 14th Int. Conf. The Jack-Up Platform—Design, Const. & Oper.*, London.

Kelleher, P., Low, H.E., Jones, C., Lunne, T., Strandvik, S. & Tjelta, T.I. 2011. Strength measurement in very soft upper seabed sediments. *Proc. 2nd Int. Symp. Frontiers in Offshore Geotech. ISFOG2010*, Taylor & Francis, London: 283–288.

Kopf, A., Stegmann, S., Krastel, S., Foerster, A., Strasser, M. & Irving, M. 2007. Marine deep-water free-fall CPT measurements for landslide characterisation off Crete, Greece (Eastern Mediterranean Sea), part 2: initial data from the western Cretan Sea. *Proc. Int. Conf. Submarine Mass Movements and Their Consequences*. Springer, Netherlands: 199–208.

Lee, J. & Randolph, M.F. 2011. Penetrometer-based assessment of spudcan penetration resistance. *J. Geotech. & Geoenv. Eng.*, ASCE, 137(6): 587–596.

Lehane, B.M., O'Loughlin, C.D., Gaudin, C., & Randolph, M.F. 2009. Rate effects on penetrometer resistance in kaolin. *Géotechnique*, 59(1), 41–52.

Low, H.E., Randolph, M.F., Rutherford, C.J., Bernard, B.B. & Brooks, J.M. 2008. Characterization of near seabed surface sediment. *Proc. Offshore Technology Conf.*, Houston, Paper OTC 19149.

Lucking, G., Stark, N., Lippmann, T. & Smyth, S. 2017. Variability of in situ sediment strength and pore pressure behavior of tidal estuary surface sediments, *Geo-Marine Letters*, 37(5): 441–456.

Mahmoodzadeh, H., Wang, D. & Randolph, M.F. 2015. Interpretation of piezoball dissipation testing in clay. *Géotechnique*, 65(10): 831–842.

Morton, J.P., O'Loughlin, C.D. & White, D.J. 2016a. Estimation of soil strength in fine-grained soils by instrumented free-fall sphere tests. *Géotechnique*, 66(12): 959–968.

Morton, J.P., O'Loughlin, C.D. & White, D.J. 2016b. Centrifuge modelling of an instrumented free-fall sphere for measurement of undrained strength in fine-grained soils. *Canadian Geotech. J.*, 53: 918–929.

Mosher, D.C., Christian, H., Cunningham, D., Mackillop, K., Furlong, A., & Jarrett, K. 2007. The Harpoon Free Fall Cone Penetrometer for Rapid Offshore Geotechnical Assessment. *Proc. 6th Int. Offshore Site Investigation and Geotechnics Conf.*, London: 195–202.

Mulhearn, P.J. 2003. Influences of penetrometer tip geometry on bearing strength estimates. *Int. J. of Offshore and Polar Eng.*, 13(1): 73–78.

Mumtaz, M.B., Stark, N. & Brizzolara, S. 2018. Pore pressure measurements using a portable free fall penetrometer. *Proc. Int. Symp. Cone Penetration Testing, CPT'18*, Delft.

Murff, J.D. & Hamilton, J.M. 1993. P-ultimate for undrained analysis of laterally loaded piles, *J. Geotechnical Eng.*, ASCE, 119 (1): 91–107.

O'Beirne, C., O'Loughlin, C.D. & Gaudin, C. 2017. A release-to-rest model for dynamically installed anchors, *J. Geotech. & Geoenv. Eng.*, ASCE, 143(9): 04017052.

O'Loughlin, C.D., Blake, A.P. & Gaudin, C. 2016. Towards a design method for dynamically embedded plate anchors, *Géotechnique*, 66(9): 741–753.

O'Loughlin, C.D., Gaudin, C., Morton, J.P. & White, D.J. 2014. MEMS accelerometers for measuring dynamic penetration events in geotechnical centrifuge tests. *Int. J. Physical Modelling in Geotech.*, 14(2): 31–39.

O'Loughlin, C.D., Randolph, M.F. & Richardson, M.D. 2004. Experimental and theoretical studies of deep penetrating anchors. *Proc. Offshore Tech. Conf.*, Houston, OTC 16841.

O'Loughlin, C.D., Richardson, M.D., Randolph, M.F. & Gaudin, C. 2013. Penetration of dynamically installed anchors in clay. *Géotechnique*, 63(11): 909–919.

Orenberg, P., True, D.G., Bowman, L., Herrmann, H. & March, R. 1996. Use of a dropped dynamic penetrometer in cohesionless soil. *Proc. Offshore Tech. Conf.*, Houston, Paper OTC 8027.

Osborne, J.J., Pelley, D., Nelson, C. & Hunt, R. 2006. Unpredicted jack-up foundation performance. *Proc. Jack-Up Asia Conf. and Exhibition*, Singapore.

Osborne, J.J., Teh, K.L., Houlsby, G.T., Cassidy, M.J., Bienen, B. & Leung, C.F. 2011. *'InSafeJIP' – Improved Guidelines for the Prediction of Geotechnical Performance of Spudcan Foundations During Installation and Removal of Jack-up Units, Final Guidelines of the InSafe Joint Industry Project Report Number EOG0574-Rev1.* RPSEnergy, Woking, UK.

Peuchen, J., Looijen, P.N. & Stark, N. 2017. Offshore characterisation of extremely soft sediments by free fall penetrometer. *Proc. 8th Int. Conf. Offshore Site Investigation and Geotechnics*, Soc. for Underwater Tech., London, 1: 370–377.

Peuchen, J. & Westgate, Z. 2018. Defining geotechnical parameters for surface-laid subsea pipe-soil interaction. *Proc. Int. Symp. Cone Penetration Testing, CPT'18*, Delft.

Pucker, T., Bienen, B. & Henke, S. 2013. CPT based prediction of foundation penetration in siliceous sand. *Applied Ocean Research*, 41: 9–18.

Randolph, M.F. 2016. New tools and directions in offshore site investigation—ISC'5 Keynote Lecture. *Australian Geomechanics*, 51(4): 81–92.

Randolph, M.F., Low, H.E. & Zhou, H. 2007. In situ testing for design of pipeline and anchoring systems. Keynote paper, *Proc. 6th Int. Conf. Offshore Site Investigation and Geotechnics*, Society for Underwater Technology, London: 251–262.

Robertson, P.K. 2016. Cone penetration test (CPT)-based soil behaviour type (SBT) classification system—an update. *Canadian Geotech. J.*, 53(12): 1910–1927.

Robertson, P.K. & Wride, C.E. 1998. Evaluating cyclic liquefaction potential using the cone penetration test. *Canadian Geotech. J.*, 35(3): 442–459.

Rocker, K. 1985. *Handbook for marine geotechnical engineering*. Naval Civil Eng. Lab., Port Hueneme, CA.

Sabetamal, H., Carter, J.P., Nazem, M. & Sloan, S.W. 2016. Coupled analysis of dynamically penetrating anchors. *Computers & Geotechnics*, 77: 26–44.

Safinus, S. 2015. *Estimation of spudcan penetration resistance in stratified soils from field piezocone penetrometer data.* PhD Thesis, University of Western Australia.

Schneider, J.A., Doherty, J.P., Randolph, M.F. & Krabbenhoft, K. 2018. Direct use of CPT data for numerical analysis of VHM loading of shallow foundations. *Proc. Int. Symp. Cone Penetration Testing, CPT'18*, Delft.

Stanier, S. & White D.J. 2015. Shallow penetrometer penetration resistance. *J. Geotech. & Geoenv. Eng.*, ASCE, 141(3): 04014117.

Stark, N., Hanff, H. & Kopf, A.J. 2009. Nimrod: a tool for rapid geotechnical characterization of surface sediments. *Sea Technology*, 50(4): 10–14.

Stark, N., Hay, A.E. & Trowse, G. 2014. Cost-effective geotechnical and sedimentological early site assessment for ocean renewable energies. *2014 Oceans—St. John's*: 1–8.

Stark, N., Wilkens, R., Ernsten, V.B., Lambers-Huesman, M., Stegmann, S. & Kopf, A.J. 2012. Geotechnical properties of sandy seafloor and the consequences for dynamic penetrometer interpretations: quartz sand versus carbonate sand. *Geotechnical and Geological Engineering*, 30: 1–14.

Stegmann, S., Morz, T. & Kopf, A.J. 2006. Initial results of a new free fall-cone penetrometer (FF-CPT) for geotechnical in situ characterisation of soft marine sediments. *Norsk Geologisk Tidsskrift*, 86(3): 199–208.

Steiner, A., L'Heureux, J.S., Kopf, A., Vanneste, M., Longva, O., Lange, M. & Haflidason, H. 2012. An in-situ free-fall piezocone penetrometer for characterizing soft and sensitive clays at Finneidfjord (Northern Norway). *Proc. Int. Conf. Submarine Mass Movements and Their Consequences*. Adv. Natural & Tech. Hazards, 31, Springer: 99–109.

Steiner, A., Kopf, A.J., L'Heureux, J.S., Kreiter, S., Stegmann, S., Haflidason, H. & Moerz, T. 2014. In situ dynamic piezocone penetrometer tests in natural clayey soils–a reappraisal of strain-rate corrections. *Can. Geotech. J.*, 51(3): 272–288.

Stephan, S., Kaul, N. & Stark, N. 2011. LIRmeter: A new tool for rapid assessment of sea floor parameters. Bridging the gap between free-fall instruments and frame-based CPT. *Proc. MTS/IEEE OCEANS 2011*. IEEE *OCEANS*.

Stoll, R.D. & Akal, T. 1999. XBP-Tool for rapid assessment of seabed sediment properties. *Sea Technology*, 40(2): 47–51.

Thompson, D., March, R. & Herrmann, H. 2002. Groundtruth results for dynamic penetrometers in cohesive soils. In *Proceedings of OCEANS 2002, MTS/IEEE—Marine Frontiers: Reflection of the Past, Visions of the Future*, (4): 2117–2123.

True, D.G. 1976. *Undrained vertical penetration into ocean bottom soils.* PhD thesis, University of California, Berkeley.

White, D.J., Gaudin, C., Boylan, N. & Zhou, H. 2010. Interpretation of T-bar penetrometer tests at shallow embedment and in very soft soils. *Canadian Geotech. J.*, 47(2): 218–229.

White, D.J. & Randolph, M.F. 2007. Seabed characterisation and models for pipeline-soil interaction. *Int. J. Offshore & Polar Engng.*, 17(3): 193–204.

White, D.J., O'Loughlin, C.D., Stark, N. & Chow, S.H. 2018. Free fall penetrometer tests in sand: Determining the equivalent drained resistance. *Proc. Int. Symp. Cone Penetration Testing, CPT'18*, Delft.

White, D.J., Stanier, S.A., Schneider, M.A., O'Loughlin, C.D., Chow, S.H., Randolph, M.F., Draper, S.D. Mohr, H, Morton, J.P., Peuchen, J., Fearon, R., Roux, A. & Chow, F.C. 2017. Remote intelligent geotechnical seabed surveys—technology emerging from the RIGSS JIP. *Proc. 8th Int. Conf. Offshore Site Investigation and Geotechnics*, Society for Underwater Technology, London, 2: 1214–1222.

White, D.J., Clukey, E.C., Randolph, M.F., Boylan, N.P., Bransby, M.F., Zakeri, A., Hill, A.J. & Jaeck, C. 2017. The state of knowledge of pipe-soil interaction for on-bottom pipeline design. *Proc. Offshore Tech. Conf.*, Houston, Paper OTC 27623.

Yan, Y., White D.J. & Randolph M.F. 2014. Cyclic consolidation and axial friction on seabed pipelines. *Géotechnique Letters*, 4: 165–169.

Yan Y., White D.J. & Randolph M.F. 2017. Elastoplastic consolidation solutions for scaling from shallow penetrometers to pipelines. *Canadian Geotech. J.*, 54: 881–895.

Yan Y. White D.J. & Randolph M.F. 2011. Penetration resistance and stiffness factors in uniform clay for hemispherical and toroidal penetrometers *Int. J. of Geomech.*, ASCE, 11: 263–275.

Young, A.G., Bernard, B.B., Remmes, B.D., Babb, L.V. & Brooks, J.M. 2011. "CPT Stinger"—an innovative method to obtain cpt data for integrated geoscience studies. *Proc. Offshore Tech. Conf.*, Houston, Paper OTC 21569.

Yuan, F., White, D.J. & O'Loughlin, C.D. 2017. The evolution of seabed stiffness during cyclic movement in a riser touchdown zone on soft clay. *Géotechnique*, 67(2): 127–137.

Taylor & Francis
Taylor & Francis Group
http://taylorandfrancis.com

Cone Penetration Testing 2018 – Hicks, Pisanò & Peuchen (Eds)
© 2018 Delft University of Technology, The Netherlands, ISBN 978-1-138-58449-5

Inverse filtering procedure to correct cone penetration data for thin-layer and transition effects

R.W. Boulanger & J.T. DeJong
Department of Civil and Environmental Engineering, University of California, Davis, USA

ABSTRACT: This paper presents an inverse filtering procedure for developing estimates of "true" cone penetration tip resistance and sleeve friction values from measured cone penetration test data in interlayered soil profiles. Results of prior studies of cone penetration in layered soil profiles are utilized for developing and evaluating the inverse filtering procedure. The inverse filtering procedure has three primary components: (1) a model for how the cone penetrometer acts as a low-pass spatial filter in sampling the true distribution of soil resistance versus depth, (2) a solution procedure for iteratively determining an estimate of the true cone penetration resistance profile from the measured profile given the cone penetration filter model, and (3) a procedure for identifying sharp transition interfaces and correcting the data at those interfaces. The details of the inverse filtering procedure presented herein were developed with a focus on liquefaction problems, but the concepts and framework should be applicable to other problems. Example applications of the inverse filtering procedure are presented for four CPT soundings illustrative of a range of soil profile characteristics. The proposed procedure provides an objective, repeatable, and automatable means for correcting cone penetration test data for thin-layer and transition zone effects.

1 INTRODUCTION

The cone penetration test (CPT) provides excellent stratigraphic detail and information for estimating a wide range of soil properties, but the spatial resolution of cone tip resistance (q_t) and sleeve friction (f_s) measurements is still limited by the physical volume of soil around a cone tip that influences those measurements. Measurements of q_t are most strongly influenced by soils within about 10–30 cone diameters (d_c) of the cone tip, which corresponds to influence zones of 0.35–1.3 m thickness for standard 10 cm^2 and 15 cm^2 cones. Measurements of q_t and f_s therefore depend on the sequence and properties of all soils within the zone of influence, such that the cone acts as a low-pass spatial filter on the true distribution of soil resistance in a soil profile. This physical low-pass spatial filtering removes information at the shorter physical wavelengths [m], corresponding to higher spatial frequencies [cycles/m], that are necessary for defining sharp interfaces between soils with different properties. The resulting spatial smoothing of information at interfaces in interbedded soil deposits is well recognized in practice (e.g., Lunne et al. 1997, Mayne 2007) and has been the focus of considerable study.

The loss of detail at shorter physical wavelengths during cone penetration in layered soil profiles may not be of importance in some areas of practice, but there are certain situations where the resulting "thin layer" and "transition zone" effects can be sufficiently important to warrant evaluating. For example, thin layer effects can be important for liquefaction methodologies, depending on the analysis procedures, soil conditions, and seismic loading (as discussed in Boulanger et al. 2016). The use of simplified one-dimensional (1D) liquefaction vulnerability indices (LVIs) can overestimate the potential for liquefaction induced deformations if the predicted intervals of liquefaction triggering are primarily associated with numerous thin layers or transition zones. In other cases, the results of 1D-LVI's may be insensitive to thin layer and transition zones if those zones are a small portion of the predicted intervals of liquefaction triggering. For nonlinear dynamic analyses (NDAs) of sites with interbedded soils, the representative properties assigned to the liquefiable interlayers can similarly benefit from accounting for thin layer and transition zone effects in some situations and be relatively unaffected in others. More commonly, thin layer and transition zone effects are just one factor among several that can contribute to an accumulation of conservatism or bias in predicted behaviors (e.g., Boulanger et al. 2016, Munter et al. 2017, Cox et al. 2017).

This paper presents an inverse filtering procedure for developing estimates of "true" cone penetration tip resistance and sleeve friction values

from measured cone penetration test data. Results of prior studies are briefly reviewed and the available theoretical and experimental data for thin layer and transition zone effects in idealized two—and three-layer soil profiles are utilized for developing the inverse filtering procedure. The inverse filtering procedure and each of its three primary components are described, including: (1) the model for how the cone penetrometer acts as a low-pass spatial filter in sampling the true distribution of soil resistance versus depth, (2) the solution procedure for iteratively determining an estimate of the true cone penetration resistance profile from the measured profile given the cone penetration filter model, and (3) the procedure for identifying sharp transition interfaces and correcting data at those interfaces. Example applications of the inverse filtering procedure are then presented for four CPT soundings illustrative of a range of soil profile characteristics. The proposed procedure, which is easy to automate and perform, is shown to work well for a range of stratigraphies. It is hoped that future experience with application of the procedure in practice will lead to further improvements.

2 PAST STUDIES OF PENETRATION IN LAYERED SOIL PROFILES

Thin layer and transition zone effects have been studied extensively, including contributions from the authors listed in Table 1. These studies have utilized elastic analyses, nonlinear analyses (cavity expansion and axisymmetric models), and physical measurements (1 g physical models, centrifuge models, field data). In all cases except the elastic analyses by Yue and Yin (1999), these studies have focused on idealized profiles with two or three uniform soil layers in different sequences; e.g., a stronger soil over a weaker soil, a weaker soil over a stronger soil, a stronger soil layer embedded in weaker soil, or a weaker soil layer embedded in a stronger soil.

The schematic in Figure 1 shows the case of a sand layer embedded in a clay deposit to illustrate both the thin layer and transition zone effects. The measured tip resistance (denoted as q^m) will smoothly increase as the cone approaches and enters the stronger layer and then smoothly decrease as the cone approaches and then enters the underlying weaker soil. The "true" tip resistance (denoted as q^t) is the value that would have been measured in this same soil if the measurement was free of the influence of the overlying and underlying weaker clay soils. The "transition" zones are those intervals near the layer interfaces over which q^m smoothly increases or decreases even though q^t abruptly changes. The thin layer effect occurs when the peak q^m becomes smaller than the corresponding q^t, with the error increasing as the stronger layer's thickness decreases. The thin layer factor (K_H), defined as q^t divided by the peak q^m for the layer, therefore increases as layer thickness decreases.

Table 1. Past studies of cone penetration in layered soil profiles.

Authors	Primary focus
Elastic analyses:	
Sayed & Hamed (1987)	Spherical and cylindrical cavity expansion in layered elastic system
Vreugdenhil et al. (1994)	Elastic solutions for stress distributions in layered elastic system
Yue & Yin (1999)	Elastic solutions for stresses in a multi-layered system
Nonlinear analyses:	
Van den Berg et al. (1996)	Axisymmetric penetration analysis in layered sand and clay
Ahmadi & Robertson (2005)	Axisymmetric penetration analysis in layered sand and clay
Xu & Lehane (2008)	Spherical cavity expansion analogue for layered sand and clay
Walker & Yu (2010)	Axisymmetric penetration analysis in layered clay
Mo et al. (2017)	Cavity expansion analysis for layered sand and clay.
Physical data:	
Treadwell (1976)	Chamber tests of cone penetration in layered sand
Meyerhof & Valsangka (1977)	Model tests of piles and cones in layered sand and clay
Foray &Pautre (1988)	Chamber tests of cone penetration in layered sand
Canou (1989)	Chamber tests of cone penetration in layered sand
Youd et al. (2001)	Interpretation of field data
Hird et al. (2003)	Chamber tests of piezocones for thin sand/silt layers in clay
Silva & Bolton (2004)	Centrifuge tests of cone penetration in layered sand
Mlynarek et al. (2012)	Chamber tests of cone penetration in layered sand and clay
Mo et al. (2015)	Centrifuge tests of cone penetration in layered sand
Tehrani et al. (2018)	Chamber tests of cone penetration in layered sand

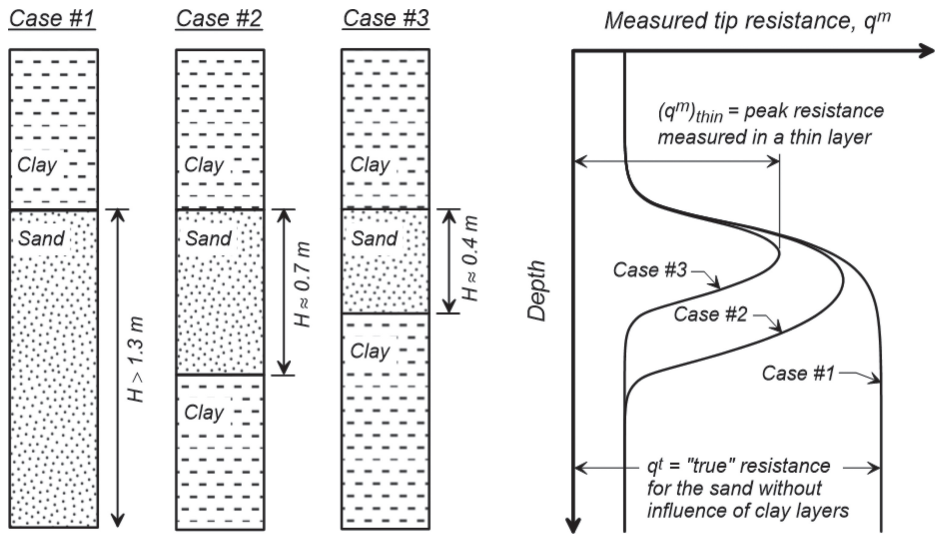

Figure 1. Schematic of thin layer effect for a sand layer embedded in a clay layer (modified from Robertson and Fear 1995).

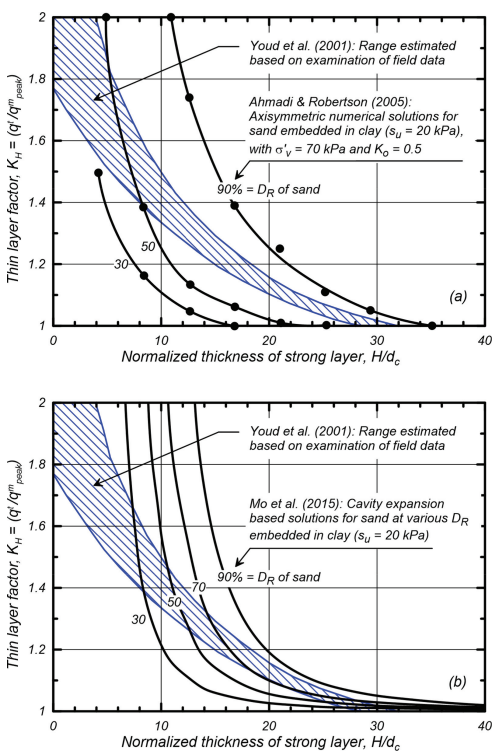

Figure 2. Thin layer factors inferred from field data (Youd et al. 2001) compared to: (a) axisymmetric numerical analyses by Ahmadi and Robertson (2005), and (b) cavity expansion based solutions by Mo et al. (2017).

Thin layer factors from three different studies are plotted versus normalized layer thickness (H/d_c) in Figures 2a and 2b to illustrate the range of findings in the literature. The range presented by Youd et al. (2001), and shown in both figures for reference purposes, was inferred from examinations of field data, although the details of the field data and interpretation method were not described. The results shown for Ahmadi and Robertson (2005) in Figure 2a are from axisymmetric nonlinear analyses of a sand layer with relative densities (D_R) of 30, 50 and 90% with σ'_v = 70 kPa and K_o = 0.5 (producing q^t of about 3.2, 5.8, and 22 MPa, respectively) embedded in soft clay with an undrained shear strength (s_u) of 20 kPa (producing a q^t of about 0.9 MPa). The corresponding thin layer factors increased with the D_R of the sand layer, which alternatively can be identified as having q^t_{strong}/q^t_{weak} ratios of about 3.6, 6.4, and 24, respectively. Ahmadi and Robertson (2005) also showed their thin layer factors to decrease with increasing effective confining stress, which is consistent with the dependence of sand dilation angle on confining stress used in their analyses. The results shown for Mo et al. (2017) in Figure 2b are based on cavity expansion analyses for a sand layer with D_R of 30, 50, 70, and 90% embedded in clay (s_u = 20 kPa), with the properties chosen to be equivalent to those used by Ahmadi and Robertson (2005). The corresponding thin layer factors are similar to those of Ahmadi and Robertson (2005), but become steeper and exceed values of 2.0 at larger values

of the normalized layer thickness. The q^t_{strong}/q^t_{weak} ratios for the cases analyzed by Mo et al. (2017) were not reported, but should be similar to those for the cases analyzed by Ahmadi and Robertson (2005). The results of these and other studies for idealized three-layer profiles produce K_H values that are less than about 1.1 when the strong layer thickness is greater than about 30 cone diameters, increase as the q^t_{strong}/q^t_{weak} ratio increases, and can exceed values of 2.0 for layers that are less than about 10 cone diameters thick if the q^t_{strong}/q^t_{weak} ratio is large enough.

Transition zones in idealized two layer profiles can also be described in terms of the sensing and development distances. When the cone tip is in the upper layer, the sensing distance is defined as the greatest distance between the cone tip and the top of the underlying layer for which q^m in the upper layer is "affected" by the underlying layer. When the cone tip is in the lower layer, the development distance is defined as the greatest distance between the top of the underlying layer and the cone tip for which q^m in the underlying layer is still "affected" by the upper layer. Specific criteria for determining sensing and development distances are often not reported, but appear to represent some degree of visually apparent effects (e.g., perhaps a few percent). Sensing and development distances and the equations describing how q^m varies from q^t_{strong} to q^t_{weak} and from q^t_{weak} to q^t_{strong} are often assumed to be mirror images of each other (e.g., Xu and Lehane 2008, Mo et al. 2015), which is an approximation that implies equal influence of the soil resistance in front of and behind the cone tip. In reality, experimental and theoretical studies (e.g., Ahmadi and Robertson 2005, Tehrani et al. 2018) show that sensing distance in a strong layer over a weak layer is greater than the development distance in a strong layer under a weak layer, which indicates that soils in front of the cone tip have a greater influence on penetration resistance than the soils behind the cone tip. Sensing and development distances in a strong layer adjacent to a weak layer increase as the ratio of the soil layer strengths increases (e.g., Xu and Lehane 2008). Sensing and development distances in a weak soil adjacent to a stronger soil are smaller than those for the stronger soil, and they decrease as the ratio of the soil layer strengths increases. For example, Walker and Yu (2010) show that q^t for a soft clay layer embedded in stronger clay can be almost fully developed in layers as thin as 2–3 cone diameters.

Application of thin-layer or transition zone corrections in practice is relatively uncommon due to a number of challenges. Their application to field situations is generally subjective, such that the corrections applied can vary significantly between different individuals analyzing the same data. The ability to consistently distinguish between sharp interfaces and graded interfaces (e.g., upward or downward fining sequences) is uncertain. The procedures are difficult to automate, and time consuming to apply in the absence of an automated processing method. These challenges, combined with the fact that the results may only have a modest effect for many design/evaluation problems, appears to be why their use is relatively uncommon.

3 INVERSE FILTERING PROCEDURE

Inverse filtering is widely used in image and signal processing for a wide range of measurement applications (e.g., Cristobal et al. 2011). Inverse filtering can help restore or improve the quality of an image or measurement if a good model can be developed for the function that "blurred" the measurement and if the signal-to-noise ratio in the measurement is favorable. Inverse filtering often responds poorly to any noise present in the measurement because noise tends to be at high spatial frequencies and the blurred measurement tends to be weakest (i.e., have the lowest signal strength) at high spatial frequencies.

The application of inverse filtering techniques to cone penetration data begins with the assumption that there is a "true" cone penetration resistance that would be obtained if the cone penetration test data were dependent solely on the soil properties at a point (i.e., measured by an infinitely small cone without particle size effects). The measured cone penetration resistance depends on soil properties within a zone of influence around the cone tip, such that cone penetration acts as a low-pass spatial filter in sampling the true profile; i.e., strong variations in soil properties over short distances correspond to short wavelengths (or high spatial frequencies) that are masked or filtered by the cone penetration process. An inverted cone penetration resistance is obtained by applying an inverse cone penetration filter to the measured cone penetration resistance profile.

It is convenient to simplify notation for cone penetration resistances for the present purposes as follows. True, measured, and inverted cone penetration resistances are identified with superscripts as q^t, q^m, and q^{inv}, respectively. The q^m refers to the resistance after any correction for unequal area effects (i.e., pore pressure behind the cone tip) has already been applied, and all three terms are normalized by atmospheric pressure. The conventional subscripts for identifying cone penetration resistances as corrected for unequal area effects or normalized by atmospheric pressure (e.g., q_{tN}) are omitted for clarity.

The filtering effect of the cone penetration process can now be expressed as,

$$q^m(z) = q^t(z) * w_c(z) \tag{1}$$

where the asterisk indicates convolution of q^t with the cone penetration filter (w_c). Convolution refers to the integral of the point-wise multiplication of the two functions as a function of the amount that one of the functions is shifted relative to the other. The spatial filtering effect can alternatively be expressed as,

$$q^m(z) = \int_{z_{\min}}^{z_{\max}} q^t(\tau) w_c(z-\tau) d\tau \tag{2}$$

The convolution integration limits, which are $-\infty$ to ∞ for the general case, are set equal to the depth limits for the CPT sounding (i.e., z_{min} to z_{max}), which also ensures that the q^m vector retains the same length as the q^t vector.

The inversion of this filtering process is complicated by the strongly nonlinear nature of w_c and limitations on the highest spatial frequencies (shortest physical wavelengths) for which the inversion is meaningful. For cone penetration, the highest spatial frequencies for which the measurements may contain meaningful information could be governed by either the data sampling interval or the physical size of the cone. Higher spatial frequencies than are measureable can exist in the field, such as those associated with discrete jumps in q^t across interfaces, but these higher spatial frequencies almost certainly cannot be reliably inverted from the measurements. For this reason, the inverse filtering procedure must include steps that remove any of these higher spatial frequency components from the solution, as discussed later.

The inverse filtering procedure proposed herein has three primary components: (1) a model for how the cone penetrometer acts as a low-pass spatial filter in sampling the true distribution of soil properties versus depth, (2) a solution procedure for iteratively determining an estimate of the true cone penetration resistance profile from the measured profile and cone penetration filter model, and (3) a procedure for identifying sharp transition interfaces and correcting the data at those interfaces. The following sections address each of these three components.

4 CONE PENETRATION FILTER MODEL

Any cone penetration filter model needs to account for the primary influencing factors, recognizing that a perfect filter model with the full complexity of factors is not yet realizable. The proposed filter model for the current study is expressed as a function of the q^t profile alone, though additional information from f_s, u_{bt}, V_s, or other measurements may prove beneficial. The function forms and parameters for the current model were developed to be consistent with the body of results from prior studies regarding thin layer effects and sensing/development distances (Table 1), including their dependencies on various soil profile characteristics as discussed in the previous section.

The cone penetration filter (w_c) model, shown in Figure 3, is the normalized product of two functions, w_1 and w_2, as,

$$w_c = \frac{w_1 w_2}{\sum w_1 w_2} \tag{3}$$

where w_c, w_1, and w_2 are all functions of z', which is the depth relative to the cone tip normalized by the cone diameter (d_c),

$$z' = \frac{z - z_{tip}}{d_c} \tag{4}$$

where z_{tip} is the current depth of the cone tip. The dependence of w_c, w_1, and w_2 on z' is omitted from notation for simplicity.

The w_1 term accounts for the relative influence of any soil decreasing with increasing distance from the cone tip as,

$$w_1 = \frac{C_1}{1 + \left(\frac{z'}{z'_{50}}\right)^{m_z}} \tag{5}$$

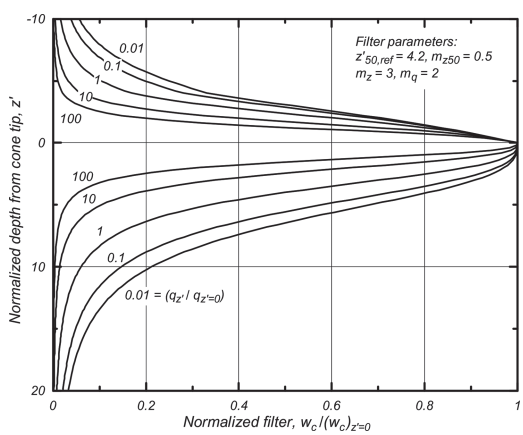

Figure 3. Normalized cone penetration filter versus normalized depth from the cone tip with lines for $q^t_{z'}/q^t_{z'=0} = 0.01, 0.1, 1, 10,$ and 100.

where z'_{50} is the normalized depth at which $w_1 = 0.5C_1$, and the exponent m_z is a parameter that adjusts the variation of w_1 with z'. The parameter C_1 is equal to unity for points below the cone tip, and linearly reduces to a value of 0.5 for points located more than 4 cone diameters above the cone tip as,

$$\begin{aligned} C_1 &= 1 \quad for \quad z' \geq 0 \\ &= 1 + \frac{z'}{8} \quad for \quad -4 \leq z' < 0 \\ &= 0.5 \quad for \quad z' < -4 \end{aligned} \tag{6}$$

The value of z'_{50} is computed as,

$$z'_{50} = 1 + 2\left(C_2 z'_{50,ref} - 1\right)\left(1 - \frac{1}{1 + \left(\frac{q^t_{z'=0}}{q^t_{z'}}\right)^{m_{50}}}\right) \tag{7}$$

where the product $C_2 z'_{50,ref}$ corresponds to the value of z'_{50} whenever $q^t_{z'}$ is equal to q^t at the cone tip (i.e., $q^t_{z'=0}$). The parameter C_2 is equal to unity for points below the cone tip, and less than unity (0.8 is used herein) for points above the cone tip. Thus, $z'_{50,ref}$ is the value of z'_{50} for points below the cone tip whenever $q^t_{z'}$ is equal to q^t at the cone tip.

The w_2 term adjusts the relative influence that soils away from the cone tip will have on the penetration resistance based on whether those soils are stronger or weaker than the soil immediately at the cone tip. If the soil at a given depth is weaker than the soil at the cone tip, its relative influence on the penetration resistance is increased, and vice versa if it is stronger than the soil at the cone tip. The w_2 term is computed as,

$$w_2 = \sqrt{\frac{2}{1 + \left(\frac{q^t_{z'}}{q^t_{z'=0}}\right)^{m_q}}} \tag{8}$$

where the exponent m_q is a parameter that adjusts the variation of w_2 with $q^t_{z'}/q^t_{z'=0}$.

The resulting filter model is shown in Figure 3 as w_c (normalized by w_c at the cone tip) versus z' for $q^t_{z'}/q^t_{z'=0}$ values of 0.01, 0.1, 1, 10, and 100 for the baseline set of parameters: $z'_{50,ref} = 4.0$, $m_z = 3.0$, $m_{50} = 0.5$, and $m_q = 2$. The soils above the cone tip receive about one half the weight received by the soils below the cone tip, all else being equal (i.e., comparing the relative areas under the w_c curves). For this parameter set, the filter model predicts that the measured penetration resistance will be controlled by soils within 2–3 diameters of the cone tip if they are far weaker than the soils further away (e.g., $q^t_{z'}/q^t_{z'=0} = 100$ at larger distances). Conversely, the measured penetration resistance will be significantly affected by soils as far as 15–20 diameters below the cone tip if the soils at these larger distances are far weaker than the soils near the cone tip (e.g., $q^t_{z'}/q^t_{z'=0} = 0.01$ at the larger distances). For more uniform soil profiles with only modest variations in q^t, the measured penetration resistance is controlled by soils within about 9 cone diameters of the tip. In addition, the asymmetry of the filter model is required to simulate the observed asymmetry in the sensing and development distances for strong layers embedded in weaker soil.

The filter convolution process is illustrated for a two-layer profile in Figure 4. For this illustration, the cone tip has reached the middle of a stronger layer embedded in a weaker soil profile, as depicted by the profile of q^t. The variation of w_c with depth is shown for that present cone tip depth. The q^t vector is point-wise multiplied by the w_c vector and the product summed to obtain the value of q^m for the present cone tip depth, which is shown as the single solid symbol on the right hand plot. This process is repeated for all other cone tip depths (with w_c shifting accordingly) to arrive at the profile of q^m shown as a dashed line on the right hand plot. For the cone tip at the middle of the stronger layer, the filter w_c decreases with distance from the cone tip in either direction for points in the stronger layer (since $q^t_{z'}/q^t_{z'=0} = 1$ throughout the layer), but steps up to larger values at the interface with the weaker soil because $q^t_{z'}/q^t_{z'=0} << 1$ for points in the weaker soil (which increases w_c as shown in Figure 3).

The numerical evaluation of the convolution integral involved two other details. First, the filter window was truncated at a length of 60 cone diameters, centered at the cone tip (i.e., $-30 \leq z' \leq 30$), for the examples presented in this paper. This truncation reduces computations and has minimal effect on results because w_c is close to zero at these distances from the cone tip. Second, the computation of w_c by Equation 3 is restricted to points that fall within the depth limits of the CPT sounding (i.e., the filter window is truncated at the data boundaries). This restriction ensures that the total area under the filter remains equal to unity near the upper and lower limits of the CPT sounding.

The behavior of the filter model is illustrated in Figure 5 showing q^t and q^m versus depth for three idealized soil profiles that each have four layers of a stronger soil interbedded in a weaker soil. The stronger soil has $q^t = 100$ in all cases, whereas the weaker soil has $q^t = 1$, 10, and 50 in Figures 5a, 5b, and 5c, respectively. The four stronger layers have thicknesses of 5, 10, 20, and 60 cone diameters in all cases. The digital data for these idealized profiles was generated with a uniform 20 mm sampling interval. The peak q^m that is computed

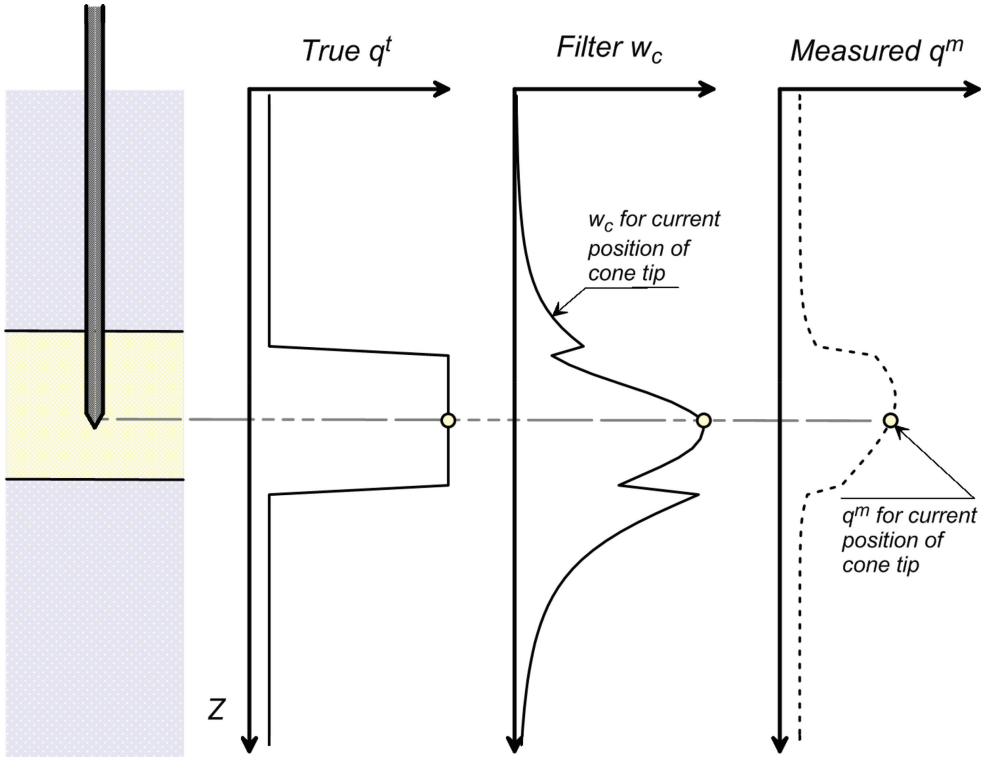

Figure 4. Illustration of the convolution of q^t with the cone penetration filter to obtain q^m at a given point in a layered profile.

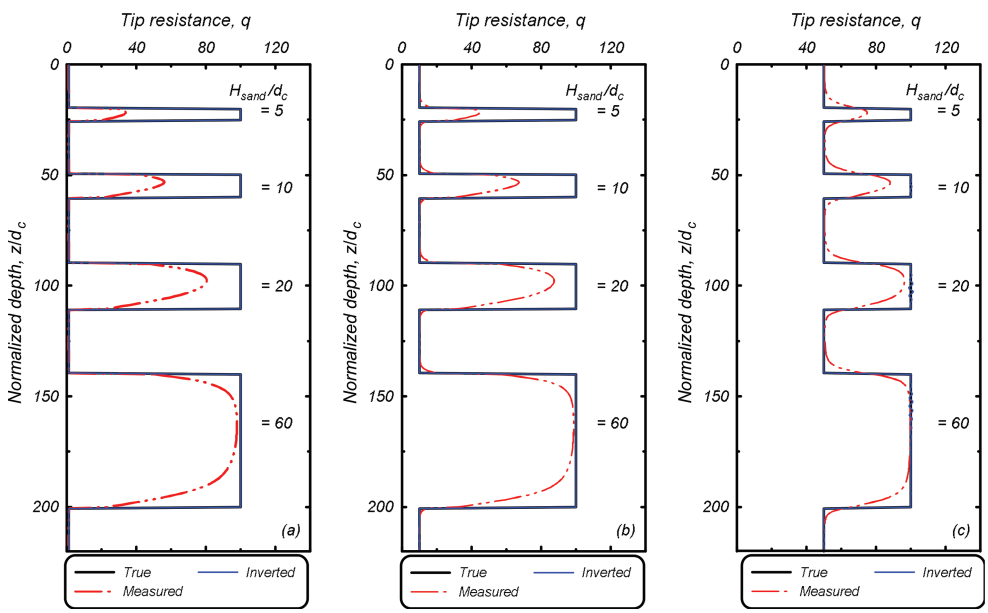

Figure 5. Values of q^t, q^m and q^{inv} for idealized profiles with interlayers of a strong soil with $q^t = 100$ embedded in a weaker soil with: (a) $q^t = 1$, (b) $q^t = 10$, and (c) $q^t = 50$. Note that q^{inv} almost perfectly overlays q^t.

to develop in the stronger layers decreases with decreasing layer thickness and decreasing strength in the surrounding soils.

Thin layer correction factors were subsequently derived using the above type of analysis for a uniform strong layer embedded in a uniform weaker deposit (e.g., Figure 1), with the results summarized in Figure 6. The derived values of K_H increase as q^t_{strong}/q^t_{weak} increases, but the rate of increase in K_H diminishes as q^t_{strong}/q^t_{weak} becomes larger. The K_H values approach unity for layers thicknesses greater than about 40 cone diameters, and are between 1.5 and 1.9 for layers about 10 cone diameters thick with q^t_{strong}/q^t_{weak} of 10–100. These K_H values are reasonably consistent with those of prior experimental and theoretical studies. The values of K_H increase rapidly as the thickness of the strong layer becomes less than about 5–10 cone diameters.

Sensing and development distances were similarly derived for an idealized two-layer system having q^t_{upper}/q^t_{lower} ratios ranging from 0.02 to 50. The sensing distance for the cone when it is in the upper layer (Δz_{sens}) and the development distance for the cone when it has entered the lower layer (Δz_{dev}), were determined as the distances from the interface where the difference between q^m and q^t was 5, 10, or 20%. The resulting values for $\Delta z_{sens}/d_c$ and $\Delta z_{dev}/d_c$ are plotted versus q^t_{upper}/q^t_{lower} in Figures 7a

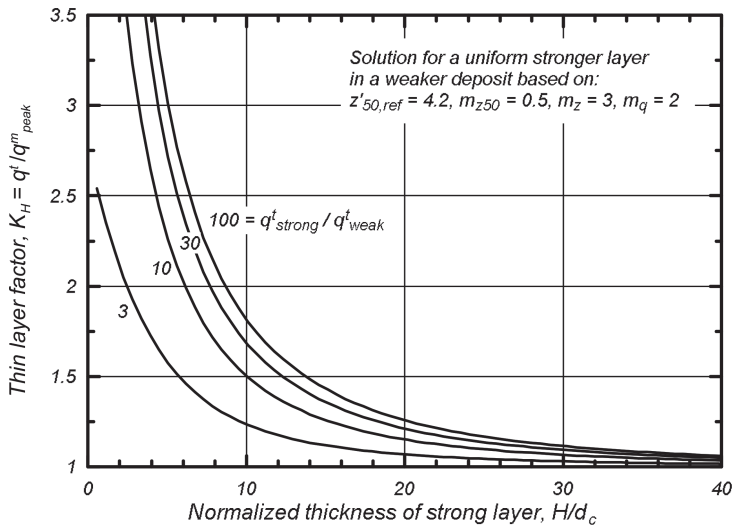

Figure 6. Thin layer correction factors computed for a uniform stronger layer of thickness H in a uniform weaker deposit.

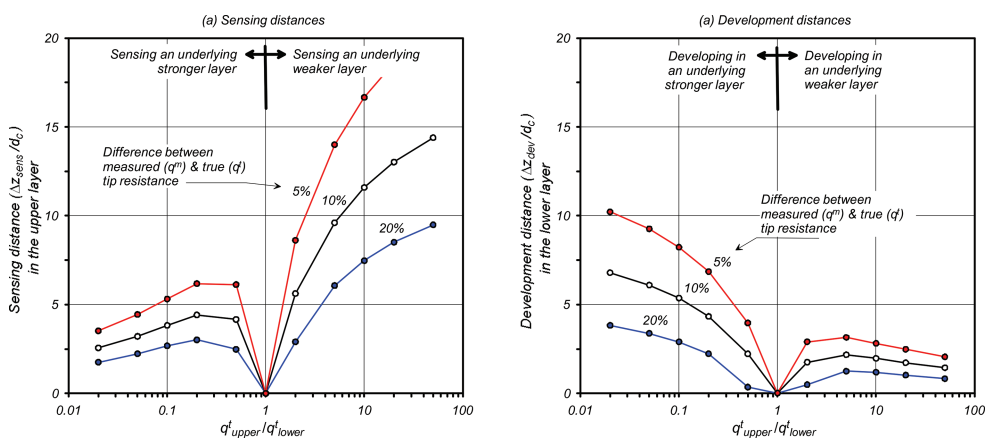

Figure 7. Sensing and development distances for a two layer system: (a) sensing distances, and (b) development distances.

and 7b, respectively. The $\Delta z_{sens}/d_c$ ranges from 2 to 6 when the cone is sensing an underlying stronger layer (left side of Figure 7a) and can be as large as 10–20 when the cone is sensing an underlying weaker layer (right side of Figure 7a). The $\Delta z_{dev}/d_c$ ranges from 2 to 10 when the cone is developing in an underlying stronger layer (left side of Figure 7b) and can be as small as 1 to 3 when the cone is developing in an underlying weaker layer (right side of Figure 7b).

The functional forms of the filter and the calibration of the filter parameters, as presented in this section, were iteratively developed to be consistent with the available experimental and theoretical data on thin layer and transition zone behaviors discussed in the previous section. The filter parameters can be adjusted to increase or decrease the thin layer effects or the sensing and development distances; for example, increasing z_{50ref} will cause the sensing/development distances to increase and the thin layer factors to increase for a given sand layer thickness. The parameter values adopted herein are considered reasonable values for general application, pending further experiences and validation studies.

5 SOLUTION PROCEDURE

5.1 *Inversion for tip resistance*

Inversion of q^m to obtain an estimate of q^t requires an iterative solution procedure because the filter is nonlinearly dependent on the unknown q^t. A method of successive substitutions as outline below was found to work well. The basic equations are first rearranged to obtain the difference between q^t and q^m as,

$$dq = q^t - q^m \tag{9}$$

where q^m is equal to the convolution of q^t with the filter, leading to

$$dq = q^t - q^t * w_c \tag{10}$$

The value of q^t can then be determined as,

$$q^t = q^m + dq \tag{11}$$

$$q^t = q^m + \left(q^t - q^t * w_c\right) \tag{12}$$

The above equation can now be solved by successive iterations as,

$$q_{n+1}^{inv} = q^m + \left(q_n^{inv} - q_n^{inv} * w_c\right) \tag{13}$$

where q_n^{inv} is the result of the nth iteration. The iteration process is initiated with the first estimate of q^{inv} set equal to q^m. Iterations continue until the following error criterion is satisfied,

$$err = \frac{\sum\left|\left(q_{n+1}^{inv} - q_n^{inv}\right)_i\right|}{\sum\left|\left(q^m\right)_i\right|} < 10^{-6} \tag{14}$$

This solution procedure, without any adjustments, is not well constrained at spatial frequencies that are higher than justifiable based on the data sampling interval or the physical size of the cone. These higher-than-justifiable spatial frequency components can also impede convergence of the solution, as shown later. Two additional steps were therefore added to the solution procedure to remove these higher spatial frequencies and improve convergence; these additional steps are introduced in sequence below, after first illustrating performance of the solution procedure without either additional step.

Performance of the above solution procedure (without the additional steps) is illustrated in Figure 5, which shows an idealized q^t profile along with a q^m computed by convolving q^t with the baseline filter model. Also shown in these plots are the q^{inv} computed iteratively from q^m with the same or "true" filter. For the cases in Figures 5a and 5b, the solution procedure converged and the differences between q^{inv} and q^t are negligible. These cases illustrate how the solution procedure is essentially perfect if the filter is known perfectly and the solution converges. For the case in Figure 5c, the solution procedure did not converge, but rather stabilized at a solution where q^{inv} included a small amount of low-level, high spatial frequency (short wavelength) noise in the stronger layers (barely visible as ripples in the q^{inv}). The wavelength of this noise is similar to the cone tip length, which is when the solution process can become less stable.

The potential effects of "noise" or the potential challenges with inverting information from very thin interlayers using the above solution procedure is further illustrated in Figure 8(a). This figure shows a profile of uniform soil with $q^m = 10$ except for thin intervals that are 1.1, 1.7, 2.2, and 3.4 cone diameters thick and have $q^m = 12$. The digital data were generated with a uniform 20 mm sampling interval, such that these depth intervals correspond to 2, 3, 4, and 6 data points with $q^m = 12$. Inversion of this q^m profile did not converge (i.e., meet the error criteria), but did stabilize at the solution shown in Figure 8a with peak q^{inv} values in the range of 30–40. These high q^{inv} values are sensitive to details of the filter model and are not reliable.

The solution procedure therefore requires an additional smoothing step that removes some of the highest spatial frequencies (shortest wavelengths) during the inversion process. After each

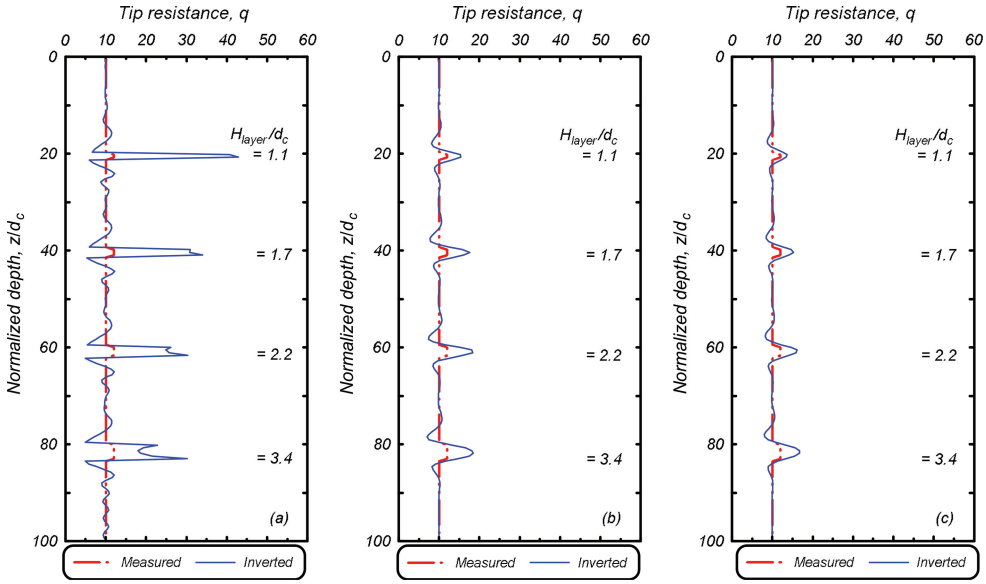

Figure 8. Inversion for a profile that has thin interlayers with $q^m = 12$ embedded in a uniform deposit having $q^m = 10$: (a) results using the first solution procedure, (b) results for the solution procedure with smoothing over the cone tip length, and (c) results for the solution procedure with smoothing followed by low-pass spatial filtering.

iteration, q^{inv} is smoothed (or low-pass spatial filtered) by taking a moving average over a window of a specified number of data points. The smoothing window is defined as the larger of either three points or the ceiling (rounding up) of the cone tip length (i.e., 0.866 d_c) divided by the data point depth spacing (i.e., Δz). The first criterion governs for a standard 10 cm^2 cone and uniform 20 mm data sampling interval, whereas the second criterion governs if the data sampling interval is much smaller (e.g., 5 mm). In this regard, the solution procedures were tested for data sampling intervals of 1–50 mm to ensure they continued to perform well for non-standard conditions. The inclusion of this smoothing step removes spatial frequencies that cannot be reliably inverted, greatly improves the convergence rate, and eliminated any cases of non-convergence. For example, application of the revised solution procedure to the profile shown in Figure 8 produced the smoother and more reasonable results shown in Figure 8b. In addition, the error term is plotted versus iteration number in Figure 9 for the solution procedures used for Figures 8a and 8b, illustrating how the inclusion of smoothing greatly improved the numerical performance of the solution procedure.

A second low-pass spatial filtering step was added to the solution procedure, although its effects are small for most situations. For this last step, the converged q^{inv} from the inversion with smoothing is convolved with another low-pass filter,

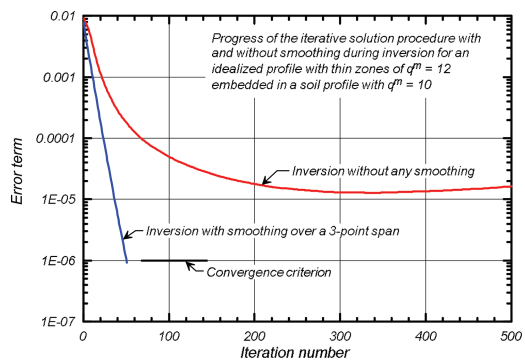

Figure 9. Progress of the iterative soil procedure with and without smoothing during inversion.

$$q^{inv} = q^{inv} * w_{c2} \tag{15}$$

where w_{c2} is the same filter model as w_c except that z_{50ref} is reduced to the length of the cone tip (i.e., 0.866 d_c). The application of this additional step in the inverse filtering of the profile shown in Figure 8 produced the slightly smoother result shown in Figure 8c. The results in Figure 8c illustrate that the overall solution procedure with smoothing during inversion followed by low-pass spatial filtering appears well-suited for handling high spatial frequency noise.

Performance of the overall solution procedure (inversion with smoothing followed by low-pass

spatial filtering) is illustrated in Figure 10 for the same idealized profiles examined previously (in Figure 5). The q^{inv} profiles still reasonably approximate the q^t profiles, though slightly rounded at the interfaces and slightly smaller than q^t for the interlayers that are only 5 cone diameters thick.

Performance of the overall solution procedure can also be expressed in terms of the "net" thin-layer factor that it produces for idealized two-layer systems, as shown in Figure 11. These net factors are computed as the peak q^{inv} in a thin layer divided by the peak q^m for that same layer, and thus are

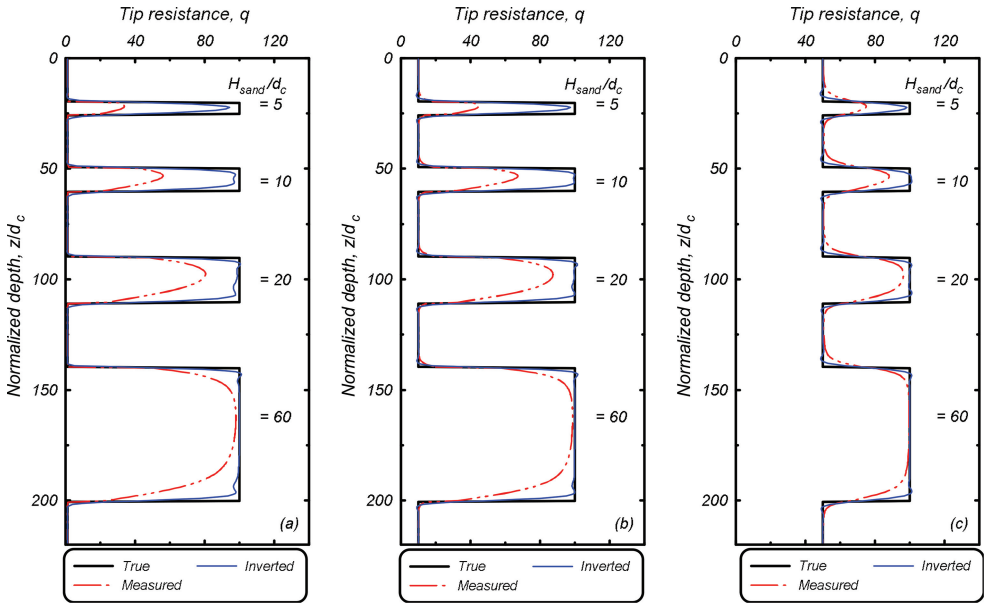

Figure 10. Values of q^t, q^m and q^{inv} for three idealized profiles using the solution procedure with smoothing followed by low-pass spatial filtering. Stronger layers have $q^t = 100$ and the weaker layers have (a) $q^t = 1$, (b) $q^t = 10$, and (c) $q^t = 50$.

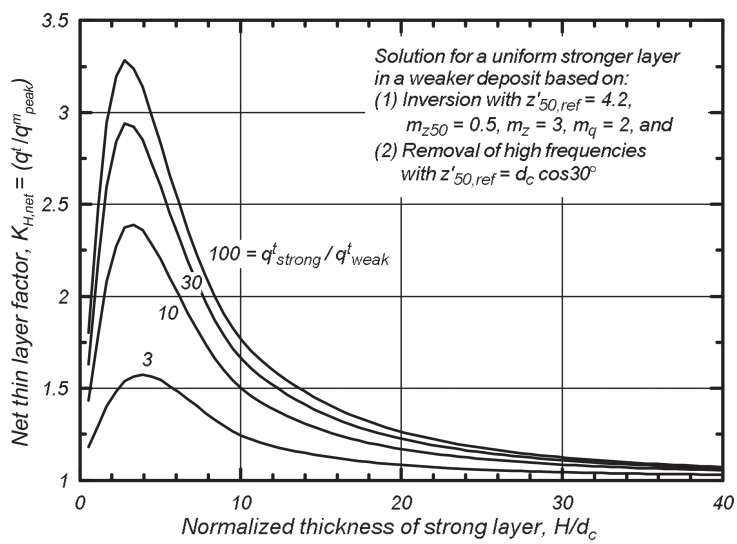

Figure 11. Net thin layer correction factors computed using inversion with low-pass spatial filtering.

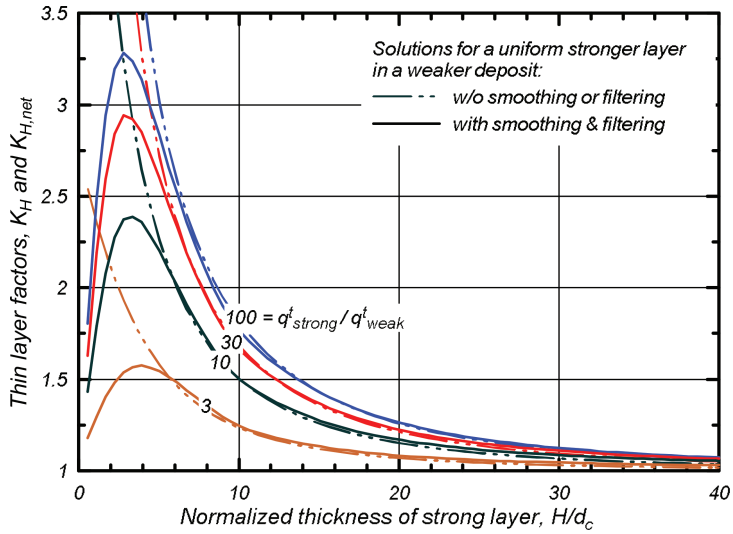

Figure 12. Comparison of the thin layer correction factors from the solutions with and without the smoothing and low-pass spatial filtering steps.

illustrative of how much amplification the inversion process may apply to the q^m in sand layers of various thicknesses. The $K_{H,net}$ curves for a range of q^t_{strong}/q^t_{weak} ratios all reach their peak values at strong-layer thicknesses of 3–4 cone diameters, and decrease toward unity with decreasing layer thickness. The fact $K_{H,net}$ tends to unity as the strong-layer thickness tends to zero reflects the fact that cone penetration measurements cannot provide meaningful information on soil properties when they vary strongly across interlayers that are less than about 2 or 3 cone diameters thick. The previously presented K_H values are overlain with the $K_{H,net}$ values in Figure 12, illustrating how the K_H values rapidly increase toward large values at these small layer thicknesses, which relates to why inversion without smoothing or low pass spatial filtering performed poorly. The solution procedure with smoothing during inversion followed by low-pass spatial filtering produces equivalent $K_{H,net}$ values that are reasonable for strong-layer thicknesses that are greater than about 3–4 cone diameters and appropriately conservative for thinner layers where inversion is not reliable.

5.2 *Inversion for sleeve friction*

The inversion of sleeve friction (f_s) profiles could conceptually follow a similar process as used for tip resistance. The filter model for f_s could have a different form and distribution. For example, examination of field data illustrates that f_s is more sensitive to thin layers than q_t, which would imply a smaller zone of influence or greater weighting of data near the sleeve. Unfortunately, there are currently limited data available to guide development of a separate filter model for f_s.

The strategy adopted herein was to develop f_s^{inv} values from the q^{inv} values. This procedure assumes that the pairs of normalized tip resistance (Q) and normalized sleeve friction ratio (F) for the inverted and measured data lie along a radial line originating from the origin of the Soil Behavior Type Index (I_c). The values of Q and F are computed as,

$$Q = \left(\frac{q-\sigma_{vc}}{P_a}\right)\left(\frac{P_a}{\sigma'_{vc}}\right)^n \tag{16}$$

$$F = \left(\frac{f_s}{q-\sigma_{vc}}\right)100\% \tag{17}$$

where σ_{vc} is the total vertical stress, σ'_{vc} is the effective vertical stress, and P_a is atmospheric pressure. The stress exponent n is computed following the relationship recommended by Robertson (2009),

$$n = \left(0.381 I_c + 0.05\sigma'_{vc} - 0.15\right) \le 1 \tag{18}$$

and the value of I_c is computed using the form recommended by Robertson and Wride (1997),

$$I_c = \left[\left(3.47-\log(Q)\right)^2 + \left(1.22+\log(F)\right)^2\right]^{0.5} \tag{19}$$

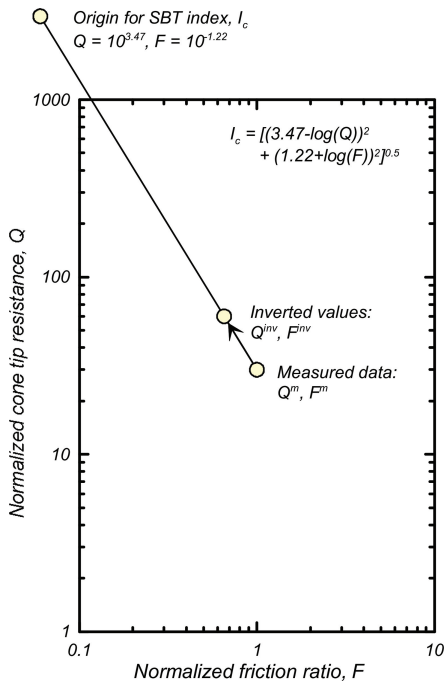

Figure 13. Procedure used to compute F^{inv} given Q^m and F^m for the field measurements and the value of Q^{inv} obtained from the inversion procedure.

The I_c value can be visualized as the radial distance between any Q-F pair and an origin point located at Q = 2,951 and F = 0.0603, as shown in Figure 13. The measured q^m and f_s^m values are used to compute Q^m and F^m values, and the inverted q^{inv} is used to compute a Q^{inv} value. The value of F^{inv} is then computed based on the assumption that the inverted point moved radially with respect to the I_c origin,

$$F^{inv} = 10^{\left\{\frac{\left(3.47-\log\left(Q^{inv}\right)\right)}{\left(3.47-\log\left(Q^{m}\right)\right)}\left(1.22+\log\left(F^{m}\right)\right)-1.22\right\}} \tag{20}$$

The above procedure is schematically illustrated for a single data point in Figure 13. The value of f_s^{inv} is then computed from F^{inv} using the definition of F.

6 INTERFACE DETECTION AND CORRECTION

The detection of sharp interfaces and correction of the data at those interfaces is a separate step because the inversion process does not reproduce the high-spatial frequencies associated with a step in the q^t profile (i.e., the smoothing during inversion followed by low-pass spatial filtering removes those spatial frequencies because they cannot be inverted reliably). Identifying sharp transitions is complicated by the fact that some interfaces may be sharp and others may be graded (e.g., upward fining sequences), and thus the criteria and process will involve some subjectivity and should be subject to confirmation by borehole sampling data or knowledge of local geology.

A sharp transition (or interface) is considered likely to exist if the rate of change in the logarithm of q^{inv} with respect to normalized depth is larger than a specified criterion. The rate of change across each discrete data sampling interval is computed as,

$$m_i = \frac{\ln\left(q_{i+1}^{inv}\right) - \ln\left(q_i^{inv}\right)}{z'_{i+1} - z'_i} \tag{21}$$

Note that the index for m corresponds to the intervals between measurement points; i.e., if there are N points in the q^{inv} vector, there are N-1 points in the m vector. The value of m that would be consistent with the existence of a sharp interface can be estimated using experimental and theoretical estimates of the sensing and development distances. For example, if q changes by a factor of more than 2 over a distance of about 6 cone diameters (214 mm for a standard 10 cm^2 cone), then m will exceed 0.12 on average. On the other hand, if q smoothly changes by a factor of less than 10 over a graded interval that is about 1 m thick (or about 28 standard cone diameters), then m may not exceed 0.08 on average. Thus, a sharp interface may be expected to exist if m exceeds a specified threshold, m_t. A reasonable value for m_t, as adopted herein, may be on the order of 0.1, subject to refinement based on site-specific sampling and geologic information.

The transition zone over which q^{inv} at a sharp interface is still blurred will also have smoothly varying m values. The m values both above and below the point where the maximum m is obtained will be smaller than the maximum m for that transition zone. For the present study, the transition zone is assumed to include any contiguous measurement points where m is greater than $m_t/5$. If the zone identified by the above criteria is less than 3 cone diameters thick, then is it is not considered a transition zone. If the zone identified by the above criteria is greater than 12 cone diameters thick where q^{inv} is increasing, then the interval is truncated to 12 cone diameters thick (centered on the original zone). If the zone identified by the above criteria is greater than 18 cone diameters thick where q^{inv} is decreasing, then the interval is truncated to

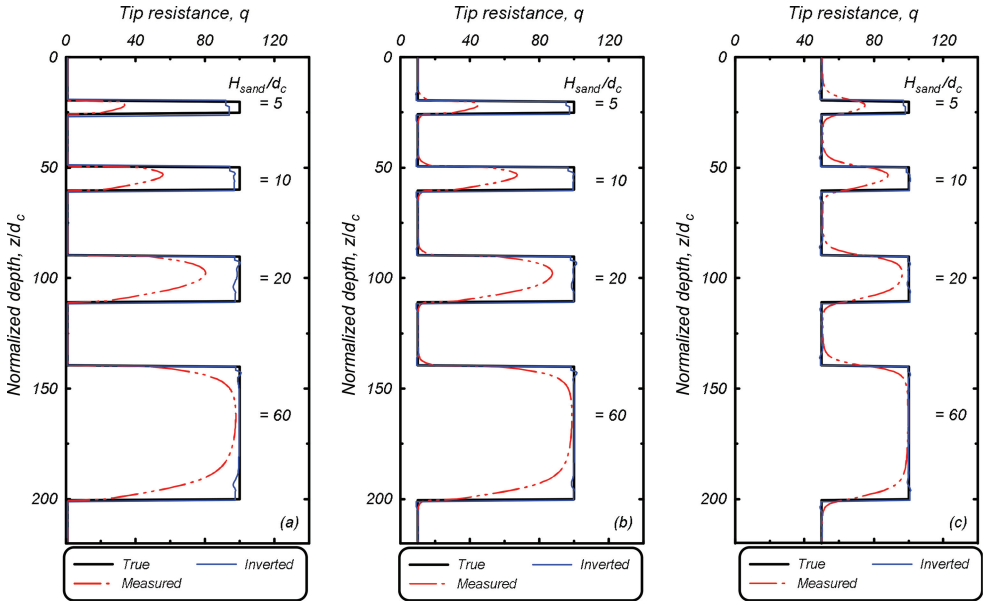

Figure 14. Values of q^t, q^m and q^{inv} for three idealized profiles using inversion with smoothing followed by low-pass spatial filtering and interface detection and correction. Stronger layers have $q^t = 100$ and the weaker layers have (a) $q^t = 1$, (b) $q^t = 10$, and (c) $q^t = 50$.

18 cone diameters thick (centered on the original zone). Once the transition zone has been defined, the q^{inv} and f_s^{inv} values at the top of the transition zone are assigned to all points in the upper 40% of the transition zone for penetration advancing into a stronger layer or the upper 60% of the transition zone for penetration advancing into a weaker layer. The q^{inv} and f_s^{inv} values at the bottom of the transition zone are assigned to all remaining points in the lower part of the transition zone.

Application of the interface detection and correction algorithm is illustrated in Figure 14 for the same idealized profiles presented in Figures 5 and 10. The interface detection and correction algorithm does not perfectly remove the transition zone, since it does not capture the slow rates of change in q at the start and end of each transition zone for this idealized profile. A greater portion of the interface could be removed by reducing m_t, but that can result in falsely identifying transition zones or computing overly thick transition zones when processing real CPT soundings.

7 INVERSION EXAMPLES FOR FIELD DATA

7.1 *Applications using the baseline model*

Application of the proposed inverse filtering procedure is illustrated in Figures 15–18 for cone soundings from four different sites. The inversion, low-pass spatial filtering, and interface detection steps are applied using the same baseline parameters specified in the previous sections. The first example (Figure 15) is CPT UC-4 along Sandholdt Road in Moss Landing, CA, USA where liquefaction-induced ground deformations were observed after the 1989 $M_w = 6.9$ Loma Prieta earthquake (Boulanger et al. 1997). The second example (Figure 16) is CPT 1–24 along Çark Canal in Adapazari, Turkey where no surficial evidence of liquefaction was observed after the 1999 $M_w = 7.5$ Kocaeli earthquake (Youd et al. 2009). The third example (Figure 17) is CPT 45185 at St. Theresa's school in Riccarton, Christchurch, New Zealand where no surficial evidence of liquefaction was observed during the 2010–2011 Canterbury Earthquake Sequence (Cox et al. 2017). The fourth example (Figure 18) is a CPT at Hinode Minami Elementary School, Urayasu, Japan where no evidence of liquefaction was observed following the 2011 $M_w = 9.0$ Tohoku earthquake (Cox et al. 2013). The data sampling intervals for these four CPT soundings were 50, 20, 10, and 25 mm, respectively. The latter three sites are of interest because some degree of liquefaction would have been expected based on common engineering liquefaction evaluation procedures, as reported in the various references. The details of liquefaction evaluations for each site are beyond the scope of the present paper, except to note that thin-layer and transition effects are considered to be one

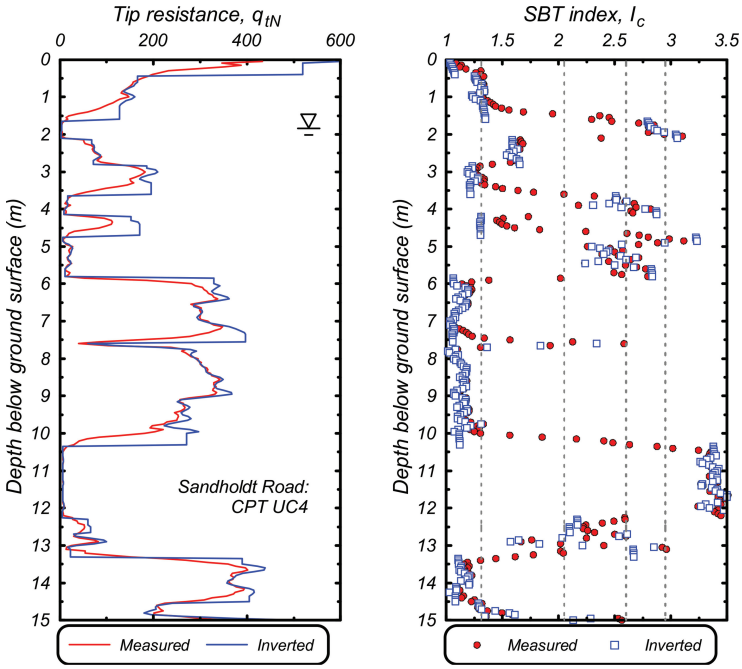

Figure 15. Measured and inverted q_{tN} and I_c profiles for CPT UC-4 at Sandholdt Road.

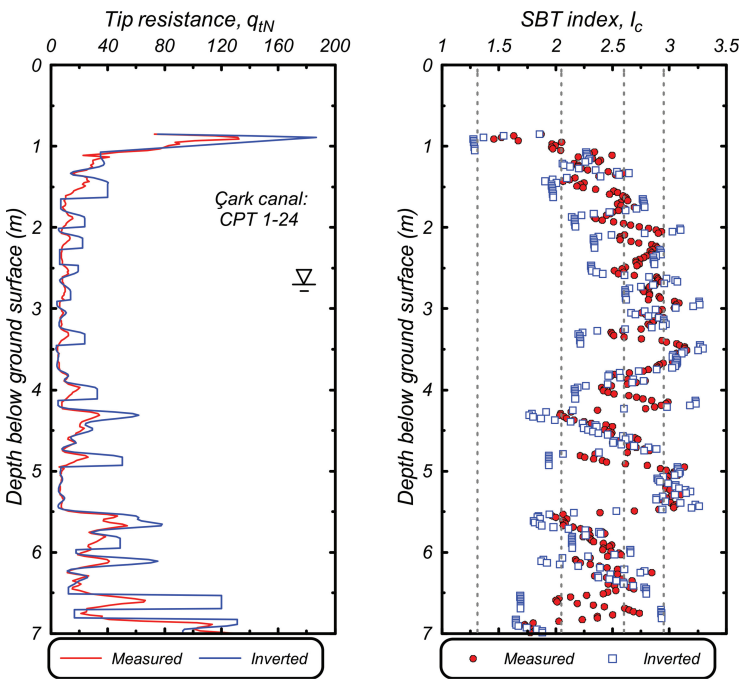

Figure 16. Measured and inverted q_{tN} and I_c profiles for CPT 1–24 at Çark Canal.

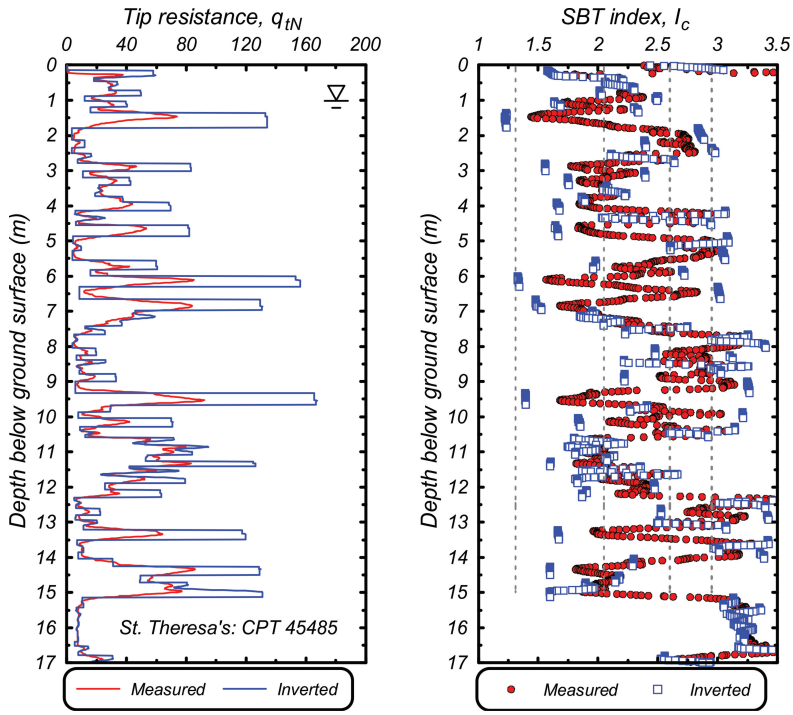

Figure 17. Measured and inverted q_{tN} and I_c profiles for CPT-45185 at St. Theresa's School.

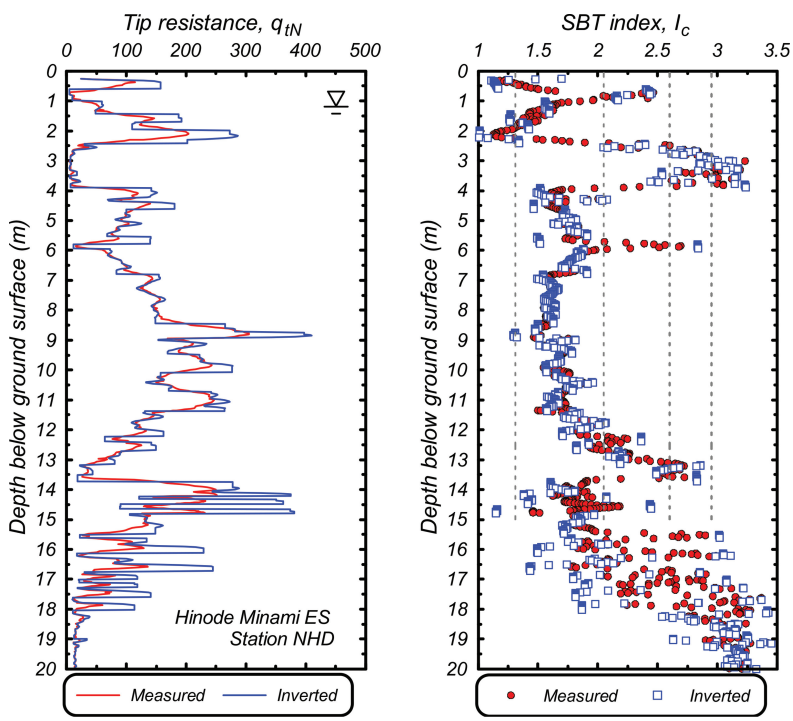

Figure 18. Measured and inverted q_{tN} and I_c profiles for Station NHD at Hinode Minami Elementary School.

of several factors that can contribute to the over-prediction of liquefaction effects (e.g., Boulanger et al. 2016).

Examination of these four examples illustrates that the proposed CPT inversion procedure is performing as expected. The inversion process has negligible effects on q or I_c in intervals where the soil type or penetration resistance is relatively uniform. The inversion procedure has the greatest effect where well-defined thin-layers of stronger material are detected. The inversion procedure increases q^{inv} (relative to q^m) by factors up to 2–3 even for the thinnest strong interlayers at the highly interbedded sites, which reflects the upper limits that the present inversion parameters will produce (e.g., as illustrated by the net thin layer factors in Figure 11) and that can be justified given conventional cone diameters. The inversion procedure was

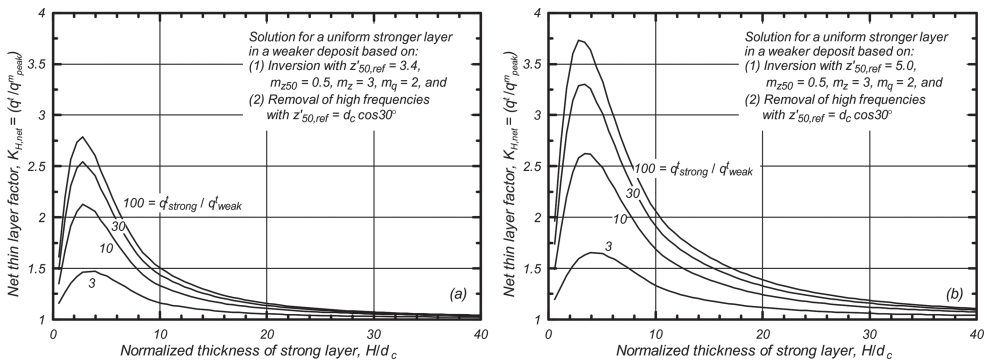

Figure 19. Net thin layer correction factors using the baseline set of filter parameters except for: (a) $z'_{50,ref} = 3.4$, and (b) $z'_{50,ref} = 5.0$

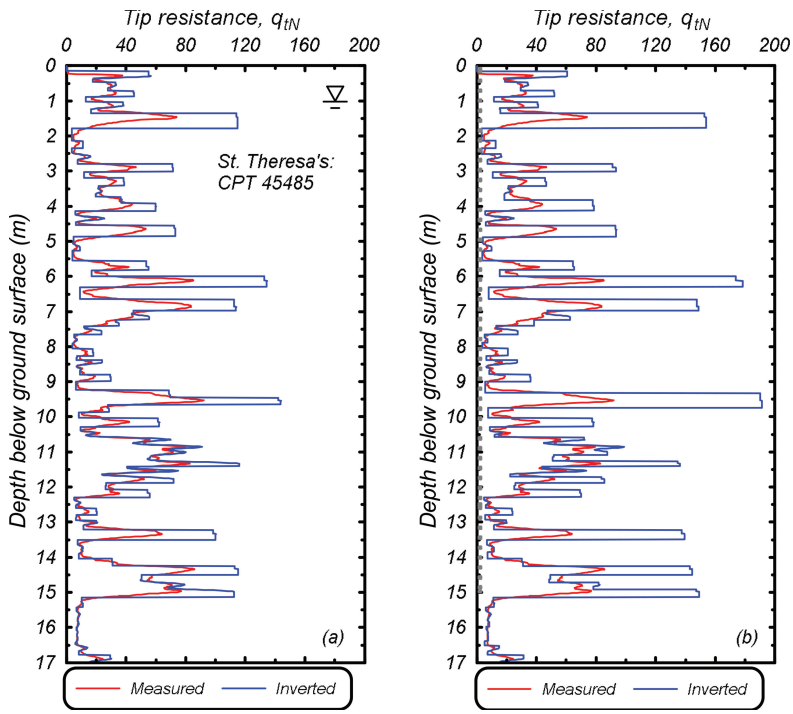

Figure 20. Measured and inverted q_{tN} profiles for CPT-45185 at St. Theresa's School using the baseline set of filter parameters except for: (a) $z'_{50,ref} = 3.4$, and (b) $z'_{50,ref} = 5.0$.

effective in removing transition zones at clearly identifiable contacts, while the detection criteria left other zones of slowly increasing penetration resistance unmodified.

7.2 *Example using alternative filter parameters*

The sensitivity of the inverse filtering procedure to alternative sets of filter parameters was also evaluated, recognizing that there is uncertainty in the filter model and individual parameters. The effect of individual parameter variations were examined in terms of how they affected the solutions for idealized problems (e.g., Figure 14), sensing and development distances for idealized two layer profiles (e.g., Figure 7), net thin layer correction factors (e.g., Figure 11), and results for field CPT soundings. Alternative sets of parameters that are consistent with the body of available experimental and theoretical data can be developed, including sets that provide more or less aggressive corrections to measured data.

For example, consider the effect of setting $z'_{50,ref}$ equal to 3.4 or 5.0 (± 19% from the baseline value of 4.2), while keeping all other parameters equal to the baseline values. The corresponding $K_{H,net}$ values, as shown in Figures 19a and 19b, are smaller for $z'_{50,ref}$ = 3.4 and larger for $z'_{50,ref}$ = 5.0, with the differences being larger for smaller layer thicknesses. For a strong layer thickness of 3–5 cone diameters, using $z'_{50,ref}$ = 3.4 reduced the $K_{H,net}$ values by 8–18% (relative to those for the baseline set of filter parameters) whereas using $z'_{50,ref}$ = 5.0 increased the $K_{H,net}$ values by 6–18%.

The effects of using the above $z'_{50,ref}$ values on the inverse filtering of a field CPT sounding are illustrated in Figures 20a and 20b for CPT 45185 at St. Theresa's school in Riccarton. The use of $z'_{50,ref}$ = 3.4 (Figure 20a) resulted in smaller q^t values in the numerous thin sand interlayers relative to those for the baseline case (Figure 17), whereas use of $z'_{50,ref}$ = 5.0 (Figure 20b) resulted in larger q^t values. The differences in the inversion results for these two cases are consistent with the differences in the corresponding net thin layer correction factors.

8 CONCLUDING REMARKS

An inverse filtering procedure for developing estimates of the "true" cone penetration tip resistance and sleeve friction values from measured cone penetration test data was presented. The inverse filtering procedure has three primary components: (1) a model for how the cone penetrometer acts as a low-pass spatial filter in sampling the true distribution of soil resistance versus depth, (2) a solution procedure to iteratively determine an estimate of the true cone penetration resistance profile from the measured profile given the cone penetration filter model, and (3) a procedure to identify sharp transition interfaces and correct the data at those interfaces. The inverse filtering procedure was shown to produce equivalent thin layer factors and sensing/development distances that are consistent with the results of prior experimental and theoretical studies. Example applications of the inverse filtering procedure to four CPT soundings illustrated that the model performs well for a range of soil profile characteristics. The inverse filtering procedure was shown to provide an objective, repeatable, and automatable means for correcting cone penetration test data for thin-layer and transition zone effects.

Further experience with application of the inverse filtering procedure can be expected to lead to improvements in components of the procedure or improved guidance for its use in practice. Issues worth further examination include how f_s and q_c may filter differently, how the filter model might depend on other specific properties (stiffness, strength, drainage conditions) or stratigraphic sequences, and how the inversion process or parameters might be adjusted based on site-specific borehole and geologic information. The present model was developed with a focus on liquefaction problems, whereas applications to other problems may identify different aspects that warrant improvement. Regardless of advances, there will be practical limits to how well inverse filtering procedures, or any other technique, can correct cone penetration test data given the nature of the cone penetration process, the infinite possible variations in geologic conditions, the presence of noise in measurements, and other complex processes that influence the measurements (e.g., partial drainage, physical dragging of soil along with the cone). In this regard, the proposed inverse filtering procedure is intended to improve or enhance the field measurements, while recognizing that any inversion process will be neither unique nor perfect.

ACKNOWLEDGMENTS

The authors appreciate the financial support of the National Science Foundation (award CMMI-1635398) and California Department of Water Resources (contract 4600009751) for different aspects of the work presented herein. Any opinions, findings, conclusions, or recommendations expressed herein are those of the authors and do not necessarily represent the views of these organizations. Dr. Mohammad Khosravi and Mr. Mathew Havey contributed to the literature review and evaluation of alternative procedures for evaluating thin-layer effects. Dr. Dan

Wilson provided valuable comments on numerical aspects of inverse filtering procedures. Professor Brady Cox provided valuable review comments that improved the clarity of the paper. The authors appreciate the above support and interactions.

REFERENCES

Ahmadi, M. M. and Robertson, P. K. 2005. Thin-layer effects on the CPT q_c measurement. Canadian Geotechnical Journal, 42(5), 1302–1317.

Boulanger, R. W., Mejia, L. H., and Idriss, I. M. 1997. Liquefaction at Moss Landing during Loma Prieta Earthquake. Journal of Geotechnical and Geoenvironmental Engineering, ASCE, 123(5), 453–467.

Boulanger, R. W., Moug, D. M., Munter, S. K., Price, A. B., and DeJong, J. T. 2016. Evaluating liquefaction and lateral spreading in interbedded sand, silt, and clay deposits using the cone penetrometer. Geotechnical and Geophysical Site Characterisation 5, B. M. Lehane, H. Acosta-Martinez, and R. Kelly, eds., Australian Geomechanics Society, Sydney, Australia, ISBN 978-0-9946261-2-7.

Canou, J. 1989. Piezocone et liquefaction des sables. Rapport de synthese des travaux realizes au CERMES, Re-search Report CERMES/ENPC, Paris, 176 p.

Cox, B. R., Boulanger, R. W., Tokimatsu, K., Wood, C., Abe, A., Ashford, S., Donahue, J., Ishihara, K., Kayen, R., Katsumata, K., Kishida, T., Kokusho, T., Mason, B., Moss, R., Stewart, J., Tohyama, K., and Zekkos, D. 2013. Liquefaction at strong motion stations and in Urayasu City during the 2011 Tohoku-Oki earthquake. Earthquake Spectra, EERI, 29(S1), S55-S80.

Cox, B. R., McLaughlin, K. A., van Ballegooy, S., Cubrinovski, M., Boulanger, R. W., and Wotherspoon, L. 2017. In-situ investigation of false-positive liquefaction sites in Christchurch, New Zealand: St. Teresa's School case history. Proc., Performance-based Design in Earthquake Geotechnical Engineering, PBD-III Vancouver, M. Taiebat et al., eds., ISSMGE Technical Committee TC203, paper 265.

Cristobal, G., Schelkens, P., and Thienpont, H. 2011. Optical and digital image processing: Fundamentals and applications. Wiley-VCH Verlag GmbH & Co KGaA, Editors: G. Cristobal, P. Schelkens, and H. Thienpont, DOI: 10.1002/9783527635245.

Foray, P. & Pautre, J-L. 1988. Piezocone et liquefaction des sables: synthese des essais sur sites en Nouvelle-Zelande et des essais en Chambre de Calibration a l'IMG, Research Report, IMG, Grenoble, 70 p.

Hird, C. C., Johnson, P., and Sills, G. C. 2003. Performance of miniature piezocones in thinly layered soils. Géotechnique, 53(10), 885–900.

Lunne, T., Robertson, P.K., and Powell, J.M. 1997. Cone penetration testing in geotechnical practice. Blackie Academic & Professional, London, UK.

Mayne, P. 2007. Cone Penetration Testing—A synthesis of highway practice. NCHRP Synthesis 268, Transportation Research Board, Washington, D.C.

Meyerhof, G. G. and Valsangkar, A. J. 1977. Bearing capacity of piles in layered soils. Proc. 9th Int. Conf. Soil Mech. Found. Engng, Japan 1, 645–650.

Mlynarek, Z., Gogolik, S., and Poltorak, J. 2012. The effect of varied stiffness of soil layers on interpretation of CPTU penetration characteristics. Archives of Civil and Mechanical Engineering, 12, 253–264.

Mo, P.-Q., Marshall, A. M., and Yu, H.-S. 2017. Interpretation of cone penetration test data in layered soils using cavity expansion analysis. J. Geotechnical and Geoenvironmental Eng., 143(1), 10.1061/(ASCE) GT.1943-5606.0001577.

Mo, P. Q., Marshall, A. M., and Yu, H. S. 2015. Centrifuge modelling of cone penetration tests in layered soils. Géotechnique, 65(6), 468–481.

Munter, S. K., Boulanger, R. W., Krage, C. P., and DeJong, J. T. 2017. Evaluation of liquefaction-induced lateral spreading procedures for interbedded deposits: Cark Canal in the 1999 M7.5 Kocaeli earthquake. Geotechnical Frontiers 2017, Seismic Performance and Liquefaction, Geotechnical Special Publication No. 281, T. L. Brandon and R. J. Valentine, eds., 254–266.

Robertson, P. K. 2009. Interpretation of cone penetration tests—a unified approach. Canadian Geotechnical Journal, 46, 1337–1355.

Robertson, P. K. and Fear, C. E. 1995. Liquefaction of sands and its evaluation. Proc., 1st Int. Conf. on Earthquake Geotechnical Engineering, Ishihara, K. (ed), A. A. Balkema.

Robertson, P. and Wride, C., 1998. Evaluating cyclic liquefaction potential using the cone penetration test. Canadian Geotechnical Journal, 35(3), 442--459.

Sayed, S. M., and Hamed, M. A. 1987. Expansion of cavities in layered elastic system. International Journal of Numerical and Analytical Methods in Geomechanics, 11(2), 203–213.

Silva, M. F., and Bolton, M. D. 2004. Centrifuge penetration tests in saturated layered sands. Proc. ISC-2 on Geotechnical and Geophysical Site Characterization, Viana da Fonseca and Mayne (eds), 377–384.

Tehrani, F. S., Arshad, M. I., Prezzi, M., and Salgado, R. 2018. Physical modeling of cone penetration in layered sand. Journal of Geotechnical and Geoenvironmental Engineering, 144(1), 04017101, DOI:10.1061/(ASCE)GT.1943-5606.0001809.

Treadwell, D.D. 1976. The influence of gravity, prestress, compressibility, and layering on soil resistance to static penetration. Ph.D. thesis, University of California at Berkeley, Berkeley, Calif.

Van den Berg, P., De Borst, R. & Huetink, H. 1996. An Eulerian finite element model for penetration in layered soil. International Journal of Numerical and Analytical Methods in Geomechanics, 20, 865–886.

Vreugdenhil, R., Davis, R. and Berrill, J. 1994. Interpretation of cone penetration results in multilayered soils. International Journal of Numerical and Analytical Methods in Geomechanics, 18(9), 585–599.

Walker, J. and Yu, H.-S. 2010. Analysis of the cone penetration test in clay. Geotechnique, 60(12), 939–948.

Xu, X. T., and Lehane, B. M. 2008. Pile and penetrometer end bearing resistance in two-layered soil profiles. Géotechnique, 58(3), 187–197.

Youd, T. L., Idriss, I. M., Andrus, R. D., Arango, I., Castro, G., Christian, J. T., Dobry, R., Finn, W. D. L., Harder, L. F., Hynes, M. E., Ishihara, K., Koester, J. P., Liao, S. S. C., Marcuson, W. F., Martin, G. R., Mitchell, J. K., Moriwaki, Y., Power, M. S., Robertson, P. K., Seed, R. B., and Stokoe, K. H. 2001. Liquefaction resistance of soils: summary report from the

1996 NCEER and 1998 NCEER/NSF workshops on evaluation of liquefaction resistance of soils, J. Geotechnical and Geoenvironmental Eng., ASCE 127(10), 817–33.

Youd, T. L., DeDen, D. W., Bray, J. D., Sancio, R., Cetin, K. O. and Gerber, T. M. 2009. Zero-displacement lateral spreads, 1999 Kocaeli, Turkey, earthquake. Journal of Geotechnical and Geoenvironmental engineering, 135(1), 46–61.

Yue, Z.Q., and Yin, J.H. 1999. Layered elastic model for analysis of cone penetration testing. International Journal for Numerical and Analytical Methods in Geomechanics, 23, 829–843.

Cone Penetration Testing 2018 – Hicks, Pisanò & Peuchen (Eds)
© 2018 Delft University of Technology, The Netherlands, ISBN 978-1-138-58449-5

Use of CPT for the design of shallow and deep foundations on sand

K.G. Gavin
Delft University of Technology, Delft, The Netherlands

ABSTRACT: A wide range of empirical correlations linking the Cone Penetration Test (CPT) end resistance q_c and the resistance of shallow and deep foundations in sand have been published. Both National and European organisations are attempting to introduce standard methods into practice that unify these approaches. In this paper experimental data and finite element analyses are reviewed to examine the mechanisms governing foundation behaviour in a bid to move towards these unified approaches. For shallow foundations and non-displacement piles, sand creep was found to affect correlations between q_c and the mobilised bearing resistance. For pile foundations direct correlations between q_c and pile end resistance that were dependent only on pile installation method are reported. In the case of shaft resistance, constant correlation factors between q_c and average shaft resistance are possible for non-displacement piles. For the case of displacement piles, correlations that include the effects of friction fatigue are recommended.

1 INTRODUCTION

Whilst conventional bearing capacity and earth pressure approaches are widely used to design shallow and deep foundation in sand, many design codes are moving towards Cone Penetration Test (CPT) based design methods. This is as a result of a significant research effort in the area of foundation design in recent years. An issue facing both designers operating internationally and causing debate for those drafting unified codes such as Eurocode 7, is that many national recommendations have been published linking CPT end resistance, q_c with the bearing resistance of shallow foundations and piles. However, these values are rarely consistent, and in some cases can vary significantly. Whilst some of these differences may be caused by geology, pile types adopted, and a wide range of methods (averaging techniques) for estimating design q_c profiles, it arises at least in part due to a lack of understanding of the mechanisms controlling foundation behavior. Even internally within some countries, there is ongoing debate surrounding CPT based design.

Recent updates to the Dutch design code have caused significant debate within the geotechnical engineering community. Based on an interpretation of static load test data from across the Netherlands, CUR report 229 proposed a 30% reduction to the pile base reduction factor that will result in larger and longer piles from January 1st 2017. These changes are largely due to a lack of reliable pile load tests data in the Netherlands as the country is unusual in that it does not routinely test the axial capacity of piles. This has been met with some resistance from industry since historical pile failure rates are very low.

In this paper, the results of experiments performed on foundations in sand and finite element analyses are compiled in an attempt to provide an insight into factors that may influence correlations between CPT q_c and the behavior of both shallow and deep foundations in sand.

2 SHALLOW FOUNDATIONS

2.1 *General description*

Routine design of shallow footings on sand is often undertaken using the conventional bearing capacity approach to calculate the ultimate bearing resistance (q_{ult}):

$$q_{ult} = 0.5\gamma\, B\, S_\gamma\, d_\gamma\, N_\gamma + \gamma D\, S_q d_q N_q \qquad (1)$$

where: = unit weight of Soil, B = foundation width, D = foundation depth, S_γ,S_q d_γ and d_q are factors to account for footing shape and depth, whilst N_γ and N_q are bearing capacity factors which depend on the friction angle (ϕ') of the soil and the footing shape.

Additional factors can be included to take account of situations such as sloping ground conditions and inclined or eccentric loading, although there is a strong argument that the latter should be treated using interaction diagrams as proposed by Gottardi and Butterfield (1993) and Houlsby and Cassidy (2002). Designers face key challenges in the application of Equation (1). These include the choice of appropriate shape and depth factors, and most importantly bearing capacity factors:

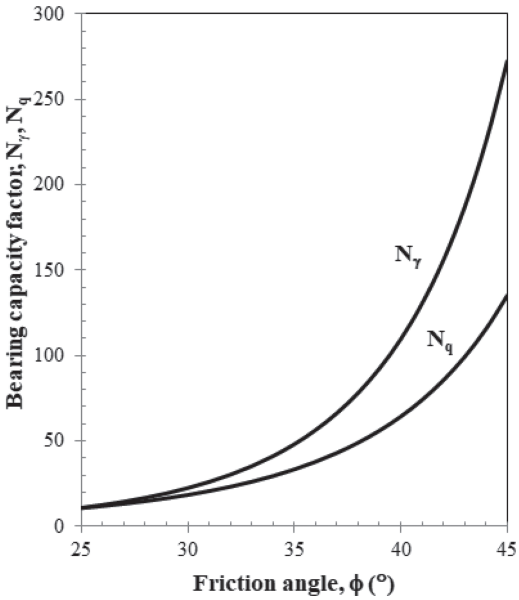

Figure 1. Typical bearing capacity factors for shallow footings.

Although Randolph et al. (2004), note that the accuracy with which bearing capacity factors can be determined has increased substantially in recent years, it is clear from Figure 1 that the values increase substantially over the range of soil strength typically encountered. Because of the difficulties in obtaining high quality samples, coupled with the challenges of interpreting soil strength parameters for the complex stress and strain paths experienced during loading at the relatively low stress levels applicable to footing design, greater reliance is placed on using empirical formulae linking ϕ' and q_c or using direct correlations linking q_c and the soil bearing resistance.

2.2 *CPT based methods for shallow foundation capacity*

In addition to the challenges outlined above, a further driver towards the use of in-situ test data in shallow foundation design was identified by Briaud (2007) from interpretation of field test data. Briaud and Gibbens (1999) report tests performed on square footings where the footing width, B varied from 1 m to 3 m. The footings were founded 0.75 m below the ground surface in recently deposited medium-dense sand. The site was in a lightly over-consolidated state (OCR ≈ 2) following the removal of about 1.0 m overburden. The mean CPT q_c resistance ranged from 5 to 7.25 MPa in the zone of influence of the footings. The pressure-settlement response (including un-load and re-load loops) of three of the footings is illustrated in Figure 2a. It is apparent that for a given settlement s, the mobilised bearing pressure, q reduced with increasing footing width. Another feature of the test was that for values of q greater than 650 kPa, significant creep settlement occurred during maintained load steps.

When the mobilised pressure was normalised by the q_c value averaged over the zone of influence, and he footing settlement divided by the footing width, a relatively unique normalised pressure-settlement response was obtained for the site, see Figure 2b. Noting that the unload-reload portions

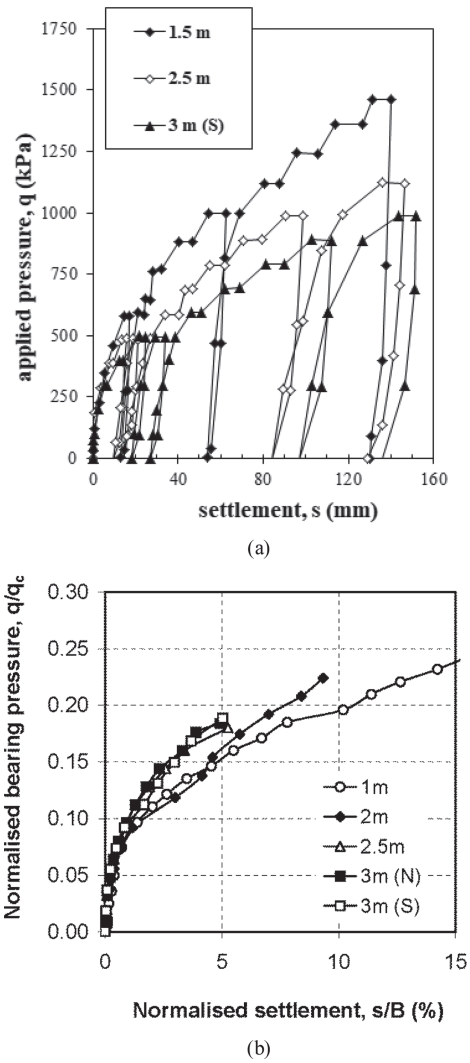

Figure 2. (a) Pressure-Settlement response for three footings (b) normalised pressure-settlement response.

of the data were removed for clarity and the maximum settlement for each load step were plotted, as it is clear from Figure 2a that the shape of the curve is affected by the load test procedure. Adopting a definition of failure as being the pressure mobilised when the footing settlement reached 10% of the footing width, $q_{0.1}$ the data suggests the adoption of a direct method for estimation of the footing resistance of the form given in Equation 2 with an α value of 0.20.

$$q_{0.1} = \alpha\, q_c \qquad (2)$$

Briaud (2007) considered data from other test sites to investigate the effect of footing depth, D and found that the normalised pressure-settlement response was independent of both footing width and relative embedment (D/B). He suggests that whilst Equation 1 would produce good estimates of q_{ult} of footings in soil profiles where the soil strength increased linearly with depth, in over-consolidated sand or in deposits where the near surface soil is unsaturated, the soils strength is often relatively constant with depth and the assumption that q_{ult} increases with footing width, B or footing depth, D is not valid.

Based on a review of footing tests from the literature, Eslaamizaad and Robertson (1996) found that the back-figured α values varied with soil density, relative embedment and footing shape. Randolph et al. (2004) summarised the results of laboratory tests, field tests and numerical analyses performed on shallow footings and buried piles. They report a relatively wide range of α values varying from 0.13–0.21. However, there was no evidence that α varied with footing width or sand state.

Finite Element (FE) analyses present an ideal environment in which to consider the mechanisms governing footing response and to perform sensitivity analyses for foundations. Lee and Salgado (2005) reported a significant study using the FE program ABAQUS in which they investigated the effect of footing width and relative density (D_r) on the mobilised bearing resistance. The CPT q_c values used to normalise the footing resistance were derived from a different program CONPOINT (Salgado and Randolph, 2001). Their analyses shown in Figure 3 indicate that α decreased when the relative density of the soil increased and the footing width reduced. The rate at which α increased with the footing width depended on the relative density of the soil, with an increase of 35% being noted for D_r = 90% when the footing width increased from 1 m to 3 m, whilst the increase was only 5% for D_r = 30%.

The variability in suggested α values from previous studies arises at least in part due to the limited

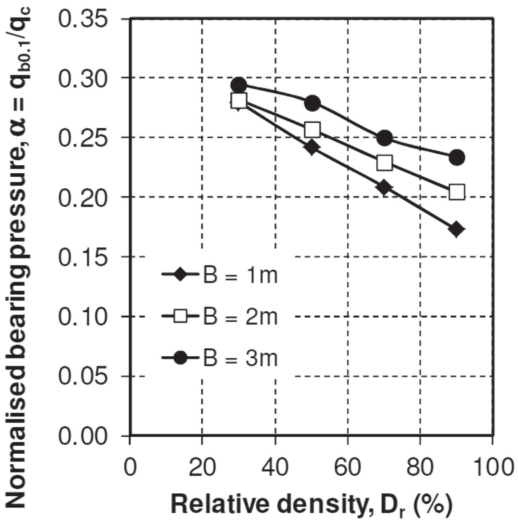

Figure 3. ormalized Base Resistance $q_{b0.1}$ /q_c versus Relative Density D_R; (after Lee and Salgado 2005).

database of footing tests from which to investigate factors which might influence the footing response. Large-scale footing tests are expensive and time consuming, and therefore, most field tests consider a relatively limited range of either footing width and/or depths in sand where the relative density is relatively constant. Gavin et al. (2009) compiled data from 22 field experiments on model and full-scale footings at five test sites. Data from the load tests performed by Briaud and Gibbens (1999) in Texas, Ismael (1985) in Kuwait, Anderson et al. (2007) at Green Cove, Gavin et al. (2009) from Blessington and Lehane et al. 2008, from Shenton Park were collated. The footing width varied from 0.1 m to 3 m, the q_c value (average over ± 1.5B) was in the range 3,330 to 14,500 kPa, and the foundation depth varied from 0.1 m to 2 m below ground level, bgl. The normalised pressure-settlement response is set out in Figure 4a.

Whilst many of the footing tests did not reach the normalised displacement level of 10%, the trend is for all sites to converge as s/B increases and tend towards α of approximately 0.2 at s/B = 10%. However, the initial stiffness response at the five sites varied considerably, and the data is recast in Figure 4b in order to examine the rate of mobilisation of the bearing resistance. The data confirms that the initial pressure-settlement response is site dependent, with a tendency for the normalised resistance to mobilise most quickly for the tests in Texas and most slowly at Shenton Park. Also included in Figure 4b are foundation settlement measurements from 23 buildings as collated by Papodopoulos (1992). The measurements relate

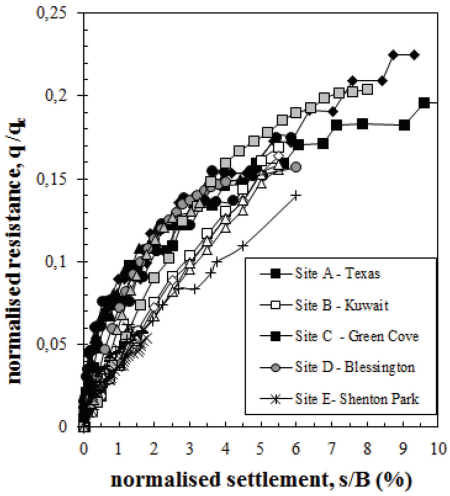

(a)

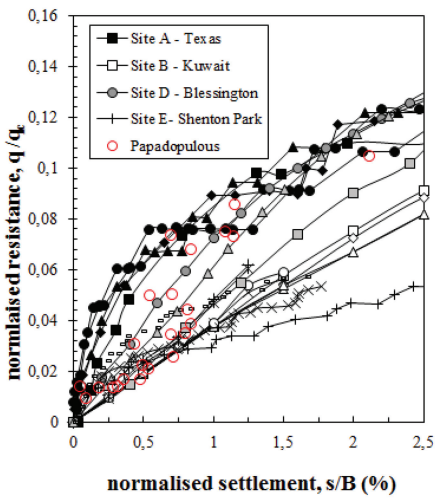

(b)

Figure 4. (a)Pressure settlement response from five test sites (b) Initial response of footing tests (after Gavin et al. 2009).

to foundations with B between 0.5 and 21.7 m, founded in sand where q_c ranged from 1800 to 19,000 kPa. Despite the range of parameters considered, the discrete measurements of maximum settlement are bounded by the experimental data presented in Figure 4b.

To gain further insight into the mobilisation rate, the rate of degradation of the secant stiffness measured at four sites where small strain stiffness data was available are compared in Figure 5. It is of interest to compare the normalised settlement level at which the secant stiffness reduces to 20% of the small strain Young's modulus ($E'_s/E_0 = 0.2$). This occurs at s/B = 0.2%, 1% and 10% at Shenton

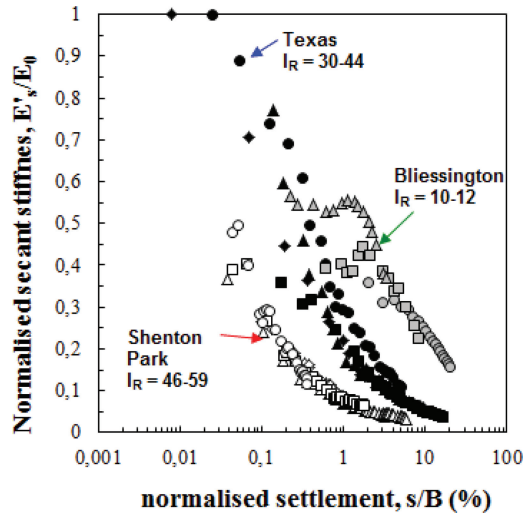

Figure 5. Variation of normalised secant stiffness with normalised settlement.

Park, Texas and Blessington respectively. The stiffness degradation rate appears to be related to the rigidity index, I_R (ratio of small strain shear modulus, G_0 to soil strength, q_c) with high I_R values resulting in rapid stiffness degradation.

The relatively low applied pressure imposed by most regular structures ensures that the factor of safety against ultimate failure of these foundations is high. As a result of this, the focus of designers is often to accurately predict settlement under working stresses. Settlement prediction models that require an estimate of the secant stiffness E'_s of sand are in common use. A number of direct correlations between E'_s and q_c have been proposed:

$$E'_s = \beta\, q_c \tag{3}$$

Das (1983) compiled β values recommended by 13 sources that ranged from 1 to 3. However, Lehane et al. (2008) and others state that at relatively small strain levels there is a weak dependence between E'_s and q_c, with the effects of stress level and ageing being dominant. Given that many foundations are designed for a maximum settlement often of the order of 25 mm, the resulting normalised settlement beneath foundations of width between 1 m and 10 m, results in s/B% in the range 0.25–2.5%. The variation of β values mobilised from the field tests described above, and shown in Figure 6, shows a very large range of operational β values at these normalised settlement levels, confirming that constant β values should be used with caution. It is worth noting that at the settlement levels typical for full-scale foundations, β values are typically higher than 3.

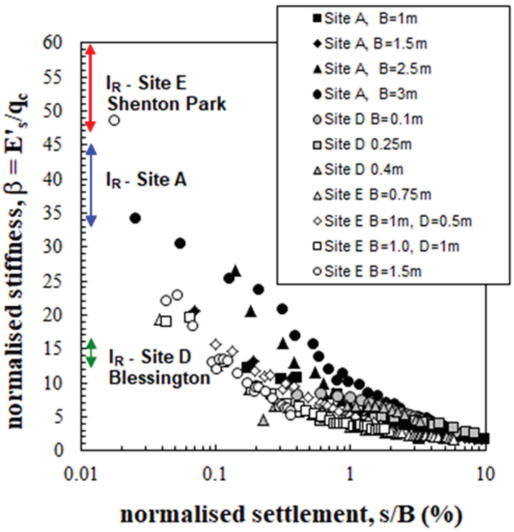

Figure 6. Variation of β (= E'_s/q_c) with normalised settlement.

2.3 *Summary*

Due to the difficulty of sampling and testing the strength and stiffness properties of sand, direct correlation between the ultimate bearing capacity and settlement response of footings on sand and in-situ testing such as CPT offers a viable alternative that appears to give consistent results.

Data from field tests presented by Gavin et al (2009) suggest that the normalised bearing pressure normalised by CPT q_c, mobilised at a footing settlement of 10% of the footing diameter, α is 0.2. This agrees reasonably well with the findings from a larger database study by Mayne et al. (2012) that considered a wider range of sand types and foundation size and concluded that a constant α value of 0.18 was appropriate. Both studies propose simple non-linear elastic models that allow the complete pressure-settlement response of the foundation to derived thus providing important insights into the operation behaviour of footings, and particularly the relatively large stiffness response at typical operation pressure levels.

3 BASE RESISTANCE OF PILES

3.1 *Background*

In many design guides and codes the end bearing resistance (q_b) mobilised by a deep footing in sand is calculated using a reduced form of Equation 1:

$$q_b = N_q \, \sigma'_v \tag{4}$$

Table 1. Recommendations for bearing capacity factors and limiting values for offshore piles (API 2007).

Density	N_q	q_b limit (MPa)
Loose	–	
Medium	20	5
Dense	40	10
Very Dense	50	12

where N_q is a bearing capacity factor and σ'_v is the vertical effective stress at the pile base. N_q factors typically vary with ϕ' or sand density as shown in Table 1. Another common feature is the adoption of limiting upper-bound values. Randolph and Gouvernec (2011) note that these limiting values are included as field data suggests that N_q reduces with increasing stress level.

The N_q values recommended for bored and cast in-place piles are typically assumed to be 50% of those derived for driven piles.

3.2 *Closed-ended driven piles*

Because of the similarities between the penetration mechanisms and the geometry of closed-ended piles and the CPT, a number of empirical correlations between the CPT end resistance q_c, and q_b have been proposed. Recent design methods for driven closed-ended or full-displacement piles in sand have been shown to have a relatively high reliability (Chow 1997, Gavin 1999 and Lehane et al. 2005) and have been widely accepted in industry. These techniques generally estimate the base resistance at relatively large pile base settlement (s_b), typically at 10% of the pile diameter, $q_{b0.1}$, using an empirical reduction factor α_p:

$$q_{b0.1} = \alpha_p \, q_c \tag{5}$$

Based on a database study Jardine et al. (2005) suggest that α_p reduced from 0.63 to 0.43 as the pile diameter increased from 200 mm to 500 mm, Lehane et al. (2005) found that an α_p value of 0.6 gave the best-fit to a database of instrumented pile load tests with diameters ranging from 0.2 m to 0.68 m. Randolph (2003) and White and Bolton (2005) argued that once appropriate averaging techniques were adopted to derive design q_c values and the effects of residual loads were accounted for, a constant α_p factor can be adopted which is independent of pile diameter and tended towards $q_b = q_c$ at large pile base displacements.

3.3 *Open-ended driven piles*

For partial displacement (open-ended) pipe piles, model and full-scale pile tests reported by Lehane

and Gavin (2001) and Foye et al. (2009) show that direct correlations between α_p (based on the average pressure mobilised over the entire pile base area) and q_c which are independent of pile diameter or sand state can be determined once the degree of plugging during pile installation are included. The plugging behaviour is best quantified through the incremental filling ratio (IFR), which compares the rate of soil intrusion during pile installation with IFR = 1 for a fully coring pile (which causes minimal disruption) and IFR = 0 for a pile with a fully formed plug, which prevents soil intrusion and results in what is effectively a closed-ended pile.

However, in reality, plug development during installation is rarely recorded and the final plug length ratio, PLR = soil plug length/pile embedment depth is only known. In the field, plugging appears to be controlled by pile diameter, sand density and installation method. The majority of large diameter (D >500 mm), piles driven offshore appears to have PLR values close to one. Significant plugging seems to occur only in the case of smaller diameter piles, or piles installed by jacking.

Gavin and Lehane (2005) present data shown in Figure 7 of plug stress mobilised during jacking strokes (closed-symbols) and static load tests (open-symbols) for pipe piles in jacked into loose sand. The normalised plug stress varies linearly with IFR from a minimum value in the range 0.15 to 0.2 that is in keeping with values suggested by Lehane and Randolph (2002) from numerical analyses of fully-coring piles. As IFR reduced, q_{plug}/q_c increased linearly. The trend was shown to be consistent over a range of installation methods (driving and jacking) and sand sate (Gavin and Lehane 2003).

Lehane and Gavin (2001) report measurements of the annular stress mobilised during installation

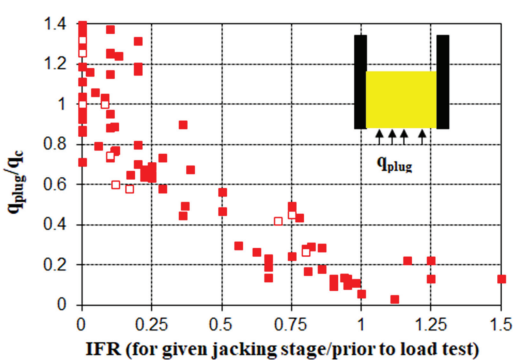

Figure 7. Effect of Incremental Filling Ratio on the plug stress mobilised by open-ended piles in sand (after Gavin and Lehane 2005).

of open-ended piles that were independent of IFR (with $q_{ann} = q_c$). Lehane et al. (2005) propose that the average base stress (combining the plug and annular components) mobilised for an open ended pile be calculated using Equation 6:

$$q_{b0.1} = 0.15 + 045\ A_{r,eff} \tag{6}$$

where $A_{r,eff} = 1 - FFR\ (D_i/D)^2$, and FFR is the IFR value at the end of driving.

Equation 6 suggests that α_p increases from ≈ 0.15 for a fully coring pile (IFR = 1) to 0.6 for a fully-plugged pile.

3.4 *Partial displacement screw injection piles*

Funderingstechnieken Verstraeten bv. performed three static compression load tests on screw injection piles installed in dense sand at a site in Terhausen, Netherlands. The piles which had shaft diameters of 0.46 m, base diameters of 0.56 m and embedded lengths of between 20.2 m and 20.3 m were instrumented with strain gauges along their length. The purpose of the test was to assess recent changes in pile capacity factors introduced in the Dutch standard NEN-EN 9997-1 introduced on January 1st 2017 that reduced the α_p values for all piles by 30%. The result was that for screw injection piles the value decreased from 0.9 to 0.63.

Estimates of the pile capacity at the test site were made using the pre-2017 design value and the piles were load tested to this capacity in an attempt to validate the old design approach. The CPT profiles at the test site are shown in Figure 8. The estimated pile capacity ranged from 5750 to 6100 kN. The load test on pile 1 was terminated an applied load of 5874 kN when the pile head settlement reached 23 mm (i.e. less than 5% of the pile diameter). The other piles were loaded up to failure at ultimate loads of 6096 kN (Pile 3) and 6312 kN (Pile 5) causing pile displacements of 60 mm.

The base pressure-settlement response of the piles is illustrated in Figure 9, showing that the initial stiffness response of the three piles was similar. Pile 1 mobilised the highest resistance, 13.7 MPa despite not reaching failure. Pile 3 mobilised an ultimate base resistance of 12 MPa and Pile 5 had the lowest resistance of 10 MPa.

The back-figured α_p value depends on the design average q_c value adopted. A comparison of values derived from the Dutch averaging method, where q_c is averaged over a distance -8B to + 4B and assuming q_c averaged over a distance ± 1.5B above the pile base are shown in Table 2. Adopting the Dutch averaging technique the measured α_p is 1.12, 80% higher than the current value (of 0.63). Using the ± 1.5B suggests that the ultimate end bearing resistance of these piles approximates q_c.

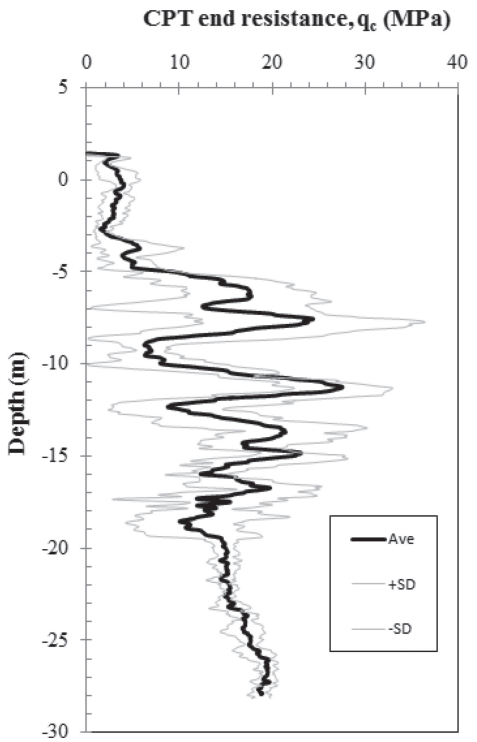

Figure 8. CPT profile at Terhausen test site.

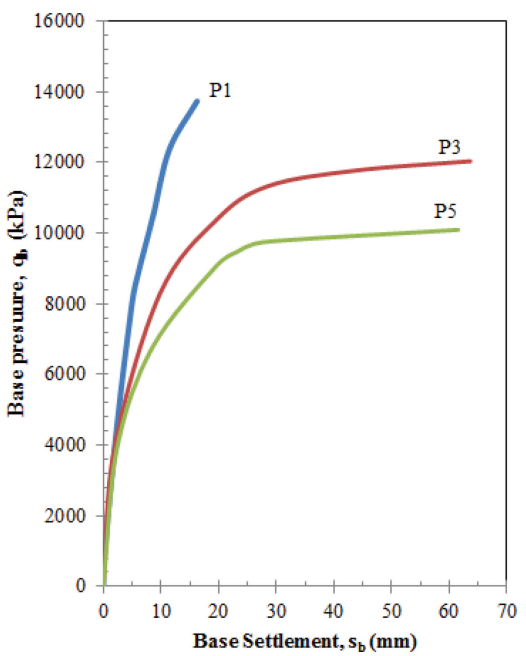

Figure 9. Base resistance mobilised by gout injection piles at Terhausen test site.

Table 2. Comparison of base capacity factors back-figured from Terhausen test site using different CPT averaging techniques.

Pile	q_c Dutch (MPa)	$\alpha_{p;Dutch}$	±1.5B	$\alpha_{p;Dutch}$
Pile 1	9.75	1.40	12	1.23
Pile 3	10.90	1.10	15	0.80
Pile 5	11.60	0.86	11.8	0.85
Average		1.12		0.96

3.5 *Bored piles*

The earliest correlation between the end bearing resistance of bored piles and q_c were suggested by (Meyerhof 1956; Meyerhof 1976; Meyerhof 1983). Based on theoretical and experimental studies on deep foundations, he introduced two reduction factors, C_1 for scale effects and C_2 to account for shallow penetration into dense strata to predict the ultimate end bearing resistance (q_{bu}) of a bored pile:

$$q_{bu} = 0.3\ q_c\ C_1\ C_2 \tag{7}$$

The LCPC or French method (Bustamante and Gianeselli 1982) was developed from a database of 197 pile tests on driven and bored piles in a range of soil conditions. An α_p value of 0.2 is recommended for bored piles in sand and gravel. The design q_c is the average from ±1.5*B* having excluded values that are in excess of ± 30% of the average. De Cock et al. (2003) compiled a review of pile design practice in Europe and found that α commonly ranged between 0.15 and 0.2, and typically did not depend on the diameter or the length of the pile. Eurocode 7, Part 2, suggests that α_p values, which although independent of footing width and depth, reduce from 0.2 for q_c values up to 15 MPa, to 0.16 for q_c = 20 MPa. Lehane (2008) reported a database study of Continuous Flight Auger (CFA) piles where the pile length varied from 4 m to 10.5 m. The database contained both straight and expanded base piles and recorded α_p values that increased from approximately 0.15 for 4 m long piles, to approximately 0.4 for a 10.5 m long pile.

Gavin et al. (2013) compiled a pile test database comprised of 20 static maintained load tests performed on non-displacement piles installed in sand where the piles were loaded to settlements in excess of 10% of the pile diameter. The diameter B of the piles ranged from 0.2 m to 1.5 m, while their length L ranged from 4 m to 26.5 m, with L/B in the range 4 to 37. They were founded in sand where the CPT end resistance, $q_{c1.5B}$ value ranged between 2 MPa and 40 MPa.

In the assessment of mobilised α_p values, the design $q_{c(1.5B)}$ was adopted. The variation of α_p with pile diameter, length, relative density and CPT q_c value is shown in Figure 10. Although there is considerable scatter in the results, there is no suggestion that α_p varied in a consistent manner with any of the parameters considered in the assessment, with an average α value for the database piles of 0.24.

Tolooiyan and Gavin (2013) performed finite element analysis using PLAXIS to investigate the factors affecting α_p for bored piles in sand. The sand was modelled using the Hardening Soil (HS) model described by Schanz et al. (1999) with the HS model parameters calibrated from lab-test data. Cavity expansion analyses were performed using a procedure described by Xu and Lehane (2008) and Tolooiyan and Gavin (2011) in order to predict the CPT q_c profile for Blessington sand. The FE generated values are compared in Figure 11 with a four typical q_c profile measured at Blessington. It is clear that the FE model provided a reasonably good albeit lower-bound estimate of the measured CPT q_c profile.

The effect of pile width, B on the bearing pressure mobilised by piles in Blessington sand was considered by analysing a pile of fixed length of 6 m with a diameter ranging from 0.2 m to 0.8 m. The piles were loaded until the settlement reached 10% of the pile diameter, see Figure 12a. The maximum end bearing resistance (≈5,500 kPa) of all piles was similar. However, the settlement required to achieve this resistance increased in proportion to the pile diameter. The normalised pressure-settlement response is shown in Figure 12b. This reveals that the normalised stiffness response for the piles was very similar, with $\alpha = 0.31$.

Considering the effect of pile length in Figure 13, a tendency for a slight reduction in α_p

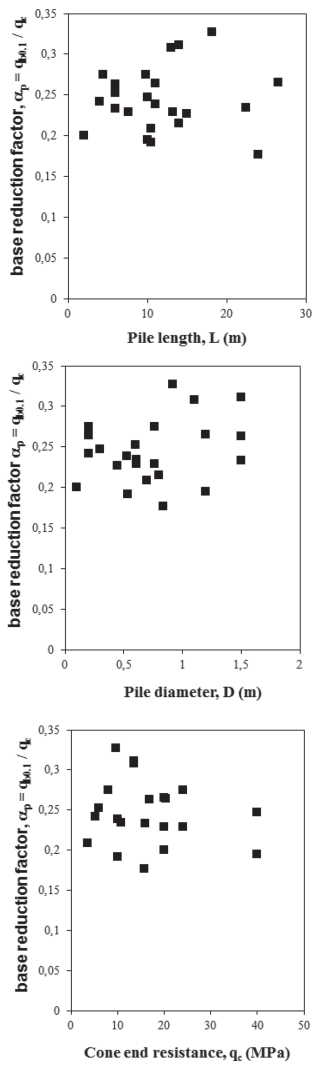

Figure 10. α_p values back-figured from load test database (a) effect of pile length, diameter, and strength.

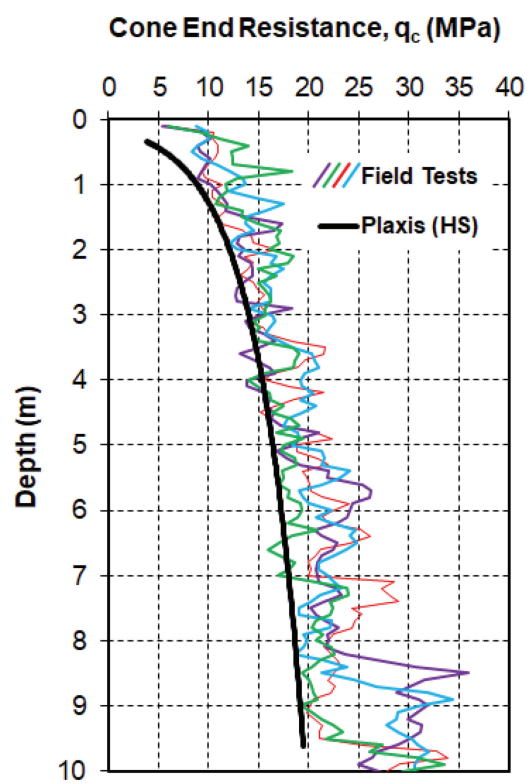

Figure 11. Measured and predicted CPT profile at Blessington.

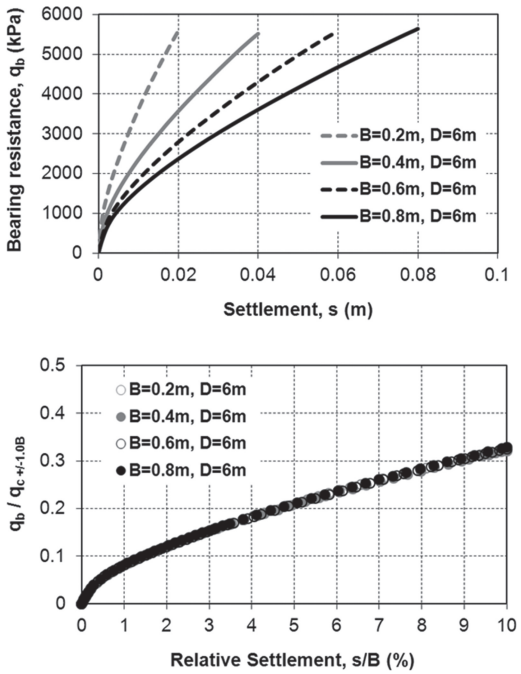

Figure 12. Bearing pressure mobilised by piles installed in Blessington (a) effect of pile width; (b) normalised pressure-settlement response.

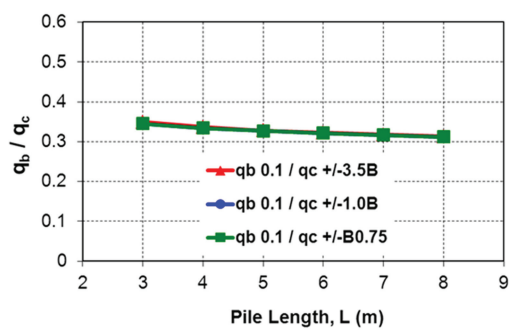

Figure 13. Effect of pile length L on normalised bearing pressure.

with depth is noted with the value decreasing from 0.34 to 0.31 as the pile length increased from 3 m to 8 m. The influence of CPT averaging technique (from ± 0.75B to ± 3.5B) technique is also considered. However, for Blessington sand the effect is negligible.

In order to investigate the effect of sand density on the mobilised α factor, sensitivity analyses were performed using three sand deposits. These were Tanta sand from Egypt which has an in-situ relative density D_r = 75% (reported by El Sawwaf (2005); El Sawwaf (2009)), Monterey sand from the United States with D_r = 65% (Wu et al. (2004) and Yang et al. (2008)), and Hokksund sand from Norway with D_r = 50% (Tefera et al. 2006). Synthetic CPT q_c profiles were derived for these deposits using the procedure as for Blessington sand. The predicted CPT q_c profiles are illustrated in Figure 14.

The sensitivity analyses were performed using a fixed pile diameter (B = 0.4 m) and a pile length which varied from 4 m to 8 m. The pressure-settlement values predicted are shown in Figure 15. The highest q_b values were measured in Tanta sand and the lowest were in Hokksund sand. The q_b values at all sites increased as the pile length increased from 4 m to 8 m. The increase was in the range 56% to 77%, with the highest increase being in Tanta sand.

When the bearing pressure mobilised at a pile base settlement of 10% was normalised by the CPT q_c value averaged over ± 1B, α_p values in the range 0.32 to 0.33 were determined. There were clear variations in the rate of mobilization at low settlement levels across the sites, with the normalised resistance developing more slowly as the relative density increased.

The influence of CPT averaging technique and pile length on α_p is considered in Figure 16. Consistent

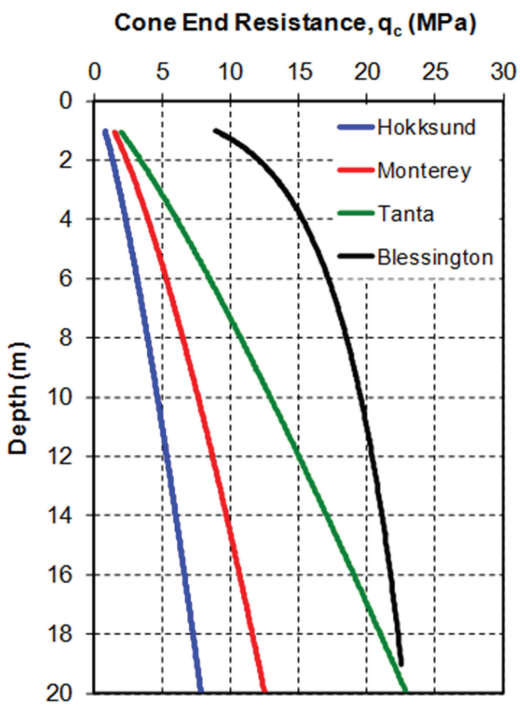

Figure 14. FE derived CPT q_c profile for Hokksund, Monterey and Tanta sand.

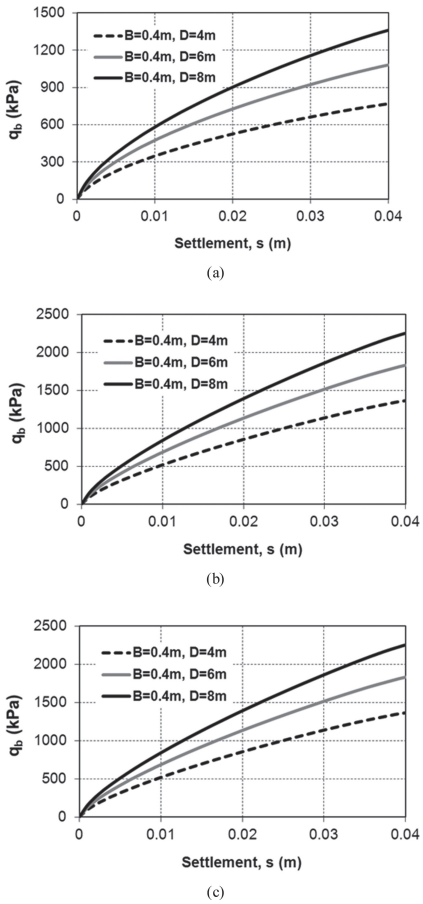

Figure 15. Pressure-settlement values predicted for: (a) Hokksund; (b) Monterey; (c) Tanta sand.

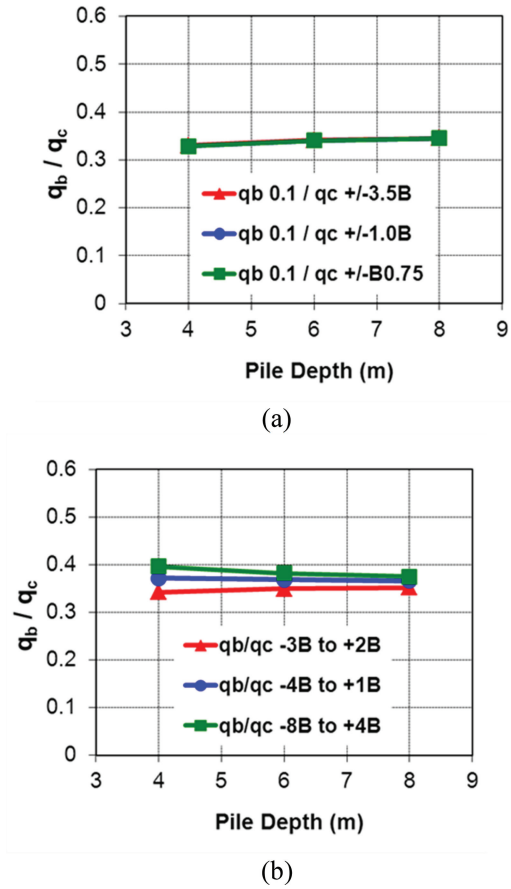

Figure 16. Effect of CPT averaging technique and pile length on α_p values in Hokksund Sand.

trends were found for all sites where α_p was reasonably constant when q_c was averaged over equal distances above and below the pile base, see Figure 16a. When q_c was averaged with a bias for values either above or below the pile base, See Figure 16b, higher variability and a more pronounced length bias was observed with the highest α_p values being inferred when using the Dutch average technique.

On the basis of these analyses, it appears that an approximate constant α_p factor of 0.3 would produce reasonable estimates of the end bearing resistance of bored piles in sand. This value is 50% higher than values typically used in practice and 20% higher than the α_p value of 0.24 inferred from the database study. To investigate one possible reason for the difference between the field response and FE analyses, it is of interest to consider the effect of loading rate on the mobilisation of α_p. Gavin et al. (2013) describe load tests performed on instrumented continuous flight auger piles installed in dense sand in Killarney, South-West Ireland. Load tests were performed on two piles, a 450 mm diameter, 15 m long pile and an 800 mm diameter, 14 m long pile. The load test procedure involved a maintained load test (MLT) followed by a fast-loading, constant rate of penetration (CRP) test. The results of the MLT portion of the load test are shown in Figure 17a where it is clearly evident that when the applied base pressure exceeded 1500 kPa, the piles experienced creep during load increments. When the normalised base displacement reached 10% of the pile diameter, the α_p factor approached 0.24.

When the piles were reloaded in the CRP test (See Figure 17b), significantly higher base resistance was mobilised. Whilst the loading history would affect the initial pressure-settlement response, the α_p factors mobilised in the fast loading tests (where

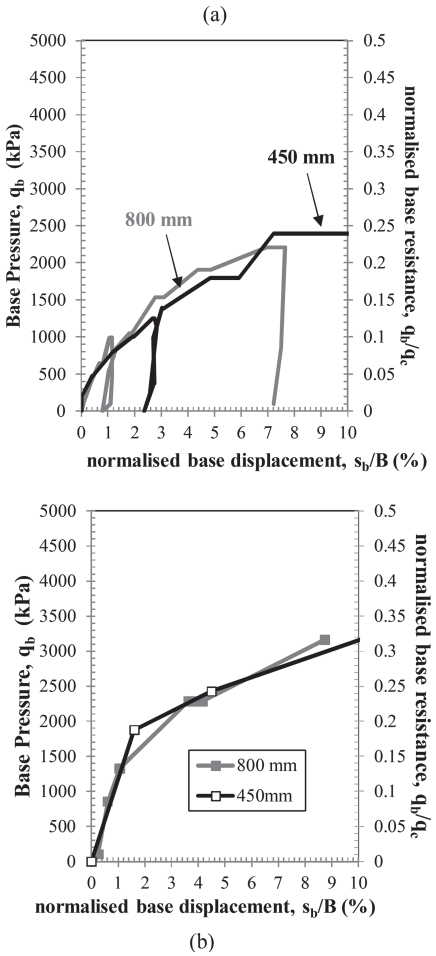

Figure 17. Effect of loading rate or test method on α_p mobilized by CFA piles in sand.

creep effects were minimised) exceeded 0.31. The soil models used in the numerical analyses did not model sand creep which clearly affected the MLT result and thus the mobilised base resistance.

4 SHAFT RESISTANCE OF PILES

4.1 *Background*

The peak unit shaft resistance (τ_f) mobilised by a pile in sand can be estimated using earth pressure theory as:

$$\tau_f = K\,\sigma'_v \tan\delta_f \tag{8}$$

where K is the earth pressure coefficient, σ'_v is the in-situ vertical effective stress, and δ_f is the soil-pile interface friction angle. As with all earth pressure approaches, the difficulty with the application of Equation 8 is in the choice of an appropriate K value for design. For bored piles, Reese and O'Neill (1999) suggest K/K_0 (where K_0, is the coefficient of earth pressure at rest), varies with the pile construction method, varying from 0.67 for a pile excavated using slurry, to 1.0 for a pile formed in a dry excavation. K_0 is notoriously difficult to measure, but may be estimated using the method proposed by Kulhawy and Mayne (1990):

$$K_0 = 1 - \sin\phi' \text{ – Normally Consolidated} \tag{9}$$
$$K_0 = (1 - \sin\phi')\,OCR^{\sin\phi'} \text{ – Over Consolidated}$$

where ϕ' is the friction angle and OCR is the Over-Consolidation Ratio.

For displacement piles, K will be changed during pile installation due to large stress changes as the pile base moves through the penetration depth and friction fatigue occurs during cyclic installation. Values in the range K = 1–2 are often used in practice. Due to uncertainties regarding input parameters such as ϕ', OCR and δ_f, and the effect of installation method, the use of CPT based design methods cone Penetration Test (CPT) are increasing:

$$\tau_f = \alpha_s\, q_c \tag{10}$$

A range of α_s values that depend on pile type are recommended in many design codes, with values typically being lowest for bored piles and highest for displacement piles. For example, in the Netherlands NEN 9997-1-2016 recommends α_s value that range from 0.06 for bored or driven open-tube piles, to 0.01 driven concrete or closed-ended steel tubes and up to a maximum of 0.014 for a driven cast-in-place piles. In Belgian practice, summarized by Huybrechts et al. (2016), α_s depends on q_c, pile type and roughness. A limiting maximum shaft resistance of 150 kPa is imposed for q_c values > 20 MPa.

Intensive research on displacement piles reported in Jardine et al. (2005) and Lehane et al. (2005) show that the local shaft resistance is given by:

$$\tau_f = (\sigma'_{hc} + \Delta\sigma'_{hd}) \tan\delta_f \tag{11}$$

where: σ'_{hc}, is the fully equalized horizontal effective stress after pile installation and $\Delta\sigma'_{hd}$ is a component derived by dilation during loading.

Chow (1997) examined profiles of σ'_{hc} recorded by an instrumented pile installed at two sites and found that σ'_{hc} values at a given location on the pile were almost directly proportional to the q_c value at that level and the distance from the level to the

pile base (h) normalised by the pile diameter (D). These findings were incorporated into the widely used design method for displacement piles known as the Imperial College (IC-05) design method (Jardine et al. 2005) and a similar approach known as the University of Western Australia (UWA) method (Lehane et al. 2005), where:

$$\sigma'_{hc} = 0.03\ q_c\ (h/D)^{-0.5} \tag{12}$$

A minimum h/D value of 2 should be used is Equation 12.

Equation 12 suggests that α_s is highest near the pile tip and reduces with increasing distance from the pile tip. Lehane (1992) suggests that the dilation induced increase in horizontal stress ($\Delta\sigma'_{hd}$) could be predicted using cavity expansion theory:

$$\Delta\sigma'_{hd} = \frac{4\,G\,\delta_h}{D} \tag{13}$$

where G is the shear modulus of the soil mass and δ_h is the horizontal displacement of a soil particle at the pile-soil interface.

The IC-05 and UWA design approaches have been shown to provide more reliable estimates of the shaft capacity of piles and accurate predictions of the distribution of mobilised local shear stress on closed-ended displacement piles by Chow (1997), Gavin (1998), Schneider (2007) and others. Given the prevalence of driven open-tube piles, particularly in the offshore sector, both the IC-05 and UWA methods allow for a reduction of shaft stress due to the lower displacement resulting from installation of these piles. Gavin et al. (2011) note that whilst the two approaches give very similar predictions for shaft capacity of closed-ended piles, differences in how they address the issue of plugging can result in significantly different estimates for open-ended piles.

4.2 *Driven cast-in-place piles*

Flynn and McCabe (2016) describe instrumented pile load tests performed on 3 driven cast-in-place piles installed at a site near Coventry, in the United Kingdom. The piles that were formed by driving a 0.32 m diameter hollow steel tube with a sacrificial circular steel plate at the base were instrumented with strain gauges at four levels. When they reached their final penetration depths of between 5.5 m and 7 m bgl. the steel tube was filled with concrete and the steel casing was withdrawn. The CPT profile at the site is shown in Figure 18. The ground conditions comprise made ground and stiff sandy clay to approximately 1.8 m bgl. underlain by medium dense to dense sand to a depth of ~ 6.5 m. Below this depth the sand becomes increasingly gravelly.

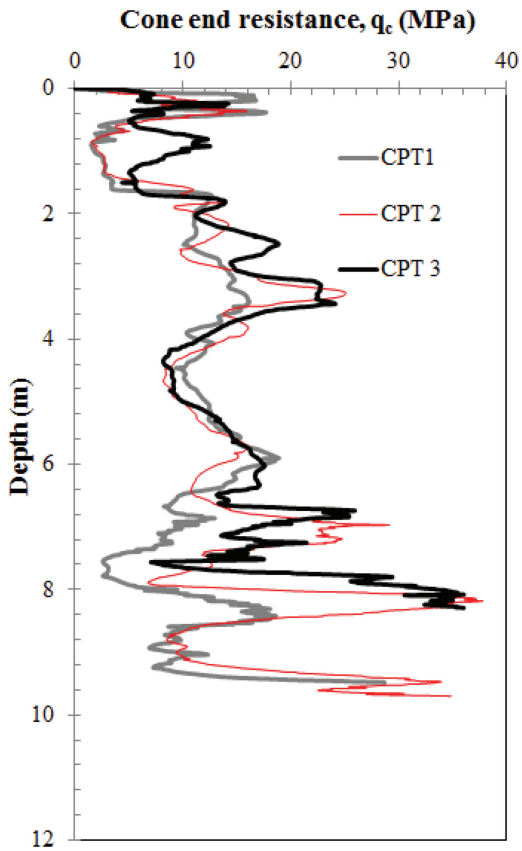

Figure 18. CPT profiles at Coventry.

The piles were load tested in compression between 19 and 23 days after installation.

The mobilisation of average shaft resistance (τ_{av} = total shaft resistance/shaft area) during the load tests is shown in Figure 19. The three piles exhibited similar initial stiffness response with peak α_s values in the range 0.094 to 0.14.

A noticeable feature of the response is that relatively large normalised dis-placement was required to mobilise the peak capacity (between 3% and 13% of the pile diameter) and in the case of Piles 1 and 3, the resistance was still increasing up to the end of the load test.

4.3 *Continuous Flight Auger (CFA) Piles*

Gavin et al. (2009) presents the results of instrumented load tests performed to study the development of shaft resistance on Continuous Flight Auger piles installed in sand. Ground conditions at the test site consist of approximately 2 m of mixed (sand, silt and clay) deposits overlying a deep deposit of sand. The CPT end resistance, q_c

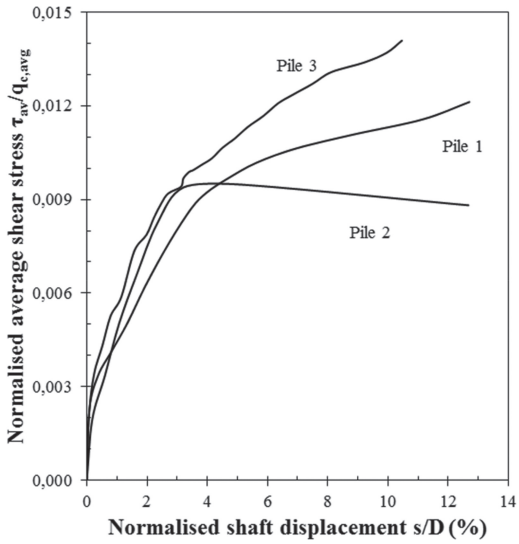

Figure 19. Normalised shaft resistance mobilised by driven cast-in-place piles (after Flynn and McCabe 2016).

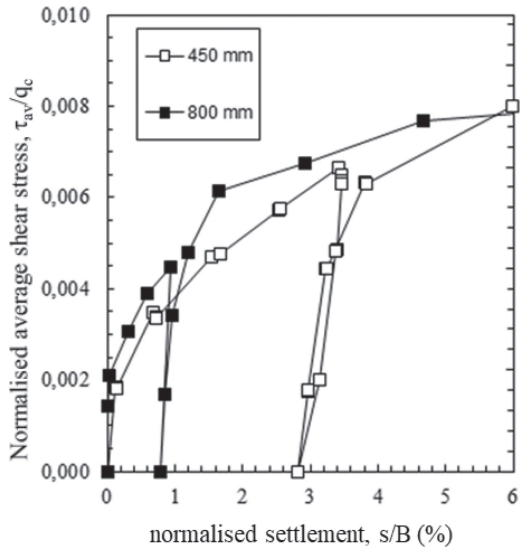

Figure 21. Normalised shaft resistance mobilised by Continuous Flight Auger Piles (after Gavin et al. 2013).

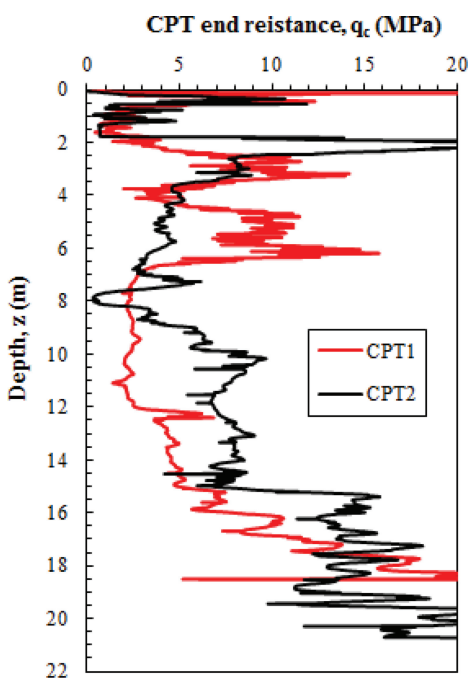

Figure 20. CPT profiles for CFA pile tests at Killarney (after Gavin et al. 2009).

measured in the vicinity of the test piles are shown in Figure 20.

Two instrumented test piles were installed at the site. The first pile was installed using an 800 mm diameter auger to 14 m bgl., and the second using a 450 mm auger to 15 m bgl. The piles were instrumented with strain gauges at four levels in order to separate base and shaft resistance components and to determine the distribution of shaft resistance along the pile.

Static load tests in compression were performed and the average shaft resistance (τ_{av}) mobilised during the static load tests of between 35 and 36 kPa was almost identical on both the 450 mm and 800 mm diameter piles suggesting that scale effects were insignificant. The resulting α_s (= τ_{av}/ q_{cav}) value of 0.008, shown in Figure 21 are similar to those used for the design of displacement piles in sand. The relatively large displacement required to mobilise the peak resistance is again a feature of the pile tests.

4.4 *Screw injection piles*

The average shaft resistance mobilised by the screw injection piles installed in dense sand at a site in Terhausen, Netherlands, described in Section 2.4 is shown in Figure 22a. The initial stiffness response of the piles which had shaft diameters of 0.46 m were remarkably similar. The load test on Pile 1 was stopped before it reached peak resistance as the pile mobilised a much higher base resistance than the other test piles, see Figure 9.

Notwithstanding this, it would seem that the ultimate shaft resistance of the piles was in the range 110 kPa to 130 kPa, However, displacements in excess of 10% of the pile shaft diam-

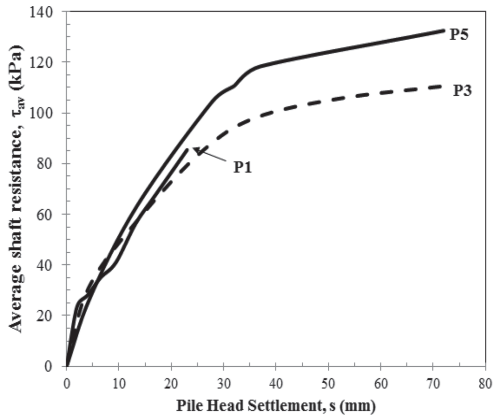

(a)

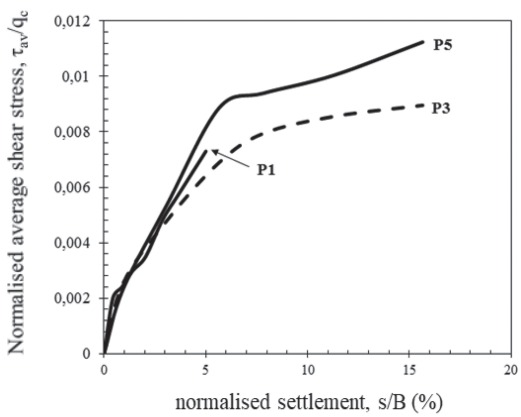

(b)

Figure 22. Shaft resistance (a) and normalised resistance mobilised (b) mobilised by Screw Injection Piles at Terhausen.

eter were required to mobilise this resistance. The back-figured α_s values shown in Figure 22b show that the Dutch standard NEN-EN 9997–1 recommended α_s value of 0.09 would provide a reasonable estimate of the fully mobilised shaft resistance for these piles.

4.5 *Distribution of normalised shaft resistance on piles in sand*

Whilst the α_s values mobilised by the test piles described above conformed broadly with the constant values proposed in many codes and seemed to depend on pile type, with higher values generally pertaining to driven piles, there remains some variation in α_s values proposed by different codes. Some insight into possible reasons for this can be determined by the instrumented load tests. The strain gauges on the piles allowed the local shear stress profiles to be determined.

The normalised local shear stress profile along the driven cast-in-place (DCIP) pile (Flynn and McCabe 2016) is compared in Figure 23 to the profile predicted using the UWA-05 approach with

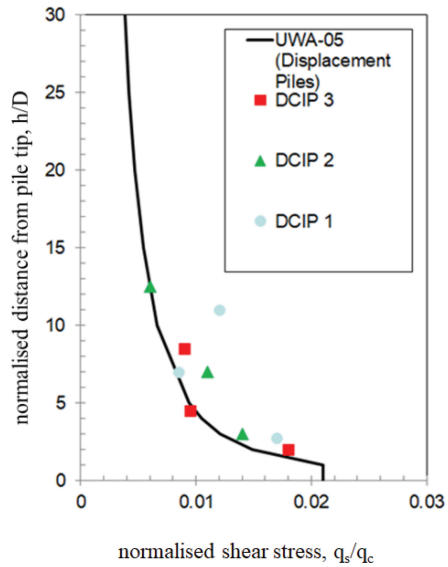

Figure 23. Comparison of distribution of shear stress on driven cast-in-place pile with prediction of UWA-05 method.

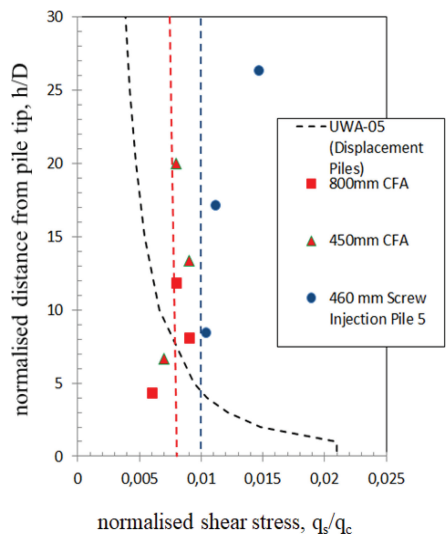

Figure 24. Comparison of distribution of normalised shear stress on CFA and Screw-Injection piles with prediction of UWA-05 method.

$\delta_f = \phi'_{cv}$). It is clear that a method which includes for the effects of friction fatigue provides a very good match to the measured response and suggests that for piles where friction fatigue occurs during installation that α_s should vary with pile geometry.

The normalised local shear stress values for the CFA piles and a typical screw injection pile are shown in Figure 24. For these piles that do not experience friction fatigue during installation, a constant α_s value is suitable to describe the shaft resistance. The value is lower than that applying to driven piles over a distance of 5D from the pile tip. Above this level the piles developed larger α_s values. Thus suggesting that non-displacement piles with deep embedment lengths could mobilise higher average α_s values than piles driven in the same deposit.

5 CONCLUSIONS

Whilst conventional earth pressure approaches remain in common use for the design of shallow and deep foundations in sand, researchers have highlighted a number of challenges related to the applicability of these methods. In all cases, obtaining high quality samples and determining operation frictional angles over the range of stress and strain relevant for design remains an issue. For over-consolidated deposits, accurately determining the earth pressure coefficient is essential and non-trivial. For shallow foundations, issues related to determining bearing capacity factors to address depth and width effects particularly for soil deposits where the strength does not increase linearly with depth have been highlighted. For pile design, the impact of installation effects; for example friction fatigue which causes complex changes to in-situ horizontal stress regime around a pile and plugging effects that results in large changes to the strength and stiffness of the sand below the pile base have been quantified in recent field tests.

Given that the CPT provides a continues indirect measurement of the strength and stiffness properties over the complete range of sand state, correlations between the cone end resistance q_c and foundation behaviour are in common use and have been embedded in the design codes in many countries. However, many of these codes give conflicting guidance on design. In this paper, results from lab and field experiments on instrumented piles and finite element analyses are used to explain the physical basis for the regional variations in CPT based approaches.

For the design of shallow foundations a number of workers have proposed α values that vary with sand state and footing dimensions. Field tests performed by Briaud (2007), Gavin et al. (2009), Mayne et al. (2012) and others suggest that unique site specific normalised resistance curves can be derived which are independent of footing geometry. A database of field tests collated in this paper suggests that at large normalised settlement levels (s/B = 5–10%), these normalised resistance curves converge and are independent of sand state. However, the initial stiffness response of the foundation is strongly dependent on the stress history and knowledge of both the strength (q_c) and small-strain stiffness parameters are crucial for design.

Considering the base resistance mobilised by piles in sand, the CPT q_c value appears to be an ideal design tool. Whilst at very large pile displacements the base resistance, q_b tends to the q_c value, see White and Bolton (2001) and Randolph (2005). The exact displacement required depends on the pile installation method and in some cases could be several pile diameters. At displacement levels typically considered in practice as representing failure, e.g. s/B = 10%, the stiffness response depends on the pile installation method. For low displacement pile types α_p (= $q_{b0.1}/q_c$) in the range of 0.15–0.2 are typically adopted in practice. For displacement piles, q_b/q_c of 0.6 is recommended for closed-ended driven steel and concrete piles. A particular feature of field tests on shallow foundations and bored pile (i.e. where pre-stressing during installation did not occur) was that significant creep occurred during maintained load tests at high stress levels. Numerical analyses of these piles using soil models that do consider creep, showed α_p values around 50% higher than those measured in maintained load tests. In quick load tests where creep was minimised, α_p values similar to those in the finite element model were mobilised. Based on these results, if effects such as loading rate, the definition of failure and residual loads are considered then higher α_p values can be adopted in design codes.

When considering shaft resistance, a number of codes suggest constant α_s (= τ_{av}/q_{cav}) values, with recommended values for displacement piles typically being higher than non-displacement piles. The case histories presented herein strongly suggest that α_s values for driven piles should incorporate a friction fatigue parameter. The absence of friction fatigue effects for non-displacement piles could result in some slender driven piles developing lower α_s than a non-displacement pile installed in the same soil deposit.

ACKNOWLEDGEMENTS

Much of the work presented in this paper was completed together with a number of former research students and collaborators who include: Prof. Barry Lahane, Dr. Ali Tolooiyan, David Cadogan,

Dr. Cormac Reale, Dr. Abidemi Adekunte and others.

The permission of Funderingstechnieken Verstraeten bv. to publish the pile load test data from Terhausen is gratefully acknowledged.

REFERENCES

Anderson, J.B, Townsend, F.C. and Rahelison, L. (2007) Load Testing and Settlement Prediction of Shallow Foundation Journal of Geotechnical and Geoenvironmental Engineering, Vol. 133, No. 12, pp 1494–1502.

API (2007) Recommended Practice for Planning, Designing and Constructing Fixed Offshore Platforms, 22nd edn. American Petroleum Institute, Washington, DC, USA, API RP2 A.

Briaud, J.L. (2007), 'Spread Footings in Sand: Load Settlement Curve Approach', *Journal of Geotechnical and Geoenvironmental Engineering, ASCE*, vol. 133, no. 8, pp. 905–920.

Briaud, J.L. & Gibbens, R. 1999. Behaviour of five large spread footings in sand. Journal of geotechnical and geoenvironmental engineering 125(9): 787–796.

Bustamante, M. & Gianeselli, L. (1982), 'Pile Bearing Capacity Predictions by Means of Static Penetrometer CPT', *Second European Symposium on Penetration Testing, ESOPT-II*, Amsterdam, The Netherlands, pp. 493–500.

Chow, F. (1997). "Investigations into the behavior of displacement piles for offshore structures." PhD Thesis, Uni-versity of London (Imperial College), London.

Das B.M. (1983) Advanced Soil Mechanics. McGraw-Hill, New York.

De Cock, F., Legrand, C. & Huybrechts, N. (2003), 'Overview of design methods of axially loaded piles in Europe', *8th European Conf. on Soil Mech. and Geotech. Eng. Report of ERTC3-Piles, ISSMGE Subcommittee*, Prague, pp. 663–715.

El Sawwaf, M. (2005), 'Strip footing behaviour on pile and sheet pile-stabilized sand slope', *Journal of Geotechnical and Geoenvironmental Engineering, ASCE*, vol. 131, no. 6, pp. 705–715.

El Sawwaf, M. (2009), 'Experimental and numerical study of eccentrically loaded strip footings resting on reinforced sand', *Journal of Geotechnical and Geoenvironmental Engineering, ASCE*, vol. 135, no. 10, pp. 1509–1518.

Eslaamizaad, S and Robertson,P.K. Cone penetration testing tests to evaluate bearing capacity of foundations in sands. Proceedings of the 49th Conference of the Canadian

Geotechnical Society, 1986, 429–438.

Foye, K.C., Abou-Jaoude, G., Prezzi, M., and Salgado, R. (2009). Resistance factors for use in load and resistance factor design of driven pipe piles in sands. Journal.of Geotechnical. Geoenvironmental. Eng., 135(1), 1–13.

Flynn, K.N. and McCabe, B.M. (2016), Shaft resistance of driven cast-in-situ piles in sand, Canadian Geotechnical Journal, Vol. 53, Issue 1, pp 49–59.

Gavin, K. (1999) Experimental investigation of open and closed ended piles in sand', [thesis], Trinity College (Dublin, Ireland). Department of Civil, Structural and Environ-mental Engineering, pp 369

Gavin, K., Adekunte, A. & O'Kelly, B. (2009), 'A field investigation of vertical footing response on sand', Proceedings of the Institution of Civil Engineers-Geotechnical Engineering, vol. 162, no. 5, pp. 257–267.

Gavin, K.G, and Lehane (2003), The Shaft capacity of pipe piles in sand The Shaft capacity of pipe piles in sand, Ca-nadian Geotechnical Journal, Vol. 40, No.1, pp36–45, (2003), doi:10.1139/t02–093

Gavin, K. & Lehane, B. (2005), Estimating the end bearing resistance of pipe piles in sand using the final filling ratio. Proceedings of the International Symposium on Frontiers in Offshore Geotechnics. ed. / M.J. Cassidy; S. Gourvenec. Vol. n/a Perth, Australia. ed. The Netherlands: CRC Press/Balkema, 2005. p. 717–723.

Gavin., K., Cadogan., D. and Casey., P (2009)The shaft capacity of CFA piles in Sand ASCE Journal of Geotech-nical and Geoenvironmental Engineering, Vol 135, Issue 6, pp 790–798.

Gavin., K., Cadogan., D., Casey., P. & Tolooiyan., A. (2013), 'The Base Resistance of Non-Dislacement Piles in Sand –: Field Tests', *ICE Journal of Geotechnical Engineering*, Vol. 166, 6, pp 540–548

Houlsby, G.T. and Cassidy, M.J.. A plasticity model for the behaviour of footings on sand under combined loading. Géotechnique, 2002, 52, No. 2, 117–129.

Huybrechts, N, De Vos, M, Bottiau, M. and Maertens, L. (2016) Design of piles—Belgian practice, ISSMGE-ETC3, International Symposium on Design of Piles in Europe, Leuven, Belgium, April eds De Vos et al.

Ismael N.F. Allowable pressure from loading tests on

Kuwaiti soils. Canadian Geotechnical Journal, 1985, 22, No. 2, 151–157.

Kulhawy, F.H., and Mayne, P.W. 1990. "Manual on estimating soil properties for foundation design." Rep. No. EL-6800, Electric Power Research Institute, Palo Alto, Calif.

Lee, J.H. & Salgado, R. (1999), 'Determination of pile base resistance in sands', *Journal of Geotechnical and Geoenvironmental Engineering, ASCE*, vol. 125, no. 8, pp. 673–683.

Lee, J.H. and Salgado, R. (2005). Estimation of Bearing Capacity of Circular Footings on Sands Based on Cone Penetration Test. Journal of Geotechnical and Geoenvironmental Engineering, Vol. 131, No. 4, April 2005, p. 442–452.

Lehane, B.M. (1992). "Experimental investigations of pile be-havior using instrumented field piles." PhD Thesis, Univer-sity of London (Imperial College), London.

Lehane, B.M. (2008), 'Relationships between axial capacity and CPT qc for bored piles in sand', *5th International Symposium on Deep Foundations on Bored and Auger Piles (BAP V)*, GHENT, BELGIUM, pp. 61–74.

Lehane, B.M and Gavin, K.G., (2001) Experimental inves-tigation of the factors affecting the base resistance of open-ended piles in sand. Journal of Geotechnical and Geoenviromental Engineering, ASCE Vol. 127, No. 6, June (2001). doi:10.1061/(ASCE)1090–0241(2001)127:6(473), p 473–480.

Lehane, B.M. and Randolph, M.F., (2002) Evaluation of a minimum base resistance for driven piles in siliceous

sand,. Journal of Geotechnical and Geoenviromental Engineering, ASCE Vol. 128, pp 198–205

Lehane, B.M., Doherty, J.P. & Schneider, J.A. (2008), 'Settlement prediction for footings on sand', *Deformational Characteristics of Geomaterials*, IOS Press/ Millpress, Rotterdam, pp. 133–150.

Lehane, B.M., Scheider, J.A. & Xu, X. (2005), *CPT based design of driven piles in sand for offshore structures*, University of Western Australia, Australia.

Mayne, P.W., Uzielli, M. and Illingworth, F. 2012. Shallow footing response on sands using a direct method based on cone penetration tests. Full Scale Testing and Foundation Design(Proceedings GSP 227 honoring Bengt Fellenius), ASCE, Reston, Virginia: 664–679.

Meyerhof, G.G. (1956), 'Penetration tests and bearing capacity of cohesionless soils', *Journal of the Soil Mechanics and Foundations Division*, vol. 82, no. SM1, pp. 1–19.

Meyerhof, G.G. (1976), 'Bearing Capacity and settlement of pile foundations', *Journal of the Geotechnical Engineering Division*, vol. 102, no. GT3, pp. 197–228.

Meyerhof, G.G. (1983), 'Scale effects of pile capacity', *Journal of Geotechnical Engineering*, vol. 108, no. GT3, pp. 195–228.

PLAXIS (2002), *Finite element code for plane strain and axi-symmetric modelling of soil and rock behaviour,* ed.^eds 8.2, Plaxis bv, The Netherlands.

Papadopoulus, B.P. (1992), Settlement of Shallow Foundations on Cohesionless Soils, ASCE Journal of geotechnical Engineering, Vol. 118, No.3 pp 377–393.

Randolph, M.F., Dolwin, J. & Beck, R. (1994), 'Design of drivenpiles in sand', *Geotechnique*, vol. 44, no. 3, pp. 427–448.

Randolph, M.F., and Gouvernec S. (2011) Offshore Geotechnical Engineering, Rouledge Publ.

Randolph, M.F., Janmiolkowski, M.B. and Zdravkovic L. (2004) Load carrying capacity of foundations. Proceedings of Advances in Geotechnical Engineering—The Skempton Conference, London, 1, 207–241.

Reese, L.C., O'Neill, M.W. and Touma, F.T. (1976) Behav-iour of drilled piers under axial loading, Journal of Ge-otechnical Engineering, ASCE, Vol 102, No.5: pp 493–51.

Salgado, R. & Randolph, M.F. (2001), 'Analysis of Cavity Expansion in Sand', *International Journal of Geomechanics*, vol. 1, no. 2, pp. 175–192.

Schanz, T., Vermeer, P.A. & Bonnier, P.G. (1999), 'The hardening soil model: formulation and verification', *Beyond 2000 in computational geotechnics: 10 years of PLAXIS International*, Rotterdam.

Schneider, J.A. (2007) Analysis of piezocone data for displacement pile design, PhD thesis, University of Western Australia

Tefera, T.H., Nordal, S., Grande, L., Sandven, R. & Emdal, A. (2006), 'Ground settlement and wall deformation from a large scale model test on a single strutted sheet pile wall in sand', *International Journal of Physical Modelling in Geotechnics*, vol. 6, no. 2, pp. 1–14.

Tolooiyan, A. & Gavin, K. (2011), 'Modelling the Cone Penetration Test in sand using Cavity Expansion and Arbitrary Lagrangian Eulerian Finite Element Methods', *Computers and Geotechnics*, vol. 38, no. 4, pp. 482–490.

Tolooiyan, A and Gavin, K.G, (2013) The base resistance of non-displacement piles in sand, Part II—Numerical Analyses, ICE Journal of Geotechnical Engineering, Vol 166, 6, pp 549–560.

White, D.J. & Bolton, M.D. (2005), 'Comparing CPT and pile base resistance in sand', *Geotechnical Engineering*, vol. 158, no. GE1, pp. 3–14.

Wu, J., Kammerer, A.M., Riemer, M.F., Seed, R.B. & Pestana, J.M. (2004), 'Laboratory Study of Liquefaction Triggering Criteria', *13th World Conference on Earthquake Engineering*, p. 14.

Xu, X. & Lehane, B.M. (2008), 'Pile and penetrometer end bearing resistance in two-layered soil profiles', *Geotechnique*, vol. 58, no. 3, pp. 187–197.

Yang, K.H., Zornberg, J.G. & Wright, S.G. (2008), *Numerical modeling of narrow MSE walls with extensible reinforcements*, Center for Transportation Research (CTR), Austin, Texas.

Taylor & Francis
Taylor & Francis Group
http://taylorandfrancis.com

CPT'18 papers

Taylor & Francis
Taylor & Francis Group
http://taylorandfrancis.com

Cone Penetration Testing 2018 – Hicks, Pisanò & Peuchen (Eds)
© 2018 Delft University of Technology, The Netherlands, ISBN 978-1-138-58449-5

Evaluating undrained rigidity index of clays from piezocone data

S.S. Agaiby & P.W. Mayne
Geosystems Group, Civil and Environmental Engineering, Georgia Institute of Technology, Atlanta, USA

ABSTRACT: A review on the evaluation of undrained rigidity index of clays ($I_R = G/s_u$) is presented, including laboratory testing, empirical correlations, and analytical methodologies. Using a hybrid spherical cavity expansion—critical state framework, an expression is derived for obtaining the operational rigidity index (I_R) directly from post-processing of CPTu data, specifically using the cone tip resistance and porewater pressure readings, or their normalized quantities. The evaluated rigidity indices are in reasonable agreement with reference laboratory tests and seismic-based in-situ approaches. The obtained values of I_R are used to calculate the yield stress (σ'_p) profiles using three separate expressions obtained from the SCE-CSSM framework, based on: (a) net cone resistance: $q_{net} = q_t - \sigma_{vo}$; (b) excess porewater pressure: $\Delta u = u_2 - u_o$; and effective cone resistance: $q_E = q_t - u_2$. The acquired value of I_R is also input into the cone bearing factor (N_{kt}) to obtain the undrained shear strength, where $s_u = q_{net}/N_{kt}$. Case studies are presented showing that the CPTu profiles of σ_p' and s_u generally agree with laboratory testing by one-dimensional consolidation and triaxial compression mode, respectively.

1 INTRODUCTION

The rigidity index (I_R) is an important input parameter for geotechnical applications involving bearing capacity, pile driving, porewater pressure generation, and piezodissipations. The value of soil rigidity index is incorporated in various theories and analytical solutions involving cavity expansion, strain path method, and finite element analyses. For piezocone penetration into clays, the magnitude of undrained rigidity index is often needed in the interpretation of coefficient of consolidation (c_{vh}) and its associated hydraulic conductivity (k).

Direct evaluation of rigidity index from its definition as the ratio of shear modulus (G) to shear strength ($I_R = G/s_u$) is quite elusive and difficult (Krage et al. 2014). The selection of the appropriate means to measure G and/or s_u is challenging and requires careful evaluation. In the simulation of the piezocone advancement into the ground, it is difficult to assign the predominant failure mode(s) that exist around the penetrometer. Hence, the selection of the correct shearing mode and testing technique is not straightforword. Keaveny (1985) and Schnaid et al. (1997) recommended the usage of CK_0UC triaxial compression test, while Konrad and Law (1987) promoted the pressuremeter test. Also, Teh and Houlsby (1991) and Yu and Mitchell (1998) deemed the triaxial compression mode as the most appropriate.

A more difficult issue lies in the selection of the correct shear modulus as its magnitude depends on the level of shear strain. The initial shear modulus ($G_0 = G_{max}$) represents the tangent modulus at very small strains, but this applies to the nondestructive region. A secant modulus ($G = \tau/\gamma_s$) represents higher strain levels with G reducing with strains (Mayne, 2007). As a compromise, Konrad & Law (1987) and Schnaid et al. (1997) chose to use a shear modulus at 50% mobilized strength (G_{50}) to give an average response.

It is evident that there are difficulties in properly selecting strength mode and mobilization level of shear modulus values using laboratory-based techniques. These are affected by issues related to sample disturbance, stress relief and high costs of obtaining and testing quality samples. Therefore, it is of great interest and benefit to develop methods of obtaining the rigidity index based on direct CPT measurements.

2 EXISTING METHODS FOR ESTIMATING UNDRAINED RIGIDITY INDEX

Keaveny and Mitchell (1986) proposed an empirical approach relating the rigidity index to the overconsolidation ratio (OCR) and clay plasticity index (PI). The methodology was based on results from triaxial CAUC test data on various clays where the

I_R was defined using $G_{50} = E_{50}/3$. The developed correlation can be expressed as:

$$I_{R50} \approx \frac{\exp\left(\frac{137 - PI}{23}\right)}{1 + \ln\left[1 + \frac{(OCR-1)^{3.2}}{26}\right]^{0.8}} \quad [1]$$

Another means to estimate the rigidity index is via original Cam Clay derivation which was obtained by Kulhawy and Mayne (1990) based on routine soil parameters. An initial modulus was evaluated by differentiation as the strain approaches zero, then using this modulus value in a normalized form to evaluate undrained rigidity index as given by the following expression:

$$I_R = \left(\frac{2}{3}\right) \cdot M \left(\frac{1+e_0}{C_c}\right) \cdot \ln(10) \frac{[1+\ln(OCR)]\exp(\Lambda)}{\Lambda(1-\Lambda)OCR^{\Lambda}} \quad [2]$$

where $M = (6 \sin\phi')/(3-\sin\phi')$ = slope of the frictional envelope for triaxial compression in $q - p'$ space, $\Lambda = (1 - C_s/C_c)$ = plastic volumetric strain potential, C_s = swelling index, C_c = virgin compression index, e_0 is the initial void ratio, and $OCR = \sigma'_p/\sigma'_{vo}$. Typically, the value of $\Lambda \approx 0.8$ from load-unload-shear lab testing, although $\Lambda \approx 1$ in many natural clays tested in recompression, especially at low OCRs (Ladd 1991).

Mayne (2001) developed an expression for estimating the rigidity index based on CPTu data in clays from the hybrid spherical cavity expansion—critical state framework (SCE-CSSM). The I_R expression was given by:

$$I_R = \exp\cdot\left[\frac{(q_t - \sigma_{vo})}{(q_t - u_2)} \cdot \left(\frac{1.5}{M} + 2.925\right) - 2.925\right] \quad [3]$$

However, as the values of net cone resistance and effective cone resistance are close, a line-by-line evaluation of data showed that the assessed I_R profile was highly variable with depth.

A recent empirical approach introduced by Krage et al. (2014) using the shear wave velocity profile and net cone tip resistance from SCPTu has been developed to evaluate I_R at 50% strain level and can be determined from:

$$(I_R)_{50} = \left[\frac{1.81 \cdot G_0}{(q_{net})^{0.75}(\sigma'_{vo})^{0.25}}\right] \quad [4]$$

With consistent units used for G_0, q_{net}, and σ_{vo}' terms.

Mayne (2016) developed an expression for rigidity index of clays from spherical cavity expansion theory which is dependent on the CPTu normalized porewater pressure parameter (B_q). The I_R expression is given by:

$$I_R = \exp\left[\frac{2.93 \cdot B_q}{(1 - B_q)}\right] \quad [5]$$

where $B_q = (u_2 - u_0)/(q_t - \sigma_{vo})$. Obtained I_R values can be restricted to the narrow range: $0.50 < B_q < 0.70$.

3 DIRECT CPTU SOLUTION FOR EVALUATING UNDRAINED RIGIDITY INDEX

3.1 *Original SCE-CSSM solution*

A hybrid formulation of spherical cavity expansion and critical state soil mechanics (SCE-CSSM) expresses the cone tip resistance (q_t) and porewater pressure (u_2) using closed-form equations, given by (Mayne 1991; Chen & Mayne 1994; Mayne 2007a):

$$q_t = \sigma_{vo} + [(4/3) \cdot (\ln I_R + 1) + \pi/2 + 1] \cdot (M/2) \cdot (OCR/2)^{\Lambda} \cdot \sigma'_{vo} \quad [6]$$

$$u_2 = u_o + [(2/3) \cdot (\ln I_R) \cdot (M) \cdot (OCR/2)^{\Lambda} \cdot \sigma'_{vo}] + [1 - (OCR/2)^{\Lambda}] \cdot \sigma'_{vo} \quad [7]$$

The hybrid SCE-CSSM model can be rearranged to express overconsolidation ratio (OCR) of the clay in three separate formulations using net cone resistance ($q_{net} = q_t - \sigma_{vo}$), excess pore pressure ($\Delta u = u_2 - u_0$), and effective cone resistance ($q_{eff} = q_t - u_2$):

$$OCR = 2 \cdot \left[\frac{(2/M) \cdot (q_t - \sigma_{vo}) / \sigma'_{vo}}{(4/3) \cdot (\ln I_R + 1) + \pi/2 + 1}\right]^{(1/\Lambda)} \quad [8]$$

$$OCR = 2 \cdot \left[\frac{(\Delta u / \sigma'_{vo}) - 1}{(2/3) \cdot M \cdot \ln(I_R) - 1}\right]^{(1/\Lambda)} \quad [9]$$

$$OCR = 2 \cdot \left[\frac{1}{1.95 \cdot M + 1}\left(\frac{q_t - u_2}{\sigma'_{vo}}\right)\right]^{(1/\Lambda)} \quad [10]$$

Combining equations [8] and [9], the value of the rigidity index can be obtained in terms of normalized CPTu measurements and friction parameter M:

$$I_R = \exp\cdot\left[\frac{1.5 \cdot Q + 2.925M \cdot (U^* - 1)}{Q \cdot M - M \cdot (U^* - 1)}\right] \quad [11a]$$

$$I_R = \exp\cdot\left[\frac{1.5 + 2.925M \cdot \left(\frac{U^* - 1}{Q}\right)}{M - M \cdot \left(\frac{U^* - 1}{Q}\right)}\right] \qquad [11b]$$

where Q = normalized tip resistance = $(q_t - \sigma_{vo})/\sigma'_{vo}$; U* = normalized porewater pressure = $(u_2 - u_o)/\sigma'_{vo}$.

Since the expression for I_R is an exponential form, the use of [11] in a line-by-line post-processing of CPTu data unfortunately results in highly variable profiles with depth, therefore a moving average is necessary for any practical use.

A stable representation for [11] is obtained in the following format:

$$I_R = \exp\cdot\left(\frac{1.5 + 2.925 \cdot M \cdot a_q}{M \cdot (1 - a_q)}\right) \qquad [12]$$

where $a_q = (U^* - 1)/Q = (u_2 - \sigma_{vo})/(q_t - \sigma_{vo})$. Hence, a_q can be determined as a single value for any clay deposit by taking the slope of a plot of the parameter (U* – 1) versus Q, or alternatively taken as the slope of $(u_2 - \sigma_{vo})$ versus $(q_t - \sigma_{vo})$. Using regression analyses, slightly different slope values for a_q are obtained.

3.2 *Effective friction angle evaluation*

The derived expression for rigidity index depends on the value of the effective friction angle (ϕ'). In the event that laboratory-measured values from triaxial tests are not available, the effective friction angle can be evaluated using the NTH method. This is an effective stress limit plasticity solution for undrained penetration developed by Senneset et al. (1989). In this method, a cone resistance number (N_m) is defined:

$$N_m = \frac{N_q - 1}{1 + N_u \cdot B_q} = \frac{q_t - \sigma_{v0}}{\sigma'_{vo} + a'} \qquad [13]$$

where $a' = c'\cot\phi'$ = attraction, c' = effective cohesion intercept, $N_q = K_p \cdot \exp[(\pi - 2\beta)\cdot\tan\phi']$ is the end-bearing factor for the cone tip resistance (q_t), $K_p = (1+\sin\phi')/(1-\sin\phi')$ is the passive stress coefficient, β = angle of plastification ($-20° < \beta < +20°$) which defines the size of the failure zone beneath the tip, and $N_u = 6 \cdot \tan\phi' \cdot (1 + \tan\phi')$ is the porewater pressure bearing factor. The full solution allows for an interpretation of a paired set of Mohr-Coulomb strength parameters (c' and ϕ') for all soil types.

For soft to firm clays, it can be adopted that $c' = 0$, thus the term N_m reduces to the well-known normalized cone resistance, $Q = q_{net}/\sigma'_{vo}$. Further simplification is achieved by taking the angle $\beta = 0$ (Terzaghi equation) for the case of undrained loading at constant volume and an approximate deterministic expression given by (Mayne 2007b):

$$\phi' = 29.5° \cdot B_q^{0.121}[0.256 + 0.336 \cdot B_q + \log Q] \qquad [14]$$

which is valid for the following parameter ranges: $20° \le \phi' \le 45°$ and $0.1 \le B_q \le 1.0$.

3.3 *Undrained shear strength evaluation*

The operational value of rigidity index I_R can be used directly to evaluate the profile of undrained shear strength of the clay with depth since it gives the cone bearing factor (N_{kt}). The strength is obtained from:

$$s_{uc} = \frac{q_{net}}{N_{kt}} \qquad [15]$$

where spherical cavity expansion theory expresses the N_{kt} in terms of the rigidity index (Vesić 1977):

$$N_{kt} = [(4/3) \cdot (\ln I_R + 1) + \pi/2 + 1] \qquad [16]$$

Notably, the same input parameters (M and I_R) can be used in [8], [9], and [10] to obtain 3 independent profiles of OCR in the clay, adopting $\Lambda = 1$.

4 CASE STUDIES VALIDATING THE I_R EVALUATION

4.1 *Ariake, Japan*

Ariake is a normally consolidated soft marine deposit located in Kyushu Island, Japan with OCR values ranging from 1.24 to 1.55 (Tanaka et al., 2001). The Ariake deposit is classified as a highly plastic clay with average water content ranging from 100 to 150% and liquid limit between 110–120%. Figure 1 presents a representative

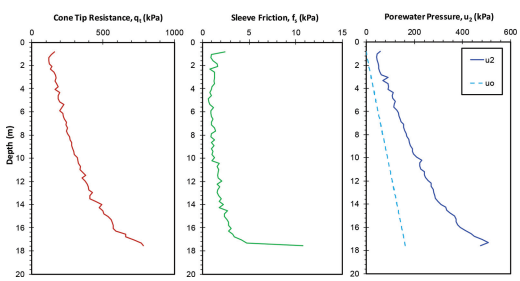

Figure 1. Piezocone sounding at Ariake: (a) cone tip resistance; (b) sleeve friction; (c) porewater pressure. (Tanaka et al., 2001).

piezocone sounding conducted by Tanaka et al. (2001). Based on the piezocone data, an effective friction angle was evaluated using the NTH method and the site has a characteristic effective friction angle $\phi' = 32.2°$, or $M = 1.2$.

Figure 2 shows the evaluation of the slope parameter a_q used in the derived I_R solution where $(u_2 - \sigma_{vo})$ is plotted versus net cone tip resistance (q_{net}), giving a parametric value $a_q = 0.455$. The slope value is used with the effective friction angle in [12] to give an operational rigidity index $I_R = 97$.

The obtained I_R value is used to evaluate the cone bearing factor (N_{kt}) per equation [16] for evaluating the undrained shear strength (s_u). The value $I_R = 97$ gives a corresponding $N_{kt} = 10$ which provides an excellent agreement with the CAUC undrained shear strength data reported by Lunne et al. (2006) for the Ariake site, as presented in Figure 3.

Applying equations [8], [9], and [10] of the hybrid SCE-CSSM solution to the CPTu results ($I_R = 97$, $\phi' = 32.2°$, $\Lambda = 1$), three assessments of stress history show consistent results, as seen in Figure 4. Overall, good agreement is observed when compared with laboratory measured σ_p' and OCR profiles reported by Tanaka et al. (2001) and Lunne et al. (2006).

4.2 *Sandpoint, Idaho*

A new bridge and approach embankments were constructed as part of a realignment project for US State Highway 95 near Sandpoint, Idaho. The soils at the site consist of post-glacial alluvial deposits includingsoft silty clays with interbedded sand layers to depths exceeding 80 m (Altaee and Fellenius, 2002). The clay at Sandpoint has the following

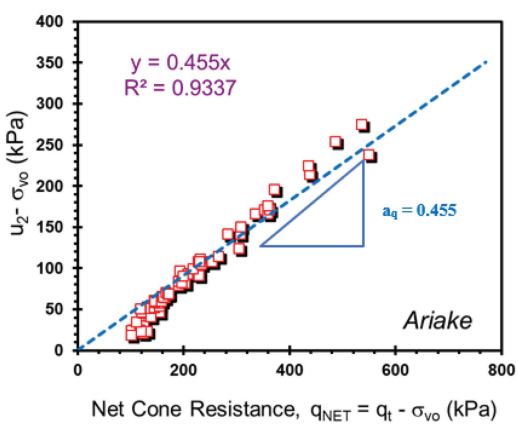

Figure 2. Evaluation of slope parameter for proposed I_R solution f [$(u_2-\sigma_{vo}) / q_{net}$] using CPTu data from Ariake, Japan.

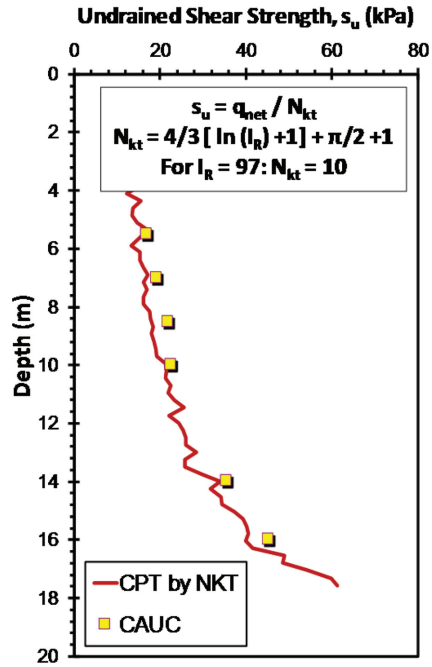

Figure 3. Undrained shear strength profile for Ariake, Japan using the SCE-CSSM operational rigidity index value for cone bearing factor N_{kt} (data from Lunne et al., 2006).

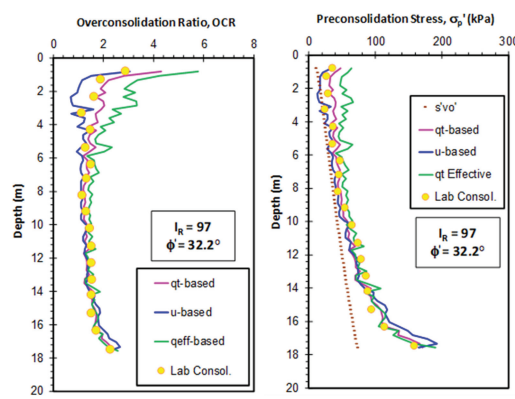

Figure 4. OCR and preconsolidation stress profiles using the SCE-CSSM framework for Ariake, Japan (data from Tanaka et al. 2001; Lunne et al. 2006).

characteristics and index values: liquid limit = 45.2 ± 6.3%, plasticity index = 19.9 ± 4.7%, and natural water content = 45.2 ± 6.4%. Figure 5 presents a deep seismic piezocone sounding (SCPTu) extending to depths of 80 m where the downhole shear wave velocity portion extends to 60 m (Mayne 2005). An average effective friction angle $\phi' = 32°$ is

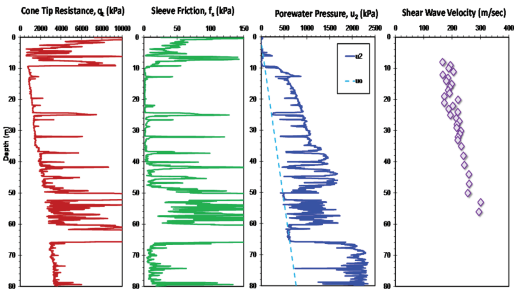

Figure 5. Seismic piezocone sounding at Sandpoint, Idaho (a) cone tip resistance, q_t; (b) sleeve friction, f_s; (c) porewater pressure, u_2; and (d) shear wave velocity, V_s (Mayne, 2005).

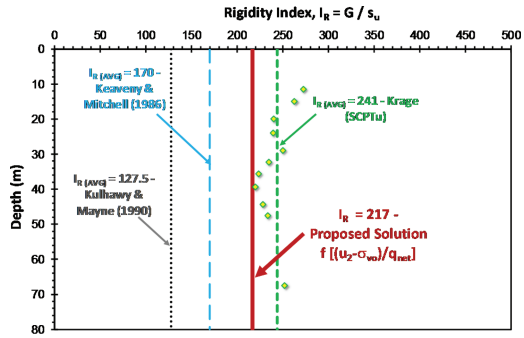

Figure 6. Comparison between different approaches for estimating rigidity index value for Sandpoint, Idaho test site.

evaluated using NTH method that compares well with CIUC triaxial tests ($\phi' = 33°$) made on undisturbed samples (Mayne 2014).

The predominant silty clay has a representative overconsolidation ratio (OCR) = 1.5 and plasticity index (PI) value of 20%. These values are used as input in the empirical equation [1] given by Keaveny and Mitchell (1986) to give an average $I_R = 170$. The same friction angle (ϕ') and OCR values are applied into equation [2] by Kulhawy and Mayne (1990) in addition to C_c value of 0.60, $\Lambda = 0.85$ and initial void ratio of 1.12 to give an average $I_R = 127.5$. The profile of the shear wave velocity is used to evaluate the small strain shear modulus (G_0) which is used in Krage et al (2014) seismic procedure presented in equation [4] along with the cone tip readings to give an average rigidity index value of $I_R = 244$.

For Sandpoint, the plot of (u_2-σ_{vo}) versus net cone tip resistance (q_{net}) determines a slope value $a_q = 0.507$. Together with the characteristic friction parameter M = 1.2, an operational rigidity index $I_R = 217$ is obtained for Sandpoint.

Figure 6 presents a comparison between the values of rigidity index obtained using four different expressions: three methods from the literature in addition to the proposed derived expression based on hybrid SCE-CSSM framework.

It is clear that the presented new solution gives rigidity index value that is reasonable, comparable and within the same order of magnitude of other expressions from the literature.

The evaluated I_R value of 217 gives $N_{kt} = 11.1$ that provides a CPTu profile of s_u in excellent agreement with the laboratory measured values from triaxial compression tests at the site, as presented in Figure 7.

Using the hybrid SCE-CSSM equations with derived parameter ($I_R = 217$ and $\phi' = 32°$), three evaluations of stress history with depth are presented in Figure 8. In the clay layers from 10 to

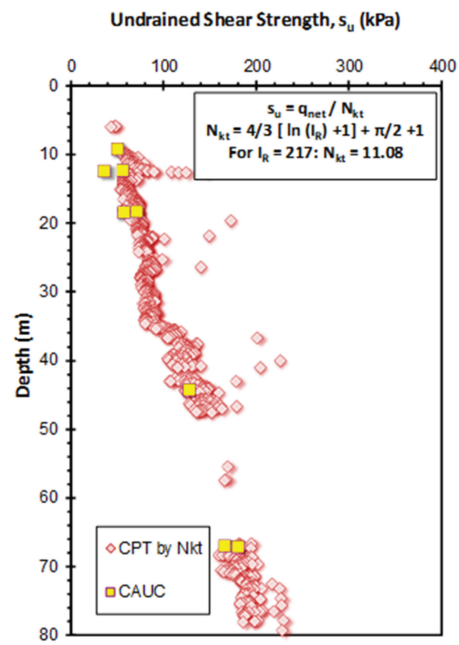

Figure 7. Undrained shear strength profile for Sandpoint, Idaho using SCE-CSSM solution and cone bearing factor N_{kt} (data from Dean Harris, 2004, personal comm.).

48 m and 66 to 80 m depth ranges, these generally agree well and compare favorably with σ_p' and OCRs obtained from one-dimensional consolidation testing.

4.3 *Ballina, Australia*

Ballina is a soft estuarine clay located in northern New South Wales in Australia. The clay has high plasticity with plasticity index value ranging 80%

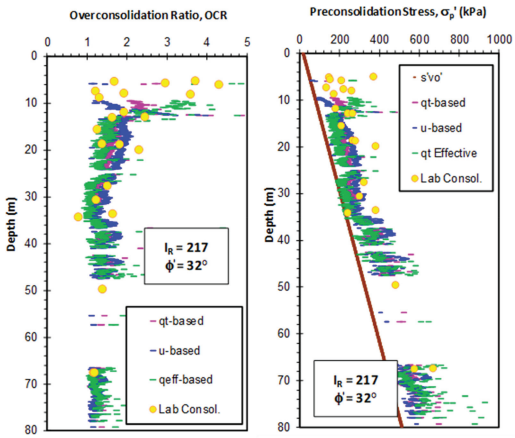

Figure 8. OCR and preconsolidation stress profiles using SCE—CSSM solution at Sandpoint, Idaho (data from Altaee and Fellenius, 2002).

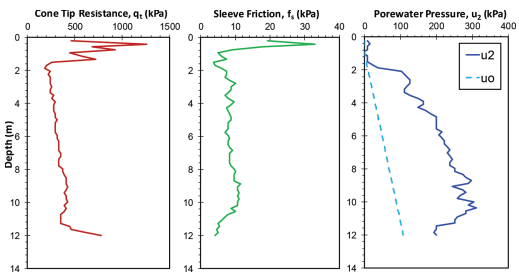

Figure 9. CPTu sounding in soft clay at Ballina, Australia: (a) cone tip resistance; (b) sleeve friction; (c) porewater pressure (data from Pineda et al. 2014).

and liquid limit value ranging 130% and water content ranging 100% (Pineda et al. 2016). The clay is characterized by its high compressibility and low undrained shear strength as measured in triaxial compression tests. Figure 9 presents the readings of a piezocone sounding conducted by Pineda et al. (2014). A characteristic effective friction angle $\phi' = 33.7°$ is evaluated the NTH method and piezocone data from the site.

By plotting (u_2-σ_{vo}) versus net cone tip resistance (q_{net}) for Ballina soft clay, a slope value of $a_q = 0.50$ is obtained. This determines an operational rigidity index $I_R = 168$. The obtained I_R value corresponds to a cone bearing factor $N_{kt} = 10.74$ that provides nice agreement with CAUC laboratory-measured s_u reference values and field vane s_u values at the site, as evident in Figure 10.

Applying the SCE-CSSM equations with $I_R = 168$ and $\phi' = 33.7°$ ($\Lambda = 1$), the three CPTu profiles give good agreement with each other at depths below 2 m, as presented in Figure 11. Very

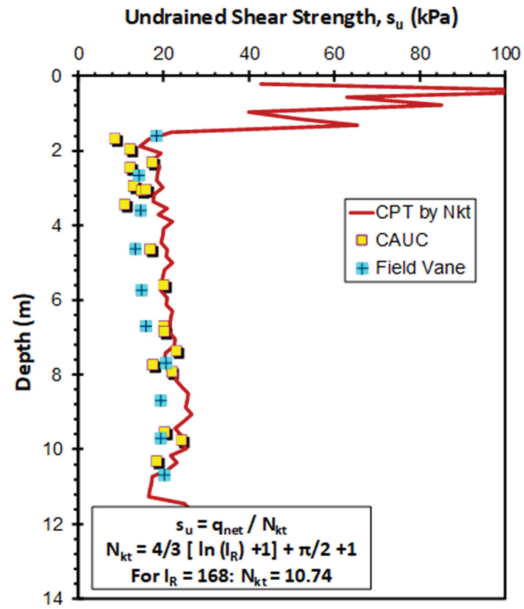

Figure 10. Undrained shear strength profile for Ballina, Australia using the SCE-CSSM operational rigidity index value and cone bearing factor N_{kt} (data from Pineda et al. 2016).

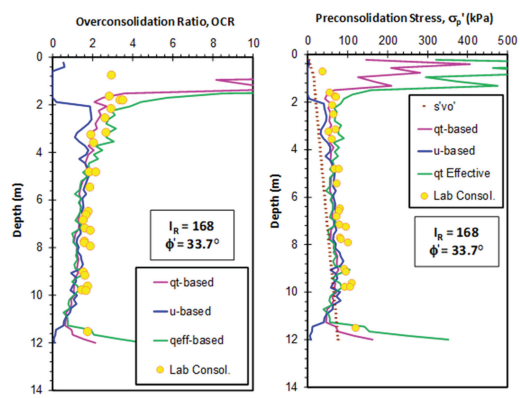

Figure 11. OCR and preconsolidation stress prediction using hybrid SCE-CSSM framework with proposed I_R expression for Ballina soft clay, Australia (data from Pineda et al. 2016).

good agreement is also observed in comparison with laboratory-measured σ_p' and corresponding OCR profiles.

5 CONCLUSIONS

Using a hybrid spherical cavity expansion—critical state framework, it is shown that an operational

value of rigidity index (I_R) is obtained from the cone tip resistance and pore water pressure readings, or their normalized quantities. Three case studies covering natural clays with different geologies are used to demonstrate the effectiveness of the methodology. The assessed I_R values are used to evaluate profiles of undrained shear strength and stress history

ACKNOWLEDGMENTS

The authors appreciate the support of ConeTec Investigations of Richmond, BC and Design House Consultancy of Dubai in support of this research.

REFERENCES

Altaee, A. and Fellenius, B.H. (2002). *Evaluation and Analysis of Results of Static Loading Test US95 Sandpoint North and South, Sandpoint, Idaho*. Report No. 0005CS193, prepared for CH2M Hill, Boise, ID by Urkkada, Ottawa, ON: 69p.

Chen, B.Y. and Mayne, P.W. (1994). *Profiling the Overconsolidation Ratio of Clays by Piezocone Tests*, Report No. GIT-CEE/GEO-94–1 submitted to National Science Foundation by Georgia Institute of Technology, Atlanta, 280 p.

Keaveny, J. (1985). *In-situ determination of drained and undrained soil strength using the cone penetration test,* Ph.D. Dissertation, University of California, Berkeley, 371p.

Keaveny, J. and Mitchell, J.K. (1986). Strength of fine-grained soils using the piezocone. *Use of In-Situ Tests in Geotechnical Engrg.* (GSP 6), ASCE, Reston/VA, 668–685.

Konrad, J.M. and Law, K. (1987). Undrained shear strength from piezocone. *Canadian Geotechnical J.* 24: 392–405.

Krage, C.P., Broussard, N.S., & DeJong, J.T. (2014). Estimating rigidity index (I_R) based on CPT measurements. *Proceedings of the 3rd International Symposium on Cone Penetration Testing,* Las Vegas: 727–735. www.cpt14.com

Kulhawy, F.H. and Mayne, P.W. (1990). *Manual on Estimating Soil Properties for Foundation Design, Report No. EL-6800,* Electric Power Research Institute, Palo Alto, CA, August 1990, 306 pages. Download from: www.epri.com

Ladd, C.C. (1991). Stability evaluation during staged construc-tion. (The 22nd Terzaghi Lecture), *Journal of Geotechnical Engineering* 117 (4): 540–615.

Lunne, T., Randolph, M., Sjursen, M.A., Low, H.E. and Gue, C.S. (2006). *Shear strength parameters determined by in-situ tests for deep water soft soils*. NGI-COFS Report 20041618–1: 558 pages.

Mayne, P.W. (1991). Determination of OCR in clays by piezo-cone tests using cavity expansion and critical state concepts. *Soils and Foundations* 31 (2): 65–76.

Mayne, P.W. (2001). Stress-strain-strength-flow parameters from enhanced in-situ tests. *Proceedings International Conference on In-Situ Measurement of Soil Properties & Case Histories* (In-Situ 200), Bali, Indonesia, 47–69.

Mayne, P.W. (2005). Integrated ground behavior: in-situ and lab tests. *Deformation Characteristics of Geomaterials*, Vol. 2 (Proc. IS Lyon'03), Taylor & Francis, London: 155–177.

Mayne, P.W. (2007a). In-situ test calibrations for evaluating soil parameters, *Characterization & Engineering Properties of Natural Soils*, Vol. 3, Taylor & Francis, London: 1602–1652.

Mayne, P.W. (2007b). *NCHRP Synthesis 368 on Cone Penetration Test*. Transportation Research Board, National Academies Press, Washington, D.C., 118 pages.

Mayne, P.W. (2014). Interpretation of geotechnical parameters from seismic piezocone tests. *Proceedings, 3rd Intl. Symp. Cone Penetration Testing*, (CPT'14, Las Vegas); edited by P.K. Robertson and K.L. Cabal): 47–73. www.cpt14.com

Mayne, P.W. (2016). Evaluating effective stress parameters and undrained shear strengths of soft-firm clays from CPT and DMT. *In Pursuit of Best Practices—Proc. 5th Intl. Conf. on Geotechnical & Geophysical Site Characterization* (ISC-5), Australian Geomechanics Society, Vol. 1: 19–40

Pineda, J.A., McConnell, A., and Kelly, R.B. (2014). Performance of an innovative direct-push piston sampler in soft clay. *Proceedings of the 3rd Symposium on Cone Penetration Testing*. Las Vegas, NV, USA: 279–288. www.cpt14.com

Pineda, J.A., Suwal, L.P., Kelly, R.B., Bates, L., and Sloan, S.W. (2016). Characterization of Ballina clay. *Géotechnique*, *66* (7): 556–577.

Schnaid, F., Sills, G.C., Soares, J.M., & Nyirenda, Z. (1997). Predictions of the coefficient of consolidation from piezocone tests. *Canadian Geotechnical J.* 34 (2): 315–327.

Senneset, K., Sandven, R., Janbu, N. (1989). Evaluation of soil parameters from piezocone tests. *Transportation Research Record* 1235, National Acad. Press, Washington DC: 24–37.

Tanaka, H., Locat, J., Shibuya, S., Soon, T. T., Shiwakoti, D.R., (2001). Characterization of Singapore, Bangkok, Ariake Clays. *Canadian Geotechnical Journal* 38(2), 378–400.

Teh, C.I. & Houlsby, G.T. (1991). An analytical study of the cone penetration test in clay. *Geotechnique* 41 (1): 17–31.

Vesić, A.S. (1977). Design of Pile Foundations. *Synthesis of Highway Practice 42*. Transportation Res. Board, National Research Council, Washington, DC: 68 p.

Yu, H. S. & Mitchell, J. K. (1998). Analysis of cone resistance: review of methods. *Journal of Geotechnical and Geoenvironmental Engineering*, *124*(2), 140–149.

Taylor & Francis
Taylor & Francis Group
http://taylorandfrancis.com

Cone Penetration Testing 2018 – Hicks, Pisanò & Peuchen (Eds)
© 2018 Delft University of Technology, The Netherlands, ISBN 978-1-138-58449-5

On the use of CPT for the geotechnical characterization of a normally consolidated alluvial clay in Hull, UK

L. Allievi, T. Curran, R. Deakin & C. Tyldsley
Arup, UK

ABSTRACT: The A63 Castle Street Improvement scheme includes an excavation approximately seven metres deep within a layer of normally consolidated alluvial clay. The collection of good quality undisturbed samples of this soil for laboratory testing proved challenging, therefore great reliance was put on site testing, especially on cone penetration tests. The procedure to calibrate and combine the data gathered from the field CPT and dissipation tests with all the ground investigation data is described. The use of CPTs provided a continuous profile with depth of the geotechnical properties of this extremely variable layer. Additional considerations are given on the effects of the use of a u1 or u2 piezocone position for the measurement of pore water pressure.

1 INTRODUCTION

Typically, the geotechnical characterisation of fine grained deposits relies greatly on the results of laboratory tests such as triaxial and compressibility tests. However, the collection of good quality samples for laboratory testing is not always possible, especially in the soft deposits with a relevant fraction of coarse grained material. In such cases cone penetration testing is a very valuable and cost effective technique to derive the in-situ properties of the soil.

This paper describes how CPT tests have been used in the A63 Castle Street Improvement project to characterise the mechanical properties of the alluvial clay.

2 THE A63 CASTLE STREET IMPROVEMENT PROJECT

The Castle Street improvement scheme is the enhancement of the A63 from the connection with the M62 to the Port of Hull, in the city of Hull, UK. The carriageway will be lowered by approximately 7 m into an underpass; a new integral road bridge will be constructed at the Mytongate junction to carry the north-south traffic across the underpass and two new footbridges will be constructed at Porter Street and Princes Quay to improve the pedestrian and cycling connectivity in a north-south direction across the A63.

The project is constrained by being into an urban area with buildings and infrastructure located directly next to the working area and by the presence of cultural heritage features. Furthermore, the A63 will need to remain operative for the entire duration of the works.

Figure 1. 3D visualization of the A63 Castle Street improvement scheme.

3 THE GROUND INVESTIGATION AND GROUND CONDITIONS

Two rounds of ground investigations were carried out for the Castle Street Improvement scheme between 2013 and 2016. The ground investigation works included exploratory boreholes and trial pits, window sampling, self-boring pressuremeter, cone penetration testing, pump testing, groundwater monitoring and laboratory testing, including triaxial and oedometer tests.

The geological conditions of the site are originated by a series of fluvial and glacial processes which have resulted in a complex superficial geology.

The bedrock is Burnham Chalk Formation from the Upper Cretaceaous. The presence of a glacial channel caused the erosion of the bedrock at the east of the site, consequently the top of

chalk drops gently from -17 mOD at the west to -25 mOD at the east.

Fluvio-glacial sands and gravels directly overly the chalk. A deposit of windblown (aeolian) sands is typically found above the glacial coarse grained deposit, however this is not present across the entire site.

Glacial fine grained deposits are found above the aeolian sand, comprising two units. The lower unit is glacio-lacustrine material, deposited in a glacial impound lake behind a moraine dam; the upper unit is glacial till deposited in a more recent glacial phase.

The thickness of the glacial deposits decreases towards the east, where a paleo-channel eroded the glacial till and subsequently deposited coarse grained alluvial material; this unit pinches out towards the center of the scheme at Mytongate Junction.

A variable thickness of estuarine alluvial clay is found on top of the glacial deposits and the coarse grained alluvium across the entire site, with a layer of peat generally recognized towards the base of the unit.

Sand lenses, bands and horizons are found irregularly within the glacial and alluvial deposits. These units are the results of fluctuations of the depositional environment and the variability of historical streams and watercourses.

Made ground material of variable thickness and nature is found across the entire site above the natural deposits.

Two main aquifers are found across the site: a shallower one within the superficial deposits and a confined and tidal-dependent one within the chalk. There is evidence that the fluvio-glacial sands and gravels and the aeolian sands are in hydraulic connectivity with the chalk; similarly, where the glacial deposits thin out at the east side of the site the coarse grained alluvium shows a slightly tidal-dependent behavior, evidence of some level of hydraulic connectivity with the deeper aquifer within the bedrock.

Of all the geological sequence, the alluvial clay is the most challenging material for the design. It is a soft deposit with high silt and coarse grained fraction and characterized by high variability both laterally and vertically across the site. Lenses and pockets of organic material are found within this deposit and a layer of fibrous peat lies towards the base of the alluvium.

4 UNDRAINED SHEAR STRENGTH OF THE ALLUVIAL CLAY

Cone penetration testing was used in combination with a number of testing techniques to derive the undrained shear strength of the alluvial clay.

4.1 *Triaxial tests*

Both unconsolidated (QUT) and consolidated undrained (CUT) triaxial tests were performed on undisturbed samples collected on site. However due to the high silt content and the presence of sand pockets within the deposits, some level of stress relief was unavoidable for these samples. This effect may have resulted in low strength results in most of the quick undrained tests.

4.2 *Cone penetration tests*

The undrained shear strength was derived from CPT tests using the expression $c_u = q_{net}/N_{kt}$, where q_{net} is the cone resistance and N_{kt} the cone factor value. It should be noted that the cone resistance was corrected to keep into account the pore pressure effects, through the relation $q_t = q_c + u2(1\text{-}a)$, where q_c is the measured cone resistance, $u2$ is the measured pore pressure and a is the net area ratio of the tip.

The value of the N_{kt} was calibrated using the shear strength derived from triaxial tests. A plot of undrained shear strength versus net cone resistance was prepared for each triaxial test; trend lines were identified across the deposit and preliminary N_{kt} values were derived from the gradient of these trend lines.

A review of the triaxial tests before the calibration allowed the elimination of unreliable results, especially those performed on samples with sand pockets or with local variations of soil characteristics. The samples tested in the triaxial apparatus were split and described after the test and the availability of these descriptions was instrumental for this stage of the ground characterization. During the calibration process, more reliance was put on the consolidated undrained triaxial tests rather than the quick undrained triaxial tests.

Having isolated the more representative triaxial tests, it was found that the best correlation between triaxial test and CPT results was based on an N_{kt} value of 20.

4.3 *Pressuremeter tests*

Two types of pressuremeter testing techniques were used during the ground investigation: Self Boring Pressuremeter (SBP) and Full Displacement Pressuremeter (FDPM). The SBP drills a borehole into the ground as wide as the pressuremeter device; in the FDPM a pressuremeter cone is used, which is a special cone mounted on a CPT apparatus and pushed to testing depth.

The limit shear strength mobilized in pressuremeter tests equals the undrained shear strength when the test is completed in undrained conditions. A review of the pressuremeter tests allowed the tests completed in undrained conditions to be distinguished

from those performed in areas with local coarse grained pockets and therefore not undrained.

4.4 *Liquidity index*

The undrained shear strength of a fine grained material can be correlated with the liquidity index. A range of correlations are available in literature; the one proposed by Skempton & Northey (1952) was used in this case.

Upper bound values of the liquidity index, resulting in lower bound undrained shear strength, were conservatively used. Based on a review of the tests results, a liquidity index increasing linearly from 0.23 at the top of the layer to 1.2 at 0 mOD and then constant with depth below 0 mOD was assumed.

4.5 *Skempton's correlation*

In literature there is a number of correlations between undrained shear strength and effective vertical stress for normally consolidated deposits. The relation $c_u = 0.11 + 0.0037PI$ proposed by Skempton & Henkel, (1953), was used.

Based on the Atterberg limits for the alluvial clay, a plasticity index (PI) of 24 was used in the correlation.

Figure 2 shows the undrained shear strength derived from all methods described above. For CPT derived shear strength, the plot shows upper and lower bound values for extreme results and the envelope of the highest density results (labelled as CPT typical envelope).

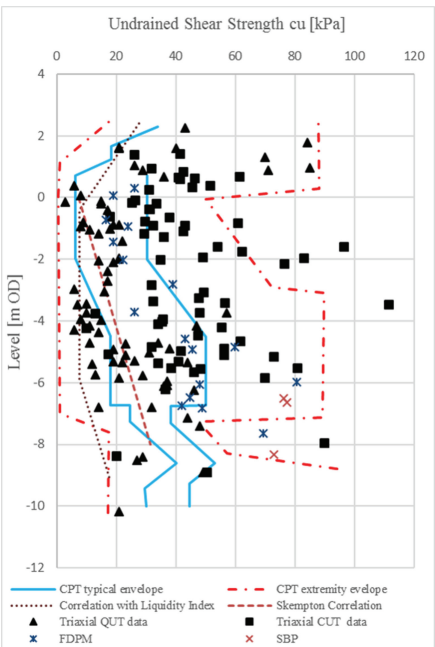

Figure 2. Shear strength of the alluvial clay.

The profile of strength derived from CPT shows that the upper part of the unit is characterized by higher strength; this corresponds to a zone of desiccated crust. Within this zone, the strength reduces linearly with depth until about 0.5 mOD; below this level, the deposit is generally very soft to soft until about -2 mOD, when a trend of strength increasing with depth begins. A step down in the strength is seen at around -5 mOD, however the trend of strength increasing with depth continues even below this level.

The majority of the shear strength values obtained with different derivation methods fall within the typical CPT envelope for depths above -3 mOD. A number of consolidated triaxial tests result in higher values of shear strength, however most of these data were obtained with consolidation pressure in excess of the in-situ pressure, and are therefore not representative of the actual soil stress conditions.

Between -3 and -6 mOD, some localized very low triaxial results can be seen within the softer zone. These results were noted from the historical data and were investigated further within the scope of the most recent ground investigation. Different sampling and testing methods confirmed the presence of localized weaker layers. It is believed that these are due to variations in the composition of lenses and thin horizons of coarser material, as seen also in the classification data.

It should be noted how of all testing methods and correlations, the Liquidity Index correlation and the Skempton curve provide the best fit with the typical lower bound CPT derived results within and below the crust respectively.

Test results, borehole descriptions and split and describe samples all agree in showing great variability in soil composition and coarse grained fraction. This is reflected in the scatter of the results obtained using the CPT data.

5 STIFFNESS OF THE ALLUVIAL CLAY

A strain level γ between 0.1% and 0.01% was assumed in the stiffness derivation for the project. This was considered an appropriate level for the design of foundations and earth retaining structures.

Two different methods of analysis of the CPT test results were used for the assessment of the stiffness of the alluvial clay: using correlations from the c_u obtained from the cone resistance and using the data gathered using seismic cone testing.

A simplified profile of the typical range of CPT derived shear strength was considered in the stiffness derivation and the correlations proposed by Kouftsoftas & Fischer (1980), based on Over Consolidation Ratio (*OCR*) and *PI*, were used. These correlations propose a ratio between shear stiffness G and shear strength c_u for different strain levels. The elastic modulus can then be derived using the relation $E = 2G(1 + \nu)$, where $\nu = 0.5$ in undrained conditions. A conservative ratio of 0.6 between drained and undrained elastic modulus was assumed.

Seismic CPT was also performed at the site. In this type of testing, the CPT cone is equipped with geophone sensors; seismic shear waves are generated at the surface and the sensors on the cone record the magnitude and arrival time of the seismic waves. A profile of the shear wave velocity with depth is obtained and this can be correlated to the soil small strain stiffness using the relation $G_0 = \rho V_s^2$, where ρ is the soil density. The degradation curves proposed by Seed & Idriss (1970) where used to derive the stiffness at the relevant strain level and undrained and drained elastic moduli were derived using the same relations proposed above.

The stiffness obtained with CPT tests was compared to that derived from pressuremeter tests. In fact, the shear modulus G can be derived from the pressure/displacement curves for different strain levels and the elastic modulus can then be derived from the shear modulus using the same elastic theory relations described above. Only the results of the SBP were considered, since the interpretation of FDPM data generally resulted in lower stiffness values, probably due to the greater level of disturbance relatively to the volume of soil tested caused during the advancement of the instrument.

Figure 3 shows the drained elastic modulus derived with the different methods. Only the results obtained below the desiccated crust are shown in the plot. CPT derived lower bound values show a good correspondence with pressuremeter data and the trend with depth is similar to what is seen for the shear strength, with softer material below the crust and strength increasing with depth below –2 mOD.

Seismic cone data show a greater scatter in the results. It is believed that this variability is a reflection of the variability of the ground conditions, which have a greater impact in the results of the seismic cone rather than the pressuremeter because of the lesser volume of soil tested with this technique. The results are mostly included within the typical CPT derived range, however, they tend to be in better agreement with the typical upper bound CPT derived values. A similar trend of increasing strength for depths greater than –2 mOD is found

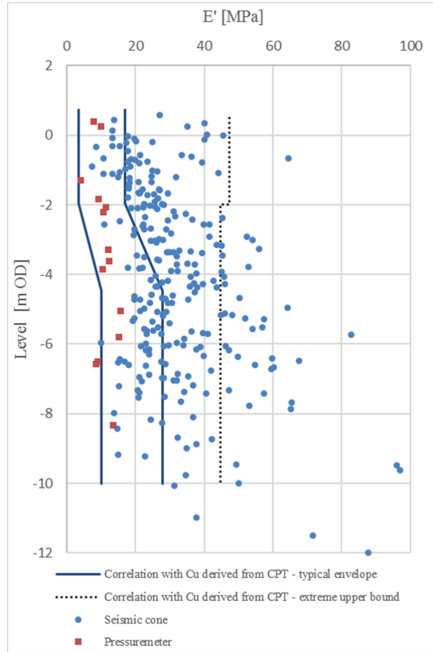

Figure 3. Drained elastic modulus of the alluvial clay.

also in the seismic cone data, however a reduction in the stiffness derived with this method is seen below -4 mOD.

A simplified upper extreme CPT envelope is also plotted on the graph. Almost the entirety of the seismic cone results falls within this envelope.

6 PERMEABILITY OF THE ALLUVIAL CLAY

As described previously, the nature of the alluvial clay is extremely varied, with silt and coarse grained lenses irregularly distributed within the deposit. The estimation of the permeability is important to predict the soil behavior during the excavation, before the construction of the permanent structures.

The permeability of the alluvial clay was estimated using dissipation tests performed during the CPT tests and using the oedometer test results. The soil permeability can be derived from the coefficient of consolidation using the relation $k = C^*\gamma_w{}^*m_v$. The coefficient of volume change m_v can be derived indirectly from the cone resistance measured during CPT tests using the relation $m_v = [\alpha_M (q_t - \sigma_{v0})]^{-1}$ (with α_c empirical factor function of the cone resistance) or directly from oedometer test results. From a comparison between the two methods, it was found that the m_v estimated with

the oedometer tests is in good agreement with the upper bound value of m_v estimated using the CPT test results.

From the dissipation tests, the coefficient of consolidation was derived using the correlation $T^* = (C^*t)/(r^{2*}\sqrt{I_r})$ proposed by Teh & Houlsby (1991), where T^* = time factor for a given degree of pore pressure dissipation, C = coefficient of consolidation, t = measured time for dissipation for the same degree as T^*, I_r = rigidity index, assumed equal to 160 for the alluvial clay, r = cone diameter.

As demonstrated by Robertson et al. (1992), the coefficient of consolidation estimated with CPT data is a good estimate of the horizontal coefficient of consolidation C_h, therefore the permeability estimated using the dissipation test results is considered to be the horizontal coefficient of permeability.

On the contrary, because of the testing method, it is believed that the coefficient of permeability estimated using oedometer tests is representative of the vertical permeability of the soil.

Figure 4 shows the value of horizontal and vertical coefficient of permeability estimated for the alluvial clay. The vertical permeability of the layer ranges typically between 10^{-6} and 10^{-7} m/s; the horizontal coefficient of permeability ranges between 10^{-5} and 10^{-6} m/s. The difference between the two is representative of the soil composition; the presence of lenses and pockets of coarser and more permeable material provides a preferential path for the horizontal dissipation of pore water pressure, however this effect is much less relevant for the water movement in vertical direction.

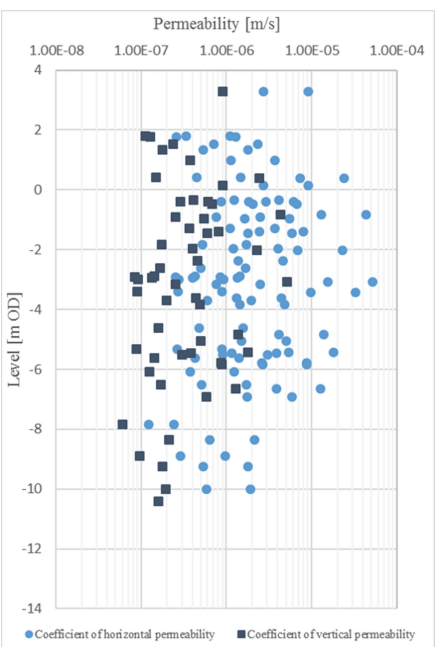

Figure 4. Permeability of the alluvial clay.

7 INFLUENCE OF PIEZOCONE POSITION

All CPT tests performed included the measurement of the pore water pressure. However, different types of piezocone were used in the different investigations A number of tests used a piezometer in u2 position, on the shoulder of the cone, and some with piezometer in u1 position, on the face of the cone.

The piezometric profile measured with u1 and u2 positions at the same location were compared and the results are showed in Figure 5. It is evident that the u1 position tends to result in significantly higher measurements of pore pressure.

Most of the correlations for CPT data available in literature have been developed for piezocone in u2 position, and the impact of using u1 rather than u2 pressure measurements is most relevant for soft clays, where the recorded tip resistance is limited. Therefore, a correction factor based on Peuchen et al. (2010) was adopted for all u1 pore pressure measurements before processing the CPT data. An example of the effect of this correction is presented in Figure 5.

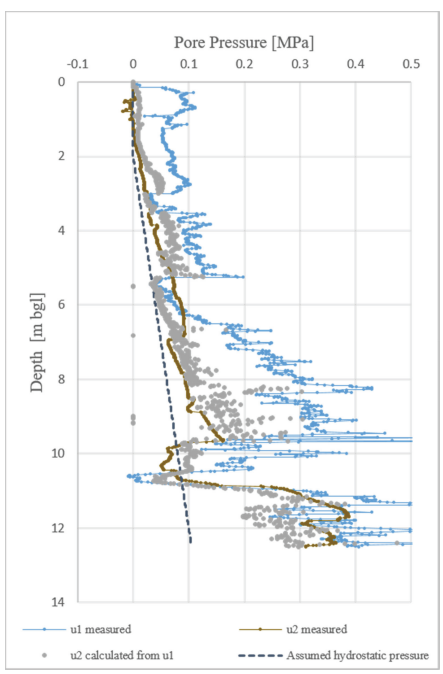

Figure 5. Pore pressure measurement from u1 and u2 piezocone positions.

8 CONCLUSIONS

When working with normally consolidated soft soils, obtaining good quality undisturbed samples for geotechnical laboratory tests can be difficult, slow and expensive and often the results obtained are not representative of the in-situ soil properties.

Cone Penetration Tests provide a simple and cost effective method to obtain a continuous profile with depth of the ground conditions. Furthermore, when combined with other in-situ and laboratory testing techniques, an example of which is the work done for the Castle Street Improvement project described in this paper, CPTs can be used to derive the soil properties, such as strength, stiffness and permeability.

When interpreting the results of CPT tests, it should be considered that because of the testing technique and instrument, the properties estimated are representative of the volume of soil immediately close to the testing zone; care should be taken in extending the results of a limited number of tests to the entire layer and in choosing the design values of the estimated parameters.

A good knowledge of the details of the test performed, such as the type of piezocone used for the measurement of the pore water pressure, is also important because this will affect the assessment of the soil properties.

REFERENCES

Koutsoftas, D. C. & Fisher, J. A. 1980. Dynamic properties of Two Marine Clays. *ASCE J. Geotechnical Division* 106 (GT6): 145–157.

Peuchen, J., VandenBerghe, J. F. & Coulais, C. 2010. Estimation of u1/u2 conversion factor for piezocone. *CPT'10: 2nd International Symposium on Cone Penetration Testing: Conference proceedings, Huntington Beach, California*

Robertson, P.K. Beach, California 2010. Soil Behaviour Type from the CPT: an update. *CPT'10: 2nd International Symposium on Cone Penetration Testing: Conference proceedings. Huntington Beach, California*

Robertson P. K. & Cabal K. L. 2015. *Guide to Cone Penetration Testing for Geotechnical Engineering, 6th edition.* Signal Hill, California: Gregg Drilling & Testing

Seed, H. & Idriss, I. M. 1970. Soil Moduli and Damping Factor for Dynamic Response Analyses. *Report number EERC 70-10* Earthquake Engineering Research Center, College of Engineering, University of California, Berkeley, California

Skempton. A.W. 1957. Discussion: Further data on the c/p ratio in normally consolidated clays. *Proceedings of the Institution of Civil Engineers* 7: 305–307

Skempton, A. W. & Northey, R. D. 1952. The sensitivity of clays. *Geotechnique* 3: 30–53

The, C.I. & Houlsby, G.T., 1991, An analytical study of the cone penetration test in clay. *Geotechnique 41 (1)*, pp. 17–34

Cone Penetration Testing 2018 – Hicks, Pisanò & Peuchen (Eds)
© 2018 Delft University of Technology, The Netherlands, ISBN 978-1-138-58449-5

New vibratory cone penetration device for in-situ measurement of cyclic softening

D. Al-Sammarraie, S. Kreiter, F.T. Stähler, M. Goodarzi & T. Mörz
MARUM-Center for Marine Environmental Sciences, University of Bremen, Bremen, Germany

ABSTRACT: A new type of vibratory cone penetration device has been developed to improve the geotechnical in-situ methods for evaluating the dynamic and cyclic properties of the soil. The new device controls displacement amplitudes in real time and is designed to test various cyclic loads that cover different configurations of vibratory pile installation and different magnitudes of earthquakes. Some soil layers reacted strongly to the induced cyclic loads with high reduction ratios *RR* of the cone resistance, while other layers did not react to cyclic loading. It was also found that even a distance of 50 cm does not guarantee a good correlation between CPT and Vibro-CPTu. Therefore two or more pairs of CPT and Vibro-CPTu should be conducted at close distances in order to minimize misinterpretations of the data, which are caused by small scale geological structures, such as the presence of inclined layers, cross bedding, or other heterogeneities.

1 INTRODUCTION

In recent years there has been an increased interest in using vibratory driving as a method for pile installation, especially for offshore structures where the well being of the sea mammals is of great concern. The method reduces noise and damage to the piles during driving as well as permits fast pile installation (O'Neill et al., 1990). Vibratory pile installation generates vertical vibrations that impose cyclic loads in the ground, which may cause the soil to liquefy (Nagomi et al., 1997). Liquefaction is the loss of soil strength due to an increase in pore water pressure and the resulting loss of shear strength during cyclic loading (Seed & Idriss, 1971). Fluidization is a type of liquefaction where the soil changes from its normal state to a quasi-fluid state under ongoing cyclic loading (Bernhard, 1967). Fluidization is related to the displacement amplitude and frequency of vibration, and it may occur during vibro piling (Rodger & Littlejohn, 1980). The prediction of the soil behavior during vibratory pile installation is uncertain and depends on empirical or combined theoretical and semi-empirical approaches (Nagomi et al., 1997). Nevertheless there have been some attempts to directly evaluate the soil dynamic behavior and the liquefaction resistance in-situ by utilizing a special type of cone penetration test, the piezovibrocone or Vibro-CPTu, that mechanically induces cyclic loads in the soil while penetrating it (Sasaki & Koga, 1983, Shibata & Teparaksa, 1988). Sasaki and Koga (1983) proposed the reduction ratio *RR* as an index for soil liquefaction resistance:

$$RR = 1 - \left(\frac{q_{cv}}{q_{cs}} \right) \tag{1}$$

where q_{cv} = vibratory cone resistance; and q_{cs} = static cone resistance (Sasaki & Koga, 1983).

Early Vibro-CPTu devices used horizontal down-hole vibrators, without a control of stress or strain (Sasaki & Koga, 1983, Sasaki et al., 1984, Shibata & Teparaksa, 1988, Tokimatsu et al., 1988, Mitchell et al. 1988). However the applied horizontal loads sometimes led to a gap at the cone-soil interface leading to debatable results. To overcome this gapping problem, vertical down-hole vibrators were used in more recent studies (Wise et al., 1999, McGillivray et al., 2000, Mayne, 2000). The only constant parameter of these vibrators is the energy. However the variation of the displacement amplitudes with depth and material was not determined. Other recent studies by Jorat et al., (2015) and Kluger et al., (2016) employed the use of distance controlled method to apply up-hole vertical cyclic loads. Since the cyclic motion of the rod was hydraulically driven up-hole, the actual cyclic movement of the cone may vary with depth. Uncertainties in the applied amplitude lead to uncertainties in the interpretation of the effect of Vibro-CPTu on the cone resistance. For this reason a new vibro cone system has been developed. The main advantage of the new system is the 500 Hz acceleration measurements in the cone, which allow to determine the displacements in situ. This study presents the first tests of the real time controlled Vibro-CPTu concept. In this paper, we

compare the results of three pairs of static CPTu and Vibro-CPTu tests, performed with two different vertical vibration amplitudes and two different frequencies. The reduction ratios for the cone resistances are calculated, and the values for the actual penetration velocity and amplitudes are presented at different penetration depths.

2 METHODOLOGY

2.1 *Vibro Crawler*

The vibro crawler has a high speed hydraulic system controlled in real time with 5 kHz (Fig. 1). The controller is compatible with bigger CPT frames—currently under construction. The cone is equipped with an inertial (navigation) system consisting of a 3-axis gyroscope and 3-axis accelerometer sensor working with 500 Hz. The presented tests were displacement controlled by a distance sensor at the hydraulic cylinder. The acceleration data was for this first study only recorded for post processing.

2.2 *Test scheme*

The test area is located in Bremen, Germany where the soil is mainly composed of dense sands, with medium to coarse grains (Fig. 2).

Three pairs of static and vibratory cone penetration tests were conducted at three locations spaced 4 m apart. The space between the static CPTu and Vibro-CPTu was 50 cm for P1 and 80 cm for P2 and P3 (Fig. 3). The used cone and the rod have a cross sectional area of 5 cm^2. In static mode, the cone is pushed at a rate of 2 cm/s. In case of vibra-

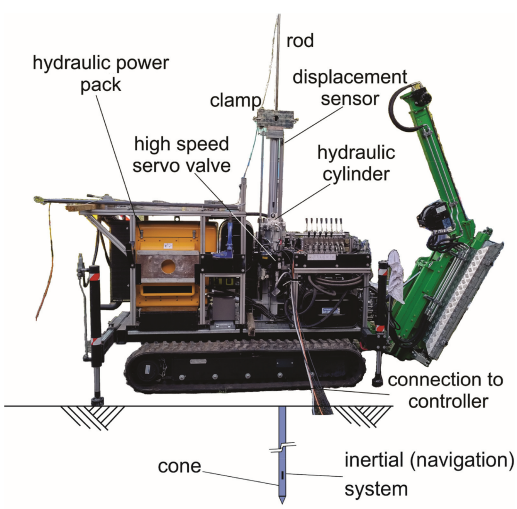

Figure 1. Vibro crawler system.

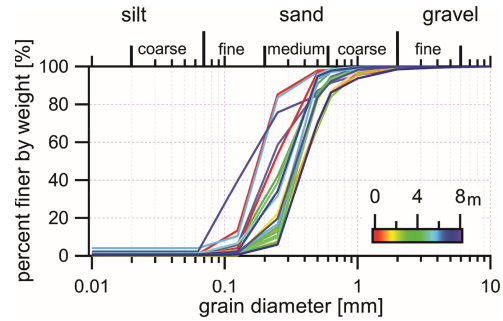

Figure 2. Grain size distribution of soil according to Triebeneck (2017).

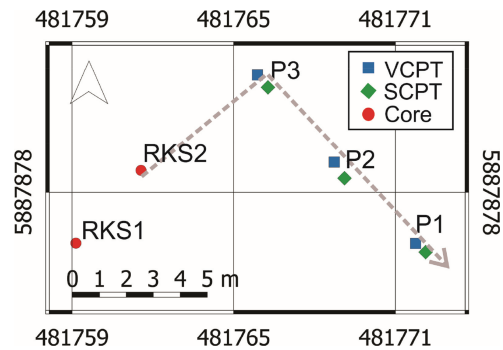

Figure 3. Map of test field using UTM zone 32. The two cores are from Triebeneck (2017). The dotted line is the correlation section shown in figure 9.

Table 1. Test scheme of Vibro?CPTu and static CPTu, where f = frequency; and ε_A = displacement amplitude.

type	f [Hz]	ε_A [mm]	Location
SCPT*			P1 P2 P3
VCPT*	15	±0.25	P1
VCPT*	10	±0.25	P2
VCPT	10	±0.5	P3

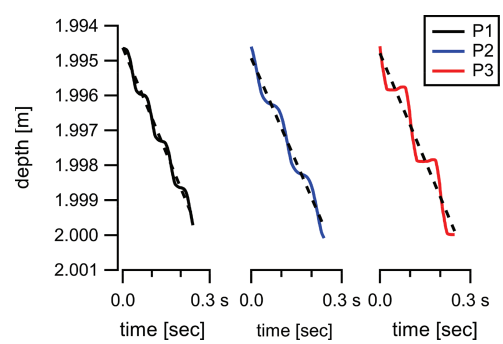

Figure 4. Displacement for the three Vibro-CPTu runs.

tory mode the sinusoidal vibration with different amplitudes is also added to an average velocity of 2 cm/s (Table 1, Fig. 4)

2.2.1 *Reduction ratio*

The reduction ratio *RR* was calculated using equation (1). *RR* values, where the lateral correlations of two tests were unclear, are omitted. The reasoning is explained in more details in the discussion.

2.3 *In-situ displacement*

The acceleration data is used to derive the in situ displacement amplitude. The displacement amplitude is obtained by double integration of the acceleration. The noise of the raw acceleration data is too high to use them directly (Fig. 5). The data is refined by exploiting the well-defined cyclic character of the vibratory push. The noise is reduced by averaging the result of multiple cycles over a certain depth interval. This requires that the cycles are measured at similar material that is only marginally changing during the rod penetration in this interval. The averaged points have all exactly the same phase in the vibration cycle. We call this "stacking" following the naming of a similar processing step in reflection seismic. The technique is also comparable to the working principle of lock-in amplifiers.

This stacking is done for three cycles in row, with a stacking factor of 100, so each point in the red curve is the average of 100 raw data points from different depths (Fig. 5). The averaged cycles were gathered over a total depth of 0.4 m, and it was established that there is no significant change in the soil behavior over that depth.

The refined data is then integrated to get the velocity and displacement. Knowing that the underlying movement is uniform, the average value of the stacked acceleration data was subtracted before integrating the data. The integration constants, initial velocity and initial displacement were obtained from the differentiated displacement data and the actual displacement data, respectively. For the comparison of the cyclic displacement amplitude, the trend of the uniform movement was subtracted.

3 RESULTS

3.1 *Vibro cone performance*

The Vibro-CPTu system is able to apply an amplitude of ±0.25 mm until 6 m depth, and there is no significant influence of the penetration depth (Fig. 6). The resulted velocities from the acceleration and displacement sensor are shown in Figure 7. The velocity derived from the

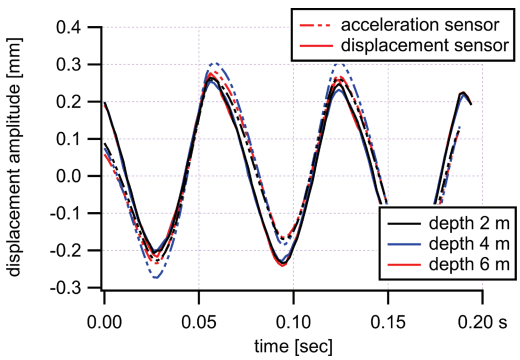

Figure 6. Amplitude of vibration at different depths derived from the displacement and acceleration sensors for P1.

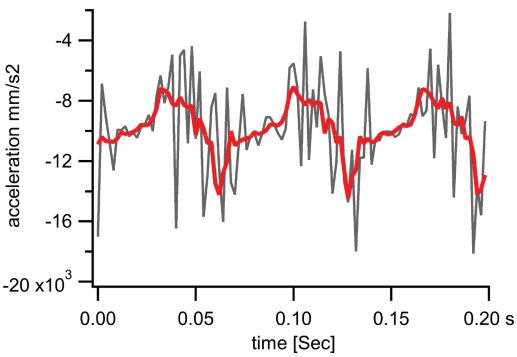

Figure 5. Raw acceleration of the first three cycles in gray and refined acceleration for 100 × 100 stacked data points in red for depth of 2–2.4 m for location P1.

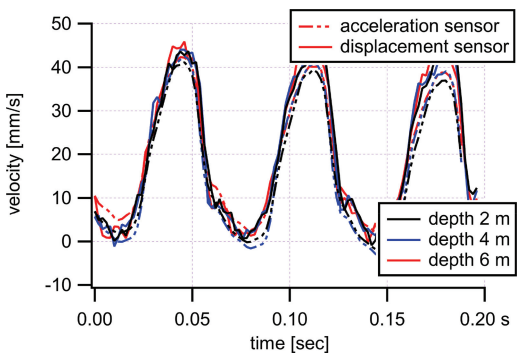

Figure 7. Velocity of vibration at different depths derived from the displacement and acceleration sensors for P1.

displacement sensor was equal to 20 mm/s and the resulted velocity from integrating the acceleration sensor had an average value of 20 mm/s at all three tested depths.

3.2 *Vibro-CPTu results*

The soil behavior type SBT has been identified according to Jefferies & Davies (1991) (Fig. 8) and is used for correlating the three SBT profiles with core RKS2 by Triebeneck (2017) (Fig. 9).

In test location P1 there are two layers that suffer from relatively high reduction in the cone resistance. The zones are shadowed in Figure 10 and named Zone 1 and Zone 2. The same zones are also evident for test location P2 in Figure 11.

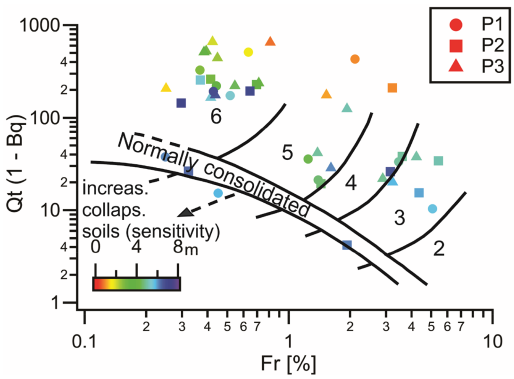

Figure 8. Soil behavior type after Jefferies & Davies (1991).

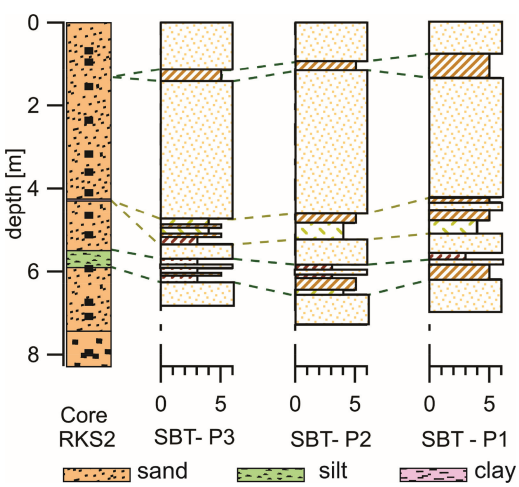

Figure 9. Correlation of soil behavior types SBTs after Jefferies & Davies (1991) with soil profile RKS2 by Triebeneck (2017). Patterns of SBTs are for visualization purposes only.

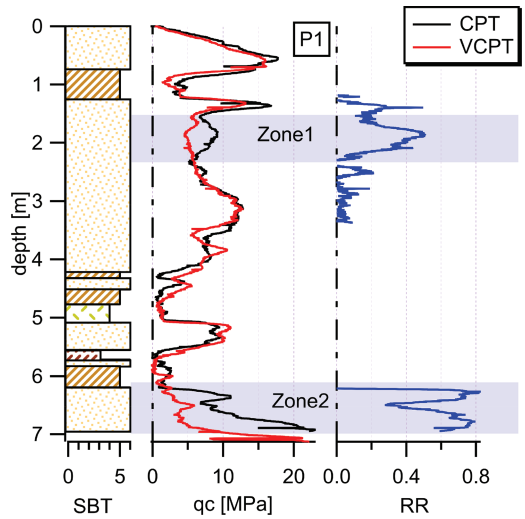

Figure 10. Soil behavior type SBT after Jefferies & Davies (1991), Cone resistance qc and reduction ratio *RR* over depth for location P1.

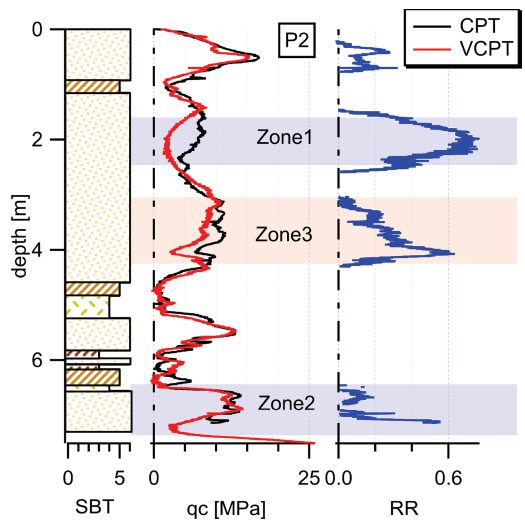

Figure 11. Soil behavior type SBT after Jefferies & Davies (1991), Cone resistance qc and reduction ratio *RR* over depth for location P2.

Although the vibration frequency was lower than for P1, the reduction ratio *RR* values are higher in the soil layers at Zone 1 and 2 (Table 2). Zone 1 in location P3 has only small *RR* values although the vibration amplitude was the highest in the study (Fig. 12, Table 2).

At the test locations P2 and P3 there is a layer with high reduction ratios shadowed and named Zone 3, which is not present in location P1.

Table 2. Maximum reduction ratio values.

Reduction ratio *RR*			
Location	Zone 1	Zone 2	Zone 3
P1	0.5	0.8	0.1
P2	0.7	0.59	0.6
P3	0.2	0.85	0.3

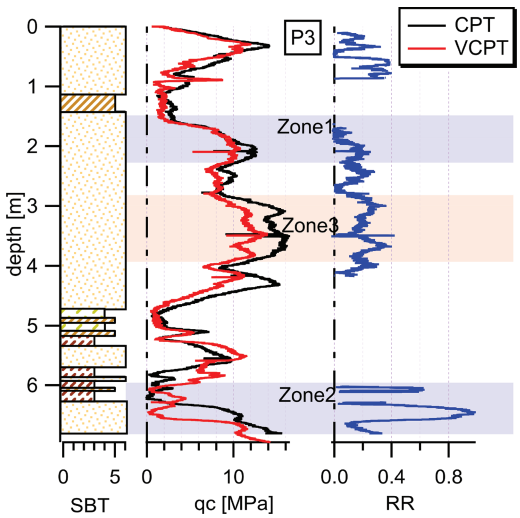

Figure 12. Soil behavior type SBT after Jefferies & Davies (1991), Cone resistance qc and reduction ratio *RR* over depth for location P3.

4 DISCUSSION

4.1 *Vibro cone*

The observed results in Figure 6 and 7 were unexpected, since it was presumed that the amplitude of the displacement cycles would decrease with increasing the depth of penetration (Kluger et al., 2016, Moore, 1987). This presumption relied on the expected increment of the axial deformation and buckling of the rod as it penetrates deeper in the ground. Therefore the 6 m depth of penetration was not deep enough to cause big deformation in the rod and thus no noticeable reduction was observed in the displacement amplitude. The total applied hydraulic force increases as the depth of penetration increases. The amplitude of cycles of the not shown hydraulic force remains surprisingly constant even though it is the displacement which is controlled. However as the cone penetrates deeper in the soil a loss in the real resulted displacement amplitude is expected, due to rod deformation. The real time controller is designed to compensate for such an amplitude loss in the future and the in situ acceleration is expected to be a sensitive tool to detect the onset of rod extensive buckling during cyclic loading

4.2 *Field tests*

Accurate values of the *RR* rely on Vibro-CPTu and CPTu within the same sediment material. Two closely positioned CPTu profiles should therefore perfectly correlate. One main result of this study is that even a distance of 50 cm does not guarantee a good correlation. This is probably caused by the high energy in the environment during the sedimentation of the sand, which led to short range local changes in material and stratigraphy. Those changes include variations in depth and thickness of the same soil layer over very small lateral distances (Biryaltseva et al., 2016, NGI, 2014, Triebeneck, 2017). These variations may include inclined sand layers, local absence or presence of certain layers and internal crossbedding of some layers which may additionally influence the correlation of CPTu and the determination of *RR*.

Local stratigraphic changes are recognized by similar patterns of two CPTu profiles at a shifted depth. Evidence of those changes is observed for the sand layer at Zone 2 at test locations P1 and P3 (Fig 10 & 12). At P1 a local increase in the static cone resistance is observed at 6.3 m, which becomes evident at 6.5 m for the Vibro-CPTu. At P3 similar observations are made below 5.9 m depth for the static and vibratory cone resistance. The high values for the reduction ratios observed for these zones, are therefore not caused by cyclic loading during Vibro-CPTu; but rather due to miscorrelation of the CPTu data. Such observations are in contrast to Zone 2 in location P2 (Fig. 11), where static and Vibro-CPTu show similar patterns, without any evidence of shift in depth. This indicates that the values of *RR* for Zone 2 in P2 are probably accurate, whereas the *RR* in P1 and P3 may be influenced by the effect of geological structure, similar to the effect described in Boulanger et al. (2016).

Good correlations are also observed in Zone 3 at test location P2 and P3 (Fig. 11 & 12); where the same pattern of CPTu and Vibro-CPTu is evident at the same depth. The considerable reduction in the cone resistance is therefore very likely caused by the cyclic loading of Vibro-CPTu.

The uncertainty of testing the same material leads us to the point, that one pair of static and vibratory CPT is in most cases insufficient for accurate conclusions on the soils cyclic behavior in sands. Two or more pairs of CPT should be conducted at small distances to allow the distinction between the cyclic soil behavior and local changes in soil state or composition. Small depth shifts in a scenario with high data density will probably allow

for even better *RR* results, especially on test sides with inclined layers.

Two pairs of CPT and Vibro-CPT profiles at P1 and P2 show the same pattern for Zone 1 (Figs. 10 & 11). A considerable reduction in the cone resistance seems to be apparent at Zone 1 for both P1 and P2. Therefore it is concluded that the sand layer at Zone 1 is weak against cyclic loading during Vibro-CPTu and has experienced cyclic softening. Nevertheless only very small reduction in the cone resistance was observed at Zone 1 for the third testing location P3 (Fig. 12), although the Vibro-CPTu at P3 used a higher amplitude. This is probably caused by a local change of the sediment material or state that lead to a lower susceptibility to cyclic soil softening of Zone 1 at P3.

5 CONCLUSION

In this study a new tool, vibro crawler, has been developed to investigate the cyclic behavior of the soil. The new device proved to generate constant amplitudes until the final depth of penetration. Two sand layers reacted to the applied cyclic loads by showing high values of the reduction ratio. It was found that local stratigraphic changes have large effect on the response of CPTu and Vibro-CPTu. One suggested way to minimize their effect, is to conduct two or more pairs of CPTu and Vibro-CPTu at small distances. This could help in differentiating between the cyclic soil behavior and local changes in soil composition or state.

ACKNOWLEDGMENT

This project was supported by the Federal Ministry for Economic Affairs and Energy (BMWi), project: Vibro Drucksondierungen, FKZ: 0325906. We thank Marc Huhndorf, Joann Schmid, Wolfgang Schunn and Joshua Albai for invaluable technical assistance during field work and construction of the Vibro-CPTu.

REFRENCES

Bernhard, R.K. 1967. Fluidization Phenomena in Soils During Vibro-Compaction and Vibro-Pile-Driving and—Pulling. Hanover, New Hampshire.

Biryaltseva, T., Mörz, T., Brandt, S., Kreiter, S., Gerdes, U. & Ossig, B. 2016. Relative Densities and Void Ratios Derived From CPT Data Using In-Situ Field Calibration. IN LEHANE, A.-M.K. (Ed. *Geotechnical and Geophysical Site Characterisation 5* Sydny, Australia.

Boulanger, R.W., Moug, D.M., Munter, S.K., Price, A.B. & Dejong, J.T. 2016. Evaluating Liquefaction and Lateral Spreading in Interbedded Sand, Silt, and Clay Deposits Using The Cone Penetrometer. *Australian Geomechanics Society*

Jefferies, M.G. & Davies, M.P. 1991. Soil Classification by The Cone Penetration Test: Discussion. *Canadian Geotechnical Journal,* 28, 173–176.

Jorat, M.E., Mörz, T., Moon, V., Kreiter, S. & De Lange, W. 2015. Utilizing Piezovibrocone in Marine Soils at Touranga Harbor. *Geomechanics and Engineering,* 9, 1–14.

Kluger, M.O., Kreiter, S., L'heureux, J.S., Stegmann, S., Moon, V. & Moerz, T. 2016. In Situ Cyclic Softening of Marine Silts by Vibratory CPTU at Orkdalsfjord Test Site, Mid Norway. IN LAMARCHE ET AL., G. (Ed. *Submarine Mass Movements and their Consequences.* Advances in Natural and Technological Hazards Research 41.

Mayne, P.W. 2000. Evaluating Ground Liquefaction Potential by Piezovibrocone. GA Tech Res Corp—GIT.

Mcgillivary, A., Casey, T., Mayne, P.W. & Schneider, J.A. 2000. An Electro-Vibrocone for Site-Specific Evaluation of Soil Liquefaction Potential. *Innovations and Applications in Geotechnical Site Characterization.* GeoDenver

Mitchell, J.K. 1988. New Developments in Penetration Tests And Equipment. *Proceeding of ISOPT-1 -Penetration Testing*, Balkema, Rotterdam, **1**, 245–261.

Moore, D.M. 1987. Evaluation Of The Vibrating Cone Penetrometer and Its Effect on Cone Bearing and Pore Pressure. *Geological Engineering* Vancouver, The University of British Columbia.

NGI 2014. Time Effects on Pile Capacity. *Summary and evaluation of test results.* Norway.

Nogami, T., Ren, F., Chen, J.W. & Mason, A. Vertical Vibration of Pile in Vibration-Induced Excess Pore Pressure Field. *J. Geotech. Geoenviron. Eng.,* 123(5), 422–429.

O'neill, M.W., Vipulanandan, C. & Wong, D. 1990. Laboratory Modeling of Vibro-Driven Piles. *Journal of Geotechnical Engineering*, 116, 1190–1209.

Rodger, A.A. & Littlejohn, G.S. 1980. A Study of Vibratory Driving in Granular Soils. *Geotechnique*, 30, 249–293.

Sasaki, Y. & Koga, Y. 1983. Vibratory Cone Penetrometer to Assess The Liquefaction Potential of The Ground. In Chung, R.M., Lew, H.S. & Kovacs, W.D. (Eds.) *Proceedings of the 14th Joint Panel Conference of the U.S.-Japan Cooperative Program in Natural Resources*

Sasaki, Y. Itoh, Y. & Shimazu, T. 1984. A Study on The Rel Tionship Between The Results of Vibratorycone Penetration Tests And Earthquake-Induced Settlement Of Embankments. *In: Proceedings, 19th Annual meeting of JSSMFE*, Tokyo, Japan.

Shibata, T. & Teparaksa, W. 1988. Evaluation of liquefaction Potentials of Soils Using Cone Penetration Tests. *Soils and Foundations,* 28, 49–60.

Tokimatsu, K. 1988. Penetration Tests for Dynamic Problems. *Proceedings Penetration Testing ISOPT–1.*

Triebeneck, P. 2017. Geotechnische und Geologische Charakterisierung des Testfeldes in Oslebshausen. *Fachbereich Geowissenschaften.* Germany, Bremen, Universität Bremen.

Wise, C.M., Mayne, P.W. & Schneider, J.A. 1999. Prototype Piezovibrocone for Evaluating Soil Liquefaction Susceptibility. *Earthquake Geotechnical Engineering*, 537–542.

Cone Penetration Testing 2018 – Hicks, Pisanò & Peuchen (Eds)
© 2018 Delft University of Technology, The Netherlands, ISBN 978-1-138-58449-5

Estimation of geotechnical parameters by CPTu and DMT data: A case study in Emilia Romagna (Italy)

S. Amoroso
Istituto Nazionale di Geofisica e Vulcanologia, L'Aquila, Italy

P. Monaco
University of L'Aquila, L'Aquila, Italy

L. Minarelli
Geotema srl, University of Ferrara spin-off company, Ferrara, Italy

M. Stefani
University of Ferrara, Ferrara, Italy

D. Marchetti
Studio Prof. Marchetti, Rome, Italy

ABSTRACT: The aim of the paper is to illustrate and compare the results of CPTu and DMT tests carried out for a case study at Mirabello (Ferrara Province, Italy), a small municipality strongly affected by liquefaction phenomena during the 2012 Emilia earthquakes. The research site, that did not liquefy, is composed by silts and sandy silts in the shallow subsurface and by clays in lower layers. The paper compares the geotechnical parameters estimated from CPTu and DMT tests. The study also investigates the CPTu-DMT correlations according to available references (Robertson 2009, Ouyang & Mayne 2017).

1 INTRODUCTION

In the field of site investigations, the last decades have seen a massive migration from the traditional practice based on drilling, sampling, and laboratory testing towards in situ testing, which often today represents the major component of an investigation. In situ tests, not requiring a borehole, are fast, economical, reproducible, highly informative, particularly the electrical cone penetration test (CPT), the piezocone penetration test (CPTu), and the flat dilatometer test (DMT). The instrumental accuracy of CPT/CPTu and DMT is "laboratory-grade", unlike "older" techniques such as the standard penetration test (SPT). In situ tests are particularly helpful and represent the state-of-practice in sands and, in general, in geomaterials difficult to recover. Obviously laboratory research remains fundamental, also for understanding and advancing the in situ techniques.

One notable emerging trend, addressed in recent papers (e.g. Marchetti 2015, Burlon et al. 2016), is the increasing diffusion of a "multi-parameter/multi-test approach" in site investigation practice, based on the combination of different in situ tests, particularly CPTu and DMT. Significant examples of in-situ multi-parameter/multi-test approach are the methods based on the combined use of DMT and CPT or CPTu for estimating the overconsolidation ratio (OCR) in sand (Monaco et al. 2014) and for liquefaction assessment (Marchetti 2016).

Despite this increasing trend, and the use of the CPT and the DMT for over 30 years, relatively little has been published regarding comprehensive correlations between the two in situ tests. The CPT-DMT relationships are investigated through the checking of CPT and DMT data consistency.

In May 2012, a wide area of the Po river plain (Emilia-Romagna region, Northern Italy) was struck by a seismic sequence, culminated into two major events of magnitude M_L 5.9 and M_L 5.8 on May 20 and 29, respectively. The earthquakes caused extensive damage to constructions over a widespread area. Large ground deformations and extensive liquefaction phenomena were reported in several areas (Caputo & Papathanasiou 2012, Emergeo Working Group 2013, Fioravante et al. 2013, Vannucchi et al. 2012, Facciorusso et al. 2016), including the small municipality of Mirabello (Ferrara). In the following months, several site investigation programs were carried out, both for research purposes and for the reconstruction/restoration of damaged buildings.

This paper illustrates and compares the results of CPTu and DMT tests carried out at a site located in Mirabello, assumed as a case study representative of soil conditions commonly found in this area. The results of previous mechanical cone penetration tests (CPTM) were also considered. The site, which did not show evidence of liquefaction during the May 2012 earthquakes, is composed by silts and sandy silts at shallow depths, followed by clay layers.

The paper compares the geotechnical parameters obtained by CPTu and DMT tests in a relatively homogeneous geological setting. The study also investigates the CPTu-DMT correlations according to available references (Robertson 2009, Ouyang & Mayne 2017).

2 GEOLOGICAL SETTING

The research site belongs to the alluvial plain of the Emilia-Romagna Region, northern Italy, corresponding to the southern portion of the Apennines foredeep basin. The compressive tectonic structures active in the area generate a significant seismic activity. During the May 2012 earthquakes, liquefaction was particularly common within fluvial paleochannel sand bodies. The study sediments were deposited into the channel of the Reno River in recent historic times. The Reno is the largest river outflowing the Northern Apennines and transported into the plain a large sediment load, particularly rich in fine grained sand and silt. Historic written record documents that the outcropping sediments (Fig. 1) and the upper portion of the analyzed terrains were deposited by the Reno River, between about the years 1500 and 1763 AD.

Correlation with adjacent continuous cores (Cibin & Segadelli 2009) supports an accurate interpretation of the study succession, which can be subdivided into several intervals. From the surface to 4 m, intercalation of prevailing silt, sand, and argillaceous silt, deposited during the abandonment phase of the Reno River channel, in the first half of the XVIII century. From 4 to 9.5 m, fine grained sand and silt, recording the main phase of fluvial activity, during the XVI and XVII centu-

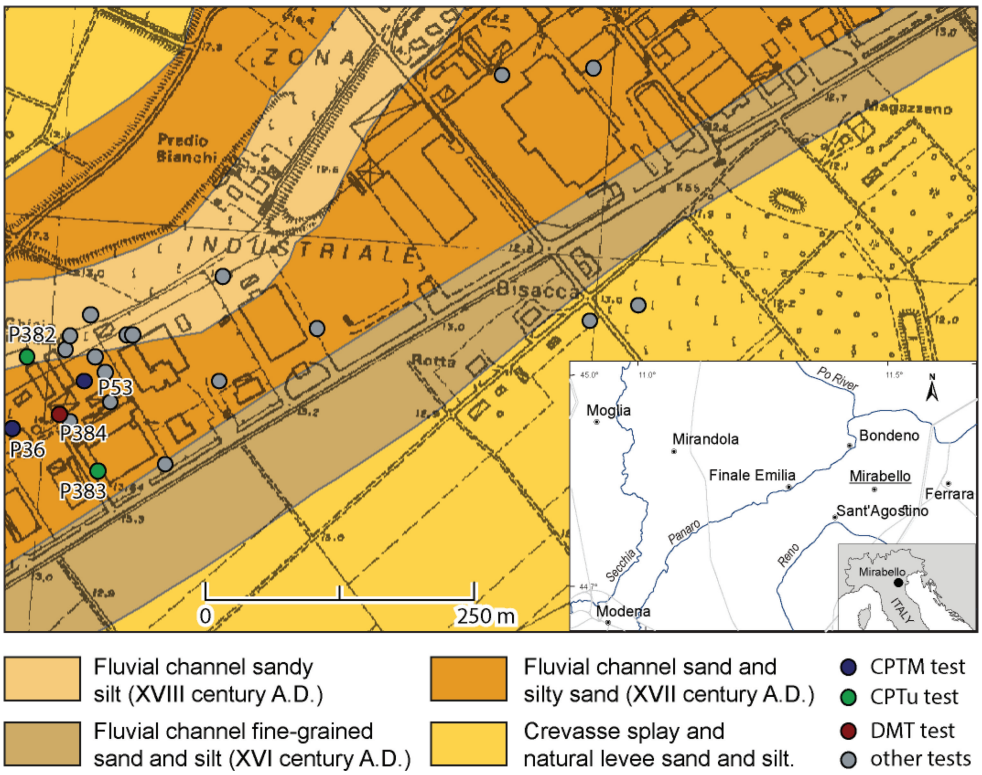

Figure 1. Geologic map of Mirabello (Italy) from the seismic microzonation study (Geotema 2014) and location of the in situ tests.

ries AD. From 9 to 15 m, argillaceous sediments deposited into moist interfluvial depressions and marshes, rich in organic clay and peat, particularly between 13 and 14 m. The unit lacks significant pedogenesis alteration. The peat interval at 14 m was dated to about 5000 yrs BP by ^{14}C in nearby cores (Cibin & Segadelli 2009). Between 15 and 20 m, silty clay and silt, deposited between 10.000 and 5000 years ago, into interfluvial plain environments, are developped. Several pedogenized horizons were described in adjacent logs. Beyond 20 m, silt and sand deposited into the synglacial plain. The top of the Glacial unit is marked by a mature palaeosol, rich in carbonate concretions.

3 SITE INVESTIGATION BY CPTU AND DMT

The Mirabello site was investigated in 2014–2016 by two CPTu soundings, to 30 m depth, and one DMT sounding, to 21.60 m depth. The results of two CPTM soundings to 7–20 m depth, previously carried out in the area, were also available.

The location of all in situ tests in the study area is shown in Figure 1. The interpretation of CPTu, CPTM and SDMT results allowed recognizing the following stratigraphic sequence from the ground surface:

- an upper soil layer, of thickness variable between 8 and 10 m, mostly composed of silts and sandy silts, corresponding to the Reno River channel deposits;
- a lower clay layer extending to the maximum investigated depth (≈ 30 m), including sand layers in the bottom portion.

The ground water level is at a depth of 1.65–2.40 m below ground surface.

Figure 2 shows the profiles of the corrected cone resistance q_t (CPTu) or of the cone resistance q_c (CPTM), of the sleeve friction resistance f_s and of the pore pressure u (CPTu) provided by all CPTu and CPTM soundings. The plot also includes results from CPTu data interpretation, i.e. the profile of the Soil Behavior Type Index I_c, calculated from the normalized cone resistance Q_{t1} and the normalized friction ratio F_r according to Robertson & Wride (1998), and of the undrained shear strength c_u in clays (Lunne et al. 1997).

Figure 3 shows the results obtained from DMT, in terms of profiles with depth of various parameters provided by the usual DMT interpretation (Marchetti 1980, Marchetti et al. 2001), i.e. the material index I_D (indicating soil type), the horizontal stress index K_D (related to stress history/ OCR), the constrained modulus M and the undrained shear strength c_u (in clay). The two negative peaks observed in the horizontal stress index diagram at about 15 and 20 m correspond to two increases of the material index. The lower one correlates with the highest measured value of the dilatometer modulus, exceeding 30 MPa. Stratigraphic correlation with adjacent cores suggests that these layers correspond to paleosol levels. The lower well developed one marks the top of the syn—and late glacial deposits and is rich in calcareous concretions, largely stiffening the geotechnical properties of the layer. Correlations with the granulometry measurements on samples suggest that the material index terminology tends to underestimate the amount of silt sized granular components, but this is reasonable, since I_D is a mechanical soil behavior index and not a grain size distribution index.

The CPTu and DMT profiles (Figs. 2 and 3) provide a consistent soil characterization in the

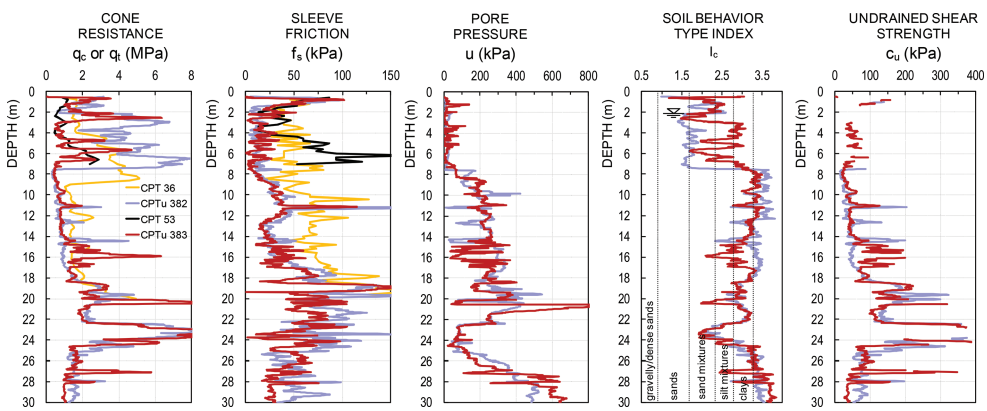

Figure 2. Profiles with depth of parameters measured by CPTu and CPTM and obtained by CPTu interpretation.

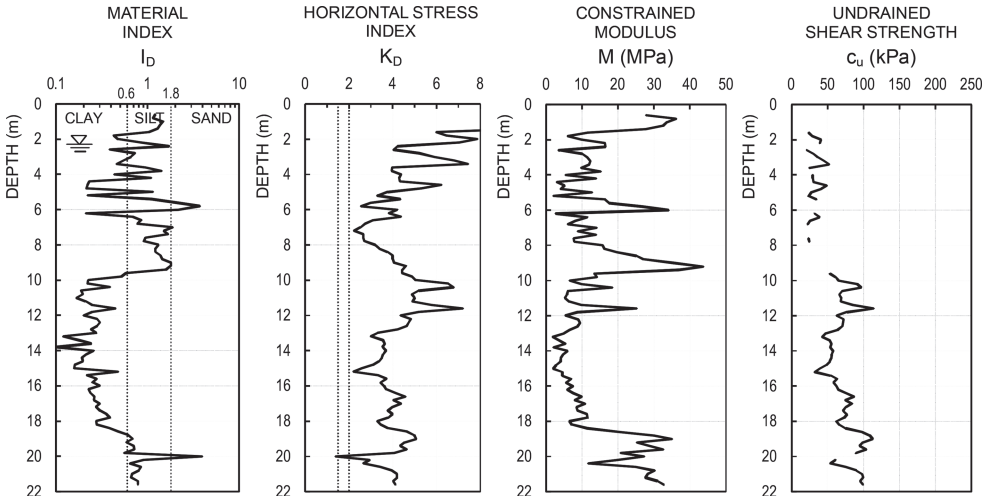

Figure 3. Profiles with depth of parameters obtained by DMT interpretation.

upper silty-sandy interval and in the lower clayey layer. The soil variability in the upper layer is justified by the local geology. In particular, the profiles of CPTu 382 clearly highlight the presence of sands, since this sounding belongs to the bed of the latest Reno paleochannel, while the other CPTu and the DMT, where the shallow soils are mostly silty sands and clays, are related to the levee of this ancient river. The interpretation of DMT results in clay indicates that the deposit is slightly overconsolidated, probably because of the subaerial exposure and strong pedogenesis alteration.

4 CPTU-DMT COMPARISONS

Robertson (2009) reviewed published results of mutually close CPT and DMT soundings, as well as existing correlations for geotechnical parameters. He proposed preliminary correlations between the main normalized parameters of the CPT and the DMT. The DMT horizontal stress index K_D and the CPT normalized cone resistance Q_{t1} were normalized in a consistent manner, using the vertical effective stress (i.e. assuming the stress exponent for stress normalization equal to 1, as originally proposed by Robertson 1990).

Correlations were tentatively established by considering the three "intermediate" DMT parameters material index I_D, horizontal stress index K_D and dilatometer modulus E_D (Marchetti 1980). These parameters were related to the CPT normalized cone resistance Q_{t1}, the normalized friction ratio F_r and the Soil Behavior Type Index I_c. The above parameters are defined as follows:

$$I_D = \frac{p_1 - p_0}{p_0 - u_0} \tag{1}$$

$$K_D = \frac{p_0 - u_0}{\sigma'_{v0}} \tag{2}$$

$$E_D = 34.7(p_1 - p_0) \tag{3}$$

$$Q_{t1} = \frac{q_t - \sigma_{v0}}{\sigma'_{v0}} \tag{4}$$

$$F_r = \left[\frac{f_s}{(q_t - \sigma_{v0})}\right] 100\% \tag{5}$$

$$I_c = \left[(3.47 - \log Q_{t1})^2 + (\log F_r + 1.22)^2\right]^{0.5} \tag{6}$$

where p_0 = corrected first DMT pressure reading, p_1 = corrected second DMT pressure reading, q_t = corrected cone resistance, f_s = sleeve friction resistance, u_0 = pre-insertion in situ equilibrium water pressure, σ_{v0} = pre-insertion in situ total vertical stress, σ'_{v0} = pre-insertion in situ effective vertical stress.

The CPT-DMT correlations proposed by Robertson (2009) can be summarized as follows:

$$I_D = 10^{(1.67 - 0.67 I_c)} \tag{7}$$

$$K_D = 0.3(Q_{t1})^{0.95} + 1.05 \text{ when } I_c > 2.60 \tag{8a}$$

$$K_D = \frac{0.144 Q_{t1}}{10^{(1.67 - 0.67 I_c)}} \text{ when } I_c < 2.60 \tag{8a}$$

$$E_D / \sigma'_{v0} = 5 Q_{t1} \tag{9}$$

The value I_c = 2.60, roughly corresponding to $I_D \approx 1$ based on Eq. (7), is assumed as an

approximate boundary between sand-like and clay-like soils (sandy silt to silty clay), according to Robertson & Wride (1998). In a general sense, CPT and DMT results are drained in sand-like soils and undrained in clay-like soils.

The Mirabello site provides a good test for the Robertson (2009) CPT-DMT correlations, since the soils range from sand, silt and sandy silt to clay. A comparison between measured and predicted DMT parameters I_D, K_D, E_D with depth based on the closest CPTu profile (CPTu 382), using Eqs. (7) to (9), is shown in Figure 4. Although CPTM 36 is even closer to DMT 384, the CPT-DMT correlations proposed by Robertson (2009) are not valid for mechanical cone penetration test results. Moreover, CPTM results are characterized by a lower accuracy when compared to CPT or CPTu data (e.g. see the high variability of the sleeve friction resistance f_s in Fig. 2). The comparison between the measured DMT parameters and those predicted from the CPTu data using the Robertson (2009) correlations show reasonable trends of correlation, particularly in the lower clay layer. Some "mismatching" in the superimposed profiles is possibly due to the different thickness of the upper silty/sandy-silty/sandy layer at the locations of the DMT and the CPTu, due to the narrow and elongated nature of the channel sedimentary body. In the upper silty layer DMT 384 and CPTu 382 cannot provide a good fit since CPTu 382 is more sandy, corresponding to the bed of the latest Reno paleochannel.

Ouyang & Mayne (2017) explored the relationships between the net cone resistance q_{net} and the excess pore pressure Δu_2, measured in a CPTu test, and the pressures p_0, p_1 measured in a DMT test, in soft clays.

The relationships proposed by Ouyang & Mayne (2017) are based on an assumed spherical cavity expansion mechanism for both devices, and supported by field measurements at 27 clay sites.

The net cone resistance q_{net}, defined as:

$$q_{net} = q_t - \sigma_{v0} \tag{10}$$

is linked to the DMT pressure readings p_0, p_1 by the following relationship:

$$q_{net} = 2.93p_1 - 1.93p_0 - u_0 \tag{11}$$

Figure 5 shows a comparison of the profiles of the net cone resistance directly measured by CPTu and predicted by DMT using Eq. (11) in the bottom clay layer. The two profiles are in rather good agreement, as observed by Ouyang & Mayne (2017) in various clays sites. The DMT data found a reasonable fit with the results obtained by CPTu 382.

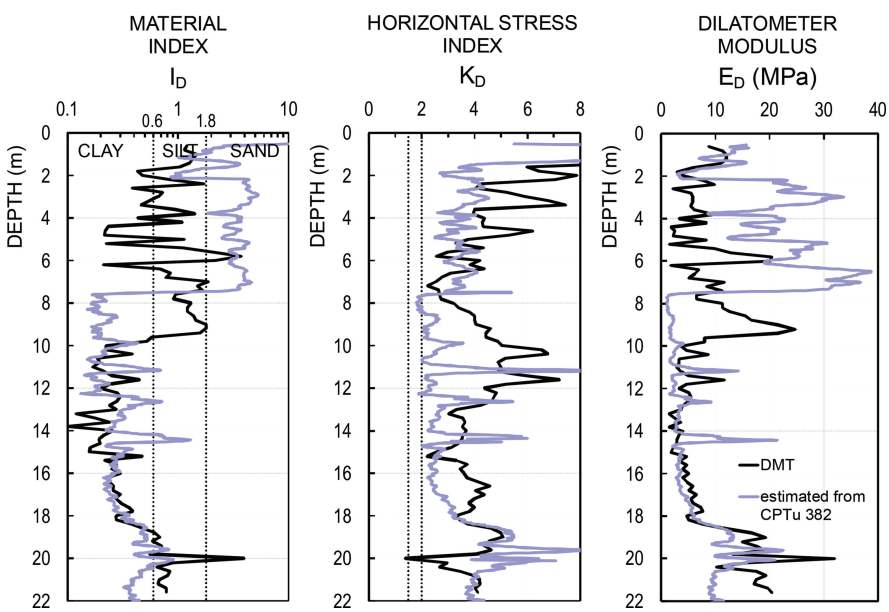

Figure 4. Comparison between profiles with depth of parameters I_D, K_D, E_D measured by DMT and predicted using the CPT-DMT correlations by Robertson (2009) at Mirabello site, Italy.

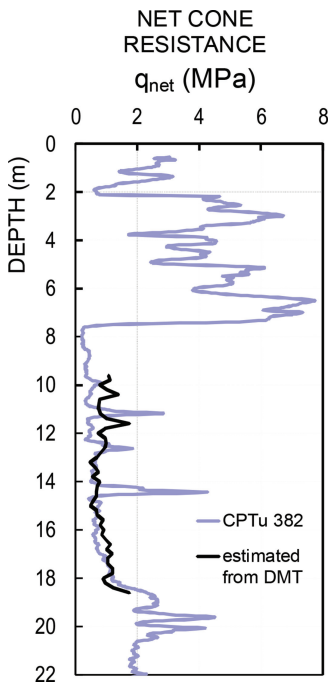

Figure 5. Comparison between profiles with depth of net cone resistance q_{net} measured by CPT and predicted using the CPTu-DMT relation by Ouyang & Mayne (2017) at Mirabello site, Italy.

5 CONCLUSIONS

The comparisons of the CPTu and DMT tests carried out for a case study at Mirabello (Ferrara Province, Italy) provide a consistent soil characterization in the upper silty-sandy clayey interval and in the lower clay one. However a certain heterogeneity is detectable in the upper layer and it is justified by the variability of the local geology.

The geotechnical parameters estimated from CPTu and DMT tests, according to available references (Robertson 2009, Ouyang & Mayne 2017), show a reasonable agreement, especially in the lower clay layer, when the electrical piezocone tip is used.

As noted by Marchetti (2011), the ultimate scope of all soil characterization studies is the determination of reliable soil parameters that the engineer can use in design. Soil information is vital for the designer, but costly to obtain, hence procedures and methods helpful for extracting as much information as possible from the field data represent a precious contribution. Correlations interconnecting the CPT or CPTu with the DMT, while not serving directly to determine design soil parameters, are useful in that translation formulas permit (1) the use of interpretation methods or charts developed for one test with the results of the other test, and (2) converting a database available for one test (e.g. liquefaction) to a database for the other test.

However, while correlations such as the ones developed by Robertson (2009) are presented as a framework for future refinements, intrinsic limits exist to the accuracy of the CPT-DMT translations, which, despite further refinements, are bound to remain of an approximate nature. This difficulty is attributed by Marchetti (2011) mostly to the different sensitivity to stress history of the representative normalized CPT and DMT parameters, being K_D from DMT much more sensitive to stress history than the normalized cone resistance, as demonstrated by several studies.

The higher sensitivity of K_D to stress history plays an important role when CPT or CPTu and DMT parameters are used in combination (not as an alternative), e.g. for estimating OCR in sand (Monaco et al. 2014) or for liquefaction assessment (Marchetti 2016), according to a most effective in-situ multi-parameter/multi-test approach.

REFERENCES

Burlon, S., Frikha, W. & Monaco, P. 2016. Session Report: Pressuremeter and Dilatometer. *Proc. 5th Int. Conf. on Geotechnical and Geophysical Site Characterization ISC'5*, Gold Coast, Australia, 5–9 September 2016, B.M. Lehane, H.E. Acosta-Martínez & R. Kelly (eds), 1: 259–269. Australian Geomechanics Society, Sydney, Australia.

Caputo, R. & Papathanasiou, G. 2012. Ground failure and liquefaction phenomena triggered by the 20 May, 2012 Emilia-Romagna (Northern Italy) earthquake: case study of Sant'Agostino—San Carlo—Mirabello zone. *Natural Hazards and Earth System Sciences* 12(11): 3177–3180.

Cibin, U. & Segadelli, S. 2009. Note Illustrative della Carta Geologica d'Italia alla scala 1:50.000, Foglio 203, Poggio Renatico. Servizio Geologico d'Italia, 104 (in Italian).

Emergeo Working Group 2013. Liquefaction phenomena associated with the Emilia earthquake sequence of May-June 2012 (Northern Italy). *Natural Hazards and Earth System Sciences* 13 (4): 935–947.

Facciorusso, J., Madiai, C. & Vannucchi, G. 2016. The 2012 Emilia earthquake (Italy): geotechnical characterization and ground response analyses of the paleo-Reno river levees. *Soil Dynamics and Earthquake Engineering* 86: 71–88.

Fioravante, V., Giretti, D., Abate, G., Aversa, S., Boldini, D., Capilleri, P., Cavallaro, A., Chamlagain, D., Crespellani, T., Dezi, F., Facciorusso, J., Ghinelli, A., Grasso, S., Lanzo, G., Madiai, C., Massimino, M.R., Maugeri, M., Pagliaroli, A., Ranieri, C., Tropeano, G., Santucci De Magistris, F., Sica, S., Silvestri, F. & Vannucchi, G. 2013. Earthquake geotechnical engineering

aspects: the 2012 Emilia-Romagna earthquake (Italy). *Proc. 7th Int. Conf. on Case Histories in Geotechnical Engineering*, Chicago, 1–34.

Geotema 2014. Microzonazione sismica Livello 2 con locali approfondimenti di Livello 3, Regione Emilia-Romagna. Comune di Mirabello (FE), Relazione illustrativa e 7 tavv. http://www.comune.mirabello.fe.it/files/00036/relazione_ms_mirabello.pdf (in Italian).

Lunne, T., Robertson, P.K. & Powell, J.J.M. 1997. *Cone Penetration Testing in Geotechnical Practice*. Blackie Academic & Professional, New York.

Marchetti, S. 1980. In Situ Tests by Flat Dilatometer. *J. Geotech. Eng. Div.* 106(GT3): 299–321.

Marchetti, S. 2011. Discussion of "CPT-DMT Correlations" by P.K. Robertson. *J. Geotech. Geoenviron. Eng.* 134(4): 443–447.

Marchetti, S. 2015. Some 2015 Updates to the TC16 DMT Report 2001. *Proc. 3rd Int. Conf. on the Flat Dilatometer DMT'15, Rome, Italy, 14–16 June 2015*. S. Marchetti, P. Monaco, & A. Viana da Fonseca (eds), 43–65.

Marchetti, S. 2016. Incorporating the Stress History Parameter K_D of DMT into the Liquefaction Correlations in Clean Uncemented Sands. *J. Geotech. Geoenviron. Eng.* 142(2): 04015072.

Marchetti, S., Monaco, P., Totani, G. & Calabrese, M. 2001. The Flat Dilatometer Test (DMT) in Soil Investigations—A Report by the ISSMGE Committee TC16. Official version approved by ISSMGE TC16 reprinted in *Proc. 2nd Int. Conf. on the Flat Dilatometer*, Washington, D.C., April 2–5, 2006, R.A. Failmezger & J.B Anderson (eds), 7–48.

Monaco, P., Amoroso, S., Marchetti, S., Marchetti, D., Totani, G., Cola, S. & Simonini, P. 2014. Overconsolidation and Stiffness of Venice Lagoon Sands and Silts from SDMT and CPTU. *J. Geotech. Geoenviron. Eng.* 140(1): 215–227.

Ouyang, Z. & Mayne, P.W. 2017. Spherical cavity expansion nexus between CPTu and DMT in soft-firm clays. *Proc. 19th Int. Conf. on Soil Mechanics and Geotechnical Engineering*, Seoul, Korea, 17–22 September, 2017, W. Lee, J.S. Lee, H.K. Kim & D.S. Kim (eds), 631–634. Korean Geomechanics Society, Seoul, Korea.

Robertson, P.K. & Wride, C.E. 1998. Evaluating cyclic liquefaction potential using the cone penetration test. *Can. Geotech. J.* 35(3): 442–459.

Robertson, P.K. 1990. Soil classification using the cone penetration test. *Can. Geotech. J.* 27(1): 151–158.

Robertson, P.K. 2009. CPT-DMT Correlations. *J. Geotech. Geoenviron. Eng.* 135(11): 1762–1771.

Vannucchi, G., Crespellani, T., Facciorusso J., Ghinelli, A., Madiai, C., Puliti, A. & Renzi, S. 2012. Soil liquefaction phenomena observed in recent seismic events in Emilia-Romagna Region, Italy. *Ingegneria Sismica* 2–3: 20–3.

Taylor & Francis
Taylor & Francis Group
http://taylorandfrancis.com

Cone Penetration Testing 2018 – Hicks, Pisanò & Peuchen (Eds)
© 2018 Delft University of Technology, The Netherlands, ISBN 978-1-138-58449-5

Cone penetration testing on liquefiable layers identification and liquefaction potential evaluation

E. Anamali
In Situ Site Investigation, Balkans

L. Dhimitri & D. Ward
In Situ Site Investigation, UK

J.J.M. Powell
Geolabs Limited, UK

ABSTRACT: This paper presents the results of liquefaction potential evaluation for various sandy sites, with high seismic risk, where soil liquefaction is a major concern for all structures supported on these kinds of soils. There are many methods available for these calculations, based on different site investigation techniques. The Cone Penetration Test (CPTU) provides ideal data for this purpose, due to its repeatability and reliability. CPTU based methods on soil liquefaction assessment are important not only to identify liquefiable layers, but also their state in situ. This paper looks at results of liquefaction analyses on different sites susceptible to liquefaction, using CPTU based methods and also compares them with methods that are Standard Penetration Test (SPT) based, but using SPT data derived from correlations to CPTU results.

1 INTRODUCTION

Evaluating the liquefaction characteristics of soils is one of the major challenges in geotechnical engineering, when it comes to the design of structures supported on saturated or partially saturated sandy and silty soils. In response to an earthquake shaking or sudden stress changes the strength and stiffness of these soils can be dramatically reduced. Over the years, many advances have occurred in evaluating the liquefaction potential of soils. Most importantly, there has been significant advancement since the early 1980s in CPT—based liquefaction potential identification procedures with the work of Robertson & Wride (1998), Moss et al. (2006) and Idriss & Boulanger (2008, 2010). Also, developments have taken place in SPT—based procedures, the most recent updates include those by Idriss & Boulanger (2008, 2010) (Idriss & Boulanger, 2014).

To evaluate the potential for soil liquefaction it is important to determine the soil stratigraphy and in-situ state of the deposits (Lunne et al. 1997). As they are able to identify all types of soils, CPTU and SPT are the most commonly used methods for site investigations in all kinds and sizes of projects. CPTU's ability to define a continuous soil profile, to identify thin layers, its repeatability and also accuracy of data acquisition makes it an ideal test for soil characterisation, and especially liquefaction potential evaluation. All methods used in this paper evaluate liquefaction potential by comparing the earthquake-induced cyclic stress ratio (CSR) with the cyclic resistance ratio (CRR) of the soil. The soil's CRR is correlated to CPTU and SPT penetration resistances after application of procedural and overburden stress corrections (Idriss & Boulanger, 2008, 2014). The liquefaction potential is evaluated by using a deterministic relationship expressed as a factor of safety (FoS), defined as the ratio of the capacity of soil to resist liquefaction, CRR, to the seismic demand imposed on it, CSR (Seed & Idriss, 1971), which predicts liquefaction of soils for values FoS≤1.0. CRR is calculated for a 7.5 magnitude earthquake and scaled to the design earthquake by a magnitude scaling factor (MSF).

In this paper, FoS has been computed applying the most widely used CPTU and SPT based liquefaction triggering procedures—for CPTU: Robertson & Wride (1998), Jefferies & Been (2006), Idriss & Boulanger (2008) and Idriss & Boulanger (2008) using fines content, FC determined from Robertson & Wride (1998). For SPT: Cetin et al. (2004), Idriss & Boulanger (2004) and Youd & Idriss

(2001). In the end, to predict the potential of liquefaction to cause near surface damage at the sites considered in this paper, the liquefaction potential index, LPI (Iwasaki et al, 1978, 1981, 1982) is calculated based on the method developed by Toprak & Holzer (2003).

This paper uses selected data from sites susceptible to liquefaction, where in situ site investigations using CPTU tests were carried out, with great success on identifying the soils' geotechnical properties and locating the liquefiable silty sandy layers within the soil profiles. The purpose of the paper is to suggest that the use of CPTU to identify liquefiable layers is reliable and the results obtained from liquefaction triggering procedures are very satisfactory, and in good agreement with SPT based methods.

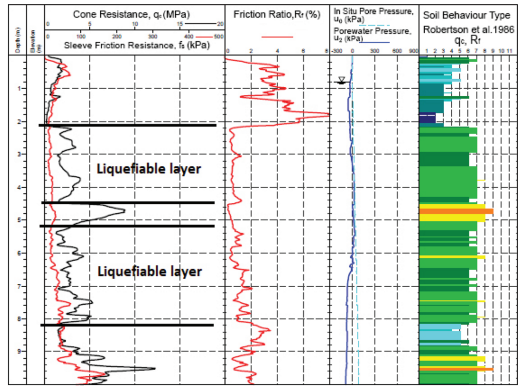

Figure 1. Typical CPTU profile (T1 CPT 01).

2 SITES SPECIFIC DATA PROCESSING

2.1 *Geotechnical conditions*

For the purpose of this paper, results from 50 CPTU tests (from 8.0 m to 40.0 m depth) carried out as part of geotechnical site investigation programs for 8 different sites, in areas susceptible to liquefaction, are considered. All sites are mainly sand and silty sand deposits with a high evaluated seismic risk. The groundwater level is measured close to the ground surface, varying from site to site from 0.8 m to 2.0 m, for all sites, except site A, where ground water level is 10.0 m below ground surface. According to geophysical test results carried out on these sites, the earthquake magnitudes vary from $M = 6.9$ to $M = 7.5$, and the peak horizontal accelerations at the ground surface generated by the earthquakes, *PGA*, vary from 0.273 g to 0.3 g.

To include a summary table for all tests, presenting the geotechnical properties and all results from liquefaction analyses, would take too much space, but full data details are available from the authors, for all interested readers. Summary tables of some important parameters are presented below.

Figure 1 shows a typical CPTU profile from one of the sites considered, where the liquefiable layers are easily distinguished.

2.2 *Soil behavior type index, I_c, fines content, FC, and penetration resistance from SPT, $(N_1)_{60}$*

The response of soils to seismic loading varies with soil type and state, including void ratio, stress history, etc. It is possible to estimate soil type and grain characteristics directly from CPTU results (Lunne et al. 1997) and also an idea of derived fines content, FC. Boulanger & Idriss (2004) correctly distinguished between *sand-like* and *clay-like* soils behaviour (Robertson & Cabal, 2015). The soil behaviour type index, I_c for the calculations in this paper is defined using Robertson & Wride (1998) method, which suggests estimating behaviour characteristics using the normalized soil behaviour chart SBT_n of Robertson (1990). Robertson & Wride (1998) suggested that the boundary between *sand-like* and *clay-like* behaviour is around $I_c = 2.60$. Furthermore, Robertson (2009) suggested that when $I_c \leq 2.50$ soils are assumed to behave as *sand-lik*e and when $I_c > 2.70$ soils behave as *clay-like*. For values in between, $2.5 < I_c \leq 2.70$, soil behaviour is represented as a transition from predominately *sand-like* to predominately *clay-like* (Robertson & Cabal, 2015). Robertson & Wride (1998) suggested zones in which soils are susceptible to liquefaction based on the normalized soil behaviour chart, Robertson (1990), and so the chart was updated showing the zones of potential liquefaction/ softening based on CPTU data (Robertson & Cabal, 2015).

All data from CPTU tests used for calculations in this paper are printed out in the updated chart, considering different values of FC, which are calculated based on 2 different methods: FC_1 by Robertson & Wride (1998) and FC_2 by Suzuki et al. (1998).

$FC \leq 15\%$, which corresponds to $I_c < 2.05$; $15\% < FC \leq 35\%$, which corresponds to $2.05 < I_c \leq 2.6$; $35\% < FC \leq 55\%$, which corresponds to $2.6 < I_c \leq 2.95$.

The SPT penetration resistance, N_{60} used in the SPT-based liquefaction triggering procedures is defined from Robertson & Wride (1998) and Jefferies & Davies (1993). Both methods derive it from CPTU data. The reason why it is preferred to derive N_{60} from CPTU, rather than SPT itself, is because the data from CPTU are *more reliable and continuous*, so giving a larger data basis.

Table 1 presents a summary of derived geotechnical parameters from the different sites that are needed to assess liquefaction potential; only data from liquefiable layers are considered.

The updated chart, Robertson & Cabal (2015), used for classification of liquefiable soils in all sites considered is based on the normalized cone resistance,Q_{tn} (see Robertson & Cabal 2015), (Figs. 2a, b, c) calculated using a stress exponent that varies with soil type via I_c, whereas the recommended chart for estimating $CRR_{7.5}$ is based on a normalized cone resistance based on a variable stress exponent, updated to allow for a variation of the stress exponent with both SBT_n, I_c and effective overburden stress (Robertson 2009, Robertson & Cabal 2015).

Soils are divided into coarse grained soils: CD & CC, cyclic liquefaction possible depending on level and duration of cyclic loading and strength loss possible depending on loading and ground geometry (I_c<2.50); and fine-grained soils: FD & FC, cyclic softening possible depending on level and duration of cyclic loading and strength loss possible depending on soil sensitivity, loading and ground geometry (I_c>2.70) (Robertson & Cabal, 2015).

The data presented in Figures 2 a, b, c, are for values of fines content varying from FC < 15%, 15%< FC ≤35% and 35%< FC ≤55%, respectively.

Table 1. Summary of geotechnical parameters.

Sites	I_c (var.)*	I_c (av.)	FC_1 (av.)	FC_2 (av.)	N_{160} (var.)*	N_{160} (av.)
A	1.74–3.49	2.61	23.07	24.59	1–26	11.25
G	1.42–3.28	2.35	13.87	17.24	1–20	10.95
H	1.53–3.25	2.39	15.94	19.12	2–20	10.04
L	1.43–2.86	2.42	28.4	28.50	5–20	10.08
P	1.39–3.41	2.40	17.13	19.55	2–28	13.11
S	1.55–3.29	2.42	36.11	32.85	1–20	4.448
T1	1.50–3.30	2.40	35.73	32.40	2–21	5.873
T2	1.81–3.63	2.72	51.05	44.37	1–21	4.730

* Variation of the values (min-max) for each site

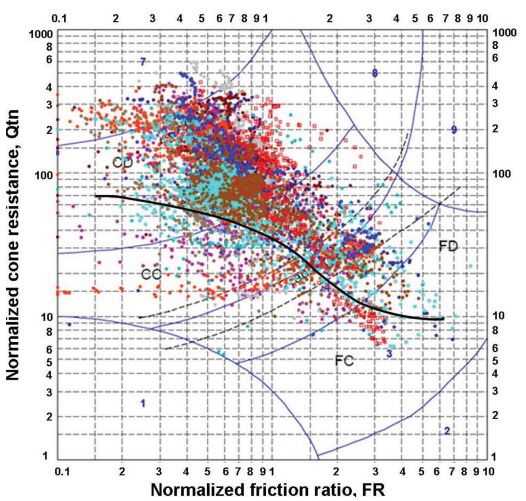

Figure 2a. Normalized SBT_n chart, Q_{tn}-FR using general large strain "soil behavior descriptors" for FC≤15%.

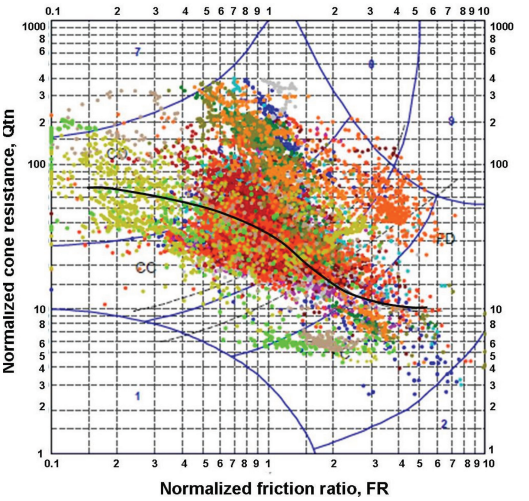

Figure 2b. Normalized SBT_n chart, Q_{tn}-FR using general large strain "soil behavior descriptors" for 15 < FC ≤ 35%.

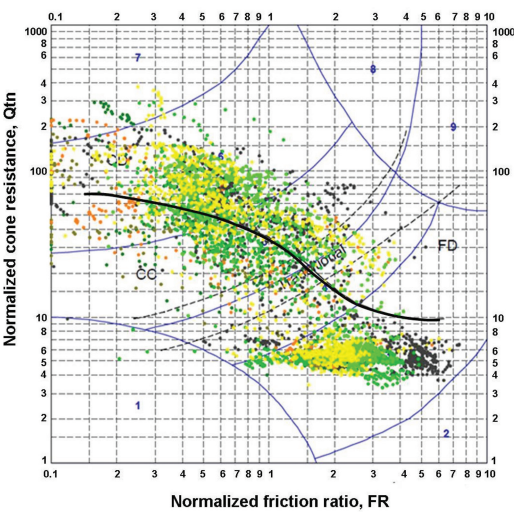

Figure 2c. Normalized SBT_n chart, Q_{tn}-FR using general large strain "soil behavior descriptors" for 35 < FC ≤ 55%.

All points plotting above the transitional zone ($2.5<I_c\leq 2.70$) represent soils under drained conditions and all points plotting below it represent soils under undrained conditions. Considering the *S* shaped line as a boundary for dilative and contractive soils, all points plotting above it represent dilative soils, whereas all points plotting below this curve represent contractive soils.

3 LIQUEFACTION ANALYSIS

3.1 *Methods and data input*

As mentioned above the liquefaction potential based on CPTU data is evaluated from the value of Factor of Safety (FoS), obtained by the following 4 methods:

1. FoS_1-Robertson & Wride (1998), which uses CSR as proposed by Seed & Idriss (1971) (called CSR_1 in the figures) and CRR, proposed by Robertson & Wride (1998), using FC_1;
2. FoS_2-Jefferies & Been (2006), which uses CSR as proposed by Seed & Idriss (1971) (called CSR_1 in the figures) and CRR proposed by Jefferies & Been (2006), using FC_2;
3. FoS_3-Idriss & Boulanger (2008), which uses CSR as proposed by Idriss & Boulanger (2008) (and called CSR_2 in the figures) and CRR proposed by Idriss & Boulanger (2008) using FC_2;
4. FoS_4-Idriss and Boulanger (2008), which uses CSR as proposed by Idriss & Boulanger (2008) (and called CSR_2 in the figures) and CRR proposed by Idriss & Boulanger (2008) using FC_1.

Liquefaction potential based on SPT values (estimated from the CPTU results) is evaluated from the value of Factor of Safety (FoS), obtained by the following 3 methods:

1. FoS_1-Cetin et al. (2004), which uses CSR proposed by Seed & Idriss (1971), where stress reduction factor, r_d is used after Cetin et al. (2014) and CRR, proposed by Cetin et al. (2004) deterministic;
2. FoS_2-Idriss & Boulanger (2004), which uses CSR and CRR proposed by Idriss & Boulanger (2004);
3. FoS_3-Youd et al. (2001), which uses CSR and CRR proposed Youd et al. (2001).

Figure 3 presents liquefaction analysis results based the data from a CPTU test.

3.2 *Results of calculations*

All CPTU data based calculations for this paper are computed using Datgel-CPT Tool gINT. All SPT data based calculations are computed using Settle^{3D} Version 4.0-Liquefaction Analysis.

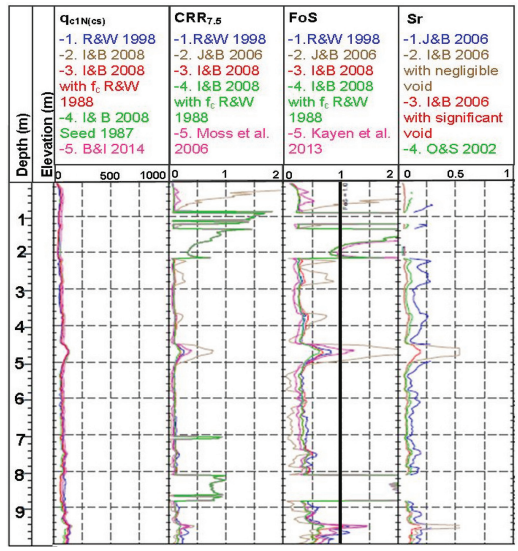

Figure 3. Results of CPTU liquefaction analysis(T1 CPT 01).

Table 2 presents a summary of the results from all sites from the liquefaction analyses, expressed by the average value of FoS from each method of calculation, based on CPTU and SPT data and Liquefaction Potential Index, LPI results derived from FoS_1 for both CPTU and SPT based methods.

The CPT—based methods used for these liquefaction analyses assess the $CRR_{7.5}$ by estimating the clean-sand equivalent normalized cone resistance, $(q_{c1\,N})_{cs}$, which depends on behaviour characteristics of the soils, fines content and many other factors, in order to avoid different results for $CRR_{7.5}$ in silty sands and clean sands. In Figure 4 is presented the distribution of data for various values of fines content, determined by I_c correlations. All the data plotted in the Figure 4 is from liquefiable layers only.

In Figure 5, results from different CPT—based methods are compared to the CRR curve derived from Idriss & Boulanger (2004). The results of these calculations are in good agreement with the triggering curve derived from Idriss & Boulanger (2004).

An updated graph from Idriss & Boulanger (2004) for our soil conditions is presented in Figure 6. The CRR curves are developed from the SPT—based methods mentioned above, using the necessary parameters for calculations, only for liquefiable layers of soils, for all sites considered in this paper. Curves 1 to 9 present the results, obtained from each calculation method for different fines content, as follows:

10%<FC < 15%; 15%<FC < 35%; 35%<FC < 55%. Curve 10 in this graph is the

Table 2. Summary of FoS and LPI from liquefaction analysis based from CPTU and SPT data.

	From CPTU analysis*					From SPT analysis*			
Sites	FoS_1	FoS_2	FoS_3	FoS_4	LPI	FoS_1	FoS_2	FoS_3	LPI
A	0.3	0.1	0.3	0.3	29	0.3	0.5	0.5	20
G	0.3	0.4	0.3	0.2	29	0.6	0.7	0.6	18
H	0.3	0.3	0.3	0.2	29	0.5	0.6	0.6	17
L	0.5	0.3	0.5	0.4	16	0.5	0.6	0.6	17
P	0.5	0.4	0.6	0.4	22	0.4	0.4	0.4	23
S	0.4	0.3	0.4	0.4	22	0.3	0.5	0.4	23
T1	0.4	0.4	0.4	0.4	26	0.3	0.5	0.4	22
T2	0.4	0.3	0.4	0.3	29	0.3	0.4	0.4	24

* Average of the values for each site, considering all liquefiable layers for each test.

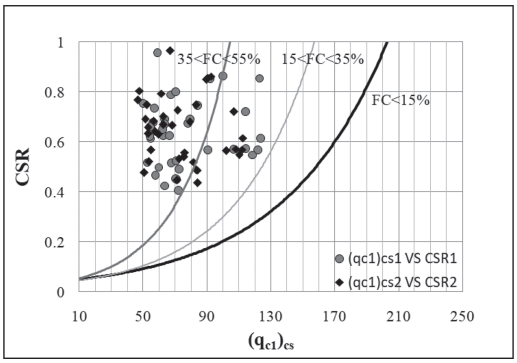

Figure 4. Results of CPT—based triggering correlations for the sites considered in this paper, for different values of FC (%) determined by I_c correlations.

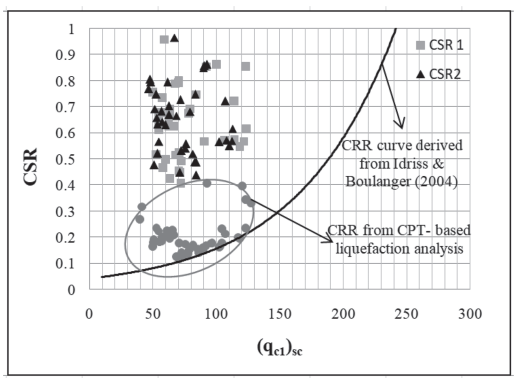

Figure 5. Distribution of data from CPT—based triggering correlations for the sites considered in this paper.

original Idriss & Boulanger (2004) curve, whereas curve 11 is obtained from SPT—based calculation methods carried out for the purpose of this

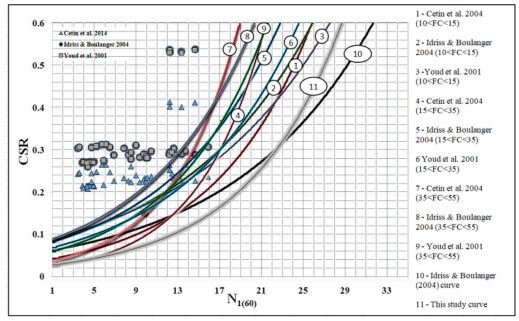

Figure 6. Results of SPT—based triggering correlations from different methods used for liquefaction potential evaluation of the sites considered in this paper, for different values of FC (%) determined by I_c correlations.

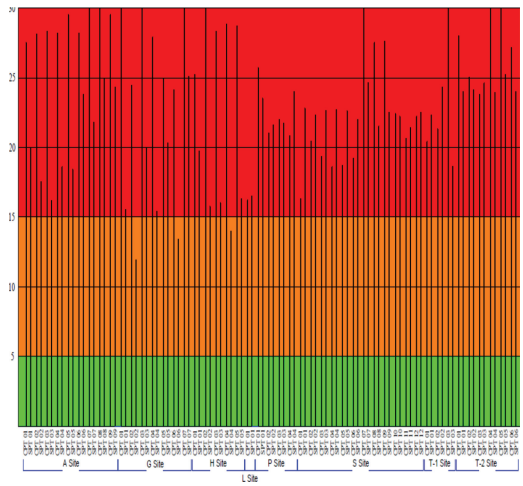

Figure 7. Distribution of LPI results obtained by Robertson & Wride (1998) method for all sites.

paper. The CRR curves shift up to the left as the FC increases, with the maximum shift occurring for fines content varying from 35% to 55%. All the data points falling in the left side of the curves represent the liquefiable soils; meanwhile the data points in the right would represent the non liquefiable soils.

To predict the potential of liquefaction to cause damage at the surface level, Liquefaction Potential Index, LPI is evaluated for each test using the predicted factors of safety, taking into account depth of the tests (the soils below 20.0 m depth are not considered in LPI evaluation) and thickness of the layers (Iwasaki et al. 1978).

In Figure 7 are presented the results obtained by the LPI evaluation, based on the method proposed by Toprak & Holzer (2003).

The risk from liquefaction phenomena, based on LPI results is categorized as:

Low risk—LPI ≤ 5- green band;
High risk- 5 < LPI ≤ 15- orange band;
Very high risk—LPI > 15- red band.

As presented in the Figure 7, the LPI mostly shows zones with high to very high risk for liquefaction potential. The results are consistent with the low factors of safety obtained by all methods of calculations based on both the CPTU and the SPT derived data.

4 CONCLUSION

Data from 50 CPTU tests, carried out in 8 different sites susceptible to liquefaction have been used to perform the analyses presented in this paper, with the main focus on the use of CPTU to identify the liquefiable layers and evaluate the liquefaction potential of sandy and silty deposits. 7 different methods to assess the liquefaction potential in terms of the factor of safety, FoS, based on CPTU and SPT penetration resistance data, were used and all results obtained were compared to each other. SPT penetration resistance was derived from CPTU data, because CPTU tests provide continuous and more reliable data in terms of penetration resistance. The input values for these calculations were corrected for soil behavior characteristics, fines content and other factors, which might affect the results for different kind of soils. All liquefiable layers along the soils profile were detected by all methods used in this paper, and similar values of FoS and LPI are obtained.

Curves derived from cyclic stress ratio (CSR) and cyclic resistance ratio (CRR) results obtained from these calculations are in good agreement with curves derived from historic CPTU and SPT data basis from Idriss & Boulanger (2004), predicting higher potential of liquefaction in cohesionless soils with higher content of fines. The CRR values obtained by CPT—based methods are higher than CRR values obtained from SPT—based methods, but also the CSR values from CPT—based methods are app. 30% higher than CSR values evaluated from SPT—based methods. For the relative performance between CPTU and SPT based methods, CPT—based liquefaction triggering procedures are less conservative, although they may lead to lower values of FoS, in cases of predicted factors of safety lower than 0.5.

To conclude, providing continuous data and having the ability to define all the thin layers within a soil profile and their geotechnical parameters makes CPTU a reliable and useful test for liquefaction potential evaluation. But, considering that all CPT—based methods are simplified procedures, the results obtained should be used carefully, in accordance with the sites and projects specifics.

ACKNOWLEDGMENTS

The authors would like to thank their colleagues at *In Situ Site Investigation* for the data basis of CPTU tests and *Datgel* who helped with the updated graphs presented in this paper.

REFERENCES

Boulanger, R.W. & Idriss, I.M., 2004. State normalization of penetration resistance and theeffect of overburden stress on liquefaction resistance. *Proc., 11th Int. Conf. on Soil Dynamics and Earthquake Engineering and 3rd Int. Conf. on Earthquake Geotechnical Engineering*, Uni. of California, Berkeley, CA: 484–491.

Cetin, K.O., Seed, R.B., Kiureghain, A.D., Tokimatsu, K., Harder, L.F., Kayen, R.E. & Moss, R.E.S. 2004. Standard penetration test-based probabilistic and deterministic assessment of seismic soil liquefaction potential. *J. Geotech.Geoenviron. Eng.* 130(12): 1314–1340.

Cetin, K.O. & Bilge H.T. 2014. Recent advances in seismic soil liquefaction engineering. *Perspectives on European Earthquake Engineering and Seismology,* 1: 585–626.

Idriss, I.M. & Boulanger, R.W. 2004. Semi-empirical procedures for evaluating liquefaction potential during earthquakes. *Proc., 11th Int. Conf. on Soil Dynamics and Earthquake Eng.*, Stallion Press, Tokyo: 32–56.

Idriss, I.M. & Boulanger, R.W. 2008. *Soil liquefaction during earthquakes*. Monograph MNO-12, Earthquake Engineering Research Institute, Oakland.

Idriss, I.M. & Boulanger, R.W. 2010. SPT-based liquefaction triggering procedures. Report no. UCD/CGM-10/02, Dept. of Civil and Environ. Eng., Uni. of California.

Idriss, I.M. & Boulanger, R.W. 2014. CPT and SPT-based liquefaction triggering procedures. Report no. UCD/CGM-14/01, California.

Iwasaki, T., Tatsuoka, F., Tokida, K., & Yasuda, S. 1978. A practical method for assessing soil liquefaction potential based on case studies as various sites in Japan. *Proc. Int. Conf. on Microzonation for Safer Construction—Research and Applicat*ion, 2: 885–896.

Iwasaki, T., Tokida, K. & Tatsuoka, F. 1981. Soil liquefaction potential evaluation with use of the simplified procedure. *Proc. Int. Conf. on Advances in Geotech. Earthquake Eng. and Soil Dynamics*, St. Louis, Missouri, Vol. 1.

Iwasaki, T., Tokida, K., Tatsuoka, F., Watanabe, S., Yasuda, S. & Sato, H. 1982. Microzonation for soil liquefaction potential using simplified methods. *3rdInt. Conf. on Microzonation for Safer Construction*, Seattle, USA: 1319–1330.

Jefferies, M.G. & Davies, M.P. 1993. Use of CPTU to estimate equivalent SPT N_{60}. *Geotech. Test. J.* ASTM. 16(4): 458–468.

Jefferies, M.G. & Been, K. 2006. *Soil liquefaction–A critical state Approach*. Taylor and Francis, London.

Kayen, R., Moss, R.E.S., Thompson, E.M., Seed, R.B., Cetin, K.O., Kiureghaian, A., Tanaka, Y. & Tokimatsu, K. 2013. Shear-wave velocity–based probabilistic and deterministic assessment of seismic soil liquefaction potential. *J. Geotech. Geoenviron. Eng*. 139(3): 407–419.

Lunne, T., Robertson, P.K. & Powell, J.J.M. 1997. *Cone Penetration Testing in Geotechnical Practice*. Blackie Academic, E & FN Spon/Routledge, New York.

Moss, R.E.S., Seed, R.B. & Olsen, R.S. 2006. Normalizing the CPT for overburden stress. *J. Geotech. Geoenviron. Eng.* 132(3): 378–387.

Olson, S.M., & Stark, T.D. 2002. Liquefied strength ratio from liquefaction flow failure case histories. *Can. Geotech. J*. 39: 629–647

Robertson, P.K. 1990. Soil classification using the cone penetration test. *Can. Geotech. J.* 27(1): 151–158.

Robertson, P.K. & Wride, C.E. 1998. "Evaluating cyclic liquefaction potential using the CPT." *Can. Geotech. J.,* 35(3): 442–459.

Robertson, P.K. 2009. Interpretation of Cone Penetration tests—a unified approach. *Can. Geotech. J.,* 46(11): 1337–1355.

Robertson, P.K. & Cabal, K.L. 2015. *Guide to Cone Penetration Testing*. 6th Edition: 96–128.

Seed, H.B., & Idriss, I.M., 1971. Simplified procedure for evaluating soil liquefaction potential. *J. Soil Mech. and Found. Div.* 97 (9): 1249–1273.

Suzuki Y., Sanematsu, T. & Tokimatsu, K. 1998. Correlation between SPT and seismic CPT. *Proc. Conf. on Geotech. Site Characterization*, Rotterdam: 1375–1380.

Toprak, S. & Holzer, T.L. 2003. Liquefaction potential index: field assessment. *J. Geotech. Geoenviron.Eng*., 129: 315–322

Youd, T.L., & Idriss, I.M. 2001. Liquefaction resistance of soils: Summary report from the 1996 NCEER and 1998 NCEER/NSF workshops on evaluation of liquefaction resistance of soils. *J. Geotech. Geoenviron. Eng.* 127(4): 297–313.

Taylor & Francis
Taylor & Francis Group
http://taylorandfrancis.com

Cone Penetration Testing 2018 – Hicks, Pisanò & Peuchen (Eds)
© 2018 Delft University of Technology, The Netherlands, ISBN 978-1-138-58449-5

Dutch field tests validating the bearing capacity of Fundex piles

S. Van Baars & S. Rica
University of Luxembourg, Luxembourg, Grand Duchy of Luxembourg

G.A. De Nijs, G.J.J. De Nijs & H.J. Riemens
BMNED, Terneuzen, The Netherlands

ABSTRACT: In 1939, Boonstra was the first to base the tip bearing capacity of foundation piles on the CPT cone resistance. Since then, many engineers and scientists have proposed improved design methods for the bearing capacity of foundation piles, such as the Dutch Koppejan method. This method holds a mistake in the q_c-averaging method. Its tip resistance is based on the cone resistance of an assumed zone between 8D above the tip and 4D below the tip, while several researchers show that this should be in a zone between 2D above the tip and 8D below the tip. In the Netherlands, Belgium and France a field test has been performed indicating that the currently used design method in the Netherlands (the Koppejan Method) was about 30% too high for the tip resistance. This, and also the current q_c-averaging method, conflict with the findings of Boonstra, Plantema, Huizinga and White & Bolton. Besides, in the field test, the residual stresses in the piles after installation were completely ignored, in fact, not even measured. Nevertheless, the Dutch Norm Commission Geo-Engineering decided to reduce the bearing capacity of foundation piles in the Netherlands, unless other field tests prove otherwise. Since this reduction is very drastic and since no serious problems due to the use of the unreduced bearing capacity were recorded, the geotechnical contracting company Funderingstechnieken Verstraeten BV has performed field tests on six Fundex piles, and asked the engineering company BMNED to assist with these tests and the design. The aim was to prove that, at least for Fundex piles, a reduction of 30% is too much. The Fundex Pile Tests in Terneuzen show that, especially for the grouted Fundex piles, the pile type factor should not be reduced in combination with the current q_c-averaging method.

1 INTRODUCTION

1.1 *Early cone penetration testing*

The cone penetrometer was initially developed around 1930 by Pieter Barentsen, who was a civil engineer at the Department of Civil Works (Rijkswaterstaat) in the Netherlands. The mechanical cone consisted of a rod, with a conical tip, inside a sounding tube. The Delft Laboratory of Soil Mechanics (now Deltares Delft) created a framework for this CPT apparatus in order to be able to make deep investigations in the soil, see Figure 1.

In 1939, Boonstra implemented even a CPT apparatus in six foundation piles (see Figure 2), in order to measure the cone resistance both before pile driving and after pile driving and also to measure the pile bearing capacity. He was also the first to conclude that the CPT cone resistance, below the tip, after the pile installation (q_b) can be higher than the CPT cone resistance (q_c) before the pile installation He also concluded that the tip bearing capacity of a foundation pile is rather similar as (the lowest values of) the CPT cone resistance $q_b \approx \min(q_c)$ (Figure 3).

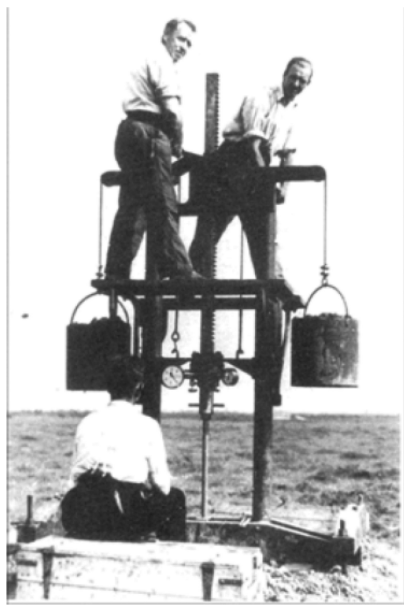

Figure 1. Dutch mechanical cone.

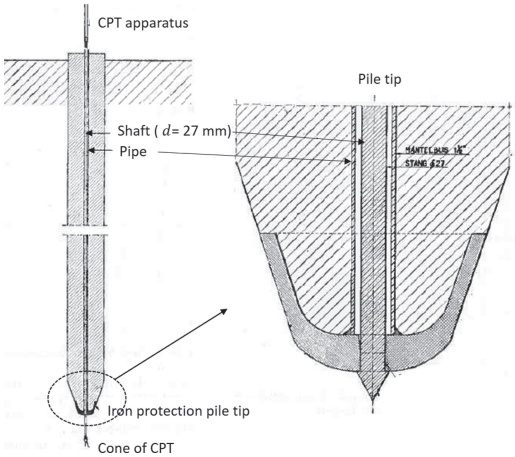

Figure 2. CPT apparatus inside a foundation pile.

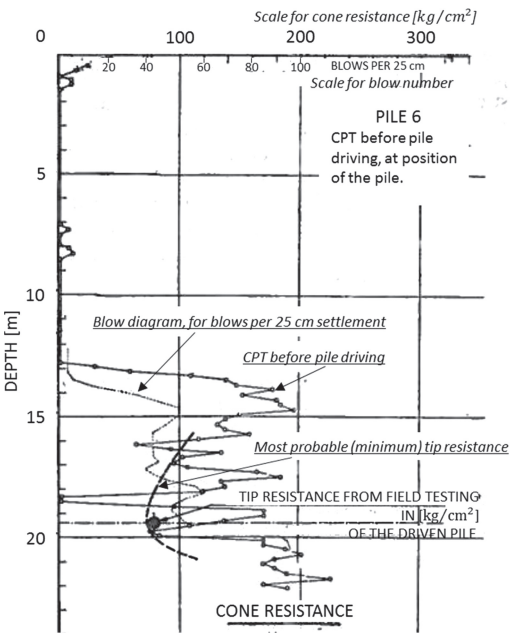

Figure 3. Tip resistance versus CPT value (Boonstra, 1939).

Plantema (1948) also concluded that $q_b \approx \min(q_c)$, based on a field test on a jacked square concrete pile.

Huizinga (1951) also found $q_b \approx \min(q_c)$ (Figure 4) and was the first who looked at a certain influence zone around the pile tip, although no specific averaging procedure was detailed by Huizinga.

In 1953, Begemann proposed to measure the shaft friction with a separate device, a friction sleeve, located just above the cone.

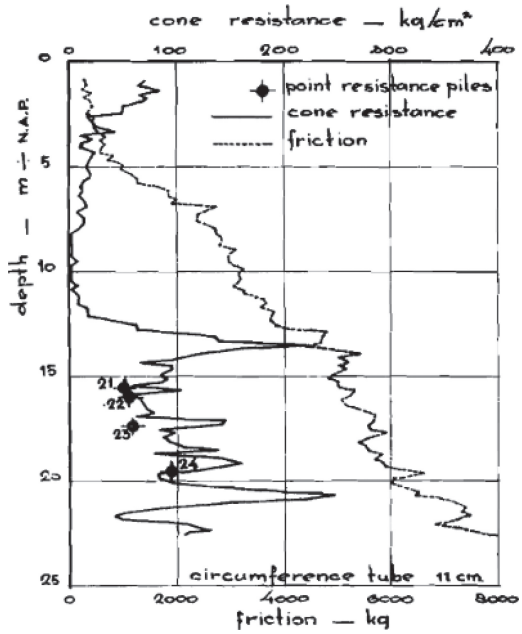

Figure 4. Tip resistance versus CPT value (Huizinga, 1951).

The friction ratio was used for the first time to classify the soil types. Fugro was first to introduce the electric cone in 1965 for routine soil investigation (Massarsch, 2014). Since then, many engineers and scientists have proposed improved design methods for the bearing capacity of foundation piles. The biggest difference between these methods is found in the definition of the influence zone.

1.2 *Dutch design method*

Prandtl (1920) gave an analytical solution for the bearing capacity of a soil under a limit pressure, p, causing kinematic failure of the weightless infinite half-space underneath, having a friction angle ϕ and cohesion c. The solution of Prandtl was extended by Reissner (1924) for a surrounding surcharge, q, and was based on the same failure mechanism. Keverling Buisman (1940) and Terzaghi (1943) extended the Prandtl-Reissner formula for the soil weight, γ.

Meyerhof (1951) was inspired by the logarithmic spiral shaped shear band in the Prandtl-Wedge, and assumed that there would be a shear band failure at the pile tip following this logarithmic spiral all the way back to the pile shaft (Figure 5).

Van Mierlo & Koppejan (1952) adopted this logarithmic spiral shaped shear band. They proposed an influence zone of 5 to 8 D above the pile tip level and 0.7 to 4 D underneath the pile tip (Figure 6).

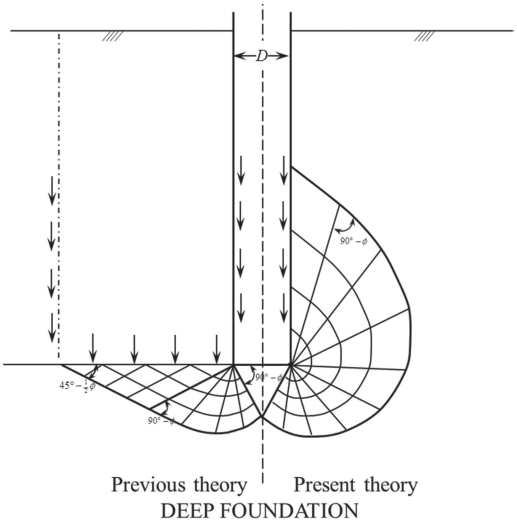

Figure 5. CPT Tip failure mechanism (Meyerhof, 1951).

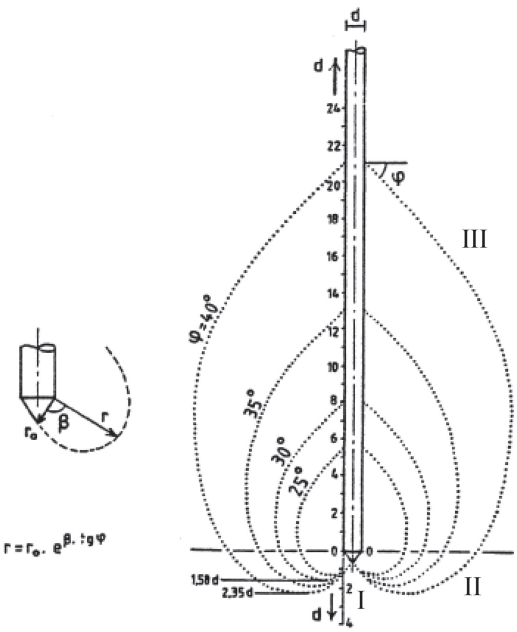

Figure 6. Logarithmic spiral shape failure mechanism around a pile tip (Van Mierlo & Koppejan, 1952).

Begemann (1963) added an averaging method, based on the following three assumptions:

1. The logarithmic spiral is subdivided into three areas: I, II and III,
2. The contribution to the pile tip resistance for area I is equally important as for area II,
3. The contribution to the pile tip resistance for area I and II is equally important as for area III.

The Dutch design code has added some correction factors, which led finally to the following equation:

$$q_b = \tfrac{1}{2}\alpha_p \beta s\left(\tfrac{1}{2}q_{c;I;avg} + \tfrac{1}{2}q_{c;II;avg} + q_{c;III;avg}\right). \quad (1)$$

where:

q_b = the pile tip (base) resistance,

$q_{c;I;avg}$ = the average value of q_c in area I, where the lowest possible result shall be chosen in the area 0.7 to 4 D,

$q_{c;II;avg}$ = the average value of the cone resistance in area II, where the cone resistance to be taken into account shall not increase the q_c values below

$q_{c;III;avg}$ = the average value of the cone resistance in area III where the cone resistance to be taken into account shall never increase the q_c values below, starting from the end-value of $q_{c;II;avg}$

α_p = the pile type factor (e.g., 1.0 for driven piles, or 0.5 to 0.6 for bored piles)

β = the pile tip factor (e.q., 1.0 for standard concrete piles and decreases for piles with an increased pile tip area)

s = the shape factor of the pile tip (1.0 for square and circular pile tips and lower for more rectangular or elliptical pile tips).

Over the years, the Begemann's averaging method got adapted in the Netherlands. This method is now named after Koppejan, even though Koppejan's paper was published in collaboration with Van Mierlo and even though the averaging method of Begemann was not implemented by Koppejan. The Koppejan method is also called the Dutch method.

The major problems with the Dutch method are that there is no scientific evidence for this method, the failure mechanism (the soil slides into the pile shaft) is kinematically impossible and the failure mechanism and location of the failure zone (with relative shear stress: τ/τ_{max} = 1.0) contradicts with numerical calculations, see Figure 7, (Van Baars, 2017), which shows that the plastic zone and most failure is not above, but below the pile tip.

1.3 *Other design methods*

Most other design methods assume an influence zone which is far lower than the Dutch influence zone. De Beer (1963), for example, used an influence zone which is completely below the pile tip (Figure 8a), which became the basis of the Belgium method. The French method uses an influence zone from 1.5 *D* below to 1.5 *D* above the pile tip. This is not only in use in France but worldwide and in other methods as well (e.g. Fugro-05). White and Bolton (2005), after studying a large amount of field tests, concluded that the influence zone is

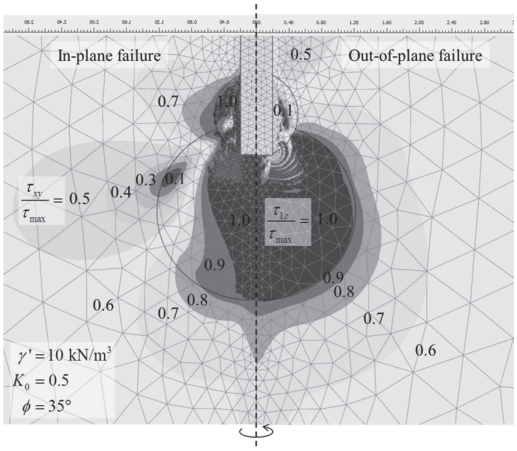

Figure 7. Relative shear stress (failure zone) around the pile tip: In-plane (left) and out-of-plane (right) (Van Baars, 2017).

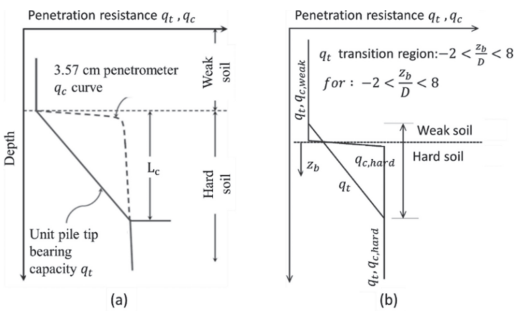

Figure 8. Influence zone: (a) De Beer (1963) and (b) White & Bolton (2005).

from 2D above the pile tip to 8D below the pile tip (Figure 8b). They also concluded that the pile type factor α_t should not be 1.0, but 0.9 for normal driven piles.

There are other well-known design methods, for example Fugro-05 (from Fugro), ICP-05 (from Imperial College), UWA-05 (from the University of Western Australia) and NGI-05 (from the Norwegian Geotechnical Institute). These methods were all published at the 1st International Symposium on Frontiers in Offshore Geotechnics in Perth, September 2005, and discussed by Clausen at all (2005).

2 FIELD TESTS AND CONSEQUENCES

2.1 *Field tests*

In order to be able to compare the pile design methods used in the Netherlands, Belgium and France, existing well instrumented field tests have been combined and re-examined. The results of these field tests are published in report CUR 229 (2010), in Van Tol et al. (2010) and in Van Tol (2012). The conclusion was drawn that the measured tip bearing capacity was 13% higher than predicted for France (but France has a pile type factor of $\alpha_t = 0.5$ for precast driven piles!), 25% too low for Belgium and 30% too low for the Netherlands (Figure 9). The authors concluded from these tests that in the Netherlands the pile type factor α_t had to be reduced for all piles with 30%.

2.2 *Consequences*

There are two very big problems with this conclusion:

1. The errors in the influence zone and in the averaging method of the Dutch method are still not solved, and these do influence strongly the predicted bearing capacity.
2. The residual stresses in the piles of the existing field tests were not measured and assumed not to play an important role. An incorrect assumption might strongly reduce the measured tip bearing capacity of the piles, and therefore the pile type factor.

The residual force is a summation of the stresses which remain at the pile tip after installation of the pile, which are balanced out by the shear stresses along the pile shaft. Because of the installation there is always a remaining stress at the pile tip (Alawneh et al, 1996). Hunter & Davisson (1969) and White & Bolton (2005) have shown that the residual force can be even as high as 40% or 45% of the total tip bearing capacity of the pile.

The ignoring of the residual stresses leads automatically to an underestimation of the tip bearing capacity of a pile and an overestimation of the

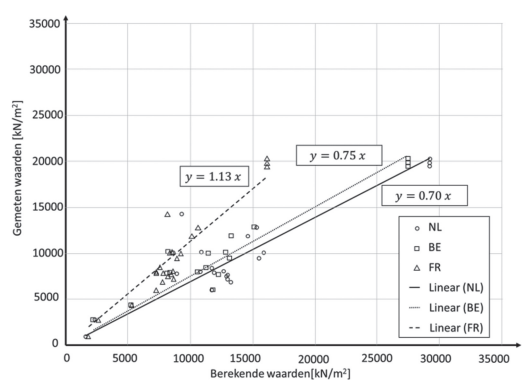

Figure 9. Tip bearing capacity for the field tests: measured values (vertical axis) versus calculated values (horizontal axis) (Van Tol et al., 2010).

shaft bearing capacity of a pile (since the measured total load at failure is known).

Despite all the field test results published by Boonstra, Plantema, Huizinga and White & Bolton, despite the mistake in the influence zone of the Dutch Method and despite the effect of the unknown residual stresses in the mentioned field tests, the Dutch Norm Commission Geo-Engineering decided nevertheless (Hannink et al, 2015) to reduce the tip resistance with 30% from January 1st, 2016, which was postponed until January 1st 2017 (Van Seters, 2015).

3 FUNDEX PILE TEST TERNEUZEN

3.1 *Pile type and test situation*

Since this reduction is very drastic and since no serious problems due to the use of the unreduced bearing capacity were recorded (Van Baars, 2015), the geotechnical contracting company Funderingstechnieken Verstraeten BV decided to perform field tests on their Fundex piles, and asked the engineering company BMNED to assist with these tests and its design. The pile tests were performed at the location of BMNED in Terneuzen, in the Southwest of the Netherlands. The aim was to prove that for Fundex piles, a reduction of 30% is too much.

Fundex piles are augered cast in place concrete full displacement piles, with a lost steel screw shaped tip (Figure 9). Six Fundex piles have been tested: three Fundex piles, type 460/560 (shaft diameter/tip diameter) without grout injection, and three identical Fundex piles with additional grout injection. For the grouted Fundex piles, the shaft becomes as wide as the tip, which gives a larger shaft and higher total shaft bearing capacity.

The pile head level was at NAP +1.3 m, the pile tip level was at NAP -18.7 m. NAP is about Main

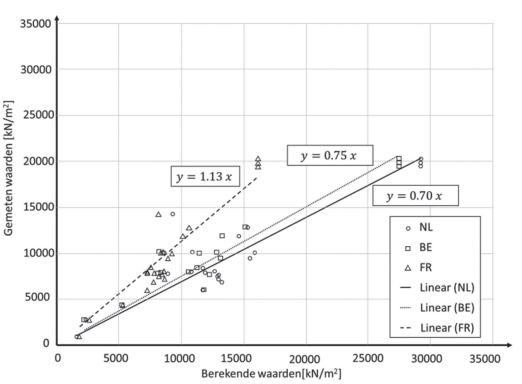

Figure 9. Boring of fundex pile.

Figure 10. CPT at test field; vertical scale is NAP +3 m to NAP –23 m; horizontal scale of left box is q_c = 0 to q_c = 20 MPa; horizontal scale of right box is R_f = 0 to R_f = 7.

Sea Level (MSL). Strain gauges were installed at 5 different levels, including near the pile head and near the pile tip.

Borings and CPT's were made, showing sand all over, with down to NAP – 5 m, sand with higher portions of silt and clay and mostly q_c < 4 MPa. Between NAP-5 to –7 m and NAP-10 to –11 m, 20 MPa < q_c < 30 MPa. Near the pile tip $q_c \approx 14$ MPa (Figure 10). Three CPT's were made for each pile.

A Kentledge system was used to load the piles (Figure 11). Three hydraulic jacks were used which can each load up to 250 tons. The failure load, or bearing capacity, is defined as the load at 10% displacement (56 mm) of the equivalent pile tip diameter.

3.2 *Test results*

Before the Dutch Norm Commission Geo-Engineering decided about the 30% tip reduction, the following parameters had to be applied for this pile: $\alpha_p = 0.9$, $\beta = 1.0$, $s = 1.0$, $\alpha_s = 0.009$.

Table 1 shows the measured bearing capacities of the three non-grouted and the three grouted Fundex piles, both absolute and in percentage of the calculated values, based on the current q_c-averaging method and the unreduced (old) Dutch design method. Both the values for the measured total bearing capacity and the measured tip bearing capacity are listed in the table.

The results from the Fundex pile tests indicate that the measured total bearing capacity is, for 5 of the 6 piles (not Pile 06) in the range of the old Dutch design method.

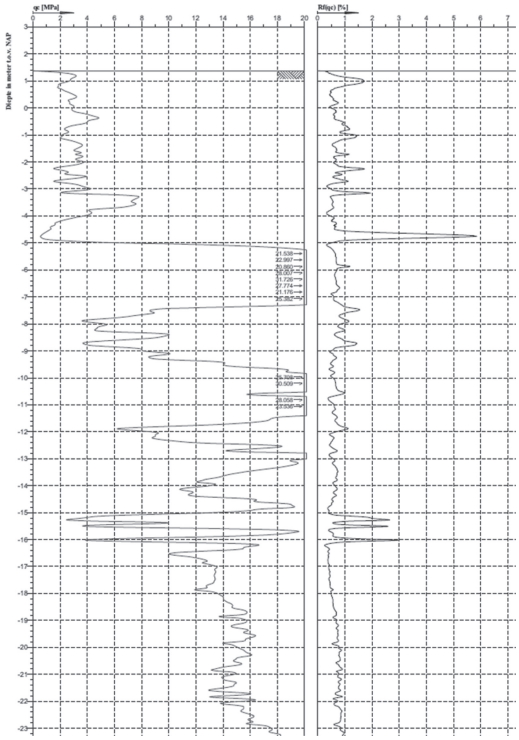

Figure 11. Applied Kentledge load system.

Table 1. Measured bearing capacities.

	Total		Tip only	
Bearing capacity	kN	%	kN	%
Pile 02 Fundex	5738	106%	2310	69%
Pile 04 Fundex	5044	94%	2385	77%
Pile 06 Fundex	3836	73%	2691	88%
Pile 01 F. Grouted*	6078	97%	–	–
Pile 03 F. Grouted	6104	100%	2931	140%
Pile 05 F. Grouted	5748	100%	2464	121%

* There were some sensor problems for Pile 01.

Looking closer to the results of only the tip bearing capacity, we see a big difference between grouted and non-grouted Fundex piles. For non-grouted Fundex piles, the pile tip is indeed underperforming and in agreement with the proposed reduction of the Dutch Norm Commission Geo-Engineering, but for grouted Fundex piles, the tip is overperforming and thus a reduction of 30% of the tip resistance will lead, to incorrect and underestimated values.

4 CONCLUSIONS

The position of the influence zone and the averaging method of the Dutch method are not correct.

The decision of the Dutch Norm Commission Geo-Engineering to reduce the tip resistance with 30%, in combination with the current q_c-averaging method, conflicts with the findings of Boonstra, Plantema, Huizinga and White & Bolton. This decision was largely based on the discussed field tests, in which the residual stresses were assumed to be near zero. This assumption can lead to an underestimation of the tip bearing capacity of a pile.

The Fundex Pile Tests in Terneuzen show for the grouted Fundex piles, that the pile type factor α_p does not have to be reduced for the current q_c-averaging method.

REFERENCES

Alawneh, A. S., & Malkawi (1996), A.I.. Residual load concept in pile foundation, Geotechnical Engineering Practice Beyond 2001, Proceedings of the Indian Geotechnical Conference. ICG-1996, Madras, India. 1996.

Barentsen, P. (1936). Short description of field testing method with cone shaped sounding apparatus. P*roc. of the 1st Int. Conference on Soil Mechanics and Foundation Engineering (ICSMFE)*. Harvard University: 6–10.

Begemann, H.K. (1953). Improved method of determining resistance to adhesion by sounding through a loose sleeve placed behind the cone. *Proc. of the 3rd Int. Conference on Soil Mechanics and Foundation Engineering*. Vol. 1, Switzerland, Aug. 1953: 213–217.

Begemann, H. P. (1963). The use of the static soil penetrometer in Holland. *New Zealand Engineering*. Vol. 18, No. 2, Feb. 1963: 41.

Boonstra, G. C. (1940). Eenige Beschouwingen over den Puntweerstand van Palen. (Some considerations about the pile tip bearing capacity). *De Ingenieur*, 55, Feb. 1940: 33–45.

Clausen, C. J. F., Aas, P. M. & Karlsrud, K. (2005). Bearing capacity of driven piles in sand, the NGI approach. *Proc. of the 1st Int. Symposium on Frontiers in Offshore Geotechnics*. Perth, Sept. 2005: 574–580.

CUR (2010). Publication 229, Axiaal draagvermogen van palen, CURNET, Gouda, the Netherlands.

De Beer, E. (1963). The scale effect in the transposition of the results of deep-sounding tests on the ultimate bearing capacity of piles and caisson foundations. *Géotechnique*. Vol. 13, No. 1, March. 1963: 39–75.

Hannink, G., De Jong, E., Lurvink M.L., Van Seters, A.J. (2015). Per 1 januari 2016 gaan de paalklassefactoren voor de paalpunt omlaag, *Geotechniek*, April 2015: 36–37.

Huizinga, T. K. (1951). Application of results of deep penetration tests to pile foundations. *Proc. of the Building Research Congress*. Vol. 1, London: 173–179.

Hunter, A., & Davisson. M. (1969). *Measurements of pile load transfer. Performance of Deep Foundations*. ASTM International, USA, Jan. 1969.

Keverling Buisman, A. S. (1935). De Weerstand van Paalpunten in Zand. *De Ingenieur*, 50 (Bt. 25–28): 31–35.

Keverling Buisman, A. S. (1940). *Grondmechanica*, Waltman, Delft, the Netherlands: 227, 243.

Massarsch, K.R. 2014. Cone Penetration Testing—A Historic Perspective. *Proc. of 3rd International Symposium of Cone Penetration Testing, CPT14*, Las Vegas, USA: 105.

Meyerhof, G. G. (1951). The ultimate bearing capacity of foundations, *Géotechnique*, 2: 301–332.

Plantema, G. (1948). Results of a special loading test on a reinforced concrete pile, a so-called pile sounding. *In Proc. of the 2nd Int. Conference on Soil Mechanics and Foundation Engineering*. Vol. 2, Rotterdam, Jun. 1948: 55–64.

Prandtl, L. (1920). Über die Härte plastischer Körper. Nachrichten von der Königlichen Gesellschaft der Wissenschaften zu Göttingen, Math..-physikalische Klasse: 74–85.

Reissner, H. (1924). Zum Erddruckproblem. *Proc., 1st Int. Congress for Applied Mechanics*, C. B. Biezeno and J. M. Burgers, eds., Delft, the Netherlands: 295–311.

Terzaghi, K. (1943). *Theoretical soil mechanics*, J. Wiley, New York, USA.

Van Baars (2015). Reaction on the open letter to the CUR-Commission 193 (Geotechniek Oktober 2014), *Geotechniek*, Jan. 2015: 8.

Van Mierlo, J.C. and Koppejan, A.W. (1952). "Lengte en draagvermogen van heipalen", *Bouw*, 3, 1952: 1–11.

Van Seters, A. (2015). Paaldraagvermogen: de weg vooruit, *Geotechniek*, Dec. 2015: 8–9.

Van Tol, A. F.(1994). *Hoe betrouwbaar is de paalfundering, Inaugeral speech* 3-6-1994, TU Delft, the Netherlands.

Van Tol, A. F., Stoevelaar, R. and Rietdijk, J. (2010). Draagvermogen van geheidepalen in international context. *Geotechniek, Funderingsdag-Special*, Dec. 2010: 4–9.

Van Tol, A. F. (2012). Draagkracht funderingspalen, een up-date. *Geotechniek, Funderingsdag-Special*. Dec. 2012: 14–18.

White, D. & Bolton, M. (2005). Comparing CPT and pile base resistance in sand. *Geotechnical Engineering*. No.158, London, Jan 2005: 3–14.

Taylor & Francis
Taylor & Francis Group
http://taylorandfrancis.com

Cone Penetration Testing 2018 – Hicks, Pisanò & Peuchen (Eds)
© 2018 Delft University of Technology, The Netherlands, ISBN 978-1-138-58449-5

Estimation of spatial variability properties of mine waste dump using CPTu results—case study

I. Bagińska & M. Kawa
Wroclaw University of Science and Technology, Poland

W. Janecki
Geosoft sp. z o.o., Poland

ABSTRACT: The paper deals with application of CPTu test results for the probabilistic modeling of lignite mine waste dump soils. The statistical measures are obtained using the results from four CPTu tests performed in a close range in the lignite mine dumping ground in Bełchatów (Central Poland). Both the tip resistance q_c as well as local friction f_s are tested. Based on the mean values, standard deviations and new classification nomogram of measured quantities, the specific zones in the dumping site profile are distinguished. For all three zones, based on normalized de-trended values for q_c and f_s both vertical and horizontal scales of fluctuation are estimated. The obtained results allow the description of dumped soil parameters using Random Fields.

1 INTRODUCTION

In the last decades there has been a growing need to reclaim or use for industrial purposes mine waste dump areas (Wysokiński 2010, O'Brien et al. 2017). This involves the development of a methodology for the geotechnical research of dumped soils. The problem applies to all areas where soil being the by-product of open-pit mines is deposited.

In the case of lignite mine waste dump soils, the basic difficulty in their management lies in their strong variability. Research and interpretation activities performed for these soils usually focus mainly on the characterization of local geological, physical and chemical characteristics of these media. The research is typically based on laboratory tests with test specimens taken separately from selected points of the waste dump area (Eswaran et al. 2002, Borecka 2007, Hawley & Cunning 2017). It seems that for such a study additional in-situ tests providing information on variability of properties of dumped soils in a continuous manner should be made. Combining information from these two sources is necessary for correct design of geotechnical structures located in waste dump areas. The randomness which is often present in the soil dumping process also indicates that in designs a probabilistic approach should be employed.

In the last decades methods based on probabilistic modeling of soil behavior have been strongly developed. The main purpose of these methods is to estimate risk associated with erecting structures on media with spatially variable properties. Recently, methods that combine Monte-Carlo simulation with Random Field Theory seem to be of particular interest (Griffiths & Fenton 2001, Fenton & Griffiths 2003). These techniques have been successfully used for natural soils. So far, they have been used to analyze the reliability of bearing capacity of strip foundations, slope stability or deep excavation support (Vessia et al. 2009, Vardon et al. 2016, Kawa et al. 2017, Puła et al. 2017).

Simultaneously, procedures allowing identification of the so-called fluctuation scales have been developed. Fluctuation scales, defined as parameters of a random field correlation model, seem to be a convenient measure of spatial variability of the field properties. Since the number of observations necessary to identify fluctuation scale is significant, some studies (e.g. Lloret-Cabot et al. 2014) suggested using tests characterized by long, continuous data series (e.g. CPT, CPTu).

The focus of the present paper is to determine the fluctuation scales for the dumping soil. Both vertical as well as horizontal scales of fluctuation are measured—the results are presented graphically and discussed. The Random Fields of soil parameters generated based on measured fluctuation scales can be further used for reliability analysis of geotechnical constructions formed in dumping site.

2 STATISTIC MEASURES OF A RANDOM FIELD

According to the Random Field Theory for the description of a random variable in the field, two sets of statistic information are needed, i.e. point value statistics and a spatial correlation function. The point statistics can be fully described knowing the probability distribution (usually given in the form of a probability density function). If the distribution is not fully known it is often assumed. For soil properties, normal, lognormal or bounded distribution are typically chosen. Their parameters, i.e. mean and variance, can be easily identified form a data series using their commonly known unbiased estimators:

$$\hat{\mu} = \frac{1}{k}\sum_{i=1}^{k} X_i, \hat{\sigma}^2 = \frac{1}{k+1}\sum_{i=1}^{k}(X_i - \hat{\mu})^2 \quad (1)$$

where X_i = the measured value of parameter; k = the number of observations; $\hat{\mu}$ = = mean value of parameter; $\hat{\sigma}$ = standard deviation.

To extend the description of the point statistics to the random field, information on the correlation structure is needed. This is often provided using a correlation function. In geostatistics a two-dimensional exponential function by Markov is often used. It can be expressed as the function of horizontal (τ_x) and vertical (τ_y) lags as:

$$\rho(\tau) = \exp\left\{\frac{-2|\tau_x|}{\theta x} + \frac{-2|\tau_z|}{\theta z}\right\} \quad (2)$$

The basic parameter for all correlation functions is the so-called fluctuation scale (Vanmarcke 1983, 2010), i.e. the length within which the correlation between two points is significant. In equation (2) it is denoted as θx and θz for the horizontal and vertical directions, respectively. Often, due to a small amount of data, the estimation of the fluctuation scale is not an easy task. This is not a problem in the case of a CPTu test, at least in the vertical direction: the test is characterized by long, vertical data series.

The detailed algorithm for determining the value of fluctuation scale based on CPT data series has been presented in the work by Lloret-Cabot et al. (2014). According to that algorithm, the value of the vertical fluctuation scale is obtained by fitting the theoretical correlation model to the experimental correlation function. The latter can be estimated as:

$$\hat{\rho}(\tau_j) = \frac{1}{\hat{\sigma}^2(k-j)}\sum_{i=1}^{k-j}(X_i - \hat{\mu})(X_{i+j} - \hat{\mu}) \quad (3)$$

where X_i = the value of the parameter (in CPTu, e.g., q_c or f_s); k = the number of observations; τ_j = depth of CPTu, as a multiplication of the observation number j = 1, 2, ..., k by length of adopted testing step $\tau_j = j\Delta\tau$.

Because it is assumed that the expected value and the variance of the random variable have the same value at all points of the field, the observations showing a trend need to be subjected to de-trending (usually linear or quadratic, e.g. Uzielli et al. (2006)) and normalizing prior to using equation (3). The same methodology, assuming a linear trend for obtained CPTu results, has been used in the present work.

The identical methodology can be also used for estimating the value of the horizontal fluctuation scale. In that case all the considered CPTu tests need to be performed in a very small area. It should be noticed that, in the case of natural soils, the value of the horizontal fluctuation scale is usually several times greater than the vertical one (Kawa & Łydżba 2015).

3 CHARACTERISTIC OF DUMPED SOIL

Dumped soil is a specific anthropogenic medium with a very diverse structure. It is produced as a result of the mining, transport and deposition of coal-bed overburden in open-pit mines. The process of formation of dumping soil can be divided into three stages. During the first stage—the mining process—the original structure of the natural soil is destroyed. In the second stage—the transport—the soil is further transformed as the result of various external factors. The third stage is the deposition process, which additionally results in accidental mixing of the soil (Dmitruk 1965, Hawley & Cunning 2017).

During all three stages described above, the soil is subject to the process of reconstruction of the original structure, loosening, agglomeration and fragmentation. The whole process results in mixing of lithologically different layers of the overburden of the bed.

Based on literature (Dmitruk 1965, Rybicki et al. 2002, Bagińska et al. 2017) three main types of mine waste dump soils can be distinguished:

- Type I—a medium with characteristics similar to granular soils, made of non-cohesive soils (sand, gravel);
- Type II—a medium with characteristics similar to cohesive soil, built of blocks of cohesive soil;
- Type III granular-cohesive medium with mixed characteristics, consisting of a mixture of granular and cohesive soils.

In order to control the current composition, conditions and spatial arrangement of the soils in

the waste dump, CPTu tests are often performed in waste dump soils after deposition. A large existing CPTu database allows the use of these results to determine the statistical measures of deposited soil.

The present paper is based on the results of 4 CPTu tests performed in close range in the area of waste dump of the lignite mine "Bełchatów" (central Poland). CPTu test points were distributed along the straight line at the distances shown in Figure 1. This specific arrangement was intentionally assumed in order to allow for the determination of the vertical and horizontal fluctuation scales of q_c and f_s.

The mean values of measured q_c, f_s and their quotient friction ratio $R_f = (f_s/q_c)100\%$ along the profile are presented in Figure 2.

As shown in Figure 2, although the tests were performed in a very "chaotic" soil they appear to be quite similar to each other. In all results, three horizontal zones with similar R_f values can be distinguished.

The results obtained in these three zones ware presented in a nomogram proposed by Bagińska et al. (2016) for the initial classification of dumped soil (Figure 3) indicating that each of the zones seem to contain different types of dumped soil.

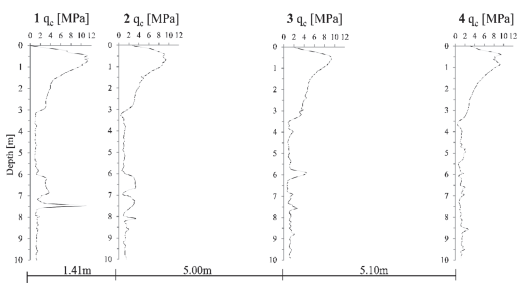

Figure 1. Arrangement of CPTu test points with q_c registration.

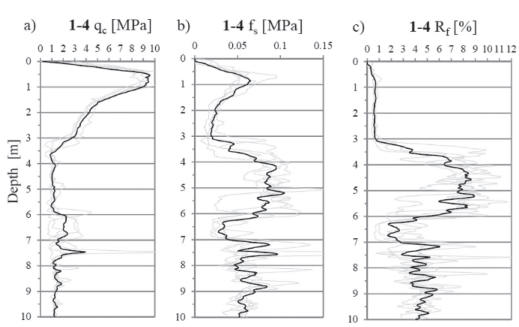

Figure 2. a) Mean q_c value; b) mean f_s value; b) mean R_f value.

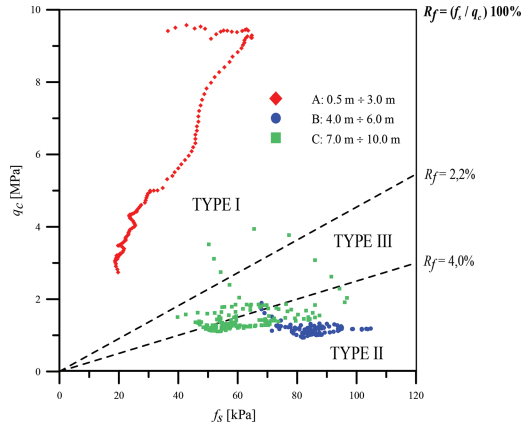

Figure 3. Classification nomogram for waste dump soils.

Table 1. Mean and standard deviation (SD) of R_f and I_{SBT} in the zones distinguished in the profile of the dump site.

Zone	Depth [m]	R_f Mean [%]	R_f SD [%]	I_{SBT} Mean [–]	I_{SBT} SD [–]
A	0.5 ÷ 3.0	0.62	0.06	2.21	0.15
B	4.0 ÷ 6.0	7.61	0.86	2.99	0.08
C	7.0 ÷ 10.0	4.46	0.71	2.82	0.09

Zone A (0.5÷3.0m) contains soil classified as type I, in zone B (4.0÷6.0m) there is soil of type II and below (7.0÷10.0m) in zone C there is soil having the characteristics between types II and III. For these three zones the variability of I_{SBT} was also analyzed. The I_{SBT} can be express as (Robertson 1990):

$$I_{SBT} = \sqrt{\left[3.47 - \log\left(\frac{q_c}{p_a}\right)\right]^2 + \left(\log R_f + 1.22\right)} \qquad (4)$$

where q_c = cone resistance; p_a = atmospheric pressure in same units as q_c; and R_f = friction ratio $R_f = (f_s / q_c)100\%$ with f_s = local friction. The result of the variability of R_f and I_{SBT} in individual zones are presented in Table 1.

4 DETERMINATION OF STATISTICAL MEASURES FOR THE DEPOSITED SOILS

Determination of all the random field parameters was performed for zones B and C of the considered dump site. Zone A was omitted in further analyzes

due the fact that it is strongly affected by passing of a stacker. As the effect of that passing significant growth of measured quantities as well strong nonlinearity of q_c and f_s trends are observed.

The obtained distributions of measured values of q_c and f_s for zones B and C are shown in the form of histograms in Figure 4. None of the distributions are symmetric. The distributions of q_c in both zones are skewed to the left, and in the case of fs the distribution is skewed to the right in zone B and skewed to the left in zone C. Asymmetry of the distributions could be caused by the presence of more than one component in the respective zones: since deposited soil is in fact a mixture of different soils, it can be assumed that, despite the distinction of "similarity" zones, within each of them more than one component can appear.

In addition to the point statistics for zones B and C, the vertical and horizontal fluctuation scales were also determined. In the first stage of the analysis a linear trend has been subtracted from the values of q_c and f_s (in order to calculate vertical scale for each test, the trend has been determined separately). The obtained values q_c and f_s, for all test points, and an average linear trend in the zones B are shown in Figure 5 and 6. In the next step, for de-trended values, the standard deviation σ_{res} has been determined and all the values have been normalized by dividing by that value (for vertical scale once again the data form each test were normalized separately). Finally, for the de-trended normalized values, the experimental correlation function (3) has been determined. The vertical scale of fluctuation has been identified by fitting Markov model (2) to the obtained mean correlation function. Experimental functions and the Markov model fits for all the zones and both q_c and f_s are shown in Figures 5c, 6c and 7. For both q_c and f_s, the obtained values of fluctuation scale are very similar.

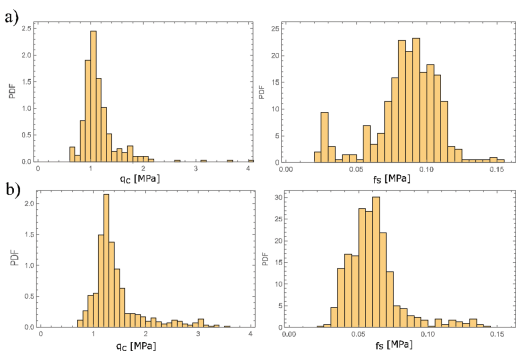

Figure 4. Histograms of q_c and f_s: a) zone B, b) zone C.

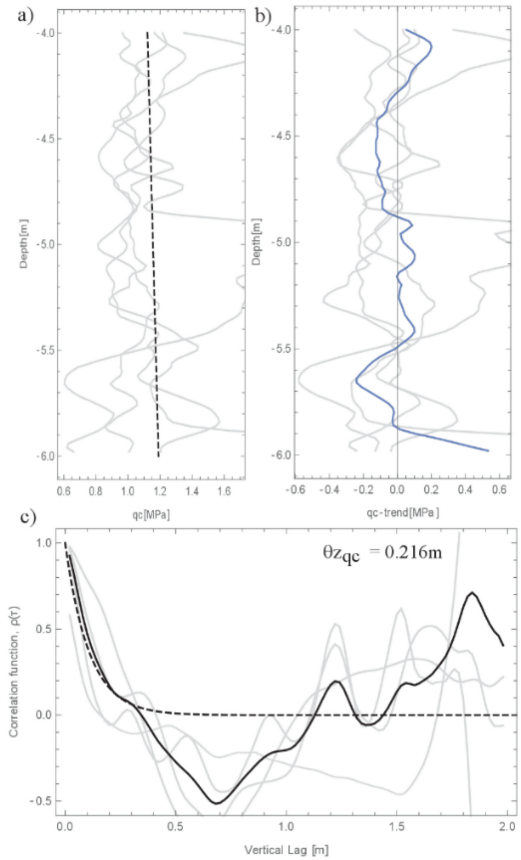

Figure 5. Zone B: a) q_c measurements with determined linear trend; b) de-trended measurements of q_c; c) estimated correlation functions for de-trended normalized q_c values (grey), their mean (black) and best fit of Markov model (dashed). Obtained values of vertical fluctuation scale θz_{qc} specified in the figure.

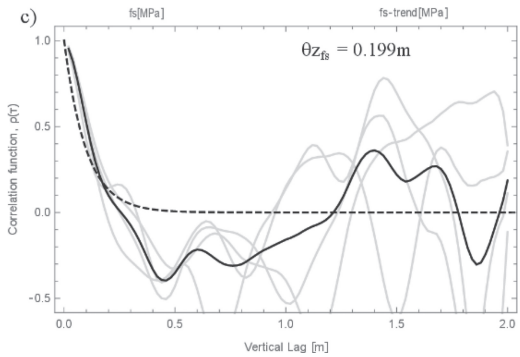

Figure 6. Zone B: estimated correlation functions for de-trended normalized f_s values (grey), their mean (black) and best fit of Markov model (dashed). Obtained values of vertical fluctuation scale θz_{fs} specified in the figure.

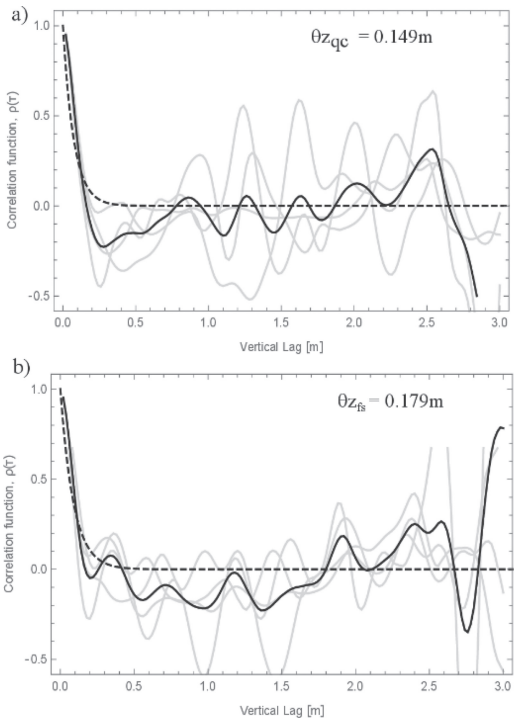

Figure 7. Zone C estimated correlation functions for de-trended normalized: a) q_c values (grey); b) f_s values (grey), their mean (black) and best fit of Markov model (dashed). Obtained values of vertical fluctuation scale θz_{qc} and θz_{fs} specified in the figure.

Horizontal scale fluctuations were obtained using the same technique. This time the de-trending was done by subtracting the average trend function from all results in the given zone, and normalization by dividing all values by a single value of standard deviation determined for the given zone (separately for q_c and f_s). De-trended and normalized (divided by their standard deviation) values were the basis for determining the value of the correlation function. Due to relatively large distances between the testing points and their small number, instead of a quasi-continuous correlation function obtained in the vertical case, here only a few point values being the mean correlation between data form points distant by a specified horizontal lag value has been obtained. The horizontal fluctuation scale was obtained once again by fitting these points with the Markov model (2). Calculations were made for both q_c and f_s. The results are shown in Figures 8, 9 and are summarized in Table 2.

Due to the already mentioned small number of points and the quite long distance between them, the obtained fit is not always a unique one. Often

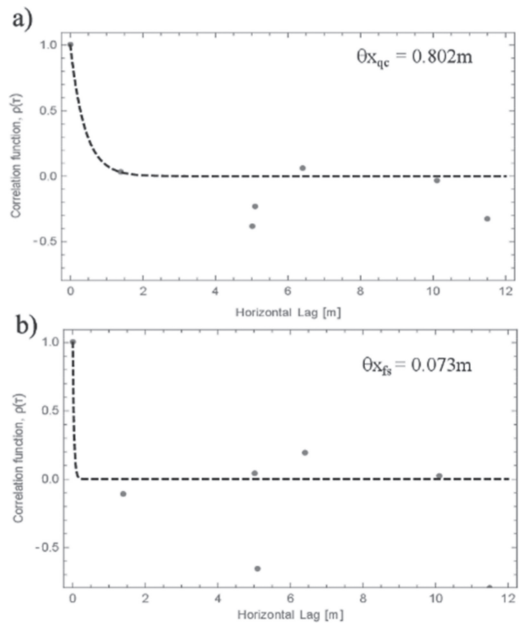

Figure 8. Obtained point values of experimental horizontal correlation function in zone B for: a) q_c; b) f_s and best fit of Markov model. Obtained values of horizontal fluctuation scale θx_{qc}, θx_{fs} specified in the figure.

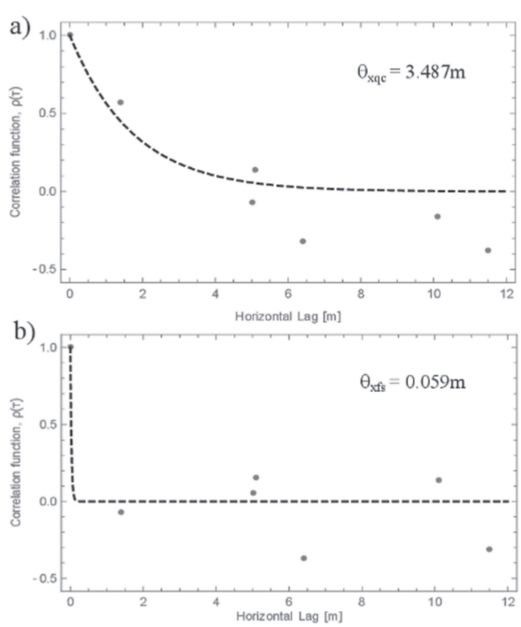

Figure 9. Obtained point values of experimental horizontal correlation function in zone C for: a) q_c; b) f_s and best fit of Markov model. Obtained values of horizontal fluctuation scale θx_{qc}, θx_{fs} specified in the figure.

Table 2. Obtained values of vertical and horizontal fuctuation scales.

Zone	Depth [m]	θz q_c [m]	θz f_s [m]	θx q_c [m]	θx f_s [m]
B	4.0 ÷ 6.0	0.216	0.199	0.802	0.073
C	7.0 ÷ 10.0	0.149	0.179	3.487	0.059

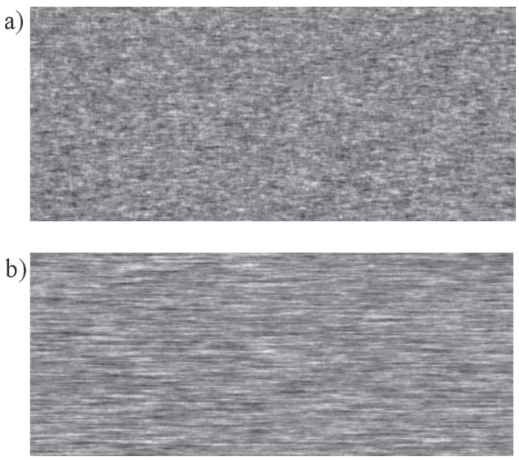

Figure 10. Random fields of q_c generated for: a) zone B; b) zone C.

the only significant point that determines the fit is the first point showing the correlation value for data distant by 1m. This point shows a strong correlation for q_c in zone C and the value of horizontal fluctuation scale obtained for that case seems to be the most reliable one. In zone B the point shows a weak but positive correlation: the horizontal scale value obtained in this zone is probable but because of the low correlation it is not certain. To improve the reliability of these results (particularly the latter one) more points with correlations for even smaller distances should be given. The results for f_s are not unique (a very similar fit can be obtained for different value of fluctuation scale); they are also significantly different than obtained for q_c and thus seem to be not reliable. They should be also checked with greater number of points.

5 RANDOM FIELDS

Based on the obtained results of the vertical and horizontal scale of fluctuation q_c value, random fields have been generated using the Fourier Series Method (Jha & Ching 2012). Although the distributions shown in Figure 4 deviate from the symmetric Gaussian distribution, for the purposes of random field presentation they are considered Gaussian.

An exemplary realization of the random field generated for the values of fluctuation scales obtained for q_c for both zones (Table 2) was presented in Figure 10. As can be seen, the obtained images differ from each other; Zone B, where the horizontal fluctuation scale is only four times higher than the vertical scale, has a much smaller horizontal orientation than zone C where the horizontal scale is 20 times higher than the vertical one.

6 CONCLUSIONS

In this paper, the procedure of identification of random fields for lignite mine waste dump soils based on results from CPTu testing has been presented. Based on the in-situ data the vertical and horizontal scale of fluctuation for the assumed Markov correlation model have been estimated.

The following conclusions can be drawn from the paper:

Lignite mine waste dump soil is a medium with strong spatial variability of parameters. In this case, the probabilistic approach within the Random Field Theory seems to be particularly adequate.

The values of vertical fluctuation scale obtained for q_c and f_s are similar (see also Bagińska et al. 2016).whereas horizontal scales for q_c and f_s have different values. The presented results show that only measurements of q_c provide a reliable source of information for determining the horizontal fluctuation scale. The phenomenon of different scale values for different parameters (particularly in the horizontal direction) requires further research;

The obtained values of vertical scales of fluctuation are comparable to values found in natural soils (Uzielli et al. 2006, Puła et al. 2017) whereas obtained horizontal scales are either similar (zone C) or different (zone B) then expected for natural soils (Cherubini 1997). The small amount of data and the procedure used can give rise to some doubts as to the correctness of the obtained values. For reliable determination of the horizontal scale of fluctuations in this case, a greater number of closer located points are needed.

The obtained histograms of q_c and f_s (Figure 4), which may indicate the presence of more than one constituent, induce the authors to further analyze the dumped soil with use of segmentation technique (Lydzba et al. 2018).

The article was based on the CPTu data measured by PGE Mining and Conventional Energy S.A. - Branch of Bełchatów Coal Mine from Poland.

REFERENCES

Bagińska, I., Frol, V. & Kawa, M. 2017. Klasyfikacja gruntów zwałowych na podstawie pomiarów sondą CPTu. In J. Bzówka & M. Łupieżowc (ed.), *Analizy i doświadczenia w geoinżynierii*: 29–38. Gliwice: Wydawnictwo Politechniki Śląskiej.

Bagińska, I., Kawa, M. & Janecki, W. 2016. Estimation of spatial variability of lignite mine dumping ground soil properties using CPTu results. *Studia Geotechnica et Mechanica*, *38*(1): 3–13.

Borecka A. 2007. Grunt zwałowy—problemy w ocenie parametrów fizyko-mechanicznych. *Geologos* 11: 131–132.

Cherubini C. 1997. Data and consideration on the variability of geotechnical properties of soils. In *Proc. of the ESREL*: 1538–1591. Conf. Lisbon.

Dmitruk S. 1965. Zadania mechaniki gruntów w wymiarowaniu zwałowisk. *Budownictwo* XXV, nr 116. Wrocław: Zeszyty Naukowe Politechniki Wrocławskiej.

Eswaran, H., Ahrens, R., Rice, T. J. & Stewart, B. A. (Eds.). 2002. Soil classification: a global desk reference. CRC Press.

Fenton, G. A. & Griffiths, D. V. 2003. Bearing-capacity prediction of spatially random c ϕ soils. *Canadian Geotechnical Journal* 40(1): 54–65.

Griffiths, D. V. & Fenton, G. A. 2001. Bearing capacity of spatially random soil: the undrained clay Prandtl problem revisited. *Geotechnique* 51(4): 351–359.

Hawley, M. & Cunning, J. (Eds.). 2017. Guidelines for Mine Waste Dump and Stockpile Design. CSIRO PUBLISHING.

Jha, S. K. & Ching, J. 2012. Simulating spatial averages of stationary random field using the Fourier series method. *Journal of Engineering Mechanics* 139(5): 594–605.

Kawa, M. & Łydżba, D. 2015. Evaluation of Bearing Capacity of Strip Footing Using Random Layers Concept. *Studia Geotechnica et Mechanica* 37(3): 31–39.

Kawa, M., Bagińska, I. & Wyjadłowski, M. 2017. The reliability analysis of sheet pile wall located in soil with random properties based on CPTu results. *Engineering Transactions*, 65(1): 193–200.

Lloret-Cabot, M., Fenton, G. A. & Hicks, M. A. 2014. On the estimation of scale of fluctuation in geostatistics. *Georisk: Assessment and Management of Risk for Engineered Systems and Geohazards 8*(2): 129–140.

Łydżba, D., Różański, A. & Stefaniuk, D., 2018. Equivalent microstructure problem: Mathematical formulation and numerical solution. *International Journal of Engineering Science* 123: 20–35.

O'Brien, P. L., DeSutter, T. M., Ritter, S. S., Casey, F. X., Wick, A. F., Khan, E. & Matthees, H. L. 2017. A large-scale soil-mixing process for reclamation of heavily disturbed soils. *Ecological Engineering* 109: 84–91.

Puła, W., Bagińska, I., Kawa, M. & Pieczyńska-Kozłowska, J. 2017. Estimation of spatial variability of soil properties using CPTu results: a case study. In Z. Młynarek & J. Wierzbicki (ed.), *In situ and laboratory characterisation of OC subsoil*: 23–32. Poznań: Wydawnictwo Exemplum.

Puła, W., Pieczyńska-Kozłowska, J. M., & Chwała, M. 2017. Search for the Worst-Case Correlation Length in the Bearing Capacity Probability of Failure Analyses. *In Geo-Risk 2017:* 534–544.

Robertson, P. K. 1990. Soil classification using the cone penetration test. *Canadian Geotechnical Journal* 27(1): 151–158.

Rybicki S., Borecka A. & Mościcki J. 2002 Nowe wyniki sondowań statycznych na zwałowiskach KWB "Turów". *Górnictwo Odkrywkowe* 44 (4): 35–39.

Uzielli, M., Lacasse, S., Nadim, F. & Phoon, K. K. 2006 Soil variability analysis for geotechnical practice. *Characterization and Engineering Properties of Natural Soils* 3: 1653–1752.

Vanmarcke, E. 1983. Random Fields: Analysis and Synthesis, MIT Press.

Vanmarcke, E. 2010. Random fields: analysis and synthesis. World Scientific.

Vessia, G., Cherubini, C., Pieczynska, J. & Pula, W. 2009. Application of random finite element method to bearing capacity design of strip footing. *Journal of GeoEngineering* 4(3): 103–112.

Vardon, P. J., Liu, K., & Hicks, M. A. 2016. Reduction of slope stability uncertainty based on hydraulic measurement via inverse analysis. Georisk: *Assessment and Management of Risk for Engineered Systems and Geohazards* 10(3), 223–240.

Wysokiński L. 2010. Rekultywacja terenów kopalni odkrywkowych i ich wykorzystanie budowlane, *Przegląd Geologiczny* 58 (9/2): 912–918.

Taylor & Francis
Taylor & Francis Group
http://taylorandfrancis.com

Cone Penetration Testing 2018 – Hicks, Pisanò & Peuchen (Eds)
© 2018 Delft University of Technology, The Netherlands, ISBN 978-1-138-58449-5

Strength parameters of deltaic soils determined with CPTU, DMT and FVT

L. Bałachowski, K. Międlarz & J. Konkol
Faculty of Civil and Environmental Engineering, Gdańsk University of Technology, Gdańsk, Poland

ABSTRACT: This paper presents the results of soil investigation in soft, normally consolidated organic soil in the estuary of Vistula river. The analysis concerns clayey mud and peat layers interbedded with loose to medium-dense sands. Several Cone Penetration Tests with pore water measurement (CPTU), Dilatometer Tests (DMT) and Field Vane Tests (FVT) were performed on the testing site. The cone factor N_{kt} was estimated using the results of FVT and peak values of undrained shear strength. The proposition of N_{kt} change due to normalized Friction ratio (F_r) has been given. The possible value of cone factor $N_{\Delta u}$ for organic soils was also suggested. The undrained shear strength of Jazowa clayey mud and peat have been compared with DMT estimates proposed by various researchers. Finally, the structural soil sensitivity of Jazowa deltaic soils was determined on the basis of residual shear strength obtained from FVT and the measurements of sleeve friction.

1 INTRODUCTION

1.1 *Aim of this research*

The research conducted at Jazowa site is related to extensive infrastructural works on soft subsoil. The aim of the study is to establish some local correlations concerning the interpretation of in situ tests in soft organic soils. Some correlations concerning the parameters of organic soils in Central Poland based on advanced in-situ tests were elaborated by Lechowicz (1997), Młynarek (2006), Rabarijoely (2008) & Zawrzykraj (2017). The set of CPTU, DMT and FVT was performed on the trial field near the S7 highway, currently under construction. The aim of the research is to calibrate the cone factors using undrained shear strength on the basis of FVT and to compare the profiles of undrained shear strength obtained with different in-situ tests. Finally, the soil sensitivity based on CPTU and FVT is additionally examined.

1.2 *Testing site description*

The trial field is localized in the delta of Vistula river near Elbląg city, Poland. Alluvial soils layers as mud and peat with sandy interbeddings can be recognized up to 14–15 m depth below ground level. Below 15 m some compacted Pleistocene sands were found. Quite regular subsoil structure was detected in the trial field area with drillings and preliminary CPTU tests. According to soil classification charts and drillings the following layers can be distinguished in the subsoil:

- 0.0–0.7 m: working platform layer,
- 0.7–1.8 m: silty and sandy clays,
- 1.8–2.7 m: clayey mud,
- 2.7–4.0 m: peat,
- 4.0–7.8 m: loose to medium-dense sand,
- 7.8–14.5 m: clayey mud layer intersected with some peat and sand inclusions
- 14.5 m the roof of dense Pleistocene sand.

The soil profile is presented in Figure 1 with typical CPTU sounding results.

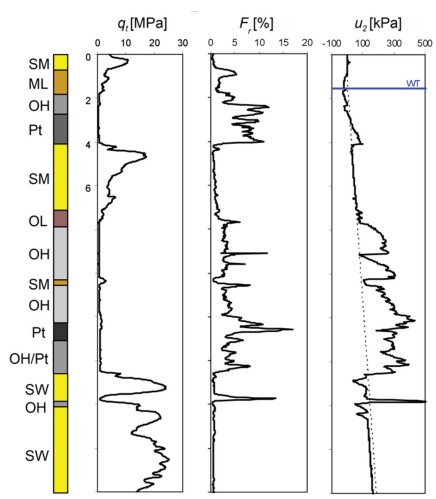

Figure 1. Typical CPTU profile for Jazowa testing site (sounding no. 4).

2 IN SITU TEST RESULTS

2.1 *CPTU and DMT soundings*

Totally 13 CPTU and 8 DMT sounding have been performed at Jazowa testing site. They were performed from the working platform in regular net with side length of 2 m. The typical results of CPTU soundings are given in Figure 1.

Typical results of DMT according to the interpretation proposed by Marchetti (2001) are given in Figure 2. One should notice that the value of lateral stress K_{DMT} for deeper clayey mud layer is close to 2 which indicate normally consolidated soil deposit. The K_{DMT} values for the upper peat and clayey mud layer suggest their slight preconsolidation.

2.2 *Vane test results*

Two electrical FVT using 7.5*13.0 cm tapper tips were conducted as supplementary field investigation at the testing site. The profiles of measured undrained shear strength with maximum and residual values are given in Figure 3a. The FVT results have been corrected due to disturbance, anisotropy and rate effects. For clayey mud layers, correction factors have been applied taking into account plasticity index and Bjerrum relation (Terzaghi 1996). For upper mud layer, with a plasticity index (*Ip*) of 49%, a factor of 0.7 was adopted while for lower layer, with plasticity index of 27.4%, a factor of 0.9 was applied. For peat inclusions the correction factor of 0.5 has been used (Gołębiewska 1983; Landva & La Rochelle 1983, Hanzawa 1994, Long 2005). The maximum and residual profiles of undrained shear strength with applied correction factors are presented in Figure 3b.

For upper soft soil deposit generally constant value of c_u can be observed and it is reasonable due to slight preconsolidation of the soil. On the other hand, for deeper mud layers nearly linear increase of undrained shear strength with depth can be seen.

3 CALIBRATION OF CONE FACTORS

For each CPTU sounding the subsoil was classified into thin layers typically 0.3–0.4m thick in the vicinity of vane tests. For each layer the average normalized friction ratio F_r and soil type behavior index I_c have been calculated.

3.1 N_{kt} *factor*

Cone factor during undrained cone penetration is defined (Lunne 1997) as:

$$N_{kt} = \frac{(q_t - \sigma_{v0})}{c_u} \tag{1}$$

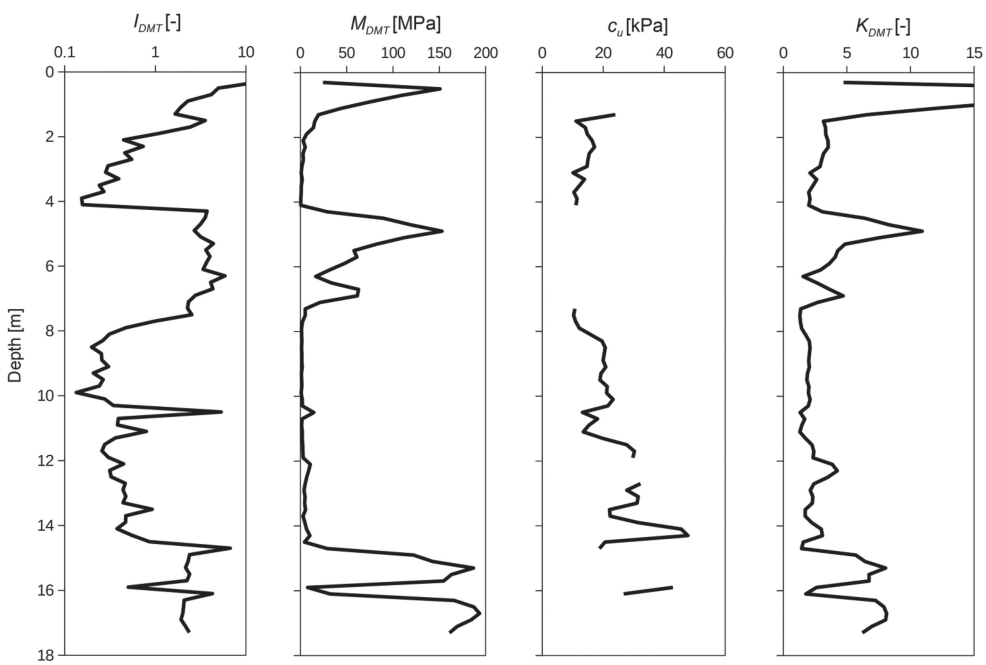

Figure 2. Typical DMT results for Jazowa trial field (sounding no.5).

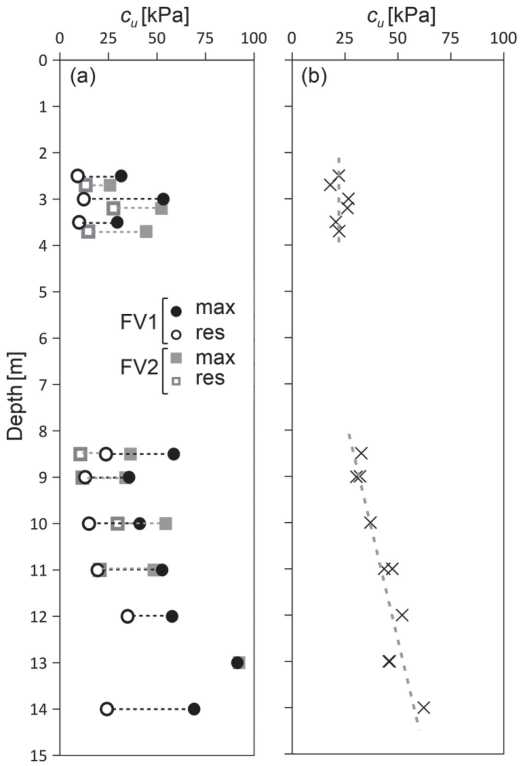

Figure 3. Uncorrected shear strength from the FVT (a) and corrected values (b).

where N_{kt} = cone factor; q_t = average corrected cone resistance; σ_{v0} = total vertical stress; c_u = undrained shear strength.

Here, the maximum shear strength after correction from FVT at the corresponding depth is used as a reference one. The N_{kt} –I_c relation obtained from sounding no.4 for given soil layers is shown in Figure 4a. It can be seen that the cone factor is generally increasing with friction ratio and N_{kt} is decreasing with soil type behavior index I_c, see Figure 4b.

To provide the sufficient relation between N_{kt} and F_r and N_{kt} and I_c the analysis have been performed on average values obtained from all 13 CPTU tests performed at the site. The average values of N_{kt} factor were calculated for each layer and the results are summarized as a function F_r in Figure 5a and as a function of I_c in Figure 5b.

As one can see, The N_{kt}—F_r provides significantly better correlation with high coefficient of determination equal to 0.871. The N_{kt}—F_r relation can be described as:

$$N_{kt} = 1.242 \times F_r + 7.803 \quad (2)$$

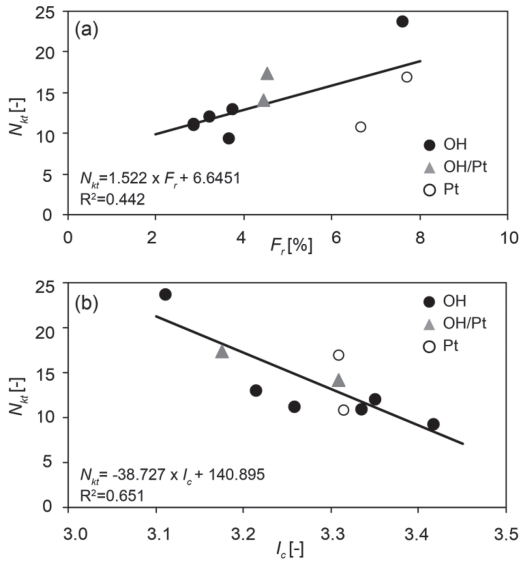

Figure 4. N_{kt} *vs.* F_r (a) and N_{kt} *vs.* I_c (b) relations.

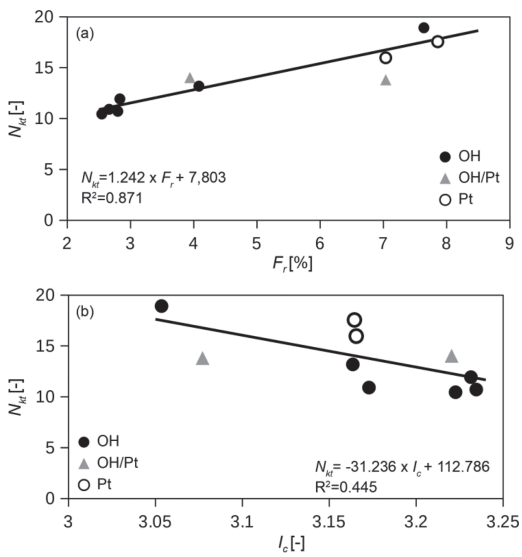

Figure 5. N_{kt}—F_r (a) and N_{kt}—I_c (b) relations based on averaged 13 CPTU soundings.

where: N_{kt} = cone factor; F_r = normalized friction ratio.

3.2 $N_{\Delta u}$ *factor*

Cone factor can be also calculated on the basis of excess pore water pressure defined as:

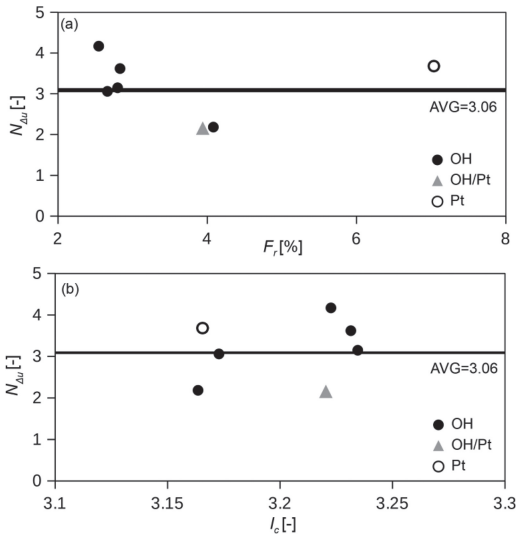

Figure 6. $N_{\Delta u}$—F_r (a) and $N_{\Delta u}$—I_c (b) relations based on averaged 13 CPTU soundings.

$$N_{\Delta u} = \frac{(u_2 - u_0)}{c_u} \tag{3}$$

where $N_{\Delta u}$ = cone factor; u_2 = average pore water pressure registered on shoulder filter element during penetration; u_0 = hydrostatic pore water pressure; c_u = undrained shear strength of soil.

The field measurements of u_2 are characterized by high scatter of data and negative registered pressure up to 3,5 m, see Figure 1 for instance. Consequently, the analysis have been performed only for the deeper clayey mud layer. As in the case of N_{kt} factor, the results are compiled for all profiles and the average values form the measurement have been used. The corrected maximum shear strength from FVT at the corresponding depth is used as a reference value.

The relationship between $N_{\Delta u}$ and F_r is shown in Figure 6a and between $N_{\Delta u}$ and I_c in Figure 6b. As can be seen, considerably higher scatter of cone factor $N_{\Delta u}$ was found due to irregularities in the registered pore water pressure u_2. In both relationships the $N_{\Delta u}$ is ranging between approximately 2.16 and 4.17 with average value of 3.06.

3.3 *Undrained shear strength*

Undrained shear strength c_u for clayey mud obtained from FVT is compared with CPTU assessment with N_{kt} after Equation 2 in Figure 7a. The additional estimations of c_u used in the comparison are based on DMT and Unconsolidated Undrained

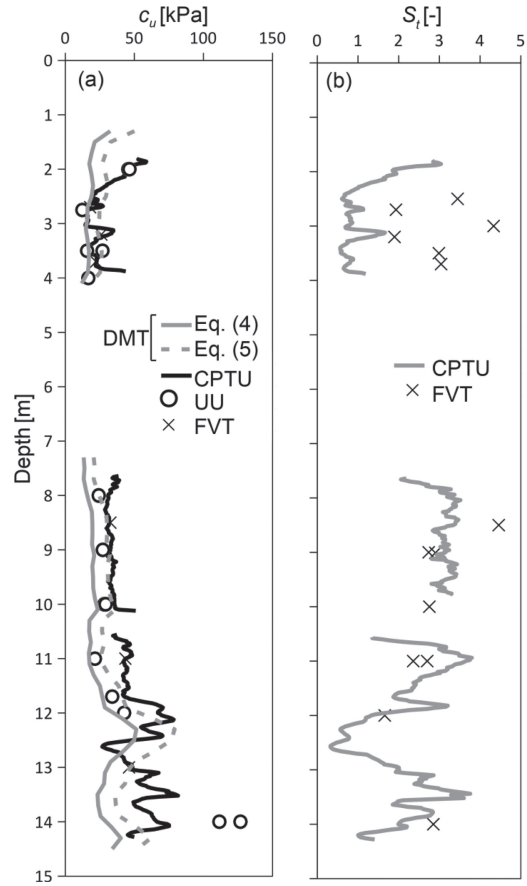

Figure 7. Undrained shear strength of Jazowa soft soil deposits estimated with different methods (a) and soil sensitivity assessed from CPTU and FVT (b).

(UU) triaxial compression tests. Two DMT estimates are based on Marchetti (2001) proposition:

$$\frac{c_u}{\sigma'_{v0}} = 0.22 \times (0.5 \times K_{DMT})^{1.25} \tag{4}$$

where c_u = undrained shear strength; σ'_{v0} = effective vertical stress; K_{DMT} = horizontal stress index, and Lechowicz (1997) equation:

$$\frac{c_u}{\sigma'_{v0}} = S \times (0.45 \times K_{DMT})^{1.20} \tag{5}$$

where c_u = undrained shear strength; σ'_{v0} = effective vertical stress; S = normalized undrained shear strength for normally consolidated state equal to 0.4 for organic soils (Lechowicz 1997); K_{DMT} = horizontal stress index.

In DMT-based estimates of c_u the average distribution of K_{DMT} is used. As one can see, the back-calculated CPTU estimation fits well into the FVT results and UU results. Lechowicz proposition also corresponds to the other results. On the other hand the Marchetti (2001) formula underestimates the c_u in the considered soft soils.

4 SOIL SENSITIVITY

The last analyzed aspect of strength parameters is related to the soil sensitivity which was estimated using two approaches. In the first one the results of FVT with the maximum and residual value of shear strength have been applied. The second approach uses the undrained shear strength estimated from the cone factor N_{kt} calibrated in the present study and the sleeve friction.

The residual shear strength is assumed as a averaged sleeve friction value in a given layer from all conducted CPTU tests. The comparison is presented in Figure 7b. One can notice that for deeper soft soil deposits the sensitivity obtained from CPTU correlation fits well the trend outlined by FVT tests. However the results for upper mud and peat layer are quite dispersed and the soil sensitivity obtained with CPTU is underestimated.

5 CONCLUSIONS

Distinct relationship between the N_{kt} and F_r (I_c) parameters for organic soils in the delta of Vistula river was found in the present study. In this particular case, the N_{kt} factor is more suitable for calculating the undrained shear strength than $N_{\Delta u}$. In case of the $N_{\Delta u}$ factor, no specific correlation between the parameters $N_{\Delta u}$ and F_r (I_c) was determined. Particular measurement points are quite dispersed and the determination of any relation between them is practically impossible, so the constant value of $N_{\Delta u} = 3.06$ was proposed. For this reason, the N_{kt} factor was used for further calculations.

In this research site, the Lechowicz (1997) DMT formula was able to correctly estimate undrained shear strength. The undrained shear strength profile from CPT test, shown in Fig. 7a, was prepared relying on the N_{kt} factor given by Equation 2. It can be noticed that they correspond to values obtained from the vane test and are similar to the triaxial UU compression test results. Similar situation is in case of the soil sensitivity. The profile obtained from CPT is close to the values outlined from FVT and the sensibility of clayey muds and peats in deeper layers is rather low and generally does not exceed 4.

ACKNOWLEDGEMENTS

The research is supported by the National Centre for Research and Development grant PBS3/B2/18/2015.

REFERENCES

Gołębiewska A. 1983. Vane testing in peat, *Proc. 7th Danube ECSMFE, Kishinev*, Vol. 1: 113–117.

Hanzawa, H., Kishida, T., Fukasawa, T. & Asada, H. 1994. A case study of the application of direct shear and cone penetration tests to soil investigation, design and quality control for peaty soils. *Soils and Foundations*, Vol. 34, No. 4: 13–22.

Landva, A.O. & La Rochelle, P. 1983. Compressibility and shear strength characteristics of Radforth Peats. *Testing of Peats and Organic Soils*. ASTM STP 820, P.M. Jarrett (ed.): 157–191.

Lechowicz, Z. 1997. Undrained shear strength of organic soils from dilatometer test. *Annals of Warsaw Agriculture University—SGGW*. Land Reclamation 28: 85–96.

Long, M. 2005. Review of peat strength, peat characterisation and constitutive modeling of peat with reference to landslides. *Studia Geotechnica et Mechanica, Vol. XXVII,* No. 3–4: 67–90.

Lunne, T., Powell, J.J.M. & Robertson, P.K. 1997. Cone Penetration Testing in Geotechnical Practice.

Mesri, G. & Ajlouni, M. 2007. Engineering Properties of Fibrous Peats. *Journal of Geotechnical and Geoenvironmental Engineering*, 133(7): 850–866.

Młynarek, Z., Tschuschke, W., Wierzbicki, J., & Marchetti, S. 2006. Interrelationship between shear and deformation parameters for gyttia and peat from CPT and DMT tests. In *Proceedings 13th Danube European Conference on Geotechnical Engineering*. Ljubljana.

Rabarijoely, S. 2008. The use of dilatometer for the determination of undrained shear strength in organic soils. *Annals of Warsaw University of Life Sciences—SGGW*. Land Reclamation No 40,2008: 97–105.

Terzaghi, K., Peck, R.B., & Mesri, G. 1996. *Soil mechanics in engineering practice*. John Wiley & Sons.

Totani, G., Marchetti, S., Monaco, P. & Calabrese, M. 2001. Use of the Flat Dilatometer Test (DMT) in geotechnical design. *International Conference On In situ Measurement of Soil*.

Zawrzykraj, P., Rydelek, P. & Bąkowska, A., 2017. Geo-engineering properties of Eemian peats from Radzymin (central Poland) in the light of static cone penetration and dilatometer tests. *Engineering Geology 226 (2017)*: 290–300.

Taylor & Francis
Taylor & Francis Group
http://taylorandfrancis.com

Cone Penetration Testing 2018 – Hicks, Pisanò & Peuchen (Eds)
© 2018 Delft University of Technology, The Netherlands, ISBN 978-1-138-58449-5

Estimation of the static vertical subgrade reaction modulus k_s from CPT

N. Barounis & J. Philpot
Cook Costello, Christchurch, New Zealand

ABSTRACT: A methodology for the estimation of the static vertical subgrade reaction modulus (k_s) for cohesionless soils from the Cone Penetration Test (CPT) has been introduced in 2013 (Barounis et al.) and 2015 (Barounis and McMahon) and has recently been integrated (Barounis and Philpot, 2017). In this paper, the conclusions from the early two papers are utilized for developing an integrated methodology based on the correlation between q_c and N_{60} (Robertson, 2012). The fundamental concepts and the theory of the proposed methodology are presented with a step-by-step procedure in this paper. The methodology returns one value termed K_F, which is the equivalent spring stiffness for any foundation depth and shape under consideration. The methodology produces values that are as conservative as the traditional SPT approach proposed by Scott (Scott, 1981). The methodology is applied on numerous sandy sites in New Zealand for different foundation typologies.

1 INTRODUCTION

As an initial step for facilitating the earthquake-resistant design of a building and its foundations, the static spring stiffness, or static vertical subgrade reaction modulus, on the surface of an assumed homogeneous half-space is typically evaluated for the given site. Then, by applying numerous dynamic modification factors to the static spring stiffness (ASCE 41–13), the dynamic spring stiffness can be evaluated. Dynamic modification factors are applied to account for the frequency of the excitation force, the embedment of the foundation and the foundation shape. The most fundamental step in this process for the structural engineer, is to determine if the foundation system under analysis is rigid or flexible. Many references are available for facilitating this step (refer to ASCE 41–13, 2014 or ACI 336). Thus, the estimation of the static spring stiffness is an important step in undertaking both static and earthquake resistant design of foundations. This paper is focused only on the static spring stiffness of flexible foundation systems.

The static vertical subgrade reaction modulus k_s is a conceptual relationship, which is defined as the soil pressure exerted σ divided by the deflection δ (Bowles, 1997).

$$k_s = -(\mathrm{MN/m^3}) \tag{1}$$

The static vertical subgrade reaction modulus is not an actual engineering property of the soil, such as Poisson's ratio, as it varies with the width and shape of the foundation (Terzaghi, 1955). The principle underlying the definition of k_s is the resistance a soil layer provides as some deflection is imposed on it due to the applied stress, analogous to a spring shortening at some imposed load. In structural engineering applications, k_s is used to model the soil stiffness in the vertical plane when soil-foundation-structure interaction considerations are included in the structural analysis. Typically, as best practice suggests, structural engineers adopt k_s values recommended by a geotechnical engineer. The structural engineer further tests the sensitivity of the model for k_s values ranging between 0.5 k_s and 2.0 k_s (ASCE 41–13, 2014). The geotechnical engineer needs to assess the k_s range for the particular situation. These values are also to be accompanied by ultimate foundation capacity estimations.

A methodology for the estimation of k_s for sands from the Cone Penetration Test (CPT), as an alternative to the conventional estimation relying on SPT as proposed by Scott (Scott, 1981) for a 300 mm plate, was proposed by Barounis et al. (2013). From recent research on the applicability of the proposed CPT methodology (Barounis and Armaos, 2016), it was demonstrated that the produced k_s values are stiffer than the values produced by Scott. The stiffer springs from CPT are conservative for the seismic response of the structure, while the softer springs from SPT are conservative for foundation deformation and their effects to the superstructure.

This paper presents an integrated methodology for the estimation of k_s values for flexible shallow foundations on cohesionless soils based on the correlation between q_c and N_{60} (Robertson, 2012). The methodology produces similar values to the SPT method proposed by Scott for the k_{300} of a 300 mm plate. The final value, corrected for foundation

shape, K_F is similar to the value produced by using the conventional SPT-based method by Scott.

For a detailed explanation of the background theory to the methodology, please refer to previous papers from Barounis et al. (2013, 2015, 2016 and 2017) on this topic. The additional theoretical basis for the method is explained in the next paragraph.

2 INTEGRATED METHODOLOGY FOR ESTIMATING THE MODULUS OF SUBGRADE REACTION K_S

2.1 *Fundamental assumptions, advantages and theoretical basis of the methodology*

The fundamental assumptions and theoretical basis for the proposed methodology and its advantages are the following:

- The methodology is applicable to cohesionless soils, only when tested with a CPT that measures penetration resistance at 10 or 20 mm increments with a 35.7 mm diameter cone.
- The theory of springs in series is assumed, modified to consider the configuration of soil layers. This means that the equivalent spring stiffness K_{eq} can be estimated by using the proposed methodology.
- The range of SPT N_{60} values is limited to between 0 and 50 blows. No extrapolation over 50 blows shall be adopted in any case. Thus, an SPT N_{60} of 50 is considered to be effective refusal.
- This upper bound value of SPT produces a maximum $K_{SPT(0.3)}$ (spring for a 300 mm plate based on Scott) value of 90 MN/m^3. Thus, any k_s value produced using this methodology for the actual foundation cannot exceed 90 MN/m^3.
- If values larger than 90 MN/m^3 need to be adopted, either for the 300 mm plate, or for the actual foundation, then actual plate load tests and further site investigations will need to be performed to prove that the subgrade modulus exceeds this value.
- The corresponding q_c (cone tip resistance in MPa) value for any soil with I_c (soil behavior type index) between 1.00 and 2.60 is related to the SPT N_{60} according to the correlation by Robertson, as shown in Figure 1. This figure shows that for increasing I_c values (increasing fines content) at effective SPT refusal, the corresponding q_c value reduces from 35.4 MPa for $I_c = 1.00$ to 12.5 MPa for $I_c = 2.60$. As the fines content increases and for a given N_{60} value, the cone resistance and the spring stiffness reduces, along with the soil stiffness E_s (refer to Figure 1).
- The methodology is applicable for circular, square, continuous or rectangular shallow foundations, founded at any shallow depth in the ground including at the ground surface. The equivalent modulus K_{eq} for any foundation shape is estimated based on the simplified formulae provided by Poulos and Davis (Xiao, 2015) that computes the vertical stress distribution beneath the centre of the foundation.
- By using the Poulos and Davis (Xiao, 2015) formulae, essentially a weighting factor is applied to every 10 mm or 20 mm long spring. Hence, the soils nearer the foundation become more critical to the overall response than the soils substantially deeper, or outside the pressure bulb of the foundation.
- The methodology considers an influence depth under any foundation configuration to be the depth at which the vertical stress increase from the foundation becomes equal to 20% of the vertical effective stress (20% rule).
- The methodology is sensitive to stiffness inversions, i.e. dense soils overlying loose soils. The methodology is also sensitive when denser soils are present at some depth from the foundation (within 20% influence depth). In general, the methodology produces good results, even for highly stratified soils or for sandwiched layers of contrasting stiffness.

Figure 1. Relationship between q_c and N_{60} for I_c between 1.00 and 2.60.

The methodology is presented in Figure 2. Detailed explanations for each step of the methodology are given in the subsequent paragraphs.

2.1.1 *1st Step: Estimation of K_{CPT} stiffness*

In this first step, the spring stiffness of the 10 mm long soil element is estimated. As per equation 1, the spring stiffness is the cone resistance q_c divided by the displacement. For a CPT with 35.7 mm diameter and a 10 mm incremental penetration:

$$K_{CPT} = 100 q_c \tag{2}$$

Step #	Equation	Units	Notes
1	For 10mm increment: $K_{CPT}=100q_c$ For 20mm increment: $K_{CPT}=50q_c$	MN/m³	CPT spring stiffness
2	$K_{CPT\,(0.3)}=0.119K_{CPT}$	MN/m³	Conversion to 300mm plate spring stiffness
3	$K_{CPT\,(SPT0.3)}= K_{CPT(0.3)}$ / CF where for 10mm increment: $CF=0.668(10^{(1.127-0.282I_c)})$ and for 20mm increment: $CF=0.334(10^{(1.127-0.282I_c)})$	MN/m³	Conversion to a similar SPT spring stiffness for a 300mm plate as per Scott's correlation, $K_{SPT\,(0.3)}=1.8N_{60}$
4	$K_{eq20\%} = \frac{\sum_{i=1}^{n} Iz_i K_i}{\sum_{i=1}^{n} Iz_i}$	MN/m³	Equivalent spring stiffness for a 300mm plate considering an influence depth as per the 20% rule that corresponds to the foundation geometry under analysis
5	$K_F=\underline{K}_{eq}$ x $(m+0.5)/(1.5m)$ where m = L/B	MN/m³	Shape correction for the given foundation geometry under analysis

Figure 2. Excerpt from Barounis et al. (2017) paper summarising the five key steps of the methodology.

This conversion is applied for every q_c measurement until the final CPT depth.

2.1.2 *2nd step: estimation of the spring $K_{CPT(0.3)}$ for a 300 mm plate by conversion from step 1*

In this step, a conversion takes place from the CPT spring to the equivalent 300 mm diameter plate spring. This is undertaken according to the formula proposed by ACI (ACI 336, 2002) and Bowles (Bowles, 1997), which relies on principles earlier presented by Terzaghi (1955):

$$K_{CPT(0.3)} = K_{CPT}\frac{D_{CPT}}{300} = K_{CPT}\frac{35.7}{300} = 0.119K_{CPT} \quad (3)$$

where D_{CPT} is the diameter of the CPT cone in mm. This is consistent with the subgrade reaction modulus theory as a greater loaded area produces lower subgrade reaction values (Terzaghi, 1955 and Bowles, 1997).

2.1.3 *3rd step: conversion to a similar SPT spring stiffness value depending on I_c by means of CF*

In this step, a reduction of the spring stiffness is undertaken by using a conversion factor CF. This reduction results in the CPT spring value coinciding with the value estimated from Scott's method.

Robertson (2012) published a correlation between q_c and SPT N_{60} with the soil behavior type index I_c (Robertson, 2015). The relationship is the following:

$$\frac{\left(\frac{q_t}{p_a}\right)}{N_{60}} = 10^{(1.127-0.282I_c)} \quad (4)$$

where $q_t = q_c$ for cohesionless soils and p_a = atmospheric pressure.

By substituting I_c values between 1.00 and 2.60 that correspond to the range of cohesionless soils, p_a of 101 kPa, and SPT N_{60} from 0 to 50 as per the assumptions in section 2.1, the relationship is depicted in Figure 1.

By dividing the $K_{CPT(0.3)}$ with $K_{SPT(0.3)}$, the stiffness ratio of the CPT spring for the 300 mm plate is compared to the SPT spring for the same 300 mm plate. This ratio can be defined as a Conversion Factor (CF):

$$CF = \frac{K_{CPT(0.3)}}{K_{SPT(0.3)}} = \frac{0.119(100q_c)}{1.8N_{60}} = \frac{11.9q_c}{1.8N_{60}} = 6.61\frac{q_c}{N_{60}} \quad (5)$$

And by solving equation (4) for q_c and substituting in (5) we have:

$$CF = 6.61\left(0.101\left(10^{(1.127-0.282I_c)}\right)\right) \quad (6)$$

$$CF = 0.668\left(10^{(1.127-0.282I_c)}\right) \quad (7)$$

Similarly, for a 20 mm incremental penetration:

$$CF = 0.334\left(10^{(1.127-0.282I_c)}\right) \quad (8)$$

This means that CF is dependent on I_c and the incremental testing depth. Applying the CF to the $K_{CPT(0.3)}$ returns a similar spring stiffness for a 300 mm plate diameter to the SPT-based method from Scott (1981). By using the symbol $K_{CPT(SPT0.3)}$ for the SPT spring stiffness produced by the CPT approach, the equation becomes:

$$K_{CPT(SPT0.3)} = \frac{K_{CPT(0.3)}}{CF} \quad (9)$$

The value of CF can be taken from equations 7 or 8 depending on the CPT incremental testing depth.

2.1.4 *4th step: Equivalent spring stiffness K_{eq} for a 300 mm plate*

The general theory of springs suggests that the equivalent spring stiffness K_{eq} of an infinite chain of springs is given by the formula:

$$K_{eq} = \frac{k_1 k_2 \ldots k_n}{k_1 + k_2 + \ldots + k_n} = \frac{\prod_{i=1}^{n} k_i}{\sum_{i=1}^{n} k_i} \quad (10)$$

It must be recognized that equation 10 is insensitive to the configuration of soil layers. In other words, the equivalent spring stiffness would return the same value regardless of the sequence with

which the soil layers are configured. The assumptions underlying this formula maybe appropriate to be used in structural mechanics; however, it does not accurately capture the soil and foundation behavior, especially when looser soils are located near the foundation level, or when very dense soils are located at some depth below the foundation, but within the 20% influence bulb. Also, from a numerical perspective, it is impossible for common software to compute the product of 100 individual springs per 1m of CPT. For these reasons, it is proposed to model and capture any layer configuration by using the Boussinesq theory in accordance with the simplified formulae proposed by Poulos and Davis (1974) as presented in Xiao (Xiao, 2015). In essence, the Boussinesq methodology is used to apply a weighting factor to every $K_{CPT(SPT0.3)}$ spring within the influence bulb of the foundation. As depth increases, the associated spring stiffness value becomes less significant for the foundation behavior. Thus, dense deeper soils may not provide substantial stiffness to the foundation, or loose deeper soils may soften the spring substantially. The weighting factor is the well-known influence factor I_z, which takes the value of 1.0 at the foundation depth and diminishes to values that tend to zero with increasing depth.

The proposed formula has the following form:

$$K_{eq20\%} = \frac{\sum_{i=1}^{n} Iz_i K_i}{\sum_{i=1}^{n} Iz_i} \tag{11}$$

Where I_{zi} is the influence factor that corresponds to a spring stiffness K_i at depth z_i. Equations 12–15 show influence factors for circular, square, continuous and rectangular foundations, respectively (Xiao, 2015):

$$z = (q - \sigma')\left[1 - \left(\frac{1}{1 + \left(\frac{B}{2z}\right)^2}\right)^{1.50}\right] \tag{12}$$

$$z = (q - \sigma')\left[1 - \left(\frac{1}{1 + \left(\frac{B}{2z}\right)^2}\right)^{1.76}\right] \tag{13}$$

$$z = (q - \sigma')\left[1 - \left(\frac{1}{1 + \left(\frac{B}{2z}\right)^2}\right)^{2.60}\right] \tag{14}$$

Table 1. Shape correction factors for various foundation shapes.

Foundation shape	Shape correction
Circular	1.0
Continuous	$(m + 0.5)/(1.5\,m)$, $m = L/B$, tends to 0.67 when $L/B \geq 5$
Square	1.0
Rectangular	$(m + 0.5)/(1.5\,m)$, $m = L/B$

$$z = (q - \sigma')\left[1 - \left(\frac{1}{1 + \left(\frac{B}{2z}\right)^{\left(1.38 + \frac{0.62B}{L}\right)}}\right)^{\left(2.60 - \frac{0.84B}{L}\right)}\right] \tag{15}$$

where B, L and z are respectively the breadth, length and depth below the foundation in metres, $(q - \sigma'_0)$ is the net applied foundation pressure in kPa, q is the gross exerted foundation pressure in kPa and σ'_0 is the effective stress at the foundation depth in kPa. Equation 11 is applied to the depth z at which the stress increase from the net applied pressure equals 20% of the vertical effective stress.

2.1.5 *5th step: correction for shape of foundation*

In this step, the final foundation spring stiffness value K_F is estimated. From the four previous steps, a similar spring stiffness value to the SPT approach has been established. The application of a correction factor for the shape of the foundation with length L and breadth B will also result in a similar corrected spring as for the SPT approach. The shape correction factors are presented in Table 1. K_F is determined from the equation:

$$K_F = S_F K_{eq20\%} \tag{16}$$

3 EXAMPLE CALCULATIONS: FOUR SANDY SITES IN CHRISTCHURCH

The proposed methodology has been applied on four different sandy sites in Christchurch, New Zealand. The foundation shape, dimensions, applied pressures and other key information are presented in Figure 3.

The summary of results from the proposed methodology are presented in Figures 4–6. Note that the $K_{CPT(SPT0.3)}$ values do not exceed 90 MN/m^3.

The results of the proposed methodology for the four sites and their agreement with Scott's approach are presented in Tables 2 and 3. The bar

Site	Foundation Shape	Length (m)	Breadth (m)	Depth (m)	Applied Pressure (kPa)	GWT Depth (m)	Influence Depth {20% Rule} (m)
1	Rectangular	10	5	0	50	0.6	7.56
2	Continuous	10	2	0	50	1.0	3.81
3	Square	5	5	0	50	1.2	5.96
4	Circular	N/A	5	0	50	1.0	5.76

Figure 3. Excerpt from Barounis et al. (2017) paper summarising foundation typologies for the four sites.

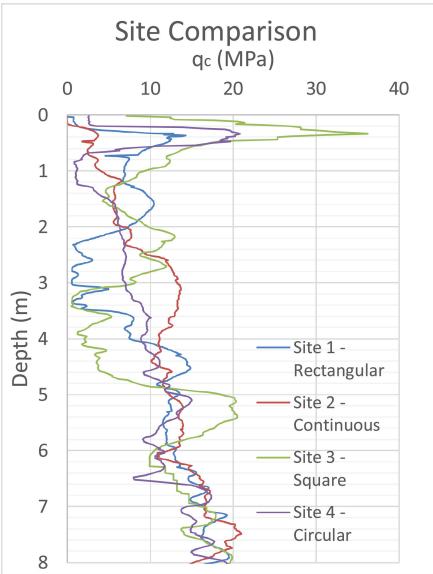

Figure 4. Comparison of q_c across all sites.

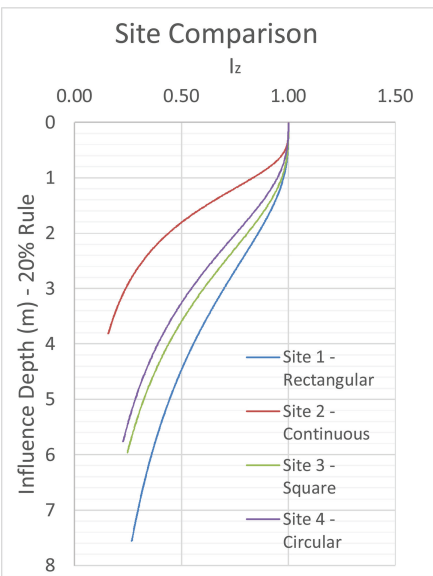

Figure 5. Comparison of influence depths (20% rule) across all sites.

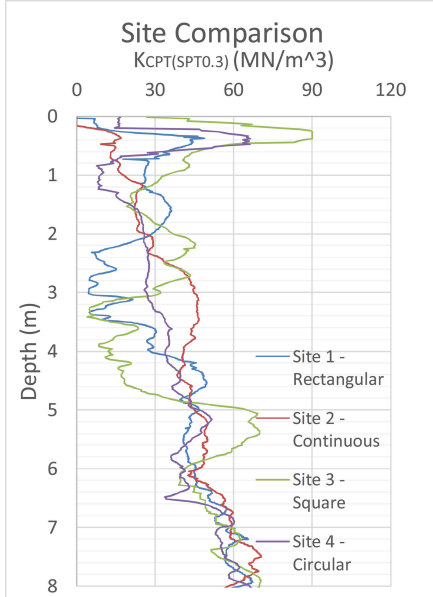

Figure 6. Comparison of $K_{CPT(SPT0.3)}$ values across all sites.

Table 2. Foundation shape, equivalent spring stiffness and foundation spring stiffness.

Site #	Foundation shape	$K_{eq20\%}$ (MN/m³)	K_F (MN/m³)
1	Rectangular	30.07	25.06
2	Continuous	21.14	15.51
3	Square	37.67	37.67
4	Circular	28.86	28.86

Table 3. Depth weighted N_{60} and q_c values and spring stiffness produced by Scott (1981) methodology.

Site #	$\overline{N_{60}}$	$\overline{q_c}$	$\frac{\overline{q_c}}{\overline{N_{60}}}$	$K_{eq}20\%$ (Scott)	K_F (Scott)
1	17	8.13	0.49	30.07	25.06
2	12	5.37	0.46	21.14	15.51
3	21	10.56	0.50	37.67	37.67
4	16	7.45	0.47	28.86	28.86

above the N_{60} and q_c values in Table 3 indicates that these are depth weighted values by using the Poulos and Davis (1974) influence factors. These values are equivalent N_{60} and q_c values for the influenced soil layers as a whole. These are plotted in Figure 7 indicating the values are consistent with the predominant soil conditions encountered at all four sites.

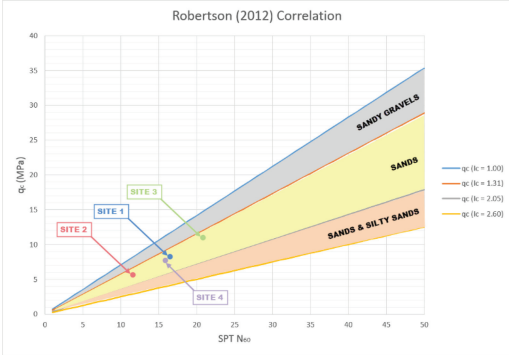

Figure 7. Relationship between q_c and N_{60} for I_c between 1.00 and 2.60 with depth weighted values plotted for all four sites.

4 CONCLUSION

An integrated methodology for the estimation of static spring stiffness from CPT has been presented for flexible shallow foundations on cohesionless soils based on the relationship between q_c and N_{60} (Robertson, 2012). The methodology can be applied to estimate the equivalent spring stiffness $K_{eq20\%}$ for a flexible shallow foundation and then subsequently estimate the K_F value for the actual foundation size and shape. The methodology can only be applied for SPT values ranging from 0 to 50, corresponding to a q_c that depends on I_c. For facilitating a Winkler foundation type of analysis applicable to flexible foundation systems, ultimate foundation capacity estimations also need to be undertaken by a geotechnical engineer as per well-established available methodologies. The methodology is expected to return similar values, in alignment with the SPT approach as per Scott (1981). However, more research, that includes sensitivity analysis for the proposed methodology, needs to be undertaken to verify the methodology returns reliable spring values for all possible soil configurations. For assessing K_F, one should not rely on one methodology. A number of methods should be applied, of which this could be one.

REFERENCES

ACI Committee 336 (2002). Suggested design procedures for combined footings and mats. Detroit: American Concrete Institute.

ASCE Standard ASCE/SEI 41–13 (2014). Seismic evaluation and retrofit of existing buildings. American Society of Civil Engineers.

Barounis, N., Saul, G. & Lally, D. (2013). Estimation of vertical subgrade reaction coefficient from CPT investigations: applications in Christchurch. Proceedings 19th NZGS Geotechnical Symposium, 2013, Queenstown.

Barounis, N. & McMahon, P. (2015). Estimation of vertical subgrade reaction modulus for sands from CPT investigations. 16th European Conference of Soil Mechanics and Geotechnical Engineering, 13–17 September 2015. Edinburgh, UK.

Barounis, N. & Armaos, P. (2016). Sensitivity of the vertical modulus of subgrade reaction, as estimated from CPT for the design of foundation and for comparison with values from SPT for a site in Christchurch. NZSEE 2016 Conference, reducing risk, increasing resilience, 1–3 April 2016, Christchurch, New Zealand.

Barounis, N. & Philpot, J. (2017). Estimation of the vertical subgrade reaction modulus k_s from CPT for shallow foundations on cohesionless soils. NZSEE 2017 Conference, Next Generation of Low Damage and Resilient Structures, 27–29 April, Wellington, New Zealand.

Bowles, J.E. (1997). Foundation analysis and design, 5th Edition. New York: McGraw-Hill.

Poulos, H.G. & Davis, E.H. (1974). Elastic solutions for soil and rock mechanics. John Wiley, New York.

Robertson, P.K. & Cabal K.L. (2015). Guide to cone penetration testing, 6th Edition. Gregg Drilling.

Scott, R.F. (1981). Foundation analysis. Prentice Hall, Englewood Cliffs, NJ.

Terzaghi, K. (1955). Evaluation of coefficients of subgrade reaction. Géotechnique, Volume 5, Issue 4, 01 December 1955, pages 297–326.

Xiao, M. (2015). Geotechnical Engineering Design. John Wiley and Sons Ltd. UK.

Cone Penetration Testing 2018 – Hicks, Pisanò & Peuchen (Eds)
© 2018 Delft University of Technology, The Netherlands, ISBN 978-1-138-58449-5

Estimation of in-situ water content and void ratio using CPT for saturated sands

N. Barounis & J. Philpot
Cook Costello, Christchurch, New Zealand

ABSTRACT: The CPT is used extensively for site characterization, soil profiling, determination of groundwater conditions and the estimation of geotechnical parameters. The geotechnical parameters that can be estimated by using the CPT include bulk unit weight, shear strength and stiffness, among many others. Best practice suggests the CPT is to be used in combination with laboratory testing, when the budget and timeframes allow for such testing to be undertaken. For low risk projects in New Zealand, such testing is not undertaken due to a restricted budget. Typical soil classification tests, such as water content, bulk unit weight, sieve analysis and plasticity index, are not commonly performed for such projects. These parameters are important for characterizing the soil behavior, in both static and dynamic conditions. This paper proposes a methodology for estimating the in-situ water content, void ratio, dry unit weight and porosity from CPT for saturated sands.

1 INTRODUCTION

The CPT is a well-established, strain-controlled failure test that is typically performed by pushing a 35.7 mm diameter penetrometer, with a conical tip and an apex angle of 60°, vertically into the ground at a penetration rate of approximately 20 mm/s. The tip resistance stress of the cone q_c and the sleeve friction resistance f_s (both in MPa), are recorded versus the testing depth. Typically, q_c is recorded against an incremental penetration of 2 mm to 10 mm. Other cone sizes and geometries are also available for pushing through dense gravels and deep soils.

The CPT is used extensively for delineating soil stratigraphy and estimating geotechnical parameters including bulk unit weight, relative density, cohesion, angle of friction and shear modulus (Robertson and Cabal, 2015) for a wide range of soils. The correlations for geotechnical parameters from CPT are semi-empirical and vary in both reliability and applicability (Robertson and Cabal, 2015). CPT is also a well-established test for evaluating the liquefaction potential (Robertson and Cabal, 2015).

This paper presents an alternative methodology for estimating water content, void ratio, dry unit weight and porosity based on the well-established bulk unit weight correlation published by Robertson & Cabal (2010). Based on this correlation, the bulk unit weight (γ) of each soil layer is estimated depending on the recorded q_t (cone resistance, corrected for pore water effects) and f_s. The correlation for the bulk unit weight is expressed by Equation 1 (Robertson & Cabal, 2010):

$$\frac{\gamma}{\gamma_w} = 0.27\left[\log R_f\right] + 0.36\left[\log\left(\frac{q_t}{p_a}\right)\right] + 1.236 \qquad (1)$$

where R_f = friction ratio = $(f_s/q_t)100\%$; γ_w = unit weight of water, in same units as γ; and p_a = atmospheric pressure, in same units as q_t.

Prediction of the soil behavior is achieved by means of the normalized Soil Behaviour Type (SBT_n) (Robertson and Cabal, 2015) for soils ranging from clays and silts to sands and gravels. Thus, a soil profile to the final testing depth can be inferred, accompanied by the corresponding bulk unit weight. This procedure enables the geotechnical engineer to produce a continuous estimate of the total overburden stress. By delineating the location of the groundwater table, effective overburden stress can be also estimated.

In the absence of laboratory results for any given project, the water content, void ratio, dry unit weight and porosity are four important parameters that are usually overlooked. These parameters are important for characterizing the soil behavior, in both static and dynamic conditions.

In this paper, a simple methodology is proposed for estimating the in-situ water content, void ratio, dry unit weight and porosity from CPT. The theoretical background, limitations and advantages of the proposed methodology are discussed in the next paragraphs.

2 THEORETICAL BACKGROUND OF THE PROPOSED METHODOLOGY

2.1 *Soil phase relationships and limitations*

The proposed methodology has the following important limitations:

- It is only applicable for non-crushable, inorganic soils: clays, silts, sands, gravels and their mixtures, for which the specific gravity G_s values can be reliably assumed, or determined. Organic soils, fill material, crushable soils and peats are excluded from applying the proposed methodology.
- It is only applicable for saturated soils below groundwater level, or in other words when the saturation ratio S_r equals 1. This is an assumption, as there may be a zone of partial saturation immediately below the water table where the saturation ratio may be slightly below 1; however, this assumption is considered to be appropriate for use in simplified analysis. For the methodology to return reliable results, the location of the groundwater table needs to be determined at any given site during testing. Best practice suggests the groundwater level to be measured by the CPT (u_2 pore pressure or dissipation tests) and/or by water level observations in boreholes, wells or standpipes. Where the budget allows, P-wave geophysical methods could be incorporated to more accurately locate the depth at which full saturation occurs and make the applicability of the proposed methodology more reliable. The methodology shall not be applied to soils located above the groundwater level.
- This paper applies the proposed methodology to two sandy sites due to the relatively high level of confidence in the assumed G_s value of 2.65 for sands. The methodology may be extended to other inorganic soils; however, it is recommended that the underlying assumptions are calibrated for different inorganic soil types. The intention is to undertake further research for the methodology to be validated in saturated inorganic fine-grained soils at a later stage. The supporting theory of the proposed methodology is based on classical soil mechanics (Bowles, 1997).

For any inorganic soil, there are five parameters that need to be determined (e, w, G_s, S_r and γ). From these five parameters, G_s can be assumed (or determined in the laboratory), and S_r is assumed to be equal to 1 below a certain depth, as explained above when the soil is fully saturated. The bulk unit weight γ can be estimated from the relationship shown in Equation 1 by Robertson & Cabal (2010). Thus, there are only two unknowns to be determined: water content w and void ratio e.

The water content w (%), saturation ratio S_r, void ratio e and the specific gravity G_s of the soil solids are interrelated by the following relationship:

$$e = \frac{wG_s}{S_r} \tag{2}$$

which, for saturated conditions ($S_r = 1$), simplifies to:

$$e = wG_s \tag{3}$$

A specific gravity of 2.65 is typically assumed for sandy soils.

For determining w and e, another relationship needs to be developed in conjunction with Equation 3. Equation 4 relates the void ratio with the dry unit weight γ_d and specific gravity:

$$\mathrm{e} = \left(\frac{G_{sw}}{{}_d}\right) - 1 \tag{4}$$

where, γ_w = unit weight of water (9.81 kN/m^3).

For any inorganic soil, the relationship between dry unit weight, the water content and its bulk unit weight is defined by Equation 5:

$$d = \frac{}{(1+w)} \tag{5}$$

By combining Equations 3, 4 and 5, the following relationship is determined:

$$wG_s = \left(\frac{G_{sw}}{\frac{}{(1+w)}}\right) - 1 \tag{6}$$

In Equation 6, the only unknown is the water content w. In essence, Equation 6 requires that the left hand side, which expresses the full saturation of the soil, must be in equilibrium with the right hand side, which expresses the water content-bulk unit weight relationship when G_s is known. The solution for the water content at full saturation then is:

$$w = \frac{(G_{sw} -)}{G_s(-_w)} \tag{7}$$

Thus, for the γ obtained from CPT, and an appropriate assumed (or determined) value for G_s, depending on the soil type, there is a unique value for the water content w that satisfies

Equation 7. The void ratio and dry unit weight can then be derived from Equations 3 and 5, respectively.

The porosity n can subsequently be estimated with Equation 8:

$$n = \frac{e}{(1+e)} \tag{8}$$

The methodology is summarized in three steps in Figure 1.

2.2 *Advantages of the proposed methodology*

The proposed methodology is simple and can be implemented for projects where there is a relatively shallow water table and the G_s values can be reliably assumed (or determined), particularly when laboratory tests are not included in the scope of the site investigations due to cost constraints. Where there is available budget for laboratory tests, the results from the proposed methodology can be checked against the laboratory results. The methodology can delineate against depth w, e, γ_d and n, and graphs for each of the estimated parameters begin at the depth where the groundwater surface was measured or inferred at the given site.

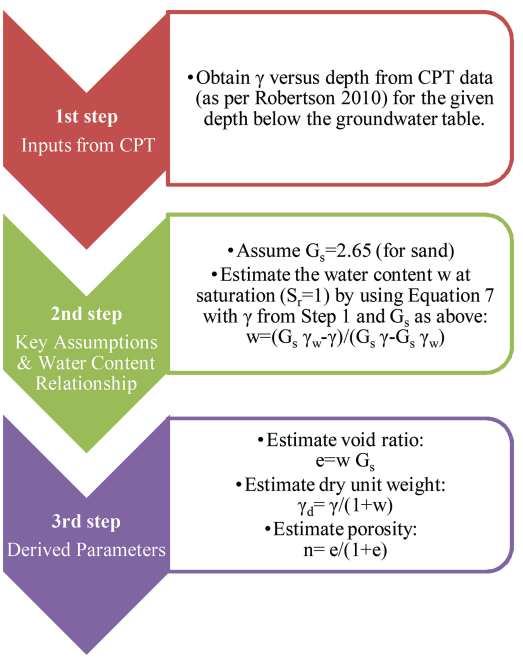

Figure 1. Flow chart summarizing the three key steps of the proposed methodology.

3 APPLICATION OF METHODOLOGY ON TWO CHRISTCHURCH SITES WITH SANDY SOIL

For applying the proposed methodology, two CPTs were downloaded from the New Zealand Geotechnical Database (NZGD). Key requirements for selecting the CPTs were that:

- The sites were known to have a relatively shallow groundwater table
- The testing was undertaken on sandy sites in Christchurch, New Zealand
- The CPTs were undertaken in close proximity to boreholes, where soil samples have been taken to the laboratory to evaluate the water content
- The number of soil samples taken at the sites was adequate to compare the proposed CPT methodology and the laboratory testing and to draw some conclusions on the applicability of the methodology

For simplicity, a specific gravity of 2.65 was adopted throughout the entire depth of the CPTs as the soil profiles were found to be predominantly sands and silty sands. This may not be an appropriate assumption for some of the fine-grained soil layers in the upper 4.4m at Site 1. The GWT depth was estimated to be 3.0m below ground level at Site 1, and 1.7m below ground level at Site 2. Five graphs have been presented for both sites including:

- Normalised SBT_n versus depth
- Water content versus depth, showing comparisons between the CPT methodology and laboratory testing results
- Void ratio versus depth
- Bulk and dry unit weights versus depth
- Porosity versus depth

3.1 *Borehole and sampling results*

A summary of borehole and laboratory testing results are presented in Tables 1–4.

Table 1. Borehole summary for Site 1.

Depth (m)	Soil description	Representative SPT N values
0.0–2.6	Sandy GRAVEL (no recovery between 0.2–2.0 m)	22
2.6–4.4	SILT	4
4.4–5.0	Silty SAND	20
5.0–19.5	SAND	13–29 (Avg. = 22)
19.5–20.0	SILT	14

Table 2. Laboratory results summary for site 1.

Depth (m)	Fines content passing 75 µm (%)	Water content (%)
6.0	5.69	23.0
9.0	5.81	25.6
12.0	6.22	24.2
15.0	4.95	22.4

Table 3. Borehole summary for site 2.

Depth (m)	Soil description	Representative SPT N values
0.0–11.0	SAND with minor silt	18–27 (Avg. = 24)
11.0–20.5	SAND with trace silt	34–47 (Avg. = 40)

Table 4. Laboratory results summary for site 2.

Depth (m)	Fines content passing 75 µm (%)	Water content (%)
3.1	6.75	28.9
4.5	2.13	29.4
6.0	2.47	31.1
7.5	2.22	26.7

3.2 *CPT results—Site 1*

CPT results and estimated parameters from the proposed methodology for Site 1 are presented in Figures 2–6 below.

3.3 *CPT results—site 2*

CPT results and estimated parameters from the proposed methodology for Site 2 are presented in Figures 7–11 below.

3.4 *Summary*

The SBT_n (Figures 2 and 7) plots have been included to provide the reader with an understanding of the soil behavior type interpretations, which indicate the soil is predominantly sandy for both sites and shows good agreement with the adjacent boreholes.

Figures 3 and 8 show comparisons between the CPT methodology for estimating water content and laboratory results. From these graphs, it can be seen that there is close agreement in the values returned by the two methods. These results indicate that the proposed CPT methodology, based on the CPT unit weight correlation (Robertson & Cabal, 2010), is accurately estimating the water content for the soil conditions encountered at the two sites. It can also be concluded that high quality results have been obtained from the laboratory.

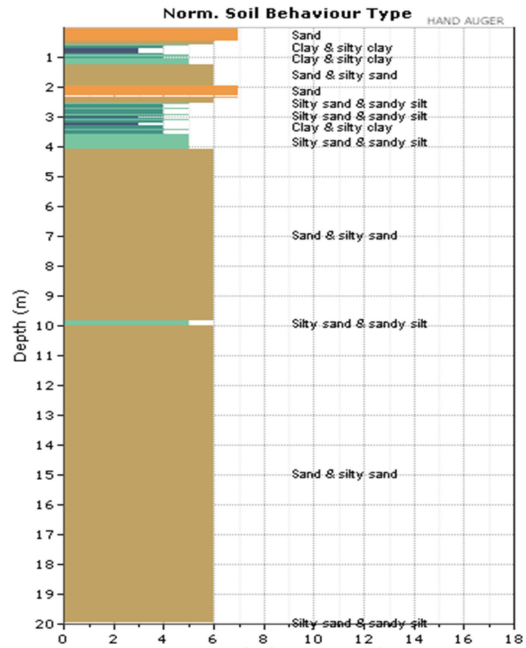

Figure 2. Site 1 SBT_n plot.

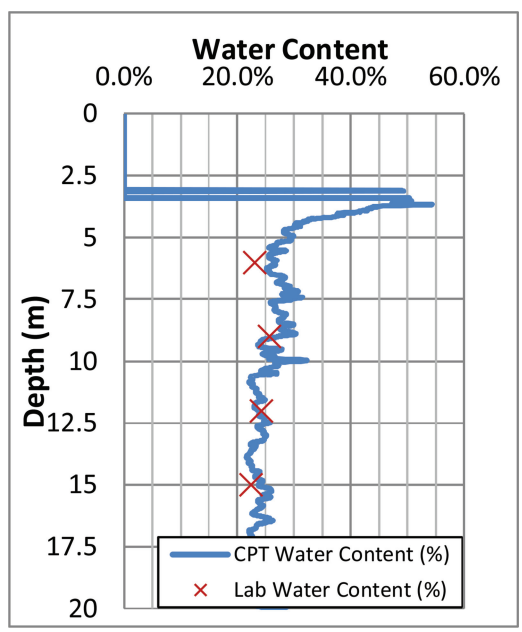

Figure 3. Site 1 water content comparison.

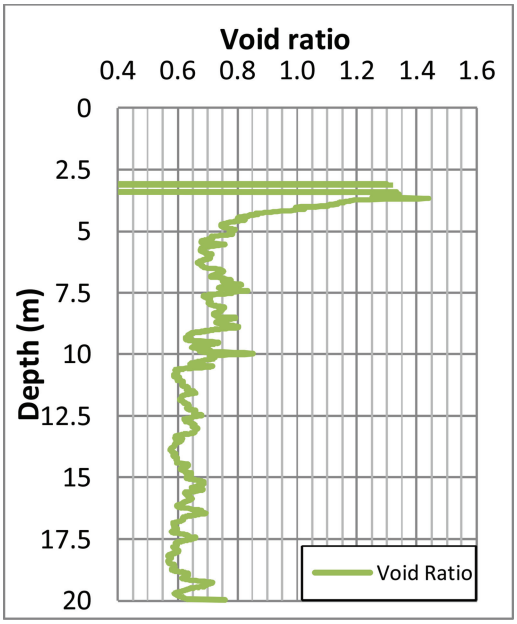

Figure 4. Site 1 void ratio.

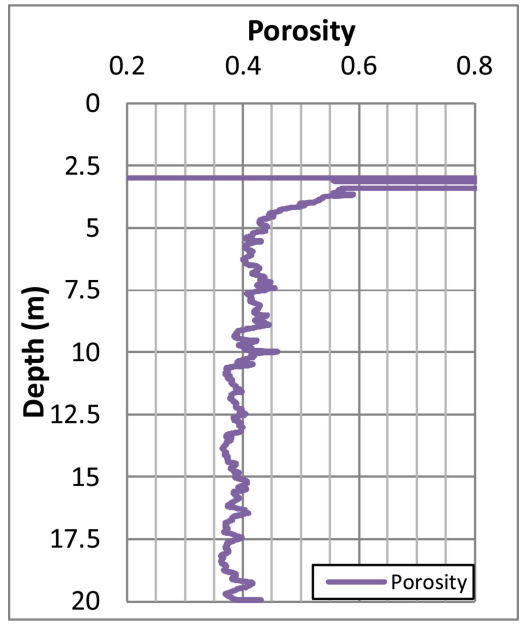

Figure 6. Site 1 porosity.

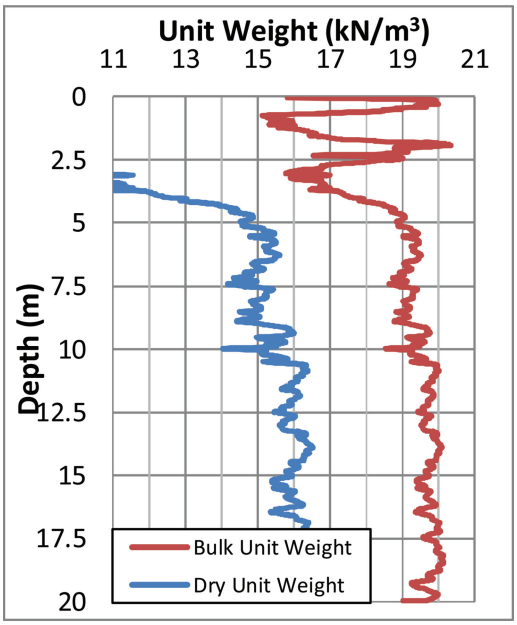

Figure 5. Site 1 bulk and dry unit weights.

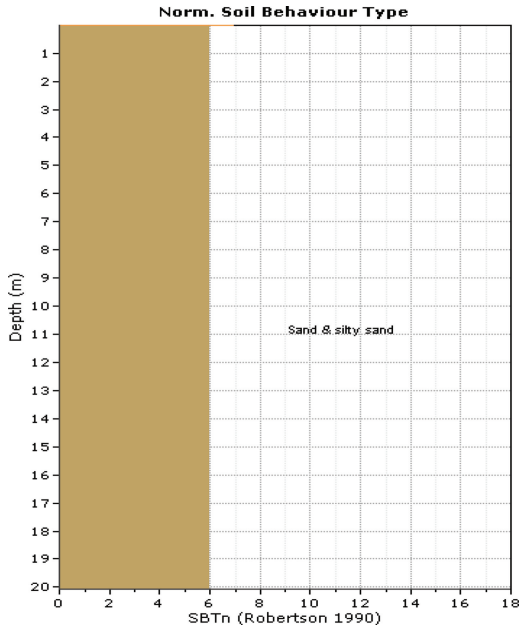

Figure 7. Site 2 SBT_n plot.

Figures 4–6 and 9–11 present the estimated void ratio, dry unit weight and porosity for the two sites. The plots for these parameters indicate values produced by the CPT methodology are consistent with typical values for the soil conditions encountered at the two sites. As these parameters have been derived based on the same assumptions as the water content, it is inferred that these estimated

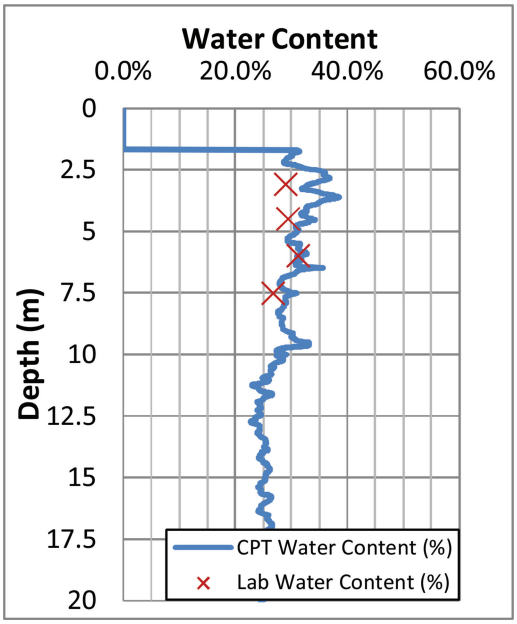

Figure 8. Site 2 water content comparison.

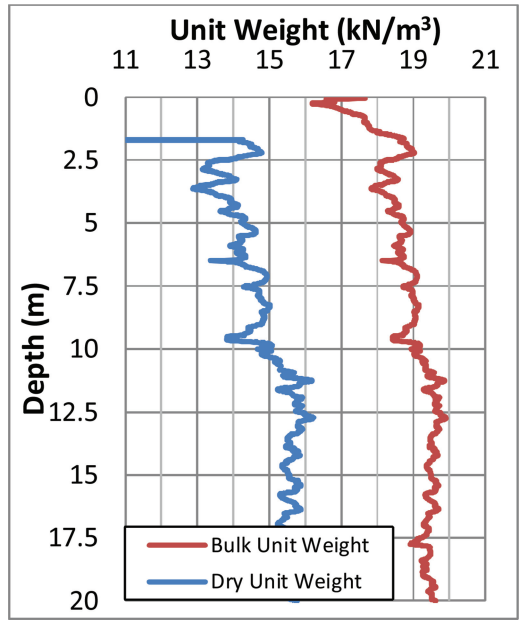

Figure 10. Site 2 bulk and dry unit weights.

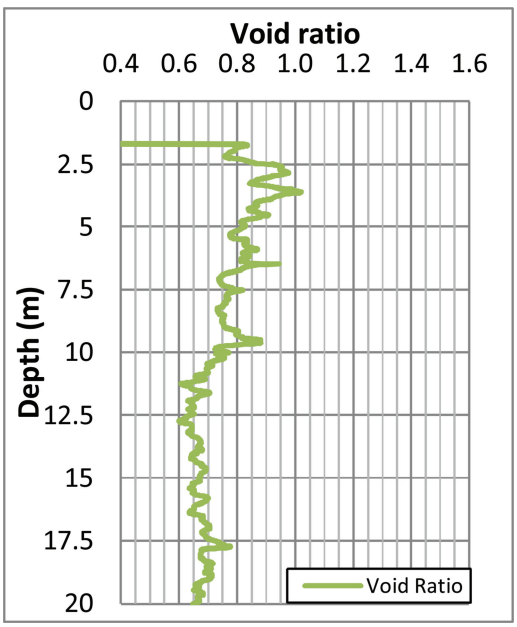

Figure 9. Site 2 void ratio.

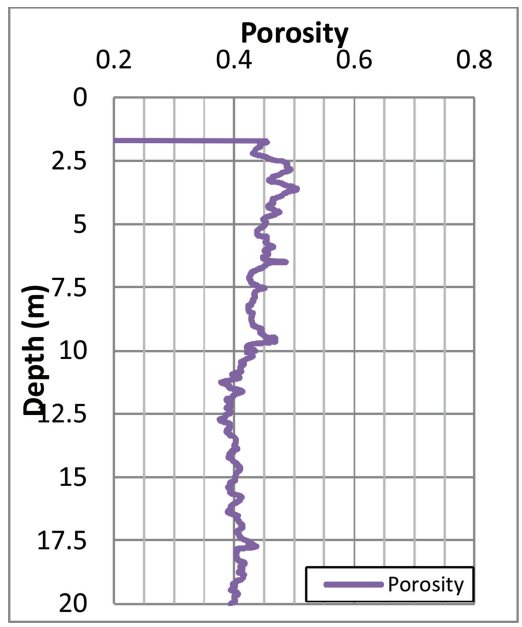

Figure 11. Site 2 porosity.

parameters have a similar degree of accuracy associated with them.

Tables 5 and 6 summarise the comparisons between the laboratory water content values and the CPT estimates at the four sampling depths for each site. An absolute difference in water content of between 0.5–3.5% (average difference of 1.8%) for Site 1, and an absolute difference of between

Table 5. Comparison between laboratory and CPT results at Site 1.

Sample depth (m)	Laboratory water content (%)	CPT water content (%)	Absolute difference (%)
6.0	23.0	26.5	3.5
9.0	25.6	27.3	1.7
12.0	24.2	23.7	0.5
15.0	22.4	23.7	1.3

Table 6. Comparison between laboratory and CPT results at Site 2.

Sample depth (m)	Laboratory water content (%)	CPT water content (%)	Absolute difference (%)
3.1	28.9	33.2	4.3
4.5	29.4	33.8	4.4
6.0	31.1	31.2	0.1
7.5	26.7	30.4	3.7

0.1–4.4% (average difference of 3.1%) for Site 2 is considered to be an encouraging result.

4 CONCLUSIONS

Based on fundamental principles of soil mechanics and the well-established published correlation for estimating bulk unit weight from CPT by Robertson & Cabal (2010), and for saturated soil conditions with an appropriate G_s value, it is possible to estimate versus depth the:

- Water content
- Void ratio
- Dry unit weight
- Porosity

The proposed methodology can only be applied to inorganic and saturated soils. This means the proposed methodology is applicable to coastal areas and other regions where the groundwater is typically near the ground surface. The proposed methodology was applied to two sandy sites in Christchurch, New Zealand, which yielded typical results for the soil conditions encountered and showed close agreement with laboratory testing results for the same sites. It is intended to undertake further research to validate the methodology for estimation of these parameters in fine-grained soils.

For projects where both CPT and laboratory testing have been undertaken, the CPT methodology can also be utilised as a quality control measure for the results obtained. If the underlying assumptions for the CPT methodology are satisfied and are sufficiently accurate for the soil conditions present at the site, there should be relatively close agreement between the water content estimated from the proposed CPT methodology and the laboratory water content results.

The four above estimated parameters can be plotted versus depth and could be used for facilitating numerical analysis with FEM and alternative methods for estimating the following:

- Assessment of shear wave velocity
- Assessment of soil natural frequency or period
- Assessment of small-strain shear modulus
- Assessment of relative density and state of packing for cohesionless soils
- Assessment of soil permeability
- Assessment of collapse potential of soil

Further research needs to be undertaken for comparing the estimated parameters from the proposed methodology against the measured laboratory results for a greater number of sites.

REFERENCES

Bowles, J.E. (1997). *Foundation Analysis and Design*, 5th Edition. New York: McGraw-Hill, 1170 pages.

Robertson, P.K. & Cabal, K. (2010). Estimating soil unit weight from CPT. *Proceedings, Second International Symposium on Cone Penetration Testing*, Vol. 2 (CPT'10, Huntington Beach, CA), Omnipress: 447–454.

Robertson, P.K. & Cabal, K. (2015). *Guide to Cone Penetration Testing*, 6th Edition. Gregg Drilling, Signal Hill, California: 140 pages.

Taylor & Francis
Taylor & Francis Group
http://taylorandfrancis.com

Cone Penetration Testing 2018 – Hicks, Pisanò & Peuchen (Eds)
© 2018 Delft University of Technology, The Netherlands, ISBN 978-1-138-58449-5

NMO-SCTT: A unique SCPT tomographic imaging algorithm

Erick Baziw & Gerald Verbeek
Baziw Consulting Engineers Ltd., Vancouver, Canada

ABSTRACT: Seismic Cone Penetration Testing (SCPT) is an important geotechnical testing technique for site characterization that provides low strain (< 10^{-5}) in-situ interval compression (*Vp*) and shear (*Vs*) wave velocity estimates. Baziw Consulting Engineers has invested considerable resources in advancing the art of SCPT, and in this paper a newly developed Normal Moveout Seismic Cone Tomographic Testing (NMO-SCTT) algorithm is introduced. This algorithm allows for two dimensional imaging of the sub-surface stratigraphy by processing acquired seismic trace arrival times derived with increasing source-sensor radial offsets. This dramatically increases the ability to characterize near-surface stratigraphy, which is very important for accurate liquefaction assessment. As opposed to crosshole tomography, the NMO-SCTT does not require any significant site disturbance aside from a single SCPT sounding, thereby greatly reducing the cost and the environmental impact. This paper outlines the mathematical and algorithmic details of the NMO-SCTT algorithm, which builds upon BCE's established FMDSM algorithm. As such it incorporates Fermat's principle when estimating SCPT interval velocities. In addition a real SCPT data tomographic data set is presented using SCPT seismic data that was acquired at offsets of 1.85 m, 5 m and 10 m, and down to a depth of 20.5 m.

1 INTRODUCTION

A fundamental goal of geotechnical *in-situ* testing is the accurate estimation of the shear and compression wave velocities (V_P and V_S, respectively) in the ground. These parameters form the core of mathematical theorems to describe the elasticity/plasticity of soils and they are used to predict the soil response (settlement, liquefaction or failure) to imposed loads (whether from foundations, heavy equipment, earthquakes or explosions). The Seismic Cone Penetration Testing (SCPT) is a common geotechnical technique for measuring *in-situ* V_S and V_P velocities. The main goal in SCPT is to obtain accurate arrival times as the source wave travels through the soil profile of interest, and from these arrival times the V_S and V_P velocities are then calculated.

Baziw Consulting Engineers has invested considerable resources in advancing the art of SCPT. A logical extension of SCPT is Seismic Travel-Time Tomography (STTT), which allows for two dimensional imaging of the sub-surface stratigraphy (Shearer, 1999; Gibowicz, and Kijko, 1994; Nolet, 1987) by processing acquired V_s and V_p arrival times. In general terms, in STTT the velocity profile is derived by seismic data inversion or iterative forward modeling, while adhering to Fermat's principle of least time. This is a particularly challenging problem in that the seismic raypaths depend upon the unknown velocity structure. A common application for STTT is Crosshole Seismic Tomography Testing (CSTT) as illustrated in Figure 1 (Gibowicz, and Kijko, 1994). In this illustration there is a linearized ray path between the source and receiver, and the discretization of the soil into blocks. The execution of CSTT requires a significant effort to create the necessary source and receiver boreholes and in addition the CSTT analysis is unwieldy due to the fact that there are many velocity blocks

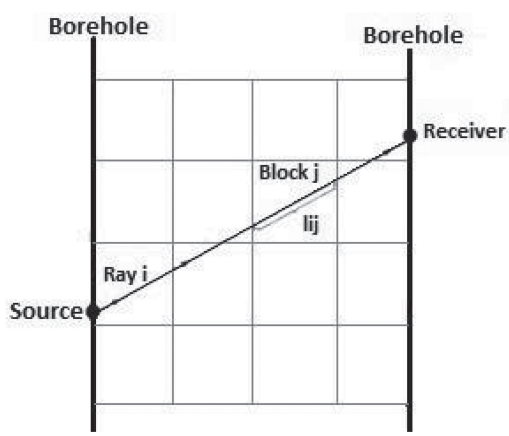

Figure 1. Schematic of a crosshole seismic tomography testing and analysis configuration (after, Gibowicz and Kijko (1994)).

with a limited number of source wave intersections, which more than likely will result in instability in the analysis equations.

This paper outlines a new approach, which facilitates the tomographic imaging of the sub-surface: the so-called Normal Moveout Seismic Cone Tomographic Testing (NMO-SCTT). In general terms, this approach allows for two dimensional imaging of the sub-surface stratigraphy by processing acquired seismic trace arrival times derived with increasing source-sensor radial offsets. This dramatically increases the ability to characterize near-surface stratigraphy, which is very important for accurate liquefaction assessment as was shown by Bray et al. (2014) through his analysis of the catastrophic liquefaction that occurred in Christchurch, New Zealand in 2010 and 2011.

2 NMO-SCTT TESTING AND ANALYSIS PROCEDURE

Figure 2 shows a schematic of the typical SCPT configuration: a seismic source is used to generate a seismic wave train at the ground surface. One or more downhole seismic receivers are used to record the seismic wave train at predefined depth increments. When triggered by the seismic source a data recording system records the response of the downhole receiver(s). Figure 3 illustrates a schematic of the NMO-SCTT testing and analysis configuration. Here the downhole seismic data sets are acquired at various radial source offsets. Figure 4 illustrates a NMO-SCTT test site where there are beam sources with pendulum hammers with radial offsets of 1.85 m, 5 m and 10 m. While analyzing the data sets 2D velocity models are derived for each subsequent offset, resulting in a dramatic lowering of the unknowns since the previously established velocity values are used whenever the ray path travels through an area that was covered before. For example, the ray path for offset X2 and

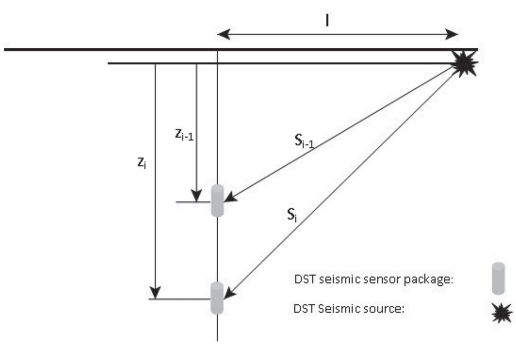

Figure 2. Schematic of the typical SCPT configuration.

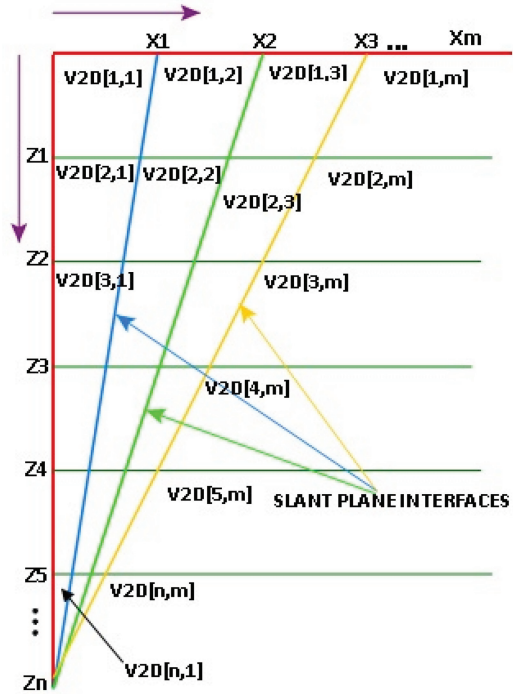

Figure 3. Schematic of a NMO-SCTT testing and analysis configuration.

Figure 4. Wiertsema & Partners of The Netherlands SCTT-NMO-SCPT site setup. SH pendulum hammer beam sources have sensor-sensor offsets of 1.85m, 5m and 10 m.

depth Z2 might travel through areas V2D[1,2], V2D[1,1] and V2D[1,2], in which case for the last two areas the velocity values obtained during the analysis of the data set for offset X1 are used and V2D[1,2] is estimated.

Methodologies employed for solving the seismic tomographic problem rely upon data inversions

and the more popular iterative reconstructive techniques such as ART-backprojection, SIRT, conjugate gradient method and LSQR (Shearer, 1999; Gibowicz, and Kijko, 1994; Nolet, 1987). It should be noted that data inversion techniques attempt to determine the solution space by inverting sparse and ill-conditioned matrices, while utilizing singular value decomposition and regularization. Oldenburg (Oldenburg and Li, 2005) has carried extensive research into the application of seismic data inversion, which has proven very challenging. For that reason it was decided to apply reconstructive techniques for the NMO-SCTT algorithm.

The suggested *NMO-SCTT* algorithm implements an iterative technique based on the same mathematical tools (e.g., Newton-Raphson technique and simplex iterative forward modeling) that are used in the single source offset Forward Modeling / Downhill Simplex Method (*FMDSM*) technique (Baziw, 2002; Baziw, E. and Verbeek, G, 2012 and 2014), but with additional slant plane interfaces for each source offset as was illustrated in Fig. 3.

In its current form the *NMO-SCTT* algorithm allows 2D interval velocity estimations for up to seven depth intervals, while for all additional intervals 1D estimations are made, which will also further enhance the accuracy of the 2D. Apart from a practical justification (to control the processing time), there is also a mathematical justification given the cone nature of the *NMO-SCTT* 2D testing environment. As the SCPT depth increases the 2D interval velocities collapse onto the first offset estimates (the apex of the analysis cone is readily approached with an increase in depth) as illustrated in Fig. 3. The performance of the NMO-SCTT algorithm was demonstrated though the processing of challenging test bed simulations (Baziw and Verbeek (2017a)).

The *NMO-SCTT* algorithm implements a Monte Carlo technique where numerous (currently 120 as a default value) searches are carried out when finding the optimal 2D interval velocities. The first search assumes that there is a Transverse Isotropic (TI) medium (i.e., no lateral variation). The subsequent estimates use the Monte Carlo technique for specifying the initial simplex for the search grid. The interval velocity results with the cost function minimum (RMS difference between the actual and derived arrival times) are used and stored within the *NMO-SCTT* tomography database. The Monte Carlo technique was adopted to address the need to search a large solution space for the interval velocities with numerous local minima. To control the processing time a 64-bit parallel processing technique has been incorporated into the algorithm so that full advantage is taken of multi-core processors and hyper-threading technology (resulting in a processing time that is less than half of that with a 32-bit configuration without parallel processing (Baziw and Verbeek (2017b)).

3 REAL DATA ANALYSIS

The NMO-SCTT data set used for this paper was acquired by Wiertsema & Partners during an investigation at a site in Northwest Europe. The SH source waves at this site were generated with pendulum sledge hammers that impacted horizontally point source steel beams located underneath the outriggers with electrical contact triggers. Figure 4 shows the site setup with radial offsets between the source and the sensor of 1.85 m, 5 m and 10 m. The data acquisition started at a depth of 2 m down to a depth of 20.5 m. The first seven test depths (2 m, 3.5 m, 5 m, 7 m, 9 m, 11 m and 12.7 m) were used for 2D analysis, while the remaining eight depths (13.5 m, 14.5 m, 15.5 m, 16.5 m, 17.5 m, 18.5 m, 19.5 m and 20.5 m) were used for 1D analysis.

Figures 5, 6 and 7 illustrate the vertical seismic profile (VSP) for the seismic data acquired at the

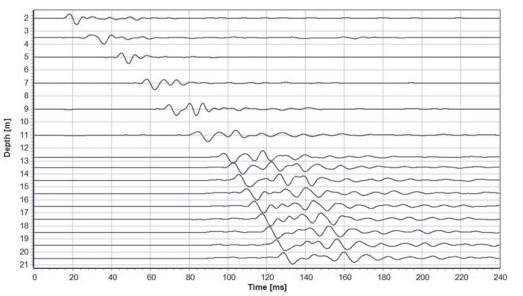

Figure 5. VSP for seismic trace recorded at a sensor-source radial offset of 1.85 m.

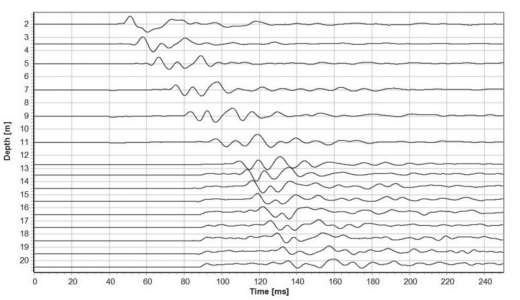

Figure 6. VSP for seismic trace recorded at a sensor-source radial offset of 5 m.

three sensor-source radial offsets after applying a 200 Hz low pass frequency filter.

Table 1 shows the estimated source wave arrival times for these VSPs, which were then fed into the NMO-SCTT algorithm to derive the interval velocities. The NMO-DSTT residual arrival time errors (difference between the actual and derived arrival times) are also illustrated in Table 1. As can be seen the residual errors increase with radial source offsets. In general terms, this is due to the fact that any errors from the smaller NMO offsets propagate to the larger NMO offsets.

The NMO-SCTT algorithm has the beneficial feature of identifying "actual" arrival times which are erroneous, e.g. due to significant measurement noise and/or interference from reflections or critically refracted rays. To illustrate this Fig. 8 shows the trace recorded at a depth of 2 m from the 10 m radial sensor-source offset. The original arrival time estimate of 90 ms resulted in a NMO-SCTT residual error of 4.6 ms, implying that an arrival time of 94.6 ms is more realistic. As is evident in Fig. 8, the arrival time of the trace recorded 2 m is difficult to ascertain and a NMO-SCTT determined arrival time of 94.6 ms is highly feasible due to the natural period of the source wave and significant first break interference.

Table 2 outlines the estimated tomographic interval velocities, showing substantial lateral variations in the interval velocities near surface (0 to 3.5 m) and becoming less pronounced for the deeper layers. Figures 9, 10 and 11 illustrate the source wave raypaths for the various sensor-source radial offsets. These figures clearly demonstrate Fermat's Principle and that source waves do not have straight raypaths, emphasizing the impor-

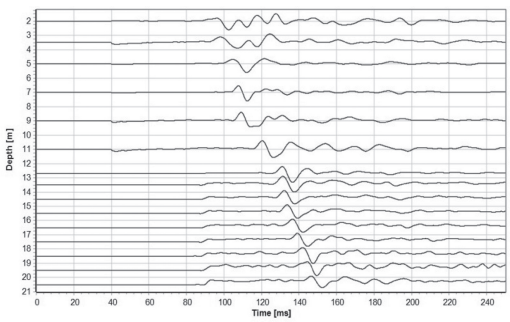

Figure 7. VSP for seismic trace recorded at a sensor-source radial offset of 10 m.

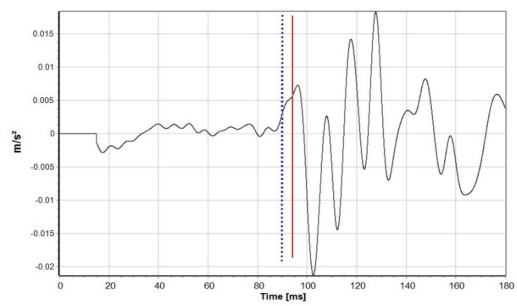

Figure 8. trace recorded at a depth of 2 m from the source with a radial offset of 10 m.

Table 1. Estimated arrival times and NMO-SCTT Residual time errors.

Depth [m]	Offset [m]	Arrival time [ms]	Residual error [ms]	Offset [m]	Arrival time [ms]	Residual error [ms]	Offset [m]	Arrival time [ms]	Residual error [ms]
2	1.85	15.28	0	5	47	*0.06*	10	94.4	–0.334
3.5	1.85	27.22	0	5	52.7	*0.21*	10	90	–0.503
5	1.85	42	0	5	61.32	*–0.27*	10	100	0.491
7	1.85	55.05	0	5	70.24	*–0.004*	10	102.71	0.222
9	1.85	66.46	0	5	78.05	*–0.114*	10	104.694	0.080
11	1.85	81.45	0	5	91.57	*0.136*	10	115.724	–0.032
12.7	1.85	94.89	0	5	104.07	*–0.022*	10	126.195	1.003
13.5	1.85	99.83	0	5	108.22	*–0.037*	10	126.606	–0.727
14.5	1.85	102.78	0	5	111.08	*1.067*	10	127.315	0.058
15.5	1.85	106.75	0	5	113.87	*0.307*	10	128.834	0.337
16.5	1.85	110.62	0	5	116.82	*–0.241*	10	131.648	0.463
17.5	1.85	114.63	0	5	120.67	*–0.087*	10	134.250	0.0871
18.5	1.85	118.23	0	5	124.25	*0.176*	10	137.051	0.361
19.5	1.85	121.99	0	5	127.32	*–0.274*	10	139.21	–0.345
20.5	1.85	125.64	0	5	130.11	*–0.934*	10	141.633	–0.856

Table 2. NMO-SCPTT Estimated interval velocities.

Depth [m]	Offset [m]	Estimated interval velocity [m/s]	Offset [m]	Estimated interval velocity [m/s]	Offset [m]	Estimated interval velocity [m/s]
2	1.85	*178.3*	5	*95.1*	10	*99.12*
3.5	1.85	*115.1*	5	*179.58*	10	*103.09*
5	1.85	*97.6*	5	*98.13*	10	*115.3*
7	1.85	*145.9*	5	*157.78*	10	*151.31*
9	1.85	*168.8*	5	*180.03*	10	*180.22*
11	1.85	*131.4*	5	*131.02*	10	*148.78*
12.7	1.85	*125.3*	5	*132.6*	10	*128.32*
13.5	1.85	*160.4*	5	*160.4*	10	*160.4*
14.5	1.85	*328.2*	5	*328.2*	10	*328.2*
15.5	1.85	*246.7*	5	*246.7*	10	*246.7*
16.5	1.85	*254.5*	5	*254.5*	10	*254.5*
17.5	1.85	*246.4*	5	*246.4*	10	*246.4*
18.5	1.85	*274.8*	5	*274.8*	10	*274.8*
19.5	1.85	*263.3*	5	*263.3*	10	*263.3*
20.5	1.85	*271.8*	5	*271.8*	10	*271.8*

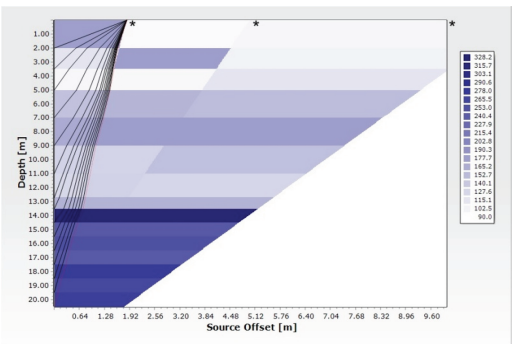

Figure 9. Estimated source raypaths for 1.85 m sensor-source radial offset.

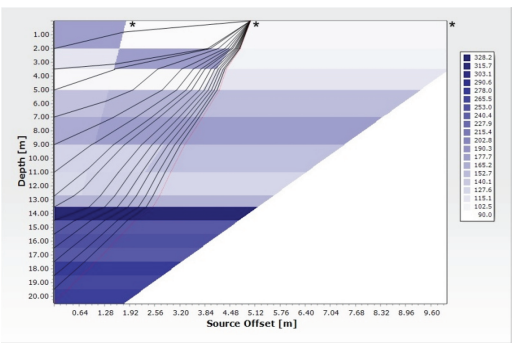

Figure 10. Estimated source raypaths for 5 m sensor-source radial offset.

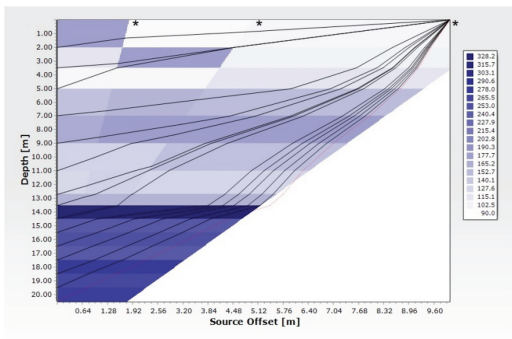

Figure 11. Estimated source raypaths for 10 m sensor-source radial offset.

tance to utilize analytical techniques which take into account raypath refraction when estimating the *in-situ* interval velocities.

4 CONCLUSIONS

The SCPT has proven to be an important geotechnical testing tool for site characterization that provides low strain in-situ interval compression and shear wave velocity estimates. This paper has outlined a newly developed Normal Moveout Seismic Cone Tomographic Testing (NMO-SCTT) algorithm which allows for the two dimensional imaging of the subsurface utilizing standard SCPT

instrumentation. As opposed to crosshole tomography, the NMO-SCTT does not require any significant site disturbance aside from a single SCPT sounding, thereby greatly reducing the cost and the environmental impact.

The NMO-SCTT algorithm allows sequentially processes acquired seismic trace arrival times derived with increasing source-sensor radial offsets. In this algorithm an iterative numerical technique is employed which is based upon the same mathematical tools (e.g., Newton-Raphson technique and simplex iterative forward modeling) that are used in the established single source offset Forward Modeling / Downhill Simplex Method (FMDSM) technique. After demonstrating great promise in processing challenging test bed simulation data sets, the NMO-SCTT algorithm was implemented on real data. This paper outlines the results of a real data NMO-SCTT analysis.

REFERENCES

Baziw, E. 2002. Derivation of seismic cone interval velocities utilizing forward modeling and the downhill simplex method. Can. Geotech. J., 39(5), pp.1181–1192.

Baziw, E., and Verbeek, G. 2012. Deriving interval velocities from downhole seismic data. Geotechnical and Geophysical Site Characterization 4 – Mayne (eds), CRC Press, 1019–1024.

Baziw, E. and Verbeek, G. 2014. Identifying critical layers using SCPT and seismic source moveout. Las Vegas, NV, USA: 3rd International Symposium on Cone Penetration Testing (CPT '14),12–14 May 2014. 357–364. http://www.cpt14.com/cpt14-papers.

Baziw, E. and Verbeek, G. 2017a. Normal moveout downhole seismic tomographic testing algorithm. http://www.bcengineers.com/images/BCE_Technical_Note_17.pdf.

Baziw, E. and Verbeek, G. 2017b. Implementation of parallel processing in BCE seismic analysis software to decrease CPU requirements. http://www.bcengineers.com/images/BCE_Technical_Note_17.pdf.

Bray, J.D., Zupan, J.D., Cubrinovski, M. and Taylor, M. 2014. CPT-based liquefaction assessments in Christchurch, New Zealand. Las Vegas, NV, USA: 3rd International Symposium on Cone Penetration Testing (CPT '14), 12–14 May 2014. 1–21. http://www.cpt14.com/cpt14-papers.

Gibowicz, S.J., and Kijko, A. 1994. *An Introduction to Mining Seismology*, Academic Press, San Diego, CA, USA.

Nolet, G. 1987. *Seismic Tomography.* D. Reidel Publishing, Holland.

Oldenburg, D.W., and Li, Y.G., 2005. Inversion for Applied Geophysics: A Tutorial. Investigations in Geophysics, Vol. 13, 2005, 89–150.

Shearer, P.M. 1999. *Introduction to Seismology*. 1st edition, Cambridge: Cambridge University Press.

Cone Penetration Testing 2018 – Hicks, Pisanò & Peuchen (Eds)
© 2018 Delft University of Technology, The Netherlands, ISBN 978-1-138-58449-5

Effect of piezocone penetration rate on the classification of Norwegian silt

A. Bihs & S. Nordal
Norwegian University of Science and Technology, Trondheim, Norway

M. Long
University College Dublin, Ireland

P. Paniagua
Norwegian Geotechnical Institute, Trondheim, Norway

A. Gylland
Multiconsult, Trondheim, Norway

ABSTRACT: Interpretation of Cone Penetration Tests (CPTU) in intermediate soils is complex due to partially drained conditions during penetration. In order to gain more insight into the material behavior of silt during a CPTU, an intensive test program was carried out in the field and several soil samples were taken and analysed. In addition a set of tests were performed in the laboratory under controlled conditions using a mini-piezocone (Fugro miniature CPTU, owned by the University of Colorado). The aim is to develop an improved interpretation basis for the CPTU in intermediate soils. The present paper gives an overview over the results obtained and shows how a change in penetration rate affects the response of the CPTU-readings. The data have been plotted into existing soil classification charts and the results from the field and laboratory investigations are compared. The Schneider et al. (2007) chart seems promising in separating the results from the different rate tests.

1 INTRODUCTION

Cone penetration testing in silty soils is difficult due to partial drainage occurring during a standard penetration rate. The CPTU is generally carried out with a rate of 20 mm/s ± 5 mm/s according to the International Reference Test Procedure (IRTP) of the International Society of Soil Mechanics and Foundation Engineering (ISSMFE). Thereby one assumes to achieve fully undrained conditions for clayey soils and fully drained conditions for sandy soils (Lunne et al. 1997). However, in intermediate soils e.g. silts, partial drainage is likely to occur during a standard penetration rate, which may lead to over- or underestimation of the geotechnical soil parameters either using analysis tools developed for fully undrained or drained behavior.

Researchers have shown that the presence of partial drainage has significant influence on the corrected cone resistance (q_t), the pore pressure (u_2) and to some extent the sleeve friction (f_s). Most of the research has been carried out under controlled conditions in the laboratory using a calibration chamber or a centrifuge and varying the penetration speed of the advancing probe using either a cone or full flow probes (Stewart & Randolph 1991, Randolph & Hope 2004, Silva & Bolton 2005, Schneider et al 2007, Paniagua 2014). Up till now, only a few field studies have been reported in the literature, as for example by Kim et al. (2008), Martinez et al. (2016), Poulsen et al. (2013) and Holmsgaard et al. (2016).

There may be several reasons for the lack of research in the field. Usually silty soils consist of a mixture of both finer and coarser materials. They often appear as small layers or lenses which makes it difficult to obtain undisturbed samples and complicates the handling of the material in the laboratory. Moreover, the interpretation of the CPTU results are complicated due to the rather complex micro fabric of the soil, e.g. Sandven (2002).

In order to study and understand the penetration processes taking place during a CPTU in intermediate soils, an intensive field study has been carried out by the Norwegian University of Science and Technology (NTNU) on a silt site in Stjørdal, close to Trondheim, Norway. In total 25 CPTU's were conducted with penetration speeds varying

between 0.5–200 mm/s using a standard 35.7 mm cone and measuring the pore pressure at the u_2 position directly behind the cone. Several dissipation tests were done at different depths of interest where the penetration is paused and the pore pressure development is logged over a certain time interval. High-quality 54 mm steel samples were taken and carefully examined in the laboratory.

In addition, a series of CPTU's were performed in the laboratory under controlled conditions using a Colorado minicone (diameter 12 mm) and a fully saturated silt specimen. The soil sample was built inside a Plexiglas cylinder (d = 100 mm) with an internally padded layer of neoprene in order to compensate for boundary effects. By using a slurry deposition method, a silt sample is built into the cylinder and an overburden pressure of 80 kPa was applied. The CPTU tests were performed using three different penetration rates: 0.06 mm/s, 6 mm/s and 50 mm/s, representing a slow, standard and fast penetration rate respectively, Paniagua (2014).

The paper gives an overview over the basic laboratory results obtained and shows CPTU curves for the different penetration rates. The results are plotted in selected existing soil classification charts and compared to the minicone results from the laboratory. The aim of the present paper is to show the influence of varying the rate of penetration in intermediate soils and how they affect the interpretation of the CPTU results. The analysis of the dissipation tests is not presented in this paper.

2 SITE DESCRIPTION

2.1 *Halsen, Stjørdal*

The research test site consists of a thick silt deposit which is situated in the Stjørdal valley about 35 km east of Trondheim in Norway. During the Quaternary period, the Scandinavian Peninsula was fully covered by a massive icecap. However several periods of warmer climate caused the icecap to retreat temporarily. During the last de-glaciation, rivers of melt-water transported clays and silts into the sea. These soils are representative for the Halsen test site where the thickness of the sediments may reach 200–300 m over bedrock. Clayey materials govern these deposits but in some parts due to increased or irregular water velocities, silts and fine sands are more dominant. This is typical for the Halsen test site where the fine sediments are dominated by silt, with layers and pockets of clay and coarse sand (Sandven 2002).

Grain size distributions have been determined and Figure 1 shows a summation plot of some of the test results including one test from the Vassfjellet silt. It is common Norwegian practice to use the recommendations made by the Norwegian Geotechnical Society (NGF) in order to classify the soil type NGF (2011). Herein the soil is defined as SILT if more than 45% of the grains are between 0.002 mm and 0.06 mm and less than 15% is clay (< 0.002 mm).

As can be seen from Figure 1, most of the soil from the Halsen test site consists of either sandy or clayey SILT with an average silt content of 55% and the majority of the particles falling into the coarse silt spectrum (e.g. 0.02–0.06 mm). The average soil grain density is about 2.66 g/cm^3. The soil gradation is middle to poorly graded with an average coefficient of uniformity of C_u = 17 which is defined as the ratio of d_{60} over d_{10}.

Figure 2 shows basic laboratory results for the Halsen test site. The water content varies between 20% and 35% with an average value of about 25%. Measurements of the bulk density are around 2.1 g/cm^3 on average. The distribution of the falling cone (fc) shear strength over depth shows a rather varied behavior with minimum values of

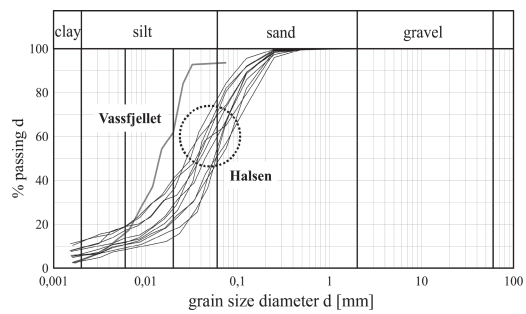

Figure 1. Grain size distribution: Halsen-Stjørdal and Vassfjellet.

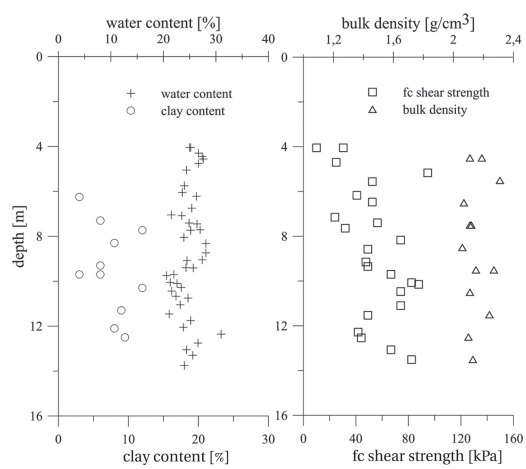

Figure 2. Overview over basic soil parameters.

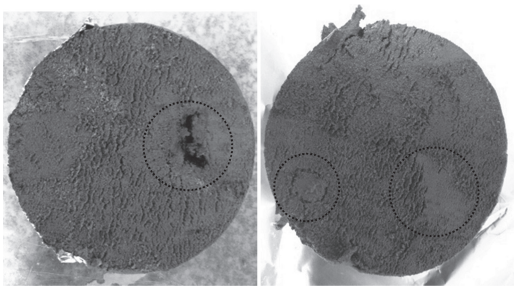

Figure 3. Cross section of soil specimen from 7.5 m, Halsen.

20 kPa and maximum values of 95 kPa. The distribution of the clay content over the depth shows an increase of clay content with depth.

In general, there is little evidence of soil properties varying with depth. Findings from the laboratory reflect the natural variation of the silty soil and underline the challenges in handling and characterizing these soils in the laboratory and in the field. Figure 3 shows a cross section of a sample from 7.5 m depth opened in the laboratory. The sand and clay lenses, which in this case seem to form vertical columns rather than horizontal layers, are clearly visible as well as cracks and holes inside and along the sample.

The laboratory results underline the geological history of the test area. To ensure the highest possible sample quality, all samples taken in the field have been analyzed within 24 hours of sampling time. The focus of the present project was on the silt layer between 4 m and down to more than 13 m. The ground water table is located at about 2.8 m which fits well with the findings from Sandven (2002).

2.2 *Vassfjellet*

The silt, which has been used in the laboratory study by Paniagua (2014), is from Vassfjellet, Klæbu, Norway, south of the Trondheim. The soil consists of a combination of glacier river deposits and peat. Due to its low cohesion, it was impossible to obtain undisturbed samples. Therefore disturbed samples were taken and rebuilt in the laboratory by a slurry deposition method.

The soil consist of a non-plastic, medium to coarse silt with a silt content of 92% and a clay content of 2.5%, see Figure 1. The silt from Vassfjellet is less sandy and clayey than the silt from the Halsen site. The soil grain density is 2.46 g/cm^3 and the organic content is lower than 2%. A maximum dry density of 1.57 g/cm^3 is obtained at 22% optimum water content and 95% saturation.

3 OVERVIEW OVER EXISTING SOIL CLASSIFICATION CHARTS

Soil classification charts, or more correctly soil behavior charts have been established since approximately 1965. It has to be stated that the application of these charts does not give accurate predictions of the soil type in terms of grain size distribution, but it is an indicator for the behavior of the present soil. Robertson (1990) stated that the classification charts are global and should only be used as a guide to define soil behavior. The general idea is that sandy soils usually generate high cone resistance and low friction ratios, whereas clayey soils have low cone resistance and high friction ratios (Lunne et al. 1997 and Robertson et al. 1986).

Ideally, all three measured parameters during a CPTU should be combined in order to achieve more reliable soil classification. Nevertheless, researchers are aware of the fact that the measured sleeve friction is often the less accurate and less reliable parameter of the three (for measurements below the groundwater table). In order to overcome the problems with the sleeve friction, Wroth (1984) and Senneset and Janbu (1985) were one of the first researchers to introduce the pore pressure parameter ratio B_q:

$$B_q = \frac{u_2 - u_0}{q_t - \sigma_{v0}} \tag{1}$$

where u_2 = measured pore pressure, u_0 = in-situ pore pressure, q_t = corrected cone resistance and σ_{v0} = total overburden stress. The original classification chart by Senneset & Janbu (1985) included the q_t against B_q whereas Senneset et al. (1989) revised the chart and used the normalized cone resistance Q_t according to Equation 2 instead of q_t.

The most widely used charts have been suggested by Robertson et al. (1986), which are based on either B_q or friction ratio versus q_t. In total 12 different soil behavior types were categorized to describe the different behavior and give a first indication of the drainage condition during cone penetration. Robertson (1990) later modified the existing charts to overcome issues related to CPTU soundings in greater depths (>30 m) by normalizing the q_t and the friction ratio F_r in the following way (see Equation 2 and 3)

$$Q_t = \frac{q_t - \sigma_{v0}}{\sigma'_{v0}} \tag{2}$$

$$F_r = \frac{f_t}{q_t - \sigma_{v0}} \tag{3}$$

where σ'_{v0} = effective vertical stress and f_t = corrected sleeve friction. Eslami & Fellenius (1997) established a classification chart used for pile design by applying data from more than 100 case histories in various soil conditions. The chart uses non-normalized parameters such as the effective cone resistance q_e ($q_e = q_t - u_2$) versus the measured friction f_t and divides the soil types into five different classes.

More recent developments are described by Schneider et al. (2008) where the classification charts are based on Q_t versus $\Delta u/\sigma'_{v0}$ and Q_t versus B_q to take into account the effects of partial consolidation and yield stress ratio. Robertson (2013) developed a revised version of the Robertson (1990) chart where it is possible to distinguish between drained and undrained penetration as well as contractive and dilative penetration behavior.

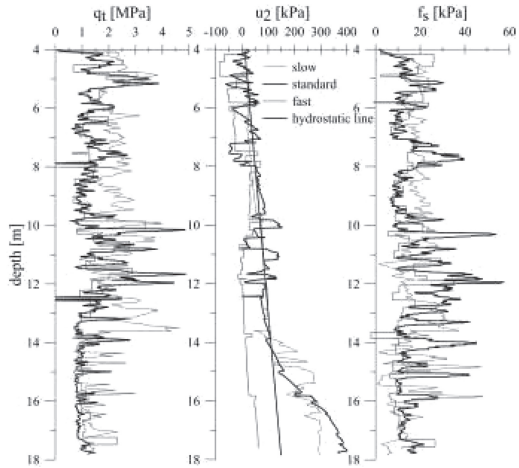

Figure 4. CPTU results Halsen (not smoothed).

4 CPTU RESULTS

4.1 *Halsen, Stjørdal*

Several CPTU soundings are carried out at the Halsen test site between 4 to 14 m. Due to a very stiff and coarse top layer, it was decided to predrill the first 4 m. Different rates of penetration have been used, but only one group of tests has been selected for the present paper: the slow test with an average penetration rate of about 0.5 mm/s representing drained conditions, the standard test at 20 mm/s and the fast test with a penetration rate of 200 mm/s corresponding to an undrained penetration. In order to facilitate the interpretation of the CPTU results, the recordings have been smoothened by applying a moving average over a measuring interval of 100 mm, similar to Holmsgaard et al. (2016).

Figure 4 shows the measured q_t, u_2 and f_s results for some of the tests carried out at Halsen. Between 4 to 14 m the soil consist of a rather coarse sandy silt layer with an average cone resistance at standard penetration rate of about 1,5 MPa and pore pressure values varying around the hydrostatic level at standard penetration rate. Below 12 m, the clay content increases resulting in a lower cone resistance and higher positive excess pore pressures exceeding the hydrostatic level when penetrating the cone at 20 mm/s (see also Figure 2).

The CPTU results pick up the different layering of the soil deposit rather precisely. The measured sleeve friction values are somewhat more scattered than the cone resistance and the pore pressure. Nevertheless, slightly higher friction values are observed during a slower penetration process. As stated by Lunne et al. (1997), the friction measurements have to be used with care due to less reliability.

Several researchers have observed similar trends for the cone resistance, i.e. increasing cone resistance values with decreasing penetration speed. This can be explained by partial consolidation effects occurring in front of the advancing cone during a slower penetration rate and allowing the pore pressure to dissipate and hence the cone resistance to increase (Kim et al. 2008 and Schneider et al. 2007). The drainage conditions during penetration change from drained (slow penetration) to partially drained (medium penetration rate) to undrained (fast penetration).

However, at Halsen the measured pore pressure profiles show opposite trends. During an increased penetration rate the pore pressure decreases and develops high negative values. During the slow rate a drained penetration is assumed by measuring almost hydrostatic pore pressures and a high cone resistance. Increasing the penetration rate leads to an increase in negative excess pore pressure. The measured pore pressure u_2 during a CPTU consists of the in situ pore pressure u_0 and the excess pore pressure Δu_2. The measured Δu_2 can further be separated into the following quantities (see Equation 4, Burns & Mayne 1998)

$$u_2 = u_0 + \Delta u_{2,oct} + \Delta u_{2,shear} \tag{4}$$

where $\Delta u_{2,oct}$ = mean octahedral normal stress component and $\Delta u_{2,shear}$ = shear component of the measured pore pressure (Wroth 1984, Baligh & Levadoux 1986 and Schneider et al. 2007). Shear induced pore pressures can have a significant effect in OC (over consolidated) clays and sandy silts, due to high negative shear occurring in the zone of intense shearing next to the penetrating cone. Further away from this zone the mean octahedral normal stress component dominates, resulting in

larger positive excess pore pressures (Schneider et al. 2007).

Furthermore, the data has been applied to some of the soil classification charts discussed in this paper. The focus is on the 4 m thick sandy silt layer that is present between 4 to 8 m. Friction based classification diagrams have not been considered due to the scattered and rather less reliable results as described above.

The top line of Figure 5 shows the Halsen CPTU data (from left to right) plotted into the Senneset et al. (1989), Robertson (1990) and the Schneider et al. (2008) chart. The Senneset et al. (1989) chart defines the soil as a stiff clay-silt or a loose sand for all penetration rates. Robertson (1990) plots the data mostly into zone 4 and 5, which are defined as silt and sand mixtures. The results for the slow tests are plotted completely in the sand mixture zone, consistent with a drained penetration. The Schneider et al. (2008) diagram shows the most distinct classification where the data is plotted mostly into zone 3 corresponding to transitional soil behavior. Nevertheless results for the slow penetration test are plotted mostly in zone 2 which is defined as a drained sand.

4.2 *Vassfjellet*

Figure 6 shows the CPTU results for the tests carried out in the laboratory for the Vassfjellet silt including three different penetration rates (Paniagua 2014).

The cone resistance shows the highest values during the fast penetration and the lowest results for the slow penetration, i.e. opposite to the Halsen test results. In contrast to the cone resistance, pore pressure values increase with increasing penetration rate, e.g. developing high negative excess pore pressure values at the fastest penetration rate, i.e.

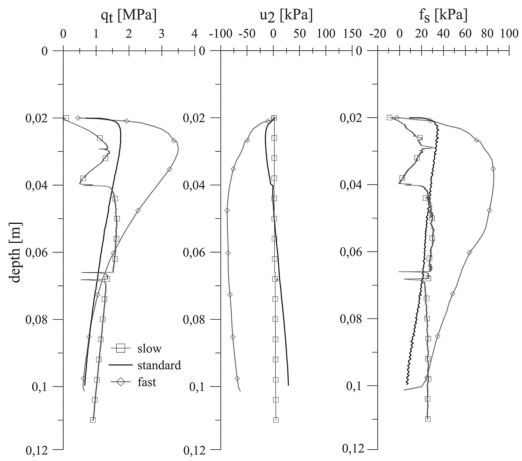

Figure 6. CPTU results Vassfjellet.

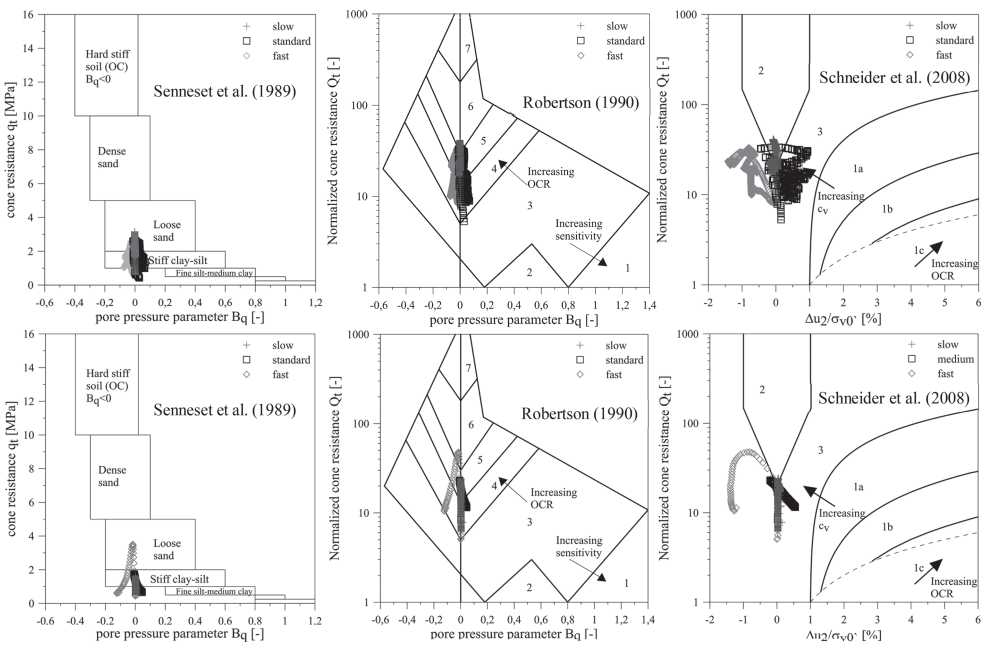

Figure 5. Soil classification charts: Halsen (top) and Vassfjellet (bottom).

similar to the results from the Halsen test site. The sleeve friction values show a similar trend as the cone resistance, e.g. high values for fast penetration and lower values for the slow penetration rate.

The bottom row of Figure 5 shows the results for the Vassfjellet silt plotted into three different soil classification charts. The Senneset et al. (1989) chart classifies the data as silt or stiff clay for the standard and fast rate whereas the data for the slow test are plotted more towards the loose sand—soil behavior. Robertson (1990) defines the soil for all three penetration rates as silt and sand mixture. Schneider et al. (2008) plots the data data into the transitional zone showing an increasing coefficient of consolidation for the increasing penetration rate, Paniagua & Nordal (2015).

5 CONCLUSIONS

The present paper gives an overview over the results obtained during variable rate CPTU tests in silty soils both in the laboratory and in the field. The results show how varying the rate of penetration effects the CPTU readings and hence the degree of drainage and the classification of the soil behavior.

Overall, during a slow penetration, the results for the Halsen test site show a contractive penetration behavior, e.g. developing high cone resistance values and close to hydrostatic pore pressures. In contrast the fast penetration tests show lower cone resistance values and high negative excess pore pressures which corresponds to a more dilative soil behavior. This can be explained by the influence of the dilative behavior giving a shear induced pore pressure component during fast penetration which results in a zone of intense shearing next to the CPTU device.

The results from the laboratory study also show a dilative penetration behavior. During a slow penetration the cone resistance is low and the pore pressures are close to the hydrostatic level. Increasing the penetration rate leads to an increase in penetration resistance and an increase in negative excess pore pressure.

Plotting the CPTU results from the Halsen test site and Vassfjellet silt onto the different soil classification charts shows a general agreement of classifying the soil as transitional and intermediate. In particular the Schneider et al. (2007) chart seems to be promising and support the use of different penetration rates allowing one to make conclusions about the degree of drainage during penetration for identifying silts.

The results show a clear rate dependency of the measured parameters and hence emphasize the need of extended research in the interpretation field of intermediate soils. Further field tests are necessary to gain more insight into the understanding of intermediate soil behavior during a CPTU and an improvement of the interpretation methods is necessary in order to increase the accuracy of developed engineering soil parameters.

REFERENCES

Baligh, M.M. & Levadoux, J.-N. 1986. Consolidation after undrained piezocone penetration. II: Interpretation. *Journal of Geotechnical Engineering* 112 (7): 727–745.

Burns, S.E. & Mayne, P.W. 1998. Monotonic and dilatory pore-pressure decay during piezocone tests in clay. *Canadian Geotechnical Journal* (35): 1063–1073.

Eslami, A. & Fellenius, B.H. 1997. Pile capacity by direct CPT and CPTu methods applied to 102 case histories. *Canadian Geotechnical Journal* (34): 886–904.

Holmsgaard, R., Nielsen, B.N. & Ibsen, L.B. 2016. Interpretation of cone penetration testing in silty soils conducted under partially drained conditions. *Journal of Geotechnical and Geoenvironmental Engineering*. ASCE 142(1).

Kim, K., Prezzi, M., Salgado, R. & Lee, W. 2008. Effect of penetration rate on cone penetration resistance in saturated clayey soils. *Journal of Geotechnical and Geoenvironmental Engineering*, ASCE 134(8): 1142–1153.

Lunne, T. Robertson, P. & Powell, J. 1997. Cone Penetration Testing in Geotechnical Practice. *Spon Press Taylor & Francis Group*, London and New York.

Martinez, M.F.G., Tonni, L., Gottardi, G. & Rocchi, I. 2016. Influence of penetration rate on CPTU measurements in saturated silty soils. *5th International Conference on Geotechnical and Geophysical Site Characterisation.* Sydney, Australia, pp. 473–478.

NGF. 2011. Veiledning for symboler og definisjoner i geoteknikk – identifisering og klassifisering av jord. *Norwegian Geotechnical Society*. Melding (2).

Paniagua, P. 2014. Model testing of cone penetration in silt with numerical simulations. *PhD thesis*. Norwegian University of Science and Technology.

Paniagua, P. & Nordal, S. 2015. Influence of variable rates of penetration on silt behavior and its SBT classification. *Proc. of 15th Pan-American Conference on Soil Mechanics and Geotechnical Engineering*, Buenos Aires, Argentina, pp. 509–516.

Poulsen, R., Nielsen, B.N. & Ibsen, L.B. 2013. Correlation between cone penetration rate and measured cone penetration parameters in silty soils. *18th International Conference on Soil Mechanics and Geotechnical Engineering*. Paris, pp. 603–606.

Randolph, M.F. & Hope, S. 2004. Effect of cone velocity on cone resistance and excess pore pressures. *Engineering Practice and Performance of Soft Deposits*. OSAKA, Japan, pp. 147–152.

Robertson, P.K., Campanella, R.G., Gillespie, D. & Greig, J. 1986. Use of Piezometer Cone Data. In-Situ `86 *Use of In-situ Testing in Geotechnical Engineering*. ASCE Specialty Conference. Reston, Virginia, pp. 1263–1280.

Robertson, P.K. 1990. Soil classification using the cone penetration test. *Canadian Geotechnical Journal* 27(1): 151–158.

Robertson, P.K. 2013. Interpretation of in-situ tests – some insights. 4th International Conference on Geotechnical and Geophysical Site Characterization. The James K. Mitchell Lecture. Pernambuco. Brazil, pp. 3–24.

Sandven, R. 2002. Geotechnical properties of a natural silt deposit obtained from field and laboratory tests. *International workshop on characterization and engineering properties of natural soils*. Singapore, pp. 1121–1148.

Schneider, J.A., Lehane, B.M. & Schnaid, F. 2007. Velocity effects on piezocone measurements in normally and overconsolidated clays. *International Journal of Physical Modelling in Geotechnics* 7(2): 23–34.

Schneider, J.A., Randolph, M.F., Mayne, P.W. & Ramsey, N.R. 2008. Analysis of factors influencing soil classification using normalized piezocone tip resistance and pore pressure parameters. *Journal of Geotechnical and Geoenvironmental Engineering*. ASCE 134(11): 1569–1587.

Senneset, K. & Janbu, N. 1985. Shear strength parameters obtained from static cone penetration tests. *Strength Testing of Marine Sediments. Laboratory and In Situ Measurements*. Symposium, San Diego, ASTM Special technical publication, STP 883, 41–54.

Senneset, K., Sandven, R. & Janbu, N. 1989. Evaluation of soil parameters from piezocone tests. *Transportation Research Record 1235,* National Academies Press, Washington D.C., pp. 24–37.

Silva, M.F. & Bolton, M.D. 2005. Interpretation of centrifuge piezocone tests in dilatant, low plasticity silts. *International Conference on Problematic Soils*. Eastern Mediterranean University, Famagusta, N. Cyprus 25: 27–34.

Stewart, D.P. & Randolph, M.F. 1991. A new site investigation tool for the centrifuge. *Proceedings of the International Conference on Centrifuge Modelling.* Centrifuge `91. Boulder, Colo. 531–538.

Sveian, H. 1995. Sandsletten blir til: Stjørdal fra fjordbunn til strandsted. *Norges geotekniske undersøkelse*. Skrifter 117.

Wroth, C.P. 1984. The interpretation of in situ soil tests. Rankine Lecture, *Géotechnique* 34 (4): 449–489.

Taylor & Francis
Taylor & Francis Group
http://taylorandfrancis.com

Cone Penetration Testing 2018 – Hicks, Pisanò & Peuchen (Eds)
© 2018 Delft University of Technology, The Netherlands, ISBN 978-1-138-58449-5

Quantifying the effect of wave action on seabed surface sediment strength using a portable free fall penetrometer

C. Bilici, N. Stark & A. Albatal
Virginia Polytechnic Institute and State University, Blacksburg, VA, USA

H. Wadman & J.E. McNinch
Field Research Facility, Coastal Hydraulics Laboratory, USACE, Duck, NC, USA

ABSTRACT: The surficial sediment strength of nearshore zone sands has previously been correlated to wave conditions in a qualitative manner. In this study, a coefficient of wave impact on sediment surface strength (*CWS*) is proposed to enable a quantitative assessment. The *CWS* was tested along a cross-shore transect in Duck, NC. The geotechnical input parameters for the *CWS* were measured using a portable free fall penetrometer. The offshore wavelength was extracted from a WaveRider buoy deployed in 17 m, and the water depth was derived from the penetrometer's pressure transducer. The results showed that the *CWS* coefficient reflects the change in sediment strength with wave-seabed interaction. Along the profile, the *CWS* ranged from 0.005 to 1.627. The *CWS* slightly increased at water depths shallower than the depth of closure (~4.5 m) and drastically increased at water depths shallower than breaker depth (~2 m), reaching a maximum value of 1.6.

1 INTRODUCTION

Sediment dynamics influence the nearshore morphology, which in turn affects the performance of engineering activities (Brown & Rashid 1975). One of to-date's most challenging issues regarding the understanding of sediment dynamics is the interaction between geotechnical characteristics of the seabed surface sediment layers, and sediment remobilization and deposition processes (Stark & Kopf 2011). Mobile sediment layers (i.e., surface sediments subjected to erosion, transport, and deposition under hydrodynamic forcing) can be identified as loose sediment top layers overlying more stable sediment layers (Dillon & Zimmerman 1970; Foster & Carter 1997; Flores & Sleath 1998; Stark et al. 2011; Stark & Kopf 2011). However, their geotechnical properties and the resulting impact on sediment dynamics are still unclear.

Portable free fall penetrometers, being an easily deployable geotechnical investigation tool, have been used to investigate sediment remobilization in areas of energetic hydrodynamics (Stark et al. 2014; Albatal & Stark 2017). In fact, the relationship between the surficial sediment strength and wave forcing has been demonstrated using a portable free fall penetrometer in a wave flume, but a direct correlation between geotechnical measurements and wave parameters is still lacking (Stark & Kopf 2011).

This preliminary study aims to fill this gap by proposing a new coefficient relating portable free fall penetrometer measurements to wave characteristics and bathymetry, and by doing so, quantify the impact of wave forcing on surficial sediment strength. The research objectives are to develop a coefficient of wave impact on sediment surface strength (*CWS*), and to test the formulated coefficient using a data set obtained using a portable free fall penetrometer at the U.S. Army Corps of Engineers' Engineering and Research Development Center, Coastal and Hydraulics Laboratory, Field Research Facility (USACE-FRF) at Duck, NC on September 22nd, 2016.

2 REGIONAL CONTEXT

The USACE-FRF is a research facility located in an intensively studied barrier island complex, Outer Banks, NC (e.g. Birkemeier 1985; Lippmann & Holman 1990; McNinch 2004). Meteorological and oceanographic measurements are conducted continuously here, and profiles of the beach and nearshore are periodically surveyed. The facility is distinguished by a 560-meter long pier that allows safe deployment of instrumentation even during energetic conditions (Fig. 1).

The nearshore surface sediments in the region are comprised of mostly quartz sands which

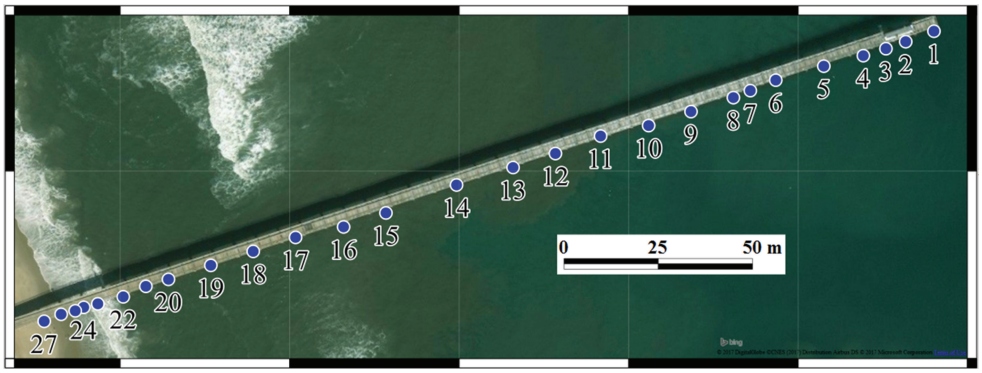

Figure 1. *BlueDrop* deployment stations along the pier located at the USACE-FRF, Duck, North Carolina (36°10'56.2" N 75°45'1.4" W).

coarsen with increasing proximity towards the swash zone (Howd & Birkemeier 1987). The mean particle size in the nearshore area ($\lesssim$150 m from the facility's local baseline) is generally 1 mm, while the offshore particles have a mean particle size of 0.1 mm (Lippmann & Holman 1990). The nearshore region is known for variations in particle size in the cross-shore direction, and with changes in hydrodynamic forcing (e.g. McNinch 2004). Sandbar formation is a common morphological feature of the area. The direction of the bar migration has been observed to be seaward during storms and shoreward during calm conditions (Elgar et al. 2001).

The region's monthly mean significant wave height ranged between 0.56–1.97 m, with a wave period of 6.2–12 s at a water depth of 25 m for the period between 1980 and 2012. The area is characterized by semi-diurnal tides with a tidal range of ~1 m (Albatal et al. 2017). The data collection effort coincided with the end of a mild storm event yielding wave heights of up to 2.5 m. During the study, the average significant wave height was 1.3 m, with a wave period of ~6.5 s (measured by a WaveRider buoy at a depth of 17.4 m for an experiment duration of 3 hr; NDBC 2016). A cross-shore bathymetric profile of the study transect was collected by the USACE-FRF 4 days after the experiment (September 26th, 2016; http://frf.usace.army.mil). It showed a nearshore slope (V: H) ranging from 1:13 to 1:160 in the survey area, and the presence of a bar at a water depth of ~3.0 m.

3 METHODS

3.1 *Portable free-fall penetrometer*

The geotechnical input parameters of the proposed coefficient were measured using the portable free fall penetrometer (PFFP) *BlueDrop*. Its mass is 7.71 kg, and the length is 63 cm. It measures vertical accelerations using five accelerometers with capacities ranging from ±2 *g* to ±250 *g*, and horizontal accelerations using a dual-axis accelerometer with a capacity of 55 *g* (*g*: gravitational acceleration). It also hosts a pressure transducer which can measure ambient pressures with a capacity of 2 MPa located behind the steel tip. Pressure readings in this study were used to confirm the water depth at each deployment location and time. More detailed information about the probe can be found in Stark et al. (2014).

The probe's displacement and velocity (during free fall, impact, and penetration) were determined from the double and single integration of the acceleration measurements, respectively. The resistance of sediment layers during penetration, represented by the equivalent of quasi-static bearing capacity (QSBC), can be estimated using Newton's second law from deceleration records, and considering the strain rate effect (Dayal & Allen 1975; Stoll et al. 2007; Stark et al. 2011). Stratification, and therefore, the thickness of a looser top layer were detected with a resolution of less than 1 cm due to a high sampling rate (2 kHz).

In this study, the PFFP was deployed at 27 cross-shore stations (3 times at each station leading to a total of 81 deployments) from the pier located at the USACE-FRF (Fig. 1). Sediment samples were collected from 9 stations.

3.2 *Coefficient of wave impact on sediment surface strength (CWS)*

The *CWS* coefficient is proposed to quantify the change of seabed surface strength with regard to the wave forcing and water depth from portable free fall penetrometer deceleration readings. The deceleration measurements of PFFPs are

representing a proxy for sediment strength (Stark et al. 2011). Therefore, the measured deceleration, $-a$, is utilized as a geotechnical input parameter. This avoids implementing further empirical factors. To account for changes in impact velocity, a ratio of the probe's deceleration achieved within the top layer, $-a_t$, and the maximum deceleration measured during the same deployment, $-a_{max}$, is applied. This also considers variations of sediment types, such as between cohesive and non-cohesive sediments for which the range of typical maximum deceleration values differ significantly (Stark & Kopf 2011). For example, deployments in marine clays often yield penetration depths of ~ 1 m and maximum deceleration of $-a_{max} < 20\ g$, while deployments in sand are usually limited to penetration depths < 20 cm and $-a_{max} > 40\ g$. Loose top layers resulting from sediment remobilization processes in sandy sediments are commonly on the order of centimeters, but may reach thicknesses on the order of tens of centimeters in soft sediments (e.g., Stark et al. 2016). For this reason, the top layer thickness, z_t, normalized by the corresponding penetration depth at a_{max}, z_{max}, are included in the *CWS* as well. Herein, the top layer thickness is defined as the thickness of a loose top layers showing low resistance to the probe during penetration which can also be associated with the active sediment layers (Fig. 2 shaded area). This layer can be clearly distinguished from a stiffer and stable substratum (Stark & Kopf 2011). Bathymetry is represented by the water depth, h, times two, and the wave characteristics by the deep water wave length

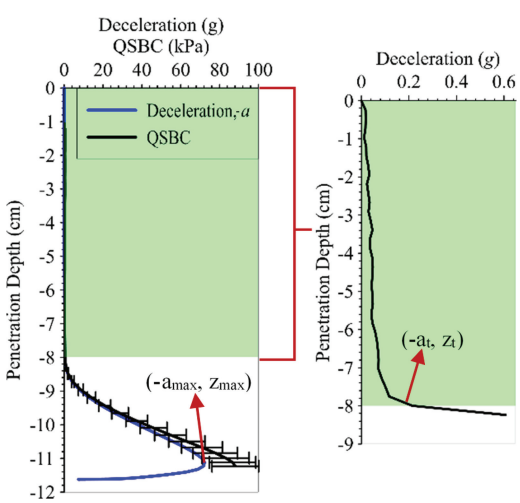

Figure 2. An example QSBC vs sediment depth profile. The QSBC error bars indicate uncertainties resulting from the strain rate correction. The shaded area represents a loose, non-cohesive top layer.

obtained from the wave buoy records, λ_0, representing a common ratio used to predict the interaction between waves and the seabed in coastal settings (Dean & Dalrymple 1991). Thus, the following expression is proposed as an initial attempt for non-cohesive sediments:

$$CWS = \frac{(a_t z_t)/(a_{\max} z_{\max})}{2h/\lambda_0} \tag{1}$$

where the numerator part of the equation reflects geotechnical properties of the soil, and the denominator part reflects the wave conditions and bathymetry. Furthermore, the numerator part expresses characteristics of the sediment surface layer with regard to the underlying substratum, i.e., how soft or loose the surface layer is compared to the substratum.

4 RESULTS

The measured $-a_{max}$ along the cross-shore profile ranged between 17.3 g and 80.6 g with an average of 53 g. The impact velocity ranged between 3.2 m/s and 6.5 m/s with an average of 4.7 m/s and a standard deviation of 0.5 m/s. Considering the strain rate effect using the approach suggested by Stark et al. (2011), the quasi-static bearing capacity (QSBC) ranged between 22.3 kPa and 131.8 kPa with an average uncertainity of ± 9.5 kPa. Penetration depths ranged from 7.3 to 33.0 cm. An example profile from deployment #1 at location #16 is provided in Figure 2.

Small variations in the $-a$ and QSBC profiles were noticed at water depths larger than about 4.5 m (Station 1-19). The maximum QSBC varied from 80 to 100 kPa at maximum penetration depths of 13 to 15 cm. The top layer thickness ranged in the same zone from 5–10 cm (Fig. 3). However, significant variations were observed from Station 22 towards the onshore, where top layer thicknesses increased up to 25 cm (Fig. 3). The maximum QSBC values decreased down to ~26 kPa at penetration depths of ~31 cm (Stations 22 to 25; Fig. 3). At the shoreline, the top layer thicknesses decreased again to a minimum thickness of 4 cm with a maximum QSBC of 74 kPa (Fig. 3; Station 27).

Collected sediment samples showed that in intermediate water (h > 1.0 m), the sediments were well-sorted medium-grained sand, while shallow water (h < 1.0 m) sediments were comprised of poorly sorted, fine to very coarse sand with gravel. Wave breaking was assessed using Miche's formula (Galvin 1972) for the mean significant wave height during the experiment period. It was estimated

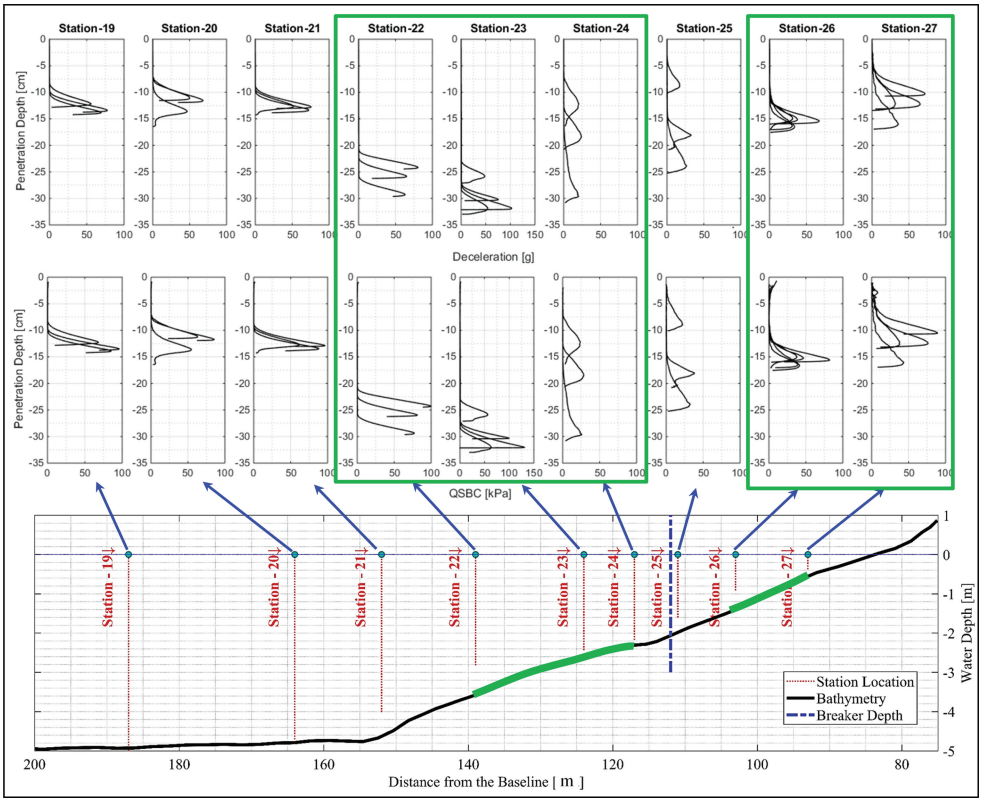

Figure 3. Selected deceleration and quasi-static bearing capacity (QSBC) vs sediment depth profiles along the cross shore bathymetry. The blue dotted line indicates the estimated breaker location at 113 m from the baseline. Green lines on the bathymetry corresponds to location of stations in the green boxes.

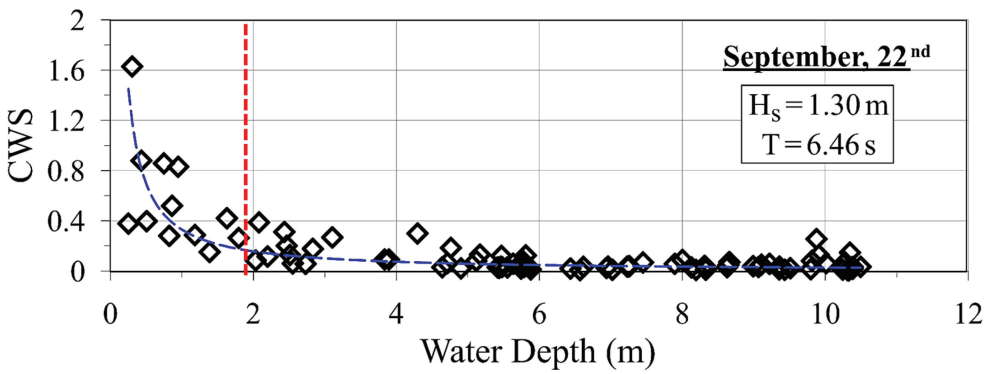

Figure 4. The coefficient of wave impact on sediment surface strength (*CWS*) vs. water depth. The red dotted line is estimated depth of wave breaking.

that wave breaking occurred at a water depth of approximately 2 m (dotted line in Fig. 3).

The *CWS* was determined for the same data set and plotted versus the water depth (Fig. 4). It remained small (< 0.06) at water depths in excess of 4.5 m (150 to 600 m from baseline; Fig. 4), but increased slightly with an average increase of 0.04 per meter in shallower water depths between 2 and 4.5 m. Additionally, the scattering increased in this zone with a standard deviation of 0.11. The trend drastically changed at a water depth ~2 m with *CWS* increasing shoreward to a maximum of 1.6.

Here, high scatter is also observed in the magnitude of the *CWS*. The standard deviation was 0.41 for water depths less than 2 m.

5 DISCUSSION

The results confirmed that the sediment strength varied along the cross-nearshore profile (Fig. 3). This is in line with the observations by Albatal and Stark (2017) from Cannon Beach, Yakutat, AK, and Albatal et al. (2017) from the same location (i.e., FRF beach). More specifically, the top layer thickness and variability in sediment strength started increasing at water depths of ~4.0 to 4.5 m towards the shore (Fig. 3).

The experiment day coincided with the end of a storm wave event (peak significant wave height ~ 2.5 m). The depth of closure is defined as the minimum water depth where no observed, significant morphological changes occur at the seabed (Birkemeier 1985; Nicholls et al. 1998). Nicholls et al. (1998) documented the depth of closure at Duck, NC, for 71storm events, and found a depth of 4–6 m for significant wave heights ranging between 2–3 m. This suggests that seabed surface disturbance would be expected at water depths of 4–6 m and shallower during our experiment. Indeed, *CWS* started to increase and showed higher variability at water depths ≤ 4.5 m, reflecting particularly an increase in top layer thickness. However, it should be explored how the sensitivity of the *CWS* to the depth of closure can be increased.

Overall, a low penetration resistance was observed in water depths of ~ 2 m. This may be a direct result of consistent wave breaking and the associated reworking of the surficial sediments down to a sediment depth of 30 cm. According to Nielsen et al. (2012), when a wave breaks, the resulting turbulence generates an increased bed shear stresses that can mobilize the sediments to a greater depth than in the non-breaking zone. The *CWS* strongly reflected this interaction between breaking waves and the seabed (Fig. 4). This increase was accompanied by relatively large scatter. One possible reason is the timing of the deployment with regard to the time of actual wave breaking. However, this assumption needs to be tested further to understand the signature of wave breaking on the geotechnical properties of surficial sediments

6 CONCLUSIONS

This study aimed to quantify the impact of wave action on geotechnical properties of the seabed, using a new coefficient (*CWS*) relating top layer strength, maximum sediment strength at maximum penetration depth, top layer thickness and total penetration depth of a portable free fall penetrometer to water depth and offshore wavelength. The results confirmed that sediment strength and layering in the nearshore zone are governed by the wave-seabed interaction. The larger the water depth for a constant wavelength, the smaller the impact of wave forcing on the seabed, i.e., smaller top layer thicknesses and larger sediment strength, leading to $CWS \rightarrow 0$. When $2h/\lambda_0 < 1$ and the interaction between the seabed and the waves is expected, the *CWS* responded by increasing, and providing values that reflect the top layer thickness and softness. The *CWS* responded strongly when approaching wave breaking and when an overall loosening of the seabed occurred.

The here presented study represents the initial development and test of the *CWS*. The coefficient was only tested using a single data set from one location. Future research will include the application of additional data sets from Duck, NC, at different times, as well as other sites. Furthermore, it will be investigated how the *CWS* can be developed to be more sensitive to the depth of closure. In addition, it will be explored if the offshore wavelength can be replaced as the input wave characteristic by wave orbital velocity, wave period or celerity to be more compatible with common hydrodynamic models.

ACKNOWLEDGMENTS

The authors acknowledge funding from the Office of Naval Research through award N00014-16-1-2590, and the National Science Foundation through award OCE-1434938. The authors would like to thank the staff of the USACE-FRF for their help with data collection processes.

REFERENCES

Albatal, A., McNinch, J.E., Wadman, H. and Stark, N., 2017. In Situ Geotechnical Investigation of Nearshore Sediments with Regard to Cross-Shore Morphodynamics. *Geotechnical Frontiers 2017*. Available at: https://doi.org/10.1061/9780784480472.042.

Albatal, A. and Stark, N., 2017. Rapid sediment mapping and in situ geotechnical characterization in challenging aquatic areas. *Limnology and Oceanography: Methods*, 15(8), pp.690–705. Available at: http://doi.wiley.com/10.1002/lom3.10192.

Birkemeier, W.A., 1985. Field data on seaward limit of profile change. *Journal of Waterway, Port, Coastal, and Ocean Engineering*, 111(3), pp.598–602.

Brown, J.D. and Rashid, M.A., 1975. Geotechnical Properties of Nearshore Sediments of Canso Strait, Nova Scotia. *Canadian Geotechnical Journal*, 12(1), pp.44–57. Available at: https://doi.org/10.1139/t75–004.

Dayal, U. and Allen, J.H., 1975. The Effect of Penetration Rate on the Strength of Remolded Clay and

Sand Samples. *Canadian Geotechnical Journal*, 12(3), pp.336–348. Available at: http://www.nrcresearchpress.com/doi/abs/10.1139/t75-038#.UOdCgG_Ezwk.

Dillon, W.P. and Zimmerman, H.B., 1970. Erosion by biological activity in two New England submarine canyons. *Journal of Sedimentary Research*, 40(2). Available at: http://jsedres.geoscienceworld.org/content/40/2/542.

Elgar, S., Gallagher, E.L. and Guza, R.T., 2001. Nearshore sandbar migration. *Journal of Geophysical Research: Oceans*, 106(C6), pp.11623–11627.

Flores, N.Z. and Sleath, J.F.A., 1998. Mobile layer in oscillatory sheet flow. *Journal of Geophysical Research: Oceans*, 103(C6), pp.12783–12793. Available at: http://doi.wiley.com/10.1029/98 JC00691.

Foster, G. and Carter, L., 1997. Mud sedimentation on the continental shelf at an accretionary margin—Poverty Bay, New Zealand. *New Zealand Journal of Geology and Geophysics*, 40(2), pp.157–173. Available at: http://www.tandfonline.com/doi/abs/10.1080/00288306.1997.9514750.

Galvin, C.J., 1972. Wave breaking in shallow water. *Waves on beaches and resulting sediment transport*, pp.413–456.

Howd, P.A. and Birkemeier, W.A., 1987. *Beach and Nearshore Survey Data, 1981–1984, CERC Field Research Facility*, US Army Engineer Waterways Experiment Station.

Lippmann, T.C. and Holman, R.A., 1990. The spatial and temporal variability of sand bar morphology. *Journal of Geophysical Research: Oceans*, 95(C7), pp.11575–11590.

McNinch, J.E., 2004. Geologic control in the nearshore: shore-oblique sandbars and shoreline erosional hotspots, Mid-Atlantic Bight, USA. *Marine Geology*, 211(1), pp.121–141.

Nicholls, R.J., Birkemeier, W.A. and Lee, G., 1998. Evaluation of depth of closure using data from Duck, NC, USA. *Marine Geology*, 148(3–4), pp.179–201.

Nielsen, A.W., Sumer, B.M., Ebbe, S.S. and Fredsøe, J., 2012. Experimental study on the scour around a monopile in breaking waves. *Journal of Waterway, Port, Coastal, and Ocean Engineering*, 138(6), pp.501–506.

Stark, N., Hanff, H., Svenson, C., Ernstsen, V.B., Lefebvre, A., Winter, C. and Kopf, A., 2011. Coupled penetrometer, MBES and ADCP assessments of tidal variations in surface sediment layer characteristics along active subaqueous dunes, Danish Wadden Sea. *Geo-Marine Letters*, 31(4), pp.249–258.

Stark, N. and Kopf, A., 2011. Detection and quantification of sediment remobilization processes using a dynamic penetrometer. In *IEEE/MTS Oceans 2011*. Waikoloa, HI., pp. 1–9.

Stark, N., Hay, A.E. and Trowse, G., 2014. Cost-effective geotechnical and sedimentological early site assessment for ocean renewable energies. In *2014 Oceans - St. John's*. IEEE, pp. 1–8. Available at: http://ieeexplore.ieee.org/document/7003004.

Stark, N., Radosavljevic, B., Quinn, B. and Lantuit, H., 2016. Application of a portable free-fall penetrometer for the geotechnical investigation of the Arctic nearshore zone. *Canadian Geotechnical Journal*. Available at: http://dx.doi.org/10.1139/cgj-2016–0087.

Stoll, R.D., Sun, Y.F. and Bitte, I., 2007. Seafloor properties from penetrometer tests. *IEEE Journal of Oceanic Engineering*, 32(1), pp.57–63.

Cone Penetration Testing 2018 – Hicks, Pisanò & Peuchen (Eds)
© 2018 Delft University of Technology, The Netherlands, ISBN 978-1-138-58449-5

Interpretation of seismic piezocone penetration test and advanced laboratory testing for a deep marine clay

M.D. Boone
Black and Veatch, Walnut Creek, California, USA

P.K. Robertson
Gregg Drilling & Testing, Inc. Signal Hill, California, USA

M.R. Lewis
Bechtel Corporation, Evans, Georgia, USA

D.E. Gerken
Bechtel Corporation, San Francisco, California, USA

W.P. Duffy
Bechtel Corporation, London, England, UK

ABSTRACT: A nearshore site investigation in a deep marine clay was performed in British Columbia, Canada. Investigation boreholes and seismic piezocone penetration test (SCPTu) soundings, including both seabed deployed and top push tests, were advanced to depths of greater than 135 meters below mudline. This paper presents the interpretation of the SCPTu data together with the results of laboratory testing on thin-wall (intact) tube samples from adjacent companion boreholes. Laboratory testing included index tests, consolidation tests, consolidated Direct Simple Shear (DSS), K_0 Consolidated Undrained Triaxial Compression tests (K_0CUTXC), and combined Resonant Column Torsional Shear (RCTS) tests. The results of the laboratory testing aided the interpretation of the SCPTu data including the development of site-specific correlations to parameters such as shear wave velocity and undrained shear strength.

1 INTRODUCTION

A nearshore site investigation performed at a project site in British Columbia, Canada included a marine geophysical survey, boreholes, SCPTu soundings, and associated laboratory testing. The water depth at the site generally ranges from about 10 to 20 m. The site soil stratigraphy typically consists of very loose silty sands ranging in thickness of about 0 to 5 m, underlain by about 20 to 100 m of lightly overconsolidated clay that approaches a normally consolidated condition with depth, underlain by dense glacial deposits including clays, silts, sands, gravels, and cobbles ranging in thickness from about 0 to 5 m. Bedrock generally consists of a slightly weathered to fresh metamorphic rock (gneiss, phyllite, and schist) occurring at depths below mudline of about 20 to 140 m.

This paper focuses on the results of the SCPTu and adjacent borehole and laboratory testing data. Kottke et al. (2017) discussed the combined resonant column and torsional shear (RCTS) laboratory tests performed for this project.

2 SITE INVESTIGATION

Twenty-three (23) boreholes were advanced through soil and rock and included the acquisition of relatively undisturbed thin-wall tube samples. Twenty (20) SCPTu locations were explored to approximately the top of either the glacial deposits or bedrock where practical refusal was encountered. The SCPTu included two types of soundings, 1) a coiled-rod seabed-deployed system to the maximum rod length of 30 m (shown here as Figure 1) and 2) a top push system using a barge-mounted drill rig to extend from the termination depth of the coiled-rod unit to final refusal on the glacial till or bedrock (shown here as Figure 2). All SCPTu soundings collected shear wave velocity measurements on one-meter depth

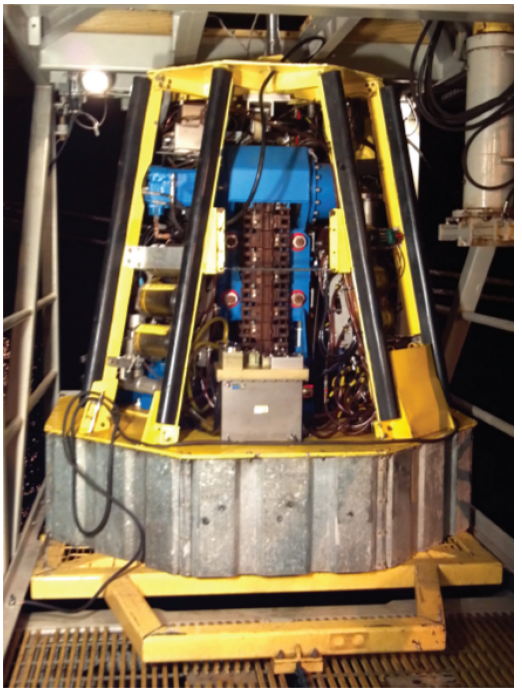

Figure 1. Seabed deployed SCPTu rig.

Figure 2. Barge mounted drill rig advancing top push sounding.

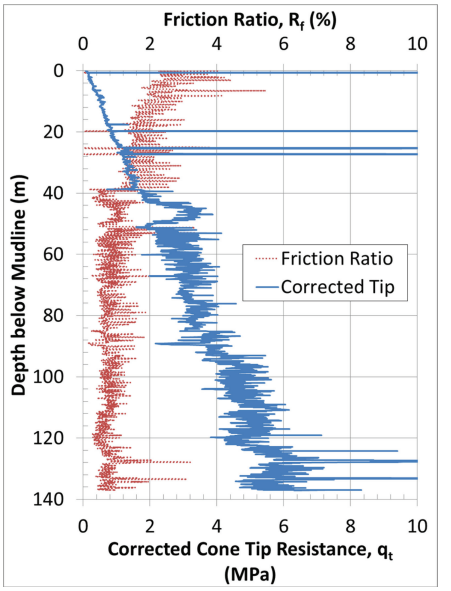

Figure 3. SCPTu corrected tip resistance and friction rato from 137 m sounding.

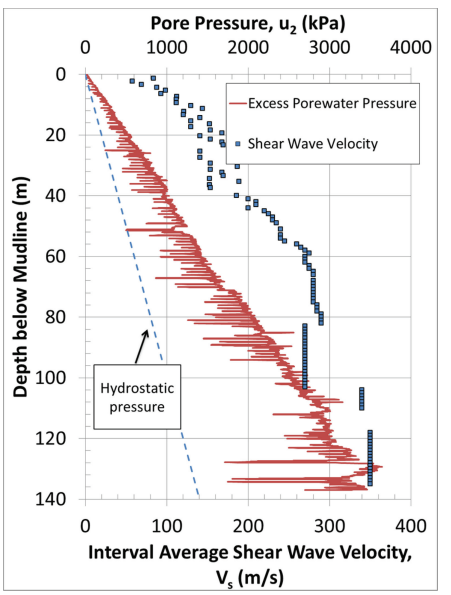

Figure 4. SCPTu pore pressure measured at cone shoulder (u_2) and interval average shear wave velocity from 137 m sounding.

intervals. A sea-bed deployed hammer unit was used to generate the shear wave. Figures 3 and 4 present the corrected tip resistance, friction ratio, pore pressure, and interval averaged shear wave velocity from the deepest SCPTu sounding.

3 LABORATORY TESTING

Laboratory testing included index testing (moisture content, unit weight, grain size distribution, organic content, and Atterberg limits) as well as consolidation testing and advanced strength testing. Figure 5 shows Atterberg limits and moisture content values versus depth below the mudline on a 5 m-depth average.

The average Atterberg Limits for the clay were: Liquid Limit 42; Plastic Limit 26 and Plasticity Index 16. The average moisture content was 40%. The average soil total unit weight for the clay was 18 kN/m^3. The results show that on average, the materials plot on the A-line, as defined by Casagrande, which indicates an inorganic clay/silt of medium plasticity and compressibility.

The moisture content was generally higher than the Liquid Limit in the upper 30 m of clay.

The advanced compressibility and strength testing relevant to this paper are described in the subsections below.

3.1 *Consolidation tests*

Forty-six (46) constant rate of strain (CRS) and 17 incremental load (IL) consolidation tests were performed on vertically oriented samples

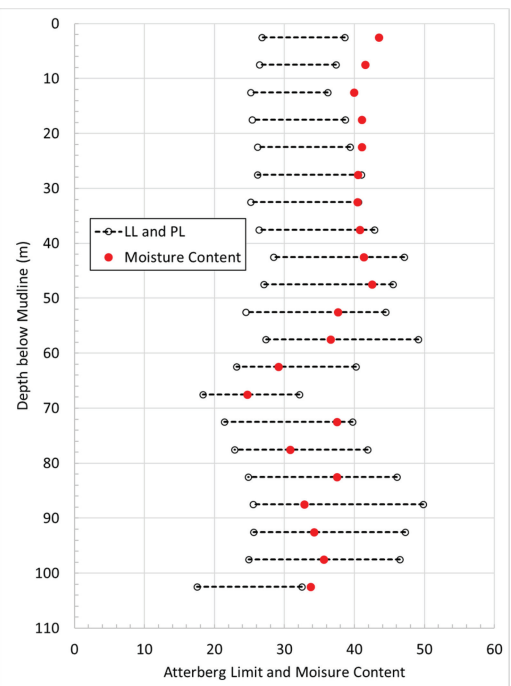

Figure 5. 5-meter average Atterberg limits and moisture content versus depth below mudline.

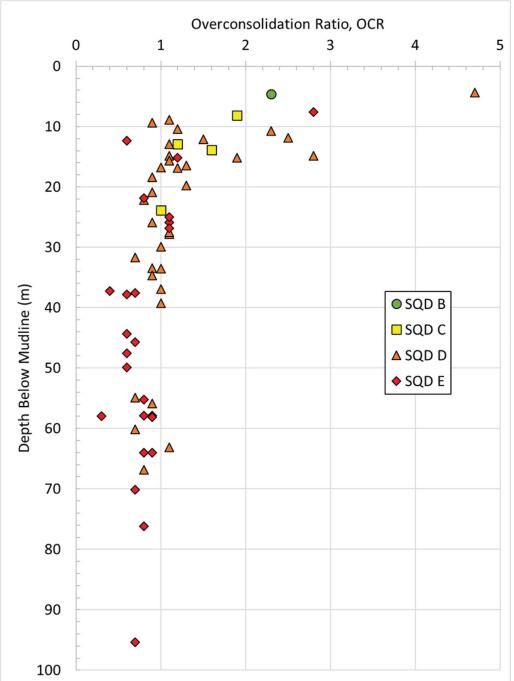

Figure 6. OCR versus depth based on laboratory test results.

to evaluate the consolidation characteristics of the subsurface materials. Figure 6 presents the overconsolidation ratio (OCR) versus depth, interpreted using the Casagrande construction. The data are segregated by symbol and color by the sample quality designation (SQD) suggested by Terzaghi et al. (1996). A review of this figure indicates lightly overconsolidated soils near the mudline, approaching normally consolidated conditions with depth. Additionally, the sample quality generally decreases with depth, as expected. The reduction in sample quality is likely attributed to stress relief associated with obtaining samples at significant depth, described by Ladd and DeGroot (2004), as well as the difficulty of sampling and transporting samples associated with offshore drilling operations.

3.2 *Consolidated undrained testing*

Laboratory K_0 consolidated undrained triaxial compression (K_0CUTXC) tests and consolidated direct simple shear (DSS) tests were performed on selected samples, over the range of plasticity encountered in the subsurface deposits, to determine the undrained shear strength of the soil using the stress history and normalized soil engineering

properties (SHANSEP) model after Ladd and Foott (1974) and summarized in Equation 1.

$$\frac{S_u}{\sigma'_{v0}} = S(OCR)^m \tag{1}$$

where S_u is the undrained shear strength, S and m are empirical parameters, and σ'_{v0} is the vertical effective stress. Generally, the samples were consolidated to about 1.5 times the in-situ preconsolidation stress, then were sheared at the laboratory manufactured OCR of 1 to confirm that the soils normalize according to the SHANSEP model. Subsequent tests were conducted similarly or were allowed to swell to a prescribed OCR. Once the SHANSEP model was confirmed, DSS were performed at laboratory manufactured OCRs of about 2, 3, and 4. K_0CUTXC were sheared only at laboratory manufactured OCR of 1 due to laboratory restrictions. These results are shown as Figure 7. Figure 8 shows the SHANSEP S and m parameters derived from the laboratory data. Note that the S parameter is derived from weighted averages of the data based on test quality, and a typical exponent "m" of 0.8 is adopted as it appears to fit the data well.

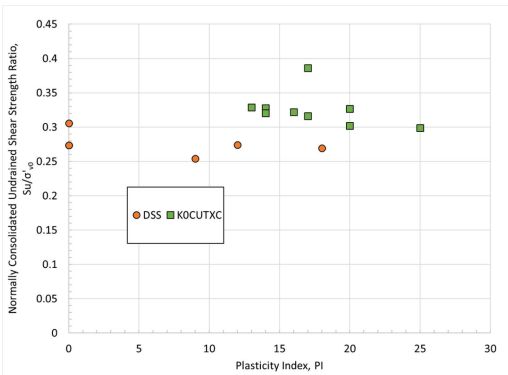

Figure 7. S_u/σ'_{v0} versus plasticity index for OCR = 1 samples.

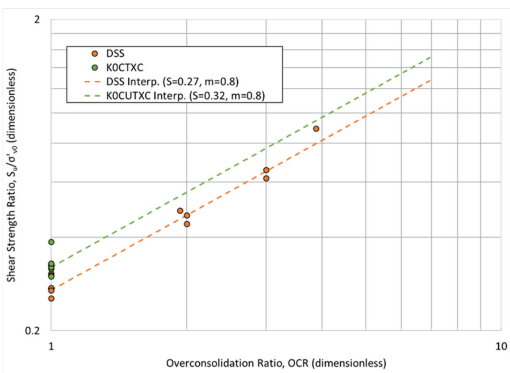

Figure 8. S_u/σ'_{v0} versus OCR.

3.3 *Resonant Column-Torsional Shear (RCTS) testing*

Laboratory RCTS tests were performed on selected samples. These tests utilize the recompression technique to minimize the effects of sample disturbance where each sample is consolidated, tested, then consolidated at a higher stress before retesting. The results of these tests can be used to construct shear wave velocity versus depth plots using Equation 2 after Hardin (1978) where σ'_0 is the mean effective stress (taken as 2/3 the vertical effective stress), P_a is atmospheric stress, and A_s and n_s are empirical parameters. Figure 9 is such a plot for four of the samples tested. Note that similar stress-shear wave velocity relations were measured in the laboratory, although the four tested samples were collected from different representative depths within the soil profile. See Kottke et al. (2017) for additional details on the RCTS testing.

$$V_s = A_s \left(\frac{\sigma'_0}{P_a} \right)^{n_s} \tag{2}$$

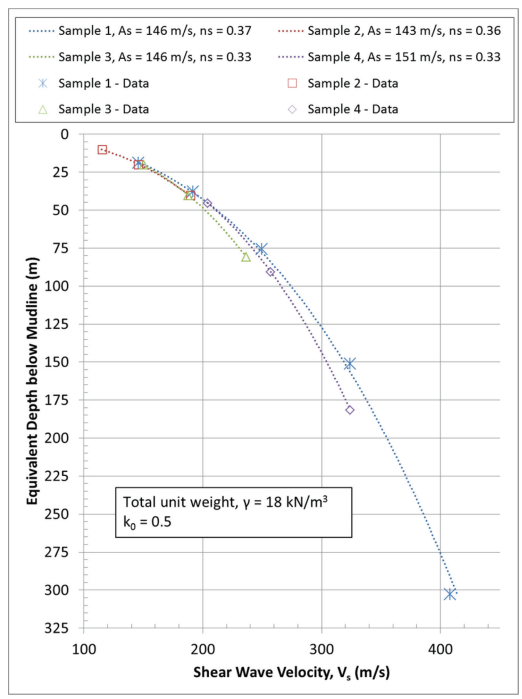

Figure 9. Shear wave velocity interpreted from RCTS data versus equivalent depth.

4 SCPTU INTERPRETATION

4.1 *Overconsolidation Ratio (OCR)*

The overconsolidation ratio (OCR) is correlated from the SCPTu data after Kulhawy and Mayne (1990) using Equation 3.

$$OCR = k\left(\frac{q_t - \sigma_{v0}}{\sigma'_{v0}}\right) = \frac{kq_{net}}{\sigma'_{v0}} \tag{3}$$

where k is an empirical constant taken as 0.33, q_t is the corrected cone tip resistance, σ_{v0} is the total overburden stress, σ'_{v0} is the effective overburden stress, and q_{net} is the corrected cone tip resistance less the total overburden stress. The interpreted OCR obtained from SCPTu's taken for this investigation are shown as Figure 10. The similarity between Figure 6 and Figure 10 is noteworthy.

4.2 *Undrained shear strength*

Peak undrained shear strength (S_u) from cone tip resistance can be calculated from Equation 4 after Aas et al. (1986) and others.

$$S_u = \frac{q_{net}}{N_{kt}} \tag{4}$$

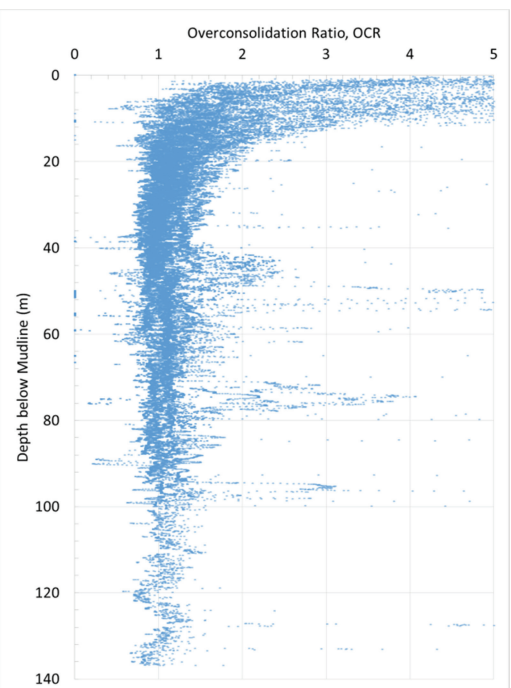

Figure 10. OCR correlated from SCPTu tip resistance versus depth (k = 0.33).

where N_{kt} is a cone factor correlating tip resistance to undrained shear strength and is calculated rearranging Equations 1, 3, and 4 resulting in Equation 5.

$$N_{kt} = k^{-m} S^{-1} \left(\frac{q_{net}}{\sigma_{v0}}\right)^{1-m} \tag{5}$$

where S and m are the SHANSEP parameters presented in Figure 8 and are selected based on mode of shearing, and k is an empirical constant taken as 0.33. The average N_{kt} values are about 10.0 for triaxial compression and about 12.5 for simple shear loading. These values are within the reported range of Low et al. (2010) of 10.0 to 14.0 for triaxial compression and 11.5 to 15.5 for simple shear loading. Alternatively, undrained shear strength can be correlated to excess porewater pressure using Equation 6 after Robertson and Cabal (2015).

$$S_u = \frac{\Delta u}{N_{\Delta u}} \tag{6}$$

where Δu is the excess porewater pressure measured at the cone shoulder, u_2 position, and $N_{\Delta u}$ is a cone factor correlating excess porewater pressure to undrained shear strength and is calculated using Equation 7 after Robertson and Cabal (2015).

$$N_{\Delta u} = B_q N_{kt} \tag{7}$$

where B_q is the measured pore pressure ratio. The average $N_{\Delta u}$ are 7 for triaxial compression and 5.5 for simple shear loading. The results are presented in Figure 11, which is a profile of undrained shear strength in triaxial compression versus depth obtained from cone tip resistance and excess porewater pressure indicating good correlation as the results from the two methods overlap, with a gradient of about 2.7 kPa/m.

As shown in Equations 1, 2 and 4, V_s and S_u can be correlated to vertical effective stress using laboratory test results. Rearranging these equations and inputting the laboratory derived empirical parameters results in Equations 8 and 9 which relate V_s and S_u assuming normally consolidated conditions. Figure 12 presents measured in-situ shear wave velocity against average undrained shear strength for the 1-meter interval correlated from SCPTu data. Curves using Equations 8 and 9 are superimposed over these data. A review of this figure indicates a good match between the laboratory derived relations and the SCPTu data.

RCTS samples range from about 7 to 46 meters below mudline which correlates to undrained shear strengths of about 17 to 110 kPa and V_s of about 70 to 130 m/s. There is a good correlation where the

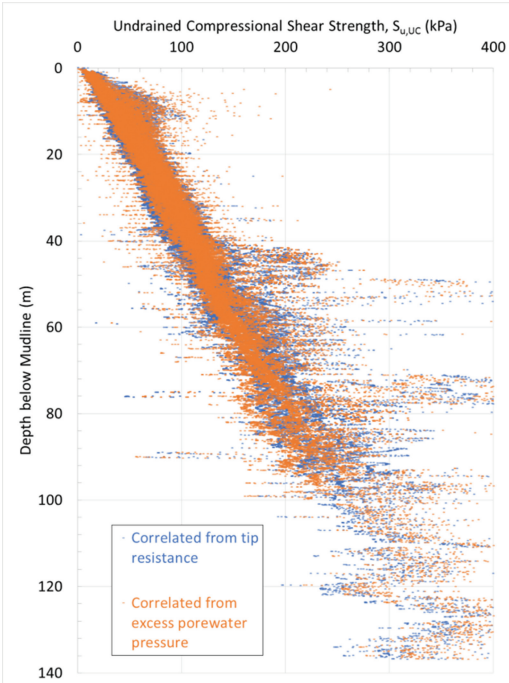

Figure 11. Undrained shear strength in triaxial compression versus depth.

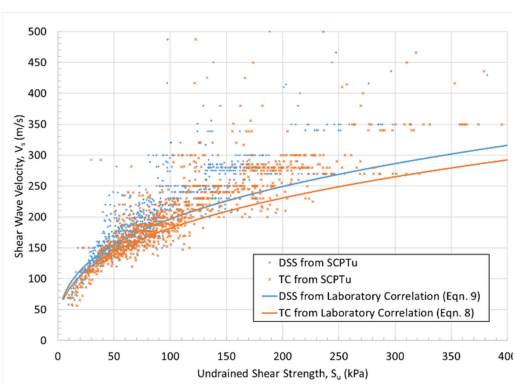

Figure 12. Undrained shear strength versus shear wave velocity assuming normally consolidated conditions.

RCTS data are interpolated and where the data are extrapolated, the correlation is not as strong. For deeper samples, at greater stress and thus greater V_s and S_u, the laboratory correlation (Equations 8 and 9) underestimate V_s. This is likely because the deeper soils have experienced additional increases in V_s due to the aging process As Wair et al. (2012) and others have noted that V_s relations from S_u or cone tip resistance are a function of age.

$$V_s = 43.3\left(S_{u,TC}\right)^{0.342} \tag{8}$$

$$V_s = 46.8\left(S_{u,DSS}\right)^{0.342} \tag{9}$$

4.3 *Shear wave velocity*

In-situ shear wave velocity (V_s) measurements from the SCPTu and the interpreted shear wave velocity profile from the laboratory RCTS tests are shown as Figure 13. A review of this figure indicates a good match between data in the upper 40 meters, with the RCTS curve predicting somewhat lower shear wave velocities than the in-situ measurements below 40 meters. Schmertmann (1991) suggested that shear modulus, and thus shear wave velocity, increase with age. It is assumed that at this site age increases with depth.

Therefore, the divergence is likely due to aging of the soil, since the laboratory curves are from more shallow, younger, samples which have not experienced the effects of aging. Note that the higher velocity "spikes" are due to V_s measured in the tills that overlie rock where the SCPTu "refused" or reached high tip resistances at shallow depths.

These points diverge from the trend because they represent the V_s of a dense till rather than a

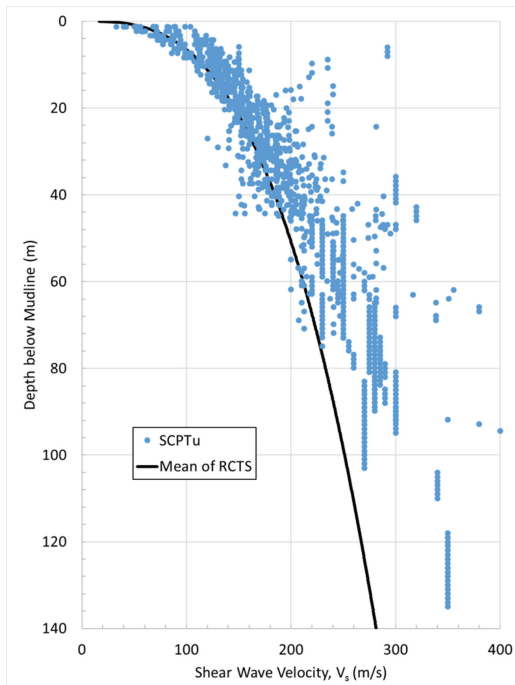

Figure 13. Shear wave velocity profile from in-situ SCPTu and laboratory measured RCTS.

normally consolidated clay. These results (spikes) are not indicative of the marine clays.

5 CONCLUSION

SCPTu's were successfully advanced to depths greater than 135 meters below mudline, providing a valuable database for evaluating the subsurface conditions at the project site. To the authors knowledge, SCPTu soundings advanced to these depths in a marine environment using surface pushing methods is unprecedented. Together with laboratory testing results, SCPTu data were very useful in evaluating the OCR and the undrained shear strength profile for this site. Additionally, the in-situ measured V_s from the SCPTu corresponds well with the laboratory measurements from the combined RCTS tests for this site.

REFERENCES

Aas, G. Lacasse, S., Lunne, T., and Hoeg, K. (1986). "Use of in situ tests for foundation design on clay." In *Use of In Situ Tests in Geotechnical Egineering*, pp. 1–30. ASCE, 1986.

Hardin, B.O. (1978). "The Nature of Stress-Strain Behavior of Soils," *Proceedings, Geotech. Eng. Div. Specialty Conference on Earthquake Eng. And Soil Dynamics*, Vol. 1 ASCE, Pasadena, June, pp. 3–90.

Kottke, A.R., Keene, A., Wang, Y., Shin, B., Stokoe, K.H., Lewis, M.R., (2017) "In-Situ and Laboratory Measured Dynamic Properties of a Deep Marine Clay", *Proceedings from Geotechnical Frontiers*, March 12–15, 2017, Orlando, FL, USA.

Ladd, C.C., DeGroot, D.J. (2014) "Recommended practice for soft ground site characterization: Arthur Casagrade Lecture." Proceedings of the 12 Pan American Conference on Soil Mechanics and Geotechnical Engineering, Massachusetts Institute of Technology, Cambridge, Massachusetts.

Ladd, C.C., Foott, R., (1977). "New design procedure for stability of soft clays." *J. Geotech. Engrg. Div.*, ASCE, 100(7), 763–786.

Low, H.E., Lunne, T., Andersen, K.H., Sjursen, M.A., Li, X., and Randolph M.F. (2010). *Geotechnique*, No. 11, 843–859 [doi: 10.1680/geot.9.P.017]

Robertson, P.K., Cabal, K.L. (2016). *Guide to Cone Penetration Testing for Geotechnical Engineering*, 6th Edition, Gregg Drilling and Testing Inc., http://www.greggdrilling.com/technical-guides

Schmertmann, J.H. (1991). "The mechanical aging of soils." *Journal of Geotechnical Engineering, 117*(9), 1288–1330.

Terzaghi, K., Peck, R.B., Mesri, G. (1996) *Soil Mechanics in Engineering Practice*. John Wiley & Sons.

Wair, B.R., DeJong, J.T., Shantz, T. (2012). *Guidelines for estimating shear wave velocity profiles*. Pacific Earthquake Engineering Research Center, Report 2012/08.

Taylor & Francis
Taylor & Francis Group
http://taylorandfrancis.com

Cone Penetration Testing 2018 – Hicks, Pisanò & Peuchen (Eds)
© 2018 Delft University of Technology, The Netherlands, ISBN 978-1-138-58449-5

CPT-based liquefaction assessment of CentrePort Wellington after the 2016 Kaikoura earthquake

J.D. Bray
University of California at Berkeley, Berkeley, CA, USA

M. Cubrinovski & C. de la Torre
University of Canterbury, Christchurch, New Zealand

E. Stocks
Tonkin & Taylor, Ltd., Wellington, New Zealand

T. Krall
CentrePort Ltd., Wellington, New Zealand

ABSTRACT: The Wellington CentrePort experienced liquefaction of reclaimed land and liquefaction-induced ground deformations that led to building and wharf damage in the 2016 M_w7.8 Kaikoura earthquake. There was evidence of lateral spreading in the fills behind the pile-supported wharves and liquefaction-induced settlement in the soils surrounding buildings supported on deep foundations. Previous attempts to perform CPTs at the port had limited success. In the reclaimed land constructed by end-dumping of quarried soils there are large gravel-size and boulder-size particles overlain by a 3-m$^+$ thick, dense compacted earth crust covered with a thick pavement. Use of a larger, more robust cone provided reliable subsurface data that characterized well the reclaimed materials at the port. Insights garnered from this site investigation of the gravelly soils are shared.

1 INTRODUCTION

CentrePort Wellington experienced significant liquefaction of reclaimed land and liquefaction-induced ground deformations that led to wharf and building damage in the 2016 M_w7.8 Kaikoura earthquake. The liquefaction caused global settlement of the fill deposits and lateral movement of the fills towards the sea. There was evidence of lateral spreading in the fills behind the pile-supported wharves and liquefaction-induced settlement in the soils surrounding buildings supported on shallow and deep foundations. After documenting the ground and structural damage from the earthquake, a comprehensive site exploration program was performed to characterize the subsurface conditions at CentrePort. Cone penetration tests (CPTs) were advanced and shear wave velocity (V_S) profiles were measured. These subsurface data add important information because few reliable quantitative subsurface data were available before the earthquake. This paper summarizes liquefaction and damage observations from the Kaikoura earthquake. CPT data from the recent subsurface investigations are discussed and current insights from the ongoing program of research are shared.

2 WELLINGTON PORT RECLAMATIONS

An aerial view of the central waterfront area of Wellington, New Zealand, which includes CentrePort, is shown in Figure 1. Wellington was developed after the European settlement in the 1850's. The original coastline from the 1850's is located approximately 200 m to 500 m inland from the current revetment line delineating a belt of reclaimed land that increases in width towards the north along the waterfront and reaches its largest extent at CentrePort.

Two methods of construction were used to reclaim land at CenterPort. The Log Yard area (top-right in Figure 2), and areas north of it (around the oval stadium shown in Figure 1 and north of the stadium) are hydraulic fills constructed using dredged material (sandy and silty soils) from the original seabed in the vicinity of the reclamation works. The remaining and larger part

Figure 1. Aerial view of Wellington highlighting CentrePort. Strong motion stations that recorded the Kaikoura earthquake are also shown (Image-Google Earth™; Cubrinovski et al. 2017).

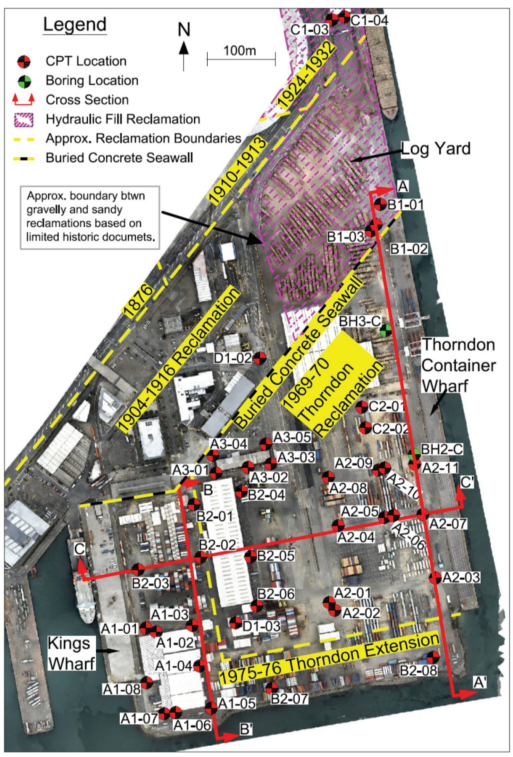

Figure 2. Overview of CentrePort showing the locations of CPTs performed for this study, some of the existing borings, and soil cross sections. The approximate boundaries of various land reclamations are shown (Cubrinovski et al. 2018).

of the reclamation was constructed by end-tipping, in which gravelly soils from nearby quarries were dumped into the sea from truck and barge operations. The CentrePort reclamation south of the buried concrete seawall (i.e. the Thorndon reclamation shown in Figure 2) was constructed by the end-tipping method between 1969 and 1976.

Based on the original records, soft sediments were first removed from the seabed by dredging, and then the quarry fill material was placed by end-tipping, creating a relatively thick fill deposit through a water sedimentation process. The thickness of the fill increases with its horizontal distance from the original coastline. The fill is about 10 m thick immediately south of the buried seawall and increases southwards reaching the maximum thickness of about 20 m along the southern edge of the Thorndon Extension. Static rollers were used to compact the top 2–3 m of the fill as soon as the fill surfaced above high water level in the construction process (Hutchison 1973); whereas, the fill below 2–3 m depth is uncompacted. The fill overlies 1–5 m thick marine sediments of interbedded sand, clay and silty clay, which sit on top of approximately 75–135 m of Wellington Alluvium composed of interbedded dense gravel and stiff to very stiff silt (Vantassel et al. 2018).

3 LIQUEFACTION AND SPREADING INDUCED DAMAGE

Following the 2016 Kaikoura earthquake, the QuakeCoRE-GEER team conducted numerous field inspections to document the damage to land and associated damage to wharves and buildings at CentrePort. The first inspections were performed three days after the main shock, while most of the perishable liquefaction evidence was observable. This initial data capture was followed by more detailed surveys that focused on obtaining additional evidence including measurements of ground displacements and relative movements between wharves or buildings and the surrounding soils. In the second part of these inspections ground-based LiDAR scanning was performed along transects of the reclamations and around CentrePort structures of interest. This section provides an overview of the damage at CentrePort. A more detailed account on the damage to the ground and structures at CentrePort caused by the 2016 Kaikoura earthquake may be found in Cubrinovski et al. (2017), and Cubrinovski & Bray (2017).

3.1 *Liquefaction ejecta*

The 2016 Kaikoura earthquake triggered widespread liquefaction in gravelly end-tipped quarry fills and sandy hydraulic fills at CentrePort. Liquefaction was manifested by substantial volumes of soil ejecta covering areas of the pavement surface at the port. The areas covered with soil ejecta were scattered and non-uniform in their spatial

distribution and thickness of the ejected soils. Liquefaction manifestation varied from traces of ejected silts and water to larger volumes of soil ejecta with thicknesses of up to 150–200 mm. Large volumes of ejecta were typically found near cracks and fissures in the pavement which allowed the liquefied soils to reach the ground surface more easily. In several cases, a larger amount of ejecta was observed near partially collapsed pavement and cavities, or along existing drainage conduits beneath the pavement.

In the Thorndon Container Terminal the ejected soils consisted generally of well-graded gravelly soils including cobble-size particles, sand, and finer fractions. Gravelly ejecta samples were collected from 15 sites at various locations of CentrePort south of the buried concrete seawall. Their grain size distribution curves are shown with solid lines in Figure 3, whereas the background shaded zone indicates the range of grain size distribution curves obtained for samples of the gravelly fill recovered from boreholes completed before the earthquake. Visual descriptions of the ejecta and the good agreement between the two sets of grain size curves indicate the end-tipped gravelly fill liquefied during the Kaikoura earthquake.

At other locations, the ejected soils consisted of sands and silts. This type of ejecta was observed typically in areas of hydraulically-placed fills north of the buried concrete seawall (e.g. in the Log Yard). However, sandy ejecta were also observed at two locations in the central area of the Thorndon Container Terminal. The observation of sandy ejecta within the end-tipped gravelly reclamation of Thorndon terminal was a noteworthy anomaly which could be explained by a temporary use of different materials in the construction of Thorndon reclamation, which is implied in the original documentation of the construction process and reclamation materials.

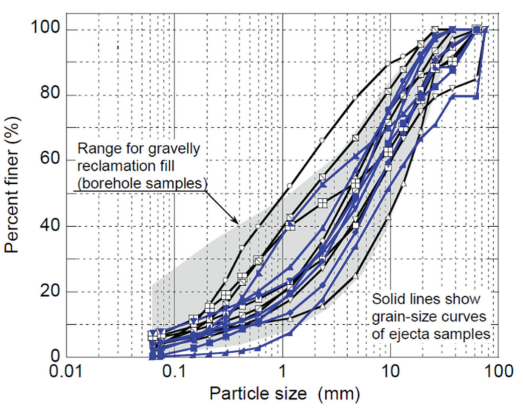

Figure 3. Grain size distribution curves from gravelly ejecta samples showing a well-graded material with 40–80% gravel (i.e. > 2 mm) and 0–10% fines. Grain size analyses of gravelly soils collected from borehole samples (i.e. shaded region) are generally consistent with those of ejecta samples.

3.2 *Land damage and movements*

Liquefaction was also manifested through large permanent displacements of the reclaimed land and associated ground cracks, fissures, and distortion. Figure 4a shows large volumes of gravelly reclamation ejected through a large fissure in the Thorndon Container Terminal. Vertical offsets on the order of tens of centimeters to above half a meter were observed between pile-supported wharves and buildings and their surrounding ground. The thick gravelly fills of the Thorndon reclamation also underwent seaward movement of the reclamation edges in all unconfined directions, with characteristic liquefaction-induced lateral

Figure 4. (a) Manifestation of liquefaction in the Thorndon Container Terminal gravelly reclamation through large volumes of ejecta and fissures in the pavement, and (b) damage to Kings Wharf bulkhead piles from lateral ground movement towards the sea exceeding 1 m and settlement of approximately 0.5 m.

spread cracking and ground distress progressing in-land.

Seaward displacements along Kings Wharf were measured to be 0.5 m to 1.4 m, along Thorndon Wharf to be 0.3 m to 1.0 m, and along Thorndon Extension to be 1.0 m to 1.5 m. The lateral movements of the wharves are also indicative of the size of lateral movements of the reclamation edge located immediately behind the wharves, as the large spreading displacements of the reclamation near the edges produced kinematic loads that pushed the piles of the wharves towards the sea. The fills reach a thickness of about 20 m along the southern perimeter and are laterally unconfined without retaining structures with armored slopes of 2H:1V extending down to the seabed. Thus, significant seaward liquefaction-induced displacements are not unexpected.

Permanent liquefaction-induced lateral displacements extended as far as 200 m behind the bulkhead within the Thorndon reclamation and the magnitude of permanent lateral displacements was particularly large within a zone of about 50 m from the bulkhead.

Vertical displacements of the ground surface of the reclamation relative to adjacent pile-supported structures were observed. Settlement of the gravelly reclamation was predominantly about 200–300 mm in the central area of the reclamation and 400–600 mm near its edges. The absolute settlement of the hydraulic fills in the Log Yard area was about 150–250 mm. The distribution of settlement also exhibits spatial non-uniformity, which is characteristic for liquefaction manifestation. The permanent settlement of pile-supported structures were small or insignificant.

3.3 *Damage to wharves*

Thorndon Container Wharf and Kings Wharf suffered substantial damage during the 2016 Kaikoura earthquake. The Thorndon Wharf is the larger and newer wharf completed in 1971. It is supported on pre-stressed reinforced concrete piles (508 × 508 mm), which are placed in 7 rows at 3.81 m spacing. The Kings Wharf was completed in 1906, and it is supported on timber piles.

Liquefaction of the reclamation and seaward movement of the fills, which was particularly large at the reclamation edges, were the principal factors in the damage to the wharves. The seaward movement of the fills displaced the Thorndon Wharf 0.3 m to 1.0 m towards the sea, which loaded the piles significantly. The lateral thrust from the displaced fill was larger for the landward piles of the wharf, which caused asymmetric loading on the wharf structure and permanent tilt of the wharf of up to 0.5° down towards the sea (Cubrinovski et al. 2017). The top of some landward Thorndon Wharf piles were sheared just below the wharf deck (Cubrinovski et al. 2017). There were large vertical offsets between the reclamation surface and pile-supported wharf decks, and ground and wharf distortion for both wharves. The large lateral displacement of Kings Wharf, which reached 1.0 m to 1.4 m at the southern end of the wharf, was accompanied with tilting of the wharf down towards the sea, and consequent splitting of the piles and failure of the connection at the pile top as shown in Figure 4b.

3.4 *Effects on buildings*

Several buildings on reclaimed soils at CentrePort were damaged by liquefaction-induced ground deformations and ground shaking. A majority of buildings were supported on pile foundations, though a few buildings were on shallow foundations. The fill surrounding the pile-supported buildings settled 50–400 mm relative to the buildings. This settlement caused abrupt offsets between the deformed ground surface/pavement and the building. Some of the low- to mid-rise buildings supported on piles, which did not appear to suffer foundation distress, were moderately to severely damaged from ground shaking.

Buildings on shallow foundations typically settled with surrounding fill. A building near the center of the reclamation, which was not affected by lateral ground movements, settled approximately 260 mm uniformly relative to the ground supported on buried piles. Another building, near the crest of the western slope, was damaged badly from lateral spreading which cracked the reinforced concrete foundation, pulled apart and tilted adjacent columns, and separated the ground floor slab at construction joints. The total width of cracks in the foundation of this building (i.e. its lateral stretch) along a wall perpendicular to the slope was approximately 350 mm in an area where lateral ground movements at the slope exceeded 1 m.

4 CPT CHARACTERIZATION OF PORT RECLAMATIONS

Recognizing the significance of CentrePort liquefaction case study and in support of the recovery of the port, the QuakeCoRE-GEER research team performed subsurface investigations at CentrePort, which included CPTs and shear wave velocity measurements. Advancing CPTs at gravelly soil sites can be difficult. In April-May 2017, 47 CPTs were successfully advanced at CentrePort by the McMillan Drilling Group working under the authors' direction at the locations shown in

Figure 2 using the equipment and procedures described in this paper.

A.P. van den Berg Icones were used with a 218 Geomil Panther 100 rig with a push force of 106 kN. Tests were performed typically with a 15 cm^2 cone because of its robustness and the reduced friction on the 10 cm^2 rods. Stainless steel and plastic filters were used for the u2 pore pressure transducers, and several pore water pressure dissipation tests were performed. After a test, cones were allowed to de-air for a minimum of 1 hour in vacuum submerged in silicone oil. Predrilling to a depth of 3 m through the dense compacted gravelly fill crust at CentrePort was performed to increase penetration depth. A plugged, small diameter casing with an extractable tip was vibrated slightly beyond the depth at which the penetration rate increased substantially. The casing had an inside diameter of 55 mm and an outside diameter of 70 mm. This method of predrilling was able to penetrate through asphalt pavement and concrete (with an open-ended barrel), produce little spoils, and provided lateral support to the CPT rods. If early refusal was encountered during a test at depths less than about 10 m, the casing was extended beyond the depth of refusal, and then cone testing was continued. Additional predrilling and two CPT attempts were required at 13 locations to reach the desired depth. Early refusal was typically met due to excessive inclination of the rods (i.e. > 15°), likely caused by deflection from cobble and boulder size particles.

Measured cone tip resistances (q_c) and computed soil behavior type index (I_c) traces (Robertson, 2016) are shown in Figure 5 for three representative locations at CentrePort. CPT B1-02 is in a hydraulic fill north of the buried concrete seawall (i.e. in the Log Yard). CPTs A2-05 and A2-11 are in the Thorndon Container Terminal reclamation. CPT A2-05 is in an area where sandy ejecta were observed, and CPT A2-11 represents a typical CPT profile obtained in the gravelly fill where gravelly ejecta were observed.

The CPT data in the hydraulic fill (e.g. CPT B1-02 in Fig. 5a) show low penetration resistances of silt-sand mixtures up to 8 m depth, overlying a 4-m thick clayey layer. From 12–20 m depth, sand layers with thickness of about 1.5 m are inter-bedded with thin silty and clayey soils. The gravelly fill at CPT A2-11 (Fig. 5c) is characterized by consistent traces of low tip resistance of q_c = 5–8 MPa and I_c values of about or slightly below 2, from 2.5–14 m depth. The I_c values imply these gravel-sand-silt fills display soil responses consistent with fine-sand coarse-silt mixtures. The CPT data confirm the earlier findings based on grain-size composition that finer fractions (sands and silts) dominate the response characteristics of the matrix of the gravelly mixture, rather than the gravel-size particles. The presence of loose-to-medium dense sand (i.e. q_c around 10 MPa) from about 5 m to 12 m depth (i.e. below gravelly reclamation) was a characteristic feature of CPT A2-05 (Fig. 5b).

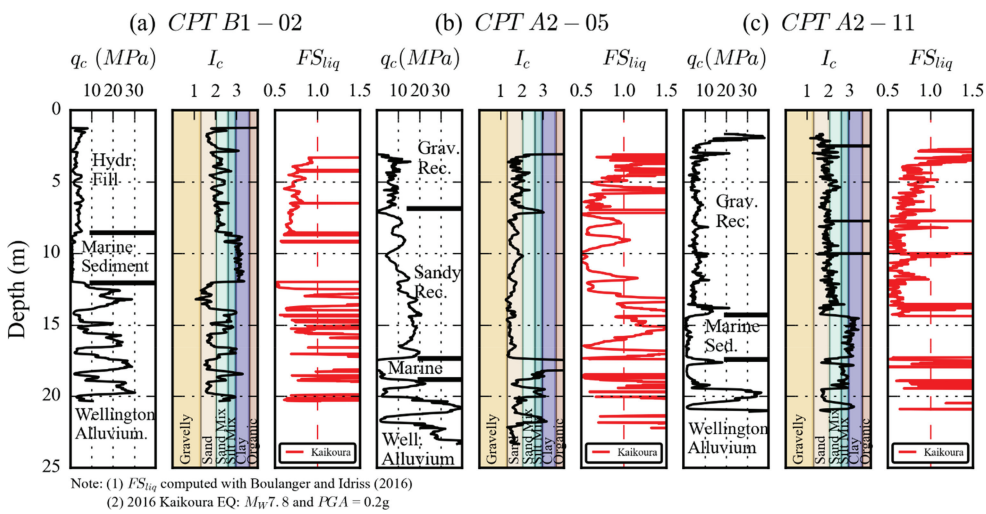

Figure 5. CPT traces of q_c and I_c with the FS_{liq} calculated with the liquefaction triggering assessment of three representative soil profiles due to the 2016 Kaikoura earthquake: (a) CPT B1-02 is in sandy hydraulic fill north of the buried concrete seawall (i.e. in the Log Yard); (b) CPT A2-05, and (c) CPT A2-11 are in the Thorndon Container Terminal; however, CPT A2-05 encountered sandy reclamation below gravelly reclamation and CPT A2-11 did not.

CPT-based liquefaction triggering analyses were performed using the deterministic Boulanger and Idriss (2016) procedure for the 2016 Kaikoura earthquake using a representative peak ground acceleration (PGA) of 0.2 g with $M_w = 7.8$ (Cubrinovski et al. 2018). The computed factors of safety (FS_{liq}) shown in Figure 5, which are well below one in much of the reclamation, indicate liquefaction should have been triggered in these areas of the port. The results of the liquefaction assessment are consistent with the observed liquefaction manifestation within the hydraulic fill, sandy reclamation, and gravelly fill at the port.

Figure 6 schematically illustrates characteristic soil profiles along three cross sections: A-A′, B-B′ and C-C′, whose locations are shown in Figure 2. These profiles summarize key features of reclamation soil units, and the underlying marine sediments and Wellington Alluvium as characterized by the CPTs. Traces of q_c for CPTs located along these cross sections are included. The inset table, and q_c and I_c numerical values embedded in the plots show characteristic ranges (25th and 75th percentiles) for typical soil units. The vertical scale of the cross sections are exaggerated to show details, which distorts the shape of the slopes and wharves. The gravelly reclamation fills show a consistent range of low tip resistance of $q_c = 4.7$–7.7 MPa and $I_c = 1.9$–2.3. The I_c values imply soil responses consistent with sand-silt mixtures. In the central part of Thorndon Container Terminal, the CPTs detected a 'mound' of loose-to-medium-dense and medium-dense-to-dense sand with $q_c = 11.6$–16.5 MPa and $I_c = 1.5$–1.7. At some CPT locations, the top part of the sand deposit consistently shows tip resistances at the low end of the above range, and at one of these locations the largest amount of clean sand ejecta was observed (i.e. at CPT A2-05).

5 CONCLUSIONS

Large capacity CPT equipment with a 15 cm^2 cone with pre-drilling and collaring systems enabled most of the CPTs to penetrate through the gravelly reclaimed fill so that effective characterization could be completed. Although the fill was found to have relatively low penetration tip resistances and the gravelly sand was first thought to be free draining, negative pore water pressures were often measured which desaturated the porous

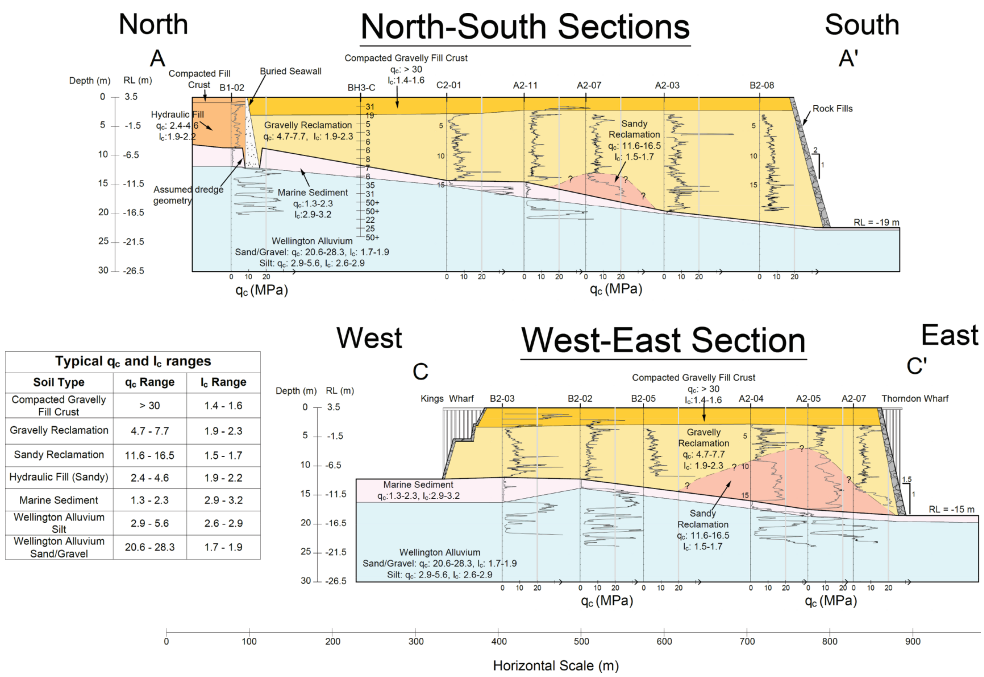

Typical q_c and I_c ranges		
Soil Type	**q_c Range**	**I_c Range**
Compacted Gravelly Fill Crust	> 30	1.4 - 1.6
Gravelly Reclamation	4.7 - 7.7	1.9 - 2.3
Sandy Reclamation	11.6 - 16.5	1.5 - 1.7
Hydraulic Fill (Sandy)	2.4 - 4.6	1.9 - 2.2
Marine Sediment	1.3 - 2.3	2.9 - 3.2
Wellington Alluvium Silt	2.9 - 5.6	2.6 - 2.9
Wellington Alluvium Sand/Gravel	20.6 - 28.3	1.7 - 1.9

Figure 6. Schematic soil cross sections depicting key soil units at CentrePort (7x vertical scale exaggeration). Refer to Figure 2 for location of cross sections and CPTs. The tabulated q_c and I_c are based on 25th to 75th percentile values for each soil unit across all representative CPTs. Slope geometry and bathymetry based on Tonkin & Taylor (2006, 2012) (from Cubrinovski et al. 2018).

stone and produced unreliable pore water pressure measurements in the fill. Pore pressure dissipation tests led to recovery of the hydrostatic water pressure, but typically only for a few centimeters of advancement. Adjacent soil borings showed the angular fine-grained matrix of the gravelly sandy fill produced these responses. CPT liquefaction triggering assessments identified loose zones of fill which likely produced the measured lateral spread deformations and vertical settlement at the port that resulted in severe damage.

In summary, the CPTs provide consistent and de-tailed characterization of the fills including clear distinction between the gravel-sand-silt mixes and pre-dominantly sandy fills, underlying marine sediment and Wellington Alluvium, and thickness of the stiff compacted fill crust. These CPT data will be further scrutinized and used to perform comprehensive liquefaction analyses using both simplified and advanced methods to elucidate the seismic performance of the reclaimed land, wharves, and buildings at the port.

ACKNOWLEDGEMENTS

NZ team reconnaissance effort was principally supported by EQC Capability Grant at the Univ. of Canterbury, and MBIE support provided for the 2016 Kaikoura Earthquake Reconnaissance. US GEER team contributors were supported by the National Science Foundation (NSF) through the Engineering for Natural Hazards program under Grants CMMI-1266418 and CMMI-1724866. CPT exploration efforts were funded through the Natural Hazards Research Platform (NHRP) grant "Kaikoura Earthquake response—geotechnical characterization of CentrePort reclamations" provided by MBIE (NZ) and NSF Grant CMMI-1724866. Any opinions, findings, and conclusions or recommendations expressed in this material are those of the authors and do not necessarily reflect the views of the NSF. The authors are grateful for the continuous collaboration provided by CentrePort Ltd. We thank Stuart Palmer, Richard Cole, Mike Jacka, and Sjoerd van Ballegooy from Tonkin+Taylor Ltd. for their assistance throughout the reconnaissance and site investigations. Iain Haycock and the McMillan Drilling Group crew performed the CPTs through challenging soil deposits and shared in the cost of the CPT work. Hugh Cowan's assistance in gaining port access is appreciated. The aerial survey data is from Cardno. This is QuakeCoRE publication number 0269.

REFERENCES

Boulanger, R.W. and Idriss, I.M. (2016). CPT- Based Liquefaction Triggering Procedures. *Journal of Geotechnical and Geoenvironmental Engineering*, 142(2), 04015065.

Cubrinovski, M., Bray, J., de la Torre, C., Olsen, M., Bradley, B., Chiaro, G., Stocks, E., Wotherspoon, L. 2017. Liquefaction effects and associated damages observed at the Wellington CentrePort from the 2016 Kaikoura earthquake. *Bulletin of the New Zealand Society for Earthquake Engineering,* 50(2), 152–173.

Cubrinovski, M., Bray, J.D., de la Torre, C., Olsen, M., Bradley, B.A., Chiaro, G., Stocks, E., Wotherspoon, L., Krall, T. 2018. Liquefaction-Induced Damage and CPT Characterization of the Reclamation at CentrePort Wellington. *Bulletin of the Seismological Society of America*, in press.

Cubrinovski, M and Bray, J. (Eds.) 2017. *Geotechnical Aspects of the 14 November 2016 Kaikoura (New Zealand) Earthquake*. QuakeCoRE – GEER Reconnaissance Report.

Hutchison, A.J.H. 1973. Reclamations in Wellington Harbour with special reference to recent developments. *New Zealand Engineering*. 15 August 1973, 217–224.

Robertson, P. 2016. Cone penetration test (CPT)-based soil behavior type SBT classification system – an update. *Canadian Geotechnical Journal,* 53(12), 1910–1927.

Tonkin & Taylor Ltd. 2006. *Harbour Quays Development Factual Geotechnical Report, Revision 2*. Prepared for CentrePort Wellington Limited. Ref No. 83725.004.

Tonkin & Taylor Ltd. 2012. *Thorndon Container Wharf Seismic Assessment Geotechnical Factual Report*. Prepared for CentrePort Limited. Ref No. 85369.001.

Vantassel, J., Cox, B., Wotherspoon, L., Stolte, A. 2018. Deep shear wave velocity profiling and fundamental site period measurements at CentrePort, Wellington and implications for locate site amplification. *Bulletin of the Seismological Society of America*, in press.

Taylor & Francis
Taylor & Francis Group
http://taylorandfrancis.com

Cone Penetration Testing 2018 – Hicks, Pisanò & Peuchen (Eds)
© 2018 Delft University of Technology, The Netherlands, ISBN 978-1-138-58449-5

Use of CPTu for design, monitoring and quality assurance of DC/DR ground improvement projects

Aymen Brik
Trevi Ground Engineering, UAE

Peter K. Robertson
Gregg Drilling & Testing Inc., USA

ABSTRACT: CPTu has proven to be an important tool with a multitude of uses throughout the life cycle of a ground improvement project, starting from design, execution and verification. The aim of this paper is to present several aspects of using the CPTu results in DC/DR ground improvement practice, including: exploration of pre-improvement sub-soil conditions, evaluation of the soil compactability and selection of the most suitable ground improvement solution based on CPT SBT_n-I_c ranges, anticipation of the required compaction energy according to soil type and required level of ground stiffness. Several ground improvement case histories shall be presented to illustrate these different aspects.

Keywords: Dynamic Compaction, Dynamic Replacement, CPTu, soil Compactability, compaction energy, cost effective

1 INTRODUCTION

Soil improvement techniques are typically implemented as value engineering solutions to foundation, liquefaction and soil replacement problems, for a wide range of projects such as infrastructure, residential buildings, oil & gas facilities, roads, railways, airports, marine structures, power plant structures and storage tanks.

For coarse-grained soils such as sands, silty sands, landfill, soil densification is a common ground improvement solution, using either Dynamic Compaction (DC), Rapid Dynamic Compaction or Vibro-Compaction techniques, according to the depth of improvement required, type of soil and project modalities.

For fine-grained soils, densification concept is not possible due to the low-permeable soils that can inhibit the dissipation of excess pore pressures and, therefore, reduce the compaction effectiveness. For this category of soils, improvement often requires substitution of the weak fine-grained soil by creating compacted columns, using gravel or sand material, through the soft soil layers, by means of Dynamic Replacement (DR) and Vibro-Replacement methods.

DC and DR techniques have benefited from many developments in recent years, which have increased its effectiveness, sustainability and range of applications.

This paper provides guidelines for evaluation, design and energy adjustment procedures for the use of DC/DR to produce ground improvement in weak soil deposits, by using CPTu as the main in-situ testing method.

Although guidelines are useful in planning and implementing DC/DR techniques, it cannot replace good judgment and adjustments during the execution stage based on the observed ground response.

2 SUMMARY OF DC/DR TECHNIQUES

DC involves dropping heavy steel pounders repeatedly on the ground at regularly spaced intervals and applicable for a wide variety of soil conditions, particularly saturated & unsaturated loose sands, non-organic fill, reclaimed fill, landfill deposits and collapsible soils.

DR is an extension of DC for fine-grained soils where the tamping energy drives granular fill material down into the compressible soils to form a large diameter soil reinforcement column with a typical diameter of 2.0 to 2.2 m. DR can be pre-excavated, and then partially backfilled with granular fill material, which is then driven into the soft layer by the drop weight to the design depth of improvement.

DR combines the advantages of DC with those of stone columns (Vibro-replacement) by creating

large-sized columns with high internal shearing resistance and stiffness as well as overall improvement of the mechanical properties of the intermediate soil.

2.1 *Improvement/Compaction energy*

The improvement/compaction energy is generally applied in phases on a grid pattern using either single or multiple passes. For each pass, a certain number of blows is applied for each impact point, which involves the use of different size pounders (tampers) and drop heights.

The total compaction/improvement energy is calculated as the sum of different levels of energy applied for different steps/passes, as follows:

Total Applied Energy:

$$E = \sum N.W.H.P/(GS)^2$$

Unit Applied Energy:

$$UE = E/D$$

N = Number of drops at each specific point location
W = Pounder weight (kN)
H = Drop height (m)
P = Number of passes
D = Depth of improvement (m)
GS = Grid spacing (m).

On typical projects, the Total Applied Energy (E) ranges from about 1 to 3 MJ/m^2 for sandy material (DC application) and 3 to 8 MJ/m^2 for cohesive soils (DR application). The Unit Applied Energy (UE) ranges from about 200 to 500 KJ/m^3 and 500 to 1000 KJ/m^3, respectively for sandy material (DC application) and cohesive soils (DR application).

The above values are indicative only and can be considered as guideline benchmarks. However, the required amount of energy should be determined (designed) taking into consideration the following main parameters:

i. Classification of the material/soil to be improved
ii. Water table conditions
iii. Depth of improvement
iv. Required degree of improvement
v. Other site conditions that might impact the application of compaction energy (presence of hard layer, site vicinity, etc.)

3 KEY SOIL PARAMETERS

A pre-improvement soil investigation campaign is always required to provide on sub-soil conditions. If soil improvement is deemed to be required, the following key parameters should be determined:

- Depth of improvement required,
- Water table conditions,
- Type of soil to be improved,
- Soil gradation (mainly coefficient of uniformity, percentages of fines and clay content), where borehole/sample data are available
- The CPT-based Normalized Soil Behavior Type (SBT_n-I_c), where CPT data are available,

The CPT has been found to be one of the best methods to assess most soil parameters required for the design and optimization of soil improvement works, due to the continuous, reliable and repeatable nature of the data.

3.1 *Introduction about CPT*

Robertson (2009) suggested that normalized CPT values were more effective to identify soil behavior type and that normalized parameters are derived from the corrected cone tip resistance (q_t) and sleeve friction (f_s) and in-situ vertical stress (σ'_{vo}). The Soil Behavior Type Index (I_c) is then calculated from normalized CPT cone resistance, as explained below:

$$I_c = \sqrt{((3.47 - \log(Q_{tn}))^2 + (1.22 + \log(F_r))^2)} \quad (1)$$

where

$$Q_{tn} = \left[\frac{q_c - \sigma_{v0}}{p_a}\right] \times CN \quad (2)$$

And

$$F_r = \left[\frac{f_s}{q_c - \sigma_{v0}}\right] \times 100\% \quad (3)$$

where Q_{tn} = Normalized cone resistance; F_r = Normalized friction ratio (%); σ_{v0} = total vertical stress at tip level; p_a = Reference stress = 100 kPa.

$$CN = \left[\frac{p_a}{\sigma'_{v0}}\right]^n \quad (4)$$

where n = 0.5 if $I_c < 1.64$; n = 1.0 If $I_c > 3.30$; n = $(I_c - 1.64)0.3 + 0.5$ if $1.64 < I_c < 3.30$

The I_c calculation is based on an iterative procedure, by assuming a stress component n = 1.0 first, which applies for clay-like soils, then iterate until the change in the stress exponent $\Delta n < 0.01$.

4 COMPACTABILITY OF SOILS

The first step in soil improvement design is to determine whether the soil can be densified or not, which has a great impact on deciding the most suited and economical soil improvement method.

Mitchell (1982) identified soils that can be compacted according to grain size distribution and suggests that most granular soils with a fines content (particles < 0.064 mm) lower than 10% can be compacted by vibratory and impact methods. The main disadvantage of this method is that grains size curves are concluded from laboratory tests on disturbed soil samples, while it is preferable to use parameters taken from in-situ tests.

The USA Federal Highway Administration (FHWA) also have criteria to evaluate compactibility using DC method based on grain-size distribution.

The FHWA guidelines suggest that soil with a fines content less than 20% are suitable for compaction using DC. FHWA also provide some guidance to predict the post-densification q_t as a function of applied energy.

Massarsch (1991) proposed criteria for vibratory compaction methods based on CPT cone resistance and friction ratio values as shown on Fig. 1. It should be noted that this diagram assumes homogeneous soil conditions. In the case of thin layers of silt and clay, the effectiveness of soil compaction will be reduced.

The CPTu can also be used to identify the occurrence of less permeable silt and clay layers.

It is worth mentioning here that DC/DR extends the range of compactable soils beyond that which is normally undertaken by conventional compaction or vibro compaction. One of the main objectives of this paper is to adjust the compactability limits, as applicable to DC/DR technique and provide guidance for suitability/compactability analysis, based on case history data collected from projects executed using DC/DR techniques.

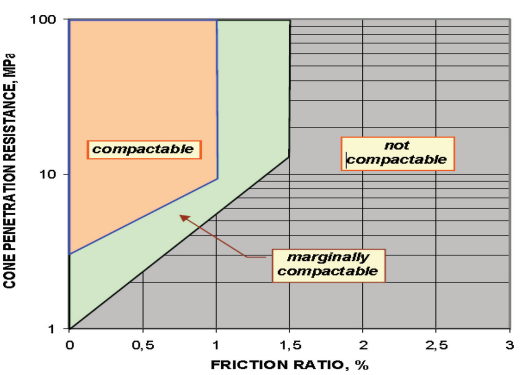

Figure 1. Soil classification for deep compaction based on CPT (After Massarsch, 1991).

4.1 *Soil compactibility based on Ic values*

Several researchers have shown that soil behavior type Index (I_c) is a better indicator of the soil compactability (e.g. Robertson, 2015), rather than using physical characteristics of the soil (e.g. Atterberg limits, grain size distribution). The CPT responds to the in-situ mechanical behavior of the soil (strength, stiffness, compressibility) and not directly to soil classification criteria based on grain-size distribution and soil plasticity measured on disturbed soil samples.

Coarse-grained soils essentially plot in SBT zones 5, 6, 7 and 8 on the normalized SBT_n chart by Robertson (2009), and can be considered as compactable soils. Soils with high fines content (> ~35%) or high soil behavior index (I_c > 2.6) are generally less compactable.

The ground behavior during ground treatment is always considered as the best indicator of the soil compactability. Typically, Heave & Penetration Test (HPT) shall be performed at the start of any DC/DR project, in order to analyze the effects of compaction and determine the optimum execution parameters to be used during the production phase. The HPT test consists of hitting the soil with the maximum energy of compaction in order to measure the ground penetration and heave (if any) after each blow, by installing topographic survey points inside and adjacent to the compaction point and measuring the change in ground elevation following each drop of the pounder.

In extremely loose deposits and/or in saturated conditions, the depth of crater (penetration) shall be limited to a certain maximum value in order to ensure the stability of the equipment, to avoid looseness of the soil at the base of crater and to avoid generating high pore water pressures in the soil.

Ground heaving is an indication that the soils are displacing plastically at no volume change rather than compacting. The energy is being transmitted through the pore water and, at this time, DC/DR is ineffective in causing densification. The ground heave adjacent to the crater shall be compared to the volumetric displacement within the crater. When the peripheral ground heave equals the change in crater volume, plastic deformation without densification is occurring. No additional energy should be applied if this condition occurs until there is a rest period to allow excess pore water pressures to dissipate.

Based on ground improvement practice in the Middle East, soils with I_c less than 1.95 can be effectively densified using Vibro Compaction, while Dynamic Compaction can work ideally up to Ic of 2.25 or even 2.6 on certain cases (mainly

Table 1. Case studies.

#	Location	G.I	Soil type	D.O.I m	W.T m
1	Zamil-KSA	DC	Sand mixtures	8	1.5
2	Dubai-UAE	DC/DR	Sands	5	3
3	AbuDhabi	DC/DR	Sand mixtures	5	2.5
4	Jizan-KSA	DC	Sands	5.5	1
5	Dammam-KSA	DC	Sands	5	1
6	Bangladesh	DC	Sand mixtures	5	2
7	Duba-KSA	DC/DR	Sand mixtures	6	2
8	Dubai-UAE	DC	Sands	7	1.5
9	Dubai-UAE	DR	Silt mixture	6	1.5
10	Jizan-KSA	DC/DR	Sand mixtures	6	5
11	AbuDhabi	DR	Silt mixtures	6	4
12	Kuwait	DR	Silt mixtures	5	1
13	Jubail-KSA	DR	Clays	8	1
14	Qahma-KSA	DR	Silt mixtures	8	2
15	Qatar	DC	Sands	8	1
16	AbuDhabi	DC	Sands	4	3
17	Jizan-KSA	DC/DR	Silt mixtures	9	2
18	Jizan-KSA	DR	Clays	5	3
19	Shuqaiq-KSA	DR	Clays	6	1

*G.I: Ground improvement technique used
D.O.I: Depth of improvement for the specified project
W.T: Water table depth from the working platform level, for the specified project

when working on unsaturated conditions). Silty/clayey soils, with I_c greater than 2.6, would require the implementation of DR method.

The above limit values are empirical and should be used only as a guide, subject to further adjustment and verification based on site conditions, such as, water table depth and overall soil stratigraphy. A trial area should be performed for each technique prior to the main soil improvement works in order to confirm its efficiency and adjust different design parameters.

5 CASE STUDIES

The present study is based on results collected from ground improvement projects carried out in the Middle East region. The case studies were selected to ensure that all data used are interpretable, accurate and reliable, starting from general information, test results, improvement energy, execution parameters and site observations. Table 1 summarizes the basic elements for each project.

6 ANALYSES

The following parameters were used for the assessment/analysis of results:

- Δq_{cB} = change (increase) in cone tip resistance, due to ground improvement, measured in between compaction points.
- Δq_{cP} = change (increase) in cone tip resistance, due to ground improvement, measured inside columns (in case of DR application)
- E: Total Applied Energy (kJ/m^2)
- UE: Unit Applied Energy (kJ/m^3)
- α = efficiency factor; $\alpha = \frac{\Delta qcB \text{ in } MPa \times 100}{UE \text{ in } kJ/m^3}$

6.1 *Compactability of soils*

The results of CPT conducted before and after ground improvement have been collected and segregated according to the on the normalized SBT_n classification and level of energy applied during DC/DR works, and then represented in form summary table hereinbelow and illustrative charts in Figures 2, 3 and 4.

The gain in cone resistance (Δq_{cB}) measured in between compaction points and efficiency factor (α) are good indicators about the soil compactability and the zones suitable for DC or DR. Marginal enhancement of the cone resistance together with low efficiency factor (less than 1) could indicate the boundary between the necessity of adding mate-

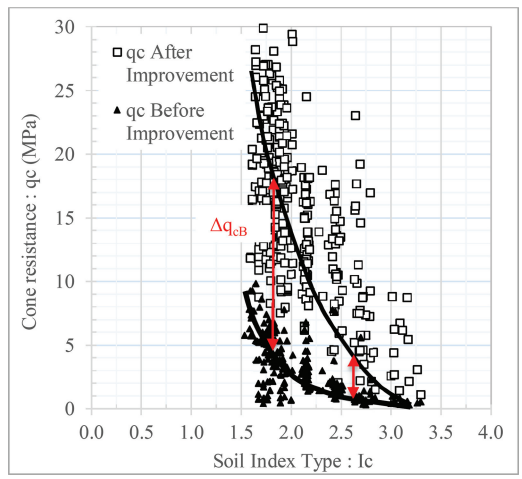

Figure 2. Improvement of cone resistance Δq_{cB} vs I_c, between compaction points.

Table 2. Δq_{cB} – summary values.

Zone	Ic	Δq_{cB}	α
1	<2.25	10–20 MPa	2.0–5.0
2	2.25–2.60	5–10 MPa	1.0–3.0
3	2.60–2.95	0–5 MPa	0.5–1.0
4	>2.95	Negligible	–

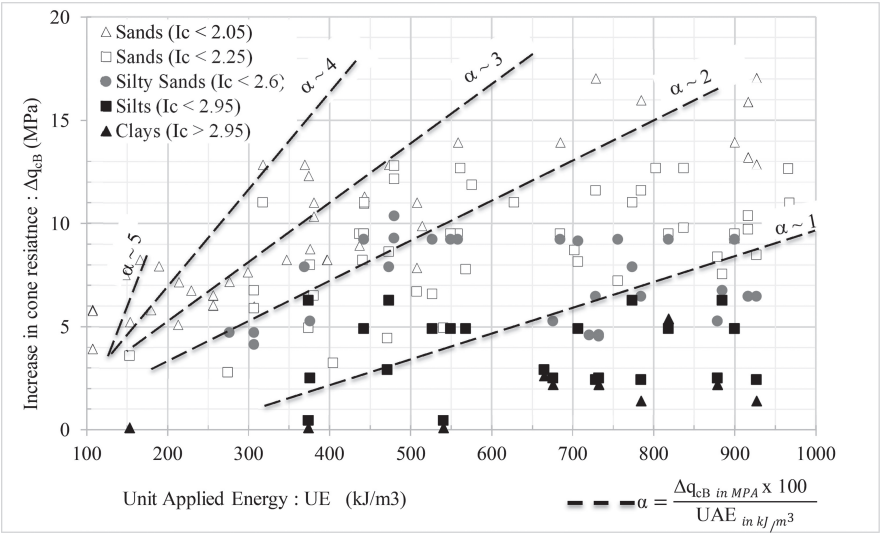

Figure 3. Gain in come resistance Δq_{cB} (MPa) between compaction points vs unit applied Energy (kJ/m^3).

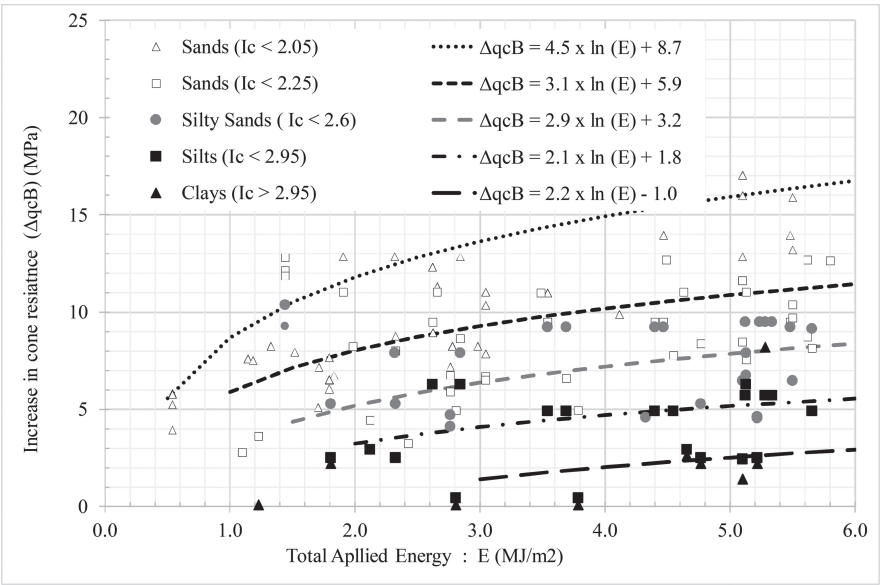

Figure 4. Improvement of cone resistance Δq_{cB} vs total applied Energy, between compaction points.

rial (DR) or densification (DC). Indeed, the strain softening behavior of the soil due to compaction energy, as it can be identified during compaction by monitoring the ground penetration & heave, can indicate the necessity to proceed with filling the columns/craters or further conventional densification.

Based on the above, the soils defined by "$I_c < 2.25$" can be clearly identified as suitable for DC, while soils defined by "$2.25 < I_c < 2.60$" appear to be the "economical" limit between DC and DR. For Ic greater than 2.60, pure densification would not be economical anymore and this zone can be classified so as suitable for Dynamic Replacement.

6.2 *Prediction of compaction/improvement energy*

The gain in soil stiffness/strength following DC/DR is difficult to predict in advance of the actual work

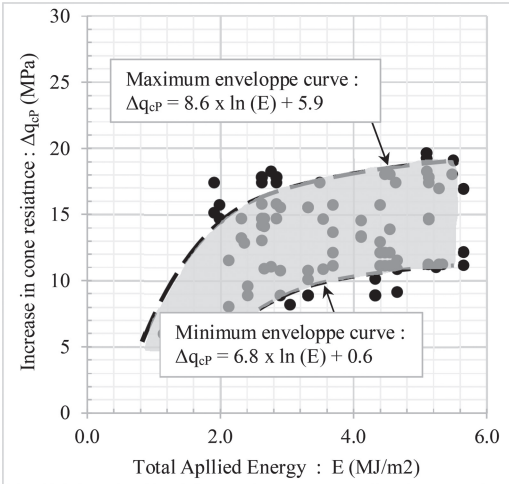

Figure 5. Improvement of cone resistance Δq_{cP} vs total applied Energy, inside columns (in case of DR application).

since the improvement depends to a large degree upon the soil reaction during improvement process and the amount of energy applied.

The pre-improvement soil parameters and experience on similar projects can provide helpful guidelines in estimating the maximum and average amount of improvement that can generally be achieved following DC/DR application.

Figure 4 shows average cone resistance values that were measured in soil between compaction points following DC/DR as a function of the soil type (represented by I_c) and total applied energy.

Figure 5 shows the average cone resistance values measured inside compacted versus total applied energy. There is considerably more scatter in the data measured inside compacted columns due to difference in the type of material used to form the DR pillars/columns for each project and due to different conditions of surrounding soil.

The average of cone resistance values were calculated over the depth of improvement for each specific project. This average is always less than the maximum amount that generally occurs at a depth of 1/2 to l/3 of the maximum depth of improvement.

7 CONCLUSION

Ground improvement techniques are used increasingly in the Middle East region, as well as other parts of the world, as value engineering solution to challenging ground conditions. In comparison to other soil improvement solutions, the implementation of DC and DR techniques requires careful design and extensive monitoring during different project phases.

Cone penetration tests (CPT) provides valuable information for design, monitoring and optimization of the DC/DR works. The cone tip resistance measurements to indicate improvement of the soil resistance. The sleeve friction combined with cone resistance can be used for soil characterization as well as to estimate changes in lateral stress due to the applied ground improvement.

In this paper, an attempt has been made to provide guidelines to evaluate soil compactability and energy requirements using the CPT. Although guidelines are useful in planning and implementing DC/DR techniques, it cannot replace good judgment and adjustments during execution stage based on the ground response. The design engineer must always use good judgment to supplement or alter the guidelines.

ACKNOWLEDGEMENTS

The authors are grateful to Trevi for providing all valuable data and information that has been used in this paper.

REFERENCES

Robertson, P.K. 2016. Cone penetration test (CPT)-based soil behaviour type (SBT) classification system — an update. *Canadian Geotechnical Journal*: 1–18.

Robertson, P.K. 1990. Soil classification using the cone penetration test. *Canadian Geotechnical Journal*: 151–158.

Robertson, P.K. 2009. CPT interpretation – a unified approach. *Canadian Geotechnical Journal*: 1337–1355.

Robertson, P.K. 2016. Suggested Quality Control for Deep Compaction using the CPT. *Proceedings of the fifth international conference on geotechnical and geophysical site characterization (ISSMGE TC-102 – ISC'5)* Volume 1: 711–715.

Robertson, P.K. 2015. CPT for Quality Control (QC) of Ground Improvement (Deep Compaction). *Webinar #13 Dec. 2015*.

Massarsch, K.R., 1991. *Deep soil compaction using vibratory probes. American Society for Testing and Material, ASTM, Symposium on Design, Construction, and Testing of Deep Foundation Improvement: Stone Columns and Related Techniques, Robert C. Bachus, Ed. ASTM Special Technical Publication*: 297–313

Ben Braiek, Aymen. 2017. Cost effective solution for improving highly heterogeneous soil. *19th International Conference on Soil Mechanics and Geotechnical Engineering proceedings*: 1–4.

Mitchell, J.K. 1982. Soil improvement-State-of-the-Art. *10th International Conference on Soil Mechanics and Foundation Engineering proceedings*: 509–565.

Lukas, Robert G. 1995. *Geotechnical engineering circular no.1 Dynamic Compaction*. Washington D.C: Federal Highway Administration.

Cone Penetration Testing 2018 – Hicks, Pisanò & Peuchen (Eds)
© 2018 Delft University of Technology, The Netherlands, ISBN 978-1-138-58449-5

Cost effective ground improvement solution for large scale infrastructure project

Aymen Brik
Trevi Ground Engineering, UAE

David Tonks
Coffey, Technical Director, UK

ABSTRACT: A safe and cost-effective solution has been applied for large scale infrastructure project in Dubai (UAE), with the use of locally available sands material to create Dynamic Replacement (DR) reinforcement columns, enabling the construction of the planned development directly on the improved ground without need for deep foundations or soil replacement measures. Significant savings in terms of construction time and cost have been achieved. Cone Penetration Testing (CPT) has been used in this project as the best suited and most reliable tool for design and monitoring of DC-DR projects. It provides valuable information and serves as a basis for design, monitoring and optimization of the ground improvement works. This paper briefly describes the use of CPT for the optimization of the ground improvement solution as well as for the entire project life-cycle.

Keywords: Dynamic Replacement, carbonate sand, shell, economical, correlation, CPT, PMT

1 INTRODUCTION

The proposed project is a multi-use development which includes residential, commercial, hotel and apartments, retail, public facilities, open spaces, roads and parks. The site is located within the Godolphin river city development of Meydan in Dubai (UAE) facing Al Khail Road on the northern boundary with a total plot area of approximately 1,000,000 sq.m, to be developed in several phases. The project phase, subject of the present paper, covers a total area of about 300,000 sq.m.

Preliminary soil investigations revealed very heterogeneous soil conditions with the presence of very loose or soft fine silty SAND, SILT and CLAY layers, with high carbonate and shell content, within the top 5–7 meters, followed by alternate layers of SILT and SAND with medium to high stiffness. Therefore, ground improvement was deemed to be indispensable in order to improve the ground conditions, eliminate the soil liquefaction risk and provide a safe platform satisfying the project requirements, in terms of allowable bearing capacity and settlement, which will enable the natural ground to safely support the foundations loads relevant to the foreseen development.

Dynamic Replacement was accepted as the most suitable and economical soil improvement technique for this project, as a global treatment procedure for the entire project plot, with the possibility of using the local available material at the ground surface, as replacement material for backfilling the created DR columns.

As for the project requirements, the improved soil conditions were to be capable of sustaining a net pressure greater than 150 kPa for shallow foundations, with settlement less than 25 mm and 50 mm, for isolated footings and mat foundations respectively. A minimum factor of safety of 1.0 was also required against liquefaction hazard posed by an earthquake of magnitude 6 and PGA of 0.15 g.

2 PRE-IMPROVEMENT SOIL CONDITIONS

A pre-improvement soil investigation campaign had been carried out at the site prior to the start of ground improvement works, in order to perform necessary field exploration, test and analysis of the sub-soil.

The main objective was to assess the prevailing geotechnical conditions at the site and derive necessary recommendations regarding the key soil parameters required for ground improvement

Table 1. Soil classification according to normalized CPT Soil Behavior Type (SBT_n) chart; (Reference CPT Guide 6th Edition by Robertson, 2009).

Zone	Soil type	Soil behavior type (Ic)
1	Sensitive, fine grained	N/A
2	Organic Soils—Clays	N/A
3	Clays—Silty Clay to clay	N/A
4	Silt Clay Mixtures	2.95–3.6
5	Sand Silt Mixtures	2.6–2.95
6	Clean Sands to silty Sands	2.05–2.6
7	Gravelly sand to dense sand	1.31–2.05
8	Sensitive, Fine grained	N/A
9	Very stiff, fine grained	N/A

design, including depth of improvement, water table conditions, type of soil to be improved, soil gradation where borehole/sample data were available and CPT-based Normalized Soil Behavior Type (SBT_n-I_c), where CPT data were available.

Several researchers have shown that soil behavior type index (SBT_n-I_c) is a better indicator of the soil compactability (e.g. Robertson, 2015), than using physical characteristics of the soil (e.g. Atterberg limits, grain size distribution). The CPT responds to the in-situ mechanical behavior of the soil (strength, stiffness, compressibility) and not directly to soil classification criteria based on grain-size distribution and soil plasticity measured on disturbed soil samples.

2.1 *Pre-improvement soil profile*

The following soil profile was abstracted as the most representative of the pre-improvement soil conditions over the area to be improved:

- From 0 to 1–2 m below the NGL: Loose to medium dense silty Sand (layer A)
- From 1–2 m to 5–7 m, below NGL: Sand and Silt mixtures, with presence of shell fragments, with cone resistance values as low as 1 MPa (layer B).
- Below 5–7 m/NGL: Dense to very dense Silty Sand, with presence of shell fragments (layer C).
- Incompressible stratum (sandstone/mudstone) generally encountered in this region at depths ranging between 10 to 15 m below the natural ground level.

The water table was encountered at depths ranging between 1 to 2 m below the natural ground level (NGL).

The soil properties, as correlated from available soil investigation data (mainly CPT), reflected the low soil strength of the soil, mainly within layers A and B.

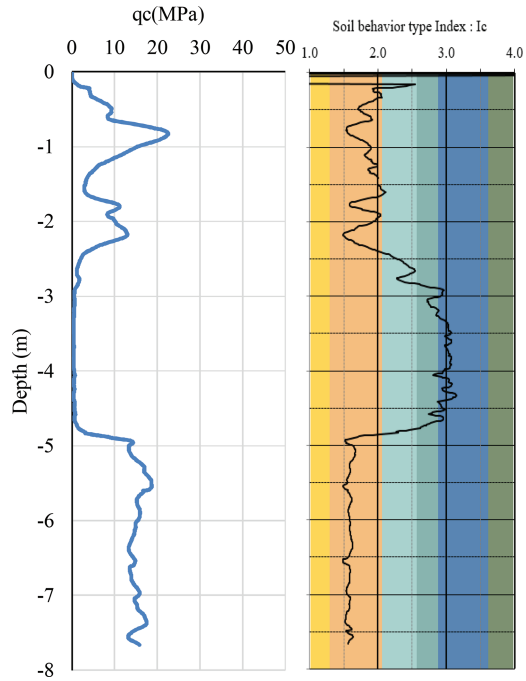

Figure 1. Example of pre-improvement CPT profile (location 1).

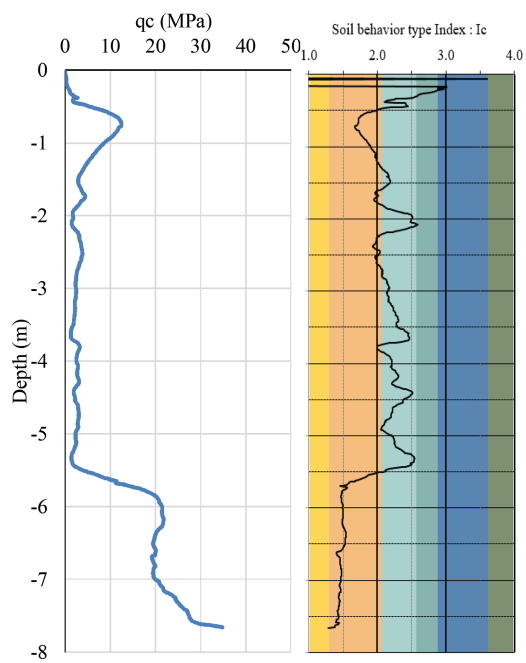

Figure 2. Example of pre-improvement CPT profile (location 2).

Table 2. Pre-improvement soil properties, location 1.

Layer	q_c MPa	f_s kPa	E_y MPa	S_u kPa	ϕ' °	N_{spt} Blows/30 cm
A-l/Sands	7.0	50	20	–	35	15
B-d/Silts	1.5	10	5	10	8	2
C-d/Sands	15.0	80	>70	–	40	>25

Table 3. Pre-improvement soil properties, location 2.

Layer	q_c MPa	f_s kPa	E_y MPa	S_u kPa	ϕ' °	N_{spt} Blows/30 cm
A-l/Sands	5.0	30	15	–	32	10
B-l/Sands	2.5	10	7.5	–	30	5
C-d/sands	20.0	100	>80	–	45	>30

l: loose; s: soft; d: dense.

The following table presents the average values for physical properties of the soil, as correlated from soil investigation data:

- q_c: cone resistance
- f_s: sleeve friction
- E_y: young modulus
- S_u: undrained shear strength
- ϕ': friction angle
- N_{spt}: SPT-N Value

Special attention was given to the presence of shell fragments at many depths (generally more than 50%), which may affect the results to be obtained after improvement. A suitable shell correction factor was duly considered and applied.

Specific analysis of the surface soil conditions (Layer A) has been performed by including results of trial pits, sieve analysis tests and correlations from CPT in order to assess the suitability of surface soil conditions for use as backfilling material to the DR columns. The following minimum specifications are considered for this purpose:

- Max. Fines content (passing sieve#200): 20% (CPT-I_c less than 2.2).
- Maximum of 10% of the particle size by weight: 300 mm
- Free from any organic matters, non-plastic
- Clay content less than 1%
- Organic content of the fill: less than 1%

In the light of the obtained results, it was concluded that the natural ground surface materials (for most of the project plot) could be used for the backfilling of DR columns by cutting for the natural platform and backfilling within the created craters, which would allow substantial saving in the cost and time of ground improvement works.

3 IMPLEMENTATION OF DR METHOD

Based on the analysis of the pre-improvement soil data and project conditions and from experience on similar projects, Dynamic Replacement (DR) technique was assessed to be the most suitable and economical soil improvement method for this project, with use of the natural sand material as available at site to create the DR columns.

DR is a real time adjustment technique, for which all production/design parameters cannot be determined/anticipated in advance of the actual site works. Heave & Penetration Tests need to be performed at the calibration stage in order to analyze the effects of compaction and determine the optimum execution parameters to be used during the production phase.

In addition to the Heave & Penetration Tests, CPT should be systemically carried out as part of the quality assurance program to monitor the ground behavior and ensure that the project requirements are met at every treated point.

Ground heave measurements can be obtained at occasional drop point locations by installing topographic survey points adjacent to the compaction points and measuring the change in elevation following each drop of the tamper. If enough observation points are established, the ground heave adjacent to the crater can be calculated. This can then be compared to the volumetric displacement within the crater itself, which is also determined from elevation readings. When the peripheral ground heave equals the change in crater volume, plastic deformation without densification is occurring. No additional energy should be applied if this condition occurs until there is a rest period to allow excess pore water pressures to dissipate.

In this project, DR was implemented through a succession of tamping by dropping a 15 to 23 tonne weight from a height of up to 20 m and backfilling in sequence. Several stages (passes) are required to allow the ground pore pressures to dissipate and then further tightening. Two to three passes of 6 to 10 blows/each were successful in forming columns at about 12–20% area ratio to depths of 5–7 m. Settlements were shown to be reduced from in excess of 70 mm predicted under 150 kPa loading to well below with 25 mm post-improvement.

Low weight pounder are usually used in the first pass, while weight & height are increased in the subsequent passes. The depth of craters was limited to 1.5 m for each pass, with a minimum thickness of 1 m above water table level during the entire process, in order to ensure safe & efficient application of DR method.

Due to the size of the project and heterogeneity of surrounding soil conditions (mainly the amount of fine grained material and depth of improvement), the total amount of energy ranged from 300 to 750 kJ/m^3 with an overall average value of 550 kJ/m^3.

4 CONE PENETRATION TESTS

The cone resistance test (CPT) is the most suited and reliable tool for design and monitoring of DR projects. It provides valuable information and serves as a basis for design, monitoring and optimization of the ground improvement works. CPT provides cone tip resistance measurements to indicate improvement of the soil resistance.

The sleeve friction combined with cone resistance can be used for soil characterization (friction ratio values) as well as to estimate changes in lateral stress due to the applied ground improvement.

Cone penetration tests were used also for the control and verification of ground improvement through comparison of the achieved post-improvement results versus pre-improvement conditions and project performance lines, which allow quick verification of the ground improvement efficiency during execution.

For this purpose, equivalent soil parameters are considered, according to the post-improvement test results achieved inside DR columns and intermediate soil:

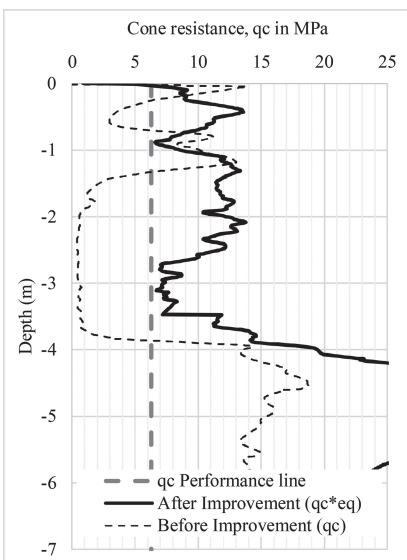

Figure 3. Example of verification of CPT-performance line at location 1 (soil type: silt/clay, treatment grid: 4.25 × 4.25 sqm).

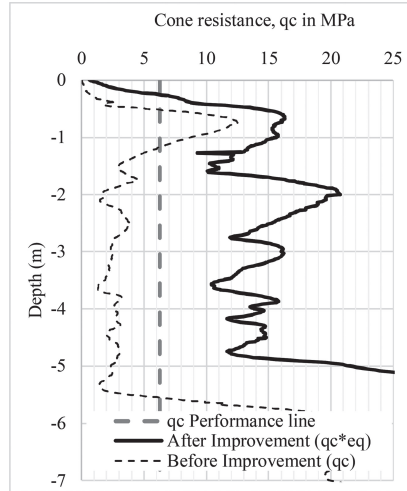

Figure 4. Example of verification of CPT-performance line at location 2 (soil type: sand/silty sand, treatment grid: 6 × 6 sqm).

$$q_{c*eq} = r \cdot q_{cP} + (1-r) q_{c*B} \tag{1}$$

where: q_{cP} is the cone resistance measured inside the DR column prints; q_{c*B} is the corrected cone resistance measured in the intermediate soil; q_{ceq} = the equivalent cone resistance; r = the treatment ratio, i.e. $r = \pi.R^2/L^2$; R = the radius of the print; L = the grid spacing.

The gain in cone resistance Δq_c (MPa), as measured in between compaction points, ranged between 5 to 8 MPa for silt/clay (location 1) and 7 to 12 MPa for sand/silty sand (location 2). Considerably higher values were achieved inside the DR columns, up to 15–20 MPa.

5 CORRELATION PMT/CPT

Many references are available from the literature giving indicative values of correlations between q_c and PMT parameters P_l, limit pressure and E_p, pressuremeter modulus or E_y, Young modulus.

Briaud et al. (1985) proposed correlations between q_c and PMT parameters P_l, limit pressure, and E_p, pressuremeter modulus, as shown in Table 4.

A preliminary correlation factor can be determined from literature, as a first step, to be further adjusted/confirmed by in-situ correlation based on the actual site conditions.

5.1 *Specific in-situ correlation*

A specific correlation has been developed as part of the calibration works, by comparing the cone

Table 4. Correlation between PMT and CPT according to Briaud et al. (1985).

Soil type	PMT parameter	Correlation to CPT
Sand	P_l	$0.2q_c$
	E_p	$2.5\ q_c$
Clay	P_l	$0.11q_c$
	E_p	$1.15\ q_c$

resistance values, to the limit pressure values and Young's modulus values, as obtained from PMT tests. As a first step, different values for shell correction factors (SCF) were considered (1, 1.2 or 1.5) for the intermediate soil, in order to take into consideration the effect of shell presence and derive a comprehensive combined correlation factor.

The second step consisted of further adjusting the obtained correlation factors, by means of iterative analysis of the bearing capacity and settlement considering different values of correlation factors, as concluded from step 1.

The final correction factor adopted for the project was determined as the one which gives the most convergence and concordance between both analyses from CPT and PMT.

A SCF of 1.2 was adopted to correct the cone resistance values measured in intermediate soil where shell soils are present. This was found to been reasonably cautious in the light of the subsequent testing, further discussed below. The concluded correlations factors for different areas are summarized below:

5.2 *Recommended values*

Based on the obtained results, the following correlation factors were concluded:

Intermediate soil (silt-clay mixtures):

- Young Modulus: $E_y/\ q_c^* = 3–5$
- Limit pressure: $P_l/\ q_c^* = 0.10–0.12$

Inside DR columns (compacted sand):

- Young Modulus: $E_y/q_c = 6–8$
- Limit pressure: $P_l/q_c = 0.15–0.2$

5.3 *Validation by zone load test*

In order to validate the above correlation factors, a zone load test (3 × 3 m square) has been performed at site. The settlement results obtained satisfactorily confirmed the above recommended values, with good safety margin.

The Young's Modulus values were verified by back calculation from the zone load test measured settlement, as per the correlation proposed by US Army Corps of Engineers, No. 9 ASCE "Settlement Analysis" as described below

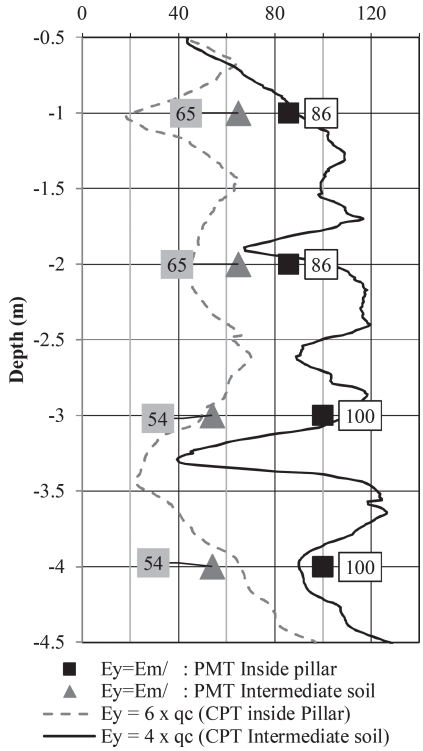

Figure 5. Example of output from correlation factor analysis (Ey/q_c^*) at location 2, Step 1.

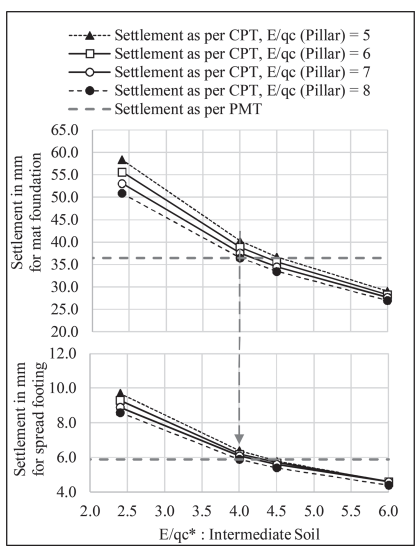

Figure 6. Example of output from correlation factor analysis ($E_y/\ q_c^*$) at location 2, Step 2.

Table 5. Correlation factors.

Zone	PMT	P_l MPa	E_m MPa	CPT	q^*_c MPa	Soil	P_l/q^*_c	E_y/q^*_c
A1	203-B	1.8	21.0	203-B	17.8	Sand	0.10	3.5
	203-P	3.2	38.5	204-p	21.2	Sand	0.15	*5.4*
A4	211-B	1.8	29.0	291-B	21.7	Sand	0.08	4.0
	212-P	2.7	31.2	292-P	19.0	Sand	0.14	*5.2*
D1	203-B	2.1	25.5	219-B	19.7	Sand	0.11	3.9
	204-P	2.7	31.4	220-P	17.3	Sand	0.16	*5.4*
	205-B	2.0	22.0	225-B	17.9	Sand	0.11	3.7
	206-P	2.7	24.8	226-P	17.4	Sand	0.16	*4.3*
A2	205-B	1.7	28.0	235-B	18.6	Sand	0.09	4.5
	206-P	3.2	44.0	236-P	21.1	Sand	0.15	*6.3*
A3	207-B	1.4	24.2	259-B	12.4	Silt	0.11	3.9
	208-P	2.7	35.9	260-P	20.4	Sand	0.13	*5.3*
	209-B	1.3	21.1	275-B	11.4	Silt	0.11	3.7
	210-P	3.5	46.7	276-P	20.5	Sand	0.17	*6.8*
	Average (P_l/q_c) inside Pillar						0.15	6.0
	Average ($P_l/q_c^{*)}$ for intermediate soil						0.10	4.0

(*) Shell correction factor of 1.2 applied to cone resistance values measured within the intermediate soil.

$$E_y = \frac{1-\mu^2}{\Delta\rho / \Delta q} \cdot B_p \cdot I_w \tag{2}$$

where E_y = Young's Modulus; μ = Poisson's Ratio = 0.3; Δρ = settlement from zone load test in inches (5.7 mm); Δq = applied pressure in psi (300 kPa);

B_p = Width of zone load test footing in inches (3 m);

I_w = Shape Factor 1 for square footing.

The correlation factor was then derived as the ratio between the Young's modulus directly obtained from ZLT results to the cone resistance average value as measured from CPT within the same location of ZLT (inside pillar).

As per the obtained results, the correlation factor (E_y/q_c) inside DR pillars, as obtained from ZLT results, is about 7.2, which reasonably validates the value assessed from trial area results.

6 CONCLUSION

Dynamic Replacement (DR) technique can be safely, sustainably and efficiently used for mitigating foundations settlement and soil liquefaction risk caused by the presence of weak soils, such as fine sand, silt or clay, with use of natural sand deposits as replacement material for the DR columns in suitable circumstances.

A proper implementation of the DR technique requires careful design, substantial suitability trials and testing and extensive validation monitoring during different project phases. This is most practicable by the use of rapid and reliable in-situ testing procedures based on CPT.

ACKNOWLEDGEMENTS

The authors would like to thank TREVI and Coffey for sharing all necessary information and data relevant to this project.

REFERENCES

Ben Braiek, Aymen. 2017. Cost effective solution for improving highly heterogeneous soil. *19th International Conference on Soil Mechanics and Geotechnical Engineering proceedings*: 1–4.

Briaud, J.L., Noubani, A., Kilgore, J. & Tucker, L.M. 1985. Correlation Between Pressuremeter Data and Other Paramaters, *Research Report. Texas A&M University*.

Douglas, B.J., and Olsen, R.S. 1981. *Soil classification using electric cone penetrometer. In Proceedings of Symposium on Cone Penetration Testing and Experience,* Geotechnical Engineering Division, ASCE. St. Louis, Missouri, October 1981.

Lukas, Robert G. 1995. *Geotechnical engineering circularno.1 Dynamic Compaction*. Washington D.C: Federal Highway Administration.

Massarsch, K.R., 1991. *Deep soil compaction using*

Mitchell, J.K. 1982. Soil improvement-State-of-the-Art. *10th International Conference on Soil Mechanics and Foundation Engineering proceedings:* 509–565.

Robertson, P.K. 1990. Soil classification using the cone penetration test. *Canadian Geotechnical Journal*: 151–158.

Robertson, P.K. 2009. CPT interpretation—a unified approach. *Canadian Geotechnical Journal*: 1337–1355.

Robertson, P.K. 2015. CPT for Quality Control (QC) of Ground Improvement (Deep Compaction). *Webinar #13 Dec. 2015*.

Robertson, P.K. 2016. Cone penetration test (CPT)-based soil behaviour type (SBT) classification system—an update. *Canadian Geotechnical Journal*: 1–18.

Robertson, P.K. 2016. Suggested Quality Control for Deep Compaction using the CPT. *Proceedings of the fifth international conference on geotechnical and geophysical site characterization (ISSMGE TC-102 – ISC'5) Volume 1*: 711–715.

Schmertmann, J.H. 1978. *Guidelines for Cone Penetration Test, Performance and Design vibratory probes. American Society for Testing and Material, ASTM, Symposium on Design, Construction, and Testing of Deep Foundation Improvement: Stone Columns and Related Techniques, Robert C. Bachus, Ed. ASTM Special Technical Publication*: 297–313

Youd and Idriss. 2001. *Liquefaction Resistance of Soils: Summary Report. From 1996NCEER and 1998 NCEER/NSF Workshops on Evaluation of Liquefaction Resistance of Soils.*

Cone Penetration Testing 2018 – Hicks, Pisanò & Peuchen (Eds)
© 2018 Delft University of Technology, The Netherlands, ISBN 978-1-138-58449-5

Evaluation of existing CPTu-based correlations for the deformation properties of Finnish soft clays

Bruno Di Buò, Juha Selänpää & Tim Länsivaara
Tampere University of Technology (TUT), Tampere, Finland

Marco D'Ignazio
Norwegian Geotechnical Institute (NGI), Norway

ABSTRACT: An extensive research program for soil testing has been conducted on five soft clay deposits located in Finland. This research project aims to collect data from high quality *in-situ* and laboratory tests and derive correlations for the strength and deformation properties specific to Finnish clays. In the literature, several authors have proposed correlation models for the deformation properties of soft clays based on CPTu measurements. However, such models are often calibrated for a specific site or a specific soil type. Consequently, these models must be validated before applying them to different soil conditions. In this paper, existing correlations for the deformation properties of soft clays based on CPTu data are compared to the test results from the investigated sites. The validity of the existing models is assessed for Finnish clays by evaluating their bias and uncertainties.

1 INTRODUCTION

The cone penetration test (CPTu) offers the ability to quickly and economically evaluate subsurface soil conditions. The traditional piezocone test provides continuous and independent measurement of three different parameters: cone tip resistance (q_c), sleeve friction (f_s), and pore water pressure (u) in saturated soils. Moreover, sensors can be added to the traditional probe to obtain additional data. For instance, with seismic piezocone (SCPTu) and resistivity piezocone (RCPTu), it is possible to profile shear wave velocity and electrical conductivity, respectively.

Even though the CPTu test is widely used in Scandinavia, the field vane (FV) shear test is still the most commonly employed *in-situ* investigation tool in Finland to determine undrained shear strength (s_u). Deformation properties, such as stiffness and/or preconsolidation pressure (σ'_p), are generally evaluated using constant-rate-of-strain (CRS) oedometer tests.

Tampere University of Technology (TUT) purchased a piezocone equipped with seismic and resistivity cones in order to establish the CPTu correlations for the strength and deformation properties of Finnish soft clays. Preliminary results have been reported by Di Buò et al. (2016).

Various empirical correlations have been proposed in the literature for determining geotechnical parameters based on CPTu data (e.g., Kulhawy and Mayne, 1990; Chen and Mayne, 1996; Karlsrud et al., 2005; L'Heureux and Long, 2017). However, in practice, the use of such correlations to evaluate local soil conditions requires validation and, possibly, calibration.

The main goal of the present study is to verify the validity of existing global and regional CPTu-based correlations for the deformation parameters of soft clays. A data set consisting of high quality laboratory and *in-situ* data gathered by TUT is exploited to verify these correlations in Finnish soil conditions. The analysis focused on the deformation parameters determined from CRS oedometer tests on soft clay samples from five sites in Finland. The bias and uncertainties of the correlations are evaluated with respect to the data set.

2 TEST SITES

This paper presents the results from the investigation conducted on five different soft clay test sites located in Southern Finland. The main geotechnical properties, including natural water content (w), plasticity index (PI), overconsolidation ratio (OCR), and sensitivity (S_t) are shown in Table 1.

The Perniö test site is located on the southwestern coast of Finland, next to the railway track connecting the cities of Helsinki and Turku. The stratigraphy consists of a 1.5 m thick dry crust layer overlaying an 8–9 m thick soft clay layer.

Table 1. Geotechnical properties of the five investigated sites.

SITE	z (m)	w (%)	PI	OCR*	S_t**
Perniö	2–3	100–120	40	2	40–60
	3–6	70–90	20–30	1.3–1.6	40–50
	6–8	90–100	40	1.3–1.4	50–70
Lempäälä	3–4	110–130	40	1.2–1.5	30–40
	4–8	60–80	20–30	1.2–1.4	30–50
Masku	3	80–90	40	1.5–1.7	20
	5	110–120	60–70	1.5	20
	8	70–80	40	1.2–1.5	20
Paimio	3–6	50–80	20	1.6–1.8	80–100
	6–9	90–110	30–40	1.3–1.4	60–80
Sipoo	2–4	80–90	40–50	1.7–1.9	20–40
	4–9	100–120	50–60	1.3–1.5	20–30

*OCR determined from the CRS tests; **S_t determined from the Fall Cone (FC) test.

The clay content varies from 60% at a depth of 3 m to 90% at a depth of 8 m. The organic content is less than 1%. The site has been previously investigated and results are reported by Lehtonen (2011) and D'Ignazio et al. (2015).

The Lempäälä site is located near the city of Tampere, along the railway track to Helsinki. The deposit consists of a 1.5 m thick layer of weathered clay crust followed by 1.5 m of organic soil overlaying soft sensitive clay. The clay content is approximately 60% and the organic content is approximately 5% above a depth of 3 m and less than 1% in the soft clay.

The Masku test site is located on the southwestern coast of Finland, near the city of Turku. The stratigraphy consists of 1.5 m of weathered clay crust over an 11 m thick soft clay deposit. Masku clay is the least sensitive (S_t = 20) among the clays presented in this study. The clay content varies between 60% and 90%. The organic content is less than 2%.

The Paimio site is located close to the city of Turku, in the southwestern region of Finland. The stratigraphy consists of a 2 m thick dry crust over a 10 m thick soft clay deposit. Two soft clay layers with different properties were found: a leaner upper clay layer and a lower layer of more plastic clay with a higher w. The clay content of the top layer ranges between 40% and 60%, increasing up to almost 100% at greater depths. The organic content of the entire deposit is less than 1%.

The Sipoo test site is located 30 km north of the city of Helsinki. Index test results reveal the presence of a deposit of homogeneous soft clay with a depth ranging between 2 m and 9 m characterized by the highest PI values among all the five investigated sites (PI = 60). The clay content increases as the depth increases, from approximately 60% at a depth of 3 m to 90% at a greater depth. The organic content is consistently lower than 2% throughout the deposit.

3 EXPERIMENTAL PROGRAM

The investigation included both *in-situ* and laboratory tests conducted on undisturbed samples from the five test sites mentioned above. The field investigation was conducted using a CPTu equipped with a seismic and resistivity cone and FV (Di Buò et al., 2016; Selänpää et al., 2017). The penetrometer consists of a standard 60° apex conical tip with a 150 cm^2 sleeve area. Excess pore pressure is measured at the shoulder above the cone tip (u_2). Details about the equipment and test procedures are described in Di Buò at al. (2016). Two different cones were used: a high capacity cone (75 MPa) and a "sensitive" cone (7.5 MPa). The latter is considered more suitable in a soft soil condition. The CPTu measurements from the Perniö site are shown in Figure 1. In particular, the corrected cone tip resistance, sleeve friction, and pore pressure are plotted versus the depth. Overall, the measurements show very good repeatability even though some scatter can be observed, especially for the high capacity cone data. Moreover, the resolution of the sleeve friction is not adequate since the sensor is not able to measure small changes of the recorded value. Therefore, improvement of the apparatus is suggested to improve the quality of the data.

The laboratory tests included classification and index tests for the remolded samples, the CRS oedometer test, the triaxial test, and the direct simple shear (DSS) test for the intact samples. In this paper, the results from the CRS tests are used to evaluate the compressibility (oedometer modulus, M_0) and stress-history (σ'_p) of the tested soils. The CRS oedometer tests were performed on samples with a 45 mm diameter and a 15 mm thickness at a constant strain rate of 0.001 mm/min (0.4%/h).

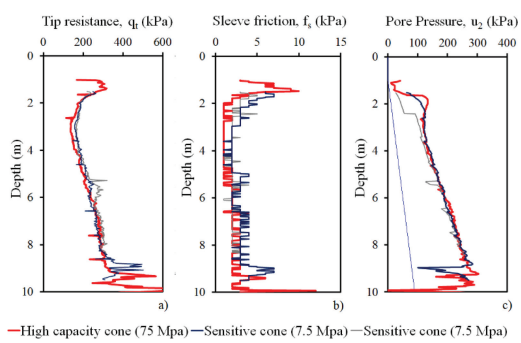

Figure 1. CPTu measurements at the Perniö site: a) corrected cone tip resistance, q_t; b) sleeve friction, f_s; c) pore pressure, u_2.

It is important to note that three different samplers were used to retrieve the soil samples: a mini-block Sherbrook sampler (Emdal et al., 2016), an open drive 132 mm diameter tube (TUT 132), and an ordinary STI 50 mm piston sampler. The tube sampler was developed at TUT in 2014 (Di Buò et al., 2016); it was inspired by the Laval tube sampler (La Rochelle et al., 1981) and its modification by the Swedish Geotechnical Institute (SGI) (Larsson, 2011). Figure 2 and Table 2 show the achieved sample quality based on Lunne et al.'s (1997) criteria. In general, the block had the highest quality of all the tested samples.

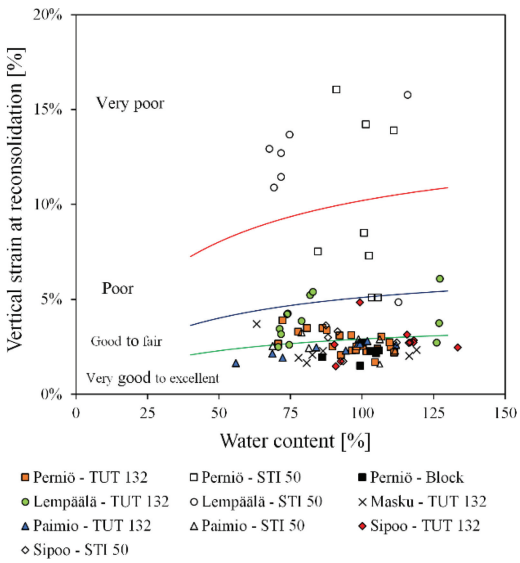

Figure 2. Sample quality based on Lunne et al.'s (1997) criteria.

Table 2. Sample quality based on Lunne et al.'s (1997) criteria.

		Number of CRS oedometer tests				
Site	Sampler	Tot.	Excellent	Good to fair	Poor	Very poor
Perniö	STI 50	8	–	2	3	3
	TUT 132	22	13	9	–	–
	Block	6	6	–	–	–
Lempäälä	STI 50	8	–	2	–	6
	TUT 132	11	3	5	3	–
Masku	TUT 132	7	6	1	–	–
Paimio	STI 50	7	6	1	–	–
	TUT 132	9	9	–	–	–
Sipoo	STI 50	6	3	3	–	–
	TUT 132	9	7	2	–	–
Total		93	53	25	6	9

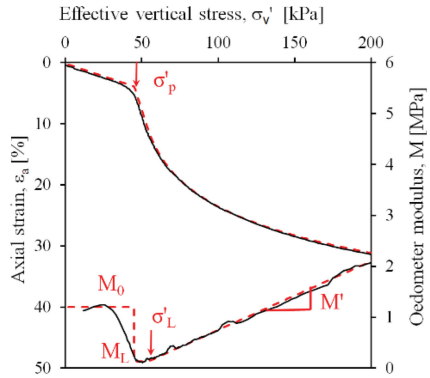

Figure 3. Schematization of Sällfors' (1975) method used to interpret preconsolidation pressure from the CRS tests.

However, good quality samples could be also obtained from the STI 50 piston sampler, especially at Paimio and Sipoo. Sample quality plays an important role in the calibration of empirical correlations since the evaluation of geotechnical parameters can be greatly affected by disturbance induced during sampling, transportation, and storage (Lunne et al., 1997; Lunne et al., 2006; Amudsen et al., 2016).

A total of 93 CRS oedometer tests were performed. However, 15 tests, which were characterized as having poor and very poor quality, were not considered in the calculations in order to obtain more reliable correlations.

The σ'_p and the oedometer moduli were evaluated using a curve fitting procedure applied to the constrained modulus proposed by Sällfors (1975), as shown in Figure 3.

In the following section, the validity of some of the existing empirical correlations for the deformation properties of clay soils is checked against the data set of the Finnish clays presented in this study. Since Finnish data were not included in the data sets from which these correlations were derived, it is expected that the data points will not always fall in the applicability domain. Therefore, this paper discusses the calibration and validation of the empirical correlations.

4 EVALUATION OF EXISTING CORRELATIONS

4.1 *Bias and uncertainties of the existing correlations*

This section presents an evaluation of the Bias factor (denoted by *b*) and coefficient of variation (*COV*) for the examined correlations based on the procedure reported by Ching and Phoon (2012). In this procedure, *b* and *COV* are calculated as

the sample mean and the coefficient of variation, respectively, of the ratio (actual target value)/(predicted target value), where the actual target value is the value measured in a test and the predicted target value is the value predicted by the correlation. If $b = 1$, the model prediction is unbiased.

4.2 *Correlations for OCR and* σ'_p

Correlations for the evaluation of *OCR* and σ'_p from CPTu are available in the literature (Kulhawy and Mayne, 1990; Larsson and Mulabdic, 1991; Chen & Mayne, 1996; Karlsrud et al., 2005).

For intact clays, a correlation to evaluate the *OCR* based on normalized cone tip resistance (Q_t) was suggested by Kulhawy and Mayne (1990) as:

$$OCR = k\left(\frac{q_t - \sigma_{v0}}{\sigma'_{v0}}\right) = kQ_t \tag{2}$$

where q_t is the corrected cone tip resistance, σ_{v0} is the total overburden vertical stress, and k is an empirical parameter. An average value of $k = 0.33$ is suggested by Kulhawy and Mayne (1990) based on statistical analysis of piezocone-oedometer data involving a variety of different clays located mainly in the United States, the United Kingdom, and Canada.

A similar correlation was proposed by Karlsrud et al. (2005) based on a database of 17 high sensitive clay deposits located in Norway:

$$OCR = \left(\frac{Q_t}{2}\right)^{1.11} \tag{3}$$

Both correlations are plotted in Figure 4, and the results are compared with the experimental data. As shown in Figure 4, Equation 2 gives an almost unbiased prediction (b = 1.07), accompanied by a low variability (COV = 0.15). However, Equation 3 seems to over-predict the *OCR* of Finnish clays by nearly 40% (b = 0.65).

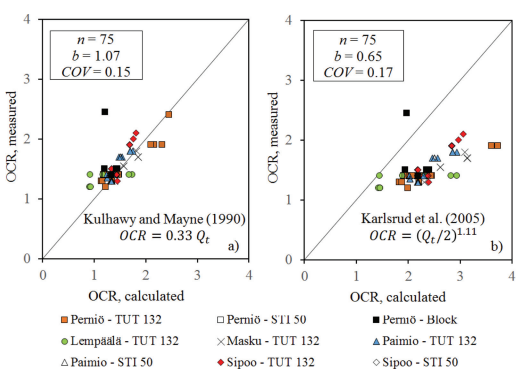

Figure 4. Comparison of the empirical correlations and the experimental data to evaluate *OCR*: a) Kulhawy and Mayne (1990); b) Karlsrud et al. (2005).

Chen and Mayne (1996) proposed simple relationships to determine σ'_p from the CPTu data as:

$$\sigma'_p = 0.53(u_2 - u_0) = 0.53\,\Delta u \tag{4}$$

$$\sigma'_p = 0.60(q_t - u_2) \tag{5}$$

Similarly, σ'_p can be evaluated from $q_{net} = q_t - \sigma_{v0}$ using the following equation:

$$\sigma'_p = \frac{q_t - \sigma_{v0}}{N_{kT(\sigma'_p)}} \tag{6}$$

where $N_{kt(\sigma'p)}$ is an adapted cone factor. For Swedish clays, Larsson and Mulabdic (1991) proposed $N_{kt(\sigma'p)}$ as a function of the liquid limit (LL) as:

$$N_{kt(\sigma'_p)} = 1.21 + 4.4\,LL \tag{7}$$

As shown in Figure 5, Equation 4 gives the lowest COV, thus indicating that an evaluation of σ'_p based on Δu is generally more reliable. While Equation 4 overestimates the σ'_p of Finnish clays by 25%

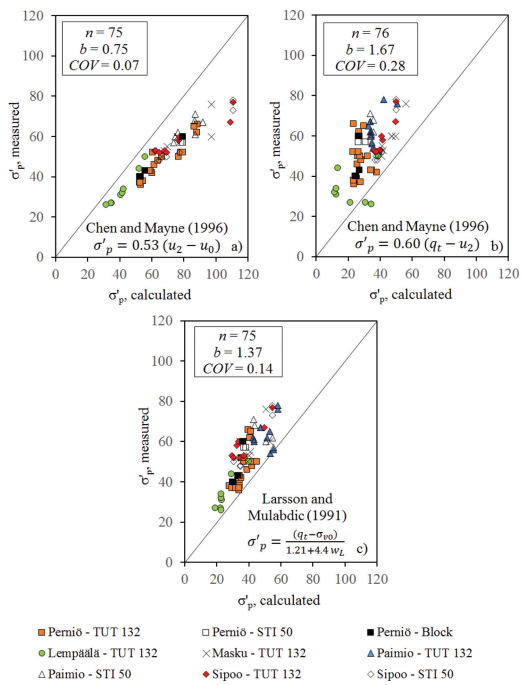

Figure 5. Comparison of the empirical correlations and the experimental data to evaluate σ'_p: a) Chen and Mayne (1996); b) Chen and Mayne (1996); c) Larsson and Mulabdic (1991).

(b = 0.75), Equation 5 and Equation 6 underestimate σ'_p by 61% and 15%, respectively. Therefore, Equations 4–6 need to be adjusted based on the calculated b values in order to be usable in Finnish clays.

4.3 *Correlations for constrained modulus*

The soil stiffness in one-dimensional compression can be expressed in terms of the constrained modulus (M), which is defined as the ratio of the change in effective stress ($\Delta\sigma'_v$) to the change in strain ($\Delta\varepsilon_v$):

$$M = \frac{\Delta\sigma'_v}{\Delta\varepsilon_v} \tag{8}$$

The constrained modulus is stress-dependent; in the overconsolidated part, a relatively high value (M_0) can be found, while the modulus drops significantly when the preconsolidation pressure is exceeded (Figure 3). In practice, the modulus in the overconsolidated part can often be modelled as a constant value. In this paper, only the constant M_0 modulus is evaluated.

Using an extensive database of silts, sands, and fine-grained soils, Mayne (2006) proposed an empirical correlation to evaluate the constrained modulus at the *in-situ* stress state (M_0) from the net cone tip resistance given by:

$$M_0 = \alpha(q_t - \sigma_{v0}) = \alpha q_{net} \tag{9}$$

The representative value of α depends on the nature of the soil. Considerably low values of α (α ≈ 1–2) are suggested for organic plastic clays from Sweden, while higher values (α >10) are expected for cemented clays. Figure 6 shows the plot of M_0 versus ($q_t - \sigma_{v0}$) for the clays investigated in the present study. As seen, the majority of data points fall between the trend lines for α that are equal to 5 and 10. Clearly, as discussed earlier, for σ'_p, the value of M is affected by the sample quality (e.g., Lunne et al., 2006; Karlsrud and Hernandez-Martinez, 2013). It is important to point out that the mean trend of the sites characterized by the highest sample quality (Paimio, Sipoo, and Masku) can be captured using α ≈ 10. However, the lower values of α seem to be more representative of the other sites. Further investigation is required to evaluate the effect of soil conditions and, possibly, sample quality on α.

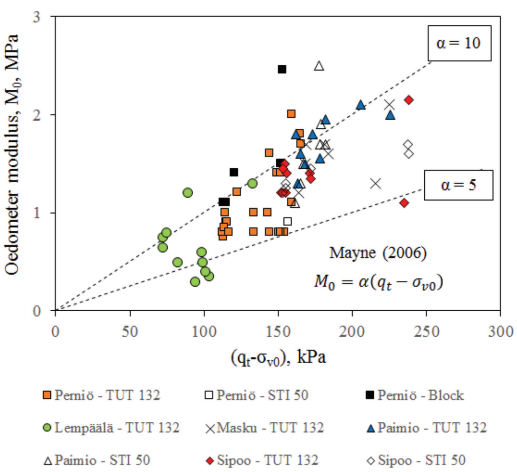

Figure 6. Comparison of the empirical correlations and the experimental data to evaluate the constrained modulus (M_0).

4.4 *Correlations between shear wave velocity and key geotechnical parameters*

The measurement of shear wave velocity (V_s) can be performed by adding geophones to the SCPTu. This provides the possibility of estimating the small-strain shear modulus (G_{max}) as:

$$G_{max} = \rho V_s^2 \tag{10}$$

where ρ is the soil density. Moreover, V_s can be used to estimate the geotechnical parameters (Mayne and Rix, 1995; Robertson, 2009; Mayne, 2014; L'Heureux and Long, 2017). In this section, the relationships between V_s and the 1D compression parameters are compared to existing correlations in the literature. In particular, the relationships between M_0, σ'_p, and V_s are analyzed. L'Heureux and Long (2017) proposed empirical correlations based on a database of 28 Norwegian clay sites. They suggested that M_0 and σ'_p increase as V_s increases, as shown by Equation 10 and Equation 11:

$$\sigma'_p = 0.00769\, V_s^{2.009} \tag{11}$$

$$M_0 = 0.00010\, V_s^{2.212} \tag{12}$$

The information presented in Figures 7a, b confirms the trends reported by L'Heureux and Long (2017) for Norwegian clays, despite the high values of b and COV. It is important to note that the correlations reported by L'Heureux and Long (2017) are based on clays that are characterized by higher OCR and S_t in comparison to the clays examined in the present study.

Equations similar to (11) and (12) can also be derived theoretically. The relationship between the oedometer modulus (M_0) and the shear modulus (G) is given by:

$$M_{oed} = \frac{2(\upsilon - 1)}{(2\upsilon - 1)} G \tag{13}$$

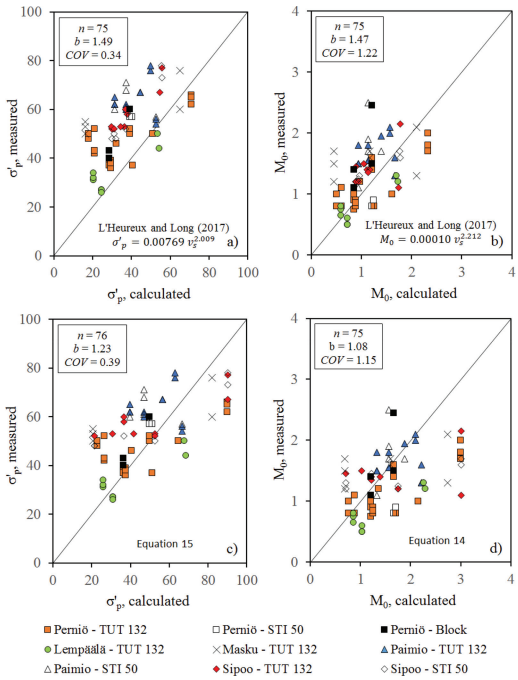

Figure 7. Comparison of the correlations based on shear wave velocity and the experimental data for the evaluation of: a) preconsolidation pressure evaluated based on L'Heureux and Long (2017); b) constrained modulus M_0 evaluated based on L'Heureux and Long (2017); c) preconsolidation pressure evaluated with Equation 14; d) constrained modulus M_0 evaluated using Equation 13.

where υ is the Poisson's ratio, which can be assumed to be 0.1 for small-strain stiffness corresponding to G_0. Considering a scaling factor of 10, to take into account the modulus degradation with increasing strain, M_0 is obtained as:

$$M_0 = \frac{1}{10}\frac{2(\upsilon-1)}{(2\upsilon-1)}\rho V_s^2 = 0.225\,\rho V_s^2 \qquad (14)$$

where ρ is the soil density assumed as constant (1500 kg/m³) in the present study.

Similarly, σ'_p can be estimated assuming that the yield stress is reached at 3% of the vertical deformation. Therefore:

$$\sigma'_p = 0.03\,M_0 = 0.00675\,\rho V_s^2 \qquad (15)$$

Both σ'_p and M_0 are expressed in Pa, while the unit measure of V_s is m/s. Equation 15 and Equation 14 are plotted in Figure 7c and 7d, respectively. Despite the high scatter, the theoretical solutions seem to fit better the mean trend of the Finnish clay data points in comparison to Equation 11 and Equation 12 (b = 1.23–1.08 vs b = 1.49–1.47).

As mentioned earlier, the influence of sample quality and the intrinsic uncertainty associated with geophysical measurements need to be further investigated before calibrating an empirical correlation valid in Finnish clay conditions.

5 CONCLUSIONS

This paper aimed to present CPTu and laboratory measurements obtained from Finnish soft clay deposits and evaluate the validity of existing empirical correlations to assess the deformation parameters of soft clays. Laboratory data from high quality samples were used. The main conclusions from this work are:

- The correlations for *OCR* from the CPTu evaluated in this study can describe the behavior of Finnish soft clays with relatively low uncertainty (*COV* = 12–14%). In particular, the correlation reported by Kulhawy and Mayne (1990) resulted in an almost unbiased prediction. A wider range of bias factors (b = 0.75–1.61) and *COVs* (8–31%) was found for the correlations based on σ'_p.
- The link between soil stiffness, expressed in terms of constrained modulus, M_0, and the net cone tip stress fits well with established empirical correlations for clays worldwide (Mayne, 2006). However, the data show significant scatter; this might be partly due to variations in the sample quality. Further investigation is required to calibrate a model valid for Finnish clays, which also accounts for the nature of the soil.
- Both preconsolidation pressure and constrained modulus can be evaluated based on the shear wave velocity. The empirical correlations reported by L'Heureux and Long (2017) seem to describe the trend between these parameters, but the scatter is quite high. The prediction could be slightly improved using similar, but theoretically derived equations.

REFERENCES

Amundsen, H.A., Thakur, V., & Emdal, A. (2016). Sample disturbance in block samples of low plastic soft clays. In *6th International Conference on Geotechnical and Geophysical Site Characterization*, Queensland, Australia.

Chen, B.S., & Mayne, P.W. 1996. Statistical relationships between piezocone measurements and stress history of clays. *Canadian Geotechnical Journal*, 33(3), 488–498.

Ching, J., and Phoon, K.-K. 2014. Transformations and correlations among some clay parameters—the global database. *Canadian Geotechnical Journal*, **51**(6), 663–685.

D'Ignazio, M., Di Buò, B., & Länsivaara, T. 2015. A study on the behaviour of the weathered crust in the Perniö failure test. *In Proceedings of the XVI European Conference on Soil Mechanic and Geotechnical Engineering*, XVI ECSMGE, Edinburgh, Scotland, ICE Publishing, 3639–3644.

Di Buò B., D'Ignazio M., Selänpää J. & Länsivaara T. 2016. Preliminary results from a study aiming to improve ground investigation data. *Proceedings of the 17th Nordic Geotechnical Meeting*: 187–197.

Emdal, A., Gylland, A., Amundsen, H.A., Kåsin, K., & Long, M. 2016. Mini-block sampler. *Canadian Geotechnical Journal*, 53(8), 1235–1245.

Karlsrud, K., & Hernandez-Martinez, F.G. 2013. Strength and deformation properties of Norwegian clays from laboratory tests on high-quality block samples. *Canadian Geotechnical Journal*, 50(12), 1273–1293.

Karlsrud, K., Lunne, T., Kort, D.A., & Strandvik, S. 2005. CPTU correlations for clays. *In Proceedings of the international conference on soil mechanics and geotechnical engineering*, Vol. 16(2), AA Balkema.

Kulhawy, F.H., & Mayne, P.W. 1990. *Manual on estimating soil properties for foundation design* (No. EPRI-EL-6800). Electric Power Research Inst., Palo Alto, CA (USA); Cornell Univ., Ithaca, NY (USA). Geotechnical Engineering Group.

L'Heureux, J.S., & Long, M. 2017. Relationship between Shear-Wave Velocity and Geotechnical Parameters for Norwegian Clays. *Journal of Geotechnical and Geoenvironmental Engineering*, 143(6), 04017013.

La Rochelle, P., Sarrailh J., Tavenas, F., Roy, M. and Leroueil, S. (1981) Causes of sampling disturbance and design of a new sampler for sensitive soils. *Canadian geotechnical journal*. 18, no. 1, 52–66.

Larsson, R. 2011. Metodbeskrivning för SGI:s 200 mm diameter 'blockprovtagare'—Ostörd provtagning i finkornig jord (In Swedish) Swedish Geotechnical Institute, SGI. Göta River Commission. GÄU. Subreport 33. Linköping.

Larsson, R., & Mulabdic, M. 1991. Piezocone tests in clay. Swedish Geotechnical Institute, Linköping, Sweden. Report No. 42.

Lehtonen, V. 2011. Instrumentation and analysis of a railway embankment failure experiment. Research report of the Finnish Transport agency 29/2011. Helsinki: Finnish Transport Agency.

Lunne, T., Berre, T., & Strandvik, S. 1997. Sample disturbance effects in soft low plastic Norwegian clay. *In Proceeding of the International Symposium on Recent Developments in Soil and Pavement Mechanics*. Rio De Janeiro, Brazil, 81–102.

Lunne, T., Berre, T., Andersen, K.H., Strandvik, S., & Sjursen, M. (2006). Effects of sample disturbance and consolidation procedures on measured shear strength of soft marine Norwegian clays. *Canadian Geotechnical Journal*, 43(7), 726–750.

Mayne, P.W. 2006. In-situ test calibrations for evaluating soil parameters. *In Characterization and Engineering Properties of Natural Soils–Proceedings of the Second International Workshop on Characterization and Engineering Properties of Natural Soils:* Taylor & Francis (pp. 1601–1652).

Mayne, P.W. 2014. Interpretation of geotechnical parameters from seismic piezocone tests. In *Proceedings, 3rd International Symposium on Cone Penetration Testing* (pp. 47–73).

Mayne, P.W., & Rix, G.J. 1995. Correlations between shear wave velocity and cone tip resistance in natural clays. *Soils and foundations*, 35(2), 107–110.

Powell, J.J.M. 2010. Session Report 1: CPT Equipment & Procedures. *In Proceeding of the 2nd International Symposium on Cone Penetration Testing*, CPT'10, California 2010.

Robertson, P.K. 2009. Interpretation of cone penetration tests—a unified approach. *Canadian Geotechnical Journal*, 46(11), 1337–1355.

Sällfors, G., 1975. Preconsolidation pressure of soft, high-plastic clays, *PhD Thesis*, Geotechnical Department, Chalmers University of Technology, Göteborg.

Selänpää, J., Di Buò, B., Länsivaara, T., & D'Ignazio, M. (2017). Problems related to field vane testing in soft soil conditions and improved reliability of measurements using an innovative field vane device. In Landslides in Sensitive Clays (pp. 109–119). Springer International Publishing.

Taylor & Francis
Taylor & Francis Group
http://taylorandfrancis.com

Cone Penetration Testing 2018 – Hicks, Pisanò & Peuchen (Eds)
© 2018 Delft University of Technology, The Netherlands, ISBN 978-1-138-58449-5

Ultimate capacity of the drilled shaft from CPTu test and static load test

M.A. Camacho & J. Mejia
Independent Engineer, Cochabamba, Bolivia

C.B. Camacho, W. Heredia & L.M. Salinas
Universidad Mayor de San Simón, Cochabamba, Bolivia

ABSTRACT: The ultimate capacity for the design of a drilled shaft is affected by several components, among them: the construction methodology, materials used, field conditions of the stratigraphy and the final constructive conditions. These components directly increase the uncertainty about the interaction between the soil and the drilled shaft, since the empirical methods of calculating the ultimate capacity from field tests assume ideal characteristics, both soil and drilled shaft. Therefore, the AASHTO LRFD standard recommends carrying out a load test in order to verify the predicted capacity of the drilled shaft. This article presents the comparison of the ultimate capacity predicted (Qp) by methods from the CPTu test with that capacity measured (Qm) through a static load test in a drilled shaft built in Cochabamba, Bolivia.

1 INTRODUCTION

The Beijing Bridge was built in Cochabamba (Bolivia) and it has three road levels. The drilled shaft studied is part of the Beijing Bridge and was built by the wet method, with a diameter of 1.20 m and a length of 20 m from the deep foundation of 2 m.

The local geology corresponds to stratigraphic conformations of sedimentary sequences of fluvio-lacustrine origin conformed by sub-horizontal strata of clays of variable plasticity between medium to low with intercalations of clays and silty sands, of formations due to hydraulic fillings typical of the valleys.

2 GEOTECHNICAL CHARACTERIZATION

2.1 *Field and laboratory test*

The geotechnical characterization was obtained by field tests of SPT (25 m) and CPTu (21 m), and laboratory tests (UU triaxial compression, characterization and consolidation tests) previously performed on the drilled shaft axis.

2.2 *CPTu*

Figure 1 shows the results of the CPTu test. The CPTu has an electrical cone with a conical tip at 60º with an area at its base of 10 cm^2 and the pore pressure has been measured above the cone (u2).

2.3 *Geotechnical conceptual model*

Figure 2 shows the evaluation of the CPTu test results using the ISBT behavior index proposed by Robertson (2010). The characterization of the soil based on the fines content (Fig. 3) proposed by F. Yi (2014) allowed an identical characterization to that obtained by means of the soil type behavior indexes (ISBT), moreover, being known the percentage of fines content present in the layer, it allowed a precise definition of the type of soil.

For the evaluation of the unit weight by means of the results obtained from the CPTu test, the equations proposed by Mayne (2012) were used. Figure 4 shows the results obtained compared with laboratory tests.

The proposal by Mayne and Kemper (1988) to evaluate the undrained shear strength is based on the N_{kt} factor.

$$s_u = \frac{q_t - \sigma_{vo}}{N_{kt}} \tag{1}$$

where: q_t = resistance to the corrected tip; σ_{vo} = initial vertical total stress; and N_{kt} = factor that varies between 10 to 20 (Ameratunga et al., 2016).

Based on 9 UU triaxial compression tests, the N_{kt} factor was calibrated for the present study. Presenting a better correlation (R^2 = 94.1%) the value of N_{kt} equal to 12.76. Figure 5 shows the results obtained compared with the laboratory tests.

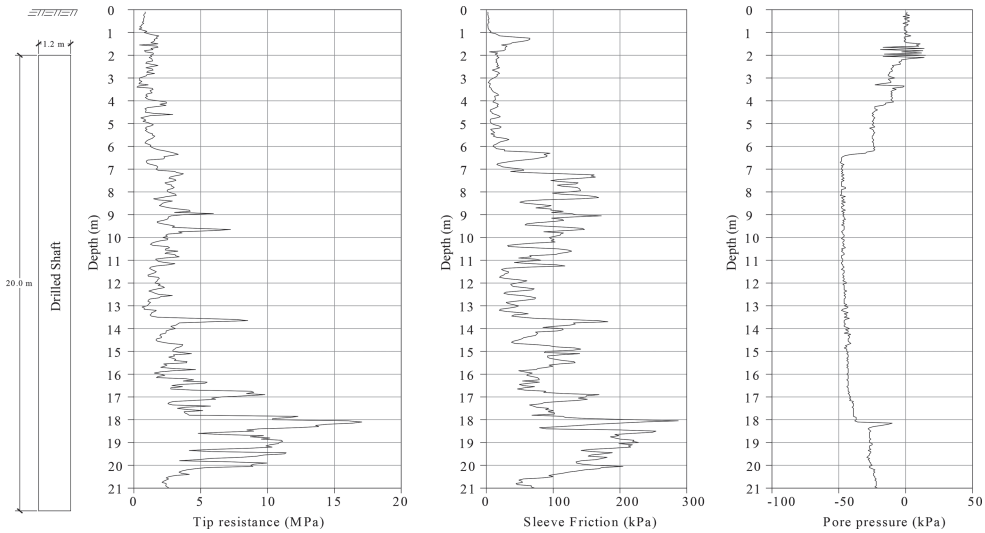

Figure 1. Results of CPTu test (Mejia, 2016).

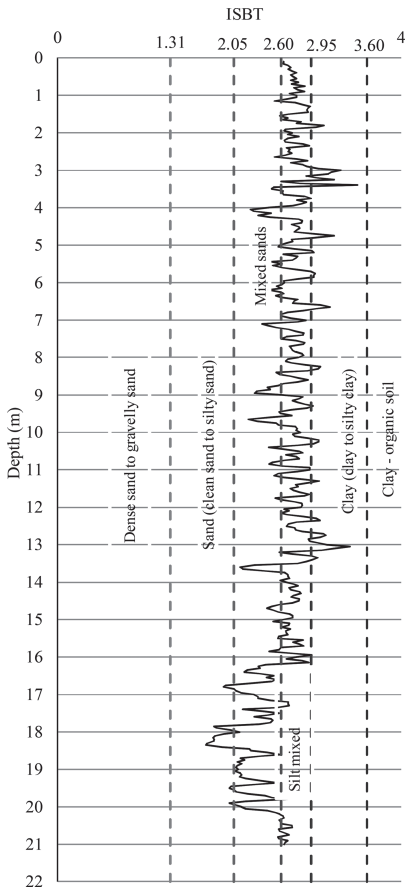

Figure 2. ISBT classification (Mejia, 2016).

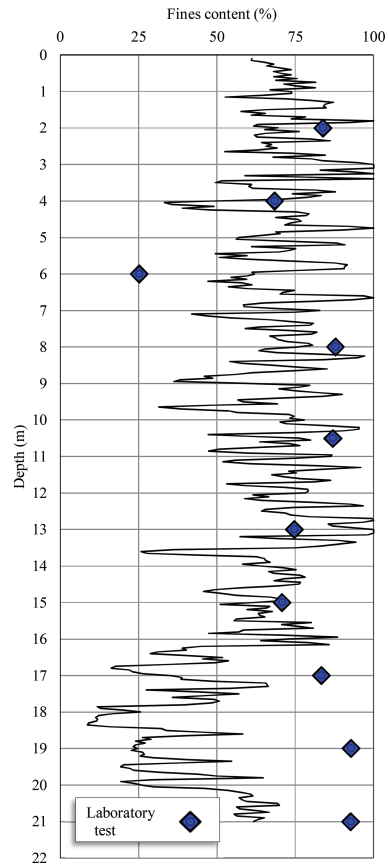

Figure 3. Comparison of fines content calculated by F. Yi and laboratory tests (Mejia, 2016).

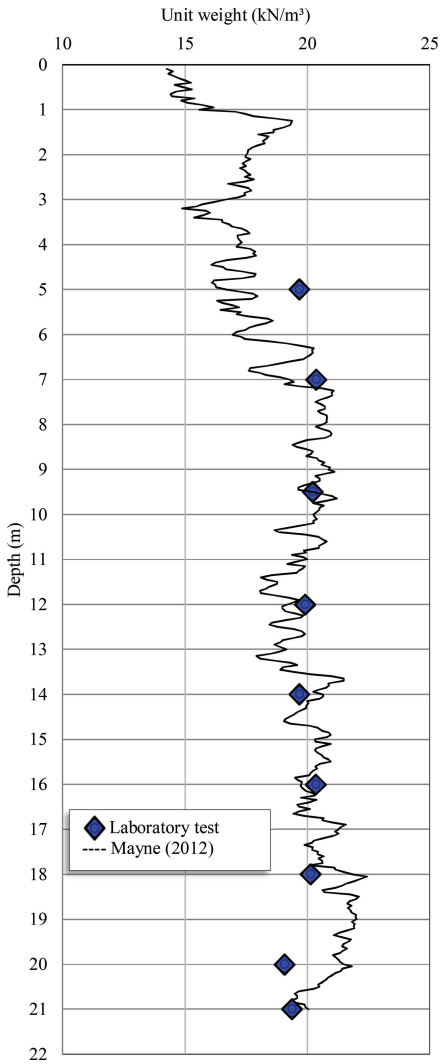

Figure 4. Comparison of the unit weight calculated by Mayne and laboratory tests (Mejia, 2016).

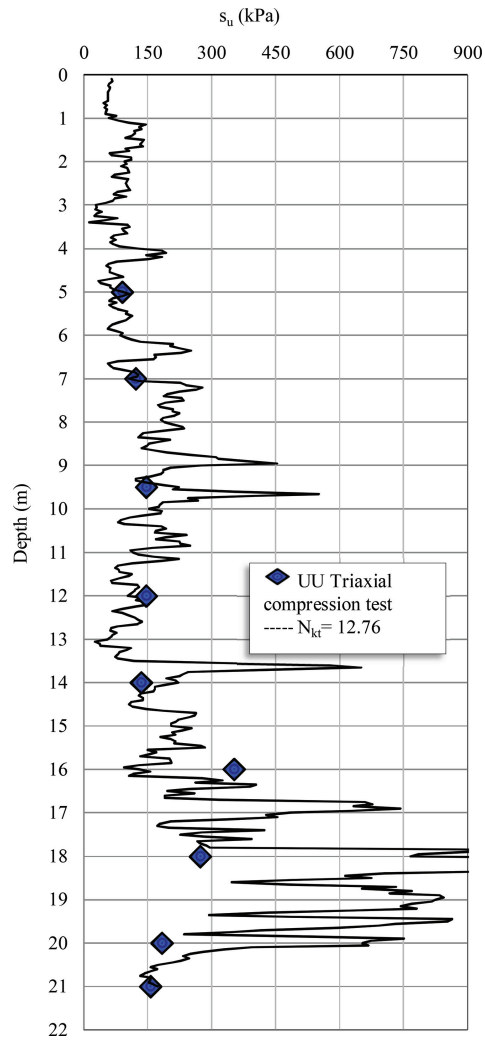

Figure 5. Comparison of the undrained resistance calculated by Mayne & Kemper and laboratory tests (Mejia, 2016).

Mayne and Kemper (1988) proposed the following relationship for the over consolidation ratio (OCR):

$$OCR = 0.37\left(\frac{q_c - \sigma_0}{\sigma'_0}\right)^{1.01} \quad (2)$$

where q_c = tip resistence from CPTu; σ_o = initial vertical total stress; and σ'_o = initial vertical effective stress.

Figure 6 shows the results obtained compared with the laboratory tests.

The geotechnical conceptual model extends from the surface up to 25 m deep, where the strata of lean clay with sand (75% of the stratigraphic profile). It is interspersed with layers of sandy silt and silty sand, resulting in a slightly plastic profile (with IP between 4.95% to 18.58% and average of 10.86% and LL between 22.18% to 37.83% and average of 30.11%). Overconsolidated soil with a low expansion and with a variable consistency, finding the water table at 2 m depth (Fig. 7). The lean clay with sand shows a rigid to very rigid consistency with values of undrained cohesion between 60 kPa to 170 kPa with average of 120 kPa.

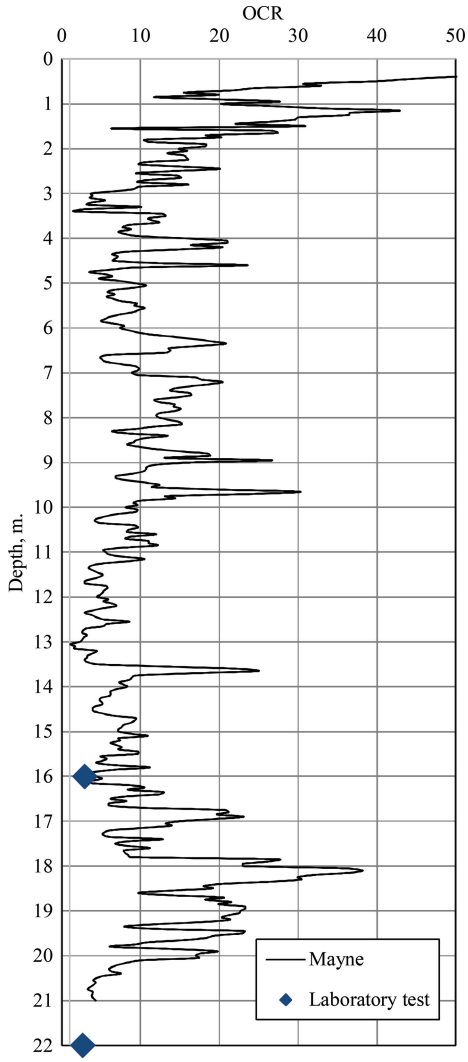

Figure 6. Comparison of the OCR calculated by Mayne & Kemper and laboratory tests (Mejia, 2016).

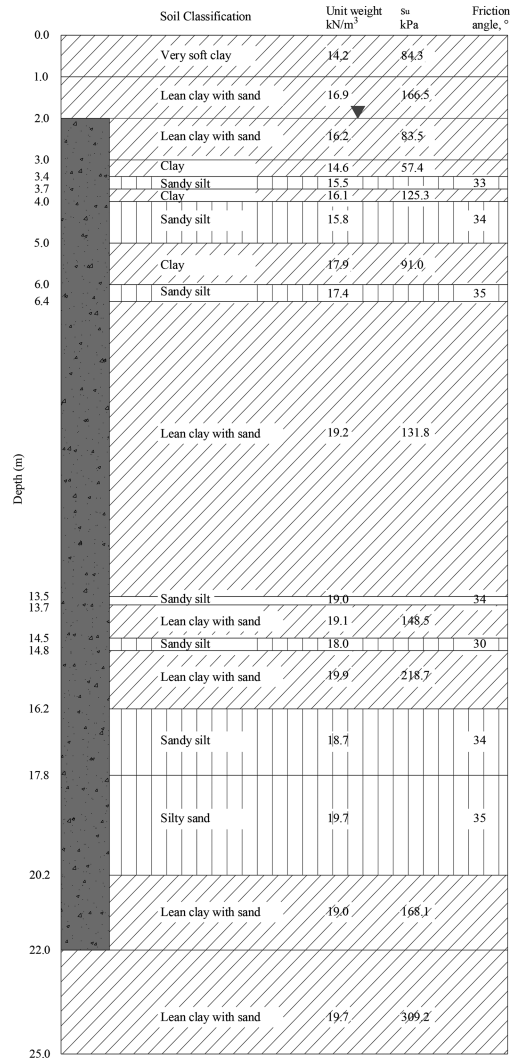

Figure 7. Geotechnical conceptual model for the drilled shaft (Camacho & Gomez, 2016).

3 ULTIMATE CAPACITY

3.1 *CPTu Methods*

Eight methods have been applied based on the CPTu (Qp) test in order to estimate the skin and base capacity. Table 1 and Figure 8 show the results obtained.

3.2 *Load test interpretation methods*

The static compression load test was performed on the top of the drilled shaft based on ASTM D1143–07. Figure 9 shows the results obtained

Table 1. Calculation of capacity by CPTu methods.

CPT	CPTu methods	Qs kN	Qb kN	Qp kN
01	Aoki y Velloso (1975)	1094	875	1969
02	Schmertmann y Nottingham (1978)	3294	826	4120
03	LCPC (1982; 1997)	2780	1171	3951
04	Price y Wardle (1982)	2928	918	3846
05	Philipponnat (1986)	2909	2492	5401
06	Frank y Magnan (1995)	1969	1224	3193
07	Eslami y Fellenius (1997)	4254	1213	5467
08	Takesue (1998) + Qb (02CPT)	4375	826	5201

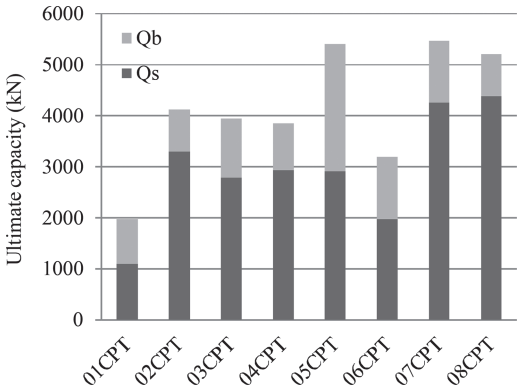

Figure 8. Calculation of capacity by CPTu methods (Camacho & Gomez, 2016).

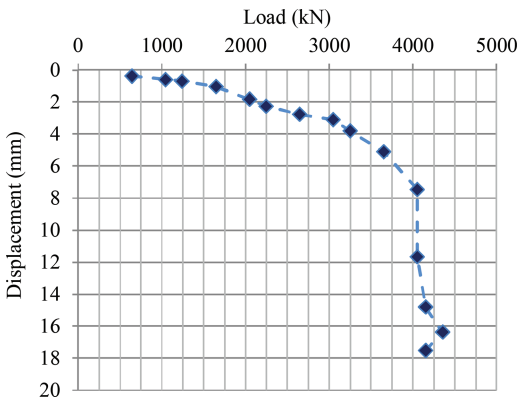

Figure 9. Load test results (Camacho & Gomez, 2016).

Table 2. Capacity calculation by load test methods.

LT	Analysis of results from the static axial loading test	Qu kN
01	The creep method, Housel (1956)	3203
02	The 80% criterion method, Hansen (1963)	4197
03	The 90% criterion method, Hansen (1963)	4046
04	The extrapolation method, Chin y Kondner (1971)	4731
05	The offset limit method, Davisson (1972)	4259
06	The intersection load, DeBeer y Walays (1972)	3903
07	The intersection method, Butler y Hoy (1977)	4048
08	The load at maximum curvature, Shen y Niu (1991)	4146
09	The extrapolation method, Decourt (2008)	4721
10	The offset limit method (AASHTO 2012)	4531

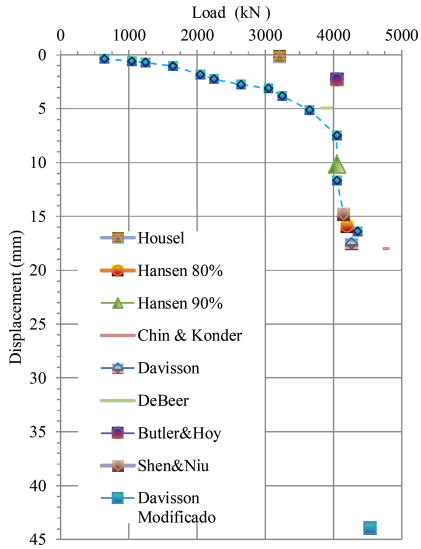

Figure 10. Variation of load test interpretation (Camacho & Gomez, 2016).

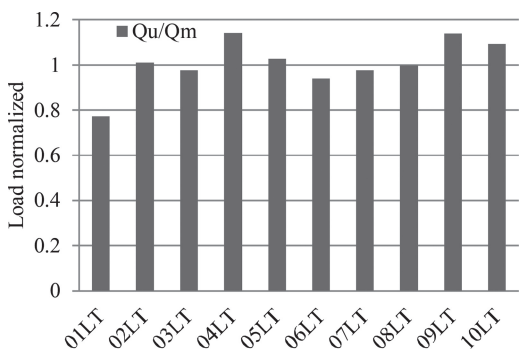

Figure 11. Normalized ultimate capacity (Camacho & Gomez, 2016).

reaching up to 4347 kN with a registered maximum displacement of 17.89 mm (1.5% strain based on the drilled shaft diameter).

The ultimate capacity of the drilled shaft has been estimated with 10 calculation methods presented by Fellenius (2016) and FHWA (2010). The results of the method interpretation analysis are presented in Table 2 and Figure 10.

4 ANALYSIS OF RESULTS

From the statistical analysis of the load test results it is concluded that 5 methods are closer to the average. Of these five methods the Shen & Niu method was chosen to normalize the results because it is the closest (Fig. 11).

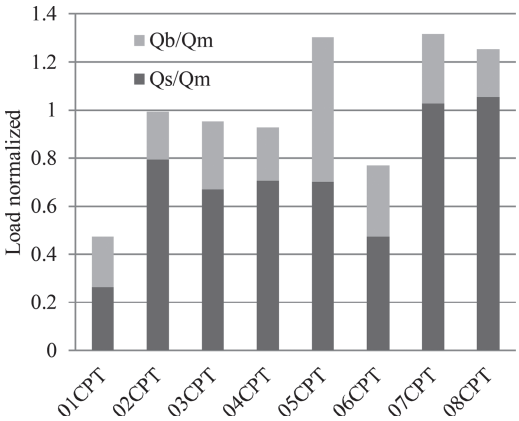

Figure 12. Comparison between the capacity predicted in the base and skin friction with the ultimate capacity measured (Camacho & Gomez, 2016).

Figure 12 shows the Qp from the CPTu normalized with Qm (i.e. Qp / Qm) and the contribution of the skin and the base capacity.

5 CONCLUSIONS

Field (CPTu and SPT) and laboratory tests (UU Triaxial compression, characterization, and consolidation test) have been carried out on the axis of the drilled shaft of 1.20 meters in diameter and 20 meters in length.

A load test was carried out until reaching a value of 4347 kN at 17.89 mm of displacement (1.5% strain based on the drilled shaft diameter).

The drilled shaft has not been equipped with base or skin friction measurements to distinguish between Qb and Qs. The result of load test shows a typical graphic of drilled shaft on fine soils.

Ten methods of interpretation have been applied for the ultimate capacity. From analysis and interpretation, the value of 4146 kN has been adopted, from the Shen and Niu method for this case study. The range of variation with the other methods is found between 0.77 to 1.14 with respect to 4146 kN.

The interpretation of data has been performed with the methods proposed from the CPTu where variations of the predicted ultimate capacity have been obtained from 0.47 to 1.32 with respect to 4146 kN. The method with the best approximation to the Qm value has been that of Schmertmann and Nottingham (1978) with a ratio of 0.99.

REFERENCES

AASHTO 2012. LRFD Bridge Design Specification. Washington: AASHTO.

Ameratunga J., Sivakugan N. & Das B. 2016. Correlations of soil and Rock Properties in Geotechnical Engineering. India: Springer.

Camacho M.A. & Gomez J.J. 2016. Determinación y comparación de la capacidad portante del pilote vaciado in situ (P2–3), a partir de ensayos de campo y una prueba de carga estática en el nudo viario Beijing. Cochabamba: Universidad Mayor de San Simón.

Fellenius, B.H. 2016. Basics of foundation design. British Columbia: www.fellenius.net.

FHWA. 2010. Drilled shafts: Construction procedures and LRFD design methods. USA: NHI.

Mayne P.W., Peuchen J. & Bouwmeester D. 2010. Soil unit weight estimation from CPTs. Atlanta: 2nd International Symposium on Cone Penetration Testing CPT.

Mejia, J. 2016. Caracterización de suelos estratificados mediante el ensayo de penetración de piezocono CPTu. Cochabamba: Universidad Mayor de San Simón.

Robertson, P.K. & Cabal K.L. 2010. Guide to Cone Penetration Testing for Geo-Environmental Engineering. California: Gregg Drilling & Testing, Inc.

Yi, F. 2014. Estimating soil fines contents from CPT data. Las Vegas: 3th International Symposium on Cone Penetration Testing CPT.

Cone Penetration Testing 2018 – Hicks, Pisanò & Peuchen (Eds)
© 2018 Delft University of Technology, The Netherlands, ISBN 978-1-138-58449-5

Interpreting properties of glacial till from CPT and its accuracy in determining soil behaviour type when applying it to pile driveability assessments

A. Cardoso & S. Raymackers
GeoSea-DEME Group, Zwijndrecht, Belgium

J. Davidson
Cathie Associates, Newcastle, UK

S. Meissl
Orsted Energy Wind Power, Gentofte, Denmark

ABSTRACT: Glacial till comprises a mixture of material which has been transported by a glacier, such as clay, silt, sand, gravel, cobbles and even boulders. Due to this widespread and variable material, accurate driveability predictions can be very difficult to begin with. This study presents a driveability assessment that was performed for the installation of monopiles at a site located offshore of England's East coast where the Swarte Bank glacial till formation can be found. Pile driveability back-calculations showed the influence of assessing the soil behaviour type, the accuracy of interpreting properties of the glacial till from CPTs when applying it to pile driveability assessment, and how CPTs should be treated with more value than borehole description when assessing soil resistance to driving on Swarte Bank glacial till.

1 INTRODUCTION

Glacial till is composed of unsorted material that has been carried out and deposited directly by a glacier. Due the heterogeneity of its composition (clay, silt, sand, gravel, cobbles and even boulders) the classification, and therefore, the behaviour prediction, can be very difficult. An interpretation of the site investigation data was carried out as a basis for the driveability assessment of the monopiles used as foundations of the windfarm. To assess the soil resistance to driving (SRD), the interpretation was based mainly on the CPT results. Borehole descriptions and laboratory tests are also taken into consideration. Driveability back-calculations were performed which showed that interpreting soil properties from CPT results should be treated with more value than borehole descriptions, when assessing soil resistance to driving in Swarte Bank glacial till.

2 GLACIAL TILL AT THE WINDFARM SITE

One of the glacial till formations found at the windfarm site is named Swarte Bank. It is the most abundant of the Quaternary units, forming the thickest sediment overlying a chalk formation, that covers the entire site and forms the infill of subglacial valleys cut during the Elsterian glaciation. It is typically composed of stiff to hard sandy gravelly clay with interbedded sand layers.

Based on the site investigation results, the Swarte Bank formation was divided in two sub-units for further analysis:

- sub-unit 1 sandy, gravelly clay;
- sub-unit 2 sand interbeds which are present within the clay sub-unit 1.

CPTs, borehole descriptions and laboratory tests were analyzed, and geotechnical classification parameters were identified for each of these sub-units.

2.1 *Swarte Bank soil behaviour type*

As described in §2, the Swarte Bank formation can have intermittent clay (cohesive) and sand (cohesionless) layers. The appropriate selection of either cohesive or cohesionless behaviour is critical when undertaking driveability calculations. Soil parameters considered when selecting either cohesive or cohesionless behaviour were the pore pressure and friction ratio. An assessment of the soil behaviour type (SBT) can be performed based on CPT data as shown in past research (i.e. Robertson (1990) as in Figure 1; Robertson and Wride (1998) as in Table 1, etc.).

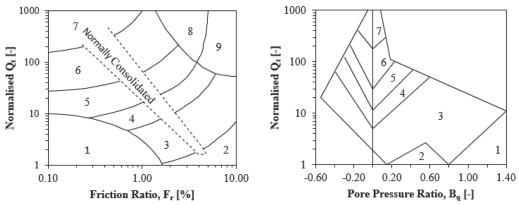

Figure 1. SBT zones Robertson (1990).

Table 1. SBT zones (Robertson and Wride, 1998).

Zone	SBT
7	Gravelly sand to sand
6	Clean sands to silty sands
5	Silty sand to sandy silt
4	Clayey silt to silty clay
3	Clay to silty clay
2	Organic soils-peats

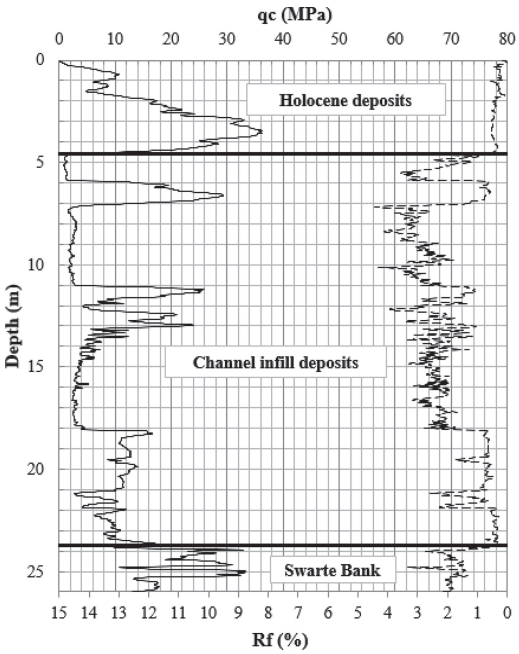

Figure 2. CPT log for Location A (qc—full line, Rf—dashed line).

It should be noted that the Swarte Bank unit was described as clay in the borehole descriptions for the majority of the locations at the site, since most CPTs refused in this unit, due to high resistance, and limited laboratory tests were performed.

Figure 2 and 3 show examples of CPT logs at 2 locations (Location A and B, respectively) where

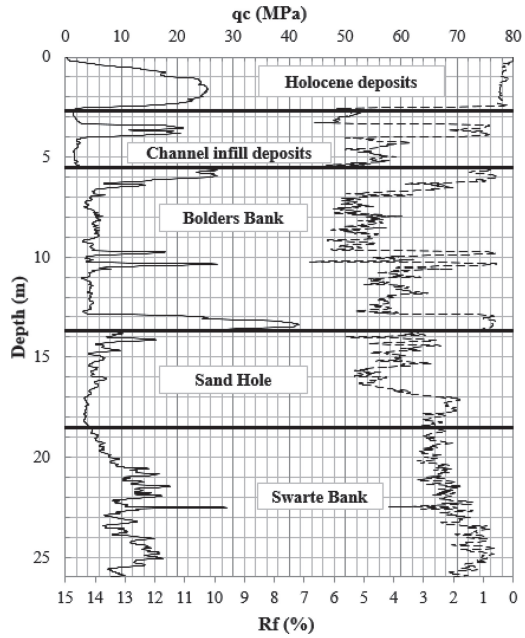

Figure 3. CPT log for Location B (qc—full line, Rf—dashed line).

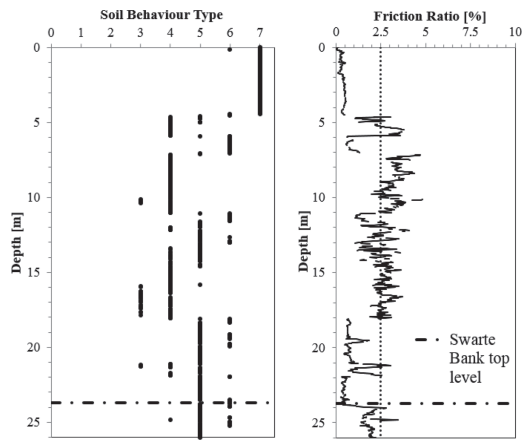

Figure 4. SBT for location A (Robertson and Wride, 1998).

the CPT did not refuse in the first meters of the Swarte Bank formation.

Based on the CPT data the SBT was derived for Locations A and B as shown in Figures 4 and 5 respectively.

Where no CPT data were available, global parameters were used for the Swarte Bank unit. These global parameters were derived based on the available consolidated undrained (CU), uncon-

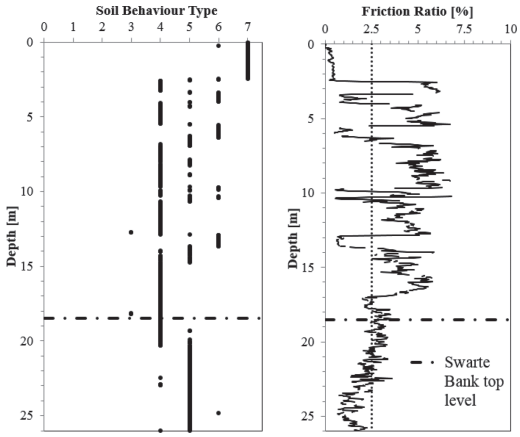

Figure 5. SBT for location B (Robertson and Wride, 1998).

solidated undrained (UU) and direct shear stress (DSS) tests.

2.2 *Geotechnical properties of the Swarte Bank sub-units*

The general properties of the two Swarte Bank sub-units identified on this site are summarized in Table 2.

The particle size distribution was determined by laboratory sieving analysis. For sub-unit 1, results are as shown in Figure 6. For sub-unit 2 only one test was performed and the result is as shown in Figure 7. Results show a sandy, gravelly clay for sub-unit 1 and a sand for sub-unit 2.

As mentioned in §2.1, where no CPT data were available the undrained shear strength values for the Swarte Bank were considered based on laboratory tests. However, values were scattered and the range of undrained shear strength obtained by laboratory tests was large; therefore, wide bounds for the undrained shear strength were adopted as shown in Figure 8 and Table 3. The best estimate (BE) and upper bound (UB) values were used for the soil profiles as the basis for assessing SRD.

For locations where CPT data were available, the undrained shear strength was derived from the q_{net} using the N_{kt} factors, as shown in equation (1):

$$Su = \frac{qnet}{Nkt} \tag{1}$$

where Su is the undrained shear strength in kPa, q_{net} is the net cone resistance in kPa and N_{kt} is the correlation factor.

Table 2. Properties of the Swarte Bank formation at the site.

Properties		Sub-unit 1 (clay)	Sub-unit 2 (sand)
Moisture content (%)		15	–
Plasticity index (%)		11	–
Effective unit weight (kN/m³)		12	10
Effective angle of friction (°)	Lower bound		34
	Best estimate		38
	Upper bound		42

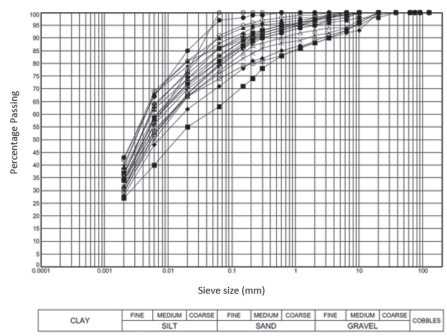

Figure 6. Sieve analysis results for sub-unit 1.

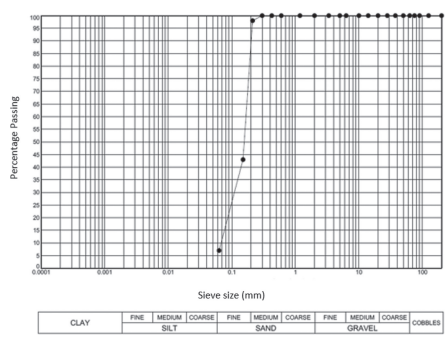

Figure 7. Sieve analysis results for sub-unit 2.

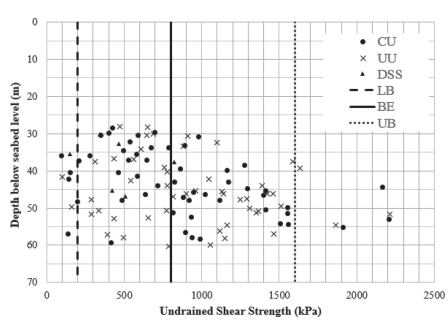

Figure 8. Undrained shear strength for Swarte Bank formation based on laboratory tests.

Table 3. Undrained shear strength bounds adopted for Swarte Bank formation at the site.

Bound	Undrained shear strength (kPa)
Lower Bound	200
Best Estimate	800
Upper Bound	1600

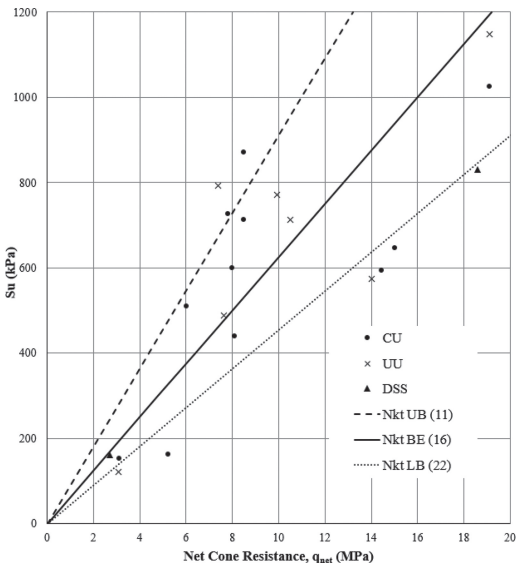

Figure 9. Calibration of N_{kt} factor for the Swarte Bank unit.

For setting up the bounds for the N_{kt} factor 11 CU, 7 UU and 2 DSS tests were available. N_{kt} factors were derived as shown in Figure 9.

3 DRIVEABILITY IN GLACIAL TILL

Monopiles were the chosen foundation solution for the wind turbines installed at the site. In order to select the most suitable hammer to be able to drive the piles to target depth, a driveability assessment was carried out. The prediction of pile driveability consists of developing a model of the hammer-pile-soil system (a wave equation model) which simulates the relationship between SRD and blow count (or pile penetration per blow).

In a separate pile analysis, the SRD was calculated based on a CPT method and used as input to GRLWEAP software (Pile Dynamics, 2010) which was used to perform the driveability assessment. In-house shaft and toe Quake and Damping parameters were used as shown in Table 4.

Table 4. Quake and damping values used in the driveability assessment.

Parameter	Value
Tip Quake	2.5 mm
Side Quake	2.5 mm
Tip Damping	0.5 s/m
Side Damping in CLAY	0.6 s/m
Side Damping in SAND	0.15 s/m

Theoretical refusal criteria significantly lower than the mechanical one was applied. This is in order to allow for some variations in soil conditions, short interruptions during driving (soil set-up) and economical pile driving.

3.1 *SRD*

There are no standardised methods for estimating SRD. Most of the better known SRD methods (Toolan and Fox, 1977; Stevens et al., 1982; Alm and Hamre, 2001) are broadly based on modifications to static pile capacity calculations. Calibration and verification of the SRD methods are based on the use of field data (measured hammer energy and blow counts) combined with wave equation modelling of the hammer-pile-soil system which provides the relationship between blow count and SRD for a given piling situation.

For this offshore wind farm SRD was assessed using a CPT method based on Alm & Hamre (2001) which calculates SRD from CPT cone tip resistance (q_c) data. It has a different method for both sand and clay and the selection of the soil type of the different layers is a manual input.

3.2 *Modelling the Swarte Bank formation*

An evaluation to assess the sensitivity of the CPT interpretation is undertaken. Back-calculations are performed by considering two different approaches for modelling the Swarte Bank formation:

Approach 1: Assess Swarte Bank as a cohesive material (clay), in line with the borehole descriptions.

Approach 2: Assess the Swarte Bank as clay when friction ratio values exceeded 2.5% and when SBT is between 2 and 4 according to Robertson and Wride (1998) (Table 1), and as sand when friction ratio does not exceed 2.5% and when SBT is between 5 and 7 according to Robertson and Wride (1998) (Table 1).

A comparison between the two approaches is presented below.

3.3 *Driveability assessment results (back-analysis)*

The pile driving records of the installed monopiles at the site were subjected to back-analysis. The stroke height was rescaled to match the applied hammer energy on site. With the rescaled theoretical stroke height a new GRL-WEAP simulation is made. Afterwards, the obtained blowcount vs depth curve is compared to the calculated ones.

Results are presented for the two locations introduced before (Locations A and B), representative of the general trend of results of the back-calculations performed for locations where the pile penetrated the Swarte Bank Unit.

The top of the Swarte Bank layer is at 23.7 m and at 18.5 m depth at Locations A and B, respectively.

3.3.1 *Swarte Bank sub-unit 1 and 2 as cohesive material*

The back-calculations performed for these two locations showed that blowcount is overpredicted on the Swarte Bank formation if this formation is assessed as clay, especially when upper bound driving conditions are considered, as shown in Figures 10 and 11.

3.3.2 *Swarte Bank sub-unit 1 and 2 depending on SBT and the friction ratio value*

For this approach, the friction ratio values, the 2.5% boundary and SBT were considered. CPT data show that at location A the friction ratio within the Swarte Bank formation (23.7 m to 26.3 m) was found to be around 2.0% and SBT was found to be between zones 5 and 6; hence this soil was modelled as sand. For Location B, since the friction ratio was found to be around 2.5% from 18.5 m to 20.5 m and thereafter to decrease to a constant value of around 2.0% for the rest of the unit, and SBT was found to be mainly in zone 5, the Swarte Bank was modelled as a clay above 20.5 m and as a sand below 20.5 m.

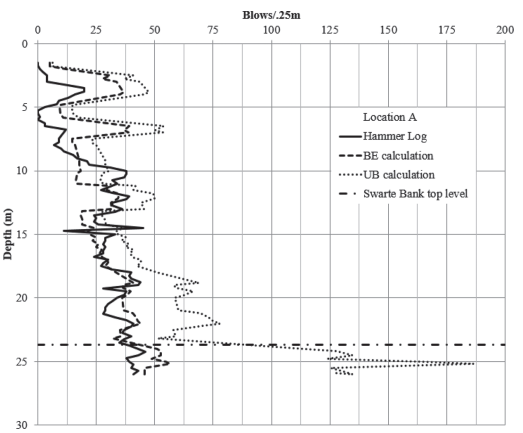

Figure 10. Back calculation location A—Approach 1.

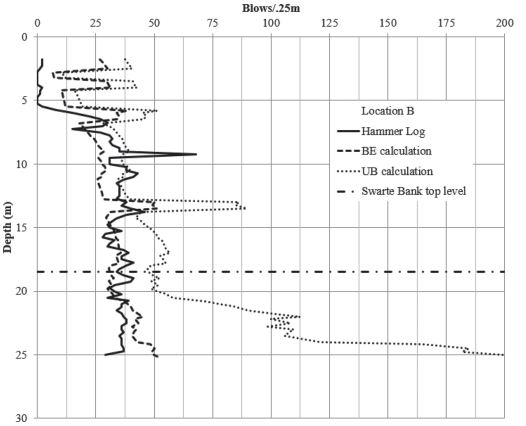

Figure 11. Back calculation location B—Approach 1.

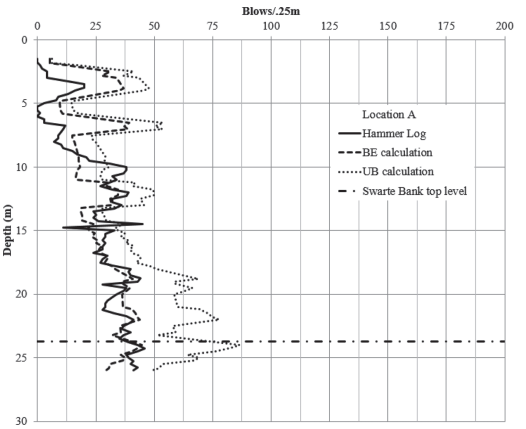

Figure 12. Back calculation location A—Approach 2.

The results are as shown in Figures 12 and 13.

As shown in Figures 10 to 13, addressing the Swarte Bank formation based on the friction ratio values and SBT (Approach 2), gives a much better fit with the measured driving results than when based on the borehole logs only (Approach 1). This is especially noticeable for Location B where a good fit with the hammer log is found by modelling the Swarte Bank formation as clay (from 18.5 to 20.5 m) and as sand (below 20.5 m).

It should also be highlighted that when the Swarte Bank formation is modelled correctly, the BE blow vs depth curve obtained by using the CPT method gives a reliable prediction.

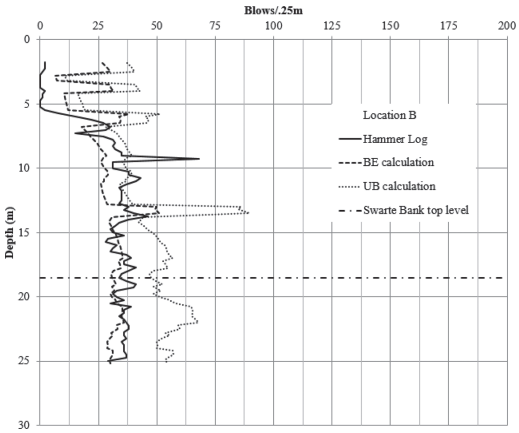

Figure 13. Back Calculation Location B—Approach 2.

4 CONCLUSIONS AND RECOMMENDATIONS

Glacial till comprises a mixture of unsorted material that has been carried by a glacier. One of the glacial till formations found at the windfarm site is named Swarte Bank. In many instances this formation is considered as "borderline" material with intermittent clay (cohesive) and sand (cohesionless) layers, which presents a challenge when describing this formation while logging the borehole cores. The selection of cohesive or cohesionless behavior for this material must be performed with caution since it can lead to an inaccurate prediction of soil resistance which is critical when undertaking driveability calculations.

Referring to the outcome of this paper, the use of the Robertson and Wride (1998) SBT index together with the friction ratio parameter, which can be applied with depth, gave an accurate representation of the method (sand/clay) to be used when predicting soil resistance in glacial till, particularly in the case of the Swarte Bank formation. By considering the SBT and the friction ration as a primary input to model the Swarte Bank formation, a better fit between the measured and the predicted blow count has been achieved. Hence, the use of CPT, especially in challenging materials such as glacial till, is promoted as it will have a positive effect on the selection of an appropriate hammer energy.

ACKNOWLEDGEMENTS

The authors would like to acknowledge the support of their respective companies especially Orsted for allowing publishing this data.

REFERENCES

America Petroleum Institute (2000). *Recommended Practice for Planning, Designing and Constructing Fixed Offshore Platforms—Working Stress Design. Recommended Practice 2A-WSD (RP 2A-WSD)*. Washington: API Publishing Services.

Alm, T. & Hamre, L. (2001). Soil Model for pile driveability predictions based on CPT interpretations. *Proceedings XV-th International Conference on Soil Mechanics and Geotechnical Engineering* Vol.3: 1297–1302

Lunne, T., Robertson, P.K. & Powell, J.J.M. (1997). *Cone Penetration testing in geotechnical practice*. London: Blackie Academic and Professional.

Pile Dynamics (2010). *GRLWEAP 2010 Background Report*. Cleveland: Pile Dynamics.

Robertson, P.K., (1990). Soil classification using the cone penetration test. *Canadian Geotechnical Journal* Vol. 27(1): 151–158.

Robertson, P.K. & Wride, C.E. (1998). Evaluating cyclic liquefaction potential using the cone penetration test. *Canadian Geotechnical Journal* Vol. 35(3): 442–459.

Stevens, R.S., Wiltsie, E.A. & Turton T.H.(1982). Evaluating pile driveability for hard clay, very dense sand and rock. *Proceedings 14th Offshore Technology Conference* paper OTC no. 4205.

Toolan, F.E. & Fox, D.A. (1977). Geotechnical planning of piled foundations for offshore platforms. *Proceedings of the Institute of Civil Engineers* Vol. 62 (1): 221–244.

Trenter, N.A. (1999). *Engineering in glacial tills*. London: CIRIA.

Cone Penetration Testing 2018 – Hicks, Pisanò & Peuchen (Eds)
© 2018 Delft University of Technology, The Netherlands, ISBN 978-1-138-58449-5

Variable rate of penetration and dissipation test results in a natural silty soil

R. Carroll & P. Paniagua
Norwegian Geotechnical Institute, Trondheim & Oslo, Norway

ABSTRACT: Variable rate of penetration over 1.2 to 1.5 m intervals were carried out in a natural clayey silt followed by dissipation tests. The tests are grouped into two main sets: an upper set from 5 to 6.5 m and a deeper set from 8.5 to 10.2 m. Index, strength and consolidation parameters are presented for reference to soil behavior and classification. This paper investigates the effect of rate on u_2, q_t and B_q using penetration rates of 2, 20, 100 and 320 mm/s. Similarly the effect of rate was investigated for assessment of dissipation tests and estimation of the time for 50% dissipation (t_{50}). Dissipation tests were predominantly dilatory at all rates and depths. Drainage conditions were evaluated at the different rates using the normalised rate of penetration (V) calculated using one method to estimate the horizontal coefficient of consolidation (c_h). Reference to B_q as a guide of drainage conditions is discussed together with V. A total of six methods to estimate t_{50} and subsequently c_h were used in this study, calculated t_{50} values are presented for all methods. One method is used for presentation of trends and consideration of which methods may yield the most representative c_h values is discussed in relation to laboratory c_v.

1 INTRODUCTION

Cone penetration tests (CPTU) in saturated intermediate materials such as silty soils typically occur under partial drainage at the standard penetration rate of 20 mm/s. Undrained penetration has been referenced in literature to be associated with normalised velocity (V) for V > 30 (Finne & Randolph 1994), V > 10 (Kim et al. 2008) and V > 20–40 (Holmsgaard et al. 2015). These values are representative of a selected number of examples from centrifuge and in situ tests. V less than the above suggested ranges are associated with partially drained to fully drained penetration depending on the V value and boundary used. Fully drained penetration is typically associated with V < 0.01. Carroll (2013) presented a detailed summary of drainage conditions and V values with reference to test type, i.e. centrifuge, in situ or calibration chamber. The summary showed that V values varied based on test type and c_h used in the normalisation.

Senneset et al. (1989) noted that the point of cut off for correlation of undrained shear strength from CPTU was at a pore pressure ratio $B_q < 0.4$ due to association with partially drained penetration. The use of B_q as a parameter associated with delineation of drainage conditions in combination with V has not been widely reported in literature.

A change in soil responses to drained, partially drained or undrained can be induced by changing the penetration rate (v) where equipment can practically reach required rates. Typically fast v are associated with undrained behavior and slow v with drained behavior. The undrained response in a soil can be contractive or dilative. This is assessed by introduction of a varied rate relative to the standard rate to assess the change in pore pressure (u_2) and cone resistance (q_t). With increased rate of penetration (v): (1) a contractive response shows an increase in u_2 and a decrease in q_t and (2) a dilative response shows a decrease in u_2 and increase in q_t. Negative u_2 (i.e. suction) may occur in some cases.

Investigation of the effect of increase and decrease of penetration rate in intermediate soils showing contractive response has been documented by DeJong & Randolph (2012), DeJong et al. (2013), Schneider et al. (2008) and Randolph & Hope (2004). While a dilative response was observed by Silva (2005), Schneider et al. (2007) and Paniagua (2014).

Regardless of penetration rate, once penetration stops Δu will vary with time and eventually reach equilibrium conditions at in situ pore water pressure (u_o). This variation with time can be either monotonic (i.e. the initial pore water pressure u_i is greater than u_o and u_i is the maximum pore water pressure measured) or dilatory (i.e. u rises with time at the start of the test, reaches a peak value u_{max}, and then decreases with time towards u_o). The rate of recovery to u_0 is a function on permeability (k) and c_h.

This paper presents data from CPTU tests at the standard penetration rate together with faster and slower rates. The tests were conducted at the silt research site, Halden; that is part of the Norwegian GeoTest Sites (NGTS) project. The NGTS project has 5 sites in total: sand, soft clay, quick clay, permafrost and silt. The sites have been characterized and are suitable for use by researchers, industry and developers of geotechnical equipment. They will be maintained for 20 years and interest to test at any of them should be expressed to the NGTS Project Manager. The Halden silt site has been characterized by Blaker et al. (2016) and Paniagua et al. (2016) presented the analysis of some dissipation tests at the site.

The present study evaluates the soil response, dilative or contractive, using a variable rate of penetration prior to dissipation tests. An assessment of the drainage condition at the various penetration rates used, and the corresponding influence of v on dissipation and c_h is discussed. Dissipation test results are presented and several interpretation methods for monotonic and dilatory decay of excess pore pressure to estimate the time for 50% dissipation (t_{50}) have been implemented and discussed. Analysis of results are presented in terms of a single method selected by the authors. The estimated c_h values are compared to laboratory derived c_v.

2 SOIL DESCRIPTION

Halden site is a natural fjord marine deposit which has a low plasticity silt. The water table is approximately 2.5 m below ground level. The silt deposit is relatively uniform between 4.5 m and 15 m, varying from a SILT, sandy clayey around 5 m depth to a SILT, clayey from 6.5 m, see Figure 1. Under anisotropic consolidation, a piston sample from 5.3 m had a dilatant response with an 'S' shaped stress path, indicating some contraction before dilation. Table 1 presents typical soil parameters for Halden silt.

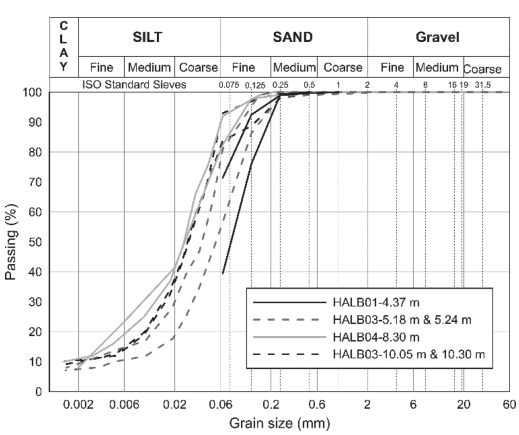

Figure 1. Grain size distribution at Halden.

Table 1. Soil parameters at Halden.

Parameter	Between 5–6.5 m	Between 8.5–10 m
Water content, w (%)	21–23	27–33
Total unit weight, γ (kN/m³)	19–19.3	18.9–19.0
Density of solids, γ_s (kN/m³)	24.6	26.3–26.5
Organic content,	<2%	<0.5%
Friction angle, φ (°)	36	35.5
Rigidity index $I_r = G_{50}/s_u$	147	126
c_v* m²/s	$0.8 \cdot 10^{-5}$	$0.7–1.0 \cdot 10^{-5}$
k* at 0% strain m/s	$1.8 \cdot 10^{-8}$	$1.3 \cdot 10^{-8}$

*Measured in CRS tests, k at 0% axial strain, c_v at in situ effective vertical stress.

2.1 *I_r determination*

The rigidity index I_r is a critical parameter for estimating c_h using cone data. Research (Teh & Houlsby 1991) has shown that I_r influences the plastic failure zone that develops during cone penetration and therefore the stresses and pore pressures associated with this process. In this paper, I_r was estimated from advanced laboratory testing and conservative undrained shear strength analysis. Comparison is made to the correlations proposed by Krage et al. (2014) based on actual laboratory measured data (Method A) and seismic in situ data (Method B). The values obtained from advanced laboratory testing are shown in Table 1. Values obtained by Method A, in the range of $205 \leq I_r \leq 217$, are higher than the ones presented in Table 1. Method B gives values ($139 \leq I_r \leq 157$) that show good agreement with the values presented in Table 1.

3 CPTU & DISSIPATION TESTS

CPTU tests at Halden were carried out using NGI's standard rig setup and an Envi cone. The penetration rate was constant for 1.0–1.5 m before the target depth of the dissipation tests. The penetration rate was in the order: 2 mm/s, 20 mm/s (standard rate), 100 mm/s and 320 mm/s. The mechanical operation for a test comprised of stopping penetration at the target depth and start logging by manual trigger by the operator. The base clamps are then engaged and the top hydraulic clamps are disengaged to avoid possible movement of the

hydraulic system with time and applying pressure on the cone. In essence there can be a short time laps of a couple of seconds between end of penetration and start of logging and some change in stress conditions due to movement of the clamps engaging and disengaging. However care and attention to these processes was made during testing to minimize possible effects on measurements. All pore pressure measurements are at the shoulder (u_2 position).

The target depths for the dissipation tests were 5 m, 6.5 m, 8.5 m and 10 m. Preceding penetration rates for each respective target depth are listed in Table 2. A total of 11 dissipation tests were carried out. The results in Table 3 show a range of u_2 values which are described under the table. Assessment of u_2^x suggests a contractive response, as with increased v there is an increase in u_2, for intervals at 5, 8.5 and 10 m using $u_{2\text{-avg}}$ as base line for standard rate. However the response of q_t does not match the associated behavior for contractive as q_t tends to increase with increased v. At the 5 and 6.5 m intervals the q_t response is not consistent with the clearer trends from deeper intervals that suggest a dilative response.

Table 3 shows the change in B_q with v and results suggest that there is little effect in this parameter from the range of rates achievable with the CPTU rig. The order of magnitude in change, where a change occurs, is 0.01–0.03. Overall B_q values are in the order of 0.1 to 0.15 at 5 to 6.5 m and 0.2 to 0.24 in the interval of 8.5 to 10.2 m. This response in CPTU is associated with partial drainage and should not be used for undrained shear strength analysis (Senneset et al. 1989).

Table 3 shows a clear increase in V with increased rate as expected. With a reduced rate, to 2 mm/s, V values move closer towards the undrained-partially drained boundary in the upper layer, with V values in the region of 14–27. For the standard rates, V is approximate 100 in the upper interval and 140–280 in the lower interval. Both intervals fit well in the undrained range based on the V values presented previously in the paper. However both cases do not agree with the reasoning suggested by Senneset et al. (1989) on partial drainage and associated B_q range. The drainage condition at the time of a dissipation test is an important consideration as theories used to evaluate the c_h are based on a fully undrained starting point.

Table 2. Penetration rate before target depth for dissipation tests.

Target depth m	u_0 kPa	Slow rate mm/s	Standard rate mm/s	Fast rate mm/s
5.0	34	2	20*	
6.5	48	2	20	320
8.5	65		20*	100
10.0	81			100 & 320

*2 tests at 20 mm/s were carried out at this depth

Table 3. Average CPTU values over 1.2–1.5 m before target depth.

Depth m	Rate mm/s	$q_{t\text{-avg}}$ MPa	$u_{2\text{-avg}}$ kPa	$u_2^{\times}$ kPa	$u_{t=0}$ kPa	u_{max} kPa	B_q -	V†	F_r %
5.00	2	1.65	106	94	94	121	0.07	29	1.33
4.96	20	1.26	101	85	92	134	0.09	111	1.17
5.01	20	1.51	104	110	95	102	0.09	178	0.98
6.50-mono	2	0.83	123	157	156	156	0.12	13	0.35
6.51	20	0.76	134	121	122	158	0.15	95	1.11
6.62	320	0.88	150	154	136	193	0.15	1200	1.26
8.50-mono	20	0.90	189	181	176	173	0.18	273	1.23
8.53	20	0.87	192	209	210	232	0.19	139	0.96
8.51	100	0.99	230	226	220	243	0.21	543	0.94
10.20	20*	0.97	222	–	–	–	0.19	180	1.11
10.20	20*	0.96	243	–	–	–	0.23	180	1.19
10.24	100	1.09	288	305	236	265	0.24	959	0.88
10.13	320	1.14	296	308	307	318	0.24	2969	NA

*Reference CPTU data, $u_{2\text{-avg}}$ and $q_{t\text{-avg}}$ values averaged over 1.5 –1.2 m before dissipation interval, × last u_2 measured before stop penetration of CPTU. $u_{t=0}$ is the measured u at start of dissipation test. u_{max} is the maximum u during dissipation.† using square root method. Mono: monotonic dissipation.

4 EVALUATION OF RESULTS

The dissipation test results are presented in Figure 2 and Figure 3 for the upper and lower depth intervals of 5 to 6.5 m and 8.5 to 10.2 m,

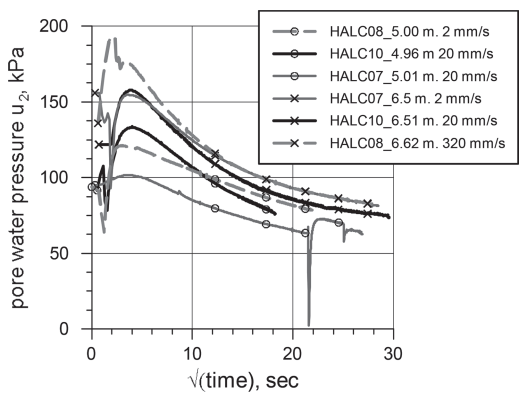

Figure 2. Measured u_2 vs. square root of time, at 5 m & 6.5 m.

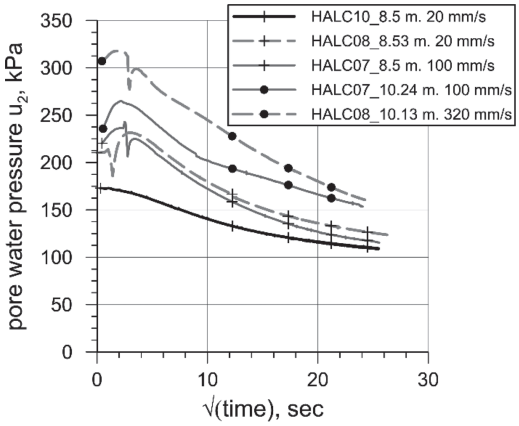

Figure 3. Measured u_2 vs. square root of time, at 8.5 m & 10 m.

respectively. A monotonic response is evident in two of the dissipation tests: HALC07–6.5 m at 2 mm/s and HALC10–8.5 m at 20 mm/s. All other tests show dilatory response. Some tests show a sudden drop in u_2 after the test has begun (about 2 to 5 s). This is particularly evident in the upper test interval while in the lower test interval this drop occurs after $u_{2\text{-max}}$ in two of the tests. The sharp reductions in u_2 are likely to be linked to rig operation with cone unloading while the increases in u_2 are thought to be linked to natural soil behavior (i.e. pore pressures redistribution) around the cone tip and shoulder.

The match between the final u measured ($u_2^{\times}$) (i.e. last point recorded before start of dissipation test) and the initial u ($u_{t=0}$) (i.e. the first u measured at the start of the dissipation test) is shown in Table 3. Results show good agreement in most cases with exception of tests at 5.01 and 6.62 m (with a difference of approximate 15 kPa) and 10.24 m (with a difference of approximate 90 kPa), the latter case shows $u_2^{\times}$ considerably greater than $u_{t=0}$. In these particular tests, undrained conditions are thought to be present based on analysis of V and results suggest that pore pressure redistribution occurs quickly. These tests show a dilatory response along with tests where there is good agreement between $u_{t=0}$ and $u_2^{\times}$. Overall the data is of good quality and shows that conditions prior to the dissipation test are in line with those of the data collected at the start of the dissipation test.

The u_{max} in dilatory test results at 5–6.5 m are approximate 30–45% greater than $u_{t=0}$, with the test at 5.01 m showing a difference of 7%. At 8.5–10.2 m, u_{max} is approx. 3–12% greater than $u_{t=0}$. This suggests that the dilatory response is amplified in the upper depth interval where soil is likely more permeable. The time to reach u_{max} is approx. 5 to 16 s in the upper interval and 3 to 10 s in the lower interval. With increased rate of penetration, the time to u_{max} reduces for dilatory response results. Overall, the dilatory response is rapid in these tests, occurring over several seconds. This highlights the need for good data collection at the start of a test, required to selection or inference of u_i used for later c_h estimation.

4.1 *Interpretation of t_{50} times by different methods*

Estimation of t_{50} was carried out using the following six procedures: (1) shoulder pore water decay (shoulder method), (2) square root method (Sully et al. 1999), (3) logarithm of time method (Sully et al. 1999), (4) Burns & Mayne (1998) method (only tests at 6.5 m target depth as fitting of parameters was considered unrealistic), (5) Mantaras et al. (2010) method and (6) Chai et al. (2012) method. Description of the methods used is summarized in Paniagua et al. (2016). The t_{50} results from each individual method are presented in Table 4.

Normalised excess pore pressure U is plotted with the modified time factor, see Figure 4 and Figure 5, which used for estimation of c_h when t_{50} or t_{50c} is estimated from U with time. Comparison of U versus T^* for the dissipation tests with the Teh & Houlsby (1991) solution shows that in Figure 4 at 20% dissipation tests are in the dilatory phase and below the theoretical curve, with the except of 6.51 m test. After 60 to 70% dissipation the results are above the theoretical solution, again with the exception of 6.51 m test which follows the theoretical solution. As to be expected there is a perfect fit at 50% dissipation for all tests.

For the depth interval 8.5 to 10 m shown in Figure 5 most tests are below theoretical Teh & Houlsby (1991) solution in the initial 20% of dissipation. However test at 8.5 m fits the trend as it is not dilating. After 60% dissipation many tests are above the solution. The lack of fit after 60% dissipation with curves generally above the theoretical line for both depths intervals suggest that the dissipation in Halden silt is slower than the estimated based on the u_i and u_o conditions applied in the analysis, i.e. the t_{50} times may be longer. There is also a lack of fit at the initial 20% dissipation leading to challenges in getting a good fit overall.

In general Mantaras et al. (2010) and Chai et al. (2012) methods show lower t_{50} times compared to the classic shoulder, square root and logarithm (log) time methods. However in the two cases at 2 mm/s, one of which is monotonic, and the monotonic test at 8.50 m, Chai et al. (2010) shows higher t_{50c} times compared to the t_{50} from tests with

Table 4. Estimated t_{50} times using different methods.

Depth m	Rate mm/s	Shoulder† s	Sq. root† s	log time† s	Burns & Mayne (1998) s	Mantaras et al. (2010) s	Chai et al. (2012) t_{50c} s	St. dev. s
5.00	2	484	391	476		286	229	102
4.96	20	258	147	242		90	67	78
5.01	20	337	237	327		143	125	89
6.50*	2	264	264	264	283	114	244	58
6.51	20	188	126	173	308	112	42	83
6.62	320	126	99	122	248	89	43	64
8.50*	20	334	335	334		147	313	75
8.53	20	253	171	244		95	92	69
8.51	100	172	133	166		145	62	39
10.24	100	329	235	324		51	171	104
10.13	320	271	228	268		340	151	63

*Monotonic dissipation. †Sully et al. (1999).

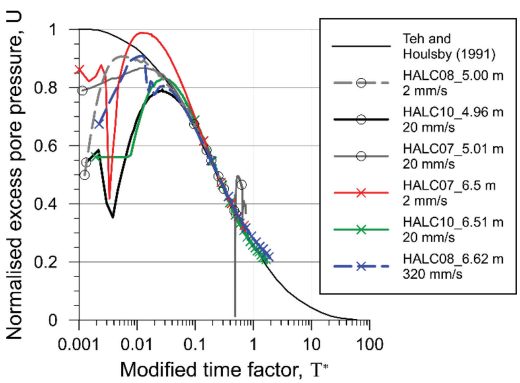

Figure 4. Normalised excess pore pressure vs. modified time factor T*, at 5 m & 6.5 m target depths.

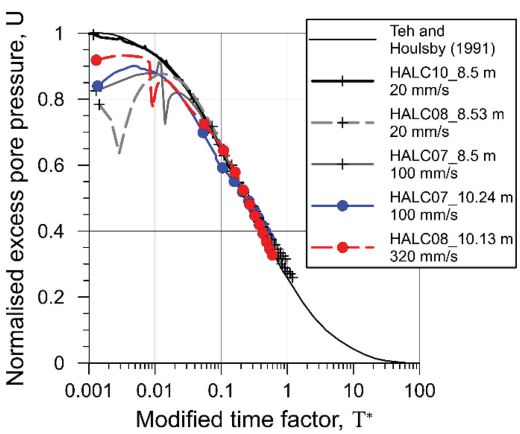

Figure 5. Normalised excess pore pressure vs. modified time factor T*, at 8.5 m & 10 m.

the standard and faster penetration rates at similar depths.

The t_{50} from the log time method is typically slightly lower than t_{50} from the shoulder method as t_0 is taken at time corresponding to u_{max} and not t_0 at the start of the test, as is used for the shoulder method. Hence the difference in t_{50} for these two is the time to u_{max} in a test. The log time method is based on a back extrapolation for u_i which estimates shorter t_{50} times compared to the shoulder and log time method. For the three results for Burns and Mayne (1998) results tend to be greater than the classic methods. Details on the methodology of the above methods is presented in Paniagua et al. (2016). The standard deviation of t_{50} based on the methods used is presented in Table 4 with values between approx. 40 and 100 s.

Overall there is a trend of increasing t_{50} with depth (without the results from 5 m as they are uncharacteristic of expected behavior due to higher sand contents and presence of the upper sand silty layer ending at 4.5 m (Blaker et al., 2016). It is possible that the monotonic test at 8.50 m at 20 mm/s shows a longer t_{50} due to missing data at the start of the test. This test was one of the two tests to show a monotonic response in the data set. The long t_{50} time is not in agreement with its neighboring test at 8.53 m which is also at 20 mm/s; which leads to likely grounds for exclusion of the monotonic tests for further analysis.

Results in Figure 6 are plotted using the square root method. This method was chosen for simplicity of visualization, it is widely known in practice as it is long established. Mean t_{50} values, based on all methods, show values reasonably close to the square root t_{50} values. Hence it is reasonable to use this method for discussion of results in the paper to assess trends with rate and depth.

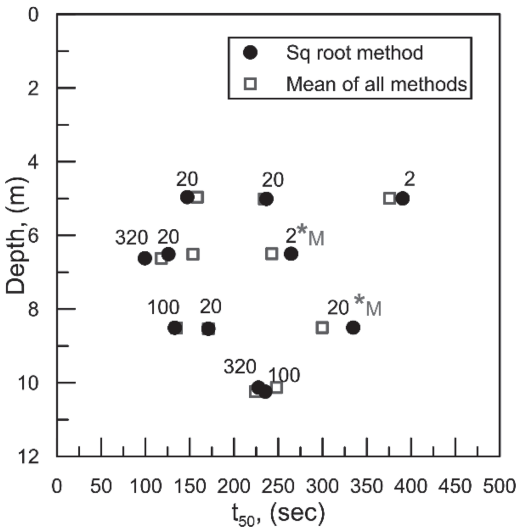

Figure 6. Estimated t_{50} using square root method with depth. Labels show the rate of penetration in mm/s. *M: monotonic tests.

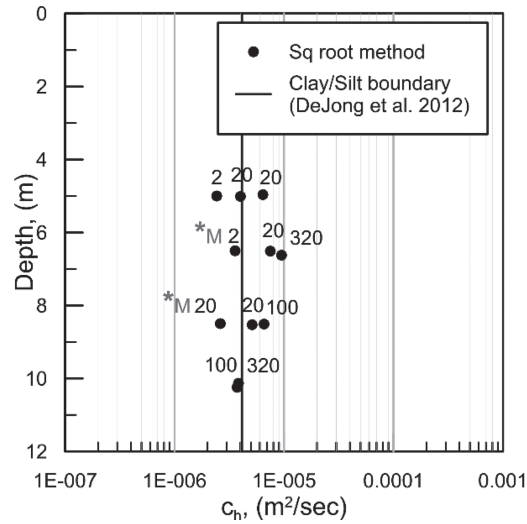

Figure 7. c_h based on estimated t_{50} using square root method with depth. Labels show the rate of penetration in mm/s. *M: monotonic tests.

4.2 *Rate effect on t_{50} times and c_h*

Table 4 shows that for rates of 320 mm/s, the standard deviation of t_{50} is lower than t_{50} at standard or slower rates. Figure 6 shows that with increased rate, t_{50} is lower. Table 3 shows that with increased rate, u_2 increased. These trends suggest that the high excess pore pressure generated during penetration at high rates dissipates faster than slower rate tests.

With decreased rate, there is increased scatter in the t_{50} values, with the values being typically longer. However based on the range of rates achievable, the order of magnitude may not have been enough to fully investigate the effect of faster or slower than standard rates.

The assessment if some tests are truly undrained using V was introduced earlier in the paper and values suggest some tests are truly undrained. For example results from 6.5 to 10.2 m that are dilatory suggest undrained soil behavior as V high. For these tests an increase in the penetration rate from 20 or 100 to 320 mm/s does not affect the interpreted t_{50} value considerably. These tests are in a uniform layer with high silt content and increasing fines and clay content with depth which contrasts to the shallower tests at 5 m with higher sand content and presence of a coarser layer directly above.

Trends for c_h will follow the behavior of t_{50} and the variation of results with depth are shown in Figure 7, based on estimated t_{50} using square root method. There is a trend of higher c_h with increasing v at 6.5 m and 8.5 m while at 10.2 m there is no change in c_h. The c_h values for the 5 m layer do not match the soil type and this confirms the assumption that these test are influenced by partial drainage and theories for use in fully undrained conditions do not apply to these tests, despite the V values shown in Table 3. In this case the B_q criteria from Senneset et al. (1989) is a good indicator. The monotonic tests suggest a c_h representative of a clay which contrasts with the c_h for tests at the same depth which are in the silty zone. Results from 10.2 m suggest low c_h values on the boundary between silt and clay. Overall for tests that are thought to be undrained, there is relatively little difference in c_h based on the rates achieved in the tests (excluding the monotonic tests).

5 CONCLUSIONS

A total of six methods were used to estimate c_h from dilatory dissipation tests following various penetration rates. The methods require input of I_r and t_{50} for estimation using the modified time factor T^* or other theoretical equations. Laboratory estimated I_r from advanced tests at this site agreed well with Krage et al. (2014) correlation which uses seismic in situ data (Method B) while the correlation using laboratory results (Method A) suggested slightly higher I_r values.

For monotonic dissipation tests the shoulder, log time, Burns and Mayne (1998) or Mantaras et al. (2010) methods may be used. Monotonic test in this paper were considered unreliable as longer uncharacteristic t_{50} times were found. It is suggested to carry out more than one test to confirm results in silty soil. Other unreliable tests were considered to be from the upper 5 m depth interval where tests were likely influenced by partial drainage and the presence of a coarser layer above. These tests were mostly dilatory.

Analysis of dilatory tests was carried out using all methods. Burns and Mayne (1998) method was limited to 3 test evaluations as unrealistic parameters were required for fitting. For cases with dilation effects, Chai et al. (2010) method estimate a short t_{50c} in comparison to alternative methods. Mantaras et al. (2010) method showed some scatter for the deeper set of test, as t_{50} from fastest test differed from t_{50} at slower rate both at similar depths. Suggesting that the monotonic tests may be unreliable. Overall the t_{50} values were somewhat greater than those estimated from Chai et al. (2010) method. These two methods gave t_{50} and subsequent c_h values that showed a reasonable match with laboratory c_v, ($0.7.10^{-5}$ to $1.0.10^{-5}$ m^2/s) compared to the lower c_h values estimated using the square root method. This suggests that these methods may capture the behavior in dilation better than the three classical empirical methods noted in the paper.

Based on the range of change in v, the response in u_2 and q_t show contrasting results for behavior of the soil from contractive to dilative respectively, as a result it is not possible to define the soil behavior.

V and B_q suggested change points from undrained to partially drained are not in agreement. If the tests at 10 m are in fact truly undrained, this would suggest that B_q in range of 0.2 to 0.24 at 20 mm/s (V = 180) is representative of an undrained response. Hence a lower threshold for use of undrained analysis in dissipation may be valid based on B_q as a guide. However further investigation of this is required for validation.

Dissipation results show that it is difficult to get a good fit for the full curve with the theoretical Teh and Houlsby (1991) solution, initial phase is conservative while later phase non conservative, e.g. after 60% dissipation curves are generally above the theoretical line. This suggests dissipation is in fact slower than what the classical methods suggest based on u_i conditions. However this is contrary to the suggestion based on c_v and comparison to the c_h estimated form Chai et al. (2010) and Mantaras et al. (2010), as noted previously.

At rates of 100 to 320 mm/s the standard deviation of t_{50} is lower than at standard or slower rates. This suggests that faster penetration rates in this silty site, with increases in u_2 as rate increases, reduces the scatter in t_{50} across the various methods investigated.

REFERENCES

Blaker, Ø., Carroll, R., L'Heureux J.-S. & Klug, M. 2016. Characterisation of Halden silt. *Geotechnical Site Characterization 5*. 25–42. Sydney; Australian Geomechanics Society.

Burns, S.E., Mayne, P.W. 1998. Monotonic and dilatory pore pressure decay during piezocone tests in clay. *Can Geotech J* 35: 1063–1073.

Carroll, R. 2013. The engineering behavior of Irish silts. Ph.D. dissertation, University College Dublin, Ireland.

Chai, J., Sheng, D., Carter, J.P. & Zhu, H. 2012. Coefficient of consolidation from non-standard piezocone dissipation curves. *Computers and Geotechnics* 41: 13–22.

DeJong, J. & Randolph, M.F. 2012. Influence of partial consolidation during cone penetration on estimated soil behaviour type and pore pressure dissipation measurements. *J Geotech Geoenviron Eng* 138: 777–788.

DeJong, J., Jaeger, R.A., Boulanger, R.W., Randolph, M.F. & Wahl, D.A.J. 2013. Variable penetration rate cone testing for characterization of intermediate soils. *Geotechnical Site Characterization 4*. 25–42. Sydney; Australian Geomechanics Society.

Finnie, I.M.S., & Randolph, M.F. 1994. Punch-through and liquefaction induced failure of shallow foundations on calcareous sediments. *Proc., Behaviour of Offshore Structures*, Vol. 1, Boston, 217–230.

Holmsgaard, R., Nielsen, B.N. & Ibsen, L.B. 2015. Interpreta-tion of cone penetration testing in silty soils conducted under partially drained conditions. *Journal of Geotechnical and Geoenvironmental Engineering*. ASCE 142(1).

Kim, K., Prezzi, M., Salgado, R., and Lee,W. 2008. Effect of penetration rate on cone penetration resistance in saturated clayey soils. *J. Geotech. Geoenviron. Eng.,* 1142–1153.

Mantaras, F.M., Odebrecht, E. & Schnaid, F. 2014. On the interpretation pf piezocone dissipation testing data. *Proc 3rd International Symposium on CPT*, Las Vegas, Nevada, USA.

Paniagua, P. 2014. *Model testing of cone penetration in silt with numerical simulations.* PhD. dissertation, NTNU, Norway.

Paniagua, P., Carroll. R., L'Heureux J.-S. & Nordal, S. 2016. Monotonic and dilatory excess pore water dissipations in silt following CPTU at variable penetration rate. *Geotechnical Site Characterization 5*. 509–514

Randolph, M.F. & Hope, S. 2004. Effect of cone velocity on cone resistance and excess pore pressures, *Proc., IS Osaka-Engineering Practice and Performance of Soft Deposits*, Osaka, Japan, 147–152.

Schneider, J.A., Lehane, B.M. & Schnaid, F. 2007. Velocity effects on piezocone tests in normally and overconsolidated clays, *Int. J. Phys. Modell. Geotech.*7 (2): 23–34.

Schneider, J.A., Randolph, M.F., Mayne, P.W. & Ramsey, N.R. 2008. Analysis of factors influencing soil classification using normalized piezocone tip resistance and pore pressure parameters. *J Geotech Geoenviron Eng* 134: 1569–1586.

Silva, M.F. 2005. *Numerical and Physical Models of Rate Effects in Soil Penetration,* PhD. thesis, Cambridge University.

Sully, J.P., Robertson, P.K., Campanella, R.G. & Woeller, D.J. 1999. An approach to evaluation of field CPTU dissipation data in overconsolidated fine grained soils. *Can Geotech J* 36: 369–381.

Teh, C.-I. & Houlsby, G.T. 1991. An analytical study of cone penetration test in clay. *Géotechnique* 41: 17–34.

Cone Penetration Testing 2018 – Hicks, Pisanò & Peuchen (Eds)
© 2018 Delft University of Technology, The Netherlands, ISBN 978-1-138-58449-5

Rapid penetration of piezocones in sand

S.H. Chow, B. Bienen & M.F. Randolph
Centre for Offshore Foundation Systems, The University of Western Australia, Australia

ABSTRACT: This study investigates the change in penetration resistance across different drainage regimes in sand using centrifuge piezocone tests. The model piezocone was jacked at various penetration rates into saturated loose and dense silica sand at gravitational acceleration of 50 *g*. In order to achieve a wider drainage regime, the sand was saturated using both water and a viscous pore fluid (methocel cellulose ether with viscosity 715 times higher than water). The results indicate the net cone resistance increases with increasing non-dimensional velocity in dense sand, but reduces with increasing non-dimensional velocity in loose sand. This rate dependency in sand can be captured using a simple harmonic backbone curve.

1 INTRODUCTION

The penetration resistance from a cone penetrometer test (CPT) is known to depend on the penetration rate, and in particular the soil drainage (or consolidation) conditions (e.g. Randolph & Hope 2004; DeJong & Randolph 2012). The effect of drainage conditions during penetration can be assessed within the established 'backbone curve' framework (Figure 1), whereby the drainage regime is related to the non-dimensional velocity, $V = vd/c_v$ or $V' = vd/c_h$ involving the velocity, v and penetrometer diameter, d and a coefficient of consolidation, either 'vertical', c_v, from laboratory oedometer tests or 'horizontal', c_h, from penetrometer dissipation tests. With increasing non-dimensional velocity, the soil behaviour will evolve from drained to partially drained, then undrained.

Rate effects on penetration resistance, arising from partial consolidation, have been studied extensively for contractive soils, such as normally consolidated or lightly overconsolidated clay. The condition for fully drained response has been established as $V_{dr} < 0.3$ and the undrained condition, $V_{un} > 30$ in normally consolidated clay (e.g. DeJong & Randolph 2012). In contractive soils, the penetration resistance, q is known to decrease with increasing V in the partially drained regime ($V_{dr} < V < V_{un}$). This is predominantly due to decreasing degree of consolidation of the surrounding soil but also with slight compensation (i.e. an increasing trend) arising from viscous rate effects. As $V > V_{un}$, viscous rate effects dominate with q increasing with increasing V (Figure 1).

On the other hand, rate effects on the penetration resistance in dilatant soil has been studied less, particularly in sand. Recent studies for dilatant soils have considered silica flour, heavily over-consolidated kaolin clay and clayey sand (e.g. Silva & Bolton 2004; Silva & Bolton 2005; Schneider et al. 2007; Suzuki & Lehane 2014). In sand, positive or negative effects of increasing penetration rate depend on the sand dilatancy, which is governed by the sand density, mineralogy and stress level (Bolton 1986). While loose sand is contractive, the penetration resistance in dense (dilatant) sand increases with increasing V (e.g. Te Kamp 1982). However, the transition between V_{dr} and V_{un} is unclear in sand as existing studies have mostly covered the drained and partially drained regimes with $V < 30$ (e.g. Finnie & Randolph 1994). In addition, the contribution of viscous rate effects remains uncertain, although commonly perceived as negligible in sand (e.g. Dayal & Allen 1975).

There is a need to examine rate effects for both loose and dense sand covering higher non-dimensional velocity, $V > 30$. Achieving high V in sand is

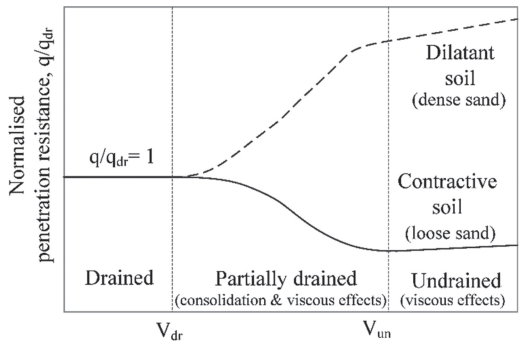

Figure 1. Drainage framework.

challenging experimentally due to the high hydraulic conductivity and stiffness (and thus c_v) of sand and technical limitations in achieving sufficiently high penetration velocity, v. To overcome this difficulty, this paper presents a centrifuge piezocone study covering V = 0.01 to 6662 in loose and dense silica sand saturated with a viscous pore fluid (methocel cellulose ether with viscosity 715 times higher than water at 20°C). The resulting reduction in consolidation coefficient, in combination with a high-speed actuator to increase the penetration velocity, v, allowed extremely high values of V to be achieved in the sand.

2 MODELLING CONCEPT USING VISCOUS PORE FLUID

In this study, modelling of $V = vd/c_v >> 30$ is achieved primarily by decreasing the coefficient of consolidation, c_v using a highly viscous pore fluid. The modelling concept of using a viscous pore fluid to satisfy similitude between physical model and prototype condition is now well accepted in geotechnical physical modelling, specifically in satisfying time scaling for dynamic events (e.g. Dewoolkar et al. 1999; Adamidis & Madabhushi 2015). The coefficient of consolidation c_v is directly related to the sand permeability k according to

$$c_v = \frac{km_v}{\rho g} \tag{1}$$

where m_v is the compressibility of the soil, ρ the density of the pore fluid and g the gravitational acceleration. The sand permeability is inversely proportional to the dynamic viscosity μ, since

$$k = \frac{K\rho g}{\mu} \tag{2}$$

where K is the intrinsic permeability of the soil.

Methocel cellulose ether Grade F450 with concentration, C = 2.2% (μ = 715 mPas at 20°C) was used as the viscous pore fluid in this study. The properties and preparation technique of the commercially available methocel F450 can be referred to Dow (2002). Methocel cellulose ether was selected here as it has been shown to produce similar constitutive behaviour as for soil saturated with water, in addition to having similar density to water (Dewoolkar et al. 1999). The viscosity of the methocel cellulose ether, a non-Newtonian fluid, is known to depend on the shear rate and temperature. These dependencies of the methocel F450 have been investigated in a series of viscometer tests considering a range of concentrations, shear rates and temperatures (Chow, unpublished data). The shear rate range considered in this study is found to have negligible influence on the measured viscosity of the methocel. The temperature dependency of the methocel F450 with C = 2.2% measured through the viscometer tests can be expressed as (Adamidis & Madabhushi 2015):

$$\frac{\mu_{T°C}}{\mu_{20°C}} = 2.44e^{-0.045T} \tag{3}$$

where $\mu_{T°C}$ is the viscosity at the desired temperature of T (°C) and $\mu_{20°C}$ the viscosity at 20°C.

3 CENTRIFUGE TEST DETAILS

3.1 *Soil properties & sample preparation*

Soil samples were prepared at two densities (loose, dense) and saturated with two different pore fluids (water, methocel) using a commercially available fine sub-angular silica sand. The index properties of the sand are summarised in Table 1. The coefficient of consolidation c_v of water-saturated sand at average relative density I_D = 50% was determined using Rowe cell tests as presented in Figure 2. The centrifuge sand samples were prepared in strongboxes with internal dimensions of 650 mm × 390 mm × 325 mm (length × width × depth). Two dense samples were prepared by air pluviation and another two loose samples were prepared by hand pouring the sand at minimal fall height into the strongbox.

Table 1. Properties of silica sand.

Specific gravity, G_s	2.67
Particle size, d_{10}, d_{50}, d_{60}	0.12, 0.18, 0.19 mm
Minimum dry density, ρ_{min}	1497 kg/m^3
Maximum dry density, ρ_{max}	1774 kg/m^3
Critical state friction angle, ϕ'_{cs}	31.6((triaxial)

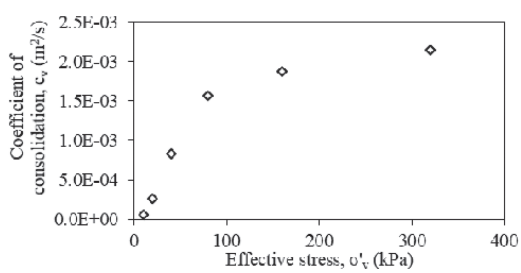

Figure 2. Coefficient of consolidation, c_v determined through Rowe cell tests.

The samples at each density were saturated using either water or methocel by gravity feed from the base of the sample. The final relative densities measured at the end of saturation are $I_D = 31\%$ and 83% for the loose and dense samples respectively. For the samples saturated with methocel, strong boxes with enlarged drainage feed of 10 mm diameter was used. An additional drainage layer of 10 mm aggregate (with height covering at least the top of the drainage feed) overlaid with a geofabric was also placed at the base of sample to further facilitate saturation with the highly viscous methocel (Figure 3). A layer of water or methocel with constant-height of 60 mm was maintained above the sand surface during testing. To avoid evaporation of the methocel during testing, a thin layer of organic oil was also placed above the methocel layer.

3.2 *Model piezocone*

The model piezocone has a cone and shaft diameter of 10 mm with a 60° cone tip (Figure 3). The stainless steel model piezocone is instrumented with tip and sleeve load cells and a pore pressure transducer located just above the cone shoulder (u_2 position). The filter for the pore pressure transducer is a 1.3 mm thick ring of polyethylene with a 35 µm pore size. The unequal area ratio, α was determined as 0.74 using a pressure chamber.

3.3 *Centrifuge test setup & procedure*

The centrifuge tests were conducted at 50 *g* gravitational acceleration using the beam centrifuge at the University of Western Australia. The use of centrifuge testing at higher gravity ensures essential similitude in soil stress between model and field conditions. The test setup is illustrated in Figure 3. The test program is summarized in Table 2. Three to four piezocone tests were conducted in each soil sample covering a range of penetration velocities, v = 0.6 to 100 mm/s using a high speed actuator. The resulting non-dimensional velocity, V (at mid-sample prototype depth z = 2.5 m) spans across 5-order of magnitudes, with V = 0.01 to 2 in the water saturated sample; and V = 1 to 1996 in the methocel saturated sample (Table 2). To ensure the reliability of the pore pressure data, saturation checks of the pore pressure transducer filter were performed before and after each test by cycling the piezocone up and down in the free water or methocel above the soil. Satisfactory saturation was indicated by a rapid response with little or no hysteresis in the data. Due to the temperature dependency of the methocel, a thermal probe was used to monitor the temperature of the pore fluid during the piezocone tests. The measured temperature maintained the same within the same piezocone test but varied between 20.2°C and 21.8°C across different tests depending on testing day and time.

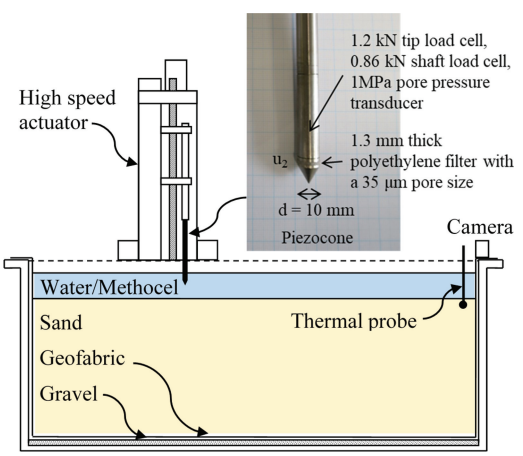

Figure 3. Centrifuge test setup and model piezocone details.

Table 2. Centrifuge test program.

Pore fluid	v (mm/s)	$V = vd/c_v$* Loose	Dense
Water	0.6	0.01	–
	6	0.1	0.2
	60	1	2
Methocel (C = 2.2%)	0.1	1	2
	6	74	120
	60	722	1198
	100	–	1996

*$c_v = 5.7 \times 10^{-4}$ m²/s at z = 2.5 m for loose samples; $c_v = 3.3 \times 10^{-4}$ m²/s at z = 2.5 m for dense samples.

4 TEST RESULTS

The test results are presented as profiles of net cone resistance, q_{net} and pore pressure at cone shoulder position, u_2 with penetration depth in prototype scale (Figure 4). The sleeve friction, f_s profiles are not discussed here due to high variability in the friction sleeve measurement. The net cone resistance, q_{net} is determined as $q_c + (1-\alpha) u_2 - \sigma_{vo}$, where q_c is the measured cone resistance and σ_{vo} is the total overburden pressure. The non-dimensional velocity, V is computed for each test by considering the coefficient of consolidation, c_v at the relevant stress level and relative density. For ease of reference, tests are identified as RVP, where

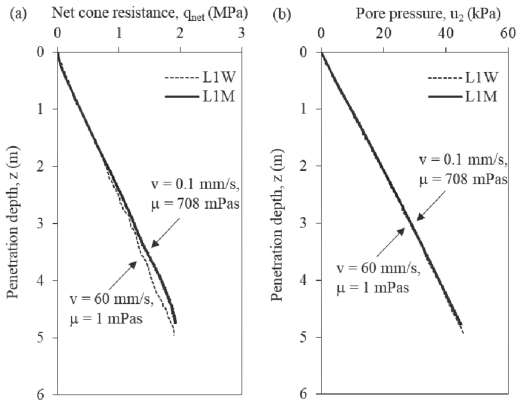

Figure 4. Validation of viscous pore fluid modelling concept.

R refers to the sample relative density (L for loose, or D for dense), V refers to the average non-dimensional velocity; and P refers to the pore fluid (W for water, or M for methocel). For instance, Test L0.1 W refers to a piezocone test at V = 0.1 in a loose sample saturated with water.

4.1 *Validation of modelling concept*

The modelling concept using viscous pore fluid discussed in Section 2 was validated using two piezocone tests conducted at the same non-dimensional velocity, V = 1, but in the loose samples saturated with different pore fluids. As demonstrated in Figure 4, good agreement was obtained with average difference of 5% between the two tests, confirming the validity of the modelling technique.

4.2 *Effect of drainage on piezocone response*

The q_{net} and u_2 profiles for all tests conducted in the loose samples are presented in Figure 5. The non-dimensional velocity, V ranges between 0.01 and 722 at mid-sample depth, z = 2.5 m of the loose samples (Table 2). As shown in the u_2 profiles in Figure 5b, the piezocone tests covering V = 0.01 to 1 produce a drained response with no development of excess pore pressure. The corresponding drained net cone resistance, $q_{net(dr)}$ at V = 0.01 to 1 appears to vary with 5 to 15% difference between the tests (Figure 5a). This variation in q_{net} could be a result of sample non-homogeneity; repeated testing on one of the tests (L0.1 W) indicated a 12% variation across the set of tests. Viscous rate effects could also contribute to the variation in q_{net} as preliminary testing using 1 g variable piezocone tests in dry sand indicated about 5% increase in cone resistance per log cycle increase in penetration velocity.

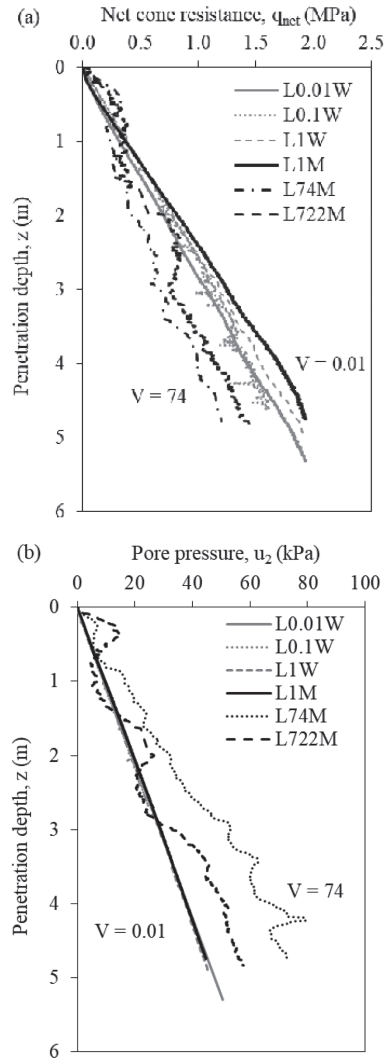

Figure 5. (a) q_{net}; and (b) u_2 profiles in loose samples.

On the other hand, the tests with V > 1 clearly exhibit a partially drained response with excess pore pressure developed in the contractive loose sand (Figure 5b). Corresponding to the generation of excess pore pressure, q_{net} at V = 74 decreases to about 67% of the drained net cone resistance. The test with the highest V = 722 also generated excess pore pressure, but to a lesser extent than the slower test with V = 74. As a result, q_{net} at V = 722 increased back to 82% of the drained net cone resistance. This rebound in q_{net} is believed to be a consequence of slight sample densification, which was later confirmed by a higher q_{net} measured in a repeat test on test L0.1M conducted at the end of the test program.

The q_{net} and u_2 profiles in the dense samples covering V = 0.2 to 1996 are presented in Figure 6. Initial comparison of the q_{net} profiles with equivalent V = 2 (tests D2 W, D2M) revealed that the water saturated sample was denser than the methocel saturated sample, despite both exhibiting drained response in the u_2 profiles. Hence examination of the drainage effects in dense sand is limited to the dense sample saturated with methocel covering V = 2 to 1996. Although missing the tests covering V < 2, it is reasonable to assume that all tests with V < 2 will exhibit essentially drained response based on the u_2 profiles in Figure 6b. In contrast to the loose sample, q_{net} increases with increasing V in the dense sample (Figure 6a). At the highest V = 1996, $q_{net(V = 1996)}$ is approximately 2.7 times higher than the drained resistance. This significant increase in q_{net} is caused by the sand dilatancy, evident in the suction generated for tests with V > 2 in Figure 6b. The suction is only observed at penetration depth, z > 0.7 m upon the full embedment of cone tip and u_2 sensor location.

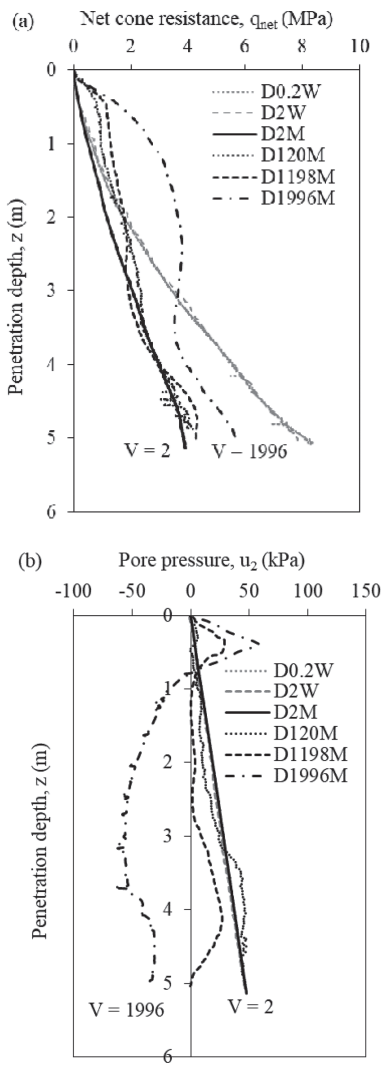

Figure 6. (a) q_{net}; and (b) u_2 profiles in dense samples.

4.3 *Backbone curves*

The rate effects in the piezocone tests in both loose and dense samples can be further examined using the backbone curve concept as shown in Figure 7. As mentioned in Section 4.2, the tests in the water saturated dense sample were excluded from Figure 7 due to the difference in sample density. The backbone curves present the variation in (a) net cone resistance normalised by the drained net cone resistance, $q_{net}/q_{net(dr)}$; and (b) excess pore pressure normalised by vertical effective stress, $\Delta u_2/\sigma'_v$ across the range of non-dimensional velocity, V considered in this study. The net cone resistance is normalised by the drained net cone resistance, $q_{net(dr)}$ here for penetration in sand, instead of the more typical normalisation by the undrained net

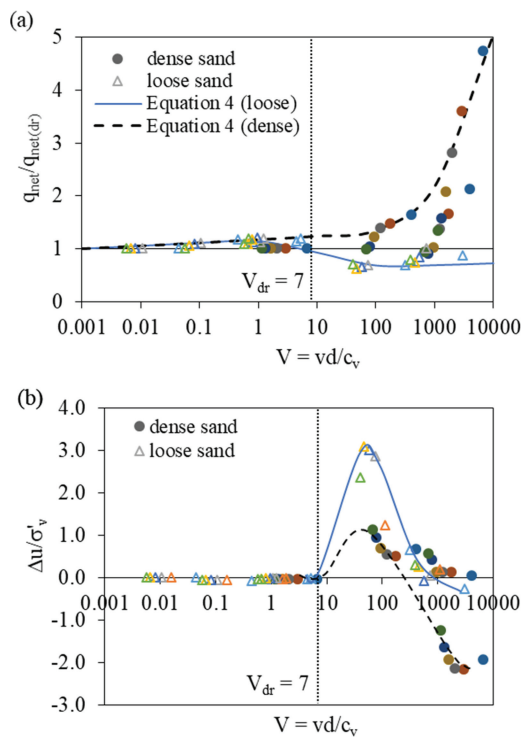

Figure 7. Backbone curves in sand: (a) $q_{net}/q_{net(dr)}$; and (b) $\Delta u_2/\sigma'_v$.

cone resistance, $q_{net(un)}$ for clay. The normalised parameters, $q_{net}/q_{net(dr)}$ and $\Delta u_2/\sigma'_v$ are computed and averaged over every 0.5 m penetration from z = 1 to 4 m. The range of penetration depth selected is to ensure the penetration resistance has achieved steady state. Taking into consideration the sample density and penetration depth range, the resulting non-dimensional velocity, V ranges between 0.01 and 4928 in loose samples and between 1.1 and 6662 in dense samples.

As shown in Figure 7, the transition from drained to partially drained condition appears to occur at $V_{dr} = 7$. This value is an order of magnitude higher than the value of $V_{dr} = 0.3$ reported for fine grained contractive soil. For $V > V_{dr}$, the loose and dense sand clearly exhibit different responses. The loose sand exhibits slight contractive behaviour with the normalised resistance decreasing to a minimum of $q_{net}/q_{net(dr)} = 0.6$ at V = 74. It is unclear whether undrained conditions have been achieved in the loose sample at the highest V investigated (V = 722). However, the normalised resistance does appear to increase slightly for V > 722. On the other hand, the dense sand clearly exhibits dilatant behaviour with $q_{net}/q_{net(dr)}$ increasing with increasing V. The most significant increase in the normalised resistance of $q_{net}/q_{net(dr)} = 4.7$ is achieved at the average penetration depth, z = 1.25 m and the highest V = 6662. The transition from partially drained to undrained conditions cannot be identified clearly here with the resistance continuing to climb in the dense sand. Hence more experimental data would be needed to determine the true V_{un} value.

In order to quantify rate effects in sand, the backbone curves in Figure 7 can be characterised as

$$\frac{q_{net}}{q_{net(dr)}} = \left[\frac{q_{net(un)}}{q_{net(dr)}} + \frac{1 - q_{net(un)}/q_{net(dr)}}{1 + (V/V_{50})^c}\right]\left(\frac{(v/d)}{(v/d)_{ref}}\right)^{\beta} \quad (4)$$

where q_{net} is the net cone resistance at V or v/d, $q_{net(dr)}$ the reference drained net cone resistance at $(v/d)_{ref}$, $q_{net(un)}$ the undrained net cone resistance at $V = V_{un}$, V_{50} the non-dimensional velocity for 50% consolidation, v/d the penetration velocity normalised by penetrometer diameter d, c a fitting coefficient and β the power law rate parameter. The first part of Equation 4 accounts for consolidation effects, whereas the second part of Equation 4 accounts for viscous rate effects using a power-law formulation.

Equation 4 is able to provide a reasonable fit to the experimental data in Figure 7. The best-fitted parameters ($q_{net(un)}/q_{net(dr)}$, V_{50}, c and β) for Equation 4 are summarised in Table 3. A unique value of V_{50} was not found between the loose and dense sand, but further validation is required using more experimental data.

Table 3. Best-fitted parameters for backbone curves.

Sample	q_{un}/q_{dr}	V_{50}	c	β
Loose	0.5	10	1.3	0.023
Dense	4	3000	1.3	0.023

5 DISCUSSION & CONCLUSIONS

This study has investigated rate effects arising from partial consolidation in piezocone tests in both loose and dense sand covering V = 0.01 to 6662. The wide range of V (spanning drained to undrained regimes) was made possible through the use of a highly viscous pore fluid. The physical modelling technique has shown promising potential in investigating partially drained to undrained behavior in sand, which will grow in importance with the recent growth in offshore renewable energy development involving shallow water depths with mainly sandy sediments.

The nature of the rate dependency in sand is found to be governed by the sand dilatancy, which is a function of sand density, mineralogy and stress level. In dense sand prevalent for field conditions, the study demonstrated significant increase in penetration resistance when V increases from drained to undrained conditions, accompanies by increasingly negative excess pore water pressure. In addition, for field application in relatively shallow water (< 30 m), it is expected the sand would cavitate, which would complicate determination of the undrained penetration resistance (Randolph et al. 2018).

The rate dependency in sand can be addressed using a simple backbone curve as expressed by Equation 4. The uncertainty in Equation 4 might be reduced by predicting the undrained resistance, $q_{net(un)}$ analytically, using the theoretical undrained shear strength of the sand based on critical state concepts (Been et al. 1991, Muir Wood 1990) and applying the relationships linking the sand dilatancy to the sand minerology, density and stress level (Bolton 1986). The framework also needs to make due allowance for cavitation for practical application in the field.

ACKNOWLEDGEMENTS

This work forms part of the activities of the Centre for Offshore Foundation Systems (COFS), currently supported as a node of the Australian Research Council Centre of Excellence for Geotechnical Science and Engineering and as a Centre of Excellence by the Lloyd's Register Foundation. The Lloyd's Register Foundation invests in science,

engineering and technology for public benefit, worldwide. The last author acknowledges support through the Fugro Chair in Geotechnics.

REFERENCES

Adamidis, O. & Madabhushi, G.S.P. 2015. Use of viscous pore fluids in dynamic centrifuge modelling. *Intern. J. of Physical Modelling in Geotechnics*, (Paper 1400022), 1–9.

Been, K., Jefferies, M.G., & Hachey, J. 1991. The critical state of sands. *Géotechnique* 41(3): 365–381.

Bolton, M.D., 1986. The strength and dilatancy of sands. *Géotechnique*, 36(1), pp.65–78.

Dayal, U. & Allen, J.H. 1975. The Effect of Penetration Rate on the Strength of Remolded Clay and Sand Samples. *Canadian Geotechnical Journal* 12: 336–348.

DeJong, J.T. & Randolph, M.F. 2012. Influence of partial consolidation during cone penetration on estimated soil behavior type and pore pressure dissipation measurements. *J. of Geotech. and Geoenviron. Eng.* 138(7): 777–788.

Dewoolkar, M.M., Ko, H.Y., Stadler, A.T. & Astaneh, S.M.F. 1999. A Substitute Pore Fluid for Seismic Centrifuge Modeling. *Geotechnical Testing Journal* 22(3): 196–210.

Dow 2002. *Methocel Cellulose Ethers: Technical Handbook*. The Dow Chemical Company, Staines, UK.

Finnie, I.M.S. & Randolph, M.F. 1994. Punch-through and liquefaction induced failure of shallow foundations on calcareous sediments. *Proc. Intern. Conf. on Behaviour of Offshore Structures*. Boston, MA, pp. 217–230.

Te Kamp, W.G.B. 1982. The influence of the rate of penetration on the cone resistance "q_c" in sand. *Proc. ESOPT*, Amsterdam, II, pp. 627–633.

Muir Wood, D.W. 1990. *Soil behaviour and critical state soil mechanics*. Cambridge University Press: England.

Randolph, M.F. & Hope, S. 2004. Effect of cone velocity on cone resistance and excess pore pressures. *IS Osaka*. The Hague, The Netherlands, pp. 147–152.

Randolph, M.F. et al. 2018. Penetrometer equipment and testing techniques for offshore design of shallow foundations, anchors and pipelines. *CPT18*, Delft.

Schneider, J.A., Lehane, B.M. & Schnaid, F. 2007. Velocity effects on piezocone measurements in normally and over consolidated clays. *International Journal of Physical Modelling in Geotechnics*, 2: 23–34.

Silva, M. & Bolton, M.D. 2004. Centrifuge penetration tests in saturated layered sands. *Proc. Intern. Conf. on Site Characterization*, pp. 377–384.

Silva, M. & Bolton, M., 2005. Interpretation of centrifuge piezocone tests in dilatant, low plasticity silts. *Proc. of Intern. Conf. on Problematic Soils*. pp. 1–8.

Suzuki, Y. & Lehane, B.M. 2014. Rate dependence of q_c in two clayey sands. CPT14, pp.411–418.

Taylor & Francis
Taylor & Francis Group
http://taylorandfrancis.com

Cone Penetration Testing 2018 – Hicks, Pisanò & Peuchen (Eds)
© 2018 Delft University of Technology, The Netherlands, ISBN 978-1-138-58449-5

Applying Bayesian updating to CPT data analysis

S. Collico, N. Perez & M. Devincenzi
Igeotest, Figueres, Spain

M. Arroyo
Department of Geotechnical Engineering, UPC, Barcelona, Spain

ABSTRACT: Evaluation of geotechnical parameters on a project site is a necessary step in geotechnical engineering. However, due to the inherent variability of soil properties and the lack of data, many unavoidable uncertainties arise during a site-specific geotechnical characterization. This challenging task can be addressed under the Bayesian framework. The aim of this paper is to apply the Bayesian approach to a reference example of friction angle evaluation in sand, using the Bayesian Equivalent Sample Toolkit (BEST). BEST is an Excel VBA program for probabilistic characterization of geotechnical properties. In particular, in this study the statistical analysis has been performed using CPT tests from reference field studies. The results obtained for one case study involving CPT are discussed.

1 INTRODUCTION

A major application of CPTu is in the evaluation of material properties for geotechnical units identified within a site. The description of a given unit property (e.g. the friction angle of a sand, ϕ') may be done in deterministic terms (a single value, eventually varying with depth) or in probabilistic terms. The latter approach is increasingly important, as the treatment of material uncertainties in geotechnical design becomes more formalized (e.g. in the selection of characteristic values for partial factor limit state design or in the application of direct reliability evaluation methods). The variability of geological processes is one fundamental component of a variation of geotechnical properties. Such variability is known in literature as inherent variability or "aleatory uncertainty". This irreducible component is increased by "epistemic uncertainty", comprising factors such as statistical error (lack of data), measurement error (inadequate equipment and/or operator errors), and transformation uncertainties (Phoon & Kulhawy 1999a). The latter component is particularly important for CPTu data, which may be directly used in design, but most frequently requires transformation models to obtain derived values. Within this context, Bayesian updating is an emerging framework (Gelman et al. 2013) well suited to handle the problem of material property evaluation under uncertainty conditions. Within geotechnics, Wang & Cao (2013) developed an equivalent sample method for Bayesian analysis in which different components of epistemic uncertainty may be treated. To do so the limited data acquired during site-specific investigation is combined with the so called prior knowledge, representing the information about the geotechnical property before any observation data are collected. The integrated knowledge (posterior knowledge), is then used to obtain a precise statistical description of the property by means of a numerical procedure known as Markov Chain Monte Carlo simulation. In order to avoid mathematical and statistical hurdles, Wang et al. (2016) developed an Excel toolkit, called Bayesian Equivalent Samples Toolkit (BEST), to evaluate the probability distribution and nominal value of the design parameters. The aim of this paper is to perform a statistical analysis, through BEST, of one design example, in which the observation data consist of four CPT tests.

2 UNCERTAINTY MODELLING

2.1 *Inherent variability*

Consider for instance a sand deposit, and its friction angle ϕ' as the design parameter X_D. According to Wang et al. (2015), which reports the probability distribution of different geotechnical parameters, inherent variability of friction angle

can be modelled using a normal random variable with a mean μ and standard deviation σ:

$$\phi' = \mu + \sigma \cdot z; \tag{1}$$

where z is a standard gaussian random variable. Note that the spatial variability of the friction angle is not considered herein.

2.2 *Transformation model*

In this study a linear semi-log regression, developed by Kulhawy & Mayne (1990), between ϕ′ and the normalized cone tip resistance q is considered (Fig. 1).

The regression equation is defined as:

$$\xi = \ln q = a\phi' + b + \varepsilon; \tag{2}$$

where q is the normalized cone tip resistance $q = (q_c/p_a)/(\sigma'_{v0}/p_a)^{0.5}$, which is a function of the effective stress σ'_{v0} and the atmospheric pressure p_a. The use of a stress-normalized regression like this implies a certain assumption about the effect of stress increases with depth on the data. The regression coefficients have values a = 0.209, b = −3.684, while the transformation error, ε, is a Gaussian random variable defined by a zero mean and a standard deviation $\sigma_m = 0.586$. It is worth noting that Equation 2 considers the transformation uncertainty of the regression model, through the ε term. Replacing Equation 1 in Equation 2 leads to:

$$\xi = \ln q = (a\mu + b) + a\sigma z + \sigma_m \varepsilon; \tag{3}$$

Thus, the normalized observation data ξ are treated as a Gaussian random variable with mean (aμ + b) and standard deviation $\sqrt{((a\sigma)^2 + \sigma_m^2)}$. The expression obtained makes clear that inherent variability (z) is independent from transformation uncertainty (ε).

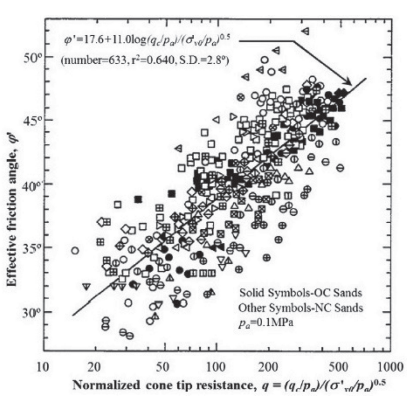

Figure 1. Regression analysis between ϕ′ and normalized cone tip resistance q (Kulhawy & Mayne 1990).

3 BAYESIAN FRAMEWORK

A key feature of Bayesian statistical approach is the integration of the prior knowledge of the model parameters (i.e. μ, σ of ϕ′) with the observation data (i.e. CPT), to obtain the posterior knowledge of the model parameters. Indeed, the latter can be expressed through Bayes theorem as (Cao & Wang 2013):

$$P(\mu, \sigma \mid Data, prior) = KP(Data \mid \mu, \sigma)P(\mu, \sigma); \tag{4}$$

where:

- Data = ξ_i with i = 1, 2 … n_c, are the observation data obtained during the site investigation in the sand layer;
- P (μ, σ) reflects the prior distribution of the model parameters μ and σ of X_D (ϕ′), without considering the observation data;
- P (Data| μ,σ) is the so called likelihood function, which expressed the probability density function (PDF) of the observation data, for a given set of μ and σ;
- $K = [\int_{\mu,\sigma} P(Data|\ \mu,\sigma)\ P(\mu,\sigma)d\mu d\sigma]^{-1}$ represents the normalizing constant which does not depend on μ and σ;
- P (μ,σ| Data,prior) is the update or posterior knowledge of the model parameters μ and σ of the design parameter X_D (ϕ′).

Note that from now on P (μ,σ| Data,prior) will be denoted as P (μ,σ| Data).

3.1 *Prior knowledge*

Two different types of prior distribution of the model parameters can be considered in the Bayesian approach:

- non informative (i.e. uniform distribution);
- informative (i.e. histogram, triangular, conjugated distribution).

The former is considered when no prior information on X_D is available for the project site. In this case a rough estimation of the prior knowledge was obtained through a literature review (Phoon & Khulawy 1999a, Cabalar 2010, Salgado et al. 2000, Naeini & Baziar 2004). Only the range of model parameters has to be considered; indeed, the prior is defined as a joint uniform distribution as:

$$P(\mu,\sigma)=\begin{cases}\dfrac{1}{\mu_{\max}-\mu_{\min}}\times\dfrac{1}{\sigma_{\max}-\sigma_{\min}}; & \text{for } \mu\in[\mu_{\min},\mu_{\max}] \\ & \text{and } \sigma\in[\sigma_{\min},\sigma_{\max}] \\ 0; & \text{otherwise}\end{cases} \tag{5}$$

Informative priors can be adopted when more information on X_D are available. As explained in the next section the use of such priors may increase the computational demands. Within the context of geotechnical engineering, a detailed analysis of available procedures for prior knowledge estimation is given in Cao et al. (2016).

3.2 *Likelihood function*

The likelihood function is defined as the PDF of the observation data for a given set of μ and σ. The Hypothesis of observation data as n_c independent Gaussian random variable, leads to:

$$P(Data\,|\,\mu,\sigma)=\prod_{i=1}^{nc}\frac{1}{\sqrt{2\pi}\sqrt{(a\sigma)^2+(\sigma_m)^2}}\times e\left(-0.5\left(\frac{\zeta_i-(a\mu+b)}{\sqrt{(a\sigma)^2+(\sigma_m)^2}}\right)^2\right) \tag{6}$$

It is worth noting that, when X_D (i.e. ϕ') is not measured directly, the likelihood is a function of both the probabilistic model M_P, used to model the inherent variability, and the transformation model M_T (Eq. 2). Hence, given a set of observation data, a comparison among different M_T can be carried out by evaluating Equation 6 for each transformation model. In this way the most suitable likelihood function for a better estimation of the posterior knowledge can be selected (Cao & Wang 2014).

3.3 *PDF of the friction angle*

Once the posterior knowledge is evaluated, the probability density function of friction angle is then obtained through the theorem of total probability as:

$$P(\phi\,|\,Data,prior)=\int_{\mu,\sigma}P(\phi\,|\,\mu,\sigma)P(\mu,\sigma\,|\,Data)d\mu d\sigma; \tag{7}$$

where P(ϕ|μ, σ) is the probability density function of the friction angle for a given set of model parameters; P(μ,σ|Data) is the posterior knowledge of model parameters. This process can be repeatedly applied. If several data sets are available (i.e. CPT, SPT), the posterior knowledge of model parameters, after CPT results are considered, may be used as prior knowledge to obtain the posterior probability distribution using the SPT values as input data. Such an approach is called Bayesian Sequential Updating (BSU) (Cao et al. 2016).

3.4 *Markov Chain Monte Carlo (MCMC) simulation*

When the prior knowledge and likelihood function are sophisticated, Equation 7 can be hard to solve explicitly or analytically due to the presence of the normalizing constant K. To bypass this inconvenience, the MCMC method is used, which, in this case, draws many equivalent sample of ϕ' from a target distribution, expressed by Equation 7. The samples drawn are then used for a statistical analysis of the parameter ϕ'. In particular, the Metropolis Hasting algorithm is used in the MCMC simulation (Hasting 1970, Wang & Cao 2013).

4 BAYESIAN EQUIVALENT SAMPLES TOOLKIT (BEST)

BEST is an Excel add-in that, using Excel VBA, implements MCMC to obtain Bayesian updates of geotechnical data statistics (Wang et al. 2016). The program is able to apply the Bayesian equivalent sample method for different soil types (i.e. clay, sand, and rock) with two different kinds of transformation models:

- built—in model;
- user—define model.

For the case of the "built-in model" option the transformation model M_T and its coefficients are already assigned. The inbuilt transformation models cover only a specific set of transformations, therefore requiring a particular set of input data. For the case of sand layers and friction angle the model 2.2 is featured, and the input data required are CPT data, and the prior knowledge of friction angle's model parameters (i.e. uniform distribution in the intervals [μ_{max}, μ_{min}], [σ_{max}, σ_{min}]). The "user-defined model" option is more flexible since is able to perform a statistical analysis of an arbitrary geotechnical parameter as long as the coefficients

and uncertainty of M_T are specified. The program also requires the input of several numerical parameters that control the MCMC algorithm operation. These include the number of Markov iterations (i.e. number of MonteCarlo runs), the number of equivalent samples obtained in each MonteCarlo run, the number of samples to discard from one step to the next of the Markov iteration. If the proposal distribution used in the Metropolis Hasting algorithm is characterized by a wrong starting point, a large sequence of equivalent samples is necessary to reach the stationarity distribution of MCMC simulation, which is called the burn-in period (Ravenzwaaij et al. 2016). Hence, the number of samples to discard should be large, since the firsts will not be reliable for the subsequent statistical analysis. BEST suggests picking up more than 31000 equivalent samples and discarding more than 1000 of them.

4.1 *Illustrative example*

The following design example is taken from Brito & Sorensen (2010). This section shows how to evaluate the probabilistic distribution of friction angle for a dense fine glacial outwash sand deposit for the construction of a pad foundation. Four CPT tests were carried out to a depth up to 8 m, whose profiles are reported in Figure 2. Note that each CPT test consist in eighty data values.

Firstly, a Bayesian equivalent samples method is carried out using the built-in model for sand. Due to the lack of information about the project site, prior knowledge is described by a joint uniform distribution of the model parameters (μ, σ) of ϕ (Eq. 5). Initially, the ranges of prior model parameters are taken from BEST under the command help (Table 1). This contains the typical range values of μ and σ for different design parameters according to the literature.

The "built-in model" for the estimation of ϕ requires the normalized cone tip resistance as input data, and these are related to the friction angle through Equation 2. Initially, one single run is considered, in which 31000 equivalent samples are selected and 1000 of them are discarded. Figure 3a and 3b show, respectively, the histogram of the friction angle values drawn, with all CPT values as input data, and the scatter plot of the equivalent sample. The 90% confidence interval is reported since BEST evaluate the 5% percentile and the 95% percentile.

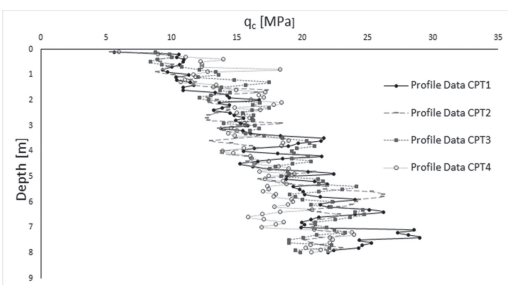

Figure 2. CPT data profiles.

Table 1. Range of prior values of μ and σ.

	μ_{max} (°)	μ_{min} (°)	σ_{max} (°)	σ_{min} (°)
Prior (BEST)	42	30	7.1	0.6
Prior (Phoon et al, 1996b)	41	35	6.97	1.27

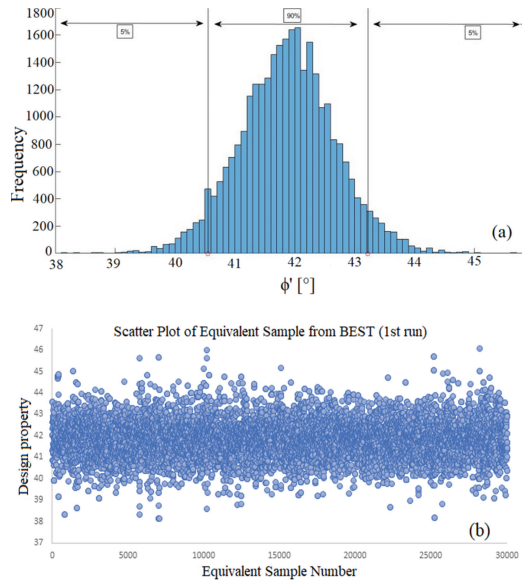

Figure 3. (a) Frequency of the friction angle drawn; (b) Scatter plot of the equivalent samples.

It is possible now to compare the obtained equivalent sample distribution to that of the original CPT data. To do so the equivalent samples generated are back-transformed into values of the measured property ξ through Equation 2 using the same coefficients a, b and σ_m adopted in the transformation model in BEST. In this way it is possible to evaluate 30000 values of the cone tip resistance q_c for a given depth D (assuming a constant bulk weight of 20 kN/m^3). The mean, the 5% percentile and the 95% percentile are plotted at each depth D alongside the measured data in Figure 4. The results show that almost all the data below 1 m are included in the 90% confidence interval. The anomaly at shallow depth points to some limitation of the transformation model M_T. Several reasons may be behind that anomaly: strength curvature at

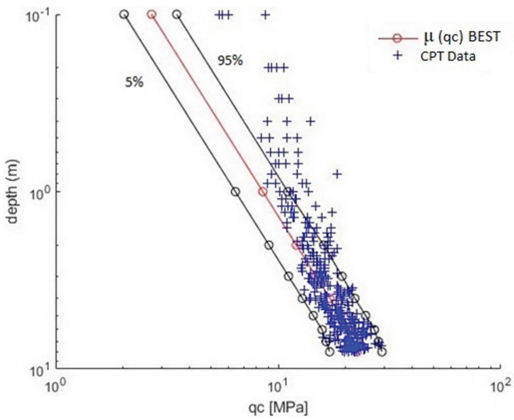

Figure 4. μ, 5% percentile, 95% percentile and data set.

very shallow stress levels, a relative increase in suction-derived effects and boundary effects on CPT tip resistance at shallow depths (Senders 2010).

4.2 *Effect of number of CPT input data*

The comparisons among the PDF and CDF of ϕ′ for different single CPT_i tests, with i = 1, 2 … 4, and the one with all the observation data, as input data, are plotted in Figure 5a and 5b respectively. The results show that, increasing the observation data the standard deviation is significantly reduced (between 12 and 18%) with respect to the estimate obtained using a single CPT. On the other hand, the estimated value of μ is approximately constant. It seems reasonable that increasing the number of observation data, if all of them are equally reliable, there is a reduction of the estimated parameter uncertainties; indeed, the likelihood function become more relevant than the prior increasing the number of data sets.

4.3 *Effect of prior knowledge*

The influence of the prior knowledge is analyzed using a different range of the model parameter μ and σ, taken from Phoon & Kulhawy (1999b) and reported in Table 1. Note that, for this comparison, all the CPT data are used as input data. The results in terms of PDF(ϕ′) and the statistics value for the two different cases are illustrated in Figure 6 and Table 3. It can be noticed that the difference between the two cases, in terms of 5% percentile, is 2.86°. Indeed, the prior distribution in BEST integrates the studies of Phoon & Kulhawy (1999b) with the ones of Cabalar 2010, Salgado et al. 2000, Naeini & Baziar 2004, in which micaceous sand, silty sand, and mixed and layered samples of sand are respectively analyzed. This provides a reduction of the prior range of the standard deviation

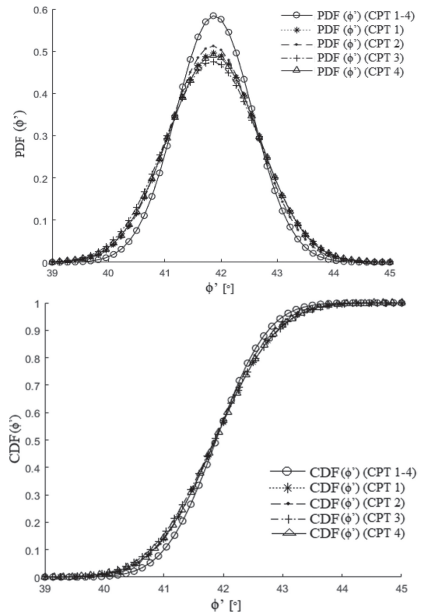

Figure 5. (a) PDF(ϕ′) for different input data; (b) CDF(ϕ′) for different input data.

Table 3. Range prior values from different sources.

Statistics	*No Prior*	*Prior* BEST	*Prior* Phoon & Kulhawy (1999b.)
μ (°)	43.3	41.87	40.93
σ (°)	1.13	0.68	1.83
5% (°)	42.02	40.73	37.87
95% (°)	45.9	43.92	43.96

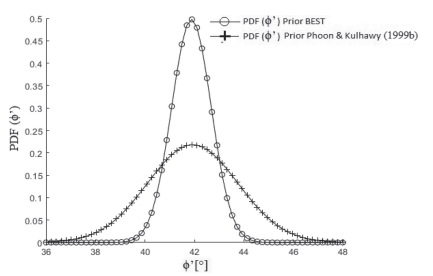

Figure 6. Probability density function of the friction angle using *prior* BEST and *prior* Phoon & Kulhawy (1999b).

and consequently a narrower estimation of PDF (ϕ′). Table 3 also includes the values that would be inferred from the data in the absence of any Bayesian updating: the friction estimate increases, skewed by the shallow data points.

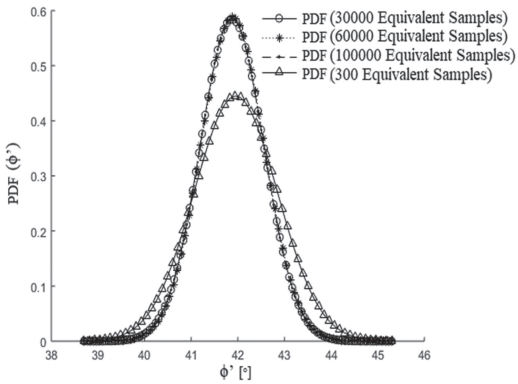

Figure 7. Probability density function of the friction angle for different sequences of equivalent samples.

4.4 *Effect of numerical parameters*

As mentioned in the previous section, a key step for the convergence of MCMC simulation is the definition of the number of equivalent samples to draw and the ones to discard for each run. The initial proposal distribution implemented in BEST, is characterized by a μ and σ equal to half of the prior mean and the standard deviation range (i.e. 36°, 3.25°), which represent a reliable starting point (Ravenzwaaij et al. 2016). To test this, several runs, with 310, 31000, 62000 and 110000 equivalent sample are conducted. The samples discarded for each run are respectively 10, 1000, 2000 and 10000. The results are illustrated in Figure 7. As suggested by BEST, 31000 equivalent samples are enough to reach convergence; indeed, no relevant difference exists among PDFs with more samples. On the other hand, as expected, a limited number of samples (i.e. 300) results in less accurate estimations, with broader probability distributions of ϕ′ and a wider 90% confidence interval.

5 CONCLUSION

In this paper, the Bayesian Equivalent Samples Toolkit, has been tested on a four CPT data set to estimate friction angle. As shown by the example analyses presented, this kind of numerical approach practically eliminates statistical error and concentrates the effort of the designer on the description of previous knowledge (prior) and in the selection of transformation models.

ACKNOWLEDGMENT

The first author's work has been supported by the European Innovating Training Network SLATE (H2020-MSCA-ITN-201).

REFERENCES

Brito, J. & Sørensen, C.S. 2010. Design Example 2.1 – Foundation with central vertical load, presentation at 2nd Int. Workshop on the Evaluation of Eurocode 7, *Pavia, Italy, recovered from www.eurocode7.com/etc10/Pavia/proceedings.html*.

Cabalar, A. 2010. Application of the oedometer, triaxial and resonant column tests to the study of micaceous sand. *Engineering Geology* 112: 21–28.

Cao, Z. & Wang, Y. 2013. Bayesian approach for probabilistic site characterization using cone penetration tests. *J. Geotech. Geoenviron. Eng*. 139 (2): 267–276.

Cao Z. & Wang, Y. 2014. Bayesian Model comparison and characterization of Undrained shear strenght. *Journal of Geotech. and Geoenviron. Engineering* (04014018) 140 (6): 1–9.

Cao, Z. Wang, Y. & LI, D.-Q. 2016. Site-specific characterization of soil properties using multiple measurements from different test procedures at different locations - A Bayesian sequential updating apporoach. *Engineering Geology* 211: 150–161.

Cao, Z. Wang, Y. & LI, D. 2016. Quantification of prior knowledge in geotechnical site characterization. *Engineering Geology* 203: 107–116.

Gelman, A. Carlin, J.B. Stern, H.S. Dunson D.B. Vehtari, A., and Rubin, D.B. 2013. *Bayesian data analysis* (third edition). Boca Raton: CRC press.

Hasting, W.K. (1970). Monte Carlo sampling methods using Markov chains and their application. *Biometrika* 57: 97–109.

Kulhawy, F.H. & Mayne, P.W. 1990. Manual on estimating soil properties for foundation design. *Report EL-6800*. Palo Alto (CA): Electric power research institute.

Naeini, S.A. & Baziar, M.H. 2004. Effects of fine content on steady-state strength of mixed and layered samples of sand. *Soil Dynamics and Erthquake Engineering* 24: 181–187.

Phoon, K.K. & Kulhawy, F.H. 1999a. Characterization of geotechnical variability. *Canadian Geotechnical Journal* 36 (4): 612–624.

Phoon, K.K. & Kulhawy, F.H. 1999b. Evaluation of geotechnical property variability. *Canadian Goetechnical journal* 36 (4): 625–639.

Ravenzwaaij, D. Cassey, P. & Scott, D.B. 2016. A simple introduction to Markov Chain Monte-Carlo sampling. Avaliable on Springlerlink.com. *Psychonomic Bulletin & Review*: 1–12.

Salgado, R. Bandini, P. & Karim, A. 2000. Shear Strength and stiffness of silty sand. *J. Geotech. Geoenviron. Eng.* 126 (5): 451–462.

Senders, M. 2010. Cone resistance profiles for laboratory tests in sand. *2nd international symposium on cone penetration testing CPT10* 2: 193–200.

Wang, Y. & Cao, Z. 2013. Probabilistic characaterization of Young's modulus of soil using equivalent samples. *Engineering Geology* 159: 106–118.

Wang, Y., Zhao, T., & Cao, Z. 2015. Site-specific probability distribution of geotechnical properties. *Computers and Geotechnics* 70: 159–168.

Wang, Y. Oluwatosin, V. & Cao, Z. 2016. Bayesian Equivalent Sample Tookit (BEST): an Excel VBA program for probabilistic characterization of geotechnical properties from limited observation data. *Georisk: Assesment and Management of Risk for Engineered System and Geohazard* 10: 251–268.

Cone Penetration Testing 2018 – Hicks, Pisanò & Peuchen (Eds)
© 2018 Delft University of Technology, The Netherlands, ISBN 978-1-138-58449-5

Geotechnical characterization of a very soft clay deposit in a stretch of road works

R.Q. Coutinho & H.T. Barbosa
Federal University of Pernambuco – UFPE, Recife, Brazil

A.D. Gusmão
Polytechnic School of the University of Pernambuco – UPE, Recife, Brazil

ABSTRACT: The practice of piezocone testing for geotechnical investigations is advantageous for rapidly obtaining parameters, continuous assessment of a soil profile and ability to estimate various geotechnical parameters. However, its results require attention regarding its implementation and interpretation, especially when the aim is to perform a geotechnical characterization of an area or deposit. This paper addresses in situ tests (SPT, vane and piezocone tests) and laboratory tests of a stretch of road works located in Pernambuco, Brazil. Stratigraphic classification, compressibility and strength parameters were obtained through piezocone tests and compared to laboratory (oedometer and triaxial) and in situ (SPT, vane) tests as benchmarks. The final results were discussed within the context of results in the literature, including the results of the Recife (Coutinho 2007) and Suape (Coutinho and Bello 2012) soft clays, confirming the potential of the piezocone test to obtain good prediction of geotechnical parameters in these soft clay deposits with correlations suited to the local/regional experience.

1 INTRODUCTION

In recent years, geotechnical engineering has evolved considerably in field investigations and modern practices, which are useful for estimating geotechnical parameters from the reference tests, such as the piezocone test (CPTu). In Brazil, there is a wealth of experience in the use of this test in soft soils, such as the articles discussed and presented by Coutinho (2007), Coutinho and Bello (2012) and Almeida and Marques (2013). Important work that brings together the main activities with the CPTu in South America, specifically Brazil, was presented by Coutinho and Schnaid (2010).

The purpose of the present study is to perform a geotechnical characterization of a soft clay deposit in a stretch of road works, using onsite and laboratory investigations, focusing on the parameters obtained and estimated by the CPTu test, mainly those related to the proposed stratigraphic classification, compressibility and strength behavior.

2 EXPERIMENTAL PROGRAM

2.1 *In situ tests*

From a comprehensive investigation involving a significant amount of SPT, vane shear, piezocone tests and Shelby tube samples, along five kilometers of road works, some tests were chosen for a sub-stretch as representative of the soft clay deposit. Two SPT boreholes, two vertical vane shear tests (VST), two vertical CPTu tests and two undisturbed Shelby tube samples (ϕ4") (Figure 1), were all run in accordance with Brazilian and international standards.

The SPT borehole identified a thick layer of very soft organic clay, approximately 12 m in depth and N_{SPT} ranging from 0/45 (no blows, only the weight of the hammer) to 2. The remaining identification tests were then carried out to characterize this deposit.

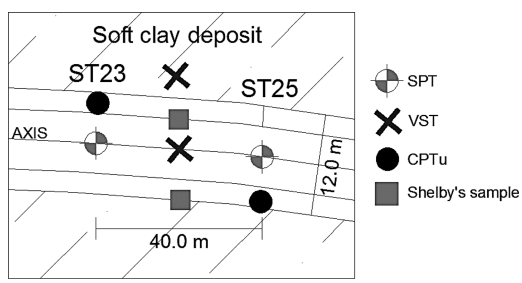

Figure 1. Experimental program—study area.

2.2 *Laboratory tests*

Based on undisturbed Shelby tube sampling (ϕ4”) in the laboratory according to Brazilian standards, tests of characterization, specific gravity (γ_n), organic matter content (OC), oedometer and triaxial UU-C were performed at depths of 2.4 m, 4.4 m, 6.4 m and 10.4 m, corresponding to layers of organic clay identified by SPT. All tests were used to compare the results of measurements and estimations of the CPTu test (Figure 4).

3 SITE CHARACTERIZATION

3.1 *Location and soil profile*

The study area is located within the Suape Industrial and Port complex, Ipojuca, Pernambuco, Brazil. The area is described as an extensive thick plain of sedimentary clay soils, saturated, with low bearing capacity, organic matter present and, in some cases, occurrence of seashells and sand lenses in the profile.

It is a practical case of state highway works that rests on soft soil deposit across a landfill with an average height of 5 m. Through the integrated analysis of all results it was possible to split the deposit profile into four (4) layers. Layer 1 (L1:0.0–2.0 m) consists of soft clayey silt; layer 2 (L2:2.0–6.0 m) very soft organic clay; layer 3 (L3:6.0–13.0 m) soft organic silt clay and layer 4 (L4:13.0–16.0 m) medium to hard clayey silt (Figure 3).

3.2 *Laboratory tests*

All laboratory tests were carried out on layers L2 and L3. The characterization tests showed that the soil in layer L2 has a clay content varying between 50% and 75%, silt between 20% and 50% and sand <10%, similar to layer L3, which had less fines at the beginning of the layer compared to the deeper levels. The natural moisture (W_n) in layer L2 varied from 159% to 185%, and layer L3 from 203% to 131%. The Atterberg limits were 70% for W_P in layer L2 and 62% in layer L3; the W_L in layer L2 ranged from 168% to 180%, and layer L3 138% to 168%. In general, the W_n values in layers L2 and L3 were close to their respective values of W_L (Figure 5), presented PI values ranging from 73% to 113%.

The analyzed samples were under the plasticity line, showing characteristics consistent with organic clays examined by Coutinho et al. (1998), which include Juturnaíba and Recife clays (Figure 2). The classification, according to USCS, for layers L2 and L3 was CH, “clay with high compressibility”.

The average organic matter content (OC) of the two layers (L2 and L3) was 12.42% ± 1.00.

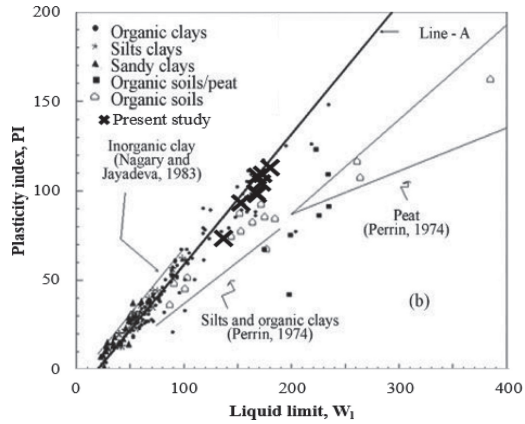

Figure 2. Casagrande plasticity chart (from Coutinho et al 1998).

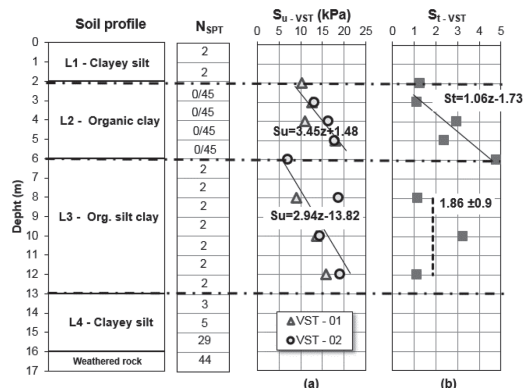

Figure 3. Results of vane shear test.

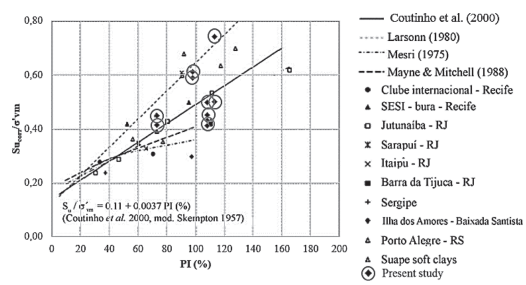

Figure 4. Resistance-ratio, S_u/σ'_{vm} (Coutinho and Bello 2012).

According to Huang et al. (2009), both layers can be classified as organic mineral soil. The oedometric tests showed that layer L2 has a rise in initial voids (e_0), and drop in layer L3. The OCR at the beginning of layer L2 was around 2.6 with a

downward trend, while layer L3 presented values of OCR of 1.6 on the surface, with the tendency to 1.0 at greater depths. In relation to the compression index (C_C), layer L2 had average values around 1.2, while the layer L3 values were close to 1.5. The values of S_u along the two layers (L2 and L3), obtained from triaxial compression tests of type UU, were around 12.75 ± 0.72 (Figure 5).

3.3 *Vane shear test (VST)*

Two S_u trends were observed for layers L2 and L3, increased linearly in both layers the values. In layer L2, $S_u = 3.45z + 1.48$, and layer L3 with values of $S_u = 2.94z - 13.82$ (Figure 3).

The layer L2 sensitivity varied linearly according to $S_t = 1.06z - 1.73$, with values close to one (1) at the beginning and reaching five (5) at the end of the layer, with ratings ranging from slightly to very sensitive clay ($1.0 < S_t < 5.0$), according to Rosenqvist (1953). In layer L3, the sensitivity showed little variability, with average value of 1.86 ± 0.9, with ratings ranging from insensitive to slightly sensitive clay.

Figure 4 shows the $Su_{VSTcorr}/\sigma'_{vm}$ x IP (%) proposed by Mesri (1975), Larsson (1980), Mayne and Mitchell (1988), Coutinho et al. (2000) modified from Skempton (1957), and Coutinho and Bello (2012), together with the mean values of various Brazilian clays, including Recife and Suape clays. The proposal by Coutinho et al. (2000) represents clays from Recife-PE, Juturnaíba-RJ, Sarapuí-RJ and satisfactorily for Suape clays (Coutinho and Bello 2012). For this analysis, S_u values were corrected according to Bjerrum (1973), with average PI of 98% corresponding to a factor of $\mu = 0.61$.

The points of the study herein matched the proposal by Coutinho et al. (2000), between the correlations of Larsson (1980) and Mayne and Mitchell (1988), forming the upper and lower limits, respectively.

3.4 *Piezocone tests*

The measures of the piezocone test, in the two verticals, were consistent with the SPT borehole profiles. It was found that layers L1 and L4 show greater resistance, not evidencing behavior in the intermediate layers (L2 and L3), identified by SPT as "Organic clay, very soft, dark grey". Figure 6 presents the measurements (q_t, f_s, u_2) and derived parameters (Q_{t1}, F_r, R_f, B_q) of CPTu testing. According to EN-ISO 22476-1, the piezocone

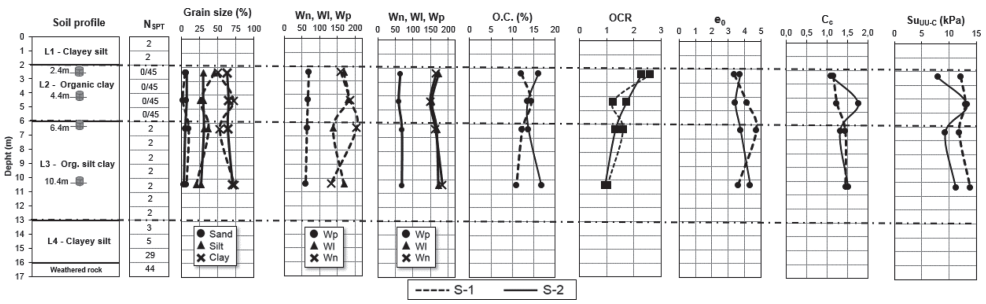

Figure 5. Profile geotechnical characteristics.

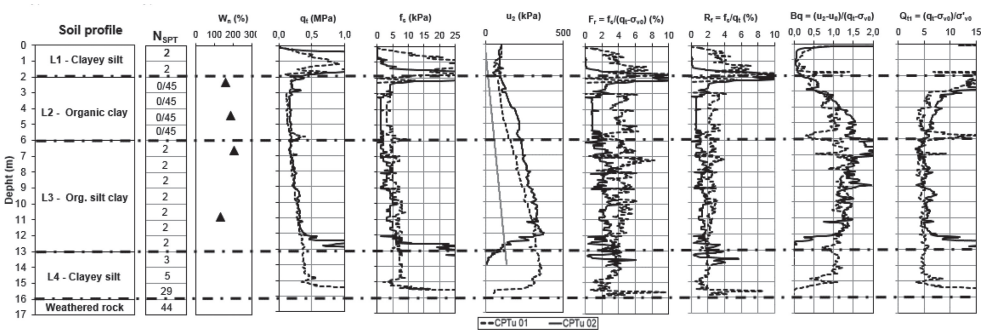

Figure 6. Measurements and derived parameters from piezocone tests (CPTu-01 and CPTu-02).

measurements of the L2 and L3 layers were in application class 1, consistent for soft soil deposits.

4 DISCUSSIONS ON PIEZOCONE TESTING

4.1 *Soil behavior type (SBT)*

The soil profile behavior was analyzed using the charts with normalized and non-normalized parameters. In order to define the layers, the non-normalized charts (Robertson, 2010) showed more consistency with the information in accordance with the SPT research and laboratory testing.

Considering the CPTu-01, the I_{SBT} profile (non-normalized) resulted in the varying its behavior from "clay to silt clay" (zone 3) in layer L1. In the layer L2 it presented behavior of "organic matter" (zone 2) and in layer L3 the I_{SBT} returned to the zone 3. In layer L4, the soil was interpreted as "clayey silt to silty clay" (zone 4) and "silty sand to sandy silt" (zone 5), a depth that showed greater strengths. For the CPTu-02, layers L1 in zones 5, 4 and 3, and layers L2 and L3 behaved as "clay to silt clay" (zone 3), and in layer L4 the I_{SBT} was between zones 4, 5 and 6, a layer that responded to the cone of higher resistance (Figure 7).

The non-normalized charts of Robertson (log q_c/p_a-log R_f and log q_t-B_q) were clear in the concentration of points of layer L2 between zones 2 and 3, indicating behavior consistent with laboratory tests results (organic clay) (Figures 8 and 9). Moreover, the charts showed that layers L1 and L4 behave differently in relation to layers L2 and L3, except for a few points that represent transition layers.

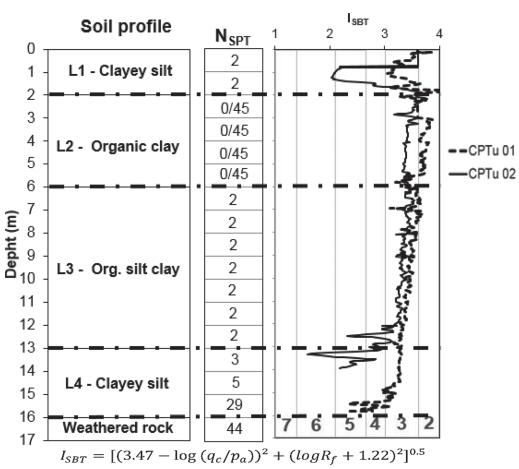

Figure 7. Non-normalized SBT index, CPTu-01 and CPTu-02, from Robertson (2010).

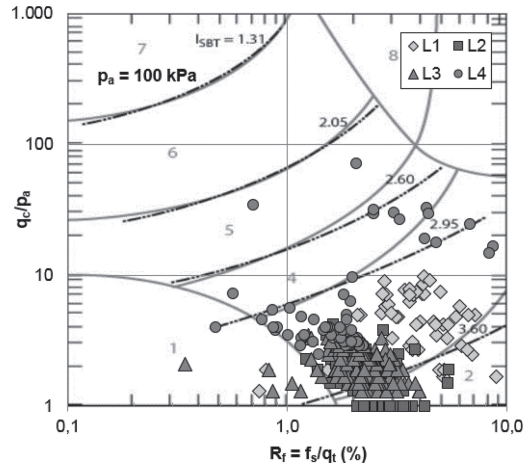

Figure 8. Non-normalized SBT chart—CPTu-01.

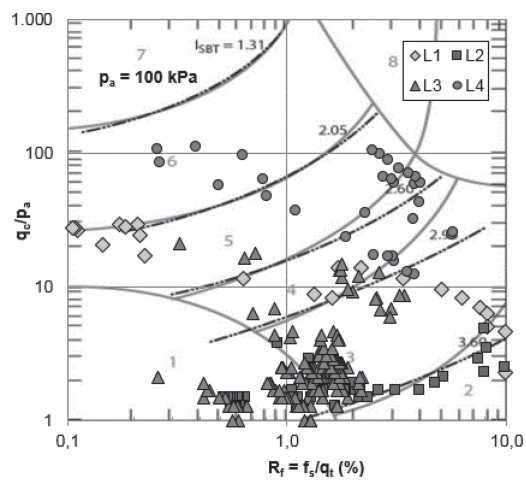

Figure 9. Non-normalized SBT chart—CPTu-02.

4.2 N_{kt}

The cone factor (N_{kt}) is a value that establishes the relationship between the undrained strength obtained by direct testing and strength measured by the CPTu test (Eq. 1).

$$N_{kt} = \frac{(q_t - \sigma_{v0})}{Su_{VST}} \tag{1}$$

where N_{kt} = cone factor, q_t = corrected cone resistance, σ_{v0} = vertical total stress in situ and S_{uVST} = undrained strength from vane shear test.

Having as benchmark the values of S_u obtained by the vane shear tests, along the profile, the value of N_{kt} in this study ranged from 7 to 13, with a

mean value of 10 ± 3, obtained by linear regression (Figure 10a). In addition to this analysis, a study was run on the variation of N_{kt} along the depth of the profile in layers of soft soil (L2 and L3). In layer L2, N_{kt} decreased linearly, namely N_{kt} = 16.41–1.72z, while layer L3 N_{kt} showed little variability, with an average value of 11.5 ± 0.9 (Figure 10b). All values found agree with results checked for Suape clays according to Coutinho and Bello (2012), close to the range presented by Coutinho (2007) for the Recife clays (N_{kt} = 12 ± 1.3) and within the average N_{kt} range for Brazilian clays (9–12) by Coutinho and Schnaid (2010).

Robertson (2012) proposed an estimation of N_{kt} from the of F_r values, according to Equation 2.

$$N_{kt} = 10.5 + 7\log(F_r) \quad (2)$$

The N_{kt} obtained as proposed by Robertson (2012) was with an average of 14.61 ± 1 (Figure 10a), slightly outside the range in the study herein and the Brazilian range.

4.3 *Estimated parameters*

Geotechnical experience confirms the efficiency of the CPTu in estimating parameters. For the present study, the preconsolidation pressure (σ'_p) was estimated as proposed by Chen and Mayne (1994) adapted by Coutinho et al. (2000) for the Recife clays, $\sigma'_p = K_1(q_t - \sigma_{v0})$ (where K_1 = 0.222 for z <4.0 m and K_1 = 0.244 for z > 4.0 m). The K_0 values were estimated by Kulhawy and Mayne (1990), $K_0 = 0.1.Q_{t1}$ and the OCR values were estimated as proposed by Kulhawy and Mayne (1990) (OCR = $\alpha.Q_{t1}$) adapted to the Suape clays by Coutinho and Bello (2012) (α = 0.17). The undrained strength (S_u) was estimated from the N_{kt} obtained by the VST test ($S_u = (q_t-\sigma_{vo})/N_{ktVST}$).

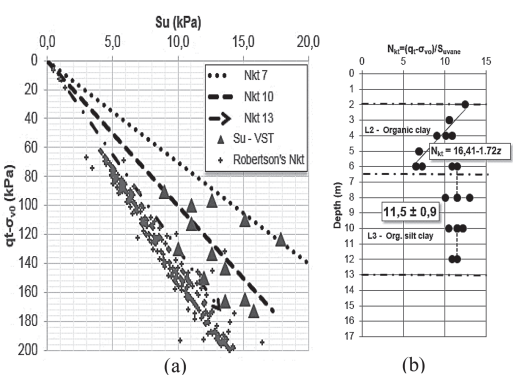

Figure 10. N_{kt} study: (a) general analysis; (b) in the profile.

The estimated preconsolidation pressure (σ'_p) in layer L2 ranged from 22 to 36 kPa, with a slight decrease to half the layer (4 m), continuing to increase after that depth, remaining in the range of laboratory values that was 20 and 30 kPa. The interface of layers L2 and L3 peaked at values of 80 kPa. In layer L3 the σ'_p increases linearly to a value of 60 kPa, following a similar trend of laboratory values (33 to 35 kPa). The CPTu-02 results were very close to the CPTu-01, but not recognizing the stronger layer at the interface of layers L2 and L3.

The OCR values in the layer L2 dropped from 2.6 to 1.0, indicating possible overconsolidation of this layer. In layer L3, OCR values were close to 1.0. The laboratory results for layer L2 varied from 2.61 to 1.24, and layer L3 from 1.60 to 1.03, showing the same tendency of the estimated results. Peak values were seen in layers L1 and L4.

The K_0 estimated by CPTu-01 had an average value of 0.51 ± 0.1 for layers L2 and L3. In the same layers, the estimated K_0 with the CPTu-02 results were 0.54 ± 0.2. In the layer L3, K_0 values were coherent with normally consolidated (NC) clays and local experiences.

The interpretation of the estimated S_u, values by means of the CPTu tests, enabled layer L2 to be split into sub-layers.

In the vertical S_u estimated by CPTu-01, two sub-layers of layer L2 were found, the first (L2.1: 2.0–5.3 m) with a slight drop to half the sub-layer, then a slight rise, with average values of 9.9 kPa ± 1.9. The second sub-layer (L2.2: 5.3–6.1 m) with values around 26 kPa ± 11.8. The layer L3 showed linear growth, S_u = 1.67z-4.38 (Figure 12a). Vertical S_u of CPTu-02, S_u in layer L2 varied according to linearity S_u = 80.14–14.29z, and layer L3, S_u = 2.33z-8.58 (Figure 12b). Similar to that observed in other estimates, Su's estimates remained close to laboratory values (Fig. 11).

Coutinho and Bello (2012) undertook an important study on Suape clays and using piezocone tests, found, in the analyzed profiles, a thick layer of organic clay. As in the study herein, the authors found OCR varying from 2 to 3 at low depths and bordering 1 for depths greater than 3 m, and estimated S_u values in the range of 9 to 16 kPa.

While not identified by SPT and laboratory tests, the CPTu-01 did show a sub-layer (L2.2), with behavior different from the thick layer of organic clay. For this layer, although presenting higher values of tip resistance and lateral friction, it cannot be argued that it is a sand lens, since the value of u_2, despite a slight decrease in this region, still remained high.

This discussion is supplemented by the results of I_{SBT}, in Figure 8, which shows that this layer did not leave zone 3, i.e. it continued to behave as "clay

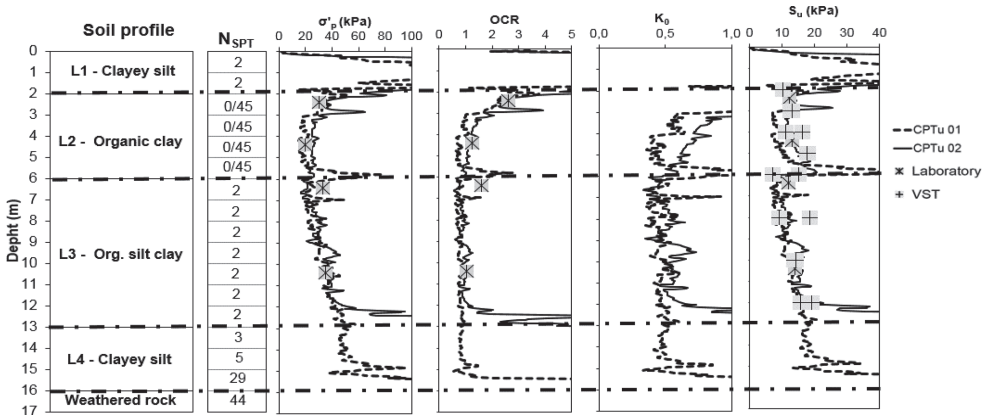

Figure 11. Estimated parameters from piezocone tests (CPTu-01 and CPTu-02).

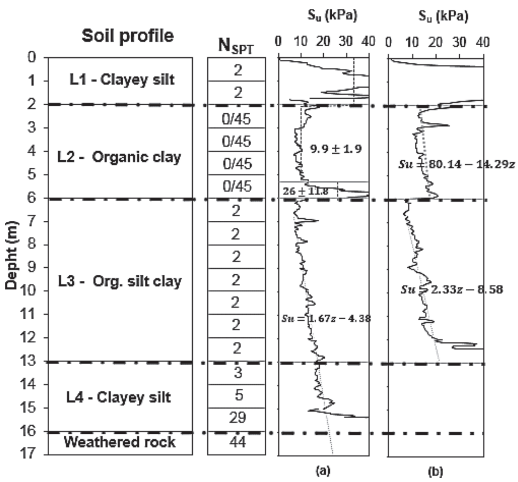

Figure 12. Estimated Su profiles from piezocone tests: (a) CPTu-01; (b) CPTu-02.

to silt clay". This behavior stresses the likely occurrence of a thin layer of overconsolidated organic clay or the presence of seashells.

De Mio et al. (2010) encountered similar behavior in CPTu test results of soft clay sediments with the presence of seashells along the Brazilian coast.

5 CONCLUSIONS

The study was able to characterize the soil layers of deposit through analysis and discussion of the results of field tests (SPT, VST and CPTu) and laboratory testing. Despite non-matching boreholes, there was a consistency of geotechnical measures along the profile. Layers L2 and L3 were below line A of the plasticity chart, consistent with organic clays. The OCR profile was in line with local studies (Coutinho and Bello 2012), with higher values at the start of the layer, tending to decrease to the value of one (1) for depths exceeding 4 m. The soft organic clay layers of the studied deposit showed high compressibility and low resistances, similar to the soft Brazilian clays. In general, the CPTu tests showed consistency in their measurements and the derived parameters with the other tests performed along the profile. The non-normalized charts, proposed by Robertson (2010), showed greater consistency in the classification of behavior throughout the profile. The average N_{kt} value obtained was 10, within the Brazilian range of 9 to 12 (Coutinho and Schnaid 2010). This study confirms how important it is to obtain parameters through laboratory and in situ tests with correlations suited to local/regional experiences. The results from in situ tests were consistent with the laboratory tests.

High compressibility and low resistance values, in general, require interventions to improve the system's behavior (landfill-soil), namely the solutions discussed by Almeida and Marques (2013).

REFERENCES

Almeida, M.S.S. & Marques, M.E.S. 2013. Design and performance of embankments on very soft soils. Taylor & Francis Group, London, UK.

Bjerrum L. 1973. Problems of soil mechanics and construction on soft clays and structurally unstable soils (collapsible, expansive and others). In: Proceedings of the 8th International Conference on Soil Mechanics and Foundation Engineering, Moscow, v. 3, p. 111–159.

Chen, B.S.-Y. & Mayne, P.W. 1996. Statistical relationship between piezocone measurements and stress history of clays. CGJ, 33(3):488–498.

Coutinho, R.Q. & Bello, M.I.M.C.V. 2012. Undrained strength and overconsolidation ratio parameters of Suape soft clays, Pernambuco. ISC'4, ISSMGE, Porto de Galinhas-Pernambuco, Brazil, v. 2. p. 1631–1639.

Coutinho, R.Q. & Schnaid, F. 2010. CPT - Regional Report for South America. CPT'10, Huntington Beach, CA. v. 1, p. 313–333.

Coutinho, R.Q. 2007. Characterization and engineering properties of Recife soft clays - Brazil. *Characterization and Engineering Properties of Natural Soils.* Tan, Phoon, Hight and Leroueil (eds), Taylor and Francis, Singapore, v.3, p. 2049–2100.

Coutinho, R.Q., Oliveira, A.T.J. & Oliveira, J.T.R. 2000. Vane test Conference: Experience, Tradition and Innovation. "*Seminar on Special Foundation Engineering and Geotechnics"*. SEFE IV, São Paulo, Brazil, v. 3, p. 53–79.

Coutinho, R.Q.; Oliveira, J.T.R. & Oliveira, A.T.J. 1998. Geotechnical site characterization of Recife soft clays. ISC'1, v.2: 1001–1006, Atlanta, USA.

De Mio, G., Giacheti, H.L., Viana da Fonseca, A., & Ferreira, C. 2010. CPTu interpretation for stratigraphic logging differences between sedimentary and residual soils., CPT'10, Huntington Beach, CA.

Huang, P.; Patel, M.; Santagata, M.C.; & Bobet, A. 2009. Classification of Organic Soils: Final Report. Indianapolis: Indiana Department of Transportation and Federal Highway Administration (FHWA/IN/JTRP-2008/2).

ISO. 2012. Geotechnical investigation and testing – Field testing – Part 1: Electrical cone and piezocone penetration tests, International Standard ISO 22476-1:2012. (With Technical Corrigendum 1, January 2013). Geneva: International Organization for Standardization.

Jefferies, M.G., & Davies, M.P. 1993. Use of CPTU to estimate equivalent SPT N Geotechnical Testing Journal, ASTM, 16(4): 458–468.

Kulhawy, F.H., & Mayne, P.H. 1990. Manual on estimating soil properties for foundation design, *Report EL-6800 Electric Power Research Institute*, EPRI, August 1990.

Larsson, R. 1980. Undrained shear strength in stability calculation of embankments and foundations on soft clays. CGJ, v. 17, n. 4, pp. 591–602.

Mayne, P.W. & Mitchell, J.K. 1988. Profiling of overconsolidation ratio in clays by field vane. CGJ, Vol. 25, pp. 150–157.

Mesri, G. 1975. Discussion: New design procedure for stability of soft clays. Journal of Geotechnical Engineering Division, ASCE, vol. 101, Nº GT4, pp. 409–412.

Robertson, P.K. 2012. The James K. Mitchell Lecture: Interpretation of in-situ tests—some insights. *ISC'4*, Porto de Galinhas-Pernambuco, Brazil, v. 1. p. 3–24.

Robertson, P.K. & Wride, C.E. 1998. Evaluating cyclic liquefaction potential using the cone penetration test. CGJ, Ottawa, 35(3): 442–459.

Robertson, P.K. 1990. Soil classification using the cone penetration test. CGJ, 27(1): 151–158.

Robertson, P.K. 2009. CPT interpretation – a unified approach, CGJ, 46: 1–19

Robertson, P.K. 2010. Soil behavior type from the CPT: an update. CPT'10, Huntington Beach, CA. v. 2, pp 575–583.

Robertson, P.K., Campanella, R.G., Gillespie, D., & Greig, J. 1986. Use of piezometer cone data. In-Situ'86 Use of In-situ testing in Geotechnical Engineering, GSP 6, ASCE, Reston, VA, Specialty Publication, pp 1263–1280.

Rosenqvist, I.T. 1953. Consideration on the sensitivity of Norwegian quick-clays. Geotechnique 3:195–200

Skempton, A.W. 1957. Discussion: The planning and design of the New Hong Kong Airport, by K. Grace and J.K.M. Henry. Institution of Civil Engineers, v. 7, p. 305–307.

Taylor & Francis
Taylor & Francis Group
http://taylorandfrancis.com

Cone Penetration Testing 2018 – Hicks, Pisanò & Peuchen (Eds)
© 2018 Delft University of Technology, The Netherlands, ISBN 978-1-138-58449-5

Analysis of drainage conditions for intermediate soils from the piezocone tests

R.Q. Coutinho & F.C. Mellia
Federal University of Pernambuco – UFPE, Recife, Brazil

ABSTRACT: This paper presents an analysis of the drainage conditions in intermediate soils, as they can be loaded by piezocone tests, at a standard rate of 20 mm/s, and may present a partially drained condition. This situation requires caution due to the lack of theoretical methodology for the interpretation of data resulting from the test. In this context, the objective of this work was to evaluate the drainage conditions in compacted intermediate soils coming from the "Barreiras Formation" geological unit present in a landfill located in the Brazilian municipality of Itapissuma, Pernambuco state (PE). Two campaigns of piezocone were carried out, with the first campaign consisting of three tests at a standard rate of 20 mm/s (CPTu-01, CPTu-02 and CPTu-03) and the second campaign consisting of two tests at a penetration rate of 10 mm/s (CPTu-01 A and CPTu-03 A) and one test at the rate of 30 mm/s (CPTu-01B). In addition, characterization and oedometer tests on undisturbed samples under flooded and natural moisture conditions near the sites of the piezocone tests contributed to the determination of the coefficient of consolidation. From the reported results, it was concluded that the studied soil, when loaded at the different cone penetration rates, presented undrained behavior.

1 INTRODUCTION

The piezocone tests (CPTu) are widely used in geotechnical engineering for the determination of stratigraphic profiles and soil constitutive parameters. The performance of these tests at their standard rate of 20 mm/s, tend to present drained behavior to granular soils and to show an undrained behavior in clayey soils. However, soils containing sand, silt and clay mixtures (intermediate soils) may present a partially drained condition. In this case, it is of fundamental importance to evaluate the drainage conditions during the piezocone test, because only in drained or undrained conditions can the correct interpretation of the results of the tests be performed.

2 LITERATURE REVIEW

To evaluate drainage conditions, several authors such as Finnie & Randolph (1994), Randolph & Hope (2004), Kim *et al.* (2006), Schnaid (2009), among others, used the normalized velocity parameter (V), expressed in equation (1), to identify drainage conditions in piezocone tests, correlating penetration rate (v), probe diameter (d) and the vertical coefficient of consolidation (C_v), initially obtained from oedometers tests in laboratory.

$$V = (v.d)/C_v \tag{1}$$

Subsequently, Dejong *et al.* (2012) considering that during piezocone penetration the pore-pressure dissipation occurs primarily in the radial direction, recommend using the horizontal coefficient of consolidation (C_h) to determine the normalized velocity parameter (Equation 2). The authors presented also a field decision chart to identify the drainage conditions with 10 cm^2 cone, from the relation between coefficient of consolidation (C_h), penetration rate (v), and normalized velocity (V).

$$V = (v.d)/C_h \tag{2}$$

For the determination of the horizontal coefficient of consolidation, pore pressure dissipation tests during the CPTU tests are recommended by several authors, including Lunne *et al.* (1997), Randolph & Hope (2004) and Dejong *et al.* (2012).

Leroueil & Hight (2003) evaluated the coefficient of consolidation in clays of Canada through several methods, being verified that the values of the coefficients of consolidation obtained by the oedometers tests in laboratory within the normal consolidation range are typically two orders of magnitude lower than the values of the coefficients of consolidation determined by the piezocone

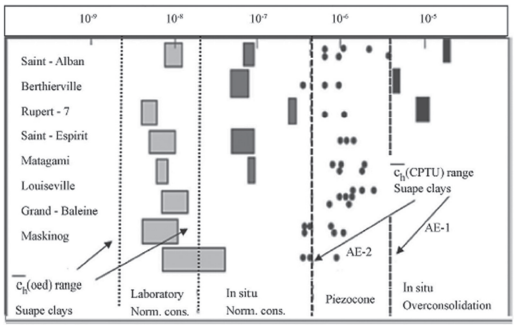

Figure 1. Coefficients of consolidation (from Leroueil & Hight, 2003) and Suape clays results (from Coutinho & Bello, 2014).

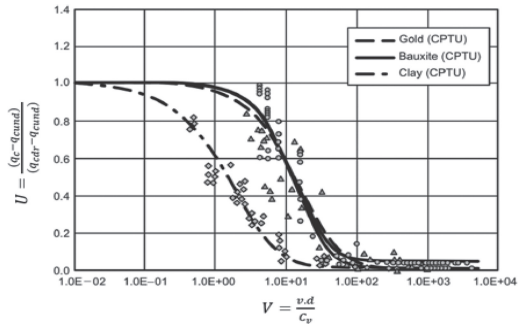

Figure 2. Identification of drainage conditions (Schnaid, 2009).

tests, as shown in Figure 1. Afterwards, Coutinho & Bello (2014) evaluated the coefficients of consolidation of Suape/PE clays and found that the ranges obtained are within the limits indicate by Leroueil & Hight (2003).

For the identification of the drainage transition points during the penetration of the piezocone test, there are several proposals in the literature.

According to Randolph & Hope (2004), for the normally consolidated clays, partial drainage occurs when V is in the range of 0.3 to 30. Schnaid (2009) reinterprets the results obtained by Randolph & Hope (2004), from the concept of degree of drainage in intermediate soils (U), which can be represented according to equation (3).

$$U = \frac{(q_c - q_{cund})}{(q_{cdr} - q_{cund})} \tag{3}$$

Where, q_{cdr} is the penetration resistance measured in a drained condition, resulting from slow tests enough that there is no excess pore pressure; q_{cund} is the resistance to penetration measured in undrained condition, resulting from faster tests, without there is any pore pressure dissipation and q_c is the penetration resistance measured at the standard rate of the test.

Figure 2 shows the relationship between the normalized velocity parameter (V) and the degree of drainage (U), obtained by Randolph & Hope (2004) through piezocone tests at different clay penetration rates and those presented by Schnaid (2009), at gold tailings and alumina tailings.

Schnaid (2009) states that the transition points of the different drainage conditions vary depending on the type of geomaterial, being a function of the rigidity index and OCR. Thus, it is recommended to avoid penetration velocities that produce normalized velocities within the range of 10^{-1} to 10^{+2}, since in this range partial drainage is likely to occur and the soil properties evaluated from the interpretation of the piezocone test may be overestimated, in particular the undrained shear strength.

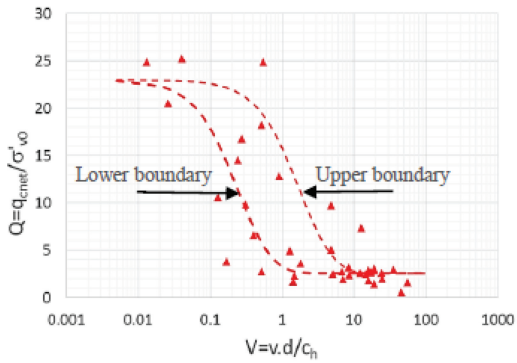

Figure 3. Rate effects in the Q versus V space (Dienstmann *et al.*, 2017).

Dienstmann *et al.* (2017) evaluated the effects of piezocone penetration rates in transient gold tailings. The results were interpreted in a graph, shown in Figure 3, which correlates the normalized velocity (V) to normalized resistance of piezocone (Q). In this new model, the normalized velocities that identify the partial drainage condition were in the range of 0.01 to 10.0. This proposal also provides a satisfactory modeling for the behavior of clays.

3 EXPERIMENTAL PROGRAM

The Landfill under study is located in the municipality of Itapissuma/PE, composed of compacted intermediate soils, coming from the geological unit "Barreiras Formation". It is a landfill with a maximum height of approximately 27.5 meters, which can have three or four levels and a slope of 1:1.5 (V:H).

The investigation program for geotechnical site characterization included in situ tests, such as, SPT

profiles, piezocone—CPTu, Guelph permeameter, disturbed and undisturbed samples collection, and laboratory tests, specifically, tests for soil grading, consistency limits, real density of grains, compacting, oedometers and drained triaxial compression (Coutinho 2015). In this paper, the piezocone tests and the oedometers tests used to evaluate the drainage conditions of the study area will be discussed, as well as the laboratory tests to characterize the material representative of the body of the landfill.

3.1 *Piezocone tests*

Two campaigns of piezocone tests were carried out.

The first campaign was carried out in September 2015, with the execution of 3 perforations at a standard rate of 20 mm/s (CPTu-01, CPTu-02, CPTu-03). The second campaign was carried out in December 2015, contemplating the execution of 3 perforations outside the standard rate for a possible attempt to analyze the landfill drainage conditions. Two verticals were performed at a rate of 10 mm/s (CPTu-01 A and CPTu-03 A) and a vertical at a rate of 30 mm/s (CPTu-01B). These were the lowest and highest rates supported by the pushing equipment.

During the execution of the CPTu-03 A test, two pore pressure dissipation tests were performed to assess conditions of drainage. However, these tests could not be analyzed due to the absence of porous element and saturation fluid suitable for the unsaturated condition of the soil, which made it impossible to obtain C_h (piezocone) directly. Thus, were used alternative studies (Leroueil & Hight, 2003 and Coutinho & Bello, 2014), in which the estimation of C_h (piezocone) is performed by correlations through data obtained in oedometers tests.

3.2 *Sampling*

The undisturbed block type samples were extracted with the minimum possible disturbance, trying to maintain their structure and conditions of humidity and natural compactness.

In total, 11 blocks of undisturbed samples, representative of compacted material from the Barreiras Formation, were extracted. However, for comparison of results between the laboratory tests and the CPTu field tests, only six blocks were selected, adopting the criterion of approximation with the piezocone tests. Blocks 6 and 7 correspond to tests CPTu-01, CPTu-01 A and CPTu-01B, blocks 4 and 5 are associated with the CPTu-02 test and blocks 10 and 11 corresponding to the CPTu-03 and CPTu-03 A tests. During the extraction of the blocks were also collected bagged deformed soil samples for the characterization and compaction tests.

3.3 *Characterization of the material*

The representative material of the blocks extracted from the landfill is generally classified into clayey sand (SC) and low compressibility sandy clays (CL). This classification was done based on the distinct granulometric composition of the material found near each block, as well as the considerable range of liquid limit (LL) and plasticity index (PI) values, as can be observed in Table 1, which presents examples of the results found during the characterization tests.

Because they are soil mixtures (intermediate soils), they may have a partial drainage condition during the penetration of the piezocone test at the standard rate. The evaluation of drainage conditions, presented and discussed in the sequence, is of fundamental importance for adequate estimation of soil constitutive parameters.

4 INTERPRETATION AND EVALUATION OF DRAINAGE CONDITIONS

The oedometers tests performed in the laboratory under flooded conditions and of natural humidity allowed the determination of the vertical coefficient of consolidation C_v (oed).

The procedure used to determine the C_v (oed) in normally consolidated condition, C_{voed} (N.C.), consisted in the realization of a mean between the two values of C_v (oed) corresponding to the tensions superior to the pre-consolidation tension (σ_{vm}), to ensure that the result, for each undisturbed block, was in normally consolidated condition.

Subsequently, the values of C_{voed} (N.C.) representative of the pair of undisturbed blocks closer

Table 1. Granulometric composition, consistency limit, real density and soil classification.

Sample	Gravel (%)	Coarse sand (%)	Medium sand (%)	Fine sand (%)	Silt (%)	Clay (%)	Specific mass of solids (g/cm^3)	LL (%)	PL (%)	PI (%)	USCS
Block 6	1,0	14,0	24,0	25,0	8,0	28,0	2,659	22,6	18,3	4,3	SC
Block 7	1,0	7,0	22,0	18,0	12,0	40,0	2,659	34,6	21,0	13,6	CL

to each CPTu test were made and averaged between them so that each piezocone test had a corresponding C_{voed} (N.C.) value.

Based on the values of C_{voed} (N.C.) corresponding to each piezocone test, it was possible to estimate C_{hoed} (N.C.) values through equation (4) (Jamiolkowski *et al.*, 1985).

$$C_h(N.C.) = \frac{k_h}{k_v} C_v(N.C.) \tag{4}$$

where: k_h/k_v is the permeability ratio in clays, according to Jamiolkowski *et al.* (1985), for homogeneous clays without defined macrostructure, this ratio ranges from 1.0 to 1.5; for clays with defined macrostructure, presence of discontinuities and permeable lenses, ranges from 2.0 to 4.0 and for deposits with several layers of permeable material, varies from 3.0 to 15.

In this study, the value of 1.25 was used for permeability ratio in clays, which corresponds to the mean value of the interval for homogeneous clays, without defined macrostructure.

Then, values of C_{hfield} (N.C.) were then obtained by means of correlation. The C_{hfield} (N.C.) values are typically being an order of magnitude higher than C_{hoed} (N.C) values (see Figure 1).

Finally, it was possible to estimate C_h (piezocone) through equation (5) (Jamiolkowski *et al.*, 1985).

$$C_h(piezocone) = \frac{CR}{RR} C_h\ field\ (N.C.) \tag{5}$$

For the estimation of C_h (piezocone), real values of the compression and decompression indices of the oedometers tests were used, using the coefficient CR/RR (average), for each two undisturbed blocks associated with the piezocone tests.

4.1 *Determination of the normalized velocity parameter*

The reported data in Tables 2 and 3 were used to determinate the normalized velocity parameter.

Table 2 shows the normalized velocities calculated for the first campaign (CPTu-01, CPTu-02, CPTu-03) at the standard rate.

Table 3 shows the normalized velocities calculated for the second campaign (CPTu-01 A, CPTu-01B, CPTu-03 A) outside the standard rate.

Considering what has been suggested by Randolph & Hope (2004), Schnaid (2009) and Dienstmann *et al.* (2017) partial drainage occurs in the V range between 0.3 to 30, 10^{-1} to 10^{+2} and 0.01 to 10, respectively. It was verified that the studied soil, when loaded at the different cone penetration rates (10 mm/s to 30 mm/s), presented undrained behavior, both for the natural humidity conditions and for the flooded conditions. The same was observed through the structure proposed by Dejong *et al.* (2012).

The tests at the rate of 10 mm/s presented closer to the partially drained condition.

In this paper, the results of the CPTu-01 test at standard rate will be presented and discussed.

Table 3. Values of the normalized velocities for the tests of the second campaign.

CPTu tests	Penetration rate v (m/s)	Probe diameter d (m)	C_h (piezocone) (m²/s)		Normalized Velocity V	
			Flooded condition	Natural humidity condition	Flooded condition	Natural humidity condition
CPTu-01A	0.01	0.0357	2.02E-06	2.33E-06	1.77E+02	1.53E+02
CPTu-01B	0.03		2.02E-06	2.33E-06	5.31E+02	4.60E+02
CPTu-03A	0.01		3.12E-06	2.86E-06	1.14E+02	1.25E+02

Table 2. Values of the normalized velocities for the tests of the first campaign.

CPTu tests	Penetration rate v (m/s)	Probe diameter d (m)	C_h (piezocone) (m²/s)		Normalized Velocity V	
			Flooded condition	Natural humidity condition	Flooded condition	Natural humidity condition
CPTu-01	0.02	0.0357	2.02E-06	2.33E-06	3.54E+02	3.07E+02
CPTu-02			2.72E-06	3.27E-06	2.62E+02	2.18E+02
CPTu-03			3.12E-06	2.86E-06	2.29E+02	2.50E+02

5 RESULTS AND ANALYSIS OF THE CPTU-01 TEST

For the CPTu-01 test, at the standard rate of 20 mm/s, are presented in Figure 4, the values of tip resistance (q_c), lateral friction (f_s), pore pressure (u_2) and material classification index (I_{SBT}) by Robertson (2010). The SPT profiles, in general, presented N_{SPT} values ≤ 10.

The frequent variation, including low and high tip resistance values, can be explained by both the limited compaction control and the heterogeneity of the material coming from the "Barreiras Formation". According to the studies by Coutinho (2015), it was verified the existence of variability in the granulometric composition, as well as in the values of maximum dry density and optimum moisture content of the samples obtained and during control.

Based on the classification of the material through SBT, it was possible to obtain a behavior profile of the studied soil, so it was verified that the profile can be classified, mostly as clay to clayey silt (zones 3 and 4), similarly to the laboratory results; in lesser extent as silty sand to sandy silt (zone 5); and a small fraction in clean sand to silty sand (zone 6).

By means of the CPTu-01 test it was also possible to estimate the undrained shear strength (S_u), using equations (6) and (7) proposed by Lunne *et al.* (1997) and Robertson (2012), respectively.

$$S_u = \frac{(q_t - \sigma_{v0})}{N_{kt}} \tag{6}$$

$$N_{kt} = 10.5 + 7log(F_r) \tag{7}$$

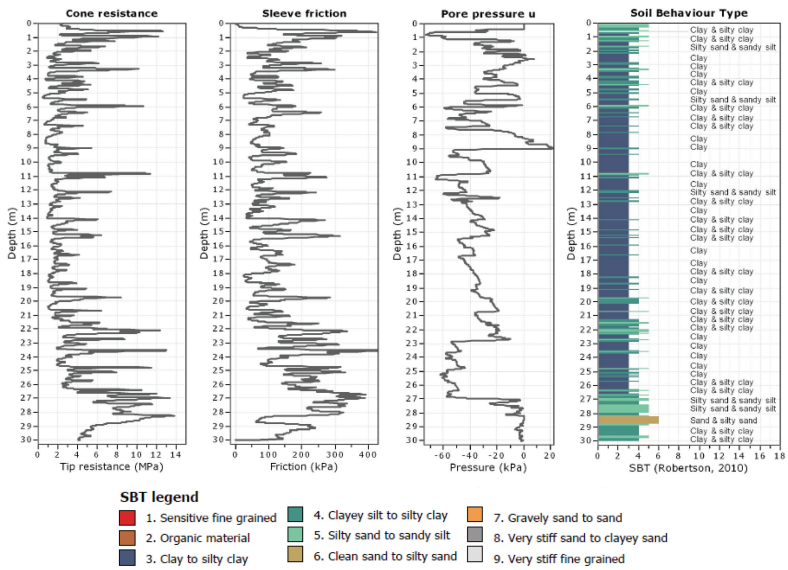

Figure 4. CPTu-01 measurements and SBT.

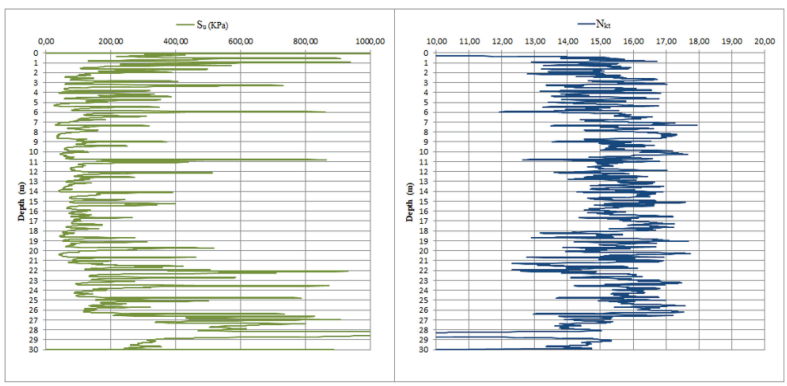

Figure 5. Typical S_u chart and N_{kt} profile from CPTu-01 test.

where: the value of q_t is the corrected tip resistance, σ_{vo} is the total vertical stress, N_{kt} is the load capacity factor and F_r is the normalized friction ratio.

Figure 5 shows the estimation of S_u and the measurements of N_{kt} along the vertical test.

For the estimation of S_u, the peaks of the graph should be disregarded, in order to avoid overestimation of this parameter.

In this case, it is considered reasonable to adopt values around 150 kPa as an adjusted estimate of S_u for the test performed.

The N_{kt} measures varied considerably along the profile, presenting an average value in the order of 15.

6 CONCLUSIONS

The objective of this work is to evaluate the results of piezocone tests in intermediate soils and to verify the drainage conditions from the concept of normalized velocity, correlating laboratory tests with the piezocone tests.

From the evaluation of the drainage conditions, through the proposals of Randolph & Hope (2004), Schnaid (2009), Dejong *et al.* (2012) and Dienstmann *et al.* (2017), it was concluded that soils when loaded by piezocone tests at penetration rate of 10, 20 and 30 mm/s, presented undrained behavior. This allowed the adequate interpretation of the data measured in the tests for the estimative of constitutive parameters of the soil in the undrained condition. However, the tests at a rate of 10 mm/s, showed the normalized velocity values closer to the boundary between the undrained and partially drained conditions, according to the Schnaid (2009) proposal.

By means of the granulometric analyzes of the disturbed samples representative of the material found in the body of the landfill, the soil was classified as a sandy clay / clayey sand—CL / SC. The classification of the material based on the SBT, through the piezocone tests, showed that the landfill material behaves mostly as soils that vary from clay to clayey silt. Then the results evidencing the tendency of the soil to present an undrained behavior.

The estimated values of the undrained shear strength parameter (S_u), for the studied material, presented an average value around 150 kPa, with N_{KT} average value in the order of 15.

ACKNOWLEDGMENTS

The authors acknowledge CAPES for their financial support, Petropolis Group Company for financing of the tests and Damasco Penna Geotechnical Engineering for their technical and operational support.

REFERENCES

Coutinho, R.Q. & Bello, M.I.M.C.V. 2014. Geotechnical Characterization of Suape Soft Clays, Brazil. *Soils and Rocks*, Vol. 37, p. 257–276.

Coutinho, R.Q. 2015. Relatório técnico de investigação de campo e ensaios de laboratório. *GEGEP, 15,* Vol. 1, 233 p.

Dejong, J.T.; Jaeger, R.A.; Boulanger, R.W.; Randolph, M.F.; Wahl, D.A.J. 2012. Variable penetration rate cone testing for characterization of intermediate soils. *In Geotechnical and Geophysical Site Characterization 4*. Edited by Coutinho and Mayne. Taylor and Francis, London, p. 25–42.

Dienstmann, G.; Schnaid, F.; Maghous, S.; Dejong, J.T. 2017. Piezocone penetration rate effects in transient gold tailings. *Journal of Geotechnical and Geoenvironmental Engineering*, ASCE.

Finnie, I.M.S. & Randolph, M.F. 1994. Punch-through and liquefaction induced failure of shallow foundations on calcareous sediments. *Proc. 7th International Conference on Behavior of Offshore Structures*, Massachusetts, USA, Vol. 1, p. 217–230.

Jamiolkowsky M., Ladd, C.C., Germaine, J.T. & Lancellotta, R. 1985. New developments of field and laboratory testing of soils. *XIICSMFE*, San Francisco, Vol. 1, p. 57–153.

Kim, K.; Prezzi, M.; Salgado, R. 2006. Interpretation of Cone Penetration tests in Cohesive Soils. Report FHWA/IN/JTRP-2006/22. Joint Transportation Research Program, Indiana Department of Transportation and Purdue University, West Lafayette, Indiana, 182 p.

Leroueil, S. & Hight, D.W. 2003. Characterization of soils for engineering. *Characterization and engineering properties of natural soils*. T.S.Tan; K.K.Phon; D.W.Hight; S.Loroueil (eds.), Singapore, Vol. 1, p. 255–236.

Lunne, T.; Robertson, P.K.; Powell, J.J.M. 1997. Cone penetration testing in geotechnical practice. Blackie Academic and Professional, Melbourne, Australia, 312 p.

Randolph, M.F. & Hope, S. 2004. Effect of cone velocity on cone resistance and excess pore pressures. *Proc. Int. Symp. On Engineering Practice and Performance of Soft Deposits*, Osaka.

Robertson, P.K. 2010. Soil behaviour type from the CPT: an update. *2nd International Symposium on Cone Penetration Testing,* CPT'10, Huntington Beach, CA, USA.

Robertson, P.K. 2012. The James K. Mitchell Lecture: Interpretation of in-situ tests - some insights. *Geotechnical and Geophysical Site Characterization 4*, ISC 4, Brazil, Vol. 1, p. 3–24.

Schnaid, F. 2009. In situ testing in geomechanics: the main tests. 1ª ed., Oxon: Taylor & Francis, Vol. 1, 329 p.

Cone Penetration Testing 2018 – Hicks, Pisanò & Peuchen (Eds)
© 2018 Delft University of Technology, The Netherlands, ISBN 978-1-138-58449-5

Behaviour of granitic residual soils assessed by SCPTu and other in-situ tests

N. Cruz & J. Cruz
Mota-Engil—Engenharia e Construção, S.A., Porto, Portugal

C. Rodrigues
Department of Civil Engineering, Polytechnic Institute of Guarda, Portugal

M. Cruz
LEMA, Mathematical Engineering Lab, ISEP, School of Engineering, Polytechnic of Porto, Portugal

S. Amoroso
Istituto Nazionale di Geofisica e Vulcanologia de Italia, Rome, Italy

ABSTRACT: Residual soils resulting from weathering processes cannot be well modelled by the classical theories of Soils Mechanics, creating several difficulties in the interpretation of in-situ test results and in the consequent geotechnical design. In fact, the presence of a cementation structure generates an extra strength component materialized by the presence of a cohesive intercept in the Mohr-Coulomb failure envelope. Moreover, when suction is present the interpretation of in-situ data becomes even more complicated, since it increases this cohesive intercept mixing both (cementation structure and suction) in one final result. In granular soils, as it is the case of granitic residual soils, three components of strength have to be considered, namely the shear resistance angle, cohesion and suction, which only can be solved if more than one field or laboratory measurement is obtained. As a consequence, Piezocone (CPTu), Marchetti Dilatometer (DMT) and Pressuremeter (PMT) tests may be considered appropriate to characterize this type of soils, while dynamic tests such as Standard Penetration (SPT) or Dynamic Probing Super-Heavy (DPSH) tests cannot be effective in this determination. On the other hand, cementation structure also affects deeply the stiffness behaviour, deviating from typical response of transported soils represented by Classical Soil Mechanics.

In the last two decades a big effort has been made in Portugal to study and characterize this kind of residual massifs in granitic environments (quite common in the North and Centre of Portugal), namely through DMT and CPTu data, materialized by several research frameworks and its consequent publications. In this paper, a methodology to evaluate the strength of these residual soils by means of SCPTu tests is presented and discussed, leading to a set of new correlations that allows for the evaluation of both cohesive and frictional contributions, hardly possible with the available interpretation models. The work was developed on the Polytechnic Institute of Guarda (IPG) experimental site, which was also previously used in the calibration of SDMT tests for the characterization of these granitic soils.

1 INTRODUCTION

The North and Centre regions of Portugal are mostly formed by granitic rock massifs, involving important residual masses that can attain considerable depths, thus creating a regular need for adequate characterization to support construction in these areas. The main research institutions located within the area have been dedicating important research on these materials behaviour (e.g. Viana da Fonseca, 1996; Rodrigues, 2003; Cruz, 2010). Furthermore, the existence of the Porto Geotechnical Map (COBA 2003), here designated as PGM, provides reliable geotechnical information on the Porto Granitic Formation, considered very useful for defining trends of behaviour and supporting characterization needs.

The residual soils arising from Portuguese granitic formations are the result of mechanical and chemical weathering, respectively by means of grain dismantling and hydrolysis of K-feldspar and Na-feldspar, which lead to the formation of kaolinite clay. In Por-to, according to PGM data (COBA, 2003), after a thin layer of top soil

(usually < 3.0 m thick) the residual profile starts with a thick layer (15 to 20 m) of medium compact residual soil, represented by N_{SPT} within 10 to 30 blows (G_2), which is sometimes followed by a compact transition layer (maximum 5 m thick) corresponding to N_{SPT} within 30 and 60 blows (G_3). In few areas or in the small pockets dispersed in the weathered mass, more intensively kaolinized soils can be found, corresponding to N_{SPT} values lower than 10 (G_1). These residual units evolve in depth from decomposed (W_5) to highly weathered (W_4) rock massif, represented by N_{SPT} values typically higher than 60, and further from medium (W_3) or slightly weathered (W_2) massif. PGM information was analyzed under the perspective of mechanical evolution through the weathering (Cruz, 2010; Cruz et al. 2015), which was particularly useful in the present context. As a whole, the massif is quite heterogeneous, as a consequence of the characteristics and distribution of inherited joint families, where the weathering starts.

From the soil identification point of view, PGM data reveals an expected increase of fine content and plasticity with weathering, as a result of the chemical weathering of feldspars into kaolinite clay. According to ASTM Unified Classification, UC (D2487 1998) soils are mainly represented by silty sands (SM), while soils with high kaolin content are represented by clayey sands (SC) and silts of low plasticity (ML).

From the mechanical point of view, the weathered massif (W_4 and W_5) and the subsequent residual soils are characterized by the presence of a cementation structure inherited from the original rock, which is progressively weakened with weathering. The presence of this structure confers a cohesive-frictional behaviour to these soils or decomposed rock masses, generating at least two different strength contributions and the development of more than one yield stress locus (Rodrigues 2003, Viana da Fonseca 1996, Cruz 2010). As so, triaxial testing is required to obtain adequate geotechnical parameters. However, laboratorial characterization depends on sampling, particularly damaging for the cementation structure, especially when the equipment and techniques used are poor. Furthermore, the fabric variations, the heterogeneity and the discontinuity of information also decreases the efficiency of laboratorial characterization, leaving a role to in-situ testing on routine analysis.

Nonetheless, sustainable methodologies for the most common in-situ tests are hardly available and the regular approaches settled for sedimentary soils do not match with the residual behaviour leading frequently to erroneous estimations of strength and stiffness parameters. In particular, strength evaluation is usually based on the concept that soils of sandy nature are characterized by a shear resistance angle, while clayey soils are characterized by its undrained cohesion. As a consequence, the sedimentary approaches applied to residual soils miss the cohesive contribution and generate a shear resistance angle that is as higher than the real one (triaxial testing) as the cohesion magnitude increases (Cruz 2010, Cruz et al. 2014). In fact, the cohesive-frictional nature of these materials implies dividing the general strength into two components (cohesion and shear resistance angle), which can only be achieved by multi-parametric tests such as DMT, CPTu or PMT. The first two can be easily used in residual soils ($N_{SPT} < 60$), while for decomposed or highly weathered materials (W_4 and W_5, characterized by N_{SPT} higher than 60) only PMT can be performed (Cruz 2010).

An earlier attempt to solve this problem in Portuguese granites was made by Cruz et al. (2004, 2006) using DMT results obtained in Porto and Minho granites, which were compared with triaxial test results. The results highlighted the sensitivity of DMT to the cementation effects on mechanical behaviour, as well as the possibility of correcting the shear resistance angles when derived from sedimentary approach. The combination of CPTu+DMT data was also considered as a possibility for solving the strength problem (more different possibilities), thus data from pairs of tests is available since the early beginning.

Due to the referred sampling disturbance (part of the cementation was permanently lost), as well as heterogeneity and micro-fabric variations, the triaxial reference used to establish the correlations did not represent well the reality in terms of cohesion. To overcome this deviation, it was settled an experimental framework that made use of artificially cemented mixtures obtained from destructured granitic soils gathered on IPG experimental site (Cruz, 2010). With this procedure, the sampling and microfabric disturbances could be avoided, giving a "true" reference for comparisons. In the end, the methodologies and the respective correlations to characterize strength and stiffness of these residual materials were settled and successfully tested in the available data of Porto and Guarda granites, revealing a good applicability.

Given the success of this calibration program, the research was extended to establish identical approaches with PMT and CPTu testing data, naturally using DMT as a reference test. In the following sections, the calibration to obtain strength parameters from SCPTu is presented and discussed, hoping to contribute to a step forward in the applicability of the test to characterize residual soils.

2 THE IPG EXPERIMENTAL SITE

The IPG experimental site involved in this program is especially rich to support the aim of finding adequate correlations with CPTu and PMT tests. In fact, the experimental site was created over the last years of the last century, starting from a full characterization of the local residual granitic massif based on a full set of laboratorial and in-situ tests (Rodrigues 2003). The Guarda Formation is characterized by a monzonitic coarse grained granite composed by quartz, potassic and sodic feldspars, biotite and muscovite. The local profile is represented by two geotechnical horizons in different weathering stages that display different mechanical responses to test solicitations.

This complete characterization allowed to understand the behaviour of Guarda granites and verify its similarity with Porto granites, as expressed in Porto Geotechnical Map (COBA 2003, Cruz et al. 2015), creating a fundamental link between the two formations and with PGM data (Cruz 2010). On the other hand, IPG owns an important laboratorial infrastructure that includes a large-scale testing device (Controlled Condition Chamber - CCC), as well as the most current in-situ tests used in Portugal. The DMT calibration experiment was performed in these facilities and it consisted in using artificially cemented samples used in triaxial testing and in the CCC, which ensured that both triaxial and DMT testing were measuring the same strength (Cruz 2010). Data from previous research performed on the naturally cemented samples (Rodrigues 2003) was used to replicate an artificial material similar to the one of the local granitic massif, namely in what concerns to void ratio, saturation conditions and magnitude of cementation strength, linking the experience with the natural ground. At the end of that framework the established correlations were tested by performing SDMT tests in the location where the artificial mixtures were obtained. Finally, data from Porto granites (Cruz et al. 2004, Cruz & Viana da Fonseca 2006) was used as testing set, confirming the sustainability of the methodology (Cruz et al. 2014) and closing the circle around the correlations based on DMT tests. Aiming the extension of this research to other tests, a new campaign was performed, consisting in six sets of SDMT, SCPTu, PMT and sample collection for triaxial tests, located along one line and with a distance of 1 m from each other.

The data obtained in this campaign was gathered with the previous phases and with the available pairs of DMT and CPTu tests performed in Porto granites (8 locations with 20 couples). Overall, more than 150 tests were involved, excluding the ones reflected in PGM data, as presented in Table 1.

Table 1. Tests performed in IPG experimental site.

Target	Tests
1. Residual mass (Rodrigues 2003)	TRX (53) UCS (12), PMT (5), CPTu (8), DMT (3), CH (1)
2. DMT calibration (Cruz 2010)	TRX (5) UCS (30), DMT in CCC (5)
3. CPTu, PMT calibration	TRX (6), SDMT(6), PMT(18), SCPTu (6)

3 CPTU CALIBRATION FRAMEWORK

For data treatment, some procedures were followed to eliminate not comparable values and ensuring a good comparison base, such as: a) all the CPTu field data was interpreted by using an interpretation software (GeoLogismiki) widely used in geotechnical practice; b) the depth fitting between CPTu and DMT for comparing the results, was made by using medians of intermediate values in CPTu (5 data sets above and 5 below of each reference depth); c) Vegetal and sedimentary caps and readings belonging to different geotechnical units (G_2 or G_3) were eliminated.

The whole package of available data was organized in 3 basic subsets, corresponding to the data used in DMT calibration (IPG Phase1), the data collected for the present calibration (IPG Phase2) and the coupled DMT and CPTu data obtained in Porto. In Tables 2 to 4, the main intervals of basic measured parameters and intermediate calculated parameters obtained in DMT, CPTu and PMT tests are presented. In those tables, data is divided according to the PGM units, namely with $10 < N_{SPT} < 30$ (G_2) and $30 < N_{SPT} < 60$ (G_3). Shear wave velocities obtained during the execution of SCPTu/SDMT tests show that these units can be respectively represented by intervals of 170 to 300 m/s and 250 to 400 m/s.

In previous analysis within this framework, Cruz et al. (2016) compared the available pairs of CPTu and DMT tests, underlining the comparability of the tests and the similar difficulties to derive strength parameters. In that context, CPTu derived results from sedimentary correlations of unit weights and permeability converge to the same geotechnical ranges observed in DMT and PGM data in the same spots, while the results on soil identification sometimes reveal discrepancies, sometimes pointing out to a clay behaviour that has no correspondence with reality.

The DMT calibration had shown that the bigger problem to be solved is the one related with strength, namely how to get shear resistance parameters? In the case of DMT, the virtual overconsolidation ratio (vOCR) was selected as the

Table 2. Basic and intermediate CPTu parameters.

N_{SPT}	q_t (MPa)	f_s (kPa)	Q_{tn}	F_R (%)	B_q
10–30	5–15	100–250	250–500	1.5–2.2	0.0–0.05
30–60	15–25	250–500	300–500	1.5–3.0	–0.05–0.0

q_t = corrected cone resistance, f_s = sleeve friction, Q_{tn} = normalized cone resistance, F_R = friction ratio, B_q = normalized pore pressure ratio.

Table 3. Basic and intermediate DMT parameters.

N_{SPT}	P_0 (MPa)	P_1 (MPa)	I_D	K_D	E_D (MPa)
10–30	0.3–1.0	1.0–2.5	1.0–3.0	15–25	25–75
30–60	1.0–2.5	2.0–5.0	1.0–3.5	10–40	60–120

p_0 = DMT corrected first reading, p_1 = DMT corrected second reading, I_D = material index, K_D = horizontal stress index, E_D = dilatometer modulus.

Table 4. PMT test parameters.

N_{SPT}	P_0 (MPa)	P_Y (MPa)	P_L (MPa)	E_{PMT} (%)
10–30	0.07–0.10	0.8–1.2	1.3–1.8	10–20
30–60	0.15–0.25	1.2–3.0	2.0–4.0	15–40

P_0 = PMT in-situ horizontal stress, P_Y = PMT yield pressure, P_L = limit pressure, E_{PMT} = pressuremeter modulus

reference to derive the cohesive parameter based and also to establish a reduction factor to correct the shear resistance angle obtained by sedimentary correlations.

In the case of CPTu data, the shear resistance angles (Robertson 2009) point out to values between 35º to 42º, within the same intervals of DMT when the correlation for sedimentary soils is used (Marchetti 1997). As expected, these values are higher than the reality represented in PGM or when the correlation proposed by Cruz (2010) for DMT's is used (33º to 37º). Once again, the observed differences could certainly be related to the cementation effects.

Before proceeding with the experimental work, it was important to evaluate if CPTu could identify the presence of cementation, for which the chart suggested by Robertson (2016) was selected (Figure 1). The chart is based in the normalized cone resistance, Q_{tn}, and the small strain rigidity index, I_G, defined as the ratio between the shear modulus (G_0) and the net cone resistance (q_n). The modified small strain rigidity index, K^*_G, of that chart can be calculated by:

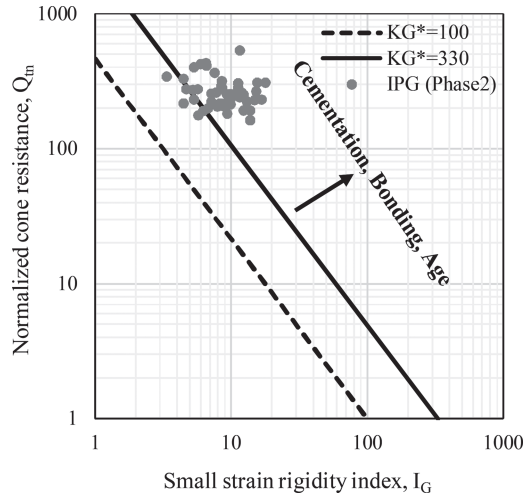

Figure 1. CPTu data of IPG (Phase 2) represented in Q_{tn} – I_G space (Robertson 2016).

$$K^*_G = \frac{G_0}{q_n}(Q_{Tn})^{0.75} \quad (1)$$

where K^*_G = modified small strain rigidity index; G_0 = small strain shear modulus; q_n = net cone resistance; Q_{tn} = normalized cone resistance.

The plotted data corresponds only to IPG data, since shear wave velocities, v_s, are scarce in Porto tested sites. Figure 1 clearly shows the efficiency of the test in the identification of the cementation structure, possibly including suction effects.

To analyse the strength response, all the available data was gathered and analyzed in the Laboratory of Mathematical Engineering of Polytechnic Institute of Porto. For global cohesion adjustments, IPG (Phase 2) and Porto Granites were used as training subsets, while IPG (Phase 1) was selected as testing subset, due to its connection with the DMT calibration and also because the respective data covers the whole range of measurements. Due to less available comparing data in the case of shear resistance angle, the training subset encompasses the whole set of observations.

Several adjustments were tested by using Q_{t1}, F_R and B_q, as well as Q_{tn}, F_R and B_q. As suspected, due to its very low variation, data analysis proved that B_q could be discarded in this calibration. The additive polynomial regression models showed good results on the training subsets, as well as on the independent test subset. Equations 2 and 3 represent the best fit to obtain a global cohesion, c'_g, while Equation 4 stands for the best fit to obtain the shear resistance angle when it is derived by sedimentary approaches:

$$c'_g = 11.5\ln(Q_{t1}) + 3.2\ln(F_R) - 30.8 \quad (2)$$

$$c'_g = 12.8\ln(Q_{tn}) + 1.6\ln(F_R) - 32.2 \quad (3)$$

$$\phi_{corr} = \phi_{sed} - 5.27\ln(Q_{t1}) - 0.99\ln(F_R) + 19.71 \quad (4)$$

where c'_g = global cohesion (cementation + suction); ϕ_{corr} = corrected shear resistance angle; ϕ_{sed} = shear resistance angle derived from sedimentary approach; Q_{t1}, Q_{tn} and F_R = CPTu normalized parameters.

The adequacy of these fits is measured by r^2 (determination coefficient), which is 0.67 for Equation 1, 0.61 for Equation 2 and 0.69 to Equation 3. A good predictor of the global results quality may be the relative errors median, represented with the main descriptive statistics of relative errors in Table 5 and Table 6, respectively for the training and test subsets.

The similarity of statistical values found in these tables are an indicator of the model robustness, which is also illustrated in Figures 2 and 3 by the high convergence of DMT and CPTu profiles for the cases of both cohesion and corrected shear resistance angles. Furthermore, the good quality of the correlations is even more promising, because of the unavoidable heterogeneity of the residual tested massifs, from where some scattering is naturally expected. Finally, it is also important to note, from the closer observation of these figures, the general decrease of global cohesion until 4 m depth, where the water level is located, which is certainly related with the suction contribution to the overall cohesive strength.

Once the correlations are validated, it is important to observe the behaviour reflected in the SBT

Table 5. Relative errors in the training subsets.

Eq.	Min (%)	1st Q (%)	Mean (%)	Med (%)	3rd Q (%)	Max (%)	Std (%)
2	0.0	5.9	18.6	13.2	24.1	133.0	19.4
3	0.2	7.3	20.8	15.0	26.5	168.9	21.3
4	0.1	4.5	17.8	12.0	23.0	188.7	24.1

Table 6. Relative errors in the test subsets.

Eq.	Min (%)	1st Q (%)	Mean (%)	Med (%)	3rd Q (%)	Max (%)	Std (%)
2	0.0	6.0	17.2	11.9	21.4	111.7	17.5
3	0.2	7.4	20.8	14.8	29.6	106.1	18.8

Min = minimum, 1stQ = first quartile, Med = median, 3 stQ = third quartile, Max = maximum, Std = standard deviation

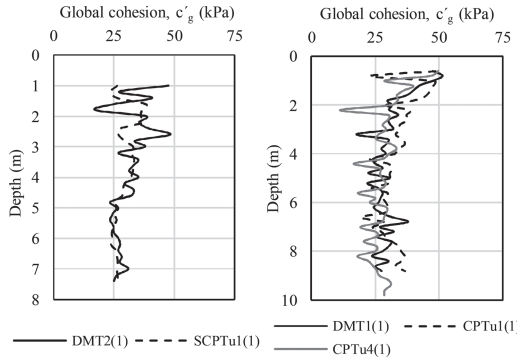

Figure 2. CPTu and DMT global cohesion profiles of the testing subset (IPG Phase1).

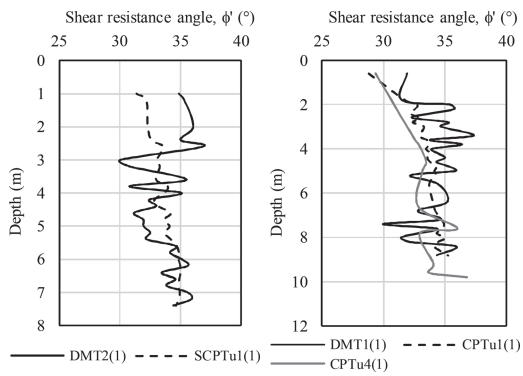

Figure 3. CPTu and DMT shear resistance angle profiles of the testing subset (IPG Phase1).

charts, given its usefulness in design considerations. Figures 4, 5 (Robertson, 2009) and 6 (Robertson, 2016) show the whole set of analysed data plotted in soil behaviour charts, where the global cohesion isolines derived from Equation 3 are also represented. As it can be observed, there is no particular differences between Porto and Guarda granites behaviour, with data points falling within zones 4, 5 and 6 of Robertson (2009) chart and identified as dilatant sandlike and claylike behaviours in Robertson (2016) chart.

The dots falling in zone 4 (Robertson, 2009) and the claylike behaviour (Robertson, 2016) are not compatible with the general behaviour of these soils that is definitively sandlike. In fact, these residual soils are mostly non-plastic silty sands to sandy silts (SM, according to ASTM Unified Classification), rarely silts, as identified by laboratorial tests and by DMT identification index (Rodrigues 2003, Cruz 2010). Furthermore, the soils show a plasticity index, IP, lower than 10% (most frequently non-plastic) and the in-situ permeability

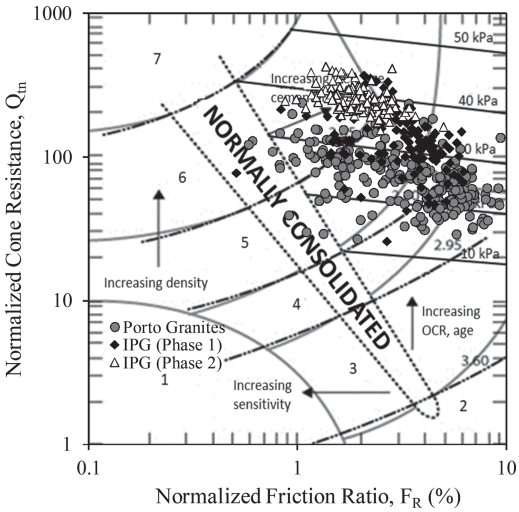

Figure 4. Representation of data on Q_{tn} – F_R chart (Robertson 2009).

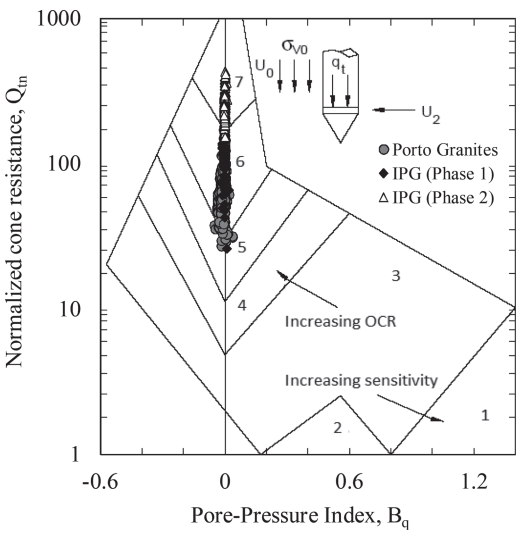

Figure 5. Representation of data on Q_{tn} – B_q chart (Robertson 2009).

typically falls within 10^{-6} to 10^{-7} m/s (Cruz 2010, Cruz et al. 2015).

Part of this observed deviation may be justified by the less efficiency of the charts when applied to cemented soils, as stressed by Robertson (2016), but it is also true that the frequency of the CPTu readings (every 1 cm against 20 cm of DMT's) may catch the concentration of more intensive weathering occurring in the close vicinity of the ancient joints.

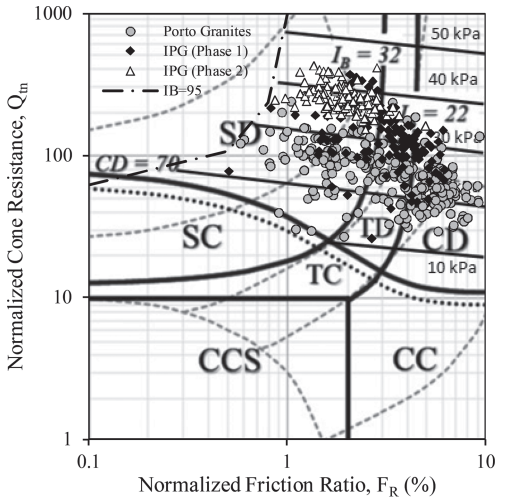

SD = Sandlike dilatant, TD = Transitional dilatant, CD = Claylike dilatant, SC = Sandlike contractive, TD = Transitional contractive, CD = Claylike contractive

Figure 6. Representation of data on Q_{tn} – F_R chart (Robertson 2016).

On the other hand, the plots reveal that the increase of cohesion magnitude pushes the soils from groups 4, 5 and 6 towards the groups 8 and 9, roughly following the curve shape of the modified soil behaviour index (I_B) represented in Robertson chart of 2016. Furthermore, the data in the same chart shows exclusively dilatant soils, with dilatancy increasing with the level of cementation, which is consistent with the findings of Rodrigues (2003) and Cruz (2010) based on triaxial testing with internal strain measurement for the same levels of local confining stresses. Finally, it is also worth note that the state parameter derived from CPTu data falls within 0 and -0.3, which is lower than the -0.5 pointed by Jefferies & Been (2006) as reference for dilatant behaviour at high strains of coarse grained soils.

4 CONCLUSIONS

In the present paper, an attempt to obtain the global cohesion and the shear resistance angles in Portuguese granitic residual soils by means of SCPTu tests was presented and discussed. The proposed methodology allows to evaluate separately the cohesive and frictional contributions for the overall strength, which is hardly possible by the current interpretation models.

The calibration is strongly based in the IPG experimental site, where a wide sort of laboratorial and in-situ tests were performed on naturally

and artificially cemented samples under controlled conditions. The site had been previously used in the calibration of DMT to characterize these residual soils (Cruz, 2010) and this test was used as reference for the present calibration. Furthermore, available pairs of CPTu and DMT tests, performed in Porto granites in earlier stages of DMT calibration process, were gathered, bringing an interesting volume of data to work with the advanced mathematic tools used in the calibration process. The obtained correlations were then validated by a testing subset, not used in the calibration.

The projection of results in two SBTn CPTu charts, allowed to follow the behaviour with cementation intensity increase and revealed some possible misinterpretations of these charts.

Finally, it is important to underline that these correlations represent well this granitic regional behaviour, but its application in other granitic environments should be tested previously. In other lithologic types new correlations should be studied.

REFERENCES

ASTM D 2487. 1998. Classification of soil for engineering purposes. *American Society for Testing Materials*.

COBA. 2003. Porto Geotechnical Map. *COBA and Faculty of Sciences of University of Porto*. Porto City Hall.

Cruz, N. 2010. Modelling geomechanics of residual soils by DMT tests. *PhD thesis, University of Porto* (*www.nbdfcruz.wordpress.com*).

Cruz, N., Cruz, J., Rodrigues, C., Cruz, M. & Martins, F. 2016. Piezocone Tests in Residual Soils. A Portuguese Experience in Granitic Soils. *5th International Conference on Site Characterization*. Brisbane, Australia.

Cruz, N., Gomes, C., Rodrigues, C. & Viana da Fonseca, A. 2015b. An approach for improving Wesley Engineering Classification. The case of Porto Granites. *XVI European Conf. on Soil Mec. and Geot. Eng*, Edimburgh, UK

Cruz, N., Rodrigues, C. & Viana da Fonseca, A. 2014. An approach to Derive Strength Parameters of Residual Soils from DMT Results. *Soils & Rocks*, Vol.37, nº3,pp. 195–209.

Cruz, N. & Viana da Fonseca, A. 2006. Portuguese experience in residual soil characterization by DMT tests. R.A. Failmezger & J.B. Anderson (eds), Flat Dilatometer Testing, *Proc. 2nd International Conference on the Flat Dilatometer*, Washington D.C. pp. 359–364.

Cruz, N., Viana da Fonseca, A. & Neves, E. 2004. Evaluation of Cohesive Intercept on Residual Soils by DMT and CPT. 2nd *International Conference on Site Characterization, ISC'2.* Porto, Portugal. Vol. 2, pp 1275–1284.

Jefferies, M.G., and Been, K. 2006. Soil liquefaction – a critical state approach. *Taylor & Francis*, ISBN 0-419-16170-8. 478p.

Marchetti, S. 1997. The flat dilatometer design applications. III *Geotechnical Engineering Conference*, Cairo University. Keynote Lecture. Vol.1, pp. 421–448.

Robertson, P.K. 2009. Interpretation of cone penetration tests – a unified approach. *Canadian Geotechnical Journal*, 46(11): 1337–1355. doi:10.1139/T09-065.

Robertson, P.K. 2016. Cone penetration test (CPT)-based soil behaviour type (SBT) classification system - an update. *Canadian Geotechnical Journal* 53: 1910–1927 dx.doi.org/10.1139/cgj-2016-0044.

Rodrigues, C. 2003. Geotechnical characterization and geomechanical behaviour analysis of a saprolite from Guarda granites. *PhD Thesis, University of Coimbra*. (in Portuguese).

Viana da Fonseca, A. 1996. Geomechanics of Porto residual soil from granite. Design criteria for direct foundations. *PhD thesis, Porto University*. (in Portuguese).

Taylor & Francis
Taylor & Francis Group
http://taylorandfrancis.com

Cone Penetration Testing 2018 – Hicks, Pisanò & Peuchen (Eds)
© 2018 Delft University of Technology, The Netherlands, ISBN 978-1-138-58449-5

Rate effect of piezocone testing in two soft clays

F.A.B. Danziger, G.M.F. Jannuzzi & A.V.S. Pinheiro
Federal University of Rio de Janeiro, Brazil

M.E.S. Andrade
Technological Federal University of Paraná, Brazil

T. Lunne
Norwegian Geotechnical Institute, Norway

ABSTRACT: The Onsøy and Sarapuí II soft clays have been studied for a number of years. In particular, piezocone tests with different rates have been conducted at both sites. Since the plasticity index and the coefficient of consolidation—which play important roles in the rate effect—are different in Onsøy and SarapuÍ II clays, an interesting comparison is possible. A bowl shaped curve was obtained for the normalized cone resistance versus penetration rate in the case of Sarapuí II clay. The cone resistance versus rate curve can be explained by the pore pressure trends, especially from the u_1 trend. Since only three rates have been used for Onsøy clay, a more complete picture cannot be obtained. However, the use of the normalized rate (or velocity), even using c_h from piezocone dissipation data, was not capable to unify the resistance-rate data for the two clays tested. Adaptations in regular rigs, allowing much smaller penetration rates, and small diameter cones, are necessary if drained conditions are to be achieved when conducting piezocone tests in deposits like Sarapuí II or Onsøy clays. No rate effect was found for penetration rates greater than the standard rate, unlike expected, due to the high I_p values in both deposits. Tests with higher rates are necessary to properly evaluate the role of I_p on rate effect on cone resistance.

1 INTRODUCTION

The piezocone test is performed with the standard rate of 20 mm/s. With this rate tests in sands are considered to be performed in drained conditions and tests in clay in undrained conditions (e.g., Lunne et al. 1997). Partially drained conditions are generally obtained in silts, and the case of tailings dams is of particular interest to be studied. Moreover, the use of penetrometers with smaller diameters than the standard 10 cm^2 base area penetrometer are becoming more frequent, especially in offshore case, and the drainage conditions are strongly dependent on the cone diameter. Therefore, the interest of properly understanding the rate effect of piezocone testing is also important for that case.

It has been recognized that the rate effect is influenced by a number of factors, and the plasticity index, I_P, is one of the most important factors when tests are carried out in undrained condition, whereas it seems that the coefficient of consolidation is very significant when the drainage condition is to be analyzed. The present study makes a comparison between rate effect in piezocone testing in two soft clays, one from Norway, Onsøy clay, and the other from Brazil, Sarapuí II clay. The Sarapuí II clay (Jannuzzi et al. 2015) is a very plastic clay (I_p in the range 60%–170%), whereas I_p values in Onsøy clay are in the range 20%–50% (Lacasse & Lunne 1982; Lunne et al. 2003). The horizontal coefficient of consolidation, c_h, obtained from piezocone dissipation data is on average 10×10^{-7} m^2/s in the case of Onsøy clay (Lunne et al. 2003) and 4×10^{-7} m^2/s in the case of Sarapuí clay (Danziger et al. 1997b).

2 THE TEST SITES

2.1 *The onsøy clay*

The Onsøy test site has been used by NGI since 1969, and several areas have been developed. Prior to 2000 all of the test areas were grouped closely together within an area of about 140 m × 120 m. However due to development of this area a new test site was established some 200 m to 300 m to the northwest. The nature of the clay deposit in both areas is essentially identical. A number of in situ and laboratory tests, as well as other studies, have been performed at the test site. Some characteristics of the clay deposit are summarized in Figs. 1 and 2, from area 2 (Lunne et al. 2003).

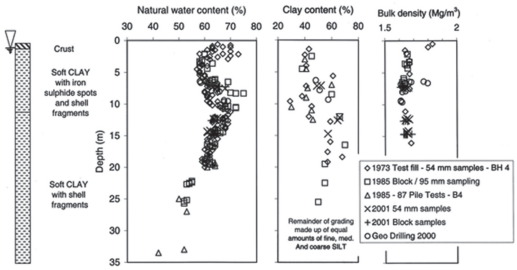

Figure 1. Natural water content, clay content and bulk density from Onsøy clay (Lunne et al. 2003).

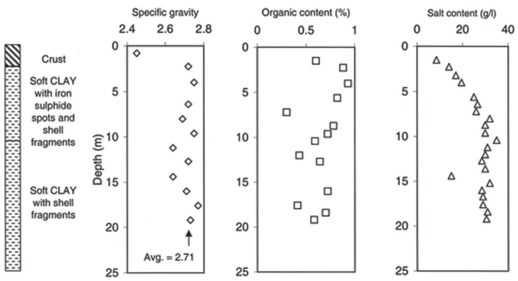

Figure 2. Specific gravity, organic and salt content from Onsøy clay (Lunne et al. 2003).

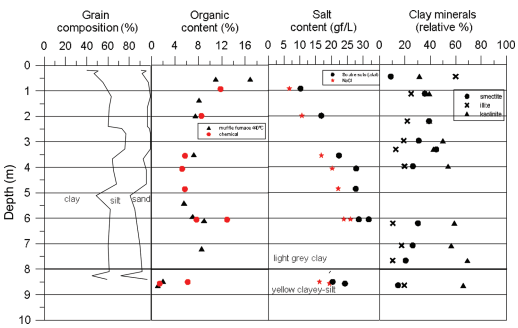

Figure 3. Grain size distribution; organic content; total salt content and NaCl content (data from Onsøy clay also included); relative percentage of clay minerals versus depth from Sarapuí II clay (adapted from Jannuzzi et al. 2015).

2.2 *The sarapuí II clay*

The Sarapuí test site has been used since mid 1970s, being the oldest test site in Brazil (e.g., Lacerda et al. 1977). As in the case of Onsøy, two areas have been used, the first one from mid 1970s until approximately 2000, and the second one, named Sarapuí II, from 2000 until today.

Comprehensive studies about Sarapuí I and Sarapuí II test sites have been provided by Almeida & Marques (2003) and Jannuzzi et al. (2015), respectively. Some characteristics of the Sarapuí II clay deposit are summarized in Figs. 3 and 4.

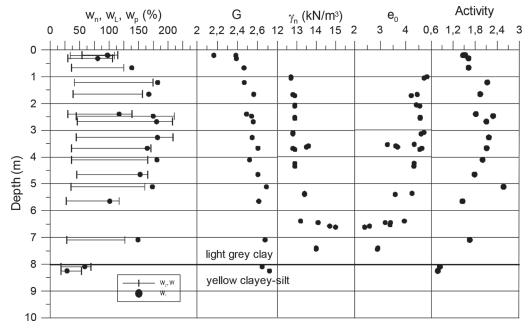

Figure 4. Liquid limit, plastic limit and natural water content; specific gravity; total unit weight; initial void ratio; activity versus depth from Sarapuí II clay (adapted from Jannuzzi et al. 2015).

Table 1. Tests performed at Sarapuí II test site.

Rate of penetration (mm/s)	Number of tests
2.5	2
5	2
10	2
20	4
40	3

It is interesting to note that the salt content in both deposits, Onsøy and Sarapuí II, is nearly the same, for unknown reasons. Moreover, the Onsøy clay is classified (by Norwegian experience) as having a high to very high plasticity. However, the Sarapuí II clay presents much higher values of liquidity limit and plasticity index, although also classified in the same way. It should be useful to define a new category in cases like Sarapuí II clay, maybe extremely high plastic clays.

3 TESTS PERFORMED

3.1 *At onsøy test site*

The tests performed at Onsøy test site have been reported by Lacasse & Lunne (1982). The piezocone used consisted of a modified 10 cm^2 Fugro cone with a 20 kN load cell capacity, and where the sleeve friction was not measured. The pore pressure measurement corresponded to the position u_2. Three rates have been used, 2 mm/s, 20 mm/s and 100 mm/s.

3.2 *At sarapuí II test site*

A 10 cm^2 penetrometer was used in Sarapauí II test site, produced by COPPE/UFRJ and Grom Eng.,

in a partnership which started in 1984. The cone and friction load capacities are 50 kN and 7.5 kN, respectively. Since the last version of this penetrometer was produced, in 1996, pore pressures u_1 and u_2 have been measured (Danziger et al. 1997a). Water is always used as the saturation fluid, thus a previous hole with casing is necessary when the water table is below ground level. This is not necessary in Sarapuí II test site, since that the water table is roughly at ground level. All transducers are calibrated before and after each test series, in the range expected to occur in the field. Thirteen tests have been performed, with the rates included in Table 1.

4 TEST RESULTS

The piezocone test results for Sarapuí II clay are presented in Fig. 5 for the standard rate of 20 mm/s, in a magnified scale, to illustrate the upper 5 m of the profile. Tests with no proper saturation, although not considered in the analysis, have also been included in the figure. For the analysis herein performed, the measured values for each quantity have been averaged in the 0.5 m interval in every meter for all penetration rates. In other words, the values indicated as corresponding to 2.5 m depth represent an average of values in the interval 2.25 m–2.75 m. Data points corresponding to change of rods have been removed. The cone resistance, q_{tn}, the friction sleeve f_{sn} and the pore pressures u_{1n} and u_{2n} for each penetration rate, n, have been normalized with respect to the average values corresponding to the standard rate of 20 mm/s, $q_{t\,20}$, $f_{s\,20}$, $u_{1\,20}$ and $u_{2\,20}$, respectively.

The normalized values $q_{tn}/q_{t\,20}$, $f_{sn}/f_{s\,20}$, $u_{1n}/u_{1\,20}$ and $u_{2n}/u_{2\,20}$ versus penetration rate are presented in Figs. 6, 7, 8 and 9, respectively, for 2.5 m depth, which presented the most consistent results and is also the region in the soil profile with the highest values of liquidity limit and plasticity index (see Fig. 4). The cone resistance in two tests performed with 40 mm/s penetration rate have not been presented due to mal-functioning of the load cell.

It can be observed in Fig. 6 that there is a reduction in the normalized $q_{tn}/q_{t\,20}$ values when the rate increases from 2 mm/s to 5 mm/s, and another reduction, although smaller, when it increases again to 10 mm/s. Then $q_{tn}/q_{t\,20}$ increases when the rate increases to 20 mm/s, and is roughly the same when the rate further increases to 40 mm/s. Other depths presented a similar behavior, however with almost the same q_{tn} values for the rates 5 and 10 mm/s.

The observed behavior is similar to the results obtained by Bemben & Myers (1974), Fig. 10, in a research which is considered by Danziger & Lunne (1997) the first paper where a complete picture on this subject was obtained. In fact, for very slow rates the behavior is predominantly drained, and

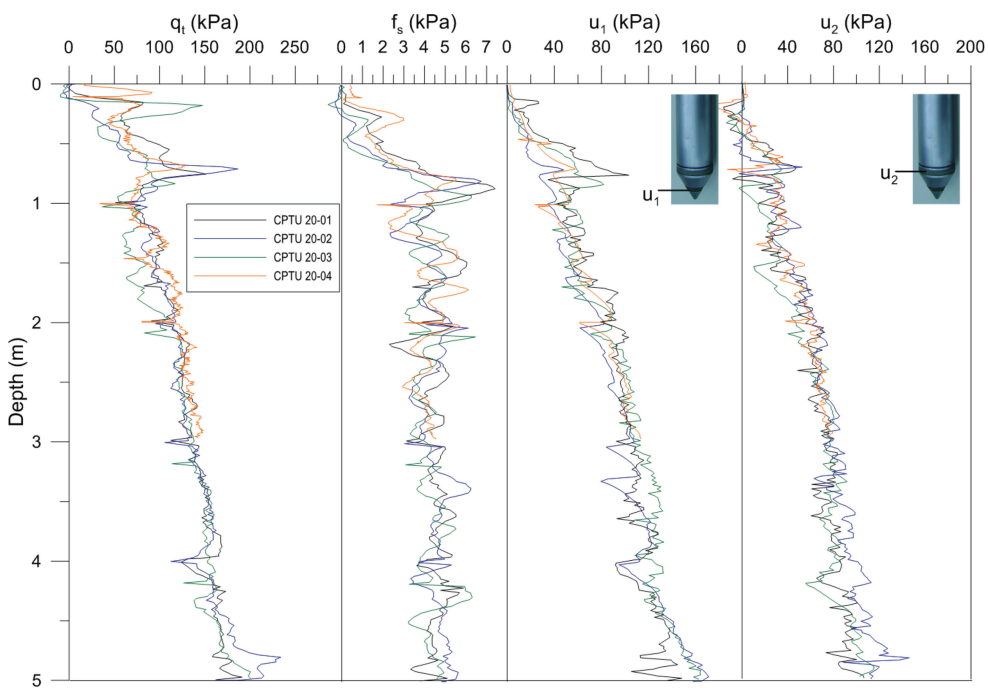

Figure 5. Piezocone test results for Sarapuí II clay, penetration rate of 20 mm/s.

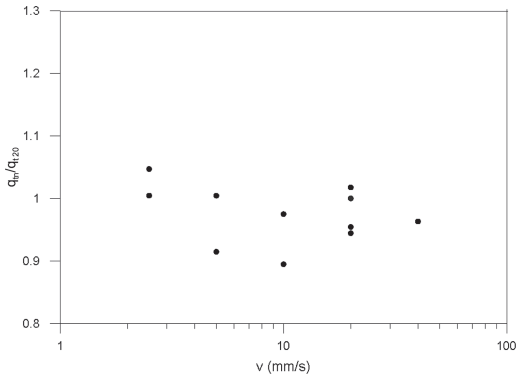

Figure 6. Normalised $q_{tn}/q_{t\,20}$ versus penetration rate, Sarapuí II clay.

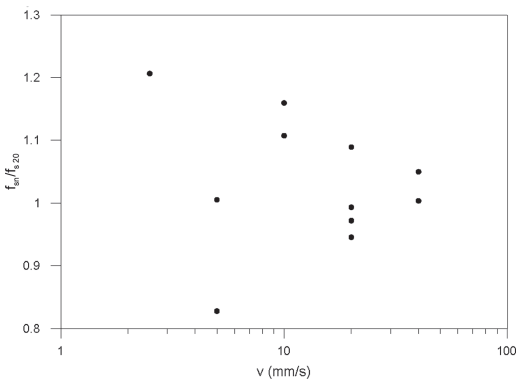

Figure 7. Normalised $f_{sn}/f_{s\,20}$ versus penetration rate, Sarapuí II clay.

as the rate increases, the cone resistance decreases due to the pore pressure generation and there is a decrease in effective stress. As the penetration rate increases furthermore, the viscous forces offset the strength reduction and the curve will pass through a minimum. Then the viscous forces will dominate the process, now in an undrained behavior (see also Roy et al. 1982; Campanella et al. 1982).

The pore pressure u_1 may be considered the most representative to analyze the cone resistance behavior, due to the position where it is measured, and the normalized $u_{1n}/u_{1\,20}$ values versus rate are shown in Fig. 8. Despite not very clear, there is a trend of u_1 increasing with increasing rate, and the region of 10 mm/s – 20 mm/s may be considered to be in undrained condition. However, the higher increase in the case of 40 mm/s has no explanation except for data scatter, since results for other materials show no pore pressure increase in the undrained condition. Further research is still needed on this subject.

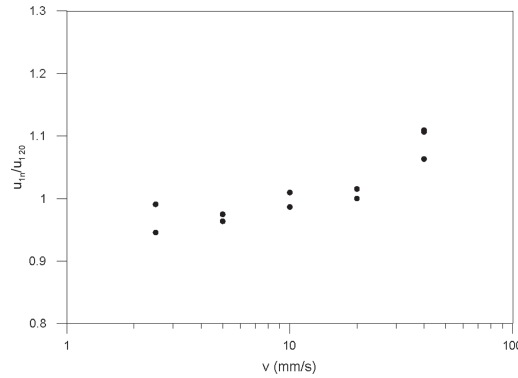

Figure 8. Normalised $u_{1n}/\ u_{120}$ versus penetration rate, Sarapuí II clay.

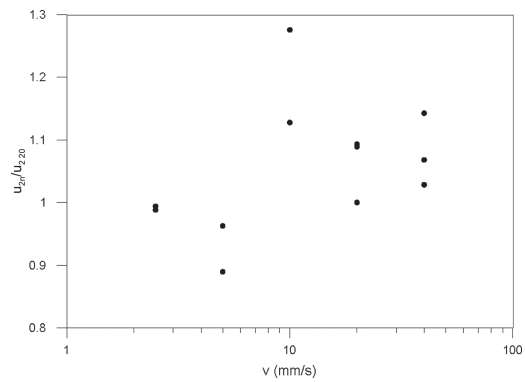

Figure 9. Normalised $u_{2n}/u_{2\,20}$ versus penetration rate, Sarapuí II clay.

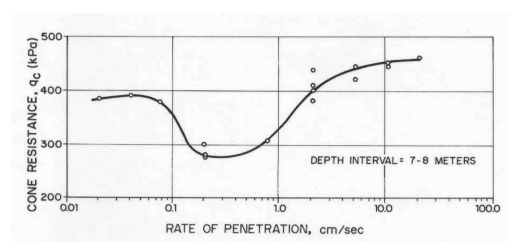

Figure 10. Influence of rate of penetration on cone resistance (adapted from Bemben & Myers 1974).

Normalized $u_{2n}/u_{2\,20}$ values (Fig. 9) present more scatter than $u_{1n}/u_{1\,20}$ values, although with the same general trend, except for 10 mm/s.

Despite the data scatter, the $f_{sn}/f_{s\,20}$ values (Fig. 7) seem to be more influenced by the rate effect than $q_{tn}/q_{t\,20}$, which has also been reported elsewhere (e.g., Campanella et al. 1982).

5 DISCUSSION

Despite the trends described above on the four piezocone quantities, the differences in the measured values are not very significant. In other words, although the measured data seem to indicate that the undrained behaviour initiates at the rate 10 mm/s, the differences with respect to the "partially drained" behaviour is not significant. It must be noted that u_1 and u_2 corresponding to the smallest penetration rate used, 2.5 mm/s, i.e. $u_{1\ 2.5}$ and $u_{2\ 2.5}$ are still much higher than the hydrostatic values (u_0), approximately 3.0–4.5 times greater than u_0 in the case of u_1 and 2.1–2.6 greater in the case of u_2. As far as excess pore pressure is concerned, u_1-u_0 is in the range 50–90 kPa (increasing with depth) and u_2-u_0 in the range 20–50 kPa. Therefore it is clear that in the case of soft clays with very low consolidation coefficients, like Sarapuí clay, it is virtually impossible to reach drained conditions in the field when using regular 10 cm^2 penetrometers.

As a consequence of this small difference in drainage conditions, there is a small difference also in the case of cone resistance and sleeve friction. If a drained condition is to be achieved, adaptations in regular rigs, allowing much smaller rates, and small diameter cones, are necessary.

In order to compare the Onsøy data with the Sarapuí II data, a normalization of the rate of penetration, v, to take into account the diameter of the penetrometer, d, and the coefficient of consolidation, c (Eq. 1) was done.

$$V = \underline{v\ a} \tag{1}$$

where V = normalized rate

Finnie & Randolph (1994) firstly proposed the use of the normalized rate (or velocity), where the coefficient of consolidation c was c_v, i.e., the vertical coefficient of consolidation, however no reference was made to the stress level considered in the analysis performed by these authors.

Other suggestions regarding the use of the proper c_v value followed (e.g., c_v at a representative stress level, House et al. 2001, at the same overconsolidation ratio, Suzuki & Lehane 2015), however this issue is outside the scope of the present paper. When the horizontal coefficient of consolidation from piezocone dissipation tests are available, they seem to be the best choice, thus those values have been used herein.

Fig. 11 presents the Sarapuí II data from Fig. 6 with the Onsøy data included. Unfortunately, only three rates have been used in Onsøy clay, thus a more complete picture cannot be obtained. However, it seems clear that the use of the normalized velocity, even using c_h from piezocone dissipation data, was not capable to unify the resistance-rate data for the two clays tested. It must be noted that this conclusion was also obtained by Suzuki & Lehane (2015), for the case of laboratory c_v values (at the same overconsolidation ratio) for kaolin and kaolin mixture in centrifuge.

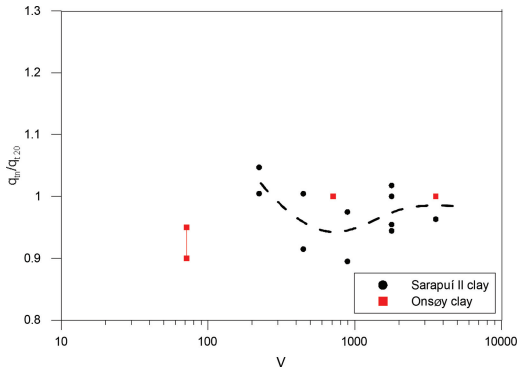

Figure 11. Normalised $q_{tn}/q_{t\ 20}$ versus normalized penetration rate, Sarapuí II and Onsøy clays.

In both deposits, rates greater than the standard rate, in the range 40–100 mm/s, did not result in increase in the normalized $q_{tn}/q_{t\ 20}$, as it could be expected from the high I_p values in both cases. Tests with higher rates are necessary to properly evaluate the role of I_p on rate effect on cone resistance.

As far as pore pressure is concerned, $u_{2\ 2}$ was approximately the same as $u_{2\ 20}$ for Onsøy clay, thus the same conclusion as Sarapuí II clay can be obtained, i.e. adaptations in regular rigs, allowing much smaller rates, and small diameter cones, are necessary if drained conditions are to be achieved for soft clays with low c_h/c_v values.

6 CONCLUSIONS

A comparison was undertaken between piezocone tests with different penetration rates in two soft clay deposits, one from Norway, Onsøy clay, and the other from Brazil, Sarapuí II clay. The Sarapuí II clay is a very plastic clay (I_p in the range 60%-170%), whereas I_p values in Onsøy clay are in the range 20%-50%.

The horizontal coefficient of consolidation, c_h, obtained from piezocone dissipation data is on average 10×10^{-7} m^2/s in the case of Onsøy clay and 4×10^{-7} m^2/s in the case of Sarapuí II clay.

Within the range of penetration rates used, 2.5 mm/s – 100 mm/s, the following conclusions can be drawn: in the case of Sarapuí II clay, there is a reduction in the normalized cone resistance $q_{tn}/q_{t\ 20}$ when the rate increases from 2 mm/s to

5 mm/s, and another reduction, although smaller, when it increases again to 10 mm/s. Then $q_{tn}/q_{t\ 20}$ increases when the rate increases to 20 mm/s, and is roughly the same when the rate further increases to 40 mm/s.

The cone resistance versus penetration rate trend may be explained by the corresponding pore pressure trend (especially u_1, but also u_2).

The friction sleeve versus penetration rate trend, although similar to the cone resistance trend, showed a higher rate effect, i.e. rate effect is more pronounced in the case of sleeve friction than in the case of cone resistance, as found by other authors (e.g., Campanella et al. 1982).

The use of the normalized rate (velocity), even using c_h from piezocone dissipation data, was not capable to unify the resistance-rate data for the two clays tested, Onsøy and Sarapuí II.

Despite the trends mentioned above, adaptations in regular rigs, allowing much lower penetration rates, and small diameter cones, are necessary if drained conditions are to be achieved when conducting piezocone tests in deposits like Sarapuí II or Onsøy clays.

No rate effect was found for penetration rates greater than the standard rate, unlike expected, due to the high I_p values in both deposits, especially in Sarapuí II clay. Tests with higher rates are necessary to properly evaluate the role of I_p on rate effect on cone resistance.

ACKNOWLEDGEMENTS

The authors would like to thank Edgard Luis dos Santos Bispo and Luiz Roberto da Rocha Marinho for assisting in the field testing and sampling.

REFERENCES

Almeida, M.S.S. & Marques, M.E.S. 2003. The behaviour of Sarapuí soft clay. In: Tan, et al. (Eds.), Characterisation and Engineering Properties of Natural Soils—Tan et al. (eds.), Swets and Zeitlinger, Lisse, v. 1, pp. 477–504.

Bemben, S.M. & Myers, D.A. 1974. The influence of rate of penetration on static cone resistance values in Connecticut river valley varved clay. Proceedings of the European Symposium on Penetration Testing, ESOPT, Stockholm, Vol. 2:2, pp. 33–34.

Campanella, R.G., Gillespie, D. & Robertson, P.K. 1982. Pore pressures during cone penetration testing. Proceedings of the Second European Symposium on Penetration Testing, ESOPT II, Amsterdam, Balkema/Rotterdam, v. 2, pp. 507–512.

Danziger, F.A.B., Almeida, M.S.S. & Bezerra, R.L. 1997a. Piezocone research at COPPE/ Federal University of Rio de Janeiro. Proceedings of the Symposium on Recent Developments in Soil and Pavement Mechanics, Rio de Janeiro, Balkema/Rotterdam, pp. 229–236.

Danziger, F.A.B., Almeida, M.S.S. & Sills, G.C. 1997b. The significance of the strain path analysis in the interpretation of piezocone dissipation data. Géotechnique 47 (5), 901–914.

Danziger, F.A.B. & Lunne, T. 1997. Rate effect of piezocone testing. NGI report 20041618-7 (unpublished).

Finnie, I.M.S. & Randolph, M.F. 1994. Punch-through and liquefaction induced failures of shallow foundations on calcareous sediments. Proceedings of the 17th International Conference on the Behaviour of Offshore Structures, Boss´94, Boston.

House, A.R., Oliveira, J.R.M.S. & Randolph, M.F. 2001. Evaluating the coefficient of consolidation using penetration tests. International Journal of Physical Modelling in Geotechnics, 1 (3), 17–25.

Jannuzzi, G.M.F., Danziger, F.A.B. & Martins, I.S.M. 2015. Geological-geotechnical characterisation of Sarapuí II clay. Engineering Geology, 190, 77–86.

Lacasse, S. & Lunne, T. 1982. Penetration tests in two Norwegian clays. Proceedings of the Second European Symposium on Penetration Testing, ESOPT II, Amsterdam, Balkema/Rotterdam, v. 2, pp. 661–669.

Lacerda, W.A., Costa Filho, L.M., Coutinho, R.Q. & Duarte, E.R. 1977. Consolidation characteristics of Rio de Janeiro soft clay. Proceedings of the Conference on Geotechnical Aspects of Soft Clays, Bangkok, pp. 231–243.

Lunne, T., Robertson, P.K. & Powell, J.J.M. 1997. Cone penetration testing in geotechnical practice. Blackie Academic & Professional, London.

Lunne, T., Long, M. & Forsberg, C.F. 2003. Characterisation and engineering properties of Onsøy clay. Characterisation and Engineering Properties of Natural Soils—Tan et al. (eds.), Swets and Zeitlinger, Lisse, v. 1, pp. 395–427.

Roy, M., Tremblay, M., Tavenas, F. & La Rochelle, P. 1982. Development of pore pressure in quasi-static penetration tests in sensitive clay. Canadian Geotechnical Journal, 19 (2), 124–138.

Suzuki, Y. & Lehane, B.M. 2015. Cone penetration at variable rates in kaolin-sand mixtures. International Journal of Physical Modelling in Geotechnics, 15 (4), 209–219.

Cone Penetration Testing 2018 – Hicks, Pisanò & Peuchen (Eds)
© 2018 Delft University of Technology, The Netherlands, ISBN 978-1-138-58449-5

A modified CPT based installation torque prediction for large screw piles in sand

C. Davidson, T. Al-Baghdadi, M. Brown, A. Brennan & J. Knappett
University of Dundee, Dundee, Scotland

C. Augarde, W. Coombs & L. Wang
Durham University, Durham, UK

D. Richards & A. Blake
University of Southampton, Southampton, UK

J. Ball
Roger Bullivant Limited, UK

ABSTRACT: Screw piles have been suggested as an alternative foundation solution to straight-shafted piles for jacket supported offshore wind turbines in deep water. The significant environmental loads in the marine environment will require substantially larger screw piles than those currently employed in onshore applications. This raises questions over the suitability of current design methods for capacity and installation torque. This paper aims to address this issue by presenting a screw pile installation torque prediction method based on cone resistance values from Cone Penetration Test (CPT) data. The proposed method, developed using centrifuge modelling techniques in dry sand, provides accurate predictions of installation torque for both centrifuge and field scale screw piles. Furthermore, unlike existing CPT-torque correlations, the proposed method is shown to be applicable to multi-helix screw piles.

1 INTRODUCTION

Although originally developed for the marine environment (Jacob, 1953, Lutenegger, 2017), screw piles have been widely adopted in numerous onshore applications such as, for guyed towers, light poles and underpinning of existing foundations. The helical plate(s), mounted on the central core of a screw pile allow for their installation by application of continuous axial and rotational forces. This installation method is significantly quieter than the pile driving methods employed in conventional straight-shafted pile installation. The effects on marine life from such noise is of growing concern and has led to strict regulations and the use of expensive mitigation techniques thus making screw piles ideal for this type of application.

The helical plates of a screw pile also generate substantial axial capacity during compression and tensile loading conditions. Furthermore, when the helices of a multi-helix screw pile are spaced apart at less than 2.5 helix diameters (Knappett et al., 2014), enhanced levels of shaft-friction are mobilized from the soil-soil shear which develops over the inter-helix interval, in comparison to the soil-steel interface associated with shaft friction along straight-shafted piles.

It is these benefits, offered by screw piles, which have led some authors (Byrne and Houlsby, 2015, Spagnoli and Gavin, 2015) to suggest their use in the offshore environment, as foundations for deep water offshore wind energy projects.

The expansion of offshore wind energy into deeper water may require alternative foundations and support structures, as concern has been raised over increasing the size of the most commonly used solution of monopile structures (Golightly, 2014). As alternative to monopiles, steel jackets founded on piles can be used. This solution is already in use in the Beatrice Offshore Wind Farm, in the Moray Firth, UK, which is sited in the deepest water to date for an offshore wind farm in the UK.

Replacing the straight-shafted piles typically used as the foundations for the jackets, with screw piles can eliminate any concerns over installation noise and potentially lead to a reduction in the amount of steel required for the foundations due to the improved efficiency of the load carrying mechanism.

To attain the in-service capacities required to sustain the forces created by the combined self-weight and environmental loads, the geometry of current screw pile designs will need to be significantly varied and upscaled. Rotating screw piles into the soil requires significant amounts of torque from the frictional resistance of the soil-steel interface. Thus, increasing the surface area of the screw pile will lead to greater installation torque requirements.

Estimating the installation torque of a screw pile is a critical factor in the development of larger pile geometries for offshore wind applications and is an active area of research (Schiavon et al., 2016, Spagnoli, 2016, Tsuha, 2016). The magnitude of the installation torque (T) of onshore piles is typically used in the verification of the axial tensile capacity (Q_t) through the empirical factor, K_t, developed by Hoyt and Clemence (1989), given in equation 1. Byrne and Houlsby (2015) have developed this further with the use of a dimensionless torque factor. However, BS 8004:2015 (British Standards Institution, 2015) states that screw piles should not be designed solely using empirical methods. Thus, predicting the torque from the axial capacity is not recommended. This would seem appropriate as Al-Baghdadi (2018) showed that the pile's core was the greatest contributor to required torque where Q_t is dictated by the helix plate diameter rather than the core diameter.

$$Q_t = K_t \mathrm{T} \tag{1}$$

Alternatively, analytical techniques developed by Ghaly and Hanna (1991) and Sakr (2015) decompose the torque into the various contributing components from the helices and core. Ghaly and Hanna (1991) had limited field verification of their method which was developed from 1g model scale tests in dry sand. However, the Sakr (2015) approach has been validated against field data for screw piles with core and helix diameters up to 0.508 and 1.016m respectively and installation depths up to 12.8m. Although, such geometries are likely to be inadequate for the loads anticipated in the deep water offshore wind sector.

Correlations between the cone resistance from Cone Penetration Test (CPT) data and the axial capacity of straight-shafted piles have been demonstrated to be potentially more reliable and accurate compared to other analytical and empirical methods. Consequently, several authors have suggested correlations which relate CPT data to the installation torque of screw piles (Gavin et al., 2013, Spagnoli, 2016, Al-Baghdadi et al., 2017).

This paper aims to provide an improvement on the method proposed by Al-Baghdadi et al. (2017), based on further centrifuge modelling of screw piles in dense sand. The method is also validated against multi-helix screw piles to address the lack of available CPT-torque prediction methods for such piles.

This work was undertaken as part of a wider project investigating the development of screw piles for offshore wind energy foundations. In addition to the physical modelling, partly discussed herein, Durham University are developing Material Point Method techniques (Wang et al., 2017) to model screw pile installation effects, while the University of Southampton will conduct field scale tests for verification of the model-scale and numerical investigations.

2 CENTRIFUGE MODELLING

All tests were conducted on the Actidyn beam centrifuge at the University of Dundee at 50g acceleration.

2.1 *Model piles*

Two 1/50 th scale model screw piles (Figure 1) consisting of single and multi-helix designs, both

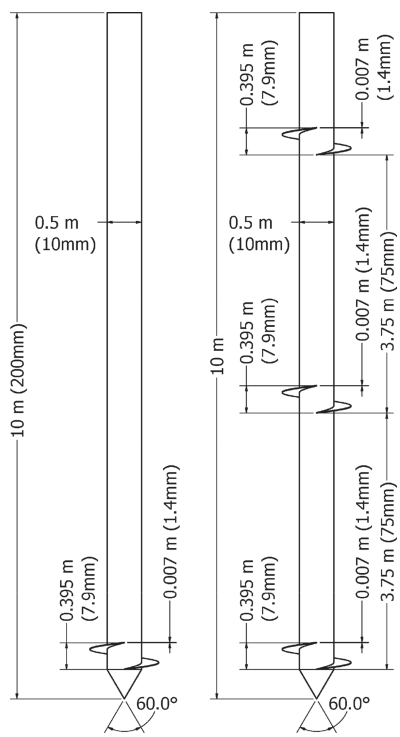

Figure 1. Model screw piles used in centrifuge tests at prototype scale (model dimensions in brackets).

Table 1. HST95 sand material properties (Al-Defae et al., 2013, Lauder et al., 2013).

Property	Value
Grading description	Fine
Effective particle size, D_{10} (mm)	0.09
Average particle size, D_{50} (mm)	0.14
Critical state friction angle, ϕ'_{crit} (°)	32
Soil-steel interface friction angle, δ_{crit} (°)	27
Angle of dilation*, ψ (°)	14
Maximum dry density, ρ_{max} (kN/m^3)	17.58
Minimum dry density, ρ_{min} (kN/m^3)	14.59

*As measured at 73% relative density (Al-Defae et al., 2013).

with 10 mm and 20 mm core and helix diameters respectively, were manufactured from mild steel. Pile shafts were closed-ended with a 60° conical tip.

2.2 *Soil properties*

All centrifuge tests were conducted using HST95 sand. The behavior and properties of this fine grained quarzitic sand are well characterised, having been used in numerous previous studies at the University of Dundee (Jeffrey et al., 2016, Al-Baghdadi, 2018). A minimum ratio of the average (d_{50}) particle size to shaft diameter of 71 satisfied the recommendations made by Garnier et al. (2007) with respect to particle size-pile diameter scaling.

2.3 *Model container and soil preparation*

A steel container with internal dimensions of 500 × 800 × 550 mm, used in all tests, allowed for two tests to be completed in one container by moving the installation/testing rig between centrifuge flights. The minimum spacing between the screw pile and container walls was greater than 10 times the largest helix diameter to ensure no boundary effects were present (Phillips and Valsangkar, 1987, Bolton et al., 1999).

The sand bed was prepared to a depth of 450 mm and a relative density of 73% using an air-pluviation method detailed in Jeffrey et al. (2016).

2.4 *Pile installation*

A custom dual-axis actuator, developed at the University of Dundee by Al-Baghdadi et al. (2016) provided the necessary rotational and vertical forces to install the screw piles. The vertical speed and revolutions per minute are linked by the pitch of the screw pile. Installation of a screw pile must occur such that the screw pile penetrates the soil by an amount equal to the helix pitch for each complete revolution to minimize soil disturbance (Perko, 2009, British Standards Institution, 2015). Thus, a displacement controlled installation, at a penetration speed of 26.3 mm/min and rotation speed of 3.33 rpm, was used for all tests.

The vertical and rotational installation forces were measured with a bespoke F310-Z combined axial loadcell and torque transducer supplied by Novatech Measurements Ltd.

2.5 *Cone penetration tests*

To acquire data to validate the CPT-torque correlation method for screw piles, CPT were conducted in-flight to measure the cone resistance (q_c) of the sand. A custom CPT probe was manufactured for this purpose from stainless steel, with a 14 mm diameter, 440 mm long shaft and a 60° conical tip mounted to a 2 kN loadcell from Novatech Measurements Ltd. The CPT probe was not designed to measure separate skin friction, with average skin friction measurements (not used in this paper) deduced from the total resistance measured at the top of the CPT shaft (via the F310-Z loadcell) minus the CPT tip loadcell readings.

At a penetration depth of 140 mm, the CPT reached the maximum permissible load of the loadcell and the test was stopped. Thus, rather than extrapolating data, the installation torque of the piles are only considered up to this depth. The cone resistance data are presented in Section 4 in the context of verification of the proposed method with field data.

3 CPT-TORQUE CORRELATION METHOD

Screw pile installation torque has been correlated to CPT cone resistance to provide a method to predict the installation torque of both single and multiple helix screw piles in dense sand. In-line with the suggestion of Bustamante and Gianeselli (1982) for pile capacity determination, the cone resistance data was averaged over a distance of 1.5 helix diameters above and below the depth of interest in the calculations.

The torque which develops from the installation of a screw pile into sand is assumed to be created by the frictional resistance between the soil and the entire surface area of the pile. In terms of the proposed CPT-torque correlation method, the torque contribution from the upper surface of the helical plates(s) to the total torque is negligible and can be ignored.

The torque required to install a screw pile with n number of helices can therefore be predicted using

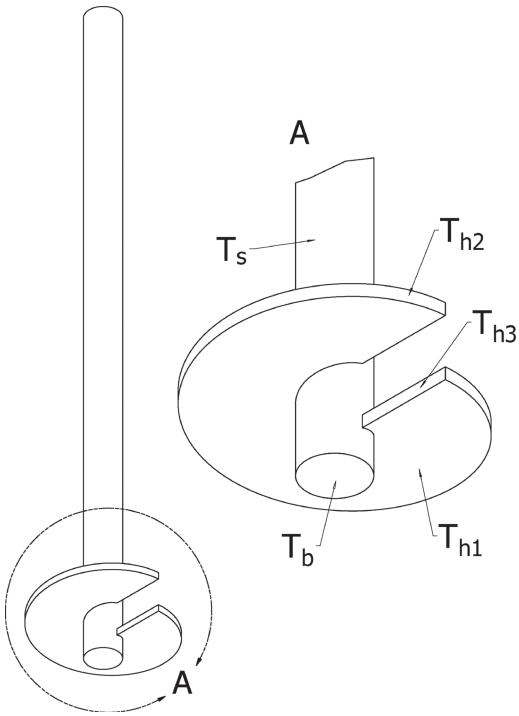

Figure 2. Installation torque resistances acting on a screw pile.

equations 2 to 11, with the components shown visually in Figure 2. In each of equations 4 to 8, the torque is calculated by integrating the relevant frictional resistance multiplied by the appropriate lever arm.

$$T = T_s + T_b + \sum_{1}^{n} T_{h(n)} \tag{2}$$

$$T_h = T_{h1} + T_{h2} + T_{h3} \tag{3}$$

$$T_s = \sum_{\Delta x=1}^{\Delta xi=L} a\overline{q}_c \tan\delta_{crit} \pi \Delta x \frac{d_c^{\,2}}{2} \tag{4}$$

$$T_b = \overline{q}_c \tan\delta_{crit} \pi \frac{d_c^{\,3}}{12} \tag{5}$$

$$T_{h1} = a\overline{q}_c \tan\delta_{crit} \pi \frac{D_h^{\,3} - d_c^{\,3}}{12k_0} \tag{6}$$

$$T_{h2} = a\overline{q}_c \tan\left(\delta_{crit} + \theta\right) \pi t \frac{d_c^{\,2}}{2} \tag{7}$$

$$T_{h3} = a\overline{q}_c t \frac{D_h^{\,2} - d_c^{\,2}}{4} \tag{8}$$

$$a = \frac{F_r}{\tan\delta_{crit}} \tag{9}$$

$$k_0 = 1 - \sin\phi \tag{10}$$

$$\theta = \tan^{-1}\left(\frac{p}{\pi}\frac{D_h - d_c}{2}\right) \tag{11}$$

where: T is the total torque resulting during installation; T_s is the torque associated with the shaft area of the central core of the pile with diameter d_c; T_b is the torque from the base of the central core; T_h is the torque resulting from the helix (with diameter of D_h, pitch of p and thickness of t), which is made up of three components - T_{h1} the friction on the underside of a helix during penetration, T_{h2} torque associated with the thin outer peripheral edge of the helix and T_{h3} from the leading edge of the helix cutting into the soil.

The torque from the shaft area of the core is calculated from the sum of intervals of length Δx over the total length of the screw pile core, L. A stress drop index (a) equal to the CPT friction ratio (F_r) divided by $\tan(\delta_{crit})$ (Lehane et al., 2005) is used to compute the radial stress acting on the screw pile. Although the Lehane et al. (2005) method is associated with driven piles, the stress drop index used was derived from CPT data and does not apply to any particular pile installation technique. To account for the inclination of the screw pile helix, the pitch angle (θ) is added to the interface friction angle (δ_{crit}). The earth pressure at rest (k_0) provides a mechanism to convert the radial stress (aq_c) into a vertical stress acting on the underside of the helices during installation. As in other torque prediction methods, any influence from temperature change during installation were disregarded.

The proposed equations differ to those suggested by Al-Baghdadi et al. (2017) in several ways. Firstly, the rotation force reduction factors required for the shaft and base components (f_1 = 0.75 and f_2 = 0.7, respectively) for force prediction during rotary installation, after Deeks and White (2008), have been omitted from equations 4 and 5. These factors were somewhat greater than those found by Deeks (2008) for installation force reduction and is it not clear why they are required for torque prediction.

Secondly, in equation 5, q_b equal to $0.6q_c$ was used. This is often adopted for pile capacity prediction where this may be below ultimate resistance or at 0.1 pile diameters. Therefore, during full flow installation, it would be more appropriate for q_b to equal q_c (Randolph and Gourvenec, 2011). Thirdly, an erroneously absent $\tan(\delta_{crit})$ term in Al-Baghdadi et al. (2017) has been correctly added to equation 5. Fourthly, equation 8 addresses an integration error and uses the radial stress instead of the full cone resistance value. Finally, the stress drop index is no longer universally assumed to equal 0.03 and is instead calculated by equation 9,

using the CPT friction ratio and interface friction angle of the screw pile.

4 CPT-TORQUE PREDICTIONS

The proposed method was used to predict the installation torque for both model screw piles from centrifuge tests and field-scale data from Gavin et al. (2013) and Spagnoli (2016). CPT cone resistance data from the centrifuge tests and field data are presented in Figure 3. The q_c values for the CPT testing in the centrifuge test were verified against the prepared relative density (checked by density pot measurements) and gave good correlations to the conventional CPT correlations for relative density by Jamiolkowski et al. (2001) at mid-height of the centrifuge container. Low values of q_c near the surface are associated with the transition to a full-flow mechanism which is not seen in the field data due to the high density or over consolidated near surface soils.

4.1 *Model-scale screw pile torque predictions*

The prediction of installation torque of the single and multi-helix screw piles in the centrifuge tests are shown in Figure 4. The predictions show a good level of correlation with the measured values from the centrifuge tests. Additionally, a prediction based on the method in Spagnoli (2016) is also shown in Figure 4a for the single helix screw pile, where an 80% over-prediction of the torque is evident at 5.5 m.

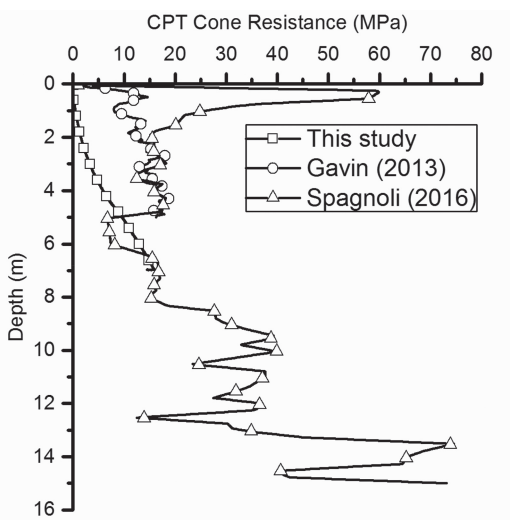

Figure 3. CPT cone resistance from: this study, Gavin et al. (2013) and Spagnoli (2016).

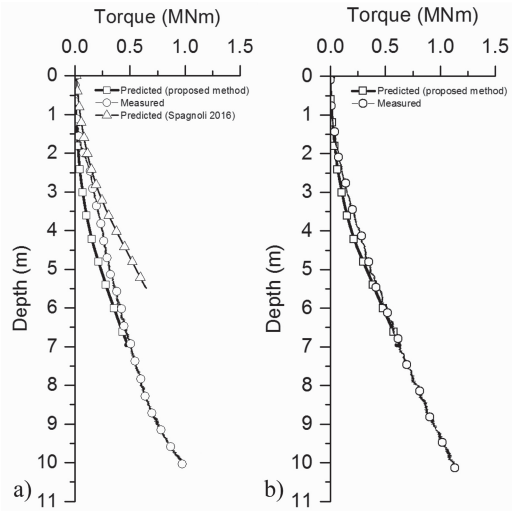

Figure 4. Predicted and measured prototype installation torque from centrifuge tests: a) single helix; b) multi-helix screw pile.

Averaging the CPT cone resistance over a distance of $\pm 1.5D_h$ requires that the CPT extends beyond the screw pile installation depth by $1.5D_h$. In all data in this study, this requirement was not met and thus, the torque predictions only extend to at a depth of $1.5D_h$ above the deepest q_c data point instead of to the full penetration depth of the screw pile.

The proposed method performs well in both cases and it is suggested that the method is applicable for multi-helix screw piles. Previous publications (Gavin et al., 2013; Spagnoli, 2016; Al-Baghdadi et al., 2017) regarding CPT-torque correlations have restricted their predictions to single helix piles only.

4.2 *Field-scale screw pile torque predictions*

Al-Baghdadi et al. (2017) presented a torque prediction based on field data for a single helix screw pile with 100 and 400 mm core and helix diameters respectively, installed to 4.5 m (Gavin et al., 2013). The process is repeated here with the proposed method.

The results (Figure 5a) show close correlations between the predicted and observed installation torque, particularly from a depth of 0.8 to 2.1 m. From 2.1 m to 4.5 m, there is an approximately 15% overprediction of the torque. This is obviously more satisfactory for design than an underprediction. Figure 6b shows a comparison to field testing from Spagnoli (2016) for 16 m long, large diameter single helix screw piles with 368 mm

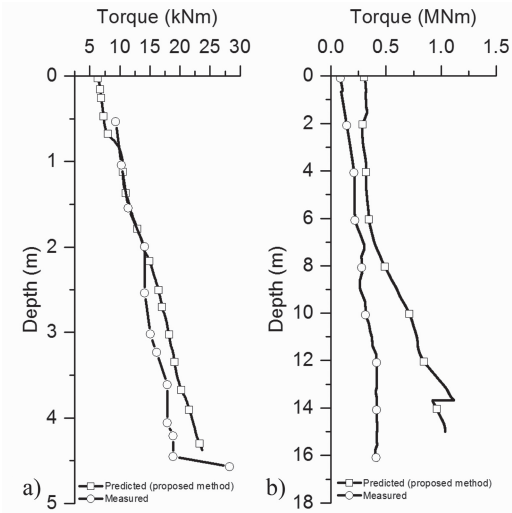

Figure 5. Predicted and measured installation torque from field scale screw piles in: a) Gavin et al. (2013); b) Spagnoli (2016).

diameter cores at a test site in Germany, where the only method available to install the screw pile with the 1500 mm helix diameter (due to torque limitations) was to "surge" the pile up and down, inevitably resulting in unwanted changes to in-situ soil conditions. This may explain the overprediction using the proposed method for the screw pile reported in Spagnoli (2016), with a 750 mm helix diameter, and highlights the need for controlled installation.

5 CONCLUSIONS

This paper presents modifications to the CPT-torque prediction method for screw pile installation proposed by Al-Baghdadi et al. (2017) based on centrifuge tests of single and multi-helix screw piles in dense, dry sand. The changes include: removal of the force rotation reduction factors, which are not deemed appropriate for torque calculations; for the base of the core, a missing $\tan(\delta_{crit})$ term is added and the full q_c value is used to reflect the full flow conditions during installation; the stress drop index used to modify the cone resistance to a radial stress is related to the interface friction angle and CPT friction ratio as well as being incorporated into the helix leading edge calculation. The updated method gives good prediction of the measured centrifuge test data and was further validated by field data from Gavin et al. (2013) and Spagnoli (2016). The modified method also provides further capability in the ability to predict installation torque of multi-helix screw piles.

ACKNOWLEDGEMENTS

This work is part of the EPSRC project EP/N006054/1: Supergen Wind Hub Grand Challenges Project: Screw piles for wind energy foundations. The authors acknowledge support from the European Regional Development Fund (ERDF) SMART Centre at the University of Dundee and thank the Iraqi Ministry of Higher Education and Scientific Research (MOHESR) for financial support to undertake part of this work.

REFERENCES

Al-Baghdadi, T. 2018. *Screw piles as offshore foundations: Numerical & physical modelling*. Ph. D. University of Dundee

Al-Baghdadi, T., Davidson, C., Brown, M., Knappett, J., Brennan, A., Augarde, C., Coombs, W., Wang, L., Richards, D. & Blake, A. 2017. CPT-based design procedure for installation torque prediction for screw piles installed in sand. *8th Int. Conf. on Site Investigation and Geotechnics*. London, UK, 12–14 September. Society for Underwater Technology (SUT OSIG).

Al-Baghdadi, T.A., Brown, M.J. & Knappett, J.A. 2016. Development of an inflight centrifuge screw pile installation and loading system. In Thorel, L., Bretschneider, A., Blanc, M. & Escoffier, S. (eds.), *3rd European Conf. on Physical Modelling in Geotechnics (EUROFUGE 2016)*. IFSTTAR Nantes Centre, France, 1–3 June.

Al-Defae, A.H., Caucis, K. & Knappett, J.A. 2013. Aftershocks and the whole-life seismic performance of granular slopes. *Géotechnique,* 63: 1230–1244.

Bolton, M.D., Gui, M.W., Garnier, J., Corte, J.F., Bagge, G., Laue, J. & Renzi, R. 1999. Centrifuge cone penetration tests in sand. *Géotechnique,* 49: 543–552.

British Standards Institution. 2015. BS 8004:2015. *Code of practice for foundations.* Milton Keynes: BSI.

Bustamante, M. & Gianeselli, L. 1982. Pile bearing capacity prediction by means of static penetrometer CPT. In Verruijt, A. (ed.) *Proc. of the 2nd European Symposium on Penetration Testing*. Amsterdam, 24–27 May 1982. CRC Press.

Byrne, B.W. & Houlsby, G.T. 2015. Helical piles: an innovative foundation design option for offshore wind turbines. *Phil. Trans. R. Soc. A,* 373.

Deeks, A.D. 2008. *An investigation into the strength and stiffness of jacked piles in sand*. Ph. D. University of Cambridge

Deeks, A.D. & White, D. 2008. Centrifuge modelling of rotary-jacked tubular piles: gyropiling. In Brown, M.J., Bransby, M.F., Brennan, A.J. & Knappett, J.A. (eds.), *Foundations—Proc. of the 2nd BGA Int. Conf. on Foundations (ICOF 2008)*. Dundee, UK, 24–27 June. IHS BRE Press.

Garnier, J., Gaudin, C., Springman, S., Culligan, P., Goodings, D., Konig, D., Kutter, B., Phillips, R., Randolph, M. & Thorel, L. 2007. Catalogue of scaling laws and similitude questions in geotechnical centrifuge modelling. *Int. Journal of Physical Modelling in Geotechnics,* 7: 01–23.

Gavin, K., Doherty, P. & Spagnoli, G. 2013. Prediction of the installation torque resistance of large diameter helical piles in dense sand. *Proc. of 1st Int. Geotechnical Symp. of Helical Foundations.* Amherst, USA.

Ghaly, A. & Hanna, A. 1991. Experimental and theoretical studies on installation torque of screw anchors. *Canadian Geotechnical Journal,* 28: 353–364.

Golightly, C. 2014. Technical Paper: Tilting of monopiles Long, heavy and stiff; pushed beyond their limits. *Ground Engineering,* January 2014: 20–23.

Hoyt, R.M. & Clemence, S.P. 1989. Uplift capacity of helical anchors in soil. *Proc. of the 12th Int. Conf. on Soil Mechanics and Foundation Engineering.* Rio de Janeiro, Brazil.

Jacob, F. 1953. A Historical Chapter: British Royal Engineers' Papers On Soil Mechanics and Foundation Engineering, 1837–1874. *Géotechnique,* 3: 242–247.

Jamiolkowski, M., Lo Presti, D.C.F. & Manassero, M. 2001. Evaluation of relative density and shear strength of sands from cone penetration test (CPT) and flat dilatometer test (DMT). *Symp. on Soil Behavior and Soft Ground Construction Honoring Charles C. "Chuck" Ladd*. Cambridge, Massachusetts, United States, 5–6 October 2001. ASCE.

Jeffrey, J.R., Brown, M.J., Knappett, J.A., Ball, J.D. & Caucis, K. 2016. CHD pile performance: part I–physical modelling. *Proc. of the Institution of Civil Engineers-Geotechnical Engineering,* 169: 421–435.

Knappett, J.A., Brown, M.J., Andrew, J.B. & Hamilton, L. 2014. Optimising the compressive behaviour of screw piles in sand for marine renewable energy applications. *DFI/EFFC 11th Int. Conf. On Piling & Deep Foundations*. Stockholm, Sweden, 21–23 May. Deep Foundations Institute.

Lauder, K.D., Brown, M.J., Bransby, M.F. & Boyes, S. 2013. The influence of incorporating a forecutter on the performance of offshore pipeline ploughs. *Applied Ocean Research,* 39: 121–130.

Lehane, B.M., Schneider, J.A. & Xu, X. 2005. The UWA-05 method for prediction of axial capacity of driven piles in sand. *Frontiers in Offshore Geotechnics*. Taylor & Francis.

Lutenegger, A.J. 2017. Support of Offshore Structures Using Helical Anchors. *8th Int. Conf. on Site Investigation and Geotechnics*. London, UK, 12–14 September. Society for Underwater Technology (SUT OSIG).

Perko, H.A. 2009. *Helical piles: a practical guide to design and installation,* Hoboken, New Jersey: John Wiley & Sons.

Phillips, R. & Valsangkar, A. 1987. *An experimental investigation of factors affecting penetration resistance in granular soils in centrifuge modelling*: University of Cambridge.

Randolph, M. & Gourvenec, S. 2011. *Offshore Geotechnical Engineering,* Abingdon, Oxon: Spon Press.

Sakr, M. 2015. Relationship between installation torque and axial capacities of helical piles in cohesionless soils. *Canadian Geotechnical Journal,* 52: 747–759.

Schiavon, J.A., Tsuha, C.H.C., Neel, A. & Thorel, L. 2016. Physical modelling of a single-helix anchor in sand under cyclic loading. In Thorel, L., Bretschneider, A., Blanc, M. & Escoffier, S. (eds.), *3rd European Conf. on Physical Modelling in Geotechnics (EUROFUGE 2016)*. IFSTTAR Nantes Centre, France, 1–3 June.

Spagnoli, G. 2016. A CPT-based model to predict the installation torque of helical piles in sand. *Marine Georesources & Geotechnology*: 1–8.

Spagnoli, G. & Gavin, K. 2015. Helical piles as a novel foundation system for offshore piled facilities. *Abu Dhabi Int. Petroleum Exhibition and Conf.* Abu Dhabi, UAE, 9–12 November. Society of Petroleum Engineers.

Tsuha, C.H.C. 2016. Physical Modelling of the Behaviour of Helical Anchors. In Thorel, L., Bretschneider, A., Blanc, M. & Escoffier, S. (eds.), *3rd European Conf. on Physical Modelling in Geotechnics (EUROFUGE 2016)*. IFSTTAR Nantes Centre, France, 1st-3rd June.

Wang, L., Coombs, W., Augarde, C., Brown, M., Knappett, J., Brennan, A., Humaish, A., Richards, D. & Blake, A. 2017. Modelling screwpile installation using the MPM. *1st Int. Conf on the Material Point Method, MPM 2017*. Delft, The Netherlands. Procedia Engineering.

Taylor & Francis
Taylor & Francis Group
http://taylorandfrancis.com

Cone Penetration Testing 2018 – Hicks, Pisanò & Peuchen (Eds)
© 2018 Delft University of Technology, The Netherlands, ISBN 978-1-138-58449-5

Effects of clay fraction and roughness on tension capacity of displacement piles

L.V. Doan & B.M. Lehane
School of Civil, Environmental and Mining Engineering, The University of Western Australia, Australia

ABSTRACT: This paper examines the effect of clay fraction and roughness on the relationship between the ratio of the CPT end resistance (q_c) to unit shaft friction (τ_f) for displacement piles in sand. Tension load tests were performed on smooth and rough model piles that were jacked into sand, sand-clay mixtures and clay. Parallel constant normal load and constant normal stiffness direct shear interface tests were conducted to assist interpretation and allow separation of effects of interface friction angle and dilation on the capacities. It is shown that even a small amount of clay within a sand mass can have a major impact on the available shaft friction. The effects of pile roughness are important for developing the pile shaft capacities in these soils.

1 INTRODUCTION

There is not a universally accepted method for estimation of the unit shaft friction of displacement piles in intermediate soils such as silts and clayey sands. Shaft friction can be severely over-estimated when applying the standard total stress α method for clay in such materials due to the effects of dilatancy on the measured undrained strength. Conversely, if a design approach for sand is adopted, effects of pore pressures generated during in-situ testing complicate the interpretation of the state of the material.

The assessment of pile capacity using direct correlations with the Cone Penetration Test (CPT) end resistance (q_t) is rapidly becoming the Industry standard partly because of the proven reliability of CPT-based methods, but also because of the ease with which capacities can be calculated without user subjectivity (Doan and Lehane 2016; Niazi and Mayne 2016). Lehane et al. (2017) reviewed the most up-to-date CPT methods namely UWA-05 (Lehane et al. 2005b), ICP-05 (Jardine et al. 2005), NGI-05 (Clausen et al. 2005), Fugro-10 (Van Dijk and Kolk 2010) and UWA-13 (Lehane et al. 2013), and concluded that CPT methods give the most reliable predictions of axial pile capacities in clay and sand. However, the same authors also highlight difficulties with application of these methods in intermediate soils.

This paper examines some of the important issues for displacement piles in intermediate soils and investigates the relationship between shaft friction and CPTu data in experiments conducted in laboratory pressure chambers in normally consolidated kaolin clay, two kaolin-sand mixtures and fine silica sand. Parallel direct shear (DS) tests employing rough and smooth interface tests assist interpretation of the contribution of dilation to the shaft friction.

2 INTERFACE SHEAR CHARACTERISTICS

Kaolin, fine silica sand and mixtures of sand combined with 5% and 25% kaolin (by dry weight) were prepared for element testing. The mixtures are referred to as kaolin (K), sand, 5%K and 25%K. The same soils were employed for the pile tests and accompanying CPTs.

Direct shear tests were performed with an initial normal effective stress of 50 kPa using rough and smooth interfaces with identical properties to those of the model test piles. The rough interface was shotblasted in order to achieve R_{max} (defined as the relative height between the highest peak and the lowest trough over a 2.5 mm gauge length) of about 100–132 µm. The normalised roughness $R_n = R_{max}/D_{50}$ (e.g. Kishida and Uesugi 1987) was such that this interface could be assumed fully rough for the sand, 5%K and 25%K soils. The smooth (aluminium) interface was polished to achieve R_{max} of 2 to 3 µm (as measured using a stylus profilometer).

Fifty soil-soil and soil-interface direct shear tests were performed under constant normal load (CNL) and constant normal stiffness (CNS) conditions using the computerised 'in house' apparatus at UWA. Both the rough and smooth interfaces

were fitted precisely into the lower half of the shear box. Both the upper and lower boxes were made from teflon to mimimise friction (Boukpeti and White 2017; Lehane and Liu 2012). This friction was corrected for using data measured in preliminary experiments (and typically amounted to about 1 kPa).

Kaolin, 5%K and 25%K samples were mixed and water was added to form slurries that were first subjected to de-airing; the water content employed was approximately two times the liquid limit of the respective mixtures. Samples were poured into Shelby tubes and pre-consolidated in stages using dead weights with a maximum stress of 20 kPa. Samples were then removed from the tubes, trimmed and placed into a ring with diameter of 71 mm and height of 20 mm. They were transferred to the upper half of the box (on the top of the interface plate) and consolidated to a normal effective stress of 50 kPa. The unit weights of the samples at the beginning of the tests had average values of 16.5 kN/m^3, 20.5 kN/m^3 and 19.5 kN/m^3 for Kaolin, 25%K and 5%K, respectively.

Shearing was conducted in a displacement-controlled mode at a nominal constant rate of horizontal displacement of 0.05 mm per minute. One test performed on kaolin included three pause periods of 24 hours at shear displacements of 0.7 mm, 1.4 mm and 3.5 mm. An identical response to that obtained with no pause periods was obtained indicating that the displacement rate of 0.05mm/min led to a fully drained response.

Results obtained in the CNL tests using smooth and rough interfaces are summarised in Figure 1, which also includes a test for sand sheared against a rough interface reported by Lehane et al. (2005a). These show that the peak stress ratios τ/σ'_n and the tendency for dilation increase as the clay fraction reduces. Peak stress ratios are approximately 0.9 for sand, 0.63 for 5%K, 0.56 for 25%K and 0.4 for Kaolin; these ratios are in good agreement with experimental observations of Suzuki (2014). It is evident that the introduction of just 5% clay into the sand causes the maximum stress ratio to drop to two thirds of the ratio developed in clean sand.

It is also apparent that the roughness has a strong influence on interface shearing characteristics. In 5%K, for example, the peak shear stress developed on the smooth interface is about 30% less than measured with the rough interface. For the same soil, significant contraction occurs when shearing against the smooth interface, whereas a dilative response is observed with the rough interface. Visual inspections of the samples at the end of the tests confirmed that the failure shear plane was within the soil for the rough interface tests, as shown on Figure 2.

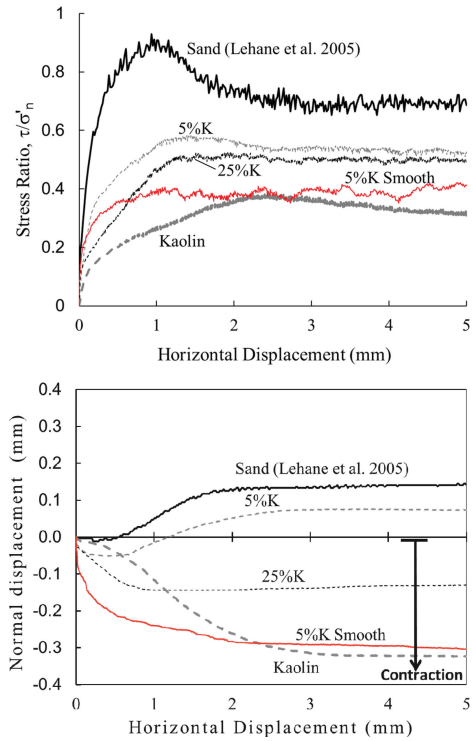

Figure 1. CNL interface tests with σ'_n of 40–50 kPa.

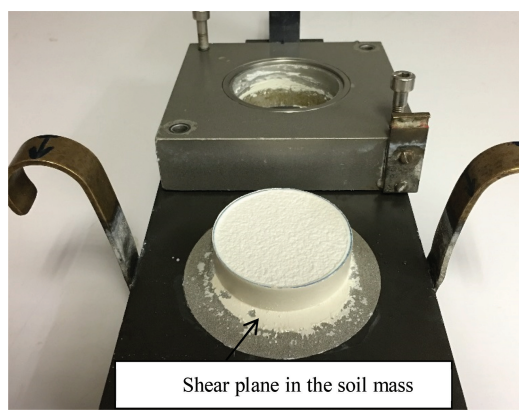

Figure 2. Shear surface for full rough interface tests.

3 CPTU AND PILE TENSION LOAD TESTS

3.1 *Experimental set-up*

CPTu and pile tension tests were performed in UWA kaolin and sand as well as in 5%K and 25%K mixtures. All ten samples tested were normally consolidated in steel pressure chambers with an

Figure 3. Setup of the experiment.

inner diameter of 395 mm and height of 400 mm (Figure 3). Details of the chamber and test set up are described by Doan and Lehane (2018a, b).

The model piles employed were aluminium rods with a diameter (D) of 10 mm. Both smooth and rough piles were tested and pile surfaces were prepared in the same manner and to the same R_{max} values used in the direct shear tests.

All soil samples were prepared from a slurry (as for the shear box tests) and first consolidated in the steel chamber to a vertical effective stress of 32 kPa. After sample consolidation (which took up to 45 days for the kaolin sample), two test piles were jacked into each sample via access holes in the top cap at a constant rate of 0.5 mm/s to a final embedment (L) of 200 mm; this gave a final (typical) pile aspect ratio (L/D) of 20. An equalization period of 24 hours was then allowed prior to tension testing of the piles, which was performed by slow extraction using an actuator at a constant displacement rate of 0.005 mm/s. A 0.5 kN capacity load cell was placed in series between the pile head connector and the actuator, as indicated in Figure 3.

3.2 *CPTu tests*

CPTu tests were performed in the samples using a 10 mm diameter piezocone with a friction sleeve area of 1162 mm^2. The pore pressure filter was situated behind the shoulder of the cone (u_2 position), which was also monitored during dissipation tests. The friction ratio (F_r) was calculated from equation (1), where f_s is the sleeve friction, q_t is the corrected cone end resistance and σ_v is the vertical total stress.

$$F_r = [f_s/(q_t - \sigma_v)]100\% \quad (1)$$

CPT q_t traces recorded in each soil type at a penetration rate of 3 mm/s are plotted on Figure 4. The normalized velocity of the cone associated with this rate is less than that of the standard cone, but Doan and Lehane (2018a) show that all of the plotted q_t and F_r values are essentially the same as the standard CPT parameters.

It is interesting to note the influence of the clay fraction on the q_t and F_r values on Figure 4. The steady state q_t value in the sand is over 5 MPa and about 5 times higher than the 5%K mixture, even though the penetration in both soils is fully

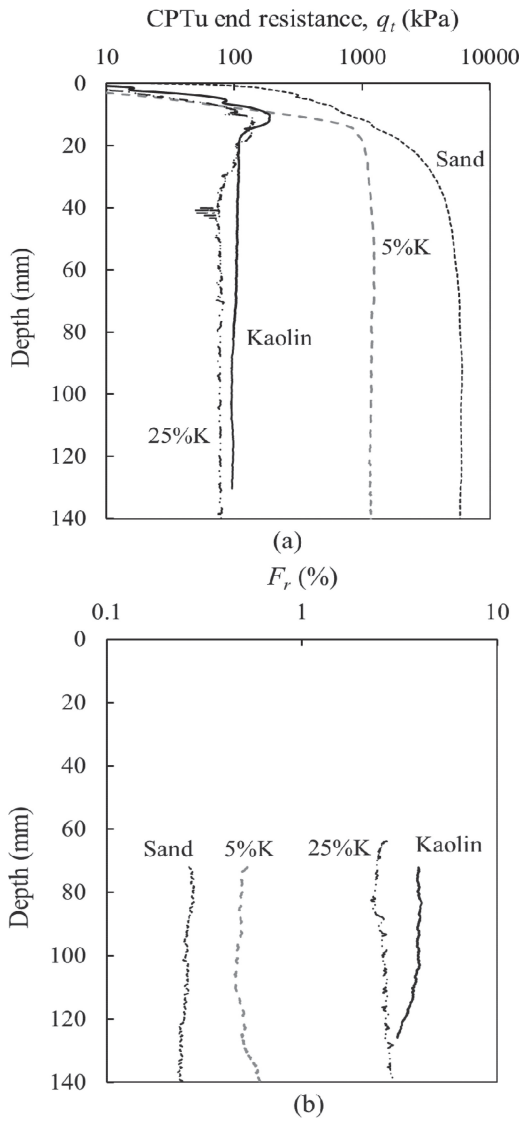

Figure 4. (a) Corrected cone resistance (q_t) and (b) Friction ratios (F_r) at penetration rate of 3 mm/s.

drained (see Doan and Lehane 2018a). The q_t values measured during undrained penetration in 25%K and K mixtures are 10 times smaller again that the 5%K soil, with slightly lower q_t values in the 25%K mixture. The effects of the clay content within a sand mass on the normalized sleeve friction (F_r) measured are illustrated on Figure 4b. It is evident that the F_r values increase with an increase in clay content. The average F_r in kaolin is 3.7%, which is about 1.5 times and 8 times the respective F_r values in the 25%K and 5%K mixtures.

Dissipation tests indicated that a period of 7 hours was required to allow full dissipation of excess pore pressure in kaolin (see Doan and Lehane 2018b). Noting that the CPT device and the piles had the same diameter, it can therefore be inferred that full dissipation of installation induced pore pressures had occurred around all the piles after the set equalization period of 24 hours.

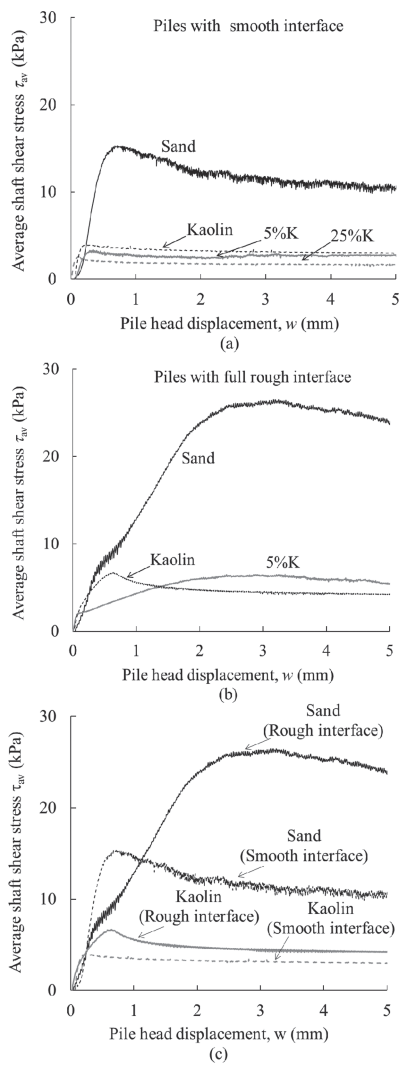

Figure 5. Average shear stress against pile head displacement curves measured in pile tension tests.

3.3 *Tension load tests*

Average shear stresses (τ_{av}), derived as the measured tension load divided by the pile shaft area, determined during some typical chamber pull-out tests are plotted against the pile head displacement (w) in Figure 5.

The dramatic effect of the addition of 5%K to the sand sample is evident, with peak shaft shear stresses (τ_{pav}) being more than 4 times less than for clean sand. The τ_{pav} mobilised in the 5%K mixture is also slightly lower than that measured in Kaolin. Figure 5 shows that the smallest τ_{pav} value is developed in the 25%K mixture. This trend could be explained by a typical strong contractive response of this material at large strains (Doan and Lehane 2018a).

The importance of roughness for these soils is also apparent. The peak shear stress developed on the smooth piles is about 45% less than that mobilised on the rough piles. A similar influence of roughness was observed by Thomas and Fahey (2007) in centrifuge model tests of piles tested in kaolin.

Peak friction develops at lower displacements against the smooth interfaces (when there is a contractive response); a similar response has been observed by Lehane et al. (2005a).

4 RESULTS AND DISCUSSION

The ratio of the average CPT q_t along a pile shaft ($q_{t,av}$) to the peak average shaft friction (τ_{av}) measured in the tension tests, referred as β_c (= $q_{t,av}/\tau_{av}$), varied from 345 in the test on the smooth pile in sand to 15 in the test on the rough pile in kaolin. These β_c ratios are plotted on Figure 6 against the soil behaviour type (SBT) index, I_c, as defined by Robertson and Wride (1998) and Robertson (2016):

$$I_c = \left[(3.47 - \log Q_{tn})^2 + (\log F_r + 1.22)^2\right]^{0.5} \quad (2)$$

$$Q_{tn} = \left[(q_t - \sigma_v)/p_a\right](p_a/\sigma'_v)^n \quad (3)$$

$$n = 0.381(I_c) + 0.05(\sigma'_v/p_a) - 0.15 \quad (4)$$

where Q_{tn} is the normalised CPT cone resistance; F_r is the normalised cone sleeve resistance obtained from equation (1); n is the stress exponent that varies with I_c; σ_v and σ'_v are the current in-situ vertical total and effective stresses and p_a is atmospheric reference pressure in the same units as q_t.

A relatively consistent variation of β_c with the SBT index, I_c, is evident on Figure 6, which uses a logarithmic scale for β_c The β_c ratios for the smooth piles are typically about double those for the rough piles for all soil types. The plotted trend lines are described by the following equations and are seen to provide a good representation of the data recorded. The legends for the tests plotted on this figure employ the symbols R and S to denote 'rough' and 'smooth' pile interfaces and use the symbol 'F' to indicate that CPT installation was conducted at a normalized velocity reasonably close to that of a standard CPT (as discussed above).

For rough interfaces:

$$\beta_c = 200 \text{ for } I_c \leq 1.8 \quad (5a)$$

$$\beta_c = 10^{3.45-0.65Ic} \text{ for } 1.8 < I_c < 3.6 \quad (5b)$$

$$\beta_c = 15 \text{ for } I_c \geq 3.6 \quad (5c)$$

For smooth interfaces:

$$\beta_c = 350 \text{ for } I_c \leq 2 \quad (6a)$$

$$\beta_c = 10^{3.45-0.65Ic} \text{ for } 2 < I_c < 3.6 \quad (6b)$$

$$\beta_c = 30 \text{ for } I_c \geq 3.6 \quad (6c)$$

Doan and Lehane (2018a) also present cone penetration q_t and F_r values recorded in the four soil types, using drained penetration velocities (e.g. velocities of 0.0005 mm/s in kaolin and 0.001 mm/s in 25%K). These drained parameters are substituted into equation (2) to derive what is referred to here as modified SBT index, given the symbol I_c*. Values of β_c are then evaluated for all the tests included in Figure 6 using both the standard q_t values and the drained q_t values and plotted against I_c* on Figure 7.

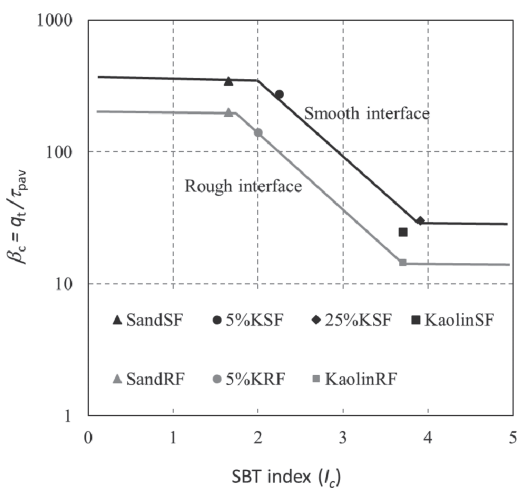

Figure 6. Variation of β_c with SBT I_c index.

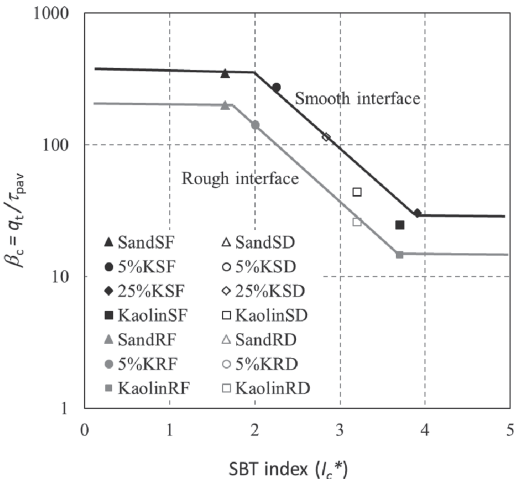

Figure 7. Variation of β_c with I_c^* index.

It is apparent on Figure 7 that the same trend lines for β_c with I_c on Figure 6 are also valid for the β_c *vs.* I_c* trend lines on Figure 7. It is seen, for example, how the reduced I_c* values in kaolin and 25%K (due primarily to higher drained cone resistances) lead to correspondingly higher β_c values. This is an important result when considering effects of partial drainage on cone penetration as it indicates that errors due to a misinterpretation of partial drainage do not arise provided that a direct correlation with the measured q_t value is employed using a formulation of the form of equation (7) for (typical) rough interfaces with a pile aspect ratio (L/D) of 20:

$$\beta_c = 200 \text{ for } I_c^* \leq 1.8 \quad (7a)$$

$$\beta_c = 10^{3.45-0.65I_c^*} \text{ for } 1.8 < I_c^* < 3.6 \quad (7b)$$

$$\beta_c = 30 \text{ for } I_c^* \geq 3.6 \quad (7c)$$

I_c^* can be substituted for I_c in equation (6) to find the corresponding formulation for smooth piles. It should also noted that these equations were derived for a single aspect ratio (L/D = 20) and methods such as Lehane et al. (2013) indicate that the friction developed on displacement piles varies mildly with L/D.

5 CONCLUSION

A series of direct shear interface, CPTu and pile tension load tests conducted in laboratory pressure chambers involving clayey sands, sand and clay indicate that:

i. The presence of even a small amount of clay within a sand mass leads to a very large reduction in the shaft capacity of displacement piles. The peak shaft shear stress of displacement piles in a 5%K mixture was more than 4 times less than that of in clean sand.
ii. Pile roughness has a critical effect on the shaft friction that can develop in sands, clayey sands and clays. The shaft friction mobilized on the 'rough' piles was typically double that of the smooth piles.
iii. The pile test data combined with CPTs performed at various rates indicate that, for piles with L/D = 20, β_c varies in a systematic manner with the modified soil behaviour type index, I_c^*. The consistent nature of this trend provides the basis for a promising approach for predicting pile capacities without the need to consider effects of partial drainage during cone penetration.

ACKNOWLEDGEMENTS

The authors would like to thank Craig at Fast Blast Co. for making the interface roughness. Thanks are also extended to Dr. Yusuke Suzuki at NGI for providing CPT digital data. The great support from staff at UWA including Jit Kheng Lim, David White, Matthew Arpin, Jim Waters, Steven, Brad Rose, Manuel Palacios, Adam Stubbs, Kelvin Leong, Ying Guo and Usha Mani as well as from postgraduate students including Reynaldi Iskandar and Gershom Ong is also gratefully acknowledged. The first author acknowledges the Australian Department of Foreign Affairs and Trade for financial support through AAS scholarships.

REFERENCES

Boukpeti, N., and White, D.J. 2017. Interface shear box tests for assessing axial pipe–soil resistance. Géotechnique **67**(1): 18–30. doi: 10.1680/jgeot.15.P.112.

Clausen, C., Aas, P., and Karlsrud, K. 2005. Bearing capacity of driven piles in sand, the NGI approach. *In* Proceedings of Proceedings of International Symposium. on Frontiers in Offshore Geotechnics, Perth. pp. 574–580.

Doan, L.V., and Lehane, B.M. 2016. The influence of pile diameter on the relationship between the unit shaft friction of bored piles in sand and the CPT end resistance. *In* 69th Canadian Geotechnical Conference—GeoVancouver 2016, Vancouver, Canada. p. #3816.

Doan, L.V., and Lehane, B.M. 2018a. Effects of partial drainage on the assessment of the soil behaviour type using the CPT. *In* Proceedings of the 4th International Symposium on Cone Penetration Testing (CPT'18), Delft, Netherlands, submitted.

Doan, L.V., and Lehane, B.M. 2018b. Shaft resistance of non-displacement piles in normally consolidated clay. *In* Proceedings of the 4th International Symposium on Cone Penetration Testing (CPT'18), Delft, Netherlands, submitted.

Jardine, R., Chow, F., Overy, R., and Standing, J. 2005. ICP design methods for driven piles in sands and clays, London: Thomas Telford.

Kishida, H., and Uesugi, M. 1987. Tests of the interface between sand and steel in the simple shear apparatus. Géotechnique **37**(1): 45–52.

Lehane, B.M., Gaudin, C., and Schneider, J.A. 2005a. Scale effects on tension capacity for rough piles buried in dense sand. Geotechnique **55**(10): 709–719.

Lehane, B.M., Li, Y.N., and Williams, R. 2013. Shaft Capacity of Displacement Piles in Clay Using the Cone Penetration Test. Journal of Geotechnical and Geoenvironmental Engineering **139**(2): 253–266.

Lehane, B.M., Lim, J.K., Carotenuto, P., Nadim, F., Lacasse, S., Jardine, R.J., and Van Dijk, B.F.J. 2017. Characteristics of Unified Databases for Driven Piles. *In* Proceedings of the 8th International Conference of Offshore Site Investigation and Geotechnics (OSIG 2017), London, UK.

Lehane, B.M., and Liu, Q.B. 2012. Measurement of Shearing Characteristics of Granular Materials at Low Stress Levels in a Shear Box. Geotech Geol Eng **31**(1): 329–336. doi: 10.1007/s10706–012-9571-9.

Lehane, B.M., Schneider, J.A., and Xu, X. 2005b. The UWA-05 method for prediction of axial capacity of driven piles in sand. *In* Frontiers in Offshore Geotechnics. Taylor & Francis.

Lehane, B.M., and White, D.J. 2005. Lateral stress changes and shaft friction for model displacement piles in sand. Canadian Geotechnical Journal **42**(4): 1039–1052.

Niazi, F.S., and Mayne, P.W. 2016. CPTu-based enhanced UniCone method for pile capacity. Engineering Geology **212**: 21–34. doi: http://doi.org/10.1016/j.enggeo.2016.07.010.

Robertson, P. 2016. Cone penetration test (CPT)-based soil behaviour type (SBT) classification system—an update. Canadian Geotechnical Journal **53**(12): 1910–1927.

Robertson, P.K., and Wride, C.E. 1998. Evaluating cyclic liquefaction potential using the cone penetration test. Canadian Geotechnical Journal **35**(3): 442–459. doi: 10.1139/t98-017.

Suzuki, Y. 2014. Investigation and Interpretation of Cone Penetration Rate Effects. PhD thesis, The University of Western Australia, Perth, Australia.

Thomas, J., and Fahey, M. 2007. Load testing of single piles in clay. *In* Proceedings of the 10th Australia New Zealand Conference on Geomechanics 2007. Carillon Conference Management Pty. Ltd. pp. 568–573.

Van Dijk, B., and Kolk, H. 2010. CPT-based design method for axial capacity of offshore piles in clays. *In* Proceedings of the International Symposium on Frontiers in Offshore Geotechnics II. Edited by S. Gourvenec and D. White. Taylor & Francis Group, London. pp. 555–560.

Cone Penetration Testing 2018 – Hicks, Pisanò & Peuchen (Eds)
© 2018 Delft University of Technology, The Netherlands, ISBN 978-1-138-58449-5

Shaft resistance of non-displacement piles in normally consolidated clay

L.V. Doan & B.M. Lehane
School of Civil, Environmental and Mining Engineering, The University of Western Australia, Australia

ABSTRACT: This paper presents results from a series of tension pile load tests on buried piles in normally consolidated kaolin and compares trends observed with shaft friction inferred from Constant Normal Load (CNL) and Constant Normal Stiffness (CNS) direct shear tests. It is shown that a CNL test with allowance for a 10% reduction in lateral effective stress during shearing provides a simple way of obtaining an accurate estimate of the available pile shaft friction. The capacities predicted using four separate of empirical methods, including more recent CPT methods, are under-predicted by a factor of between 1.5 and 2.2.

1 INTRODUCTION

CPT-based methods for predicting the axial capacity of driven piles are rapidly becoming the industry standard. Chandler and Martins (1982), Francescon (1983), Mochtar and Edil (1988), and others examined the response of piles in kaolin. There is, however, a relative shortage of experiments performed under well-controlled conditions in the laboratory to test the validity of CPT methods for non-displacement piles and to compare measured capacities with the simple Coulomb friction law. This paper addresses this scarcity of data by presenting results from tension pile tests conducted on buried piles in normally consolidated kaolin in a laboratory pressure chamber and in the centrifuge. CPT q_t, f_s and u_2 data were recorded in the same kaolin deposits used for the pile tests. Parallel constant normal load (CNL) and constant normal stiffness (CNS) direct shear interface tests are presented to assist interpretation of the pile tests. All piles and interfaces tested were fully rough.

The relief in lateral stress during boring operations is thought to be compensated for the application of the head of concrete during shaft construction and therefore lateral stresses acting on the pile shaft are approximately unchanged from their initial K_0 condition (O'Neill 2001). For this reason, the observations made in this paper for buried piles are also considered applicable to standard bored piles.

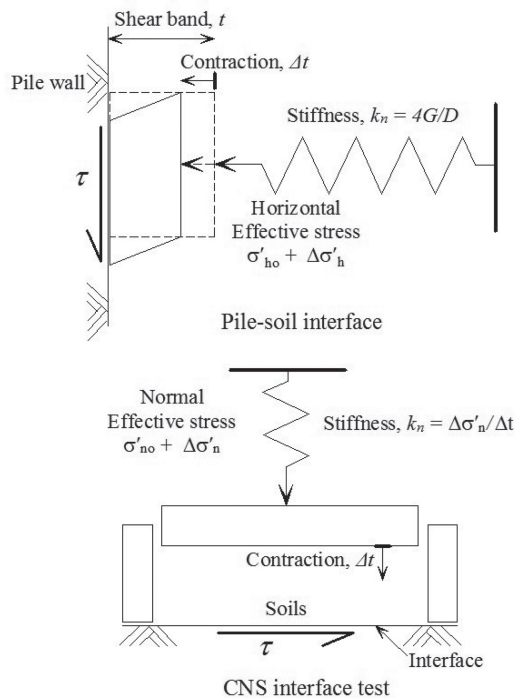

Figure1. Analogy between a pile-soil interface and a CNS test.

2 MODEL FOR PILE SHAFT RESPONSE

Static pile load testing is usually performed at a drained rate of displacement. Under these conditions, as illustrated in Figure 1, the soil at the soil-pile shaft interface will either contract or dilate during shear and hence lead to a reduction or increase in lateral effective stress ($\Delta\sigma'_h$) acting on the shaft due to the constraint provided by the surrounding soil mass. This mechanism is similar to that of a soil element subjected to interface shear under CNS conditions (e.g. Airey et al. 1992).

The change in lateral stress ($\Delta\sigma'_h$) on a cylindrical pile shaft of diameter D due to a change in shear band thickness (Δt) can be replicated in CNS interface shear box test as follows using a CNS stiffness of k_n, by considering elastic cavity expansion (Boulon and Foray 1986)

$$\Delta\sigma'_h = \frac{4G\Delta t}{D} = k_n \Delta t \tag{1}$$

where G is the operational shear modulus of the soil around the pile.

3 CNL AND CNS INTERFACE SHEAR TESTS

Five direct shear tests were performed with initial normal effective stresses of 25 kPa and 50 kPa using rough interfaces with identical properties to those of the model test piles. The rough interface was shotblasted in order to achieve R_{max} (defined as the relative height between the highest peak and the lowest trough over a 2.5 mm gauge length) of about 100–132 μm. The normalised roughness $R_n = R_{max}/D_{50}$ (e.g. Kishida and Uesugi 1987) was such that this interface could be assumed fully rough for the clay.

Soil-interface direct shear tests were performed at at normal stiffnesses (k_n) of 0 kPa/mm (i.e. a CNL test), 100 kPa/mm, 200 kPa/mm and 1000 kPa/mm using the computerised 'in house' apparatus at UWA. The rough interfaces were fitted precisely into the lower half of the shear box. Both the upper and lower boxes were made from teflon to mimimise friction (Boukpeti and White 2017; Doan and Lehane 2018a; Lehane and Liu 2012). This friction was corrected for using data measured in preliminary experiments (and typically amounted to about 1 kPa).

Kaolin clay with respective liquid and plastic limits of 61% and 27% was used in all tests. The kaolin was mixed under a vacuum for 1 day at a water content of two times the liquid limit (about 120%) to form a homogeneous slurry. Samples for the shear box tests were poured into Shelby tubes and pre-consolidated in stages using dead weights with a maximum stress of 20 kPa. Specimens were then removed from the tubes, trimmed and placed into a ring with diameter of 71 mm and height of 20 mm. They were subsequently transferred to the upper half of the box (on the top of the interface plate) and then consolidated to initial normal effective stresses ($\Delta\sigma'_{no}$) of 25 and 50 kPa.

Figure 2 summarises the results obtained in interface tests on rough interfaces. The shear displacement required to mobilise peak stresses is a little smaller in CNS tests, but was typically about 2 mm for the CNL and CNS tests. All samples contract under shear with peak stresses mobilized just prior to when samples attain constant volume conditions. The ratios of shear stresses (τ) to current

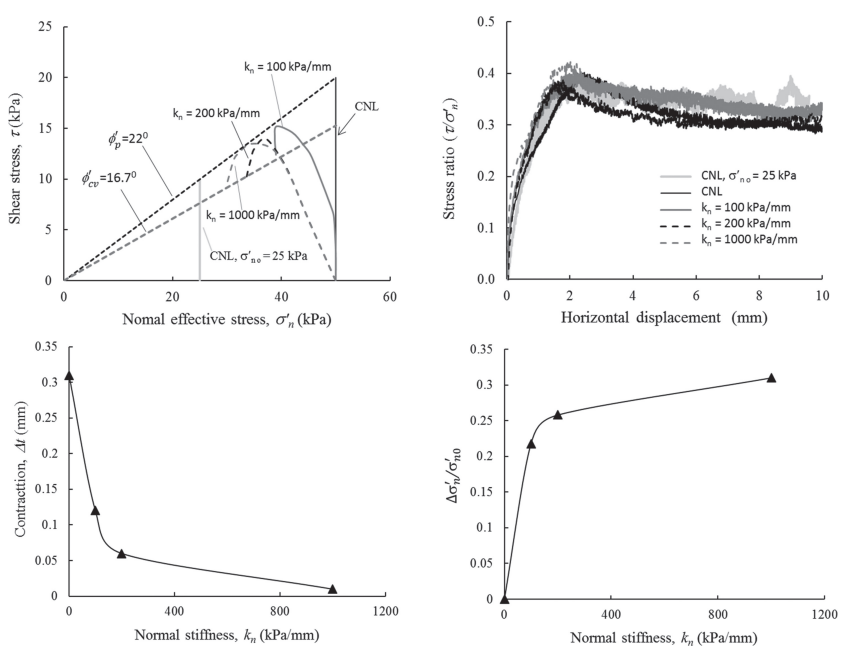

Figure 2. Interface shear test results for Kaolin using rough interface with σ' of 25 kPa and 50 kPa.

normal effective stresses (σ'_n) at peak and ultimate conditions are comparable for all CNS and CNL tests. The mean peak and ultimate stress ratios observed are 0.4 and 0.3 respectively.

It is apparent that the contraction and the decrease in normal effective stresses ($\Delta\sigma'_n$) acting on the interface at peak are higher with higher values of k_n (Figure 2). Significantly higher maximum shear stresses are mobilised under CNL conditions as, in contrast to the CNS tests, there is no decrease in normal effective stress during shear. An unrestrained maximum contraction of 0.31 mm is observed in the CNL tests, whereas the maximum (Δt) value is only 0.01 mm for the samples sheared with $k_n = 1000$ kPa/mm. Figure 2 shows the $\Delta\sigma'_n / \Delta\sigma'_{no}$ ratios plotted against the normal stiffness (k_n). The highest $\Delta\sigma'_n / \Delta\sigma'_{no}$ ratio of about 0.3 is obtained for the CNS test with $k_n = 1000$ kPa/mm.

4 CPTU AND PILE TENSION LOAD TESTS

4.1 *Experimental set-up*

CPTu and pile tension tests were performed in normally consolidated kaolin in the geotechnical beam centrifuge and in a number of laboratory pressure chambers at the University of Western Australia (UWA).

4.1.1 *UWA beam centrifuge*

One of the samples tested in the UWA centrifuge was normally consolidated in a rectangular strongbox with internal plan dimensions of 390 mm by 650 mm and a height of 325 mm. The strongbox weighs about 70 kg and permits models with up to 250 mm of saturated soil (about 200 kg) to be tested at maximum acceleration level of 200*g* (Figure 3). A complete technical description of the facility is given by Randolph et al. (1991).

The model tension pile employed was a hollow, closed-ended, aluminium rod with a diameter of 8 mm. The embedded length of the pile in the sample was 100 mm. The pile surface was prepared in the same manner as the rough interface in the direct shear tests. The model pile was embedded in kaolin slurry and positioned using a pin with a plate at the top of the strongbox, as indicated on Figure 3; this pin also facilitated vertical movement of the pile. The weight of pile was designed to equal the weight of the displaced kaolin to ensure that no relative displacement between the pile and the soil took place during in-flight consolidation of the kaolin. These procedures ensured no negative skin friction on the pile and lateral stresses acting on the pile shaft prior to axial loading that closely approximated normally consolidated K_0 conditions.

The kaolin sample (including the pile) was consolidated at an acceleration of 100*g* for 4 days. To

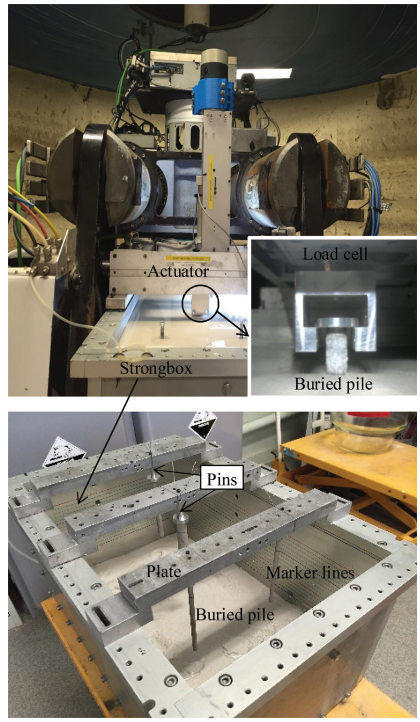

Figure 3. Setup of UWA beam centrifuge for tension load tests.

ensure that the sample was fully consolidated, the soil settlement was monitored and compared with marker lines inside of the strongbox, as indicated in Figure 3. A 20 mm layer of free water was maintained above the sample throughout testing. After the sample consolidation completed, the pile was then tension load tested by applying a constant displacement rate of 0.0005 mm/s to the pile head using a 8 kN capacity load cell connected to the actuator.

4.1.2 *UWA pressure chamber*

All three samples tested were normally consolidated in steel pressure chambers with an inner diameter of 395 mm and height of 400 mm. Details of the chamber and test set up are described by Doan and Lehane (2018a, b).

The model piles were buried in a kaolin slurry sample, which was then consolidated to a vertical effective stress of 32 kPa over a period of 45 days (at which point no creep settlement of the kaolin samples was detectable). A load cell and two laser LVDTs were used to monitor the applied stress and soil settlement during testing. The water level was always maintained about 20 mm above the top plate to ensure that the samples were fully saturated.

The model tension piles employed were solid aluminium rods with diameters of 8 mm, 14 mm

and 20 mm, each with an embedded length of 200 mm. All model piles were tied to the top cap using split clamps via access holes with clearance of 1 mm around the piles during the sample consolidation. The procedures could avoid relative displacements between the pile and the soil during the test. When sample consolidation was completed, split clamps were removed before piles tests. The pile tension load tests were performed by slow extraction using an actuator at a constant displacement rate of 0.005 mm/s. A 0.5 kN capacity load cell was placed in series between the pile head connector and the actuator.

4.2 *CPTu tests*

CPTu tests were performed at various penetration rates in both the geotechnical beam centrifuge and the laboratory pressure chambers. The cone penetrometer had a diameter of 10 mm and a friction sleeve area of 1162 mm^2. The pore pressure filter was located at the shoulder (u_2 position) of the cone.

Apart from the upper 30 mm of the sample where cone penetration was not steady-state, the CPTu tests in the chambers indicated uniform conditions with virtually constant q_t and u_2 values of 95 kPa and 40 kPa, when tested at an undrained rate of penetration. The q_t values in the centrifuge reach their respective steady state gradient of 16.7 kPa/m (Randolph and Hope 2004). A more detailed description of CPTu results at various penetration rates is provided by Doan and Lehane (2018b).

4.3 *Tension load tests*

Average shear stresses (τ_{av}), derived as the measured tension load divided by the pile shaft area, determined during the chamber and centrifuge pull-out tests are plotted against the pile head displacement (w) in Figure 4. Peak average shear stress (τ_{pav}) on these rough piles develop at pile head displacements corresponding to a w/D ratio of 5%. The magnitudes of τ_{pav} are independent of pile diameter (D), for the investigated D range of 8 mm to 20 mm, although the higher pile displacements are required for larger pile diameters, as indicated in Figure 4.

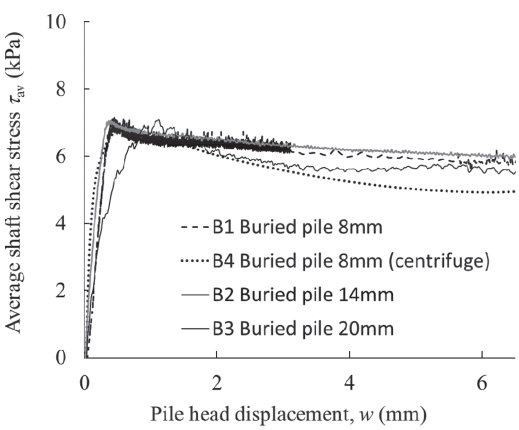

Figure 4. Typical shear stress displacement curves measured in pile tension tests.

5 RESULTS AND DISCUSSION

5.1 *Predicting the pile shaft friction using results obtained in CNL and CNS interface tests*

The peak ultimate shaft friction (τ_f) on a non-displacement pile may be obtained from Coulomb's friction equation as:

$$\tau_f = \sigma'_{hf} \tan \delta_p = K_0 \sigma'_{vo} (1 + \Delta\sigma'_h/\sigma'_{ho}) \tan \delta_p \qquad (2)$$

where σ'_{hf} is the lateral effective stress at peak unit skin friction and δ_p is the peak interface friction angle between the soil and the pile shaft. The value of σ'_{hf} differs from the in-situ lateral effective stress (σ'_{h0}) due to the changes in lateral effective stress that arise during shearing at the pile-soil interface ($\Delta\sigma'_h$).

The inferred values of $\Delta\sigma'_h$ derived using equation (2) are normalised by the mean initial lateral effective stress (σ'_{h0}) and current lateral effective stress (σ'_h) provided in Table 1. The K_0 value was assumed equal to 0.6 and tan δ_p was taken as 0.4 using the mean ratio observed in the CNL and CLS direct interface tests (Figure 2).

Table 1 indicates a mean reduction of 8% in horizontal effective stress during loading of test piles. This result is similar to the stress reduction during shearing inferred by Chandler and Martins (1982) in laboratory model pile tests and is also comparable to the mean reduction of 15% measured by Lehane and Jardine (1994) for displacement piles in soft clay.

The mean lateral effective stress at peak shear stress (σ'_{hf}) was calculated assuming a 10% reduction in lateral stress from the K_0 stress and

Table 1. Test results.

Piles	D (mm)	τ_{pav} (kPa)	σ'_{h0} (kPa)	$\Delta\sigma'_h$ (kPa)	$\Delta\sigma'_h/\sigma'_{h0}$
B1	8	7.2	19.5	1.6	0.08
B2	14	7.1	19.5	2.0	0.1
B3	20	7.1	19.5	2.0	0.1
B4*	8	7.7	19.8	0.8	0.04

*Performed in UWA beam centrifuge.

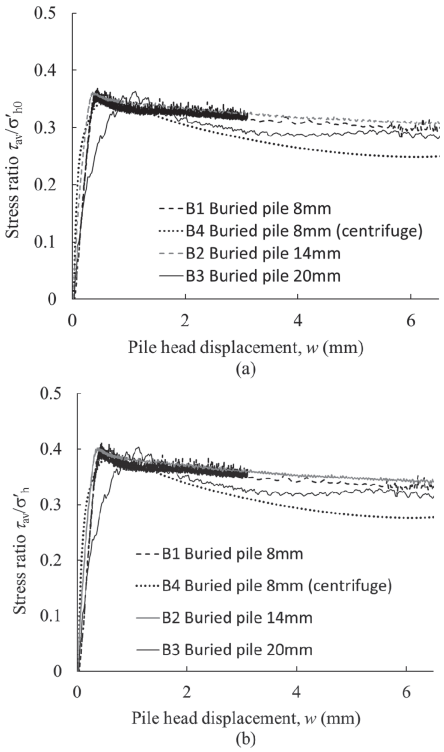

Figure 5. Stress ratios against pile head displacement (w).

ratios of average peak shear stress (τ_{pav}) to these σ'_{hf} values are plotted against the pile head displacement on Figure 5. It is evident that Figure 5 closely resembles Figure 2, confirming direct interface tests can be used directly in pile capacity predictions.

5.2 *Comparison of measured capacities with existing methods*

The pile capacities measured in the chamber and centrifuge tests are compared in this section with popular existing design methods. One of the most popular methods is the α method where α is typically taken equal to 0.5 for bored piles (Tomlinson and Woodward 2014). Lehane et al. (2009) show that the undrained strength ratio (for simple shear strength) of the kaolin used in the experiments is 0.25 and this ratio combined with $\alpha = 0.5$ was used to estimate the ratio of the calculated to measured pile capacities (Q_c/Q_m). The average Q_c/Q_m ratio obtained using this approach for the four pile tests is 0.56, as indicated in Table 2.

Another popular method is the LCPC method proposed by Bustamante and Gianeeselli (1982)

Table 2. Mean Q_c/Q_m ratios for four test piles in kaolin.

Methods	Q_c/Q_m
Direct shear test (CNL with $\Delta\sigma'_h/\sigma'_{h0} = 0.1$)	0.97
Total stress method (α)	0.56
Bustamante and Gianeeselli (1982)	0.45
Eslami and Fellenius (1997)	0.62
Niazi and Mayne (2016)	0.67

where peak friction is directly related to the CPT q_c value for bored piles in soft clay as:

$$\tau_p = q_c / 30 \tag{3}$$

As indicated in Table 2, this method also significantly under-predicts the pile capacities with a mean Q_c/Q_m value of 0.45 for the four test piles.

Eslami and Fellenius (1997) proposed an improvement on the LCPC method by correlating capacities with CPTu parameters using 102 full-scale pile loading tests. They proposed the following formulation for bored piles in soft sensitive clays:

$$\tau_p = 0.08(q_t - u_2) \tag{4}$$

where q_t is the pore pressure corrected q_c resistance. As indicated in Table 2, this method performs better than the LCPC method but under-estimates capacity by about 40%.

A more recent method proposed by Niazi and Mayne (2016) based on data from 153 pile load tests gives the following expression for bored pile under tension loading mode at a constant rate of penetration:

$$\tau_p = 0.78 \times (10^{0.73 I_c - 3.6})(q_t - u_2) \tag{5}$$

where I_c is the soil behaviour type index defined by Robertson (2016). Adopting the I_c value of 3.6 provided by Doan and Lehane (2018b) for kaolin leads to a mean Q_c/Q_m ratio of 0.67 which is an improvement on the two other CPT methods examined.

Table 2 clearly indicates that best predictions are obtained using the stress ratio measured in a direct shear interface test combined with the assessed K_0 value of 0.6 and a 10% reduction in lateral effective stress during shearing. Further research is required to improve the empirical methods considered.

6 CONCLUSION

The following conclusions are obtained from a series of static tension tests on buried piles in

normally consolidated kaolin, coupled with parallel constant normal load and constant normal stiffness direct shear interface tests.

i. The pile diameter (D) does not affect the magnitudes of the shaft frictions developed (with D ranging from 8 mm to 20 mm).
ii. A CNL test with allowance for a 10% reduction in lateral effective stress during shearing provides a simple way of obtaining an accurate estimate of the available pile shaft friction, if the in-situ horizontal stress can be reasonably estimated.
iii. Existing empirical methods relating capacity with the CPTu parameters as well as clay undrained strength perform poorly for the buried piles and underestimate capacity by a factor of between 1.5 and 2.2.

ACKNOWLEDGEMENTS

The authors would like to thank Craig at Fast Blast Co. for making the interface roughness. The great support from staff at UWA including Jit Kheng Lim, David White, Matthew Arpin, Jim Waters, Steve Hobden, Brad Rose, Manuel Palacios, Adam Stubbs, Kelvin Leong, Ying Guo and Usha Mani as well as from postgraduate students including Reynaldi Iskandar and Gershom Ong is also gratefully acknowledged. The first author acknowledges the Australian Department of Foreign Affairs and Trade for financial support through AAS scholarships.

REFERENCES

Airey, D., Al-Douri, R., and Poulos, H. 1992. Estimation of Pile Friction Degradation from Shearbox Tests.

Boukpeti, N., and White, D.J. 2017. Interface shear box tests for assessing axial pipe–soil resistance. Géotechnique **67**(1): 18–30. doi: 10.1680/jgeot.15.P.112.

Boulon, M., and Foray, P. 1986. Physical and numerical simulation of lateral shaft friction along offshore piles in sand. *In* Proc. 3rd International Conference on Numerical methods in offshore piling, Paris, France. pp. 127–148.

Bustamante, M., and Gianeeselli, L. 1982. Pile bearing capacity prediction by means of static penetrometer CPT. *In* Proc. of Second European Symposium on Penetration Testing (ESOPT II), Amsterdam. pp. 493–500.

Chandler, R.J., and Martins, J.P. 1982. An experimental study of skin friction around piles in clay. Géotechnique **32**(2): 119–132. doi: doi:10.1680/geot.1982.32.2.119.

Doan, L.V., and Lehane, B.M. 2018a. Effects of clay fraction and roughness on tension capacity for displacement piles. *In* Proceedings of the 4th International Symposium on Cone Penetration Testing (CPT'18), Delft, Netherlands, submitted.

Doan, L.V., and Lehane, B.M. 2018b. Effects of partial drainage on the assessment of the soil behaviour type using the CPT. *In* Proceedings of the 4th International Symposium on Cone Penetration Testing (CPT'18), Delft, Netherlands, submitted.

Eslami, A., and Fellenius, B.H. 1997. Pile capacity by direct CPT and CPTu methods applied to 102 case histories. Canadian Geotechnical Journal **34**(6): 886–904.

Francescon, M. 1983. Model pile tests in clay: Stresses and displacements due to installation and axial loading. PhD thesis, University of Cambridge.

Kishida, H., and Uesugi, M. 1987. Tests of the interface between sand and steel in the simple shear apparatus. Géotechnique **37**(1): 45–52.

Lehane, B.M., and Jardine, R.J. 1994. Displacement-pile behaviour in a soft marine clay. Canadian Geotechnical Journal **31**(2): 181–191. doi: 10.1139/t94–024.

Lehane, B.M., and Liu, Q.B. 2012. Measurement of Shearing Characteristics of Granular Materials at Low Stress Levels in a Shear Box. Geotech Geol Eng **31**(1): 329–336. doi: 10.1007/s10706–012–9571–9.

Lehane, B.M., O'loughlin, C.D., Gaudin, C., and Randolph, M.F. 2009. Rate effects on penetrometer resistance in kaolin. Géotechnique **59**(1): 41–52. doi: doi:10.1680/geot.2007.00072.

Mochtar, I., and Edil, T. 1988. Shaft Resistance of Model Pile in Clay. Journal of Geotechnical Engineering **114**(11): 1227–1244. doi: 10.1061/(ASCE)0733-9410(1988)114:11(1227).

Niazi, F.S., and Mayne, P.W. 2016. CPTu-based enhanced UniCone method for pile capacity. Engineering Geology **212**: 21–34. doi: http://doi.org/10.1016/j.enggeo.2016.07.010.

O'Neill, M. 2001. Side Resistance In Piles and Drilled Shafts. Journal of Geotechnical and Geoenvironmental Engineering **127**(1): 3–16.

Randolph, M., and Hope, S. 2004. Effect of cone velocity on cone resistance and excess pore pressures. *In* Proceedings of the IS Osaka—Engineering Practice and Performance of Soft Deposits. Yodogawa Kogisha Co. Ltd. pp. 147–152.

Randolph, M., Jewell, R., Stone, K., and Brown, T. 1991. Establishing a new centrifuge facility. *In* Proc. Int. Conf. on Centrifuge Modelling, Centrifuge 91. Boulder, Colo., Boulder, Colo. pp. 3–9.

Robertson, P. 2016. Cone penetration test (CPT)-based soil behaviour type (SBT) classification system—an update. Canadian Geotechnical Journal **53**(12): 1910–1927.

Tomlinson, M., and Woodward, J. 2014. Pile Design and Construction Practice, Sixth Edition. 5 ed. Taylor & Francis Inc, CRC Press Inc, Hoboken.

Cone Penetration Testing 2018 – Hicks, Pisanò & Peuchen (Eds)
© 2018 Delft University of Technology, The Netherlands, ISBN 978-1-138-58449-5

Effects of partial drainage on the assessment of the soil behaviour type using the CPT

L.V. Doan & B.M. Lehane
School of Civil, Environmental and Mining Engineering, The University of Western Australia, Australia

ABSTRACT: This paper presents the results from a series of CPTs performed at various penetration rates in kaolin, two kaolin-sand mixtures and fine silica sand. The CPTs were conducted in laboratory pressure chambers at penetration velocities varying from 0.0002 to 3 mm/s. The measured dependence of cone end resistance (q_t), sleeve friction (f_s) and pore pressure (u_2) on penetration rate is used to examine implications for the assessment of soil behavior type from CPT parameters. Element tests using triaxial and direct interfaces tests are used to assist interpretation of the test results.

1 INTRODUCTION

The standard penetration rate of 20 mm/s employed in a CPT typically results in drained penetration in sand, undrained penetration in clay and partially drained penetration in silts and clayey sands. Partial drainage effects are an important consideration when assessing the soil behaviour type from charts such as those of Robertson (2009). Understanding these effects in silts and clayey sands is also vital in foundation engineering for examples such as the prediction of the embedment of large diameter spudcans using CPT data (Erbrich 2005).

Variable rate CPTs (or 'twitch tests') have been proposed by Randolph et al. (2007), and others, as a means of assessing effects of partial drainage. Lunne et al. (2011) also reviewed the benefits of the variable-rate penetration tests in evaluating strain rate dependency of in-situ soil strength and consolidation characteristics.

CPT rate effects in clayey soils and kaolin have been investigated successfully by many researchers (DeJong et al. 2012; Kim et al. 2008; Schneider et al. 2007; Suzuki and Lehane 2015). However, the effects of different penetration rates on the assessed soil behavior type and on the Robertson I_c index (Robertson 2009) have not been evaluated for a wide range of soils.

This paper presents CPTu results conducted in laboratory pressure chambers with measurements of end resistance (q_t), cone sleeve friction (f_s) and pore pressure at the cone shoulder (u_2) at different penetration rates in kaolin clay, two kaolin-sand mixtures and fine silica sand; each soil was normally consolidated. Previous investigations of this kind at the University of Western Australia (UWA) did not measure cone sleeve friction and did not enable assessment of the soil behaviour type or I_c index.

2 SOIL PROPERTIES

UWA kaolin, fine silica sand and mixtures of sand mixed with 5% and 25% kaolin (by dry weight) were prepared for element tests and CPTs performed in a pressure chamber. The mixtures are referred to as kaolin (K), sand, 5%K and 25%K.

Isotopically consolidated undrained (CIU) triaxial compression tests with consolidation radial effective stresses of 50 and 100 kPa were performed as part of this study and to supplement simple shear tests performed on other kaolin-sand mixtures reported by Suzuki and Lehane (2015). Stress paths measured in these tests are shown on Figure 1 and indicate a highly contractive response before phase transformation, after which strong dilation is observed.

Direct shear tests employing rough and smooth interface tests with an effective normal pressure of 50 kPa were also performed for the 5%K soil with a unit weight of 19.5 kN/m^3 and a water content of 20%. The rough interface was shotblasted to a centre line average roughness (R_{CLA}) of about 18.5 µm or R_{max} of about 100–132 µm. The smooth interface was similar to that of the CPT friction sleeve interface (R_{max} ~ 2–3 µm). The test results are shown on Figure 2 and indicate that, as seen in the triaxial tests, an initially contractive response followed by dilation occurs for the 5%K sample sheared against a rough interface.

However the response of the 5%K when sheared against a relatively smooth interface is contractive and the mobilized shear resistance is about 25%

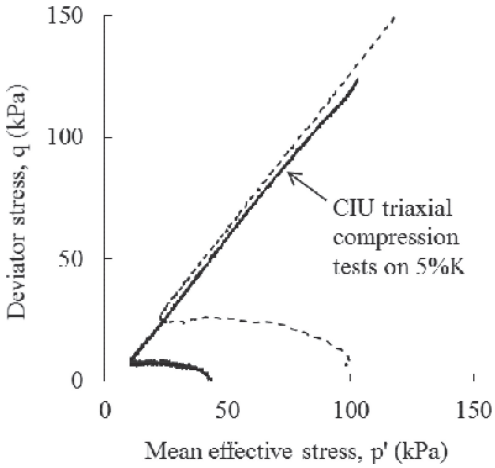

Figure 1. Stress paths measured in CIU triaxial compression tests on 5%K.

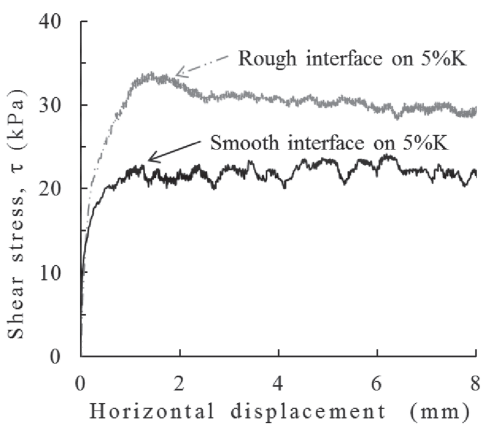

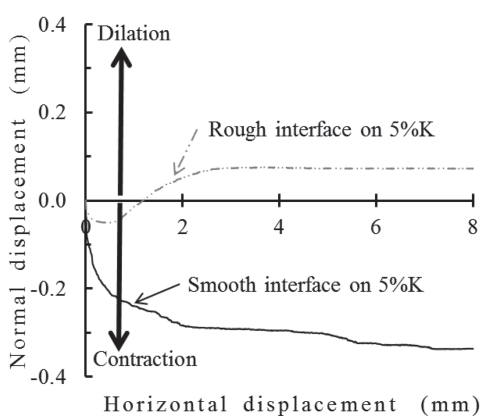

Figure 2. Smooth and fully rough interface test results on 5%K with initial normal effective stress of 50 kPa.

less than for the case of a rough interface. It is evident that the shear strength and dilative behaviour increase with increasing roughness; a similar response has been observed by Hu and Pu (2004) and Pra-ai (2013). This observation has important implications for the interpretation of cone friction sleeve measurements.

A more detailed description of the properties of UWA sand and kaolin and of the 5%K and 25%K mixtures is provided by Lehane et al. (2005; 2009) and Suzuki and Lehane (2015).

3 CPT TESTS IN PRESSURISED CHAMBERS

A series of CPTu tests was performed in normally consolidated UWA kaolin and sand as well as in 5%K and 25%K mixtures. All nine samples tested were normally consolidated in steel pressure chambers with an inner diameter of 395 mm and height of 400 mm (Figure 3). Details of the chamber and test set up are described by Lim and Lehane (2014) and (Doan and Lehane 2018a, b).

The aluminum plate located on the top surface of the samples was 20 mm thick and included a 13 mm diameter circular opening that facilitated the insertion of a removable cap. The cap was fixed to the top plate using two screws during soil consolidation and then removed to enable CPTu penetration. A teflon coating was applied to the inner wall of the steel chamber and to the top plate to minimize friction. A constant normal consolidation stress (σ'_v) of 32 kPa was applied to samples using dead weights (DWs) and a lever system, as indicated in Figure 3. A load cell was placed in line with the load transferring rod and top plate to measure the stress applied to the sample.

Figure 3. Setup of the experiment.

An actuator was used to insert the cone at penetration rates ranging from 0.0002 to 3 mm/s. The miniature piezocone comprised a standard 60° cone tip, with a cone and shaft diameter of 10 mm, a friction sleeve area of 1162 mm^2 and a pore pressure filter situated behind the shoulder of the cone (u_2 position). The cone unequal area ratio correction factor (α) of 0.8 was measured when calibrated both by direct loading and within a pressure chamber.

Kaolin, 5%K and 25%K samples were mixed and water was added to form slurries that were first subjected to de-airing; the water content employed was approximately two times the liquid limit of the respective mixtures. The slurry samples were poured on top of two sheets of geotextiles placed at the base of the chambers. The sand samples were created by water pluvation to achieve a relative density of ~42%. The unit weights of these samples were measured at the end of the test with average values of 16.5 kN/m^3 for Kaolin, 20.5 kN/m^3 for 25%K, 19.5 kN/m^3 for 5%K and 19.7 kN/m^3 for sand. The upper aluminium plate was located on the top of the samples, which were then consolidated in stages to the required normal stress of 32 kPa. A load cell and two laser LVDTs were used to monitor the applied stress and soil settlement. The CPTu penetration was started after the LVDT reading showed no change for a period of at least three days. The water level was maintained about 20mm above the top plate during the consolidation and penetration testing. The procedures employed ensured that the samples were fully saturated and consolidated.

4 RESULTS AND DISCUSSION

4.1 *CPTu testing results*

The testing program comprised CPTu penetrations in nine separate chamber experiments to investigate the effects of various penetration rates on the CPT parameters in clay-sand mixtures. A standard (relatively fast) rate of 3 mm/s was selected as a reference rate in this study. Steady state deep penetration was attained at depths between 25 and 60 mm depending on the soil stiffness. The higher soil stiffness (arranged in order of sand, 5%K, 25%K and kaolin) required a deeper depth for CPT penetration to stabilize and reach the steady state.

The following normalized CPTu parameters have been proposed by Robertson (2016) and Schneider et al. (2008):

$$Q_m = [(q_t - \sigma_v) / p_a](p_a / \sigma'_v)^n \quad (1)$$

$$F_r = [f_s / (q_t - \sigma_v)]100\% \quad (2)$$

$$U_2 = (u_2 - u_0) / \sigma'_v = \Delta u_2 / \sigma'_v \quad (3)$$

where q_t is the corrected cone resistance and equal to $[q_c + u_2(1 - \alpha)]$; σ_v and σ'_v are the current in-situ vertical total and effectives stresses; u_2 is the penetration pore pressure on the cone shoulder; u_0 is the current in-situ equilibrium water pressure; Δu is the excess penetration pore pressure; f_s is the cone sleeve friction; p_a is atmospheric reference pressure in the same units as q_t; n is the stress exponent that varies with soil behaviour type (SBT) defined by:

$$n = 0.381(I_c) + 0.05(\sigma'_v / p_a) - 0.15 \quad (4)$$

where $n \leq 1.0$; I_c is a SBT index initially proposed by Jefferies and Davies (1993) and modified by Robertson and Wride (1998) to apply to the Robertson (2009) Q_t - F_r chart, as defined by:

$$I_c = \left[(3.47 - \log Q_{tn})^2 + (\log F_r + 1.22)^2\right]^{0.5} \quad (5)$$

Equation (5) is used to calculate this index at different velocities and is referred to here at I_c^* to distinguish it from the I_c value measured in a standard CPT. Figure 4 summarises the CPTu results at various penetration rates measured in the chamber tests. It is clear that a higher kaolin content leads to a lower cone resistance, except for the case of the 25%K mixture for which cone resistances in excess of 0.5 mm/s fall below those of pure kaolin.

In 25%K and kaolin, the data suggest that penetration at velocities less than 0.001 mm/s is fully drained with Δu_2~0 i.e. u_2 was virtually identical to u_0. The calculated normalized drained CPT end resistance with a variable stress exponent (Q_{tnD}) is approximately 8 in 25%K, which is 60% higher than Q_{tnD} in kaolin. In contrast, the normalized undrained CPT end resistance with a variable stress exponent (Q_{tnUD}) in kaolin (at velocities in excess of about 0.5 mm/s) is about 20% higher than for the 25% K mixture while corresponding Δu_2 values are about 25% lower.

For the 5%K soil, no significant differences in Δu_2 were observed for penetration rates between velocities of 0.002 and 3 mm/s. Although the absence of excess pore pressure suggests that penetration at these rates is largely drained, a slight increase in Q_{tn} is evident as penetration velocities decrease. As expected for the sand, Q_{tn} values are independent of the penetration rate (over the range investigated) and excess pore pressures are essentially zero.

The effect of the cone velocity on the normalized sleeve friction (F_r) measured in the four soils investigated is illustrated on Figure 4c. It is seen that F_r is virtually constant at about 0.3 ± 0.1% for

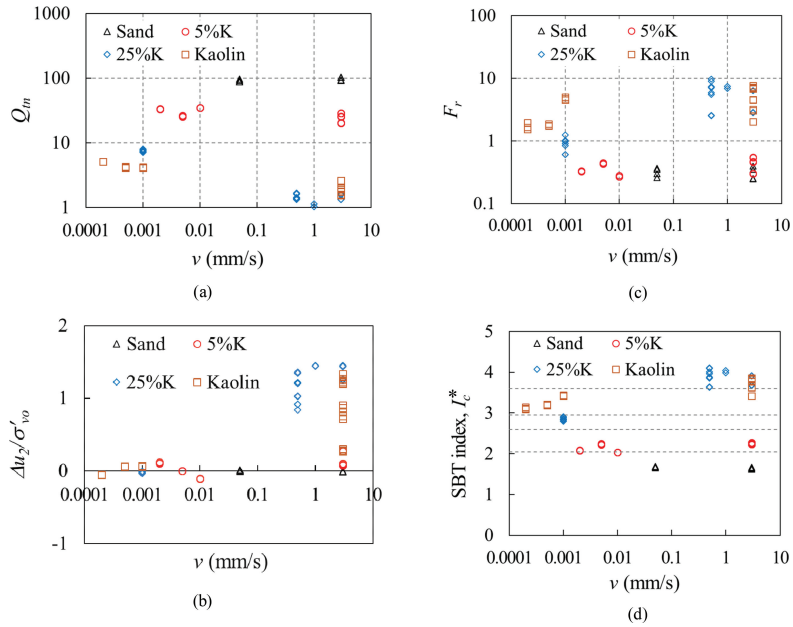

Figure 4. Effects of different penetration velocities on: (a) Q_{tn}, (b) $\Delta u_2/\sigma'_v$, (c) F_r and (d) I_c^*.

all velocities for the 5%K and sand. However, the F_r values decrease with slowing penetration velocities for the samples with higher kaolin contents (albeit with some scatter). The average F_r ratio reduces by a factor of between 3 and 7 as the penetration rate reduces from an undrained to a drained rate.

The variation of I_c^* calculated using equation (5) at different cone penetration velocities is illustrated in Figure 4d. It is seen that I_c^* remains independent of cone velocity for the sand and the 5%K mixture, averaging at 1.7 and 2.1 respectively. In kaolin, I_c^* shows a relatively small reduction with velocity (which varies by four orders of magnitude) reducing from 3.7 for undrained conditions to 3.2 in drained conditions i.e. the index and the assessment of SBT is not overly sensitive to the cone velocity. Greater sensitivity of I_c^* is exhibited by the 25%K soil, which reduces from a value of 4 during undrained penetration to 2.8 at a drained velocity. This change in index shifts the data point on Robertson's SBT chart from Zone 2 to Zone 4 (see Figure 6c). However, it is important to note that the SBT chart of Robertson (2009) relates to the standard cone penetration velocity of 20 mm/s for a standard area cone (10 cm^2).

4.2 *Effect of CPTu penetration rate on end resistance (q_t)*

The CPTu measurements in this study are combined with results obtained in the UWA drum centrifuge and 1_g chamber reported by Suzuki and Lehane (2015) to examine the effect of a wider range of penetration velocities on CPT end resistance (Figure 5). A normalized velocity (V) is defined by Finnie and Randolph (1994)

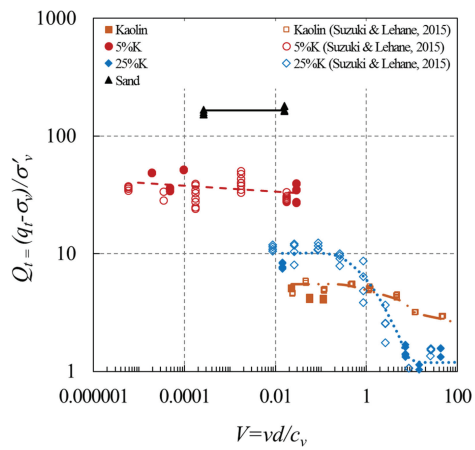

Figure 5. Normalized cone resistance (Q_t) against normalized velocity (V).

$$V = \frac{vd}{c_v} \tag{5}$$

where v is the cone velocity; d the cone diameter; and c_v is the vertical coefficient of consolidation measured in a one-dimensional consolidation test.

The c_v values employed here are reported by Suzuki and Lehane (2015) for the four soils investigated.

Figure 5. presents results of normalized end CPT resistance (Q_t) against V for the combined database.

In sand, the Q_t value of 170 ± 10 is independent of V. For 5% K mixture, a reduction in Q_t of only about 20% is observed as V increases from 10^{-5} (v = 0.01 mm/s) to 0.03 (v = 3 mm/s). This reduction occurs even though Δu_2 was zero at all velocities.

In the 25%K mixture, fully drained penetration occurred at $V < 0.01$ and fully undrained penetration required $V > 7$. The ratio of normalized drained end cone resistance (Q_{tD}) to normalized undrained end cone resistance (Q_{tUD}) is 10 ± 2, which is similar to the ratio measured by both Kim et al. (2008) and Jaeger et al. (2010). In kaolin, the partially drained penetration occurs at a different normalized velocity range between 0.08 and 100 and the average Q_{tD}/Q_{tUD} ratio of 2.2 is about 4 times lower than for 25%K soil; this ratio is in good agreement with CPTs performed in centrifuge tests by Randolph and Hope (2004). The very low Q_{tUD} values in the 25%K mixture (and resulting high Q_{tD}/Q_{tUD} ratio) is attributed by Suzuki & Lehane (2015) to a highly contractive response, as seen also in element tests on the material.

4.3 *Soil behaviour type*

The data from the variable rate penetration tests are plotted on the most up-to-date Soil Behaviour Type (SBT) charts on Figure 6. The results obtained by Suzuki and Lehane (2015), Kim et al. (2008) as well as in this study show that data recorded at rate of 3 mm/s with a 10 mm diameter cone are similar to those of the standard 36 mm diameter CPTu performed at 20 mm/s (noting respective normalized velocities differ by a factor of 24). This is confirmed on Figure 6a which shows the sand, the 5%K mixture and kaolin classifying as sand (Zone 6), sand-mixtures (Zone 5) and clay (Zone 2) respectively. It is interesting to note that despite the high sand content, this chart classifies the 25%K mixture as a clay; this classification is in keeping with the material's mechanical characteristics measured in element tests.

The Q_{tn} vs. F_r chart of Figure 6a also includes a "*CD*" line above which material is expected to be dilative and below which the material is contractive. This line is compatible with the known characteristics of the sand, 25%K and kaolin samples but classifies the 5%K soil as contractive, despite the strongly dilative response of this material at large strains, as seen in undrained triaxial compression in Figure 1. Penetration of the cone in the 5%K mixture was essentially drained for all velocities investigated (see Figure 4b) and therefore the interface shear response observed in drained direct shear plotted on Figure 2 can assist interpretation. This figure indicates that there is likely to be a contractive response at the smooth friction sleeve of a cone and therefore Robertson's assessment of a contractive material is correct. If, however, a rough friction sleeve was employed, Figure 2 indicates that there would a dilative response at the interface and friction would increase by 30%. Such an increase in friction would move many of the data points for 5%K into the dilation zone above the state parameter $\psi = -0.05$ (≡ CD) line shown on Figure 6a.

Figure 6b shows the Q_{tn} - U_2 chart provided by Schneider et al. (2008) and updated by Robertson (2016) by replacing Q_t with Q_{tn}. The effects of rate are also apparent on this figure, although it is seen that the 5%K mixture classifies as dilative and both the kaolin and 25%K soils plot within a transitional zone even at the higher (undrained) velocities of 3 mm/s.

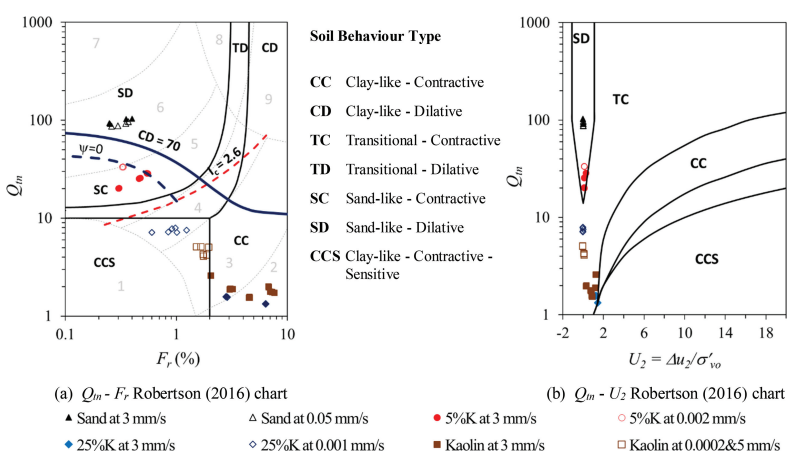

Figure 6. Effects of various penetration velocities on CPT-based soils classification charts.

5 CONCLUSION

A series of CPTu employed in laboratory pressure chambers involving clayey sands, sand and clay indicate that:

i. The soil behavior type charts of Robertson (2009, 2016) are successful in predicting the nature of mechanical characteristics of the materials investigated.
ii. The presence of just 5% clay within a sand deposit can have a significant effect on the response to shear, as observed in element tests. CPT data show lower cone tip resistance in these materials and a fully drained response. Friction ratios in these materials are sensitive to the roughness of the friction sleeve and can affect interpretation.
iii. Undrained CPT end resistances measured in sand with a kaolin clay fraction of 25% are almost a factor of 2 lower than pure kaolin. Cone parameters in these kinds of materials are particularly sensitive to the penetration rate.

ACKNOWLEDGEMENTS

The authors would like to thank Craig at Fast Blast Co. for making the interface roughness. Thanks are also extended to Dr. Yusuke Suzuki at NGI for providing CPT digital data. The great support from staff at UWA including Jit Kheng Lim, David White, Matthew Arpin, Jim Waters, Steven, Brad Rose, Manuel Palacios, Adam Stubbs, Kelvin Leong, Ying Guo and Usha Mani as well as from postgraduate students including Reynaldi Iskandar and Gershom Ong is also gratefully acknowledged. The first author acknowledges the Australian Department of Foreign Affairs and Trade for financial support through AAS scholarships.

REFERENCES

DeJong, J., Jaeger, R., Boulanger, R., Randolph, M., and Wahl, D. 2012. Variable penetration rate cone testing for characterization of intermediate soils. Geotechnical and geophysical site characterization **4**: 25–42.

Doan, L.V., and Lehane, B.M. 2018a. Effects of clay fraction and roughness on tension capacity for displacement piles. *In* Proceedings of the 4th International Symposium on Cone Penetration Testing (CPT'18), Delft, Netherlands, submitted.

Doan, L.V., and Lehane, B.M. 2018b. Shaft resistance of non-displacement piles in normally consolidated clay. *In* Proceedings of the 4th International Symposium on Cone Penetration Testing (CPT'18), Delft, Netherlands, submitted.

Erbrich, C. 2005. Australian frontiers–spudcans on the edge. *In* Proc., 1st Int. Symp. on Frontiers in Offshore Geotechnics. Taylor & Francis Group London. pp. 49–74.

Finnie, I., and Randolph, M. 1994. Punch-through and liquefaction induced failure of shallow foundations on calcareous sediments. *In* Proceedings of International Conference on Behaviour of Offshore Structures, Boston, MA. pp. 217–230.

Hu, L., and Pu, J. 2004. Testing and Modeling of Soil-Structure Interface. Journal of Geotechnical and Geoenvironmental Engineering **130**(8): 851–860. doi: doi:10.1061/(ASCE)1090–0241(2004)130:8(851).

Jaeger, R., DeJong, J., Boulanger, R., Low, H., and Randolph, M. 2010. Variable penetration rate CPT in an intermediate soil. *In* Proceedings of the International Symposium on Cone Penetration Testing, Huntington Beach, Calif.

Jefferies, M.G., and Davies, M.P. 1993. Use of CPTU to estimate equivalent SPT N 60. ASTM **16**(4): 458–468.

Kim, K., Prezzi, M., Salgado, R., and Lee, W. 2008. Effect of Penetration Rate on Cone Penetration Resistance in Saturated Clayey Soils. Journal of Geotechnical and Geoenvironmental Engineering **134**(8): 1142–1153. doi: 10.1061/(ASCE)1090-0241(2008)134:8(1142).

Lehane, B.M., Gaudin, C., and Schneider, J.A. 2005. Scale effects on tension capacity for rough piles buried in dense sand. Geotechnique **55**(10): 709–719.

Lehane, B.M., O'loughlin, C.D., Gaudin, C., and Randolph, M.F. 2009. Rate effects on penetrometer resistance in kaolin. Géotechnique **59**(1): 41–52. doi: doi:10.1680/geot.2007.00072.

Lim, J.K., and Lehane, B.M. 2014. Set-up of pile shaft friction in laboratory chamber tests. International Journal of Physical Modelling in Geotechnics **14**(2): 21–30.

Lunne, T., Andersen, K.H., Low, H.E., Randolph, M.F., and Sjursen, M. 2011. Guidelines for offshore in situ testing and interpretation in deepwater soft clays. Canadian geotechnical journal **48**(4): 543–556.

Pra-ai, S., Pra-ai. 2013. Behaviour of soil-structure interfaces subjected to large number of cycles. Application to modeling of piles cyclically loaded. Université de Grenoble.

Randolph, M., and Hope, S. 2004. Effect of cone velocity on cone resistance and excess pore pressures. *In* Proceedings of the IS Osaka—Engineering Practice and Performance of Soft Deposits. Yodogawa Kogisha Co. Ltd. pp. 147–152.

Robertson, P. 2016. Cone penetration test (CPT)-based soil behaviour type (SBT) classification system—an update. Canadian Geotechnical Journal **53**(12): 1910–1927.

Robertson, P.K. 2009. Interpretation of cone penetration tests—A unified approach. Canadian Geotechnical Journal **46**(11): 1337–1355. doi: 10.1139/t09–065.

Robertson, P.K., and Wride, C.E. 1998. Evaluating cyclic liquefaction potential using the cone penetration test. Canadian Geotechnical Journal **35**(3): 442–459. doi: 10.1139/t98-017.

Schneider, J.A., Lehane, B.M., and Schnaid, F. 2007. Velocity effects on Piezocone measurements in normally and over consolidated clays. International Journal of Physical Modelling in Geotechnics **7**(2): 23–34. doi: doi:10.1680/ijpmg.2007.070202.

Schneider, J.A., Randolph, M.F., Mayne, P.W., and Ramsey, N.R. 2008. Analysis of Factors Influencing Soil Classification Using Normalized Piezocone Tip Resistance and Pore Pressure Parameters. Journal of Geotechnical and Geoenvironmental Engineering **134**(11): 1569–1586. doi: doi:10.1061/(ASCE)1090-0241(2008)134:11(1569).

Suzuki, Y., and Lehane, B.M. 2015. Cone penetration at variable rates in kaolin–sand mixtures. International Journal of Physical Modelling in Geotechnics **15**(4): 209–219. doi: doi:10.1680/ijpmg.14.00043.

Cone Penetration Testing 2018 – Hicks, Pisanò & Peuchen (Eds)
© 2018 Delft University of Technology, The Netherlands, ISBN 978-1-138-58449-5

Analysis of CPTU data for the geotechnical characterization of intermediate sediments

M.F. García Martínez, L. Tonni & G. Gottardi
Department DICAM, University of Bologna, Italy

I. Rocchi
Department of Civil Engineering, Danish Technical University, Denmark

ABSTRACT: The intermediate soil (e.g. silt, sandy silt, clayey silt) response at the standard cone penetration (CPT) velocity of 20 mm/s is generally partially drained, falling between that of sand and clay. As a result, a proper interpretation of CPT (or CPTU) in such mixed soils is not always straightforward. In order to properly analyse the in situ soil response and avoid incorrect estimates of soil parameters, the preliminary assessment of drainage conditions is essential. In this paper, changes in normalized CPTU measurements caused by changes in cone velocity are analysed. Penetration rate effects are assessed by means of No. 8 piezocone tests, with penetration rates ranging from about 0.9 to 61.7 mm/s. Tests were performed at a site located at the southern margin of the Po river valley (Northern Italy), where the subsoil mainly consists in a clayey silt deposit. Limitations on the applicability of some widely used empirical correlations, proposed for sands, are investigated and some preliminary results are shown.

1 INTRODUCTION

Cone penetration testing, with or without pore water pressure measurements (CPTU/CPT), is the most widely used in-situ technique for stratigraphic profiling and evaluation of soil parameters. Compared to sampling and laboratory testing, it allows fast and economical data acquisition and interpretation.

It is generally accepted that the soil response to the standard penetration rate (20 mm/s) is fully drained in sands and fully undrained in clays. By contrast, partially drained response is very likely to occur in silts and other natural soil mixtures (i.e. silty or clayey sands, sandy silts), with significant implications on the appropriate interpretation of field measurements for geotechnical characterization. Current engineering practice lacks of standardized recommendations concerning both testing procedures and data interpretation in such intermediate soils, whilst a significant amount of knowledge is nowadays available for sands and clays.

Over the last years, a number of studies (e.g. Randolph 2004, Schnaid et al. 2004) have stressed the crucial importance of a preliminary assessment of the actual drainage conditions around the advancing cone in order to suitably interpret CPTU data in silty sediments. In this regard, according to the experience of various Authors (e.g. Randolph & Hope 2004, Schneider et al. 2007), cone penetration tests carried out at variable rates are nowadays recognized as an effective way to identify the transition point from undrained to partially drained and drained responses. A dimensionless velocity V (Finnie & Randolph 1994), given by:

$$V = \frac{v \cdot d}{c_v} \tag{1}$$

is generally used to interpret field data, being v the cone penetration rate, d the cone diameter and c_v the vertical coefficient of consolidation. Some Authors have also observed that the horizontal coefficient of consolidation c_h should be used in Equation (1) instead of c_v, since the primary direction of pore water flow is horizontal (Chung et al. 2006).

Although the matter is at present far from being satisfactorily solved, the significant amount of experimental research carried out so far, including both laboratory studies with miniature penetrometers and field scale tests (e.g. Randolph & Hope 2004, Chung et al. 2006, Oliveira et al. 2011, Kim et al. 2008, Tonni & Gottardi 2009, Schnaid et al. 2010, Suzuki et al. 2013, Krage et al. 2014, García et al. 2014, García et al. 2016b), has led to the identification of probable consolidation patterns as function of cone penetration rate. However, the available research results seem to suggest that there is not a unique drained nor undrained transitional

value of V, being dependent on the fine content of soils (Suzuki & Lehane 2015).

Significant difficulties have been typically encountered in the interpretation of variable rate field scale tests, due to a variety of reasons, such as limitations in equipment capability to vary and control the penetration velocity, additional time and costs related to field testing (Suzuki & Lehane 2014) and, particularly, natural soil heterogeneity and the unavoidable spatial variability of soil deposits.

This paper presents the analysis of a set of variable rate CPTU tests carried out in a clayey silt deposit located in the southern margin of the Po river valley near Forlì, Italy. The identification of a probable consolidation trend as function of cone velocity is first examined in order to establish the actual drainage degree during a standard CPTU. Besides, based on a few available laboratory test results, limitations on the applicability of some widely used empirical approaches for geotechnical characterization are discussed and a preliminary attempt to account for partial drainage effects in correlations for the estimate of the friction angle is presented.

2 SITE DETAILS AND FIELD TESTS

The dataset used in this study includes No. 8 adjacent CPTU tests, typically 1 to 2 m distant from each other, performed at penetration rates from 0.9 mm/s to 61.7 mm/s. All tests were pushed to over 15 m in depth. A 35.7 mm diameter cone with pore pressure recorded at the shoulder position (u_2) was employed. For further details on this campaign, readers may refer to García Martínez et al. (2016a, b).

The stratigraphic conditions of this site, as revealed by a deep borehole carried out in a previous investigation campaign as well as by standard CPTU results, mainly consist of a macro-unit of about 29 m of silty-clayey sediments, followed by gravels. Local interbedded silty sand/sandy silt levels, 1 to 3 m thick, are encountered from ground level to 29 m in depth.

Table 1 summarises some basic physical properties of such sediments, together with a few results from direct shear tests and oedometer tests carried out on undisturbed samples.

According to grading characteristics and Atterberg limits, the tested samples range from silty sands (15–15.5 m in depth) to silts-sandy silts (12.3–12.5 m) with approximately 10% of fine content and also high plasticity clays (6.2–6.7 m and 18.0–18.5 m in depth). According to both CPTU and borehole logs, a certain variability in fine content can be at times detected at decimetric level.

Table 1. Physical and mechanical properties.

Depth (m)	γ_n (kN/m³)	w_n (%)	w_L (%)	w_P (%)	S (%)	M (%)	C (%)
6.2–6.7	19.8	25	57.6	21	–	65	35
12.2–12.3	19.2	31.3	25	17	25.6	59.4	15
12.3–12.5	19.2	31.3	20	19	41.1	48.9	10
15.0–15.5	20.6	22.2	–	–	68	32	
18.0–18.5	19.2	31.5	50.8	23.1	–	60	40

Depth (m)	M* (MPa)	c_v* (m²/s)	ϕ'** (°)
6.2–6.7	8.6	–	20.8
12.3–12.5	4.8	$3.1 \cdot 10^{-6}$	34.6
15.0–15.5	–	–	38.9
18.0–18.5	6.3	$1.5 \cdot 10^{-7}$	23.43

S: sand; M: silt; C: clay;
* from oedometric tests (stress interval 70–145 kPa);
** from direct shear tests.

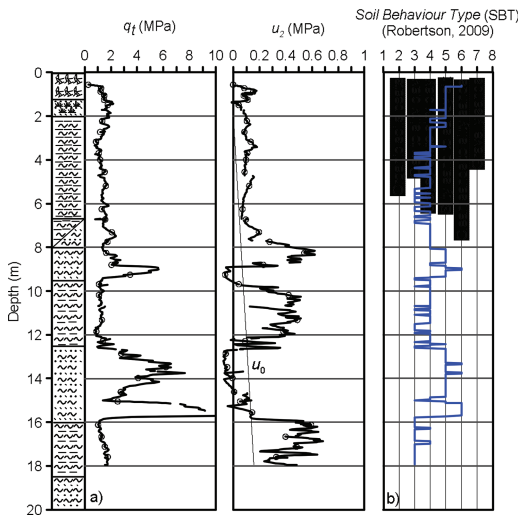

Figure 1. a) CPTU1 log profiles and b) SBT profile according to Robertson (2009).

Figure 1 shows the q_t and u_2 profiles obtained from standard cone penetration test CPTU1. The equilibrium pore pressure profile, corresponding to a water table located at approximately 2 m in depth, has been also plotted in Figure 1 for useful comparison with u_2.

The Soil Behaviour Type (SBT) profile depicted in column (b) has been derived from the value of the material index I_{cn}, according to the well-known CPTU-based classification method proposed by Robertson (2009). Such classification results have been more extensively commented in García Martinez et al. (2016b). A reasonable agreement

between results in terms of Soil Behaviour Type and soil lithology from borehole BH1, also reported in Figure 1, can be appreciated.

The q_t and u_2 profiles from the set of piezocone tests performed at various penetration rates have been plotted in Figure 2. Lower (0.9 mm/s) and upper (61.7 mm/s) values of test velocity were established based on the technical limits of the equipment.

The figure shows that in the upper 7 m, cone resistance remains almost unvaried, whereas pore pressure appears to be slightly more sensitive to penetration rate effects. In any case, such response seems to suggest that penetration in these shallow sediments, basically classified as SBT = 4 or SBT = 3, is predominantly undrained. At greater depth, q_t generally decreases and u_2 increases as the rate of penetration is decreased. It is worth noting that the pore pressure at 0.9 mm/s follows a hydrostatic profile from 12.7 to 16 m, thus indicating fully drained penetration. Again, from 16 m up to the end of the tests, where almost all the sediments are classified as clay, q_t profiles are substantially coincident (García et al. 2016b).

Dissipation tests have been also carried out during the CPTU campaign. As an example, Figure 3 shows the dissipation curves obtained from tests CTPU1 (20 mm/s) and CPTU8 (58 mm/s) at about 12.2 m in depth. As it will be discussed later, test CPTU8 is likely to be ascribed to fully undrained initial conditions. Accordingly, the coefficient of consolidation for this silt has

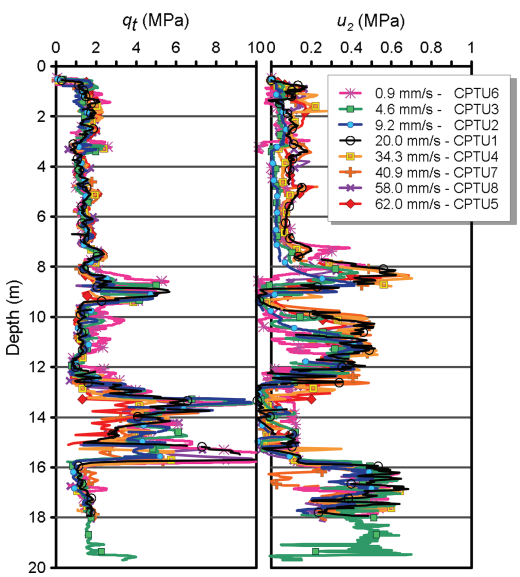

Figure 2. CPTU profiles from adjacent tests at variable rate.

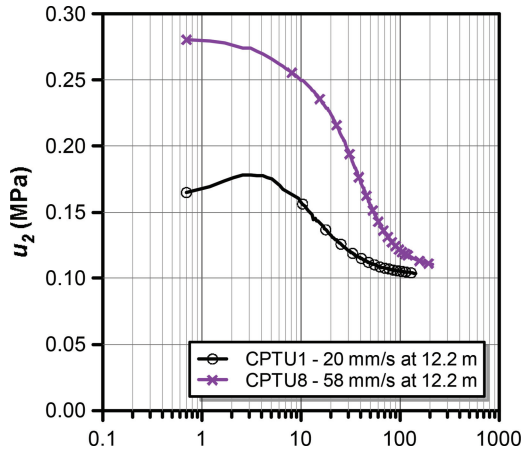

Figure 3. Dissipation tests at 12.2 m.

been determined by applying to CPTU8 dissipation data the well-known Teh & Houlsby (1991) method, this latter being based on the assumption of fully undrained penetration. Assuming the rigidity index I_r ($= G/s_u$) equal to 130, c_h turned out to be equal to $2.9 \cdot 10^{-5}$ m²/s.

Such estimate of the horizontal coefficient of consolidation is about one order of magnitude higher than the value of c_v obtained from the oedometer tests carried out on a soil sample taken at the same depth (see Table 1). As observed by various Authors, differences between c_v and c_h are basically due to anisotropy of soil permeability k in the vertical and horizontal directions, which may result in values of the ratio k_h/k_v up to 10–15 in highly stratified deposits or silts with continuous permeable layers (Jamiolkowski et al. 1985, Mayne 2007). On the other hand, it is often considered as acceptable that accuracy in the estimate of the coefficient of consolidation may vary within one order of magnitude (Robertson 2015). It is worth remarking here that the application of the Teh & Houlsby (1991) method to the dissipation test carried out during standard CPTU1 (i.e. in partial drainage conditions) resulted in $c_h = 4.4 \cdot 10^{-5}$ m²/s.

In what follows, the computed c_h from CPTU8 dissipation test has been used to normalize cone penetration velocities, according to DeJong & Randolph (2012).

3 ANALYSIS OF RATE EFFECTS

In order to perform a preliminary analysis of rate effects on the piezocone measurements, the variations with velocity of normalized tip resistance, $Q_t = ((q_t - \sigma_{vo})/\sigma'_{vo})$, and normalized excess pore pressure, $\Delta u/\sigma'_{v0}$, in a few selected thin

homogeneous layers of sandy silts to silty sands (8–8.5 m, 14.8–15.2 m) and clayey silts (10–10.3, 11.8–12.2 m) have been first examined. In Figure 4, the median and the first and third quartile of Q_t and $\Delta u_2/\sigma'_{v0}$ are plotted, for each velocity v. A rather pronounced scatter of data can be appreciated in sandy silts/silty sands, especially at 14.8–15.2 m in depth, suggesting a certain intrinsic heterogeneity of these soil layers. As it will be shown in the following, intrinsic heterogeneity, coupled with the unavoidable horizontal spatial variability, makes the interpretation of field data more complex to be performed and consolidation trends more difficult to be identified.

According to the plots of Figure 4, clayey silts from 10 to 10.3 m show increasing values of Q_t for $v < 20$ mm/s, whereas those from 11.8 to 12.2 m only show higher values of Q_t for $v < 4.6$ mm/s. Regarding the $\Delta u_2/\sigma'_{v0} - v$ plots, the trend is similar at both depths: a transition point from undrained to partially drained response seems to be close to 40.9 mm/s.

With regard to the sandy silt/silty sand layers, trends at 8–8.5 m are similar to those identified for the clayey silts, although normalized values are generally higher. By contrast, Q_t at 14.8–15.2 m decreases with velocity over the entire investigated range, whilst pore pressures remain almost uninfluenced. In this latter layer, it is very unlikely that fully undrained conditions might have been reached at the maximum cone velocity of 62 mm/s, whilst approximately fully drained penetration may have occured at $v_{min} = 1$ mm/s.

Data from the selected intervals of clayey silts (10–10.3 and 11.8–12.2 m) have been also interpreted in terms of the normalized velocity V, taking the consolidation trend proposed by DeJong & Randolph (2012) as a base. According to such approach, the so-called *"backbone curve"* is given by:

$$\frac{Q}{Q_{ref}} \approx 1 + \left(\frac{Q_{drained} / Q_{ref} - 1}{1 + \left(V / V_{50} \right)^c} \right) \tag{2}$$

where the subscript *'ref'* denotes normalized measurements in undrained conditions whilst the coefficients $Q_{drained}/Q_{ref}$, V_{50} and c are the normalized drained resistance, the normalized velocity at 50% degree of drainage and the maximum rate of change of Q/Q_{ref} with V, respectively. It is worth emphasizing that Equation (2) only describes the consolidation process during cone penetration and therefore ignores effects of viscosity on tip resistance, which are conversely included in other formulations of the backbone curves, such as the one proposed by Randolph (2004).

Interpretation of the available data in the framework described by Equation (2) is not straightforward, especially with regard to the evaluation of the ratio $Q_{drained}/Q_{ref}$. Indeed, extremely slow penetration tests, not performed in this experimental study, would be required in order to attain fully drained conditions around the advancing cone and thus to obtain a value of $Q_{drained}$ which might be considered as representative of this deposit. Furthermore, according to the data shown in Figure 5, the consolidation trend exhibited by sediments at 10–10.3 m seems to differ notably from that observed at 11.8–12.2 m. In any case, $Q_{drained}$ would

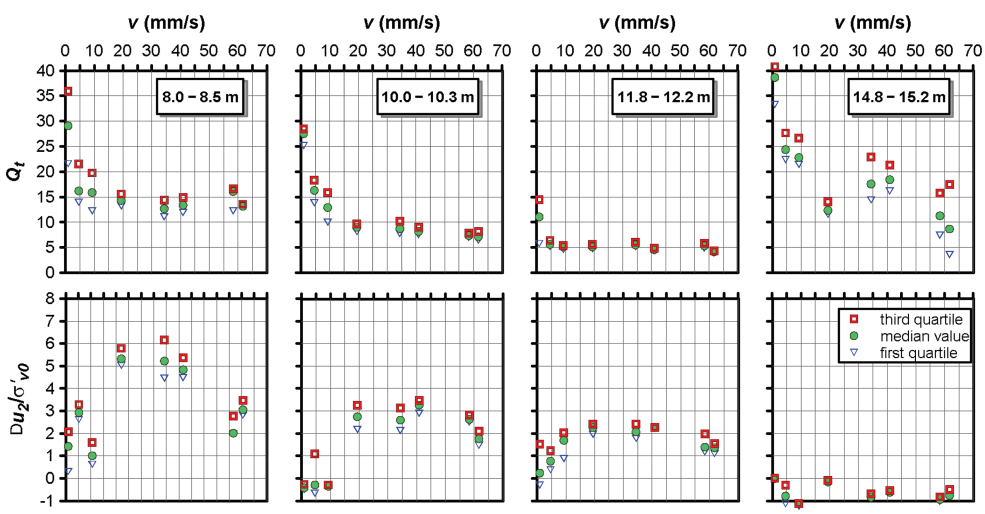

Figure 4. Q_t and $\Delta u/\sigma'_{v0}$ variations with penetration velocity within thin homogeneous layers.

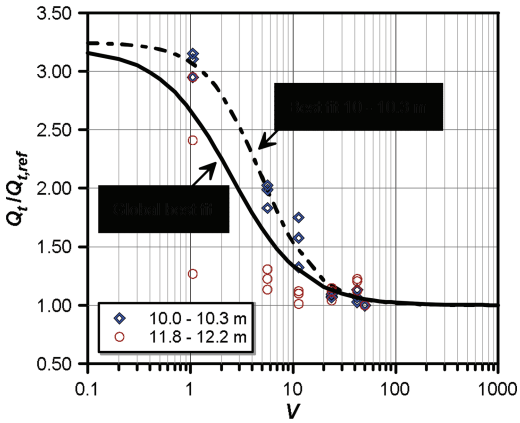

Figure 5. Normalised resistance variations with V within thin homogeneous clayey silt layers and fitted backbone curves.

be certainly located at $V < 1$, while the transition point from partially drained to fully undrained cone penetration has been assumed at V 50.

It is worth remarking here that if c_h obtained from the dissipation test following standard penetration ($c_h = 4.4 \cdot 10^{-5}$ m²/s) had been used, the consolidation trend would have shifted to the left, thus giving lower velocity transition points.

The best fit to data collected in the shallowest clayey silt has been attained by assuming $V_{50} = 4.82$, $c = 1.60$ and $Q_{drained}/Q_{ref} = 3.25$. This latter turns out to be consistent with the values obtained in other experimental studies, both in the laboratory (Oliveira et al. 2011) and in the field (Krage & DeJong 2016, Suzuki et al. 2013), where $Q_{drained}/Q_{ref}$ was found to vary approximately between 2.5 and 4, though higher values have been also detected in a few non-standard soils (DeJong et al., 2013).

At the same time, the regression analysis on the only cone resistance data at 11.8–12.2 has resulted in a significantly high, and thus rather questionable value of $Q_{drained}/Q_{ref}$ (≈28). More data would be probably required in order to identify a reliable consolidation trend. A global consolidation curve, matching all data points, has been obtained for $Q_{drained}/Q_{ref} = 3.20$, $V_{50} = 2.51$ and $c = 1.24$.

4 ASSESSMENT OF PEAK FRICTION ANGLE FROM CPTU-BASED CORRELATIONS

Most of the CPTU-based empirical correlations for the assessment of peak friction angle ϕ'_p have been calibrated on sands, thus potentially resulting in invalid estimates when applied to silts and sandy silts, due to potential partially drained conditions in standard CPT. In what follows, different correlations for the estimate of the effective shear resistance in granular soils are examined and the computed values of ϕ'_p are compared with a few available laboratory results.

Figure 6 shows the peak friction angle profiles obtained from the application to piezocone data in silts-sandy silts of the well-known correlations described by Equation (3) and Equation (4), as proposed by Robertson & Campanella (1983) and Kulhawy & Mayne (1990) respectively:

$$\phi'_p(^\circ) = \frac{180}{\pi} \arctan\left[\log\left(\frac{q_c}{\sigma'_{v0}}\right) + 0.29\right] \quad (3)$$

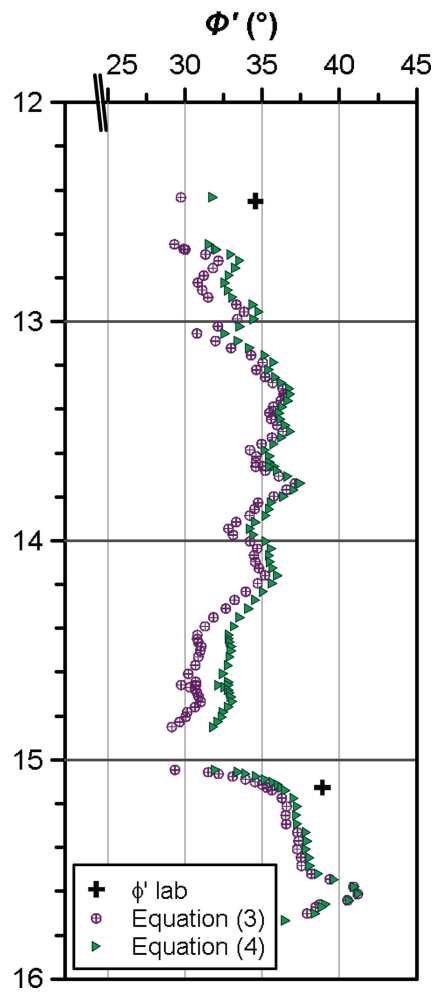

Figure 6. CPTU-based estimates of ϕ' and results from laboratory tests.

$$\phi'_p(^\circ) = 17.6 + 11.0 \cdot \log\left[\frac{(q_t / \sigma_{atm})}{(\sigma'_{v0} / \sigma_{atm})^{0.5}}\right] \quad (4)$$

Profiles are shown for the depth interval 12.4–15.7 m, where a predominance of SBT = 5 has been found. Both correlations appear to be in good agreement. A certain variability of the computed values over the soil layer can be appreciated, as a consequence of its intrinsic heterogeneity.

By comparing such estimates with values of ϕ'_p obtained from direct shear tests (Table 1), also plotted in the figure at 12.4 and 15.1 m in depth, Equations (3) and (4) seem to underestimate the effective shear resistance of these intermediate sediments.

Following the approach recently proposed by Holmsgaard et al. (2016), the laboratory values of ϕ' have been used to adjust the cone resistance at the standard rate v = 20 mm/s and thus to obtain the $q_{t,dr}$ and the stress-normalized $Q_{t,dr}$, corresponding to fully drained conditions. The resulting normalized resistance assumed to apply at fully drained penetration, Q_{dr}, has been found to be ~ 32 at 12.4 m and ~ 70 at 15.1 m. Consequently, the ratio between the normalized drained resistance and that at standard velocity, Q_{dr}/Q_t, turned out to be 3.2 and 1.3 respectively. Holmsgaard et al. (2016) expressed such ratio in terms of non-normalized cone resistances $q_{t,dr}$ and $q_{t,20mm/s}$, obtaining $q_{t,dr}/q_{t,20mm/s}$ = 1.4 for some silty soils of a test site in Dronninglund (Denmark).

It is obvious that such combined interpretation of field data and direct shear test results must be considered as a first attempt to account for partial drainage in geotechnical characterization and that a larger database from the laboratory would be necessary in order to confirm such preliminary analysis.

At the same time, the above interpretation has been also used to help in identifying a more reliable value of the normalized drained resistance $Q_{drained}/Q_{ref}$ in silt mixtures at 11.8–12.2 m and thus overcome uncertainties mentioned in section 3. Indeed, assuming a $Q_{drained}$ equal to 32, the ratio $Q_{drained}/Q_{ref}$ has turned out to be on average 6.8, Q_{ref} (~ 4.7) being obtained from field data (see Fig. 4). This outcome confirms that the value ($Q_{drained}/Q_{ref}$ = 28) previously obtained from regression analysis is probably overestimated.

5 CONCLUSIONS

This paper has presented the results of a set of variable rate CPTUs conducted in a silty deposit located at a site in Northern Italy, with the aim of having a better insight into the drainage degree during testing and its effect on field measurement and geotechnical characterization. Indeed, partial drainage may prevail in intermediate soils when CPTU are performed at the standard rate (20 mm/s).

Despite difficulties in interpreting field data, comparisons between the available tests revealed that decreasing penetration velocity generally results in increasing tip resistance, whereas pore pressure tends to decrease.

From the analysis in terms of normalised CPTU measurements within selected depth intervals of the clayey silt layer, a consolidation trend has been identified. The transition point from undrained to partially drained conditions is likely to occur at a normalised velocity V 50. By contrast, significant difficulties have been encountered in detecting fully drained conditions. According to the analyses, also relying on laboratory data, $Q_{drained}/Q_{ref}$ has been found to vary from 3.25 to approximately 6.8 in the predominantly silty layer. The amplitude of such range is presumably due to intrinsic heterogeneity of the soil unit. On the other hand, the estimated values turn out to be in substantial agreement with results from similar experimental studies.

As a consequence of partial drainage, careful attention should be paid when empirical CPTU correlations, developed for sands or clays, are used to estimate geotechnical parameters in intermediate soils. In particular, peak friction angle ϕ' in silts to sandy silts appears to be underestimated when some well-known expressions are applied to the standard test. Comparisons between the estimated and the measured ϕ' have suggested a ratio between the drained normalized and the standard resistance, Q_{dr}/Q_t, ranging between 3.2 and 1.3. Additional laboratory results would be required to confirm such preliminary results and to update empirical correlations.

REFERENCES

Chung, S.F., Randolph, M.F. & Schneider, J.A. 2006. Effect of cone penetration rate on penetrometer resistance in clay. *J. Geotech. Geoenviron. Eng.* 132(9): 1188–1196.

DeJong, J.T. & Randolph, M. 2012. Influence of partial consolidation during cone penetration on estimated soil behaviour type and pore pressure dissipation measurements. *J. Geotech. Geoenviron. Eng.* 138(7): 777–788.

Finnie, I. & Randolph, M.F. 1994. Punch-through and liquefaction induced failure of shallow foundations on calcareous sediments. *Proc. Int. Conf. on Behavior of Offshore Structures, Boston (USA)*: 217–230.

García Martínez, M.F., Tonni, L. & Gottardi, G. 2016a. On the interpretation of piezocone tests in natural silt

and sand mixtures. *Proc. 1st IMEKO TC-4 International Workshop on Metrology for Geotechnics, Metrogeotechnics2016, Benevento (Italy)*: 63–68.

García Martínez, M.F., Tonni, L. & Romagnoli, F. 2014. Variable rate CPTU in liquefaction-prone silty sand deposits of the Emilia-Romagna Region (Italy). *3rd Int. Symposium on Cone Penetration Testing*, *Las Vegas (USA)*: 737–744.

García Martínez, M.F., Tonni, L., Gottardi, G. & Rocchi, I. 2016b. Influence of penetration rate on CPTU measurements in saturated silty soils. *Proc. 5th Int. Conf. on Geotech. and Geophysical Site Characterisation (ISC'5), Gold Coast (Australia)* (1): 473–478.

Holmsgaard, R. Nielsen, B.N. & Ibsen, L.B. 2016. Interpretation of cone penetration testing in silty soils conducted under partially drained conditions. *J. Geotech. Geoenviron. Eng*. 142(1): 04015064.

Jarniolkowski, M., Ladd, C.C., Germaine, J.T., & Lancellotta, R. 1985. New developments in field and laboratory testing of soils. *Proc. 11th Int. Conf. on Soil Mechanics and Foundation Engineering, San Francisco* 1: 57–153.

Kim, K., Prezzi, M., Salgado, R. & Lee, W. 2008. Effect of penetration rate on cone penetration resistance in saturated clayey soils. *J. Geotech. Geoenviron. Eng.* 134(8): 1142–1153.

Krage, C.P. & DeJong, J.T. 2016. Influence of drainage conditions during cone penetration on the estimation of engineering properties and liquefaction potential of silty and sandy soils. *J. Geotech. Geoenviron. Eng.* 142(11): 04016059.

Krage, C.P., DeJong, J.T. & Wilson, D.W. 2014. Variable Penetration Rate Cone Testing in Sands with Fines. *Geo-Congress 2014*, GSP 234: 170–179.

Kulhawy, F.H. & Mayne, P.W. 1990. Manual on estimating soil properties for foundation design. *Rep. EL-6800, Electric Power Research Institute, Palo Alto, CA*.

Mayne P.W. 2007. Synthesis 368 on Cone Penetration Test. *(NCHRP), Transportation Research Board, National Academy Press, Washington DC, www.trb.org.*

Oliveira, J.R.M.S., Almeida, M.S.S., Motta, H.P.G. & Almeida, M.C.F. 2011. Influence of penetration rate on penetrometer resistance. *Journal of Geotech. and Geoenviron. Eng.* 137(7): 695–703.

Randolph, M. 2004. Characterisation of soft sediments for offshore applications. *Proc. ISC-2, Porto (Portugal)* 1: 209–232. Millpress, The Netherlands.

Randolph, M.F. & Hope, S. 2004. Effect of cone velocity on cone resistance and excess pore pressures. *Proc. Int. Symp. on engineering practice and performance of soft deposits*, *Osaka (Japan)*: 147–152.

Robertson, P.K. & Campanella, R.G. 1983. Interpretation of cone penetration tests. Part I: sand. *Can. Geotech. J*. 20(4): 719–733.

Robertson, P.K. 2009. Interpretation of cone penetration tests—a unified approach. *Can. Geotech. J*. 46 (11): 1337–1355.

Robertson, P.K. 2015. *Guide to cone penetration testing*. 6th Edition, California: Gregg Drilling & Testing Inc.

Schnaid, F., Bedin, J. & Costa Filho, L.M. 2010. Drainage characterization of tailings from in situ tests. *Proc. 2nd Int. Symp. on Cone Penetration Testing, Huntington Beach (USA)*.

Schnaid, F., Lehane, B.M. & Fahey, M. 2004. In situ test characterization of unusual geomaterials. *Proc. 2nd Int. Conf. on Site Characterization* 1: 49–74.

Schneider, J.A., Lehane, B.M. & Schnaid, F. 2007. Velocity effects on piezocone measurements in normally and overconsolidated clays. *Int. J. Physical Modelling in Geotechnics* 2: 23–34.

Suzuki, Y. & Lehane, B.M. 2014. Field observations of CPT penetration rate effects in Burswood clay. *Proc. 3rd Int. Symp. on Cone Penetration Testing, Las Vegas*: 403–410.

Suzuki, Y. & Lehane, B.M. 2015. Cone penetration at variable rates in kaolin–sand mixtures. *Int. J. of Physical Modelling in Geotechnics* 15(4): 209–219.

Suzuki, Y., Lehane, B.M. & Fourie, A. 2013. Effect of penetration rate on piezocone parameters in two silty deposits. *Proc. ISC'4*: 809–815.

Teh, C.I. & Houlsby, G.T. 1991. An analytical study of cone penetration test in clay. *Géotechnique* 41(1): 17–34.

Tonni, L. & Gottardi G., 2009. Partial drainage effects in the interpretation of piezocone tests in Venetian silty soils. *Proc. of the 17th International Conf. on Soil Mechanics and Geotech. Eng., Alexandria (Egypt)* 2: 1004–1007.

Taylor & Francis
Taylor & Francis Group
http://taylorandfrancis.com

Cone Penetration Testing 2018 – Hicks, Pisanò & Peuchen (Eds)
© 2018 Delft University of Technology, The Netherlands, ISBN 978-1-138-58449-5

Detection of soil variability using CPTs

T. de Gast, P.J. Vardon & M.A. Hicks
Section of Geo-Engineering, Faculty of Civil Engineering and Geosciences, Delft University of Technology, Delft, The Netherlands

ABSTRACT: The variability of soil is well known to affect the geotechnical performance of structures. As probabilistic design methods become more commonly used, the ability to measure the variability of soil becomes more important. However, by using only the point statistics of soil parameters in design (e.g. the mean and standard deviation), typically an over-estimation of failure probabilities occurs, leading to over-conservative designs. By looking at the spatial correlation (e.g. scales of fluctuation) a more accurate representation can be achieved. This paper presents a method to use vertical Cone Penetration Tests (CPTs) to detect both the vertical and horizontal scales of fluctuation. An extensive numerical and experimental investigation has been undertaken to understand how spatial variation can be estimated and to quantify the accuracy in that estimation. The impact of being able to quantify the uncertainty is illustrated via a simple slope stability example.

1 INTRODUCTION

Soil properties are intrinsically variable and addressing these variations in design is one of the main challenges in geotechnical engineering (Honjo 2011). The impact of soil variability has been shown to be significant in many types of geotechnical analyses, including: shallow, strip and pile foundations (Jaksa et al. 2005, Naghibi et al. 2016); retaining walls (Sert et al. 2016); liquefaction of hydraulic sand fills (Popescu et al. 1997, Wong 2004, Hicks & Onisiphorou 2005); and slope stability (Griffiths & Fenton 2000, Spencer & Hicks 2007, Hicks & Spencer 2010, Li & Hicks 2014, Vardon et al. 2016). Using embankments as an example, it has been shown that the spatial variation of material properties in combination with the problem geometry plays an important role in the slope stability and failure mode (Hicks & Samy 2002, Hicks et al. 2014, Li et al. 2015, 2016).

Comprehensive theoretical overviews on the quantification of the spatial variation in soils are given by Vanmarcke (1977a), Campanella et al. (1987) and Wickremesinghe & Campanella (1993), and later discussed by Fenton (1999a, 1999b) and Griffiths et al. (2007). The scale of fluctuation can be estimated using a range of techniques and, in particular, by using an auto-correlation function (e.g. de Gast et al. (2017)).

However, little experimental evidence that considers the scale of fluctuation, especially in the horizontal direction, is available. In this paper, the auto-correlation function is reviewed for its accuracy in obtaining the spatial correlation in synthetic data and proposes a method to estimate the accuracy in measuring the spatial correlation. In this way a CPT campaign can be designed to measure horizontal scales of fluctuation using limited CPT data.

This paper summarises the method proposed by de Gast et al. (2018) and gives an example of how to apply it.

2 THEORETICAL BACKGROUND

Soil properties are variable, although they are generally correlated to the properties of material in close proximity. A convenient measure of the spatial variability is the auto-correlation length θ, often referred to as the scale of fluctuation (SoF). Loosely speaking, it is the distance within which material properties are significantly correlated. Conversely, the properties at two points separated by a distance greater than θ will be largely uncorrelated (Griffiths & Fenton 1997). The scale of fluctuation has been defined by Vanmarcke et al. (1986) as

$$\theta = 2\int_0^{\infty} \rho(\tau)\, d\tau \tag{1}$$

where $\rho(\tau)$ is the auto-correlation function describing the spatial auto-correlation structure and τ is the lag distance, i.e. the distance separating two points. Hence, θ is the area under the auto-correlation function over the range $-\infty \le \tau \le \infty$, and, while it can have different orientations, for soils it is commonly considered to be different in the vertical and horizontal directions due to deposition processes.

An experimental auto-correlation function can be obtained from

$$\hat{\rho}(\tau) = \frac{\hat{\gamma}(\tau)}{\hat{\gamma}(0)} \tag{2}$$

where $\hat{\gamma}(\tau)$ is the experimental covariance function. This is given by Vanmarcke (1983) as

$$\hat{\gamma}(\tau) = \frac{1}{(t-1)} \sum_{j=1}^{t} \left(y_j - \hat{\mu}\right)\left(y_{j+\Delta j} - \hat{\mu}\right) \tag{3}$$

where $\hat{\mu}$ is the estimated mean (or trend) of the dataset, j is a counter representing the first of a data pair at lag distance τ, $j + \Delta j$ represents the second of the data pair, and t is the number of pairs at lag distance τ. By using, for example, the following Markov theoretical auto-correlation function,

$$\rho(\tau) = e^{\frac{-2|\tau|}{\theta}} \tag{4}$$

and finding the minimum of the error given by

$$E(\theta) = \sum \left(\rho(\tau) - \hat{\rho}(\tau)\right)^2 \tag{5}$$

an estimate for the scale of fluctuation may be obtained.

As with any sampled data, a sample from a population is taken and the accuracy of the method depends on the amount and r epresentativeness of the data available. It has been observed that as more data (CPTs) are considered, the better the mean auto-correlation function is (Lloret-Cabot et al. 2014), especially at larger lag lengths. This feature is investigated in detail in the following section.

3 INVESTIGATION USING SYNTHETIC DATA

The effectiveness of the experimental auto-correlation function for a set of data was investigated using computer generated data, i.e. data where the scale of fluctuation and auto-correlation were known a priori. 1D strings of data of varying length, data spacing and correlation length, representing CPT profiles, were generated using covariance matrix decomposition (Davis 1987, van den Eijnden & Hicks 2017). The data were generated using a mean of zero, a standard deviation of unity and a Markov auto-correlation function with a scale of fluctuation of 5 (units of length).

In order to test the effectiveness of estimating the auto-correlation function from equations (2)-(5), different variables were investigated: (1) the number of datasets—which is, in the vertical direction, analogous to the number the number of CPT profiles; (2) the number of data points used per dataset—which is analogous to the total number of data points in single CPT profile; (3) the value of θ; (4) the effect of grouping data at larger intervals—in the horizontal direction, this is analogous to having several CPT profiles in groups with a significant space between groups, or, in the vertical direction, it is analogous to having a data gap in the CPT profile.

Multiple datasets were generated representing different combinations of the four variables, and these are presented in detail in de Gast et al. (2018). Figure 1 shows the impact of increasing the number of datasets on the estimated θ, which has the largest impact on the coefficient of variation (COV) of θ. By increasing the number of datasets, the COV decreases rapidly as indicated by the broken line.

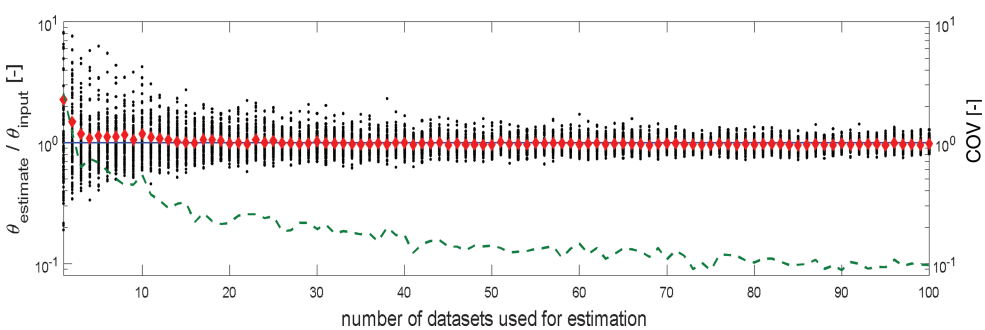

Figure 1. Example analysis investigating the accuracy in calculating θ as a function of the number of datasets. Each dot is a single estimation of θ, normalized by the input $\theta = \theta_{input}$; the horizontal line equal to 1 is the normalized input θ; the red diamonds are the calculated average from the individual estimates; and the broken line is the calculated coefficient of variation (COV = σ/μ) of the estimated θ.

4 ESTIMATING THE VARIATION

It has been found that the coefficient of variation of the measured horizontal or vertical scale of fluctuation is related to the actual scale of fluctuation, the number of datasets, the domain size and the distribution (i.e. spacing) of CPT profiles. The following equation has been proposed to predict the COV of θ (de Gast et al. 2018):

$$COV = \underbrace{1.1}_{\substack{fitting\\coefficient}} \times \underbrace{\tan^{-1}\left(\frac{5\theta}{D_g}\right)}_{factor\ for\ \theta < D_g} \times \underbrace{\frac{1}{\sqrt{nf}}}_{factor\ for\ no.of\ datasets} \times \underbrace{\left(1+\frac{in}{ng\times\theta}\right)}_{factor\ for\ spacing} + \underbrace{\frac{\theta}{5nf\times D_t}}_{factor\ for\ \theta > D_t} \tag{6}$$

where:

$$nf = \begin{cases} \dfrac{D_p}{\theta_p}; & D_p > \theta_p \\ 1; & D_p \le \theta_p \end{cases} \tag{7}$$

and in which θ is the scale of fluctuation, nf is the number of datasets (with a minimum of 1), in is the space interval between the groups, ng is the number of groups (if the data have different intervals), D_t is the total domain length (the length over which the data points are obtained), D_g is the domain length of the groups (if $D_t = D_g$, in is the interval between data points), D_p is the domain length perpendicular to the investigated direction and θ_p is the scale of fluctuation perpendicular to the investigated direction.

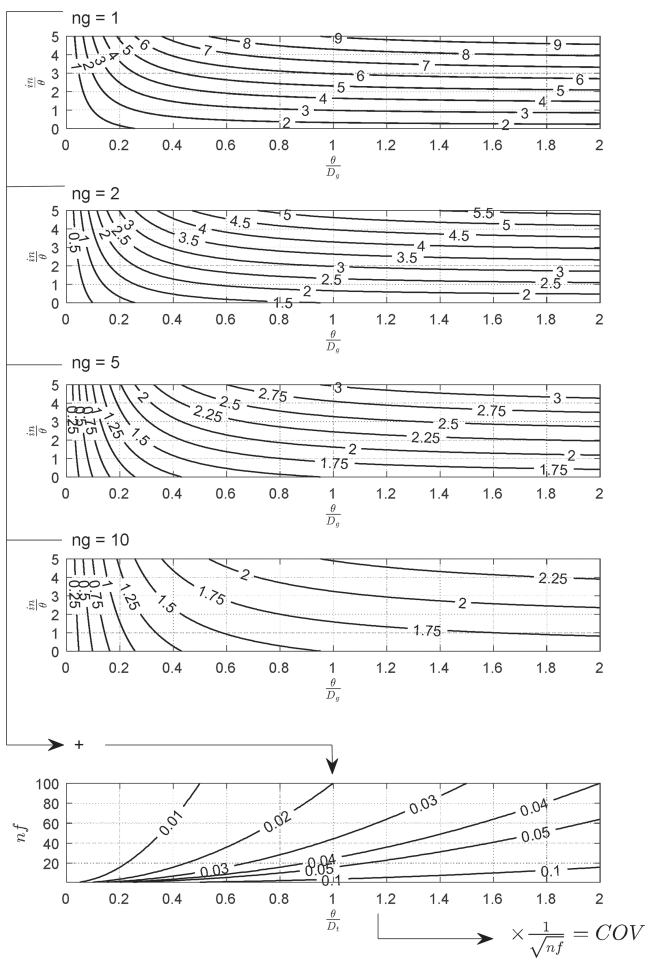

Figure 2. Method of estimating COV of the scale of fluctuation using groups of data.

Equation (6) can be rearranged to aid graphical interpretation as:

$$COV = \frac{1}{\sqrt{nf}}\left(\frac{\theta}{5\sqrt{nf}\times D_t}+1.1\left(1+\frac{in}{ng\times\theta}\right)\tan^{-1}\left(\frac{5\theta}{D_g}\right)\right) \tag{8}$$

and is graphically presented in Figure 2, which can be used after first calculating the scale of fluctuation using equations (2)-(5). In the first four subfigures in Figure 2, which represent the last term in equation (8) with different values of ng, the contour lines can be assumed to be horizontal at the right-hand side, i.e. if $\theta / D_g > 2$, the value can be evaluated at $\theta / D_g = 2$.

For example, consider 10 CPTs grouped in $ng = 5$ groups of 2 CPTs, with a spacing of $D_g = 2.5$ m between CPTs within each group and a spacing between groups of $in = 25$ m, giving a total domain of $D_t = 112.5$ m. If the horizontal scale of fluctuation is estimated to be $\theta = 50$ m, the first part of the figure gives a contour value of between 1.75 and 2.0, and the second part of the figure gives a contour value below 0.05; adding these numbers together gives a value between 1.8 and 2.05, and dividing by the square root of $nf = 20$ ($D_p = 5$ m, $\theta_p = 0.25$ m) yields an estimated COV of 0.40–0.46; using equation (6) yields an estimated COV of 0.43.

5 EFFECT ON DYKE STABILITY

Considering a hypothetical study of the stability of a dyke, the impact of the sampling has been investigated. The analytical model of Vanmarcke (1977b) is used, which considers 3D effects and has been examined in detail by Li et al. (2015) and Varkey et al. (2017). It is summarised by the following equations:

$$F_{b,\mu} = F\left(1+\frac{d}{b}\right) \tag{9}$$

$$F_{b,\sigma} = F\Gamma(L_a)\Gamma(b)V_s \tag{10}$$

$$\Gamma(b) = \begin{cases} \sqrt{\dfrac{\theta_h}{b_c}}; & b_c > \theta_h \\ 1; & b_c \le \theta_h \end{cases} \tag{11}$$

$$\Gamma(L_a) = \begin{cases} \sqrt{\dfrac{\theta_e}{L_a}}; & L_a > \theta_e \\ 1; & L_a \le \theta_e \end{cases} \tag{12}$$

$$b_c = \begin{cases} \dfrac{F}{F-1}d; & b_c > \theta_h \\ \theta_h; & b_c \le \theta_h \end{cases} \tag{13}$$

$$d = 2\frac{A}{L_a} \tag{14}$$

where F is the mean 2D factor of safety, $F_{b,\mu}$ is the corrected mean for 3D end effects, d is related to the cross-sectional sliding area A and failure arc length L_a, b_c is the critical failure length in the third dimension, $F_{b,\sigma}$ is the standard deviation of the 3D safety factor, $\Gamma(L_a)$ and $\Gamma(b)$ are variance reduction factors depending on θ, V_s is the coefficient of variation of the strength point statistics, θ_h is the horizontal scale of fluctuation, and θ_e is the equivalent scale of fluctuation obtained by a weighted average of the horizontal and vertical components of the scale of fluctuation along the 2D slip circle.

In this example analysis, it is assumed that a budget for 10 CPTs is available to assess the stability of a 5 m high dyke with a length of 150 m. It is also assumed that the following are calculated: $F = 1.5$, $V_s = 0.3$, $L_a = 11.25$ m, $A = 16$ m^2 and $\theta_v = 0.25$ m. θ_v is measured using an interval of 0.01 m between measurements down to 5 m depth for all CPTs. The CPTs are either evenly distributed (i.e. ungrouped) over the length of the dyke at 16.7 m spacing, or in five groups of 2 CPTs, with a distance of 2.5 m between the 2 CPTs in each group and a spacing of 34.4 m between each group.

To illustrate the effect of CPT positioning and the corresponding uncertainties obtained from equation (6), two scenarios have been considered, where the horizontal scales of fluctuations are (a) $\theta_h = 50$ m and (b) $\theta_h = 5$ m. Using the COV obtained from equation (6), three likely outcomes of θ_e have been calculated (following the approach of Li et al. (2015)) for the following combinations of $(\theta_h+\sigma, \theta_v+\sigma)$, (θ_h, θ_v) and $(\theta_h-\sigma, \theta_v-\sigma)$. For each combination, the five percentile factor of safety $F_{b,5\%}$ has been calculated, following the procedure of equations (9)-(14).

In Table 1 the results of the different scenarios and CPT groupings are presented. For a large θ_h (scenario 1), the difference between the grouped and ungrouped data is not apparent as they yield almost the same $F_{b,5\%}$. For a small θ_h (scenario 2), there is a clear advantage in grouping the CPTs; this is because the small scale of fluctuation can then be measured, whereas, for the ungrouped data, this is not the case and the calculated θ_h has a minimum value equal to the CPT spacing (16.7 m). Table 1 shows that based on the same point statistics, a large range of $F_{b,5\%}$ can be found, from 1.24 to 1.90, depending on the value of θ_h and the distance between the CPT locations.

As the scale of fluctuation is not generally known a priori, it is more useful to use grouped CPTs, as then both large and small scales of fluctuation can be estimated using the same number of CPTs. Comparing any pair of calculated safety

Table 1. Effect of CPT positioning (ungrouped or grouped) and θ_h (scenario 1 or 2) on the 5 percentile factor of safety.

Scenario/ positioning	Mean calculated θ_h [m]	COV θ_h	$F_{b,5\%}$		
			$\theta_e+\sigma$	θ_e	$\theta_e-\sigma$
1.Ungrouped	50	0.34	1.26	1.32	1.40
1.Grouped	50	0.44	1.24	1.32	1.44
2.Ungrouped	16.7*	0.25	**1.57**	1.60	1.64
2.Grouped	5	0.86	**1.72**	1.78	1.90

*the minimum distance between the CPTs in the horizontal direction equals 16.7 m; as this is therefore the smallest θ_h that can be found, CH036_118-E035.eps m is used

factors (for the same scenario and same calculated θ_e), e.g. the data in bold text, it is possible to calculate up to an 10% increase in the five percentile factor of safety.

6 CONCLUSIONS

A method is presented to quantify the uncertainty in the measured values of the spatial scale of fluctuation (which characterises the soil heterogeneity). In a simple example used to illustrate the calculation process, it has been demonstrated that, by careful design of the site investigation, the factor of safety of an embankment may be increased by ~10%.

ACKNOWLEDGEMENTS

This research was supported under project number 13864 by the Dutch Technology Foundation STW, which is part of the Netherlands Organisation for Scientific Research (NWO), and which is partly funded by the Ministry of Economic Affairs.

REFERENCES

Campanella, R.G., Wickremesinghe, D.S. & Robertson, P.K. 1987. Statistical treatment of cone penetrometer test data. *Proceedings of 5th International Conference on Applications of Statistics and Probability in Soil and Structural Engineering*, Vancouver, Vol. 2, pp. 1011–1019.

Davis, M.W. 1987. Production of conditional simulations via the LU triangular decomposition of the covariance matrix. *Mathematical Geology* 19(2): 91–98.

De Gast, T., Vardon, P.J. & Hicks, M.A. 2017. Estimating spatial correlations under man-made structures of soft soils. *Proceedings of Geo-Risk 2017*, Denver, pp. 382–389.

De Gast, T., Vardon, P.J. & Hicks, M.A. 2018. Measuring vertical and horizontal variability in soils—Submitted for publication.

Fenton, G.A. 1999a. Estimation for stochastic soil models. *Journal of Geotechnical and Geoenvironmental Engineering* 125(6): 470–485.

Fenton, G.A. 1999b. Random field modeling of CPT data. *Journal of Geotechnical and Geoenvironmental Engineering* 125(6): 486–498.

Griffiths, D.V. & Fenton, G.A. 1997. Three-dimensional seepage through spatially random soil. *Journal of Geotechnical and Geoenvironmental Engineering* 123(2): 153–160.

Griffiths, D.V. & Fenton, G.A. 2000. Influence of soil strength spatial variability on the stability of an undrained clay slope by finite elements. *Proceedings of Geo-Denver 2000*, Denver, pp. 184–193.

Griffiths, D.V., Fenton, G.A. & Denavit, M.D. 2007. Traditional and advanced probabilistic slope stability analysis. *Proceedings of Geo-Denver 2007*, Denver, pp. 1–10.

Hicks, M.A. & Onisiphorou, C. 2005. Stochastic evaluation of static liquefaction in a predominantly dilative sand fill. *Géotechnique* 55(2): 123–133.

Hicks, M.A. & Samy, K. 2002. Influence of heterogeneity on undrained clay slope stability. *Quarterly Journal of Engineering Geology and Hydrogeology* 35(1): 41–49.

Hicks, M.A. & Spencer, W.A. 2010. Influence of heterogeneity on the reliability and failure of a long 3D slope. *Computers and Geotechnics* 37(7–8): 948–955.

Hicks, M.A., Nuttall, J.D. & Chen, J. 2014. Influence of heterogeneity on 3D slope reliability and failure consequence. *Computers and Geotechnics* 61: 198–208.

Honjo, Y. 2011. Challenges in geotechnical reliability based design. *Proceedings of 3rd International Symposium on Geotechnical Safety and Risk (ISGSR 2011)*, Munich, pp. 11–28.

Jaksa, M.B., Goldsworthy, J.S., Fenton, G.A., Kaggwa, W.S., Griffiths, D.V., Kuo, Y.L. & Poulos, H.G. 2005. Towards reliable and effective site investigations. *Géotechnique* 55(2): 109–121.

Li, Y. & Hicks, M.A. 2014. Comparative study of embankment reliability in three dimensions. *Proceedings of 8th European Conference on Numerical Methods in Geotechnical Engineering*, Delft, Vol. 1, pp. 467–472.

Li, Y.J., Hicks, M.A. & Nuttall, J.D. 2015. Comparative analyses of slope reliability in 3D. *Engineering Geology* 196: 12–23.

Li, Y.J., Hicks, M.A. & Vardon, P.J. 2016. Uncertainty reduction and sampling efficiency in slope designs using 3D conditional random fields. *Computers and Geotechnics* 79: 159–172.

Lloret-Cabot, M., Fenton, G.A. & Hicks, M.A. 2014. On the estimation of scale of fluctuation in geostatistics. *Georisk: Assessment and Management of Risk for Engineered Systems and Geohazards* 8(2): 129–140.

Naghibi, F., Fenton, G.A. & Griffiths, D.V. 2016. Probabilistic considerations for the design of deep foundations against excessive differential settlement. *Canadian Geotechnical Journal* 53(7): 1167–1175.

Popescu, R., Prevost, J.H. & Deodatis, G. 1997. Effects of spatial variability on soil liquefaction: Some design recommendations. *Géotechnique* 47(5): 1019–1036.

Sert, S., Luo, Z., Xiao, J.H., Gong, W.P. & Juang, C.H. 2016. Probabilistic analysis of responses of cantilever wall-supported excavations in sands considering vertical spatial variability. *Computers and Geotechnics* 75: 182–191.

Spencer, W.A. & Hicks, M.A. 2007. A 3D finite element study of slope reliability. *Proceedings of 10th International Symposium on Numerical Models in Geomechanics (NUMOG X),* Rhodes, pp. 539–543.

Van Den Eijnden, A.P. & Hicks, M.A. 2017. Efficient subset simulation for evaluating the modes of improbable slope failure. *Computers and Geotechnics* 88: 267–280.

Vanmarcke, E.H. 1977a. Probabilistic modeling of soil profiles. *Journal of the Geotechnical Engineering Division-ASCE* 103(11): 1227–1246.

Vanmarcke, E.H. 1977b. Reliability of earth slopes. *Journal of the Geotechnical Engineering Division-ASCE* 103(11): 1247–1265.

Vanmarcke, E.H. 1983. *Random fields: Analysis and synthesis.* M.I.T. Press, Cambridge, Massachusetts.

Vanmarcke, E., Shinozuka, M., Nakagiri, S., Schueller, G.I. & Grigoriu, M. 1986. Random-fields and stochastic finite-elements. *Structural Safety* 3(3–4): 143–166.

Vardon, P.J., Liu, K. & Hicks, M.A. 2016. Reduction of slope stability uncertainty based on hydraulic measurement via inverse analysis. *Georisk: Assessment and Management of Risk for Engineered Systems and Geohazards* 10(3): 223–240.

Varkey, D., Hicks, M.A. & Vardon, P.J. 2017. Influence of spatial variability of shear strength parameters on 3D slope reliability and comparison of analysis methods. *Proceedings of Geo-Risk 2017*, Denver, pp. 400–409.

Wickremesinghe, D. & Campanella, R.G. 1993. Scale of fluctuation as a descriptor of soil variability. *Proceedings of Probabilistic Methods in Geotechnical Engineering*, Canberra, pp. 233–239.

Wong, S.Y. 2004. *Stochastic characterisation and reliability of saturated soils.* PhD Thesis, University of Manchester.

Cone Penetration Testing 2018 – Hicks, Pisanò & Peuchen (Eds)
© 2018 Delft University of Technology, The Netherlands, ISBN 978-1-138-58449-5

MPM simulation of CPT and model calibration by inverse analysis

P. Ghasemi & M. Calvello
Department of Civil Engineering, University of Salerno, Fisciano, Italy

M. Martinelli & V. Galavi
Deltares, Delft, The Netherlands

S. Cuomo
Department of Civil Engineering, University of Salerno, Fisciano, Italy

ABSTRACT: The Material Point Method (MPM) has been employed in the study of many geotechnical large deformation problems. This study aims at showing: the effectiveness of MPM in simulating a CPT, and the possibility to calibrate the model input parameters by inverse analysis. The MPM schematization adopted to implement the CPT boundary value problem uses a moving mesh concept to model the cone as a rigid body penetrating into the soil. A gradient-based non-linear regression analysis is used to calibrate the input parameters of the constitutive law adopted to model the soil. To this aim, a synthetic case study has been set up, using the model results of a "base" simulation as observations and, in particular, the cone resistance values computed at 24 different depths. The results of the performed sensitivity, parametric and inverse analyses highlights few important aspects related to the use of optimization algorithms to calibrate the input parameters of MPM models of CPTs.

1 INTRODUCTION

Cone penetration tests always produce large displacements, rotations and deformations of soil elements, as well as a complex response of the soil to the displacements imposed by the penetration process (e.g. Arshad et al., 2014).

In recent years, the numerical simulation of this complicated mechanism has been the subject of many research contributions (Gens et al., 2016). These researchers addressed the issue of modelling a boundary value problem exhibiting very large deformations in a significant portion of the control volume by adopting different numerical techniques: arbitrary Lagrangian-Eulerian finite element approach (e.g. Lu et al., 2004; Tolooiyan and Gavin, 2011); discrete element method (e.g. Arroyo et al., 2011; Butlanska et al., 2013); particle element method (e.g. Monforte et al., 2016).

The material point method (MPM), successfully used in the study of a number of geotechnical large deformation problems (e.g. Coetzee et al., 2005; Andersen and Andersen, 2010), recently found its first applications also in the study of cone penetration (Beuth, 2012; Kafaji, 2013; Ceccato et al., 2016). The main aims of the study presented herein are: to confirm the effectiveness of MPM in simulating a CPT; to show the possibility to calibrate the model input parameters by a combination of parametric, sensitivity and inverse analyses.

2 NUMERICAL MODEL

2.1 *Material point method formulation*

The Material Point Method was developed by Schreyer, Sulsky and co-workers for solving problems of solid mechanics (Sulsky *et al.*, 1994) and it has been later applied to granular materials by Więckowski et al., (1999). It came into the field of geotechnical engineering only recently (Beuth *et al.*, 2007; Zabala & Alonso, 2011; Kafaji, 2013).

The MPM can be considered as an extension of the widely-used Updated Lagrangian Finite Element Method (UL-FEM). Similar to the UL-FEM, the MPM makes use of a Lagrangian finite element mesh in which nodes are attached to a deforming body and consequently moving through space with the material. To prevent mesh distortion, all computational data, such as state parameters and stresses, are stored in the material points at the end of each time step and the Lagrangian mesh is reset. At the beginning of the next step, the stored data in the material points are mapped to the mesh based on the new locations of the material points. Therefore the material points

move through the underlying finite element mesh. This approach entails that the finite element grid extends across the entire region of space where the material is expected to move into. However, only nodes attached to finite elements that contain material points are considered when setting up the equilibrium equations. Spatial integration is only performed over the volume inside the finite element mesh that is covered by material. The larger mesh therefore does not lead to an additional computational effort.

The solution adopted herein is based on the modified Lagrangian algorithm proposed by Sulsky et al. (1994) using the Euler-Cromer explicit time integration scheme (Kafaji, 2013). The numerical simulation of a CPT can be carried out in a less expensive way, if the effect of rotational symmetry of the pile and the surrounding soil is taken into consideration in the formulation of the material point method. This results in an extended formulation, originally developed by Sulsky & Schreyer (1996), which is based on a two dimensional axisymmetric framework. This formulation can significantly reduce the number of elements and material points compared to a three dimensional one. The details of this formulation are described in Galavi *et al.* (2018).

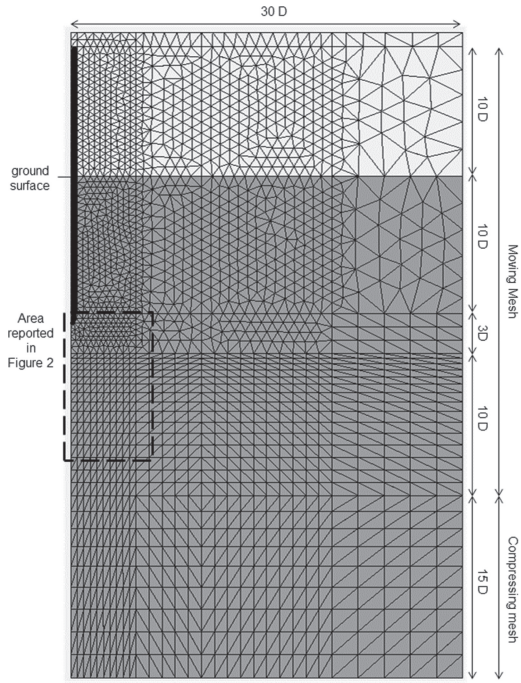

Figure 1. Scheme of the MPM model of CPT.

2.2 *Schematization of CPT*

The MPM schematization adopted to implement the CPT boundary value problem is shown in Figure 1. The finite mesh has a total of 3992 elements including the initially inactive elements. The inactive elements above the soil surface may be activated during the calculation process if material points move into the empty space they occupy. Triangular elements with a linear interpolation of the displacements are used. The number of material points is 13,810.

The numerical simulations are performed using an axisymmetric geometry. To avoid boundary effects, the side boundary is placed at a distance of 30 D from the symmetry line (D being the diameter of the cone). This space is divided in three parts with mesh sizes getting larger and the number of particles per elements decreasing as the distance from the symmetry line increases. Displacements at the side boundary are constrained in the radial direction and free in the vertical direction. The bottom boundary is fully fixed. The stresses in the soil are initialized using a typical K_0-procedure and a surcharge of 10 kPa is applied at the ground surface, equivalent to a 1 m thick soil layer above that surface. The cone penetrometer "pile" is modelled as a rigid body penetrating into the soil. The pile, which is initially embedded below the soil surface for a length equal to 10 D, is pushed into the soil for an additional 7 D. The penetration of the pile into the soil is modelled by applying a prescribed velocity, herein equal to 0.02 m/s, a value common in standard practice. The MPM moving mesh concept is adopted in all simulations (Kafaji, 2013). The cone is slightly curved at the transition from shaft to conical to avoid numerical difficulties due to locking. The simulations are performed considering a submerged one-phase material in drained conditions.

An elastic perfectly plastic constitutive law, based on the Mohr-Coulomb failure criterion, is used to simulate the behavior of the soil. It adopts 5 input parameters: stiffness modulus (E); Poisson's ratio (ν); cohesion (c); friction angle (ϕ); and dilatancy angle (ψ). In addition to these, two other parameters are also needed to define the initial conditions of the soil: porosity (n); and specific gravity of the soil grains (Gs), which is equal to 2.65 in all the numerical simulations performed herein. The values of the soil parameters assumed for the base case ("Base" in Table 1) are considered representative of the behavior of loose well-graded sands. A contact algorithm is used to model the frictional contact between the pile and the soil. The adopted friction angle value (11°), is representative of a sand to polished steel contact (Murray and Geddes, 1987). Considering the above conditions, the time needed to run one model simulation is equal to 20'.

Table 1. Input parameter values of the parametric analysis.

ID	E (kPa)	υ	c (kPa)	φ [°]	ψ [°]	n
Base	6000	0.2	1	30	0	0.2
SET1	4000	0.2	1	30	0	0.2
SET2	8000	0.2	1	30	0	0.2
SET3	6000	0.15	1	30	0	0.2
SET4	6000	0.25	1	30	0	0.2
SET5	6000	0.2	2	30	0	0.2
SET6	6000	0.2	5	30	0	0.2
SET7	6000	0.2	1	27	0	0.2
SET8	6000	0.2	1	33	0	0.2
SET9	6000	0.2	1	30	–1	0.2
SET10	6000	0.2	1	30	+1	0.2
SET11	6000	0.2	1	30	0	0.15
SET12	6000	0.2	1	30	0	0.25

2.3 *Parameter sensitivity and inverse analysis*

Inverse analysis algorithms can be effectively employed to calibrate the input parameters of numerical models for different geotechnical boundary value problems. The advantages of automated optimization analysis over trial-and-error procedures to calibrate the parameters of a given model are many, including: ability to automatically calculate parameter values that produce the best fit between observations and computed results; simultaneous calibration of multiple parameters; providing statistics that quantify the quality of calibration, data shortcomings and reliability of parameter estimates and predictions; possible time-saving; identification of issues that are easily overlooked during non-automated calibration (Finno and Calvello, 2005).

The sensitivity and inverse analysis have been herein conducted using UCODE (Poeter and Hill, 1997), a model independent algorithm designed to allow inverse modeling posed as a parameter estimation problem. The error function to minimize, called weighted least-squares objective function S($\underline{b}$), is expressed by:

$$S(b) = \left[\underline{y} - \underline{y}'(\underline{b})\right]^T \underline{\omega}\left[\underline{y} - \underline{y}'(\underline{b})\right] = \underline{e}^T \underline{\omega}\underline{e} \qquad (1)$$

where: $\underline{b}$ is a vector containing values of the parameters to be estimated; $\underline{y}$ is the vector of the observations being matched by the regression; $\underline{y}'(\underline{b})$ is the vector of the computed values which correspond to observations; $\underline{\omega}$ is the weight matrix; $\underline{e}$ is the vector of residuals.

To update the input parameters of a model, UCODE performs a gradient-based non-linear regression analysis adopting a modified Gauss-Newton algorithm. The relative importance of the input parameters being simultaneously estimated is defined using parameter statistics, such as: the sensitivity of the predictions to changes in parameter values, the variance-covariance matrix, confidence intervals and coefficients of variation. Herein, the composite scaled sensitivities (*css*), and the correlation coefficients (*cor*), will be used to evaluate, respectively, the sensitivity of the predictions to parameters changes and the degree of correlation between different input parameters.

The described inverse analysis algorithm will be used, herein, to calibrate the input parameters of the constitutive law adopted in the MPM model of the CPT. It's worth noting that the parameter optimization requires multiple runs of the MPM code, i.e. a number of iterations for the convergence of the regression analysis. More details on the calibration of soil constitutive laws by inverse analysis using UCODE can be found in Calvello (2014).

3 RESULTS

3.1 *Forward model*

Figure 2 shows the deviatoric strain and the deviatoric stress at penetration depths equal to two and six times the cone diameter, for the portion of mesh highlighted in Figure 1. The cone is pushed to its final depth from an initial position below the ground surface. This was done for two main reasons: to avoid numerical instabilities related to the presence of significant strains at low stress levels; to reduce the computational time, given that multiple iterations of the model are needed for the inverse analysis.

At the beginning of the simulation the soil mainly deforms from the initial position of the cone to about 2 to 3 D below and around the tip of the cone. As expected, no noticeable deformations are observed in the rest of the domain, including in the material particles along the CPT shaft above the initial position of the cone. The inner portion of this volume, extending for about 1 D below the tip and about 2 D laterally, exhibits deformations of the order of 10%. At the end of the simulation it is very clear that the soil deformations follow downward, as expected, the cone displacements. The highest deformations influenced a volume of soil extending from the initial position of the cone to about 2 to 3 D below its final position. The values of the deviatoric stress are less homogeneous around the cone, yet the size of the soil volume influenced by significant stresses extends laterally and downwards in a similar way at both penetration depths. These values are consistent with data reported in the literature (e.g. Van der Linden, 2016).

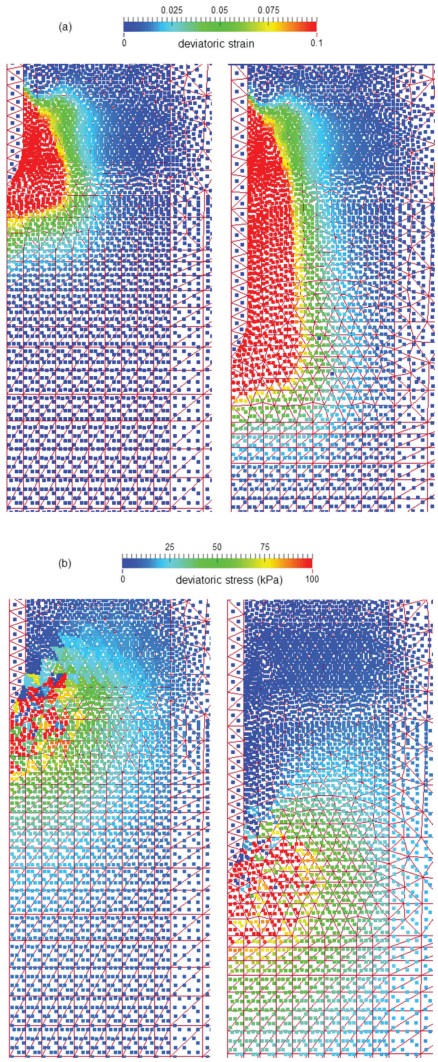

Figure 2. Results of the MPM model at penetration depths 2D and 6D: a) deviatoric strain; b) deviatoric stress.

The values of the cone tip pressure are plotted in Figure 3 as a function of the cone penetrometer depth (see "Base" simulation). As expected the cone resistance monotonically increases with depth with a trend asymptotically reaching, after a penetration depth of about 4 to 6 diameters, an almost constant value. The final value of the ratio between the resistance force and the cone area is equal to about 700 kPa, which can be associated to the average cone resistance within the soil layer extending from the initial position of the cone to about 2 D below the cone tip. Therefore, as already mentioned, the model only allows to retrieve a

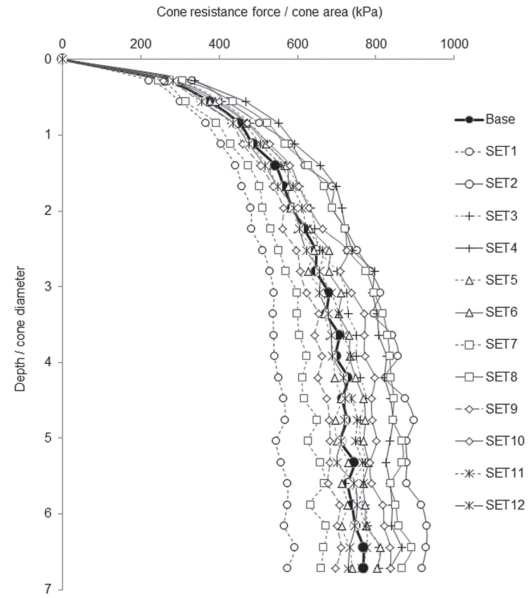

Figure 3. Results of the parametric analysis: cone resistance pressure vs. dimensionless depth.

single force representative of the average cone resistance in a layer of soil about 10 D thick. This value is comparable to the values reported by Salgado and Prezzi (2007) for the sand with a similar stress state.

3.2 *Parametric analysis*

A parametric analysis is carried out to evaluate the sensitivity of the cone resistance profile to changes in the values of the model input parameters. Table 1 shows the values of the parameters adopted. Besides the base case, 12 simulations were conducted by decreasing and increasing, one at the time, the values of the six input parameters keeping the rest of them constant. The minimum and maximum parameter values were defined considering reasonable ranges around the base case for the considered soil type. The results of the 13 numerical simulations are plotted in Figure 3 in a graph showing the modelled cone resistance versus the ratio between the penetration depth and the cone diameter. All the simulations produce a cone resistance pressure non-linearly increasing with depth and reach a maximum value of cone resistance before the final penetration depth. This behavior confirms that the depth reached by the numerical model is adequate. Only four simulations (sets 1, 2, 7 and 8) significantly differ from the base case, while the rest produce similar cone resistance results at all depths. This in turn means that the model results

are mainly sensitive to only two input parameters, i.e. E (sets 1 and 2) and ϕ (sets 7 and 8).

3.3 *Inverse analysis*

The results of the parametric analysis indicate that the two input parameters mostly affecting the MPM model results are E and ϕ. The inverse analysis is thus carried out to evaluate the capability of a gradient-based optimization algorithm to estimate the optimal value of these two input parameters, given a set of observations coming from the results of a CPT. To this aim, a synthetic case study has been set up, using the model results of the "base" simulation as observations and, in particular, the cone resistance values computed at 24 different depths (see Fig. 3).

Table 2 shows the main statistical indicators resulting from a set of eight sensitivity analyses performed for different initial values of the two input parameters. The soil stiffness (E), and the friction angle (ϕ), are respectively ranging from 4000 kPa to 8000 kPa and from 27° to 33°. The values of the composite scale sensitivities (css), indicate that the model results are sensitive to both parameters for all the considered values. The values of the correlation coefficients, ranging from 0.92 to 0.96 for six of the eight considered cases, indicate that the two parameters are, in most cases, very highly correlated. The latter indicates that it is unlikely that they can be estimated simultaneously within a single regression analysis. Considering the previous results, the first two regression analyses only consider one parameter at the time (Figure 4). Two initial values are considered for each one of the parameters. In both cases and for both parameters, the regression converges to the optimal "true" values using a small number of iterations, from 2 to 4. The capability of the optimization algorithm to find the global minimum of the error function is thus proved, irrespective of the initial values assumed for the parameter being calibrated.

Table 2. Main statistical indicators of the sensitivity analysis.

E (kPa)	φ (°)	css (E)	css (°)	Correlation coefficient
4000	27	4.32	9.91	0.78
4000	33	7.09	12.32	0.92
5000	28.5	5.72	13.09	0.94
5000	31.5	7.40	14.49	0.96
7000	28.5	6.02	18.44	0.92
7000	31.5	8.04	19.67	0.92
8000	27	6.64	18.81	0.95
8000	33	11.62	25.30	0.75

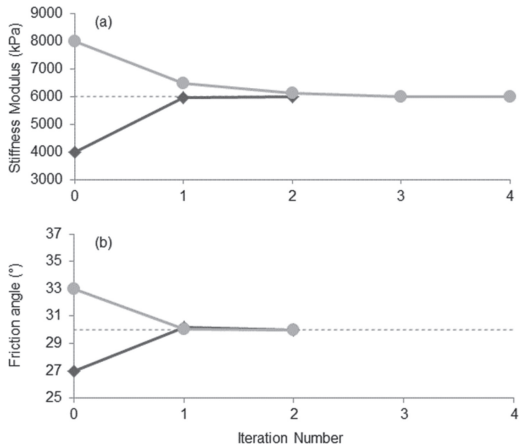

Figure 4. Parameter values during the regression analysis when it is conduced to calibrate on one parameter at the time: a) soil stiffness, E; b) friction angle, ϕ.

The results are different, as expected, when both the input parameters are calibrated simultaneously. Two initial set of values are herein considered, respectively assuming the two parameter values are either both higher than the optimal ones ("upper bound" simulation) or both lower than the optimal ones ("lower bound" simulation). It's worth noting that the two sets are the only ones for which the sensitivity analysis did not yield correlation coefficients between E and ϕ higher than 0.9. The results are presented by showing the values of the parameters (Figure 5) and the related error functions (Figure 6) at each iteration of the regression analysis until the final convergence of the optimization algorithm. In the lower bound simulation the optimization ends when the error function assumes almost negligible values, i.e. the solution converges towards a global minimum representing the true solution of the case study. On the contrary, in the upper bound simulation the optimization algorithm finds a solution that represents a local minimum of the error function with values of the two input parameters very different from the optimal values of the case study. Despite that, also in this case the error function decreases significantly during the optimization and reaches a minimum value of 2.65 after only two iterations, 1.00 being the value of the error function consistent with the accuracy of the information conveyed by the observations (Calvello, 2017). The latter can be visually confirmed by looking at the cone resistance profile with depth (Figure 7), which is much better than the initial one and not too different from the base case. In this case, the optimization got "trapped" in a local minimum of the error function possibly because the two parameters,

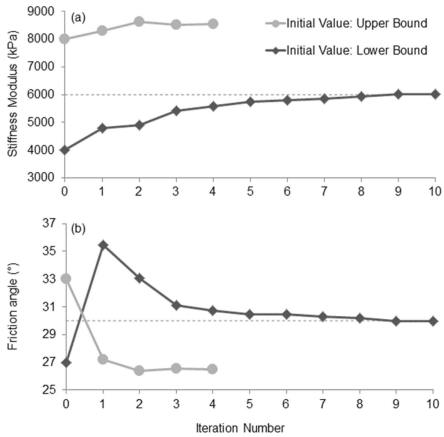

Figure 5. Parameter values during the regression analysis when it is conduced to calibrate both parameters simultaneously: a) soil stiffness, E; b) friction angle, ϕ.

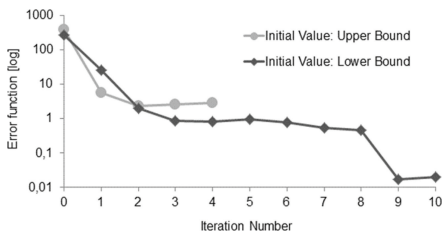

Figure 6. Error function during the regression analysis when it is conduced to calibrate parameters E and ϕ simultaneously.

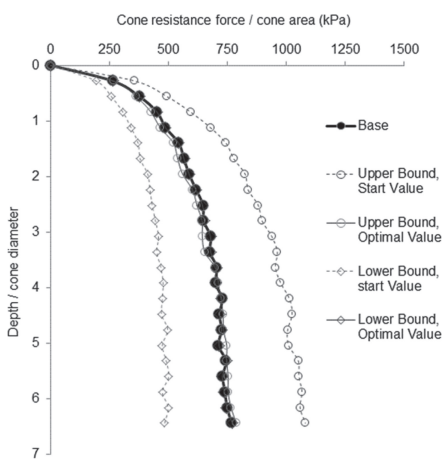

Figure 7. Cone resistance profile with depth for the initial and optimal values of the input parameters in the regression analysis conducted to calibrate parameters E and ϕ simultaneously.

moderately correlated when the regression started, became highly correlated after one iteration (being E close to 8000 kPa and ϕ close to 27°) and the gradient-based methods do not perform satisfactorily in calibrating multiple parameters when this happens.

4 CONCLUSIONS

The results of the performed inverse analyses highlight a few important aspects related to the use of optimization algorithms to calibrate the input parameters of MPM models of CPTs. Globally, the regression problem must be well-posed, which means: the observations must be sufficient for the adopted constitutive law and the numerical implementation of the CPT boundary value problem; the computed results must be sensitive to the parameters being calibrated; the parameters do not have to be highly correlated. When this happens, a gradient-based optimization algorithm, such as the one adopted herein, can be effectively used to optimize the model parameters so that the computed results match CPT observations. Of course, more research is needed to extend these findings to: situations employing real CPT data and not synthetic ones; observations related to full CPT profiles and not to a 10 D thick soil layer.

ACKNOWLEDGEMENTS

This work is partly funded by "Topsector Energiesubsidie van het Ministerie van Economische Zaken", the Netherlands.

REFERENCES

Andersen, S., & Andersen, L. 2010. Modelling of landslides with the material-point method. *Computational Geosciences*, *14*(1), 137–147.

Arroyo, M., Butlanska, J., Gens, A., Calvetti, F., & Jamiolkowski, M. 2011. Cone penetration *tests* in a virtual calibration chamber. *Géotechnique*, *61*(6), 525–531.

Arshad, M. I., Tehrani, F. S., Prezzi, M., & Salgado, R. 2014. Experimental study of cone penetration in silica sand using digital image correlation. *Géotechnique*, *64*(7), 551–569.

Beuth, L. 2012. Formulation and application of a quasi-static material point method. PhD. Thesis, Universität Stuttgart.

Beuth, L., Benz, T., Vermeer, P. A., Coetzee, C. J., Bonnier, P., & Van Den Berg, P. 2007. Formulation and validation of a quasi-static material point method. In *Proceedings of the 10th international symposium on numerical methods in Geomechanics (NUMOG), Rhodes, Greece*: 189–195.

Butlanska, J., Arroyo, M., Gens, A., & O'Sullivan, C. 2013. Multi-scale analysis of cone penetration test (CPT) in a virtual calibration chamber. *Canadian geotechnical journal*, *51*(1), 51–66.

Calvello, M, 2014. Calibration of soil constitutive laws by inverse analysis. In M.A. Hicks & C. Jommi (eds), *ALERT Doctoral School 2014 – Stochastic Analysis and Inverse Modelling*: 239–262.

Calvello, M. 2017. From the observational method to "observational modelling" of geotechnical engineering boundary value problems. In C. Hsein Juang et al. (eds) *Geotechnical Safety and Reliability*: 101–117.

Ceccato, F., Beuth, L., & Simonini, P. 2016. Analysis of piezocone penetration under *different* drainage conditions with the two-phase material point method. *Journal of Geotechnical and Geoenvironmental Engineering*, *142*(12), 04016066.

Coetzee, C. J., Vermeer, P. A., & Basson, A. H. 2005. The modelling of anchors using the material point method. *International journal for numerical and analytical methods in geomechanics*, *29*(9), 879–895.

Finno, R. J., & Calvello, M. 2005. Supported excavations: observational method and inverse modeling. *Journal of Geotechnical and Geoenvironmental Engineering*, *131*(7), 826–836.

Galavi V., Tehrani F. S., Martinelli M., Elkadi A., Luger D. 2018. Axisymmetric formulation of the material point method for geotechnical engineering applications. *9th Conf. on Numerical Methods in Geotechnical Engineering*, Porto, Portugal. Submitted.

Gens, A., Arroyo, M., Butlanska, J., Monforte, L., Carbonell, J. M., Ciantia, M., & O'Sullivan, C. 2016. Simulation of the cone penetration test: discrete and continuum approaches. *Australian Geomechanics Journal*, *50*(4), 169–182

Kafaji, I. K. A. 2013. Formulation of a dynamic material point method (MPM) for geomechanical problems., PhD thesis, Universität Stuttgart.

Lu, Q., Randolph, M. F., Hu, Y., & Bugarski, I. C. 2004. A numerical study of cone penetration in clay. *Géotechnique*, *54*(4), 257–267.

Monforte, L., Carbonell, J. M., Arroyo, M., & Gens, A. 2017. Performance of mixed formulations for the particle finite element method in soil mechanics problems. *Computational Particle Mechanics*, *4*(3), 269–284.

Murray, E. J., & Geddes, J. D. 1987. Uplift of anchor plates in sand. *Journal of Geotechnical Engineering*, *113*(3), 202–215.

Phuong, N. T. V., Van Tol, A. F., Elkadi, A. S. K., & Rohe, A. 2016. Numerical investigation of pile installation effects in sand using material point method. *Computers and Geotechnics*, *73*, 58–71.

Poeter, E. P., & Hill, M. C. 1997. Inverse models: A necessary next step in ground-water modeling. *Groundwater*, *35*(2), 250–260.

Salgado, R., & Prezzi, M. 2007. Computation of cavity expansion pressure and penetration resistance in sands. *International Journal of Geomechanics*, *7*(4), 251–265.

Sulsky, D., & Schreyer, H. L. 1996. Axisymmetric form of the material point method with applications to upsetting and Taylor impact problems. *Computer Methods in Applied Mechanics and Engineering*, *139*(1–4), 409–429.

Sulsky, D., Chen, Z., & Schreyer, H. L. 1994. A particle method for history-dependent materials. *Computer methods in applied mechanics and engineering*, *118*(1–2), 179–196.

Tolooiyan, A., & Gavin, K. 2011. Modelling the cone penetration test in sand using cavity expansion and arbitrary Lagrangian Eulerian finite element methods. *Computers and Geotechnics*, *38*(4), 482–490.

Van der Linden, T. I. 2016. Influence of multiple thin soft layers on the cone resistance in intermediate soils. *Master Thesis, TU Delft.*

Więckowski, Z., Youn, S. K., & Yeon, J. H. 1999. A particle-in-cell solution to the silo discharging problem. *International journal for numerical methods in engineering*, *45*(9), 1203–1225.

Zabala, F., & Alonso, E. E. (2011). Progressive failure of Aznalcóllar dam using the material point method. *Géotechnique*, *61*(9), 795–808.

Taylor & Francis
Taylor & Francis Group
http://taylorandfrancis.com

Cone Penetration Testing 2018 – Hicks, Pisanò & Peuchen (Eds)
© 2018 Delft University of Technology, The Netherlands, ISBN 978-1-138-58449-5

Challenges in marine seismic cone penetration testing

P. Gibbs, R.B. Pedersen & L. Krogh
Ørsted Wind Power, Copenhagen, Denmark

N. Christopher & B. Sampurno
Fugro, Wallingford, UK

S.W. Nielsen
COWI, Copenhagen, Denmark

ABSTRACT: Current advancements in foundation design methodologies have given a new focus on acquiring *in situ* G_0 data to compliment current laboratory testing methods and to provide G_0 profiles for design in a parameter bound framework. Seismic CPTU (SCPTU) data was acquired from sites within the North Sea both in drilling and non-drilling mode. An assessment of the data showed significant scatter in the interpreted results. Current standards provide little guidance on what is 'accurate and reliable' data, hence an assessment was initiated to better understand the reasons for the scatter observed and what is to be considered reliable data. This paper discusses the assessments that have been undertaken and covers: the seismic testing set-ups, how the data was acquired; how the data was interpreted; offers suggestions on what can be causing the scatter; and provides commentary on how to gain confidence in the data acquired. This study highlights the need for greater understanding of SCPTU data and closer client-contractor collaboration. It is recommended that project specifications clearly define SCPTU reporting beyond the standard requirements, where comprehensive information of the seismic data acquired and the methods used to derive the v_s is needed to improve confidence on data evaluation and interpretation for the design purpose.

Keywords: seismic velocity, CPT, small strain shear modulus

1 INTRODUCTION

As a method for providing strength and small strain stiffness measurements of the subsurface the Seismic Cone Penetration Test (SCPTU) has been available for a significant period of time. Onshore, as well as offshore, the technique has delivered interval velocities of shear waves, v_s, for determining the initial shear modulus, G_0. Recent developments within offshore foundation design have identified the need for high quality and accurate in-situ and laboratory G_0 data to inform detailed design parameters. To obtain in-situ stiffness measurements during geotechnical site investigations, one go-to tool is the Seismic Cone Penetration Test.

It is recognized that, historically, the SCPTU type test has been used for delivering relative values for developing ground models and identifying stratigraphy, whilst the need of today's geotechnical design engineers is a specific value for use within design.

This paper will present examples of results from offshore investigations at neighbouring sites located within the North Sea, and will discuss the learnings from these investigations, undertaken for detailed offshore wind farm development. Data originates from both drilling mode and non-drilling mode SCPTU set-ups. Non-drilling mode SCPTUs provided the projects with, on average, 12–15 m of penetration, whilst the drilling mode SCPTUs were carried out typically between 20–40 m below seabed.

On receipt and interpretation of the acquired data, significant scatter was seen in the results. Recognizing this scatter, it was acknowledged that an increased focus is needed to understand the variance in the v_s results, and what might be causing this, before considering their applicability for generating G_0-values.

With the lack of guidance for what is quality and accurate data within current standards, a study was initiated to investigate 'what is reliable data' that can be taken forward into design. The study proved it not possible to quantitatively determine the accuracy and precision of the v_s data and therefore the first task was to establish confidence in the results obtained. For the geotechnical engineer assessing the data as well as the engineer carrying out the geotechnical design, it is important to have the confidence in the v_s measurements obtained. Confidence being defined as having an understanding

of how the data is acquired, processed and interpreted and with knowledge of the limitations and assumptions that have been made when generating the v_s value taken forward in design. The intention of this paper is to initiate a dialog between client, contractors and suppliers on how to improve the tools, acquisition, interpretation and evaluation of v_s data to develop a robust method for acquiring confident v_s results from SCPTU.

2 INVESTIGATION METHODS

2.1 *Marine soils investigation*

The investigation works were performed to ISO 19901–8 (2014) standard. This includes *in situ* testing using either drilling mode and/or non-drilling methods. In non-drilling mode (seabed) tool penetration is initiated at the seafloor and penetrated in a single stroke to refusal or to a predetermined depth. In drilling mode (downhole), the tool is lowered down a predrilled borehole, and *in situ* testing is initiated at the bottom of the borehole.

2.2 *Seismic cone penetration testing (SCPTU)*

The penetrometer for a SCPTU consists of 10 cm^2 or 15 cm^2 piezocone, which provides continuous measurements of cone resistance (q_c), sleeve friction (f_s) and induced pore pressure (u_2), with additional instrumentation above the cone to measure seismic waves. The cone is pushed into the ground at a nominal rate of 20 mm/s (ISO 19901–8, 2014).

Measurements are made using geophones to detect shear wave velocities and pressure wave velocities, v_p, using an SCPTU. The shear wave is recorded in three axes by three geophones in the x, y and z directions, referred to as a geophone array as illustrated in Figure 1. The seismic cone is pushed into the soil and stopped at regular intervals to carry out testing.

A seismic velocity test (SVT) consists of several shots, which may be stacked to improve the signal to noise ratio (SNR). The moment the source is triggered, the data acquisition unit starts recording seismic response of the geophone array to the shear wave produced.

From analysis of the signal traces recorded, the arrival time of the shear wave can be estimated. The difference in the shear wave arrival times between tests at different depths can be used to calculate interval velocities. When a cone with a single geophone array is advanced through the soil, the calculated interval velocities are regarded as pseudo interval velocities. This is because separate shots have been used to infer the difference in the arrival times and subsequently calculate the interval velocity. If two geophone arrays are used, spaced at a known distance from each other within the tool,

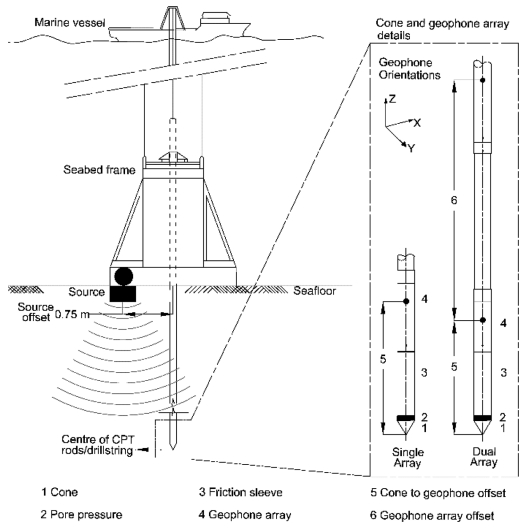

Figure 1. Offshore setup and SCPTU cone details.

then the actual difference in the arrival time from a single shot can be measured; this is the true interval velocity (Rice, 1984). One main advantage when using a dual geophone array is that the results are much less affected by any error in the trigger timing and the start of data recording.

3 SCPTU DETAILS

3.1 *Seismic source*

The source for the seismic tests was Fugro's hydraulic underwater shear wave hammer (HUSH) box fixed to the base of modified seabed frames. The source setup was the same for both modes with an offset of 0.75 m from the centre of the seabed frame and CPT rod as detailed in Figures 1. Alignment of geophone axis with the source was not possible with the offshore set up.

3.2 *Data acquisition—Non-drilling mode*

Continuous push of SCPTU in non-drilling mode were performed using Fugro's SEACALF® system. A single geophone array seismic piezocone was used as detailed in Figure 1. The cone penetration was paused approximately every 1 m to perform SVTs. Pseudo interval velocities over 1 m could then be derived. Relative penetration depth accuracy for this interval is in the order of ± 0.02 m.

3.3 *Data acquisition—Drilling mode*

Drilling mode SCPTU were performed using Fugro's WISON® system. The downhole SCPTU

equipment had a maximum penetration length of 3.0 m. A dual geophone array seismic piezocone (0.5 m fixed array offset) was deployed as detailed in Figure 1. True interval velocities were calculated with this method. Nominally, penetration was paused at 1.5 m to perform a SVT and then again after maximum penetration.

If penetration refusal occurred, then a SVT was performed at this point. True interval velocities over 0.5 m could then be derived approximately every 1.5 m.

For true interval velocity measurement, the depth accuracy is less critical due to the fixed offset of the geophone array.

3.4 *Seismic velocity test (SVT) procedure*

Each SVT consisted of a minimum of four shots. The form of the seismic trace was reviewed after each shot to identify the approximate shear wave arrival. Additional shots were performed when random noise or inconsistencies were identified to ensure enough data was acquired before advancement of the cone to the next SVT depth. SVTs continued until the shear waves could not be easily identified in the seismic traces.

3.5 *SVT data processing*

Individual shots were reviewed using seismic data analysis software, SC3-RAV (BCE, 2015). Shots free of significant random noise and unexpected arrival times were stacked to improve the SNR. A digital filter was then applied to remove any unwanted frequencies. The unfiltered data was then compared to ensure that no significant phase time shifts had occurred.

Reference shear wave arrival times were identified using the peak to peak method.

3.6 *Interval shear wave velocity calculation*

Shear wave velocity was calculated using the method detailed in the main text of the ASTM D7400 (2014). This method assumes a direct travel path from the centre of the source to the centre of the receiver (Figures 2a and 2b). The uncertainty associated with this assumption is not explored in this paper, however, the standard recommends methods to estimate the true travel path.

3.7 *Data review*

The calculated interval shear wave velocities were then assessed based on the ranges expected for the given soil strata. Of the many correlations between v_s and CPTU data that have been published, Robertson (2009) provided a close match with the derived v_s values and was useful in assessing the data set. Any results identified as unusual were then reprocessed and the location data set was then reassessed.

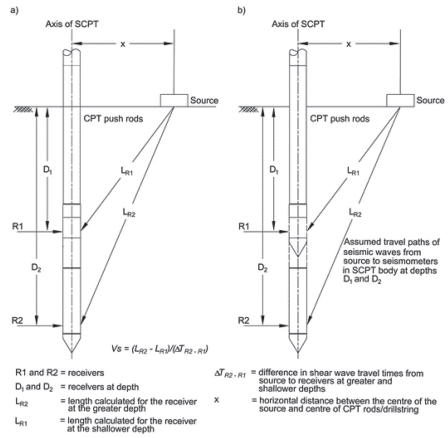

Figure 2. Seismic cone schematics (adapted from ASTM D7400, 2014): a) Single geophone array cone; b) Dual geophone array cone.

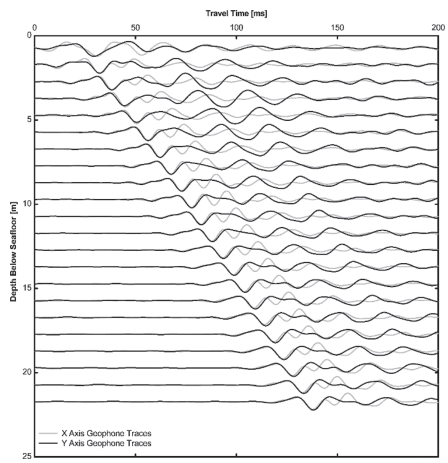

Figure 3. Non-drilling mode example location normalised amplitude seismic traces.

The review happened in two stages the first was performed offshore in advance of preliminary deliverables and the second was performed onshore in advance of the final data reports.

3.8 *Non-drilling mode results*

In general, the v_s results calculated using geophones in the x and y directions showed close agreement. Strong correlations between the derived v_s, from the SCPTU, and the v_s estimated from the traditional CPTU parameters was also observed. Figure 3 shows seismic traces from an example non-drilling mode location. Figure 4 shows the calculated v_s for this example location. Note that the reliability of derived v_s in the upper 2 m to

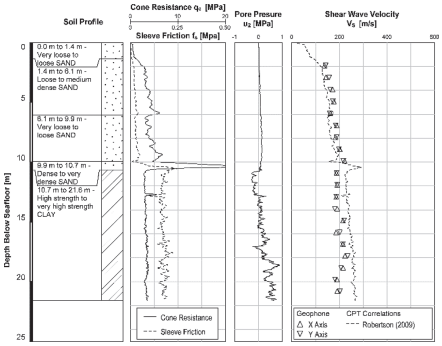

Figure 4. Non-drilling mode example location v_s data.

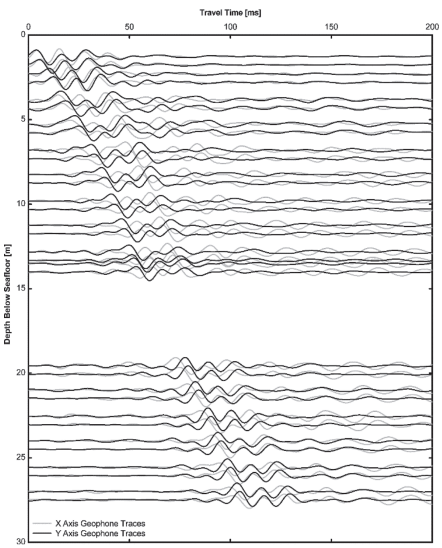

Figure 5. Drilling mode example location normalised amplitude seismic traces.

5 m (ISO 19901–8:2014) may not be representative depending on the system characteristics and site conditions, however, for the example given the results from 2 m are consistent with subsequent tests at greater depth.

3.9 *Drilling mode results*

In general, the v_s results calculated using geophones in the x and y directions were inconsistent. Figure 5 shows seismic traces from an example drilling mode location with variable stratigraphy. Figure 6 shows the calculated v_s for this example location from both axes in addition to the v_s derived using CPTU data. Results from 2.5 m are consistent with subsequent tests at greater depth.

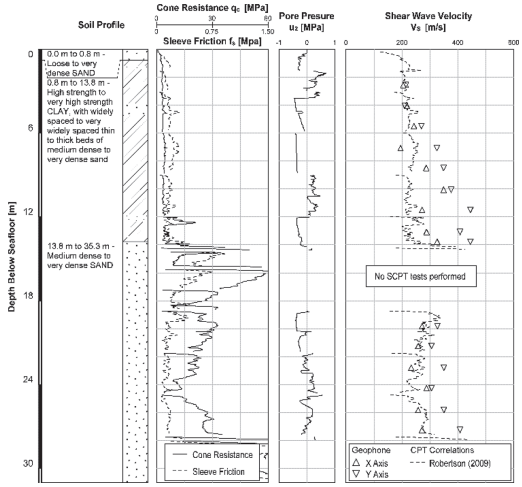

Figure 6. Drilling mode example location v_s data.

4 V_S DATA INTERPRETATION AND EVALUATION

In trying to assess the quality of the data, it became apparent that for both drilling and non-drilling modes, there is no agreed standard for quantitative estimates of accuracy. Instead, users have to rely on comparisons with known reasonable values and insight into the raw data and processing sequence to build confidence in the results.

The scatter of the drilling mode logs is too large for the results to be used with confidence (Figure 6), although it is acknowledged that a slightly more mixed geology might complicate the conclusions further. By going back through the processing steps a number of factors can be identified that influence the quality of the calculated velocities can be identified.

The highly scattered final velocities correspond with large deviations between the velocities calculated for the x and y geophone components. One factor influencing the results is the uncertainty of first arrival picks. The accurate picking of first arrivals is limited by noise in the data traces masking the arriving signal, see Figure 5.

4.1 *Noise*

There are mainly two different types of distortions of the transmitted signal that may result in difficulties interpreting the received records: Random noise and coherent noise.

Random noise is usually coming from external sources and is not related to the seismic source itself. It will change from one shot to the next and can therefore be reduced by stacking of several

recordings. Random noise can be expected to increase with depth relative to the signal as the signal path gets longer and the seismic waves get dampened and spread out over a larger area.

In the end, a depth will be reached when the SNR will be too low and the source signal can no longer be identified with the required accuracy in time, if at all.

Coherent noise, on the other hand, is related to the signal from the source. It can be a by-product from the source itself, or it can be the result of disturbances along the signal path. Examples can be waves travelling along the drill string or casing, typically with higher velocity than in the surrounding soil. Coherent noise typically does not change between shots and cannot be reduced by stacking.

In non-drilling mode, very little variation is seen between the unstacked traces providing evidence of a low level of random noise. The SCPTUs reach refusal before getting the depth where the signal gets dampened significantly. Distinct first arrivals can be identified in the majority of the traces and no significant signs of coherent noise can be identified (Figure 7a).

In drilling mode, the greater maximum penetration depth means that some traces are influenced by low SNR and the unstacked traces show larger variations due to random noise (Figure 7b). The overall signal quality, also for traces with little random noise, is lower with less distinct first arrivals. The received waveform varies little with depth, and it is therefore unlikely that the distortions are caused by the variations in the geology. The distortion of the signal is attributed mainly to coherent noise generated by signals travelling in the drilling mode equipment and disturbances of the soil created during drilling.

At greater depth, the signal is dampened and random noise starts to dominate reducing the signal to noise ratio. Random noise will eventually deteriorate the signal enough that no interpretation can be done.

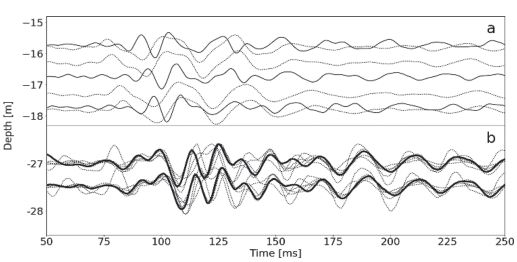

Figure 7. a) Comparison of traces recorded in drilling mode (dotted line) and non-drilling mode (solid line) at the same location. b) Random noise in deep drilling mode traces. Dotted lines are the unstacked traces and the solid lines are the stacked traces.

4.2 *Deviations between the horizontal components*

The S-waves recorded are horizontally polarized and are recorded by two horizontal receivers placed perpendicular to each other.

The signal will be distributed between the two receivers depending on their orientation relative to the source. This orientation changes if the seismic cone is rotated around its own axis (Figure 8). In some setups rotation can happen while the cone is pushed down. A change in orientation will change the relative signal strength of the receivers, but not the timing of the signal arrival. If both receivers' have enough signal strength for the record to be interpreted they should agree on the v_s value. Any difference will reflect the uncertainty on the derived v_s.

The relatively broad and indistinct first arrivals of the drilling mode data make accurate picking of the first arrival times difficult. This increases the uncertainties of the calculated v_s values resulting in significant scatter and deviation between the two components.

4.3 *Receiver array distance*

The SVT velocity values are calculated from differences in travel time to different depths. There are two options for obtaining the records from the two depths needed to find the travel time difference: They can be recorded simultaneously using two receiver arrays (true interval), or one after the other by moving a single receiver array (pseudo interval).

The advantages of the single array system are that it requires less equipment and the receivers take up less space along the SCPTU tool.

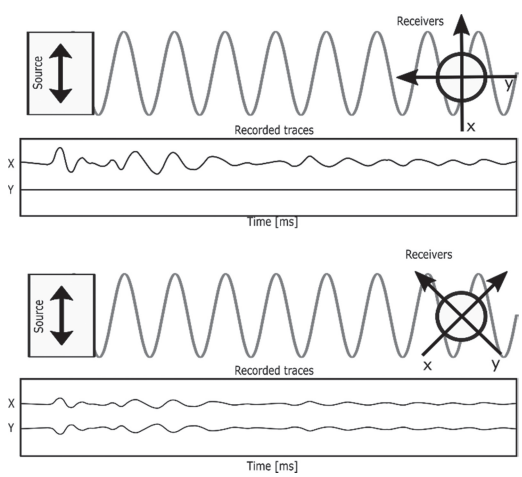

Figure 8. Two examples of receiver orientation in relation to the direction to the s-wave source, showing how the rotation influences the distribution of the signal between the perpendicular receiver components.

The main advantage of using the dual array setup is the elimination of the error on the distance measurement between the two receiver depths as well as the influence from variations in the timing of the shots. Timing variations will still have a negative impact on trace stacking.

In the present data set the dual array setup was only used in drilling mode. Due to space constraints in the equipment the distance between the dual receiver arrays was limited to 0.5 m, as opposed to the 1 m distance used for the non-drilling mode data.

The choice of receiver array distance, apart from practical constraints, is a trade-off between depth resolution and accuracy of the calculated v_s velocities.

In principle, the dual receiver array used in drilling mode should be more accurate than the single array used in non-drilling mode, as the dual array minimizes any uncertainty in the trigger timing and the distance between the receiver arrays. However, for the drilling mode data the improvement in distance accuracy (fixed 0.5 m) does not compensate for the difficulties in accurately determining the shorter time delay between the traces. Under the conditions of the two surveys presented, the 0.5 m receiver spacing may have been too small and contributed to the scatter in the v_s values.

4.4 *Confidence as a substitute for accuracy*

Some insight into the data confidence can be gained by calculating signal to noise ratios of records. However, these parameters do not easily translate into quantitative estimates of the accuracy of the resulting v_s values.

Assessing the quality of the seismic results has therefore mainly relied on three characteristics: Consistency between the two components, amount of variation between adjacent v_s values and evaluation of the raw data and first break picks.

5 CONCLUSIONS

Non-drilling mode and drilling mode methods can provide v_s data. The main challenge is that no common practice is available to define quality, accuracy, uncertainty and reliability of the measured and derived data.

During the review process, the understanding of the following was found to be critical when evaluating the data:

- The techniques used;
- Nature of noise within traces;
- Variation in the v_s derived from the geophone components (x & y); and
- Impact of geophone arrays and interval distance.

It has become apparent to the authors that collaboration and an in-depth understanding of the procedures and equipment used cannot be underestimated. The end user of the v_s results cannot refer to a quality measure and therefore needs to know the derivation of the results to have confidence.

6 RECOMMENDATION

The community must work together and agree on a standardised method for operational testing setups, data evaluation and reporting in order to provide reliable and trustworthy results for further use.

Lacking quantitative measures of v_s accuracy means that gaining insight into the raw data and the data processing is essential to create confidence in the results. This raises the level of detail required in the reporting phase and demands a greater insight into the data acquisition and interpretation by the end users of the processed results. It is thus recommended that current project specifications clearly detail requirements to SCPTU reporting beyond standard requirements.

REFERENCES

ASTM International, 2014. D7400-14 Standard Test Methods for Downhole Seismic Testing. Geneva. West Conshohocken: ASTM International.

Baziw Consulting Engineers Ltd (BCE), 2015. SC3-RAV 2015 - Seismic Data Analysis Software Version 15.3.1. Vancouver: Baziw Consulting Engineers Ltd.

International Organization for Standardization (ISO), 2012. ISO 22476-1:2012 Geotechnical investigation and testing—Field testing—Part 1: Electrical cone and piezocone penetration test. Geneva: ISO.

International Organization for Standardization (ISO), 2014. ISO 19901-8:2014 Petroleum and natural gas industries – Specific requirements for offshore structures – Part 8: Marine soil investigations. Geneva: ISO.

Rice, A. 1984. The seismic cone penetrometer, thesis submitted in partial fulfilment for Master of Applied Science, Department of Civil Engineering, University of British Columbia.

Robertson, P.K. 2009. Interpretation of cone penetration tests—a unified approach. Canadian Geotechnical Journal, Vol. 46(11): 1337–1355.

Cone Penetration Testing 2018 – Hicks, Pisanò & Peuchen (Eds)
© 2018 Delft University of Technology, The Netherlands, ISBN 978-1-138-58449-5

Numerical simulation of cone penetration test in a small-volume calibration chamber: The effect of boundary conditions

M. Goodarzi
MARUM—Center for Marine Environmental Sciences, University of Bremen, Bremen, Germany
Geo-Engineering.org GmbH, Bremen, Germany

F.T. Stähler & S. Kreiter
MARUM—Center for Marine Environmental Sciences, University of Bremen, Bremen, Germany

M. Rouainia
School of Engineering, Newcastle University, Newcastle upon Tyne, UK

M.O. Kluger
MARUM—Center for Marine Environmental Sciences, University of Bremen, Bremen, Germany

T. Mörz
MARUM—Center for Marine Environmental Sciences, University of Bremen, Bremen, Germany
Geo-Engineering.org GmbH, Bremen, Germany

ABSTRACT: In this study, laboratory Cone Penetration Tests (CPTs) were conducted in the MARUM Calibration Chamber (MARCC) with three lateral boundary conditions: (BC), constant stress, constant strain and the simulated field conditions with constant stiffness. Cuxhaven-Sand was studied in the chamber tests and tip resistance-relative density ($q_c - D_r$) relationships were generated for each BC. Laboratory experiments were carried out to estimate the mechanical properties of the Cuxhaven-Sand. Multiple numerical analysis have then been undertaken to simulate the calibration chamber results. First, the soil model was calibrated against laboratory soil parameters and a CPT result of the calibration chamber with fixed lateral boundaries, then, a numerical penetration analysis in an infinite soil mass was performed to evaluate the implemented constant stiffness boundary condition in the chamber. Good agreement between experimental and numerical cone resistances demonstrates the possibility of using the advanced small volume MARCC for producing controlled CPT results applicable in true field test conditions.

1 INTRODUCTION

Calibration chambers (CCs) play a crucial role in the interpretation and analysis of cone penetration test (CPT) results. The advantage of cone penetration tests in a CC is that material properties and the stress state of the sample can be controlled. Therefore, uncertainties in the dependency of cone resistances on soil and stress state are less ambivalent than in field tests. The conventional boundary conditions of the sample in a CC are either constant stress or constant strain in lateral and vertical directions. Two widely used boundary conditions are BC1 and BC3. In both cases the vertical stress boundary is applied, the lateral boundary in BC1 applies a constant stress, while in BC3 the lateral displacement is fully constrained, which results in a constant strain (Salgado et al., 2001). Despite the advantages of CC tests, the limited size of the sample or chamber may impose boundary effects on the measured cone resistance. This phenomenon was observed when different chambers or cone sizes were adopted for tests under BC1 and BC3 along with defined materials or stress conditions (Jamiolkowski et al., 1985). Moreover, the boundary effect may also be related to the soil density. For example, Schnaid & Houlsby (1991) reported an increase of boundary effect with increase in relative density (D_r) under BC1 conditions.

The calibration of field CPT data with laboratory CC experiments requires either the sample to be large enough or the measured q_c to be corrected for boundary effects. Parkin and Lunne (1982) concluded that the boundary effect is negligible when the ratio of sample to cone diameter (R_d) is larger than 50 and Jamiolkowski et al. (2003)

recommended a R_d of at least 70. Working with such big CC is technically and economically more challenging regarding the amount of materials needed and the time spent on sample preparation. Therefore, some studies attempted to establish correction factors for the q_c values measured in small volume CC by comparing the values of CC with field tests (Mayne & Kulhawy, 1991; Jamiolkowski et al., 1985; 2003; Butlanska et al., 2009). A problem associated with these studies is that the correction factors are determined for specific samples, cone sizes or sands. Therefore, they cannot be generally used for all CC test. Another approach to tackle the size effect is to impose a constant stiffness on the lateral boundary of the sample and to simulate an infinite soil mass. Huang & Hsu (2005), following the work of Ladanyi (1972), proposed a stress-strain relation for the lateral stiffness boundary utilizing the equilibrium equation in cylindrical coordinates. The stress-strain response of the soil is first determined by compressing the sample in the lateral direction and then the obtained radial stress-strain relationship is used to replicate the stress on a sample embedded in an infinite soil mass. This boundary condition is called BC5 or simulated field boundary condition. Their sample in CC is confined with several rings and each ring controls the required stress strain relationship independently.

In this study, a small volume CC (Fleischer et al., 2016) with a R_d of 25 was equipped with three circumferential strain sensors. The approach initially proposed by Ladanyi (1972), which has the aim to determine the undrained shear strength of clay using a pressuremeter, was reformulated for CC in order to estimate the imposed stress at the sample boundary under BC5. An important step is to validate this new boundary condition and to prove that the stress state inside the chamber is comparable to the stress of an infinite soil mass. For this purpose, several chamber tests were conducted under BC1, BC3 and BC5 and the q_c-D_r relationships were generated for these boundary conditions. Cuxhaven-Sand, an onshore material analogous to Pleistocene Southern North Sea sand was used as the sample material. Then, numerical models of the chamber with these three boundary conditions were generated using the commercial finite element (FE) software ABAQUS (Abaqus manual version 6.11). Mohr-Coulomb soil parameters were obtained from triaxial testing and then the soil model was calibrated using CC test with the constant strain boundary condition of BC3. The numerical results were compared with the CC tests under both BC1 and BC5 in order to evaluate the capability of the CC in reproducing q_c, comparable with CPT tests in an infinite soil mass.

2 THE SMALL VOLUME CALIBRATION CHAMBER

2.1 *Overview*

A small volume CC was developed in Marine Engineering Geology working group of the Center for Marine Environmental Sciences (MARUM), University of Bremen (Fleischer et al., 2016). The MARUM CC (MARCC) is similar to a large triaxial cell with a sample of 300 mm in diameter and 550 mm in height placed in a latex membrane (Fig. 1). An in-house designed small cone with a 12 mm diameter is used for the tests resulting in a R_d of 25. The chamber is equipped with three LVDT circumferential sensors to measure the lateral strain of the sample throughout the tests. The LVDT sensors are placed at vertical distances of 150, 250 and 350 mm from the top of the sample.

2.2 *Boundary conditions*

MARCC has different vertical and lateral boundaries. The top boundary of the sample is a fixed sintered steel plate, while the lower boundary is a stress-controlled water filled cushion and applies a constant pressure. The lateral boundary can be fully fixed by using a rigid steel casing, which is used for boundary condition BC3 (Fig. 2). The BC1 is realized by regulating constant pressure around the latex membrane of the sample in CC.

The complexity, however, lies in the implementation of the simulated field boundary condition BC5 in the MARCC. In an ideal scenario, the BC5 should reproduce the stress and strain at the sample lateral boundary in such a way that the sample is embedded in an infinite soil mass (Fig. 3).

While BC1 and BC3 are independent of soil properties and the sample size, BC5 simulates the material dependent displacement and induced

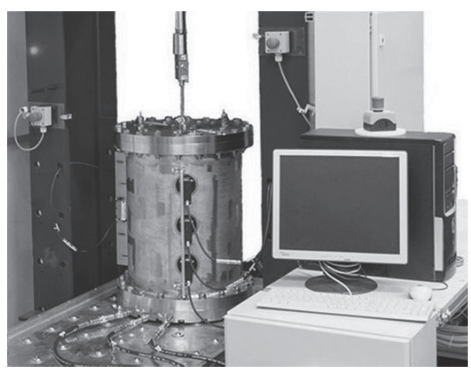

Figure 1. An overview of the calibration chamber facility MARCC at MARUM, University of Bremen.

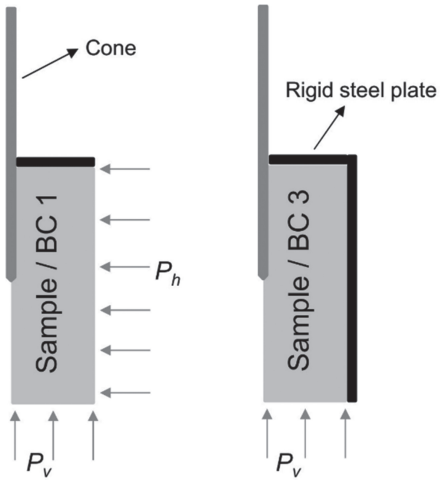

Figure 2. Axisymmetric schematic drawing of the BC1 and BC3 in the CC.

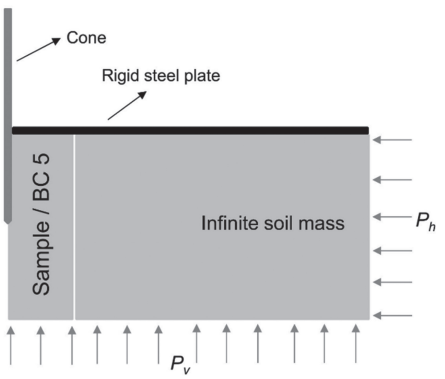

Figure 3. Axisymmetric schematic drawing of an ideal BC5 in the CC.

stress at the lateral boundary. The actual lateral stress in BC5 thus depends on how the soil deforms during penetration. In order to derive an analytical expression for the stress-strain response around a cylindrical cavity expansion, Ladanyi (1972) proposed to use the equilibrium equation in cylindrical coordinates with no body forces and no vertical stress variation as follows:

$$\frac{d\sigma_r}{dr} + \frac{\sigma_r - \sigma_\theta}{r} = 0 \tag{1}$$

where r is the radius and σ_r and σ_θ are the total principle stresses in radial and tangential directions, respectively. As the σ_r and σ_θ are the principal stresses, the term σ_r - σ_θ is a deviatoric stress, q.

The equilibrium equation should be satisfied at any point inside the sample and on the boundary. During penetration the cavity radius expands, Equation 1 is then integrated for any incremental change in the sample radius for r_i to r_{i+1} as follows:

$$\int_i^{i+1} d\sigma_r = \int_i^{i+1} \frac{q_{i,i+1}}{r} dr \tag{2}$$

where $q_{i,i+1}$ is the deviatoric stress at increment i to $i+1$. Assuming a constant $q_{i,i+1}$ through each incremental radius change. After some mathematical calculation, Equation 2 can be rewritten as:

$$\sigma_r^{i+1} = -q_{i,i+1}(\ln(1+\varepsilon_r^{i+1}) - \ln(1+\varepsilon_r^{i})) + \sigma_r^{i} \tag{3}$$

where ε_r is the radial strain and the superscript i is the increment number.

Equation 3 is an analytical expression of radial stress and radial strain around the axis of symmetry of the sample. The term $q_{i,i+1}$ is a function of the stress level, the distance from the center of cavity expansion and the soil mechanical response. If it is assumed that the elastic response of the soil under small deformation at the chamber boundary is similar in both compression and expansion, $q_{i,i+1}$ can be evaluated by an initial lateral compression of the sample. Therefore, after the preparation and consolidation of the sample, the lateral stress is incrementally increased by 10 kPa/min until a maximum radial strain of 0.08% is reached. The radial strain is derived from the circumferential LVDTs and allows a relationship between $q_{i,i+1}$ and ε_r to be established.

When the cone penetrates under BC5, the required incremental increase in the lateral stress is calculated for each increment of radial strain and its corresponding $q_{i,i+1}$ using Equation 3.

Within the MARCC, the increase in lateral stress is controlled by the maximum radial strain recorded with the three LVDTs. This potentially introduces some artefacts, as the stress increases around the whole height of the chamber uniformly and the radial strain measurement is only at three levels. The effectiveness of this approach for incorporating simulated field boundary condition in calibration chambers is discussed in Section 6.

3 MECHANICAL PROPERTIES OF CUXHAVEN SAND

The mechanical properties of the Cuxhaven-Sand are needed to perform numerical analysis of the CPTs in MARCC. A linear elastic-perfectly plastic behaviour with Mohr-Coulomb failure envelope was chosen for this study, requiring the elastic parameters, the internal friction angle and dilation angle of Cuxhaven-Sand.

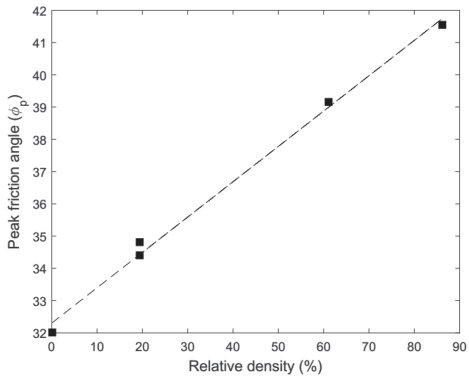

Figure 4. Peak friction angle as a function of relative density.

A correlation between the peak/critical friction angle and relative density for Cuxhaven sand was derived by a sequence of monotonic triaxial compression tests and sand cone pluviation tests, following procedures outlined in Wichtmann (2005) (Fig. 4). The critical friction angle is 32 degree and the dilation angle is estimated using

$$\psi = \varphi'_P - \varphi'_C \,, \tag{4}$$

where φ'_p and φ'_c are the peak and critical friction angles and ψ is the dilation angle (Susila and Hryciw, 2003).

The Young's modulus, of the soil significantly controls the concentration of induced stress around the cone. The Young's modulus is nonlinear and known to be affected by the mean effective stress (Susila & Hryciw, 2003; Tolooiyan & Gavin, 2011). Therefore, CPT results are used to calibrate this parameter for the Cuxhaven-Sand.

In order to estimate the relative density of the Cuxhaven-Sand inside the chamber, the maximum and minimum void ratio was determined following DIN 18126 (1996) and the relative density is calculated as:

$$D_R = \frac{e_{\max} - e}{e_{\max} - e_{\min}} = \frac{0.82 - e}{0.82 - 0.48} \tag{5}$$

where e_{max}, e_{min} and e are the maximum, minimum and actual void ratio, respectively.

4 CPT IN MARCC WITH DIFFERENT BOUNDARY CONDITIONS

The q_c-D_r relationships of the Cuxhaven-Sand for BC1, BC3, and BC5 conditions were established for initial relative densities ranging from dense to very dense based on several tests per boundary condition (Fig. 5).

All samples were prepared by air pluviation to relative densities between $D_R = 0.75$ and $D_R = 0.95$. Air-pluviated samples were vacuum saturated in MARCC by allowing de-aired and demineralized water to slowly percolate from the bottom to the top of the sample. A Skempton B-value of at least 0.95 was reached for all tests. Vertical and radial consolidation stresses of 300 kPa and 190 kPa were applied, respectively and a back pressure of 100 kPa was realized. These conditions represent a burial depth of around 18 m to 20 m, which is important for offshore wind turbine foundations. All saturated and consolidated samples were penetrated by a 12 mm cone under drained conditions with a constant penetration speed of 2 cm/s.

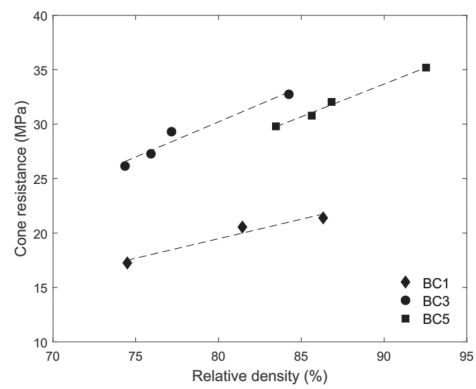

Figure 5. CPT results in Cuxhaven sand obtained in MARCC with different boundary conditions.

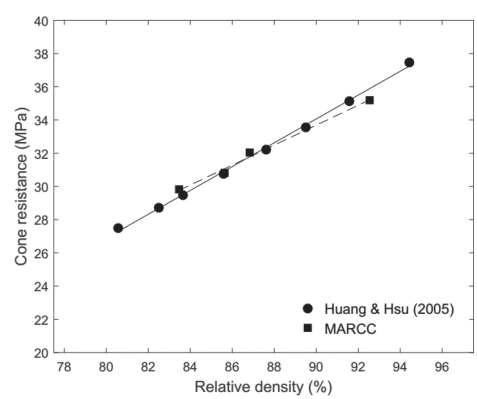

Figure 6. Comparison between CPT results obtained in Huang & Hsu's (2005) chamber and MARCC under BC5.

Figure 5 provides the $q_c - D_r$ relationships obtained with different boundary conditions. One data-point for CPT represents the steady-state cone resistance over a penetration depth of usually 150–300 mm. As expected, the constant stress boundary condition BC1 results in the lowest q_c values and the constant strain boundary condition BC3 gives the highest. The simulated field boundary condition, BC5 shows values between BC1 and BC3.

The larger CC of Huang & Hsu (2005) with its independent circumferential rings is, despite our use of only one lateral stress and the use of a different sand, in good agreement with the results presented in this study (Fig. 6).

5 NUMERICAL MODELLING OF CALIBRATION CHAMBER TESTS

The numerical analyses of the CC tests were carried out using the commercial finite element package, ABAQUS (Abaqus manual version 6.11). The symmetry around the cone axis allows an axisymmetric formulation for the model set up. Suitable mesh refinement around the cone is an important numerical parameter, which needs to be determined in order to avoid mesh-dependency in the results. As there is no rule of thumb, the appropriate mesh size is evaluated by repeated runs with a stepwise mesh refinement until the value of q_c stays constant.

The penetration process of CPT involves large deformation of the soil around the cone. Therefore, the arbitrary Lagrangian-Eulerian (ALE) formulation, implemented in ABAQUS, is used as a means to avoid the excessive mesh distortion around the cone, which could terminate the solution. This method allows for the adjustment of the aspect ratio of elements around the cone where excessive deformation takes place (see Hu &Randolph, 1998). The ALE formulation is only applied to a zone round the penetration path.

The soil mass is considered to be weightless and elastic-plastic using the Mohr-Coulomb failure criteria. The solution is explicit dynamic so axisymmetric linear elements (CAX4R) are used. The cone and rod is assumed to be rigid, therefore an analytical rigid surface is adopted to represent them. As the tests are static CPT in highly permeable sand, it is assumed that the system is drained. Therefore, based on the values of pore pressure and total stresses mentioned in Section 4, the numerical analyses are conducted with the effective stresses of 200 kPa and 90 kPa for vertical and lateral boundaries, respectively. The contact friction between the cone and the sand is assumed half of the internal friction angle of the soil (Susila & Hryciw, 2003).

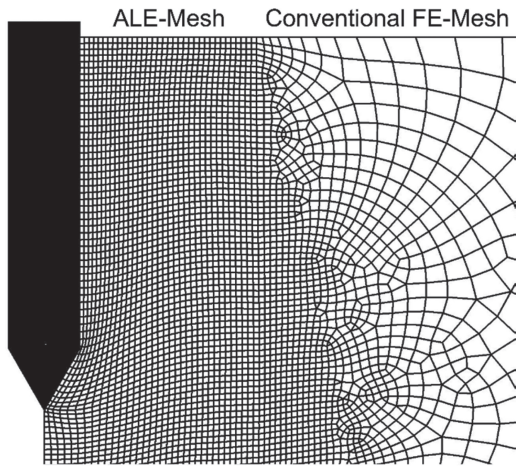

Figure 7. Deformed mesh around the cone in the FE model.

The BC1 and BC3 boundary conditions are applied as constant stress or fixity at the boundaries. However, in order to test the BC5 of the MARCC in the numerical model, an infinite soil mass is required in the lateral direction of the chamber. Therefore, the lateral boundary is extended (see Figure 3) four times leading to $R_d = 125$, which is beyond the recommended value of 70 for CC. The employed mesh refinement around the cone and the quality of the deformed mesh with ALE formulation is presented in Figure 7.

6 NUMERICAL ANALYSES OF CPTS IN MARCC

6.1 *Calibration of the stiffness of Cuxhaven-Sand with CPT results*

BC3 is the best-defined boundary condition consisting of a top and circumferential fixity with only the lower boundary being subjected by variable but constant stresses. Therefore, BC3 tests were selected for the purpose of model calibration using the soil stiffness for the Cuxhaven-Sand as a variable. A relative density was chosen for the calibration and its corresponding mechanical properties are derived from experimental results, whereas the Poisson's ratio (υ) is assumed (Table 1).

Several attempts with different elastic modulus values were conducted in order to calibrate this parameter for a relative density of 82% and the best result is presented in Figure 8 along with two other trials. An E of 50 MPa results in a cone resistance of almost 31 MPa, which is similar to the measured cone resistance in the CC test. It is also observed that the Young's modulus of the

Table 1. Experimental data for the selected relative density.

Parameters	Values
Relative density (D_r)	82%
Peak friction angle (φ'_p)	41
Critical friction angle (φ'_c)	32
Dilation angle (ψ)	9
Young's modulus (E')	?
Poisson's ratio (υ)	0.3
Cone resistance, q_c (MPa), in MARCC with:	
BC1	20.2
BC3	31
BC5	29

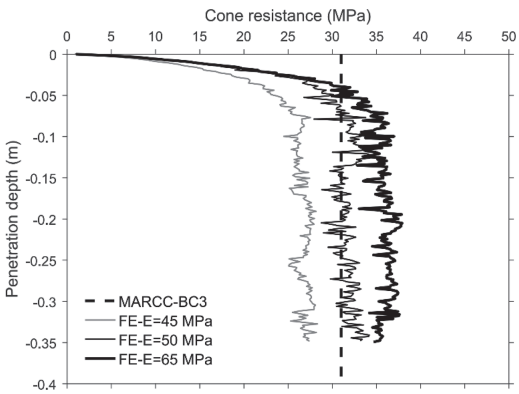

Figure 8. Three trial numerical CPT curves for CC test under BC3 with soil parameters presented in Table 1 and different Young's moduli, the straight-line represents the average value of the steady state part of the experimental CPT curve.

Cuxhaven-Sand has a significant effect on the simulated q_c due to its influence on the induced stress concentration around the cone.

The value of 50 MPa for this sand for a mean effective stress (p') of 126.7 kPa is in good agreement with the experimental graph of p'-E reported by Tolooiyan & Gavin (2011) for Blessington Sand, which gives $E = 50.6$ MPa for the same p'.

6.2 *Prediction of the CPT results in MARCC under BC1 and BC5*

The set of mechanical properties of Cuxhaven-Sand with relative density 82%, achieved in the previous section, is used in order to predict the cone resistance in CC with BC1 and BC5. Comparing the numerical result with the CC test is important in two aspects. First, it is interesting to see how well the boundary effects are reproduced in FE analyses. This could potentially help to determine boundary

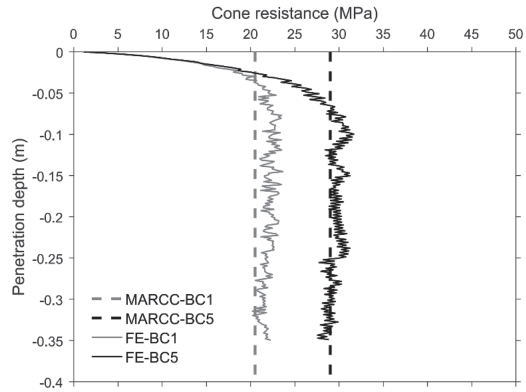

Figure 9. Numerical and experimental results for the uncalibrated CPTs in CC under BC1 and BC5. The straight-lines represent the average values of the steady state part of the experimental CPT curves.

effect correction factors for the CC results using finite element analysis. Second, as the numerical CPT with BC5 has an actual infinite lateral boundary, it allows us to evaluate the performance of the implemented BC5 in MARCC.

Figure 9 shows the numerical CPT curve versus the q_c measured in MARCC with both uncalibrated boundary conditions BC1 and BC5. A good agreement between FE analyses and the experimental results is observed. It can be concluded that the less sophisticated set-up in MARCC for the simulated field boundary is effective enough to produce CC's results, which are comparable to CPTs in infinite soil mass. A slight error in reproducing CPT results under BC1 condition can be seen. This issue could potentially be due to the simplicity of the soil model or caused by friction on the lateral boundary in the MARCC test, which was considered as frictionless in the numerical model.

7 CONCLUSION

In this study, the small volume calibration chamber MARCC was equipped with circumferential strain gauges and a servo-control lateral pressure system in order to reproduce the so-called simulated field boundary conditions BC5. This boundary condition allows production of CPT results comparable to field tests in calibration chambers. A numerical analysis was then used to evaluate the performance of the implemented boundary conditions.

Through several numerical and experimental CPTs with Cuxhaven-Sand, it was shown that numerical modelling captures the effect of different boundary conditions in the calibration

chamber. This could potentially be a way to correct the calibration chamber's results for the boundary effect. In addition, the implemented BC5 in MARCC was validated by this numerical analysis. It is observed that—despite the simplicity of the MARCC—the measured cone resistance with simulated field boundary conditions is in good agreement with a more sophisticated calibration chamber in the literature and also matches well with the numerical CPT results in an infinite soil mass. This finding is of great importance, as it allows for the use of MARCC's output for engineering practice with more confidence.

ACKNOWLEDGMENT

The Authors would like to acknowledge the support of the project "Vibro Drucksondierungen", FKZ: 0325906 A by the Federal Ministry for Economic Affairs and Energy (BMWi) and the MARUM—Center for Marine Environmental Sciences, University of Bremen. The crucial help and assistance of the engineering and technician team of the geotechnical laboratory at MARUM, Marc Huhndorf, Joann Schmid, Wolfgang Schunn, and Tim Stanski are also greatly appreciated.

REFERENCES

Abaqus/Explicit User's Manual, Version 6.11 (2011) Dassault Syste`mes Simulia Corporation. Providence, Rhode Island, USA.

Butlanska, J., Arroyo, M. & Gens, A. 2009. Virtual calibration chamber CPT on Ticino sand. Second International Symposium on Cone Penetration Testing, CPT'10, At Humtington Beach, California, USA, Volume: 2.

DIN 18126 (1996) Bestimmung der Dichte nichtbindiger Böden den bei lockerster und dichtester Lagerung. Baugrund, Untersuchung von Bodenproben, vol DIN 18126:1996–11. Deutsches Institut für Normung, Berlin.

Fleischer, M., Kreiter, S., Mörz, T. & Hundorf, M. 2016. A Small Volume Calibration Chamber for Cone Penetration Testing (CPT) on Submarine Soils. Submarine Mass Movements and their Consequences, Advances in Natural and Technological Hazards Research 41.

Hu, Y., & Randolph, M.F. 1998. A practical numerical approach for large deformation problems in soil.. *Int. J. Numer. Anal. Meth. Geomech.,* 22: 327–350.

Huang, A.B. & Hsu, H.H. 2005. Cone penetration tests under simulated field conditions. *Geotechnique,* 55(5): 345–354.

Jamiolkowski, M., Presti, D.C.F. & Manassero, M., 2003. Evaluation of relative density and shear strength of sands from CPT and DMT. Symposium on Soil Behavior and Soft Ground Construction Honoring Charles C. "Chuck" Ladd.

Ladanyi, B. 1972. In Situ determination of undrained stress-strain behavior of sensitive clays with the pressuremeter. *Canadian Geotechnical Journal*, 9:313–319.

Mayne, P.W. & Kulhawy, F.H. 1991. Calibration chamber database and boundary effects correction for CPT data. Proceedings of the First International Symposium on Calibration Chamber Testing/ISOCCTl, Potsdam, New York.

Parkin, A.K. & Lunne, T. 1982. Boundary effects in the laboratory calibration of a cone penetrometer for sand. Proceeding of 2nd European symposium of penetration testing, Amsterdam, the Netherlands, 761–768.

Salgado, R. & Jamiolkowski, M. 2001. Calibration chamber size effects on penetration resistance in sand. *Journal of Geotechnical and Geoenvironmental Engineering*, 878–888.

Schnaid, F. & Houlsby, G.T. 1991. An assessment of chamber size effects in the calibration of in situ tests in sand. *Geotechnique,* 41(3): 437–445.

Susila, E. & Hryciw, R.D. 2003. Large displacement FEM modelling of the cone penetration test (CPT) in normally consolidated sand. *Int. J. Numer. Anal. Meth. Geomech.,* 27: 585–602.

Tolooiyan, A. & Gavin, K. 2011. Modelling the cone penetration test in sand using cavity expansion and arbitrary Lagrangian Eulerian finite element methods. *Computers and Geotechnics*, 38: 482–490.

Wichtmann, T. 2005. Explicit accumulation model for non-cohesive soils under cyclic loading, Inst. für Grundbau und Bodenmechanik Bochum University, Germany.

Taylor & Francis
Taylor & Francis Group
http://taylorandfrancis.com

Cone Penetration Testing 2018 – Hicks, Pisanò & Peuchen (Eds)
© 2018 Delft University of Technology, The Netherlands, ISBN 978-1-138-58449-5

Transition- and thin layer corrections for CPT based liquefaction analysis

J. de Greef & H.J. Lengkeek
Witteveen+Bos, Deventer, The Netherlands

ABSTRACT: Liquefaction potential of the subsoil is often assessed by performing an automated CPT based liquefaction triggering procedure. Due to a bias in the measured cone penetration resistance erroneous prediction of the liquefaction potential can be expected at the transition of soft, non-liquefiable and stiffer, liquefiable layers. This too is the case for relatively thin liquefiable layers interbedded in soft soil layers. A simple procedure is proposed that provides a solution to both issues in an automated liquefaction potential screening.

1 INTRODUCTION

1.1 *Problem description*

Liquefaction potential of the subsoil is often assessed by performing an automated CPT based liquefaction triggering procedure. These triggering procedures are established rather well for sand-like and clay-like materials. On the interface of the two however, there exists a discreet boundary (Robertson, 2009). Close to this boundary the soil can be interpreted in two ways: either the soil is not liquefiable at all (clay with a relatively high cone tip resistance), or the liquefaction potential is very large (fine sands with a relatively low cone tip resistance). As such the triggering assessment may give an erroneous prediction of the liquefaction potential and consequential expected settlements or lateral displacements. This is the case at interbedded sandy soil layers and in the proximity of layer transitions.

Youd et al. (2001) recommend an often referred to lower bound relationship, which can be used to account for the effect of thin interbedded sandy soil layers that are affected by surrounding soft soil layers. This procedure does however require human interference upon application.

Erroneous prediction of the actual relative densities close to the proximity of layer transitions can be addressed by performing two steps. First identifying these transition zones, e.g. by establishing a criterium of the rate of change of the soil behavior type with depth. Second is then deleting them from the analysis results. This could in practice also lead to deleting soil layers with a low relative density that happen to be located close to a transition.

1.2 *Scope*

Boulanger et al. (2016) note that there exists a potential bias from the thin layer effects and corrections are not uniformly applied or relied upon. Ideally bias should be removed from the analysis in a repeatable procedure. The scope of this paper is doing exactly that by relying closely on the original recommended relationship by Youd et al. (2001). It is stressed that further laboratory testing schemes are required to increase the understanding of the physical aspects of the problem.

The formulation of the thin layer correction by Youd et al. (2001) is given by Equation 1.

$$K_H = 1 + 0.25\left(\frac{1}{17}\left(\frac{H}{d_c}\right) - 1.77\right)^2 \tag{1}$$

Herein:

K_H is the correction factor applied to the cone resistance of an entire sandy soil layer that is embedded in two soft soil layers
H is the thickness of this sand layer
D_c is the diameter of the cone from which the cone resistance is measured

Equation 1 can be applied to an ideal situation of an interbedded sand layer. As the thickness of H decreases to 0 m, the factor K_H in the limit approaches a maximum value of 1.78. The maximum interbedded layer thickness for which a correction is still applied is approximately equal to 30 times the cone diameter d_c. Formally, the boundary condition for using Equation 1 is $H/d_c \leq 17 \cdot 1.77 \approx 30$.

2 PROPOSED PROCEDURE

2.1 *Formulation*

In reality the expected influence of the soft soil layer on the cone resistance will be largest at the boundaries of the soft soil layer, and smallest in the center of the interbedded layer. From this perspective the following formulation is proposed:

$$K_z = 1 + 0.25\left(\frac{1}{17}\left(\frac{2z}{d_c}\right) - 1.77\right)^2 \tag{2}$$

Herein:

K_z is the correction factor applied to the cone resistance of each CPT measurement interval,
z is the shortest distance to a boundary between the considered sand layer and a soft soil layer.

Using this formulation, independent of the total thickness of the interbedded layer H, there will always be a correction near the transition of soft and sandy soils. As z approaches 0 in this case, the correction at the intersection is exactly the maximum value of K_H of 1.78. In the middle of an interbedded layer (z = 0.5H) the correction factor is equal to the correction factor that follows from the original formulation by Youd et al. (2001) in Equation 1. The boundary condition for implementing Equation 2 is $z/d_c \leq 17/2 \cdot 1.77 \approx 15$.

2.2 *Theoretical example*

Suppose that there exists a soil profile with a depth of 2 meters in which there are two soil layers: a soft soil layer represented by a cone resistance of 1 MPa and an interbedded sand layer represented by a cone resistance of 3 MPa. By assuming a fictive cone tip diameter of 33.2 mm the correction factor K_H reduces exactly to 1.0 at an interbedded layer thickness of 1.00 m. The difference between

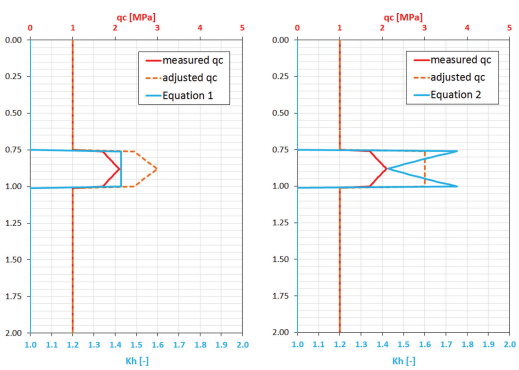

Figure 1. Thin layer correction according to Equation 1 and Equation 2 for an interbedded layer thickness of 0.25 m.

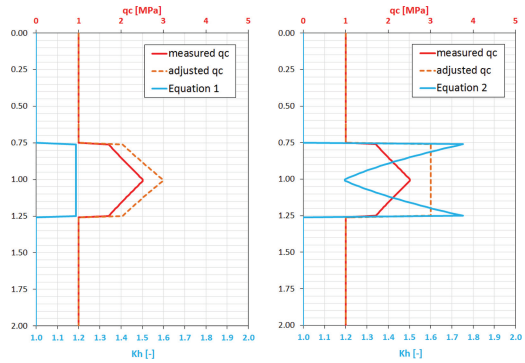

Figure 2. Thin layer correction according to Equation 1 and Equation 2 for an interbedded layer thickness of 0.50 m.

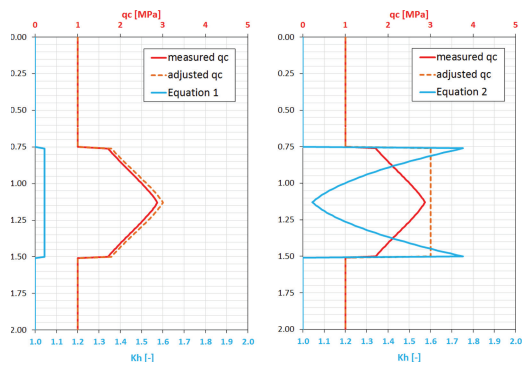

Figure 3. Thin layer correction according to Equation 1 and Equation 2 for an interbedded layer thickness of 0.75 m.

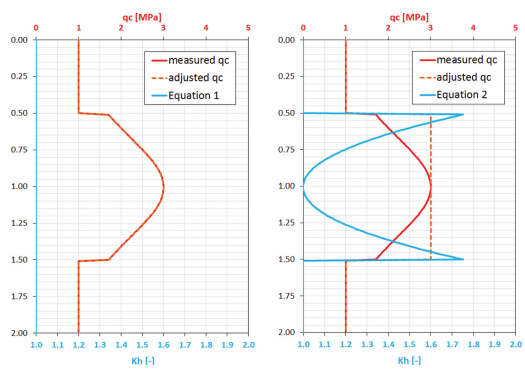

Figure 4. Thin layer correction according to Equation 1 and Equation 2 for an interbedded layer thickness of 1.00 m.

Equations 1 and 2 is shown in Figures 1 to 4 for interbedded layer thicknesses of respectively 0.25, 0.50, 0.75 and 1.00 m.

2.3 *Relative layer thicknesses*

Using the proposed formulation from Equation 2, there still are some issues that need to be addressed:

- In the ideal situation a perfectly clean sand layer is interbedded in perfectly clean clay layers. In reality a boundary should be defined to determine whether a soil is 'clay-like' or 'sand-like'.
- It is assumed that the correction at the boundary of a sandy soil layer is independent of the thickness of the clay layer. Intuitively this assumption is incorrect as a clay lamination with a thickness of 2 cm is expected to have a smaller influence than a clay layer with a thickness of 2 m.

As a boundary between clay-like and sand-like behavior the soil behavior type index I_c by Robertson (2009) can be adopted. As a first guess a value of 2.6 will depict the boundary between liquefiable and non-liquefiable soils and thus the soil types, but it is recommended that locally an I_c plot will be compared with a borehole description to establish whether this value is indeed appropriate. Note that the sleeve friction f_s is inherently averaged over the length of the sleeve. As a consequence there are in practice limitations to correctly identifying layers with a thickness less than the sleeve length.

To implement the thickness of the surrounding soft soil layers in the approach, the formulation from Equation 2 is extended further:

$$K_{z_e} = 1 + 0.25\left(\frac{1}{17}\left(\frac{2z_e}{d_c}\right) - 1.77\right)^2 \tag{3}$$

Herein z_e represents the effective distance to a layer boundary. If the thickness of a soft soil layer Δ is large compared to the distance of an interbedded layer, z_e should approach z. If the thickness of a soft soil layer is small compared to the distance from that layer, z_e should approach infinity (although the limit $z_e/d_c \leq 15$ still applies). Given these boundary conditions Equation 4 is proposed wherein a and b are fitting parameters that can be chosen on a basis of expert judgment (see Figure 5) or can be verified based on back-calculation of case history data.

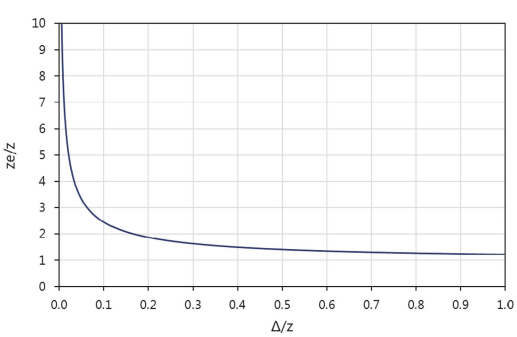

Figure 5. Implication of Equation 4 using a = b = 0.5.

$$Z_e = z\left(1 + a\frac{2}{\Delta}\right)^b \tag{4}$$

2.4 *Implementation in spreadsheet*

In this paragraph the implementation of Equation 2 into an Excel spreadsheet environment is presented.

Table 1 shows the different column descriptions after which Equation 5.C to 5.H give the formulae that can be implemented in a spreadsheet. These should be entered in Row #1 and can then be dragged down to Row #1000, assuming a total of 1000 CPT data entries starting at Row #1. It is noted that the reference level in Column A should contain values that are decreasing with increasing depth.

Note that for the implementation of Equation 3 a similar set of equations can be used. If the bottom of the clay layer is known, all thicknesses are available. By comparing the distance z to a clay layer with a certain thickness Δ, Equation 4 can be applied. By doing so at the top and bottom of a sand layer, Equation 5.H can be applied to determine K_{Ze}.

Table 1. Implementation of Equation 2 to Excel.

Column	Description	Equation
A	reference level	–
B	id soil type	–
C	top of sand layer	5.C
D	top of clay layer	5.D
E	bottom of sand layer	5.E
F	H/z from top of layer	5.F
G	H/z from bottom of layer	5.G
H	correction factor K_Z	5.H

= IF(B1 = "sand";IFERROR(LOOKUP(2;1/($B$1:B1 = "clay");$A$1:A1);MAX($A$1:$A$1000)+5);0) (5.C)
= IF(B1 = "clay";IFERROR(LOOKUP(2;1/($B$1:B1 = "sand");$A$1:A1);MAX($A$1:$A$1000));0) (5.D)
= IFERROR(INDEX(D1:$D$1000;MATCH(TRUE;INDEX (D1:$D$1000<>0;);0));MIN($A$1:$A$1000)-5) (5.E)
= IF(B1 = "sand";(C1-A1)/d_cone;0) (5.F)
= IF(B1 = "sand";(A1-E1)/d_cone;0) (5.G)
= IF(B1 = "clay";1;1+0.25*(MIN(2*F1;2*G1;1.77*17)/17–1.77)^2) (5.H)

3 METHOD APPLICATION

3.1 *Application to CPT*

In this chapter the proposed automated procedure will be evaluated. This is done by comparing for multiple CPTs the lateral displacement indices as reported by Boulanger et al. (2016). Herein it is reported that by simply applying a liquefaction triggering analysis the LDI index indicates that significant liquefaction effects are expected to occur along part of the Çark canal in the 1999 Kocaeli earthquake (M_w = 7.5 and PGA 0.4 g). In reality these effects were not observed and therefore the conclusion is drawn that using default analysis parameters in this case results in a conservative estimation of the liquefaction potential. An attempt is made to identify the factors that lead to the erroneous prediction. These factors are thin—and transitional layer corrections, site-specific fines calibration and site-specific soil behavior index calibration.

Equation 2 is applied to the same case study to verify the outcome with the results from the paper. For this purpose the CPT-based triggering procedure by Boulanger & Idriss (2014) is used. The LDI is calculated by depth-integration of the γ_{max} values from Yoshimine et al. (2006) using the limit value γ_{min} as suggested by Idriss & Boulanger (2008).

The calculated LDI values for the different CPTs are presented in Table 2. The intermediate analysis results in terms of a depth profile are presented in Figure 6 and Figure 7 for CPT-1–23.

The range of outcomes from the default analysis closely resembles the range noted by Boulanger et al. (2016) of 56–123 cm. The reported median values are 76 cm, 53 cm and 36 cm for respectively the default approach, after thin—and transitional layer corrections, and after adding a site-specific fines calibration using C_{FC} = 0.27. Although these values are slightly lower than the median values from Table 2 of 86 cm, 62 cm and 46 cm, the percentual decrease for each step is very similar.

At CPT-1–21 and CPT-1–24 the phreatic levels were not reported. For both locations it was assumed that the phreatic level was at 3 meters below surface level, which closely resembles the average of the other three CPTs. Particularly at CPT-1–21 this assumption has a great influence on the outcome.

Table 2. LDI values [cm] for the different CPTs.

	Default	+ Eq. 2	+ C_{FC}	+ $PoE_{50\%}$
CPT-1–21*	111.5	83.7	47.4	43.0
CPT-1–22	57.0	47.5	33.0	31.8
CPT-1–23	73.7	55.2	39.7	38.5
CPT-1–24*	85.9	62.4	45.7	44.0
CPT-1–25	97.3	66.0	51.4	47.5

* The phreatic level at these locations was not available.

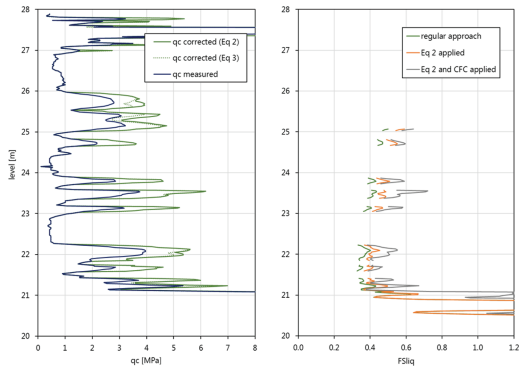

Figure 6. Cone tip corrections and calculated liquefaction safety factors at CPT-1–23.

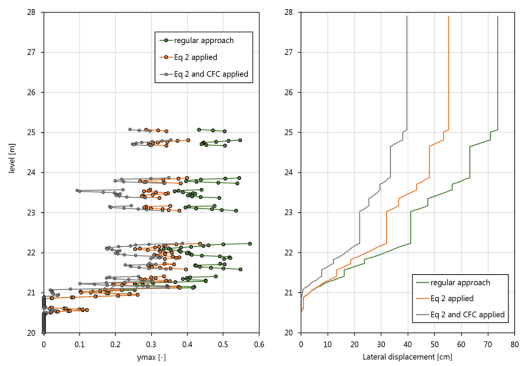

Figure 7. Maximum shear strain at each 2 cm interval and culumative lateral displacement at CPT-1–23.

By default the liquefaction triggering analysis is performed at an exceedance probability of 16%. When looking at expected values in the case of field observations an exceedance probability of 50% seems more appropriate. Given the low values of FS_{liq} for the potentially liquefiable layers as presented in Figure 6, the influence on the analysis outcome is marginal. For lower magnitude earthquakes where values of FS_{liq} are close to F_{α} the exceedance probability may have a significant influence on the calculated lateral displacement indices.

3.2 *Application to laboratory test results*

In 2015 multiple laboratory test were performed by Deltares to examine the effect of thin layers and layer transitions on the measured cone tip resistances. The details of these tests are documented in the master thesis by Van Der Linden (2016).

The results of the tests 5-TEST1 and 6-TEST1 are presented below respectively in Figure 8 and Figure 9. The tests consisted of driving a cone with a tip diameter d_c of 25.2 mm through clean sand with a relative density of 55% and multiple thin clay layers with varying thicknesses.

In test 5-TEST1 the thickness of the clay layers and the distance between the clay layers was 80 mm, in test 6-TEST1 the thickness of clay layers and the distance between the clay layers was 20 mm. No overburden pressure was applied, so the tests were performed at relatively low effective stress levels.

In Figure 8 and Figure 9 the automated cone tip corrections from Equation 2 and Equation 3 are presented. Herein also the cone tip resistances are presented that can be estimated by applying the relation from Baldi et al. (1982), given the relative density of the sand and the vertical effective stress level.

Due to the low (effective) stress level, commonly applied CPT correlations for estimating the saturated unit weight and soil behavior types are not accurate. For application of the thin layer correction therefore the a-priori known clay layer boundaries are used.

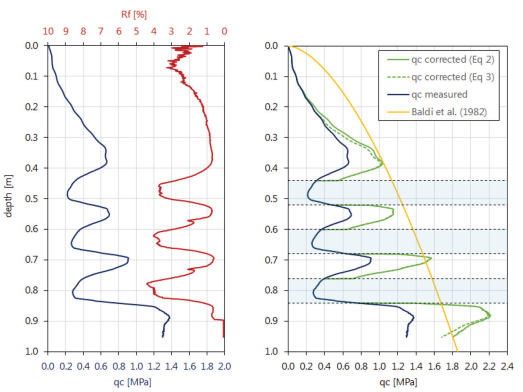

Figure 8. Results for test 5-TEST1.

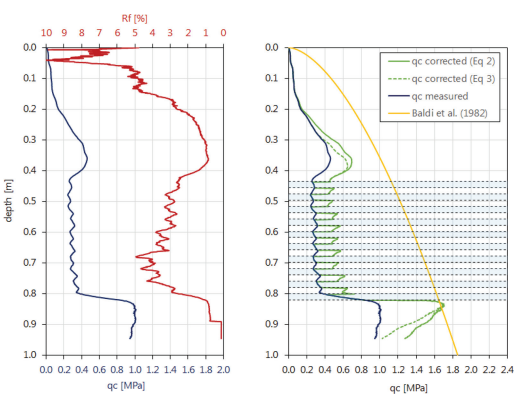

Figure 9. Results for test 6-TEST1.

4 CONCLUSIONS AND RECOMMENDATIONS

- A repeatable transition—and thin layer correction procedure is proposed which is in line with the recommended relation by Youd et al. (2001).
- The proposed procedure gives very similar results to transition—and thin layer corrections as reported by Boulanger et al. (2016).
- Accounting for thickness of clay layers using a formulation like Equation 3 seems logical, but for now lacks substantiation. The correction will be less, whereas the LDI from the case study should even be lower.
- From lab tests a clear asymmetry between the decrease in cone resistance at the top and the bottom of the sandy soil layer can be observed. The proposed procedure does not account for this.
- For 5-TEST1 the proposed correction seems to be appropriate, although other correlations for estimating the relative density may provide less convincing results given the low effective stress level and varying stress exponents in other correlations.
- In laminated soils with layer thicknesses of about d_c and less, it is very difficult to distinguish between the layers in-situ. Moreover, if the distinction can be made the maximum applicable correction factor of 1.78 seems inappropriate. For these soils it is recommended to perform (large size) cyclic tests to assess the liquefaction potential.
- At known case history sites where transitional—and thin layer effects play a significant role it is recommended to evaluate the proposed method in combination with liquefaction severity indices other than the LDI too, such as the LSN or the recently developed LPI_{ISH} by Maurer et al. (2015).

ACKNOWLEDGEMENTS

The authors are very grateful to Piet Meijers from Deltares for providing us with the measurement data that helped substantiating our proposed method.

REFERENCES

Boulanger, R.W., Idriss. I.M. 2014. CPT and SPT Based Liquefaction Triggering Procedures, Report

No. UCD/CGM-14/01. *University of California, Davis, California, USA.*

Boulanger, R.W., Moug, D.M., Munter, S.K., Price, A.B., DeJong, J.T. 2016. Evaluating Liquefaction and Lateral Spreading in Interbedded Sand, Silt and Clay Deposits using the Cone Penetrometer. *Australian Geomechanics* 51(4): 109–128.

Baldi, G., Bellotti, R., Ghionna, V., Jamiolkowski, M., Pasqualini, E. 1982. Design parameters for sands from CPT. *Proceedings of the Second European Symposium on Penetration Testing, Amsterdam, 24–27 May 1982.*

Idriss, I.M., Boulanger, R.W. 2008. Soil Liquefaction During Earthquakes. *Earthquake Engineering Research Institute (EERI), Oakland, California, USA.*

Maurer, B.W., Green, R.A., Taylor, O.S. 2015. Moving towards an improved index for assessing liquefaction hazard: Lessons from historical data. *Soils and Foundations* 55(4): 778–787.

Pacific Earthquake Engineering Research Center. 2017. *Geotechnical Site Investigation at Lateral Spread Sites*. http://peer.berkeley.edu/publications/turkey/adapazari/phase4/cark/index.html, accessed November 2017.

Robertson, P.K. 2009. Discussion of "Evaluation of Cyclic Softening in Silts and Clays" by Ross W. Boulanger and I.M. Idriss. *Journal of Geotechnical and Geoenvironmental Engineering* 135(2): 306–307.

Van Der Linden, T.I. 2016. Influence of Multiple Thin Soft Layers on The Cone Resistance in Intermediate Soils. *M.Sc. Thesis at Delft University of Technology.*

Youd, T.L., Idriss, I.M., Andrus, R.D., Arango, I., Castro, G., Christian, J.T., Dobry, R., Finn, W.D.L., Harder, L.F., Hynes, M.E., Ishihara, K., Koester, J.P., Liao, S.S.C., Marcusson, W.F., Martin, G.F., Mitchell, J.K., Moriwaki, Y., Power, M.S., Robertson, P.K., Seed, R.B., Stokoe, K.H. 2001. Liquefaction Resistance of Soils: Summary Report from the 1996 NCEER and 1998 NCEER/NSF Workshops on Evaluation of Liquefaction Resistance of Soils. *Journal of Geotechnical and Geoenvironmental Engineering* 127(10): 817–833.

Yoshimine, M., Nishizaki, H., Amano, K., Hosono, Y. 2006. Flow deformation of liquefied sand under constant shear load and its application to analysis of flow side of infinite slope. *Soil Dynamics and Earthquake Engineering* 26: 253–264.

Cone Penetration Testing 2018 – Hicks, Pisanò & Peuchen (Eds)
© 2018 Delft University of Technology, The Netherlands, ISBN 978-1-138-58449-5

Soil classification of NGTS sand site (Øysand, Norway) based on CPTU, DMT and laboratory results

A.S. Gundersen, S. Quinteros, J.S. L'Heureux & T. Lunne
Norwegian Geotechnical Institute (NGI), Oslo, Norway

ABSTRACT: The Norwegian GeoTest Site project (NGTS) established five research sites in Norway in 2016. The sites are referred to as sand, soft clay, quick clay, silt and permafrost. The project is funded by the Research Council of Norway and the aim of the project is to establish, characterize, share digital data and manage the use of the test sites in the coming 20 years. The sites are open to other researches for developing and calibrating new tools and techniques. The focus of this paper is the soil classification of the NGTS sand site at Øysand based on Cone Penetration Tests (CPTUs) and Dilatometer Tests (DMT). The fluvial and deltaic deposit at Øysand consists of a 20–25 m fine silty sand with occasionally high content of gravel. The deposit is generally normally consolidated in loose to medium dense states. The *in situ* test data is further supported by laboratory test results from a 20 m long and continuous borehole. This paper presents the results of two CPTUs and one DMT in addition to laboratory test results, all from the same location at the research site. The prediction of *soil behavior type* and unit weights from CPTU and DMT tests, based on existing correlations, are compared qualitatively to the soil classification from grain size distribution and unit weights from laboratory measurements.

1 INTRODUCTION

1.1 *Background*

Loose sandy soils are challenging materials in geotechnical engineering with many difficulties associated with sampling undisturbed material and interpretation of *in situ* and laboratory test data. To this aim, the Norwegian Geotechnical Institute (NGI) and its partners, the Norwegian University of Science and Technology (NTNU), SINTEF Building and Infrastructure, the University Centre in Svalbard (UNIS), and the Norwegian Public Roads Administration (NPRA) recently established a research site on a natural sand deposit at Øysand, Norway. This site is part of a larger research project called the Norwegian GeoTest Site (NGTS), funded by The Research Council of Norway (L'Heureux et al. 2016, 2017).

1.2 *Site location*

The Øysand research site is located in central Norway, approximately 15 km south of Trondheim (Figure 1). The area available for geotechnical investigations at Øysand is about 35,000 m^2 and is used only for agricultural purposes. The deposit at the site consists of fluvial material, underlain by deltaic material deposited at the mouth of the Gaula River. Today the Gaula River borders the site to the east.

1.3 *Aim of the study*

The purpose of this study is to present preliminary results summarizing the geotechnical properties of the Øysand research site. Focus is given to the interpretation of soil type and unit weight based on piezocone (CPTU) and dilatometer (DMT) tests. The results are compared qualitatively to the grain size distributions (GSD) and unit weights measured in the laboratory. The results will form a useful reference to engineers working on similar intermediate soils worldwide and will be used as reference for further research planned at this site.

2 DATA AND METHODS

2.1 *Field data and methods*

Field tests including state of the art techniques for field characterization e.g. seismic CPT and DMT, multichannel analysis of surface waves, MASW, symmetrical resistivity profiling, SRP, Multi-sensor core logging, MSCL, electrical resistivity tomography, ERT, ground penetrating radar, GPR, etc. were carried out in 2016 and 2017. However, this paper only presents the CPTU and DMT results from locations nearby borehole OYSB09, as illustrated in Figure 1.

NGI retrieved disturbed samples at borehole OYSB09 using a 54 mm GEONOR piston sampler. Continuous sampling was carried out to

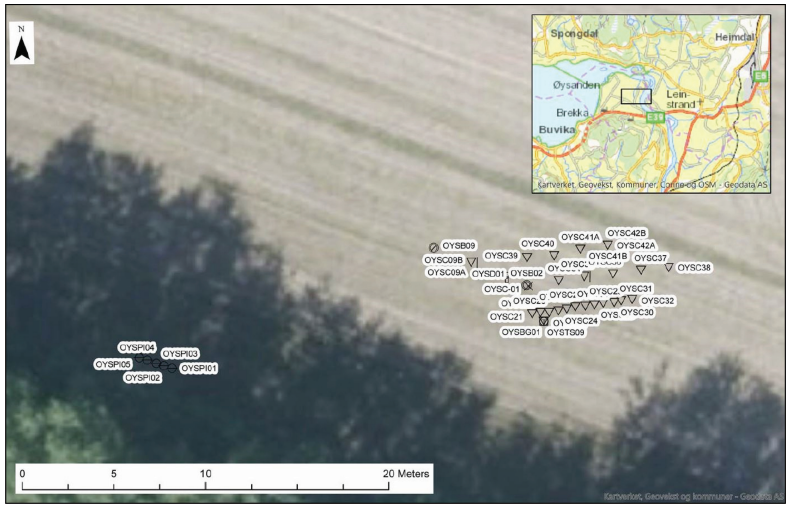

Figure 1. Location of soil investigations.

20 m below ground level except in the depth range between 4 to 5 m, where a hard layer of gravelly material was drilled through.

CPTU tests were performed to 20 m depth using standard 10 cm^2 Geotech cones at the locations identified as OYSC02 and OYSC09. The CPTUs had area ratios of 0.857 and 0.844 respectively. CPTUs where performed following ISO 22476-1:2012. The tests included predrilling to a depth of 1 m and 2 m respectively to avoid damaging the cone while penetrating trough the top gravelly layer. Moreover, predrilling was also needed during the CPTU test at OYSC09 between ca. 4 m and 6 m depth because of a gravelly layer, which could have damaged the cone. The total depth of the CPTU tests was 20 m.

The same DMT test setup as described by TC16 (2001) and Marchetti (1980) was used at Øysand, while ASTM D6635–01 (2007) testing procedures were followed. Two days of testing were required (Oct. 27th and Nov. 2nd, 2016) for the DMTs, because of the need to predrill through the gravel layer between 3.5 m and 6.0 m depth. The total achieved depth of the DMT test was 18 m.

2.2 *Laboratory data and methods*

NGI's main laboratory in Oslo, Norway, carried out index testing to establish the water content, W, unit weight, UW, and grain size distributions, GSD, of the 54 mm diameter samples from borehole OYSB09. This borehole was located at about 5 m from the CPTs and DMT locations. Table 1 provides an overview of the number of tests carried out and testing procedures followed. As seen in this table, a representative amount of tests has been performed.

Table 1. Summary of relevant laboratory tests.

Type of test	No. of tests	Reference
W	19	NS 8013
UW	36	NS 8011
GSD	20	NS 8005

Samples that contained mainly sand and gravel were subjected to dry sieve analysis, while materials containing more than 5% silt and clay particles were wet sieved on a 75 mm sieve before dry sieving as per the standard mentioned in Table 1. The falling drop method described in Moum (1965) was used for samples containing mainly silt or clay.

3 GENERAL STRATIGRAPHY AND IN-SITU CONDITIONS

3.1 *Stratigraphy*

The overall stratigraphy at the site represents a general coarsening upward sequence as typically observed in deltaic sequences. A snap of the site stratigraphy, using field and lab data is shown in Figure 2. Two main soil units are identified down to 20 m below the ground surface. Unit 1 at the top is up to ca. 10 m thick and consists of a fine to coarse sand with presence of gravel. Unit 2 consists of finer material comprising medium silty sand and sandy silt with traces of organic material.

3.2 *Groundwater level and pore pressures*

Piezometers were installed at several depths intervals down to 20 m below the surface near borehole

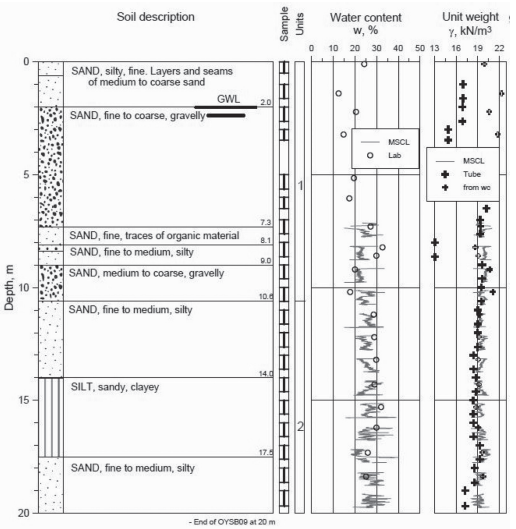

Figure 2. Borehole log OYSB09.

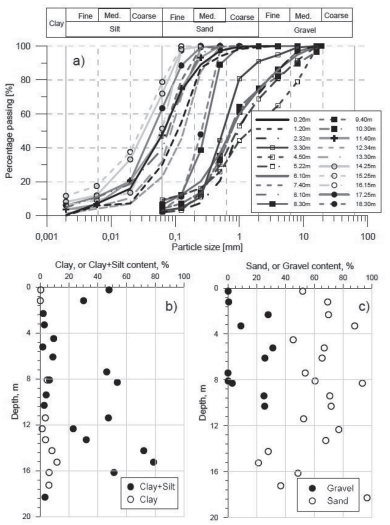

Figure 3. Grain size distribution from borehole OYSB09.

OYSB09 in 2017. The results show mostly constant values in time with hydrostatic pore pressure from 2 m below ground level where the groundwater level is found.

4 LABORATORY TEST RESULTS

GSD curves of samples from borehole OYSB09 are shown in Figure 3a. Figures 3b and 3c show the fines and coarse contents per depth respectively. The GSDs results form the basis of the soil description in the borehole log presented in Figure 2. From this figure, it can be inferred that gravel to silt can be found at Øysand. The predominant soil being silty sand.

Figure 2 shows also values of UW calculated based on W, derived from Magnetic Susceptibility Core Logging (MSCL) readings and estimated using the sampled 54 mm piston tubes. Note that the estimated UW from piston samples is expected to be less reliable in the gravel soil, because during the sampling process dense soil may be loosened and heavily disturbed. Good agreement between all measurements of UW by the three presented methods is found below 5 m depth, where the representative value is 19 kN/m^3. Above 5 m depth, UW from WC is consistently higher than the obtained from the piston samples. However, the representative value of UW was used when interpreting DMT and CPTU readings.

5 IN SITU TEST RESULTS

CPTs have been available to geotechnical engineers since the 1930s as a mechanical test. The incorporation of electric strain-gauged load cells was introduced in the 1960s. A recent ISO standard (ISO 22476-1:2012) covers equipment, procedures and reporting which has been applied for soil investigations at Øysand. Lunne et al. (1997) presented methods for interpretation, which are used herein.

Figure 4 shows the CPTU results including cone resistance, q_c, unit sleeve friction resistance, f_s, and the pore pressure measured behind the cone, u_2. Figure 5 illustrates the DMT results from sounding OYSD01 close to borehole OYSB09 where I_D is the material index, K_D is the horizontal stress index and E_D is the dilatometer modulus as defined in TC 16 (2001). These parameters can be regarded as intermediate parameters calculated from the corrected first and second DMT readings, p_0 and p_1, as follows:

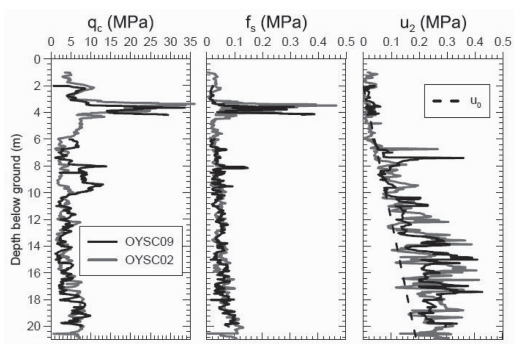

Figure 4. CPTU results OYSC02 and OYSC09.

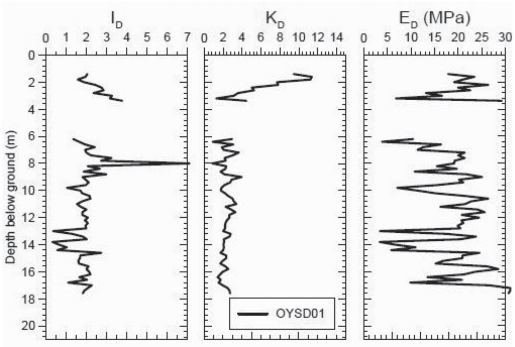

Figure 5. DMT results OYSD01.

$$I_D = (p_1 - p_0)/(p_0 - u_0) \quad (1)$$

$$K_D = (p_0 - u_0)/\sigma'_{v0} \quad (2)$$

$$E_D = 34.7(p_1 - p_0) \quad (3)$$

Here u_0 is the pre-insertion pore pressure and σ'_{v0} is the pre-insertion effective overburden stress calculated assuming a total unit weight of 19 kN/m^3.

It is worth mentioning that three independent measurements (q_c, f_s, u_2) are obtained from a CPTU test, while only two (A and B reading) are obtained from a DMT test (excluding penetration resistance record and C-readings). In addition, the CPT provides close to continuous data while the DMT provides data every 20 cm.

6 SOIL CLASSIFICATION & UNIT WEIGHT

6.1 *Soil classification and unit weight from CPT and DMT results*

Based on the work of Wroth (1984), Robertson (1990) suggested the following normalized CPTU parameters to identify soil behavior types:

$$Q_{tn} = (q_t - \sigma_{v0})/\sigma'_{v0} \quad (4)$$

$$F_r = f_s/(q_t - \sigma_{v0}) \quad (5)$$

$$B_q = (u_2 - u_0)/(q_t - \sigma_{v0}) \quad (6)$$

where: q_t is the corrected cone resistance and σ_{v0} and σ'_{v0} are the pre-insertion *in situ* total and effective vertical stress respectively.

Robertson (1990) suggested two charts based on the combination of either Q_{tn} & F_r or Q_{tn} & B_q, but recommended that the $Q_{tn} - F_r$ chart was generally more reliable.

Jefferies & Davies (1993) identified that a soil behavior type index, I_c, could approximate the material boundaries in the $Q_{tn} - F_r$ chart where I_c is simply the radius of concentric circles. According to Robertson & Wride (1998), the circles can be described using the following equation:

$$I_c = [(\log F_r + 1.22)^2 + (\log Q_{tn} - 3.47)^2]^{0.5} \quad (7)$$

CPTU and DMT tests are mechanical in nature and both Robertson (1990) and Marchetti (1980) suggested the soil classification based on these tests indicates the *soil behavior type (SBT),* and not a strict soil classification like that obtained from GSD. Comparison should therefore be qualitative, rather than quantitative. Moreover, the classification from CPTU and DMT are generally empirical and care should be exercised when a dataset is outside the domain of the data from which the empirical method was developed, like for the gravelly sand layers at Øysand.

Robertson (1990) observed that most uncemented, normally consolidated, young soils tend to follow an approximately diagonal line between the upper left corner and the lower right corner in the Q_{tn}-F_r chart. Figure 6 shows how the results from Øysand display the same property except for the more overconsolidated sand towards the top of the stratigraphy.

Similarly, Marchetti (1980) noted that in normally consolidated cohesive soils where the soil has not been influenced by aging, structure or cementation, the value of K_D is approximately 2. As seen in Figure 5, K_D from DMT test at Øysand approaches the value of 2 below 6 m depth, which is consistent with the CPTU results and geological history of the site.

From Figure 6, it is also observed that the deposit falls mainly into zones 4 to 6, hence described as silt mixtures to sands. The estimated UW, normalized by the unit weight of water, γw,

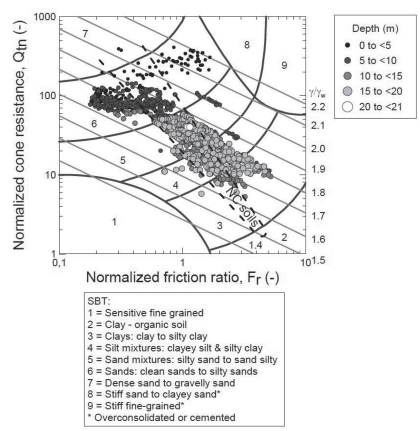

Figure 6. SBT after Robertson (1990) for OYSC02 & OYSC09.

are generally in the range of 1.7–1.9. This is on the low side of the results from laboratory testing shown in Figure 2. The estimation of UW based on CPT, shows significant scatter (see Fig. 6), especially towards the top of the stratigraphy, where no obvious trend seems to exist. The assumption of a single UW is certainly not possible from the CPTU interpretation, and hence in disagreement with the general trend of laboratory and MSCL results (Figure 2).

Marchetti & Crapps (1981) proposed a log-log chart, based on I_D and E_D, for estimating the soil type and UW. E_D distinguishes mud/peat from other soil types and relates to the material unit weight as presented in Figure 7. The material index differentiates between clays, silts and sand soil types. Figure 7 shows the interpreted DMT results from Øysand. As seen in this figure, sandy silt or silty sand, in terms of their behavior, are identified. The occasionally high content of gravel is not indicated. The results propose a material unit weight mainly in the range of 18 to 19 kN/m^3, which is in good agreement with the general trend from laboratory and MSCL.

Table 2 summarizes the boundaries for the SBT indices in the CPTU and DMT frameworks proposed by Robertson (1990) and Marchetti & Crapps (1981). This table gives a better overview of the expected values of both I_C and I_D for identification of the soil behavior type.

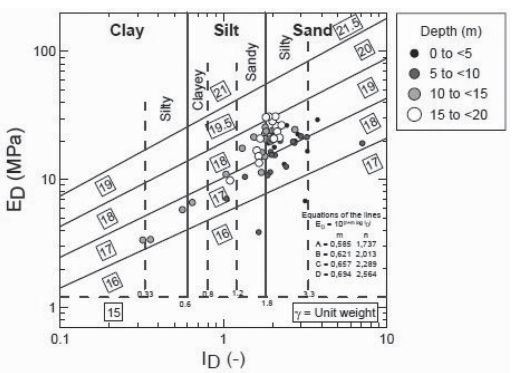

Figure 7. DMT-SBT chart after Marchetti & Crapps (1981) for DMT test OYSD01.

Table 2. Soil behavior type boundaries for I_C (CPT) & I_D (DMT).

Soil behavior type	I_C (CPT)	I_D (DMT)
Clay	Ic > 2.95	$0.1 < I_D < 0.6$
Silt	$2.05 < I_C < 2.95$	$0.6 < I_D < 1.8$
Sand	$I_C < 2.05$	$1.8 < I_D < 10.0$

6.2 *Comparison of soil classification and unit weight from CPT and DMT with laboratory results*

To compare the classification from DMT and CPTU as function of depth, a simple linear transformation of the DMT material index has been made. The equation is given below:

$$I_D^* = 0.75 I_D + 1.6 \quad (8)$$

where: I_D^* has the same soil behavior boundary values between clay and silt and silt and sand as the CPTU material index I_c. The uniqueness of the criteria, proposed by Marchetti (1980), is preserved.

Figure 8 displays the transformed DMT material index from OYSD01 and the CPTU index from OYSC02 and OYSC09 with depth. It can be seen that both the DMT and CPTU predict well the overall SBT at Øysand although the high contents of gravel are not identified. At greater depths both the DMT and CPTU reflects the change in soil behavior from highly drained to more undrained to some degree.

The trend of higher content of silt and clay particles around 14 m depth is also evident from the laboratory tests. It is further noted that the DMT seems to identify the material as generally coarser than the CPTU.

The two CPTUs show consistency in the interpretation of soil behavior type. At 9 meters depth, the two CPTUs show a difference in the SBT which

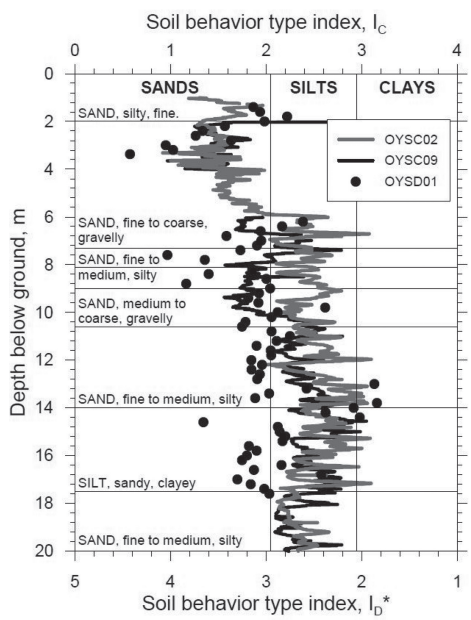

Figure 8. SBT-indices with depth for OYSB09.

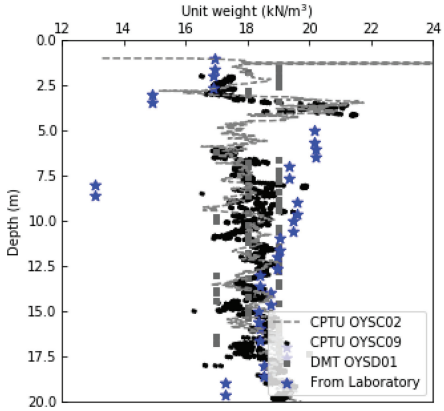

Figure 9. Unit weight from CPT (Robertson, 1990), DMT (Marchetti & Crapps, 1981) and 54 mm tube samples.

is thought to be due to lateral variability in the soil conditions of the site.

It can also be seen that the soil behavior type index, I_C, does not predict as much clay behavior as the Q_{tn}-F_r chart. This is due to the definition of I_C, which is not able to match the soil behavior chart exactly. For Øysand, the CPTU soil behavior index seems to give a more correct picture of the soil conditions than the soil behavior chart.

Figure 9 illustrates the unit weight from in situ tests and laboratory measurements with depth. It can be seen that the values from CPTs are generally lower than the unit weights from laboratory measurements on 54 mm tube samples between 5 and 15 m depth. DMT results show similar tendency between 5 and 15 m depth while it displays higher unit weight at shallow depth compared to the 54 mm tube.

7 CONCLUSION

The Norwegian GeoTest Site project (NGTS) established five research sites in Norway in 2016. These are referred to as sand, soft clay, quick clay, silt and permafrost sites. This paper presents laboratory and *in situ* test results (CPT, DMT and MSCL) for the sand site with focus on soil classification.

Soil classification based on grain size distribution, CPTU (Robertson 1990) and DMT (Marchetti & Crapps 1981) have been presented and compared qualitatively. The CPTU and DMT results support the assumption that the site is a close to normally consolidated loose sand deposit. The interpretation of the in situ results show that the soil behavior type is generally sandy silt or silty sand, which is consistent with the laboratory results. In situ tests failed to identify the occasional high content of gravel, but the correlations are able to reflect the change from highly drained to more undrained material to some degree. This demonstrates how the existing correlations can be used to estimate soil behavior type with confidence for this site.

Existing correlations made it possible to compare the interpreted total unit weights from CPTU and DMT with values measured in the laboratory. The results from the DMT test matched the laboratory test results slightly better than the CPTU. Both DMT and CPTU predictions generally fall on the low side of the measured values from the laboratory. Some further refinement in the correlations may be necessary to better predict the unit weight from CPTU and DMT test results.

REFERENCES

ASTM D6635-01. 2007. Standard Test Method for Performing the Flat Plate Dilatometer. ASTM International, West Conshohocken, PA.

ISO 22476-1:2012. Geotechnical investigation and testing – Field testing – Part 1: Electrical cone and piezocone penetration test.

Jefferies, M.G. & Davies, M.P. 1993. Use of CPTU to estimate equivalent SPT N60. Geotechnical Testing Journal. 16(4). 458–468.

L'Heureux, J.S., Caroll, R., Lacasse, S., Lunne, T., Degago, S., Instanes, A., Nordal, S. & Sinitsyn, A. 2016. The Norwegian Geo-Test Sites (NGTS) project – A preliminary overview. Geo-Vancouver.

L'Heureux, J.S., Lunne, T., Lacasse, S., Caroll, R. Strandvik, S.O., Ozkul, Z., Instanes, A., Sinitsyn, A., Degago, S. & Nordal, S. 2017. Norway's National GeoTest Site Research Infrastructure (NGTS). In Unearth the Future, Connect beyond. Proceedings of the 19th International Conference on Soil Mechanics and Geotechnical Engineering.

Lunne, T., Robertson, P.K. & Powell J.J.M. 1997. Cone Penetration in geotechnical practice. Routledge, New York.

Marchetti, S. 1980. In-situ tests by flat dilatometer. Journal of Geotechnical Engineering. 106(3). 299–321.

Marchetti, S. & Crapps, D.K. 1981. Flat dilatometer manual. GPE incorporated.

Moum, J. 1965. Falling drop used for grain-size analysis of fine-grained materials. Sedimentology, 5(4), 343–347.

Robertson, P.K. 1990. Soil classification using the cone penetration test. Can. Geotech. J. 27(1). 151–158.

Robertson, P.K. 2009. CPT-DMT Correlations. Journal of Geotechnical and Geoenvironmental Engineering. Vol. 135, No. 11, November 1, 2009.

TC16 2001. The Flat Dilatometer Test (DMT) in Soil Investigations. A Report by the ISSMGE Committee TC16. May 2001, 41 pp.

Wroth, C.P. 1984. The interpretation of in-situ soil tests. Rankine Lecture. Geotechnique. 4. 449–489.

Cone Penetration Testing 2018 – Hicks, Pisanò & Peuchen (Eds)
© 2018 Delft University of Technology, The Netherlands, ISBN 978-1-138-58449-5

Numerical study of anisotropic permeability effects on undrained CPTu penetration

L. Hauser & H.F. Schweiger
Institute of Soil Mechanics, Foundation Engineering and Computational Geotechnics, Graz University of Technology, Graz, Austria

L. Monforte & M. Arroyo
Department of Geotechnical Engineering, Universitat Politècnica de Catalunya – BarcelonaTech, Barcelona, Spain

ABSTRACT: The numerical simulation of Cone Penetration Tests (CPT) is a challenging field in geotechnics. Both the underlying physical model and the numerical method need to be capable of taking into account large deformations and displacements within the problem domain. Researchers at the Polytechnic University of Catalonia (UPC) and the International Center for Numerical Methods in Engineering (CIMNE) have developed a Particle Finite Element Method (PFEM) code named G-PFEM which conducts fully coupled analysis of penetration problems in saturated porous media. An updated Lagrangian description is used in order to formulate the governing equations. The PFEM is based on frequent remeshing of critical regions of the problem domain adding additional computational cost to the solving process. Therefore, the use of linear elements in combination with a stabilized mixed formulation of the governing equations helps to reduce the computational effort and at the same time cope with the phenomenon of volumetric locking associated with linear elements. Within the present work, anisotropic permeability is introduced and tested by means of consolidation of an elastic soil layer. Furthermore, recalculations of an available in-situ CPT are performed allowing the examination of the influence of changing boundary conditions, such as anisotropic permeability of the soil or penetration velocity of the cone, on the measured tip resistance, sleeve friction and pore water pressure. It was found that the recalculation with G-PFEM provides comparable results for undrained conditions and anisotropic permeability.

1 INTRODUCTION

The characterization of soils is an integral part of geo-technical engineering. In-situ investigation methods, such as cone penetration testing (CPT), have gained in popularity, especially when dealing with sensitive soils where the specimen is easily disturbed during recovery. In cone penetration testing hydraulic and mechanical soil properties are derived from the measured tip resistance, sleeve friction and pore water pressure, whereby the quality of the empirical correlations plays a decisive role. Experience has shown that CPT provides reasonable results for applications in sand or clay where either drained or undrained behaviour governs the penetration process. However, correlations for partial drainage, as it occurs during penetration in silts, are still an ongoing research topic.

Recent advances in the numerical simulation of large deformation problems based on a Particle Finite Element Method (PFEM, see Oñate et al. 2011) allow to model this kind of penetration problems where a rigid cone penetrates a fully water saturated soil body. Thereby, the focus lies on investigating partial drainage and gaining a more profound understanding of the mechanical behaviour during penetration by numerical means.

This paper aims to give a brief explanation of the model, introduce an anisotropic permeability tensor to the problem and present a first recalculation of in-situ CPTs under undrained conditions with the focus on anisotropic permeability.

2 MODEL

The simulations are carried out using the platform G-PFEM, short for Geotechnical-Particle Finite Element Method (Monforte et al. 2017a, Monforte et al. 2017b), which has been developed within the Kratos framework (Dadvand et al. 2010) at the Polytechnic University of Catalonia (UPC) and the Center for Numerical Methods in Engineering (CIMNE).

2.1 *G-PFEM platform*

In G-PFEM, the quasi-static linear momentum and mass balance equations are formulated for a solid and fluid phase adopting an updated Lagrangian description. The basic idea behind the PFEM is a continuous remeshing of critical regions of the domain, where new nodes can be added and old ones removed, in order to deal with large deformations and avoid excessive mesh distortion. This strategy results in an increased computational cost and therefore low order elements in combination with a mixed, stabilized formulation of the problem are used.

In this way, the computation time is reduced and the issue of locking associated with low order approximation is addressed. Monforte et al. (2017b) implemented and tested different mixed formulations, where an additional degree of freedom—the determinant J of the deformation gradient or the mean pressure p—is introduced on top of the displacement and water pressure fields **u** and p_w, respectively. It was found that the mixed **u**-J-p_w formulation performs well and thus the formulation is adopted within this work. Furthermore, the problem is stabilized using the Polynomial Pressure Projection. The interested reader is referred to Monforte et al. (2017a) and Monforte et al. (2017b) for a more detailed outline of the PFEM.

2.2 *Anisotropic permeability*

In natural soil deposits the water flow is often governed by a highly anisotropic hydraulic permeability. In order to model CPTs in a realistic way the anisotropy is an important aspect to consider. According to Larsson & Larsson (2002) Darcy's law in the spatial configuration is given as:

$$\boldsymbol{v}_d = -\boldsymbol{k}_p(\nabla p_w - \rho_w \boldsymbol{g}) \tag{1}$$

with the relative Darcian velocity of the fluid phase $\mathbf{v}_d$, the spatial permeability tensor $\mathbf{k}_p$, the water pressure p_w, the water density ρ_w and gravity **g**. Furthermore, $\mathbf{k}_p$ can be expressed depending on the initial permeability tensor $\mathbf{K}_{p,0}$:

$$\boldsymbol{k}_p = J^{-1}\boldsymbol{F} \cdot \boldsymbol{K}_{p,0} \cdot \boldsymbol{F}^t \tag{2}$$

where **F** is the deformation gradient and J its determinant. Thus, the principal directions of the tensor—initially defined by a horizontal and vertical permeability—rotate with the deformation of the soil (Larsson & Larsson 2002).

2.3 *Consolidation of an elastic finite soil layer*

The analytical solution for consolidation problems in multi-layered half space with anisotropic permeability by Chen (2004) serves as validation for the anisotropy feature in G-PFEM. Thereby, a homogeneous, fully saturated, elastic soil layer is bedded on a rigid, rough and impervious base and subjected to a circular load (see Figure 1). The radius of the load and the thickness of the soil layer are equal, resulting in a = H. Assuming weightless soil and water, Chen (2004) provides solutions for the dimensionless surface settlement $\mu w(r,z,T)/(qa)$ at the centre point (r = z = 0) depending on the dimensionless time factor $T = k_{p,v}\mu t/a^2$ and for the dimensionless pore water pressure p/q along the normalized centre axis z/H where μ stands for the shear modulus of the soil. The solutions are based on Poisson's ratio of 0.25, the elastic water bulk modulus $K_w = 4.5 \cdot 10^{10}$ Pa and permeability ratios $\gamma^2 = k_h/k_v$ of 0.01, 1, 10 and 100.

Figure 2 shows the development of the normalized surface settlement at the centre point of the domain over time. The numerical results agree very well with the analytical solution, not only in terms of the initial and final settlements but also regarding the consolidation curves for different anisotropy ratios.

Furthermore, the pore pressure profiles over depth at the time instances T equal to 0.001 and 0.01 are displayed in Figure 3 and again good

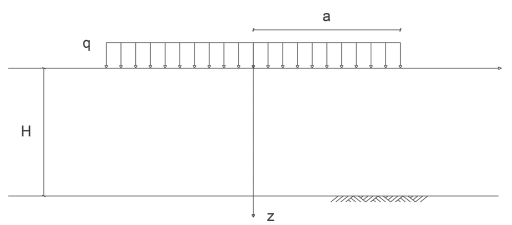

Figure 1. Axisymmetric model for consolidation problem.

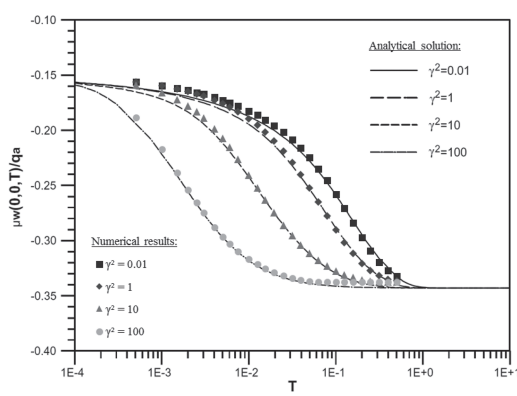

Figure 2. Comparison of normalized displacement over time factor T for different permeability ratios γ^2 (Chen 2004).

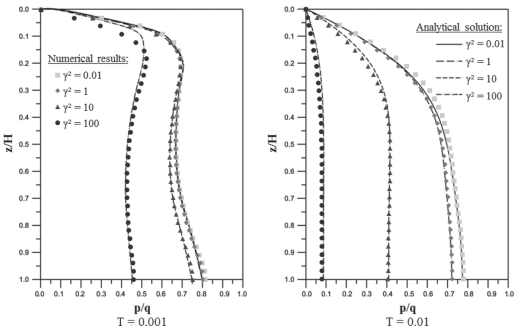

Figure 3. Comparison of normalized pore pressure over dimensionless depth at given T (Chen 2004).

overall agreement between numerical and analytical results is obtained. Free drainage at the top of the layer results in a steep initial pressure gradient which decreases during consolidation. Both the evaluation of the surface settlement and the pore pressure profile show that horizontal water flow is dominant within the system.

3 SIMULATION OF CPT

3.1 *Modelling of CPT*

Modelling a CPT involves an ideally rigid cone that penetrates a deformable two-phase medium at a constant velocity. This leads to an axisymmetric model consisting of a rectangular box with a height of 1.1 m and a width of 0.5 m. The cone radius R measures 1.78 cm with a tip angle of 60° corresponding to the standard geometry (base area of 10 cm^2). The penetration starts from an initial position where the cone is located at a depth of 10 cm. The lateral and lower boundaries are fixed in normal direction while an overburden pressure can be applied at the top of the domain. Moreover, free drainage is allowed at the boundaries except along the symmetry axis. Figure 4 shows the basic model.

From a mathematical point of view, the contact between cone and soil body is described by a set of constraints and a penalty method is considered for the realization. The contact algorithm is explained in detail in Monforte et al. (2017a).

The constitutive behaviour of the soil is described by means of the Modified Cam Clay (MCC) model whereby the elastic regime follows the hyperelastic model by Houlsby.

3.2 *Recalculation of in-situ CPTu*

Based on the available data from Sachsenhofer (2012) a recalculation of a CPTu is performed. Thereby, the in-situ soil parameters (in terms of

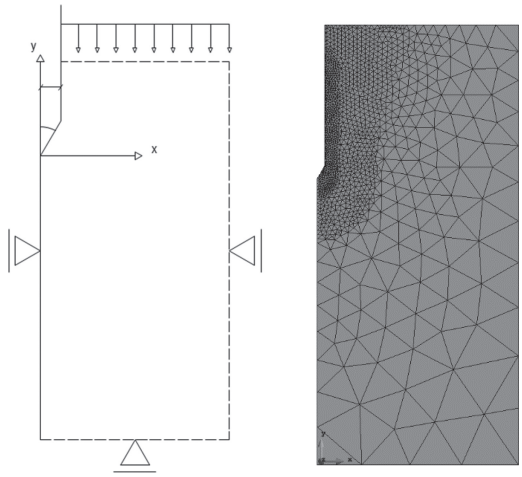

Figure 4. Axisymmetric model (left) and refined mesh during penetration process (right).

Table 1. Input parameters for MCC model.

ρ_s [kg/m^3]	ρ_w [kg/m^3]	λ^* [–]	κ^* [–]	φ' [°]	M [–]	G_0 [kPa]	α [–]
1700	1000	0.015	0.005	22.5	0.88	2900	0
OCR [–]	p_{c0} [kPa]	K_w [kPa]	k_v [m/s]	k_h [m/s]	K_0 [–]	φ_{int} [°]	e_0 [–]
1	100	$1 \cdot 10^8$	$2 \cdot 10^{-8}$	$2 \cdot 10^{-7}$	0.7	7	0.5

the specific weight γ_s, the Oedometric stiffness E_s and the effective friction angle φ') and the CPTu profiles for the tip resistance q_c, the sleeve friction f_s and the pore water pressure u_2 at the shoulder position are given. Additionally, Poisson's ratio of 0.3, a vertical hydraulic permeability k_v of $2 \cdot 10^{-8}$ m/s and a permeability ratio k_h/k_v of 10 are estimated for a clayey silt and the soil parameters are averaged over a 5 m thick layer located at a depth of 13 to 18 m. The derived input parameters for the MCC model are summarized in Table 1. Note that the friction on the interface between cone and soil is taken into account assuming an interface friction angle φ_{int} roughly equal to $\varphi'/3$.

The simulations are carried out for 3 different penetration velocities of 1, 2 (standard velocity) and 3 cm/s. The recorded tip resistance q_c, sleeve friction f_s and the water pressures u_1, u_2 and u_3 are shown in Figure 5 as normalized depth profiles. Generally, all measured quantities tend to reach a stationary level after an initial transient phase. Note that the pore pressure profiles at the shoulder position u_2 show the strongest oscillations which is due to the fact that the measuring point is at a

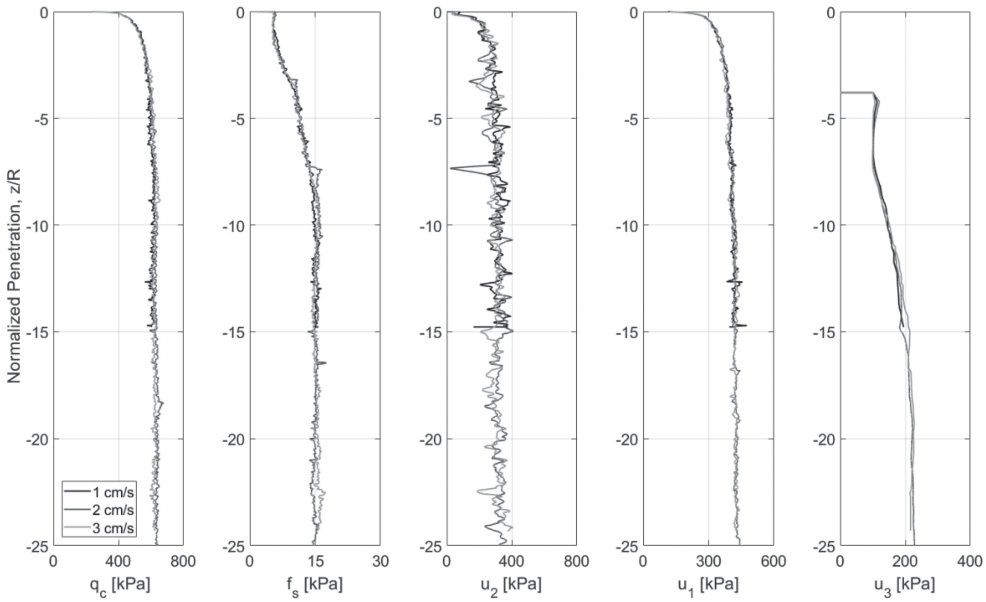

Figure 5. CPT profiles for tip resistance q_c (with the averaged mean value $\overline{q}_c = 635$ kPa) sleeve friction f_s ($\overline{f}_s = 15$ kPa) and pore pressures u_1, u_2 ($\overline{u}_2 = 320$ kPa) and u_3 for varying penetration velocities.

geometric non-linearity where high pressure gradients occur. Apparently, a variation of penetration velocity has no impact on the system behaviour suggesting undrained conditions for all 3 cases. Thus, the resulting pore pressure represents a maximum value reached during undrained loading. At the shoulder position, the stationary average of u_2 (being the total pore water pressure) yields approximately 320 kPa. Burns & Mayne (1998) suggest an analytical way to calculate the undrained excess pore pressure based on cavity-expansion theory and the Modified Cam-Clay model. Equation (3) gives the total pore pressure u_m depending on the initial water pressure u_0, the effective, initial, vertical stress σ'_{v0}, the critical stress ratio M, the over consolidation ratio, the shear modulus G, the undrained shear strength s_u (summarized in the rigidity index $I_r = G/s_u$) and the plastic volumetric stain ratio $\Lambda = 1 - C_s/C_c$. The latter is based on the swelling and compression indices of the soil.

$$u_m = \frac{4}{3}\left[\sigma'_{v0}\frac{M}{2}\left(\frac{OCR}{2}\right)^{\Lambda}\right]\ln I_r + \left[1-\left(\frac{OCR}{2}\right)^{\Lambda}\right] + u_0 \tag{3}$$

Eventually, the calculated u_m yields 350 kPa and shows good agreement with the maximum undrained pore pressure of 320 kPa from the numerical calculations.

Furthermore, Sheng et al. (2014) proposed a critical ratio between the penetration rate v and the (isotropic) soil permeability k suggesting that values of 10^6 or larger lead to undrained behaviour. For the penetration velocities of 1, 2 and 3 cm/s, the ratios v/k_v of $0.5 \cdot 10^6$, $1.0 \cdot 10^6$ and $1.5 \cdot 10^6$ and v/k_h of $0.5 \cdot 10^5$, $1.0 \cdot 10^5$ and $1.5 \cdot 10^5$ are obtained, respectively. Thus, it appears reasonable to assume almost undrained behaviour with the onset of partial drainage due to the increased horizontal permeability.

However, the initial goal was to recalculate an actual in-situ CPTu by numerical means and compare the results for q_c, f_s and u_2. With the in-situ results only being available on a large scale (Sachsenhofer 2012) the comparison is made in terms of averaged values at the depth of 13 to 14 m and summarized in Table 2. Note that the measured and calculated values $\overline{q}_c$ and $\overline{f}_s$ show the same order of magnitude whereas almost one order lies between the calculated and measured $\overline{u}_2$. The numerical simulations reproduced undrained system behaviour which results in increased pore pressure and reduced tip resistance while in-situ for this kind of soil (clayey silt) some partial drainage can be expected. Thus, the numerical approach provides reasonable results for the undrained case and forms the basis for future investigation of partial drainage where the tip resistance is expected to increase as the pore pressure decreases.

Table 2. In-situ and numerical results for $\bar{q}_c$, $\bar{f}_s$ and $\bar{u}_2$.

Averaged values	$\bar{q}_c$ [kPa]	$\bar{f}_s$ [kPa]	$\bar{u}_2$ [kPa]
In-situ	800	20	35
Numerical	635	15	320

3.3 *Anisotropy under undrained conditions*

The recalculation in section 3.2 showed that undrained system behaviour is obtained for different penetration velocities, however the role of anisotropic permeability during undrained penetration is not yet clear. Therefore, two test cases based on the set up from section 3.2 are simulated with standard penetration velocity of 2 cm/s, a smooth interface between cone and soil and inverted anisotropic permeability. Test case (a) considers an increased horizontal permeability with $k_h = 2{\cdot}10^{-7}$ m/s and $k_v = 2{\cdot}10^{-8}$ m/s while case (b) includes the opposite case ($k_h = 2{\cdot}10^{-8}$ m/s and $k_v = 2{\cdot}10^{-7}$ m/s).

The modified anisotropy is crucial for the hydraulic behaviour and prescribes the preferred flow direction which is horizontal for case (a) and vertical for case (b). Now the profiles of q_c and u_2 are compared in Figure 6 and in both cases (a) and (b) the expected undrained behaviour with u_2 of around 320 kPa and q_c of 600 kPa is observed. However, a closer look reveals that test case (a) gives a slightly lower pore pressure (315 kPa and 330 kPa) and a higher tip resistance (610 kPa and 585 kPa) compared to case (b): These observations are consistent with the assumption of a preferred flow direction due to anisotropy. As the cone penetrates the soil radial (or rather horizontal) flow is dominant caused by the geometric boundary conditions of the test.

Thus, for case (a) the preferred flow directions due to anisotropy and problem geometry coincide which leads to increased drainage of the system. For case (b) the opposite occurs and the main flow direction is vertical. Consequently, the overall behaviour is rather undrained with regard to case (a) and u_2 increases while q_c decreases. Of course, on a large scale both cases are still considered to be in the undrained regime.

Furthermore, the effect of anisotropic permeability on the pore pressure field is shown in Figure 7. Thereby, one observes that the order of magnitude of the occurring water pressures is the same, again as expected for undrained conditions, but the distribution differs. Then again, for case (b) the pressure bulb has an increased vertical extension along the preferred drainage direction. Additionally, different effective stress fields are found for test cases (a) and (b) whereas the total stress field remains the same. The latter observation is consistent for undrained behaviour where the soil-water body acts as a one-phase medium.

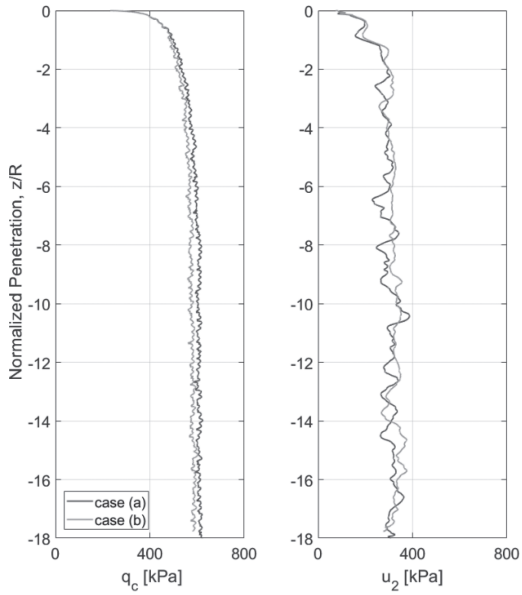

Figure 6. Comparison of q_c and u_2 for inverted anisotropic permeabilities; case (a) with $k_v = 2 \cdot 10^{-8}$ m/s, $k_h = 2 \cdot 10^{-7}$ m/s and case (b) with $k_v = 2 \cdot 10^{-7}$ m/s, $k_h = 2 \cdot 10^{-8}$ m/s.

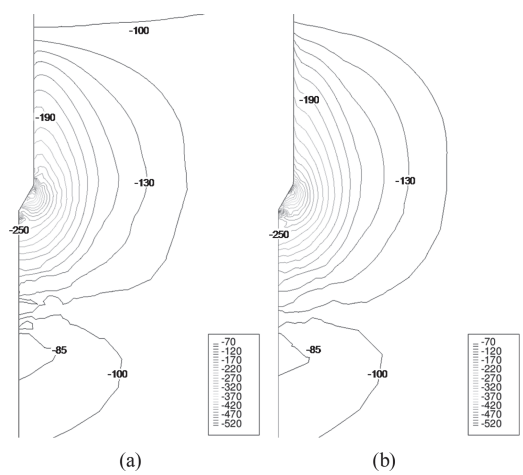

Figure 7. Pore pressure fields for inverted anisotropic permeabilities; case (a) with $k_v = 2 \cdot 10^{-8}$ m/s, $k_h = 2 \cdot 10^{-7}$ m/s and case (b) with $k_v = 2 \cdot 10^{-7}$ m/s, $k_h = 2 \cdot 10^{-8}$ m/s.

4 CONCLUSION

The results suggest that G-PFEM is an appropriate tool for simulating CPT. The application considers

anisotropic permeability and the comparison with the analytical solution for consolidation of an elastic soil layer with anisotropic permeability (Chen 2004) showed very good results.

Furthermore, an in-situ CPTu was recalculated whereby, apart from the standard penetration velocity of 2 cm/s, additional velocities of 1 and 3 cm/s were considered. Eventually, all three calculations led to the same profiles for q_c, f_s, u_1, u_2 and u_3 suggesting predominant undrained system behaviour. The calculated water pressures are up to one order of magnitude higher compared to the in-situ measurement while the calculated tip resistance is lower than the in-situ reference value but shows the same order of magnitude. However, the comparison is consistent because it can be assumed that the in-situ behaviour is partially drained.

It was also shown that anisotropy influences the pore pressure and effective stress fields under undrained conditions depending on the preferred flow direction due to anisotropy and the dominant horizontal drainage direction during cone penetration. In both cases the soil-water body behaves as a one-phase medium, and thus the total stresses remain unaffected.

REFERENCES

Burns, S.E. & Mayne, P.W. 1998. Monotonic and dilatory pore-pressure decay during piezocone tests in clay. *Canadian Geotechnical Journal* 35(6): 1063–1073.

Chen, G.J. 2004. Consolidation of multi-layered half space with anisotropic permeability and compressible constituents. *International Journal of Solids and Structures* 41: 4567–4586.

Dadvand, P.; Rossi, R.; Oñate, E. 2010. An Object-oriented Environment for Developing Finite Element Codes for Multi-disciplinary Applications. *Arch Comput Methods* Eng 17(3): 253–297.

Larsson, J. & Larsson, R. 2002. Non-linear analysis of nearly saturated porous media: theoretical and numerical formulation. *Comput. Methods Appl. Mech. Engrg.* 191: 3885–3907.

Monforte, L.; Arroyo, M.; Carbonell, J.M.; Gens, A. 2017a. Numerical simulation of undrained insertion problems in geotechnical engineering with the Particle Finite Element Method (PFEM). *Computers and Geotechnics* 82: 144–156.

Monforte, L.; Carbonell, J.M.; Arroyo, M.; Gens, A. 2017b. Performance of mixed formulations for the particle finite element method in soil mechanics problems. *Computational Particle Mechanics* 4(3): 269–284.

Oñate, E.; Idelsohn, S.R.; Celigueta, M.A.; Rossi, R.; Marti, J.; Carbonell, J.M.; Ryzakov, P.; Suárez, B. 2011. Advances in the particle finite element method (PFEM) for solving coupled problems in engineering. *Particle-Based Methods* 25: 1–49.

Sachsenhofer, M. 2012. Comparison of correlations from CPTu, SDT, DP. Master's Thesis. Technische Universität Graz.

Sheng, D.; Kelly, R.; Pineda, J.; Bates, L. 2014. Numerical study of rate effects in cone penetration test. In *3rd International Symposium on Cone Penetration Testing*: 419–428.

Cone Penetration Testing 2018 – Hicks, Pisanò & Peuchen (Eds)
© 2018 Delft University of Technology, The Netherlands, ISBN 978-1-138-58449-5

Evaluating undrained shear strength for peat in Hokkaido from CPT

H. Hayashi & T. Yamanashi
Civil Engineering Research Institute for Cold Region (CERI), Sapporo, Japan

ABSTRACT: In case of evaluating stability of soft ground using circular slip analysis, it is very important to determine the undrained shear strength (S_u) of the ground. Meanwhile, fibrous and high organic peat is distributed widely in Hokkaido, the northernmost island of Japan. As peat is accumulated heterogeneously, unconfined compression tests, vane shear tests and other tests performed for only a few samples lack validity. The electric Cone Penetration Test (CPT) is more reasonable and valid than these, in that CPT can estimate average S_u from in-situ tests, which continuously provide information. A series of K_0 consolidated-undrained triaxial compression tests (K_0CUC tests) on undisturbed peat soil collected at several sites in Hokkaido was conducted. Also the CPT was performed at the same sites. This report describes the relationship between S_u obtained from the K_0CUC tests and CPT cone resistance (q_t), and proposes a method for estimating S_u in peat soil from q_t.

1 INTRODUCTION

When embankment such as road and river levee is constructed over soft ground, the stability of the ground is commonly evaluated by the safety factor obtained from circular slip analysis. In this analysis, it is very important to determine the undrained shear strength (S_u) of the ground. As peat, which is a widely distributed soft and problematic soil in Hokkaido, Japan, is accumulated heterogeneously (Noto, 1991), unconfined compression tests, vane shear tests and other tests performed for only a few samples lack validity. The electric cone penetration test (CPT) is more reasonable and valid than these, in that CPT can estimate average S_u from in-situ tests, which continuously provide information. Therefore, the aim of this study is to establish a method for estimating the S_u of peat ground by performing CPT.

A series of K_0 consolidated-undrained triaxial compression tests (K_0CUC tests) on undisturbed peat soil collected at several sites in Hokkaido was conducted. Also the CPT was performed at the same sites. This report describes the relationship between S_u obtained from the K_0CUC tests and CPT cone resistance (q_t), and a method for estimating S_u in peat soil from q_t.

2 INVESTIGATION METHOD

2.1 *Investigation site*

A series of CPT and collection of undisturbed samples for the laboratory tests were conducted at the four sites (Shinotsu, Ebetsu city; Asajino, Sarufutsu village; Riyamunai, Kyowa town and Kitashima, Eniwa city) in peat ground in Hokkaido, Japan (Fig. 1). The undisturbed samples were collected using a thin-wall sampler with a fixed piston (JGS 1221; JGS, 2015). Table 1 shows the soil types and the engineering properties of the sampling soils at the investigation sites. The sampling soils at the Asajino site and the Riyamunai site were classified as fibrous peat. For comparison, undisturbed clay soil, which was underlying of peat, was collected at the Kitashima site.

2.2 *CPT*

Figure 2 shows the dimension of the CPT cone used. The penetration velocity was set at 2 cm/s, and q_t, skin friction (f_s) and pore water pressure (u) were continuously measured at each 1 cm of penetration. The q_t obtained from the CPT is a value that takes into account the influence of water pressure at the filter, as determined by Equation (1), where q_{ce} is the measured cone resistance (kN/m^2), A_e is the effective cross-sectional area of the cone (m^2), A_p is the area of the base of the cone (m^2) and u is the pore water pressure (kN/m^2).

$$q_t = q_{ce} + (1 - A_e/A_p)\, u \tag{1}$$

2.3 *K_0 consolidated-undrained triaxial compression test*

To obtain the undrained shear strength of peat, the K_0CUC test (JGS0525: JGS, 2011) was performed for undisturbed soil samples (Fig. 3). Each sample

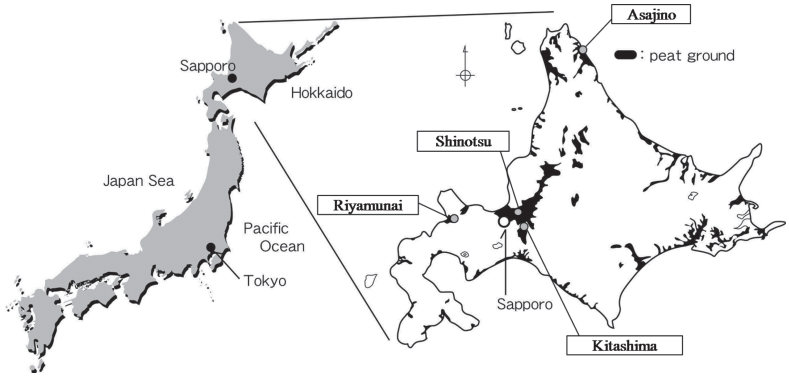

Figure 1. Location of the investigation sites (Peat distribution in Hokkaido; Noto, 1991).

Table 1. Engineering properties of the soil samples.

Site	Sample Ref.	Soil type	Natural water content W_n (%)	Ignition loss Li (%)	Degree of decomposition von Post	In-situ void ratio e_0	Conmpression index C_c	S_u obtaied from K_0-consolidated triaxial compression test S_u (kN/m^2)
Shinotsu	No. 1	Peat	459	66	H5	9.3	5.1	20.7
	No. 2	Peat	424	58	H5	7.2	4.0	18.0
	No. 3	Peat	327	37	H5	7.0	4.2	21.5
Asajino	No. 1	Fibrous peat	860	92	H2	14.8	9.3	11.1
Riyamunai	No. 1	Fibrous peat	834	94	H3	13.5	10.0	7.4
	No. 2	Fibrous peat	724	82	H3	14.5	9.5	8.1
Kitashima	No. 1	Peat	387	55	–	–	–	20.3
	No. 2	Clay	142	9.5	–	–	–	13.5

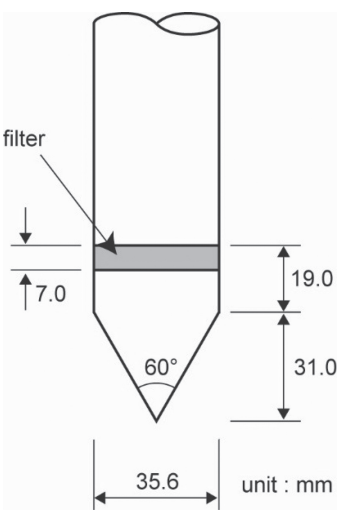

Figure 2. Dimension of the CPTU cone used in this study.

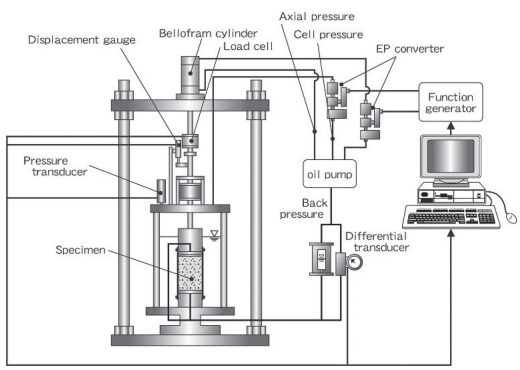

Figure 3. Set up of the K_0 consolidated-undrained triaxial compression test used in this study.

was 75 mm in diameter and 150 mm in height. The samples were carefully trimmed and set on the test device to avoid unnecessary disturbance. As the S_u of the soil is significantly affected by the con-

fining pressure, K_0 consolidation was conducted with a pressure equivalent to the in-situ stress. This means that the in-situ anisotropic consolidation was reproduced in the laboratory. After the K_0 consolidation, compression (0.1%/min of strain rate) under an undrained condition was done. Additionally, an oedometer test and physical index tests were conducted.

3 RESULTS AND DISCUSSION

3.1 *CPT profile*

Figure 4 shows the depth distribution results of the CPT at the Shinotsu site. This is the typical CPT profile (q_t, f_s and u) of this study. The geologic columnar section obtained from drilling at the Shinotsu site was added to the figure. The q_t in the peat layer (q_t = 0.33–0.71 MN/m^2) was lower than that in the other soil types, which indicates that the peat layer is very soft. Large excess pore water pressure, which was caused by the cone penetration, was generated in the peat layer and the clay layer.

3.2 *Relationship between cone resistance and undrained shear strength*

To calculate the S_u of the ground from CPT, Equation (2) is commonly applied. Where, the S_u and q_t are both expressed in units of kN/m^2, σ_{v0} is the total overburden pressure (kN/m^2), and N_k is a correction coefficient called the cone coefficient (no dimension).

$$S_u = (q_t - \sigma_{v0})/N_k \tag{2}$$

Konrad & Lan (1987) reported that N_k in Equation (2) greatly varies by soil property. Figure 5 shows the relation between (q_t − σ_{v0}) and S_u obtained from the K_0CUC test, to reveal the N_k of peat. As shear strength does not peak along compression strain in the K_0CUC test on peat, S_u was assessed by assuming 15% of the compression strain as failure. Overall, the S_u in peat was only between 5–20 kN/m^2, and S_u increased linearly with increase in (q_t − σ_{v0}). Noto (1991) pointed out that the N_k of peat is 20, based on the cone resistance obtained from a mechanical cone penetration test. Konrad & Lan (1987) reported that the N_k of

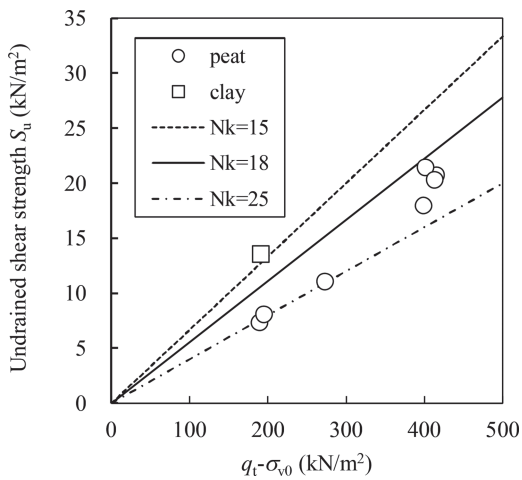

Figure 5. Relationship between (q_t-σ_{v0}) and undrained shear strength for peat.

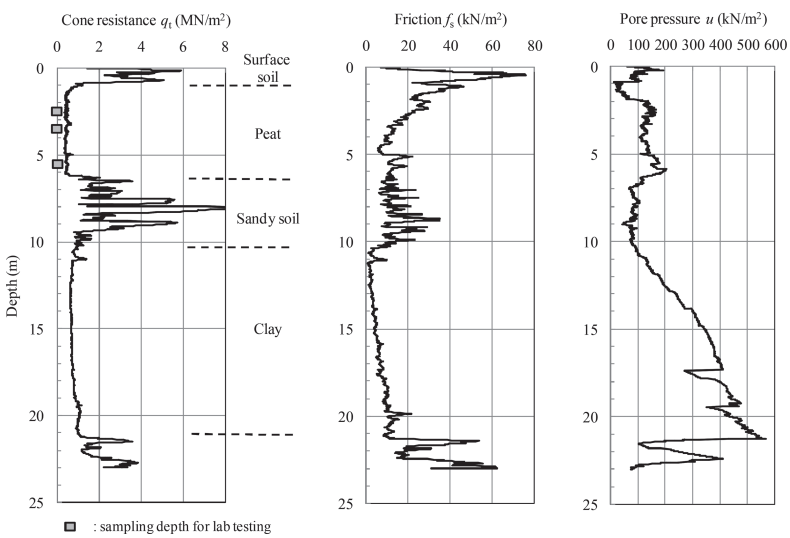

Figure 4. Depth distribution results of the CPT at the Shinotsu site (Hayashi & Hayashi, 2016).

clay is between 10 and 20. In this study, the N_k of peat almost ranged from 15 to 25, and was found to be greater than that of clay.

Figure 6 shows the relationship between ignition loss (L_i), indicating content of organic matter in soil, and N_k calculated by Eq. (2) and experimental data as shown in Fig. 5. The N_k increased linearly with increase in L_i. This indicates that the N_k of peat is not constant value, and is affected by the content of organic matter. The relationship

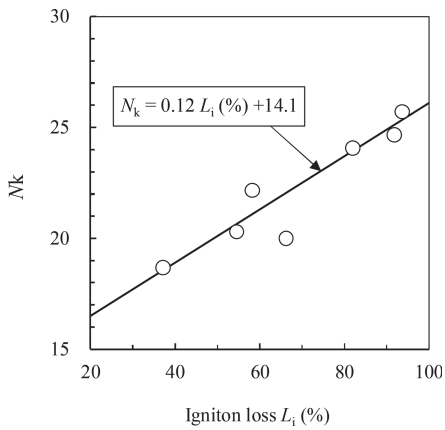

Figure 6. Relationship between ignition loss and N_k.

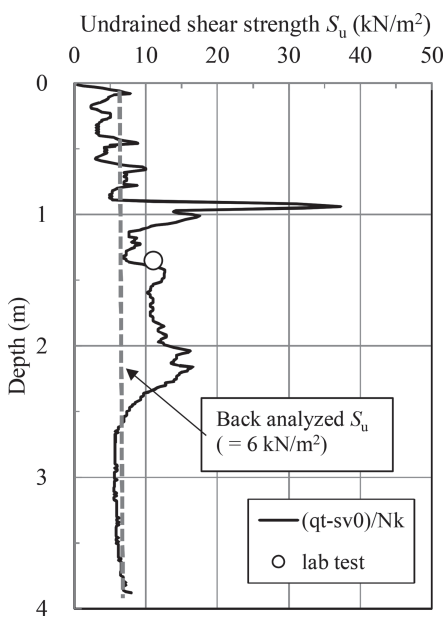

Figure 7. Undrained shear strength calculated using Eqs. (2) and (3), and obtained from the K_0 consolidated-undrained triaxial compression test at the Asajino site (after Hayashi & Hayashi, 2016).

can be approximated by Equation (3), where L_i is expressed in%.

$$N_k = 0.12\ L_i\ (\%) + 14.1 \tag{3}$$

Figure 7 shows the depth distribution of S_u, calculated by Eq. (2) based on the q_t measured at the Asajino site. For the calculation, N_k value, which is obtained from Eq. (3) and L_i of collected peat samples at the site, was used. It was found that the S_u obtained from K_0CUC test almost corresponded to the calculated value. At the Asajino site, sliding failure happened during embankment construction unfortunately. Back circular slip analysis was performed based on this fact of the sliding failure, which led S_u of the peat layer to be 6 kN/m². This roughly corresponds with the S_u calculated by Eqs. (2) and (3). These indicate that it is possible for Eqs. (2) and (3) to estimate S_u in peat ground.

4 CONCLUSIONS

To clarify the estimation method of undrained shear strength (S_u) for peat ground, a series of electric cone penetration tests (CPT) and laboratory tests were conducted for peat ground in Hokkaido, Japan. The main results can be summarized as follows:

1. The S_u in peat was only between 5–20 kN/m², and S_u increased linearly with increase in ($q_t - \sigma_{v0}$).
2. The N_k of peat almost ranged from 15 to 25, and was found to be greater than that of clay.
3. The N_k increased linearly with increase in L_i, and the relationship can be approximated by "$N_k = 0.12\ L_i\ (\%) + 14.1$".
4. It is possible to estimate of S_u value for peat ground using this relationship.

REFERENCES

Hayashi, H. and Hayashi, T. 2016. Estimation of undrained shear strength for peat using CPT, Proc. of International Conference on Geotechnical and Geophysical Site Characterisation, Gold Coast, USB.

Japanese Geotechnical Society. 2015. Japanese Geotechnical Society Standards – Geotechnical and Geoenvironmental Investigation methods.

Japanese Geotechnical Society. 2009. Japanese Geotechnical Society Standards – Laboratory Testing Standards of Ge-omaterials.

Konrad, J.M. and Lan, K.T. 1987. Undrained shear strength from piezocone tests, Canadian Geotechnical Journal, 24(3), pp. 392–402.

Noto, S. 1991. Peat Engineering Handbook, pp. 24–66.

Cone Penetration Testing 2018 – Hicks, Pisanò & Peuchen (Eds)
© 2018 Delft University of Technology, The Netherlands, ISBN 978-1-138-58449-5

Interpreting improved geotechnical properties from RCPTUs in KCl-treated quick clays

T.E. Helle
Directorate of Public Roads, Trondheim, Norway

M. Long
University College Dublin, Dublin, Ireland

S. Nordal
Norwegian University of Science and Technology, Trondheim, Norway

ABSTRACT: In January 2013, Potassium Chloride (KCl) wells were installed in a highly sensitive quick clay deposit at Dragvoll, Trondheim, Norway. The geotechnical properties significantly improved in the following years due to increased salt content and changed pore-water chemistry. Several Resistivity Cone Penetration Tests (RCPTU) were conducted around the wells to map the salt-plume extent, and to interpret improved geotechnical properties. The RCPTUs effectively mapped the salt plume extent around the wells, and the increased tip resistance clearly indicated improved properties in the salt-treated clay. Commonly used correlations for Norwegian clays are used herein for interpreting the geotechnical properties in the original quick clay and the salt-treated clay. The interpreted Over Consolidation Ratio (OCR) and shear strength (c_u) are compared to laboratory determined geotechnical properties on high quality downsized Sherbrooke samples (mini-blocks). The tip resistance in the salt-treated clay increased significantly due to increased remolded shear strength and increased resistance to deformations. Improved OCR and c_u in the salt-treated clay at Dragvoll are determined from the CPTU data applying existing correlations based on bearing factor for net tip resistance (N_{kt}). The existing correlations for Norwegian clays work reasonably well, but ideally specific local correlations should be developed.

1 INTRODUCTION

Geotechnical properties are often interpreted from CPTU tests as they are cost-efficient, and considered reliable. In Norway, geotechnical engineers often deal with highly sensitive quick clays, defined by a remolded shear strength (c_{ur}) of less than 0.5 kPa (Norwegian Geotechnical Society, 2011). The Norwegian clays are characterized as having high sensitivity (S_t) > 30, medium S_t in the interval 8–30, and low S_t < 8. The resistance to penetration is smaller in highly sensitive clays than in clays with lower sensitivity. Therefore, the measured tip resistance is generally low, and the measured pore pressure high in highly sensitive quick clays compared to in clays with higher c_{ur} and low S_t. The CPTU correlations for Norwegian clays developed by Karlsrud et al. (2005), are based on empirical correlations between CPTU data and high-quality block samples. Most of the included sites are in the south-eastern part of Norway. A clear advantage of the correlations is that they aim to differentiate between clays with high and low S_t by including two frameworks dividing clays into S_t above and below 15. Therefore these correlations are widely used amongst Norwegian geotechnical engineers as CPTU is one of the most used site investigation tools on clay sites in Norway. These correlations are used herein for interpreting improved geotechnical properties in highly sensitive quick clays treated with potassium chloride (KCl).

Six salt wells filled with KCl were installed at the research site Dragvoll, Trondheim in Mid-Norway in January 2013, aiming to improve the geotechnical properties in the highly sensitive quick clay deposit. The salt migrated into the quick clay volume, with time resulting in increased remolded shear strength (c_{ur}) and plasticity index (IP), and decreased liquidity index (IL) and S_t (Helle et al., 2017a). In addition, the apparent pre-consolidation stress (p_c') increased and the deformations at loads just beyond p_c' were significantly reduced (Helle et al., 2018).

Increased plasticity due to an increased liquid limit may indicate decreased compressibility, i.e. decreased volume change at increasing loads

(Bjerrum, 1967; Sridharan and Nagaraj 2000). Furthermore, increased over-consolidation ratio (OCR) may indicate increased peak undrained shear strength (e.g. Bjerrum, 1967; Ladd and Foot, 1974; Karlsrud and Hernandez-Martinez, 2013). The tip resistance (q_t) increases with decreasing compressibility as the resistance against penetration increases (Lunne et al., 1997b). The plasticity index in the salt-treated clay is increased, and the deformations at loads exceeding p_c' are decreased. Improved OCR and undrained shear strength (c_u) may therefore be detected by increased q_t.

Resistivity cone penetration tests (RCPTU) were conducted to map the extent of the salt plumes by changes in the soil conductivity, and for detection of improved properties (Fig. 1) (Helle et al. 2017b). The conductivity profiles showed that the salt migrated slightly non-symmetrical and off-centered from the wells. Improvement of c_{ur} > 1 kPa commenced at very low salt contents and was caused by favorable changed pore-water chemistry; from being sodium dominated in the quick clay to having more than 20% of potassium, magnesium and calcium in the salt-treated improved clay even at salt contents less than 2 g/L. Therefore, the conductivity in the low-saline improved clay did not increase, and no unique correlations were obtained distinguishing improved salt-treated clays from non-treated quick clays based on conductivity. However, improved properties were detected at low salt contents when the normalised cone factor ($N_m = q_n/(\sigma'_{v0}$ + attraction)) improved beyond 3.5, and the pore pressure parameter ($B_q = (u_2 - u_0)/q_n$) decreased below 0.9.

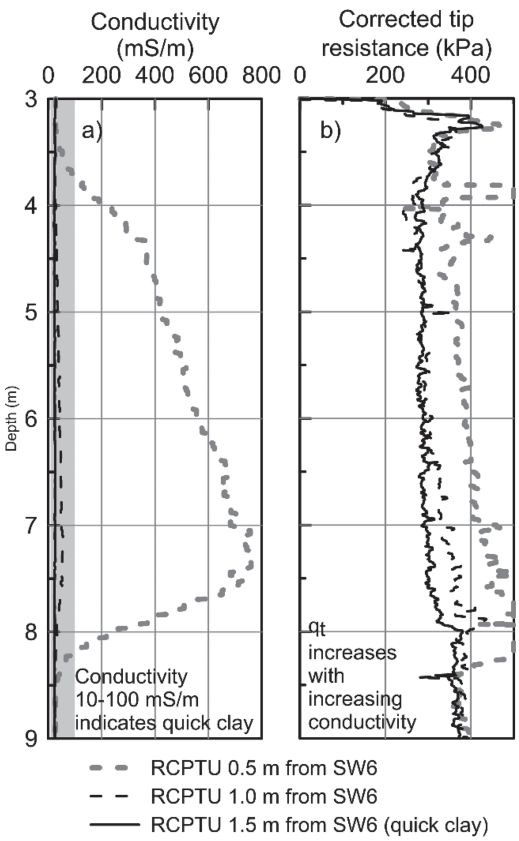

Figure 1. a) Conductivity profiles and b) corrected tip-resistance (q_t) with distance from salt-well no. 6, 3 years and 5 months after installation. The q_t increases as the soil conductivity increases as a result of increased remolded shear strength.

This paper presents the interpreted OCR and c_u profiles in the original quick clay and the salt-treated clay. The interpreted properties are compared to laboratory test results from clay samples extracted from nearby boreholes. The applicability of the correlations developed by Karlsrud et al. (2005) on interpreting geotechnical properties in the quick clay and salt-treated clay at Dragvoll is evaluated and discussed.

2 CPTU CORRELATIONS COMMONLY USED FOR NORWEGIAN CLAYS

Norwegian quick clays are highly sensitive, often with a S_t, i.e. ratio between undisturbed and remolded shear strength, of more than 30. The correlations developed by Karlsrud et al. (2005) differentiates between clays with S_t > 15 and S_t < 15 (Table 1).

The cone factor (Q_t), and shear strength based on bearing factors for excess pore water pressures ($c_{u,N\Delta u}$) and net tip resistance ($c_{u,Nkt}$) are determined by Equations 1–3 (Lunne et al. 1997b).

$$Q_t = (q_t - \sigma_{v0}) / \sigma'_{v0} \tag{1}$$

$$c_{u,N\Delta u} = (u_2 - u_0) / N_{\Delta u} \tag{2}$$

$$c_{u,Nkt} = (q_t - \sigma_{v0}) / N_{kt} \tag{3}$$

The interpreted c_u profiles are often compared to c_u profiles obtained from "Stress History

Table 1. Bearing factors for excess pore water pressures ($N_{\Delta u}$) and net tip resistance (N_{kt}). OCR for clays with S_t below and above 15 suggested by Karlsrud et al. (2005). The IP is in%.

	St < 15	St > 15
$N_{\Delta u}$	6.9 – 4.0 · log(OCR) + 0.07 · IP	9.8 – 4.5 · log(OCR)
N_{kt}	7.8 + 2.5 · log(OCR) + 0.082 · IP	8.5 + 2.5 · log(OCR)
OCR	$(Q_t/3)^{1.20}$	$(Q_t/2)^{1.11}$

Table 2. Range of α and m for Norwegian clays. From Karlsrud and Hernandez-Martinez (2013).

	α	M
Average	0.30	0.70
Lower	0.25	0.65
Upper	0.35	0.75

And Normalized Soil Engineering Properties" (SHANSEP) developed by Ladd and Foott (1974) (Equation 4).

$$c_{u,SHANSEP} = \alpha \cdot \sigma'_{v0} \cdot OCR^m \quad (4)$$

where constants $\alpha = (c_{uc}/\sigma_{v0}')$ at OCR = 1, and m may be determined from laboratory tests. Karlsrud and Hernandez-Martinez (2013) suggest α and m for Norwegian clays based on laboratory tests on high-quality block samples within the ranges given in Table 2.

3 CPTU SOUNDINGS, SAMPLING AND LABORATORY TESTS

Resistivity cone penetration tests (RCPTU) were conducted both in the original quick clay and the salt-treated clay around the installed salt wells, using a 5 ton GeoTech CPTU Nova and 2 ton Envi CTPU, both with tip areas of 10 cm^2.

Mini-block samples, downsized Sherbrooke samples (for further description see Emdal et al. (2016)), were extracted from the Dragvoll quick clay, and 54 mm steel-tube piston samples were extracted from the salt-treated clay around the salt wells. Water content, Atterberg limits, fall cone undrained and remolded shear strength and density were determined on all samples. Constant rate of strain oedometer tests (CRS) with a strain rate of 0.75%/hr were conducted on some of the samples. All samples were tested in the laboratory within 48 hours to minimize storage effects on the results.

4 LABORATORY DETERMINED GEOTECHNICAL PROPERTIES IN THE DRAGVOLL CLAY

4.1 *Quick clay*

The c_{ur} is < 0.1–0.5 kPa (Fig. 2), and a S_t based on fall cone tests is in the range of 32–143. The quick clay is of low plasticity with a plasticity index (IP) in the range of 4.4–6.3%. The liquid limit is well below the natural water content, and the IL is in the range of 3.4–4.3. The sample quality of the oedometer tests were evaluated based on the difference in void ratio from the start of the test (e_0) to the void ratio at in-situ effective overburden stress ($\Delta e/e_0$) (Lunne et al. 1997a). CRS were conducted on samples of very good to excellent quality ($\Delta e/e_0$ = 0.025–0.038). The OCR decreases from 2.2 at 4.1 m depth to 1.2 at 5.9 m depth.

4.2 *Salt-treated clay*

In the samples extracted from 5.4 m depth around salt-well no. 7, IP and c_{ur} increase to 21.9–24.0% and 4.7–5.1 kPa respectively. The CRS tests conducted on these samples were of good to fair quality ($\Delta e/e_0$ = 0.040–0.042). The p_c' increases and deformations decrease at loads just beyond p_c', and the OCR increases from 1.2 in the quick clay to 1.7 and 2.1 in the salt-treated clay having salt contents of 9.7 and 27.7 g/L respectively.

Unfortunately, the measured pore pressures (u_2) in the RCPTUs conducted around salt-well no. 7 were affected by the close proximity to the open sampling boreholes. The measured u_2 was in the order 50–100 kPa lower than in the original quick clay Therefore one of the RCPTU soundings nearby salt-well no. 3 is used for interpretation of the geotechnical properties in the salt-treated clay. The clay around salt-well no. 3 (Fig. 3) has about the same salt content, fall-cone undrained and remolded shear strength as found in the clay around salt-well no. 7.

5 INTERPRETED PROPERTIES IN THE QUICK CLAY AND SALT-TREATED CLAY

5.1 *Quick clay*

The corrected tip-resistance is low in the quick clay (Fig. 4a). The interpreted soil profiles in the original quick clay show that the OCR is overestimated when applying the equation for clays with higher S_t than 15 (Fig. 4b). The c_u is underestimated by 25–30% (Fig. 4c). Surprisingly, the interpreted OCR and $c_{u,N\Delta u}$ profiles match the laboratory results in the highly sensitive Dragvoll quick clay when applying the relationships for S_t < 15. The $c_{u,Nkt}$ profiles are the same using both the relationships, and fit reasonably well with c_{uc} found in the triaxial tests (Fig. 4d). The SHANSEP c_u profile (grey thick solid line) match the c_{uc} by applying the interpreted OCR profile for clays with S_t < 15, and the constants α of 0.38 ($= c_{uc}/\sigma_{v0}'$ = 27.7 kPa/73.6 kPa at 7.9 m depth), and m of 0.75.

5.2 *Salt-treated clay*

The measured pore pressure (u_2) is slightly decreased compared to that in the quick clay down to about 6 m depth, possibly also resulting in a

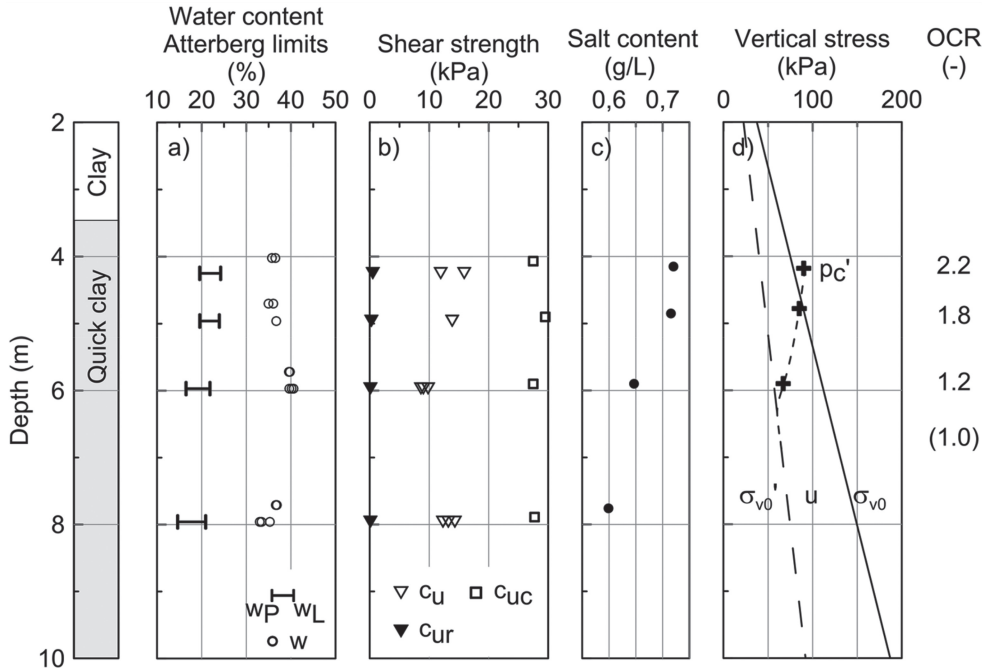

Figure 2. Geotechnical properties in the original quick clay. a) Water content (w), plastic (w_P) and liquid limit (w_L). b) Fall-cone c_u and c_{ur}, and peak-undrained shear strength (c_{uc}) from triaxial tests. c) Salt content. d) Total (σ_{v0}) and effective (σ_{v0}') vertical stress, p_c' and OCR.

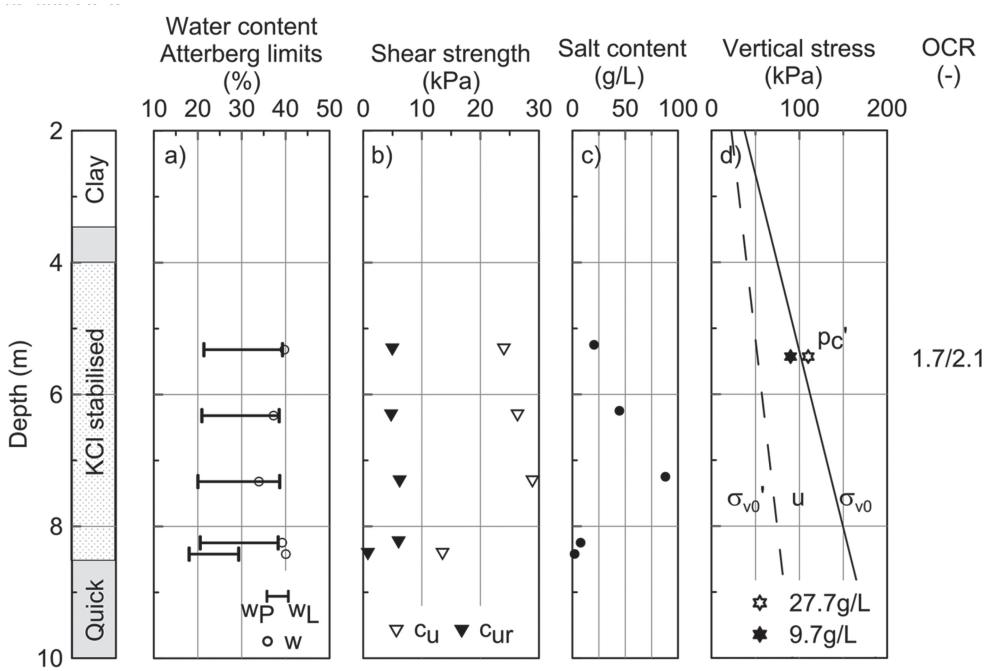

Figure 3. Geotechnical properties in salt-treated clay 0.5 m from salt-well no. 3. a) w, w_P and w_L. b) Fall-cone c_u and c_{ur}. c) Salt content. d) Vertical stresses and p_c' found on samples from around salt-well no. 7.

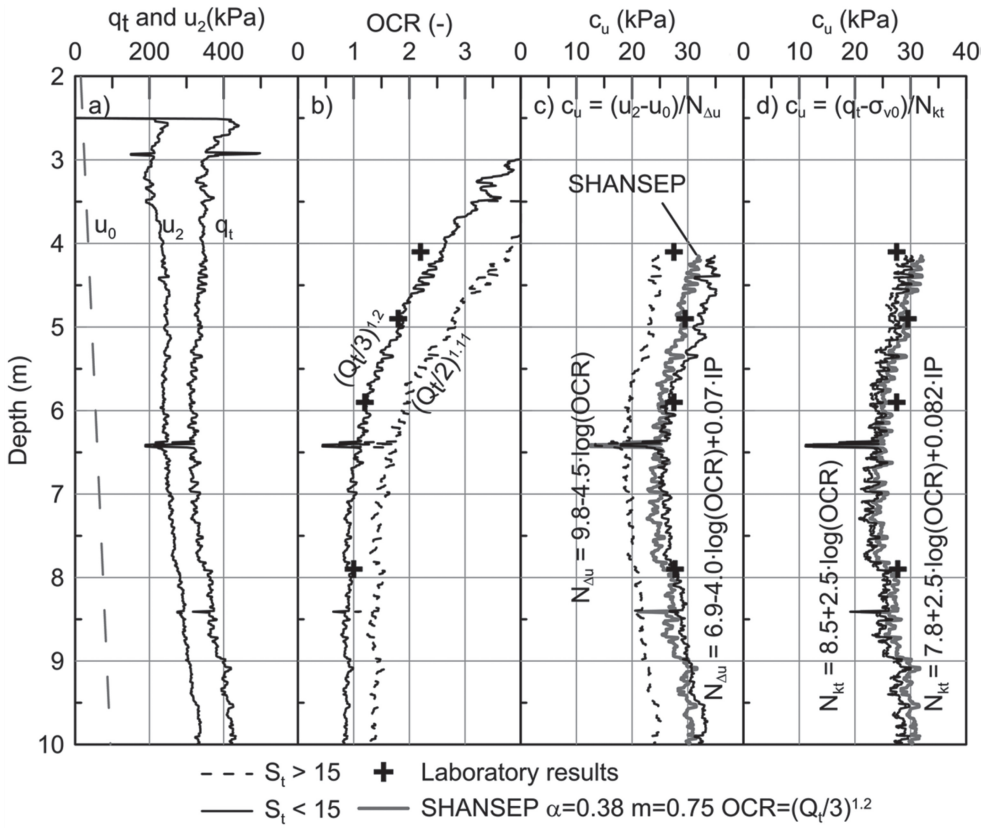

Figure 4. Interpreted geotechnical properties in the original quick clay for S_t above and below 15. a) Corrected tip resistance (q_t), pore pressure behind the cone (u_2) and in-situ pore pressure (u_0). b) Interpreted OCR, and OCR from CRS tests (symbols). c) Shear strength profiles based on $N_{\Delta u}$, and c_{uc} from CAU_c tests (symbols). d) Shear strength profiles based on N_{kt}, and c_{uc} (symbols). The grey thick solid lines in c) and d) show the SHANSEP c_u profile interpreted by applying OCR = $(Q_t/3)^{1.2}$ (S_t < 15) in b).

decreased corrected tip resistance (q_t) (Fig. 5a). The sounding was conducted at a distance of 0.5 m from the well, so this reduction in pore pressure was caused by the well installation. Nevertheless, q_t clearly increases in the salt-treated clay (black thick solid line in Fig. 5). The interpreted OCR increases and correlates well with the OCR found in the salt-treated clay with a salt content of 27.7 g/L (open star in Fig. 5b). Even though increasing OCR should induce increased shear strength (c_u), the $c_{u,N\Delta u}$ is practically unchanged compared to the quick clay due to almost no changes in u_2. The $c_{u,Nkt}$, however, increases by 10–45% compared to the original quick clay due to increased q_t.

The SHANSEP c_u profile for the salt-treated clay (dashed grey line in Fig. 5c and d) is developed by applying the same constants as found for the quick clay. As the interpreted OCR profile in the quick clay fits reasonably well with the CRS tests, the interpreted OCR based on the cone factor was applied in the SHANSEP profile for the salt-treated clay. SHANSEP c_u is slightly higher than the $c_{u,Nkt}$.

In addition to conducting laboratory tests on in-situ treated clay, CRS and undrained anisotropically consolidated compression tests (CAU_c) tests were conducted on undisturbed mini-block samples submerged in KCl slurry (Bryntesen, 2014; Helle et al. 2015). The salt content in the pore water after storage was of 170–260 g/L. The samples were stored for several months, and were allowed to swell. Nevertheless, the deformation curves from the CRS tests corresponded well to the curves from the CRS tests conducted on the in-situ salt-treated quick clays which imply decreased brittleness. Furthermore, the peak undrained shear strength of the samples stored in the containers was slightly improved to the order of 26–32 kPa; fairly consistent with the $c_{u,Nkt}$ profile (black thick solid line in Fig. 5d).

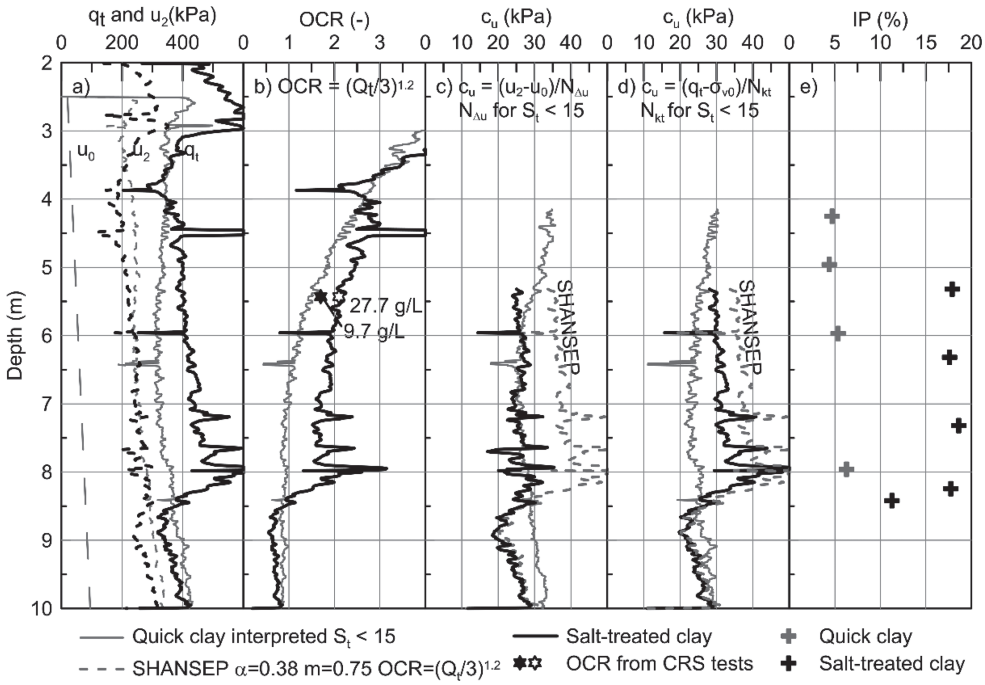

Figure 5. Figure 5. Interpreted geotechnical properties in salt-treated clay 0.5 m from salt-well no. 3. a) Corrected tip resistance (qt) and pore pressures in the original quick clay (grey line) and the salt-treated clay (thick black line). b) Interpreted OCR for the original quick clay and salt-treated clay. Both interpreted by the relation for sensitivity (St) less than 15. CRS determined OCR at 5.43 m for in-situ salt-treated clays with salt contents of 9.7 g/L (black filled star) and 27.7 g/L (open star). c) Undrained shear strength (c_u) interpreted by $N_{\Delta u}$. d) c_u interpreted by N_{kt}. The grey dashed line in c) and d) show the SHANSEP cu profile interpreted by applying the interpreted OCR for the salt-treated clay in b). e) Plasticity index (IP) in the original quick clay (grey symbols) and salt-treated clay (black symbols).

6 DISCUSSIONS AND CONCLUSIONS

The RCPTUs effectively map the salt-plume extent at the same time detecting improved geotechnical properties in the salt-treated clay. Interpreting the parameters of the Dragvoll quick clay by applying the CPTU correlations for clays with sensitivity (S_t) higher than 15, overestimates the over consolidation ratio (OCR) and underestimates the shear strength (c_{uc}) by as much as 25–30% compared to laboratory tests on high-quality mini-block samples. Such underestimates may create large costs in projects. Applying the equations for $S_t < 15$ for the quick clay, the interpreted OCR and $c_{u,N\Delta u}$ profiles fit the laboratory results, whereas the $c_{u,Nkt}$ profile is slightly lower. The SHANSEP c_u profile fits reasonably well with the laboratory results with the assumptions α of 0.38 and m of 0.75, and applying the interpreted OCR profile for $S_t < 15$.

Treating the clay with potassium chloride (KCl) increases the OCR. The CPTUs show no change in the measured pore pressure (u_2) compared to in the quick clay, and the bearing factor for excess pore pressures ($N_{\Delta u}$) is about the same as in the original quick clay even though both OCR and the plasticity index (IP) increase. Therefore, the $c_{u,N\Delta u}$ profile shows no sign of improvement. The corrected tip resistance (q_t) is increased, which is included in the $c_{u,Nkt}$. It is therefore recommended to interpret the c_u profile in salt-treated clays by $c_{u,Nkt}$ (Equation 3) rather than $c_{u,N\Delta u}$ (Equation 2).

The CPTU correlations developed by Karlsrud et al. (2005) differentiating between clays with sensitivity lower and higher than 15 have been most valuable, and have eased the interpretation of geotechnical properties from CPTUs in Norwegian clays. The correlations are widely used amongst Norwegian geotechnical engineers. However, the number of quick-clay samples included in the study of Karlsrud et al. (2005) is limited, and most of them are from sites in south-eastern Norway. There are discussions on whether these correlations apply for clays found in Mid-Norway as these clays tend to have higher silt content. To improve correlations for clays especially in Mid-Norway, a research project collecting data from sites where

CPTU results are correlated to high-quality mini-block or block samples has been initiated in the Norwegian Public Roads Administration.

The results presented herein show the importance of making local correlations between laboratory tests on high-quality samples and CPTU results for interpreting the mechanical properties. This was also emphasized in Karlsrud et al. (2005). The interpreted profiles in the original Dragvoll quick clay fit better to $c_{u,N\Delta u}$ where $N_{\Delta u}$ is determined based on the equation for $S_t < 15$, even though the quick clay has S_t in the range of 32–143. Applying the $N_{\Delta u}$ for interpreting c_u from CPTU in clays is often considered the best approach. However, as the pore-pressure response is unchanged in the salt-treated clay whereas q_t increases, interpreting the c_u profile based on N_{kt} is considered a better approach for salt-treated clays.

ACKNOWLEDGMENTS

This work was made possible thanks to the generous support from the research program "Natural hazards: infrastructure for floods and slides" (NIFS).

REFERENCES

Bjerrum, L. 1967. Engineering Geology of Norwegian normally-consolidated marine clays as related to settlements of buildings. *Géotechnique* 17(2): 83–118.

Bryntesen, R.N. 2014. Laboratory investigation on salt migration and its effect on the geotechnical strength parameters in quick clay mini-block samples from Dragvoll. Master's thesis, Norwegian University of Science and Technology, Trondheim, Norway, pp. 1–105.

Emdal, A., Gylland, A.S., Amundsen, H.A., Kåsin, K. & Long, M. 2016. Mini-block sampler. *Canadian Geotechnical Journal* 53(8), 1235–1245.

Helle, T.E., Bryntesen, R.N., Amundsen, H.A., Emdal, A., Nordal, S. & Aagaard, P. 2015. Laboratory setup to evaluate the improvement of geotechnical properties from potassium chloride saturation of a quick clay from Dragvoll, Norway. *Proceedings for GeoQuebec2015 - Challenges from North to South, Quebec, Canada, 20–23 September 2015*.

Helle, T.E., Aagaard, P. & Nordal, S. 2017a. In-situ improvement of highly sensitive clays by potassium chloride migration. *Journal of Geotechnical and Geoenvironmental Engineering ASCE* 143(10).

Helle, T.E., Long, M., Nordal, S. & Aagaard, P. 2017b. Effectiveness of RCPTU to detect improved properties in salt-treated highly sensitive clay. *Proceedings of the Institution of Civil Engineers – Ground Improvement* 170(3): 173–184.

Helle, T.E., Nordal, S. & Aagaard, P. 2018. Improved geotechnical properties in salt-treated highly sensitive landslide-prone clays. *Proceedings of the Institution of Civil Engineers - Geotechnical Engineering, published online ahead of print.*

Karlsrud, K., Lunne, T., Kort, D.A. & Strandvik, S. 2005. CPTU correlations for clays. In *Proceedings of the 16th International Conference on Soil Mechanics and Geotechnical Engineering. Osaka, Japan. Amsterdam*: IOS Press BV.

Karlsrud, K. & Hernandez-Martinez, F.G. 2013. Strength and deformation properties of Norwegian clays from laboratory tests on high-quality block samples. *Canadian Geotechnical Journal* 50(12): 1273–1293.

Ladd, C.C. & Foott, R. 1974. New design procedure for stability of soft clays. *Journal of the Geotechnical Engineering Division ASCE* 100(7): 763–786.

Lunne, T., Berre, T. & Strandvik, S. 1997a. Sample disturbance effects in soft low plastic Norwegian clay. In Marcio (ed.) *Proceedings of Recent Developments in Soil and Pavement Mechanics. Rio de Janeiro, Brazil, 25–27 June 1997.* Amsterdam: A.A. Balkema.

Lunne, T., Robertson, P.K. & Powell, J.J.M. 1997b. *Cone penetration testing in geotechnical practice*. Spon Press.

Norwegian Geotechnical Society 2011. Veiledning for symboler og definisjoner i geoteknikk: Identifisering og klassifisering i jord. Norwegian Geotechnical Society, Oslo, Norway, NGF-notification no. 2 2nd revision, first published in 1982. pp. 1–54.

Sridharan, A. & Nagaraj, H.B. 2000. Compressibility behaviour of remoulded, finegrained soils and correlation with index properties. *Canadian Geotechnical Journal* 37(3): 712–722.

Taylor & Francis
Taylor & Francis Group
http://taylorandfrancis.com

Cone Penetration Testing 2018 – Hicks, Pisanò & Peuchen (Eds)
© 2018 Delft University of Technology, The Netherlands, ISBN 978-1-138-58449-5

Some experiences using the piezocone in Mexico

E. Ibarra-Razo & R. Flores-Eslava
InGeum Ingeniería SA de CV, Ciudad de México, México

I. Rivera-Cruz
Thurber Engineering, Ltd., Vancouver, BC, Canada

J.L. Rangel-Núñez
Universidad Autónoma Metropolitana, Azcapotzalco, Ciudad de México, México

ABSTRACT: The use of the Cone Penetrometer Test sounding (CPT) in geotechnical exploration in Mexico goes back to the 1970s, during which time a great deal of experience and a set of empirical correlations with different mechanical properties of the soils have been obtained; however, that local experience has been limited almost exclusively to the measurement of tip resistance (qc) in soft clay deposits, especially in the Valley of Mexico. In recent years, new versions of cones have been made available in our country that allow digital measurements and visual checks on real time, not only of end resistance against depth but also of sleeve friction and pore pressure during driving, *i.e.*, the piezocono test (CPTu). In this paper, we present several case histories of the application of the digital piezocone (CPT-u) in various geotechnical environments; In soft clayey stratified soils with hard layers, in clean sands and in tailings deposits. It highlights the advantages and disadvantages of this new generation of electrical cones, mainly on aspects of field execution, equipment operation and interpretation of recorded data.

1 INTRODUCTION

The use of the Cone Penetrometer sounding test (CPT) in geotechnical exploration in Mexico goes back to the 1970s, during which time a great deal of experiences and a set of empirical correlations with different mechanical properties of the soils was obtained; however, local experience has been limited almost exclusively to the measurement of tip resistance (q_c) in soft clay deposits, especially in the Mexico City. In recent years, new versions of cones have been made available in our country that allow digital measurements of tip resistance (q_T), sleeve friction (f_s) and excess pore pressure (u_2), as well as the inclination and the driving speed. In accordance with international standard ISO 22476-1:2012, the piezocone is driven at a constant velocity of 2 cm/s. In addition to these new cones, specifically designed hydraulic machines are used. These have greater capacity (up to 200 kN) and speed control, which has allowed for the reduction of uncertainties in the test and has extended the potential of use of this exploration tool not only to soft clayey soils, but to sandy soils, tailing dams, and soft soil with hard layers, among others.

In this paper, three case histories of the application of the digital piezocone (CPT-u) in various geotechnical environments are presented; in soft clayey stratified soils with hard layers, in clean sands and in tailings deposits. This paper highlights the advantages and disadvantages of this new generation of electrical cones, mainly in the aspects of field execution, equipment operation and interpretation of recorded data.

2 CASE HISTORIES

2.1 *Alvarado project*

This project is located in a coastal zone of Mexico, where an industrial plant will be built on a 10-hectare lot. The subsoil is made up of a clean sand deposit with different degrees of compactation and with a deep water level table, with no risk of liquefaction problems. In order to ensure proper behavior of the platforms for the industrial nave, the first 13 mts of the deposit will be improved using Vibrocompactation. Vibrocompactation is applied in a square pattern with 5 m to each side, improving the four corners and a fifth point found at the center of the pattern (Fig. 1).

In order to evaluate the efficiency of the Vibrocompactation, exploration was performed using piezocones driven to a depth that varied between

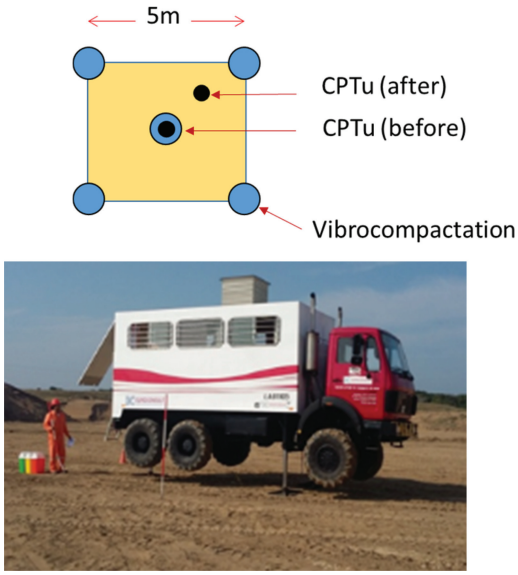

Figure 1. Pattern for improvement of soil using Vibrocompactation method.

8 and 20 m, in which q_T, f_s and u_2 were measured before and after the improvement. In accordance with the company that performed the improvement (Keller, 2016), the level of improvement was established taking into account the relative density, determined indirectly based on the piezocone sounding, as per expression 1.

$$D_r = 100 * \sqrt{\frac{Q_{tn}}{C_{DR}}} \tag{1}$$

where, C_{DR} is a constant (≈350)

$$Q_{tn} = \frac{q_T - \sigma_{vo}}{p_a}\left(\frac{p_a}{\sigma'_{vo}}\right)^n$$

σ_{vo}, σ'_{vo} and p_a are total and effective vertical stress, and atmospheric pressure, and

$$n = 0.38(I_c) + 0.05\left(\frac{\sigma'_{vo}}{p_a}\right) - 0.15;$$

$$I_c = \left[\left(3.47 - log(Q_{t1})\right)^2 + \left(log(F_r) + 1.22\right)^2\right]^{0.5};$$

$$Q_{t1} = \frac{(q_T - \sigma_{vo})}{\sigma'_{vo}};\ F_r = \frac{f_s}{q_T - \sigma_{vo}}$$

Here are the results obtained in the two sites studied, in which the improvement was inadequate (Fig. 2) and efficient (Fig. 3), presented as examples.

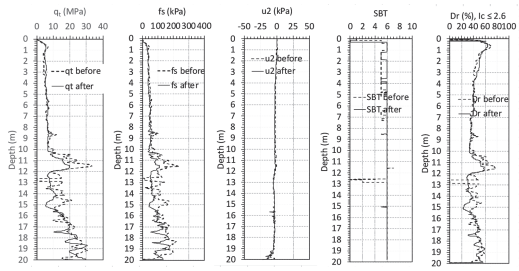

Figure 2. Site where improvement was inadequate.

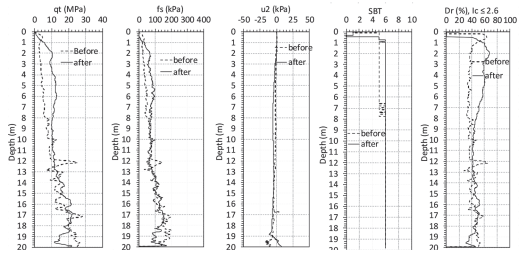

Figure 3. Site where improvement was efficient.

In the first case, we can see that the measurements of q_T and f_s, taken before and after the improvement, are practically the same, concluding that the subsoil at this site was not improved. On the other hand, in Fig. 3 we can see results where the improvement was efficient, seeing that there is an important increase in values of q_T, f_s and D_r after the improvement of the first 10 m.

Based on the results of the campaign performed with piezocones, sites where improvement was inadequate were identified and a second improvement was performed, but this time using the dynamic compactation technique.

The application of the piezocone in the assessment of the quality of the improvement has the following advantages: it is fast (8 piezocones were performed per day at the site), it is practical (only one truck was used, with no need for secondary equipment and the option for use of lightweight equipment in case of difficult access) and the results obtained can be clearly interpreted.

2.2 *Soft clayey stratified soil*

The subsoil of Mexico City is made up of a very soft soil deposit with alternating hard lenses/layers. Figure 4 shows a typical probe of the area of a virgin lake to the depth of the first hard layer.

The use of the piezocone in this type of soil has proven favorable since it characterizes in detail the clay deposit and it is possible to determine the mechanical properties using correlations. However,

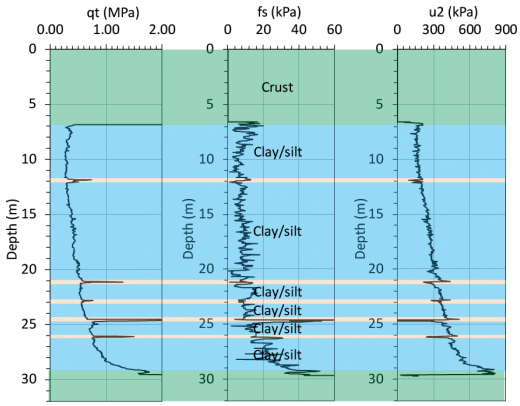

Figure 4. Probes using typical digital piezocones in the lacustrine zone.

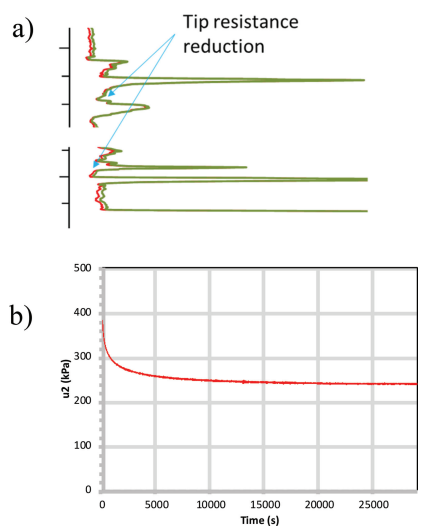

Figure 5. Some problems faced when the piezocone is driven into soft soil deposits. A. Alternation between hard lenses/layers and very soft ones, and B. Pore pressure.

use in this type of subsoil has the following problems (Fig. 5):

- *Crossing the alternating soft soils layers and hard lenses*. These alternations cause sudden changes in the resistance of the tip, from very high values to very low ones, happening repeatedly. This means that the instrumentation must guarantee low hysteresis in order to obtain trustworthy data.
- *The measurement of friction in the shaft*. In very soft soils, where the water content is near the liquid limit, the drive of the cone remolds the soil causing thixotropy. In such conditions, the soil behaves as a liquid, so it is difficult to measure parameter f_s. This problem has been solved by using special sheaths (shaft striation) and increasing the resolution of the equipment.
- *Hard layers that are less than 0.5m thick*. The drive of the cone in very soft soil deposits is interrupted when it comes to a hard layer. When trying to go through this layer, no matter the thickness, the tooling has lost its verticality and on occasions the bars have broken. This factor generates a decrease in the performance of the exploration since a different technique must be used to cross or to explore the hard layer. The stretch where the cone was driven also must be shored in order to continue driving the cone to the lower part of the hard layer. This causes an increase in time and cost of the exploration, due to the need for more equipment and another perforation method to cross through the hard layer.
- *Measuring pore pressure*. In very soft soils where the permeability coefficient is very low, determining equilibrium pore pressure using pore pressure dissipation testing has a disadvantage in that the time it takes to reach equilibrium in the reading is over 6 hours, so it is not possible to perform continuous driving. Besides, leaving the cone in the soil for long periods of time causes the soil to stick to the cone shaft and to the entire length of the tubing, making extraction difficult and occasionally causing the loss of the entire tooling. In the case of Mexico City, during cone driving only dynamic pore pressure is measured and the static pore pressure of the soil is determined by recoverable Viber Wire piezometers.
- *Fissures*. The presence of fissures in clay deposits randomly causes abrupt drops in the reading of parameters q_T and f_s. Unfortunately, these drops can be associated with errors in measurements and not attributed to the presence of fissures.

Another interesting aspect is the determination of mechanical properties. In the specific case of very soft soils in Mexico City, there are correlations with the following mechanical parameters (eq 2 to 5; Rangel *et al*, 2017): non-drained shear resistance (s_u) in normally consolidated soils, remolded cutting resistance (s_{rem}) and compressibility modules in virgin stretches and in discharge (C_c y C_r).

$$s_u = \frac{q_T}{N_k(\approx 13)} \tag{2}$$

$$s_{rem} = f_s \tag{3}$$

$$C_c = 217.6(q_T)^{-0.6} \tag{4}$$

$$C_r = 6.4(q_T)^{-0.45} \tag{5}$$

Usually the period of geostatic vertical stress is included in the correlation $q_T.vs.s_u$, however, in the case of clays in Mexico City, this parameter is

of no greater influence, so it is often omitted. As well, the correlation index obtained for the relation q_T.vs.C_r is very low, so the value of C_r is only indicative.

2.3 *Tailing deposits*

Tailing deposits are mining residues that have generally been through a process of mechanical disintegration, and so are made up mainly of granular materials. The characterization of these materials is complex, due to the heterogeneity of the deposit, in depth and horizontally, and because unaltered sampling is difficult.

In order to define the stratigraphic characteristics and to have an order of the magnitude of the mechanical parameters of tailing deposits, two piezocone soundings were performed, one in the area where the tailings contain fines (Fig. 6a, CPTu-03), and another where the tailing is mainly granular (Fig. 6b, sounding CPTu-05).

In Fig. 6 we can see the continuous variation in parameters q_T, f_s and u_2 up to 50 m deep, as well as a strongly oscillatory behavior produced mainly by the heterogeneous composition of the tailing. Just as in clay and sandy soils, the records show a tendency in which values q_T and f_s grow proportionally to the depth and when examining the curves in detail it is possible to distinguish the sequence of depositing of tailings when the tendency is inverted.

The CPT-u has a high-level potential due to the fact that using lightweight equipment (100 kN penetrometer) the tooling has been able to drive this tool into areas that are difficult to access and perform soundings to a depth of 50 m.

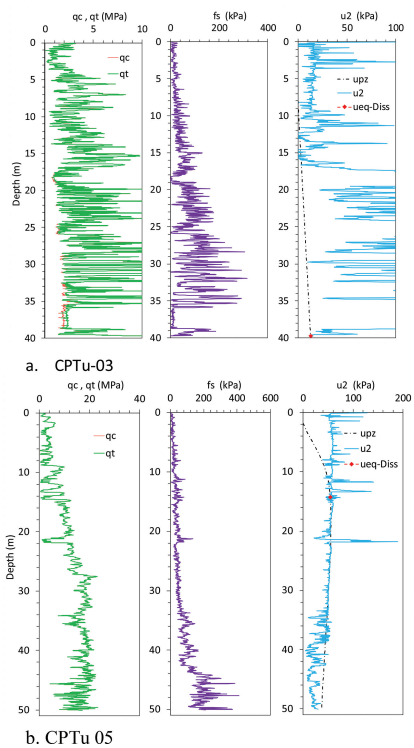

Figure 2.6. CPTU carried out in fine and granular zones (a and b, respectively).

3 CONCLUSIONS

From what we have examined previously, we can make the following conclusions:

- Three cases of the use of the piezocone in Mexico are presented: In clean sand deposits, in soft clayey stratified soils with hard layers and in tailings deposits.
- In the case of clean sand deposits, the efficiency of the improvement of the deposits using Vibrocompactation was evaluated. Two cases were presented, one in which the improvement was efficient and one in which it was inadequate. The evaluation of the improvement was done by comparing the measurements of D_r before and after the improvement. There are three main advantages to using the piezocone as a measure of control in compactation: speed, simplicity and clarity in the interpretation of results.
- The use of the piezocone in very soft soils allows for the stratigraphy to be detailed and for mechanical property values to be obtained using correlations. However the implementation has the following challenges: when crossing through alternating layers of soft and hard soils there are errors in the measurements of parameters q_T and f_s, there is difficulty in the measuring of shaft friction, f_s, caused by remolding during cone drive, the impossibility to cross hard lenses/layers that have a thickness of more than 0.5 m, it isn't possible to measure static pore pressure due to low soil permeability, and the cracking of the soil causes errors in measurement.
- Stratigraphic characteristics were evaluated for tailings using the piezocone. This technique has great potential since it is possible to perform deep explorations with lightweight equipment.

REFERENCES

Keller, 2016. "Subsoil improvement at site Alvarado", personal communication.

Rangel-Núñez J.L., Rivera, I, Ibarra E & Flores, R., 2017. Experiences acquired in the use of the seismic flat dilatometer (SDMT) and piezocone (CPTu) for an enhanced site characterization of Mexico City soft clay, *Proceedings of the 19th International Conference on Soil Mechanics and Geotechnical Engineering*, Seoul 2017.

Cone Penetration Testing 2018 – Hicks, Pisanò & Peuchen (Eds)
© 2018 Delft University of Technology, The Netherlands, ISBN 978-1-138-58449-5

Evaluation of complex and/or short CPTu dissipation tests

E. Imre
Alternative Energy Techn, Knowledge Center, Obuda University, Budapest, Hungary

T. Schanz
Ruhr University of Bochum, Germany

L. Bates & S. Fityus
University of Newcastle, Newcastle, Australia

ABSTRACT: A case-study of evaluating nine u_2 CPTu dissipation tests (I to V types) of small t_{50} with 3 published methods is presented. One method is a one-point fitting method, based on I_r and t_{50}. The two newer methods implies automatic, multi-point curve fitting, with output for not only c but also for the initial condition, the parameter error and some reliability information. The results indicate that the dissipation tests are good tools to identify soil property/layer boundary information, the new methods can be used to study the partly drained penetration and to get c value using tests shorter than the t_{50} testing time.

1 INTRODUCTION

Nine, partly drained u_2 dissipation tests (Robertson, 2017) with various shapes (from type I to type V) were evaluated using three methods; a t_{50} method and two newer ("fast and slow") methods, to determine the coefficient of consolidation c. The dissipation test data were used for soil identification. The two newer methods were also applied to truncated tests (tests shorter than t_{50}).

The values of c identified using the complete dissipation test showed the usual, similar pattern indicating that the newer methods can be used in practice, like to the t_{50} method.

Concerning shorter tests than t_{50}, the values of the c identified using the fast method showed that c became constant after a so called minimum testing time t_{min} with larger t_{50}-t_{min} for less dilatory tests.

The identified initial condition gave some information on partly drained penetration (see eg., Sheng et al, 2014).

2 METHODS

2.1 *The evaluation methods*

The method of Teh-Houlsby (1988) is based on a two-dimensional consolidation model and one-point fitting, using I_r information, typically based on t_{50}.

The assumed initial pore pressure distribution is determined by the strain path method, in soft, normally (NC) to lightly over-consolidated (OC) soils. However, in OC soils the solution provide a poor estimate of the initial distribution of pore pressure, it cannot always handle if t_{50}< 50 s, and if the dissipation is starting from less than u_0 values. No reliability information is given (e.g. goodness of fit, uniqueness and parameter error).

In the newer methods, called "fast" and "slow" methods (some second long and some 10 minute long, resp., Imre et al, 2013, see the App.), the c and the initial pore pressure distribution is identified with an automatic, conditional minimisation in two different ways, with different computer time. The output includes parameters (c, initial condition), parameter error, uniqueness and goodness of fit information in both cases. The newer, routine methods are not using I_r information but the c result is needed to be adjusted for r_1 (varying with filter position, see section 4.1.2.).

In the fast method-versions ("fast 1,.. fast k"), the coefficients of a k-jet of the infinite series analytical solution are identified. The so resulted initial condition is limited by the number of terms in the jet (for k = 1, it is monotonic, for k > 1 it is non-monotonic), less than about 5 terms are used in practice since the method is numerically unstable for larger jet term number k than about k = 5 in at present state.

In the slow method k = 200 coefficients are determined beforehand for a non-monotonic, physically admissible, parametric shape function series of the initial pore pressure distribution (see

the App.) The shape functions with four integer parameters (s, n_1, n_2, sign) describe both the negativity and the widths of the shear zone (with parameters n_1 and s, resp.), and the positivity outside the interface shear zone, with parameters n_2). The shape functions vary over a wide range, the mirror images are related to the negative multipliers while c is identified.

2.2 *Soil types on the basis of dissipation data*

Three CPTu profiles were made up to a depth of 18 m at a site in California, with nine dissipation tests (Fig. 1). The dissipation tests were represented forming two groups, in Figure 2, using their initial excess pore pressure Δu and $\Delta u/u_0$ data as follows.

Tests 4, 7, 8 are with $t_{50} < 1$ min, are type III and V, with small initial pore water pressure at the shaft $\Delta u < 100$ kPa, with $-12 < \Delta u/u_0 < 1.7$. These tests are basically drained. In the classification of distribution of pore pressures in granular soils (Fig. 3), type V tests are loose sand, type III are loose silt. The $\Delta u/u_0 = -12$ extreme value is caused by the small u_0.

Tests 1, 3 are transitional in terms of drainage parameters, being possibly silty soils. Test 1 is type

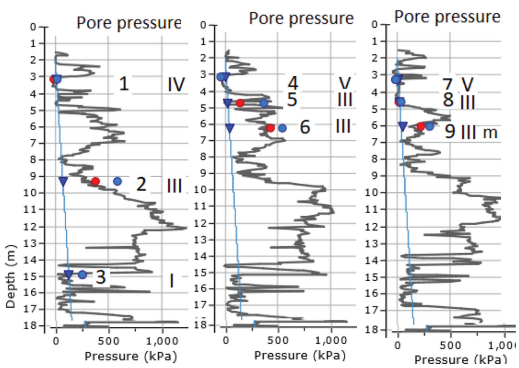

Figure 1. Dissipation tests 1 to 9 in CPT1 to CPT3.

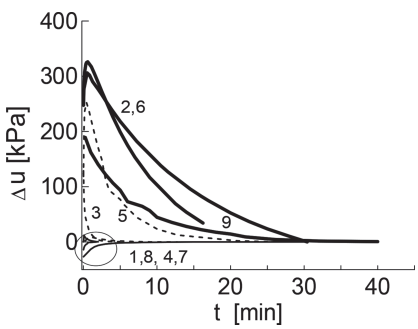

Figure 2. Dissipation curves.

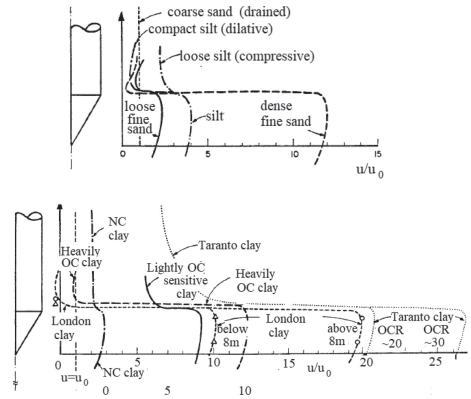

Figure 3. Distribution of initial pore pressures in granular soils (upper) and plastic+ soils (lower). Robertson et al, 1986.

Table 1. The list of dissipation tests.

	t [min]	t_{50} [min]	u_0 [kPa]	$\Delta u/u_0$	$u - u_0$ [kPa]	Ir
1	7	1,30	8,2	**–0,5**	12,2	100
2	22	5,47	79,1	7,6	520,9	200
3	7	0,15	130,0	2,0	130,0	100
4	15	0,55	3,4	–10,2	38,4	100
5	25	1,95	24,9	14,9	345,1	100
6	30	11,63	41,6	13,2	508,4	200
7	5	0,13	4,7	–0,5	22,7	100
8	6	0,27	27,0	1,6	17,0	100
9	45	4,12	50,0	6,2	260,0	200

IV with $t_{50} < 1{,}5$ min with small $\Delta u < 100$ kPa and with negative $\Delta u/u_0 = -0{,}5$. It can be OC or can be situated close to a more permeable layer boundary. Test 3 is type I, with $t_{50} < 1$ min, but with medium stress 100 kPa $< \Delta u <$ 150 kPa, with $\Delta u/u_0 = 2$, can be near NC.

Test 5 is with high stress and medium $t_{50} \sim 2$ min, $\Delta u/u_0 = 15$, possibly the soil is OC clayey silt. Tests 2, 6 and 9 are likely lightly OC to OC clays, the penetration is undrained or slightly drained, with $t_{50} > 4$ min, with $\Delta u > 150$ kPa, with $6 < u/u_0 < 14$.

Real negative pressures occurred in three cases modifying the Figure 3 upper diagram. The I_r was selected approximately, as 100 for all non-clay soils, and as 200 for clays (Table 1, Figs. 2, 3).

3 RESULTS

3.1 *Comparing c values of long tests*

The identified c values are represented in Figure 4, in Tables 2 and 3. The c_{fast} improved with k for

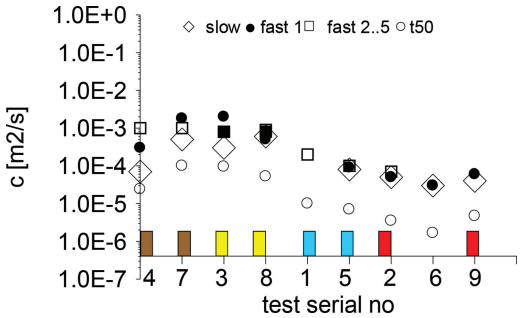

Figure 4. Identified c, rearranged from granular to plastic.

Table 2. Identified fast c compared to slow $c[c_{fast}/c_{slow}]$.

Sign, soil		Fast $k = 1$	Fast, max k
4 - CPT2/1	V	4,3	0,3
7 - CPT3/1	V	3,6	0,3
3 - CPT1/3	I	6,7	0,3
8 - CPT3/2	III	0,8	1,6
1 - CPT1/1	IV	14,3	0,6
5 - CPT2/2	III	1,1	1,1
2 - CPT1/2	III	1,0	1,4
6 - CPT2/3	III	1,0	1,0
9 - CPT3/3	III/I	1,5	0,3

clays: 1 to 1.5, clayey soils: 1 to 1.13, silt-sand: 1 to 2

Table 3. Newer methods c compared to c of t_{50} $[c_{new}/c_{t50}]$.

		Slow	Fast $k = 1$	Fast last k
4 - CPT2/1	V	2,9	12,5	4,2
7 - CPT3/1	V	5,0	18,0	5,0
3 - CPT1/3	I	3,2	21,1	6,3
8 - CPT3/2	III	11,4	9,5	15,2
1 - CPT1/1	IV	0,7	10,0	6,0
5 - CPT2/2	III	11,4	12,9	14,3
2 - CPT1/2	III	14,3	14,3	20,0
6 - CPT2/3	III	17,6	17,6	17,7
9 - CPT3/3	III/I	8,5	12,8	4,3

granular soils, the ratio values given for granular soils were related to the largest k with the best solution in Tables 2, 3.

The ratio c_{fast}/c_{slow} for the new methods was equal to 1–1.5 for clays, 1–1.2 for clayey mixtures, 1–2 for silt-sands.

The c of the t_{50} method compared with c of new methods showed the following. For granular soils the new methods have larger c by about a factor of 3 to 6 (if the k values for the fast method were larger than 1).

In clay the new method c was greater by generally a factor of 10 to 20 except for the near-monotonic test where this factor was 8. (Where the t_{50} method c differed more from the slow method c, the initial condition was generally non-optimal).

3.2 *The c values of the truncated tests*

Truncated data with test duration less than the t_{50} time were evaluated for the tests with $t_{50} > 4$ min (Figs. 5, 6) with the slow method and the fast 1 method. Only the fast 1 method gave monotonic results with t, there was a minimum testing time t_{min} such that for $t > t_{min}$ the identified c value was about constant. The $t_{min} < t_{50}$ was met for each case. In the near-monotonic test 9, a one-minute long test gave the proper c value. In tests 2 and 6 $t_{min} = t_{50} - d$ was found with increasing d for increasing monotonicity.

3.3 *Evaluation details – newer methods*

For sandy soils (tests 4 and 7) with 0.55 and 0.13 min t_{50} times and with type V dissipation (Fig. 7, Tables 1 to 4), the initial pore water pressure shape functions identified with the slow method are negative; and are also negative with the

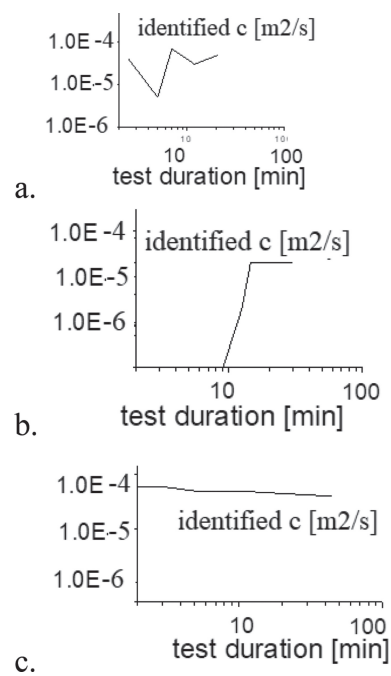

Figure 5. Truncated data, slow method, tests 2, 6, 9.

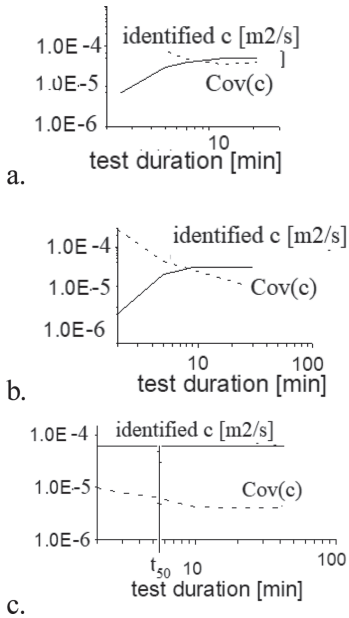

Figure 6. Truncated data, fast 1 method, tests 2, 6, 9.

Table 4. Identified shape function parameters, slow method.

	s [–]	n_1 [–]	n_2 [–]	sign	
4 - CPT2/1	6	2	2	–	V
7 - CPT3/1	1–	3	3	–	V
3 - CPT1/3	1–	2	3	+	I
8 - CPT3/2	5	3	5	+	III
1 - CPT1/1	7+	5+	1-	+	IV
5 - CPT2/2	7+	2	8	+	III
2 - CPT1/2	7+	2	9+	+	III
6 - CPT2/3	7+	2	7	+	III
9 - CPT3/3	6	2	5	+	III/I

+/– boundary value (25% silt-sand, 66% clay, 100% silt).

fast $k = 1$ methods, partly positive for the fast $k > 2$ method (which is probably qualitatively the best).

For assumingly transitional soil with types IV or I dissipation (test 1 and 3), with t_{50} of 1.2 and 0,15 min (Figs 8 and 9, Tables 1 to 4), the initial condition is starting to be positive but is non-optimal with the slow method for test 1, the s value is too small.

Three tests (2, 6, 9) are III, III and III~I type tests in clay with t_{50} of 5.47, 11.63, 4.12 min. The initial condition is non-optimal in cases 2 and 6. In Figures the results related to 10 and 11 tests 9 and 2 are shown, the fast 1 and 2 methods gave realistic initial conditions, resp.

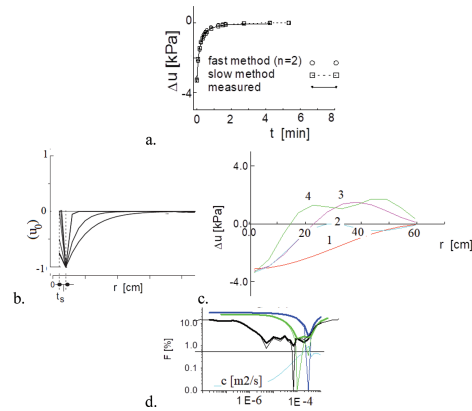

Figure 7. Test 4. Type V dissipation. (a) Measured and fitted data. (b) to (c) Identified initial condition (slow method, $n_1 = 3$. $n_2 = 3$. $s=1$, fast method $k = 1..4$). (d) Merit function sections for the reliability tests (from left to right: slow, fast $k = 2$, fast $k = 1$).

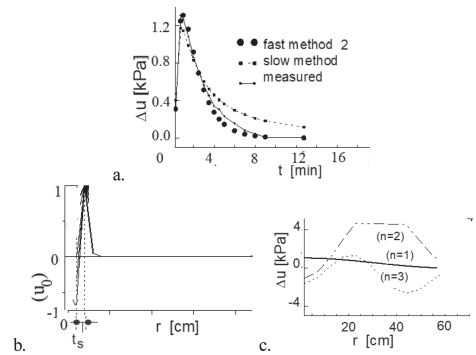

Figure 8. Test 1, type IV dissipation. (a) Measured and fitted data, slow method and fast method. (b) and (c) Identified initial condition (slow method, $n_1 = 5$, $n_2 = 1$. s = 7, fast method k = 1..3).

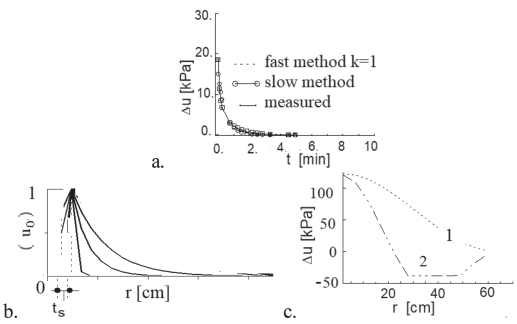

Figure 9. Test 3, type I. (a) Measured and fitted data. (b) and (c) Identified initial condition (slow method, parameters: $n_1 = 2$, $n_2 = 3$. s = 1, fast method k = 1,2).

4 DISCUSSION

4.1 *Initial condition in partly drained cases*

4.1.1 *Shear zone in sand*

The results indicate that the initial pore water pressure for loose silts-sands can be (real) negative with type V dissipation curves (Figs. 3 and 7).

The rebound around the shaft after a large drained compression below the tip may cause OC state in the originally loose sand. The OC clay and the OC sand behaviour differ in the extent of negativity, since the deformation of the soil grains in clay may be large but this is not the case for sands.

The hypothesis that the (negative) pore water pressures may be influenced by the undrained deformability of the grains and pore fluid, follows from the identification results of several conventional compression tests (see eg., Imre et al, 2013(a)).

Moreover, earlier results indicate that the shear zone thickness s may increase with decreasing plasticity or with increasing OC state (see the correlation trends between the fitted parameters n_1, n_2 and s, with the parameter c of 70 dissipation tests undertaken at Hunter river, Australia, Bates et al, 2013).

The shape functions were identified with negative sign (Tables 4, 5) for granular soils. This may have occurred due to the large negative and small positive part of the initial condition, indicating large shear zone size parameter s, also.

4.1.2 *The displacement domain*

In the newer methods, the pair $n = (r_1 - r_0)/ r_0 = 36$ for $I_r = 150$ (from Baligh, 1986) are used in u_3. Using the approximate time factor, a model law applies (see App., Imre et al, 2010) since in filter position u_2 the n is different, and all c values are needed to be divided by a constant of 1 to 1.5. The effect of the rigidity index I_r can be taken into account if the time factor of Teh and Houlsby is combined with the time factor derived in the consolidaton modelling of the newer methods (see the App.) as follows:

$$n^2 = (r_1 / r_0 - 1)^2 = T^{T-H} / T^1 * I_r^{1/2} \quad (1)$$

From Eq (1), the value of $n = (r_1 - r_0)/ r_0$ is dependent on the rigidity index I_r, n and r_1 is smaller for less I_r than for larger I_r. For $I_r = 100$ and 200; n = 32,53 and n = 38,49 are valid, resp., in filter position u_3.

Table 5. Uniqueness, initial condition optimality, fit "by eye".

		Unique slow	Bad fit quality			Optimality	
			Slow	k = 1	k > 1	Fast	Slow
4 CPT2/1	V	Yes					
7 CPT3/1	V	No				–	
3 CPT1/3	I	Yes		+	+	–	–
8 CPT3/2	III	No		+		–	
1 CPT1/1	IV	No	+	+			–
5 CPT2/2	III	Yes		+			–
2 CPT1/2	III	Yes		+			–
6 CPT2/3	III	No	+	+		–	–
9 CPT3/3	~I	Yes					

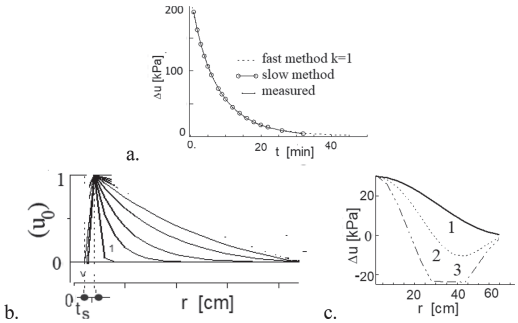

Figure 10. Test 9, type III~I (near type I) dissipation. (a) Measured and fitted data. (b), (c) Identified initial condition (shape function parameters: $n_1 = 2$, $n_2 = 3$. s = 1).

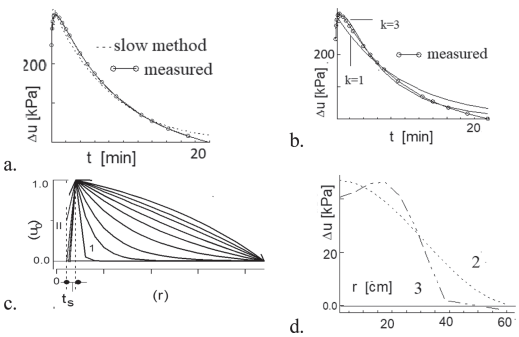

Figure 11. Test 2, type III dissipation. (a), (b) Measured and fitted data. (c), (d) Identified initial condition (shape function parameters: $n_1 = 2$, $n_2 = 9$. s = 7, fast method k = 1..3).

5 SUMMARY, CONCLUSIONS

5.1 *General results with the three methods*

Concerning the comparison of the three methods, the results can be summarized as follows.

The coefficient of consolidation (c) result of the three methods showed similar pattern here and in the previous studies (Imre et al, 2005, 2014). The newer methods gave higher c values, than

the t_{50} time method. This result indicates that the newer methods are reliable. The differences can be explained by the approximate, non-optimal initial conditions of the newer methods, and by the approximate I_r information (the shear modulus may decrease with strains by a factor of 20 or 30, Mayne, 2007).

5.2 *Some notes on the newer methods*

5.2.1 *Uniqueness, goodness fit, initial condition*

The slow method did not have unique solution in less than half of the cases (Table 5), in those cases the unique solution of the fast 1 method was used to select the good solution for the slow method.

The fit of the slow/fast methods was good for all or 75% of the silt-sands, for 66% or all clays and, was not good for transitional test 1 in either case (Table 5). The fast method had good fit in clays with for $k = 1$ or 2, in granular soils for larger k.

The limitations of the newer methods can be attributed to the non-optimal initial conditions, both methods need extension (additional shape functions: slow method, fast method: larger k values).

The shape functions were acceptable for slightly OC clay dissipation curves, were limiting for more dilatory curves and not acceptable with positive sign for granular soils (Tables 4, 5).

Results show that the shear zone thickness s may increase with decreasing plasticity or increasingly drained penetration, which also follows from earlier non-monotonic evaluations.

5.2.2 *Truncated tests*

By evaluating truncated tests with test duration t shorter than the t_{50} time, the c - t function was determined. The c - t function identified for the fast 1 method was monotonic, and the c was constant for larger test durations t than a limit time t_{min}. The t_{min} was smaller if the dissipation test was less dilatory.

The short computer time of the fast 1 method allows the identification the c value in each minute of a dissipation test. The so determined c - t function can be used to terminate the dissipation test after t_{min}, when the identified c value becomes constant. Further research is suggested on this, and on the minimization of dilatory nature of the dissipation.

5.3 *The dissipation tests in the geotechnical design*

By representing the dissipation curves in this work (Fig. 2), the subgraph area gave soil type information based on the simple fact that both parameters Δu, t_{50} are increasing with plasticity (except in the presence of a layer boundary). The ratio $\Delta u/u_0$ gave information to density or NC-OC state (Fig. 3).

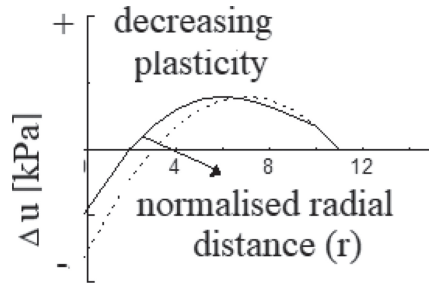

Figure 12. The change in the initial excess pore water distribution for more drained penetration or for less plastic soil.

In this work real negative pressures occurred in three granular soils, modifying the upper diagram in Figure 3, indicating that the initial pore water pressure distribution is not fully known for sands at present. The initially loose silts-sands may behave as OC soils due to the large compression below the tip. However, the initial condition may differ from the OC clay case, due to the different grain material compressibility.

Further research is suggested on silts-sands (eg., using DEM, and real measurements) and, on the initial condition in case partly drained penetration.

ACKNOWLEDGEMENT

The support of Professor Peter K. Robertson is used for this research which is greatly acknowledged.

REFERENCES

Baligh, M.M. (1986). Undrained deep penetration, II. pore pressures. *Geotechnique*, 36(4): 487–503.

Bates L, Bishop D, Fityus S, Hegedüs M, Imre E The joint evaluation of some pore water pressure and cone resistance dissipation test records. *ISC–4. Porto de Galinhas, Brazília*, CRC Press – Taylor and Francis Group, 2013. 881–889. (ISBN:978-0-415-62136-6).

Imre, E.; Rózsa, P.; Bates, L.; Fityus, S (2010) Evaluation of monotonic and nonmonotonic dissipation test results.

Computers and Geotechnics, 37, Issues 7–8, 885–904. DOI: 10.1016/j.compgeo.2010.07.008.

Imre, E., Vijay P. Singh and Fityus S. 2013(a). The modelling of some point-symmetric tests 166–185. *Proc. of the 3rd Kézdi Conference. Budapest, Hungary*, 2013.05.28.ISBN 978-963-313-081-0.

Imre E, Schanz T, Hegedűs Cs 2013. Some thoughts in non-linear inverse problem solution. In: EURO:TUN 2013. Bochum, 04.17-2013.04.19. pp. 357–365.

Imre E, Firgi T, Juhász M, Hazay M, Hegedűs M, Bakacsi Zs, Singh V 2014. CPTu pore water pressure dissipation tests in saline environment. *3rd*

International Symposium on Cone Penetration Testing. Las Vegas, pp. 675–682.
Mayne P.W. 2007. In-Situ Test Calibrations for Evaluating Soil Parameters. *Proc. characterization and Engineering Properties of Natural Soils (2007), Singapore December 2006.* Volume 3. p.1. (Balkema) ISBN: 9780415426916.
Sheng, D, Kelly, R, Pineda, J, Bates, L. Gregg Drilling; 2014. Numerical study of rate effects in cone penetration test. *3rd International Symposium on Cone Penetration Testing. Las Vegas.* 419–428.
Robertson P.K Campanella R G, Gillespie D.G. Greig J. 1986. Use of piezometer cone data. *ASCE Specialty conference IN-SITU'86.* SM 92.1263–1280.
Robertson P.K. 2016. Fallon Dissipation test Report. Manuscript.
Teh, C.I. and Houlsby, G.T. 1988. Analysis of the cone penetration test by the strain path method. *Proc. 6th Int. Conf. on Num. Meth. in Geomechanics, Innsbruck.* 1:397–400.

APPENDIX: SUMMARY OF NEWER METHODS

Consolidation model

The analytical solution of the spherical coupled 1 model (Table A1) for the pore water pressure u and its derived time factor T:

$$u(t,r)=\frac{1}{\sqrt{r}}\sum_{k=1}^{\infty}C_k e^{-\gamma_k^2 \cdot c_h \cdot t}\left\{\begin{matrix}[J_{0.5}(\lambda_k r)+\mu_k Y_{0.5}(\lambda_k r)]\\ -[J_{0.5}(\lambda_k r_1)+\mu_k Y_{0.5}(\lambda_k r_1)]\end{matrix}\right\} \quad \text{(A1)}$$

$$T=\frac{ct}{(r_1-r_0)^2} \quad \text{(A2)}$$

where r is space coordinate, t is time, J_n and Y_n are Bessel functions, c is coefficient of consolidation, the λ_i, μ_i depend on r_0 and r_1 and C_i ($i = 1$ to k) on the initial condition, T time factor.

Evaluation methods

The two methods (slow, fast) differ in computer work which is smaller by about 2 order of magnitudes for the fast method.

In the fast method, the output includes the C_i ($I = 1$ to k) linearly dependent coefficients for a few terms, the c nonlinearly dependent parameter and, the parameter error is computed for the linearized model. For $k = 1$, the method is monotonic and has unique solution, for $k > 1$ non-monotonic.

In the slow method, output includes the c and the identified, initial condition shape function (Fig. A1). Every shape function parameter is nonlinearly dependent except the scaling, resulting in large numerical work. The C_i ($i = 1, 2\ldots 200$) values for each shape function are built in, being determined beforehand.

Table A1. One dimensional linear models (Imre et al., 2010).

Type	Spherical	Cylindrical
Uncoupled	Torstensson	Soderberg
Coupled 1	Imre-Rózsa	Imre-Rózsa
Coupled 2	Imre-Rózsa	Randolph-Wroth

The initial condition shape functions

The initial excess pore water pressure u_0 is the sum of a negative part due to the interface shear in a thin zone along the shaft and a positive part due to the penetration normal stresses. The first part is described by one of 5 linear functions within the shear zone (between r_0 and r_s) (Fig. A1, I to V). The second part ($r_s < r \le r_1$), is given the function described by:

$$u_0(F,r)=\left(1-e^{\frac{r-\eta}{F}}\right)/\left(1-e^{-\frac{\eta-r_s}{F}}\right) \quad F\neq 0;\ F\neq\infty \quad \text{(A3)}$$

with fixed F values. Seven r_s values (varying between $0.1r_0$ and $2r_0$) were used, given in Table A2. Hence, 350 shape functions are resulted. For negative scaling, 350 mirror image shape functions are resulted.

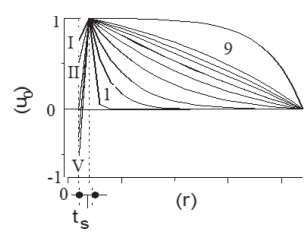

Figure A1. Shape functions. The $n_1 = 1$ to 5 correspond to I to V linear functions in the sheared zone, $s = 1$ to 7 is related to the ts sheared zone thickness ts, $n_2 = 1$ to 9 for the positive part, and a positive or negative scaling constant is used to adjust.

Table A2. Thickness values of the interface shear zone

s [–]	t_s [cm]	$r_s = r_o + t_s$ [cm]	$s = t_s/r_o$[–]
1	0.1	1.85	0.05
2	0.21	1.96	0.12
3	0.42	2.17	0.24
4	0.84	2.59	0.48
5	1.89	3.64	1.08
6	2.94	4.69	1.68
7	3.36	5.11	1.92

Taylor & Francis
Taylor & Francis Group
http://taylorandfrancis.com

Cone Penetration Testing 2018 – Hicks, Pisanò & Peuchen (Eds)
© 2018 Delft University of Technology, The Netherlands, ISBN 978-1-138-58449-5

New Russian standard CPT application for soil foundation control on permafrost

O.N. Isaev & R.F. Sharafutdinov
Gersevanov NIIOSP, Moscow, Russia

N.G. Volkov
Fugro Group, Moscow, Russia

M.A. Minkin & G.Y. Dmitriev
FUNDAMENTPROIECT, Moscow, Russia

I.B. Ryzhkov
BGAU, Ufa, Russia

ABSTRACT: In 2016 in Russia, a new Standard STO 36554501–049–2016 "CPT Application for Soil Foundation Control on Permafrost" was developed and enacted. The standard determines the basic requirements for CPT (Cone Penetration Testing) application for geotechnical control and investigation of the foundations located on permafrost soils. The standard applies to soils which are dispersive, natural and man-made, frozen/freezing and thawed/thawing. The composition and condition of these soils should allow continuous penetration of a penetrometer used for CPT. Many chapters of the standard are relevant and applicable for performing geotechnical site investigation for foundation design purposes. Particular attention is paid to the CPT probe applications with additional sensors.

1 INTRODUCTION

In 2016 in Russia, a new Standard STO 36554501-049-2016 "CPT Application for Soil Foundation Control on Permafrost" was developed by N.M. Gersevanov NIIOSP involving Fugro Consultants Inc., Houston, USA, "GEOINZHSERVICE" LLC, "FUNDAMENTPROJECT" JSC, BGAU and "PIKA-TECHNOSERVICE" STC (Standard 2016).

The standard establishes requirements for CPT procedure using electrical probes for geotechnical control and investigation (further—control) of the foundations of buildings and structures (further—structures) under construction and operated ones, located on permafrost soils.

2 RELEVANCE AND OBJECTIVES OF STANDARD DEVELOPMENT

Control over the foundations of buildings and structures under construction and operated ones, located on permafrost soils is a challenge that must be met by surveyors, designers, builders and building operation and maintenance services.

Despite the relevance of this problem and the efforts made in recent years in Russia to develop and improve new approaches, techniques and equipment, it has not been handled yet. The current standards do not adequately illustrate the issues concerning control over the foundations, and the potential and experience of the new in-situ express methods are not sufficiently used for soils.

CPT holds a special place among the in-situ express methods (Lunne et al. 2004; Minkin 2005; Ryzhkov & Isaev 2016). The studies carried out in Russia (Volkov & Isaev 1983; Isaev 1989; Isaev et al. 1995; Dlugach et al. 1995; Isaev & Ryzhkov 2010; Isaev 2011a, 2011b, 2012a, 2012b; Sokolov et al. 2016) and abroad (Ladanyi 1976; Blouin et al. 1979; Ladanyi 1982; Woeller et al. 1991; Buteau et al. 2005; Fortier & Yu 2012; McCallum et al. 2014, 2014a) showed the applicability and effectiveness of CPT application on permafrost soils, particularly when using electrical probes equipped with additional sensors and devices.

3 STRUCTURE AND CONTENT OF THE STANDARD

The document consists of seven chapters, which reflect: the standard application limitations; normative references; terms and definitions, requirements for equipment, instruments, preparation and testing; main principles for the geotechnical control of foundations by CPT.

The sections of the standard contain conditions on the CPT application for the geotechnical control: soil types; soil temperature and temperature for monitoring well installation; state of soils and detection boundaries between frozen and non-frozen soils; groundwater mineralization and salinity of soil; groundwater level; corrosiveness of soils; consolidation of thawing soils; seismic soil liquefaction; site seismicity; thermophysical properties of soils; mechanical properties of frozen/non-frozen soils; mechanical properties of frozen soils after thawing; pile bearing capacity; pile driving capability to specified level.

Appendices, supporting and detailing the content of the main sections of the Standard, are: additional sensors in CPT cones; types of CPT cones and measured parameters; applicability of CPT cones depending on task of geotechnical control; applicability of CPT cones depending on soil conditions; design of special CPT cone with temperature sensor; diagram for determination of soil condition (frozen/non-frozen) according to CPT data; electrode location in special CPT cone equipped with an electrical resistivity sensor; CPT depth correction by inclinometer; examples for CPT locations on a studied site, depending on the number of test cycles; recommended CPT depth when controlling foundations of various engineering structures, etc.

4 GENERAL

The following are the most important provisions of the standard:

a. A list of additional sensors and devices, including the measured parameters and performed functions; the following types of special probes (Table 1). The cone tips may additionally include: a temperature sensor (T-CPT, RT-CPT, HT-CPT, T-CPTU); a temperature sensor and a heat element (HT-CPT); a pore pressure sensor (CPTU, T-CPTU, R-CPTU, S-CPTU); an electrical resistivity sensor (R-CPT, RT-CPT, R-CPTU); a seismic-acoustic sensor (S-CPT, S-CPTU); a gamma radiation sensor (GR-CPT); a gamma-gamma radiation sensor (GGR-CPT); a neutron-neutron radiation sensor (NNR-CPT).

Table 1. Types of special probes and measured parameters.

	Measured parameters											
Probe	q_c	f_s	α	T_c	u_2	J_e	v_p	v_s	I_γ	$I_{\gamma\gamma}$	I_{nn}	H
T-CPT	x	x	x	x								
R-CPT	x	x	x			x						
RT-CPT	x	x	x	x		x						
HT-CPT	x	x	x	x								x
S-CPT	x	x	x				x					
GR-CPT	x	x	x						x			
GGR-CPT	x	x	x							x		
NNR-CPT	x	x	x								x	
CPTU	x	x	x		x							
T-CPTU	x	x	x	x	x							
R-CPTU	x	x	x		x	x						
S-CPTU	x	x	x		x		x					

Note: Measured parameters: q_c – cone resistance; f_s – sleeve friction; α – inclination of the cone tip determined by inclinometer; T_c – cone tip temperature; u_2 – pore pressure between the cone and friction sleeve; J_e – current strength between the isolated electrodes; v_p and v_s – velocities of the primary and secondary seismaic waves; I_γ – flux density of the natural gamma radiation; $I_{\gamma\gamma}$ – flux density of the dissipated primary gamma radiation; I_{nn} – flux density of the moderated neutrons during dissipation in soil. H – heat element

b. Depth requirements (Tables 2 and 3) and requirements for the number and location of the CPT points taking into account the types of buildings and structures (local or linear, under construction or operated), the type of foundation and soil (plastic-frozen or hard-frozen), the principle of using soils as foundations (frozen, thawed or thawing soils are used).
c. Applicability of electrical probes (Table 4) depending on the type of probe, degree of soil dispersion (gravel-pebble, sandy, clays) and state of soil (thawed, plastic-frozen, hard-frozen). Probes incorporating a heat element (HT-CPT), which is located in the cone, are most used in frozen soils.

The standard considers controlling over the following (Table 5): types and varieties of soils and engineering geological sections; groundwater level; soil temperatures and thermometric wells; condition of soils; boundaries between thawed and frozen soils; salinity of soils and detection of cryopegs; corrosiveness of soils; consolidating of thawing and hardening of freezing soils; possible liquefying of thawed sands in dynamic and seismic effects; parameters of seismic microzoning of permafrost and thawed soils; physical and thermophysical properties of soils; strength and deformation properties of soils; mechanical prop-

Table 2. Recommended depth for CPT when controlling foundations of independent buildings and structures.

Type of foundation	Depth for CPT for soil foundation, frozen (Principle I) and non-frozen (Principle II): Principle I		Principle II	
Plastic-frozen soils				
Strip foundations with loads on a foundation (kN/m):				
– up to 500	10–12 m	from the foundation base	10–12 m	from the foundation base (but 5 m min. below the designed depth of soil thawing)
– up to 700	12–15 m		12–15 m	
– up to 1000	15–20 m		15–20 m	
Separate piers with loads on a pier (kN):				
– up to 2500	8–10 m	from the foundation base	10–12 m	from the foundation base (but 5 m min. below the designed depth of soil thawing)
– up to 5000	10–12 m		12–15 m	
– up to 10,000	10–12 m		12–15 m	
– up to 15,000	12–15 m		15–20 m	
– up to 20,000	15–20 m		20–25 m	
Pile foundations	5 m below the pile tip		5 m below the pile tip, but 5 m min. below the designed depth of soil thawing	
Slab foundations	3–5 m below the depth of the compressible thickness		5 m below the designed depth of soil thawing, but 7–10 m min. from the foundation footing	
Hard-frozen soils				
Strip foundations and separate piers	7–10 m from the foundation footing		–	
Pile foundations	3–5 m below the pile heel, but 10–12 m minimum.			
Slab foundations	12–15 m minimum.			

NOTE: Lower depths are taken for foundation soils with low ice content, greater ones—for icy ones and for foundation soils with high ice content.

Table 3. Recommended depth and distance between CPT locations for control of linear structure foundations.

Type of a linear structure	Distance between CPT points, m	Depth for CPT when using dispersed foundation soils on the principle: I	II
Railways and highways	50–200	3–5 m below the designed depth of soil seasonal thawing	3–5 m below the designed depth of soil thawing under the mass of the embankment, but 10–12 m max.
Bridges, viaducts, elevated roads and overhead power lines	Piers on-site, by 1–2 points	5 m below the pile heel	5 m below the pile heel, but 5 m min. below the designed depth of soil thawing
Engineering underground networks (water pipeline, sewage, heating networks, gas pipeline)	50–150	10–15	3–5 m below the designed depth of soil thawing, but 12–15 m min.
Main pipelines (oil and gas pipelines): – above-ground routing (on piers);	50–100, piers on-site	3–5 m below the depth of pier installation	3–5 m below the designed depth of soil thawing under the pier, but 3 m min. below the pier installation depth
– in the embankment, underground routing	50–100	7–10 m below the pipeline	3–5 m below the designed depth of soil thawing

Note: Lower depths are taken for foundation soils with low ice content, greater ones—for icy ones and for foundation soils with high ice content.

Table 4. Applicability of electrical probes with regard to soil conditions.

Probe	Dispersed soils						
	Thawed			Frozen			
	Gravel-pebble	Sands	Clays	Plastic-frozen sands	Plastic-frozen clays	Hard-frozen soils	Icy soils
Probes without heat elements CPT, T-CPT, R-CPT, RT-CPT, S-CPT, GR-CPT, GGR-CPT, NNR-CPT, CPTU, T-CPTU, R-CPTU, S-CPTU	C	A-B	A-B	C-D	B	C-D	C-D
Probe with a heat element HT-CPT	C	A-B	A-B	B-D	A-B	B-C	B-C

Notes: The table illustrates domestic and foreign experience on applicability (possible pushing) of an electrical probe in various soil conditions. Applicability: «A» – high, «B» – medium, «C» – low; «D» – the probe is not used.

Table 5. Applicability of electrical probes with regard to the objectives of control over foundations.

Type of probe	Type of soil, section	Groundwater level	Soil temperature	Thermometric wells	State of soil (thawed or frozen)	Boundary between thawed and frozen soils	Cryopegs	Salinity of soil	Corrosiveness	Consolidation of thawing soils	Parameters of seismic microzoning	Possible liquefying of thawed sands	Soil density	Soil moisture	Thermophysical properties	Modulus of deformation	Modulus of shearing in small deformations	Consolidation ratio	Soil permeability	Strength properties	Properties of frozen soils in thawing	Pile bearing capacity
1	2	3	4	5	6	7	8	9	10	11	12	13	14	15	16	17	18	19	20	21	22	23
CPT	B/C	–	–	C/B	B	C	B	–	–	B	–	C	C/–	–	–	B	–	–	C/–	B	–	A
T–CPT	B	–	A	C/B	A	A	A	–	–	B	–	C	C/–	–	C	B	–	–	C/–	B	–	A
R–CPT	B/C	B	–	C/B	B	C	A	B	B	B	–	C	C/–	C	–	B	–	–	C/–	B	–	A
RT–CPT	B	B	A	C/B	A	A	A	B	B	B	–	C	C/–	C	C	B	–	–	C/–	B	–	A
HT–CPT	B	–	A	C/B	A	A	A	–	–	B	–	C	C/–	–	B	B	–	–	C/–	B	B	A
S–CPT	A/C	–	–	C/B	B	C	B	–	–	B	B	B	C/–	–	–	B	–	–	B/–	B	–	A
GR–CPT	A/C	–	–	C/B	B	C	B	–	–	B	–	C	C/–	–	–	B	–	–	C/–	B	–	A
GGR–CPT	B/C	–	–	C/B	B	C	B	–	–	B	–	C	A/B	–	–	B	–	–	C/–	B	–	A
NNR–CPT	B/C	A	–	C/B	B	C	B	–	–	B	–	C	C/–	A/B	–	B	–	–	C/–	B	–	A
CPTu	A/C	–	–	C/B	A–B	C	B	–	–	B	–	C	C/–	–	–	B	–	B	B/–	B	–	A
T–CPTu	A/C	–	A	C/B	A	A	A	–	–	B	–	C	C/–	–	C	B	–	–	C/–	B	–	A
R–CPTu	A/C	B	–	C/B	A–B	C	A	B	B	B	–	C	C/–	C	–	B	–	B	B/–	B	–	A
S–CPTu	A/C	–	–	C/B	A–B	C	B	–	–	B	B	B	C/–	–	–	B	–	B	B/–	B	–	A

Notes:
1.Applicability: “A”, “B”, “C” – the probe is used; “-” – the probe is not used.
2.Applicability: “A” – high, “B” – medium, “C” – low.
3.In the numerator—for thawed soils, in the denominator—for frozen soils.

erties of frozen soils with regard to their thawing; load-bearing capacity of foundation soils; quality of geotechnical works in foundation engineering.

REFERENCES

Blouin S., Chamberlain E., Sellmann P. and Garfield D. 1979. Determining subsea permafrost characteristics with a cone penetrometer. *Cold Regions Science and Technology*. № 1, pp. 3–16.

Buteau, S., Fortier, R. and Allard, M. 2005. Rate-controlled cone penetration tests in permafrost. *Can. Geotech. J*. 42, pp. 184–197.

Dlugach, A., Loktev, A., Okko, O., and Rokos, S. 1995. Soil mechanical properties and in situ temperature from arctic offshore CPT data. *In Proceedings of the International Symposium on Cone Penetration Testing, Linköping, Sweden, 4–5 October 1995. Swedish Geotechnical. Society, Linköping, Sweden*. Vol. 2, pp. 167–172.

Fortier, R. & Yu, W. 2012. Penetration rate-controlled electrical resistivity and temperature piezocone penetration tests in warm ice-rich permafrost in Northern Quebec (Canada). *15th International Conference on Cold Regions Engineering, Quebec, Canada*. pp. 1–11.

Isaev, O.N. 1989. Principal tasks in CPT development in permafrost soils. *All-Union Scientific Conference "Problems of engineering-geological investigations in cryolite zone". Magadan,* pp.180–182.

Isaev, O.N. & Ryzhkov, I.B. 2010. TCPT in permafrost: penetrometer—soil thermophysical interaction. *Proceedings of the Second International Symposium on Cone Penetration Testing. CPT`10, Huntington Beach,* USA.

Isaev, O.N. 2011a. Identification of the thawed and frozen states of soils by CPT. *Proceedings of the IX International symposium on engineering Permafrost. Mirny (Russia), September 3–7,* pp. 63–67.

Isaev, O.N. 2011b. Methods of frozen soil static sounding. Proceedings of the IX International symposium on engineering Permafrost. Mirny (Russia), September 3–7, pp. 69–73.

Isaev, O.N. 2012a. Ground state and determination of the strength and compressibility characteristics of plastic frozen soils with the help of the static probing method. *Proceedings of the Tenth International Conference on Permafrost (ICOP)*, 10, Volume 4, pp. 226–227.

Isaev, O.N. 2012b. CPT and TCPT in permafrost: constant rate and relaxation-creep penetrometer test procedures. *Proceedings of the 4th International Conference on Site Characterization. ISC-4 – Pernambuco, Brazil*.

Isaev O.N., Shvarev V.V., Konstantinov A.V., Tichomirov C.M. and Sadovsky A.V. 1995. Progress of the method of static sounding in the investigation of geotechnical properties of frozen soils. *Proc. of the Int. Simp. on Cone Penetration Testing, CPT'95 Linköping, Sweden, October 4–5*, vol. 2, pp. 179–186.

Ladanyi, B. 1976. Use of the static penetration test in frozen soils. *Canadian Geotechnical Journal*, 13(2): pp. 95–110.

Ladanyi, B. 1982. Determination of geotechnical parameters of frozen soils by means of the cone penetration test. *Proc. of the Second European Symposium on Penetration Testing. Amsterdam*, vol.1, pp. 671–678.

Lunne, T., Robertson P.K. and Powell J.J.,M. 2004. *Cone penetration testing in geotechnical practice*. London and New York: Spon Press, 312 p.

McCallum, A.B., Barwise, A. and Santos, R.S. 2014. Is the cone penetration test (CPT) useful for arctic site investigation? *Proceedings of the ASME 2014 33rd International Conference on Ocean, Offshore and Arctic Engineering. OMAE2014. San Francisco, USA*. 5 p.

McCallum, A.B. 2014a. A brief introduction to cone penetration testing (CPT) in frozen geomaterials. *Annals of Glaciology 55(68) 2014*. pp. 7–14.

Minkin, M.A. 2005. *Methodology and methods of engineering-geocryological investigations*. Uhta: Institute of Management, Information and Business. 252 p.

Ryzhkov, I.B. & Isaev, O.N. 2016. *Cone penetration testing of soils in geotechnics*. Stockholm, Sweden: Bokforlaget Efron & Dotter AB, 408 p.

Sokolov, I., Volkov, N. and Isaev, V. 2016. Cone Penetration Testing for Railways on Permafrost. *Proc. of the XI International Conference on Permafrost, Potsdam, Germany*.

Standard STO 36554501-049-2016 *"CPT Application for Soil Foundation Control on Permafrost. General guidelines"*. NIIOSP. Moscow. 54 p.

Volkov, F.E. & Isaev, O.N. 1983. Possibility of CPT application in plastic-frozen soils by S-832M CPT rig. Pile Foundations: *Collected scientific papers. NIIpromstroy, Ufa*, pp. 90–94.

Woeller, D.J., Weemees, I., Kurfurst, P.J., and Robertson, P.K. 1991. Penetration Testing for Arctic Soil and Permafrost Conditions. *In Proceedings of the Geotechnical Engineering Congress, Boulder, Colorado. American Society of Civil Engineers, New York*. Vol. 1, pp. 76–83.

Taylor & Francis
Taylor & Francis Group
http://taylorandfrancis.com

Cone Penetration Testing 2018 – Hicks, Pisanò & Peuchen (Eds)
© 2018 Delft University of Technology, The Netherlands, ISBN 978-1-138-58449-5

Thermophysical finite element analysis of thawing of frozen soil by means of HT-CPT cone penetrometer

O.N. Isaev, R.F. Sharafutdinov & D.S. Zakatov
Gersevanov NIIOSP, Moscow, Russia

ABSTRACT: The paper presents the results of the FE-based numerical thermophysical analysis of geocryological factors (soil type, temperature and moisture) and constructive-technological factors (power, heating and cooling time) having an effect on the thawing area size around the HT-CPT cone penetrometer. Based on the results obtained, the empirical dependencies are proposed to predict the depth and diameter of thawing area around the HT-CPT cone penetrometer.

1 INTRODUCTION

For the first time, CPT on permafrost soils was tested in 1974 by the Canadian researcher B. Ladanyi (Ladanyi, B. 1976). He showed technical feasibility and serviceability of CPT to study permafrost soils.

Today CPT is often used for geotechnical investigations or scientific research of permafrost soils (in particular, plastic-frozen), ice and snow.

Studies carried out in USSR and Russia (Volkov & Isaev 1983; Isaev 1989; Isaev et al. 1995; Dlugach et al. 1995; Minkin 2005; Isaev 2011a, 2011b, 2012a, 2012b; Ryzhkov & Isaev 2016; Sokolov et al. 2016) (65% of Russia's land is covered by permafrost) and abroad (Ladanyi 1976; Blouin et al. 1979; Ladanyi 1982; Lunne et al. 1997; Buteau et al. 2005; Fortier & Yu 2012; Adrian et al. 2014) have revealed high efficiency and serviceability of CPT. It makes it possible to evaluate the following: pile load-bearing capacity, modulus of deformation, equivalent adhesion, piling up to the specified depth, soil condition (thawed or frozen), etc.

CPT is efficiently used in permafrost if cone penetrometers are equipped with special sensors and devices—temperature sensor (T-CPT, RT-CPT, T-CPTU); temperature sensor and heat element (HT-CPT); pore pressure sensor (CPTU, T-CPTU, R-CPTU, S-CPTU); electrical resistivity sensor (R-CPT, RT-CPT, R-CPTU); seismic-acoustic sensor (S-CPT, S-CPTU); gamma radiation sensor (GR-CPT); gamma-gamma radiation sensor (GGR-CPT); neutron-neutron radiation sensor (NNR-CPT). Almost the whole of these cone penetrometers are in mass production of A.P. VANDENBERG, FUGRO, GEOTECH, PAGANI, PEAK-TECHNOSERVICE, VERTEK and other companies.

A cone penetrometer equipped with a temperature sensor and a heat element (HT-CPT) is the only one that is not manufactured anywhere and has not been studied until recently. HT-CPT cone penetrometer can make it possible to meet a number of challenges which cannot be met by other cone penetrometers:

- to push the cone penetrometer into low-temperature hard-frozen soil layers by their repeated local thawing;
- to evaluate frozen/thawed soil resistance to CPT during intermittent actions;
- to determine strength and deformation properties of frozen soils, taking into account their thawing;
- to evaluate thermophysical properties of frozen soils.

Numerical thermophysical studies and laboratory tests carried out at Gersevanov NIIOSP (Moscow) resulted in approaches and methods used to solve these problems. The report presents the results of numerical studies on various factors having an effect on the thawing area parameters of frozen soil around the HT-CPT cone penetrometer.

2 METHODOLOGY OF THERMOPHYSICAL FINITE ELEMENT ANALYSIS

Mathematical simulation of thermophysical interaction of the "HT-CPT cone penetrometer—frozen soil" system was performed using "GeoStudio TEMP/W" software package in the axisymmetric set.

Physical and thermophysical characteristics of permafrost soils were taken after Appendix B of Building Code SP 25.13330.2012.

The cone penetrometer was modeled in its full size with dimensions as per IRTP. It included a

cone tip and a push rod. The cone base diameter was 36 mm, the apex angle of the cone – 60°.The holes were modeled in the cone (Figure 1) for the heat element (30 mm in length and 6 mm in diameter) and the temperature sensor (23 mm in length, 3 mm in diameter).

Calculation was carried out in two stages: the first one—heating of the cone penetrometer within 120 minutes, the second one—cooling of the cone penetrometer within 120 minutes after switching off the cone penetrometer.

Heating was modeled by the heat flow radiating from the heat element.

The finite element grid was spaced in intervals of 0.05 m. For greater accuracy of calculations, grid spacing decreased to 0.01 m in the soil area adjacent to the cone penetrometer; the cone penetrometer itself was set out with a grid spacing of 0.005 m. The calculated model with the finite element grid is shown in Figure 3.

The calculated area was chosen from the condition of the changed temperature attenuation in the soil due to heating by the cone penetrometer. The experiments revealed that the dimensions of the calculated area did not influence interaction of the cone penetrometer with the adjacent soil if the dimensions of the calculated area were 2.5 m along the X axis and 2 m along the Y axis. That is why these dimensions of the calculated area were used in simulation.

The boundary conditions at the boundary of the calculated area were set by the frozen soil temperature.

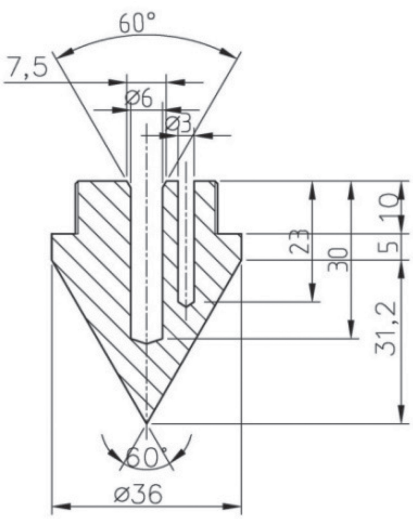

Figure 1. Schematic illustration of the cone with holes for the heat element and temperature sensor.

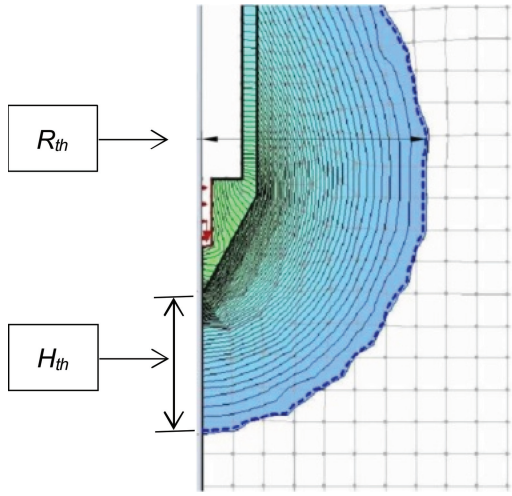

Figure 2. Calculated area of thawing in the vicinity of the cone: $H_{thaw.}$ – depth of thawing, $R_{th.}$ – radius of thawing.

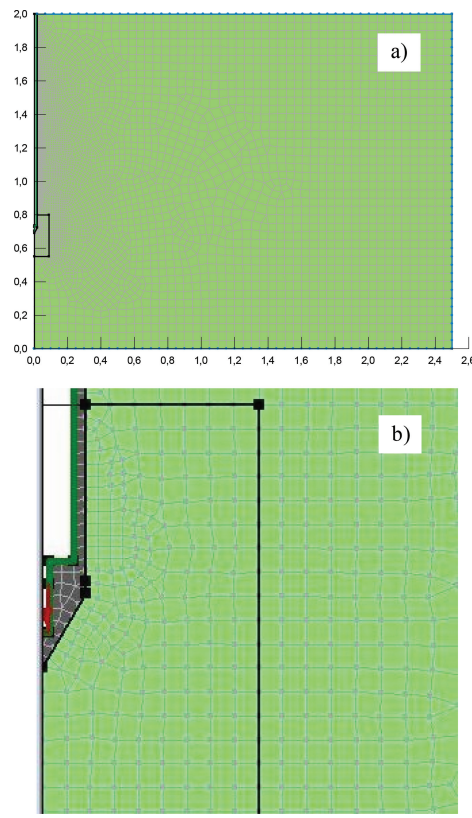

Figure 3. Calculation scheme with FE grid: *a* – the whole calculation scheme; b—expanded fragment of the calculation scheme in the vicinity of the cone.

The following parameters were considered:

- soil type (sand, clay sand, loam and clay);
- soil temperature (–0.3; –0.5; –1.0; –2.5; –4.0; –5.5; –7.0°C);
- soil moisture (5…25% for sands; 5…35% for clay sands; 5…40% for loams and clays);
- heat element power (20, 40, 60, 100 W); heating time of the cone penetrometer (10, 30, 60, 90, 120 min); cooling time (10, 30, 60, 90, 120 min).

A series of numerical experiments simulating the given calculated situations were performed after a specially developed plan. When studying a particular parameter, the values of the rest parameters were taken to be equal to their mean values.

Then the analysis of the obtained depth and diameter of the frozen soil thawing around the HT-CPT cone was performed. The values of the depth and diameter of thawing were recorded according to the scheme shown in Figure 2.

3 RESULTS OF THERMOPHYSICAL FINITE ELEMENT ANALYSIS

The calculations resulted in the graphs showing the nature and extent of constructive-technological and geocryological factors having an effect on the maximum depth and diameter of thawing area (Figure 4).

A comparative analysis of the graphs makes it possible to note the following.

The influence of the factors under study on the parameters under evaluation were relatively equal for clays and loams, so they were combined into a single group later.

Heating and cooling time. When heating was performed within 120 min, the depth of thawing was 4.5 cm for sands, 3.7...3.9 cm—for clay soils, i.e. 19% less. The greatest intensity of thawing was observed at the initial moment of heating, and then it slightly decreased. During the last 30 min

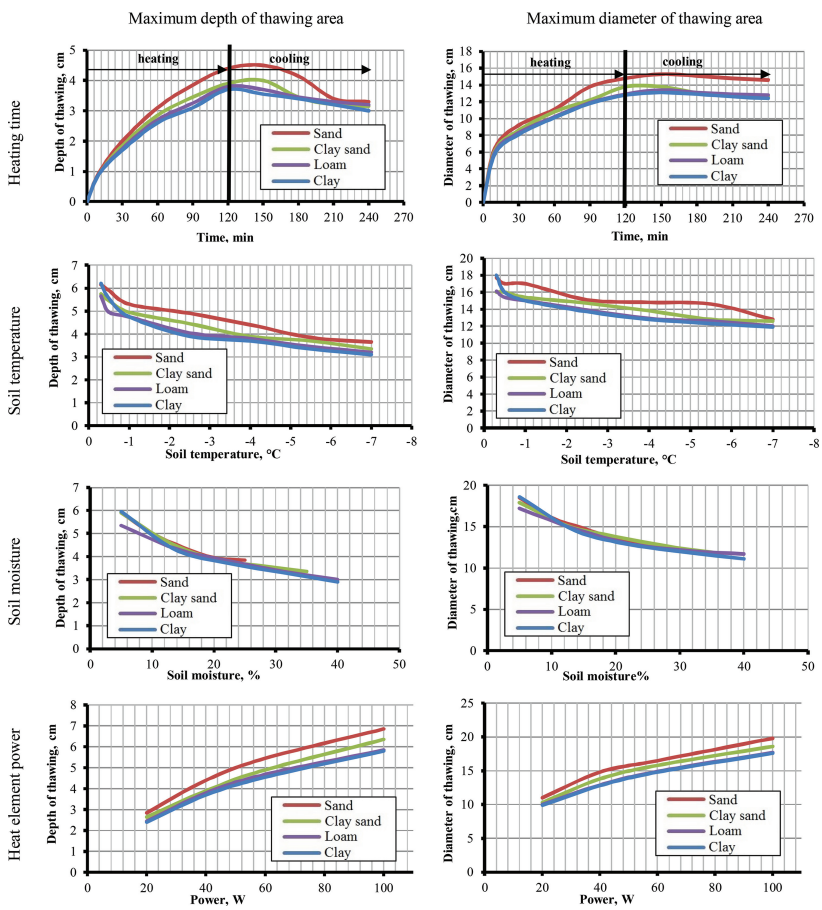

Figure 4. Graphs of constructive-technological and geocryological factors versus the maximum depth and diameter of the thawing area.

of heating, the depth of thawing increased in direct proportion to the heating time.

When heating was stopped, the depth of thawing (sands and clay sands) continued to increase by 3…5% and reached its maximum within 30 min. For loams and clays it decreased by 0.1...0.2 cm within 30 min. In 120 min, when heating was stopped, the depth of thawing for all soils became relatively equal to each other – 3.0...3.3 cm.

When heating was performed within 120 min, the maximum diameter of thawing was 15.3 cm for sands, 12.7...14.0 cm—for clay soils, i.e. 8…17% less. The greatest intensity of thawing (0.5 cm/min) was observed at the initial moment of time and it significantly decreased after 15 min, and then the diameter of thawing increased in direct proportion to the heating time at a speed of 0.06 cm/min.

When heating was stopped, the diameter of thawing slightly changed during 120 min for the whole of soils, i.e. by 7...12%, and reached 14.7 cm for sands and 12.5 cm—for clays.

Soil temperature. When heating was performed within 120 min, and the initial soil temperature decreased from -0.3 to -7.0 ⊠, the depth of thawing decreased from 5.6...6.2 cm to 3.1...3.7 cm; the diameter of thawing decreased from 16.0...18.0 cm to 12.0...13.0 cm. Thus, the area of thawing depends most strongly on the initial soil temperature in the range from -0.3...-1.0 ⊠, and then it changes approximately linearly. In here, the more dispersed the soil is, the smaller depth of thawing area is observed.

Soil moisture. When heating was performed within 120 min with soil moisture increased from 5 to 40%, the depth of thawing decreased from 5.3...6.0 cm to 3.0…3.8 cm, i.e. by 76...100%, and the diameter of thawing decreased from 17.0...18.2 cm to 11.0...12.0 cm, i.e. approximately by 50%. The type of soil almost does not affect this dependence—the whole curves are very close to each other.

Heat element power. When heating was performed within 120 min with the heat element power increased from 20 to 100 W, the depth of thawing increased significantly—from 2.2...2.9 cm to 5.7...6.8 cm, i.e. by 134...160%, and the diameter of thawing—from 10.0...12.2 cm to 17.4...18.9 cm, i.e. by 55...74%. The type of soil greatly affects this dependence; given the same heat element power, the more dispersed the soil is, the smaller depth of thawing area is observed.

It is necessary to note that cone temperature increases up to 170 ⊠ if heat element power is high (100 W); it is not permissible in in-situ testing of frozen soils with HT-CPT cone penetrometers, since evaporation of moisture and soil pressure increase will occur and hence, natural soil conditions will be violated.

4 EMPIRICAL DEPENDENCIES OF THE THAWING AREA SIZES UPON CONSTRUCTIVE-TECHNOLOGICAL AND GEOCRYOLOGICAL FACTORS

Based on the statistical analysis of the data obtained, regression equations were developed in the form of the second degree polynomials to determine the maximum depth H_{th} and diameter D_{th} of thawing. The regression equation coefficients were selected separately for sands, clay sands and clays/loams using IBM SPSS Statistics program. The input parameters of equations are presented in Table 1.

The regression equations are as follows:

$$H_{th} = a_1T^2 + a_2T + a_3 + b_1W_{tot}^2 + b_2W_{tot} + c_1t^2 + c_2t + d_1P^2 + d_2P \quad (1)$$

$$D_{th} = a_1T^2 + a_2T + a_3 + b_1W_{tot}^2 + b_2W_{tot} + c_1t^2 + c_2t + d_1P^2 + d_2P \quad (2)$$

The empirical coefficients were tabulated for convenience (see Tables 2, 3). All regression equations can only be used when they substitute factor values in the ranges of the experimental data that were used to compile the equations!

In order to determine the accuracy and applicability of the regression equations for predicting

Table 1. Input parameters of equations.

Parameter	Symbols	Dimension of quantity
Soil temperature	T	°C
Soil moisture	W_{tot}	%
Heating time	t	Min
Heat element power	P	W

Table 2. Empirical regression equation coefficients to determine $H_{th.}$

	Soil type		
Coefficient	Sand	Clay sand	Loam/clay
a_1 =	0.023	0.026	0.042
a_2 =	0.391	0.391	0.531
a_3 =	1.187	1.285	1.792
b_1 =	0.004	0.002	0.002
b_2 =	–0.181	–0.128	–0.124
c_1 =	–0.00019	–0.00017	–0.00016
c_2 =	0.057	0.053	0.049
d_1 =	–0.00026	–0.00021	–0.00021
d_2 =	0.066	0.056	0.053

the thawing area sizes, the depths and diameters of these areas were calculated from the empirical equations (1), (2) and obtained in numerical simulation. The obtained values were compared and are shown in Figure 5.

The graphs show that the convergence of the results is rather good for engineering calculations. The results obtained were processed using mathematical statistics methods. It has been concluded that the developed technique is sufficiently reliable and can be used to predict the thawing area sizes of the frozen soil heated by the HT-CPT cone penetrometer.

Table 3. Empirical regression equation coefficients to determine the D_{th}.

Coefficient	Soil type		
	Sand	Clay sand	Loam/clay
a_1 =	–0.030	0.041	0.084
a_2 =	–0.003	0.687	1.079
a_3 =	4.110	6.716	8.074
b_1 =	–0.0095	0.0043	0.00424
b_2 =	0.264	–0.311	–0.316
c_1 =	–0.0004	–0.00039	–0.00039
c_2 =	0.127	0.122	0.118
d_1 =	0.000048	–0.00056	–0.0005
d_2 =	0.0011	0.1378	0.1276

5 CONCLUSIONS

The results of numerical studies of thermophysical interaction between the HT-CPT cone penetrometer and thawing soils make it possible to conclude:

1. The study resulted in determining the regularities and nature of the constructive-technological and geocryological factors having an effect on the thawing area sizes of frozen soils heated by the HT-CPT cone penetrometer. The following regularities can be noted. The effects of the factors under study are relatively equal for clays and loams. The thawing area sizes are most affected by the power and duration of heating. Soil moisture also affects significantly. Soil type and temperature affect less. When heating is performed, the intensity of thawing area increase is much higher than the intensity of its decrease in initial frozen soil temperature recovery. When heating is stopped, the thawing area

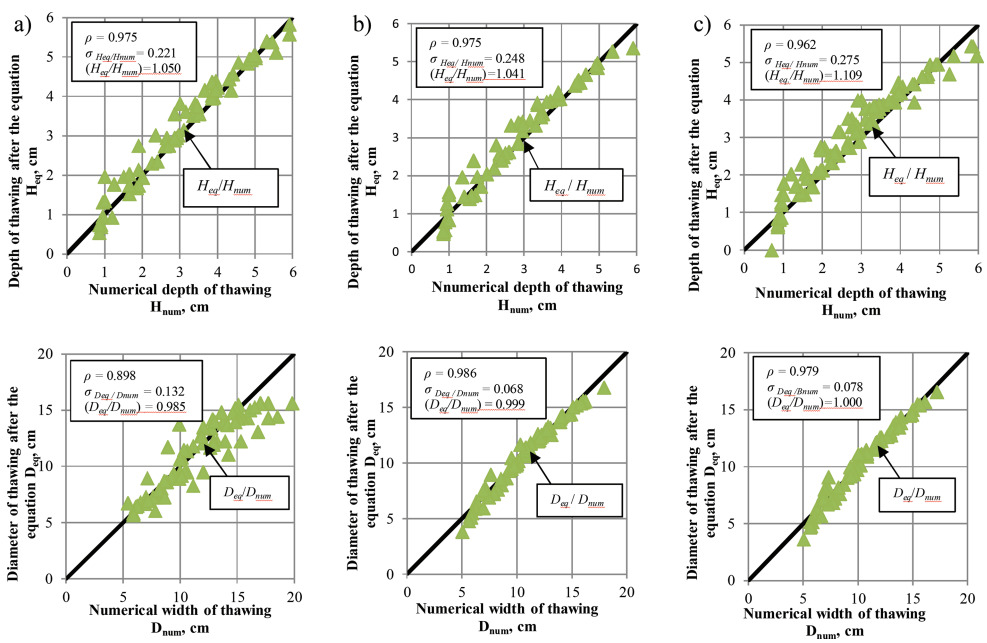

Figure 5. Compared values of the depth and diameter of thawing for sands (a), clay sands (b), loams and clays (c) calculated by the empirical equation obtained after numerical simulation: H_{eq} and H_{num} – depth of the thawing area calculated by the empirical equation (1) and obtained in simulation; D_{eq}/D_{num} – diameter of the thawing area calculated by the empirical equation (2) and obtained in simulation; ρ – correlation coefficient; σ – sample standard deviation; (D_{eq}/D_{num}) – arithmetical average D_{eq}/D_{num}.

sizes are stabilized for a certain period, and then they decrease.

2. As a result of statistical calculations, the empirical equations obtained for frozen sands, clay sands and clays/loams have made it possible to determine the depth and diameter of the soil thawed by the HT-CPT cone penetrometer taking into account the soil type, its temperature and moisture, power and heating time. The equations obtained allow predicting the thawing area sizes of frozen soils heated by the HT-CPT cone penetrometer with sufficient accuracy to be used in practice.

REFERENCES

Adrian B. McCallum, Andy Barwise, Roi S. Santos 2014. Is the cone penetration test (CPT) useful for arctic site investigation? *Proceedings of the ASME 2014 33rd International Conference on Ocean, Offshore and Arctic Engineering. OMAE2014. San Francisco, USA.* 5 p.

Building Code SP 25.13330.2012 2012. *Soil bases and foundations on permafrost soils*. – Moscow, 117 p.

Buteau, S., Fortier, R., and Allard, M. 2005. Rate-Controlled Cone Penetration Tests in Permafrost. *Canadian Geotechnical Journal*, 42 (1): pp. 184–197.

Blouin S., Chamberlain E., Sellmann P. and Garfield D. 1979. Determining subsea permafrost characteristics with a cone penetrometer. *Cold Regions Science and Technology*. № 1, pp. 3–16.

Building Code SP 25.13330.2012 (2012) *Soil bases and foundations on permafrost soils*. – Moscow, 117 p.

Dlugach, A., Loktev, A., Okko, O., and Rokos, S. 1995. Soil Mechanical Properties and In Situ Temperature from Arctic Offshore CPT Data. *In Proceedings of the International Symposium on Cone Penetration Testing, Linköping, Sweden, 4–5 October 1995. Swedish Geotechnical. Society, Linköping, Sweden*. Vol. 2, pp. 167–172.

Fortier, R & Yu, W. 2012. Penetration rate-controlled electrical resistivity and temperature piezocone penetration tests in warm ice-rich permafrost in Northern Quebec (Canada). *15th International Conference on Cold Regions Engineering, Quebec, Canada*. pp. 1–11.

Ivan Sokolov, Nikolay Volkov, Vladislav Isaev. 2016. Cone Penetration Testing for Railways on Permafrost. *Proc. of the XI International Conference on Permafrost, Potsdam, Germany*.

International Reference Test Procedure (IRTP) for the Cone Penetration Test (CPT) and the Cone Penetration Test with pore pressure (CPTU): *Report of the ISSMGE Technical Committee 16 on Ground Property Characterisation from In-situ Testing 1999 (corrected 2001) – TC 16, ISSMGE*, 29 p.

Isaev, O.N. 1989. Principal tasks in CPT development in permafrost soils. Abstract at All-Union *Scientific Conference "Problems of engineering-geological investigations in cryolite zone". Magadan*, pp. 180–182.

Isaev O.N., Shvarev V.V., Konstantinov A.V., Tichomirov C.M., Sadovsky A.V. 1995. Progress of the method of static sounding in the investigation of geotechnical properties of frozen soils. *Proc. of the Int. Simp. on Cone Penetration Testing, CPT-95 Linköping, Sweden, October 4–5, vol. 2*, pp. 179–186.

Ladanyi, B. 1976. Use of the static penetration test in frozen soils. *Canadian Geotechnical Journal, 13(2)*: pp. 95–110.

Ladanyi B. 1982. Determination of geotechnical parameters of frozen soils by means of the cone penetration test. *Proc. of the Second European Symposium on Penetration Testing. Amsterdam, vol.1*, pp. 671–678.

Lunne T., Robertson P.K. and Powell J.J.,M. 1997. *Cone penetration testing in geotechnical practice. London and New York: Spon Press,* 312 p.

Minkin M.A. 2005. *Methodology and methods of engineering-geocryological investigations. Uhta: Institute of Management, Information and Business.* 252 p.

Ryzhkov I.B. & Isaev O.N. 2016. *Cone penetration testing of soils in geotechnics. Stockholm, Sweden: Bokforlaget Efron & Dotter AB,* 408 p.

Sylvie Buteau, Richard Fortier and Michel Allard. 2005. Rate-controlled cone penetration tests in permafrost. *Can. Geotech. J. 42*, pp. 184–197.

Volkov F.E., Isaev O.N. 1983. Possibility of CPT application in plastic-frozen soils by S-832M CPT rig. *Pile Foundations: Collected scientific papers. NIIpromstroy, Ufa*, pp. 90–94.

Cone Penetration Testing 2018 – Hicks, Pisanò & Peuchen (Eds)
© 2018 Delft University of Technology, The Netherlands, ISBN 978-1-138-58449-5

Large deformation modelling of CPT probing in soft soil—pore water pressure analysis

J. Konkol & L. Bałachowski
Faculty of Civil and Environmental Engineering, Gdańsk University of Technology, Gdańsk, Poland

ABSTRACT: This paper presents the results of finite element modelling with Updated Lagrangian formulation of the Cone Penetration Test in soft soil deposit located in Jazowa, Poland. The numerical calculations are carried out for homogenous, normally consolidated, organic soil layer. The Modified Cam Clay constitutive model for soft soil and Coulomb model for interface are used. The study compares the registered pore water pressure distributions for type-2 piezocone observed during in-situ penetration and corresponding numerical model. The numerical dissipation test is carried out and the results are confronted with in-situ registered data. The influence of orthotropic soil hydraulic conductivity on pore water pressure development at shoulder filter element during dissipation tests is examined. Finally, the distribution of pore water pressures around the piezocone obtained from numerical simulations is compared with high quality literature database.

1 INTRODUCTION

Piezocone is one of the most widely and successfully used site investigation tool. It enables to measure the pore water pressure development during cone penetration into the subsoil as well as pore water pressure dissipation at stationary cone position. Dissipation tests are commonly used to estimate the horizontal coefficient of permeability or horizontal coefficient of consolidation. However, the above mentioned variables are usually determined by empirical correlations based on statistical analysis with scatter data and its applicability is often limited (e.g., Robertson et al., 1992).

In recent years, the rapid development of numerical methods introduces the new possibilities in analysis of pore water pressure distributions around the piezocone (e.g., Burns & Mayne, 1998). These studies mainly concern on developing of new methods of coefficient of consolidation estimation (e.g., Chai et al., 2012) or the horizontal coefficient of consolidation determination (e.g., Ansari et al., 2014). The parametric studies which link the coefficient of consolidation with strength and consolidation parameters of the soil have been also carried out (e.g., Mahmoodzadeh et al., 2014). The influence of partial drainage on dissipation curves was also in terms of interests (e.g., Sheng et al., 2014; Ceccato et al., 2016). However, in most of these studies isotropic soil permeability is applied (e.g., Chai et al., 2012, 2014; Ansari et al., 2014; Ceccato et al., 2016). The influence of orthotropic coefficient of permeability is usually neglected and it is rarely investigated.

In this paper the case study of numerical modelling of piezocone penetration and dissipation test for soft soil deposit located in Jazowa, Northern Poland is presented. In the first part of this paper the applicability of numerical methods in terms of Updated Lagrangian (UL) for CPT penetration prediction is shown. Next, the influence of anisotropy of the coefficient of permeability on dissipation curve is investigated. On the basis of numerical tests the empirical correlation for horizontal coefficient of permeability presented by Robertson (2010) is calibrated on the purpose of Jazowa clayey mud case. Finally, the pore water pressure distributions obtained from numerical calculations for Jazowa site are compared with available database.

2 REFERENCE FIELD TESTING SITE

The Jazowa testing site is chosen as the reference site and it is located in Vistula Marshlands, 50 km southeast of Gdańsk, Poland, within the S7 highway. Jazowa testing site is supervised by Gdańsk University of Technology and Menard Polska under the cooperation within the National Centre of Research and Development grant. For purpose of this paper 14 piezocone penetration tests (CPTu) and 4 dissipation tests are used as reference field tests. The authors decide to model

Table 1. Jazowa clayey mud parameters.

Parameter	Symbol	Value	Unit
Soil dry bulk density	ρ_d	1.074	g/cm^3
Void ratio	e_0	1.416	–
Coefficient of permeability	k	2.74×10^{-10}	m/s
Shear modulus	G	4000	kPa
Undrained shear strength obtained in UU test	$c_{u,UU}$	29	kPa
Logarithmic elastic modulus	κ	0.0359	–
Logarithmic plastic modulus	μ	0.1890	–
Mean preconsolidation stress	p_c	55	kPa
Stress ratio in p'-q plane	M	1.5	–
Lateral earth pressure at rest coefficient	K_0	0.54	–
Overconsolidation ratio	OCR	1.0	–

numerically the CPTu probing from 8 to 9 m depth below ground level and to perform dissipation test at the 9 m depth, where 4 field reference dissipation tests have been carried out.

The soil parameters used in the numerical study are based on laboratory testing, see Table 1. The initial soil conditions in terms of earth pressure at rest coefficients are determined from 8 flat dilatometer test (DMT) soundings that have been carried out at Jazowa site. The coefficient of permeability has been estimated from isotropically consolidated soil sample in triaxial apparatus. This value has been verified using dissipation curves and Robertson formula (2010):

$$k_h = \left(1.67 \times 10^{-6}\right) \times 10^{\left(1-\log\left(t_{50}\right)\right)} \times \gamma_w / \left(Q_t^2 \times \sigma'_{v0}\right) \tag{1}$$

where k_h = horizontal coefficient of permeability; t_{50} = time corresponding to 50% of consolidation; γ_w = water unit weight; $Q_t = (q_t - \sigma_{v0}) / \sigma_{v0}$; q_t = corrected cone resistance; σ_{v0} = total vertical stress; and σ'_{v0} = effective vertical stress.

Equation 1 returns $k_h = 3.6 \times 10^{-10}$ m/s for Jazowa CPTu dissipation and probing data.

3 NUMERICAL MODEL DEVELOPMENT

The numerical calculations are performed with UL formulation as it is implemented in Abaqus 6.14. The UL formulation is provided in Abaqus Standard when the nonlinear geometry option (NLGEOM) is toggled on. UL formulation uses the reference domain from the previous time increment, which facilitates the analysis when large deformations occur (e.g., Mahmoodzadeh et al., 2014). The axisymmetric soil domain is 2.2 m high and 1.0 m wide and it is discretized with 6936 quadratic, second order elements with reduced integration, see Figure 1. The cone is pre-bored at the depth of 5 cm in the soil and it is jacked with standard velocity of 2 cm/s using zipper type technique. In this technique, the rigid cone is connected with tube that is in frictionless contact with soil domain and which moves downward with cone (Mabsout & Tassoulas, 1994). The overburden pressure and the pore water pressure are applied to simulate in-situ conditions. The penetration stroke is 1 m and the final level corresponds to approximately 9 m depth in field. Then, the numerical dissipation test is carried out.

The Modified Cam-Clay (MCC) model is used to simulate the soil behavior with the parameters presented in Table 1. However, some minor changes have been applied and they are discussed below. The soil parameters calibration procedure on TX samples suggests the reduction of plastic surface size on the wet side of critical state line (CSL) by 30% (Dassault Systèmes, 2014). The plastic surface in π-plane is not modified and is kept as a circle. The coefficient of permeability is increased to $k = 2 \times 10^{-9}$ m/s due to isotropic consolidation calibration tests. However, this modification still preserves the undrained conditions which are commonly accepted for $k \leq 10^{-8}$ m/s for clayey soils (e.g., Ceccato et al., 2016; Suzuki, 2015). As the piezocone is pressed into the subsoil with much higher rate than it is achieved during standard Unconsolidated Undrained (UU) triaxial compression tests, the MCC model must also reflect the rate dependency. Kulhawy and Mayne (1990) have shown that the undrained shear strength increases with the strain rate after formula:

$$c_u = c_{u0} \times \left(1 + 0.1 \times \log\left(\dot{\varepsilon}\right)\right) \tag{2}$$

where c_u = actual undrained shear strength; c_{u0} = reference undrained shear strength corresponding to strain rate of 1%/h; and $\dot{\varepsilon}$ = strain rate.

Preliminary laboratory testing of Jazowa clayey mud has confirmed the rate dependency of the material. For strain rate of 1%/h the reference c_{u0} is equal to 25 kPa. According to Equation 2, the c_u obtained in UU triaxial test with $\dot{\varepsilon} \approx 60$%/h should be equal to 29.5 kPa and similar value was measured directly in laboratory, see Table 1. For CPTu penetration the strain rate is approximately 200000%/h, which results in $c_u = 1.5\ c_{u0}$. Consequently, the MCC parameters should simulate the undrained behavior corresponding to c_u equal to 37.5 kPa. To achieve this goal only the preconsolidation pressure p'_c will be modified. Worth (1984) have shown that c_u can be derived from MCC parameters when the same plastic surface size for wet and dry side of the CSL is used. However, Worth's derivation can be easy expanded for different sizes of plastic surfaces on the dry and wet side of CSL (Konkol, 2017) and consequently, the preconsolidation pressure that supports the corresponding c_u for undrained shearing can be defined as:

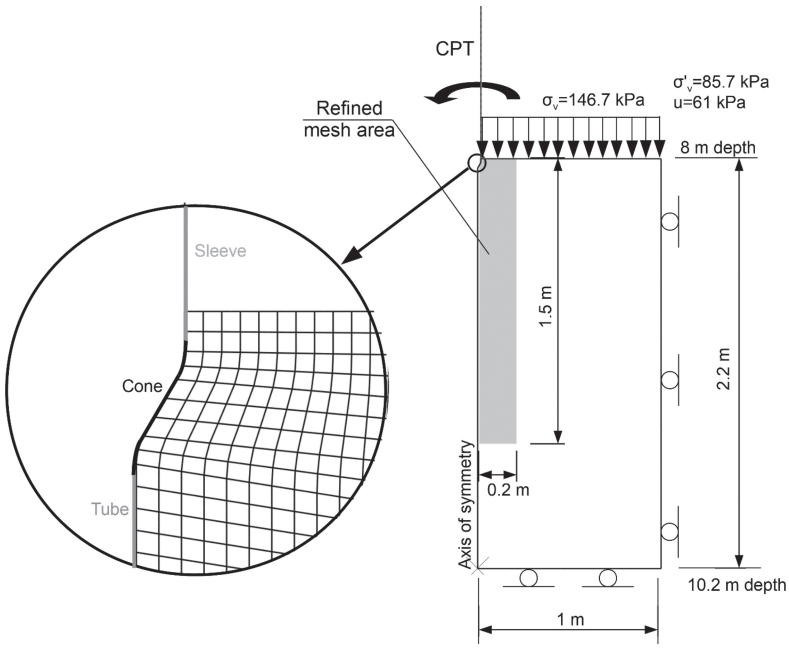

Figure 1. UL model geometry and boundary conditions.

$$p'_c = \left(\frac{2 \times (1+\beta) \times c_u}{M} \times \left((1+\beta) \times p'_0 \right)^{-\kappa/\lambda} \right)^{\frac{\lambda}{\lambda-\kappa}} \quad (3)$$

where: p'_c = preconsolidation pressure corresponding to c_u; M = stress ratio in p'-q plane; β = size of the Figure 1. UL model geometry and boundary conditions plastic surface on the wet side of CSL; c_u = undrained shear strength; p'_0 = initial mean effective stress; κ = logarithmic elastic modulus; and λ = logarithmic plastic modulus.

To provide the c_u equal to 37.5 kPa, the Equation 3 returns p'_c = 82 kPa. Consequently, this value is used in the numerical model to satisfy the shear rate influence instead of the value provided in Table 1. The last modification of the parameters is related to large deformation problem where rigidity index G/c_u is usually around 50 (Vardanega & Bolton, 2013). To satisfy this condition G = 2000 kPa is assumed in numerical models.

The last modelling issue is the interface behavior between cone and the soil. In Abaqus tangential contact between soil and cone is used in terms of effective stresses. This is a widely used assumption as a smooth contact between water and cone is considered. However, this implies a problem in modelling when undrained shearing occurs at the interface and where adhesive contact should be applied. Laboratory direct shear tests on smooth steel—Jazowa clayey mud interface suggest the effective angle of interface friction δ_f as equal to 10° and adhesion $\alpha \approx 0.36$. Assuming c_u = 37.5 kPa, the limit interface shear stress is equal to 13.5 kPa. The frictional contact have been applied with Coulomb friction coefficient of 0.176 (corresponding to δ_f = 10°) in order to accurately model the cone—soil interface during penetration. To include the adhesion contact, the maximum allowable shear stress at the interface is limited to 13.5 kPa. During CPTu dissipation test, no shear stress limit is defined due to drained analysis.

In this paper the results of 5 cases are presented and the testing program is summarized in Table 2. Test-1 (default) is preliminary calculation with isotropic soil hydraulic conductivity. In Test-2 to Test-5 the orthotropic coefficients of permeability are applied. The boundary value of $k_h = 10^{-8}$ m/s is chosen to maintain undrained condition during piezocone penetration. The tested ratios of coefficients of permeability are in agreement with available databases for cohesive soils (e.g., Robertson et al., 1992).

4 RESULTS ANALYSIS

4.1 *Field measurements versus numerical ones*

Due to undrained penetration of piezocone all tests show almost the same response during probing. The numerical results of corrected cone resistance q_t, sleeve friction f_s and pore water pressures

Table 2. Numerical testing program for Jazowa clayey mud piezocone.

Test no	Soil coefficient of permeability [m/s]		
	Vertical	Horizontal	k_h/k_v
1	2×10^{-9}	2×10^{-9}	1
2	2×10^{-9}	4×10^{-9}	2
3	2×10^{-9}	6×10^{-9}	3
4	2×10^{-9}	8×10^{-9}	4
5	2×10^{-9}	10^{-8}	5

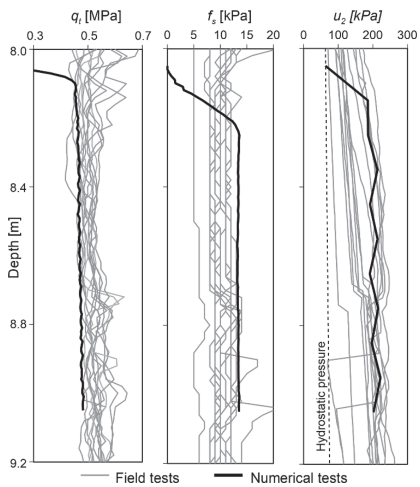

Figure 2. Numerical results of CPTu penetration compared with in situ measurement.

u_2 are compared with the field measurements in Figure 2. The numerical readings start from 8.05 m depth due to cone pre-installation. The pore water pressure reading cannot be obtained automatically from numerical model. As a result, the u_2 value is read out with 10 cm interval manually at mesh node in the vicinity of filter location. As can be seen, very satisfactory results have been achieved. The numerically obtained q_t is the lower bound of the field measurement while f_s is the upper bound. The previous research on numerical modelling of penetration has shown that q_t is sensitive to rigidity index G/c_u (e.g., Van den Berg, 1994). As c_u cannot be changed due to modelling assumptions, the perfect fit for q_t authors achieved when G ≈ 3000 kPa which corresponds to G/c_u = 80. The friction sleeve is constant and equal to 13.5 kPa. This is in agreement with the assumption presented in section 3, where the shear stresses at the interface have been limited to this value. However, the field tests at Jazowa site with different penetration rates suggest that rate dependency on interface is not so obvious and further studies in this area are required. Consequently, the assumption of rate dependency of interface shear strength used in section 3 may be questionable. The field measurement of u_2 is characterized by a large scatter which may be caused by many factors (Campanella et al., 1986). However, very satisfactory fit between field measurement and numerical results has been achieved in terms of u_2 distributions, especially for the last 40 cm of probing. Consequently, it can be assumed that the numerical modelling in a very accurate way reflects the field measurements performed at Jazowa site.

4.2 *Influence of the permeability coefficient anisotropy*

The application of the orthotropic coefficient of permeability results in a faster pore water pressure dissipation and a lower maximum calculated values of u_2, see Figure 3. The dissipation curves presented in Figure 3 prove that the horizontal coefficient of permeability plays a key role in pore water pressure dissipation behavior and even slight deviation in k_h/k_v from isotropic distribution results in visible reduction of dissipation time. However, the rate of this process decreases with increasing k_h/k_v. The k_h/k_v between 4 and 5 seems to reflect the in-situ conditions. Moreover, the conducted UL tests allow for the calibration of Robertson (2010) formula in terms of horizontal coefficient of permeability. The back calculation revels the conversion of empirical factor 1.67×10^{-6} to 4.0×10^{-5}. Consequently, k_h for Jazowa site can be calculated as:

$$k_h = \left(4 \times 10^{-5}\right) \times 10^{\left(1 - \log\left(t_{50}\right)\right)} \times \gamma_w / \left(Q_t^2 \times \sigma'_{v0}\right) \quad (4)$$

where k_h = horizontal coefficient of permeability; t_{50} = time corresponding to 50% of consolidation; γ_w = water unit weight; $Q_t = (q_t - \sigma_{v0})/\sigma_{v0}$; q_t = corrected cone resistance; σ_{v0} = total vertical stress; and σ'_{v0} = effective vertical stress.

Equation 4 returns $k_h = 8.6 \times 10^{-9}$ m/s for Jazowa CPTu data. The results of calibration are similar to the results of numerical research on normally consolidated soil presented by Ansari et al. (2014). According to the procedure described by Ansari et al. $k_h = 9.4 \times 10^{-9}$ m/s has been obtained.

4.3 *Pore water pressure distribution around the piezocone*

The distribution of pore water pressures around the cone and sleeve at the end of piezocone penetration has been compared with the available database of pore water pressure measurements in soft, normally consolidated soils (Chen & Mayne, 1994). The four possible filter locations have been

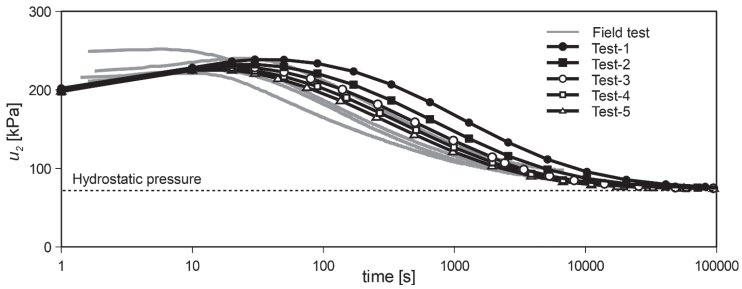

Figure 3. Numerical results of dissipation tests versus field measured ones.

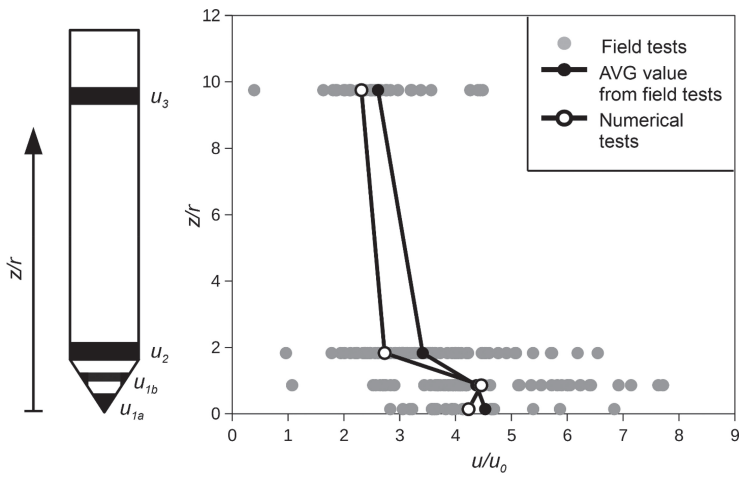

Figure 4. Pore water pressure distribution around the piezocone obtained from numerical tests and compared with database (Chen & Mayne, 1994).

considered in numerical models to provide sufficient comparison, see Figure 4. As one can see, the numerical modelling results of CPTu penetration in Jazowa clayey mud are in the range of other in-situ measurements. Further, the pore water pressures calculated in each filter location in numerical models are similar to the trend outlined by average values from database.

5 CONCLUSIONS

The numerical studies performed have shown that UL formulation as it is implemented in Abaqus can be successfully used for the CPTu penetration problem and the two-phase soil model. The satisfactory results achieved with UL formulation and presented in this paper as well as in previous research (e.g., Chai et al., 2012; Mahmoodzadeh et al., 2014) are sufficient to conclude that UL formulation is well-established method for large deformation problems.

The results of numerical analysis of CPTu probing in Jazowa clayey mud have been verified by field tests conducted at the site. Some final remarks about introduced studies can be formulated. Firstly, the simplification in terms of limitation of maximum shear stress at the interface can be used to simulate the adhesive contact for undrained penetration. However, the pure friction contact behavior is based on effective pressures and the change in friction behavior results in practically the same pore water distributions during cone penetration regardless the limit shear stresses at the interface are defined or not. This is proper model response due to smooth steel-water interface. Nevertheless, the laboratory tests on clay-steel interfaces have shown that increasing interface roughness results in increasing pore water pressures at the interface (Tsubakihara & Kishida, 1993). The same mechanism in observed when total stress analysis in used (e.g., Beuth & Vermeer, 2013). Consequently, further studies in this area are required. Secondly, the orthotropic soil hydraulic conductivity strongly

influences the dissipation response measured at u_2 position. The horizontal coefficient of permeability also influences the shape of the dissipation curve as it was shown in Figure 3. However, it was found that dissipation time decrease weakens with increasing k_h/k_v ratio. Consequently, UL modelling of CPTu can be used as an additional tool to calibrate the orthotropic hydraulic conductivity of soil as it was shown for Jazowa clayey mud. The numerical tests also enable to calibrate and to match the commonly accepted formulas for k_h estimation to the local soft soil deposits as it has been shown in this paper. Finally, the numerical modelling presents the reasonable values of pore water pressure at u_1 and u_3 positions in accordance to the collected database. Therefore, the u_1 and u_3 pressures obtained from the numerical modelling can be treated as a representative and accurate values for Jazowa clayey mud.

Summing up, the numerical tests performed in this paper have confirmed the applicability of UL formulation. The influence of anisotropy of coefficient of consolidation on the dissipation tests results has been analyzed and the empirical equation for k_h initially presented by Robertson (2010) has been calibrated for the purpose of Jazowa clayey mud case. Consequently, the advanced numerical methods find its place as an additional tool for more precise geotechnical site investigation.

ACKNOWLEDGEMENTS

The research is supported by the National Centre for Research and Development grant PBS3/B2/18/2015. The calculations were carried out at the Academic Computer Centre in Gdańsk (CI TASK).

REFERENCES

Ansari, Y., Merifield, M. & Sheng, D. 2014. A piezocone dissipation test interpretation method for hydraulic conductivity of soft clays. *Soils and Foundations*, 54(6): 1104–1116.

Beuth, L. & Vermeer, P.A. 2013. Large deformation analysis of cone penetration in undrained clay. In M.A. Hicks et al. (eds.), *Installation effects in geotechnical engineering, Proc. intern. conf., Rotterdam, The Netherlands, 24–27 March 2013.* London, UK: Taylor & Francis.

Burns, S.E. & Mayne, P.W. 1998. Monotonic and dilatory pore-pressure decay during piezocone tests in clay. *Canadian Geotechnical Journal*, 35(6): 1063–1073.

Campanella, R.G., Robertson, P.K. & Gillespie, D. 1986. Factors affecting the pore water pressure and its measurements around the penetrating cone. In *Proceedings of 39th Canadian Geotechnical Conference.* Ottawa, Canada.

Ceccato, F., Beuth, L. & Simonini, P. 2016. Analysis of Piezocone Penetration under Different Drainage Conditions with the Two-Phase Material Point Method. *Journal of Geotechnical and Geoenvironmental Engineering*, 140(12): 04016066.

Chai, J., Hossain, M.J., Carter, J.P. & Shen, S.-L. 2014. Cone penetration-induced pore pressure distribution and dissipation. *Computers and Geotechnics*, 57: 105–113.

Chai, J., Sheng, D. & Zhu, H. 2012. Coefficient of consolidation from non-standard piezocone dissipation curves. *Computers and Geotechnics*, 41: 13–22.

Chen, B.S.Y. & Mayne, P.W. 1994. *Profiling the overconsolidation ratio of clays by piezocone tests*. Internal Report GIT-CEEGEO-94–1. Atlanta: Georgia Institute of Technology.

Dassault Systèmes. 2014. Abaqus 6.14 Documentation.

Konkol, J. 2017. *Numerical analysis of pile installation effects in cohesive soils*. PhD Thesis. Gdańsk: Gdańsk University of Technology.

Kulhawy, F.H. & Mayne, P.W. 1990. *Manual on estimating soil properties for foundation design*. Palo Alto, California, USA: Electric Power Research Institute.

Mabsout, M.E. & Tassoulas, J.L. 1994. A finite element model for the simulation of pile driving. *International Journal for Numerical Methods in Engineering*, 37(2): 257–278.

Mahmoodzadeh, H., Randolph, M.F. & Wang, D. 2014. Numerical simulation of piezocone dissipation test in clays. *Géotechnique*, 64(8): 657–666.

Robertson, P.K. 2010. Estimating in-situ soil permeability from CPT & CPTu. In *Proceedings of 2nd International Symposium on Cone Penetration Testing*. Pomona, California, USA: California State Polytechnic University.

Robertson, P.K., Sully, J.P., Woeller, D.J., Lunne, T., Powell, J.M.M. & Gillespie, D.G. 1992. Estimating coefficient of consolidation from piezocone tests. *Canadian Geotechnical Journal*, 29(4): 539–550.

Sheng, D., Kelly, R., Pineda, J. & Bates, L. 2014. Numerical study of rate effects in cone penetration test. In *Proceedings of 3rd International Symposium on Cone Penetration Testing*. Las Vegas, Nevada, USA.

Suzuki, Y. 2015. *Investigation and interpretation of cone penetration rate effects*. PhD Thesis. Perth, Australia: University of Western Australia.

Tsubakihara, Y. & Kishida H. 1993. Frictional behaviour between normally consolidated clay and steel by two direct shear type apparatuses. *Soils and Foundations*, 33(2): 1–13.

Van den Berg, P. 1994. *Analysis of soil penetration.* PhD Thesis. Delft, Netherlands: Delft University of Technology.

Vardanega, P.J. & Bolton, M.D. 2013. Stiffness of clays and silts: Normalizing shear modulus and shear strain. *Journal of Geotechnical and Geoenvironmental Engineering,* 139(9): 1575–1589.

Wroth, C.P. 1984. Interpretation of in situ soil tests. *Géotechnique*, 34(4): 449–489.

Cone Penetration Testing 2018 – Hicks, Pisanò & Peuchen (Eds)
© 2018 Delft University of Technology, The Netherlands, ISBN 978-1-138-58449-5

The use of neural networks to develop CPT correlations for soils in northern Croatia

M.S. Kovacevic
Faculty of Civil Engineering, University of Zagreb, Zagreb, Croatia

K.G. Gavin & C. Reale
Faculty of Civil Engineering and Geosciences, Delft University of Technology, Delft, The Netherlands

L. Libric
Faculty of Civil Engineering, University of Zagreb, Zagreb, Croatia

ABSTRACT: The evaluation of soil parameters for design is best undertaken through comprehensive laboratory test programmes. However, due to sampling difficulty, time and cost constraints correlations between in-situ tests and physical-mechanical properties of soils are routinely applied in practice. This paper presents data collected from five sites in Northern Croatia at which Cone Penetration Tests (CPT) and comprehensive laboratory test data was available. One of the advantages of using CPT data in preference to other types of in-situ tests for establishing correlations, is the large volume of high-quality data available at each probe location allows for the application of advanced statistical approaches. In this paper, the use of neural networks in developing such correlations is demonstrated. Using a database of 216 data pairs, obtained from the five sites, a correlation between CPT q_c and soil unit weight is established. A validation exercise was performed in which the correlation was tested against data from the recent Veliki vrh landslide that occurred in the same geographical region as the database sites. In addition, by using the soil behaviour type index, *Ic*, normalised cone tip resistance, *Qtn*, and normalised sleeve friction, *Fr*, the results can be compared to correlations developed for soils from geotechnical diverse regions to check for consistency in the derived correlations.

1 INTRODUCTION

Evaluating design values for soil parameters in a laboratory environment is a time consuming, challenging task, which involves painstaking attention to detail and numerous retests to validate results and ensure representation of reality. As with any methodology, there are advantages and disadvantages to such an approach. Some of the advantages of laboratory testing include repeatability, high accuracy and precision, and importantly the explicit measurement of the parameter in question. While the disadvantages include significant cost, substantial processing time, sampling difficulty, and the perennial problem of determining whether the laboratory investigation adequately represents site conditions.

In-situ CPTs can easily overcome these disadvantages, while still providing high accuracy and repeatability and although they may not provide explicit measurements of critical geotechnical parameters many correlations (Librić et al., 2017; Mayne, 2014; Robertson, 2009) have been developed over recent years indirectly relating CPTs to various geotechnical parameters. Additionally, CPTs generate large volumes of near continuous data during testing which means that the sample size of CPT based correlations is much higher than that of laboratory tests, thus greatly reducing the influence of erroneous tests. CPT based correlations greatly streamline the construction process allowing for savings in both time and money. They are typically developed using either statistical approaches or curve fitting or both. However, it is important to note that while these correlations typically perform well, they are not exact solutions and consequently are not infallible and need to be applied with caution by experienced geotechnical engineers.

This paper investigates the use of both statistical regression and a machine learning technique, artificial neural networks (ANN), for developing CPT based correlation between cone tip resistance, q_c, depth, z, sleeve friction, f_s, and soil unit weight, γ_t. These correlation are developed using a database of 216 pairs of corresponding CPT and laboratory

results, obtained from five sites across Northern Croatia. The resultant correlations are verified using results from a separate test site in the same geographical region, Veliki vrh, a site which was not used in the initial development of the models.

2 SELECT EXISTING CORRELATIONS

CPT based soil correlations and classification charts are typically expressed in terms of normalised piezocone parameters, to evaluate normalised piezocone parameters it is first necessary to evaluate the total and effective overburden pressure, both of which first require an estimate of the soil unit weight. Naturally, the precise measurement of soil unit weight involves a laboratory test, however, in an attempt to expedite the process and save both time and money, many authors have developed CPT correlations to describe soil unit weight.

Mayne (2007) described a relationship between sleeve friction and total unit weight by linking the relationships between shear wave velocity and sleeve friction and shear wave velocity and total unit weight. The database used contained a wide variety of soil types ranging from soft clays to gravel. The relationship can be seen in Equation 1.

$$\gamma_t = 2.6\log f_s + 15G_s - 26.5 \tag{1}$$

where G_s is the specific gravity of the soil solids in question. Mayne et al. (2010) expanded this relationship using data from 44 sites to incorporate depth, z, and cone resistance corrected for pore pressure, q_t, see Equation 2 and 3. An R^2 value of 0.72 was obtained using the relationship.

$$\gamma_t = 11.46 + 0.33\log z + 3.1\log f_s + 0.7\log q_t \tag{2}$$

$$q_t = q_c + u_2(1 - a) \tag{3}$$

where u_2 is the pore pressure measured behind the cone and a is the cone area. Robertson & Cabal (2010) proposed a similar relationship which utilises the friction ratio ($R_f = \left(R_f = (f_s/q_t)100\right)$ instead of directly using the sleeve friction, their relationship presented in Equation 4, was trialled using published data from around the world and generally reported a good fit.

$$\frac{\gamma_t}{\gamma_w} = \left[0.27\log R_f + 0.36\log\frac{q_t}{P_a} + 1.236\right]\frac{G_s}{2.65} \tag{4}$$

where P_a is atmospheric pressure and γ_w is the unit weight of water. Mayne & Peuchen (2012) proposed a regression method that takes account of unit weight variations with depth. They accomplished this using a parameter m_q which is the change in normalised cone resistance with depth $(\Delta q_t/\Delta z)$, see Equation 5.

$$\frac{\gamma_t}{\gamma_w} = 0.886\left(\frac{q_t}{\sigma_{atm}}\right)^{0.072}\left[1 + 0.125\frac{m_q}{\gamma_w}\right] \tag{5}$$

Ghanekar (2014) noted that these relationships work much better in uniform soil deposits and typically break down when used in layered soil profiles.

3 NEURAL NETWORKS

Artificial neural networks are an advanced machine learning technique developed by computational scientists (Basheer and Hajmeer, 2000; Rojas, 2013; Rosenblatt, 1958) based on how we perceive the human brain and nervous system to interpret information and perform calculations. Mimicking real life brain neurons, interconnected artificial neural elements work together, passing information to and fro so as to establish the relationship between different parameters within a system, in order to learn or emulate how it functions. The major advantage of neural networks lies in their ability to adapt and update hypotheses when supplied with new data. Neural networks can be used to perform regression analysis, classification analysis and predict future system response. Every connection between a neuron and another neuron receives a weighting. These weightings determine how the neural network responds and adapts by assigning more or less importance to relationships of note. These systems of weightings are trained by mapping inputs onto some output or outputs, and optimising the weightings until the neural network reacts as the system does.

Neural networks are typically arranged into an input layer; a hidden layer or layers, and an output layer (see Figure 1). The number of input and output nodes required is typically dictated by the underlying engineering problem. While the number of hidden neurons needed is a lot more subjective and requires investigation on a problem by problem basis. Too many hidden neurons and the neural network will be slow to converge while also at the same time being at an increased risk of over-training. Too few, and the neural network will be too general and will be inconsistent with unseen data. A multi-layer feed forward neural network with a sigmoid activation function for hidden neurons and a linear activation function for output neurons was used in this example. In a feed-forward neural network, information only moves in one direction from the input nodes through the hidden nodes to the output nodes, i.e. there is no recursive programming involved.

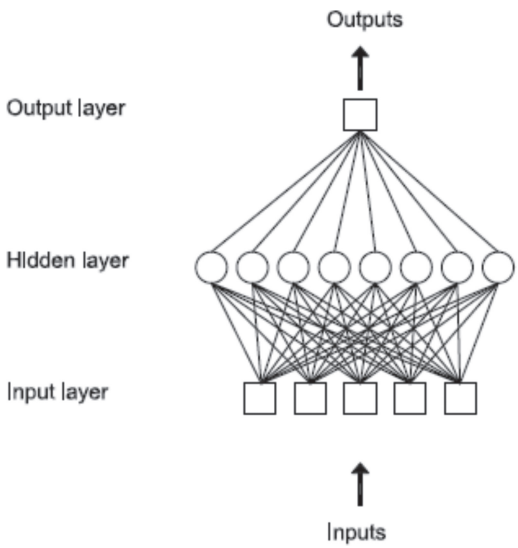

Figure 1. General schematic of a feed-forward artificial neural network.

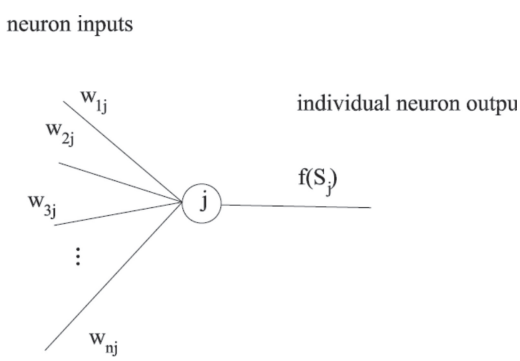

Figure 2. Close up of an individual neuron and how it interacts with the neurons around it.

During training, both the inputs and outputs of the specified problem are given. The weightings are then developed automatically without human intervention in the hidden layer by the ANN. This process is shown in Equation 6, where j represents an individual neuron, w_{ij} represents the individual weighting between input neuron i and hidden neuron j i.e. the factor by which every value passing from node i to node j is multiplied. These weightings are then summed at each node and a bias term w_{0j} is added, See Equation 6. An activation function needs to then be applied to this term (S_j) to generate the individual neuron's output, see Figure 2. Any function can be used for this purpose, but if backpropagation is used to train the model then the function needs to be continuously differentiable. The sigmoid function is the activation function most commonly used in feedforward neural networks and is shown in Equation 7. The two layer feed forward neural network used in this study was trained using the Bayesian Regularisation backpropagation algorithm.

$$S_j = \sum_{i=1}^{n} w_{ij} u_j + w_{0j} \tag{6}$$

$$f(x) = \frac{1}{1+e^{-x}} \tag{7}$$

This training phase continues until the ANN can adequately model the system response or until all available training data has been exhausted. The ANN should then be validated using a new set of input data, which had not previously been used during model training. If the ANN can determine the outputs of this dataset, then it can be said to model the system accurately. Provided enough input and output data has been provided during training, an ANN model should be able to determine the significance each individual parameter has on the outcome.

The ANN developed in this study used q_L depth, and f_s as inputs, to predict the soil unit weight γ_t as an output. Three hidden layers were utilised in this application.

4 TEST SITES

Five test sites from Northern Croatia were used to train, validate, and test the developed neural network model, while a sixth site Veliki vrh was used as an external unseen verification measure. Four of the 6 sites consisted of highly over consolidated soil, while the remaining two *Biđ-Bosut* and *Ilok port* were found to be slightly over consolidated (Reale et al., 2018). The initial dataset used to train, develop, and test the model consisted of 216 pairs of CPT/ Laboratory results. A short overview of each test site and the geotechnical testing carried out at each site is given below. All laboratory unit weight tests were carried out in accordance with the European Standard (HRS CEN ISO/TS 17892–2:2004) for the determination of density of fine grained soil (Tehni and Specifikacija, 2013).

4.1 *Biđ-Bosut Irrigation canal*

A 14 km long irrigation canal was constructed as of the multi-purpose Danube-Sava canal. The canal geometry consists of two stepped slopes the upper slope has a 1:2 gradient while the lower slope is at 1:3. The total excavation is approximately 7 m deep and a relatively wide step exists between the

two slopes. The geotechnical site investigation at the site consisted of 12 m deep boreholes at 300 m centres with core classification and extraction of representative soil samples for lab tests (consistency levels, particle size distributions, and direct shear tests). At 150 m intervals, 4 to 5 m deep trial pits were excavated along the canal route. Representative samples were extracted from each pit and tested in the laboratory. Cone Penetration Tests and standard penetration tests (SPT) were carried out at each borehole together with two hold tests to measure pore pressure dissipation on the CPT cone. 15 piezometers were installed to a depth of 8 m, to monitor trial pumping conducted in exploration wells. In total 75 pairs of laboratory tests and CPT, results were obtained at the site.

4.2 *Ilok port*

Ilok port which is currently under construction will be located on the right bank of the Danube 1296.5 to 1297.0 km, downstream from the Ilok-Bačka Palanka Bridge, in the Danube inundation area. The geotechnical investigation carried out at the site consisted of a total of 9 exploration wells with continuous coring to a maximum depth of 30 m. Dynamic (SPT) and static (CPTU) testing, geophysical testing using seismic refraction, multichannel analysis of surface waves (MASW), seismic static cone penetration test (SCPT), together with laboratory tests. The site yielded 36 pairs of laboratory testing and CPT results.

4.3 *Krsišće landslide*

The Krsišće landslide occurred on the southern slopes of the Medvednica Mountain, in the Markuševec area, at an altitude of approximately 300 meters. On Kršišće street, an unstable slope was detected, adjacent to house no. 43. Soil movement at the site occurs periodically along the interface between the Clay and Marl materials, where excess pore pressures develop during wet periods. Investigation work included 5 boreholes, with continuous coring to a maximum depth of 8 m, dynamic (SPT) and static (CPTU) testing, together with laboratory tests. 20 pairs of laboratory and CPT results were obtained at the site.

4.4 *Mirogoj landslide*

The Mirogoj landslide is located on the southern slope of the Medvednica Mountain. Adjacent to the Mirogoj cemetery is a slope that drops uniformly towards the north-east. The slope inclination in the area affected by the landslide is between 20° and 25°. A total of 5 borings were made, with continuous coring to a depth of 8 m, dynamic (SPT) and static (CPTU) testing was carried out in conjunction with laboratory testing. 25 pairs of laboratory tests and CPTs were gathered from the site.

4.5 *Krematorij landslide*

The Krematorij landslide is located east of Kameniti stol street, in the Gornji grad—Medveščak area, on the southern, more cavernous slopes of the Medvednica mountain. The unstable area is located between 250 and 225 m above sea level. The geotechnical investigation carried out at the site comprised of 5 exploration wells with continuous coring to a maximum depth of 12 m, dynamic (SPT) and static (CPTU) testing, together with laboratory tests. 60 pairs of laboratory testing and CPT results were obtained from the site.

4.6 *Verification site: Veliki vrh landslide*

The site located on the southern slopes of Medvednica Mountain, at an altitude between 205 and 225 metres, is a shallow translational landslide. The landslide was the result of pore pressure build up along the contact zone between Clay and Marl layers after heavy rainfall. The site investigation consisted of 4 boreholes with continuous coring to a depth of 12 m, dynamic (SPT), and static (CPTU) testing in conjunction with laboratory tests. In total 19 pairs of laboratory tests and CPT, results were gathered at the site. Table 1 shows the results of the CPT and laboratory tests for the site.

5 NEW CORRELATION

Using the data obtained from the five test sites, this paper proposes another log regression model similar in formulation to the model proposed by Mayne et al. (2010), but with a higher initial intercept value and lower constants for z, f_s, and q_t respectively. Initially, it was proposed to develop the model using just q_t and f_s, as it was postulated that the depth trend would already be accounted for within the CPT results. While this approach yielded similar accuracy and regression values, it was significantly less precise than a regression model containing z. The best fit relationship found in this study is shown in Equation 8. Both Mayne et al.'s relationship and the proposed have very similar regression values when applied to the dataset, however, as can be seen from Figure 3: The statistical correlation developed in this study, with Mayne et al. (2010) for comparison et al's equation significantly overpredicts unit weight magnitude but captures the relative increase reasonably well. The relationship from this paper effectively reduces the magnitude of Mayne et al's relationship to more closely approximate reality.

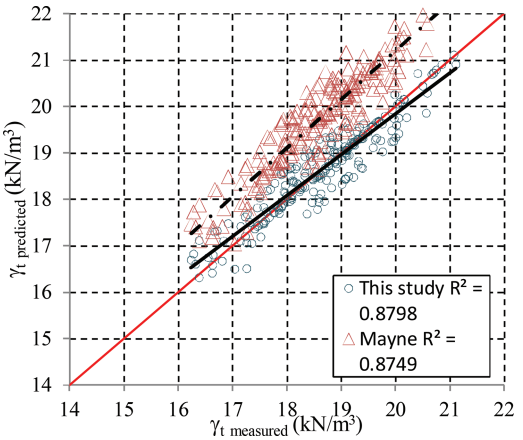

Figure 3. The statistical correlation developed in this study, with Mayne et al. (2010) for comparison.

$$\gamma_t = 11.849 + 0.109 \log z + 2.595 \log f_s + 0.561 \log q_t \tag{8}$$

6 ANN RESULTS AND DISCUSSION

The model development dataset which comprised of sleeve friction, depth, and corrected tip resistance as inputs and soil unit weight as an output was split randomly into the following proportions 80% for training, 10% for testing, and 10% for validation. For training, the ANN had access to both inputs and outputs allowing it to learn the sensitivity of each variable and understand each parameters effect on the system response. The next 10% was used as a test set, during the testing process only the inputs were supplied to the model. At the end of the testing phase, the neural network performed a system recalibration on itself so that system inputs could be more accurately mapped onto system outputs based on the test results. Following completion of the testing phase the final 10%, or the validation set, was sent to the neural network. Only inputs are sent in the validation phase, thus allowing the direct comparison of outputs from the validation set to actual measured values. Provided a good correlation has been achieved the neural weightings are saved and the entire data set is subsequently inputted blind. The resultant outputs are compared to actual outputs, see Figure 4. A regression coefficient of 0.8853 was achieved for the entire dataset, with a correlation coefficient of 0.94. As can be seen from Figure 3, there is very little data scatter, and importantly no extreme outliers. Therefore while a misclassification could occur, an extreme difference between predicted soil unit weight and measured soil unit weight is unlikely.

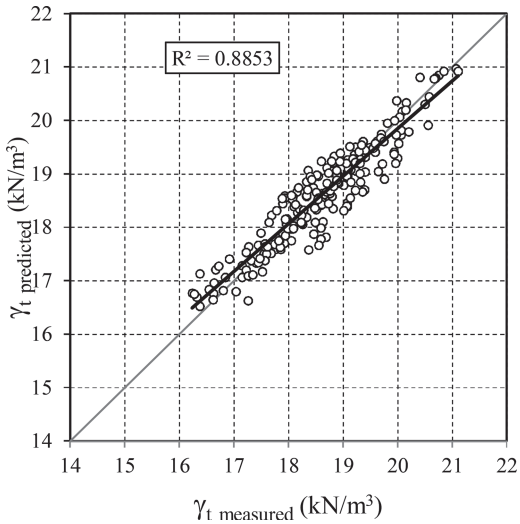

Figure 4. ANN predicted unit weight for five test sites used in model development.

Table 1. Unit weight and CPT results from Veliki vrh.

GB/CPTU	Sample no	z [m]	q_t [MPa]	f_s [kPa]	γ_t [kN/m³]
B 1/CPTU 1	1	2.20	1.63	116.00	**19.05**
	2	2.80	0.74	62.00	**18.20**
	3	3.30	0.60	38.00	**17.61**
	4	5.00	3.38	172.00	**19.72**
B 2/CPTU 2	5	2.10	1.55	93.00	**18.84**
	6	2.80	0.79	72.00	**18.72**
	7	3.60	0.62	55.00	**18.52**
	8	4.40	1.29	69.00	**18.76**
	9	5.60	1.12	90.00	**18.73**
	10	6.60	1.51	101.00	**18.90**
	11	7.20	1.58	96.00	**18.90**
B 3/CPTU 3	12	1.60	0.81	54.00	**17.43**
	13	2.20	0.62	26.00	**17.18**
	14	3.80	4.69	188.00	**20.46**
	15	5.80	2.24	104.00	**18.62**
B 4/CPTU 4	16	1.80	2.04	122.00	**19.11**
	17	2.20	1.99	84.00	**18.79**
	18	3.10	4.99	193.00	**19.27**
	19	3.70	6.59	203.00	**19.99**

To ensure the model was working correctly input data from an additional site within the same geographic region, Veliki vrh was supplied to the model. This data which can be seen in Table 1, consisted of 19 pairs of CPT and laboratory unit weight results.

An extremely good R^2 of 0.8495 was obtained for this external verification with a correlation coefficient of 0.92. The predicted unit weight versus measured unit weights is shown in Figure 5.

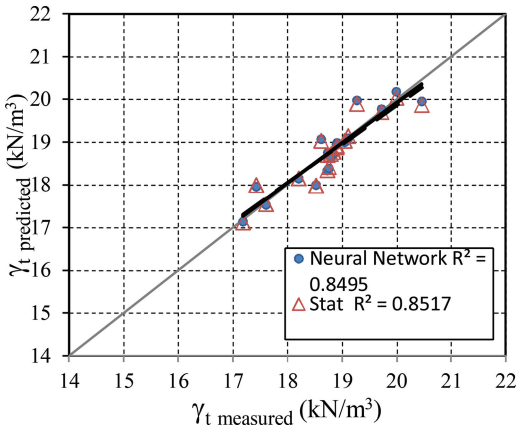

Figure 5. predicted unit weights for Veliki Vri using closed loop ANN and regression approach.

The statistical approach proposed earlier in Equation 8 performed equally well on the unseen dataset, Veliki vrh, achieving an R^2 of 0.8466. Both are shown in Figure 5, giving virtually identical results.

7 CONCLUSION

This paper presents two approaches, regression and neural network, for automatically calculating soil unit weight using CPT measurements as inputs. Both approaches could easily be performed automatically onsite as the CPT is ongoing, thus allowing for an extremely fast interpretation of soil unit weight. This would reduce the quantity of laboratory tests needed per site thus saving time and money. An additional benefit of such an approach is that any laboratory tests that are carried out can then combined with their respective CPT soundings become additional data entries for both the regression and ANN models, thus improving their future accuracy. In this way, the models can continue to evolve over time, gradually increasing in both accuracy and precision.

The approaches were developed using 216 pairs of CPT/laboratory unit weight tests from five different locations across Northern Croatia. An entirely separate sixth site Veliki vri was used as an external verification measure for the saved neural networks. The models performed extremely well on both the initial dataset and the subsequent verification dataset.

Unfortunately, ANN-based models have some drawbacks, of particular concern is the black box nature of the results, which makes proof of concept hard to verify, while also making their standalone implementation a risky process for the engineer involved. The authors think that much of this can be mitigated by testing a small number of samples from every site in the laboratory for local verification. Thus, allowing the training database to continue to grow in size over time making incorrect classifications less likely to occur. Over time reducing the cost, time, and labour involved.

This study confirms the functional link between CPT results, and soil unit weight..The developed neural network and regression models performed admirably for a wide range of soil types closely predicting soil unit weights between 16 and 21 kN/m³. The close prediction between the neural networks and the regression model is a testament to the accuracy of log regression models for predicting soil unit weights and further validates their use in everyday design situations, given their simplicity and transparency. One caveat which needs mentioning is all soils tested were either heavily or slightly over consolidated and the correlations may not perform as well in normally consolidated deposits.

REFERENCES

Basheer, I., Hajmeer, M., 2000. Artificial neural networks: fundamentals, computing, design, and application. J. Microbiol. Methods 43, 3–31.

Ghanekar, R.K., 2014. Evaluation of CPT unit weight correlations on Indian offshore calcareous fine-grained soils, in: 3rd International Symposium on Cone Penetration Testing (CPT`14). pp. 347–356.

Librić, L., Jurić-Kaćunić, D., Kovačević, M., 2017. Application of cone penetration test (CPT) results for soil classification. Građevinar 69, 11–20.

Mayne, P.W., Peuchen, J. & Bouwmeester, D., 2010. Soil unit weight estimation from CPTs., in: 2nd International Sym—Posium on Cone Penetration Testing CPT 10. Huntington Beach, pp. 169–176.

Mayne, P., 2014. Interpretation of geotechnical parameters from seismic piezocone tests. 3rd Int. Symp. Cone Penetration Test. 47–73.

Mayne, P.W., 2007. NCHRP Synthesis 368: Cone penetration testing. Washington D.C.

Mayne, P.W., Peuchen, J., 2012. Unit weight trends with cone resistance in soft to firm clays, in: Geotechnical and Geophysical Site Charactization 4, Vol 1. CRC Press, London, pp. 903–910.

Reale, C., Gavin, K., Librić, L., Jurić-Kaćunić, D., 2018. Automatic classification of fine grained soils using CPT measurements and Artificial Neural Networks. Adv. Eng. Informatics In Press.

Robertson, P., 2009. Interpretation of cone penetration tests—a unified approach. Can. Geotech. J. 46, 1337–1355.

Robertson, P.K., Cabal, K.L., 2010. Estimating soil unit weight from CPT, in: 2nd International Symposium on Cone Penetration Testing. p. 8 p.

Rojas, R., 2013. Neural networks: a systematic introduction.

Rosenblatt, F., 1958. The perceptron: A probabilistic model for information storage and organization in the brain. Psychol. Rev. 65, 386.

Tehni, H., Specifikacija, K.A., 2013. HRS CEN ISO / TS 17892–2:2004.

Cone Penetration Testing 2018 – Hicks, Pisanò & Peuchen (Eds)
© 2018 Delft University of Technology, The Netherlands, ISBN 978-1-138-58449-5

CPT in thinly inter-layered soils

D.A. de Lange & J. Terwindt
Deltares, Delft, The Netherlands

T.I. van der Linden
Royal HaskoningDHV, Amersfoort, The Netherlands

ABSTRACT: The interpretation of CPT within intervals consisting of multiple sequences of thin soil layers holds large uncertainty. For multi-layer systems, it is expected that the cone resistance would be influenced by the layer thickness (relative to the cone diameter), the number of layers within the zone of influence and the characteristic cone resistances of the individual layers. The Dutch method for determination of the pile base resistance can be used to simulate the cone resistance in thinly inter-layered soils and to come up with correction factors as function of the aspects mentioned above. A test program (parametric study) is defined in order to validate the proposed modified Dutch method. The proposed simulation method fits reasonably well with the interim test results.

1 INTRODUCTION

The resolution of CPT (Cone Penetration Testing) in delineating stratigraphic layers is related to the size of the cone tip and the friction sleeve and the sample recording rate relative to the penetration rate. A transition zone can be defined around the interface between two different soil layers, since the measured resistance will be affected by both the under—and overlying layers. The dimensions of such a transition zone are, inter alia, a function of the cone tip size. The CPT interpretation within these intervals holds large uncertainty, especially for deposits containing multiple thin layers, since the cone resistance will be affected by several surrounding layers (Van der Linden et al. 2017). For several applications a better understanding of CPT in thinly layered soils is desired. One may think of the estimation of the liquefaction potential of thin sand layers and the shear strength of thin soft layers. Current methods for correction of "thin" layers are based on analytical linear elastic solutions (e.g. Vreugdenhil et al. 1994; Robertson and Fear 1995; Joer et al. 1996) or numerical analysis for single intermediate layers only, having a thickness larger than the cone diameter (Ahmadi and Robertson 2005; Mo et al. 2016).

This paper presents a selection of interim results of a study undertaken to devise a correction method which will determine more realistic engineering properties of thin sand layers within thinly inter-layered zones. Thin layers are defined as layers which are thinner than the diameter of the penetrometer. The measured cone resistance needs to be converted to a 'clean sand' resistance, hereafter referred to as characteristic resistance. CPT has been performed in artificially constructed deposits containing multiple soil layers. The test results are simulated with the analytical method based on the Dutch method as described in Van der Linden et al (2017).

2 LITERATURE OVERVIEW

Numerical work regarding the effect of soil layering on cone resistance, compared to a uniform soil formation with the same physical properties, has been extensively investigated (e.g. Vreugdenhil et al. (1994), Robertson & Fear (1995), Van den Berg et al. (1996), Youd & Idriss (2001), Ahmadi & Robertson (2005), Walker & Yu (2010), Mo et al. (2016)), also often in combination with physical modelling, (e.g. Van den Berg (1994), Joer et al. (1996), Ahmadi (2000), Silva and Bolton (2004), Młynarek et al. (2012), Mo (2014), Tehrani et al. (2017)). However, none of the studies addressed the effect of multiple thin layers. Van der Linden et al. (2017) provides a more detailed discussion on the content of before mentioned authors.

From the literature mentioned above it can be concluded that the size and the location of the transition zone depends on the ratio between the characteristic resistances in the stiff and soft soil layer. It can be also concluded that more penetration is needed to reach the full steady state cone resistance in a sand layer than in a clay layer. Furthermore, it can be concluded that the difference

between the measured and the characteristic cone resistance in a "thin" sand layer, interbedded in soft layers, increases with increasing density index of the sand. Therefore, for multi-layer systems, it is expected that the cone resistance would be influenced by the layer thickness (relative to the cone diameter), the number of layers within the zone of influence and the characteristic cone resistances of the individual layers, which depend on, inter alia, the porosity and the stress level.

3 DUTCH METHOD

Van der Linden et al. (2017) conclude that the Dutch method for determination of the pile base resistance can be used to simulate the cone resistance in thinly inter-layered soils. However, different approaches are proposed for layer thicknesses greater and smaller than the cone diameter. The method considers the variation of the cone resistance in the range of $4D_{eq}$ (the equivalent pile diameter) below and $8D_{eq}$ above the base level and is derived from a combination of empirical data and theoretical influence shapes. The procedure of this method is set up such that a conservative approximation of the path of least resistance will be found.

Three trajectories are defined for which a governing cone resistance has to be determined by averaging, see Figure 1. The distance below the pile base over which averaging takes place (trajectory I and II) varies between $0.7D_{eq}$ and $4D_{eq}$, depending on the distance over which the minimum value will be met. The procedure to determine the governing cone resistance for the trajectories II and III is such that the q_c taken into account cannot be higher than the q_c at deeper levels of these trajectories. The distance above the pile base over which averaging takes place (trajectory III) is fixed at $8D_{eq}$.

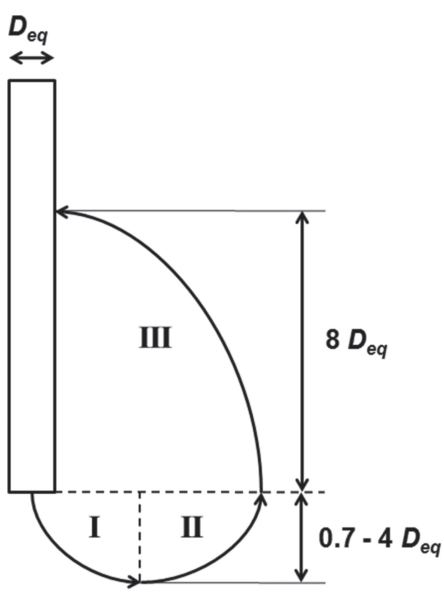

Figure 1. Schematization of the trajectories taken into account in the Dutch method.

The following relations are proposed to approach the measured cone resistance in thinly interlayered zones:

$$\text{for } H > d_{cone} : q_b = q_{c;I;av} \quad (1)$$

$$\text{for } H < d_{cone} : q_b = 0.25q_{c;I;av} + 0.25q_{c;II;av} + 0.5q_{c;III;av} \quad (2)$$

where q_b represents the measured cone resistance, H the layer thickness and d_{cone} the penetrometer diameter. The characteristic cone resistance of the individual layers has to be used as input for the calculations.

4 PHYSICAL MODELLING

4.1 *Testing program*

A test program (parametric study) was defined in order to validate the proposed modified Dutch method. The test program is a continuation of earlier work (Van der Linden, 2016). Different layer configurations, bulk density indices (I_d), stress levels and cone diameters are applied in order to investigate the influence of these parameters. CPT was performed on saturated layered soil deposits, which were artificially built up in a cylindrical container. The layered units of multiple clay and sand layers, each having an equal thickness, were sandwiched between two thicker sand layers. For each I_d a uniform sand model was prepared in addition to the layered models in order to serve as a reference. Table 1 provides details about the variations applied (not all possible combinations are tested).

4.2 *Sample preparation*

Model preparation followed the same methodology as Van der Linden (2016, 2017), i.e. pluviation of dry sand in a partially water-filled container.

Table 1. Testing variables.

Variable	Value	Unit	Value	Unit	Value	Unit
Penetrometer	25.3	mm	35.8	mm		
Density index	0.30	–	0.60	–		
Layer thickness	20	mm	40	mm	80	mm
Vertical stress	25	kPa	50	kPa	100	kPa

Table 2. Soil properties.

Parameter	Symbol	Unit	Value[1]
Cohesionless material			
Mass-Median-Diameter	d_{50}	mm	0.136
Coefficient of uniformity	d_{60}/d_{10}	–	1.4
Particle density	ρ_{grains}	kg·m^{-3}	2650
Minimum porosity	n_{min}	–	0.356
Maximum porosity	n_{max}	–	0.471
Cohesive material			
Water content	W	%	23.5 ± 0.3
Undrained shear strength[2]	$s_{u,pp}$	kPa	11.7 ± 0.9
	$s_{u,tv}$	kPa	17.3 ± 1.4
Liquid limit	LL	%	32.3
Plastic limit	PL	%	15.8
Plasticity index	PI	%	16.5
Liquidity index	LI	%	46.7
Coefficient of consolidation	c_v	m·s^{-1}	1.8 · 10^{-8}

1) Plus-minus values refer to one standard deviation. 2) Undrained shear strength index testing has been determined with pocket penetrometer (pp) and torvane (tv).

This method of preparation has been described by De Lange et al. (2016), and results in a fully saturated sand-sample. The density of the sand is controlled by periodically tamping the sand surface during pluviation. Clay layers were placed after trimming prefabricated clay bricks to the required dimensions. Densification of the sand during the placement of the clay was limited by temporarily lowering the phreatic level. By lowering the phreatic level the capillary action provides apparent cohesion to the sand. The employed sand and clay are Baskarp and Vingerling K147, respectively. Table 2 provides details on the applied soils.

During preparation the bulk density was closely monitored by measuring the sample height. Upon completion of the cone penetration tests the soil model was excavated and volume-mass density measurements were performed at various positions and depths in the model.

4.3 *Testing equipment*

The test setup itself is a further development of the setup discussed by Van der Linden et al. (2016). It consists of a cylindrical steel cell with a 0.90 m inner diameter and is 0.96 m in height. The cell wall is lined with a rubber membrane and the space in between can be filled with a film of water (a geotextile was placed in between to ensure this). In this way the horizontal stress can be controlled. The horizontal stress applied is equal to 0.5 times the vertical stress. Vertical stress is applied by a flexible water-filled cushion which is placed on top of the soil model.

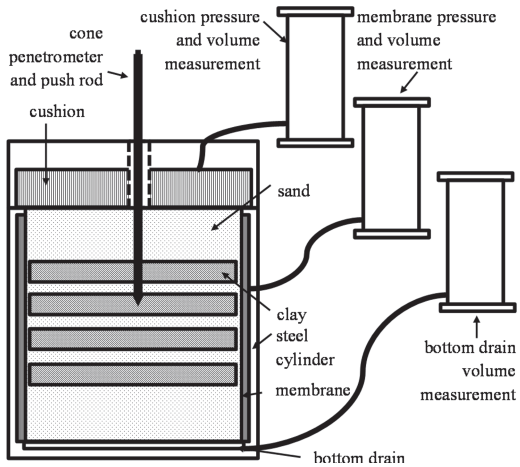

Figure 2. Schematized test setup.

The employed cone penetrometer is either a 35.8 mm or a 25.3 mm (corresponding to a cone face area of 10 cm^2 and 5 cm^2, respectively), depending on the test, and were manufactured by Fugro. The penetrometers were installed by a hydraulic jacking unit at a rate of 4 mm·s^{-1} with a measurement frequency of 4 Hz, resulting in a data point every 1 mm.

In situ vertical soil stress was monitored using a total stress transducer while the applied horizontal and vertical stress was measured using pressure transducers. Any change in volume of the soil model was monitored by measuring the volume change in the water supply of both the membrane and the cushion and any water dissipated through the bottom drain of the test setup. Figure 2 shows a schematic overview of the test setup.

4.4 *Measurement uncertainty*

The measurement uncertainty of the cone resistance has been estimated with the uncertainty provided in the calibration certificates. In the softer clay layers of about 500 kPa cone resistance the measurement uncertainty is about 35 kPa (or 7.0% of the indicated value). In loose sand with a cone resistance of about 3.5 MPa, the measurement uncertainty is assessed to be about 45 kPa (or 1.3% of the indicated value).

Uncertainty for (bulk) density index measurements in cohesionless material has been assessed using guidelines presented in EA-4/02 (2013). For small, but accurately known, volume-mass density measurements, such as performed during the excavation of the model, the measurement uncertainty was assessed to be about 6% I_d. For bulk I_d measurements during preparation, the uncertainty

strongly depends on the sample height. Because diameter and mass of the sample are accurately known compared to the sample height, the height is the governing parameter influencing the uncertainty. The uncertainty of bulk density index for the full preparation height of 0.96 m is about 2.5% I_d. For smaller intervals of, say, 0.05 m, the uncertainty increases to about 20% I_d.

4.5 *Interim results*

Only some of the results can be presented in this paper, since the investigation was still ongoing at the time of writing. It has been chosen to present the CPT results in two artificial soil samples: sample 2 and 3. Sample 2 contained a layered unit of 4 clay layers and 3 sand layers, each having a layer thickness of 4 cm, while sample 3 contained a layered unit of 6 clay layers and 5 sand layers, each having a layer thickness of 2 cm. An initial bulk density index of around 30% has been applied for these samples. Multiple CPTs (2 or 3) were performed at the same soil model. First, the desired stress level has been applied and after reaching a sufficient degree of consolidation a CPT has been performed. Subsequent tests were performed at different locations and stress levels, leaving the previous cone(s) in place. The CPTs were performed at 300 mm from the container wall and a distance between the CPT locations of 260 mm has been applied.

Figure 3 shows the measured cone resistance in sample 2 for two stress levels (vertical stress applied to the top of the sample is 25 kPa and 50 kPa, respectively). The individual layers can be clearly distinguished. Also the effect of the applied stress level can be observed resulting in higher a cone

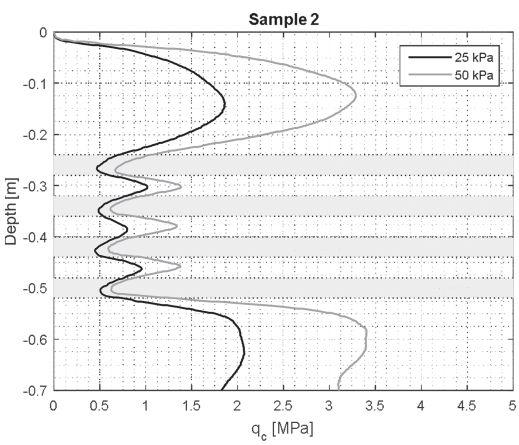

Figure 3. Test results sample 2 (the four 4 cm thick clay layers are indicated in gray).

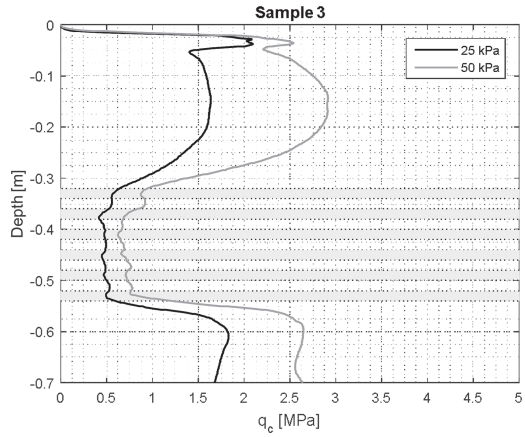

Figure 4. Test results sample 3 (the six 2 cm thick clay layers are indicated in gray).

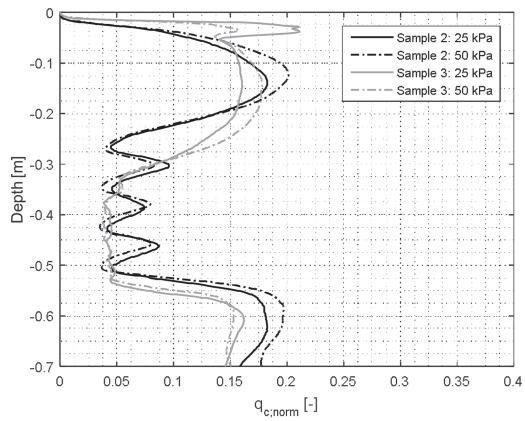

Figure 5. Normalized cone resistance of the four tests presented in this paper.

resistance for higher a stress level. Figure 4 shows the measured cone resistance in sample 3 for the same stress levels. In this case, the individual thin layers can be hardly distinguished. The initial peak in cone resistance at about 5 cm depth is an artifact of a cylindrical tube which was in place to protect the cushion.

Figure 5 shows the cone resistance in sample 2 and 3 normalized for the applied stress level using the following equation (based on Lunne et al.1997):

$$q_{c;norm} = \frac{q_c}{\sigma_v^{0.71}} \tag{3}$$

In which σ_v is the applied vertical stress level.

5 NUMERICAL SIMULATION

Simulations are made by calculating the tip resistance at each mm by the method as described in section 3. In order to get a more realistic simulation the moving average over a height of 27 mm (the cone height) has been calculated. The average of the measured cone resistance in the upper and bottom sand layer is used as characteristic cone resistance for the sand layers. For the clay layers a value of 0.035 is used, based on the test results. Figure 6 shows the simulation of the tests performed at sample 2. The normalized test results are also plotted in this graph. A good fit is obtained with the proposed method.

Figure 7 shows the simulation of the tests performed at sample 3 with the normalized test results. A good fit is obtained for the layered unit, while the simulation deviates strongly from the measurements for the transition zones between the layered unit and the upper and bottom sand layers. However, since the difference between the maximum measured resistance within a layer and the characteristic resistance is of interest in this investigation, the proposed method can still be used.

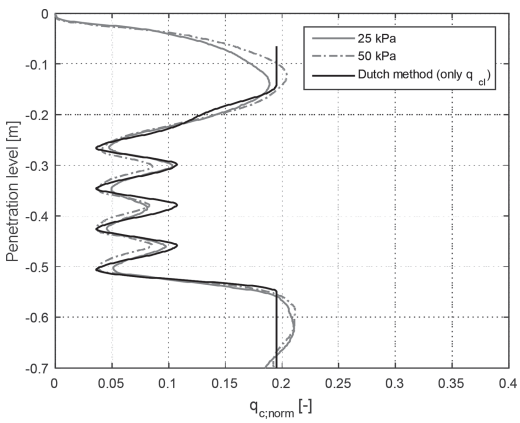

Figure 6. Simulation of CPTs at sample 2.

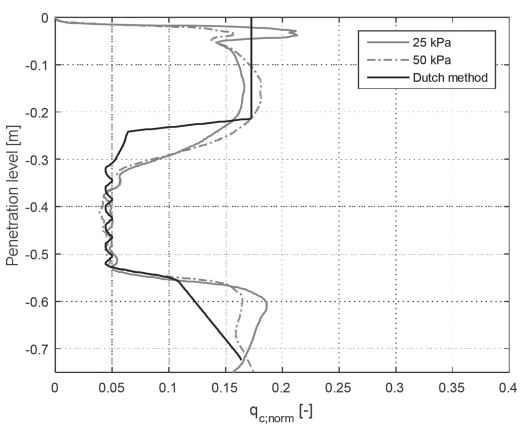

Figure 7. Simulation of CPTs at sample 3.

6 DISCUSSION

It should be noted that the penetration rate applied in the experiments (4 mm/s) differs from the standard rate applied in the field (20 mm/s). Furthermore, the cone resistance has not been corrected since no pore pressure measurement was performed. The effects of both these aspects are considered to be minimal.

Local variation in void ratio was observed in the artificially constructed soil samples, since it was hard to control the density index during preparation of saturated layered samples. This aspect has to be taken into account in the further analysis of the results and in order to come up with a correction method for CPT in thinly inter-layered soils.

It should be noted also that the tested multi-layered samples contained sand and clay layers of equal thickness. This is certainly not always the case in the field. Therefore, the results cannot simply be applied to all thinly inter-layered soils.

7 CONCLUSION AND FUTURE WORK

A test program (parametric study) is defined in order to validate the proposed simulation method for CPT in thinly inter-layered soils. The proposed simulation method fits reasonably well with the interim test results. The simulation method can be used to set-up a correction method. Such a method should incorporate the influence of the layer thickness (relative to the cone diameter), the number of layers within the zone of influence and the characteristic cone resistances of the individual layers. The recognized uncertainties have to be taken into account as well.

ACKNOWLEDGMENTS

The authors would like to acknowledge the NAM (Nederlandse Aardolie Maatschappij B.V.) for financing the research, M. Korff and R. Stoevelaar for their review and F.M. Schenkeveld and R. Zwaan for their invaluable assistance and input with regards to development of the test setup and model preparation.

REFERENCES

Ahmadi, M.M. & Robertson, P.K. 2005. Thin-layer Effects on the CPT q_c Measurement. *Canadian Geotechnical Journal* 42:1302–1317.

Ahmadi, M.M. 2000. Analysis of cone tip resistance in sand. *Ph.D. thesis.* University of British Columbia, Vancouver, B.C., Canada.

De Lange D.A., Van Beek V.M., Schenkevel F.M. et al. (2016) Preparation techniques for unconventional sand samples. In Proceedings of the 3rd European Conference on Physical Modelling in Geotechnics (EUROFUGE 2016), Nantes, France, pp. 61–66.

EA. 2013. Evaluation of the uncertainty of measurement in calibration, EA-4/02. *European Co-operation for Accreditation of Laboratories*, 75 p.

Joer, H.A., Randolph, M.F. & Liew, Y.H. 1996. Interpretation of Cone Resistance in Layered Soils. Proceedings 7th Australia New Zealand Conference on Geomechanics (Jaska MB, Kagawa WS and Cameron DA (eds)). Institution of Engineers, Australia, pp. 92–97.

Lunne T., Robertson P.K. and Powell J.J.M. (1997) Cone Penetration Testing in Geotechnical Practice. *First edition, Blackie Academic & Professional, ISBN 0751403938.*

Młyranek, Z., Gogolik, S. & Półtorak, J. 2012. The effects of varied stiffness of soils layers on interpretation of CPTU penetration characteristics. *Archives of Civil and Mechanical Engineering* 12:253–264.

Mo, P.Q. 2014. Centrifuge Modelling and Analytical Solutions for the Cone Penetration Test in Layered Soils. *Ph.D. thesis*, The University of Nottingham, Nottingham, UK.

Mo, P.Q., Marshall, A.M. & Yu, H.S. 2016. Interpretation of Cone Penetration Test Data in Layered Soils Using Cavity Expansion Analysis. *Journal of Geotechnical and Geoenvironmental Engineering* 143(1), ISSN 1943–5606

Poel, J.T., & Schenkeveld, F., 1998. A preparation technique for very homogeneous sand models and CPT research. In *Proc. of the int. conf. Centrifuge 98*, Tokyo, 149–154.

Robertson, P.K. & Fear, C.E. 1995. Liquefaction and its evaluation. *In Proceedings First International Conference on Earthquake Geotechnical Engineering (Ishihara ed.)*, Balkema, Rotterdam, pp. 1253–1289.

Silva, M. & Bolton, M.D. 2004. Centrifuge penetration tests in saturated layered sands. In *Proceedings ISC-2 on Geotechnical and Geophysical Site Characterization* (Viana da Fonseca and Mayne (eds)), Millpress, Rotterdam, pp. 337–384.

Tehrani, F.S., Arshad, M.I., Prezzi, M., and Salgado, R 2018. Physical Modeling of Cone Penetration in Layered Sand. *To be published in Journal of Geotechnical and Geoenvironmental Engineering Volume 144 Issue 1 - January 2018*

Van den Berg, P., De Borst, R. & Huétink, H. 1996. An Eulerian Finite Element Model for Penetration in Layered Soil. *International Journal for Numerical and Analytical Methods in Geomechanics* 20:865–886.

Van der Linden, T.I., 2016. Influence of multiple thin soft layers on the cone resistance in intermediate soils. *MSc thesis*. Delft University of Technology, Delft, the Netherlands.

Van der Linden, T.I., De Lange, D.A., & Korff, M., 2017. Cone Penetration Testing in Thinly Inter-Layered Soils. *Geotechnical Engineering.* Advance online publication. doi: 10.1680/jgeen.17.00061

Vreugdenhil, R., Davis, R. & Berrill, J. 1994. Interpretation of Cone Penetration Results in Multilayered Soils. *International Journal for Numerical and Analytical Methods in Geomechanics* 18:585–599.

Walker, J. & Yu, H.S. 2010. Analysis of the cone penetration test in layered clay. *Géotechnique* 60(12):939–948

Youd, T.L. & Idriss, I.M. 2001. Liquefaction Resistance of Soils: Summary Report from the 1996 NCEER and 1998 NCEER/NSF Workshops on Evaluation of Liquefaction Resistance of Soils. *Journal of Geotechnical and Geoenvironmental Engineering* 127(4):297–313.

Cone Penetration Testing 2018 – Hicks, Pisanò & Peuchen (Eds)
© 2018 Delft University of Technology, The Netherlands, ISBN 978-1-138-58449-5

CPT based unit weight estimation extended to soft organic soils and peat

H.J. Lengkeek
Delft University of Technology, Delft, The Netherlands
Witteveen+Bos, Deventer, The Netherlands

J. de Greef
Witteveen+Bos, Deventer, The Netherlands

S. Joosten
Delft University of Technology, Delft, The Netherlands

ABSTRACT: A reliable estimate of the saturated soil weight from CPT analysis can be useful for various purposes. An often used relation that gives a reasonable first approximation is presented by Robertson & Cabal (2010). In The Netherlands very soft and highly organic soils are omnipresent and these types of soil are absent in the aforementioned relation. In this paper a new relation is proposed that can be used to estimate the saturated soil unit weight for a wider range of soils, from sands to highly organic soils.

1 INTRODUCTION

1.1 *Problem description*

Cone penetration testing has a widespread application in The Netherlands, from code regulated pile foundation and dike design, and in recent years liquefaction triggering assessments in Groningen related to induced earthquakes.

CPT based parameter estimation is applied in a wide variety of geotechnical projects. The quantity of complementary laboratory tests in general depends on the risks involved in a project. Due to increased computer performance more and more analyses are being performed and will be automated. Since a CPT provides continuous data in a vertical soil profile, the obtained data lends itself for automated interpretation.

The use of CPTs in the design of dikes in The Netherlands has intensified with the Dijken op Veen method (Zwanenburg & Jardine, 2015). In this method a layer specific empirical cone factor (N_{kt}) is determined and applied directly to the CPTs to derive the undrained shear strength (S_u). In order to do so, laboratory test are required to determine the in-situ undrained shear strength, the undrained shear strength ratio (S), the unit weight (γ) and the pre-consolidation stress (p_c). These tests are normally performed on undisturbed samples taken from a few boreholes with an adjacent CPT. This allows for correlating the aforementioned parameters. The large natural variability associated with geotechnical soil properties is taken into account by applying the correlation to each individual CPT.

In practice it turns out that the identification of soil type and in particular the estimation of unit weight for soft organic soils and peats is often not very accurate. Most existing methods are validated for, and therefore applicable to mineral soils only. Applying these correlations will lead to an overestimation of the unit weight and consequentially and erroneous prediction of stresses and strength.

1.2 *Scope*

By combining soil properties obtained from laboratory testing with fairly constant CPT results, layer-, site- or region-specific correlations can be obtained between CPT measurement data and geotechnical properties of the soil. When automating this process for all measurement points or multiple CPTs, it is preferable to have a direct reliable relation between the measurement data and the estimated soil unit weight, so that human interference is limited to a minimum. Moreover, because many soil properties (and thus the applicable correlations) depend on the stress level, it is paramount to have an indication of the stress profile over depth. For this purpose use of lookup tables (such as provided in the Dutch version of Eurocode 7) is not preferable.

1.3 *Approach*

The approach is based on matching laboratory tests results with CPT data. The CPT data is taken from the same level as the samples, where a maximum distance between borehole and CPT of 1 meter is applied. Soil investigation programs at the locations from Table 1 across the Netherlands have been used.

For the definition of the CPT Class reference is made to ISO 22476-1:2012 which is effectively in use in The Netherlands since February 2013.

In Table 2 an overview of both the number of samples and the minimum and maximum values of the observed values are presented.

Chapter 2 will further elaborate on the unit weight of organic soils as measured in the laboratory. A new correlation is presented in order to estimate the organic content based on the water content. This correlation can be useful in practice because most often the organic content or specific gratify is not determined.

Chapter 3 will elaborate on a new framework correlation for the unit weight based on the cone resistance and friction ratio, calibrated with laboratory measurements.

Table 1. Overview of CPT locations.

Location	Number of CPTs	Class
Amsterdam	42	2
Bergambacht	19	2
Delfzijl	32	2
Eemdijk	42	1
Eemshaven	52	2
Katwoude	36	1
Krimpen aan den IJssel	11	1
Leeuwarden	6	2
Rotterdam	6	2
Terneuzen	46	2
Uitdam	8	2

Table 2. Overview number of samples.

Property		Number of samples	Minimum value	Maximum value
q_t	[MPa]	300	0.10	33.05
R_f	[%]	300	0.22	10.54
u_2	[MPa]	218	–0.06	1.67
γ_{sat}	[Mg/m³]	300	10.05	21.33
γ_{dry}	[Mg/m³]	257	0.81	18.29
Water content	[%]	294	16.6	1145
Loss on ignition	[–]	78	0.0	89.5
Specific gravity	[–]	9	1.45	2.33

2 UNIT WEIGHT OF ORGANIC SOILS

2.1 *Organic clays and peats*

Large parts of The Netherlands have Holocene deposits with organic soils such as peat. The specific gravity in organic soils is affected by the organic constituents, and cannot simply be set to somewhere near 2.7 as in mineral soils. Cellulose has a specific gravity of approximately 1.6, while for lignin it is approximately 1.4. These low values reduce the compounded specific gravity of organic soils (Den Haan & Kruse, 2006). Consequently the density of organic soils is lower than mineral soils.

The organic content is unfortunately not always measured in practice. A collection of measurements from various soil investigation programs across the Netherlands is presented in Figure 1. Herein the measured loss on ignition (closely related to the organic content) is plotted measured saturated water content. Equation 1 presents the best fit to the data and is a slight adjustment to the correlation presented by Mitchell & Soga (2005).

$$N = 0 < \frac{(W - 18.3)}{6.35} < 90 \quad (1)$$

In which:

N is the loss on ignition [%]

W is the saturated water content [%]

Equation 1 can be used in case the field classification indicates organic soils and no measurements of organic content has been performed. Once the loss on ignition is known the specific gravity (ρ_s) of the solids can be determined. In Figure 2 the measurement loss on ignition is plotted against the

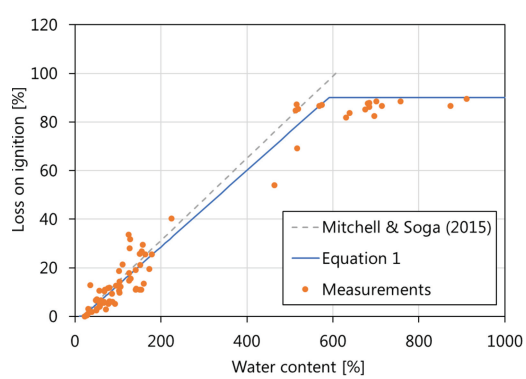

Figure 1. Measurements versus correlation Mitchell & Soga.

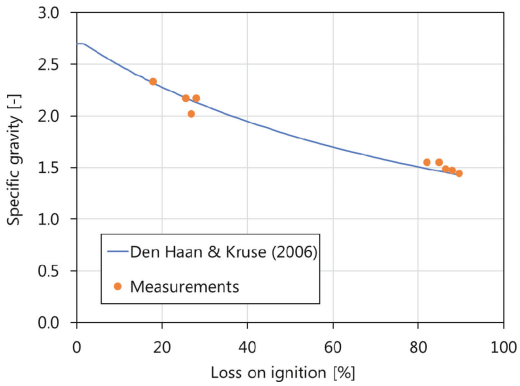

Figure 2. Measurements versus correlation Den Haan & Kruse.

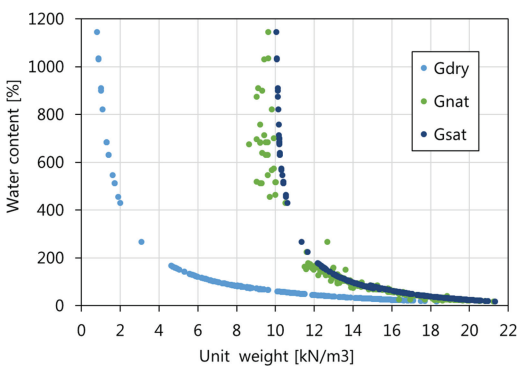

Figure 3. Measured unit weights.

specific gravity together with Equation 2 as presented in Den Haan & Kruse (2006).

$$\frac{1}{\rho_s} = \frac{N}{1.354} + \frac{(1-N)}{2.746} \tag{2}$$

The data fits very well with the existing equation and data of Den Haan & Kruse (2006). This is probably the reason why this test is not often performed in practice. The specific gravity is required to calculate the correct densities and other classification parameters, in particular the void ratio. In Figure 3 the measured dry and natural unit weights are presented together with the calculated saturated unit weight. From Figure 1 to Figure 3 it can be observed that there is practically an absence of data on organic clays and peats with a saturated unit weight between 11.0–12.0 kN/m^3, dry unit weights between 2.0–4.5 kN/m^3, water content between 200–400%, loss on ignition between 30–70% and specific gravity between 1.6–2.0 [-]. Apparently these soils are less present in the Holocene deposits in The Netherlands.

3 PROPOSAL NEW FRAMEWORK AND UNIT WEIGHT CORRELATION

3.1 *Existing methods*

Estimating the soil unit weight from CPT measurement data is required to determine the total and effective stresses in a soil profile. As such this step is at the basis of further CPT data interpretation and evaluation as for many relations correcting for the in-situ (effective) stress level is required.

One way to determine unit weights and an initial stress profile is by using look-up tables. After having identified a certain soil type from the raw measurement data, e.g. Douglas & Olsen (1981) and Robertson et al. (1986), a discrete unit weight value can be assigned to each soil type after which the total and effective vertical stresses can be computed. Using a continuous rather than a discrete function is however preferable because also intermediate states and densities can be accounted for.

Robertson & Cabal (2010) proposed a continuous function where the saturated unit weight is a function of the cone tip resistance q_t and the friction ratio R_f. The downside of their formulation is that it is only derived for clays and sands that have saturated unit weights of 15 kN/m^3 and higher. As can be observed from the dotted curves in Figure 4, the estimated unit weight increases with increasing friction ratio for all soil types. For soft clays and organic soils typically the opposite is observed, namely that the saturated unit weight is expected to decrease as the friction ratio increases as a consequence of the increase of the organic content in the soil.

Mayne et al. (2010) used a regression analysis on a wider array of soil types including soft clays and silts with a minimum considered γ_{sat} of about 12 kN/m^3. Their regression analysis resulted in the formulation presented by Equation 3.

$$\gamma_{sat} = 1.95 \cdot \gamma_w \cdot \left(\frac{\sigma'_{vo}}{\sigma_{atm}}\right)^{0.06} \cdot \left(\frac{f_s}{\sigma_{atm}}\right)^{0.06} \tag{3}$$

Although this relation captures the range of interest better, an iteration or first estimate of the vertical effective stress is required which is surmountable, but undesirable nonetheless. The same holds for relations that depend on the shear wave velocity, unless SCPT measurement data is available. As the latter is most often not the case, the application range of such relations is less desirable.

Mayne (2014) furthermore suggests a relation that is solely dependent on the sleeve friction f_s which gives reasonable results to the soft clay domain. When organic soils are considered the relation seems clearly off. By considering the graphical interpretation of f_s relation introduced

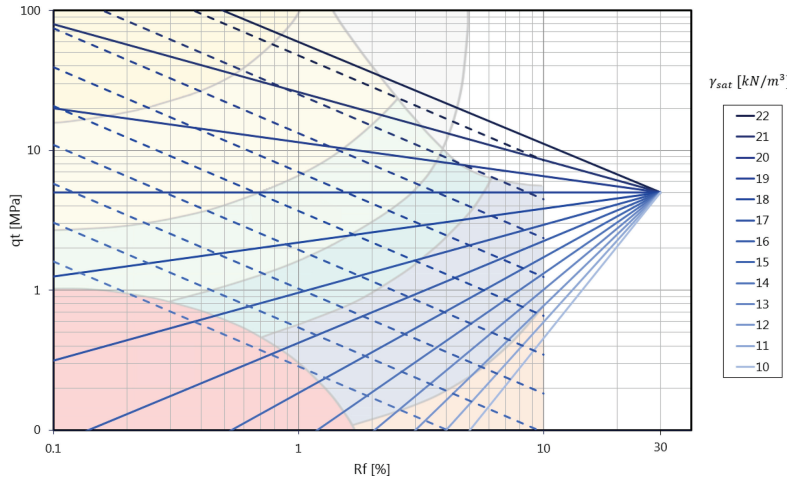

Figure 4. Graphical representation of the framework by Robertson & Cabal (dotted) and the proposed framework (continuous).

by Mayne (2014) it can be seen clearly that organic peats do not fall within the desired range.

3.2 *Formulation*

A new formulation is proposed to estimate the soil unit weight from CPT measurement data, having the following expedient properties:

- The saturated unit weight is a continuous function of the standard CPT measurement data
- No iterative procedure is required
- The application domain is extended to the soft and organic soils typically found in The Netherlands

The analytical formulation is given by Equation 4. Similar to the proposed relation by Robertson & Cabal (2010), contours of equal unit weight can be drawn in the q_t-R_f plane (see Figure 4).

$$\gamma_{sat} = \gamma_{sat,ref} - \beta \cdot \frac{\log\left(\frac{q_{t,ref}}{q_t}\right)}{\log\left(\frac{R_{f,ref}}{R_f}\right)} \tag{4}$$

Herein:

$\gamma_{sat,ref}$ is the reference unit weight at which the cone resistance is constant regardless of R_f.
$q_{t,ref}$ is the reference cone resistance at which the unit weight is constant regardless of friction ratio.
$R_{f,ref}$ is the reference friction ratio at which the apex of all lines of equal unit weight is located.
β is a measure for the inclination of the equal unit weight contours.

The functional form of Equation 4 implies that for all cone tip resistances lower than $q_{t,ref}$ the saturated unit weight decreases with increasing friction ratio. Although the functional form allows for the calculation of values of γ_{sat} lower than 9.81 kN/m^3 (bottom right corner of Figure 4) it is recommended to use this value as a practical cut-off since the saturated unit weights will never be far less than the unit weight of water. Peats however often contain gas and therefor the natural unit weight can be as low as 9.0 kN/m^3 as shown in Figure 3.

The basic formulation is such that the reference values can easily be chosen and the inclination parameters easily be fitted. This can be done for a specific soil type, a site specific layer or in general for projects or even large regions as done here.

3.3 *Verification with data*

To verify the proposed framework and Equation 4, values of saturated unit weight obtained from laboratory measurements are compared with CPT measurement data at mid sample depths. Data is obtained at multiple locations and at various depths. Requirement for this verification procedure is that the borehole from which the sample is taken and the CPT are in close proximity (at maximum 1 m) and the variation in CPT measurement data is not too large. On some locations this turned out to be an issue because the Holocene deposits in The Netherlands show significant variation in vertical and horizontal direction and the layer thickness is limited.

Using the proposed framework the whole range of soils and unit weights can be addressed as is shown in Figure 4 to Figure 6. By combining

a regression analysis with expert judgment the adopted values to be implemented in Equation 4 are presented in Table 3. For this purpose the 300 data points mentioned in Table 2 are used.

A comparison between the measured and the calculated saturated unit weights is also made for other available correlations. Graphically this is presented in Figure 5, where for the sake of clarity the correlation by Mayne (2014) is not shown. The observed trend, namely that the calculated values are too high when organic soils are considered, is equal. Table 4 gives the R^2 values and slopes for the four considered methods. From these values it is obvious that over the whole considered range the proposed framework is superior to the correlations.

The general trend (Pearson R^2 and slope [1:x]) of the proposed correlation has improved significantly. The variation is large but the standard error on regression (Sxy) is reduced. As noted earlier in the method by Robertson & Cabal (2010) no values of γ_{sat} below 15 kN/m³ were considered and Mayne

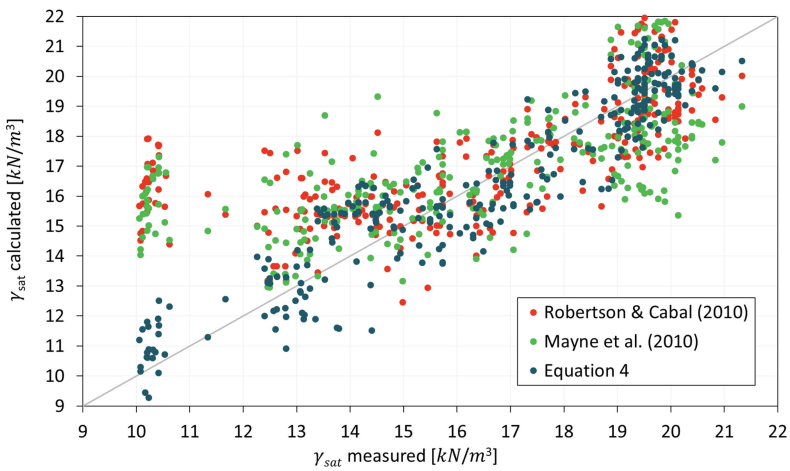

Figure 5. Measured versus calculated saturated unit weights using some of the different correlations from Table 4. Note that herein no cut-off value is applied for the minimum value of the calculated unit weight.

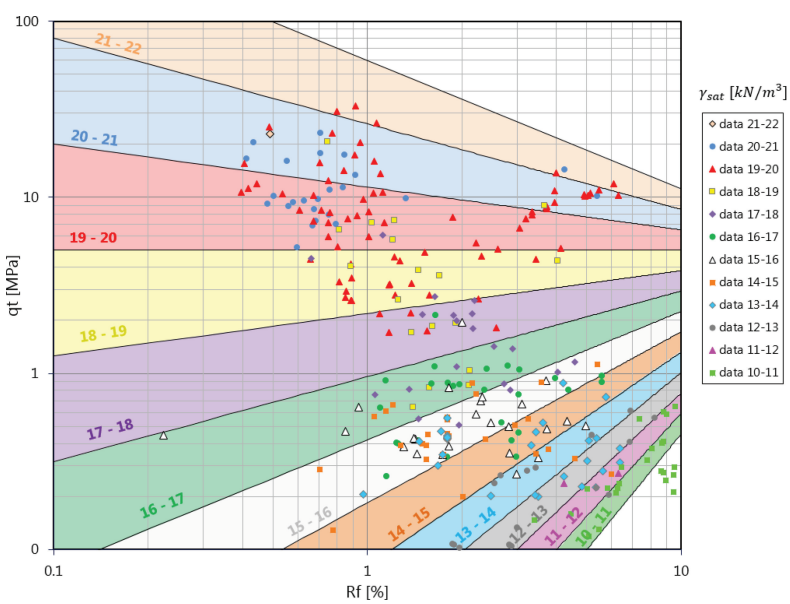

Figure 6. Graphical representation of the measurement data in the proposed framework at discrete unit weight intervals.

Table 3. Proposed parameters for Equation 4.

Parameter	Adopted best fit values
$\gamma_{sat,ref}$	19.0
$q_{t,ref}$	5.0
$R_{f,ref}$	30.0
β	4.12

Table 4. Results for multiple methods.

Method	R^2	slope [1:X]	Sxy
Equation 4	0.88	0.95	1.13
Robertson & Cabal (2010)	0.49	0.45	1.46
Mayne et al. (2010)	0.45	0.47	1.65
Mayne (2014)	0.39	0.42	1.68

et al. (2010) focus mainly on soft clays and silts with a minimum considered γ_{sat} of about 12 kN/m^3.

Therefore a comparison is also made for measured $\gamma_{sat>}$ 15 kN/m^3 based on 193 measurements. The R^2 is 0.77 for Equation 4 compared to 0.28–0.60 for the existing correlations. This means that also for non-organic soils a better estimation is found.

The standard error of the estimated unit weight is typically ± 1 kN/m^3. This error is first of all caused by the distance between CPT and borehole and the variation in lateral and vertical direction. Furthermore the measurement accuracy of the CPTs, in particular for peats with very low cone resistance and sleeve friction. But also the accuracy of the laboratory tests as it turned out that in about 5% of the samples the measured unit weight and water content were inconsistent. Finally the error is inherent to the variation in soil types, effective stress, over-consolidation, aging, organic content, saturation etc.

In addition a comparison has been made between Class 1 and Class 2 CPTs for $\gamma_{sat<}$ 15 kN/m^3. The R^2 is respectively 0.71 and 0.78. The difference is not much but still it is surprising that the Class 1 CPTs have a lower R^2. This could be explained by the very low measured q_c and f_s values of peats that where mainly investigated by Class 1 CPTs.

4 CONCLUSIONS AND RECOMMENDATIONS

- The correlations by Mitchell & Soga (2005) and Den Haan & Kruse (2006) are confirmed, where it appears that the former can be slightly improved. This will enhance better prediction of the density and classification parameters of organic soils.
- The new framework and proposed equation for estimating the saturated unit weight based on q_t and R_f measurements can be applied to the entire range of firm sandy soils to organic soils and peat, as typically can be found in Holocene sedimentary deposits in The Netherlands.
- For the considered soil data, the proposed relationship outperforms other considered correlations. The variation in the estimation is however still considerable and comparable to earlier studies.
- It is recommended that care is taken when applying the relation to other non-sedimentary soils. The authors are curious to see how the proposed framework performs for other type of soils as the framework allows for adjusting the fitting parameters.

ACKNOWLEDGEMENTS

This work is part of the Perspectief research programme All-Risk with project number P15–21, which is (partly) financed by NWO Domain Applied and Engineering Sciences. The authors would like to thank Professor S.N. Jonkman of Delft University of Technology for his review.

REFERENCES

Den Haan, E.J., Kruse, G.A.M. 2006. Characterisation and engineering properties of Dutch peats, Report No. UCD/CGM-14/01. Proceedings of the 2nd international workshop on characterisation and engineering of natural soils, Singapore, vol. 3: 2101–2133.

Douglas, B.J., Olsen, R.S. 1981. Soil classification using electric cone penetrometer. Proceedings of ASCE conference on Cone Penetration Testing and Experience, St. Louis, Missouri, USA.

International Organization for Standardization. 2012. Geotechnical investigation and testing - Field testing - Part 1: Electrical cone and piezocone penetration test.

Mayne, P.W., Peuchen, J., Bouwmeester, D. 2010. Soil unit weight estimation from CPTs. Proceedings, 2nd International Symposium on Cone Penetration Testing, Huntington Beach, California, USA.

Mayne, P.W. 2014. Interpretation of geotechnical parameters from seismic piezocone tests. Proceedings, 3nd International Symposium on Cone Penetration Testing, Las Vegas, Nevada, USA.

Mitchell, J.K., Soga, K. 2005. Fundamentals of Soil Behavior, 3rd Edition, Page 182, Figure 10.12.

Robertson, P.K., Campanella, R.G., Gillespie, D., Greige, J. 1986. Use of piezometer cone data. Proceedings of ASCE Specialty Conference In-Situ '86: Use of In-situ Testing in Geotechnical Engineering.

Robertson, P.K., 2009. Interpretation of cone penetration tests – a unified approach. *Canadian Geotechnical Journal, vol.46*: *1337–1355.*

Robertson P.K, Cabal K.L. 2010. Estimating soil unit weight from CPT. Proceedings, 2nd International Symposium on Cone Penetration Testing, Huntington Beach, California, USA.

Zwanenburg C., Jardine R.J. 2015. Laboratory, in situ and full-scale load tests to assess flood embankment stability on peat. *Géotechnique 65(4): 309–326.*

Cone Penetration Testing 2018 – Hicks, Pisanò & Peuchen (Eds)
© 2018 Delft University of Technology, The Netherlands, ISBN 978-1-138-58449-5

Impact of sample quality on CPTU correlations in clay—example from the Rakkestad clay

J.S. L'Heureux, A.S. Gundersen, M. D'Ignazio, T. Smaavik, A. Kleven, M. Rømoen, K. Karlsrud, P. Paniagua & S. Hermann
Norwegian Geotechnical Institute (NGI), Oslo, Norway

ABSTRACT: As part of the zoning plan for the new 30 km long highway, E16, from Nybakk to Slomarka, an extensive laboratory and field testing campaign was conducted by NGI. The deposit along the highway is a normally to slightly overconsolidated clay with a water content in the range of 30–45% and a plasticity index ranging between 7–25%. 72 mm diameter piston samples at 70 localities were taken and CPTUs were carried out at over 120 locations. About 180 CRS oedometer tests and 360 triaxial tests were performed. These results generally show good to excellent sample quality. However, due to the interpreted lower values of undrained shear strength from local CPTU correlations, 9 block samples were retrieved at 3 locations and additional laboratory testing was performed. The active undrained shear strength obtained from the block samples was up to 53% higher. Based on this data set, correlations were established to optimize the engineering solutions for the new road and to address the impact of sample disturbance on geotechnical engineering parameters. The results lead to important economical saving for the project and highlight the need for local and high quality samples for CPTU correlations in soft and sensitive clays.

1 INTRODUCTION

All building and construction works require reliable and proper determination of geotechnical design parameters. A careful consideration of the most appropriate investigation method is likely to result in improved understanding of soil behaviour and, therefore, in more cost-effective and sustainable solutions for the construction, transport and energy sectors. There is a need for better understanding of the behavior of soft and sensitive clays in order to improve geotechnical design, make it more innovative, and to reduce risks related to e.g. landslides and excavation failures.

NGI was recently involved in the elaboration of the detailed zoning plan for the new highway, E16, from Nybakk to Slomarka (approximately 50 km northeast of Oslo, Norway). Samples were collected using a piston sampler (Ø72 mm) at c. 70 localities and CPTU soundings were carried out at over 120 locations. About 180 CRS oedometer tests and 360 triaxial tests were carried out to assess the strength and stiffness properties of the Rakkestad clay along this E16 section. The results generally show good to excellent sample quality. However, the undrained shear strength interpreted from local CPTU correlations and based on the laboratory results was about 15% less than expected from previous experience.

To evaluate the impact of sample quality on the CPTU correlations, nine block samples (Sherbrooke type; Ø250 mm) were retrieved at three locations and additional laboratory testing was performed on the clays. This would allow for an optimization of the chosen design parameters and thereby optimize engineering solutions in connection with the construction of the new road.

The goals of the present paper are to demonstrate and document the impact of sampling methods on the stiffness and strength properties of the Rakkestad Clay, and to give recommendations on the most appropriate CPTU correlations for assessing the strength and stiffness properties of this clay. The results lead to important economical saving for the project and highlight the need for local and high quality samples for CPTU correlations in soft and sensitive clays.

2 STUDY AREA AND DATA INCLUDED IN THIS STUDY

The location of the planned highway, E16, from Nybakk to Slomarka is shown in Figure 1. The soil conditions in the study area are fairly homogenous and can be generalized with three layers. The top layer consists of a 0.4 m thick cropland overlying a layer of desiccated clay or dry crust underneath.

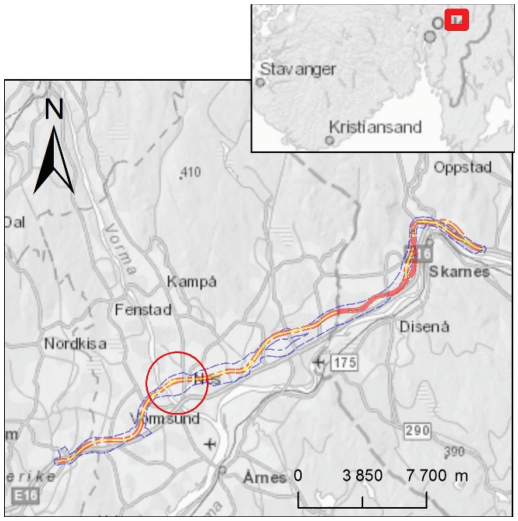

Figure 1. Location of the study area with the planned highway E16. The red circle shows the location where block samples were taken in the study area.

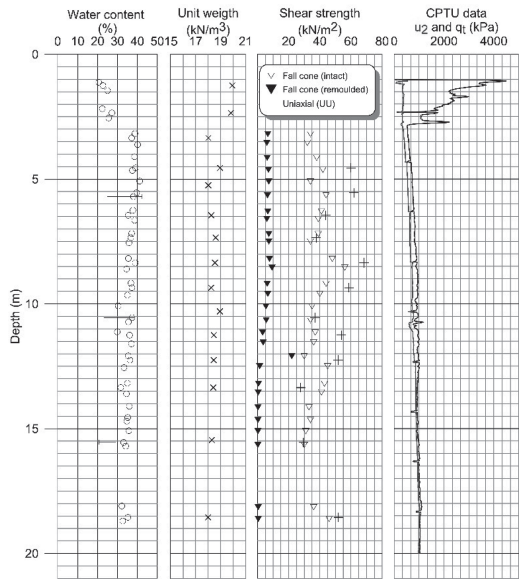

Figure 2. Typical borehole log (2371) in the study area showing results from index tests, strength tests and CPTU.

The dry crust generally extends 3–4 m below the ground surface. Further down, a normally consolidated and sensitive marine clay is found. The sensitivity (S_t) of the clay varies in this deeper layer (S_t up to 230) and the clay is also found to be quick (i.e. remolded undrained shear strength; $s_{ur} < 0.5$ kPa) at certain localities and depths. Aging may have led to some overconsolidation in the clay. The thickness of the marine clay deposit varies from approximately 20 to 45 m below the ground surface.

A high number of undisturbed samples were retrieved from 102 boreholes with an Ø72 mm GEONOR piston sampler. The compiled database with results from tests on 72 mm samples is further referred to as the *Reference database.*

To evaluate the effect of sample quality on the strength and stiffness characteristics of the clay, Ø250 mm Sherbrooke block samples were retrieved at three locations along the planned E16. These locations are referred to by their borehole identification numbers which are 2371, 2411 and 2284. All block samples were carved at similar depths as the previously retrieved 72 mm samples and are representative of the general soil conditions in the study area.

3 GEOTECHNICAL PROPERTIES OF THE CLAY

3.1 *Index properties*

The water content of the clay samples in the study area ranges from 30–45% while the total unit weight varies between 17.5 and 19.5 kN/m^3 (Fig. 2). The plasticity index (Ip) is generally in the range of 7–25%. An example of a geotechnical profile with index properties for borehole 2371 is shown on Figure 2.

3.2 *Effective stresses and stress history*

From the geological history of the area, no exceptional loading events are known; only normal sedimentation processes. Some overconsolidation is however observed at some locations in the study area due to unloading caused by erosion from creeks and rivers over the past. Groundwater level is 1–2 m below the ground surface. The pore water pressures were measured at several depth intervals and locations throughout the study area. The data generally show pore water pressures equal to 60–85% of hydrostatic conditions.

The preconsolidation pressure (or yield stress), p'_c, has been measured from CRS oedometer tests on the 72 mm and 250 mm samples. In general the overconsolidation ratio (OCR) in the clay ranges from 1.3 to around 6 at some locations. Figure 3 shows typical CRS results for tests carried out on block and 72 mm piston samples in the study area. CRS results on the block samples clearly show a better distinction between the over consolidated stress range and the normally consolidated stress range. Hence the reliability in the selection of p'_c and OCR is better from the CRS test results on block samples.

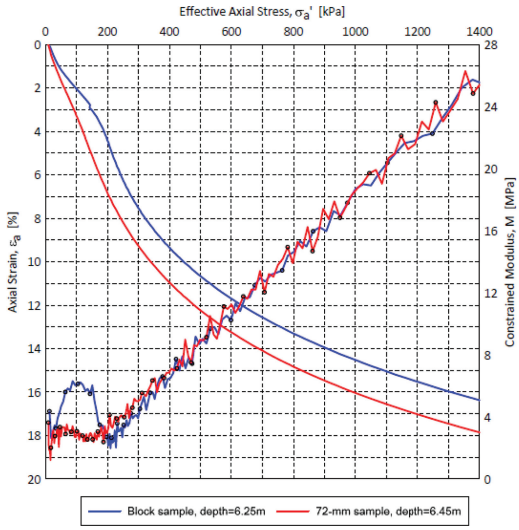

Figure 3. Example of oedometer test results from samples collected with a 72 mm sampler and a 250 mm block sampler in the study area. Test results are from borehole location 2371.

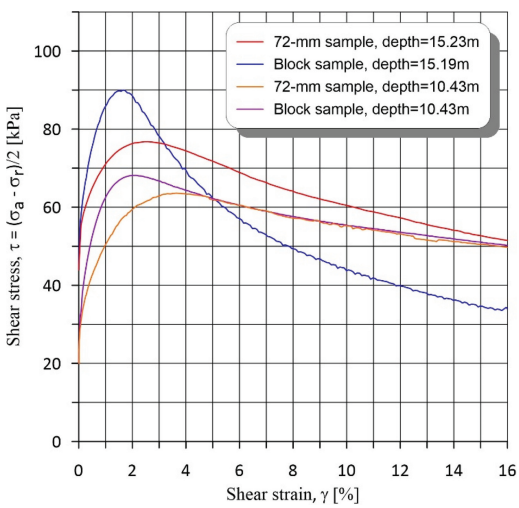

Figure 4. Example of CAUC triaxial test results from samples collected with a 72 mm piston sampler and a 250 mm block sampler in the study area. Test results are from borehole location 2371.

3.3 *Strength properties*

Typical results from anisotropically consolidated triaxial tests sheared in compression (CAUC) are shown in Figure 4 for both 72 mm samples and block samples from the same location and depth. According to the sample quality criteria proposed by Lunne et al. (1997) all samples were categorized as being of good to excellent quality. All stress-strain curves on Figure 4 show a strain softening behavior for the Rakkestad clay. However, results from CAUC tests on block samples show a higher peak shear strength and a more brittle behavior than those on the 72 mm samples (Fig. 4). The difference in peak strength can be important and was observed to be up to 53.8% at some locations (Table 1).

Table 1. Relative increase in undrained shear strength from block samples with respect to 72 mm samples.

Borehole no.	Depth m	s_u^C 72 mm kPa	s_u^C Block kPa	% increase %
2371	5.43	57.3	61.9	8.0
2371	10.43	63.6	68.2	7.2
2371	15.23	76.8	89.9	17.2
2411	6.21	45.1	56.6	25.5
2411	10.45	–	61.1	–
2411	12.06	48.0	73.8	53.8
2284	6.25	28.7	44.0	53.3
2284	11.36	–	51.1	–
2284	12.4	34.9	48.7	39.5

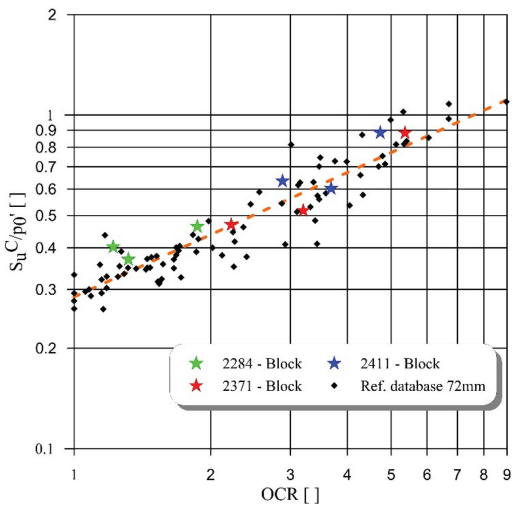

Figure 5. Normalized undrained shear strength ratio (s_u^c/p_0') from triaxial tests (CAUC) as a function of OCR.

Figure 5 illustrates the undrained shear strength normalized by the in situ effective stresses (p'_0) against OCR for CAUC laboratory tests. The normalized strength results from block samples show less variation than the 72 mm reference database. Also, the block samples generally give higher undrained shear strength ratio than that obtained from tests on 72 mm samples from same locations and depth.

4 CPTU CORRELATIONS

4.1 *Correlations for OCR*

CPTU correlations for assessing OCR in Norwegian clays have previously been established by Karlsrud et al. (2005). These correlations were established based on CPTU cone factors such as $N_{\Delta u}$, N_{kt} and N_{ke}, and a large database of block samples with overall similar soil conditions as those found herein. However, in this study, all form of correlations between OCR and the CPTU cone factors were found to be poor (i.e. very low regression coefficient; r^2). The best fit regression result was obtained between the normalized cone parameter Q_t and OCR (Fig. 6) through the following equation:

$$OCR = 0.35 + 0.645Q_t \qquad r^2 = 0.95 \qquad (1)$$

where $Q_t = (q_t - \sigma_{vo})/\sigma'_{vo}$, q_t with being the corrected cone resistance, σ_{vo} the total vertical stress and σ_{vo}'the vertical effective stress.

As shown on Figure 6, the trendline of Equation 1 is very similar to the Q_t-OCR trendline defined by Karlsrud et al. (2005) for clays with sensitivity higher than 15. One can also note little variation in the block sample data compared to the 72 mm data points. For a given a value of Q_t, the best regression line for the 72 mm reference database provides a much lower OCR value (i.e. black line in Fig. 6).

Figure 7 presents a regression of data based on the pore pressure parameter B_q, Ip, and the OCR. The regression analysis shows a fairly high regression coefficient, only slightly lower than r^2 for Equation 1. The best fit is given as:

$$OCR = 16.5 \cdot Bq^{-2.85} \cdot Ip^{-0.75} \qquad r^2 = 0.84 \qquad (2)$$

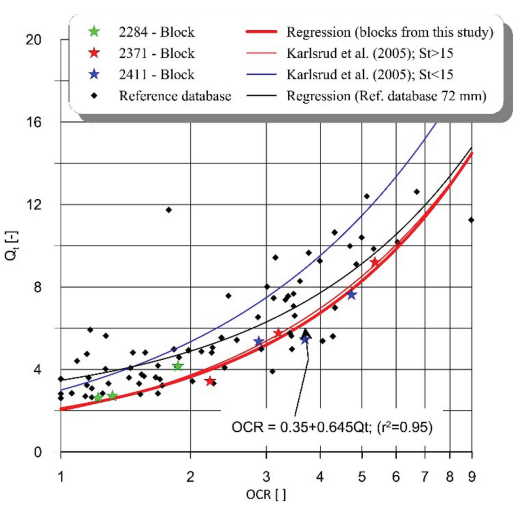

Figure 6. Normalized cone parameter Q_t against OCR.

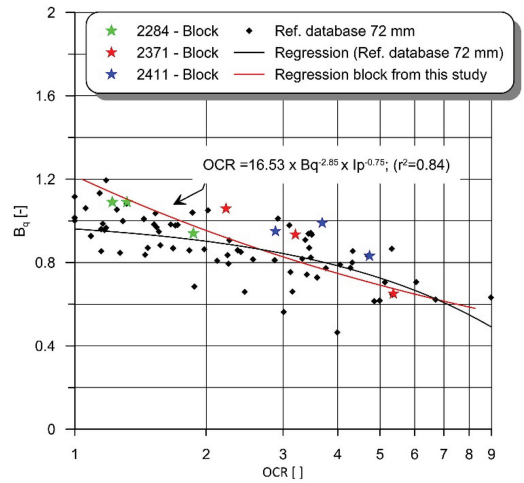

Figure 7. Pore pressure parameter B_q against OCR.

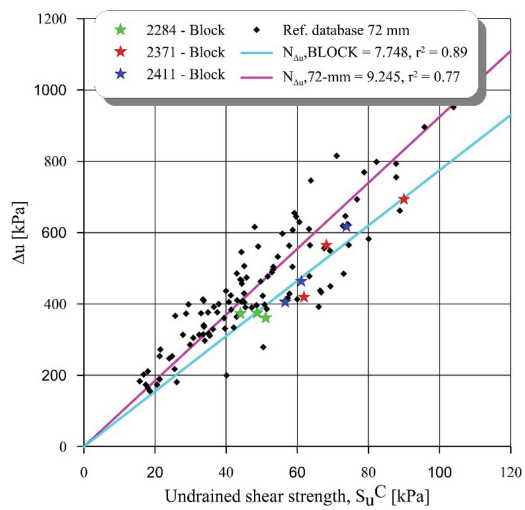

Figure 8. Excess pore pressure Δu measured at location u_2 against undrained shear strength from CAUC triaxial tests.

Once again, the results from block samples show more consistent results than those from the 72 mm reference database.

4.2 *Correlations for undrained shear strength in compression (s_u^c)*

Figures 8 and 9 illustrate the excess pore pressure and the net cone resistance against the measured undrained shear strength in compression (s_u^C) from the study area. From these figures, one can see that the undrained shear strength data correlates better (higher coefficient of determination; r^2) with the Δu parameter. On these figures, a larger scatter

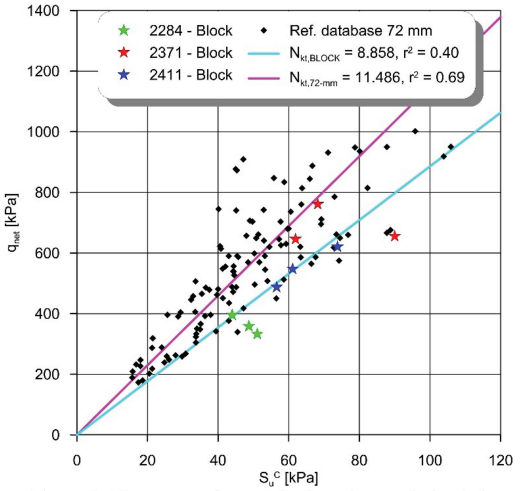

Figure 9. Net cone resistance (q_{net}) against undrained shear strength from CAUC triaxial tests.

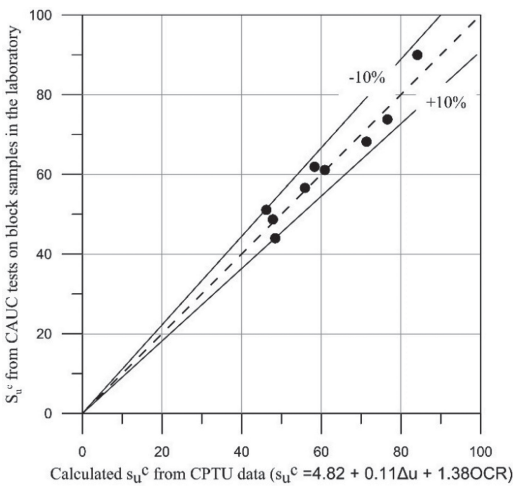

Figure 10. Calculated versus measured undrained shear strength in compression using Eq. 3.

can also be observed in the reference database compared to the larger diameter block samples data set.

To evaluate the most appropriate equation form for the interpretation of s_u^C from CPTU data in the study area, a series of regression analyses were performed.

The two best fits were obtained by using i) the Δu parameter with OCR, and ii) the q_{net} parameter with OCR. The resulting best fit equations are given as follows:

$$s_u = 4.82 + 0.11\Delta u + 1.38OCR \qquad r^2 = 0.93 \qquad (3)$$

$$s_u = 0.39OCR^{-0.17} \cdot q_{net}^{0.83} \qquad r^2 = 0.74 \qquad (4)$$

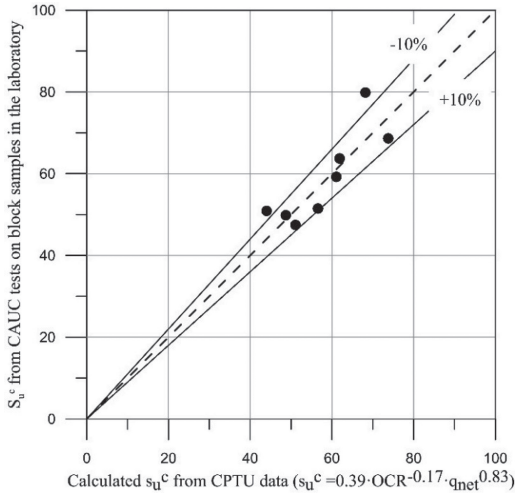

Figure 11. Calculated versus measured undrained shear strength in compression using Eq. 4.

As shown from the r^2 coefficients above, the best statistical fit is obtained with Equation 3 on the basis of the Δu parameter and OCR data. Figures 10 and 11 shows that both Equations 3 and 4 gives reliable estimates of s_u^C in the study area, within +/– 10% of that measured in the laboratory from CAUC on block samples.

5 DESIGN CONSIDERATIONS

A typical example of the use of Equations 1–4 in the study area is shown in Figure 12 for a CPTU test carried out at location 2371. On this figure, the OCR and s_u^C interpretations are compared to results from other empirical correlations normally used in design in Norway (i.e. Karlsrud et al. 2005) and to correlations based on laboratory results from 72 mm samples. The latter is based on the best fit $N_{\Delta u}$ correlation (i.e. $N_{\Delta u} = \Delta u/s_u^C$) shown in Figure 8.

As expected, a better match with the relationships based on the block sample correlations is obtained. The Karlsrud et al. (2005) relationship seems to underestimate the OCR of Rakkestad clay. The differences are significant throughout the profile (Figure 12).

Differences are also observed in the case of the interpreted undrained shear strength (Figure 12). Here the difference can be up to 30–40% when compared to the interpretation based on the 72 mm reference database. Also, at depths larger than 10 m, the estimated shear strength from Equations 3–4 is generally higher (up to 30%) than that obtained from the Karlsrud et al. (2005) methodology.

The major difference between the undrained shear strength estimated from the 72 mm reference data-

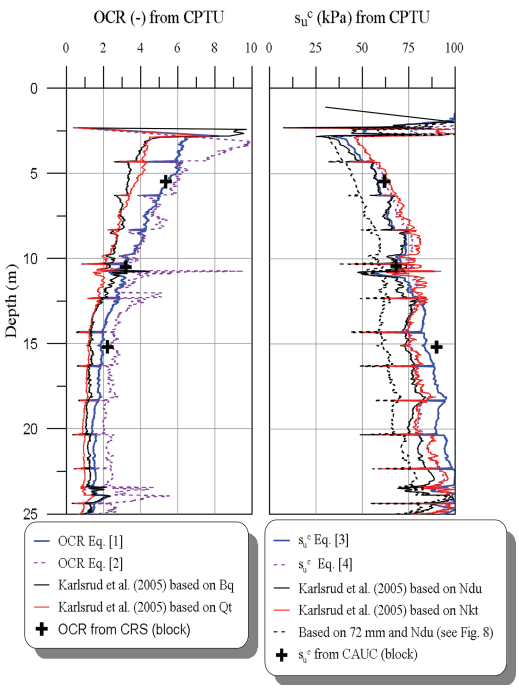

Figure 12. Interpretation of OCR and s_u^C of Rakkestad clay at borehole 2371 based on correlations by Karlsrud et al. (2005) and on the best fit empirical correlations obtained from this study (i.e. both 72 mm and block samples).

base and that based on the block samples is associated with sample quality and sampling technique. Throughout this project, the laboratory results on the block samples showed consistently superior quality than those acquired on the 72 mm samples, which resulted in a notable difference in undrained shear strength. This seems to agree with other studies documenting the impact of sampling processes in soft and sensitive clays (e.g. Berre et al. 2007).

Results from this study show with little doubt that one can use a higher undrained shear strength profile in design for the Rakkestad clay along the planned E16 highway. At some locations along the highway, the difference between the previously recommended design line and the new design criterion from block samples can be important (i.e. up to 40% in active undrained shear strength). The results are expected to lead to important economic savings for the E16 project and highlight the need for local and high quality samples for CPTU correlations in soft and sensitive clays. A first assumption is that the findings will lead to a saving of approximately 30% of costs associated with lime-cement stabilization of road cuttings along the E16 highway project.

6 CONCLUSIONS

A high quality database including results from CPTU and laboratory tests performed on Ø72 mm piston samples and Ø250 mm block samples collected along the planned new highway, E16, from Nybakk to Slomarka, in southeastern Norway was assembled. The laboratory results on block samples show a superior quality compared to 72 mm samples, a higher peak undrained shear strength and less scatter in the other important geotechnical parameters such as preconsolidation stress and overconsolidation ratio.

Based on regression analyses, the database allowed the development of empirical correlations between CPTU parameters and the undrained shear strength and the overconsolidation ratios for the Rakkestad clay. The recommended CPTU correlations in the study area show up to 40% increase in undrained shear strength when compared to previously established CPTU correlations for Norwegian clays, or to correlation based on laboratory tests performed on 72 mm samples.

Results presented herein clearly show the importance of establishing site specific correlations when assessing geotechnical parameters from CPTU tests. In soft and sensitive clays, it is also particularly important that the correlations are established from large diameter samples of very high quality. For the E16 project, a small investment in the field campaign to collect large diameter block samples will lead to cost-effective solutions and savings of approximately 30% associated with the lime-cement stabilization of road cuttings.

ACKNOWLEDGEMENTS

This work was funded in part by the Norwegian Research Council through the Strategic Research Project SP8-GEODIP at NGI, and by the Norwegian Public Road Administration (NPRA).

REFERENCES

Berre, T., Lunne, T., Andersen, K.H., Strandvik, S., & Sjursen, M. (2007). Potential improvements of design parameters by taking block samples of soft marine Norwegian clays. *Canadian Geotechnical Journal*, *44*(6), 698–716.

Karlsrud, K., Lunne, T., Kort, D.A., & Strandvik, S. (2005). CPTU correlations for clays. In Proceedings of the international conference on soil mechanics and geotechnical engineering (Vol. 16, No. 2, p. 693). AA Balkema Publishers.

Lunne, T., Berre, T., & Strandvik, S. (1997). Sample disturbance effects in soft low plastic Norwegian clay. In *Symposium on recent developments in soil and pavement mechanics*. Rio de Janeiro, Brazil.

Cone Penetration Testing 2018 – Hicks, Pisanò & Peuchen (Eds)
© 2018 Delft University of Technology, The Netherlands, ISBN 978-1-138-58449-5

Use of the free fall cone penetrometer (FF-CPTU) in offshore landslide hazard assessment

J.S. L'Heureux & M. Vanneste
Norwegian Geotechnical Institute, (NGI), Trondheim and Oslo, Norway

A. Kopf
MARUM, University of Bremen, Germany

M. Long
University College Dublin (UCD), Dublin, Ireland

ABSTRACT: Free Fall penetrometer (FF-CPTU) testing can provide significant advantages over conventional CPTU investigation for shallow sub-surface offshore site investigations. Much work has been done on soil characterisation and on determination of the undrained shear strength (s_u) from FF-CPTU testing. However, little data has been published on analysis of FF-CPTU dissipation testing. Here, FF-CPTU data from two Norwegian fjords with evidence of recent landsliding are presented, and the techniques used to analyse and correct the data are described. At Hommelvika, relatively high residual excess pore pressures (15–17 kPa) were found in the vicinity of a large pockmark identified on the fjord bed from multibeam data. At Finneidfjord, the residual excess pore pressures are lower and are in agreement with long-term piezometer data from the area. Reliable estimates of the coefficient of consolidation (c_h) were also be obtained from the FF-CPTU dissipation tests.

1 INTRODUCTION

Near-shore and submarine landslides are hazards along Norwegian fjords and in other similar environments worldwide. One particular issue is the occurrence of excess pore water pressure in relatively thin soil layers that undermines the stability of slopes. This phenomenon has led to a number of significant slope failures, including the well-documented 1996 Finneidfjord landslide (Longva et al. 2003). As the investigation of the seafloor conditions using conventional CPTU or drilling techniques is difficult and expensive, an alternative, less expensive and faster approach for investigating these situations using the free fall piezocone penetrometer (FF-CPTU) is presented herein. As pointed out by Strout & Tjelta (2005) and others, offshore dissipation testing and interpretation of the results are challenging.

The focus of this paper lies therefore on the use of overnight dissipation tests in order to determine the pore pressure regime in specific soil layers. Dissipation test data and the analysis workflow applied from two offshore sites at Finneidfjord and Hommelvika in Norway are examined. The analysis of the data allows for the determination of the excess pore water pressures as well as the coefficient of consolidation. Finally, some implications of the findings for landslide hazard assessment are discussed.

2 INSTRUMENT AND DEPLOYMENT METHOD

Standard CPTU testing is the main method of obtaining *in situ* offshore data. This method requires a suitably equipped and relatively large vessel or drilling platform, and therefore, the method is expensive. Reasonable weather conditions are also generally required. FF-CPTU instruments utilise a more simple gravity-driven deployment style. They can be installed from relatively small vessels by two people. Instrument recovery can be facilitated by a battery powered portable winch.

Many FF-CPTU devices have been developed recently (see Chow & Airey 2013, Chow & Airey 2014). These devices are primarily used to characterise the undrained shear strength of the sediments. However, these devices are also useful to study dissipation of excess pore water pressures and the consolidation characteristics of the soils (Chow et al. 2014). Lucking et al. (2017) describe how the pore pressure response during FF-CPTU

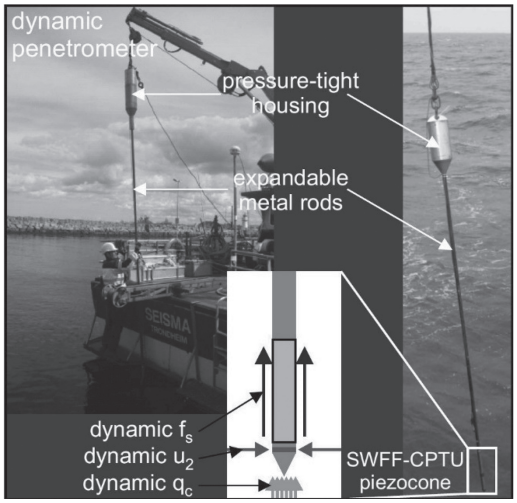

Figure 1. Free-fall penetrometer instrument (modified after Steiner et al. 2013).

penetration can be used to help characterising near-shore sediments.

The FF-CPTU instrument used in this study was developed at MARUM (Center for Marine Environmental Sciences, University of Bremen, Germany), see Figure 1. A full description of the device is given by Stegmann et al. (2006a) and Stegmann et al. (2006b). It is designed to free-fall through the water column, impact the seabed and record penetration data at a high sample rate.

The instrument uses a 15 cm^2 / 10 MPa GEOMIL subtraction piezocone measuring cone resistance (q_c), sleeve friction (f_s), pore pressure behind the tip during penetration (u_2), but also tilt, and *in situ* temperature. It has a modular design and the length can vary between 1.5 m (short mode) and 7.5 m (long mode) by adding 1 m long rods. The length of the probe used in this study was 7.5 m. Depending on the sediment strength, modular weight pieces (15 kg each) can be added in order to achieve deeper penetration (up to 4 × 15 kg-pieces). The weight of the instrument ranges from 45 kg in short mode to a maximum of 170 kg in long mode.

Data logging frequency is variable but is typically set to 40 Hz. Binary data are temporarily stored on a micro flash card and then downloaded to a computer.

3 SITE DESCRIPTIONS

Data from two Norwegian sites at Finneidfjord and Hommelvika are presented here. A short description of each site follows.

3.1 *Finneidfjord*

The 1996 landslide at Finneidfjord and the subsequent investigations and analyses are well described by Longva et al. (2003), Lecomte et al. (2008), Cassidy et al. (2008) and L'Heureux et al. (2012a), amongst others. Steiner et al. (2012) described the use of the FF-CPTU at 38 locations across or in the immediate vicinity of the landslide area to characterize the strength of the soft layers at this site (Figure 2).

Ground conditions in the Finneidfjord area comprise beach deposits (sand and gravel) overlying a thick sequence of clayey silts resting on bedrock (Fig. 3). Significant pockets of very sensitive clay and quick clay were found at several locations along the shoreline and also offshore (Fig. 3).

L'Heureux et al. (2012a) suggest that this landslide initiated within a weak layer in the fjord-ma-

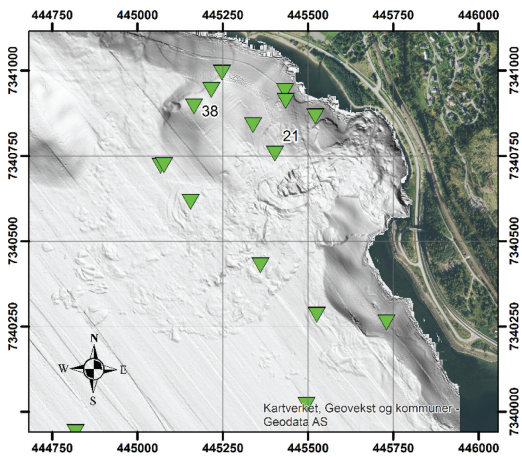

Figure 2. Swath bathymetry image of the Finneidfjord study area showing the location of free-fall penetrometer tests (green triangles) performed in 2010. Piezometers were also installed at FF-CPTU location 21.

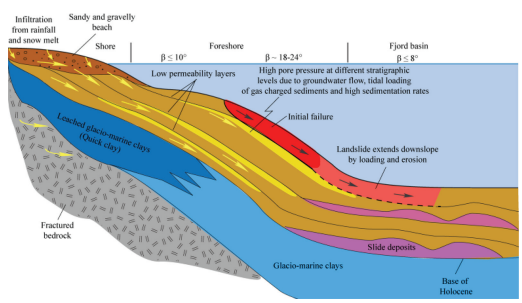

Figure 3. Conceptual stratigraphical model and slope failure mechanism at Finneidfjord (modified after L'Heureux et al. 2012).

rine sediments before developing retrogressively across the shoreline. They explain that, through the integration of results from sediment cores, free-fall cone penetrometer tests and high-resolution 3D seismic data, the slide-prone layer is a regional bed likely sourced from clay-slide activity in the catchment of the fjord. The sediments in this regional layer are softer and more sensitive than the typical fjord-marine deposits, which explain their role in slope instability.

3.2 *Hommelvika*

The bay of Hommelvika is located approximately 20 km northeast of Trondheim, Norway. Ground conditions in the Hommelvika area comprise a complex distribution of sandy silts overlying silty clay. The clays are generally of medium sensitivity. The FF-CPTU work at Hommelvika was designed to investigate large pockmarks (Figure 4). The purpose of the FF-CPTU testing was to characterise the nature of the materials and their undrained shear strength. In addition, the possible presence of excess pore pressure inside and close to the large pockmarks was of interest (Figure 4). The pockmarks are up to 75 m in diameter and 5 m deep. They can be an indication of groundwater seepage.

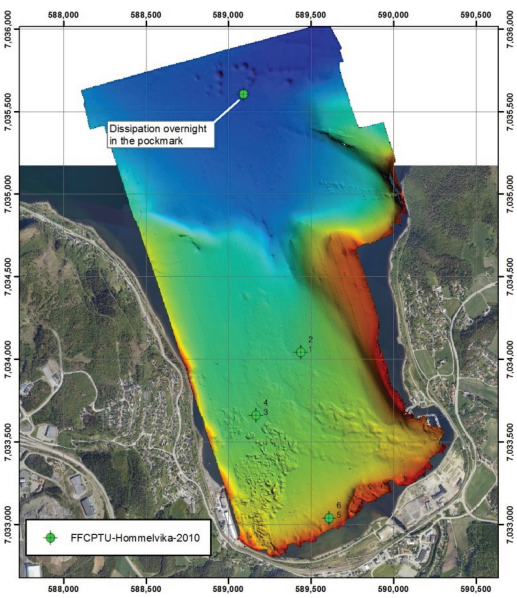

Figure 4. Swath bathymetry image of the Hommelvika study area showing the location of free-fall penetrometer tests performed in 2010. Landslide debris and large pockmarks are also observed on the fjord bottom.

The excess pressure likely originates from groundwater infiltration in the near-shore sediments due to the significant topographic gradients in the region. Similar processes and pockmarks are often observed in other lakes and fjords in Norway e.g. Lake Botnen at Rissa; L'Heureux et al. (2012b).

4 DATA PROCESSING

4.1 *Strategies for FF-CPTU tests*

Generally, three options are available for FF-CPTU tests. Type A testing aims at a high-resolution vertical record (1 kHz logging frequency) of the sediment properties. The FF-CPTU instrument is lowered at 1.0 to 2.0 m/s winch speed to a level 10 m to 15 m above the seafloor. It is then released in free–fall mode until the probe impacts the seafloor and dynamically decelerates until its terminal depth is reached. The instrument is recovered immediately after the FF-CPTU probe comes to a complete halt. Due to the short time length of the test, no dissipation data for pore pressure is recorded.

Type B testing is initially similar to Type A (same test parameters). However, it aims at the recording the absolute pore pressure evolution once the FF-CPTU instrument is embedded in the sediment. Pore pressure dissipation is usually recorded for 20 minutes to 25 minutes.

Type C testing focuses on the logging of the absolute pore pressure evolution overnight (pore pressure dissipation for 12 hours to 15 hours) using a recording frequency of 10 Hz. The deployment is basically similar to Types A and B. Only pore pressure is recorded. As of yet, the system does not allow recording pore pressure response and other parameters for extended periods of time.

4.2 *Examples of Type B dissipation tests*

Some examples of Type B, short term dissipation tests, for the Hommelvika site are shown on Figure 5. The location of the tests is shown on Figure 4.

On impact with the fjordbed, negative excess pore pressures develop. These reach a minimum value at the end of the FF-CPTU penetration and then slowly rise to reach a maximum after a while. Seifert et al. (2008) classify this pattern of pore pressure behaviour as a "Type B1" signal and suggest the development of the negative excess pore pressure is due to a combination of factors, including the dilatory response of the soil due to some silt and sand content and also the presence of gas in the sediments. The tests were of insufficient

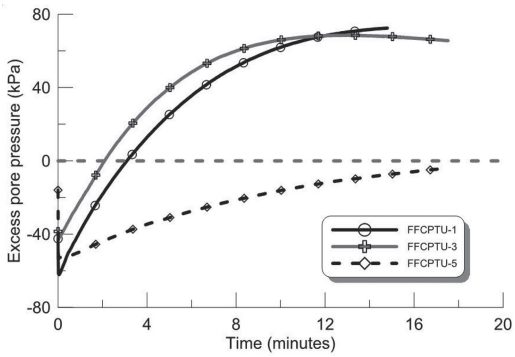

Figure 5. Short term dissipation tests for Hommelvika.

length for any subsequent dissipation of the excess pore pressure to be observed. Thus, for these tests, it is not possible to obtain the *in situ* excess pore water pressure.

Tests 1 and 3, located towards the center of the bay, show very similar results. Test 5, close to the edge of the bay, shows a much slower recovery of pore pressure.

4.3 *Long term Type C dissipation tests*

Results from three Type C tests at Finneidfjord and one at Hommelvika are also available. Due to the overnight duration of these tests, the data require corrections to take into account tidal effects and atmospheric pressure variations. These corrections can be either positive or negative.

Values for the absolute pore pressure were recorded by the instrument every tenth of a second over the 13 to 19 hour period during the long-term dissipation testing at the three locations. Due to the large amount of data recorded during testing, values of absolute pore pressure corresponding to 10 minute intervals were selected for plotting. As for the Type B tests, the pore pressure initially decreases as expected and then reaches a maximum before dissipating slightly and then rises again. The subsequent rise in pore pressure after the initial decline confirms that correction of the data is required.

The correction required to be applied to the data due to tidal effects is calculated as follows:

$$p_{tide} = \rho_{sw} g h \tag{1}$$

where:

p_{tide} = correction to measured pore pressure reading
ρ_{sw} = density of seawater = 1030 kg/m^3
g = acceleration due to gravity = 9.81 m/s^2
h = mean tide level during test—actual tidal observation (referenced to "zero" datum)

A similar approach was adopted for corrections in atmospheric pressure variations (p_{air}). The standard reference value of atmospheric pressure (taken to equal 101.325 kPa) was subtracted from the measured value of the air pressure (corresponding to the same time as the pore pressure value under study).

Finally the corrected pore pressure value is determined as follows:

$$u_{2,corrected} = u_{2,measured} + p_{tide} + p_{air} \tag{2}$$

Excess pore pressure (Δu) is obtained from:

$$\Delta u = u_{2,corrected} - u_0 \tag{3}$$

where:

u_0 = *in situ* hydrostatic pore water pressure corresponding to mean tide level.

In any case, none of the test results were corrected for fluid dynamic effects such as Bernoulli.

5 RESULTS AND DISCUSSION

5.1 *Excess pore pressures (EPP)*

The results of the three long term dissipation tests, with the results corrected as described above, are shown on Figure 6.

The residual excess pore pressure values are:

- Hommelvika FFCPTU-7 = 15–17 kPa
- Finneidfjord FFCPTU-21 = 2–4 kPa
- Finneidfjord FFCPTU-38 = 5–7 kPa

5.2 *Comparison with piezometers*

In order to assess the accuracy of these calculated *in situ* values, we compare the results with long-

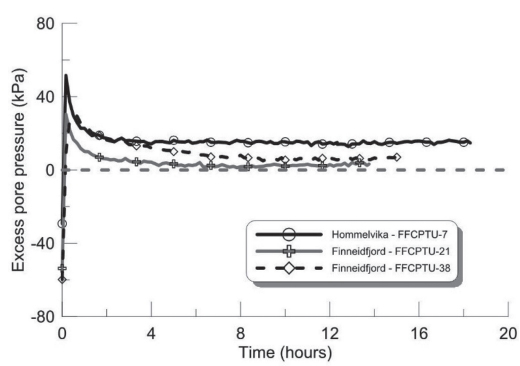

Figure 6. Long term dissipation tests at Hommelvika and Finneidfjord.

term piezometer tests carried out at a nearby location in Finneidfjord (red circle; Fig. 2). Three set of piezometer data are available for Finneidfjord. These instruments were connected to logging stations located onshore. Data is logged hourly and transmitted once per day.

Figure 7 shows an example of the data from PZ2.3. The average *in situ* excess pore pressure in July 2013 is around 4 kPa and varies throughout the year [figure only shows 1 month] between 2–5 kPa. Thus, the piezometer results agree very well with the data from the FF–CPTU tests. Figure 7 also presents information about temperature, rainfall, tidal variation and total pressure variation during the measured time period. The excess pore pressure ratio R_u ($R_u = \Delta u/\gamma_{tot} \cdot z$ where γ_{tot} is the total unit weight of the soil and z the depth below seafloor) is also shown and ranges from 0.19–0.26.

5.3 *Comparison with seabed features*

At Hommelvika, relatively high excess pore pressures occur in the vicinity of a large pockmark (Figure 4). The presence of excess pore pressure inside the pockmark could be an indication of groundwater seepage as a key part of its formation. The

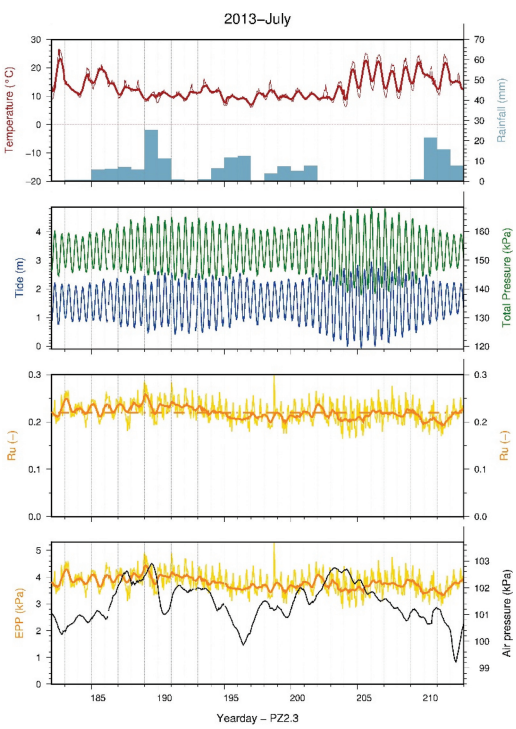

Figure 7. Long term interpretation of piezometer data for a selected period (July 2013) at the Finneidfjord site. EPP: residual excess pore pressure.

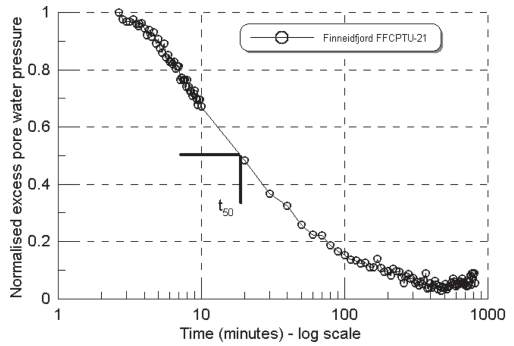

Figure 8. Example of calculation of c_h from long-term dissipation test data.

excess pressure from the groundwater seepage may be sourced from high pore pressure gradients in the near-shore sediments as is the case with pockmarks in Lake Botnen in Rissa, Norway (L'Heureux et al. 2012b). Comparisons with piezometers located along the shoreline at Hommelvika confirm that significant hydraulic gradients exist.

5.4 *Coefficient of consolidation*

Long-term dissipation test data can also be used to determine the coefficient of consolidation c_h. Several methods are available for performing these calculations. In the example shown on Figure 8 (Finneidfjord test FF-CPTU-21) the classic technique outlined by Teh & Houlsby (1991) is used to determine c_h by obtaining the time for 50% consolidation of excess pore pressure (t_{50}) from the test data. The following values of c_h were determined:

- Hommelvika FF-CPTU-7 = 47 m^2/yr.
- Finneidfjord FF-CPTU-21 = 60 m^2/yr
- Finneidfjord FF-CPTU-38 = 10 m^2/yr.

6 CONCLUSIONS AND IMPLICATIONS

Free-fall penetrometer tests provide a valuable and time-efficient method for shallow offshore geotechnical site investigation. One particular issue in such environment is the potential occurrence of excess pore water pressures that—if present—would undermine the stability of slopes. Using a simple analysis workflow including, amongst other things, corrections for tidal effects and atmospheric pressure variations, results obtained from two study sites at Hommelvika and Finneidfjord in Norway compared well with piezometer data and morphological seafloor features. At Hommelvika, relatively high residual excess pore pressures

(15–17 kPa) were found in the vicinity of a large pockmark. At Finneidfjord, the excess pore pressures are lower and are in agreement with long-term piezometer data from the area. The analysis of the data also allows determining the coefficient of consolidation in the clays.

ACKNOWLEDGEMENTS

The authors would like to acknowledge the efforts of Alois Steiner and Late Mathias Lange previously at MARUM for help with data acquisition and processing. A special thanks also to the NGU crew (Oddvar Longva and John Anders Dahl) aboard the research vessel RV Seisma during data acquisition. The authors are also grateful to two UCD MSc students Laura McElduff and Darren Mullins for their help and contribution.

REFERENCES

Cassidy, M.J, Uzielli, M., Lacasse, S. 2008. Probability risk assessment of landslides: A case study at Finneidfjord. Canadian Geotechnical Journal 45 (9):1250 1267.

Chow, S.H. & Airey, D.W. 2013. Soil strength characterisation using free-falling penetrometers. Géotechnique 63 (13):1131–1143.

Chow, S.H. & Airey, D.W. 2014. Free-falling penetrometers: a laboratory investigation in clay. Journal of Geotechnical and Geoenvironmental Engineering ASCE 140 (1):201–214.

Chow, S.H., O'Loughlin, C.D., Randolph, M. 2014. Soil strength estimation and pore pressure dissipation for free-fall piezocone in soft clay. Géotechnique 64 (10):817–827.

L'Heureux, J.S., Longva, O., Steiner, A., Hansen, L., Vardy, M.E., Vanneste, M., Haflidason, H., Brendryen, J., Kvalstad, T.J., Forsberg, C.F., Chand, S., Kopf, A. 2012a. Identification of weak layers and their role for the stability of slopes at Finneidfjord, northern Norway. In: Y. Yamada et al. (eds). Submarine Mass Movements and Their Consequences, Advances in Natural and Technological Hazards Research, 29, Springer, Dordrecht (The Netherlands). 321–330.

L'Heureux, J.S., Eilertsen, R.S., Glimstad, S., Issler, D., Solberg, I.-L., Harbitz, C.B. 2012b. The 1978 quick clay landslide at Rissa, mid-Norway: subaqueous morphology and tsunami simulations. In: Y. Yamada et al. (eds). Submarine Mass Movements and Their Consequences, Advances in Natural and Technological Hazards Research, 29, Springer, Dordrecht (The Netherlands). 507–516.

Lecomte, I., Bano, M., Hamran, S.E., Dalsegg, E., Nielsen, K.M. 2008. Mapping quick clay sites for geohazard assessment: the Finneidfjord case study, Norway. Paper presented at the Near Surface 2008–14th European Meeting of Environmental and Engineering Geophysics Kraków, Poland, September 2008.

Longva, O., Janbu, N., Blikra, L.H., Bøe, R. 2003. The 1996 Finneidfjord slide: seafloor dynamics. In *Submarine mass movements and their consequences* (pp. 531–538). Springer, Dordrecht.

Lucking, G., Stark, N., Lippmann, T., Smyth, S. 2017. Variability of in situ sediment strength and pore pressure behavior of tidal estuary surface sediments. Geo-Marine Letters 37:441–456. doi:10.1007/s00367-017-0494-6.

Seifert, A., Stegmann, S., Mörz, T., Lange, M., Wever, T., Kopf, A. 2008. In situ pore-pressure evolution during dynamic CPT measurements in soft sediments of the western Baltic Sea. Geo-Marine Letters (2008) 28:213–227. doi:10.1007/s00367-008-0102-x

Stegmann, S., Mörz, T., Kopf, A. 2006a Initial results of a new free fall-cone penetrometer (FF-CPT) for geotechnical in situ characterisation of soft marine sedimentsVo l. 86, No. 3, pp. 199–208. Norsk Geologisk Tidskrift (Norwegian Journal of Geology) 86 (3):199–208.

Stegmann, S., Villinger, H., Kopf, A. 2006b. Design of a modular, marine free-fall cone penetrometer. Sea Technology 47 (2):27–33.

Steiner, A., Kopf, A., L'Heureux, J.S., Kreiter, S., Stegmann, S., Hafliadason, H., Moerz, T. 2013. *In situ* dynamic piezocone penetrometer tests in natural clayey soils – a reappraisal of strain-rate corrections. Canadian Geotechnical Journal 51:272–288.

Steiner, A., L'Heureux, J.S., Kopf, A., Vanneste, M., Longva, O., Lange, M., Haflidason, H. 2012. An in-situ free-fall piezocone penetrometer for characterizing soft and sensitive clays at Finneidfjord (Northern Norway): Free-fall CPTU at Finneidfjord. In: *Submarine Mass Movements and Their Consequences, Advances in Natural and Technological Hazards Research*, 29, Spinger, Dordrecht (The Netherlands). pp. 99–109. 978-94-007-2161-6

Strout, J.M. & Tjelta, T.I. 2005. *In situ* pore pressures: What is their significance and how can they be reliably measured? Marine and Petroleum Geology 22 (1–2):275–285.

The, C.I. & Houlsby, G.T. 1991. Analytical study of the cone penetration test in clay. Géotechnique 41 (1):17–34.

Vanneste, M., Longva, O., L'Heureux, J.S., Vardy, M.E., Morgan, E., Forsberg, C.F., Kvalstad, T.J., Strout, J.M., Brendryen, J., Hafliadason, H., Lecomte, I., Steiner, A., Kopf, A., Mörz, T., Kreiter, S. 2013. Finneidfjord, a field laboratory for integrated submarine slope stability assessments and characterization of landslide-prone sediments: a review. Paper presented at the Offshore Technology Conference (OTC).

Cone Penetration Testing 2018 – Hicks, Pisanò & Peuchen (Eds)
© 2018 Delft University of Technology, The Netherlands, ISBN 978-1-138-58449-5

Fibre optic cone penetrometer

P. Looijen, N. Parasie, D. Karabacak & J. Peuchen
Fugro, Nootdorp, The Netherlands

ABSTRACT: This paper presents a novel prototype cone penetrometer for piezocone penetration tests (CPTU). It is equipped with Fibre Optic (FO) sensors for measuring cone resistance (q_c) and sleeve friction (f_s). The FO sensors replace the classical, electric strain-gauges. Field results, laboratory calibration and uncertainty assessment show capability of achieving q_c and f_s values that are well within Application Class 1 of ISO 22476-1 "electrical cone and piezocone penetration test". This makes the FO cone penetrometer particularly suitable for use in very soft clays, silts and peat, i.e. Soil A and Interpretation H of ISO 22476-1. The cone penetrometer has potential to meet a significantly more stringent, Dutch Application Class 1+.

1 INTRODUCTION

Drawing on extensive fibre optics experience, Fugro developed a prototype fibre optic (FO) cone penetrometer which is capable to perform piezocone penetration tests (CPTU) well within ISO 22476-1 Application Class 1.

The FO cone penetrometer is intended for onshore use in soft clays, silts and peat, i.e. Soil A and Interpretation H of ISO 22476-1. The FO cone penetrometer should also meet the Application Class 1+ accuracies particularly developed for dike stability inspections in The Netherlands (Stoevelaar & van Duinen 2016). It is noted that the Class 1+ concept is experimental and it is currently not entirely clear how to interpret the Class 1+ requirements.

The FO cone penetrometer fits within Fugro's process for metrological confirmation, including the ISO/IEC 17025 accredited calibration laboratory (Peuchen et. al., 2017) and including seamless upload of calibration data into the cone penetrometer itself.

FO cone penetrometers are expected to be available for commercial use by the second half of 2018.

2 TECHNOLOGY

The prototype FO penetrometer has a tip area of 1 500 mm^2 and a net area ratio of 0.77. The FAZ Technology (2017) interrogator is used to convert optic signals into physical units, for cone resistance (q_c), sleeve friction (f_s), pore pressure (u_1 or u_2), inclination (bi-axial) and temperature. The fibre optic sensors for measuring q_c and f_s have maximum ranges of 10 MPa and 0.5 MPa respectively. These ranges imply that this FO cone penetrometer can be used for soft soils only. Other ranges will follow once the prototype is optimized. The FO cone penetrometer is of the type "cone resistance and sleeve friction load cells in compression", as defined by Figure 1 of ISO 22476-1.

Figure 1. Prototype FO cone penetrometer.

This paper focuses on the performance of the q_c-sensor, for which testing is largely completed (2017). The required dynamic range of the optic signals of the q_c-sensor is more challenging than for the f_s-sensor. Fine-tuning of the f_s-sensor design is currently (2017) in progress. FO pore pressure and inclination sensors will follow later.

3 PERFORMANCE

3.1 *Resolution*

Figure 2 demonstrates q_c resolution of the FO cone penetrometer by a laboratory test where the cone tip was loaded by adding (dead weight) masses of 200 g, 100 g, 50 g and 20 g steps corresponding to equivalent q_c values of 1.31 kPa, 0.65 kPa, 0.33 kPa and 0.13 kPa respectively. The difference in the zero load reading before and after this test is 0.01 kPa. Similar dead weight tests have shown that load steps equivalent to q_c values as small as 0.07 kPa (10 g) can be distinguished.

The FO cone penetrometer performs data acquisition at 500 Hz. Figure 3 presents results of a field test which demonstrates the difference between 500 Hz the classical 2 Hz data acquisition. Higher sampling frequency provides a possibility to detect very thin soil layers more accurately.

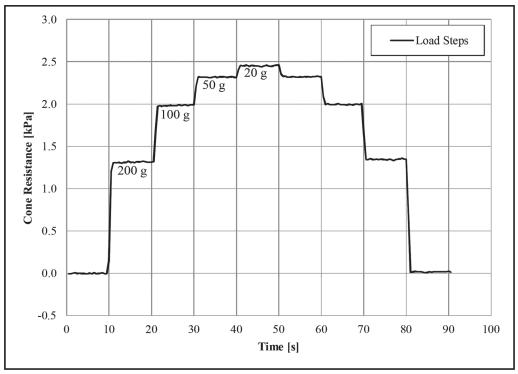

Figure 2. FO cone penetrometer resolution.

3.2 *Influence of ambient and transient temperatures*

As per ISO 22476-1, the FO cone penetrometer is designed in such a way that temperature changes are predominantly mechanically compensated. In addition compensation by calibration is applied, as is common for strain-gauge cone penetrometers.

Figure 4 shows a laboratory test where the FO cone penetrometer is preheated to 20°C and subsequently lowered into a 5°C cold water bath. The temperature shock caused a maximum drift in cone resistance of 33 kPa. The zero load drift of the test was approximately 1 kPa. This is equivalent to a hydrostatic water head of 0.1 m.

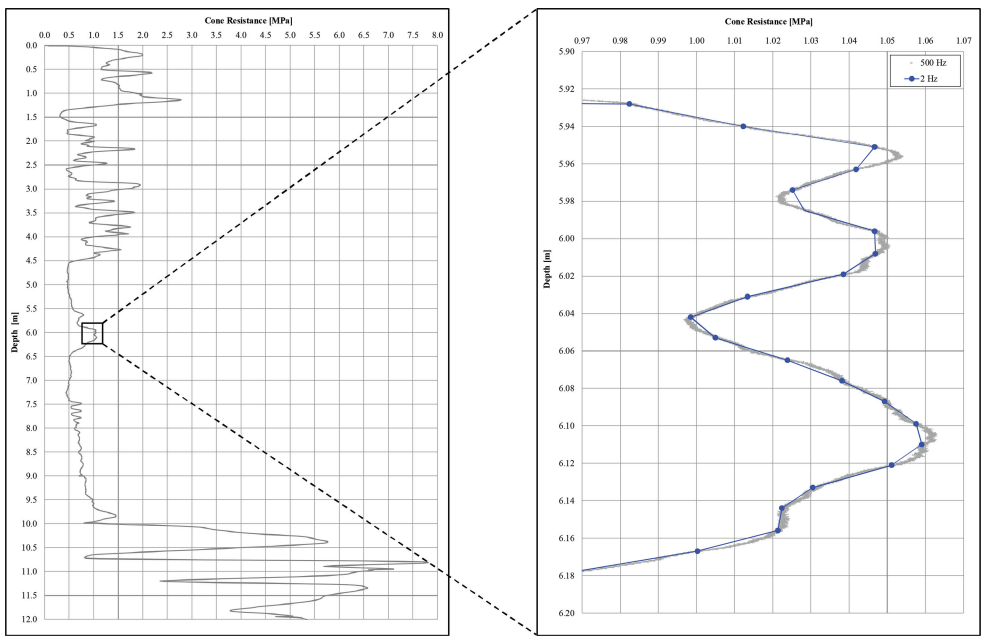

Figure 3. Test results for FO cone penetrometer.

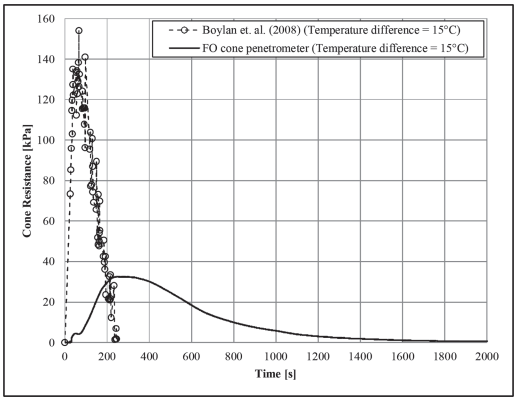

Figure 4. Cone resistance output upon transient temperature shock of 20°C to 5°C.

Somewhat comparable laboratory tests with strain-gauge cone penetrometers showed a q_c drift of approximately 50 kPa to 150 kPa for a temperature difference of 15°C (Boylan et. al, 2008)

One of the future development plans for the FO cone penetrometer is to fit a temperature sensor in the FO cone penetrometer. This sensor will target heat flux and may provide a possibility for correction of transient temperature effects.

3.3 *Influence of bending of cone penetrometer*

As per ISO 22476-1, the measured error of cone resistance due to probe bending should be considered. This error depends on the direction of the applied load. Laboratory test results for the FO cone penetrometer showed a maximum error of cone resistance due to probe bending of 0.35 kPa/Nm. This value is approximately 8 times smaller than values for double bridge cone penetrometers, as presented by Peuchen & Terwindt (2014). To determine the error of cone resistance due to probe bending, the FO cone penetrometer was loaded close to the tip with a moment of 9.0 Nm. The cone resistance output was recorded while rotating the cone penetrometer 360°. Note that FO technology also allows for distinction between (bending) load direction and magnitude.

4 CONCLUSION

Test results indicate that the prototype fibre optic (FO) cone penetrometer is capable to perform piezocone penetration tests (CPTU) well within ISO 22476-1 Application Class 1.

For the prototype penetrometer, the fibre optic sensors for measuring q_c and f_s have maximum ranges of 10 MPa and 0.5 MPa respectively. This implies applicability for onshore soft clays, silts and peat, i.e. Soil A and Interpretation H of ISO 22476-1. The FO cone penetrometer has potential to meet a significantly more stringent, Dutch Application Class 1+.

Laboratory test results for the FO cone penetrometer show favourable performance for transient temperature change and penetrometer bending.

Additional development and qualification activities are ongoing (2017). It is expected that the FO cone penetrometer will be available for commercial use by the second half of 2018.

ACKNOWLEDGEMENTS

The authors are indebted to many dedicated colleagues and gratefully acknowledge Fugro's persistent commitment to excellence in cone penetration testing. The opinions expressed in this paper are those of the authors. They are not necessarily shared by Fugro.

REFERENCES

Boylan, N., Mathijssen, F., Long, M. and Molenkamp, F. 2008. Cone penetration testing of organic soils. Proceedings, *Baltic Geotechnical Conference, September. Gdansk, Poland.*

FAZ Technology 2017. *FAZT I4 Interrogator.* [online] Available at: www.faztechnology.com [Accessed 10 October 2017].

International Organization for Standardization, 2005. ISO 17025:2005 General requirements for the competence of testing and calibration laboratories. Geneva: ISO.

International Organization for Standardization, 2012. ISO 22476-1:2012 Geotechnical Investigation and Testing – Field Testing – Part 1: Electrical Cone and Piezocone Penetration Tests. Geneva: ISO.

Peuchen, J., Kaltsas, D. & Sinjorgo G. 2017. Calibration of cone penetrometers in accredited laboratory. In 4*th International Symposium on Cone Penetration Testing CPT18: May 21–22, 2018 – Delft, The Netherlands*.

Peuchen, J. and Terwindt, J. 2014. Introduction to CPT accuracy. In 3rd International Symposium on Cone Penetration Testing CPT14: May 12–14, 2014 – Las Vegas, Nevada, 45 pp.

Stoevelaar, R. & van Duinen, A. 2016. Protocol Sonderen Voor Su-bepaling. *Report 1220083-010-GEO-0006. Delft: Deltares*, 33 pp (in Dutch).

Taylor & Francis
Taylor & Francis Group
http://taylorandfrancis.com

Cone Penetration Testing 2018 – Hicks, Pisanò & Peuchen (Eds)
© 2018 Delft University of Technology, The Netherlands, ISBN 978-1-138-58449-5

Some considerations related to the interpretation of cone penetration tests in sulphide clays in eastern Sweden

A.B. Lundberg
ELU Konsult AB, Stockholm, Sweden

E.A. Alderlieste
SPT Offshore BV, Woerden, the Netherlands

ABSTRACT: Holocene clays that contain a significant amount of sulphide are regularly discovered during site investigation programs carried out along the East coast of Sweden. Cone Penetration Tests (CPTs) are frequently executed during such investigations, and the mechanical properties of the soil is subsequently interpreted from the CPTs. The mechanical behaviour of the sulphide clays is somewhat similar to other high-plasticity Scandinavian clays, including shear-strength anisotropy, and a high level of strain-rate and temperature dependency. These factors make the interpretation of the soil properties complicated, since the testing conditions and the testing methods have a large influence on the soil behaviour. Sample disturbance and the temperature of laboratory direct simple shear tests also influence the interpretation, since these have been used as a reference for in-situ tests. The boundary conditions of the soil during both the in-situ and laboratory tests are consequently mixed in the interpretation, resulting in significant uncertainty about the correct soil properties. The design shear strength is typically chosen conservatively, but studies show a significant variation in the resulting cone factors for sulphide clays from empirical correlations. There are however some cases where a low undrained shear strength is not conservative, and in which design guidelines create some confusion. A case study of Cone Penetration tests in sulphide clay in Eastern Sweden is examined and some factors which influence the soil behaviour are discussed, including the strain-rate, temperature and anisotropic strength.

1 INTRODUCTION

Sulphide clays are frequently present in the Holocene sediments along the East coast of Sweden. The sulphide and organic content are especially high along the Bothnian bay, but clays with sulphide content are also present all over Eastern Sweden, including Stockholm. Such clays are highly strain-rate and temperature dependent, (Larsson et al 2007, Leroueil et al 1985, Leroueil & Soares Marques 1996). Cone penetration tests are frequently carried out as part of a site investigation program to assess the strength and deformation properties of these clays. Empirical cone factors $N_{kt} > 20$, correlated to direct simple shear (DSS) tests for the undrained shear strength in direct shear c_u^{DSS} are recommended for design, (Larsson et al 2007, Westerberg et al 2015). This results in low evaluated shear strengths in design, especially in comparison to typical Scandinavian clays, as demonstrated in Lunne et al (1976). There is also significant uncertainty in the determination of the soil properties, and correlation studies also show low correlation factors for the suggested empirical cone factors, (Larsson et al 2007). Since the designation of the clay sample as sulphide clay is frequently done by inspection in the laboratory, the sulphide content is not known for most samples. In addition, the reference DSS tests are often carried out in room temperature (20°C), which reduces the undrained shear strength of clay, (Westerberg et al 2015). Sulphide clays are also quite sensitive to temperature changes, which indicates that the laboratory reference tests carried out in room temperature would result in significantly lower shear strengths, (Leroueil & Soares Marques 1996). Sample disturbance also influence laboratory testing of Holocene clays, (Lundberg 2017). The shear strength in triaxial extension (c_u^P) has been also shown to be larger than the DSS strength (c_u^{DSS}) as evaluated from DSS tests in Scandinavian high-plasticity clays, implying that the DSS test results are somewhat conservative, and maybe be influenced by sample disturbance, (Karlsson & Karstunen 2017). A large laboratory study of different sulphide clays display a factor of at least 2 between the shear strength in triaxial compression (c_u^a) and the DSS strength (c_u^{DSS}), which suggests

that sample disturbance can have a large influence on the reference DSS-tests, (Larsson et al 2007).

There are consequently many factors which influence the undrained shear strength of sulphide clays. This is frequently taken into account in design by choosing a conservative characteristic value. A conservative assessment of the undrained shear strength of a clay normally results in a design on the safe side. There are however some practical cases where such conservatism results in a design which is non-conservative, or on the unsafe side:

- Structural analysis (e.g. of bridges) with the soil modelled as elastic springs, in which the spring stiffness is correlated to the rigidity index G/c_u. The structural forces are calculated for different load cases in such models, frequently including temperature expansion models, and a conservative assessment of the undrained shear strength in such a load case will therefore result in a higher stiffness in the real surrounding soil, and different estimated forces in the structural members.
- Ground improvement by triggered slides, in which surcharge is added to trigger a limited slide (e.g. intended to minimize the amount of material going to a recycling deposit). The conservative assessment of c_u underestimates the surcharge needed to trigger a slide.
- Assessment of undrained shear strength from correlations from field full scale tests, which are frequently carried out quite fast. The high strain rate overestimates the strength of the clay, and contradicts the in-situ and laboratory tests.

In the current study, some CPTs in a sulphide clay from Eastern Sweden are examined to illustrate some of the main features of sulphide clay during cone penetration relative other in-situ and laboratory testing. The site is located in Eastern Sweden, and provides additional information about the geographical distribution of sulphide clays alongside the samples discussed in Larsson et al (2007) which originate from the North of the country along the Bothnian Bay. The CPT data is analyzed in comparison to some other standard methods to determine the undrained shear strength of clays in direct shear, c_u^{DSS}.

2 CHARACTERISTICS OF SULPHIDE CLAYS

Sulphide clays are characterized by the presence of sulphide, commonly in the form of FeS and FeS^{2+}. Such soils mainly occur in tropical regions, but they are also present along the Northern and Eastern coast of Sweden. They are characterized by the dark colour of the FeS content and a normally low content of H_2S, resulting a characteristic smell, (Larsson et al 2007). Sulphide clays are the result of sedimentation in an anaerobic environment, and the sulphide content originates from organic components in the clay sediments, (Yu 1993). The anaerobic decomposition of the organic substances in the sediments occurs because of low water circulation, and results in Sulphur Hydrogen (H_2S), which reacts with the iron content is the soil (Fe^{2+}), producing iron-mono-sulphide (FeS). During extended time periods FeS is transformed into FeS_2, (Westerberg et al 2005).

The geological conditions resulting in sedimentation of sulphide clays have historically been present in parts of the Baltic sea, where the hydrodynamic conditions produced low circulation for such extended geographical areas, especially during the extension of the Littorina sea across the coastline around 9000 B.C.E. The warmer geological periods and the consequent increase in organic growth between 4000–8000 B.C.E. resulted in growth of large amounts of organic matter which was subsequently deposited along the coastline. The isostatic rise of the Fennoscandian shield means that these areas are currently located above the present sea level, (Eriksson 1989, Larsson et al 2007). A detailed geological and chemical description of sulphide clay is given in Georgala (1980). The sulphide content of these clays varies along the coastline; higher levels of FeS and FeS_2 are found in the Northern part of the coastline, and degree of composition also displays strong variation. An outline of the region where sulphide clays dominate the Holocene soil layers is displayed in Figure 1.

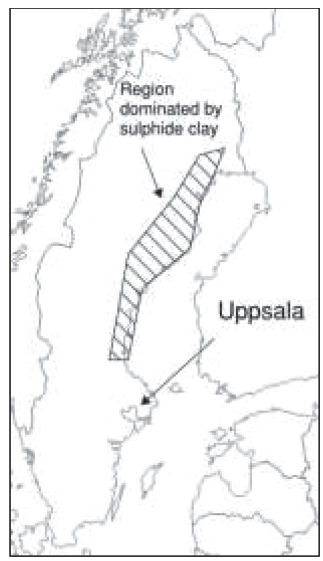

Figure 1. Location of sulphide clays along the Bothnian bay in Sweden.

Sulphide clays, however, also frequently occur in the Stockholm region further South, especially in large geological basins where significant amounts of organic clays have been deposited, (Larsson et al 2007). Assessment of the mechanical properties of sulphide clays is consequently a frequently occurring feature in practical geotechnical design in Eastern Sweden.

The sensitivity S_t of the sulphide clays is mostly 10–20, (Westerberg et al 2015). This level of sensitivity is similar to other Scandinavian Holocene clays. The cause of the comparably high sensitivity the creation of bonds during sedimentation, which are subsequently destructurated during remoulding, resulting in high sensitivity (Larsson et al 2007).

3 CONSIDERATIONS IN ASSESSMENT OF SULPHIDE CLAYS

3.1.1 *Mechanical behaviour*

The mechanical behaviour of sulphide clays has been described in several studies, e.g. Holtz & Holm (1979), Eriksson (1989), Larsson et al (2007). Sulphide clays are related to some of the main characteristics of Scandinavian Holocene clays as outlined by Bjerrum (1979). The sedimentation process has resulted in an anisotropic yield surface. The yield surface is dependent on the strain rate and temperature, resulting in an expansion of the yield surface with an increasing strain rate and a contraction of the yield surface with an increase in temperature, (Eriksson, 1989; Yu, 1993). This is illustrated schematically in Figure 2 which shows an alteration of the anisotropic yield surface with any change in strain rate and temperature during shearing.

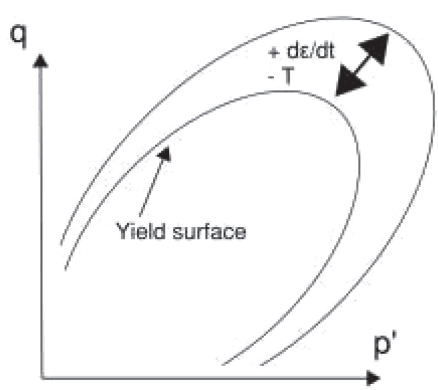

Figure 2. Alteration of anisotropic yield surface with strain rate and temperature changes.

3.1.2 *Mechanical response during soil testing*

The strain rate and temperature dependence of the yield surface influences the mechanical response of sulphide clay during soil testing. The high-strain rate during in-situ testing increases the undrained shear strength, (Schnaid 2009). On the other hand, laboratory tests are influenced by soil sample disturbance and the laboratory temperature. The influence on the temperature has been well-documented in laboratory experiments, (Eriksson 1989). The influence of sample disturbance is not fully known for sulphide clays, but can be significant in laboratory testing of other high-plasticity clays, (Lundberg 2017).

3.1.3 *Spatial variability*

The spatial variability of the soil strata governs the reliability of any geotechnical design if fixed LRFD partial factors are used, e.g. in Eurocode 7 (Lundberg & Li 2015). The spatial variability is consequently of interest in practical design. The horizontal and vertical scale of fluctuation for sulphide clays has been discussed in the literature, (Larsson et al 2007, Westerberg et al 2015). However, no systematic study of sulphide clays has been carried out. Since empirical cone factors N_{kt} are referenced to DSS tests carried out at finite locations in the soil strata, this has some influence on the applicability of correlations used in practical design.

4 A CASE STUDY OF CPT MEASUREMENTS IN EASTERN SWEDEN

4.1 *Site location and local geology*

Cone Penetration Testing was carried out as part of a site investigation program for residential development in Uppsala, Eastern Sweden, shown in Figure 1. The site is located South of the area dominated by sulphide clay in Figure 1, but during site investigation a large extent of the soil strata (from 9 m to 23 m depth) was found to consist of sulphide clay. The sulphide clay was located at around the same depth at all boreholes, suggesting homogeneous strata.

The clay deposit is around 50–60 m deep and located in the center of a valley formation, resulting in uniform marine soil deposition of the clay sediments. The soil layers are described in Table 1. The top soil layer consists of organic high-plasticity clay, with around 5% organic content, followed by the sulphide clay. These layers were formed during the post-glacial period which started around 10000 years BCE (Georgala 1980). The clay was deposited in marine-brackish conditions. Beneath these sediments, a layer of varved high-plasticity

Table 1. Index properties of the soil strata.

Layer	Properties
Organic post-glacial high-plasticity clay	Depth: 3–9 m Liquid limit: 60–65% Water content: 60–70% Bulk density: 1.6 t/m^3 Sensitivity: 10–18 OCR: 1.2–2
Sulphide clay	Depth: 9–23 m Liquid limit: 80–100% Water content: 60–90% Bulk density: 1.45–1.60 t/m^3 Sensitivity: 8–14 OCR: 1.2 Sulphuric content: 1–1.5%
Glacial varved high-plasticity clay	Depth: 23–60 m Liquid limit: 45–70% Water content: 35–60% Bulk density: 1.60–1.90 t/m^3 Sensitivity: 3–8 OCR: 1.2

clay extends to a 1–2 m layer of moraine deposited on the rock face. The clay basin extends for a couple of kilometers around the city of Uppsala and follows local rock faults located in the Western part of the Fennoscandian shield in the Eastern part of Sweden.

The plastic limit is normally not evaluated during standard laboratory testing of high-plasticity clay in Sweden. Consequently, the plasticity index in not much used in soil classification, and the liquid limit is typically used instead, (Larsson et al 2007). The plasticity index for typical clays ranges from 25–60, (Westerberg et al 2005). The sulphide clay layer has a very high natural water content, as shown in Table 1. The clay is normally consolidated with an OCR of around 1.2 because of creep in the clay since deposition after the glacial period, which is commonly occurring in the Scandinavian region (Bjerrum 1973).

4.2 *Cone penetration testing*

10 CPTs and two Field Vane Tests (FVTs) were carried out at the site. Soil compressibility in the vertical direction was assessed through Constant rate of Strain (CRS) tests performed at eight levels along the strata at four different boreholes. The sampling was carried out with a 50 mm Swedish St II piston sampler, described in Lundberg (2017). Fall Cone tests (FCs) were also executed on the clay samples. Both the strength and deformation properties were therefore evaluated through different methods, forming part of the yield surface shown in Figure 2. Here only the penetration in the upper 25 m are discussed. CPT 1 is examined in detail to describe the features of the sulphide clay.

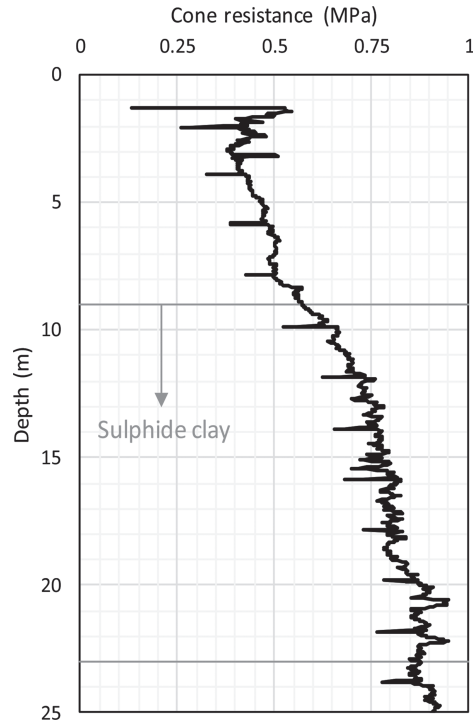

Figure 3. CPT 1: Cone resistance.

Figure 3 shows the Cone resistance of CPT 1. The extent of the sulphide clay is displayed in the Figures. Figure 4 and 5 show the pore pressure development (u_2) and sleeve friction of CPT 1. Figure 6 displays the friction ratio of CPT 1, suggesting a somewhat uniform response during the cone penetration of the sulphide clay layer.

The sleeve friction and friction ratio also show that the sulphide clay is fairly uniform from 12–22 m depth, where is reached a plateau, and transforms from the shallow high-plasticity organic clay above to the high-plasticity varved glacial clay beneath it. The relatively high friction ratio indicates the organic content of the soil, following Lunne et al. (1997).

The corrected cone resistance q_t of all 10 CPTs that were carried out in the area are displayed in Figure 7, showing the uniformity of the soil layer. The distance between the CPTs were 50–150 m for a total area of around 250 x 500 m^2.

4.3 *Interpretation of undrained shear strength*

The main objectives of CPT interpretation include the assessment of the undrained shear strength using empirical cone factors N_{kt}, (Lunne et al 1997). An average CPT profile was assembled to assess the recommended N_{kt} value of 20.2 from Westerberg et al (2015). This profile of the

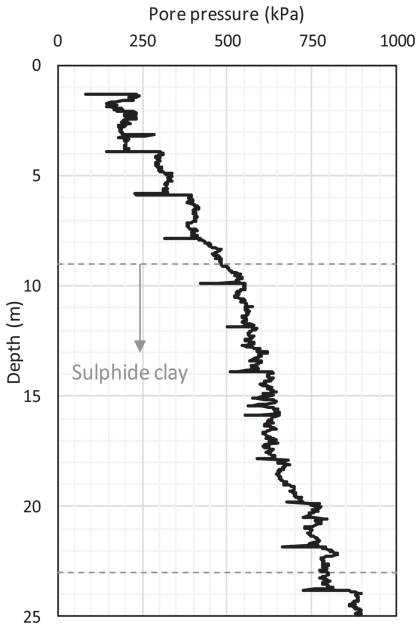

Figure 4. CPT 1: Pore pressure u_2.

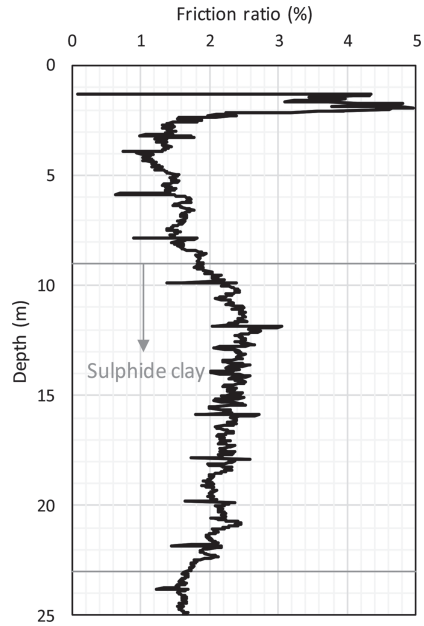

Figure 6. CPT 1: Friction ratio.

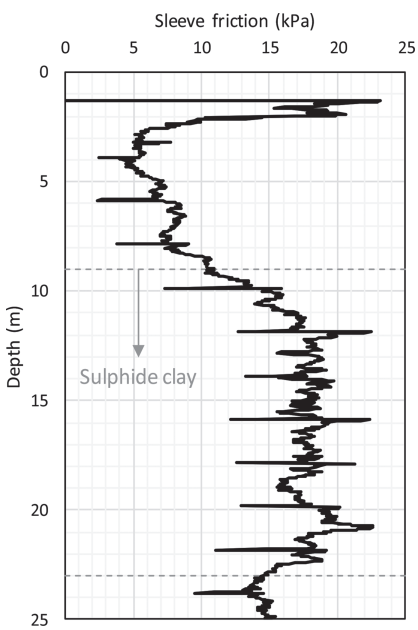

Figure 5. CPT 1: Sleeve friction.

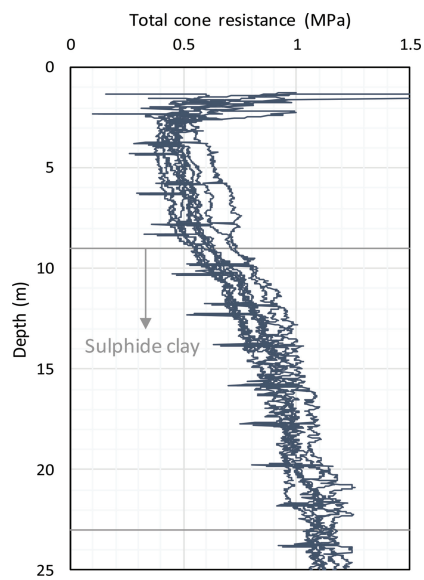

Figure 7. Corrected cone resistance q_t of the 10 CPTs.

undrained shear strength in direct shear c_u^{DSS} in the sulphide clay layer was compared to the measured and correlated values of the undrained shear strength obtained through the correlations discussed in Larsson et al. (2007). These include a correction factor for the undrained shear strength in direct shear c_u^{DSS} assessed from the Field Vane Tests (FVT) and Fall Cone Tests (FC), as well as a correlation with the preconsolidation pressure from Jamiolkowski et al (1985). The undrained shear strength in direct shear c_u^{DSS} estimated by these methods and the suggested cone factor for

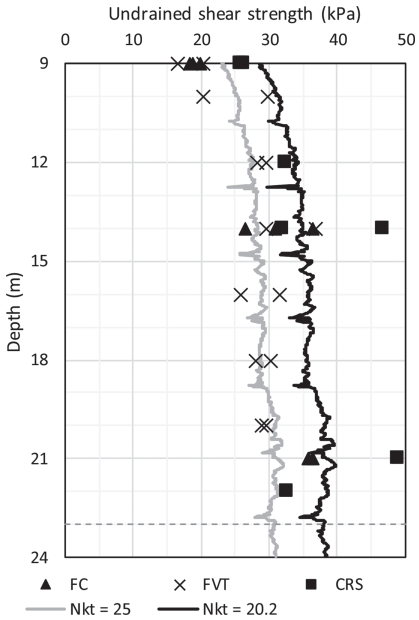

Figure 8. Interpreted undrained shear strength in direct shear c_u^{DSS} with cone factors N_{kt} = 20.2 and 25).

the CPT are shown in Figure 8 for the sulphide clay layer. Figure 8 also shows the depth of the sulphide clay layer and the evaluated undrained shear strength c_u^{DSS} from the mean CPT for a cone factor N_{kt} = 20.2 and N_{kt} = 25. The large variation in undrained shear strength c_u^{DSS} evaluated by the different methods indicate the need for site-specific calibration for the cone factor N_{kt}, since the value of N_{kt} = 20.2 suggested by Westerberg et al (2015) might be unconservative for the specific site compared to the other test methods, consisting of FVTs, FCs and CRS-correlations.

5 CONCLUSIONS

CPT interpretation in sulphide clays remain a challenge due to the complicated material behaviour of these soils. An example of a sulphide clay from Eastern Sweden was exhibited to display some main characteristics during cone penetration. The high friction ratio in the sulphide clay is noticeable. It is also shown that an empirical cone factor obtained from correlations with DSS tests carried out on soil samples from Northern Sweden is somewhat low, and that a cone factor of 25 provide more conservative fit with the standard methods to estimate the undrained shear strength in direct shear c_u^{DSS} sulphide clays, and that site-specific correlations are needed in practical design.

REFERENCES

Bjerrum, L. 1973. Problems of soil mechanics and construction of soft clays and structurally unstable soils. In *Proc. 8th. Intl. Conf. on SMFE, Moscow, 1973*. 118–159.

Eriksson, L.G. 1989. Temperature effects on consolidation properties of sulphide clays. In *International Conference on Soil Mechanics and Foundation Engineering, 1989*. 2087–2090. Balkema Publishers, AA/Taylor & Francis.

Georgala, D. 1980. Paleoenvironmental studies of postglacial black clays in north-eastern Sweden, Stockholm, Almqvist & Wiksell.

Holtz, R.D., & Holm, G. 1979. Test embankment on an organic silty clay. In *Proceedings of the 7th European Conference on Soil Mechanics and Foundation Engineering, Brighton, England.* British Geotechnical Society, Vol. 3: 79–86

Larsson, R., Westerberg, B., Albing, D., Knutsson, S., & Carlsson, E. 2007. *Sulfidjord: geoteknisk klassificering och odränerad skjuvhållfasthet*. Luleå tekniska universitet. (In Swedish).

Jamiolkowski, M., Ladd, C.C., Germaine, J.T. & Lancelotta, R. 1985. New developments in field and laboratory testing of soil. Proceedings of the international conference of soil mechanics and foundation engineering, 57–153

Karlsson, M., & Karstunen, M. 2017. On the Benefits of Incorporating Anisotropy in Stability Analyses in Sensitive Clays. In *Landslides in Sensitive Clays*. Heidelberg: Springer International Publishing.

Leroueil, S., Kabbaj, M., Tavenas, F. & Bouchard, R. 1985. Stress–strain–strain rate relation for the compressibility of sensitive natural clays. *Geotechnique*, 35(2), 159–180.

Leroueil, S., & Soares Marques, M.E. 1996. Importance of strain rate and temperature effects in geotechnical engineering. In *ASCE Special Publication No. 61: Measuring and modeling time dependent soil behavior*, 1–60. Philadelphia: ASCE.

Lundberg, A.B. 2017. Sample Disturbance in Deep Clay Samples. In *Landslides in Sensitive Clays* (pp. 133–143). Springer International Publishing.

Lundberg, A.B., & Li, Y. 2015. Probabilistic characterization of a soft Scandinavian clay supporting a light quay structure. *Geotechnical safety and risk* V. IOS Press, Heidelberg, 170–175.

Lunne, T., Eide, O., & Ruiter, J.D. 1976. Correlations between cone resistance and vane shear strength in some Scandinavian soft to medium stiff clays. *Canadian geotechnical journal*, *13*(4): 430–441.

Lunne, T., Robertson, P.K., & Powell, J.J.M. 1997. Cone penetration testing. *Geotechnical Practice*. London: Taylor & Francis.

Schnaid, F. 2009. In situ testing in geomechanics: the main tests. Toronto: CRC Press.

Westerberg, B., Müller, R., & Larsson, S. 2015. Evaluation of undrained shear strength of Swedish fine-grained sulphide soils. *Engineering Geology*, *188*: 77–87.

Westerberg, B., Albing, D., & Larsson, R. 2005. Research on strength and deformation properties of Swedish fine-grained sulphide soils. *In International Conference on Soil Mechanics and Geotechnical Engineering, 2005.* Vol. 2: 623–626.

Yu, Y. 1993. Testing and modelling of silty and sulphide-rich soils, Luleå, Luleå tekniska universitet.

Cone Penetration Testing 2018 – Hicks, Pisanò & Peuchen (Eds)
© 2018 Delft University of Technology, The Netherlands, ISBN 978-1-138-58449-5

Effect of cone penetrometer type on CPTU results at a soft clay test site in Norway

T. Lunne, S. Strandvik, K. Kåsin & J.S. L'Heureux
Norwegian Geotechnical Institute, NGI, Oslo, Norway

E. Haugen, E. Uruci, A. Veldhuijzen, M. Carlson & M. Kassner
Norwegian Public Road Administration, NPRA, Oslo; Pagani, Italy
Geomil, The Netherlands
Geotech, Sweden
Adam Mickiewicz University in Poznan, Poland

ABSTRACT: Seven different cone penetrometers from 5 manufacturers have been used in a comparative testing program at the Norwegian GeoTest Site (NGTS) on soft clay in Onsøy, Norway. Tests with all cone types give very repeatable penetration pore pressure, u_2. When comparing tests with different cone types, six of the cones give very similar u_2 values. One cone type give consistently higher u_2 values. Measured cone resistance, q_c, generally varies somewhat more, both regarding tests with the same cone, and when comparing results of one cone type with another. Some of the cone types give good repeatability for sleeve friction, f_s, readings, while some show relatively large variation. When comparing f_s from different cone types the variation is quite large, which is in line with previous experience. An attempt has been made to understand the reasons for the large f_s variations.

1 INTRODUCTION

It is a well-known fact that even if cone penetrometers adhere to the international standards (e.g. ISO 22476–1:2012), results of tests using equipment from different manufacturers can give different results (e.g. Lunne et al.1986, Gauer et al. 2002, Powell & Lunne 2005, Tigglemann & Beukema 2008, Lunne 2010, Cabal & Robertson 2014). This is particularly a problem when soil investigation contractors using different cones operate in the same area, and especially on the same project. Lunne et al. (1986) carried out a comprehensive laboratory and field study comparing tests results from cone penetrometers from 8 different manufacturers. In that study it was shown that all three parameters q_c, f_s and u_2 could vary significantly, depending on the equipment used.

A later study by NGI (Gauer et al. 2002) based on a number of different cone penetrometers tested in Onsøy clay showed that the situation had improved. The cone resistance showed relatively small scatter, and the penetration pore pressure was even more repeatable from one cone type to another. However, the scatter in the measured sleeve friction, and hence the friction ratio, was very significant.

Powell & Lunne (2005) showed that if calibration of all cone penetrometers used was done in a consistent manner by one organization who also carried out all tests, then the variation in results will be reduced.

Over the last few years further improvements in cone design and electronics have occurred by some cone manufactures. The establishment of 5 new national test sites in Norway (L'Heureux et al. 2017) has given the opportunity to revisit the problem of uncertainties in CPTU test results by inviting several companies to do testing at 4 of the sites.

This paper includes only results of tests from the soft clay site at Onsøy, a later paper will include test results from all 4 test sites.

For the tests reported herein the calibrations were carried out by each cone manufacturer. It is thought that the test results will then be more representative for general practice in the soil investigation industry. Each cone manufacturer has tried to follow requirements and recommendations in international standards and guidelines.

2 ONSØY TEST SITE

The Onsøy test site is located about 100 km south of Oslo. It consists of a 25–35 m thick marine deposit which has never been subjected to higher vertical stresses than today, but it has an over consolidated ratio due to ageing. The Onsøy test site has been used by NGI for more than 40 years, including testing out of *in situ* tools and testing many types of samplers (Lunne et al. 2003). Due to development of the area for industrial purposes several locations at Onsøy have been used over the years. The present site appears to be slightly less uniform compared to the previous locations (L'Heureux et al. 2017). A soil profile is shown in Figure 1.

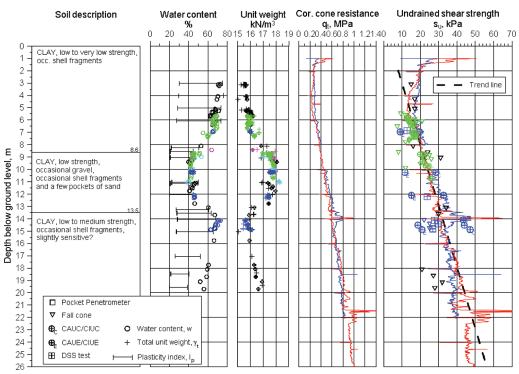

Figure 1. Soil profile at Onsøy.

3 DESCRIPTION OF CONE PENETROMETERS USED

Seven different cone penetrometers from five manufacturers were used in the present study. Some key dimensions and other information about the cone penetrometer is given in Table 1.

As can be seen from Table 1 six of the cone penetrometers are of the compression type with both cone resistance, q_c, and sleeve friction, f_s, being measured by separate compression load cells. One of the cones is of the subtraction type where one compression load cell measures q_c, and another load cell measures $q_c + f_s$. Then f_s can be calculated by subtraction.

The penetration pore pressure is measured at the location just above the conical part, u_2.The pore pressure measurement systems vary as shown in Table 2 where the filter type and saturation fluid are summarized. Six of the cones use filter made of bronze, brass or stainless steel. Five of these use silicon oil as saturation fluid and one uses glycerin. One of the cone penetrometers use a so-called slot filter. As described in ISO 22476–1:2012, in this system the pore pressure is measured by an open system with a 0.3 mm slot immediately behind the conical part. The slot communicates with the pressure chamber through several channels. De-aired water, antifreeze (glycol) or other liquids can be used to saturate the pressure chamber, whereas the channels are saturated with gelatin or a similar liquid.

Table 1. Dimensions and other relevant information regarding the cone penetrometer used in this study.

Cone type	D1	D2	h	L1	Ac	Asb	Ast	As	a-nom	b-nom	Cone type	Capacity qc	fs	ua
1	35.76	35.78	10	134	1003.84	200	200	15014	0.80	0.0	Comp	50	1.6	2.5
2	35.90	36.00	10	135	1012.23	163	163	15155	0.85	0.0	Comp	25	0.5	2
3	36.00	36.10	10	135	1017.36	279	279	15000	0.80	0.0	Subtr	100	1	2
4	36.00	36.10	10	135	1017.36	279	279	15000	0.80	0.0	Comp	100	1	2
5	36.00	36.10	10	135	1017.36	279	279	15000	0.80	0.0	Comp	50	0.5	2
6	36.00	36.00	10	135	1017.36	297	168	15268	0.69	0.008	Comp	50	1	2
7	35.70	35.90	10	133.8	1006.6	208	208	15090	0.75	0.0	Comp	75	1	2

Table 2. Pore pressure measurement systems for the various cone penetrometer used in this study.

Cone type	Filter type	Saturation fluid	Date performed	Number of tests
1	Bronze	Silicone ISOVG 100	04092017	4
2	Bronze	Glycerine	17112017	3
3	Brass 38 micron (SIKA B-20)	Silicone oil 200 fluid 50 cSt	18092017	2
4	Brass 38 micron (SIKA B-20)	Silicone oil 200 fluid 50 cSt	18092017	4
5	Brass 38 micron (SIKA B-20)	Silicone oil 200 fluid 50 cSt	18092017	4
6	Slot	Grease/oil	13112017	3
7	Stainless steel, S/S 10 micron	Silicone oil, DC200, 50 cSt	14112017	2

4 TEST PROGRAM AND MEASURED PARAMETERS

The tests included in this paper were carried out between 4th September and 17th November 2017 within an area of 5 m by 12 m. All tests were carried out to a depth of 25 m below ground level except for cone 1 which was stopped at 21 m. Pore pressure measurements show that the water table has been at about 0.5 m throughout the testing period. Due to various circumstances a various amount of soundings (2–4) were carried out with each of the cone penetrometers. Predrilling to 1 or 2 m was used for the tests with cones 2, 6 and 7.

Figure 2 shows the results of all tests from the seven cone penetrometer types, in terms of measured q_c, u_2 and f_s. The following immediate observations can be made from visual inspection:

- For all cone penetrometers except cone 3, u_2 show very good repeatability. The two profiles with cone 3 are deviating 10–60 kPa from each other in the depth interval 5–20 m. The large deviation between 21 and 25 m is possibly caused by the sounding being influenced by a neighbor CPT hole.
- For all cones the measured q_c exhibit reasonably good repeatability, but not as good as u_2
- Most variations occur for f_s; especially for cones 1, 2, 3 and 7.

All dimensions in mm; All areas mm^2; Capacity q_c, f_s and u_2 sensors in MPa; nominal means average values given by manufacturer, D_1 = diameter of cylindrical part of cone tip; D_2 = diameter of sleeve; h = height of cylindrical part of cone tip, L_1 = length of friction sleeve, A_c = cross-sectional

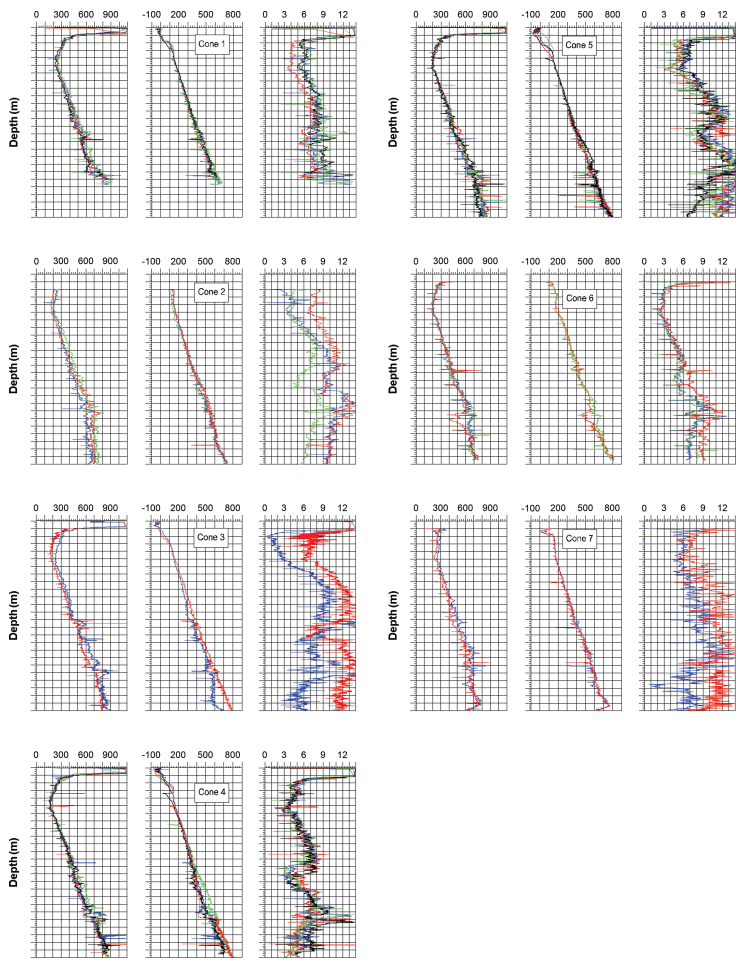

Figure 2. Measured q_c, u_2 and f_s vs depth for all CPTU profiles included in study.

area of cone tip, A_{sb} = area where pore water pressure can act at bottom of friction sleeve; A_{st} = area where pore water pressure can act at top of friction sleeve; A_s = area of sleeve; a = area ratio of cone; b = are ratio of sleeve

5 COMPARISON BETWEEN THE DIFFERENT CONE TYPES

5.1 *Measured parameters*

For all types of cones used a representative profile has been chosen. Average values have been worked out for all three basic measurements. Obvious erroneous results caused by poor saturation, like for cones 4 and 5 have been excluded as well as some other anomalies. One test with cone 7 was not included due to large zero shift observed at test completion. As mentioned in the introduction, details in calibration of CPTU sensors can potentially vary between different cone manufacturers, especially in the lower range of values as in soft clay. At 10 m for instance a u_2 value of 300 kPa is typically measured and the nominal capacity of the pore pressure sensor is 2000 kPa, this means that about 15% of the capacity is utilized. q_c with capacity of 100 MPa about 0.3% is typically utilized at same depth. And for f_s with a typical load cell capacity of 1 MPa about 0.8% is utilized. It can be expected that the u_2 reading may be more accurate and consistent since a larger part of the capacity of the measurement sensor is utilized compared to q_c and even more so f_s.

In addition to the general calibration which is normally carried out at room temperature sensitivity of zero readings to change in temperature can also be important.

Figure 3a compares the representative profiles of the measured parameters (q_c, u_2 and f_s), without any corrections for the 7 cone types.

It should be noted that the a-factor has been measured in a calibration vessel for each cone used and may deviate slightly from the nominal values given in Table 1. The q_c profiles in Figure 3 for cones 1, 3 and 4 showed much lower values than the other tests. The a values for these cones were not much lower than the others so this effect cannot explain the differences in q_c. Based on previous experience it was suspected that zero shift caused by different temperature at ground level (generally about 15 °C, but in a few cases as low as 0 °C) and soil temperature (7 °C) could occur. Laboratory calibration tests by two of the manufacturers (cones 1, 3, 4 and 5) showed that zero shifts due to change in temperature from 15 to 7°C could cause measured q_c to be too low by 50–100 kPa. For f_s temperature zero shifts were 1–4 kPa for the same cones. For u_2 the temperature zero shifts were not significant. Cone 7 gives

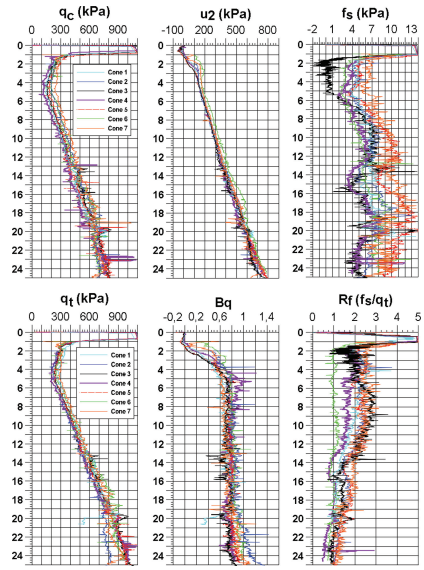

Figure 3. Comparison of representative values of q_c, u_2, f_s, q_t, B_q and R_f for all cones.

higher q_c, even though the two profiles carried out with this cone gave very similar q_c as shown in Figure 2. This can only partly be explained by an observed zero shift, which is 21 kPa for the average profile for cone 7.

For cones 1, 3, 4 and 5 corrections for temperature zero shifts have been made before computing the derived parameters. For cone 2 zeroing before tests was done in a bucket with temperature as in ground. For cone 7 the air temperature was quite close to ground temperature, No corrections were required for the tests with these two cones.

Except for cone 6, u_2 shows remarkably good comparison among the cone types. Cone 6 is the only cone using a slot (filter) instead of a filter. This may be an explanation why u_2 is higher (20–80 kPa in depth interval 5–15 m) compared to the other cones. However, neither NGI nor NPRA, who have many years of experience with using slot filters have observed such deviations earlier.

5.2 *Derived parameters*

Derived parameters q_t, R_f and F_r are also shown in Figure 3b. The derived parameters are defined as follows:

$$q_t = q_c + (1 - a) * u_{2;}\ R_f = f_s/q_t,\ \% \qquad (1)$$

Considering q_t the range has narrowed down considerably when compared to the measured q_c values. Computed B_q values are as expected for a soft clay and generally within a range of 0.65–0.80.

The range for R_f is larger, indicating that for soft clay B_q can be a more reliable classification parameter compared to R_f. Lunne & Andersen (2007) summarised the potential main reasons for lack of accuracy in f_s:

1. Pore pressure effects on ends of the sleeve.
2. Tolerance in dimensions between the cone and the sleeve.
3. Surface roughness of the sleeve.
4. Load cell design and calibration.

Due to limited space, only factors 1 and 2 will be discussed in the following. To correct sleeve friction for pore pressure effects it is necessary to know the pore pressure in the u_3 position (behind the sleeve). Sleeve friction corrected for pore pressure effects:

$$f_t = f_s - (u_2 * A_{sb} - u_3 * A_{st})/A_s \quad (2)$$

NGI has previously carried out triple element CPTU at Onsøy which showed that on average $u_3 = 0.77 \cdot u_2$. This has been used here for calculating f_t. Previous studies, e.g. Gauer et al. (2002) and Powell & Lunne (2005) have shown that the pore pressure correction has resulted in lower variation in f_t compared to f_s.

Figure 4 shows f_s (corrected for temperature zero shifts for the cone types mentioned above) and f_t vs depth. For all cones except cone 6 the pore pressure correction is very small due to the following facts: i) equal end areas at both end of sleeves, ii) relatively small end areas and iii) u_3 is quite small compared to u_2. And when comparing f_s with f_t in Figure 4 the differences in the ranges for f_s and f_t are indeed small. For cone 6 the correction is larger due to difference in end areas at the upper and lower ends of the friction sleeve. Estimates of pore pressure effects do not explain the differences in f_s.

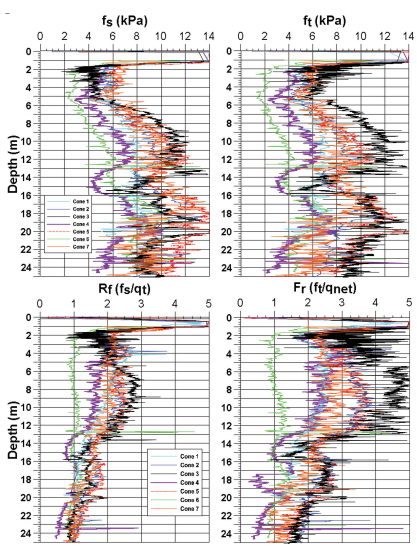

Figure 4. Comparison of f_s, f_t, R_f and F_r for all cones. f_s is corrected for temperature effects.

The effect of variations in sleeve diameter and cone diameter have been demonstrated by Holtrigter & Thorp (2016) and Cabal & Robertson (2014). Holtrigter & Thorp (2016) showed that if the friction sleeve diameter is larger than the cone diameter this can have a significant influence on f_s, even if the sleeve diameter is within the tolerances given in the international standards (ASTM 2012, ISO 2012). Figure 5 shows the results at the Huapai (clay) site. The cone diameter in Holtrigter & Thorp's work was 35.7 mm and sleeve diameters ranged from 35.7 to 36.15 mm. Based on the results shown in Figure 5 and results at 4 other sites, Holtrigter & Thorp suggested correction factors to take into account the effect of larger diameter of sleeve compared to cone. Assuming that Holtrigter & Thorp's correction factor for their Huapai clay can also be used for Onsøy clay, and using the diameters given in Table 1, the following corrections can be applied to the present f_s values: cones 1 and 6: 1.0; cones 2, 3, 4 and 5: 0.9; cone 7: 0.8.

The overall range for the measured f_s is 5.3 to 9.4; applying the correction factors suggested by Holtrigter & Thorp for Huapai clay the range reduces somewhat to 5.0 to 8.1.

The above indicate that for the present test series the variation in measured f_s values can only to some limited extent be explained by the effects of oversized friction sleeve diameter.

Figure 4 shows that R_f varies as expected for one type of cone to another. At 10 m R_f varies

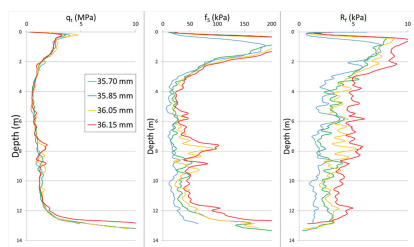

Figure 5. Results of tests with different sleeve diameters Huapai clay from Holtrigter & Thorp (2016).

Table 3. Average values at 10 m depth, kPa.

	Cone 1	Cone 2	Cone 3	Cone 4	Cone 5	Cone 6	Cone 7
fs mea.	6.8	9.0	7.1	5.6	9.3	5.3	9.4
fs corr.	6.8	8.1	6.4	5.0	8.4	5.3	7.5

from about 1.0 to 2.8%. If cone 6 is excluded this reduces to 1.7 to 2.8%.

5.3 *Final remarks*

The above discussion indicate that equipment related issues cannot explain all the variation in CPTU readings experiences in this study. A recent study by Kardan et al. (2016) showed that procedures and operator skill can have significant effects on the test results, in addition to the equipment. Thus uncertainties related to the test results can be caused by both the equipment and procedure details as well as operator skill.

In the present study, tests with cone types 3, 4 and 5 were carried out by the same personnel using one rig. Tests with all the other cone types were carried out by different personnel and rigs. It cannot be excluded that this also has had an influence on the results of tests with different cone types.

The problems with the zero shifts caused by different air and ground temperature could have been avoided if the zero readings at the start of the tests had been carried out with the cone in a bucket with the same temperature as the ground. This procedure was followed for the tests with cone type 2.

6 SUMMARY AND CONCLUSIONS

Seven different cone penetrometers from 5 manufacturers have been used in comparative testing program at the Norwegian GeoTest Site (NGTS) on soft clay at Onsøy, Norway. Two to four tests were carried out with each cone type and the results have been systematically compared. The main findings are:

1. Tests with all cone types gave very repeatable penetration pore pressure, u_2. When comparing tests with different cone types, six of the cones give very similar u_2 values. One cone type using a slot filter gave consistently higher u_2 values.
2. Measured cone resistance, q_c, generally varies somewhat, regarding test with the same cone, and more when comparing one cone type with another. This is expected since the cones have different a-factors. Taking zero shifts for different air and ground temperatures into account, and correcting for pore pressure effects, improved significantly the comparison between the q_t values for the different cone types.
3. Some of the cone types give good repeatability for sleeve friction, f_s, readings, while some show relatively large variation. When comparing f_s from different cone types the variation is quite large, which is in line with previous experience. An attempt has been made to understand the reasons for the large f_s variations, but there are still unanswered questions.

ACKNOWLEDGEMENTS

Pagani, Geotech and Geomil contributed by performing the tests with their CPTU equipment. NPRA and NGI carried out the remaining tests using other CPTU equipments. The authors would like to acknowledge the Research Council of Norway (RCN) for funding the Norwegian GeoTest Site project (No. 245650/F50).

REFERENCES

ASTM D5778–12. 2012. Standard Test Method for Performing Electronic Friction Cone and Piezocone Penetration Testing of Soils, ASTM International. www.astm.org.

Cabal, K. & Robertson, P.K. 2014. Accuracy and Repeatability of CPT Sleeve Friction Measurements. Proc. CPT'14, Las Vegas, Nevada, USA.

Gauer, P., Lunne, T., Mlynarek, Z., Wolynski, W. & Croll, M. 2002. Quality of CPTu -Statistical analyses of CPTu data from Onsøy. NGI Report No.: 20001099–2, Oslo.

Holtrigter, M. & Thorp, A. 2016. Correction for CPT fs errors due to variation in sleeve diameter. .Proc. ISC'5, Gold Coast, Australia, Proc. Vol. 1, pp. 303–309.

ISO. 2012. Geotechnical investigation and testing – Field testing – Part 1: Electrical cone and piezocone penetration tests, International Standard ISO 22476-1:2012.

Kardan, C., Viking, K., Nik, L. & Larsson, S. 2016. Influence of operator performance on quality of CPTU results. Proc. Of 17th Nordic Geotechnical Meeting, Reykajvik May 2016.

L'Heureux, J.S., Lunne, T., Lacasse, S., Carrol, R., Strandvik, S.O. & Ozkul, Z. 2017. Norway's National Geo-Test Sites Research Infrastructure. Proc. 19th International Conference on Soil Mechanics and Geotechnical Engineering. Seoul 2017.

Lunne, T., Eidsmoen, T., Gillespie, D. & Howland, J.D. 1986. Laboratory and field evaluation on cone penetrometers. Proceedings of ASCE Specialty Conference In Situ'86: Use of In Situ Tests in Geotechnical Engineering. Blacksburg, ASCE, 714–729.

Lunne, T. & Andersen, K.H. 2007. Soft clay shear strength parameters for deepwater geotechnical design. Proceedings 6th International Conference, Society for Underwater Technology, Offshore Site Investigation and Geomechanics, London, 151–176.

Lunne, T., Long, M. & Forsberg, C.F. 2003. Characterization and engineering properties of Onsøy clay. Characterization and engineering properties of natural soils. Ed. by T.S. Tan et al. Balkema 2003. Proceedings of the International Workshop, Singapore 2002, Vol. 1, pp. 395–427.

Lunne, T. 2010. The CPT in Offshore Soil Investigation – a historic perspective. Proc. CPT'10, Los Angeles, May 2010, pp.71–113.

Powell, J.J.M. and Lunne, T. (2005). A comparison of different piezocones in UK clays. Proc. ISSMGE Conference, Osaka, 2005.

Tigglemann, L. & Beukema, H.J. 2008. Sounding Ring Investigation. Proc. ISC-3, Taiwan, pp. 757–762.

Cone Penetration Testing 2018 – Hicks, Pisanò & Peuchen (Eds)
© 2018 Delft University of Technology, The Netherlands, ISBN 978-1-138-58449-5

Evaluation of CPTU N_{kt} cone factor for undrained strength of clays

P.W. Mayne
Georgia Institute of Technology, Atlanta, Georgia, USA

J. Peuchen
Fugro, The Netherlands

ABSTRACT: The evaluation of undrained shear strength of clays (s_u) is most often sought using the net cone resistance ($q_{net} = q_t - \sigma_{vo}$) and a cone factor ($N_{kt}$) such that $s_u = q_{net}/N_{kt}$. While site-specific calibration of N_{kt} with laboratory reference values (i.e. triaxial compression, simple shear) or field benchmark (i.e. vane) is the best approach, this requires considerable extra time and funding to accomplish. In the approach covered herein, a database involving 407 high-quality triaxial compression tests (CAUC) was used to review strengths from a wide variety of clays ranging from intact soft to firm to stiff to hard and fissured geomaterials. The study considered a total 62 clays, categorized into five groups: soft offshore, soft-firm onshore, sensitive, overconsolidated, and fissured clays. The backfigured N_{kt} factors ranged from 8 to 25 and found to decrease with pore pressure ratio, $B_q = (u_2 - u_0)/q_{net}$.

1 INTRODUCTION

1.1 *Undrained strength*

The undrained shear strength ($s_u = c_u$) of clays is a predominant geoparameter used to evaluate foundation bearing capacity, including shallow footings, rafts, and pilings, as well as input to short-term stability of excavations, slopes, and embankments. In conceptual terms within the classical understanding on the stress-strain behavior of soils, the undrained strength can be taken as the maximum shear stress (τ_{max}) for a stress path at constant volume. Yet, because of the complex effects of anisotropy, strain rate, direction of loading, and boundary conditions, assigning a single value of s_u to a given clay is not possible. Instead, a family of s_u values must be considered, including shear in compression and extension under various modes.

The various strength modes can be evaluated by laboratory tests on intact, undisturbed soil samples, for instance: anisotropically-consolidated triaxial (CAUC and CAUE), plane strain (PSC and PSE), as well as simple shear (SS), direct simple shear (DSS), torsional shear (TS), and other modes (e.g., CIUC, true triaxial, hollow cylinder, directional shear, etc.).

1.2 *Strength modes*

Constitutive soil models help in establishing a general hierarchy of the test modes. For instance, the Wroth-Prevost hybrid model establishes the modal order in terms of normalized undrained shear strength to effective overburden stress for normally-consolidated (NC) clays: $S = s_u/\sigma_{vo}'$, as shown by Figure 1 (Mayne 2008). In this framework, the values of S for all modes are expressed as functions of the effective stress friction angle (ϕ') of the clay.

The general hierarchy of the strength modes is borne out by laboratory tests on natural clays, as shown by Kulhawy & Mayne (1990), Ladd & DeGroot (2003), Karlsrud et al. (2005), and others.

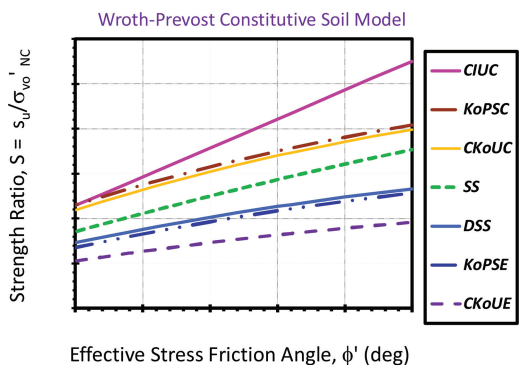

Figure 1. Normalized strength ratios for various shearing modes for Wroth-Prevost hybrid constitutive soil model (after Mayne 2008).

1.3 *Strength evaluation by piezocone tests*

Field testing by piezocone penetration testing (CPTU) in clays is standardised by e.g. ASTM (2012), ISO (2012) and ISO (2014). For marine environments, including rivers and lakes, consideration can also be given to a free fall tool equipped with a cone penetrometer (e.g. Dayal 1980; Peuchen et al. 2017).

While several expressions are available for interpreting the in-situ undrained shear strength in clays from CPTU results, the most common and reliable is given by:

$$s_u = \frac{q_t - \sigma_{vo}}{N_{kt}} = \frac{q_{net}}{N_{kt}} \quad (1)$$

where σ_{vo} = total overburden stress, q_{net} = net cone resistance and N_{kt} = cone factor.

The appropriate choice of N_{kt} can be made on the basis of theoretical, experimental, and/or statistics relationships. Site-specific calibration of the CPTU with either selective laboratory strength testing performed on high-quality samples and/or selective field vane shear testing (VST) is the best approach, albeit requires considerable time and financial expense because of the more involved testing program, specifically added costs of drilling, sampling, transport, and testing. Moreover, the effects of sample disturbance on laboratory results are essentially inevitable and unavoidable in most instances (e.g. ISO 2006; ISO, 2014).

Guidance on the empirical selection of N_{kt} factors have been given for various clays. For CPTUs in soft to firm clays, Lunne et al. (2005) recommend a value N_{kt} = 12 for the CAUC undrained shear strength, s_{uc}. A study of piezocone data on 3 onshore and 11 offshore clays by Low et al. (2010) found the range: $8.6 \leq N_{kt} \leq 15.3$, with a mean value of N_{kt} = 11.9 for the triaxial compression mode. Similarly, a study of 17 soft to firm intact clays found a mean value of N_{kt} = 11.8 for s_{uc} corresponding to the CAUC triaxial mode (Mayne et al. 2015).

For differing shearing modes, other operational values of N_{kt} must be used. For instance, Low et al. (2010) found a mean N_{kt} = 13.6 for the laboratory average strength (s_{uAVE}) from triaxial compression, direct simple shear, and triaxial extension (range: $10.6 \leq N_{kt} \leq 17.4$), which is close to the direct simple shear mode (s_{uDSS}). For calibration with the field vane (s_{uv}), they determined N_{kt} averages 13.3 with a range $10.8 \leq N_{kt} \leq 19.9$.

For several sensitive Norwegian clays tested in CAUC mode, Karlsrud et al. (2005) show the cone factor is lower and within the ranges: $7.5 \leq N_{kt} \leq 11.5$. Similarly, for a soft sensitive clay in Québec, Wang et al. (2015) reported that an N_{kt} = 10.5 was needed to match VST results.

In contrast, for overconsolidated and fissured clays, Powell & Quarterman (1988) showed that a much higher N_{kt} factor ($20 < N_{kt} < 30$) was necessary to match reference values of s_u obtained from laboratory triaxial compression tests and field plate load test results.

Theoretical solutions for N_{kt} are readily available, including expressions based on limit plasticity (e.g. Konrad & Law 1987), cavity expansion theory (e.g. Mayne 2016), and strain path method (Teh & Houlsby 1991), as well as algorithms that approximate the results from numerical finite element simulations (Lu et al. 2004). Yet, these approaches require additional input geoparameters that must be assessed beforehand, such as rigidity index ($I_R = G/s_u$), cone roughness (α_c), lateral stress state ($K_0 = \sigma_{ho}'/\sigma_{vo}'$), friction angle ($\phi'$), and/or other variables.

As a consequence of the aforementioned uncertainties and lack of guidance towards an available and reliable means for selecting N_{kt}, a detailed database approach was devised, with the results reported by Mayne (2014).

2 CPTU-CAUC DATABASE

2.1 *Clay data*

The database focused on a total of 62 clays that were categorized into five main groupings: (a) 17 offshore soft-firm clays that are normally-consolidated (NC) to lightly-overconsolidated (LOC); (b) 30 onshore clays that are NC-LOC, (c) 5 sensitive clays that are NC-LOC, (d) 5 overconsolidated (OC) intact clays, and (e) 5 OC fissured clays.

A listing of these individual clays is given in Figure 2, including assignment of a separate

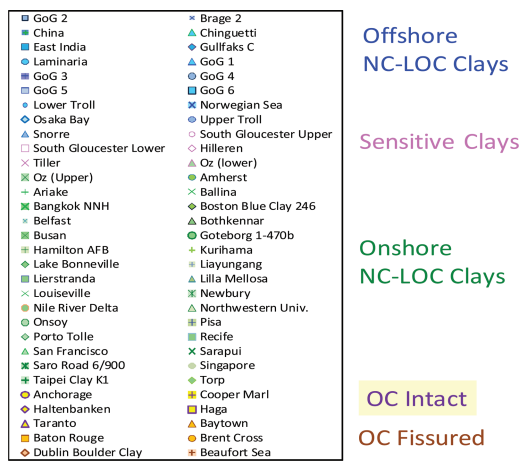

Figure 2. List of 62 clays with CAUC-CPTU data.

Table 1. Summary of CAUC s_{uc} versus CPTU q_{net} for clays.

Clay Group	No. sites N	No. data n	Statistical Regressions Slope m	Coef.[a] r^2	Factor = 1/m N_{kt}	Mean B_q
Offshore NC-LOC	17	115	0.0812	0.980	12.32	0.51
Onshore NC-LOC	30	191	0.0833	0.867	12.00	0.53
Sensitive NC-LOC[b]	5	43	0.0968	0.507	10.33	0.84
OC Intact	5	36	0.0737	0.862	13.57	0.49
OC Fissured[c]	5	22	0.0445	0.393	22.47	–0.01
All Clays	62	407	0.0750	0.923	13.33	0.55

[a]Note: r^2 = coefficient of determination (for N_{kt} only),
[b]Note: confidence level for sensitive clays is low,
[c]Note: uncertainty level for OC fissured clays is high.

symbol for each site. For tracking purposes, the clay symbols are also grouped by color according to each category: offshore (blue), onshore (green), sensitive (pink), intact OC clays (purple dot with yellow infilling), and fissured OC clays (brown symbol with orange infilling). The results and findings herein are based on a review of high-quality laboratory and field data obtained from the open literature and private unpublished technical reports.

The strength data for these sites were obtained from high-end laboratory tests, including consolidated triaxial tests, and in selected cases, also direct simple shear mode. In addition to the strength results, index parameter values and other information were also collected about each of these sites, including: water content (w_n), liquid limit (LL), plasticity index (PI), unit weight (γ_t), preconsolidation stress (σ_p') and overconsolidation ratio ($OCR = \sigma_p'/\sigma_{vo}'$), as well as other available data (i.e. groundwater table, calcium carbonate content, etc.), where reported.

For both the NC-LOC offshore and onshore series, the in-situ OCRs generally ranged between 1 and 2.5. These 47 soft-firm clays represent the bulk of the dataset with $n = 306$ paired sets of data and are characterized by an average $B_q = 0.52$.

2.2 *Laboratory test procedures*

For each of the 62 clays considered, a reference value of s_{uc} was evaluated from a CAUC or CK_0UC test, or test series program, performed on an individual specimen obtained from undisturbed sampling. Corresponding CPTu data were acquired at the same site at elevations consistent with the sampling depths.

One important issue is that the testing laboratories used different reconsolidation techniques to restore in-situ stress states on the specimens, including: direct recompression to σ_{vo}' and σ_{ho}', true K_0 conditions versus general anisotropic states (K_c), unloading-type SHANSEP, and recompression-type SHANSEP methods, as well as other variants (Lunne et al. 2006). In some cases, the differences in s_{uc} obtained from different laboratory procedures may be small (say CAUC versus CK_0UC). For some clays, the use of classical SHANSEP testing destructures the specimens by consolidating past the in-situ yield stress or preconsolidation stress (σ_p'), giving quite a different strength in comparison to recompression-type series of tests that do not exceed σ_p' (Le et al. 2008). Also, both types of SHANSEP approaches rely on laboratory one-dimensional consolidation testing and approximate interpretation models for estimating the OCR at each elevation, which in turn is utilized to provide the undrained shear strength via normalized strength ratio power law trends established by the testing program (Ladd & DeGroot 2003).

These s_u/σ_{vc}' versus OCR trends somewhat assume that vertical and lateral variability of the soil deposit is negligible, where in fact there may be significant or subtle changes across the site. In some instances, the traditional normalized strength plots have shown to vary with water content (Finno & Chung 1992).

Note, in the cases involving the few fissured clays, the CAUC types of tests have rarely been performed. Hence, the majority of s_u reference data for fissured clays were procured from the results of isotropically-consolidated triaxial tests (CIUC) which are believed still valid since $K_0 > 1$ for these geomaterials. Regardless, the characterization of fissured clays represents a major challenge in practice, e.g. Vitone and Cotecchia (2011). The work presented here is less reliable in fissured clays and therefore should be used with care.

2.3 *Piezocone data*

For the offshore series, most CPTu data were obtained using Fugro equipment, thus comparable results in high quality and reliable measurements. For the onshore series, the published results came from a variety of different commercial systems and it was not possible to scrutinize these for their design, maintenance & wear, analog-digital resolution, compliance with ASTM/ISO standards, preparation of filter elements, saturation, and other factors.

In all but one case (Osaka Bay), all three CPTu readings (q_c, f_s, u_2) were obtained for each site.

The test depths ranged from 1.4 m to 245.6 m below ground surface, with a mean test depth of z = 17.1 m. Cone resistances ranged from 112 kPa to 10.7 MPa, with a mean q_{net} = 1082 kPa. Sleeve friction values ranged from 0.5 kPa to 167 kPa with a mean f_s = 19 kPa. Penetration pore pressures varied from –22 kPa to 7.2 MPa, with a mean u_2 = 567 kPa. Using the CPTU soil behavior type (SBT) charts established by Robertson (2009), the range of soil behavior type index was determined as $2.3 \leq I_c \leq 3.7$, with a mean I_c = 3.12 and S.D. = 0.24. The corresponding soil zone was 3 (clay).

Note that the table excludes cemented clays, carbonate geomaterials, and weak rock showing I_c values on the order of 3. These geomaterials provide specific challenges for CPTU interpretation. It is also noted that CPTU u_2 measurements can be problematic for high OC and fissured clays. In such cases, acquisition of u_1 measurements should be considered (Robertson et al. 1986; Peuchen & Terwindt 2014), with approximate conversion to u_2 (e.g. Peuchen et al. 2010).

3 UNDRAINED STRENGTH FROM CPTU

3.1 *Database results*

The total collection of 407 paired sets of undrained shear strengths obtained from triaxial compression mode tests (s_{uc}) versus the net cone resistance (q_{net}) are presented in Table 1 and sorted according to clay category as shown. The table also shows mean values for pore pressure ratio $B_q = (u_2 - u_0)/q_{net}$. Figure 3 provides the summary graphical results for each of the groups.

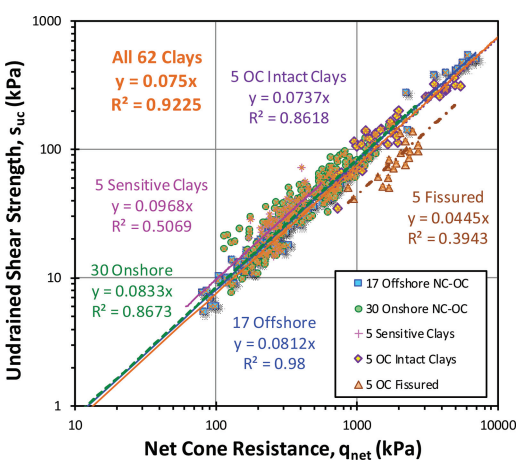

Figure 3. CAUC undrained shear strength versus net cone resistance for the five clay groups.

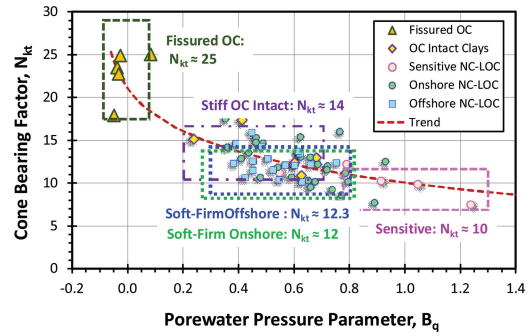

Figure 4. Trend of N_{kt} with B_q for the five clay groups.

Figure 4 presents the N_{kt} - B_q relationship for s_{uc} for the five clay groups. Following the approach used by Low et al. (2010) whereby a single N_{kt} is recommended for preliminary studies, each clay group could be assigned a typical value such as listed in Table 1, or by guidance in Figure 4: N_{kt} = 10 (sensitive clays); N_{kt} = 12 (NC-LOC soft-firm onshore clays); N_{kt} = 12.3 (NC-LOC offshore clays); N_{kt} = 14 (OC intact clays); and N_{kt} = 25 (OC fissured clays).

Within each group, however, there is considerable range and variance for the specified N_{kt} that could be associated with sample disturbance, clay mineralogy, fabric, organic content, and other variables.

3.2 N_{kt} *trend with* B_q

One well-known relationship indicates that N_{kt} decreases with B_q (Lunne et al. 1985; Skomedal & Bayne, 1988; Lunne et al. 1997; Hong et al. 2010; Knappett & Craig 2012; Mayne et al. 2015). Figure 5 presents this direct trend for the database of Table 1. In this case, each of the 62 clays is given weighting by a single point, so as to not bias the relationship obtained by regression analyses. Adopting a continuous function between the clay groups, then s_{uc} is obtained from:

$$N_{kt} = 10.5 - 4.6 \cdot \ln(B_q + 0.1) \qquad (2)$$

which only applies when $B_q > -0.1$.

For the NC-LOC offshore group, the derived N_{kt} factor = 12.3 is close to the value N_{kt} = 12 recommended by Low et al. (2010). Similarly, the NC-LOC onshore group gave N_{kt} = 12.0. For other clay groups, the N_{kt} can be smaller (sensitive clays, where B_q > 0.75) or higher (fissured OC clays, where B_q < 0.5).

Negative or low B_q values are often characteristic in fissured OC clays. Negative B_q values for

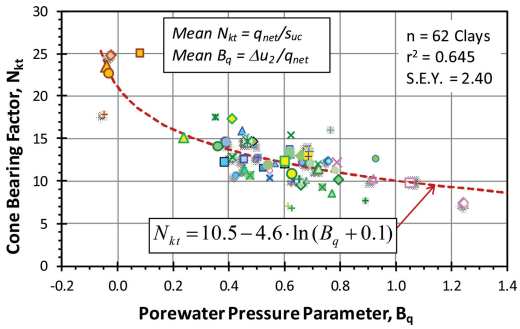

Figure 5. Overall trend of N_{kt} with B_q for 62 individual clays.

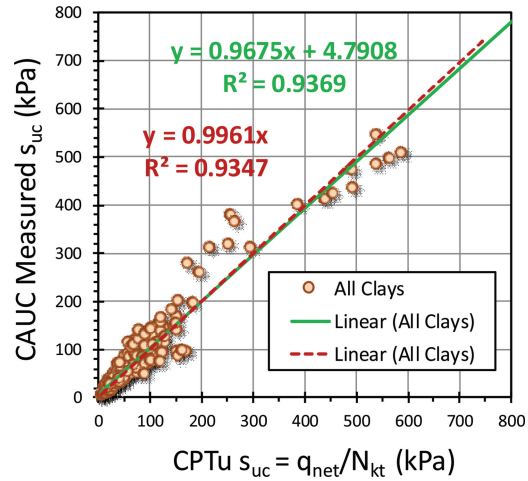

Figure 6. Measured CAUC strength versus CPTU-evaluated strength with N_{kt} = fctn (B_q) for all 62 clays.

onshore clays are limited by cavitation but considerable negative B_q values are possible in an offshore setting. Therefore, the limiting value of $B_q > -0.1$ is forced by the logarithmic algorithm. Also, no paired TC-CPTU tests were available to extend into that range.

Fugro software includes automated profiling of N_{kt} values according to the above equation. The algorithm allows manual selection of a range of I_c values. It also allows profiling for a bandwidth of N_{kt} values, by applying range factors such as 0.8 N_{kt} and 1.15 N_{kt}. The range factors can be selected to match regional knowledge, expected data variability and site-specific laboratory test values.

Using the database, reverse statistics can be conducted to evaluate the reliability of the methodology. The laboratory-derived s_{uc} versus the CPTU data for the entire dataset of 406 triaxial compression tests are shown in Figure 6. Two sets of statistical measures have been performed, as listed in Table 2: (a) arithmetic; and (b) regressions using both least squares and best fit lines. Statistics are done for three groupings: (1) soft-firm onshore & offshore clays (plus 5 sensitive clays); (2) NC and OC intact clays; and (3) all clays.

For the arithmetic statistics (dashed red line of Fig. 6), the ratio of measured-to-estimated values gives a mean value μ, with desired best results at 1.00. Also, the standard deviation (S.D.) and coefficient of variation (COV = S.D./μ) are given. A COV as close to 0.0 is ideal. For the regressions (solid green line of Fig. 6), the best fit line provides a slope, while the least squares equation provides a slope and intercept. In all 3 groupings, a small intercept of around 6 kPa or less was obtained and slopes of both best fit line and least squares linear equation were within 3% of each other. Also given are the values of coefficient of determination with r^2 averaging about 0.95 and the standard errors of the y-estimator (S.E.Y.) ranging from 13.2 to 16.1.

Table 2. Statistics on N_{kt} from B_q methodology.

Parameter	Soft-Firm NC-LOC clays	Intact NC-OC clays	All clays: NC, OC, and fissured[a]
No. of data, n	356	386	406
μ = ratio of measured/ estimated	1.093	1.091	1.087
S.D.	0.279	0.272	0.279
COV = S.D./μ	0.255	0.250	0.256
Regression slope m	0.947	0.964	0.996
Coefficient r^2	0.965	0.963	0.935
S.E.Y.	13.21	14.68	16.05

[a]Note: Caution should be applied when using these results in fissured clays

3.3 *Strength anisotropy*

As noted in Section 1.2, clays exhibit strength anisotropy, often with the hierarchy: $s_{uc} > s_{uDSS} > s_{ue}$. For a given deposit, a reasonable means to quantify its strength anisotropy is to run parallel sets of compression, direct simple shear, and extension tests on undisturbed samples taken at various depths. In review of lab data collected herein, Fig. 7 shows trends for 157 sets of data where all three modes were available.

Using the compression mode (s_{uc}) as the reference, the ratios $K_{45} = s_{uDSS}/s_{uc}$ and $K_s = s_{ue}/s_{uc}$ can be used to represent loading at 45° and 90° (horizontal), respectively. Despite prior studies showing that K_s increases with PI (Kulhawy & Mayne 1990) and K_s increases with natural water content (Karlsrud

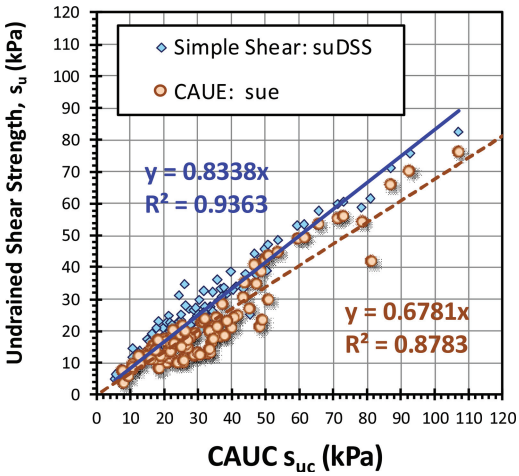

Figure 7. Strength anisotropy results from clay database.

et al. 2005), no such trends were observed with this database. Won (2013) presented similar findings.

The strength anisotropy data from this study indicate the average relationships:

$$s_{uDSS} = 0.834\ s_{uc} \qquad (r^2 = 0.936) \qquad (3)$$

$$s_{ue} = 0.678\ s_{uc} \qquad (r^2 = 0.878) \qquad (4)$$

Also, the following average trends were observed:

$$s_{uAVE} = 0.999\ s_{uDSS} \qquad (r^2 = 0.976) \qquad (5)$$

$$s_{uAVE} = 0.839\ s_{uc} \qquad (r^2 = 0.977) \qquad (6)$$

4 CONCLUSIONS

A high-quality database consisting of 407 laboratory triaxial compression tests paired with field piezocone data from 62 clays was grouped into five categories: offshore, onshore, sensitive, overconsolidated, and fissured geomaterials. A general trend to handle soft to firm to stiff to hard intact clays and fissured clays was observed indicating N_{kt} decreasing with pore pressure parameter, B_q.

The results are considered highly valuable for use as a reference database for assessing N_{kt}. However, caution should be applied when using the database at new sites containing limited high-quality laboratory data, particularly when sensitive clays or overconsolidated fissured soils exist.

REFERENCES

ASTM. 2012. Standard test method for electronic friction cone and piezocone penetration testing of soils, Vol. 04.08, ASTM D5778-12. ASTM Intl., West Conshohocken.

Dayal, U. (1980). Free fall penetrometer: a performance evaluation. *Applied Ocean Research*, 2(1), 39–43.

Finno, R.J., & Chung, C-J. 1992. Stress-strain-strength responses of compressible Chicago glacial clays. *Journal of Geotechnical Engineering* 118 (10): 1607.

Hong, S.J., Lee, M.J., Kim, J.J. & Lee, W.J. 2010. Evaluation of undrained shear strength of Busan clay using CPT. *Proc., 2nd Intl. Symp. on Cone Penetration Testing*, Vol. 2 (CPT'10, Huntington Beach, CA), Omnipress: 313–320.

ISO 2006. Geotechnical investigation and testing – sampling xxx ISO 22475-1:2006. Geneva: International Organization for Standardization.

ISO 2012. Geotechnical investigation and testing – Field testing – Part 1: Electrical cone and piezocone penetration tests, International Standard ISO 22476-1:2012. (With Technical Corrigendum 1, January 2013). Geneva: International Organization for Standardization.

ISO 2014. Petroleum and Natural Gas Industries - Specific Requirements for Offshore Structures – Part 8: Marine Soil Investigations, International Standard ISO 19901-8:2014.

Karlsrud, K., Lunne, T., Kort, D.A. & Strandvik, S. 2005. CPTU correlations for clays. *Proc. 16th ICSMGE* (Osaka); Vol. 2, Millpress, Rotterdam: 693–702.

Knappett, J.A. & Craig, R.F. 2012. *Craig's Soil Mechanics*, 8th Edition, Spon Press-Taylor & Francis, London: 570 pages.

Konrad, J-M. & Law, K.T. 1987. Undrained shear strength from piezocone tests. *Canadian Geotechnical Journal*, 24 (3): 392–405.

Kulhawy, F.H. & Mayne, P.W. 1990. Manual on Estimating Soil Properties for Foundation Design. *Report EL-6800*, Electric Power Res. Inst., Palo Alto, 306 p. www.epri.com

Ladd, C.C. & DeGroot, D.J. 2003. Recommended practice for soft ground site characterization. *Soil & Rock America 2003*, Vol. 1 (Proc. 12th Pan American Conference, MIT), Verlag Glückauf Publishing, Essen: 3–57.

Le, M-H., Nauroy, J-F., DeGennaro, V., Delage, P., Flavigny, E., Thanh, N., Colliat, J-L., Puech, A., & Meunier, J. 2008. Characterization of soft deepwater West Africa clays: SHANSEP testing is not recommended for sensitive structured clays. *Proceedings Offshore Technology Conference* (Paper 19193), Houston, TX.

Low, H.E., Lunne, T., Andersen, K.H., Sjursen, M.A., Li, X. & Randolph, M.F. 2010. Estimation of intact and remoulded undrained shear strengths from penetration tests in soft clays. *Geotechnique* 60 (11): 843–859.

Lu, Q., Randolph, M.F., Hu, Y. & Bugarski, I.C. 2004. A numerical study of cone penetration in clay. *Géotechnique* 54 (4): 257–267.

Lunne, T., Christoffersen, H.P. & Tjelta, T.I. 1985. Engineering use of piezocone data in North Sea clays. *Proc. 11th ICSMGE,* Vol. 2 (San Francisco), Balkema, 907–912.

Lunne, T., Robertson, P.K., & Powell, J.J.M. 1997. *Cone Penetration Testing in Geotechnical Practice*, Blackie Academic/London, Routledge, New York: 312 p.

Lunne, T., Randolph, M.F., Chung, S.F., Andersen, K.H. & Sjursen, M. 2005. Comparison of cone and t-bar factors in two onshore and one offshore clay sediments. *Frontiers in Offshore Geotechnics* (Proc.

ISFOG-1, Perth), Taylor & Francis Group, London: 981–989.

Lunne, T., Berre, T., Andersen, K.H., Strandvik, S. & Sjursen, M. 2006. Effects of sample disturbance and consolidation procedures on measured shear strength of soft marine Norwegian clays. *Canadian Geot. J.* 43 (7): 726–750.

Mayne, P.W. 2007. *NCHRP Synthesis 368: Cone Penetration Testing*. Transportation Research Board, National Academies Press, Washington, DC: 118 p. www.trb.org

Mayne, P.W. 2008. Piezocone profiling of clays for maritime site investigations. *Geotechnics in Maritime Engineering*, Vol. 1 (Proceedings, 11th Baltic Sea Geotechnical Conference, Gdansk), Polish Committee on Geotechnics: 333–350.

Mayne, P.W. 2014. Development of an automated methodology for evaluation of undrained shear strength of offshore clays from piezocone penetration tests. *Report 122931* submitted by Georgia Tech Research Corp. (Project: 2006U94) to Fugro Engineers, Leidschendam, The Netherlands, 192 p.

Mayne, P.W., Peuchen, J. & Baltoukas, D. 2015. Piezocone evaluation of undrained strength in soft to firm offshore clays. *Frontiers in Offshore Geotechnnics III*, Vol. 2 (Proc. ISFOG, Oslo), Taylor & Francis, London: 1091–1096.

Mayne, P.W. 2016. Evaluating effective stress parameters and undrained shear strengths of soft-firm clays from CPT and DMT. *Australian Geomechanics Journal* 51 (4): 27–55.

Peuchen, J., Vanden Berghe, J.F. & Coulais, C. 2010. Estimation of u_1/u_2 conversion factor for piezocone. *Proc. 2nd International Symposium on Cone Penetration Testing,* Vol. 2 (CPT'10, Huntington Beach, CA): Omnipress: 15–22.

Peuchen, J. & Terwindt, J. (2014), Introduction to CPT accuracy, *Proc. 3rd International Symposium on Cone Penetration Testing* (CPT'14, Las Vegas, NV): 1–46. www.cpt14.com

Peuchen, J., Looijen, P. & Stark, N. 2017. Offshore characterisation of extremely soft sediments by free fall penetrometer. Offshore Site Investigation and Geotechnics: Smarter Solutions for Future Offshore Developments: *Proc. 8th Intl. Conf.* Royal Geographical Society, Volume 1. London: Society for Underwater Technology: 370–377.

Powell, J.J.M. & Quarterman, R.S.T. 1988. The interpretation of cone penetration tests in clays with particular reference to rate effects. *Penetration Testing 1988*, Vol. 2 (Proc. ISOPT-1, Orlando), Balkema, Rotterdam: 903–909.

Robertson, P.K., Campanella, R.G., Gillespie, D. & Greig, J. 1986. Use of piezometer cone data. *Use of In Situ Tests in Geotechnical Engineering.* (*Proc. In Situ '86, Blacksburg, Virginia),* GSP No. 6, ASCE, Reston/VA: 1263–1280.

Robertson, P.K. 1991. Closure to: Soil classification using the cone penetration test. *Canadian Geot. J.* 28 (1): 176–178.

Robertson, P.K. 2009. Interpretation of cone penetration tests: a unified approach. *Canadian Geot. J.* 46 (11): 1337–1355.

Teh, C.I. & Houlsby, G.T. 1991. An analytical study of the cone penetration test in clay. *Géotechnique* 41 (1): 17–31.

Vitone, C. & Cotecchia, F. 2011. The Influence of Intense Fissuring on the Mechanical Behaviour of Clays. *Géotechnique*, Vol. 61, (12), 1003–1018.

Wang, B., Brooks, G.R. & Hunter, J.A.M. 2015. Geotechnical investigations of a large landslide site at Quyon, Québec. *Proc. GeoQuébec 2015*, Paper ID 355, Canadian Geotechnical Conference.

Won, J.Y. (2013). Anisotropic strength ratio and plasticity index of natural clays. *Proc. 18th* ICSMGE (Paris), 445–448: www.issmge.org

Taylor & Francis
Taylor & Francis Group
http://taylorandfrancis.com

Cone Penetration Testing 2018 – Hicks, Pisanò & Peuchen (Eds)
© 2018 Delft University of Technology, The Netherlands, ISBN 978-1-138-58449-5

Applying breakage mechanics theory to estimate bearing capacity from CPT in polar snow

A.B. McCallum
Faculty of Science, Health, Education and Engineering (FOSHEE), University of the Sunshine Coast, Australia

ABSTRACT: Demand for polar infrastructure is increasing and accurate determination of bearing capacity from CPT data is increasingly useful. Breakage mechanics theory has been applied to enhance pile end-bearing capacity predictions in crushable soils. Because polar snow can also be considered a crushable geomaterial, this technique may be useful in enhancing bearing capacity predictions using polar snow CPT data. This technique was preliminarily examined to investigate its application in determining bearing capacity from polar snow CPT data. Application of contemporary soil behavioural theories to polar snow undergoing penetration does not routinely occur and insights not typically examined by glaciologists can be obtained. However, extensive controlled laboratory testing is necessary to further refine the application of this technique to accurately deduce bearing capacity from CPT in polar snow.

1 INTRODUCTION

Increasing strategic political interest in the polar regions has increased the amount of science conducted in these areas. This has resulted in a corresponding need for increased development of polar infrastructure, particularly in areas removed from the coast where rock or soil cannot be used to found infrastructure.

McCallum (2013) conducted significant amounts of fieldwork in Antarctica examining particular facets of analysis of CPT in polar snow; many of these investigations have been reported (McCallum (2013); McCallum (2014a); McCallum (2014b); McCallum (2017) etc.). McCallum (2012) preliminarily examined the derivation of bearing capacity from CPT data in polar snow. However, further examination of the direct determination of bearing capacity from CPT data obtained in polar snow remains valuable.

Einav (Einav (2007a); Einav (2007b)) outlined a comprehensive theory termed continuum breakage mechanics (CBM) that described the crushing behaviour of granular materials (such as dry polar snow) under compression and Zhang, Nguyen, & Einav (2013) went on to apply this theory to the establishment of a reliable bearing capacity equation for piles penetrating into sand. Zhang et al.'s theory considers "the grain crushability as well as other critical factors (e.g. GSD, friction coefficient, and elastic stiffness)". Polar snow is also a porous crushable geomaterial (McCallum, 2013); therefore, this technique may be applicable to derive bearing capacity from CPT data in polar snow.

Application of breakage mechanics theory using FEM as described within Zhang, Nguyen, & Einav (2013) is outside the scope of this work and PSDs are not routinely collected in glaciological / snow mechanics observations.

However, one facet of Zhang et al.'s work (Zhang, Nguyen, & Einav, 2013), application of their derived constitutive model, is examined herein, along with comparison with existing techniques to assess whether application of this technique may be useful in generating more accurate bearing capacity estimates from CPT data obtained from polar snow.

2 METHOD

Zhang, Nguyen, & Einav (2013) define an equation for the yield condition in terms of triaxial stresses as:

$$y = \frac{\theta}{2E_c}\left(\frac{p^2}{K} + \frac{q^2}{3G}\right)\left(\frac{1-B}{1-\theta B}\right)^2 + \left(\frac{q}{Mp}\right)^2 - 1 \le 0$$

where:

- θ is a physical grading index that relates initial to ultimate particle size distribution,
- E_c is the Critical Breakage Energy (MPa) that can be calculated from the Critical Comminution Pressure, p_c (MPa), the pressure at which grain crushing commences during isotropic compression,
- p (MPa) is the mean (effective) stress,

- q (MPa) is the triaxial shear stress,
- G (MPa) is the shear modulus,
- K (MPa) is the bulk modulus, and
- M equals (q_f /p_f) and is the friction ratio at critical state between the ultimate mean and triaxial shear stress, p_f and q_f respectively.

This equation results from the degenerate Legendre transformation for first order homogeneous functions and is used to change the independent variables in a function of two variables by application of the product rule; in this case, to capture the internal energy of the system undergoing compaction that is subject to breakage.

The term B, Breakage, is a scalar internal breakage variable, varying from 0 to 1.0 that represents the evolution of the cumulative Grain Size Distribution (GSD) of a material undergoing compaction.

The evolving cumulative GSD by mass (F(x, B)) can be expressed in terms of B by assuming a linear scaling between the initial (F_0(x)) and ultimate (F_u(x)) GSDs (Zhang, Nguyen, & Einav, 2013):

$$F(x,B) = (1-B)F_0(x) + BF_u(x)$$

For estimated material parameters (Ec, K, G and M), values for q can be ascertained for various p, with yield occurring when y = 0. Further explanation on each of these terms can be found within Zhang, Nguyen, & Einav (2013) and breakage mechanics theory is presented in Einav (2007a) and Einav (2007b). Zhang, Nguyen, & Einav (2013) further outline non-associated flow rules defining incremental elastic volumetric and shear strains associated with this yield condition, but these are not considered further herein.

3 RESULTS AND DISCUSSION

3.1 *Yield criterion*

After verifying numerical model performance using typical values for sand, as presented within Zhang, Nguyen, & Einav (2013), typical values for snow of initial density ~ 450 kg m^{-3} (Table 1) were used to examine shear stresses, q (MPa) at the yield condition for various initial confining stresses, p (MPa). Initially, no grain breakage was assumed thus $B = 0$ and $\theta = 1$.

Bulk and shear moduli values are from Mellor (1975) and Critical State Friction Ratio (M) is derived from Santamarina & Cho (2001). p_c is obtained from Petrovic (2003) and E_c is calculated using Equation 3 (Zhang, Nguyen, & Einav, 2013):

$$E_c = \frac{p_c^2\theta}{2K}$$

Table 1. Typical values for snow.

Term	Description	Value
K	Bulk modulus	300 MPa
G	Shear modulus	160 MPa
E_c	Critical Breakage Energy	0.00468 MPa
P_c	Critical Comminution Pressure	10 MPa
B	Breakage	0
θ	Grading Index	1
M	Critical State Friction Ratio	1.42

For a typical initial confining stress at a depth of 1 m of ~ 20 kPa, application of Equation 1 results in a shear stress at yield of ~ 30 kPa.

Although many of the terms used in calculating this shear strength are not well-developed for snow, this result is consistent with values for dry polar snow of density ~ 450 kg m^{-3} found at Halley Station Antarctica by McCallum (2012) and agree with historical values presented within Mellor (1975).

Preliminary sensitivity testing showed that this value was unresponsive to variations in the Grading Index; this is because the Critical Breakage Energy (E_c) also depends on θ. Limited sensitivity was also evident for variations in Critical Comminution Pressure (p_c).

Varying Breakage from 0 to 1.0 for θ ranging from 0 to 1.0 also resulted in no change to the yield condition. This is because the second term in Equation 1 (dependent on p, q, K and G) approaches zero, thereby nullifying the effect of variations to both B and θ in the equation's third term. However, altering the Friction Ratio (derived from the Critical State Friction Angle) by 10% resulted in shear variations of ~ 10%.

Additional laboratory testing is necessary to further examine the values and effect of these variables in polar snow undergoing compression.

3.2 *End-bearing capacity factor*

Zhang, Nguyen, & Einav (2013) then went on to apply this technique to estimate the end-bearing capacity of piles in crushable soils through the derivation of a new formula for the end-bearing capacity factor. Analysis of numerical analysis data showed that the end-bearing capacity factor N_{q*} was dependent on both the confining and critical comminution pressures "through a sort of overconsolidation ratio, p_0/p_c" (Zhang, Nguyen, & Einav, 2013).

From these data Zhang, Nguyen, & Einav (2013) established the following relationship (Equation 4):

$$N_q^* = \alpha\left(\frac{p_c}{p_0}\right)^{2\beta}$$

where N_{q*} is the end-bearing capacity factor and α and β are parameters that depend on material stiffness (G and K) and the friction parameter (M) (Zhang, Nguyen, & Einav, 2013).

Zhang, Nguyen, & Einav (2013) resolved that β approached a constant value of 0.42 at steady state (for crushable soils); this was determined through both FEM and parametric analyses. Whereas α was determined to vary as a function of M, G and K (Equation 5) (Zhang, Nguyen, & Einav, 2013):

$$\alpha = M^3 + 14\left(\frac{G}{K}\right)$$

By then relating G and K in terms of Poisson's ratio v, using the standard approximation M = 6 sinφ/(3 − sinφ) and incorporating the dependence of the critical comminution pressure p_c on θ, Equation 6 can be established utilising parameters from the breakage model (Zhang, Nguyen, & Einav, 2013):

$$N_q^* = \left[\left(\frac{6\sin\varphi}{3-\sin\varphi}\right)^3 + 7\left(\frac{3-6v}{1+v}\right)\right]\left(\frac{2KE_c}{\theta p_0{}^2}\right)^{0.42}$$

Substituting representative values for dry polar snow from Table 1 into equation 6 results in a value for N_{q*} of 13.34.

This is substantially lower than the values for Nq obtained for Dog's Bay sand (Zhang, Nguyen, & Einav, 2013) and is much lower than typical values for Dog's Bay sand established by Zhang, Nguyen, & Einav (2013) for high p_0/p_c ratios, that approach 1–200. This significant variation may be because of the order of magnitude variation in bulk and shear moduli between the crushable soils used to establish the breakage model and dry snow.

For assumed snow density of ~ 450 kg m^{-3}, McCallum 2012 estimated that surface bearing capacity in homogeneous snow was approximately equal to average cone tip resistance divided by 3 ($q_{cavg}/3$).

Results described above suggest that the end bearing capacity of piles (q_p) in homogeneous snow of density ~ 450 kg m^{-3} is approximately equal to N_q * p_0 where p_0 is the initial effective confining pressure (Zhang, Nguyen, & Einav 2013).

How may q_p and q_{cavg} be related to enable comparison?

Insufficient testing has occurred into CPT in polar snow to enable a robust empirical expression to be presented relating these two parameters; the only work that has been conducted is that by McCallum, described herein and similar.

A simple quantitative comparison may be sufficient to suggest the value or otherwise of the application of breakage mechanics to estimate bearing capacity in polar snow.

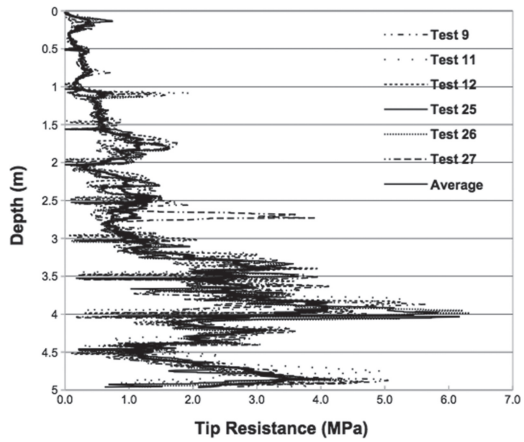

Figure 1. All CPT data from tests conducted adjacent to snow test pit 1. The bold black line is the mean resistance value generated from all tests. Snow of density ~ 450 kg m^{-3} existed between depths of ~ 1 to 1.4 m.

For assumed snow density of ~ 450 kg m^{-3} the effective confining pressure at a depth of 1 m may be equal to 20–30 kPa. For a value of Nq* of 13.34, this results in a value for q_p of ~ 260–400 kPa. Via McCallum's expression (McCallum 2012), this should equate to a q_{cavg} of ~ 1 to 1.2 MPa.

Figure 1 shows CPT tip resistance data for a test conducted in dry polar snow in Antarctica; homogeneous snow of density ~ 450 kg m^{-3} existed between depths of ~1 to 1.4 m.

This preliminary comparison suggests that a value of N_{q*} equal to 13.34, whilst very different to values for sand published by Zhang, Nguyen, & Einav 2013 may be a representative N_{q*} value for polar snow.

4 CONCLUSION

This paper introduces the concept of Breakage Mechanics as conceived by Einav (2007a) and briefly suggests how it may be applied to compaction in dry polar snow. Dry polar snow is in many ways similar to crushable soil and this preliminary investigation shows that application of the Breakage Mechanics model (Einav, 2007a) in a manner presented by Zhang, Nguyen, & Einav (2013) may have merit in describing the behaviour of dry polar snow under compaction.

However, more work is necessary to ensure that the morphological behaviour described is firstly appropriate for snow and secondly, that accurate estimation of necessary parameters can be

achieved. Additional controlled laboratory testing is necessary to further refine the application of this technique to accurately deduce bearing capacity from CPT in polar snow.

ACKNOWLEDGEMENTS

Discussions with Itai Einav and Francois Guillard, from University of Sydney, Australia and correspondence with Chunshun Zhang, from Monash University, Australia, contributed to my further understanding of the processes discussed within this manuscript.

REFERENCES

Einav, I. (2007a). Breakage mechanics - part 1: Theory. Journal of the Mechanics and Physics of Solids 55, 1274–1297.

Einav, I. (2007b). Breakage mechanics - part ii: Modelling granular materials. Journal of the Mechanics and Physics of Solids 55, 1298–1320.

McCallum, A.B. (2012). Cone Penetration Testing in Polar Firn. Ph. D. thesis, Scott Polar Research Institute, University of Cambridge.

McCallum, A.B. (2013). Cone penetration testing (CPT): a valuable tool for investigating polar snow. Journal of Hydrology (New Zealand) 52, 97–113.

McCallum, A.B. (2014a). Cone penetration testing (CPT) in antarctic firn: an introduction to interpretation. Journal of Glaciology 60(219), 83–93.

McCallum, A.B. (2014b). Direct estimation of snow density from CPT. In P.K. Robertson and K.I. Cabal (Eds.), 3rd International Symposium on Cone Penetration Testing, Las Vegas. ISSMGE Technical Committee TC 102.

McCallum, A.B. (2017). Assessing mass balance using the cone penetration test (CPT). Journal of Glaciology 63(239), 565–567.

Mellor, M. (1975). A review of basic snow mechanics. In International Symposium on Snow Mechanics, Volume International Association of Hydrological Sciences Publication 114, Grindewald, pp. 251–291. International Association of Hydrological Sciences.

Petrovic, J.J. (2003). Mechanical properties of ice and snow. Journal of Materials Science 38, 1–5.

Santamarina, J.C. & G.C. Cho (2001). Determination of critical state parameters in sandy soilssimple procedure. Geotechnical Testing Journal 24(2).

Zhang, C., G.D. Nguyen, & I. Einav (2013). The end-bearing capacity of piles penetrating into crushable soils. Geotechnique 63(5), 341–354.

Cone Penetration Testing 2018 – Hicks, Pisanò & Peuchen (Eds)
© 2018 Delft University of Technology, The Netherlands, ISBN 978-1-138-58449-5

Empirical correlations to improve the use of mechanical CPT in the liquefaction potential evaluation and soil profile reconstruction

C. Meisina
Department of Earth and Environmental Sciences, University of Pavia, Italy

S. Stacul & D.C. Lo Presti
Department of Civil & Industrial Engineering, University of Pisa, Italy

ABSTRACT: CPT-based simplified methods are the common used approaches to determine the liquefaction hazard and they require cone penetration test with electrical tip. However, in some countries, as Italy, penetrometric tests are carried out with mechanical tip (CPTm). The cone—shape effects on sleeve friction (fs) have the greatest influence on soil classification in terms of SBT, underestimating the grain size of loose soils (e.g. sands) with respect to CPTu. An empirical correlation between the fs measured with CPTm and CPTu was tested. Moreover, another correlation was developed to determine a ΔIc value as function of the cone resistance in the case of silty sands and sandy silts non correctly identified by the SBT classification systems. The correlation was applied to tests carried out in the area interested by the 2012 Emilia earthquake (Italy), where liquefaction phenomena have occurred. The procedure makes possible to use huge existing database (CPTm) for liquefaction risk assessment.

1 INTRODUCTION

Liquefaction mainly occurs in saturated sandy soils and causes the loss of shear strength, which in turn leads to an almost complete loss of bearing capacity. As a consequence, the structures experience high differential settlements, tilting, or overturning. Eventually, in the free field conditions, sand ejection and pore water pressure increase can damage infrastructures and lifeline systems. Recent examples of these effects include damage produced during the 2012 Emilia and 2010–2011 Canterbury earthquakes (Lo Presti et al. 2013; Bray et al. 2014). The identification of the area prone to liquefaction is therefore an important task for land use planning. It provides to decision makers useful information about site-specific geotechnical investigation and the identification of areas requiring ground improvement.

The most known methods for liquefaction hazard assessment are simplified empirical (or semi—empirical) procedures (Liquefaction Evaluation Procedures—LEPs) (Seed & Idriss 1971; Boulanger & Idriss 2014; Robertson & Wride 1998).

Simplified procedures evaluate the liquefaction potential of soils computing the factor of safety (FSL) against liquefaction at a given depth in the soil profile and consist of two steps: 1) Evaluation of the earthquake-induced shear stress through an estimate of the cyclic stress ratio (CSR) (Seed & Idriss, 1971) and 2) Evaluation of the soil strength to liquefaction usually accomplished through an estimate of the cyclic resistance ratio (CRR). Because of the difficulty of sampling, CRR is generally determined via in situ tests, such as standard penetration test (SPT) (Seed & Idriss 1971; Youd et al. 2009), cone penetration test (CPT) (Idriss & Boulanger 2006; Robertson & Campanella 1985; Juang et al. 2003), shear wave velocity (Vs) (Andrus & Stokoe 2000), flat dilatometer tests (DMTs), and self-boring pressuremeter (SBPT). Once the safety factor against liquefaction has been computed at various depths, numerical indicators or qualitative criteria to define the liquefaction severity at ground level can be used such as the LPI index (Iwasaki et al. 1978) or the LSN parameter (Tonkin & Taylor 2013).

CPT based LEPs were developed with reference to the results of electrical tests (i.e. cone tests with piezocone). On the other hand, in some countries, as Italy, huge databases of cone tests with mechanical tip (CPTm) are available.

The different equipment of CPTm and electrical CPT lead to differences between the two typologies of tests. While the cone—shape effects on tip resistance (qc) are not very relevant, those on the sleeve friction (fs) can strongly influence the FSL calculation, especially in the case of silty sands; fs measured with the mechanical tip is always greater than the one measured with the electrical tip (the difference is practically negligible for clay). The use of classification methods which were developed to

interpret CPTu, mainly causes the lack of identification of sandy to silty liquefiable layers.

Meisina et al. 2017 developed a relationship establishing empirical correlation between the sleeve friction measured with mechanical tip and that measured with electrical cone (piezocone) in order to correct CPTm results. The authors compared the SBT classes, evaluated according to Robertson 1990, to that given by Schmertmann (1978) classification chart for a large CPTm database. They found an empirical correction of the Ic index (Soil Behaviour Type Index), so that the Robertson SBT class coincide with that of Schmertmann (1978).

The aim of the paper was to apply corrections of fs and Ic proposed by Meisina et al. 2017 to CPTm in order to verify the effectiveness of the proposed methodology in 1) liquefiable layers identification; 2) build subsoil model for liquefaction hazard assessment.

Table 1. Correspondence between Schmertmann (1978) and Robertson (1990) approaches (classes 1 and 9 of Robertson approach were not considered).

Schmertmann (1978)	SBTn (Robertson 1990)
Organic clay and mixed soils	2
Insensitive non fissured inorganic clays	3
Sandy and silty clays	4
Clayey sands and silts	5
Silt—sand mixtures	5
Sands	6–7
Dense or cemented sands	8
Very shell sands, limerocks	8

2 MATERIALS AND METHODS

2.1 *Materials*

Pairs of text CPTm and CPTu not used for the development of the correlation of Meisina et al. (2017) were analysed. They were carried out in the Po Plain in Northern Italy and belong to the database of the Emilia Romagna region interested by the seismic sequence of May–June 2012 (Regione Emilia Romagna 2011). This seismic sequence is an example of a moderate earthquake yielding the most prominent extensive liquefaction phenomena of the last century in Italy (Emergeo Working Group 2013). Liquefaction related phenomena and associated ground failures caused damages and extensive problems mainly to infrastructures (roads, wells, lifelines, etc.) while the foundation system of very few buildings was damaged. Most of the liquefaction sites are located on elevated fluvial ridges.

2.2 *Methods*

Using the results of the tests that have been carried out at Pisa (Central Italy) and those of four pairs of CPTm/CPTu from Emilia-Romagna Region database (2011), a correlation function between the fs(CPTm) and the fs(CPTu) was found by Meisina et al. 2017.

The measured sleeve friction is corrected according to the following equations

$$fs(CPTu) = \left[0{,}0797\, fs(CPTm)\right]^{2.504} \quad (1)$$

if fs(CPTm) < 65 kPa

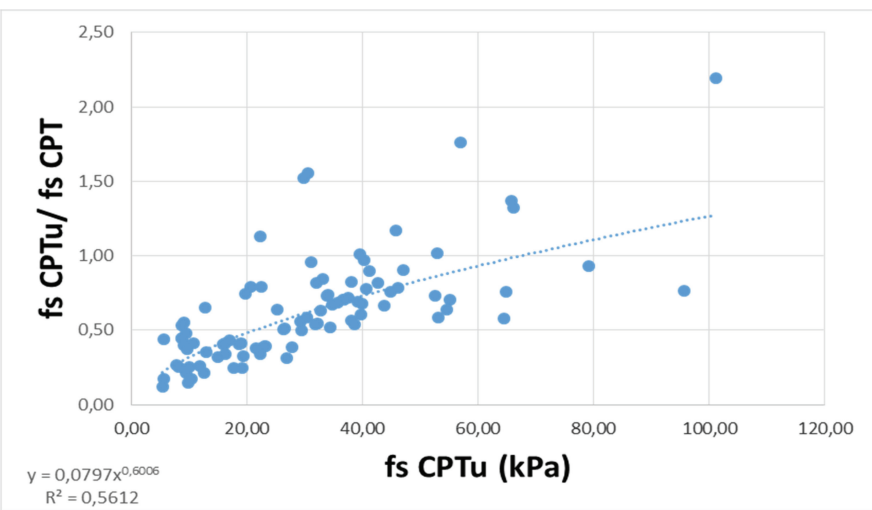

Figure 1. Correlation function between fs(CPTm) and fs(CPTu).

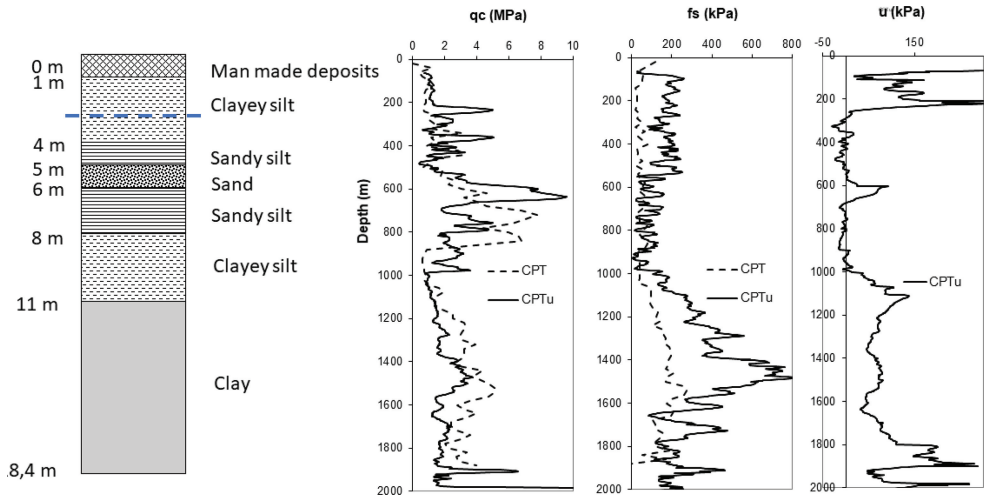

Figure 2. Case history 1. Simplified borehole, CPTm and CPTu qc, fs and u.. In blue the Ground Water Table.

$$fs(CPTu) = fs(CPTm) \quad (2)$$

if fs(CPTm) > = 65 kPa.

The Ic index is also corrected according to the following equation:

$$\Delta Ic = -0.296 \ln(qc) + 0.8568 \quad (3)$$

$$Ic\ (correct) = Ic(Robertson, 1990) - \Delta Ic \quad (4)$$

The correction was obtained by comparing soil classes of the Schmertmann (1978) approach to those inferred by using the Robertson (1990) SBTn (Tab. 1). Mainly the use of Robertson (1990) for interpreting CPTm leads to an underestimate of soil granulometry. The proposed correction applies only when the Robertson (1990) classification underestimate that of Schmertmann (1978b).

Normalized class description: 2: Organic soils, peats; 3: Clays: clay to silty clay; 4: silt mixtures: clayey silt to silty clay; 5: Sand mixtures: silty sand to sandy silt; 6–7: Sands: clean sand to silty sand; Gravely sands to sands; 8: Very stiff sand to clayey sand; Very stiff sand to clayey sand.

3 RESULTS

3.1 *Application of the developed methodology*

The methodology of correction was applied to different pairs of tests CPTm-CPTu, representative of the following conditions:

a. Level of sand interbedded within layers of sandy silt (Case history 1);
b. Level of sandy silts and silty sand (Case history 2).

The liquefiable layers consist on sand and silty sand with FC (materials passing a number 200 sieve ASTM) = 18–28%.

The pairs CPTm and CPTu are at a distance less than 100–200 m from liquefaction phenomena (sand boils). They have a relative distance of 50–30 m. For each pair of test a reference borehole, with a maximum distance of 9–50 m from the considered CPT, was selected in order to define a reference stratigraphic profile. The area is characterized by a strong lithological heterogeneity. Nevertheless, the pairs of tests and the reference borehole were selected so that they belong to the same geomorphologic unit and have therefore the same behavior with respect to liquefaction.

The first step consisted in the borehole simplification in order to obtain simplified soil profiles allowing to identify the critical layers responsible for liquefaction.

In a second step for each layer Ic (normalized soil behavior index) values are calculated following the method of Robertson, 1990. It was assumed that liquefiable soils are characterized by Ic < = 2.6 (Cubrinovski et al. 2017). Factors of safety against liquefaction were computed according to the procedures proposed by Boulanger & Idriss (2014) method.

For the interpretation of CPTm and CPT the software CPT PaGE, developed by University of Pisa, was used (Stacul et al. 2017).

3.2 *Case history 1*

The stratigraphy of the subsoil is characterized by non liquefiable layers (clayey silt and silt and clay) in the first 4 m. The potential critical layers for soil liquefaction develop between 4 and 8 m and

it is constituted by silty sand (4–5 m), sand (5 to 6 m), followed by two meters of sandy silt (Fig. 2). Clayey silt and clay are present till 18 m followed by sandy silt. The depth to the water table is 3.5 m.

Differences of qc and fs can be also related to local heterogeneity of the soil stratigraphy (Fig. 2).

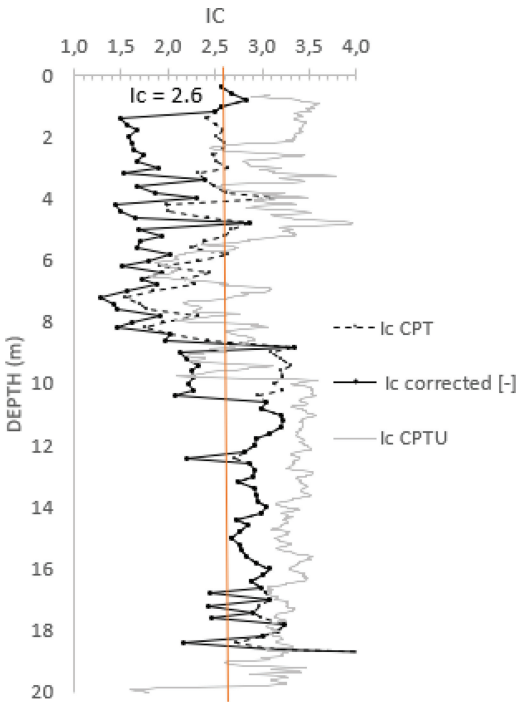

Figure 3. Case history 1. Ic variation with depth.

The Ic, calculated through CPTu, assumes values generally greater than 2.6, except for the layer of sand (5–6 m) for which 1.8 < Ic < 2.55.

In the CPTm the most surficial sandy silt layer has non corrected Ic values from 2.1 and 2.6, for the sand Ic ranges between 1.9 and 2.45; meanwhile the deeper sandy silt layer presents values from 1.62 and 2.02 (Fig. 3).

The CPTu test identify liquefiable horizons between 5–6 m (sand).

The Ic values calculated through CPTm indicate that for mechanical penetrometric test the liquefiable horizon is thicker and includes also sandy silt and silty sand.

The application of the correction for CPTm further reduces the values of Ic, which are always lower than 2.1 (from 1.3 to 1.9 for the sandy layer).

In this case the Ic seems to be underestimated especially for soils between 8 and 10 meters. This lead to evaluate as prone to liquefaction clay and silty soils.

3.3 *Case history 2*

The subsoil is composed by the alternation of silty sand and sandy silt and silty sand till 8.8 m overlying clayey silt (Fig.4).

The depth to the water table is 2.7 m.

Ic calculated though mechanical CPTm in the interval 3.1 to 8.8 m ranges between 1.98 and 2.55 (Fig.5).

For CPTu Ic is greater than 2.6 except between 3.7 and 5 where it has values between 1.84 and 2.6 (sandy silt and silty sand).

The correction of CPTm allows to obtain Ic lower than 2.6.

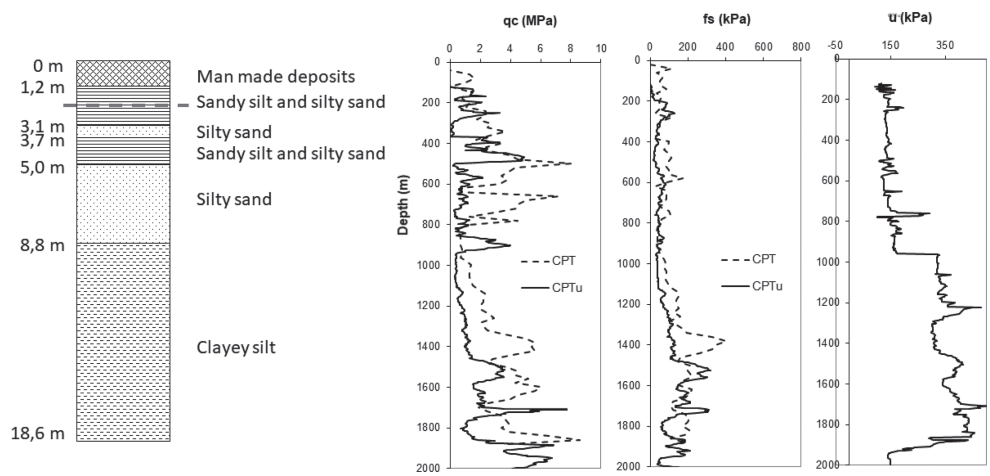

Figure 4. Case history 2. Simplified borehole, CPTm and CPTu qc, fs and u. In blue the Ground Water Table.

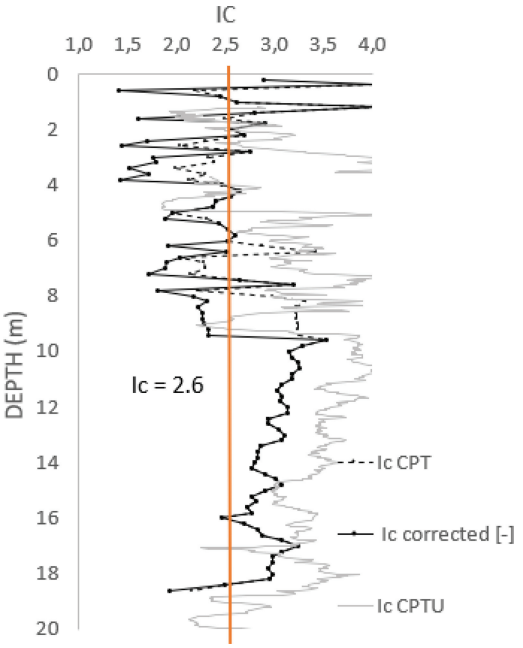

Figure 5. Case history 2. Ic variation with depth.

Also in this case the CPTu test identify thinner liquefiable horizons between 3.7 and 5 m (sandy silt). The Ic values calculated through CPTm indicate that for mechanical penetrometric test the liquefiable horizon is thicker and includes also sandy silt and silty sand.

The application of the correction for CPTm bring to an underestimation of Ic, with value less than 2.6 also for clay and silty soils.

4 CONCLUSIONS

A procedure developed by Meisina et al.2017 for correcting mechanical CPTm parameters (sleeve friction and Ic) was applied to a certain number of mechanical CPTm in the Emilia Romagna area interested by the seismic sequence of May 2012. Liquefiable horizons are composed by sand containing a certain amount of silt.

Results, in the case history documented in this study, demonstrated that:

1. All the tests detect liquefiable horizons (layers having Ic < 2.6 were assumed to be potentially liquefiable) but with different thickness, generally CPTu can misleading the interpretation of transitional soils as silty sand.
2. The correction of CPTm could in some cases underestimated the Ic and this lead to consider potentially liquefiable also clay and silty soils.
3. The Ic 2.6 threshold separating liquefiable and non liquefiable soils requires more analysis in the study area.

REFERENCES

Andrus, R.D. & Stokoe, K.H., 2000. Liquefaction Resistance of Soils from Shear-Wave Velocity. *Journal of Geotechnical and Geoenvironmental Engineering*, 126 (11): 1015–1025.

Boulanger, R. W., & Idriss, I. M. (2014). *CPT and SPT based liquefaction triggering procedures*. Report No. UCD/CGM-14/01, Center for Geotechnical Modeling, Department of Civil and Environmental Engineering, University of California, Davis, CA, 134 pp.

Bray, J.D., Zupan, J.D., Cubrinovski, M., Taylor, M., 2014. *CPT-based liquefaction assessments in Christchurch*, New Zealand. Papers of the 3rd International Symposium on Cone Penetration Testing, Las Vegas, Nevada.

Cubrinovski, M., Rhodes, A. & Ntritsos, N., 2017. *System response of liquefiable deposits*. PBD-III, Earthquake Geotechnical Engineering, Vancouver, July 16–19, 2017.

Emergeo Working Group, 2013. Liquefaction phenomena associated with the Emilia earthquake sequence of May-June 2012 (Northern Italy). *Natural Hazards Earth System Sciences*, Vol. 13, p. 935–947.

Boulanger, R. W., &Idriss, I. M., 2014. *CPT and SPT based liquefaction triggering procedures*. Rep. No. UCD/CGM-14/01, Univ. of California, Davis, CA.

Idriss, I. M., & Boulanger, R. W., 2006. Semi-empirical procedures for evaluating liquefaction potential during earthquakes, *J. Soil Dynamics and Earthquake Eng*. 26: 115–30.

Iwasaki, T., Tokida, K., Tatsuko, F., and Yasuda, S., 1978. *A practical method for assessing soil liquefaction potential based on case studies at various sites in Japan*. Proceeding of the 2nd International Conference on Microzonation for Safer Construction-Research and Application, San Francisco, California, Vol. 2, 885–896.

Lo Presti, D. C. F., Sassu, M., Luzi, L., Pacor, F., Castaldini, D., Tosatti, G., Meisina, C., Zizioli, D., Zucca, F., Rossi, G., Saccorotti, G., Piccinini, D.,2013. *A report on the 2012 seismic sequence in Emilia (Northern Italy)*. Seventh International Conference on case Histories in Geotechnical Engineering, April 29-May 4, 2013 Chicago. ISBN 1–887009–17–5.

Meisina, C., Persichillo, M.G., Francesconi, M., Creatini, M., Lo Presti, D.C., 2017. Differences between mechanical and electrical cone penetration test in the liquefaction hazard assessment and soil profile reconstruction. ICCE International Conference of Civil Engineering, 12–14 October 2017, Tirana, Albania, 95–105.

Regione Emilia Romagna (Italy), 2011. La banca dati geognostica. See http://ambiente.regione.emilia-romagna.it/geologia/cartografia/webgis-banchedati/banca-dati-geognostica.

Robertson, P.K., 1990. Soil Classification Using the Cone Penetration Test. *Canadian Geotechnical Journal*, 27: 151–158.

Robertson P.K. & Wride C.E. (1998). Evaluating Cyclic Liquefaction Potential Using the Cone Penetration Test, *Canadian Geotechnical Journal*, 35: 442–459.

Robertson, P.K. & Campanella, R.G., 1985. Liquefaction potential of sands using the cone penetration test, *Journal of Geotechnical Division of ASCE*, 22(3): 277–286.

Schmertmann J.H., 1978. *Guidelines for Cone Penetration Test*. Performance and Design, U.S. Department of Transportation, Washington.

Seed, H. B. & Idriss, I. M., 1971. Simplified Procedure for Evaluating Soil Liquefaction Potential. *Journal of the Soil Mechanics and Foundations Division*, ASCE, Vol. 97, No SM9, Proc. Paper 8371, September 1971, 1249–1273.

Stacul, S., Giusti, I. & Lo Presti, D., 2017. CPT PaGE, CPTU (CPTm) Interpretation and use, User Manual, University of Pisa.

Tonkin & Taylor, 2013. Liquefaction Vulnerability Study. Tonkin e Taylor Ltd.

Youd, T.L. et al., 2001. Liquefaction resistance of soils: Summary report from the 1996 NCEER and 1998 NCEER/NSF workshops on evaluation of liquefaction resistance of soils, Journal of Geotechnical and Geoenvironmental Engineering, 127: 817–833.

Cone Penetration Testing 2018 – Hicks, Pisanò & Peuchen (Eds)
© 2018 Delft University of Technology, The Netherlands, ISBN 978-1-138-58449-5

Rigidity index (I_R) of soils of various origin from CPTU and SDMT tests

Z. Młynarek
University of Life Sciences in Poznan, Poland

J. Wierzbicki & K. Stefaniak
Institute of Geology, Adam Mickiewicz University in Poznan, Poland

ABSTRACT: The paper presents an analysis of the qualitative impact of soil properties of varied origin on the rigidity index variability. This coefficient is defined as the ratio between the shear modulus *G* and undrained shear strength su. In order to determine values of this coefficient in four genetically varied soil groups, CPTU and SDMT tests were performed. The article discusses the concepts of evaluating the *G* modulus based on the values measured with the SDMT test, as well as the coefficient $I_R' = G_0 \cdot s_u^{-1}$. The results have revealed that the significant influence on the I_R variation, apart from the characteristic soil properties, such as type of soils or plasticity index, is displayed by the cementation and over consolidation effects, and the anisotropy of macrostructure of certain sediments.

1 INTRODUCTION

The rigidity index is frequently used to describe changes in subsoil stiffness. Due to the fact that this coefficient consists of two independent components, which are undrained shear strength and shear modulus *G*, the rigidity index can be also used for design purposes in determining undrained shear strength changes. The components of the rigidity index are determined by two test methods that record the test parameters at substantially different deformation values (Mayne 2001). CPTU static penetration test is commonly used to evaluate the undrained shear strength values, while SDMT-type dilatometer test or SCPTU-type static penetration test are used to determine the shear modulus. Variables related to the subsoil properties affect the parameters measured both in the CPTU test and the SDMT or SCPTU tests (Młynarek 2007, Młynarek, et al. 2012, Hardin 1978), but their qualitative influence may vary. For this reason, the rigidity index, which is the empirical coefficient marking the proportion between shear modulus *G* and undrained shear strength, is not a constant value. Mayne (2001) indicated that the determination of the rigidity index requires knowledge of the *OCR* preconsolidation coefficient and the plasticity index *PI*. An interesting question arises of what is the qualitative contribution of these variables in shaping the rigidity index values, and how this contribution is related to the soil origin. The aim of this paper is to find answer to those questions.

2 GEOLOGICAL CHARACTERISTICS OF INVESTIGATED SOILS

Investigations were conducted on 10 plots located in northern, western and southern Poland. In each locations the CPTU and seismic downhole type tests (SDMT) were carried out as well as borings for investigations of basic geotechnical and geological properties. The total number of 234 geotechnical data sets,, was obtained as a result. Such arrangement of research areas combined with clearly distinguished geological structures of Poland's surface layers enabled the assembly of data on genetically varied material.

The oldest soil investigated was overconsolidated Pliocene clay, located in the vicinity of Bydgoszcz and Warsaw (Kumor 2008, Barański et al. 2012). The aged glacial till formed in the Mindel glaciation, located in Derkacze, were also included in this group. On the other side glacial sediments of the youngest glaciation on the area of Poland, the Weicheslian glaciation, were divided into two groups, depending on the phase of formation. The Posnanian phase soils form Jarocin and Marszew were assumed as overconsolidated but not aged, and the Pomeranian phase soils form Batkowo, Rzepin and Boryszew, were assumed as normally consolidated and slightly overconsolidated. The next group, silty aeolian loess and loess-like soils form Łańcut, are the normally consolidated soil. However, in the case of this soil, due to strong calcium carbonate $CaCO_3$ cementation, the upper

Table 1. Range of values of the selected physical parameters of the analyzed soils.

Genetic group	Parameters			
	LI [–]	*PI* [%]	*OCR* [–]	$CaCO_3$ [%]
Pliocene clay[1]	0.00–0.30	25–32	11.4–22.9	7.21
Pliocene sandy clay[2]	0.00–0.05	16–18	12.1–13.6	4,50
aged & OC till	0.00–0.42	7–9	2.0–10.5	10.81
OC till[3]	0.08–0.28	14–24	1.4–14.2	11.06
OC till[4]	0.00–0.56	5–17	1.1–9.8	7.12
loess uncemented	0.10–0.52	6–18.5	1.0–7.9	6.23
loess cemented	0.15–0.54	6–13	1.1–13.4	18.49
young & NC till	0.15–0.50	14–16	1.2–5.5	4.12
young till[5]	0.00–0.37	13–18	3.1–8.2	3.12
young till[6]	0.15–0.36	12–25	1.2–8.1	3,47
organic & NC clay	0.25–0.75	11–28	1.2–4,8	–

LI – Liquidity index, *PI* – Plasticity index, *OCR* – Overconsolidation ratio, $CaCO_3$ content, [1] –Bydgoszcz, [2] – Warszawa, [3] – Jarocin, [4] – Marszewo, [5] – Rzepin, [6] – Boryszewo cities.

part of the loess profile can be assumed as a quasi-preconsolidated (Frankowski et al. 2010, Młynarek et al. 2015). The separate group consists of cohesive and organic soil, deposited under the conditions of proglacial plains and postglacial lakes in northern Poland, in early Holocene. these soils are characterized by high porosity and considerable content of organic matter. In this group the silty clays and low organic and organic soil dominate. Concise characteristic of the basic properties of the soil are summarized in Table 1.

3 METHODOLOGY OF DETERMINATION OF PARAMETERS FOR CALCULATION OF RIGIDITY INDEX

The rigidity index is defined with the formula (Lunne et al. 1997, Vesic 1972):

$$I_R = G/s_u \tag{1}$$

where: G – shear modulus for selected deformation, s_u – undrained shear strength.

In order to determine the s_u values, various reference tests are used. Based on these tests, diverse values of undrained shear strength are obtained (De Groot 2014, Mayne 2006). In the conducted tests, s_u was determined from the CPTU test with use of the formula (Lunne et al. 1997):

$$s_u = (q_t - \sigma_{v0})/N_{kt} \tag{2}$$

where: q_t – corrected cone resistance, σ_{v0} – total vertical stress, N_{kt} – cone factor.

The key parameter to determine the s_u value from the Equation 2 is coefficient N_{kt}. The values of this coefficient were assumed according to the type of soil origin and degree of overconsolidation (Młynarek et al. 2018): 18 for Pliocene clay, 16 - loess, 14.5 - aged till, 14 - young till, 12 - organic soil. The coefficient has been related to the undrained shear strength from the vane test.

The second component of the Equation 1, the shear modulus G, is defined according to two concepts. In the first one, the coefficient α is used to calculate the G-modulus on the basis of the measured initial shear modulus G_0:

$$\alpha = G/G_0 \tag{3}$$

With respect to the α coefficient there are several proposals for defining its "computational" value. Since the value of the modulus G depends on the degree of deformation γ (Drnevich & Massarsch 1979), it is important to assume a specific deformation level for determination of this modulus. Hardin (1978), Massarsch (2004) acknowledge that the value $\gamma = 0.5\%$ is correct for geotechnical analyses. This value also corresponds to the deformations observed in the subsoil during penetration tests such as DMT (Mayne 2001). Based on seismic in situ tests, the G_0 values can only be determined with very small deformations $\gamma = 10^{-6}$. As a result, a need arises to correct the obtained results with the G/G_0 relationship, which has been repeatedly investigated, also in the context of soil load type (Vucetic & Dobry 1991, Massarsch 2004). In the instruction books for design purposes of specific constructions, a constant value of this ratio appears. Authors of the Guidelines for Design of Wind Turbines—DNV / Risø 2002 recommend $\alpha = 0.35$. A similar value is suggested by Mayne (2006), while Robertson (2009), as well as Recommendations for design, calculation, installation and inspection of wind turbine foundations (Working Group "Wind turbine foundations", Rev. Francaise de Geotechnique No. 138-139, 2012), recommend values in the range of 0.30–0.38. It should be noted that the adoption of a constant value of the coefficient α is related to the typical, for a given construction, degree of subsoil deformation. This fact documents the adoption of the deformation level for the G and G_0 moduli, which are respectively 10^{-2} and 10^{-4}. Massarsch (2004) indicates that the α coefficient depends significantly on the soil type, and the value of the plasticity index in particular. Therefore, the analysis assumes that the value of the coefficient $\alpha = G/G_0$, denoted as R_M (Massarch 2004), will be determined from the formula (4) (Massarsch 2004).

$$R_M = 0.0043PI + 0.103 \tag{4}$$

The R_M values for soils used in this analysis, together with the basic statistical distribution parameters, are illustrated in Fig. 1.

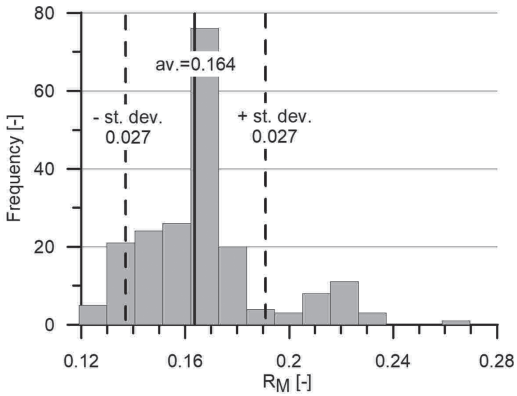

Figure 1. Histogram of R_M values used in the analysis, with marked average and standard deviation values.

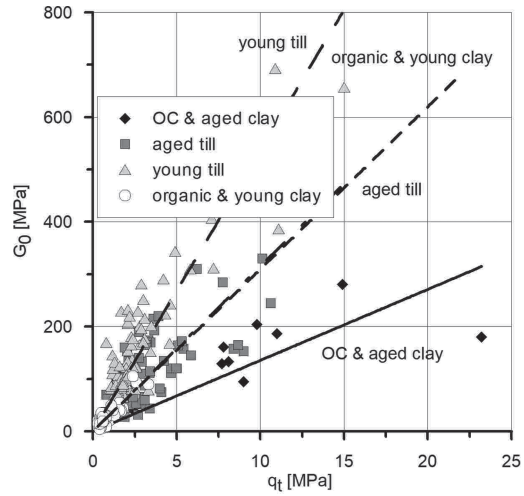

Figure 2. Relationship between the shear modulus G_0 and the cone resistance q_t.

Data for calculating the rigidity index and the G modulus from the Equation 4 were prepared as pairs of G_0-s_u measurements, at the average stress value σ_{v0} in the subsoil profile for the individual homogeneous soil layer. The values of liquidity index and plasticity index, close to a constant in the layer, have been adopted as the homogeneity criterion. In total, 220 pairs of s_u and G_0 measurements were used.

In order to determine the qualitative influence of the soil properties on the rigidity index, the multivariate analysis of variance was used.

4 CONCEPT OF DATA PREPARATION FOR ANALYSIS

The modified Hardin (1978) Equation 5 reveals that the shear modulus G_0 is influenced by a number of subsoil properties, related to its structure (θ), lithology (PI), stress state (σ'_{v0}), consistency (LI), and origin (σ'_p) (5).

$$G_0 = f(LI, PI, OCR, \sigma'_p, \sigma'_{v0}, \theta) \quad (5)$$

Similar characteristics, although in different ways, influence the cone resistance values in CPTU test (Młynarek et al., 2012). On this basis, a preliminary analysis of the collected data was performed through comparing the seismic and CPTU results for all separated layers. The data was prepared for analysis according to the rule presented in section 3. The obtained results (Fig. 2) indicate the presence of an evident relationship between G_0 and q_t. This relationship, however, is distinct for individual test sites. It follows that one of the primary factors influencing the relationship between the cone resistance and the G_0 shear modulus is the soil origin and the effect of post-depositional processes (cementation, preconsolidation). In order to account for the so-called "locality", it was necessary to adopt the geological-genetic criterion in the data division. As a result, all the data were categorized into 4 main genetic groups (Fig. 2). Obtained categories constituted the basis for further analysis of the effect of other measurable properties of the subsoil on its rigidity.

Table 2. Values of linear correlation coefficient obtained in multidimensional regression analysis for different genetic groups.

Genetic group	Correlation coefficient R^2
OC & aged clay	0.96
Aged till	0.69
Young till	0.81
Organic & young clay	0.71

Accuracy of the performed division, in the context of influence of the remaining soil properties on the analyzed dependency, can be confirmed by the results of the multivariate regression analysis. These results indicate a significant correlation between G_0 and q_t in the respective groups (Table 2).

5 DATA ANALYSIS

As far as the assessment of the rigidity index variability is concerned, two elements are highlighted. The first one is, as already mentioned, the assessment of the mean value of the I_R coefficient for

the population of its value in the separated soil groups. This type of analysis makes it possible to address the range of I_R variability in particular soil groups. The second element concerns the hierarchy of the influence of variables from Equation 4 on the rigidity index variability.

In order to determine the mean of rigidity index it was assumed that the distribution of this index, as of the shear strength parameter and deformation modulus, was normal (Lumb 1974). In this case, the range of I_R variability can be described by specification of confidence intervals at the level of $\alpha = 0.05$. For each soil group, the following mean values of I_R were obtained (Table 3).

A very wide range of I_R variability proves that the variables recorded in Equation 5 have a varied and significant effect on the rigidity index variability. This fact is well supported by the location of the I_R values from the whole data set in the space described by *PI* and *LI* coordinates. Figure 3 indicates that the variability of I_R strongly correlates with the variability of plasticity index and liquidity index. Figure 4 shows the sample variability of the rigidity index associated with the change in liquidity index for particular soil groups.

Table 3. Mean rigidity index values and 95% I_R confidence intervals determined for individual genetic groups.

	Data number N	Mean $\bar{x}$	–95% confidence interval	+95% confidence interval
OC & aged clay	11	76.97	39.19	114.76
Aged till	68	99.28	86.34	112.22
Young till	93	166.68	153.38	180.57
Organic & young clay	48	167.05	135.83	198.28

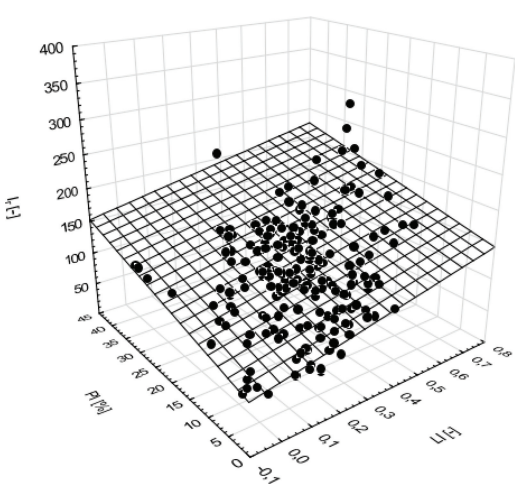

Figure 3. 3-dimensional ilustration of the relationship between I_R, *PI* and *LI* determined for the entire data set.

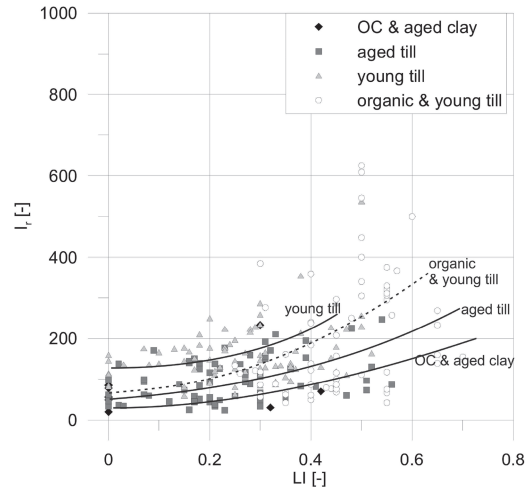

Figure 4. Rigidity index I_R vs liquidity index *LI*.

A qualitative assessment of the influence of the three basic variables from Equation 5 on the rigidity index variability can be obtained by means of multivariate regression analysis (Draper & Smith 1981). The following approximate solution of the Equation 5 were obtained for each individual soil group:

OC & aged clay:

$$I_R = 3.81PI - 38.16\ LI + 231.78;\ R^2 = 0.64 \quad (6a)$$

$$I_{R(RM=0,35)} = 361.79\ LI + 3.58\ PI + 1.84;\ R^2 = 0.56 \quad (6b)$$

aged till:

$$I_R = 8.80\ PI - 7.89\ OCR - 7.21\ LI + 149.19;\ R^2 = 0{,}54 \quad (7a)$$

$$IR(RM = 0{,}35) = 317{,}15\ LI + 15{,}24\ PI - 44{,}72\ OCR - 17{,}34;\ R2 = 0{,}47 \quad (7b)$$

young till:

$$I_R = 386.05\ LI + 0.60\ \sigma'_{v0} + 9.45\ OCR - 128.05\ PI + 4.75;\ R^2 = 0{,}26 \quad (8a)$$

$$I_{R(RM=0,35)} = 1.18\sigma'_{v0} + 840.83\ LI + 3.29\ PI + 13.43\ OCR - 149.52;\ R^2 = 0{,}28 \quad (8b)$$

organic & young clay:

$$I_R = 4.73\ PI - 4.78\ OCR - 14.04\ LI + 151.74;\ R^2 = 0{,}51 \quad (9a)$$

$$I_{R(RM=0,35)} = 267.33\ LI + 3.63\ PI - 3.17\ OCR + 75.67;\ R^2 = 0{,}45 \quad (9b)$$

The *OCR* values in the aged clay group underwent little change, hence the influence of this variable on the rigidity index was statistically insignificant (Eq. 6a, 6b). For aged clay and aged till, the rigidity index variability was primarily related to the liquidity index variability. As far as young organic clay and young till are concerned, all the variables from equations 8 and 9 strongly determine variability of the rigidity index.

Crucial information is derived from the calculated value of the multivariate regression coefficient R^2 in individual soil groups. The R^2 values indicate that the rigidity index variability in the range from 45 to 64% is related to the variability of the parameters in Equations (6) to (9), irrespective of the values of the coefficient α or R_M. This means that there are other variables involved in the variability of the rigidity index in the subsoil. This result confirms the statement that the rigidity index also depends on the cementation effect, the calcium carbonate content, and the anisotropic macrostructure of sediments. This process is particularly noticeable in young till sediments. The anisotropy of the macrostructure is connected with the occurrence of the thin layers of fine sand in the clay or boulder loam layers. The influence of these factors also on the values of constrained modulus and initial shear modulus G_0 had already been demonstrated by Młynarek et al. (2012).

The fact that correlations used to calculate the rigidity index for the tested soils from Poland available in the literature are useful is very important.. These relationships include formulas created by Keaveny & Mitchel (1980) (Eq. 10) or Krage et al. (2014).

$$I_R = 0.26\left(\frac{G_0}{\sigma'_{vo}}\right)\left(\frac{1}{0.33\left(0.33Q_t\right)^{0.75}}\right) \tag{10}$$

where: Q_t – normalized cone resistance.

$$I_R \approx \frac{\exp\left(\frac{137-PI}{23}\right)}{1+\ln\left[1+\frac{\left(OCR+1\right)^{3.2}}{26}\right]^{0.8}} \tag{11}$$

Figure 5 indicates that in the zone of rigidity index values up to the level of 200, the I_R values calculated from Equations 6 to 9 and Krage et al. (2014) are very close and concentrated near the 1:1 straight line of calibration. Outside of the *IR* zone of 200, the trend of changes in the rigidity index determined with the different formulas varies dependently on the soil groups.

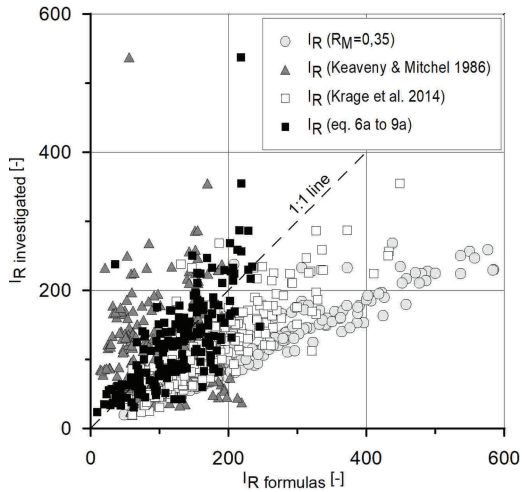

Figure 5. Comparison of changes in rigidity index determined with different formulas.

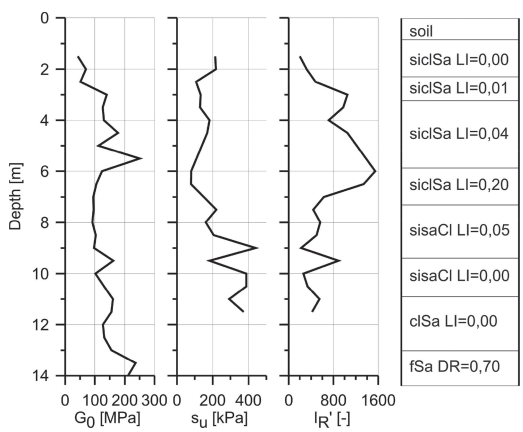

Figure 6. Changes in shear modulus G_0, undrained shear strength and I_R' with depth in young till subsoil (location: Batkowo).

The G_0 shear modulus and the rigidity index in the form of $I_R' = G_0 \cdot s_u^{-1}$ are frequently used to predict changes in the subsoil in the G_0 modulus, based on undrained shear strength s_u, unless a seismic test is performed. In most cases, the s_u value from the CPTU test is applied for this dependency. Figure 6 reveals that I_R' is as dependent on the soil properties as the I_R. However, to assume I_R' values at constant levels e.g. 2600 (e.g. Guidelines for the design of wind turbines—DNV/Risø) is highly risky, especially in the subsoil characterized by great variability of macrostructure, and effects of cementation and preconsolidation.

6 CONCLUSIONS

The main conclusion arising from the conducted tests is that the tests confirmed the hypothesis formulated by several authors (e.g., Keaveny and Mitchel 1986, Mayne 2006, Krage et al. 2014) that variability in rigidity index is related to variability in parameters that determine soil properties. The investigation also explicitly revealed that the influence of these parameters is qualitatively differentiated and dependent on the soil origin. In the case of soils in Poland, the essential influence on the rigidity index value was displayed by such factors as cementation and anisotropy of macrostructure of certain sediments. This leads to the conclusion that the most effective correlations for determining the rigidity index are local correlations (e.g. Fig. 3). These correlations account for varied origin and properties of different soil groups that occur in the tested area.

REFERENCES

Barański M., Godlewski T. & Szczepański T. 2010. Determination of Soil Stiffness Parameters on Chosen Test Sites, Using in situ Seismic Methods. In E. Dembicki, J. Komisarek (eds.) Soil parameters from in situ and laboratory tests: 149–157. Poznan: Wyd. Uniw. Przyrodniczego.

De Groot D. 2014. Evaluation pf soft clay properties from interpretation of CPTU data within a SHANSEP framework. In Z. Młynarek & J. Wierzbicki *CPTU and DMT in soft clays and organic soils*: 79–94. Poznan: Exemplum.

Draper N.R., Smith H. 1981. Applied regression analysis. New York: Wiley.

Drnevich, V. P. & Massarsch, K. R. 1979. Sample Disturbance and Stress—Strain Behaviour. *ASCE Journal of the Geotechnical Engineering Division,* Vol. 105 No GT 9: 1001–1016.

Frankowski, Z., Majer, E. & Pietrzykowski P. 2010. Geological and geotechnical problem of loess deposits from south-eastern Poland. *Proceedings of the International Geotechnical Conference Geotechnical challenges in megacities, Vol. 2, Moscow 2010*: 546–553.

Hardin B.O. 1978. The nature of stress-strain behavior for soils. *Proc. ASCE Geotechnical Div. Specialty Conf. on Earthquake Engng. and Soil Dynamics*, Pasadena Vol. 1:3–90.

Keaveny, J. & Mitchell, J.K. 1986. Strength of fine-grained soils using the piezocone. *Use of In-Situ Tests in Geotechnical Engrg. (GSP 6), ASCE, Reston/VA*: 668–685.

Krage C.P., Broussard N.S. & DeJong J.T. 2014. Estimating rigidity index (I_R) based on CPT measurements. *Proc. 3rd International Symposium on Cone Penetration Testing, Las Vegas, Nevada, USA – 2014*: 727–735.

Kumor M. K. 2008. Selected geotechnical problems of expansive clays in/the area of Poland. *Arch. Civ. Eng. Environment. No 4, The Silesian Univ. of Technology.*

Lumb P. 1974. Applications of Statistics in Soil Mechanics. In J. K. Lee (ed.) *Soil Mechanics-New Horizons. Chapter 3.* London: Newness-Batterworth.

Lunne, T., Robertson, P.K., & Powell, J.J.M. 1997. Cone penetration testing in geotechnical practice. New York: Blackie Academic, EF Spon/Routledge Publ.

Massarsch, K. R. 2004. Deformation properties of fine-grained soils from seismic tests. In Viana da Fonseca & Mayne (eds.) Geotechnical and Geophisical *Site Characterization. Proc. International Conference on Site Characterization, ISC'2, 19–22 Sept. 2004, Porto*: 133–146. Rotterdam: Millpress.

Mayne P.W. 2001. Stress-strain-strength-flow parameters from enhanced in-situ tests. *Proc., International Conference on In-Situ Measurement of Soil Properties & Case Histories [In-Situ 2001], Bali, Indonesia, May 21–24, 2001*: 27–48.

Mayne P.W. 2006. In-Situ Test Calibrations for Evaluating Soil Parameters. In T.S. Tan, K.K. Phoon, D.W. Hight & S. Leroueil (eds.) *In Characterisation and engineering properties of natural soil. Proc. In-Situ Testing—Singapore Workshop, Nov. 29- Dec. 01,2006:* 1–56.

Młynarek, Z. 2007. Site investigation and mapping in urban area. In V. Cuellar et. al (eds.) *Geotechnical Engineering in Urban Enviornment,* Vol. 1: 175–202. Rotterdam: Millpress.

Młynarek Z., Wierzbicki J. & Stefaniak K. 2012. Deformation characteristics of overconsolidated subsoil from CPTU and SDMT tests. In R. Q. Coutinho & P.W. Mayne (eds.). *Proc. of 4th International Conference on Geotechnical and Geophisical Site Investigations, Porto de Galinhas, Brazil:* 1189–1193. London: Taylor & Francis Group.

Młynarek, Z., Wierzbicki, J. & Mańka, M. 2015. *Geotechnical parameters of loess soils from CPTU and SDMT. Proceedings of International Conference on the Flat Dilatometer DMT'15, Rome 2015*: 481–489.

Młynarek Z., Wierzbicki J. & Stefaniak K. 2018 (in print). Interrelationship between undrained shear strength from DMT and CPTU tests for soils of different origin. *Geotechnical Testing Journal*.

Robertson, P.K. 2009. Interpretation of cone penetration tests—a unified approach. *Canadian Geotechnical Journal*, 46: 1337–1355.

Vesic, A.S. 1972. Expansion of cavities in infinite soil mass. *J. Soil Mech. And Found. Div., ASCE*, 98 (3): 265–290.

Vucetic, M. & Dobry, R. 1991. Effect of Soil Plasticity on Cyclic Response. *Journal of the Geotechnical Engineering Division, ASCE* Vol. 117, No. 1. Jan: 89–107.

Cone Penetration Testing 2018 – Hicks, Pisanò & Peuchen (Eds)
© 2018 Delft University of Technology, The Netherlands, ISBN 978-1-138-58449-5

A state parameter-based cavity expansion analysis for interpretation of CPT data in sands

P.Q. Mo
China University of Mining and Technology, Xuzhou, China

H.S. Yu
University of Leeds, Leeds, UK

ABSTRACT: Cone Penetration Testing (CPT) serves as a useful in-situ tool for site investigation and soil characterization, while the end-bearing and shaft capacities of driven piles could be directly related to the CPT measurements. In terms of interpretation of CPT data, state parameter concept has been employed largely owing to its good indication of soil behaviour at different stress levels and densities. Drained cavity expansion solution in a unified state parameter model for clay and sand (CASM) is adopted in this paper for the applications to CPT in sands regarding to in-situ soil state. The effects of initial stress condition, friction angle and soil compressibility on the correlations between cone tip resistance, sleeve friction and state parameter are presented and discussed. The proposed method indicates the influence of initial state parameter on the evaluation of normalised penetration resistance, and the state parameter is directly related to the soil behaviour type index. The analysis contributes to the theoretical background of the framework for interpretation of CPT data.

1 INTRODUCTION

The cone penetration test (CPT) has become a widely used in situ soil testing method, owing to its repeatability and accuracy at relatively low cost (IRTP, 1999; Robertson, 2009; Shuttle & Jefferies, 1998). Interpretation of CPT data aims to obtain soil parameters from the CPT continuous soundings by solving the inverse boundary value problem, which is usually replaced by empirical correlations determined from calibration chamber tests. Based on geometric similarity, CPT-based design methods for driven piles have been developed with examination of relationships between cone tip resistance and pile capacity in siliceous sands (e.g. Fugro-05, ICP-05, NGI-05, UWA-05). However, penetration mechanism is not well understood yet because penetration in soils is a complicated process in which soil flows around the penetrometer, large strains and stress distributions are generated, together with the hardening/softening of soils. In consideration of a soil model with strain hardening, numerical simulations have been conducted to analyze various boundary value problems, including cone penetration test and pile installation (e.g. Dijkstra et al., 2007; Kouretzis et al., 2014; Ahmadi & Golestani Dariani, 2017), while analytical solution is rather difficult and limited. In terms of available analytical solutions, cavity expansion methods have been proved to be suitable for analysis of penetration problems (Mo et al., 2017; Mo & Yu, 2017), whereas numerical techniques are usually employed for more realistic situations (Shuttle & Jefferies, 1998; Suzuki & Lehane, 2015).

Compared to the conventional interpretation methods using the relative density or void ratio, the state parameter (ψ, difference between the void ratio in the current state and that at the critical state for the same stress condition, after Been & Jefferies, 1985, see Figure 1a) is of a more fundamental importance to practicing engineers due to its correlations with friction/dilation angles derived from the critical state soil mechanics, as well as some indication of potential soil liquefaction. The use of state parameter has also been reported by many researchers for interpreting CPT data (Been et al., 1986; Ghafghazi & Shuttle, 2008; Reid, 2015). The correlations between normalised cone tip resistance and initial state parameter were found to be arguably unique for sand with various conditions. The interpretation of CPT data with the state parameter concept is therefore preferred for characterizing sand behaviour, and the state parameter-based prediction of pile bearing capacity in sands using CPT measurements is potentially an effective approach. However, the current correlations for CPT data interpretation are still heavily

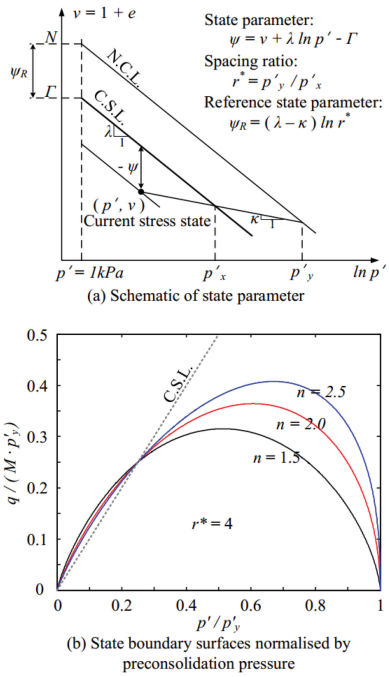

Figure 1. Illustration of CASM after Yu (1998): (a) schematic of state parameter, (b) state boundary surfaces.

relying on empirical methods, which remain the lack of theoretical explanations and hold the limitations for implication on variety of soil types.

This paper aims to develop the interpretation with a more sophisticated soil model and the cavity expansion theory, which could contribute to the establishment of framework for interpretation with following investigations. In this study, a newly developed drained cavity expansion solution is adopted for the investigation of CPT data in sands using state parameter concept. After applying the large strain analysis with critical state soil model CASM, the cone tip resistance is predicted from the spherical cavity expansion solution. The effects of initial stress condition, friction angle, and soil compressibility are investigated in associated with the influence of initial state parameter.

2 CAVITY EXPANSION SOLUTION AND INTERPRETATION APPROACH

In this study, the drained cavity expansion solution in sands is provided by Mo & Yu (2018), in which the unified state parameter soil model CASM (Yu, 1998) is applied. The model, adopting the critical state concept, was developed based on the original Cam-clay model and formulated in terms of the state parameter, which is illustrated in Figure 1(a). Comparing to the original Cam-clay model, two additional parameters (spacing ratio r^* and stress-state coefficient n) were introduced to propose a general stress-state relation for both clay and sand by modifying the state boundary surfaces (see Figure 1b), which was then validated to capture overall behaviour of various soils under both drained and undrained loading conditions. The details on parameter determination and the comparisons with experimental data could also be found in Yu (1998).

Based on the developed cavity expansion solution in sandy soils, an initial cavity with a radius of a_0, embedded in an infinite geomaterial with isotropic stress condition, is uniformly expanded to an arbitrary size of a. The increased cavity pressure corresponding to the process of expansion is thus utilized for the analyses of cone tip resistance and sleeve friction, where spherical cavity expansion is assumed around the cone tip based on the analogous observation of soil deformation (Mo et al., 2015). The penetration of a probe is modeled as an expansion of cavity with radius from 0.1mm (equivalent to grain size level) to 17.8mm (radius of a standard CPT probe), and the relation between cavity pressure and cone tip resistance can be given by Eq. (1), following Ladanyi & Johnson (1974) and Suzuki & Lehane (2015).

$$q_c = \sigma_{r,wall,sph}^{a_0 \to a} \times \left(1 + \sqrt{3}\tan\phi_{sph}\right) \tag{1}$$

The sleeve friction (τ_s) of penetrometer could be predicated by Eq. (2), following the UWA-05 CPT based design method for driven piles in siliceous sand (Xu, 2007).

$$f_s = \left\{0.03\, q_c \left(h/D\right)^{-0.5} + 4G_0 \Delta y / D\right\} \times \tan\delta_y \tag{2}$$

where h is penetration depth of the probe, G_0 is shear modulus from the cavity expansion solution ($G_0 = [3(1-2\mu)\nu_0\, p_0] / [2(1+\mu)\,\kappa]$, following Mo & Yu, 2018), Δy is the radial displacement during penetrometer loading $\Delta y \sim 0.02$ mm), and δ_y is the interface friction angle ($\delta_y \sim 15°$).

3 PARAMETRIC STUDY FOR INTERPRETATION OF CPT DATA

As the solution utilized the state parameter as an important property determining soil behaviour, the interpretation of CPT data gains its benefits. Previous experimental and numerical study have also shown the correlations between state parameter and CPT measurements. Results of paramet-

ric study are presented in this section to investigate the effects of initial stress condition, friction angle, critical state parameter λ, as well as the initial state parameter. The sand model parameters in this paper are selected for Ticino sand (after Yu, 1998 and Mo & Yu, 2018): $\mu = 0.3$, $\Gamma = 1.986$, $\lambda = 0.024$, $\kappa = 0.008$, $\phi_{tx} = 32°$, $r* = 108.6$, $n = 2.0$. The effect of initial state parameter on the computed behaviour of drained triaxial compression tests on Ticino sand was provide by Yu (1998) and shown in Figure 2. The selection of Ticino sand is also because of its extensively investigations from laboratory elementary tests and CPT tests. For spherical scenario, the critical-state friction angle is assumed as $\phi_{sph} = \phi_{tx}$, and the friction constant is then determined with $M = 6\sin\phi_{sph} / (3 - \sin\phi_{sph})$. State parameter ($\psi$) is taken as an important indicator for the interpretation of CPT data, and the variation of ψ_0 ranges from -0.3 to 0.075 ($\psi_R = (\lambda - \kappa)\ln r^* = 0.075$ as the reference state parameter) in this study. Note that sand with negative value of ψ_0 is located at the 'dry' side of the critical state line, indicating a denser initial condition with a high value of overconsolidation ratio. Figure 3 shows the stress paths of cavity expansion with variation of initial state parameter for tests under a constant initial stress

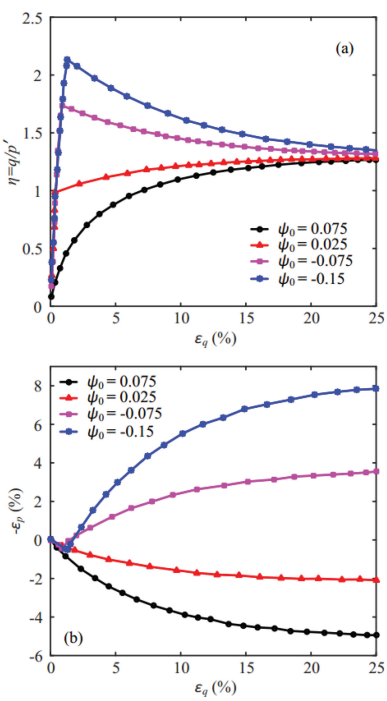

Figure 2. Estimation of responses of drained triaxial compression tests for Ticino sand: (a) stress ratio against deviatoric strain; (a) volumetric strain against deviatoric strain (after Yu, 1998).

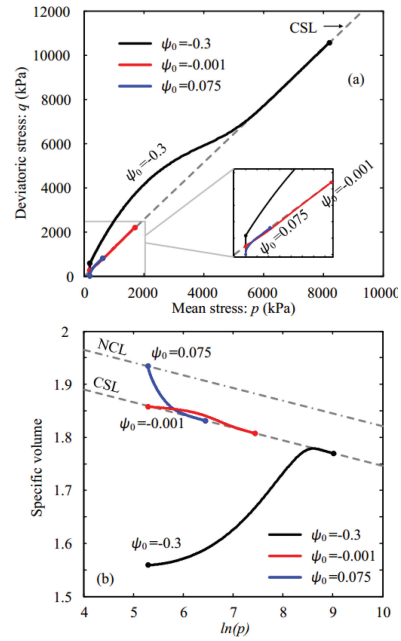

Figure 3. Relationships of (a) spherical cavity pressure and (b) normalised cone tip resistance against initial state parameter with various initial stress condition.

condition $p_0 = 200\ kPa$. The ultimate stresses after expansion decrease with the state parameter, and the ultimate specific volume is higher for a larger value of initial state parameter. The difference on stresses is over an order of magnitude from $\psi_0 = -0.3$ to $\psi_0 = 0.075$ thus the influence of initial state parameter is obviously significant.

3.1 *Effect of initial stress condition*

The effect of initial stress condition is examined by varying p_0 from 200 kPa to 1000 kPa in this section. Increased initial stress condition relates to a high magnitude of shear modulus, resulting to the growth of spherical cavity pressure, as presented in Figure 4(a). The decrease of cavity pressure with state parameter shows non-linear behaviour. Applying the correlation between q_c and $\sigma_{r,wall,sph}$ (Eq. 1), the normalized cone tip resistance is defined as Eq. (3), according to Robertson (1990) and Been et al. (1986).

$$Q_{t1} = \frac{q_c - p_0}{p_0} \tag{3}$$

It can be found from Figure 4(b) that the normalized cone tip resistance is hardly affected by the initial stress condition, in contrast to the trends

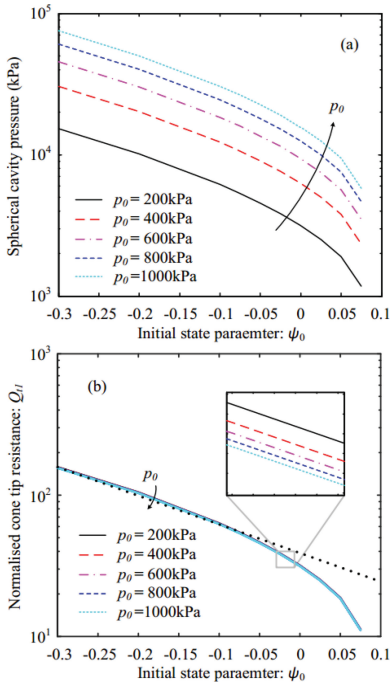

Figure 4. Relationships of (a) spherical cavity pressure and (b) normalised cone tip resistance against initial state parameter with various initial stress condition.

of cavity pressure. This phenomenon indicates the direct relationship between Q_{t1} and ψ_0, irrespective of stress condition and relative density, which is also confirmed by numerical simulation of cone penetration tests (Kouretzis et al., 2014). The linear expression between ψ_0 and $\log Q_{t1}$ was reported by Been et al. (1988), providing an expression of $Q_{t1} = k \cdot \exp(-m \cdot \psi_0)$. The results show that m value increases with ψ_0, and linear curve fitting provides the soil-specific coefficients as: $k = 39$ and $m = 4.67$ for $\psi_0 < -0.05$.

Considering the nonlinear increase of q_c with p_0 for various soils, the normalization of cone resistance is suggested with a variable stress exponent n (approximated by the SBTn index and effective overburden stress, after Robertson, 2009), where

$$Q_{tn} = \frac{(q_c - p_0)/p_a}{(p_0/p_a)^n} \tag{4}$$

and p_a is the atmospheric pressure. The normalised tip resistance Q_{tn} shows a slight decrease with initial stress condition (see Figure 5). Finite element simulation of calibration chamber testing in Ticino 4 sand was reported by Ghafghazi & Shuttle (2008), indicating the relation between Q_{tn}

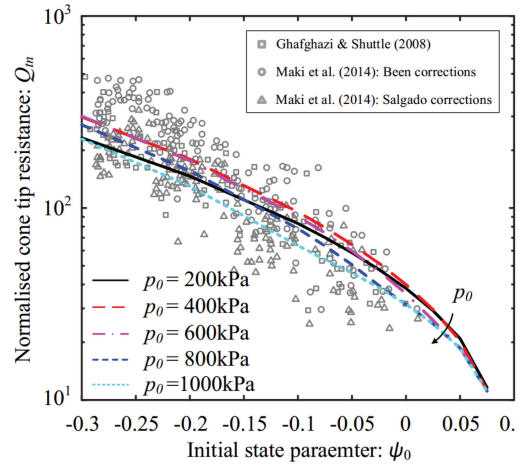

Figure 5. Normalised cone tip resistance Q_{tn} against initial state parameter with comparisons of numerical simulation for Ticino sand.

and ψ_0. Additional, experimental data from Maki (2014) was originally derived from calibration chamber tests of Ticino sand by Been et al. (1986), and both calibration chamber corrections by Been et al. (1986) and Salgado et al. (1998) were applied. The predictions on the basis of the proposed cavity expansion solution shows good comparisons with experimental and numerical results, as illustrated in Figure 5. In short, the determination of state parameter based on the normalised cone tip resistance seems to be obtained from the correlations as long as the soil parameters are known. This also confirms the direct interpretation of in situ state of soil based on the CPT data.

Together with the prediction of sleeve friction (Eq. 2), the SBT chart (Robertson, 2009) is employed to examine the variation of stress condition and initial state parameter, as shown in Figure 6. The normalised sleeve friction is defined as $F_r = \left[f_s / (q_c - p_0) \right] \times 100\%$. The effect of p_0 *seems to be negligible in* $Q_{tn} - F_r$ *space, whereas higher state parameter results in a smaller value of Qtn* and a larger F_r *for a given stress condition. When the variation of* ψ_0 from -0.3 to 0.075, the trend is almost linear in the SBT chart, with increase of the soil behaviour type index, I_c, as defined by Robertson (2009).

3.2 *Effects of friction angle and critical state parameter* λ

The measured CPT data is normally interpreted to obtain soil properties, including friction angle, density and elastic parameters. Since the concept of critical state has enabled the significant

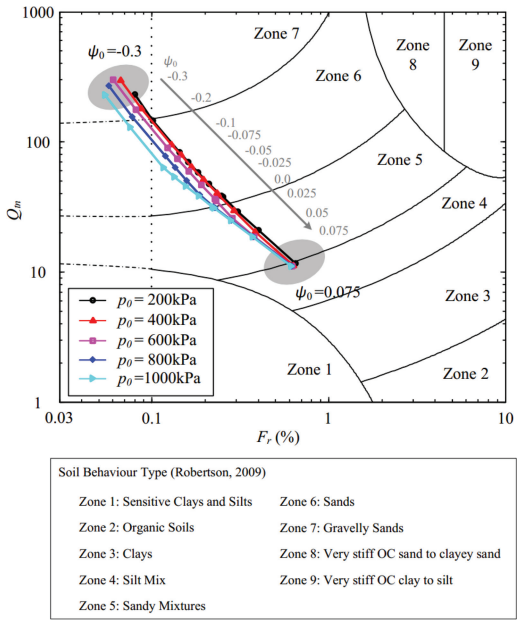

Figure 6. Effects of initial stress condition and state parameter on the SBT chart.

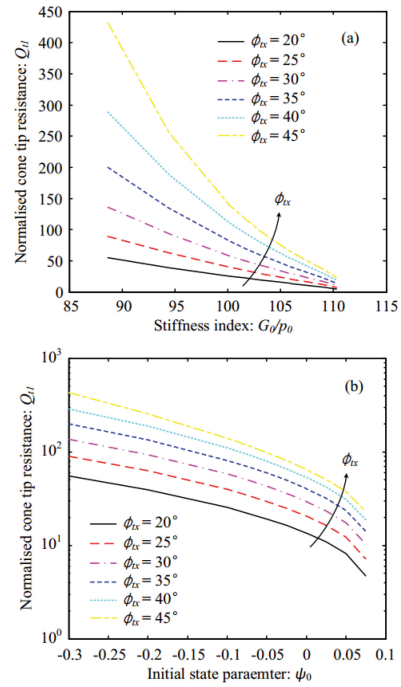

Figure 7. Effect of friction angle: (a) normalised cone tip resistance against stiffness index, (b) normalised cone tip resistance against initial state parameter.

development of soil constitutive models with consideration of volumetric changes, the critical state parameters are becoming important to geotechnical engineers. Friction angle is correlated to the critical state friction ratio M. The influence of friction angle on the normalised cone tip resistance is examined and presented in Figure 7. Note that this test series keeps the constant initial confining stress with $p_0 = 500kPa$. Based on the aforementioned definition of G_0, the stiffness index G_0 / p_0 is directly related to initial specific volume, and thus to initial state parameter with constant p_0. The trends in both $Q_{t1} - G_0 / p_0$ and $Q_{t1} - \psi_0$ spaces show non-linear increases of Q_{t1} with friction angle.

Critical state parameter λ (slope of critical state line in $v - \ln p$ space) indicates the soil compressibility, and the impact of compressibility was reported to be significant to CPT data. Shuttle & Jefferies (1998) noted that the relationship between Q_{t1} and ψ_0 is weakly reliance on λ, whereas Reid (2015) stated that the relationship of Q_{t1} and ψ_0 is dependent of λ and M, with λ the dominant factor. The effect of λ is investigated in this study with interpretation of state parameter, as illustrated in Figure 8(a). The significant influence on the relations between Q_{t1} and ψ_0 is observed, and the decreasing rate of tip resistance with state parameter decays as the value of λ increases. When a linear curve fitting in $Q_{t1} - \psi_0$ space is applied,

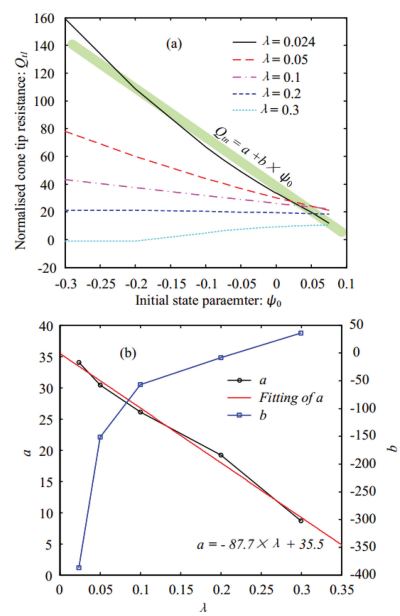

Figure 8. Effect of friction angle: (a) normalised cone tip resistance against stiffness index, (b) normalised cone tip resistance against initial state parameter.

the parameters varying with λ are shown in Figure 8(b). The results also provide the possible estimation of λ based on CPT data, in addition to sample tests in laboratory.

In general, it can be found the clear indication of initial state parameter for the interpretation of CPT data in sands. While the results of CPT measurements are dependent of soil inherent and state parameters, further study on variety of sands is still needed, together with the analysis of sleeve friction and soil behaviour type index. The cavity expansion solution with an applicable soil model and concept of state parameter could serve as an effective tool and provide a theoretical background for the interpretation of CPT data and CPT-based pile design methods. However, the interpretation of CPT data is actually dealing with the estimation of soil properties, corresponding to an inverse analysis of cavity expansion. By adopting a more sophisticated soil model like CASM, the number of soil parameters is usually larger than that of measurements, and therefore the derivations of direct correlations between CPT data and soil parameters are not available. Further techniques, including stochastic analysis, probabilistic analysis and neural network methods, are required to incorporate with the current analysis for the development of framework for interpretation of CPT data.

4 CONCLUSIONS

A state parameter based method was developed in this paper for the interpretation of CPT data using cavity expansion solution, which could also be extended to the prediction of bearing capacity of closed-ended piles. Drained cavity expansion solution in a unified state parameter model was adopted for the analyses owing to the benefits of state parameter concept. The presented investigation showed that the relationship between normalised cone tip resistance and state parameter is independent of stress condition, whereas the effects of friction angle and soil compressibility constant are relatively significant. The prediction of sleeve friction indicated that the effect of stress condition *is nearly negligible and the state parameter seems to increase with the* soil behaviour type index in the exponent space of normalised penetration resistance against normalised sleeve friction. The derivation of state parameter based on CPT measurements was therefore obtained from the correlations as long as the soil model parameters are known. To obtain correlations between CPT data and soil properties, further study on variety of soils is required with more investigations on penetration resistance and sleeve friction, together with probabilistic methods. It was concluded that the state parameter based cavity expansion analysis with the unified soil model provides further insight into our understanding of the measured results from in-situ soil tests and pile foundations.

ACKNOWLEDGEMENTS

The first author would like to acknowledge financial support from Natural Science Foundation of Jiangsu Province (no. BK20170279), China Postdoctoral Science Foundation (no. 2017M621866), and Postdoc Research Funding of Jiangsu Province (no. 1701196B).

REFERENCES

Ahmadi, M.M. & Golestani Dariani, A.A. 2017. Cone penetration test in sand: A numerical-analytical approach. Computer and Geotechnics 90: 176–189.

Been, K. & Jefferies, M. G. 1985. A state parameter for sands. Geotechnique 35, No. 2: 99–112.

Been, K., Crooks, J. H. A., Becker, D. E. & Jefferies, M. G. 1986. The cone penetration test in sands: Part I, state parameter interpretation. Geotechnique 36, No. 2, 239–249.

Dijkstra, J., Broere, W. & van Tol, A.F. 2007. Numerical simulation of the installation of a displacement pile in sand. In: Pande Pietruczak, editor. Numerical models in geomechanics NUMOG X. Taylor and Francis; p. 461–6.

Ghafghazi, M. & Shuttle, D.A. 2008. Interpretation of Sand State from Cone Penetration Resistance. Géotechnique, 58(8): 623–634.

IRTP. 1999. International reference test procedure (IRTP) for the cone penetration test (CPT) and the cone penetration test with pore pressure (CPTU). Proceedings of the 12th European conference on soil mechanics and geotechnical engineering, pp. 2195–2222. Rotterdam, the Netherlands: Balkema.

Kouretzis, G.P., Sheng, D.C. & Wang D. 2014. Numerical simulation of cone penetration testing using a new critical state constitutive model for sand. Computer and Geotechnics 56: 50–60.

Ladanyi, B. & Johnston, G. H. 1974. Behaviour of circular footings and plate anchors embedded in permafrost. Canadian Geotechnical Journal 11: 531–553.

Maki, I. P., Boulanger, R. W., DeJong, J. T. & Jaeger, R. A. 2014. State-Based Overburden Normalization of Cone Penetration Resistance in Clean Sand. Journal of Geotechnical and Geoenvironmental Engineering, 140(2): 1–12.

Mo, P. Q. & Yu, H. S. 2017. Undrained cavity expansion analysis in a unified state parameter model for clay and sand. Géotechnique 67(6): 503–515.

Mo, P. Q. & Yu, H. S. 2018. Drained cavity expansion analysis with a unified state parameter model for clay and sand. Canadian Geotechnical Journal. DOI: 10.1139/cgj-2016–0695.

Mo, P. Q., Marshall, A. M. & Yu, H. S. 2015. Centrifuge modelling of cone penetration tests in layered soils. Géotechnique, 65(6): 468–481.

Mo, P. Q., Marshall, A. M. & Yu, H. S. 2017. Interpretation of Cone Penetration Test Data in Layered Soils Using Cavity Expansion Analysis. Journal of Geotechnical and Geoenvironmental Engineering, 143(1): 04016084–1-12.

Randolph, M. F., Dolwin, J., & Beck, R. 1994. Design of driven piles in sand. Géotechnique, 44(3): 427–448.

Robertson, P. K. 1990. Soil classification using the cone penetration test. Canadian Geotechnical Journal 27(1): 151–158.

Robertson, P. K. 2009. Interpretation of cone penetration tests-A unified approach. Can. Geotech. J., 46(11): 1337–1355.

Salgado, R., Mitchell, J. K. and Jamiolkowski, M. 1998. Calibration chamber size effects on penetration resistance in sand. Journal of Geotechnical and Geoenvironmental Engineering 124(9): 878–888.

Shuttle, D. & Jefferies, M. 1998. Dimensionless and unbiased CPT interpretation in sand. International Journal for Numerical and Analytical Methods in Geomechanics 22: 351–391.

Suzuki, Y. & Lehane, B.M. 2015. Analysis of CPT end resistance at variable penetration rates using the spherical cavity expansion method in normally consolidated soils. Computers and Geotechnics 69: 141–152.

Vesic, A. S. 1977. Design of pile foundations. Technical report, Transport Research Board.

White, D. J. 2003. Field measurements of CPT and pile base resistance in sand. Technical Report CUED/D-SOILS/TR327, University of Cambridge.

Xu, X. T. 2007. Investigation of the end bearing performance of displacement piles in sand. PhD thesis, The University of Western Australia.

Yu, H. S. 1998. CASM: A unified state parameter model for clay and sand. Int. J. Numer. Analyt. Methods Geomech. 22, No. 8: 621–653.

Taylor & Francis
Taylor & Francis Group
http://taylorandfrancis.com

Cone Penetration Testing 2018 – Hicks, Pisanò & Peuchen (Eds)
© 2018 Delft University of Technology, The Netherlands, ISBN 978-1-138-58449-5

Permeability estimates from CPTu: A numerical study

L. Monforte, M. Arroyo & A. Gens
Universitat Politècnica de Catalunya—BarcelonaTech, Barcelona, Spain

C. Parolini
Politecnico di Milano, Milan, Italy

ABSTRACT: Realistic numerical simulations of CPTu in soft soils are now becoming possible thanks to methods like the Particle Finite Element Method (PFEM). They may be used to systematically explore the traditional methods of CPTu interpretation, identify their limitations and propose alternatives. This paper discusses a series of tests simulation CPT installation and subsequent dissipation tests in soils represented by the Modified Cam Clay model. Simulation outputs obtained for different input permeabilities are examined to obtain direct estimates of permeability using different methods proposed in the literature; additionally, a method to estimate the hydraulic conductivity during the piezocone penetration is also used. These estimates are then compared with the known input permeability value to assess their reliability.

1 INTRODUCTION

The cone penetration test (CPTu) is one of the most widely used geotechnical site investigation methods. During the test an instrumented cone is pushed into the ground at a controlled rate. Tip resistance and sleeve friction are always recorded, and, very frequently, the pore water pressure at several standard positions is also measured. From these measurements, stratigraphy and constitutive soil parameters are estimated based mostly on empirical correlations (Robertson, 2009).

Traditionally, the evaluation of coefficients of consolidation of fine grained soils has been of much interest for geotechnical design. CPTu based methods for obtaining consolidation coefficients were researched intensively almost since the instrument became available (Tortensson, 1977; Baligh & Levadoux, 1986; Teh & Houlsby, 1991). The operational procedure requires a dissipation test: the cone is halted and the variation in time of water pressure is measured. The interpretation of dissipation tests frequently needs other constitutive parameters that also require approximation.

A coefficient of consolidation combines unit weight, permeability and soil stiffness. Because soil stiffness is dependent, amongst other variables, on stress level, strain level and loading path relating co-efficients of consolidation obtained from CPTu dis-sipation curves with those controlling behavior in a given geotechnical problem is not always easy.

When, as it is increasingly frequent, numerical methods are used to study consolidation problems models typically require separate inputs for stiffness and permeability (following common usage we employ here "permeability" instead of the more precise "hydraulic conductivity"). Consolidation coefficients may be then bypassed and the designer will be more interested in permeability, a parameter that has also direct application in other geotechnical problems (dewatering, drainage design, hydraulic heave, etc.). It is therefore increasingly necessary to evaluate permeability from CPTu records.

In this work, the current available procedures to evaluate permeability form CPTu results are assessed using results from numerical simulations of piezocone penetration and dissipation.

2 ESTIMATING PERMEABILITY WITH CPTU

2.1 *Methods based on dissipation results*

Several methods have been proposed to estimate permeability from piezocone records. Most of them require a dissipation test and relate the time to half dissipation, t_{50}, to permeability, k.

Parez & Fauriel (1988) presented data supporting an empirical relation between these two parameters. The relation was presented in graphic form; Mayne (2007) approximated it by

$$k_h = \left(\frac{1}{251\, t_{50}} \right)^{1.25} \tag{1}$$

where t_{50} is expressed in s and k_h is a laboratory measured coefficient of horizontal permeability,

expressed in cm/s. Robertson et al. (1992) presented another graphical empirical relationship between the same variables, showing larger scatter.

Robertson (2010) presented a formula that, based on results by Houlsby & Teh (1991), summarized the relationship between coefficient of horizontal consolidation, c_h, and t_{50} as follows

$$c_h = 1.67 \cdot 10^{-6} \cdot 10^{1-\log(t_{50})} \tag{2}$$

where t_{50} has units of minutes and c_h of m²/s. Horizontal permeability is then obtained as

$$k_h = \frac{\gamma_w}{M} 1.67 \cdot 10^{-6} \cdot 10^{1-\log(t_{50})} \tag{3}$$

where γ_w is the unit weight of water and M a 1-D constrained modulus. Robertson (2010) proposed to estimate M from the CPT results. The formula relevant here (valid for $Q_t < 14$) reads:

$$M = \sigma'_{v0} \, Q_t^2 \tag{4}$$

where Q_t is a normalized net tip resistance that, for fine grained soils, is given by

$$Q_t = \frac{q_t - \sigma_{v0}}{\sigma'_{v0}} \tag{5}$$

2.2 *On-the-fly method*

Building up on previous work by Elsworth and Lee (2005, 2007), Chai et al (2011) proposed an explicit equation to evaluate the hydraulic conductivity of soils from piezocone soundings performed at undrained or partially drained conditions. The method does not require a dissipation phase, as it estimates permeability directly from the product $Q_t B_q$, of normalized tip resistance and normalized excess pore pressure,

$$B_q = \frac{\Delta u}{q_t - \sigma_{v0}} \tag{6}$$

3 NUMERICAL SIMULATIONS

3.1 *Simulation method*

Numerical simulations have been carried out by means of the numerical code G-PFEM (Geotechnical Particle Finite Element Method), specifically developed for the analysis of large strain contact problems in geomechanics (Monforte et al, 2017, 2018). The code is able to accurately simulate the interaction between fluid-saturated porous media and rigid structures.

Table 1. Constitutive parameters adopted for the simulation of the CPT penetration in a Modified Cam Clay soil.

κ	λ	e_0	G (kPa)	M
0.02	0.2	1.94	10000	1.07
OCR	K_0	ρ_s(kg/m³)	ρ_w(kg/m³)	
1.1	0.765	2000	1000	

The material is described by a Modified Cam Clay constitutive model. The cone has the standard dimensions (R = 1.78 cm; cone angle 60°) and is assumed rigid and smooth. Soil parameters, listed in Table 1, describe a quasi-normally consolidated clayey deposit.

At the beginning of the simulation the cone is wished-in-place in the tip at a depth of 2 cone radii. The weight of the soil is considered and, at the top boundary a vertical stress of 100 kPa is imposed. The penetration at the standard velocity (v = 0.02 m/s) is simulated to the depth of z = 20R. After stopping penetration a dissipation tests is simulated.

The results presented correspond to a set of simulations in which the permeability is varied five orders of magnitude (from $k = 10^{-7}$ m/s to 10^{-12} m/s). For that range of permeability the penetration phase takes place in practically undrained conditions. The normalized cone velocity (Schneider et al, 2007) for the simulation with the higher permeability is $V = 47.8$. Permeability is assumed isotropic.

3.2 *Simulation results: penetration phase*

Figure 1 presents the penetration curves. Because of the continuous remeshing that is characteristic of the PFEM approach numerically induced oscillations appear on the penetration curves. These have been smoothed in the penetration curves using a moving average over a distance of 1R.

The results show that, within this undrained range, tip resistance and pore pressure show little sensitivity to permeability. Indeed differences in net cone resistance at steady state between simulations are within a range of 6%. For all cases volumetric deformation was minimal, thus confirming the expected undrained behaviour.

Table 2 presents the main results of the tests for the 6 different simulations. In particular, the table shows the normalized tip resistance and pore water pressure ratio, Q_t and B_q respectively. To filter out remeshing induced noise the steady state values for each test are obtained as the average value for depths between 10 and 20 penetration radius.

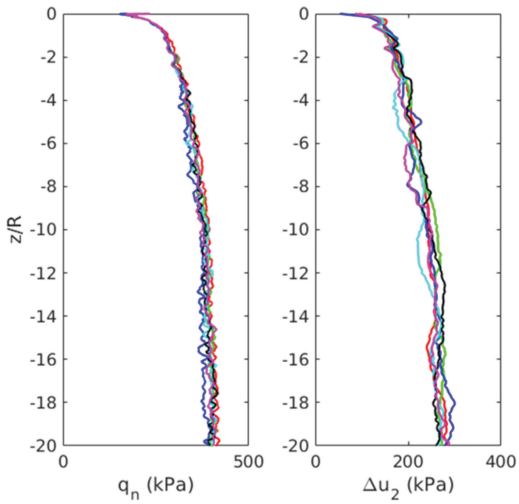

Figure 1. Computed net cone resistance and excess water pressure at the u_2 position in terms of the normalized penetration, z/R.

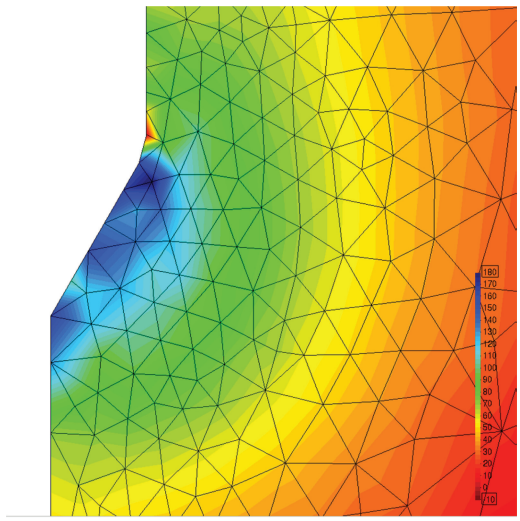

Figure 2. Excess water pressure in the vicinity of the cone.

Table 2. Results of the simulation of the Cone penetration test.

K (m/s)	Q_t	B_q	t_{50} (s)
10^{-7}	3.86	0.64	$1.38 \cdot 10^{1}$
10^{-8}	3.79	0.65	$1.43 \cdot 10^{2}$
10^{-9}	3.61	0.61	$1.83 \cdot 10^{3}$
10^{-10}	3.77	0.58	$1.79 \cdot 10^{4}$
10^{-11}	3.75	0.63	$1.61 \cdot 10^{5}$
10^{-12}	3.77	0.63	$1.60 \cdot 10^{6}$

3.3 *Simulation results: Dissipation phase*

Figure 3(a) depicts the dissipation curves at the u_2 position for all the simulated cases. As expected the curves shift to higher times as permeability decreases. The value of the initial excess pore pressure varies significantly (between 220 and 310 kPa). The reason beneath this variation is numerical: pore pressure is only available at nodes, continuous remeshing results in slight variations in the relative node positions with respect to the cone shoulder (Figure 2). This means that the record of dissipation, always interpolated from the nodes closest to the u_2 position, corresponds to slightly different positions in different meshes. This numerical procedure induces variability which is compounded by the well-known fact (Teh & Houlsby, 1991) that the highest gradients of excess pore pressure during penetration are induced at the cone shoulder position.

To overcome this problem the reference value for dissipation curves is taken as the steady-state

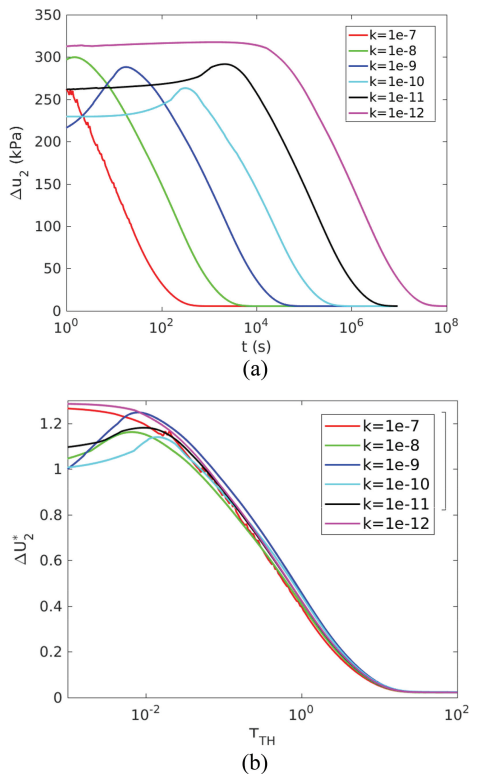

Figure 3. Dissipation curves at the u_2 position. On the top, (a), results of the simulation; on the bottom, (b), time is normalized by the method proposed by Teh & Houlsby (1991) whereas the water pressure is normalized using the steady state value during penetration.

value for the penetration phase, Δu_{2ss}. The time to half dissipation, t_{50} corresponds to the time in which the dissipation curve reaches half Δu_{2ss} The values of t_{50} thus obtained are reported in Table 2.

Figure 3(b) shows the dissipation curves where the excess water pressure has been normalized by Δu_{2ss}; additionally, time has been normalized according to the formula proposed by Teh & Houlsby (1991):

$$T_{TH} = \frac{c_v\, t}{r\, I_r^{0.5}} \tag{7}$$

where c_v is the coefficient of consolidation and I_r is the rigidity index. For simplicity, the values of c_v and I_r corresponding at the initial state are considered. It appears that the normalization works well in that all the curves converge after the normalized excess pore pressure passes below 0.95.

4 ESTIMATION OF PERMEABILITY DURING PENETRATION

Elsworth and Lee (2005, 2007) proposed a methodology to estimate the permeability of soils during cone penetration based on the product of the normalized resistance and normalized excess water pressure. Based on this product, a non-dimensional index, directly proportional to the permeability, might be evaluated. The authors (Elsworth and Lee, 2007) restricted the applicability of the method to partially drained conditions, thus excluding materials such as those considered here. Using cavity expansion theory they identified the transition from undrained to partially drained conditions in the range $1.2 < Q_t B_q < 5.6$. The precise value of this limit depends on soil constitutive parameters and the vertical effective stress.

Chai et al (2011) extended the previously highlighted interpretation technique to practically undrained conditions. The authors linked the product of $Q_t B_q$ to a dimensionless hydraulic conductivity index $K_D = 2k\sigma'_{v0}\left(r\,\gamma_w v\right)^{-1}$ (where r is the probe radii and $v$is the penetration velocity) through a bilinear model, shown in Figure 4. As such, the permeability may be directly estimated from the product of two cone normalized metrics. The authors validated their model with a set of field and laboratory data from clay sites.

Figure 4 shows the numerical results plotted in the interpretation chart proposed by Chai et al (2011). The numerical results plot in an almost straight line: the mean value of the product $Q_t B_q$ is 2.34 and the standard deviation is 0.12; this product does not show any trend with permeability. By using this method, a permeability equal to $k = 1.17 \cdot 10^{-8}$ m/s is estimated for the mean value

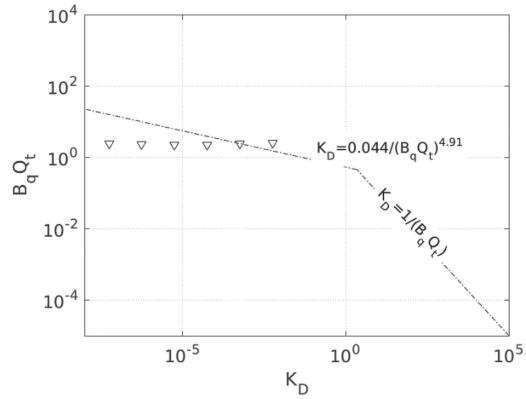

Figure 4. Numerical results in the $K_D - Q_t B_q$ interpretation chart proposed by Chai et al (2011).

of the product $Q_t B_q$. This value is in the range of permeability values that separate undrained conditions from partially-drained conditions.

5 ESTIMATION OF PERMEABILITY DURING DISSIPATION

5.1 *Parez & Fauriel method*

In Figure 5 the values of t_{50} are plotted against the input permeability. The figure also includes the correlation proposed by Parez & Fauriel as formulated by Mayne (2007). The estimated value of permeability is always within a factor of 5 from the input value.

The correlation underestimates somewhat the larger values of permeability and does the opposite for the smaller values. Most permeability values in the database supporting the original correlation were close to 10^{-6} cm/s and this is also where the fit with the numerical results appears better.

5.2 *Robertson method*

Figure 6 plots the numerical results in the interpretation chart proposed by Robertson (2010). The permeability vs half dissipation plots appear well aligned with the predicted trend, but offset from the theoretical position that would be assigned according to their compressibility.

In the upper panel, following the suggestion of Robertson, the constrained modulus is estimated based on the CPT penetration steady state values and Equation (4). In the lower panel the chart is directly labelled using values of constrained modulus.

The average value of Q_t for the simulations is 3.8 and the corresponding line is highlighted in the upper panel. It appears that the Robertson correla-

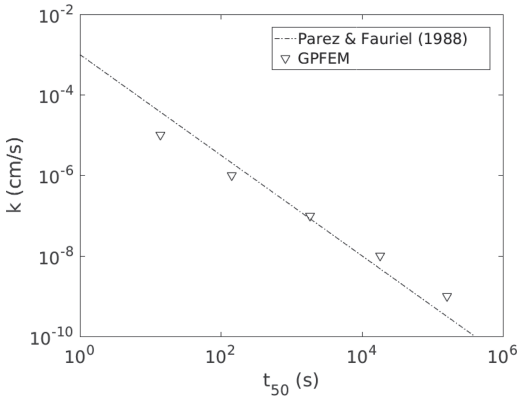

Figure 5. Comparison of numerical results with Parez & Fauriel (1988) correlation.

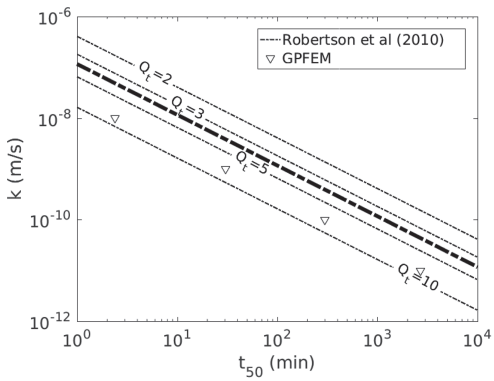

(a)

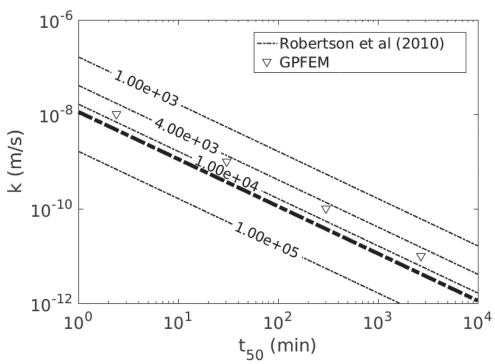

(b)

Figure 6. Numerical results in the $t_{50} - k$ interpretation chart proposed by Roberston et al. (2010). On top, approximating the constrained modulus by the CPT log. The thick line represents the mean normalized tip resistance obtained in the simulations, $Q_t = 3.76$. On the bottom the constrained modulus is directly an input parameter; the thick line stands for the input parameter of the numerical simulations.

tion, if applied in this manner, would estimate a permeability value about 4 times larger than the input value.

In the lower panel the line highlighted corresponds to the value of the tangent constrained modulus at initial state, which is $M = 1.45 \cdot 10^4$ kPa. In this case the correlation would underestimate the input permeability approximately by a factor of 3.

Of course, the tangent stiffness at the initial state is not representative of that of the soil after penetration, during the dissipation phase. Interestingly, the results obtained suggest that the operative stiffness during dissipation is smaller than that of the intact soil but larger than that obtained with the tip resistance correlation.

6 CONCLUSION

In this work, several techniques to interpret the permeability for clayey materials have been assessed against a set of data obtained from numerical analysis. The piezocone penetration and subsequent dissipation has been simulated in a quasi-normally consolidated Modified Cam Clay soil, in which the only parameter that has been changed is the permeability. In all the simulations practically undrained conditions are found.

Unfortunately, the results obtained do not support the on-the-fly technique proposed by Chai et al (2011). That may be a side effect of the approximations involved in the numerical solution; it is true, however, that the original range of application of the underlying theory was that of partially undrained penetration rather than fully undrained, as it is the case here. Exploration of this method in partially undrained conditions is ongoing.

On the other hand, dissipation-based methods appear far more sensitive to permeability. The simple correlation of Parez & Fauriel produces results that are in the correct order of magnitude. The more elaborate technique developed by Robertson (2010) improves slightly on those results, its limits essentially given by the difficulty in estimating the precise value of operative stiffness during consolidation.

All the results presented here assume isotropic permeability. Anisotropic permeability has been already implemented in G-PFEM (Hauser, 2017) and a systematic exploration of its effects on permeability estimates is ongoing. The effects of overconsolidation, plastic compressibility and strength are also topics of ongoing work.

ACKNOWLEDGMENTS

The financial support of the Ministry of Education of Spain through research grant BIA2014-59467-R is gratefully appreciated.

REFERENCES

Baligh, M.M., & Levadoux, J.N. (1986). Consolidation after undrained piezocone penetration. II: Interpretation. Journal of geotechnical engineering, 112(7), 727–745.

Chai, J.C., Agung, P.M.A, Hino, T., Igaya, Y. & Carter, J.P. 2011. Estimating hydraulic conductivity from piezocone soundings. *Géotechnique*: 61(8): 699–708.

Elsworth, D. & Lee, D.S. 2005. Permeability determination from On-the-Fly piezocone sounding. *Journal of Geotechnical and Geoenvironmental Engineering.* 131(5): 643–653.

Elsworth, D. & Lee, D.S. 2007. Limits in determining permeability from on-the-fly uCPT souding. *Géotechnique.* 57(8): 679–685.

Hauser, L. (2017) Numerical simulation of cone penetration tests using G-PFEM, MSc thesis, Technischen Universitat Graz

Mayne, P.W. (2007). Cone penetration testing (Vol. 368). Transportation Research Board.

Monforte, L. Arroyo, M., Carbonell, J.M. & Gens, A (2017a) Numerical simulation of undrained insertion problems in geotechnical engineering with the Particle Finite Element Method (PFEM). *Computers and Geotechnics.* 82:144–156.

Monforte, L. Arroyo, M., Carbonell, J.M. & Gens, A (2018) Coupled effective stress analysis of insertion problems in geotechnics with the Particle Finite Element Method. *Submitted*.

Monforte, L. Carbonell, J.M., Arroyo, M. & Gens, A (2017b) Performance of mixed formulations for the particle finite element method in soil mechanics problems. *Computational Particle Mechanics.* 4(3): 269–284.

Parez, L., & Fauriel, R. (1988). Le piézocône améliorations apportées à la reconnaissance des sols. Revue française de géotechnique, (44), 13–27.

Robertson, P.K. 2010. Extimating in-situ soil permeability from CPT & CPTu. *2nd International Symposium on Cone Penetration Testing*.

Robertson, P.K., Sully, J.P., Woeller, D.J., Lunne, T., Powell, J.J.M & Gillespie, D.G. 1992. Estimating coefficient of consolidation from piezocone test. *Canadian Geotechnical Journal*: 29: 539–550.

Schneider, J, Lehane, B.M & Schnaid, F. 2007. *Velocity effects on piezocone measurements in normally and over consolidated clays.* International Journal of Physical Modelling in Geotechnics. 7(2): 23–34.

Teh, C.I. & Houlsby, G.T. 1991.An analytical study of the cone penetration test in clay. *Géotechnique*: 41(1): 17–34.

Torstensson, B.A. (1977). The pore pressure probe. Nordiske Geotekniske Mote, 34(34), 1–34.

Cone Penetration Testing 2018 – Hicks, Pisanò & Peuchen (Eds)
© 2018 Delft University of Technology, The Netherlands, ISBN 978-1-138-58449-5

Pore pressure measurements using a portable free fall penetrometer

M.B. Mumtaz, N. Stark & S. Brizzolara
Virginia Polytechnic Institute and State University, Blacksburg, VA, USA

ABSTRACT: Pore pressure measurements during penetrometer deployments can complement measurements of strength resistance, and provide additional information about the soil. However, for high-velocity impacts, hydrodynamic forces lead to complex pressure recordings during the free fall and penetration. To investigate these effects, a Computational Fluid Dynamics model (CFD) has been developed. Based on initial results from the CFD model, a quasi-steady approach based on a velocity-dependent correlation is proposed to correct for dynamic effects and shape dependent pressure gradients acting on the FFP, and thus, also on the pore pressure readings. Finally, the results are discussed with regard to opportunities for future research.

1 INTRODUCTION

Free Fall Penetrometers (FFP) are gaining popularity as a convenient early site investigation tool for surficial seabed sediments (sediment depths on the order of decimeters to meters). Modern FFP frequently house pressure transducers in addition to other sensors. In conventional cone penetration testing (CPT), the pore pressure behavior of soils has been used to obtain insights into in-situ properties of the seabed such as strength measurement, relative density, stress history, consolidation and permeability of the soil (Lunne *et al.*, 1997). However, conventional CPTs can be difficult to deploy in nearshore environments or other areas of difficult access. Free fall penetrometers have the advantage of being easy to deploy, and some enable deployment from small vessels. This makes them considerably less costly than conventional CPTs. However, they are subject to hydrodynamic forces that affect the pressure measurements. This leads to complex pressure signals, especially during the free fall and during the penetration into surficial seabed layers at high velocities (> 2 m/s) (Lucking et al. 2017; Stark & Ziotopoulou 2017). Therefore, the accurate prediction of the hydrostatic pressure during the free fall is an important initial step to correct pore pressure recordings for hydrodynamic effects from high speed penetration. Additionally, the accurate prediction of water depth from the penetrometer may become crucial to assess consolidation of the soil, or the accurate impact position in areas of complex morphologies.

In summary, there is a need for correcting the pressure signal for fluid dynamic effects during high speed deployments of free fall penetrometers. The objective of this study is to investigate these effects using basic fluid dynamics principles during the descent through the water column and a velocity dependent quasi-steady correction.

2 BACKGROUND/METHODS

2.1 *Free-fall penetrometers*

The portable FFP *BlueDrop* was used for this study. It was designed with an approximately streamlined shape to stabilize and optimize the fall through the water column even in energetic hydrodynamic conditions. The penetrometer measures acceleration and tilt using 5 vertical and 2 horizontal micro-electro-mechanical system (MEMS) accelerometers with a sampling rate of 2 kHz. The data logging and analysis methods are explained in detail by (Stark *et al.*, 2015) and are not repeated here.

The FFP *BlueDrop* houses a pore pressure transducer that measures ambient pressures up to about 2 MPa. The sensor is located behind a pore pressure filter just behind the cone in the u_2 position. To ensure the proper saturation of the filter ring, it is submerged in water overnight before initiating the survey, or saturated using mineral oil. Fluids can be injected through a bypass from the inside through the filter ring to the outside to ensure full saturation. This study will focus on the analysis of the pressure data.

2.2 *Field survey*

A field survey was performed in the York River near Yorktown, VA (37.2388° N, 76.5097° W) in June 2017, with 30 free fall penetrometer deployments around the George Coleman Memorial

Bridge. Deployments were made by submerging the FFP in water from the side of a boat, and manually releasing the FFP with a rope attached to retrieve it later.

The surficial layers of the seabed in the surrounding area are mostly composed of soft organic mud (Hartman *et al.*, 2008). Low maximum deceleration values measured by the penetrometer during impact and penetration (more than 90% are lower than 10*g*, with *g* being gravitational acceleration), and visual observation of mud retrieved using a sediment sampler confirmed soft clays (Albatal & Stark, 2017).

2.3 *Fluid dynamic effects*

Lucking et al. (2017) argued that the pressure measurement during the free fall of the penetrometer through the water column is affected by fluid dynamic forces governed by the particular shape of the penetrometer and velocity. To obtain a pressure signal equal to ambient hydrostatic pressure, a correction must be applied. Bernoulli's principle explains the changes in pressure due to the motion of a fluid, and was applied here to attempt a correction (Lucking et al. 2017; Stark & Ziotopoulou, 2017). A quasi-steady approach, solving for the pressure distribution around the body, in steady viscous flow was adopted, thus ignoring added mass and transient viscous effects (on pressure forces).

Following the Galilean invariance principle, the problem of the body falling down at constant velocity v_B is assimilated to a problem of a fixed body immersed into an upward flow stream with uniform velocity v_B.

Due to the slender and approximately streamlined shape of the penetrometer (Figure 1), a thin boundary layer exists around the body. Outside this thin layer, the flow can be well approximated by an inviscid, irrotational flow of an incompressible fluid, such as water, and the Bernoulli equation can be applied, following the quasi-steady approximation of the transient flow.

Two points in the potential flow region were selected (Figure 1): Point 1 is chosen just outside the boundary layer, at the location of the pressure sensor on the penetrometer surface. Point 2 lies outside the perturbed flow field created by the probe, at the same water depth as point 1. The Bernoulli's equation between these two points reads:

$$p_1 + \frac{\rho v_1^2}{2} + \rho g z_1 = p_2 + \frac{\rho v_2^2}{2} + \rho g z_2 \tag{1}$$

where ρ is density of the fluid, p is pressure, v is velocity of fluid and z is elevation of the chosen point. The flow velocity of water at point 2 v, is equal to the free-stream velocity, v_B. The velocity v_1 of water particles immediately outside of the boundary layer at the location of point 1 can assumed to be a fraction α of the free-stream velocity, depending on the actual shape of the body and the position of the point 1:

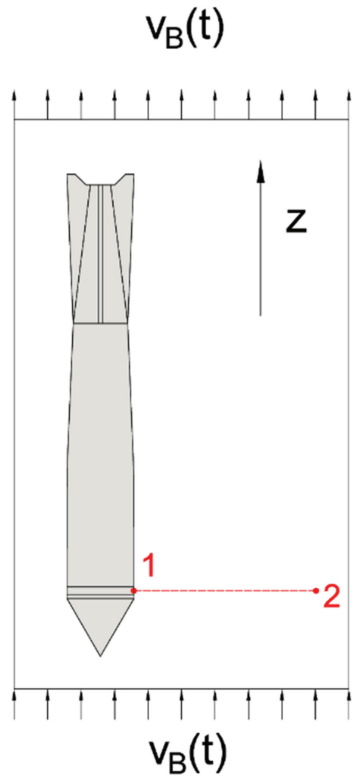

Figure 1. Schematic sketch of BlueDrop in a uniform flow stream of velocity v_B.

$$v_1(t) = \alpha \cdot v_B(t), \quad v_2 = v_B(t) \tag{2}$$

Point 1 and 2 are located at the same depth, so that:

$$z_1 = z_2 \tag{3}$$

$$\rho g z_1 = \rho g z_2 \tag{4}$$

Pressure at point 2, p_2 represents the hydrostatic pressure, whereas the pressure at point 1, p_1 will be affected by the motion of the fluid. So:

$$p_1 = p_{tot}; \quad p_2 = p_{stat} \tag{5}$$

Here, the pressure coefficient C_p is introduced, which is a non-dimensional measure of the pressure felt on an object in a flow field, calculated in steady

flow at point 1 of the given body. In potential flow, according to (1) with conditions (2) and (3), the pressure coefficient can be related to the local flow speed measured at point 1:

$$C_p = \frac{p_{dyn}}{\frac{1}{2}\rho v_B^2} = \frac{p_{tot} - p_{stat}}{\frac{1}{2}\rho v_B^2} = \frac{\frac{1}{2}\rho(v_B^2 - v_1^2)}{\frac{1}{2}\rho v_B^2}$$
$$= 1 - \frac{v_1^2}{v_B^2} = 1 - \alpha^2 \quad (6)$$

Simplifying (1):

$$p_{stat} = p_{tot} + \frac{1}{2}\rho(\alpha \cdot v_B)^2 - \frac{1}{2}\rho v_B^2 = p_{tot} + \frac{1}{2}\rho v_B^2(\alpha^2 - 1) \quad (7)$$

$$p_{stat} = p_{tot} - \frac{1}{2}\rho v_B^2 C_p \quad (8)$$

The second term on the right hand side of equation (8) represents the magnitude of the decrease in pressure due to the local velocity measured out of the boundary layer.

To investigate the relative pressures on the pressure transducer of *BlueDrop*, a computational fluid dynamic (CFD) model was developed. For the CFD simulation, the Galilean invariance was deployed, i.e. the body was kept fixed, and flow velocity varied in accordance with the changes in fall velocity of the penetrometer. The model was developed with the actual body geometry and was solved using a steady Reynolds-Averaged Navier-Stokes Equation (RANSE) solver for a flow of 6 m/s. The solution provides pressure coefficients C_p along the body of the FFP. A velocity of 6 m/s was chosen, because it was the most commonly observed maximum velocity achieved during the free fall of the FFP at the study site. In the field, the velocity started decreasing to about 4–5.5 m/s at impact after achieving a maximum, due to the increase in rope drag.

The pressure profile measured during a deployment is then corrected using equation 8. The velocity of the penetrometer v_B is calculated by the integration of the acceleration profile. The profile start point is set at the point of release when the acceleration starts. The profile end point is set at the point where the FFP comes to a rest in the sediment.

3 RESULTS

3.1 *CFD model results*

For this study, a series of steady flow solutions have been run on the body at different flow speeds with a fully turbulent RANSE segregated flow solver, using a two-layers (Rodi, 1991), realizable (Shih *et al.*, 1994) k-ε turbulence model. This type of turbulence model gives a good estimate of the thin boundary layer thickness around a streamlined body with prevalently attached flow. The finite-volume RANSE solver allows for non-structured polyhedral elements to discretize the physical domain. SIMPLE method is used to conjugate the pressure field and velocity field, and the AMG (Algebraic Multi-Grid) solver to accelerate the convergence of the solution of the momentum and continuity equations at each iteration. A total number of about 300 iterations were sufficient to reach convergence of the solution (i.e. stable residuals with relative magnitude lower than 10^{-6}). The solver has been validated in the past on a number of different hydrodynamic problems, including steady turbulent free surface flows around complex bodies such as ship hulls (Brizzolara & Villa, 2010) or un-steady flow around propellers (Gaggero *et al.*, 2010).

Due to the probe body symmetry, only 1/4 of the penetrometer body has been discretized, using symmetric boundary conditions on both longitudinal planes. The domain, presented in Figure 2 spans about 20 body lengths along the flow direction and about 10 body diameters in the transverse direction. The mesh counts 200k cells and three prisms layers around the body surface were to capture resolve the thin boundary layer flow around the body. No particular refinement is used in the wake since the attention of the study was primarily in the entrance-body of the probe, where the pressure sensor is located.

Results in terms of pressure distribution on the probe body surface and velocity distribution in the surrounding fluid are given in Figure 3 for a simulated inflow speed of 6 m/s. As evident, the probe is disturbing the flow only in a small region around its body. The deceleration around the tip and in the

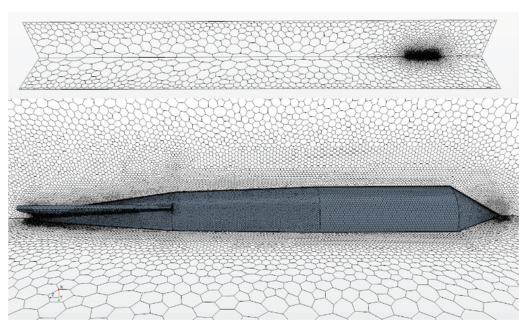

Figure 2. Domain extension (top) and detail of the polyhedral mesh created around the probe (bottom) for the RANSE simulations.

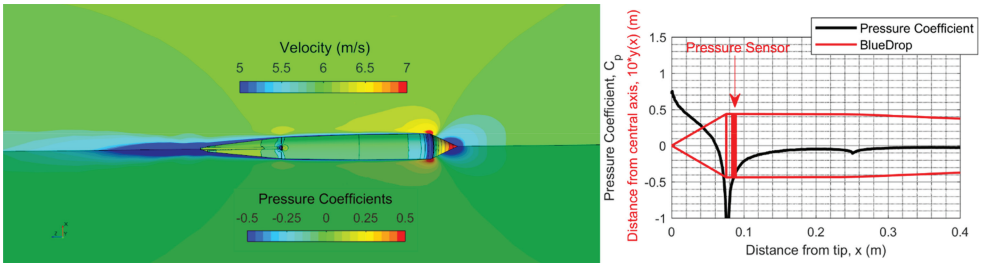

Figure 3. (Left) Results of the RANSE simulations at 6 m/s: velocity magnitude flow field on the symmetry planes and pressure coefficient distribution on the penetrometer. Only 1/4 of the body is presented. (Right) Pressure coefficients (represented by black line) on the body of BlueDrop (represented by red lines), as a function of distance from the tip. The vertical distance from central axis of BlueDrop is multiplied by 10 for a better display.

wake of the probe is evident, as well as the acceleration around the maximum area section at the base of the cone, where the pressure sensor is located. This acceleration of the flow determines the negative dynamic pressure that reduces the actual pressure measured by the sensor with respect to the hydrostatic pressure of the surrounding fluid.

A detailed pressure distribution curve along a meridian (longitudinal) section of the probe in between two fins is given in Figure 3. The pressure filter located just behind the cone, experiences suction forces under flow ($C_p < 0$), resulting from the shape transition from cone to shaft. The C_p equals ~ − 0.5 around the pressure filter area. The negative value is due to the acceleration of the flow in response to the increase of the cross section area from the pointed leading edge to the area of the maximum section, just upstream the porous ring, where the pressure sensor is located. The negative C_p leads to a measured pressure smaller than the actual hydrostatic pressure.

This calculated C_p value is used with equation 8 to obtain the correct pressure values as following:

$$p_{stat} = p_{dyn} + \frac{1}{2}\rho v_B^2 * 0.5 \tag{9}$$

3.2 *Corrected pressure signal*

The pressure measurements obtained during free fall through the water were corrected using equation 9. This has been applied to multiple deployments from the survey, and has provided matching results. An example deployment is shown in Figure 4. The FFP was submerged at a water depth of ~ 1 m, and then released falling under its own weight. It impacted the seabed at water depth of ~10 m, and was eventually brought to a stop by the resisting forces of the seabed sediments after ~1 m of seabed penetration. The recorded pressure during free fall was noticeably lower than the hydrostatic pressure as shown in Figure 4(a), being in agreement with observations by Lucking et al. (2017) and Stark & Ziotopoulou (2017) from other locations. The corrected pressure signal (Figure 4-red lines) matched the hydrostatic pressure until entering the seabed.

Insertion into the seabed was accompanied by a short period of subhydrostatic pressures. This is in line with observations by Stegmann et al. (2006), Seifert et al. (2008), Chow et al. (2014) and Stark et al. (2015). However, this phase may be overestimated if no correction of the measured pressure is applied. Considering the correction, the pressure signature changes to suprahydrostatic with positive excess pore pressure of up to ~ 9 kPa within the upper 10 cm of penetration of the pressure transducer (Figure 4(b)). Allowing a direct application of the CPT concept that undrained shear strength s_u can be estimated from excess pore pressure divided by an empirical cone factor $N_{k\Delta u}$ (Lunne *et al.*, 1997) and using $s_u = 8.1$ after a suggestion by Rémai (2013) would lead to an estimate of $s_u = 1.1$ kPa at a penetration depth of 0.8 m. While this has not been validated, it appears as a reasonable value based on the type of sediment. A preliminary analysis can be made on the basis of undrained shear strength ratios. Many authors have reported the undrained shear strength ratios of organic muds/clays to lie in the range of 0.4–0.65 (Chandler, 1988; Edil & Wang, 2000). Using an intermediate value of shear strength ratio of 0.5 and a saturated unit weight of 12.8 kPa as measured by Faas (1973), undrained shear strength values of about 1.2 kPa are estimated, matching well with the value calculated from the excess pore pressure. While the proposed correction converges to the actual measurements when the FFP approaches its maximum penetration depth, the correction appears crucial if pore pressure analysis is conducted throughout the penetration profile. However, it must be considered that

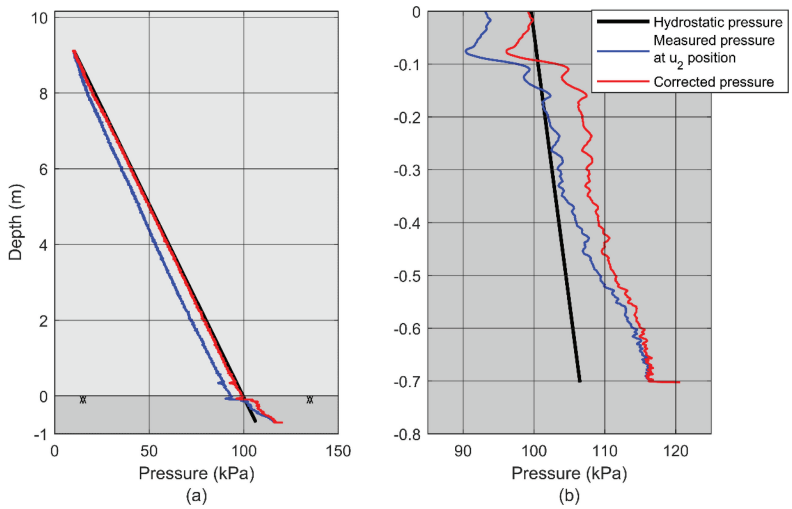

Figure 4. Measured and corrected pressure profiles from an example BlueDrop deployment during (a) the complete fall and (b) inside seabed. Zero depth indicates the seabed. Hydrostatic pressure calculated by estimating the depth, at the start point of deployment, inside water column from the pressure data. Increase in pressure beyond hydrostatic in (b) indicates the build-up of pore pressure in the sediments during penetration,.

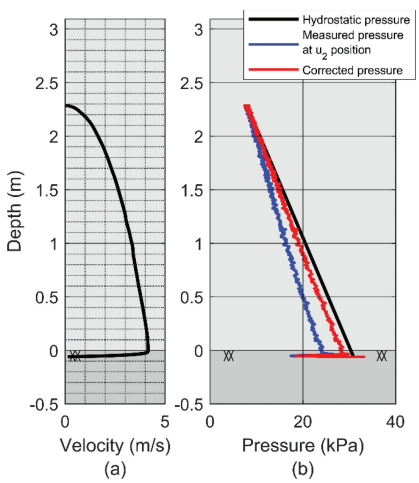

Figure 5. Deployment in water depth of about 3m: (a) Velocity profile and (b) pressure profile. The mismatch in corrected and hydrostatic pressure due to the low velocity is evident.

further corrections need to be applied, due to the change in "fluid" properties and resulting changes in fluid dynamic effects when entering the soft sediment.

The effect of changing velocity, however, was visible in some of the deployments. Figure 5 shows data from a deployment performed at a relatively shallow water depth of about 3 m achieving an impact velocity of ~ 4 m/s. Since the velocity profile (Figure 5(a)) never achieves 6 m/s, the pressure profile still lags behind the actual hydrostatic pressure. It is apparent that the pressure coefficients calculated for a flow of 6 m/s does not work very well in this case. More CFD models need to be run that simulate flow at other speeds to estimate pressure coefficients for other speeds.

4 DISCUSSION

Dynamic cone penetration testing, or in this case, portable free fall penetrometer testing is subject to additional velocity effects compared to a conventional quasi-static cone penetration test. The investigation and proper understanding of these effects is important to make correct interpretations of the results. The pressure recording behind the cone with the water and potentially soft soil flowing past the pressure transducer inlets results in measurements of pressures that are lower than expected hydrostatic pressures. This was also observed by Lucking et al. (2017), and can be explained by Bernoulli's equation which quantifies the change in pressure due to the velocity of fluid. The steady Bernoulli equation in combination with the concept of pressure coefficients has been used to develop a correction for the pressure signal in the form of equation 9. The steady Bernoulli equation is a simplification of the actual scenario, since it assumes a constant velocity. However, the velocity of the FFP after initial acceleration remains almost constant or within a fairly narrow

range over the free fall, and it provided an accurate estimation of the correct pressures. Overall, using the Bernoulli's equation and pressure coefficients from a CFD dynamic model of the FFP resulted in pressure profiles in close agreement with hydrostatic pressure.

At shallower depths, where the velocity never reached a value of 6 m/s, the correction will require pressure gradients estimated for the specific maximum velocity (Figure 5(b)), stressing the dependence of these pressure coefficients to the fall velocity. The unsteady Bernoulli equation would account for the effects of changing acceleration throughout the fall. However, the accurate solution of an unsteady Bernoulli equation has traditionally been a difficult task. Additionally, the rope tied to the FFP during all deployments adds an influencing factor during the fall through the water column due to the increasing rope drag with increasing depth, which results in the FFP experiencing a decelerating force from the rope. This makes it challenging to use an unsteady Bernoulli correction, particularly considering the good match that was achieved using the steady Bernoulli correction with the maximum velocity. Therefore, it appears more feasible to develop a chart or correlation expressing suitable pressure coefficients for a realistic range of velocities for the specific penetrometer.

Impact into the seabed usually resulted in a sudden drop in the pressures to sub-hydrostatic. This has also been observed in previous studies on high-velocity impacts into the seabed (Stegmann et al. 2006; Seifert et al. 2008; Chow et al. 2014; Stark et al. 2015). It has been hypothesized that the sub-hydrostatic pressures are developed because of the rapid outward displacement of sediment and water (Seifert *et al.*, 2008; Lucking *et al.*, 2017). The observation of sediment particles moving at high speeds around the cone tip during high-velocity penetration supports this hypothesis (Omidvar & Iskander, 2017).

Large deformation problems in very soft soils have been commonly treated with the soil modelled as a non-Newtonian fluid especially at large strain rates (Boukpeti *et al.*, 2012). A CFD model for very soft soils, modelled as a fluid of varying density and viscosity is in development and is expected to provide more insights into the pore pressure behavior, under high-velocity dynamic loading. The primary limitation of CFD modelling is its inability to model some of the in-situ soil properties such as anisotropy and stress history, and its assumption of soil as a uniform and homogenous mass. In estuarine environments, however, deposition and frequent remobilization of sediments usually results in freshly deposited, normally consolidated sediment deposits, and such deposits do not exhibit significant anisotropy, or any stress history and thus, the use of CFD modelling is valid. Raie & Tassoulas (2009) have successfully used CFD models to predict penetration depths of torpedo anchors in soft silts and normally consolidated clays.

5 CONCLUSIONS

The importance of accurate pore pressure measurements in cone penetration testing is well-known (Lunne *et al.*, 1997). This article presents a proof of concept that pressure corrections using basic fluid dynamic principles such as the Bernoulli equation and pressure coefficients obtained from CFD modelling can represent an accurate and reliable method to correct for fluid dynamic effects in the water column.

To make an accurate interpretation of the pore pressure signal from surficial seabed sediments in marine environments from free fall penetrometers, it appears essential that the pressure signal is corrected for fluid dynamic effects. The pore pressure response of soils during loading has conventionally been proved to be dependent on the stress history and stiffness of fine-grained soils (Burns & Mayne, 1998) and on the relative density of coarse-grained soils (Seed & Lee, 1967), among many other factors. Thus, pore pressure measurements may be used as indicators of important in-situ characteristics. However, the unique pressure behavior observed due to the dynamic nature of the free-fall penetration test is still an area of active research. More research is planned to investigate and incorporate the rheological and viscosity characteristics of very soft muds into the correction to account for dynamic effects during penetration of the seabed at high velocities.

ACKNOWLEDGMENTS

The authors acknowledge funding through the Fulbright Foreign Student Program administered by International Institute of Education (IIE) and the United States Educational Foundation in Pakistan (USEFP), the National Sciences Foundation (NSF) through grant OCE-1434938, the Office of Naval Research (ONR) through grant N00014-17-1-2344, and Virginia Tech's Institute for Critical Technology and Applied Sciences (ICTAS). The authors also thank Dan Stilwell and Cagdas Bilici (both VT) for their support in the field, and Stephen Smyth (blueCDesigns) for discussions regarding pore pressure effects.

REFERENCES

Albatal, A. & Stark, N. (2017) 'Rapid sediment mapping and in situ geotechnical characterization in challenging aquatic areas', *Limnology and Oceanography: Methods*, 15(8), pp. 690–705.

Boukpeti, N., White, D.J., Randolph, M.F. & Low, H.E. (2012) 'Strength of fine-grained soils at the solid–fluid transition', *Géotechnique*, 62(3), pp. 213–226.

Brizzolara, S. & Villa, D. (2010) 'Multiphase URANS Simulations of Surface Combatant using StarCCM+', in *Proceedings of the Workshop on Numerical Ship Hydrodynamics*. Gothenburg, Sweden.

Burns, S.E. & Mayne, P.W. (1998) 'Monotonic and dilatory pore-pressure decay during piezocone tests in clay', *Canadian Geotechnical Journal*, 35(6), pp. 1063–1073.

Chandler, R. (1988) 'The In-Situ Measurement of the Undrained Shear Strength of Clays Using the Field Vane', in *Vane Shear Strength Testing in Soils: Field and Laboratory Studies*. West Conshohocken, PA: ASTM International, pp. 13–44.

Chow, S.H., O'Loughlin, C.D. & Randolph, M.F. (2014) 'Soil strength estimation and pore pressure dissipation for free-fall piezocone in soft clay', *Géotechnique*, 64(10), pp. 817–827.

Edil, T. & Wang, X. (2000) 'Shear Strength and K', in *Geotechnics of High Water Content Materials*. West Conshohocken, PA: ASTM International, pp. 209–225.

Faas, R.W. (1973) 'Sedimentational Regimes of the York River, Southeastern Virginia, As Shown By Mass Properties', *Chesapeake Science*, 14(3), pp. 181–187.

Gaggero, S., Villa, D. & Brizzolara, S. (2010) 'RANS and PANEL method for unsteady flow propeller analysis', *Journal of Hydrodynamics, Ser. B*, 22(5), pp. 564–569.

Hartman, J.J., Pepe, Jr., F. & Castelli, R.J. (2008) 'Widening of the George P. Coleman Memorial Bridge', in *GeoCongress 2008*. Reston, VA: American Society of Civil Engineers, pp. 976–983.

Lucking, G., Stark, N., Lippmann, T. & Smyth, S. (2017) 'Variability of in situ sediment strength and pore pressure behavior of tidal estuary surface sediments', *Geo-Marine Letters*, 37(5), pp. 441–456.

Lunne, T., Robertson, P.K. & Powell, J.J.M. (1997) *Cone penetration testing in Geotechnical practice*, *Blackie Academic*. New York: EF Spon/Routledge Publishing.

Omidvar, M. & Iskander, M. (2017) 'Soil Deformations during Finless Torpedo Installation', in *Geotechnical Frontiers 2017*. Reston, VA: American Society of Civil Engineers, pp. 389–397.

Raie, M.S. & Tassoulas, J.L. (2009) 'Installation of Torpedo Anchors: Numerical Modeling', *Journal of Geotechnical and Geoenvironmental Engineering*, 135(12), pp. 1805–1813.

Rémai, Z. (2013) 'Correlation of undrained shear strength and CPT resistance', *Periodica Polytechnica Civil Engineering*, 57(1), p. 39.

Rodi, W. (1991) 'Experience with two-layer models combining the k-epsilon model with a one-equation model near the wall', in *29th Aerospace Sciences Meeting*. Reno, NV: American Institute of Aeronautics and Astronautics.

Seed, H.B. & Lee, K.L. (1967) 'Undrained strength characteristics of cohesionless soils', *Journal of the Soil Mechanics and Foundations Division*. New York, NY, United States, 93(SM6), pp. 333–360.

Seifert, A., Stegmann, S., Mörz, T., Lange, M., Wever, T. & Kopf, A. (2008) 'In situ pore-pressure evolution during dynamic CPT measurements in soft sediments of the western Baltic Sea', *Geo-Marine Letters*, 28(4), pp. 213–227.

Shih, T.-H., Liou, W.W., Shabbir, A., Yang, Z. & Zhu, J. (1994) A New K-epsilon Eddy Viscosity Model for High Reynolds Number Turbulent Flows: Model Development and Validation, Computers & Fluids.

Stark, N., Quinn, B., Ziotopoulou, K. & Lantuit, H. (2015) 'Geotechnical Investigation of Pore Pressure Behavior of Muddy Seafloor Sediments in an Arctic Permafrost Environment', in *Volume 1: Offshore Technology; Offshore Geotechnics*. ASME, p. V001T10A017.

Stark, N. & Ziotopoulou, K. (2017) 'Undrained Shear Strength of Offshore Sediments from Portable Free Fall Penetrometers: Theory, Field Observations, & Numerical Simulations', in *Offshore Site Investigation & Geotechnics Committee 8th International Conference*. London, UK: Society for Underwater Technology.

Stegmann, S., Mörz, T. & Kopf, A. (2006) 'Initial Results of a new Free Fall-Cone Penetrometer (FF-CPT) for geotechnical in situ characterisation of soft marine sediments', *Norwegian Journal of Geology*, 86, pp. 199–208.

Taylor & Francis
Taylor & Francis Group
http://taylorandfrancis.com

Cone Penetration Testing 2018 – Hicks, Pisanò & Peuchen (Eds)
© 2018 Delft University of Technology, The Netherlands, ISBN 978-1-138-58449-5

Influence of soil characteristics on cone and ball strength factors: Case studies

T.D. Nguyen
Infrastructure Engineering Program, Vietnam Japan University, Hanoi, Vietnam
Formerly, Department of Civil Engineering, Dong-A University, Busan, South Korea

S.G. Chung
Department of Civil Engineering, Dong-A University, Busan, South Korea

ABSTRACT: This paper presents a comparative study on the influence of some typical soil characteristics on the cone and ball factors (N_{kt} and N_{ball}). Experimental data from CPTU and ball penetration test (BPT) on Busan (two sites), Ariake, and Mihara clays were taken into analysis. In contrary to the conclusions from existing FE analysis and experimental results at limited sites that N_{ball} is independent on rigidity index (I_r) and normalized stress difference (Δ), N_{ball} was found to clearly increase with the increase in I_r and to increase or decrease with Δ. This disagreement is attributed to different inherent characteristics of natural clays. Both N_{kt} and N_{ball} decrease pronouncedly with the increase in normalized shear strength (s_{uFV}/s'_{v0}), however the factors expose to have no definite correlations with sensitivity (S_{tFV}) and plasticity index (I_p) at the investigated sites.

1 INTRODUCTION

In soft to very soft clays, especially those under high pore pressure conditions, ball penetration test (BPT) exposes to have several advantages over the traditional cone concentration test (CPTu) (Randolph, 2004; DeJeong et al. 2011). Although the BPT has been developed and used recently, relative understandings from a number of numerical studies (e.g. Lu et al. 2000, Zhou and Randolph 2009) and experimental studies (e.g. Low et al. 2010, DeJong et al. 2011) has led to development of essential recommendations for penetrometer design, testing procedures, and data analysis (DeJong et al. 2010; Lunne et al. 2011).

One of the key applications of the BPT in very soft to soft clays is to evaluate the undrained shear strength (s_u) of the deposits. Similar to the use of cone resistance, the indirect BPT-based s_u value of any target site should also be determined using an adopted ball strength factor (N_{ball}). Unlike the cone factor (N_{kt}), which is influenced by a number of soil characteristics such as rigidity index ($I_r = G/s_u$, where G is shear modulus of soil), the normalized in situ stress difference between vertical (σ_{v0}) and horizontal (σ_{h0}) stresses ($\Delta = (\sigma_{v0} - \sigma_{h0})/s_u$), friction ratio ($\alpha_f = \tau_f/s_u$, where τ_f is limiting shear stress on penetrometer surface), and strength anisotropy ($\rho = s_{ue}/s_{uc}$, where s_{ue} and s_{uc} are undrained shear strength in extension and compression, respectively) (Teh & Houlsby 1991, Lu et al. 2004), the N_{ball} factor obtained from numerical study (Lu et al. 2000) and limited experimental data (Low et al. 2010) was shown to have ignorable dependence on certain soil characteristics, especially on the I_r and Δ. The less dependence on soil characteristics of N_{ball} essentially means that an established range of N_{ball} would be applicable to more soil types compared with that of N_{kt}. Since studies on variation of experiment-based N_{ball} with soil characteristics are rarely reported in the literature, it is still desired to have more experimental studies to verify this important feature of N_{ball}.

This study presents a comparison on the variation of experimental N_{ball} and N_{kt} factors with several soil characteristics, including I_r, Δ, normalized shear strength (s_u/σ'_{v0}), sensitivity (S_{tFV}), and plasticity index (I_p). For this, experimental data from BPT, CPTU, and field vane test (FVT) at two test sites in the Nakdong River Delta, Busan, S. Korea and from two test sites in Japan were used for the analysis. In addition, experimental data points of N_{ball} and N_{kt} versus I_r at another two test sites reported in Low et al. (2010) were also included in part of the analysis to obtain a more representative trend of the factors versus I_r.

2 SITE DESCRIPTION

2.1 *Site location and geological characteristics*

The first two study sites, namely, DIS-2 and DIS-5 (approximately 1.2 km apart), are located in the floodplain (i.e., marginal basin) of the Nakdong River Delta, west of Busan City, South Korea. Besides, BPT results from Ariake and Mihara sites in Japan (Nakamura et al. 2009) are also included into the analysis. The Ariake site is located in Kyushu Island and faces the Ariake Sea, whereas the Mihara site is located in Ebetsu district, near Sapporo, Hokkaido.

At the DIS-2 and DIS-5 sites, late Quaternary deposits are distributed with four sedimentary units closely related to the sea level change. The units of both sites, which have similar characteristics but slightly different thicknesses, are summarized as follows (from bottom to top): the fluvial channel (FC), the lower tidal flat (TF(L)), the inner shelf (IS), and the upper tidal flat (TF(U)). The geological conditions of the sites were described in detail by Chung et al. (2012).

Geological and geotechnical characteristics at Ariake site have been extensively investigated for many years (e.g. Hanzawa et al. 1990, Tanaka et al. 2001). Based on the variation of physical properties (i.e. w_n, I_p, ρ_t) with depth, Hanzawa et al. (1990) divided the clay at the site into upper clay (from ground surface to 12.0 m) and lower clay (12.0 to 18.5 m). Unlike the Ariake site, there have been a few studies on the geological and geotechnical characteristics at Mihara site (e.g. Nakamura et al. 2009; Hayashi et al. 2012). Geologically, the soil profile at Mihara site consists of the following layers: a surface peat layer from 0 to 6.5 m, a sand layer from 6.5 to 11.0 m, a silty clay layer from 11.0 to 19.0 m, and a silty sand layer from 19.0 to about 28.0 m.

2.2 *Geotechnical characteristics*

Geotechnical characteristics at DIS-2 and DIS-5 are rather similar as typically shown in Figure 1 for DIS-2. A typical feature at this site is that the sensitivity based on the field vane ($S_{t,FV}$) in the upper part (from 5 m to 12 m) of the IS unit is significantly higher than that of DIS-5 at the same levels, and this was resulted from leaching effect at DIS-2 (Nguyen & Chung 205). The clay at the sites is classified as normally consolidated (NC) to slightly overconsolidated soil with *OCR* values ranging from 1.3 to 2.0 (Singh & Chung 2015).

Geotechnical characteristics of Ariake have been described in detail in many references (e.g. Tanaka et al. 2001). Briefly, the natural water content (w_n) of the clay is very high ($w_n > 100\%$) and exceeds the liquid limit (w_L) along the entire depth, leading to

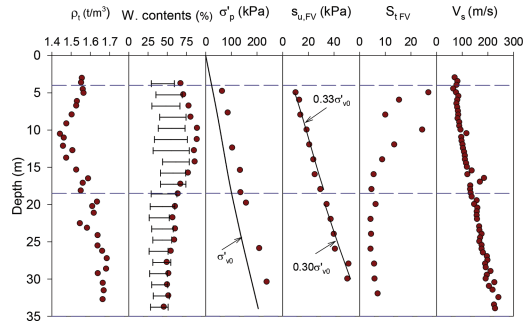

Figure 1. Basic geotechnical properties at DIS-2.

very high values of I_p (45% to 90%) and *IL* (1.4 to 1.8). The clay is classified as very high plasticity. The w_n values of Mihara site are almost equal or less that the w_L, leading to I_p of 30% – 44% and *IL* of slightly less than 1.0. Similar to Busan clay, the clays at both the sites are NC to slightly overconsolidated with OCR varying from 1.2 to 1.6 at Ariake site and from 1.2 to 1.4 from Mihara site.

3 FIELD TEST

3.1 *BPT*

BPT with four different ball sizes (A_r = 0.15 to 1.0, where A_r = shaft-ball area ratio) was first carried out at DIS-5 using a Geomil track-mounted CPT machine with a capacity of 20 tons. After the analysis of the test results for DIS-5, a ball with smaller area ratio ($A_r = 0.1$) was found necessary to enhance the interpretation of the test results. Thus, the BPT with the previous four balls and the new ball was conducted at DIS-2. The balls made of duralumin were not sandblasted to achieve a specific roughness but were normally polished in the factory. Thus, all the balls were assumed to have the same surface roughness. More information on the shape and dimensions of the balls are given in Nguyen & Chung (2015).

As the ball penetrometer, the cone tip of a 15 cm^2 Geomil cone type (i.e., 43.7 mm in diameter) was replaced by balls screwed at the filter location of 25 mm above the top of the balls. The BPT test at both sites was conducted at a constant speed of 20 mm/s following the procedure recommended by the International Society of Soil Mechanics and Geotechnical Engineering (ISSMGE 1999). Penetration resistances were recorded at intervals of 10 mm.

The BPT with a similar series of four different ball sizes ($A_r = 0.1$ to 1.0) was conducted at Ariake and Mihara sites by a geotechnical research group leading by Prof. H. Tanaka of Hokkaido Univer-

Table 1. Specifications of the penetrometers.

Specification	DIS-5	DIS-2	Ariake	Mihara
Ball diameter, D_{ball} (cm^2)	11.28	13.82	11.28	11.28
Ball area, A_{ball} (cm^2)	100.0	150.0	100.0	100.0
Shaft area, A_{shaft} (cm^2)	15.0	15.0	10.0	10.0
Shaft-ball area ratio, A_r	0.15	0.10	0.10	0.10

sity, Japan. For these two sites, the test was carried out at a constant speed of 1.0 m/min (16.7 mm/s) following the standard of Japanese Geotechnical Society for CPT (JGS 1435 2003). More details on the BPT at these sites are described in Nakamura et al. (2009). The BPT experimental data at the Ariake and Mihara sites were personally given by Prof. H. Tanaka (2012). Table 1 shows specifications of the cones (or shafts) and balls having smallest A_r used at the four sites and experimental data from these penetrometers will be used for the analysis herein.

3.2 *Other field tests*

CPTU was conducted at DIS-5 and DIS-2 sites using the same CPT rig and cone probe used for the BPT

(A_{shaft} = 15 cm^2). The cone was electrical type, with a 60° apex and a porous element (filter) mounted immediately behind the cone shoulder to measure induced pore water pressure (u_2). The average penetration rate for the CPTU was 20 mm/sec, following the procedure recommended by the ISSMGE (1999). Similarly, CPTU with cone area of A_{shaft} = 10 cm was also performed at Ariake and Mihara following the same speed and procedure applied to the BPT.

FVT was also performed at all the sites. For Busan clay, a Geonor vane (H-10) with the blade of 55 mm wide, 100 mm high, and 2 mm thick was used to advance directly (without a pre-borehole) into the ground and then stopped at 50 cm above the test depth. The blade connected to the inner rod was then pushed down to the test depth. After 5 min, the test was performed at a constant speed of 0.1 °/s until the residual resistance became constant. The remolded test was also conducted at all test depths to evaluate the sensitivity. For Ariake and Mihara clays the FVT was also conducted using the same standard rotation speed. However, the vane was slightly smaller (with the blade of 40 mm in diameter and 80 mm in height). Aside from FVT and CPTU, Dilatometer/Seismic Dilatometer test (DMT/SDMT) were alternatively performed at DIS-5 and DIS-2 at intervals of 0.5 m. For the Japanese sites, only SCPT was available at Ariake site as reported in Tanaka et al. (2001).

4 RESISTANCES AND STRENGTH FACTORS

4.1 *Definition of net resistance*

The net cone penetration resistance, q_{net}, is defined as follows:

$$q_{net} = \left[q_b + (1-a)u_2\right] - \sigma_{v0} = q_t - \sigma_{v0} \tag{1}$$

where q_c and q_t are the measured and corrected cone resistances; a is the cone area ratio (Lunne et al. 1997); u_2 is the pore pressure at the cone shoulder; and σ_{v0} is the in-situ total overburden pressure at the cone tip.

The net ball penetration resistance, $q_{net(b)}$, is defined as follows (DeJong et al. 2010):

$$q_{net(b)} = q_b - \left[\sigma_v - (1-a)u_2\right]A_r \tag{2a}$$

And an alternative is

$$q_{net(b)} = q_b - \left[\sigma_{v0} - (1-a)u_0\right]A_r \tag{2b}$$

where q_b is the measured ball resistance (an analogy of q_c); σ_{v0} and σ_v are total overburden pressures at the ball level in in-situ and ball-penetrated conditions, respectively; u_0 and u_2 are hydrostatic (in situ) and induced pore pressures, respectively, at the connection between the ball and the shaft; A_r is the ratio of the cone (shaft) area to the projected area of the ball, i.e., $A_r = A_{shaft}/A_{ball}$. In this study, Equation 2b is used to calculate the net ball resistance following reasons recommended in DeJong et al. (2010).

4.2 *Strength factors*

The cone factor (N_{kt}) and ball factor (N_{ball}) are generally defined as follows:

$$N_{kt} = \frac{q_{net}}{s_u} \tag{3a}$$

$$N_{ball} = \frac{q_{net(b)}}{s_u} \tag{3b}$$

where s_u is the reference undrained shear strength. In this paper, the undrained shear strength from the field vane test (s_{uFV}) is taken as the reference value for all analyses.

5 TEST RESULTS AND DISCUSSIONS

5.1 *Net cone and ball resistances*

The net cone and ball resistances obtained from the four study sites are shown in Figure 2. A shown, $q_{net(b)}$ is normally smaller than q_{net} (except in the IS unit at DIS-2) and the discrepancy increases with the increase in depth. These profiles are good examples to explain that for the same clay N_{ball} is often smaller than N_{kt}. Note that at DIS-5 site there was a shell interbedded sub-layer varying unevenly from depths of 16.5 m to 23.5 m, and all experimental data from these depths were excluded in the analysis herein.

Note also that $q_{net(b)}$ profile at DIS-5 was obtained from the ball having $A_r = 0.15$. To get a unified set of data from all balls having $A_r = 0.1$ for analysis in next section, $q_{net(b)}$ values at specific depths (e.g., s_{uFV}, V_s tested depths) at DIS-5 site were manually extrapolated to get equivalent values at $A_r = 0.1$. The extrapolated values were obtained based on the actual variation trend of resistances with A_r (Nguyen & Chung 2015). That is, at any particular depth the extrapolated $q_{net(b)}$ value at $A_r = 0.1$ should fall onto a smooth parabola-like curve following the trend defined from measured resistances at $A_r = 0.15$, 0.25, 0.5, and 1.0. As a result, the ratio of $q_{net(b)}$ at $A_r = 0.10$ to $q_{net(b)}$ at $A_r = 0.15$ from all extrapolated points varies from 1.06 to 1.18.

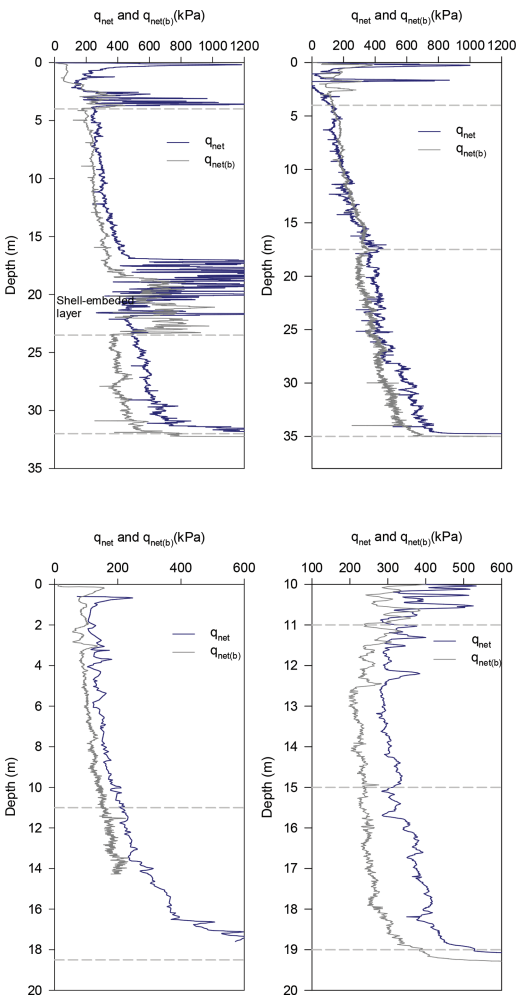

Figure 2. q_{net} and $q_{net(b)}$ profiles at: (a) DIS-5; (b) DIS-2; (c) Ariake; (d) Miahara.

5.2 *Strength factors versus soil characteristics*

The variation of N_{kt} and N_{ball} with rigidity index (I_r) was first taken into analysis. The index $I_r = G/\tau_f$, where τ_f ($= s_u$ in undrained case) is shear strength at failure, was originally suggested by Vesic (1973) and it was associated with the assumed elastic-ideal plastic behavior of soil. That is, G is a constant value until plastic failure happens. However, in modern soil mechanics G has been well recognized to degrade nonlinearly with the increment of induced shear strains. Around a penetrometer, G varies from the maximum value (G_0) at some distance from the penetrometer to much smaller value ($G << G_0$) in the completely disturbed zone near the penetrometer surface. For practical applications, the shear modulus at 50% mobilized strength (G_{50}) is often recommended as an average one used for evaluating I_r (Mayne 2001). In this study, sine G_{50} from triaxial-based stress-strain curves was not available, an average value of $G_{50} = 0.26G_0$ was adopted following recommendation by Krage et al. (2014). In other approach, G_{50} might roughly be evaluated from degradation curve of G, which is often expressed in a modified hyperbolic form of $G/G_0 = 1-f(\tau/\tau_{max})^g$ (Fahey & Carter 1993, Mayne 2007), where coefficients f and g possibly vary from 0.75 to 1.0 and 0.2 to 0.4, respectively. If $f = 0.91$ and $g = 0.30$ are taken as typical values, then $G_{50} = 0.26G_0$ is obtained at $\tau/\tau_{max} = 0.5$ (50%). The value of $G_0 = \rho V_s^2$ was evaluated using measured shear wave velocity (V_s) for DIS-5, DIS-5, and Ariake sites and adopted correlation $V_s = 1.75q_t^{0.627}$ (Mayne 2007) for Mihara site.

Figure 3 shows the variation of N_{kt} and N_{ball} versus I_r at the four sites as well as that at Onsoy and Burswood sites reported in Low et al. (2010). As shown in the figure, except some data points from the TF(L) unit of DIS-5 and DIS-2, both N_{kt} and N_{ball} appear to increase with the increase in I_r, and the factors vary in large ranges of 8.0 to 18.0 ($\Delta N_{kt} = 9.0$) and 6.0 to 15.0 ($\Delta N_{ball} = 9.0$), respectively, for the six test sites (I_r = 50 to 400).

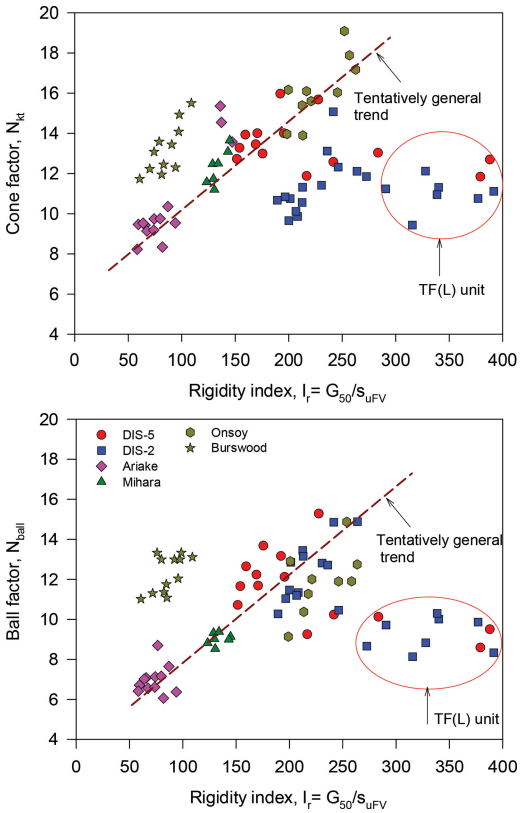

Figure 3. Variation of: (a) N_{kt} vs I_r; (b) N_{ball} vs I_r at the sites.

The out-of-trend data points circled in the figure can mainly be attributed to special feature of net resistances in the TF(L) sub-layer, especially in the depths of 23.5 m to 28.0 m (DIS-5) and 17.5 m to 27.0 m (DIS-2). As shown in Figure 2, the net resistances, especially $q_{net(b)}$, increase marginally with depth whether V_s increase almost linearly following the trend of the IS sub-layer. As a result, this results in smaller strength factors and larger I_r in these depths.

The dependence of N_{ball} on I_r as shown in Figure 3b contrasts with conclusions from numerical analysis (Lu et al. 2000) and limited experimental data (Low et al. 2010) that N_{ball} is independent on the index. The disagreement with the numerical analysis results may mainly be attributed to the soil model, among other possible reasons, adopted in the FE analysis. In fact, natural clays from different depositional environments (i.e. different physical and mechanical characteristics) are expected to have different behavior whereas the soil in the FE analysis was modeled as homogeneous elastic-perfectly plastic material obeying a Tresca or Von Mises criteria. In addition, if results at only Onsoy and Burswood sites (Fig. 3b), which have relatively similar ranges of N_{ball} at different ranges of I_r, are examined the independence of N_{ball} on I_r might be misinterpreted.

The variation of N_{kt} and N_{ball} with Δ was then taken into analysis. To evaluate the total horizontal stress σ_{h0} ($= K_0\sigma'_{v0}+u_0$), the coefficient of earth pressure at rest (K_0) was interpreted from DMT-based horizontal stress index (K_D) for Busan and Ariake clays using equation of $K_0 = 0.34K_D^{0.55}$ (Powell & Uglow 1988). This equation, among several common recommended equations in the literature, was adopted because the interpreted K_0 values for the clays are very close to the K_0 reported in Chung et al. (2012) and Hanzawa et al. (1990). A constant $K_0 = 0.64$ of Mihara site was directly taken from experimental result (Hayashi et al. 2012).

Figure 4 shows the variation of N_{kt} and N_{ball} versus Δ at the four sites. In a general view, N_{kt} tends to gently increase with the increase in Δ whereas N_{ball} exposes to have no general trend. However, if view is focused on DIS-5 and DIS-2 sites specifically,

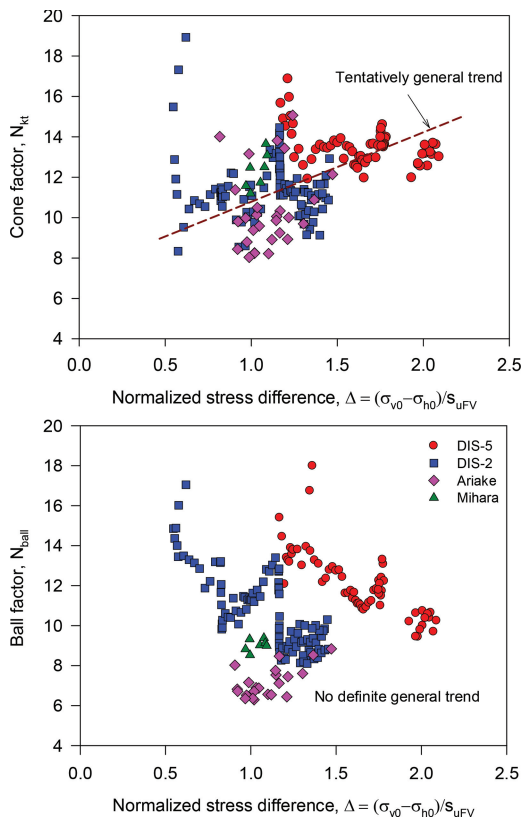

Figure 4. Variation of: (a) N_{kt} vs Δ; (b) N_{ball} vs Δ at the sites.

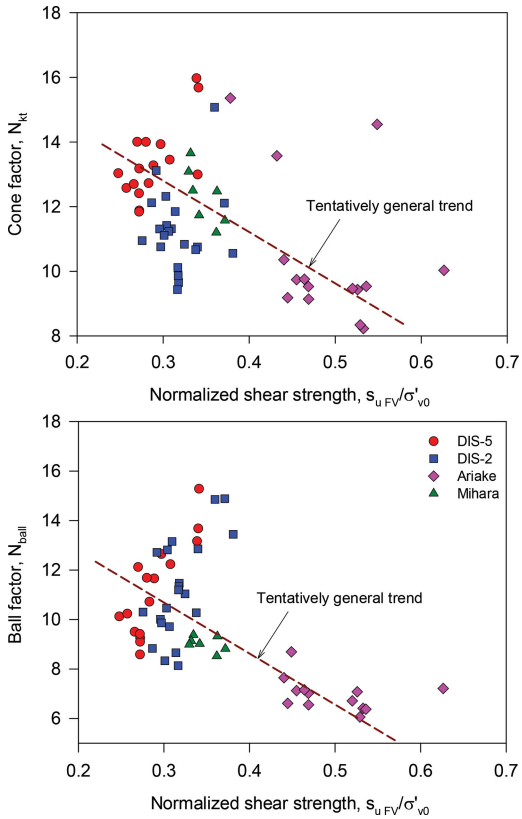

Figure 5. Variation of (a) N_{kt} and (b) N_{ball} vs s_{uFV}/σ'_{v0}.

N_{kt} of the sites appears relatively constant with the increase of Δ whereas N_{ball} tends to decrease pronouncedly. Both N_{kt} and N_{ball} of Ariake site tend to increase with the increase of Δ.

Figure 5 shows the variation of N_{kt} and N_{ball} versus normalized shear strength (s_{uFV}/σ'_{v0}) at the four sites. As shown, both N_{kt} and N_{ball} decrease pronouncedly with the increase of s_{uFV}/σ'_{v0}. This general trend was also noted in the numerical analysis (Zhou & Randolph 2009) and experimental study (Nguyen & Chung 2015). That is, at the same A_r value, soil having larger s_{uFV}/σ'_{v0} ratio results in smaller N_{ball}. The variation of N_{kt} and N_{ball} versus sensitivity (S_{tFV}) and plasticity index ($I_p = w_L$-w_P) was also investigated for the four test sites. However, no definite trends were found for these correlations and due to space limitation the figures are not presented herein.

6 CONCLUSION

This paper presents a comparative study on the influence of some soil characteristics (i.e. rigidity index (I_r), normalized stress difference (Δ), normalized shear strength (s_{uFV}/σ'_{v0}), sensitivity (S_{tFV}), and plasticity index (I_p)) on cone (N_{kt}) and ball (N_{ball}) factors. CPTU and BPT experimental data on Busan clay at two sites, Ariake clay and Mihara clay were taken into analysis. Although more experimental data are needed to generalize the dependence of the strength indexes on the investigated soil characteristics, the following conclusions might be drawn from the study: (*i*) in contrast with conclusion from existing FE analysis and limited experimental data that N_{ball} is independent on I_R, N_{ball} obtained from six study sites exposes to increase pronouncedly with increase in I_r; (*ii*) data from four investigated site showed that in general N_{kt} tends to increase gently with the increase in Δ but N_{ball} appears to have no definite trends; (*iii*) both N_{kt} and N_{ball} decrease at a similar gradient with the increase in s_{uFV}/σ'_{v0}; (*iv*) N_{kt} and N_{ball} from the sites appear to have no definite correlation trends with S_{tFV} and I_p.

ACKNOWLEDGEMENT

This study was supported by the Korea Science and Engineering Foundation Programs through the National Research Foundation of Korea (NRF) funded by the Ministry of Science, ICT, and Future Planning (No. 2016R1A2A2A05005131) and by the Ministry of Education (No. 2016R1A6A1A03012812). Prof. H. Tanaka at Hokkaido University, Japan, Dr. Han Eng Low at Advanced Geotechnics Pty Ltd., Australia are appreciated. The graduate students of Dong-A University, Busan, gave valuable assistance in the laboratory and field tests.

REFERENCES

Chung, S.G., Ryu C.K., Min S.C., Lee J.M., Hong YP & Odgerel E. 2012. Geotechnical characterization of Busan clay. *KSCE Journal of Civil Engineering*, **16**(3): 341–350.

DeJong J., Yafrate N, DeGroot D., Low H.E. & Randolph, M.F. 2010. Recommended practice for full flow penetrometer testing and analysis. *Geot. Testing J.*, **33**(2): 1–13.

DeJong J.T., Yafrate N.J. & DeGroot, D.J. 2011. Evaluation of undrained shear strength using full-flow penetrometers. *J. of Geotechnical and Geoenvironmental Engineering*, ASCE, **137**(1): 14–26.

Fahey, F. & Carter, J.P. 1993. A finite element study of the presuremeter test in sand using nonlinear elastic plastic model. *Canadian Geotechnical J.*, **30**: 348–362.

Hanzawa, H., Fukaya, T. & Suzuki, K. 1990. Evaluation of engineering properties for an Ariake clay. *Soils and Foundations*, **30**(4): 11–24.

Hayashi, H., Yamazoe, N., Mitachi, T., Tanaka, H. & Nishimoto, S. 2012. Coefficient of earth pressure at rest for normally and overconsolidated peat ground in Hokkaido area. *Soils and Foundations*, 52(2): 299–311.

ISSMGE 1999. International reference test procedure for cone penetration test (CPT) and cone penetration test with pore pressure (CPTU), *Proceedings of the Twelfth European Conference on Soil Mechanics and Geotechnical Engineering*, Amsterdam, Barends et al. (ed.), Vol.3, pp. 2195–2222.

JGS 1435 2003. Electric cone penetration test, site investigation method and explanation, *Japanese Geot. Society.*

Krage, C.P., Broussard, N.S. & DeJong, J.T. 2014. Estimating rigidity index (I_R) based on CPT masurements. Proceedings of the 3rd Int. Symp. on CPT, Nevada, USA: 727–735.

Low, H.E., Lunne, T., Andersen, K.H., Sjursen, M.A., Li X. & Randolph, M.F. 2010. Estimation of intact and remolded undrained shear strengths from penetration tests in soft clays. *Géotechnique*, **60**(11): 843–859.

Lu, Q., Hu, Y. & Randolph, M.F. 2000. FE analysis for T-bar and spherical penetrometers in cohesive soil. *Proceedings of the 10th International Offshore and Polar Engineering Conference:* 617–623.

Lu, Q., Randolph, M.F., Hu, Y. & Bugarski, I.C. 2004. A numerical study of cone penetration in clay. *Geotechnique*, 54(4): 257–267.

Lunne, T., Robertson, P.K. & Powell J.J.M. 1997. *Cone Penetration Testing in Geotechnical Practice*. Blackie Academic & Professional, London, UK.

Lunne, T., Andersen, K.H., Low, H.E., Randolph, M.F. & Sjursen, M. 2011 Guidelines for offshore in situ testing and interpretation in deepwater soft clays. *Canadian Geotechnical J.*, **48**(4): 543–556.

Mayne, P.W. 2001. Stress-strain-strength-flow parameters from enhanced in-situ test. Proceedings of Int. Conf. on In-situ Measurement of Soil Properies and Case Histories, Bali, Indonesia, pp. 21–24.

Mayne, P.W. 2007. Cone penetration testing, NCHRP synthesis No. 368.

Nakamura, A., Tanaka, H., & Fukasawa, T. 2009 Application of T-bar and ball penetration tests to soft clayey grounds. *Soils and Foundations*, **49**(5): 729–738.

Nguyen, T.D. and Chung, S.G. 2015. Effect of shaft area on ball resistances in soft clay, *Geotechnical Engineering*, ICE, **168**(GE2): 103–119.

Powell, J.J.M. & Uglow, I.M. 1988. The interpretation of the Marchetti dilatometer test in UK clays. Penetration testing in the UK, ICE, Paper 34: 269–273.

Randolph M.F. 2004. Characterisation of soft sediments for offshore applications. *Proceedings of the 2nd Int. Conf. on Geot. and Geoph. Site Charact. (ISC-2)*, pp. 209–231.

Singh, V.K. & Chung, S.G. 2015. Evaluation of overconsolidation ratios from laboratory and in situ tests on Busan clay, *Engineering Geology*, **199**(2015):38–47.

Tanaka, H., Locat, J. Shibuya, S., Soon, T.H. & Shiwakoti, D.R. 2001. Characterization of Singapore, Bangkok, and Ariake clays. *Canadian Geotechnical J.*, **38**: 378–400.

Teh, C.I. and Houlsby, G.T. 1991. An analytical study of the cone penetration test in clay. *Geotechnique*, 41(1): 17–34.

Vesic, A.S. 1973. Analysis of ultimate loads of shallow foundations, *J. Soil Meachnics & Found. Div*. ASCE **99**(SM1): 45–73

Zhou, H. & Randolph, M.F. 2009. Effect of shaft on resistance of a ball penetrometer. *Geotechnique*, **61**(11): 973–981.

Taylor & Francis
Taylor & Francis Group
http://taylorandfrancis.com

Cone Penetration Testing 2018 – Hicks, Pisanò & Peuchen (Eds)
© 2018 Delft University of Technology, The Netherlands, ISBN 978-1-138-58449-5

A method for predicting the undrained shear strength from piezocone dissipation test

E. Odebrecht
State University of Santa Catarina, Joinville, Brazil

F.M.B. Mantaras
Geoforma Engenharia Ltd., Joinville, Brazil

F. Schnaid
Federal University of Rio Grande do Sul, Porto Alegre, Brazil

ABSTRACT: A method developed to correlate the measured piezocone dissipation excess pore-water pressure (Δu) to the soil undrained shear strength (s_u) has been presented by Mantaras et al. (2015). In the proposed approach, a mathematical closed form solution was derived linking the ratio of normalized maximum excess pore pressure and the normalized undrained shear strength. In the preset paper the predicted s_u values obtained from the from dissipation tests are calibrated against field vane shear strength in both normally consolidated and lightly overconsolidated soils (OCR of up to 5). Data from 5 cm^2 and 10 cm^2 piezocone cross section areas are evaluated to demonstrated that reported results are consistent and encourage the use of the method in engineering practice.

1 INTRODUCTION

Piezocone penetrometers are instrumented with pressure transducers mainly located at the tip or shoulder of the cone to measure the pore water pressure generated during penetration. In clay pore pressure in excess to hydrostatic values allows assessment of geoenvironmental parameters including the coefficient of consolidation and the coefficient of hydraulic conductivity. Interpretation is based on modelling dissipation test response using cavity expansion or strain path methods (Torstensson, 1977; Randolph & Wroth, 1979; Levadoux & Baligh, 1986; Teh & Houlsby, 1991; Burns & Mayne, 1998). One example is the cavity expansion-critical state solution proposed by Burns & Mayne (1998) that can model the monotonic and dilatory pore pressure responses with regard to time, allowing both the octahedral and shear-induced components during penetration to be calculated as a function of OCR, ϕ' and I_r (= G/s_u). Incidentally, the undrained shear strength ratio s_u/σ'_{vo} is also a function of the same variables (e.g. Wroth, 1984; Jamiolkowski et al., 1985; Ladd, 1991). Mantaras et al (2014, 2015) combined these concepts to derive a mathematical expression correlating the ratio of normalized maximum excess pore pressure and the normalized undrained shear strength. It has been shown that the ratio of normalized values fluctuates around a mean value, being affected by soil strength and stiffness and independent on stress history. The present paper illustrates the applicability of the approach to normally consolidated and lightly overconsolidated clays.

2 BACKGROUND

The mathematical solution proposed by Burns & Mayne (1998) is based on the cavity expansion-critical state framework for the monotonic and dilatory response with regard to time. Departing from this solution, the *undrained pore pressure ratio* ($\Delta u_{max}/s_u \cdot log(I_r)$) can be expressed as (Mantaras et al, 2015):

$$\left(\frac{\Delta u_{\max}}{S_u \cdot \log(I_r)}\right) = \frac{\dfrac{\alpha\left[\dfrac{OCR}{2}\right]^{\Lambda}}{1+50\cdot T^*_{\max}} + \dfrac{1-\left[\dfrac{OCR}{2}\right]^{\Lambda}}{1+5000\cdot T^*_{\max}}}{\dfrac{1}{2}\sin(\phi)\cdot OCR^{\Lambda}\cdot\log(I_r)} \quad (1)$$

where Δu_{max} is the piezocone maximum dissipation excess pore-water pressure, OCR the overconsolidation ratio, ϕ' the effective friction angle, $M = (6sin\phi')/(3-sin\phi')$, Ir the rigidity index, Λ the compressibility ratio (1-CC/CR) and T^* the dimensionless modified time factor $T^* = [c_h t/(r^2\ Ir^{0.75})]$. The derived formulation shows little sensitivity to variations on OCR, but is influenced by ϕ' and Ir.

Assuming typical representative values of M = 1.2 (corresponding to $\phi' = 30°$), $Ir = 100$ and $\Lambda = 1.0$, equation (1) becomes, equation 2:

$$S_{u(\Delta u max)} = \frac{\Delta u_{max}}{N_{\Delta u_{max}}} = \frac{\Delta u_{max}}{4.2(\pm 0,2)\cdot log(I_r)} \frac{\Delta u_{max}}{8.4} \qquad (2)$$

3 CASE STUDY

A site investigation campaign carried out at the Tubarão Experimental Testing Site is described to illustrate the applicability of equation (2) in estimating the undrained shear strength. As part of this project, tests were carried out with as a standard 10 cm^2 piezocone and a small piezocone having a cross section area of 5 cm^2 capable of recording pore pressures at the cone tip (u_1) and the cone shoulder (u_2). The 5 cm^2 piezocone is shown in Figure 1.

Sediments in the upper 20 m are predominantly normally consolidated, formed during the last 8,000 years in the Holocene period after the most recent glaciation (Odebrecht & Schnaid, 2017; Schnaid et al, 2016). Typical CPTu profiles showing corrected cone resistance (q_t) and pore pressure (u_2) are presented in Figure 2. The water table at the site is about 0.6 m below ground level and the piezometric profile is approximately hydrostatic.

Typical piezocone dissipation tests are shown in Figure 3 for measurements recorded at both the u_1 and u_2 filter locations. The excess pore water

Figure 1. Piezocone 10 cm2 e 5 cm2 cross-section areas.

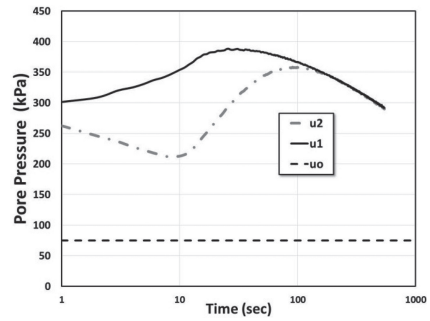

Figure 3. Dissipation pore water pressure for piezocone tip and shoulder locations (8.5 m depth – Profile 3).

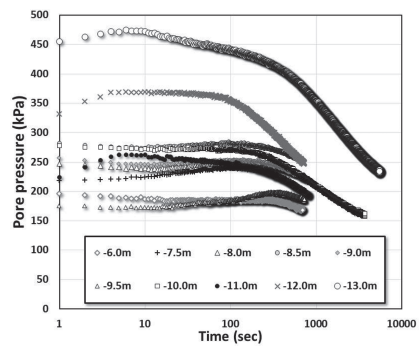

Figure 4. u_2 recorded at short dissipation tests (Profile 2).

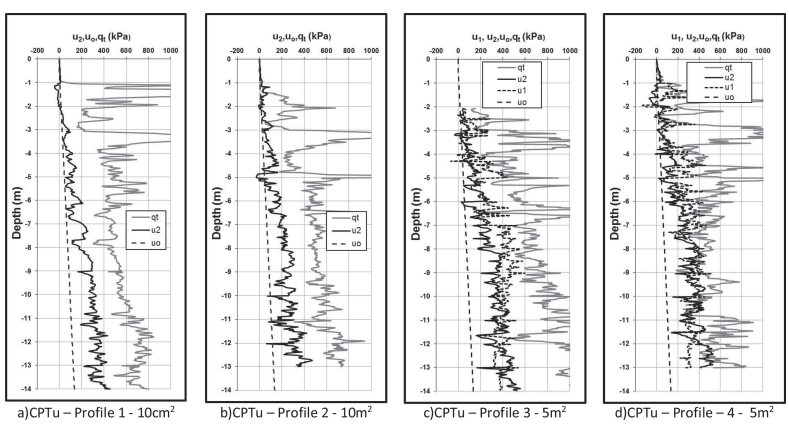

Figure 2. Typical piezocone profiles at the Tubarão Experimental Testing Site.

pressure of u_1 was larger than that of u_2. An initial drop of excess pore water pressure was first observed (except for the first 10 s at the u_2 location) and were followed by monotonic dissipation. At about 100 s the magnitude of the 2 readings converged and showed the same trend thereafter.

The major attractiveness of the approach is related to the fact that maximum dissipation excess pore-water pressure can be recorded within a couple of minutes after halting the piezocone at a given depth. In principle, Δu_{max} can be measured at every depth, while connecting a rod for a further 1 m stroke, without increasing overall costs of the test. Some examples are given in Figure 4 to 6 and are used to illustrate the predicted undrained shear strength in Figure 7. Field vane shear tests performed in a boring located near the center of the piezocone soundings were used for comparisons. The undrained shear strength estimated from vane, piezocone tip resistance and dissipation pore pressures yield s_u values in close agreement along the soft clay layer. It is worth noticing that very little scatter is observed among the different methods which reduces the uncertainties in predicting s_u.

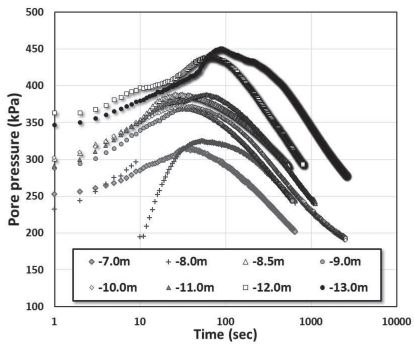

Figure 5. u_2 recorded at short dissipation tests (Profile 3).

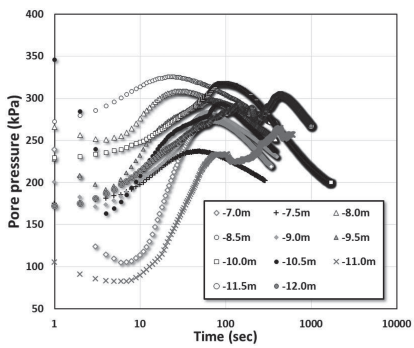

Figure 6. u_2 recorded at short dissipation tests (profile 4).

Typical piezocone dissipation tests are shown in Figure 3 for measurements recorded at both the u_1 and u_2 filter locations. The excess pore water pressure of u_1 was larger than that of u_2. An initial drop of excess pore water pressure was first observed (except for the first 10 s at the u_2 location) and were followed by monotonic dissipation. At about 100 s the magnitude of the 2 readings converged and showed the same trend thereafter.

Figures 4 to 6 present all short dissipation test for each profile and Table 1 to 3 the s_u estimation.

Table 1. s_u Estimated from profile 2.

Depth (m)	$u_{2\,max}$ (kPa)	u_o (kPa)	s_u (kPa)
–6.0	196	50	18,3
–7.5	242	65	22,1
–8.0	252	70	22,7
–8.5	284	75	26,2
–9.0	257	80	22,1
–9.5	200	85	14,3
–10.0	278	90	23,5
–11.0	263	100	20,3
–12.0	369	110	32,4
–13.0	475	120	44,4

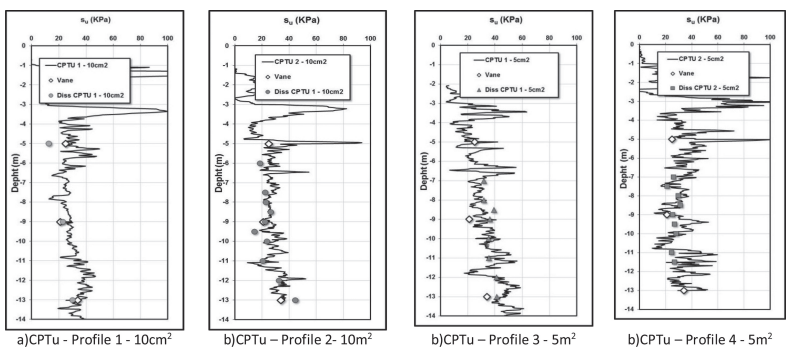

Figure 7. Predicted undrained shear strength in normally to slightly overconsolidated clay.

Based on experimental results gathered in the past 4 years, partially reported in the previous discussion, it is assured that the method gives results that are very consistent with other in situ test predictions in normally consolidated to lightly overconsolidated clays. Data summarized in Figure 9 report the experience in 9 different sites where the undrained shear strength is compared to a reference value and plotted against OCR (s_{uref} is a reference value obtained from field vane tests or laboratory triaxial tests).

Table 2. s_u Estimated from profile 3.

Depth (m)	$u_{2\,max}$ (kPa)	u_o (kPa)	s_u (kPa)
–7.0	315	60	31,8
–8.0	325	70	31,9
–8.5	388	75	39,2
–9.0	369	80	36,1
–10.0	373	90	35,3
–11.0	388	100	36,0
–12.0	439	110	41,1
–13.0	450	120	41,3

Table 3. s_u Estimated from profile 4.

Depth (m)	$u_{2\,max}$ (kPa)	u_o (kPa)	s_u (kPa)
–7.0	273	60	26,6
–7.5	237	65	21,5
–8.0	308	70	29,8
–8.5	325	75	31,3
–9.0	283	80	25,4
–9.5	298	85	26,6
–10.0	317	90	28,4
–11.0	346	100	30,8
–11.5	264	105	19,9
–12.0	304	110	24,3

Data from 6 of the reported sites have been obtained from tests performed and supervised by our own personnel, following strictly IRTP (1988) recommendations. Besides the Tubarão experimental testing site, data comprises 5 locations distributed along the Brazilian Coast. The sources of data are CPTU and laboratory consolidation and shear strength tests. In addition, 2 other locations have been included from tests reported in the literature (Sully at al 1999; Ha at al 2008) – their use required some judgment in predicting parameters that might have introduced small errors in the analysis. From these databases it is seen that the $s_u/s_{u,ref}$ ratio is 1 ± 0.2 indicating that this type of approach may be useful in giving redundancy to site investigation predictions. The reported data from Figure 8 is summarized in Table 4, including the characteristic values of *Su* and OCR.

4 CONCLUSION

The applicability of an analytical solution developed to correlate the maximum dissipation excess pore-water pressure and the undrained shear strength in normally too lightly overconsolidated clay is discussed in this paper. The solution is supported by cavity expansion and critical state soil mechanics following early studies by Burns & Mayne (1998). Results from pore pressures recorded at the cone tip (u_1) and the cone shoulder (u_2) using 5 cm^2 and 10 cm^2 piezocones provided the required database for interpretation. Based on cumulative experience, it has been demonstrated that for saturated clays in the OCR range of 1 to 5, the measured Δu_{max} provides estimates of s_u in agreement with values calculated from other tests. It offers the benefit of providing additional data for spatial interpolating and extrapolation of results from vane and triaxial tests with minimal cost increase. Additionally, comparing and pre-

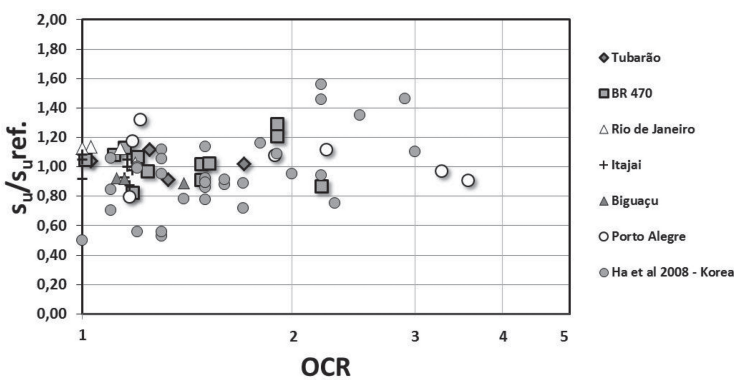

Figure 8. Variation of undrained shear strength ratio with OCR.

Table 4. Data results – (*)own results; (**) Ha et al. (2008).

Site	Deep (m)	γt (kN/m^3)	u_2(max) (kPa)	u_o (kPa)	Δ u_2(max) (kPa)	$s_u$ref (kPa)	s_u (kPa)	OCR	Reference test	OCR reference	s_u/s_uref. °
Tubarão - SC (*)	–5,0	13,0	151,4	49,4	102,0	13,0	12,8	1,71	Vane	Consolidation	1,02
	–9,0	14,0	273,4	89,4	184,0	21,0	23,0	1,33	Vane	Consolidation	0,91
	–13,0	15,0	372,4	129,4	243,0	34,0	30,4	1,25	Vane	Consolidation	1,12
	–17,5	15,0	505,4	174,4	331,0	43,0	41,4	1,03	Vane	Consolidation	1,04
BR 470 - Navegantes - SC (*)	–14,0	15,0	391,0	140,0	251,0	34,0	31,4	1,11	Vane	Consolidation	1,08
	–5,0	13,0	141,0	49,0	92,0	13,0	11,5	1,15	Vane	Consolidation	1,13
	–25,0	15,0	351,0	249,0	102,0	13,0	12,8	1,48	Vane	Consolidation	1,02
	–3,0	13,0	143,0	29,0	114,0	13,0	14,3	1,48	Vane	Consolidation	0,91
	–10,0	14,0	435,0	99,0	336,0	43,0	42,0	1,52	Vane	Consolidation	1,02
	–10,0	14,0	371,0	99,0	272,0	28,0	34,0	1,18	Vane	Consolidation	0,82
	–5,0	13,0	233,0	49,0	184,0	20,0	23,0	2,20	Vane	Consolidation	0,87
	–12,4	14,0	367,0	123,0	244,0	32,0	30,5	1,01	Vane	Consolidation	1,05
	–6,0	13,0	195,0	59,0	136,0	22,0	17,0	1,90	Vane	Consolidation	1,29
	–6,0	13,0	191,0	59,0	132,0	16,0	16,5	1,24	Vane	Consolidation	0,97
	–7,0	13,0	219,0	69,0	150,0	20,0	18,8	1,20	Vane	Consolidation	1,07
	–6,4	14,0	235,0	63,0	172,0	26,0	21,5	1,90	Vane	Consolidation	1,21
Rio de Janeiro - RJ (*)	–7,0	12,0	218,0	70,0	148,0	19,0	18,5	1,19	Vane	Consolidation	1,03
	–12,0	13,0	310,0	120,0	190,0	27,0	23,8	1,03	Vane	Consolidation	1,14
	–16,0	13,0	423,0	160,0	263,0	37,0	32,9	1,13	Vane	Consolidation	1,13
	–19,5	14,0	337,0	195,0	142,0	20,0	17,8	1,00	Vane	Consolidation	1,13
Itajaí - SC (*)	–3,0	14,0	197,0	29,0	168,0	22,0	21,0	1,00	Vane	Consolidation	1,05
	–4,0	15,0	135,0	39,0	96,0	13,0	12,0	1,00	Vane	Consolidation	1,08
	–5,0	15,0	145,0	49,0	96,0	11,0	12,0	1,00	Vane	Consolidation	0,92
	–6,0	15,0	171,0	59,0	112,0	13,0	14,0	1,15	Vane	Consolidation	0,93
	–7,0	15,0	205,0	69,0	136,0	17,0	17,0	1,16	Vane	Consolidation	1,00
	–8,0	15,0	207,0	79,0	128,0	14,0	16,0	1,17	Vane	Consolidation	0,88
	–9,0	15,0	249,0	89,0	160,0	21,0	20,0	1,16	Vane	Consolidation	1,05
	–10,0	16,0	263,0	99,0	164,0	20,0	20,5	1,18	Vane	Consolidation	0,98
Biguraçu - SC (*)	–4,0	14,0	183,0	39,0	144,0	16,0	18,0	1,40	Vane	Consolidation	0,89
	–5,5	14,0	158,0	54,0	104,0	12,0	13,0	1,12	Vane	Consolidation	0,92
	–10,5	15,0	296,0	104,0	192,0	22,0	24,0	1,15	Vane	Consolidation	0,92
Porto Alegre - RS (*)	–4,5	14,0	183,0	44,0	139,0	23,0	17,4	1,21	Vane	Consolidation	1,32
	–6,0	14,0	229,1	59,1	170,0	25,0	21,3	1,18	Vane	Consolidation	1,18
	–3,0	14,0	235,0	29,0	206,0	25,0	25,8	3,27	Vane	Consolidation	0,97
	–4,0	14,0	185,0	39,0	146,0	14,5	18,3	1,17	Vane	Consolidation	0,79
	–6,0	14,0	194,7	58,7	136,0	19,0	17,0	2,24	Vane	Consolidation	1,12
	–3,2	14,0	181,1	31,1	150,0	17,0	18,8	3,57	Vane	Consolidation	0,91
	–4,5	14,0	222,0	44,0	178,0	24,0	22,3	1,89	Vane	Consolidation	1,08
Daejeo (*8)	–3,2	14,0	113,0	12,0	101,0	17,1	12,6	2,50	Cam Clay	Consolidation	1,35
	–8,7	15,0	254,0	66,0	188,0	26,9	23,5	1,90	Cam Clay	Consolidation	1,15
	–12,1	16,0	329,0	98,0	231,0	38,2	28,9	1,80	Cam Clay	Consolidation	1,32
	–14,0	17,0	437,0	118,0	319,0	43,7	39,9	1,60	Cam Clay	Consolidation	1,10
	–16,0	18,0	500,0	137,0	363,0	52,2	45,4	1,50	Cam Clay	Consolidation	1,15
Yangsan #1 (**)	–16,0	16,0	494,0	147,0	347,0	39,7	43,4	1,60	Cam Clay	Consolidation	0,92
	–20,0	16,0	601,0	186,0	415,0	46,3	51,9	1,50	Cam Clay	Consolidation	0,89
	–25,0	18,0	760,0	235,0	525,0	74,3	65,6	1,50	Cam Clay	Consolidation	1,13
	–30,0	18,0	894,0	316,0	578,0	60,4	72,3	1,10	Cam Clay	Consolidation	0,84
	–37,4	18,0	1060,0	357,0	703,0	109,3	87,9	1,50	Cam Clay	Consolidation	1,24
Yangsan #3 (**)	–5,0	14,0	135,0	39,0	96,0	10,7	12,0	1,50	Cam Clay	Consolidation	0,89
	–10,0	16,0	295,0	88,0	207,0	23,6	25,9	1,40	Cam Clay	Consolidation	0,91
	–14,7	17,0	382,0	134,0	248,0	35,7	31,0	1,30	Cam Clay	Consolidation	1,15
	–20,4	18,0	555,0	190,0	365,0	47,8	45,6	1,10	Cam Clay	Consolidation	1,05
	–24,8	18,0	597,0	233,0	364,0	57,6	45,5	1,10	Cam Clay	Consolidation	1,27

(*Continued*)

Table 4. (*Continued*).

Site	Deep (m)	γt (kN/m³)	u_2(max) (kPa)	u_o (kPa)	Δ u_2(max) (kPa)	$s_u$ref (kPa)	s_u (kPa)	OCR	Reference test	OCR reference	s_u/s_uref. °
Yangsan	–2,8	15,0	90,0	27,0	63,0	7,3	7,9	2,30	Cam Clay	Consolidation	0,93
#4 (**)	–8,3	16,0	226,0	81,0	145,0	17,9	18,1	1,50	Cam Clay	Consolidation	0,99
	–11,6	17,0	397,0	114,0	283,0	25,7	35,4	1,30	Cam Clay	Consolidation	0,73
	–13,6	18,0	445,0	133,0	312,0	32,3	39,0	1,20	Cam Clay	Consolidation	0,83
	–15,6	20,0	520,0	153,0	367,0	39,8	45,9	1,00	Cam Clay	Consolidation	0,87
Yangsan	–20,6	17,0	601,0	143,0	458,0	63,9	57,3	1,30	Cam Clay	Consolidation	1,12
#2 (**)	–24,6	17,0	734,0	182,0	552,0	72,8	69,0	1,30	Cam Clay	Consolidation	1,06
	–37,3	17,0	1064,0	307,0	757,0	94,6	94,6	1,20	Cam Clay	Consolidation	1,00
	–39,9	17,0	1139,0	333,0	806,0	99,9	100,8	1,20	Cam Clay	Consolidation	0,99
Namak 1 (**)	–6,1	15,0	194,0	60,0	134,0	12,0	16,8	1,70	Cam Clay	Consolidation	0,72
Namak 2	–6,0	15,0	228,0	49,0	179,0	24,7	22,4	3,00	Cam Clay	Consolidation	1,10
(**)	–11,9	18,0	502,0	107,0	395,0	33,1	49,4	1,30	Cam Clay	Consolidation	0,67
Namak 3 (**)	–5,7	15,0	206,0	36,0	170,0	18,9	21,3	1,70	Cam Clay	Consolidation	0,89
Namak 4	–3,5	13,0	102,0	25,0	77,0	12,0	9,6	2,90	Cam Clay	Consolidation	1,25
(**)	–9,0	16,0	313,0	78,0	235,0	31,0	29,4	2,20	Cam Clay	Consolidation	1,06
Incheon 2	–26,0	12,0	545,0	176,0	369,0	61,6	46,1	2,10	Cam Clay	Consolidation	1,33
(**)	–28,6	14,0	874,0	202,0	672,0	93,2	84,0	2,20	Cam Clay	Consolidation	1,11
Gunsan (**)	–5,0	15,0	171,0	39,0	132,0	15,7	16,5	2,00	Cam Clay	Consolidation	0,95

dicting a constitutive parameter such as s_u from independent measurements enhances the reliability in estimating soil properties.

Further studies are required to validate the approach in heavily overconsolidated soils. Caution is required on the interpretation of tests in silty-clay, fissured clay or in the vicinity of sand lenses, where partial drainage can affect piezocone dissipation testing data.

REFERENCES

Baligh, M.M. & Levadoux, J.N. 1986. Consolidation after undrained piezocone penetration. II: Interpretation. *J. Soil Mech. Found. Engng. Div., ASCE*. 11(7), 727–745.

Burns, S.E. & Mayne, P.W. 1998. Monotonic and dilatory pore-pressure decay during piezocone tests in clay. *Can. Geotech. J*., 35(6): 1063–1073.

Ha, T.G; Chung, c.k.; Kwon, H.M; Cho, S.M; Jung, J.H. 2008. Finite difference analysis of dilatory dissipation on piezocone test in overconsolidated cohesive soil. Proc. Of the Eigteenth Inte. Offshore and Polar Engineering Conference. Vancouver, BC, Canada. 504–511.

Jamiolkowski, M., Ladd, C.C., Germaine, J.T. & Lancellotta, R. 1985. New developments in field and laboratory testing of soils. *11th Int. Conf. on Soil Mech. and Found. Engng*., San Francisco, 1: 57–153.

Ladd, C.C.1991. Stability evaluation during staged construction. J. Geotech Engng Div, ASCE, 177(4): 540–615.

Levadoux, J.N., and Baligh, M.M. (1986). "Consolidation after undrained piezocone penetration. I: Prediction." J. Geotech. Engrg. Div., ASCE, 112(7), 707–726.

Mantaras, F.M.B; Odebrecht, E.; Schnaid, F. 2014. Using piezocone dissipation test to estimate the undrained shear strength in cohesive soil. *CPT'14; 3rd International Symposium on Cone Penetration Testing.* Las Vegas.

Mantaras, F.M.B; Odebrecht, E.; Schnaid, F. 2015. Using piezocone dissipation test to estimate the undrained shear strength in cohesive soil. *Can. Geotech. J.* 52: 318–328.

Odebrecht, E. & Schnaid, F. 2017. Assessment of the stress history of Quaternary clay from piezocone tests. Soil and Rock, submitted for publication.

Schnaid, F.; Odebrecht, E.; Sosnoski, J.; Robertson, P.K.; Effects of Test Procedure on Flat Dilatometer Test (Dmt) Results in Intermediate Soils. 2016. *Canadian Geotechnical Journal*, 53(8): 1270–1280.

Sully J.P.; Robertson. P.; Campanella, R.G.; Woeller, D.J. 1999. An approach to evaluation of field CPTU dissipation data in overconsolidated fine-grained soils. Canadian Geotech. Journal 36:369–381.

Randolph, M.F. & Wroth, C.P. 1979. An analytical solution for the consolidation around a driven pile. *Int. J. for Numerical and Analytical Methods in Geomech.*, 3: 217–229.

Teh, C.I. &Houlsby, G.T. 1991. An analytical study of the cone penetration test in clay. *Geotechnique*, 41(1): 17–34.

Torstensson, B.A. 1977. The pore pressure probe. *Norsk Jord-Og Fjellteknisk Forbund. Oslo, Foredrag* 34.1–34.15, Trondheim, Norway.

Wroth, C.P. 1984. The interpretation of in situ soil test. 24th Rankine Lecture. *Géotechnique*, 34(4): 449–489.

Cone Penetration Testing 2018 – Hicks, Pisanò & Peuchen (Eds)
© 2018 Delft University of Technology, The Netherlands, ISBN 978-1-138-58449-5

Realistic numerical simulations of cone penetration with advanced soil models

Zhandos Y. Orazalin
Singapore-MIT Alliance for Research and Technology, Singapore

Andrew J. Whittle
Massachusetts Institute of Technology, Cambridge, MA, USA

ABSTRACT: The analysis of soil penetration represents a challenging class of geotechnical problems due to large deformations, high gradients of the field variables (stresses, strains, pore pressures, etc.) around the penetrometer, the various drainage conditions and complex constitutive behavior of soils. Most prior research using large deformation Finite Element (FE) methods has been limited to simplified assumptions on drainage conditions and constitutive behavior. Following earlier work by Hu & Randolph (1998), we propose a finite element analysis procedure using automated remeshing and solution mapping within a commercial FE solver (ABAQUS Standard) in order to simulate quasi-static piezocone penetration using advanced effective stress soil models. Predictions of piezocone penetration using the proposed FE analyses are evaluated through comparison with undrained *steady state* analytical solutions obtained from the Strain Path Method and with field measurements from Boston. Predictions of partially drained penetration are compared with recently published 2-phase MPM analyses and with data from laboratory (1g and centrifuge) model tests in kaolin.

1 INTRODUCTION

Piezocone testing is widely used in geotechnical engineering to investigate subsurface stratigraphy and to estimate engineering properties of pertinent soil units based (primarily) on measurements of tip resistance and penetration pore pressures. Most quantitative interpretations of the data are based on empirical classification schemes and correlations. The theoretical basis for estimating parameters such as undrained shear strength in homogenous, low permeability clays is also well established using the Strain Path Method (SPM; Baligh, 1985; Teh & Houlsby, 1991) in conjunction with relevant constitutive models. However, there is clearly a need for more comprehensive predictive capabilities for interpreting penetration in soils of transitional permeability and in interpreting piezocone signatures in layered soil systems.

Finite element analyses offer a general framework for tackling these large deformation problems. Special procedures are needed to control mesh distortions when using conventional Lagrangian FEM, (e.g., RITSS; Hu & Randolph, 1998) while more advanced methods (ALE: van den Berg, 1984; MPM: Beuth et al., 2012) mitigate this problem by considering the Eulerian flow of soil particles through a mesh. Nearly all of the published studies for cone penetration use total stress analyses and highly simplified models of soil behavior (e.g., linearly elastic perfectly-plastic, EPP). Only two studies have specifically considered partial drained piezocone penetration: 1) Yi et al. (2012) use a conventional updated Lagrangian formulation for coupled consolidation (ABAQUS/Standard; with local controls on mesh distortion) together with an EPP model; while 2) Ceccato et al. (2016) use a two-phase mixture MPM program (Anura3D, 2017) with the Modified Cam Clay soil model (MCC; Roscoe & Burland, 1968).

This paper proposes a numerical procedure for simulating large deformation piezocone penetration using an *automated* mesh-to-mesh solution mapping procedure in Abaqus/Standard™ (Simulia, 2016) which is conceptually similar to RITSS (Remeshing and Interpolation Technique with Small Strain). This method enables simulation of partially-drained coupled consolidation with advanced effective stress soil models.

2 METHODOLOGY

Figure 1 illustrates the general algorithm proposed for finite element analyses of cone penetration. The procedure combines conventional Lagrang-

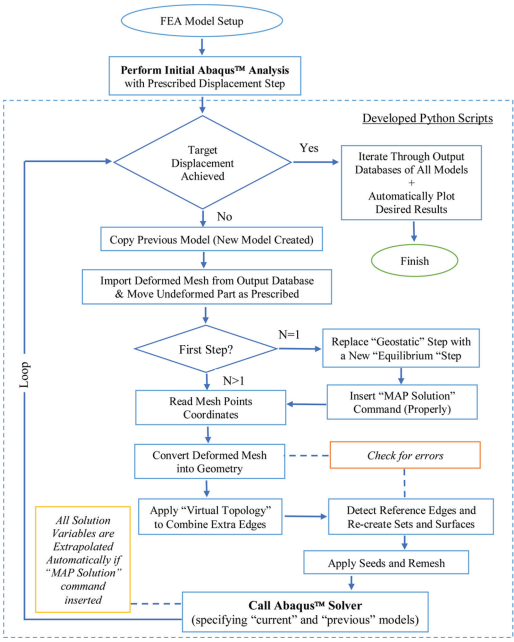

Figure 1. General algorithm for automated re-meshing and solution mapping in FE analysis (Orazalin, 2017).

ian FEM with separate remeshing (of the entire domain) and solution mapping and interpolation of the solution variables (stresses, pore pressures, state variables, etc.), using the mesh-to-mesh feature available in Abaqus/Standard.

This is controlled through a scripting interface (that uses the same syntax and operators as Python) that allows users to bypass Abaqus Environment's Graphical User Interface and communicate directly with the program kernel. After each remeshing step, a single Command is needed to initiate creation of the new FE model:

mdb.Model(name = *newmodel*, objectToCopy = mdb.models[*oldmodel*])

The accuracy of the analysis depends on the success of the interpolation employed to map the solution variables. This is especially important for complex models with (discontinuous) history-dependent state variables. The only required input is the frequency of remeshing which can be tailored to the specific problem of interest.

Figure 2a shows the geometry of the FE model for simulating axisymmetric cone penetration. Coupled consolidation within the soil mass is represented using 4-noded triangular elements (CAX4P) with bilinear interpolation of displacements and pore pressures and full integration of element stresses. The model uses an unstructured mesh constructed using an advancing front method-Delaunay algorithm (Borouchaki et al., 2000). The penetrometer is specified as a rigid shell with a rounded tip geometry (Fig. 2b) which approximates the simple pile geometry (Baligh, 1985). Previous studies (Aubeny, 1992) have found this to be a good approximation for the standard 60° conical tip while mitigating potential numerical problems associated with singular stress points.

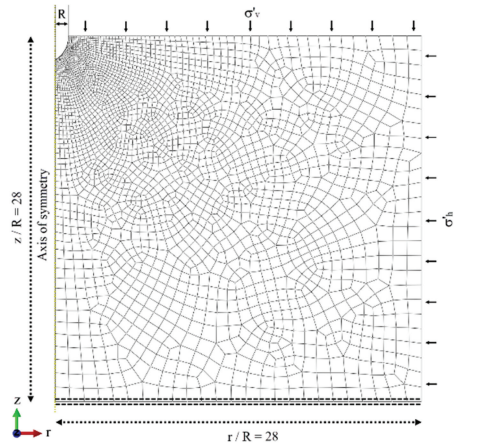

a) Initial FE mesh

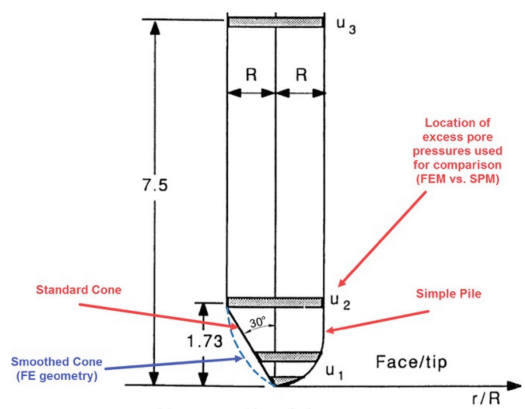

b) Details of tip geometry

Figure 2. Finite element model of axisymmetric piezocone penetration.

Contact between the penetrometer and soil is tracked using a finite sliding formulation (Simulia, 2016) which requires that the master surface (penetrometer) has a continuous surface normal at all points in order to avoid numerical convergence problems. Abaqus automatically smooths the transition between element facets along the master surface using a control parameter, f:

$f = \alpha_1/l_1 = \alpha_2/l_2$

where l_1 and l_2 are the lengths of the adjacent facets and α_1, α_2 the associated transition lengths.

In order to maintain accuracy in tracking the contact surface through multiple cycles of re-meshing and interpolation, the analyses use f = 0.01, with re-meshing conducted at fixed penetration intervals, $\Delta y/R = 0.1$. The current analyses assume smooth, frictionless contact between the penetrometer and the soil ($\delta = 0°$).

The FE model represents a standard piezocone (R = 1.78cm) moving vertically at specified displacement rate, v, within a homogenous element of soil (0.5m high with radius 0.5m; i.e., z/R = 28 = r/R). The model simulates a calibration chamber configuration (i.e., uniform initial stress state) with an initial vertical effective stress, σ'_{v0} = 100kPa applied as a surcharge at the top surface and K_0 conditions (controlled by stress history). The far boundaries (lateral and base) are free draining (zero excess pore pressures), while the top surface is assumed to be impermeable. The current analyses assume that the tip of the penetrometer is embedded within the clay (i.e., there is a perturbation of the initial stress field to achieve drained equilibrium), in order to simplify the computations.

The proposed procedure has proved to provide a robust framework that can be used in conjunction with a range of advanced effective stress models of soil behavior. Here, we compare predictions for two rate independent elasto-plastic models, Modified Cam Clay (MCC; Roscoe & Burland, 1968) and MIT-E3 (Whittle & Kavvadas, 1994) using parameters corresponding to resedimented BBC (Boston Blue Clay). The MIT-E3 model is able to describe aspects of the non-linear and anisotropic stress-strain-strength properties measured in laboratory element tests (Whittle et al., 1994). All of the analyses assume a constant hydraulic conductivity, $k = 1 \times 10^{-7}$ cm/s. The two soil models are integrated within Finite Element solvers through UMAT (user-defined material model) subroutines (Hashash, 1992; Akl, 2010; Orazalin, 2015) and have been compared in prior analyses of penetrometer tests in clays using the Strain Path Method (Aubeny, 1992; Aubeny & Whittle, 1992).

3 UNDRAINED PENETRATION

Figure 3 shows the remeshing process and typical predictions of the excess pore pressures at several different tip depths. The results in Figure 4 compares finite element predictions for standard piezocone penetration (v = 2cm/s) in K0-consolidated BBC using the MCC and MIT-E3 soil models. Automatic remeshing (and interpolation) has been carried out at fixed intervals in these analyses ($\Delta z/R = 0.1$), such that there is no apparent distortion in the meshes shown in Figure 3, while effects

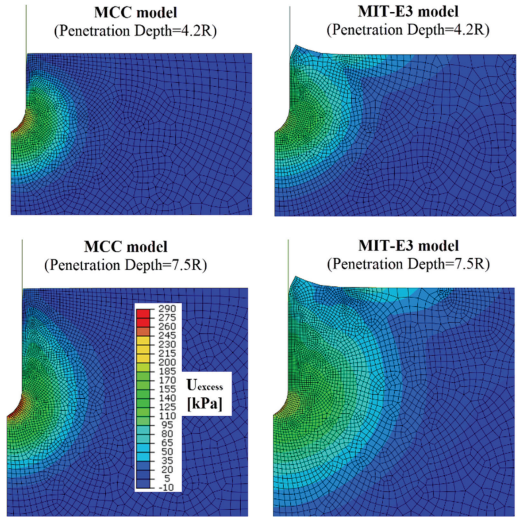

Figure 3. Excess pore pressure fields for undrained penetration in K_0-normally consolidated BBC (MCC and MIT-E3 models).

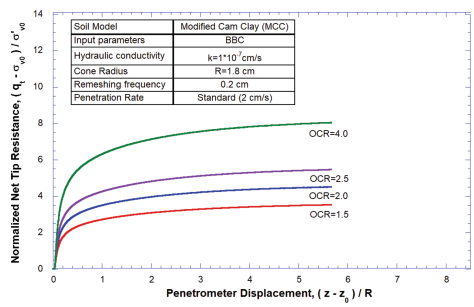

a) MCC model predictions

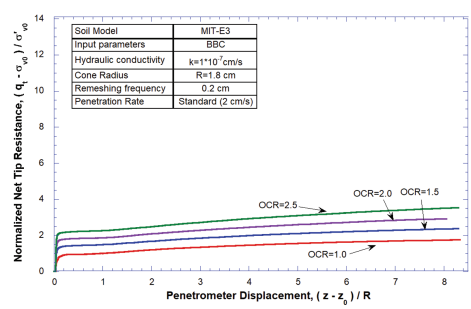

b) MIT-E3 model predictions

Figure 4. Effect of soil model and stress history on predictions of undrained penetration resistance.

of the initial embedment are seen in the excess pore pressures near to the top surface. There is minimal migration of pore water within the model (this is readily checked by increasing the displacement

rate). The computed excess pore pressures around the tip of the penetrometer at z/R = 5.5 are in close agreement with prior Strain Path analyses using the same soil models (Aubeny, 1992).

Figure 4a shows the computed net tip resistance, $(q_t\text{-}\sigma_{v0})/\sigma'_{v0}$ as a function of the penetration depth for the MCC soil model with OCR's ranging from 1.0–4.0. These results show rapid convergence towards steady state penetration conditions. In contrast, predictions for MIT-E3 (Fig. 4b) show the tip resistance increasing more gradually with penetration depth. This result can be attributed to the effects of non-linear shear stiffness at small strains, that generate a much larger zone of excess pore pressures around the penetrometer. The current analyses were extended to a total depth, z/R = 8.25, at which point the excess pore pressures were affected by proximity to the base boundary in the model.

Figure 5a compares the net tip resistance from the current finite element and prior steady state Strain Path analyses (presented by Aubeny, 1992).

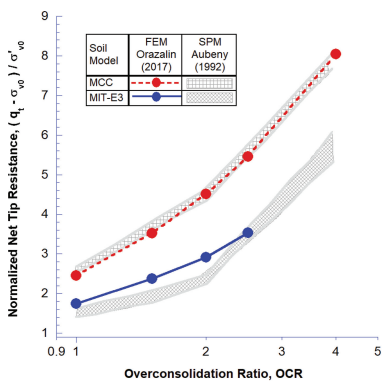

a) Comparison with predictions from Strain Path Method (Aubeny, 1992)

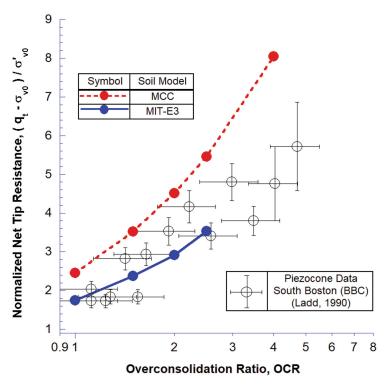

b) Comparison with measured piezocone data, South Boston (Whittle & Aubeny, 1992; Ladd et al., 1998)

Figure 5. Evaluation of FE predictions of undrained penetration resistance in BBC.

There is excellent agreement between the two sets of analyses for MCC (for OCR = 1.0–4.0). The FE predictions for MIT-E3 (interpreted at the final penetration depth) are also in reasonable agreement with the prior SPM analyses but further refinements are needed to establish steady state conditions in the FE model.

Differences in the computed tip resistance from the two soil models can be linked to the undrained strength anisotropy of MIT-E3. The two models exhibit similar shear strength in triaxial compression, but MIT-E3 predicts lower strength in the direct simple shear and extension models (s_{uDSS}/s_{uTC} = 0.65, s_{uTE}/s_{uTC} = 0.64, respectively, at OCR = 1.0).

There are several well documented sets of piezocone data in BBC. Figure 5b compares results from tests published by Ladd et al. (1998) from the CA/T Special Test Site in South Boston. The results show the mean and standard deviation of the net cone resistance and OCR computed over 3m (10ft) intervals through the full depth (43+m) of the clay. The data show significant scatter in net tip resistance with OCR. However, it is apparent that the MCC model generally overestimates the measured behavior, while MIT-E3 is in better agreement with the data (especially at low OCR).

4 EFFECTS OF PARTAL DRAINAGE

Partial drainage refers to the situation where there is concurrent generation and dissipation of excess pore pressures during steady penetration. McNeilan and Bugno (1984) showed that resistance (of a standard 10cm^2 cone at 2cm/s) was closely correlated with the hydraulic conductivity of silts at four sites where k ranged from 10^{-7}–10^{-4} cm/s. The reported tip resistance for drained penetration (k > 10^{-4}cm/s) were a factor of 7 larger than that measured in undrained situations (k ≤ 10^{-7}cm/s). Suzuki and Lehane (2014) investigated partial drainage in lightly overconsolidated Burswood clay by varying the penetration rates in the range v = 2 × 10^{-5}–2.0cm/s. Their data showed a factor of 2 difference between drained and undrained penetration. The highest tip resistance at the slowest penetration rate (fully drained) but the lowest tip resistance occurred in the range 0.02–0.2cm/s suggesting that penetration properties are also influenced by rate-dependent soil behavior.

Partial drainage effects can be readily simulated in the proposed FE analyses by varying either the penetration rate, hydraulic conductivity or size of the cone. Results in Figure 6 show typical predictions of penetration tip resistance (in the calibration chamber model, Fig. 1) using the MCC soil model for normally consolidated BBC at penetra-

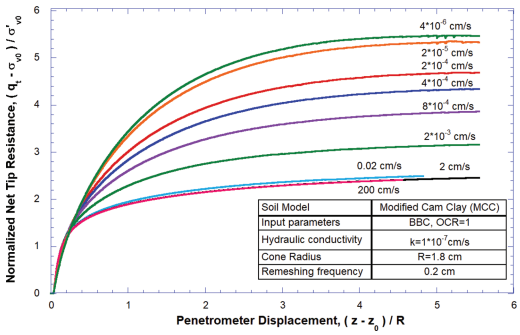

Figure 6. Effect of penetration rate on computed penetration resistance using MCC soil model.

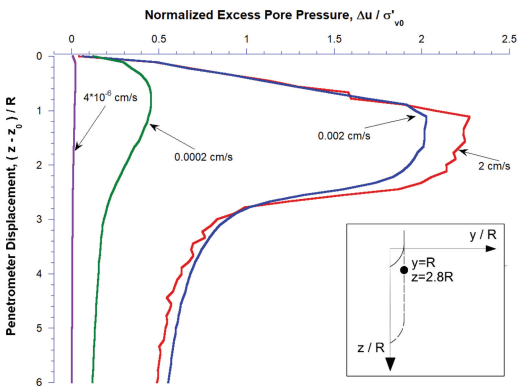

Figure 7. Effect of penetration rate on computed penetration resistance using MCC soil model.

tion rates varying from 4×10^{-6}–200cm/s. Each simulation was conducted to a minimum penetration depth, z/R = 5 with at least 50 automated remeshing steps.

The steady state penetration resistance is well defined in each of these simulations. The results show that drained penetration ($[q_t-\sigma_{v0}]/\sigma'_{v0} = 5.47$) occurs for $v \leq 2 \times 10^{-5}$cm/s; while undrained behavior is found in all case with $v \geq 0.02$cm/s ($[q_t-\sigma_{v0}]/\sigma'_{v0} = 2.45$). Partial drainage effects are observed for intermediate values of v. Figure 7 shows the computed excess pore pressures at a fixed point in the FE model (r/R = 1; z/R = 2.5). These results show that maximum excess pore pressures occur close to the base of the cone for undrained penetration, while there are no excess pore pressures in the fully drained penetration.

In order to validate the proposed FE analyses, we have attempted to replicate recent numerical simulations of piezocone tests reported by Ceccato et al. (2016) using the Material Point method (MPM). Ceccato et al. (2016) also use the MCC soil model with input parameters selected for K_0-normally consolidated kaolin. They report results corresponding to selected values of a normalized velocity, V[-] = vD/cv (after Randolph & Hope, 2004) where D is the one diameter and c_v is a constant coefficient of consolidation. In general, the stiffness of the surrounding soil will vary with the penetration induced stresses (and is therefore not constant). Ceccato et al. (2016) select a reference value (based on compression properties of NC kaolin):

$$c_v = \frac{k(1+e_0)}{\lambda \gamma_w} \sigma'_{v0} \tag{1}$$

where k is the hydraulic conductivity, e_0 and σ'_{v0} are specified initial void ratio and vertical effective stress (1.41, 50 kPa), λ is the virgin compression index (0.205) and γ_w the unit weight of water.

Figure 8 compares the FE and MPM predictions of penetration resistance for NC kaolin at selected values of V. The results show excellent agreement between the two analyses for undrained conditions (V = 501). However, the FE analyses predict higher tip resistance at lower values of the normalized velocity. For the fully drained case the FE analyses predict that a net tip resistance ($[q_t - \sigma_{v0}]/\sigma'_{v0} = 4.1$) that is 25% higher than the values reported by Ceccato et al. (2016). The source of this discrepancy requires further investigation but may be related in part to difference in the tip geometry (the MPM analyses uses a 60° conical tip, while the FE use a rounded geometry as shown in Fig. 1).

Ceccato et al. (2016) also show that there the interface friction between the cone and soil can have a large effect on penetration resistance, particularly for drained penetration. We plan to extend the current FE analyses to include effects of tip geometry and interface shear resistance.

There are a variety of laboratory tests that have been used to investigate cone resistance in nor-

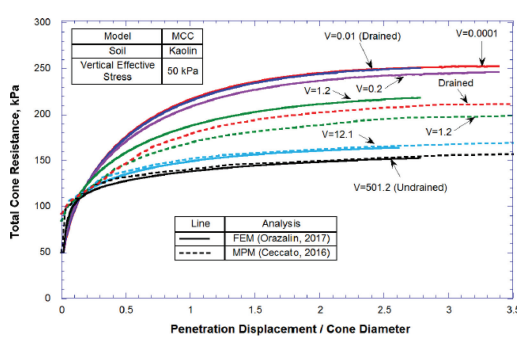

Figure 8. Comparison between proposed FE analyses and results reported using MPM method (μ = 0) using MCC model for NC Kaolin.

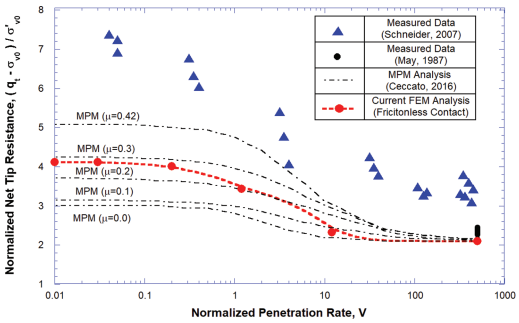

Figure 9. Comparison of computed and measured effects of partial drainage on piezocone tip resistance in kaolin.

mally consolidated kaolin including data from 1-g calibration chamber tests and centrifuge model tests. May (1987) performed a suite of tests at different penetration rates using miniature piezocones (A = 1cm^2 and 5cm^2) in 1g calibration chamber specimens with V = 480–1050 (based on lab measurements of c_v) i.e., tests in the undrained range where viscous effects are expected. Schneider et al. (2007) report results of centrifuge tests with a miniature piezocone (A = 0.079cm^2) at velocities v = 0.3 4 × 10^{-5}cm/s (V = 0.05–500, based on the reference value of c_v, Eqn. 1).

Figure 9 compares the measured net tip resistance from these experiments with the predictions from the current FE analyses and the prior MPM analyses by Ceccato et al. (2016) using a range of interface friction coefficients (μ = 0 = 0.42). In undrained conditions the FE analyses (V ≥ 50), the proposed FE analyses are in very good agreement with net tip resistance measurements in the calibration chamber, but generally underestimate the data from the centrifuge model tests. This discrepancy becomes more pronounced in slow penetration tests (drained conditions, V ≤ 0.1) where the measured tip resistance 6.9–7.4 (vs 4.1 predicted). MPM analyses of partially drained penetration predict lower tip factors than the current FE analyses (when compared with a smooth interface, m = 0). When interface friction is included the MPM model can match the measured drained tip resistance for μ 0.3.

These comparisons should be viewed as preliminary. On-going research is now focused on the role of more advanced soil model in simulating partially (and fully) drained penetration.

5 CONCLUSIONS

This paper has proposed an automated procedure for remeshing and interpolation in conjunction with a standard Lagrangian FE method to simulate large deformations caused by quasi-static piezocone penetration in soil. This methodology enables practical calculations of steady state penetration conditions with partial drainage using advanced effective stress soil models. The current paper demonstrates the accuracy of the proposed FE analysis for representing undrained penetration in clays using the MCC and MIT-E3 soil models, through comparison with prior Strain Path analyses and field measurements. Simulations of partially drained penetration (that would typically occur in transitional soils) are represented by using the MCC model to represent penetration in kaolin at a range of penetration velocities. Discrepancies from prior MPM analyses of drained penetration may be related to modeling of tip geometry and interface friction, while future studies will focus on implementations with advanced models that can represent the behavior of silts.

REFERENCES

Akl, S.A. 2010. *Wellbore instability mechanisms in clays*. PhD thesis, Massachusetts Institute of Technology, 341p.

Anura3D. 2017. *Scientific Manual for Anura3D MPM Software*, MPM Community, Ed. M. Martinelli.

Aubeny, C.P. 1992. *Rational interpretation of in-situ tests in cohesive soils*. PhD Thesis, Massachusetts Institute of Technology, 433p.

Baligh, M.M. 1985. Strain Path Method. *ASCE Journal of Geotechnical Engineering*, 111(GT9), 1131–1146.

Beuth L. 2012. *Formulation and application of a quasi-static material point method*. PhD thesis, Univ. of Stuttgart, Stuttgart, Germany.

Borouchaki, H., Laug, P. & George, P.L. 2000. Parametric surface meshing using a combined advancing-front generalized Delaunay approach. *International Journal for Numerical Methods in Engineering*, 49(1–2): 233–249.

Ceccato, F. 2015. *Study of large deformation geomechanical problems with the Material Point Method*. PhD Thesis, University of Padova.

Ceccato, F., Beuth, L., & Simonini, P. 2016. Analysis of Piezocone Penetration under Different Drainage Conditions with the Two-Phase Material Point Method. ASCE *Journal of Geotechnical and Geoenvironmental Engineering*, 142(12), 04016066-1

Hashash, Y.M.A 1992. *Analysis of deep excavations in clay*. PhD thesis, Massachusetts Institute of Technology, 344p.

Hu, Y. & Randolph, M.F. 1998. A practical numerical approach for large deformation problems in soil. *International Journal for Numerical and Analytical Methods in Geomechanics 22*(5): 327–350.

Ladd, C., Young, G.A., Kraemer, S. & Burke, D. 1999. Engineering properties of Boston Blue Clay from Special Testing Program. In *Special Geotechnical testing: Central Artery/Tunnel Project in Boston, Massachusetts, ASCE GSP 91,* 1–24.

Lu, Q., Randolph, M.F., Hu, Y. & Bugarski, I. 2004. A numerical study of cone penetration in clay. *Géotechnique 54*(4): 257–267.

May, R. 1987. *A study of the piezocone penetrometer in normally consolidated clay*, PhD Thesis, Oxford University.

McNeilan, T.W., & Bugno, W.T. 1985. Cone penetration test results in offshore California silts. Strength Testing of Marine Sediments: Laboratory and In Situ Measurements, ASTM STP 883: 55–71.

Orazalin, Z.Y. 2017. *Analysis of large deformation offshore geotechnical problems in soft clay*. PhD Thesis, MIT, 303p.

Orazalin, Z.Y., Whittle, A.J. & Olsen M.B. 2015. Three-Dimensional Analyses of Excavation Support System for the Stata Center Basement on the MIT Campus. *Journal of Geotechnical and Geoenvironmental Engineering*, 141(7).

Roscoe, K. & Burland, J.B. 1968. On the Generalized Stress-Strain Behavior of 'Wet' Clay. In *Engineering Plasticity, Cambridge University Press*, 535–609.

Schneider, J., Lehane, B.M., & Schnaid, F. 2007. Velocity effects on piezocone measurements in normally and over consolidated clays. *International Journal of Physical Modelling in Geotechnics 7*(2): 23–34.

Simulia. 2016. *Abaqus Documentation* by Dassault Systemes.

Teh, C.I., & Houlsby, G.T. 1991. An analytical study of the cone penetration test in clay. *Géotechnique*, 43(1): 17–34.

van den Berg, P. 1994. *Analysis of soil penetration*. PhD thesis, Delft University of Technology.

Whittle, A.J. & Aubeny, C.P. 1992. The effects of installation disturbance on interpretation of in-situ tests in clays. *Predictive Soil Mechanics*, Proceedings of the Wroth Memorial Symposium, Thomas Telford, London, 742–768.

Whittle, A. & Kavvadas, M. 1994. Formulation of MIT-E3 constitutive model for overconsolidated clays. *ASCE Journal of Geotechnical Engineering 120*(1), 173–198.

Whittle, A.J., DeGroot, D.J., Ladd, C.C. & Seah, T-H. 1994. Model prediction of the anisotropic behavior of Boston Blue Clay. *ASCE Journal of Geotechnical Engineering*, 120(1): 199–225.

Yi, J.T., Goh, S.H., Lee, F.H. & Randolph, M.F. 2012. A numerical study of cone penetration in fine-grained soils allowing for consolidation effects. *Géotechnique*, 62(8): 707–719.

Taylor & Francis
Taylor & Francis Group
http://taylorandfrancis.com

Cone Penetration Testing 2018 – Hicks, Pisanò & Peuchen (Eds)
© 2018 Delft University of Technology, The Netherlands, ISBN 978-1-138-58449-5

Calibrating NTH method for ϕ' in clayey soils using centrifuge CPTu

Z. Ouyang & P.W. Mayne
Georgia Institute of Technology, Atlanta, USA

ABSTRACT: An existing effective stress limit plasticity solution for piezocone penetration tests (CPTu) developed at the Norwegian Institute of Technology (NTH) is calibrated to evaluate the effective stress friction angle ϕ' for clayey soils subjected to centrifuge model testing. Results from previously conducted in-flight mini-piezocone tests by various institutes were compiled for study, including readings taken from 13 series of centrifuge chamber tests on artificially prepared clays, mainly kaolin and kaolinitic-silica mixtures. Effective stress friction angles from companion triaxial compression tests (CAUC or CIUC) and/or Direct Simple Shear (DSS) tests on these soil deposits were adopted as the benchmark reference to verify the reasonableness of the NTH method in assessing ϕ' at constant penetration rates, as well as a few special tests conducted at variable rates.

1 INTRODUCTION

The use of laboratory testing and artificially-prepared soils helps mitigate the issues of inherent variability and scatter from natural soil deposits when evaluating results from field tests. Also, it is possible to minimize the uncertainty involved in interpreting in-situ test results by verifying, in a calibration chamber, any analytical, theoretical numerical, or empirical relationship between a measured quantity and the reference soil parameters (Ouyang & Mayne 2016).

This study illustrates the interpretation of ϕ' from clays in centrifugal model chamber tests containing artificially-prepared soils under various accelerations and subjected to mini-piezocone penetration tests (CPTu). Results from a total of 13 centrifuge model test series on manufactured clayey soils, mainly kaolinitic clay deposits and silica-kaolin mixtures.

The data are taken from in-flight mini-piezocone penetrometer testing at constant penetration rates, as well as a few variable penetration rate tests (twitch testing). The total cone tip resistance (q_t) and penetration porewater pressure (u_2) at the shoulder position from the miniature penetrometers were recorded. Details on centrifuge model test dimensions, accelerations, piezocone diameters, test rate and soil parameters such as moisture content, liquid limit, plasticity index, and stress history were reviewed and tabulated.

The interpretation of the effective stress friction angle ϕ' from CPTu is carried out using an existing undrained limit plasticity solution from the Norwegian Institute of Technology (Senneset et al. 1989, Senneset & Janbu 1985). The evaluated effective stress friction angle ϕ' from the centrifuge CPTu soundings are compared with benchmark values primarily obtained from laboratory CAUC and/or CIUC triaxial tests on the corresponding soils to examine the validity of the solution.

2 CENTRIFUGE MODEL TESTING

2.1 *Principles of centrifuge modeling*

The geotechnical centrifuge is a useful tool to study the mechanical behavior of soils for very large physical structures in order to allow modelling at large strains where failure is too costly to conduct at full scale (Schofield 1980). The centrifuge applies an increased gravitational acceleration to small-scale physical models to produce identical self-weight stresses in the model that simulate those in the prototype. Thus, results from the centrifuge model tests can be utilized to validate and calibrate analytical and/or numerical methods. Details on the principles and operations of the centrifuge, scaling laws, equipment, and procedures are given by Springman et al. (2010).

2.2 *Geomaterials used in centrifuge tests*

The centrifuge series reviewed in this study were collected from laboratory programs established at the University of Western Australia, Cambridge University, National University of Singapore, University of Colorado Boulder, and Zhejiang University, which have different equipment, acceleration capacities, and dimensions.

For this study, the focus was on clayey type soils and the geomaterials that were subjected to centrifuge modeling are mainly kaolinitic type clay deposits and silica-kaolin and or clay-sand mixtures, which are prepared initially as a slurry and then consolidated in the model chambers. For the majority of the soils studied in this paper, the stress histories applied in the chamber tests focused on normally consolidated (NC) to lightly-overconsolidated (LOC) clay deposits. A special series of tests by Cinicioglu et al. (2006) investigated a range of tests with $1 \leq OCRs \leq 150$, where $OCR = \sigma'_p / \sigma'_{vo}$ = overconsolidation ratio.

Table 1 shows the summary information on the centrifuge series including accelerations, clay types, and their data reference sources.

Table 2 illustrates the geotechnical index parameters of the clay deposits which was prepared, such as water content, liquid limit, plasticity index, and overconsolidation ratio. The initial water contents (w_n) of the soils before the consolidation stage ranged from 30% to 136%, the liquid limit (LL) was between 27% to 80%, and the plasticity index (PI) varied around 2% to 35%.

2.3 *Mini-piezocone penetration tests in centrifuge*

Each of the soil deposits was tested using miniature piezocone penetrometers. Most of the probes had a diameter of d = 10 mm, except the penetrometers adopted by Zhou et al (2014) and Silva & Bolton (2005) where d = 12 mm, and Cinicioglu et al. (2006) used a mini cone with d = 11.3 mm. The equivalent prototype depth was calculated as the product of the model depth times the acceleration.

Two sets of CPTu test series are analyzed to observe the influence of penetration rate: (a) inflight penetration with a constant push rate test, and (b) a limited series of twitch tests with variable penetration rates. Table 3 lists the details about the centrifuge chamber sizes (rectangular shape chamber/cylindrical chamber), penetrometer probe dimensions, and the corresponding penetration rates that were adopted for analysis in these test series.

Table 1. Centrifuge model test series reviewed in this study.

No.	a_g	Clay type	Reference
1	100	Kaolin 1	Teh et al (2007)
2	100	Sandy Kaolin	Teh et al (2006)
3	160	Kaolin 2	Schneider (2008)
4	110	Kaolin 3	Mahmoodzadeh & Randolph (2014)
5	160	Kaolin 4	Randolph & Hope (2004)
6	100	Pisa Clay 1	Burland et al. (2003)[1]
7	100	Pisa Clay 2	Burland et al. (2003)[1]
8	100	Pisa Clay 3	Burland et al. (2003) [1]
9	150	Speswhite Kaolin	Cinicioglu et al. (2006)[2]
10	30	Clayey Sand	Zhou et al. (2014)
11	50	Silica flour	Silva & Bolton (2005)
12	100	K75-S25[3]	Fitzgerald (2009)
13	75	China Kaolin	Esquivel and Silva (2000)

Notes: a_g = centrifuge acceleration in g;
[1]Additional data from Jamiolkowski & Pepe (2001);
[2]Additional information from Cinicioglu et al. (2007);
[3]Mixture of 75% kaolin + 25% sand.

Table 2. Geotechnical parameters of the clayey soils in the centrifuge series.

No.	Clay type	Indices			
		w_n (%)	LL (%)	PI (%)	OCR
1	Kaolin 1*	120	61	27	1.0
2	Sandy Kaolin	120	80	35	1.0
3	Kaolin 2	120	61	34	1.0
4	Kaolin 3*	120	61	27	1.0
5	Kaolin 4*	120	61	27	1.0
6	Pisa Clay 1	88	71	29	1.6
7	Pisa Clay 2	88	52	24	1.2
8	Pisa Clay 3	88	56	23	1.1
9	Speswhite Kaolin	136	53	21	1.0
10	Clayey Sand	NA	NA	27	1.0
11	Silica flour	31	27	2	NA
12	K75-S25	92	46	22	NA
13	China Kaolin	106	53	21	1.0

*same type of kaolin used.

Table 3. Chamber sizes and penetrometer information.

Soil no.	Equipment and test parameters			
	Chamber size[1]	d (mm)	v (mm/s)	V
1	650 · 390 · 340	10	1	64
2	500 · 370[2]	10	2.5	40
3	650 · 390 · 325	10	3	630
4	650 · 390 · 325	10	0.0045 to 1	160[3]
5	650 · 390 · 325	10	1	120
6	850 · 400[2]	10	1	NA
7	850 · 400[2]	10	1	NA
8	850 · 400[2]	10	1	NA
9	606 · 537[2]	11.3	20	400
10	730 · 350 · 300	12	1	NA
11	850 · 400[2]	12	2 to 8	>40
12	650 · 390 · 325	10	1	62
13	NA	12.7	NA	NA

[1]Rectangular chamber: Length · Width · Height (mm);
[2]Cylindrical chamber: Diameter · Height (mm);
[3]V varies from 1 to 160 based on different push rate.

A non-dimensional velocity parameter $V = v \cdot d/c_v$, where v = push rate, d = cone diameter and c_v = coefficient of consolidation has been defined to determine the drainage regime of the soils during testing (DeJong et al 2013, Randolph & Hope 2004), where a V > 30 indicates undrained penetration. For most of the centrifuge testing series investigated in this paper, it is believed that the geomaterial undergo undrained penetration process, except for the twitch test series studied in the later section of the paper, which simulate different drainage regimes.

3 EFFECTIVE FRICTION ANGLE FROM CPTU

Soft to firm to stiff intact clays will exhibit excess porewater pressures during penetration tests ($\Delta u > 0$). An effective stress limit plasticity solution from NTH was derived for the CPTu (Senneset & Janbu 1985) towards the evaluation of ϕ' during undrained penetration. The full solution allows for an interpretation of a paired set of effective stress Mohr-Coulomb strength parameters (c' and ϕ') for all soil types, including: sands, silts and clays, as well as mixed soils (Sandven 1990).

Ouyang and Mayne (2016) reviewed data from 11 series of 1-g clay chamber tests using miniature cone and piezocone penetrometers and found that the NTH solution gave good evaluations of ϕ' for prepared deposits of clays, mostly having used kaolin and/or kaolinite-sand mixtures in these testing programs. In a larger study, Ouyang and Mayne (2017) helped to verify the limit plasticity NTH solution by calibrating the theory with data from 105 field sites underlain by natural clays and clayey silts that were subjected to both field CPTu and laboratory triaxial testing.

For the specific case ($c' = 0$, $\beta = 0°$), a closed-form version of the analytical solution was derived for calculating the effective stress friction angle ϕ' for clays, silty clays, and clayey silts in the following mathematical format:

$$Q = \frac{\tan^2(45° + \phi'/2) \cdot \exp(\pi \cdot \tan\phi') - 1}{1 + 6 \cdot \tan\phi' \cdot (1 + \tan\phi) \cdot B_q} \qquad (1)$$

where the original NTH cone resistance number (N_m) is equal to $Q = q_{net}/\sigma'_{v0}$ = normalized cone tip resistance, and $B_q = \Delta u/q_{net}$ = porewater pressure parameter, $q_{net} = q_t - \sigma_{v0}$ = net cone resistance, and $\Delta u = u_2 - u_0$ = measured excess porewater pressure.

A full inversion of Equation (1) is not possible, yet an approximate solution can be developed over an expected range of effective stress friction angles ($20° \le \phi' \le 45°$) and limited values of porewater pressure parameter ($0.1 \le B_q \le 1.0$):

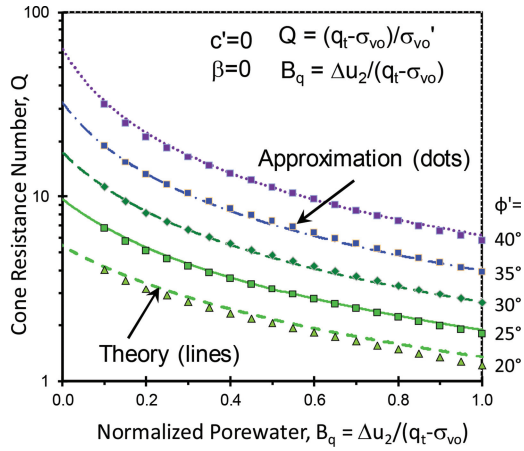

Figure 1. NTH method for evaluating ⊠' from CPTu in intact clays and clayey silts using approximate and exact solutions.

$$\phi' \approx 29.5° \cdot B_q^{0.121} [0.256 + 0.336 \cdot B_q + \log Q] \qquad (2)$$

The approximate expression is compared with the actual closed-form analytical solution in Figure 1 and seen to be in reasonable agreement over the specified ranges of ϕ' and B_q.

4 APPLICATION TO CENTRIFUGE SERIES

Most of the data from in-flight mini-piezocone tests in centrifuge series were taken at constant rates of penetration. In a few special series, termed "twitch tests", the piezocone series recorded the penetration readings at variable rates of penetration. Selected examples are presented in the following subsections to illustrate the application of the NTH method.

4.1 *Constant rate piezocone testing in centrifuge*

Centrifuge testing on kaolin (Soil ID No. 3) was performed using the beam centrifuge at the University of Western Australia (UWA). The clay samples were prepared in 325 mm high strong boxes with plan dimensions of 390 mm by 650 mm. Normally-consolidated kaolinitic clay having a liquid limit of 61%, plasticity index of 34%, and initial water content of around 55% to 70% was prepared as slurry and consolidated. Afterwards, the deposit was subjected to an acceleration of 160 g and inflight piezocone tests made with a constant probe push rate of 3 mm/s. Miniature piezocone penetration test were conducted using a 10 mm diameter penetrometer with a 60 degree tip angle, which has a polypropylene filter element behind the 1 mm high

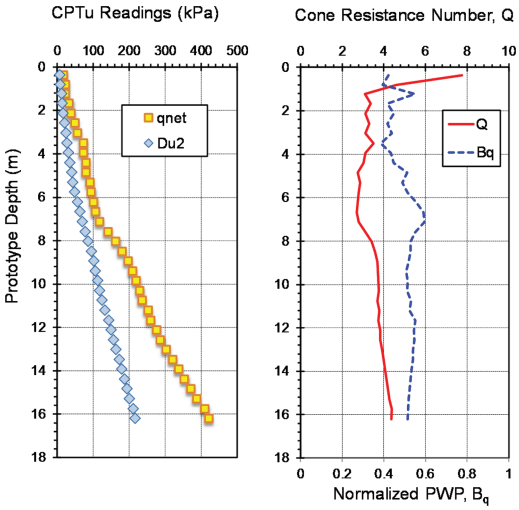

Figure 2. Profiles of q_{net}, Δu, Q and B_q in NC kaolin in centrifuge testing (data from Schneider 2008).

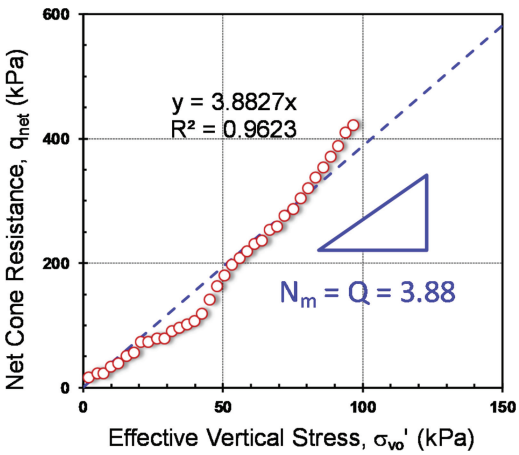

Figure 3. Derivation of the cone resistance number Q for kaolin 2 (data from Schneider 2008).

cone shoulder to measure u_2. The cone did not have a friction sleeve (Schneider 2008).

Figure 2 illustrates the profiles of the net cone resistance ($q_{net} = q_t - \sigma_{vo}$) and the excess pore water pressures ($\Delta u = u_2 - u_0$) measured during the centrifuge piezocone penetration test. The corresponding profiles of cone resistance number Q and normalized porewater pressure B_q are also shown in the figure.

The input parameters Q and B_q for calculating the friction angle ϕ' using the NTH solution can also be found by the following process. The cone resistance number Q is found as the slope from plotting net cone resistance q_{net} vs. effective overburden stress σ'_{v0}, as illustrated in Figure 3.

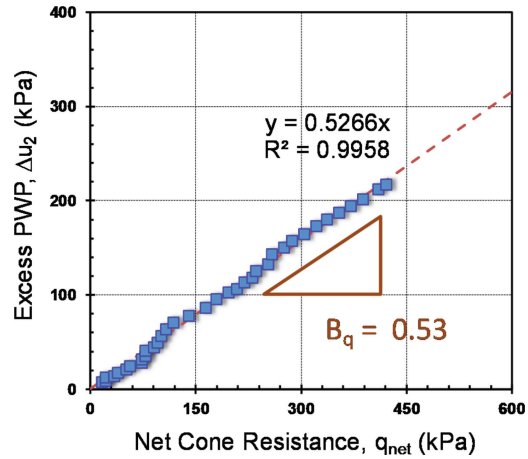

Figure 4. Derivation of porewater pressure parameter B_q for kaolin 2 (data from Schneider 2008).

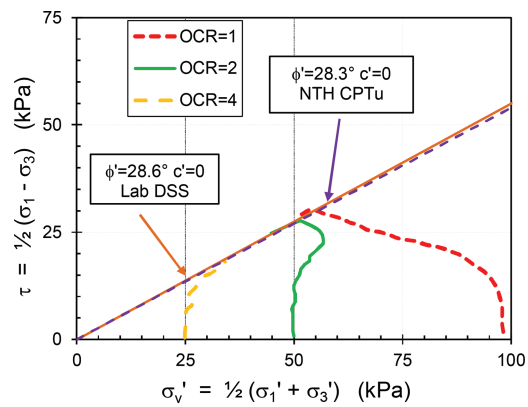

Figure 5. Comparison of NTH evaluated effective friction angle ϕ' from CPTu with lab DSS (data from Schneider 2008).

In this example, we force the line through the origin (assuming $c' = 0$) to obtain Q = 3.88. By the same token, the normalized porewater parameter B_q is determined as the slope of measured excess porewater pressure $\Delta u = (u_2 - u_0)$ versus net cone resistance q_{net}, giving the value of $B_q = 0.53$ for this sounding, as indicated by Figure 4. The paired Q-B_q are the input for friction angle calculation and according to Figure 1, the evaluated ϕ' from the CPTu sounding is $\phi' = 28.3°$. This value compares well with a measured value of $\phi' = 28.6°$ obtained from laboratory direct simple shear test (DSS) on the same soil, as confirmed by Figure 5.

4.2 *CPTu twitch test at 110g acceleration*

A special series of CPTu soundings that are conducted at variable penetration rates are termed

twitch tests (Randolph 2004; DeJong et al. 2013). Twitch testing is known to influence the measured magnitudes of cone resistance q_t and porewater pressure u_2 and was devised to study the quantify the effects of partial drainage, viscous behavior, and dissipation response of soils (Randolph & Hope 2004). In low permeability soils, by varying the CPTu penetration rate during centrifuge testing, one can monitor the consolidation conditions from undrained to partially-drained to fully drained. In this case study, a series of centrifuge CPTu of various probe push rates on normally consolidated kaolin under an acceleration of 110 g were done by UWA to examine the sensitivity of the NTH method in evaluating ϕ'.

As reported by Mahmoodzadeh and Randolph (2014), a commercial dry kaolin (clay ID No. 4 in Table 1) was mixed under a vacuum at an initial water content of 120% before being placed above a sand drainage layer in the centrifuge strongbox. Consolidation was applied in steps with the final sample height recorded at 230 mm and corresponding to a prototype depth of 25.3 m.

Penetration rates for these six twitch test series varied from 1 mm/s to 0.0045 mm/s and the effect of the testing rate on the interpretation of the soil parameters were analyzed. The change of the penetration rate could indicate the change of the drainage condition during the penetration for the kaolin clays subjected to CPTu, with the fastest rate of 1 mm/s to be undrained penetration and the lowest rate 0.0045 mm/s to be drained. Table 4 lists the information about the twitch testing ID, the corresponding penetration rate, the net cone resistance q_{net} at the final test depth, the excess porewater pressure Δu at the final test depth, the cone resistance number Q, the normalized porewater pressure parameter B_q and the evaluated ϕ' using the NTH approximate solution. It is observed that the magnitude of Q increases and B_q decreases as the penetration rate decreases (undrained to drained). However, when the paired sets of Q and B_q are plotted on the NTH solution chart given by Figure 6, they all follow the same friction angle contour ($\phi' = 23°$), indicating agreement with the NTH solution for effective stress penetration.

Table 4. Measured q_{net} and Δu plus derived B_q and Q from CPTu centrifuge twitch testing on kaolin (data from Mahmoodzadeh & Randolph 2014).

ID	v *	q_{net} (kPa)	Δu (kPa)	B_q	Q	NTH ϕ'
PC-1	1	207	146	0.71	2.0	22.2°
PC-2	0.45	249	148	0.59	2.4	22.9°
PC-3	0.15	300	126	0.42	2.8	22.6°
PC-4	0.045	405	71	0.18	3.8	21.4°
PC-5	0.015	495	28	0.06	4.7	19.7°
PC-6	0.0045	501	9	0.02	4.7	17.0°

* Piezocone probe push rate in mm/s

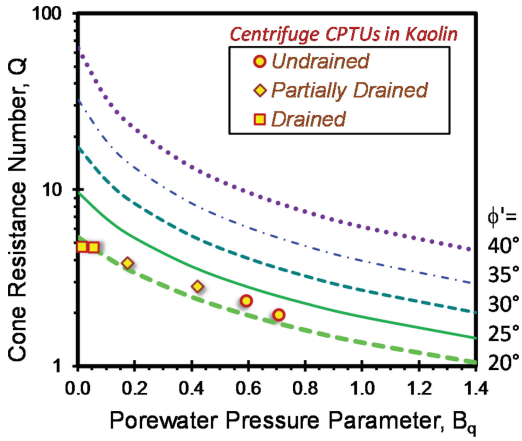

Figure 6. NTH CPTu evaluated ϕ' for kaolin subjected to centrifuge twitch testing (data from Mahmoodzadeh & Randolph 2014).

Table 5. Laboratory measured friction angles and NTH parameters from the centrifuge CPTu soundings.

		Lab and CPTu parameters			
No.	Clay type	Lab ϕ'	B_q	Q	NTH ϕ'
1	Kaolin 1	23.0°	0.18	5.35	25.1°
2	Sandy Kaolin	23.0°	0.29	3.73	23.5°
3	Kaolin 2	28.6°*	0.54	3.9	28.3°
4	Kaolin 3	23.0°	0.71	2.0	22.2°
5	Kaolin 4	23.0°	0.57	2.43	23.0°
6	Pisa Clay 1	23.5°	0.34	3.95	25.0°
7	Pisa Clay 2	28.0°	0.71	3.16	28.1°
8	Pisa Clay 3	27.0°	0.59	3.1	26.2°
9	Speswhite Kaolin	25.2°	0.92	1.87	24.4°
10	Clayey Sand	31.0°	0.05	20	32.3°
11	Silica flour	36.6°	0.01	100	37.1°
12	K75-S25	25.0°	0.37	4.22	26.4°
13	China Kaolin	23.0°	0.45	3.46	25.0°

Notes: (a) lab reference ϕ' from triaxial compression tests (b) *from lab DSS tests shown in Figure 5.

4.3 *Database Summary*

For all 13 series of CPTu centrifuge tests at constant penetration rates, Table 5 provides the individual cone resistance number (Q) and normalized porewater pressure readings (B_q) with their corresponding NTH effective friction angle ϕ' and the measured benchmark ϕ' from laboratory testing.

Figure 7 presents a summary plot for the measured laboratory friction angle values versus the CPTu-determined values from centrifuge tests.

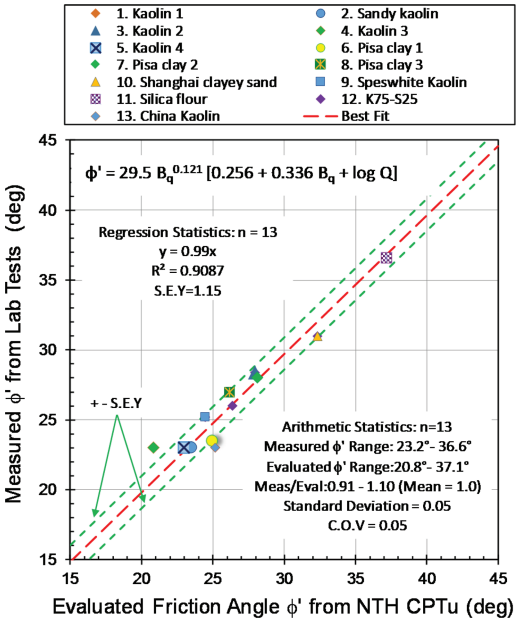

Figure 7. Comparison of laboratory benchmark measured ϕ′ versus NTH-evaluated ϕ′ from centrifuge CPTu series.

Two sets of statistical measures were made on the data set, including: (a) arithmetic statistics, and (b) regression statistics, as indicated on the figure. The measured laboratory ϕ′ cover the range from 23.2° to 36.6° and the CPTu-evaluated ϕ′ values range from 20.8° to 37.1°. From the arithmetic measures, the ratio of measured/evaluated values ranges from 0.91 to 1.10 with an overall mean of 1.0 and standard deviation = 0.05, giving a corresponding COV (coefficient of variation) = 0.05. From the regression evaluations of laboratory vs. field values, the slope m = 0.99 with a coefficient of determination of $r^2 = 0.921$ and standard error of the Y-estimate SEY = 1.15 for a best fit line. The above statistics generally support that the NTH method gives a reasonable evaluation of the effective friction angle when compared with the laboratory reference value.

5 CONCLUSIONS

Data from 13 series of in-flight mini-piezocone penetrometer tests in centrifuge deposits were reviewed for verifying the NTH limit plasticity solution (Sandven 1990; Senneset et al. 1989) in assessing the effective friction angle of normally consolidated to lightly over-consolidated clays and clayey silts. The majority of artificially-prepared deposits of clays included kaolinites or kaolin-sand mixtures. Primarily, the friction angle ϕ′ from laboratory triaxial compression tests served as the reference benchmark value. Results from constant penetration rate CPTu soundings gave good agreement with laboratory determined ϕ′. In addition, one series of CPTu twitch tests on kaolin clay at variable rates showed that as the behavior varied from undrained to partially drained to fully drained, the changes in Q and B_q correspondingly followed the same ϕ′ contours established by the NTH solution.

ACKNOWLEDGMENTS

The authors appreciate the funding and support provided by ConeTec of Richmond, BC and Design House Consultancy of Dubai, UAE towards research activities on in-situ testing.

REFERENCES

Burland, J.B., Jamiolkowski, M., & Viggiani, C. 2003. The stabilisation of the Leaning Tower of Pisa. *Soils and Foundations*, 43(5), 63–80.

Cinicioglu, O., Znidarčić, D., & Ko, H.Y. 2006. A new centrifugal testing method: Descending gravity test. *Geotechnical Testing Journal*, 29(5), Paper ID GTJ100213, 355–364

Cinicioglu, O., Znidarcic, D., & Ko, H.Y. 2007. New structure-based model for estimating undrained shear strength. *Journal of Geotechnical & Geoenvironmental Engrg*, 133(10), 1290–1301.

DeJong, J.D., Jaeger, R.A., Boulanger, R.W., Randolph, M.F. & Wahl, D.A.J. 2013. Variable penetration rate cone testing for characterization of intermediate soils. *Geotechnical & Geo-physical Site Characterization 4*, Vol. 1 (Proc. ISC-4, Per-nambuco 2012), Taylor & Francis Group, London: 25–42.

Esquivel, E.R. and Silva, C.H. (2000). Miniature piezocone for use in centrifuge testing. *Innovations & Applications in Geotechnical Site Characterization,* GSP No. 97, ASCE, Reston/Virginia, 118–129.

Fitzgerald, M.R. 2009. Influence of drainage state on direct-push permeability profiling methods. *PhD Thesis*, College of Earth and Mineral Sciences, Pennsylvania State University, State College, PA: 140p

Jamiolkowski, M., & Pepe, M.C. 2001. Vertical yield stress of Pisa clay from piezocone tests. *Journal of Geotechnical and Geoenvironmental Engineering*, 127(10), 893–897.

Lunne, T., Robertson, P.K., and Powell, J.J.M. 1997. *Cone Penetration Testing in Geotechnical Practice.* Blackie Ac-ademic/Chapman-Hall Publishers, UK: 312 pages.

Mahmoodzadeh, H. & Randolph, M.F. 2014. Penetrometer testing: effect of partial consolidation on subsequent dissipationresponse. *J. Geotechnical & Geoenvironmental. Engrg*. Vol. 140 (6), 04014022, 1–12.

Mayne, P.W. 2007. *Synthesis 368 on Cone Penetration Test*. National Cooperative Highway Research Program (NCHRP), Transportation Research Board, National Academies Press, Washington, DC: 118 pages: www.trb.org

Ouyang, Z., Mayne, P.W. & Sharp, J. 2016. Review of clay chamber tests using miniature cone and piezocone penetrometers, *Proc. GeoVancouver 2016,* (69th Canadian Geotechnical Conference): www.cgs.ca

Ouyang, Z., Mayne, P.W. 2017. Effective friction angle of clays and silts from cone piezocone penetration tests. *Canadian Geotechnical Journal*, in press.

Randolph, M.F. 2004. Characterization of soft sediments for offshore applications. *Geotechnical & Geophysical Site Characterization*, Vol. 1 (Proc. ISC-2, Porto), Millpress, Rotterdam: 209–232.

Randolph, M.F. & Hope, S. 2004. Effect of cone velocity on cone resistance and excess pore pressures, *Proc., Intl. Symp. Engineering Practice and Performance of Soft Deposits*, Osaka, Japan, 147–152.

Robertson, P.K. 2009. Interpretation of cone penetration tests – a unified approach. *Canadian Geotechnical Journal*, Vol. 46 (11): 1337–1355.

Robertson, P.K. 2016. Cone penetration test-based soil behaviour type classification system - an update. *Canadian Geotechnical Journal* 53 (12): 1910–1927.

Sandven, R. 1990. Strength and deformation properties ob-tained from piezocone tests, *PhD Thesis*, Norwegian University of Science & Technology, Trondheim: 342 pages

Sandven, R. and Watn, A. 1995. Theme lecture: interpretation of test results. Soil classification and parameter evaluation from piezocone tests. Results from Oslo airport. *Proc. Intl. Symposium on Cone Penetration Testing*, Vol. 3, Swedish Geotechnical Society Report SGF 3:95, Linköping: 35–55.

Schneider, J.A. 2008. Analysis of piezocone data for displacement pile design. *Doctoral Dissertation*, University of Western Australia: 340 pages

Schofield, A.N. 1980. Cambridge geotechnical centrifuge operations. *Geotechnique*, 30(3), 227–268.

Senneset, K. & Janbu, N. 1985. Shear strength parameters obtained from static cone penetration tests. *Strength Testing of Marine Sediments.* Special Technical Publication No. 883, ASTM, West Conshohocken, PA: 41–54.

Senneset, K., Sandven, R. and Janbu, N. 1989. Evaluation of soil parameters from piezocone tests. *Transportation Research Record 1235,* National Academy Press, Washington, DC: 24–37.

Silva, M.F. and Bolton, M.D., 2005. Interpretation of centrifuge piezocone tests in dilatants, low plasticity silts. *Proc., Int. Conf. on Problematic Soils.* Vol. 3, Eastern Mediterranean University Press, Cyprus: pp. 1277–1284.

Springman, S., (Ed.), Laue, J. (Ed.), Seward, L. (Ed.) (2010). *Physical Modelling in Geotechnics*, (Proc. 7th IC on Physical Modeling in Geotechnics, Zurich), Two Volume Set. CRC Press/Taylor & Francis, London: 1552 p.

Teh, K.L., Leung, C.F., & Chow, Y.K. 2006. Characterization of layered soil using miniature piezocone. *Proc. 6th Int. Conf. on Phys. Modelling in Geotechnics*, Hong Kong: 209–304.

Teh, K.L., Leung, C.F., Chow, Y.K., Cassidy, M.J., & Foo, K.S. 2007. Miniature penetrometers responses in sand overlying clay. *Proc. 16th Southeast Asian Geotechnical Conference*, Kuala Lumpur, Malaysia: 405–410.

Zhou, Y.G., Liang, T., Chen, Y.M., Ling, D.S., Kong, L.G., Shamoto, Y., & Ishikawa, A. 2014. A two-dimensional miniature cone penetration test system for centrifuge modelling. *Proceedings of the 8th International Conference on Physical Modelling in Geotechnics (ICPMG2014)*, Perth, Australia, 301–307.

Taylor & Francis
Taylor & Francis Group
http://taylorandfrancis.com

Cone Penetration Testing 2018 – Hicks, Pisanò & Peuchen (Eds)
© 2018 Delft University of Technology, The Netherlands, ISBN 978-1-138-58449-5

CPT interpretation and correlations to SPT for near-shore marine Mediterranean soils

S. Papamichael & C. Vrettos
Technical University of Kaiserslautern, Germany

ABSTRACT: CPT and SPT field data from the Mediterranean Region comprising onshore and offshore sands, silts, clays and organic soils were analyzed and cross-correlated for the purpose of this research. Laboratory tests on retrieved samples were utilized to aid the evaluation of the applicability of CPT as a site investigation tool. Identification of soil types was carried out using different empirical diagrams and compared with laboratory classification. The applicability of existing empirical CPT-SPT correlations was examined and a site-specific correlation was proposed. The results show that the available empirical charts work well for the majority of soils. Nonetheless, a refinement is required for the transition zones. Robust correlations between the cone resistance of CPT and the N-value of SPT are still missing and available approximations should be applied with caution.

1 INTRODUCTION

Modern site characterization is usually accomplished by means of CPT testing and back analysis based on empirical charts or even explicit expressions derived from case studies or calibration chamber tests. Despite the advances of the last decades in in-situ testing, SPT is still widely used in many countries. Tip cone resistance q_c or blow-count number N_{SPT} are then used to estimate soil mechanical properties. In most projects, only one of these two options is available mainly due to cost control. Designers are then enforced to determine equivalent values from SPT to CPT or reverse. However, reliable correlations are either site-specific or based on a limited number of testing results. Still, there is no consensus on the soil parameters to be used in such correlations. Initially, the ratio q_c / N_{SPT} was expressed in terms of the mean grain size diameter D_{50} (Robertson 1983). Various attempts have been made since then to identify other more suitable parameters to replace D_{50} as the relevant independent variable.

In the frame of the design of the Preveza-Aktio immersed tunnel on the western coast of Greece with considerable liquefaction potential, an extensive field investigation survey was carried out including CPT and SPT tests along the tunnel alignment (Vrettos & Savidis 2004) in order to enhance reliability that is crucial in seismic design. The prevailing ground conditions comprise a wide spectrum of marine and near-shore soils, thus providing a seldom opportunity i) to evaluate the applicability of CPT as a site investigation tool and ii) to cross-correlate the relevant values of CPT and SPT. In the following, soil classification derived from laboratory testing is compared to the predictions by CPT charts, existing CPT-SPT correlations are reviewed, and a site-specific correlation is presented.

2 SOIL CONDITIONS AND FIELD TESTING

Data on the soil conditions derive from fourteen boreholes distributed along the tunnel axis: eight onshore and six offshore. Exploration depth reached 80 meters below seabed level in the center of the strait. The limestone bedrock was not identified. The deepest layers penetrated in the boreholes are Pliocene/Pleistocene deposits comprising hard clays, silts and marls with inclusions of sand layers. They are overlain by inhomogeneous Holocene marine sediments that comprise layers of sands, silts and clays, partially with a high content of organic matter.

SPT testing was carried out at specific depths in the boreholes by recording the blow count number N_{SPT}. Adjacent to each borehole, one CPTu test was performed. Near each onshore borehole an additional CPT was executed to complement the data.

SPT tests were carried out according to the international reference test procedure and no further corrections were required to account for

rod length effects and rod energy ratio, sampling method or borehole diameter. The measured N_{SPT}-values correspond to the normalized values at 60% energy N_{60}.

CPTu tests on land were conducted using twenty-ton capacity hydraulic penetrometer equipment mounted on a heavy truck ballasted to provide a reaction weight of twenty-three tons. A five-ton capacity electric piezocone instrument was employed. The additional CPT tests on land were made using a fifteen tons capacity electric cone. The offshore CPTu tests were made using an AP van der Berg, 4 Module Roson Seabed Penetrometer, ballasted to provide a maximum thrust of sixteen tons. A sixteen-ton capacity electric piezocone instrument was used for the tests, which gave measurements of cone end resistance, local side friction and dynamic pore-water pressure. The rate of penetration was kept constant at a nominal 2 cm/s except when penetrating very dense or hard layers. Simultaneously, the results were recorded on the computer hard disc at 10 mm depth intervals. Due to equipment limitations, the maximum depths investigated by the CPTu were up to 30 m both onshore and offshore.

Results were recorded in terms of cone end resistance q_c, sleeve friction f_s, and pore water pressure u_2 measured behind the cone. Effects of pore water pressure on the measured values were negligible, and further analysis was carried out with the uncorrected raw values q_c and f_s, i.e. assuming that the corrected cone resistance value q_t equals q_c.

Field testing was complemented by data from an extensive laboratory investigation program on retrieved samples from the boreholes. The tests that were conducted for all soils included i) grain size distribution with mean grain diameter D_{50}, uniformity coefficient C_u and fines content percentage FC%, and ii) Atterberg limits and organic content for the cohesive soils. Soil classification was made according to the Unified Soil Classification System USCS. The data were the basis for the definition of the stratigraphy in the tunnel design, and are used herein for the assessment of the available CPT-based soil classification charts.

3 CLASSIFICATION CHARTS CONSIDERED

3.1 *CPT-based soil classification*

The stratigraphic profile can be interpreted using different empirical diagrams. Due to the strong variability of the soil along the depth, it was essential to have accurate information on the topography of the seabed level at the positions of the CPT soundings.

In design practice, the most commonly used classification procedure is based on the normalized soil behavior type SBTn chart by Robertson (1990, 2010). The non-normalized SBT chart is still widely used, as it can be utilized for real-time data interpretation. Within the context of the present study, the collected field data were first transformed to yield the input values for the three different charts suggested by Robertson (1990, 2010), namely the SBT, SBTn and Q_t - B_q charts. A first screening can be accomplished solely by using the soil behavior index I_c which has been proposed by Robertson & Wride (1989) to capture six of the designated zones of the SBTn-chart that cover the basic soil types encountered in practice, cf. Table 1. Likewise, a similar soil behavior index I_{SBT} that corresponds to the SBT chart could be used (Robertson 1990). The advantage is that I_{SBT} can be used directly for real-time interpretation because it requires only the raw values of CPT. I_{SBT} is defined as follows:

$$I_{SBT} = \left[\left(3.47 - \log \frac{q_c}{p_a} \right)^2 + \left(\log R_f + 1.22 \right)^2 \right]^{0.5} \quad (1)$$

where p_a = atmospheric pressure and

$$R_f = \frac{f_s}{q_c} \times 100\% \quad (2)$$

is the friction ratio.

When using the charts for a more precise identification, the following additional parameters are required:

$$F_r = \frac{f_s}{q_t - \sigma_{v0}} \times 100\% \quad (3)$$

$$B_q = \frac{u_2 - u_0}{q_t - \sigma_{v0}} \quad (4)$$

Table 1. Soil type behavior type based on I_c.

Zone	Soil behavior type	I_c
1	Sensitive, fine grained	NA
2	Organic Soils—Clays	>3.6
3	Clay—silt clay to clay	2.95–3.6
4	Silt mixtures—clayey silt to silt clay	2.60–2.95
5	Sand mixtures—silty sand to sandy silt	2.05–2.60
6	Sands—clean sand to silty sand	1.31–2.05
7	Gravely sand to dense sand	1.31
8	Very stiff sand to clayey sand*	NA
9	Very stiff fine grained*	NA

*heavily overconsolidated or cemented

$$Q_t = \frac{q_t - \sigma_{v0}}{\sigma'_{v0}} \quad (5)$$

$$Q_{tn} = \left(\frac{q_t - \sigma_{v0}}{p_a}\right)\left(\frac{p_a}{\sigma'_{v0}}\right)^n \quad (6)$$

$$I_c = \left[\left(3.47 - \log Q_{tn}\right)^2 + \left(\log F_r + 1.22\right)^2\right]^{0.5} \quad (7)$$

$$n = 0.381 I_c + 0.05\left(\frac{\sigma'_{v0}}{p_a}\right) - 0.15 \le 1.0 \quad (8)$$

where F_r = normalized friction ratio; B_q = normalized pore pressure parameter; Q_t = normalized cone resistance (n = 1); Q_{tn} = normalized cone resistance; I_c = soil behavior index; n = stress normalization exponent; σ_{v0} = in-situ initial vertical stress; σ'_{v0} = in-situ initial vertical effective stress; u_0 = in-situ equilibrium water pressure.

The in-situ stresses can either be calculated assuming appropriate values of the soil unit weight or estimated directly using the following equation (Robertson & Cabal 2015):

$$\frac{\gamma}{\gamma_w} = \left[0.27\log R_f + 0.36\log\left(\frac{q_t}{p_a}\right) + 1.236\right]\frac{G_s}{2.65} \quad (9)$$

where γ = unit weight of soil; γ_w = unit weight of water; G_s = specific gravity of the soil material.

In order to be able to identify the zones 1, 8 and 9 of the SBTn chart by a set of equations, which is not possible solely by the use of I_c, Mayne (2014) suggested the following equations 10 and 11. Equation 10 separates zone 1 from the other zones; equation 11 represents zone 8 for 1.5% < F_r < 4.5% and zone 9 for F_r > 4.5%:

$$Q_{tn} \le 12\exp\left(-1.4F_r\right) \quad (10)$$

$$Q_{tn} \le \frac{1}{0.005\left(F_r - 1\right) - 0.0003\left(F_r - 1\right)^2 - 0.02} \quad (11)$$

Another classification chart considered herein is that suggested by Eslami & Fellenius (2004) that requires merely the values of the measured sleeve friction f_s and the effective cone resistance q_E where

$$q_E = q_t - u_2 \quad (12)$$

3.2 *CPT-SPT correlations*

Reliable correlations between CPT and SPT are in general difficult to be derived due to the different type of sounding involved. Initially, the ratio q_c/N_{SPT} was linked to the mean grain size D_{50} (Robertson et al. 1983); other engineering soil properties have been suggested subsequently such as the soil behavior index I_c, the fines content FC% or the relative density as summarized by Shahien & Albatal (2014). The following relationships that have been considered were: Those suggested by Kulhawy & Mayne (1990)

$$\frac{q_c/p_a}{N} = 5.44\left(D_{50}\right)^{0.26} \quad (13)$$

$$\frac{q_c/p_a}{N} = 4.25 - \frac{FC\%}{41.3} \quad (14)$$

and that by Robertson & Cabal (2015) which incorporates soil type effects in a single parameter, the soil index I_c

$$\frac{q_c/p_a}{N_{60}} = 10^{\left(1.1268 - 0.2817 I_c\right)} \quad (15)$$

A similar relation of the ratio q_c/N_{60} dependent on I_c has initially been suggested by Jefferies & Davies (1993).

4 RESULTS

4.1 *CPT-based soil classification*

Figures 1 to 4 show the CPT data plotted on the different empirical charts presented in Section 3. Generally, all the charts work well for the majority of soils: stratigraphy derived from the charts is in good agreement with the one obtained from the direct soil classification determined on samples from the boreholes. Comparing Figures 1 and 2, it

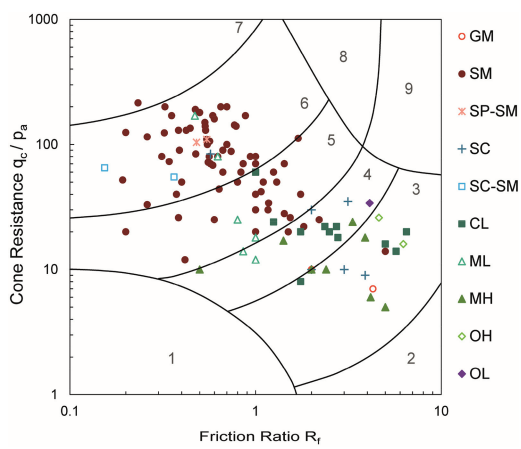

Figure 1. Soil classification in the SBT chart.

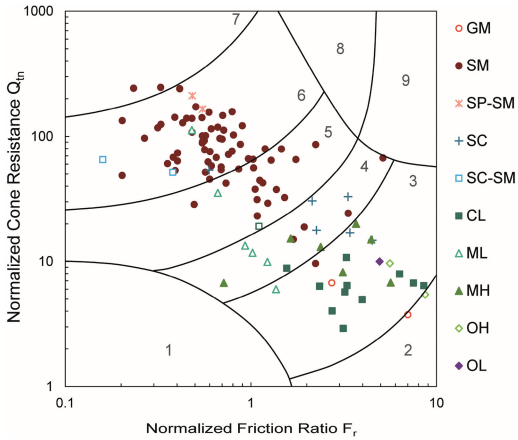

Figure 2. Soil classification in the SBTn chart.

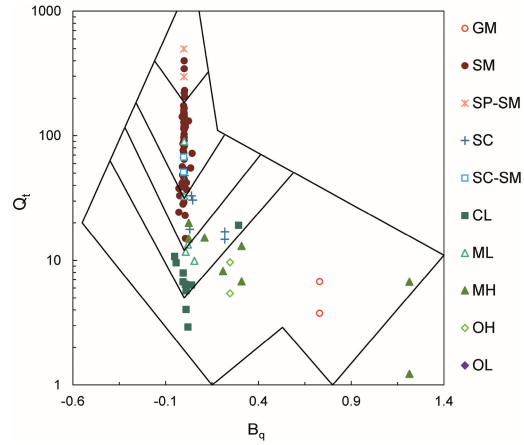

Figure 3. Soil classification in the B_q-Q_t chart.

can be inferred that the normalized SBTn graph provides a slight improvement in the interpretation accuracy, in particular for some of the organic soils. Use of the Q_t-B_q chart does not provide any additional advantage for the investigated soils. Note that this chart is very sensible with respect to the pore water pressure, which in practice is often difficult to measure with sufficient accuracy.

Silty gravels are falsely plotted in the zone 3 in all charts. Silty sand is plotted quite well on the corresponding zones, although a few data sets are plotted in zones 3, 4 and 7 instead. Clayey sand is incorrectly plotted in zones 3 to 6 instead of zone 8. A couple data sets for clays are inaccurately placed in zone 4 or 5. For clays, an improvement is observed when the classification is based on the SBTn rather than on SBT or on the Q_t-B_q chart with almost all clays plotting in the corresponding zone 3.

Clayey silts are plotted correctly on zone 4, but partially also on zone 5 which corresponds to silty sands and sandy silts. An accurate distinction is still difficult.

Elastic silts are well plotted on the corresponding region both in the SBT and in the SBTn chart whereas a few data sets are incorrectly interpreted by the $Q_t - B_q$ chart. The above deviations should be interpreted considering the fact that the above empirical charts are intended to provide information on the behavior of soils rather than reproducing soil categories defined in classification systems.

Figure 4 displays the CPT data plotted on the Eslami-Fellenius chart. Silty gravels are incorrectly plotted in the silt/clay region. The same holds for many of the silty sands which are interpreted as sands or sandy silts. Furthermore, clayey silt is plotted on the sandy silt/silty sand/sand regions. Elastic silts, as well as clays, are correctly identified by the chart.

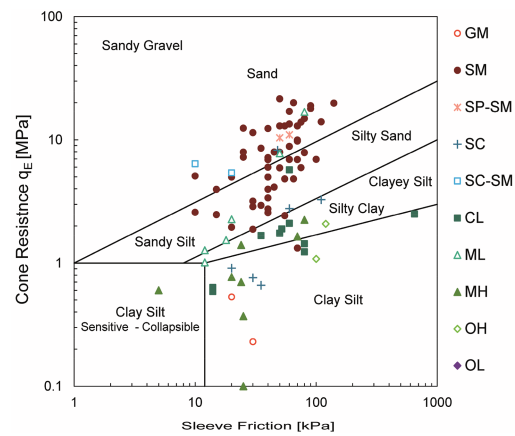

Figure 4. Soil classification using the Eslami- Fellenius chart.

It should be mentioned that the present case study includes a vast number of silty sands and sandy silts and provides a unique opportunity to assess the capability of the empirical charts to distinguish between them. It can be concluded that the transition between zones 5 and 6 requires further refinement.

Similar inaccuracies arise between zones 4 and 5 in the charts where clayey silt is turning directly to sandy silt without any transition zone.

Classification using only the numerical value of the I_c, in conjunction with Table 1 provides sufficient interpretation accuracy for the majority of soils encountered in routine design.

4.2 *CPT-SPT correlations*

In the context of the present study, the applicability of the correlations summarized in Section 3

is investigated by graphically comparing them against the measured q_c and N_{SPT} data sets. D_{50} and FC are chosen as independent parameters in Figures 5 and 6, respectively. The dependency on D_{50} and FC is confirmed but a reliable functional correlation between the results of the two in-situ tests cannot be established. Note that the amount of data points is small due to the fact that the number of soil samples taken at the location of the SPT soundings was limited, as is the case in most projects.

Using equation 15 with I_c as the governing parameter provides better estimates. The need for establishing local site-specific correlations to improve the reliability of the correlations between CPT and SPT becomes evident. Based on the available data of the current research, a site-specific correlation is derived by linear regression for $5 \leq N_{SPT} \leq 50$, as depicted in Figure 7:

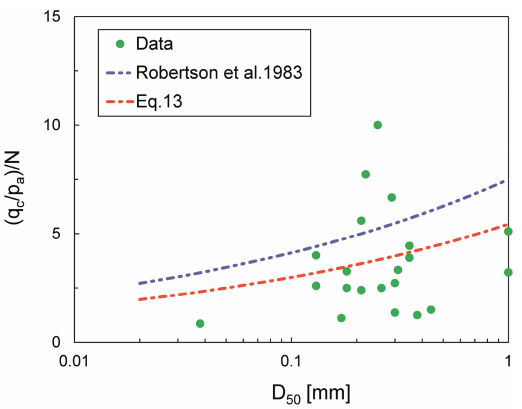

Figure 5. CPT-SPT correlation in dependence on D_{50}.

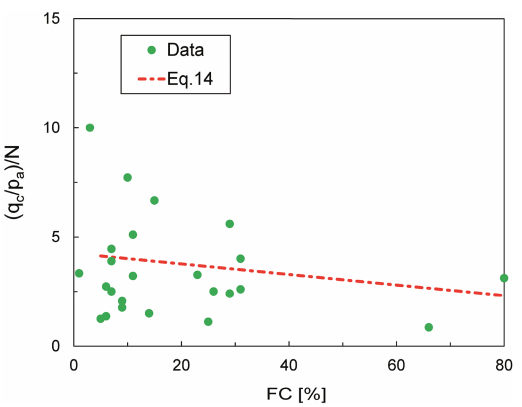

Figure 6. CPT-SPT correlation in dependence on FC%.

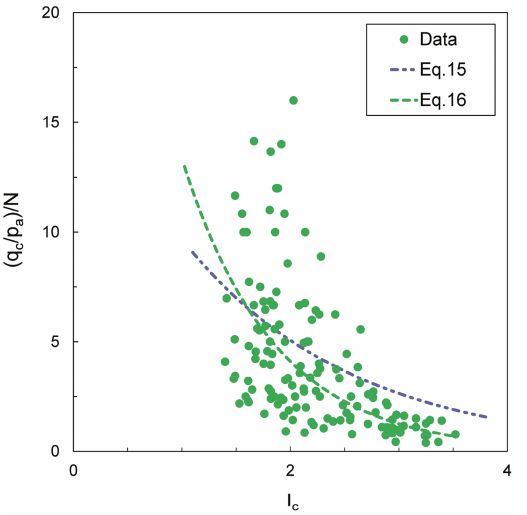

Figure 7. CPT-SPT correlation utilizing the soil index I_c.

$$\frac{q_C / p_a}{N_{60}} = 43.44 \exp(-1.18 I_c) \tag{16}$$

with a correlation coefficient $R^2 = 0.47$ which is satisfactory taking into consideration the different penetration mechanisms of the tests.

A further comparison is made utilizing the well-known liquefaction triggering charts suggested by Boulanger & Idriss (2014). The explicit equations for the cyclic stress ratio depending on q_{c1Ncs} and $(N_1)_{60cs}$ for clean sands in conjunction with the corrections factors to account for FC% were adopted to derive a relation between q_{c1N} and $(N_1)_{60}$ utilizing the stress normalization factor C_N as suggested, where

$$q_{c1N} = C_N \frac{q_c}{p_a} \tag{17}$$

$$(N_1)_{60} = C_N N_{60} \tag{18}$$

Figure 8 displays the comparison with the project data for different fine content values. The project data show large scatter for FC ≤ 5%, and exhibit in general for all FC% consistently lower values than the ones derived from the liquefaction triggering charts without any specific pattern.

Hence, a direct correlation between CPT and SPT is quite tricky and requires attention when implemented in practice. It should be stressed, however, that there is a need for converting CPT values to SPT in order to utilize SPT-based charts and procedures established in codes of practice for various design purposes.

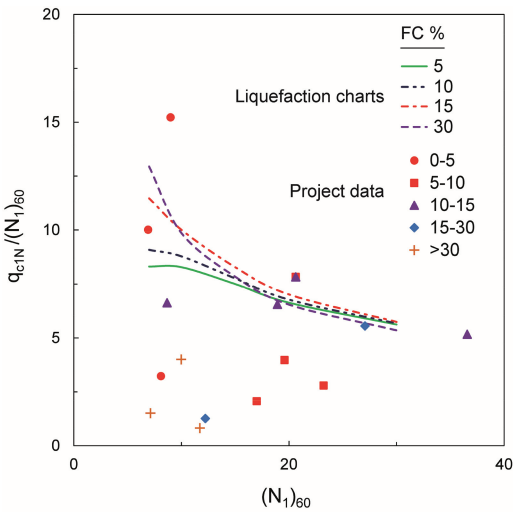

Figure 8. CPT-SPT correlation implied by the liquefaction triggering charts compared to the project data.

5 CONCLUSIONS

The present study confirmed that empirical diagrams as used in routine design for soil characterization are sufficiently accurate for complex stratigraphies comprising a large variety of soils. The suggested charts by Robertson yield comparable results, yet the SBTn chart is shown to be more accurate. The Eslami & Fellenius chart provides also satisfactory interpretation. Refinements are required in the transition zones between silty sands and sandy silts as well as between clayey silts and sandy silts. Linking the ratio between CPT cone tip resistance and SPT blow count number with granulometric soil parameters yielded poor correlation coefficients, whereas the soil behavior index seems to be a promising alternative.

ACKNOWLEDGEMENTS

This work was supported by the Helmholtz Alliance ROBEX.

REFERENCES

Boulanger, R.W. & Idriss, I.M. 2014. *CPT and SPT based liquefaction triggering procedures*. Rep. No. UCD/CGM-14/01. Davies, California: University of California.

Eslami, A. & Fellenius, B.H. 2004. CPT and CPTu data for soil profile interpretation: Review of methods and proposed new approach. *Iranian Journal of Science and Technology* 28: 69–86.

Jefferies, M.G. & Davies, M.P. 1993. Use of CPTu to estimate equivalent SPT N_{60}. *Geotechnical Testing Journal* 16(4): 458–468.

Kulhawy, F.H. & Mayne, P.W. 1990. *Manual on Estimating Soil Properties for Foundation Design*. Palo Alto, California: Electric Power Research Institute.

Mayne, P.W. 2014. Interpretation of geotechnical parameters from seismic piezocone tests. In *Proc. 3rd Intl. Symposium on Cone Penetration Testing*, Las Vegas, Nevada, www.cpt14.com.

Robertson, P.K., Campanella, R.G. & Wightman, A. 1983. SPT-CPT correlations. *Journal of Geotechnical Engineering, ASCE* 109(11): 1449–1459.

Robertson, P.K. 1990. Soil Classification using the cone penetration test. *Canadian Geotechnical Journal* 27(1): 442–459.

Robertson, P.K. & Wride, C.E. 1998. Evaluating cyclic liquefaction potential using the cone penetration test. *Canadian Geotechnical Journal* 35(1): 151–158.

Robertson P.K. 2010. Soil Behavior Type from the CPT: an update. In *2nd Int. Symp. on Cone Penetration Testing*, Huntington Beach, USA.

Robertson, P.K. & Cabal, K.L. 2015. *Guide to Cone Penetration Testing for Geotechnical Engineering*. Signal Hill, California: Gregg Drilling & Testing, Inc.

Shahien, M.M. & Albatal, A.H. 2014. SPT-CPT correlations for Nile Delta silty sand deposits in Egypt. In *3rd Int. Symp. on Cone Penetration Testing*, Las Vegas, pp. 699–708.

Vrettos, C. & Savidis, S. 2004. Stone column ground improvement against liquefaction for the Preveza-Aktio immersed tunnel. In *Proc. 5th Int. Conf. on Case Histories in Geotechnical Engineering*, New York, NY, Paper No. 12A-14.

Cone Penetration Testing 2018 – Hicks, Pisanò & Peuchen (Eds)
© 2018 Delft University of Technology, The Netherlands, ISBN 978-1-138-58449-5

Characterization of a dense deep offshore sand with CPT and shear wave velocity profiling

J.G. Parra, A. Veracoechea & N. Vieira
Geohidra, Caracas, Venezuela

ABSTRACT: In some areas of the northern South American continental shelf, 89 m below the sea floor a stratum of dense to very dense siliciclastic sand has been identified. Given the properties of the overlying soil layers, this sand is the most competent foundation strata for offshore jacket structures. The proper geomechanical characterization of this sand poses some challenges, among them: the maximum pushing capacity available in the wireline CPT system used in offshore geotechnical exploration, and the extent of the perturbed zone beneath the end of the borehole. This work describes an attempt to overcome those limitations by means of the use of shear wave velocity (Vs) profiling with a P-S logging tool, together with known correlations between Vs and CPT point resistance (qt) to generate more reliable "virtual" CPT records. A MonteCarlo simulation was performed with the objective of assessing the sensitivity of the axial capacity of the proposed foundation piles to the derived CPT records.

1 INTRODUCTION

This paper presents an example of an attempt to overcome some of the limitations in the use of wireline CPTU *in situ* testing for the geomechanical characterization of deep offshore dense sands by means of the use of shear wave velocity (Vs) data obtained from a P-S logging tool. The wireline CPTU is the most used method for in situ testing of offshore soils and in particular has been extensively used in some prospective areas of the Caribbean Sea. In the presented case a deep sand was identified during the field exploration. The proper characterization of this sand is necessary as it is expected that the heavy fixed jacket structures to be built will need to have piles installed and founded on this stratum.

2 BASIC SAND CHARACTERISATION

2.1 *Geological framework*

The study area is located in the Caribbean Sea at the junction of the northeastern section of the South American plate with the southeastern portion of the Caribbean plate, at about 100 m water depth. The site comprises a variable sequence of Holocene, Pleisto and Pliocene sediments deposited in an environment that has been subjected to significant changes of the sea level, sediment source and depositional energy. The top most section corresponds to 10 m of very soft clay that overlays a variable thickness (20–30 m) of bioclastic carbonate sand, followed by a significant layer (50–89 m) of soft to stiff high plasticity clay. Finally, at the bottom of the explored depth, from about 89 m down to 120 m a fine, dense to very dense siliciclastic sand was identified. This paper examines the geomechanical characterization of this sand.

2.2 *Description of recovered samples*

Several sand samples were recovered using thick-walled Shelby tubes pushed with a heave compensated wireline hydraulic tool deployed from a four-point moored geotechnical vessel. The recovered material corresponds to a dense, brown, occasionally silty, siliciclastic sand. At about 102–103 m some organic content was identified. The fine content is variable from 7–17% in the upper section and lowering to 2–6% in the lower portion, corresponding to a non-plastic silt. The grains were examined under low magnification microscope. In general they present high sphericity (0.7–0.9) and variable roundness, around 0.7 in the upper section and lowering towards 0.3–0.1 in the lower section (sphericity and roundness as given by Santamarina 2001). The median values of grain size d50 = 0.35 mm, uniformity coefficient cu = 3.6 and curvature coefficient cc = 1.1. Following ASTM (D2487) the classification would be SM to SP-SM.

2.3 *CPT profiles*

One CPTU log was taken along the deep sand using a heave compensated wireline system. The tools used were able to apply a maximum push-

ing capacity of 100 kN in strokes of 1 m, on cones with 10 cm^2 area, for a theoretically maximum cone tip pressure (qc) of 100 MPa. The data acquisition system allows recording data points (tip pressure qc, friction fs and pore pressure u2) at 20 mm intervals. Figure 1 shows the corresponding records of qc.

2.4 *Shear wave (Vs) velocity profile*

In addition to samples and CPTU records, a shear wave velocity (Vs) profile was acquired using an OYO suspension P-S logging system. The system consists of a tool that is deployed at the bottom of the borehole once the drilling operation is finished (and after extending the borehole depth to accommodate the lower portion of the tool).

The borehole was kept stable by the use of a drilling mud based on a mixture of Guar Gum and Barite, no casing was used and no borehole instability issues were reported. The tool is raised from the bottom of the borehole while it registers the arrival of upward travelling P and S waves from a source located at the lower end of the tool. Above the source there is a pair of geophones located 1.0 m apart. By picking the first arrival of the P and S waves in the sensors an accurate determination of wave travel times and velocities are obtained. The latter are reported at the depth of the midpoint between the sensors. The time resolution of the acquisition system is 10 µsec. The space resolution is controlled the dominant wave length of the signal (<0.25 m for the typical frequency content of the source signal) and by the fixed distance of the geophones (1.0 m) (OYO Corporation 2002). Figure 2 shows a schematic of the test and Fig 3 depicts the actual registered data superposed over the CPTU qc records (Vs values plotted every 0.5 m). The P-S logging test is an established procedure for measuring P and S wave velocity. Even with the uncertainties associated with the correct picking of the arrival times, noise in the signals and their time and space resolution, it has been shown to produce results similar to other methods like downhole or seismic CPT (Diehl, 2010).

The original purpose of this data acquisition was to assess the small strain shear stiffness of

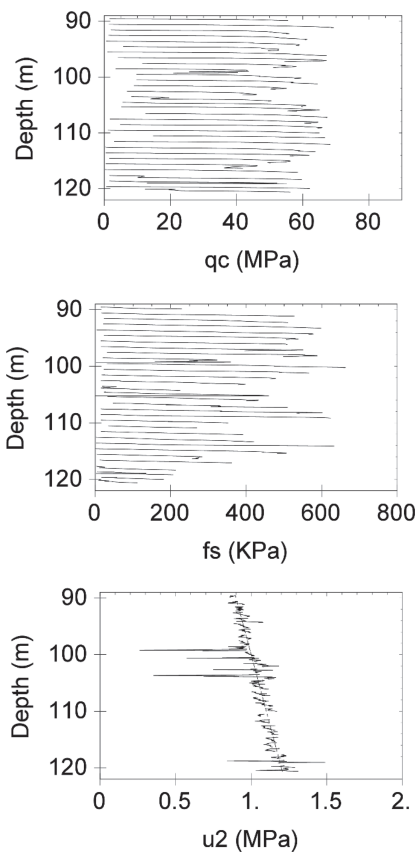

Figure 1. CPT profile in the deep sand.

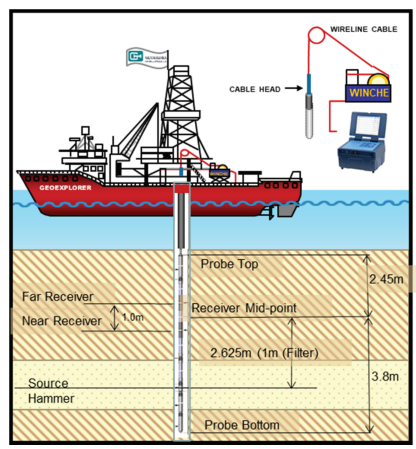

Figure 2. Suspension PS logging.

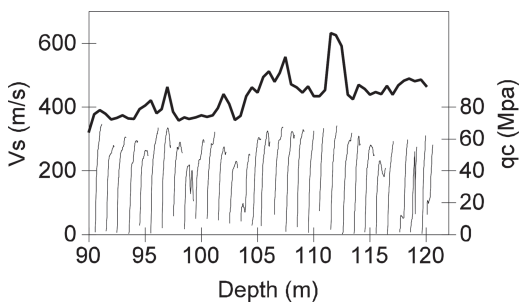

Figure 3. Shear wave velocity (Vs) profile.

the soil profile in order to carry dynamic response analysis of the deposit and derive seismic response spectra, given the high seismicity of the investigated area.

3 CPT RECORDS DERIVED FROM SHEAR WAVE PROFILES

3.1 *Limitations of the presented CPTU records in the deep sand*

The set of CPT records in Figure 1 have several characteristics that limit their usefulness for mechanical characterization of the sand. The length of each "subrecord" is smaller than the available stroke of the CPT tool, and vary between 0.3 to 0.8 m with a mean value of 0.7 m. In all of them the maximum safe capacity of the hydraulic pushing system of the CPTU tool was reached. In some sub-records the last data points show an increasing tendency that was interrupted by the operator to protect the hydraulic system. In others a maximum was reached followed by a very short, irregular decrease. There are some reasons which may affect the reliability of these last decreasing sections in some sub-records: sliding of the clamps in the sea bed frame; slight play in the latching system; effect of the decompression of hydraulic oil after interruption of the pushing operation; and delay in the interruption of the depth acquisition. And finally and most importantly, a significant portion of the length of these sub-records are showing the tip resistance (qc) of a sand subjected to the perturbation of the drilling operation and a significantly reduced effective stress state. Every time the borehole is advanced and the wireline CPTU tool is latched into position, the sand immediately beneath the end of the drill pipe is unloaded to a very low vertical effective stress. Due to the boundary conditions and the stiffness of the sand at these depths (90–120 m below sea floor) the sand regains an effective stress state similar to the in situ undisturbed state only after a recording length of 2 to 4 borehole diameters (8.5 "). This means that a portion between 50–100% of the length of each sub-record could be affected, hence showing a lower qc and fs value than that expected for a sand at the real in situ undisturbed effective stress state (Figure 4). For all these reasons it is believed that most of the qc (and fs) values given in the records shown in Fig. 1 do not represent a reliable estimate of the cone penetration resistance, and even the data points with the highest recorded qc values probably provide a lower bound with an unknown degree of conservatism.

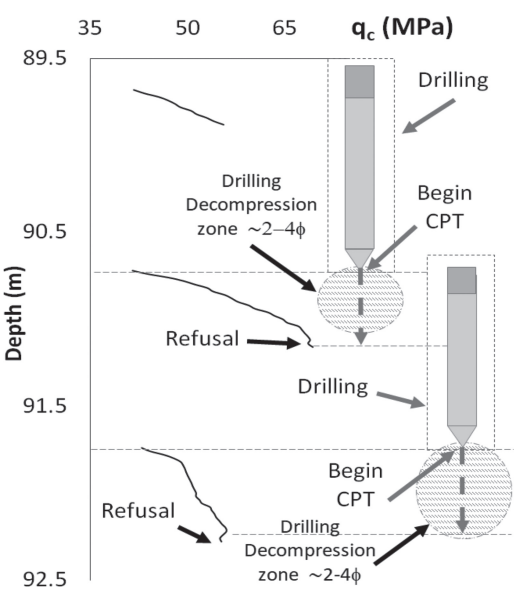

Figure 4. Effect of unloading at the bottom of the borehole.

3.2 *Soil behavior type*

Following Robertson's (2009) methodology for behavior characterization, Figure 5 presents the (Fr,Qtn) values plotted on the Soil Behavior Type classification normalized chart. The following equations are used:

$$Qt1 = \frac{(qt - \sigma_{vo})}{\sigma'_{vo}} \quad (1)$$

$$Ic = \left[(3.47 - Log(Qtn))^2 + (Log(Fr) + 1.22)^2 \right]^{0.5} \quad (2)$$

$$n = 0.381 * Ic + 0.05 \left(\frac{\sigma'_{vo}}{pa} \right) - 0.15 \quad (3)$$

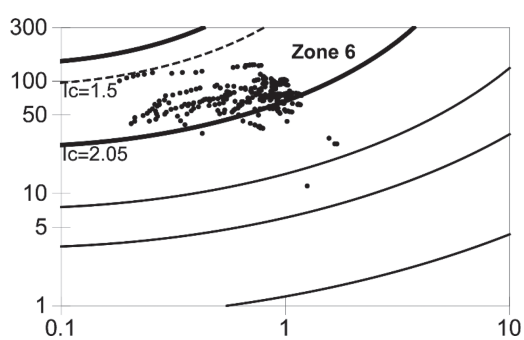

Figure 5. Selected CPTU data points plotted in the soil behavior type classification normalized chart.

$$Qtn = Qt1 * \left(\frac{\sigma'_{vo}}{pa} \right)^{1-n} \quad (4)$$

$$Fr = f_s / (qt - \sigma_{vo}) * 100\% \quad (5)$$

where qt is corrected tip resistance; σ_{vo} and σ'_{vo} are total and effective vertical stress; fs = friction resistance; pa = atmospheric pressure; Qt*n* = normalized cone resistance; n normalizing exponent. The presence of Qtn in equation (2) requires the use of an iterative procedure (Zhang et al. 2002).

The following observation applies: i) the CPTU data points have the limitations stated in the previous section, ii) only the last 10 data points of each sub-record are included in the plot, iii) the stress normalization factor calculation considers that the in situ vertical stress (σ'_{vo}) is equal to the free field value (i.e. no borehole).

Most of the selected points have a Soil Behavior Index (Ic) value between 1.80 to 2.05, landing in Zone 6 (1.31 < Ic < 2.05) of clean to silty sands in the Robertson chart. This soil type corresponds to the classification described in Section 2.2 from the recovered samples. *It is believed that if a continuous record with an ideal higher pushing capacity CPTU tool was available the Qtn values would be higher than those shown.*

3.3 *Correlation of Vs with qt*

To overcome the limitations of the CPTU records stated in Section 3.1, an attempt to estimate a more representative tip resistance qt from the available shear wave velocity data is described below (at these depths and considering the soil type, qt is indistinguishable from qc). Following Robertson (2009): "… Vs depends on the response under very small strains and it is sensitive to the number and quality of the grain-to-grain contacts, which in turn depend on the relative density, effective vertical stress state, the rearrangement of the particles due to age and cementation. Cone penetration resistance is also controlled by relative density, effective stress state and to a lesser degree to age and cementation".

Following Robertson (2009) and Andrus (2007):

$$Vs_1 = Vs \left(\frac{\sigma'_{vo}}{pa} \right)^{-0.25} \quad (6)$$

$$Vs_1 = k \left(\alpha * Qtn \right)^{0.5} \quad (7)$$

$$\alpha = 10 \wedge (0.55 * Ic + 1.68) \quad (8)$$

where Vs_1 = stress corrected shear wave velocity; α = shear wave cone factor (in $(m/s)^2$); and k the age/cementation factor. The k value accounts for effects such as age, cementation and others that may affect Vs values much more than qt values. For instance, if the mechanical strength of the cementation is weak, Vs would be much more sensitive to it than cone tip resistance qt (Santamarina 2001). Andrus (2007) & Robertson (2009) suggest values of k = 1.0 for Holocene uncemented sands and a range of k from 1.22 to 1.26 for Pleistocene sands.

Initially, k was assumed equal to 1.25 for the whole sand stratum as it is known that the sand was deposited in the Pleistocene. For the limited set of CPTU values shown in Figure 5 the ratio of Vs values measured to calculated (using equations 6, 7 and 8) are shown in Figure 6. Keeping in mind the limitations of the CPTU values used, the plot shows that there are two distinct zones: from the top of the stratum (89 m) to approximately 103–104 m the measured Vs values are lower than the calculated ones (median of the ratio = 0.82) whereas from 104 m to the base of the stratum (120 m) the measured values are higher than the calculated ones (median of the ratio = 1.15). This suggests that there are two sands with distinct features. After a careful review of the laboratory data it was found that the fine content (grain size smaller than #200 sieve) of the upper sand varies between 7–17% whilst the fine content of the lower sand varies between 2–6%. At about 103 m depth a thin sand layer with organic matter was identified which could indicate a change in the sediments source. Additionally, from the examination of the microphotographs of the sand grains a systematic difference in the grain texture was identified, with smoother and more rounded grains in the upper sand (higher roundness) versus more angular grains in the lower section (lower roundness), which also showed some evidence of cementation (Fig. 7). All this suggest that even if the sand was broadly deposited in the same geological age they may correspond to different depositional environments. From this it is considered more appropriate

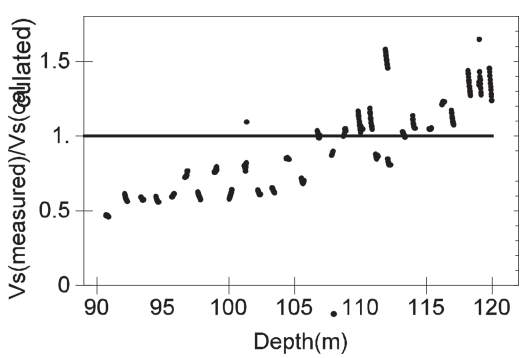

Figure 6. Ratio between measured and calculated Vs.

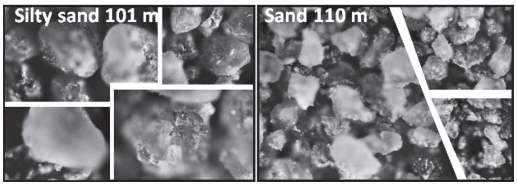

Figure 7. Sample of grain microphotographs.

to use two different values of the k factor: a lower one, possibly closer to 1–1.05 in the top substratum; and a higher one, possibly close to 1.25, in the lower stratum. In the next section this hypothesis is further explored.

3.4 *qt derived from Vs*

Ideally from the original data set of Andrus (2007) it would be possible to derive an inverse correlation of qt from the Vs data (accounting for the higher resolution of the CPTU as compared to the Vs values). As the data is not available for more statistically rigorous calculations, the approximation of just solving the Vs-qt correlation in terms of qt was used. From equations 1 to 7 the following is obtained:

$$Qt1 = \left(\frac{Vs^2}{\alpha k^2}\right)\left(\frac{\sigma'_{vo}}{pa}\right)^{-1.5+n} * \varepsilon(z) \tag{9}$$

$$q_t = Qt1 * \sigma'_{v0} + \sigma_{v0} \tag{10}$$

ε(z) is a residual function explained later. The α factor depends on Ic which in turn depends on Qtn and fs which are in principle unknown. In order to simplify calculations a constant Ic value was assumed for the complete sand layer below 89 m. This is based on the characteristics of the sand in the recovered samples and the observation that qt values higher than those measured in the field are expected. All this translates in likely Ic values lower than the range given in Section 3.2, but still within SBTn zone 6 (clean to silty sands). Therefore, an initial value of Ic = 1.5 was assumed. For the k values (age/cementation factor), and based in the discussion in Section 3.3, a variable k = 1.05 if z < 102 m (upper sub stratum), 1.25 if z > 104 m (lower sub stratum) and intermediate values at the transition zone in between were chosen. In Figure 8 the derived qt values are shown (together with the cases of constant k = 1.05 and k = 1.25). It seems reasonable to conclude that two values of k give a reasonable set of derived qt records

A MonteCarlo simulation was performed in order to estimate the sensitivity of the derived (virtual) qt profiles to the assumptions made for k and

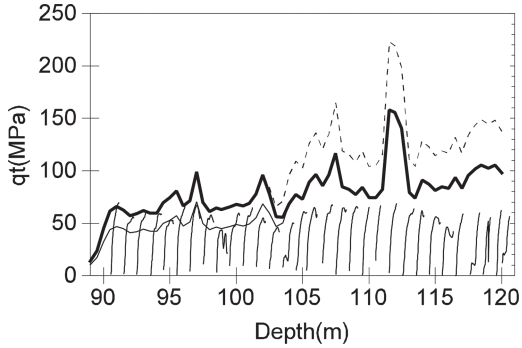

Figure 8. Derived qt records for Ic = 1.5. Thin line: k = 1.25; dashed: k = 1.05, thick: variable k.

Ic. Ic was considered independent from the k values, constant along the stratum and having a triangular probability density function with a minimum of 1.2, median and mode of 1.5 and maximum value of 1.8. The spread would be higher than that given in section 3.2. Two independent random variates ku (upper sand) and kl (lower sand) with uniform distributions were assumed for the upper and lower substratum k values: ku between 0.95 and 1.15 and kl between 1.15 and 1.35. Their mean values follows from Section 3.3. Their spread around their means tries to replicate that reported by Andrus (2007). The assumption of Ic independent from the k seems appropriate as the effect that k is measuring affects mostly Vs but not qt.

In order to simulate the typical variability in qt (and Qt1) values in sand and some of the uncertainty associated with the spread of the correlation, each complete derived record of qt from equation (8) were considered as a "trend" which is multiplied by a realization of a residual function ε(z) = Exp[η(z)]. This residual function is the exponential of a stationary, zero mean random Gaussian process η(z) with variance = σ^2 and a normalized autocorrelation function Exp[-(r/r_o)^2], where r is the separation between data points and r_o is the autocovariance distance. (Lune et al, 1997). From the statistics of the field envelope shown in Fig 11 and recommended values in literature (Uzielly et al 2005) σ = 0.1 and r_o = 1.1 m were used. A total of 1000 CPT records were derived.

In Figure 9 the corresponding 10%, 50% and 90% percentiles of the derived qt values are shown (continuous lines), together with the percentiles obtained considering only the variation in Ic with constant ku = 1.0 and kl = 1.5 (dashed lines).

In Figure 10. the same 10%, 50% and 90% percentile of the derived qt values are shown, together with the percentiles obtained considering only the variation in ku and kl with constant Ic = 1.5 (dashed lines). It can be seen that under the given

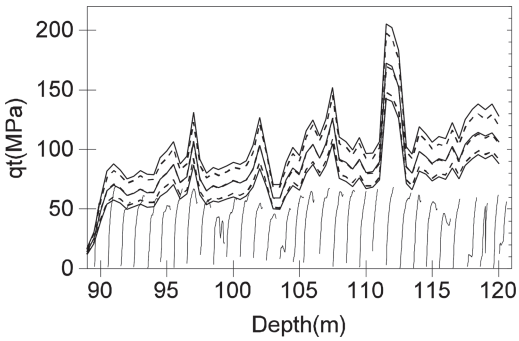

Figure 9. 10%, 50% and 90% percentiles of the derived qt values (continuous line full variation, dashed lines only variation in Ic).

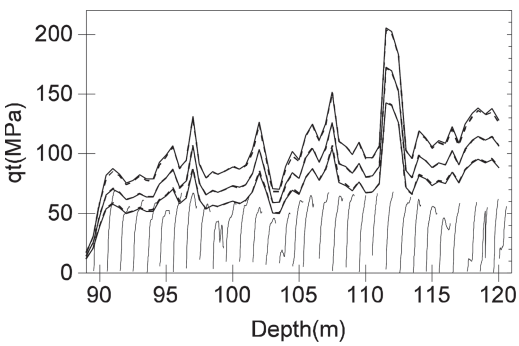

Figure 10. 10%, 50% and 90% percentiles of the derived qt values (continuous line full variation, dashed lines only variation in k).

assumptions the spread from the k values (ku, kl) are slightly larger than the spread from Ic values.

The most notable feature in the derived records is the zone of very high qt values around 112 m which more or less correspond to a zone in which the field CPT sub-records show a sudden interruption while the values were increasing. Similarly there are peaks around 97, 102 and 107 m that corresponds (within 1 m) to interrupted field sub-records. Beyond 117 m the field sub-records also shown the same interruption and the derived qt values are increasing. Additionally, some of the maximum qt values in the sub-records that show a maximum followed by a limited decrease are similar to the 10% percentile of derived qt. This probably indicates that several of the limitations of the recorded CPTU values stated in Section 3.1 come into play.

4 AXIAL PILE CAPACITY

The sensitivity of the axial pile capacity to the derived set of CPT records in the dense deep sand generated in the previous MonteCarlo simulation was assessed by combining them with the (fixed) field record of CPT values from sea floor to 89 m. This is not a complete uncertainty analysis as only the effect of one variable (CPT values in the deep sand) is being assessed.

In order to calculate the axial pile capacities the ICP method (Jardine et al, 2005) was used. The common practice is to trace an envelope of the actual peaks in qt, possibly on the conservative side. Fig. 11 shows an example of such an envelope. For a pile of 2134 mm OD, 28 mm wall thickness and 110 m length, the calculated axial capacity would be 77.6 MN. An unplugged base capacity was assumed given the large pile diameter. The tip of this pile is above the zone of large CPT values seen in the Vs based CPT records. Using this set of 1000 records the histogram for the total axial capacity shown in Figure 12 is obtained. The mean value is 95.4 MN, the 10% percentile is 87.3 MN, the 90% percentile is 103.6 MN and the coefficient of variation COV = 0.065. This COV is only measuring the uncertainty associated with the possible set of CPTU records in the sand from the Vs data. It cannot be compared with the total uncertainty in axial pile capacity prediction due to all the influencing

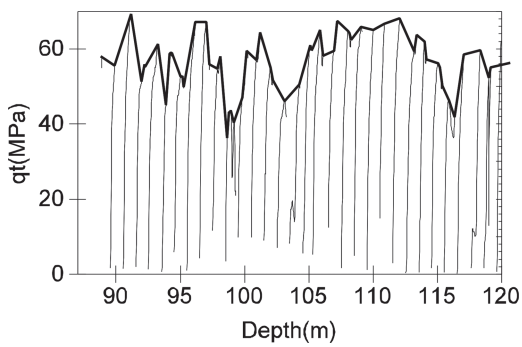

Figure 11. Possible envelope of field recorded CPT values.

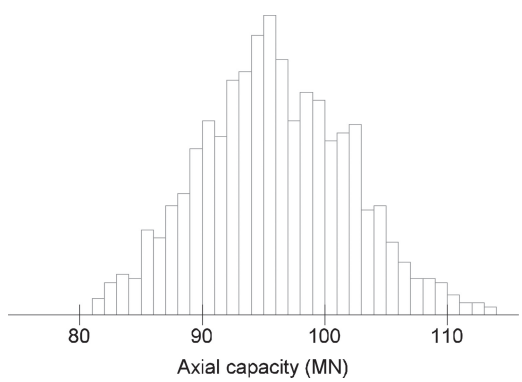

Figure 12. Histogram of axial capacity values.

factors (including the reliability of the pile capacity method used), which has a COV of the order of 0.15 or approximately ± 30% (Randolph, 2003). From this is seems that the total spread (considering all sources of uncertainty) around the mean value is not necessarily much larger by using the CPT derived records, but in this case the increase in the mean is substantial. The axial capacity from the typical envelope is 19% lower than the mean and 11% lower than the 10% percentile. This increase could provide for savings in the pile design and should be accounted for in the drivability analysis to avoid underestimating the hammer requirements.

5 CONCLUSIONS

The use of shear wave (Vs) velocity data from a suspension PS-log probe, together with valid correlations between CPTU qt values and Vs provides additional information that can overcome the limitations of the pushing capacity of wireline CPTU tools when used in deep dense sands. The key aspects of this approach are the estimation of a representative soil behaviour type index Ic and correction factor (k) in the Vs-qt correlations. The latter properly account for age, cementation and other effects that may affect the Vs value but not significantly the qt values. In this respect it is essential to consider the geological conditions and to recover samples to help in the assessment of Ic and k values. In the presented case the use of derived qt values from Vs data led to an increase in the mean axial capacity of piles of the order of 19%.

ACKNOWLEDGEMENTS

The authors would like to acknowledge the contribution from Adriana Gonzalez and Diana de Ponte in discussing the geological aspects of this work.

REFERENCES

Andrus, R; Mohanan, N; et al (2007) Predicting Shear-Wave Velocity from Cone Penetration Resistance. *4th International Conference on Earthquake Geotechnical Engineering.* Proc June 25–28, 2007. No. 1454. Greece. Thessaloniki.

ASTM D2487 (2015), Vol. 04.08. *ASTM International,* West, Conshohocken, Philadelphia.

Diehl, J. Borehole Geophysics for Geotechnical Engineering. 4th North American Chinese Geotech. Eng. Assoc. workshop. January, 2010. http://www.nac-gea.org

Jardine. R. et al, (2005). ICP Design methods for driven piles in sands and clays. *Imperial College*, London.

Lunne,T.; Robertson,P. & Powell, J. (2001). Spon Press. *Cone penetration testing in geotechnical practice.* Chapter 5. UK.

OYO Cooperation. (2002). Materials for the technical meeting on the suspension PS log. http://geo.cv.nctu.edu.tw/EngGeo/download/Downhole_Suspension_Sonic.pdf

Randolph M.F. (2003) Science and empiricism in pile foundation design. *43th Rankine Lecture. Geotechnique 53. No 10*, 847–875.

Robertson, P.K. (2009). Interpretation of cone penetration test – a unified approach. *Canadian Geotech. Journal*. 46: 1337–1355.

Santamarina, C.J. (2001). John Wiley and Sons Ltd (ed). *Soils and waves: Particulate materials behavior, characterization and process monitoring.* Chapter 4. Hoboken, United States

Uzielli, M.; Vannuchi, G. & Phoon, K. (2005) Random field characterization of stress-normalised cone penetration testing parameters. *Geotechnique 55. No 1*, 3–20.

Zhang, G. Robertson, P. & Brachman, R (2002). Estimating liquefaction-induced ground settlements from CPT for level ground. *Canadian Geotechnical Journal*. 39: 1168–1180.

Taylor & Francis
Taylor & Francis Group
http://taylorandfrancis.com

Cone Penetration Testing 2018 – Hicks, Pisanò & Peuchen (Eds)
© 2018 Delft University of Technology, The Netherlands, *ISBN 978-1-138-58449-5*

Calibration of cone penetrometers in accredited laboratory

J. Peuchen, D. Kaltsas & G. Sinjorgo
Fugro, Nootdorp, The Netherlands

ABSTRACT: Calibration of a penetrometer is an important step in the metrological confirmation of cone penetration testing. This paper summarises experience of Fugro's calibration laboratory based in The Netherlands. This laboratory performs calibrations for about 3000 cone penetrometers used worldwide. The calibration laboratory is accredited to ISO/IEC 17025:2005 "general requirements for the competence of testing and calibration laboratories". This accreditation status is unique for cone penetration test equipment and implies rigorous quality standards.

1 INTRODUCTION

The cone penetration test (CPT) is the premier in-situ test for geotechnical investigation of soils. Its global profiling meterage is possibly in the order of 1000 km per year, which is equivalent to about 50 000 000 data points annually. Consistent reliability of the data points is key to the success of CPTs. It is also key to the success of test methods that make use of cone penetrometers, particularly the pore pressure dissipation test and the (marine) free fall penetrometer equipped with a (CPT) cone penetrometer (Randolph 2016).

The cone penetration test is standardised by many national and international standards. The common international standards are ASTM D5778-12 (ASTM, 2012), ISO 22476-1:2012 (ISO, 2012) and ISO 19901-8:2014 (ISO, 2014). These standards include specific guidance about the management of the measurement process for CPTs. A key consideration in this guidance is the calibration of cone penetrometers, which is the subject of this paper. It is noted that ASTM D5778-12 refers informatively to ASTM D3740-12 (ASTM, 2012), "Standard practice for minimum requirements for agencies engaged in testing and/or inspection of soil and rock as used in engineering design and construction". Similarly, ISO 22476-1 and ISO 19901-8 refer to ISO 10012:2003 (2003) "Measurement management systems—Requirements for measuring processes and measuring equipment". ISO 10012 refers to an early version of ISO/IEC 17025 "General requirements for the competence of testing and calibration laboratories", for example in a section on traceability: "Traceability is usually achieved through reliable calibration laboratories having their own traceability to national standards. For example, a laboratory complying with the requirements of ISO/IEC 17025 could be considered reliable."

Fugro provides and interprets CPT results worldwide. The results are acquired by deploying about 3000 cone penetrometers, including spares, resulting in about 2500 calibrations per year. The calibrations are performed by Fugro's calibration laboratory in The Netherlands. This laboratory is accredited (Fig. 1) for the calibration of cone penetrometers according to ISO/IEC 17025:2005

RAAD VOOR ACCREDITATIE

The Dutch Accreditation Council RvA, by law appointed as the national accreditation body for The Netherlands, hereby declares that accreditation has been granted to:

Fugro Engineers B.V.
Transducer Workshop
Nootdorp

The organisation has demonstrated to be able to generate technical valid results in a competent way and work according to a management system.

This accreditation is based on an assessment against the requirements as laid down in ISO/IEC 17025:2005.

The accreditation covers the activities as specified in the authorized annex bearing the registration number.

The accreditation is valid provided that the organisation continues to meet the requirements.

The accreditation with registration number:

K 167

is granted on 26 October 2016

This declaration is valid until
1 November 2020

The accreditation has been granted for the first time on
26 October 2016

The Chief Executive

Ir. J.C. van der Poel

Figure 1. Accreditation certificate.

(2005). Such accreditation status is unique for cone penetration test equipment. It also applies to tools such as the ball penetrometer and T-bar penetrometer, which include sensors calibrated within the range of accredited measurement capabilities.

ISO/IEC 17025sets rigorous quality standards, including traceability to (inter)national measurement standards. For example, force calibration for a cone penetrometer is traceable to Dutch NMi (Nederlands Meet-instituut) that is certified by the Dutch RvA (Raad voor Accreditatie), which is a member of the International Laboratory Accreditation Cooperation (ILAC). This complies with most, if not all, standards for cone penetration testing, worldwide.

The following sections provide further details by means of explanations of a calibration certificate and by comments on the calibration process and facilities.

2 CALIBRATION CERTIFICATE

A calibration certificate and supplementary information consist of eight to nine pages of text, tables and graphics, depending on the number of sensors incorporated in the cone penetrometer. The first five pages present and explain results of the calibration of sensors, while the rest are dedicated to the penetrometer geometry including net area ratios. For example, the certificate for a piezo-cone penetrometer covers: (1) the force sensors for cone resistance (q_c) and sleeve friction (f_s), (2) the pressure sensor for pore pressure (u), (3) the inclinometer for inclination from vertical (i), and (4) the geometry. The certificate also presents information about the calibration laboratory, the environmental conditions during calibration, and an explanation of adopted uncertainty analyses. References are made to detailed calibration procedures.

Figure 2 illustrates general information shown on the certificate, particularly a unique identification of the type of cone penetrometer (CP10-CF50PB20-P1E1M1-V1) and its serial number.

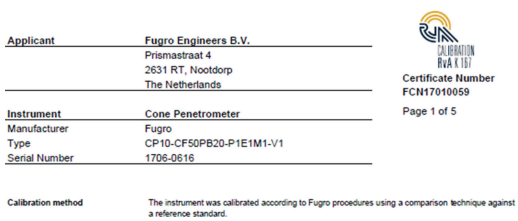

Applicant	Fugro Engineers B.V.
	Prismastraat 4
	2631 RT, Nootdorp
	The Netherlands

Instrument	Cone Penetrometer
Manufacturer	Fugro
Type	CP10-CF50PB20-P1E1M1-V1
Serial Number	1706-0616

Calibration method: The instrument was calibrated according to Fugro procedures using a comparison technique against a reference standard.

CALIBRATION RvA K 157
Certificate Number FCN17010059
Page 1 of 5

Figure 2. Example of general information in calibration certificate for a piezocone penetrometer with a nominal cross-sectional area of 1000 mm^2.

Table 1 presents a part of the certificate giving information about the controlled environmental conditions applicable to the calibration. Section 3 illustrates some of the required activities to achieve such control of environmental conditions.

Figure 3 exhibits parts of the certificate providing information about calibration of the sensor for cone resistance. Note the tracking of the electronics, including node type and hardware/software versions embedded in the cone penetrometer. The "Reference" section is about the reference force system with traceability to Dutch Nmi. The uncertainty (in kN) of the reference force system used for this example calibration is expressed as $0.003\ F_w + 0.015$ [kN], where F_w is the applied force in kN. This represents a CMC, i.e. one of the accredited Calibration and Measurement Capabilities. The section about "Calibration Details" includes another software reference, in this case software used for the calibration itself and for seamless uploading of the calibration results and other tracking information into the (digital) cone penetrometer. The "Characteristics" section of Figure 3 summarises the actual results of the calibration, expressed in units of [kN]. The meaning of terms such as "Max accuracy error (q)" are explained in the calibration certificate. Particularly, accuracy error is defined as the difference between the average indicated value by the instrument and the applied value. Repeatability error is the maximum difference between the measurements of the instruments and the applied value. Reversibility error is defined as the difference between the average indicated value by the instrument at a certain applied value when it was increased and

Table 1. Example of information on environmental conditions in calibration certificate.

Environmental	Conditions
Temperature during calibration	20.5 ± 3°C
Atmospheric pressure during calibration	1000 ± 100 mbar

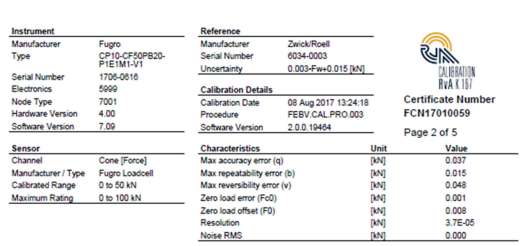

Instrument	
Manufacturer	Fugro
Type	CP10-CF50PB20-P1E1M1-V1
Serial Number	1706-0616
Electronics	5999
Node Type	7001
Hardware Version	4.00
Software Version	7.09

Sensor	
Channel	Cone [Force]
Manufacturer / Type	Fugro Loadcell
Calibrated Range	0 to 50 kN
Maximum Rating	0 to 100 kN

Reference	
Manufacturer	Zwick/Roell
Serial Number	6034-0003
Uncertainty	0.003-Fw+0.015 [kN]

Calibration Details	
Calibration Date	08 Aug 2017 13:24:18
Procedure	FEBV.CAL.PRO.003
Software Version	2.0.0.19464

Characteristics	Unit	Value
Max accuracy error (q)	[kN]	0.037
Max repeatability error (b)	[kN]	0.015
Max reversibility error (v)	[kN]	0.048
Zero load error (F0)	[kN]	0.001
Zero load offset (F0)	[kN]	0.008
Resolution	[kN]	3.7E-05
Noise RMS	[kN]	0.000

CALIBRATION RvA K 157
Certificate Number FCN17010059
Page 2 of 5

Figure 3. Example information about calibration of cone resistance.

when it was decreased. Furthermore, noise RMS is defined as the quadratic mean when the sensor is not subjected to force.

Figure 4 illustrates a part of the certificate showing graphics on the results of calibration of cone resistance. The dual-scale graph shows the applied force on the x-axis. The two y-axes show the measured average force and the accuracy error. The measured force refers to the green curve and the accuracy error to the dashed red curve.

Table 2 corresponds to Figure 4. It provides tabular values and additional quantification of uncertainty for each load interval. The expanded uncertainty is that of the average indicated quantity and includes the entire calibration method, including the reference and the calibrated sensor, but excludes the difference between average indicated value by the instrument and the applied value. It can be seen that three values of measured force (*Fa,1 Fa,2* and *Fa,3*) are presented for each applied force. The numerical values of error (q, b and v) and expanded uncertainty (U) apply to the measured average force (*Fa*).

Figure 4 and Table 2 apply to a cone penetrometer with a cross sectional area of 1 000 mm^2. For this case, Fw = 1 kN is equivalent to q_c = 1 MPa. The values of accuracy error q and expanded uncertainty U can thus be compared with the allowable minimum accuracies (or allowable maximum uncertainties) given by the ISO standards. For example, Application Class 1 of ISO (2012) considers an allowable minimum accuracy of q_c = 0.035 MPa for a CPT profile with measured values of q_c < 0.7 MPa. The allowable minimum accuracy is 0.05 q_c for 0.7 MPa < q_c < 3 MPa. For a measured value q_c = 3 MPa, the allowable maximum uncertainty is then equivalent to q_c = 0.15 MPa.

It can be observed that Table 2 shows accuracy errors q of up to 0.037 kN (q_{qc} = 0.037 MPa) for a calibrated range of Fw = 0 to Fw = 50 kN (q_c = 50 MPa). Even better values of q apply to low q_c values. Furthermore, a comparison of the values for q and expanded uncertainty U shows that the values of U are dominated by the uncertainty of the accredited reference at low values of Fw. This is as discussed by e.g. Peuchen and Terwindt (2014): "*Laboratory calibration for a cone penetrometer is typically for loading/ unloading against a reference load cell. Note that a high quality cone penetrometer has characteristics equivalent to a high-quality reference load cell, i.e. calibration results may be limited by the reference load cell. Low range data may be obtained by incremental application of mass*". For example, at Fw = 0, the value of U for the reference is U = 0.015 kN (Figure 3) compared to U values for the cone penetrometer of 0.016 kN and 0.015 kN (2nd row and last row of Table 2). This confirms that the actual accuracy of the cone penetrometer at low values of q_c is significantly better than the expanded uncertainty U presented on the calibration certificate.

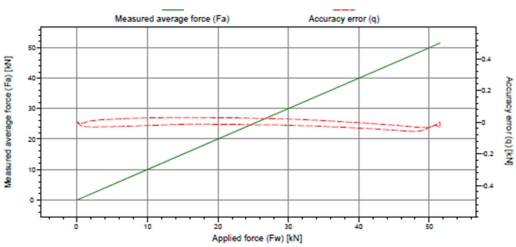

Figure 4. Example results of calibration of cone resistance, expressed in units of force [kN].

Table 2. Tabular values of example graphics shown on Figure 4.

Applied force (Fw) [kN]	Measured force 1 (Fa, 1) [kN]	Measured force 2 (Fa, 2) [kN]	Measured force 3 (Fa, 3) [kN]	Measured average force (Fa) [kN]	Accuracy error (q) [kN]	Repeatability error (b) [kN]	Reversibility error (v)	Expanded uncertainty (U) [kN]
0.000	0.003	–0.002	–0.001	0.000	0.000	0.005		0.016
10.000	9.976	9.978	9.984	9.979	–0.021	0.008	0.048	0.095
20.000	19.981	19.988	19.991	19.987	–0.013	0.010	0.042	0.096
30.000	29.974	29.981	29.986	29.981	–0.019	0.012	0.039	0.118
40.000	39.957	39.964	39.967	39.963	–0.037	0.011	0.034	0.145
50.000	49.969	49.960	49.975	49.968	–0.032	0.015		0.170
40.000	39.990	39.998	40.002	39.997	–0.003	0.013		0.139
30.000	30.014	30.021	30.024	30.020	0.020	0.010		0.108
20.000	20.022	20.030	20.034	20.029	0.029	0.011		0.078
10.000	10.021	10.028	10.032	10.027	0.027	0.010		0.048
0.000	0.001	0.001	0.000	0.001	0.001	0.001		0.015

3 CALIBRATION PROCESS AND FACILITIES

The calibration certificate is an outcome of a largely automated calibration process that includes management of the calibration facilities. This section provides comments.

Figure 5 illustrates example records used for control of environmental conditions in the calibration laboratory. The records comprise measured temperature fluctuations on a typical day for three sensors: one placed against a wall and two attached to reference loadcells of calibration devices.

Figure 6 shows a rubber joint in the floor of the calibration laboratory. The part of the building beyond this joint, where the calibration apparatus stands, has a separate foundation and is not connected to the rest of the building to further eliminate the vibrations from activities in other parts of the building. This is particularly important for the accuracy of calibrations.

A cone penetrometer which is returned to the calibration laboratory after use is subjected to a so-called post-fieldwork validation, or PFW. This takes place prior to actual re-calibration. For example, the PFW for cone resistance covers three load cycles up to the originally calibrated range, using the original calibration data. PFW information provides an indication of the condi-

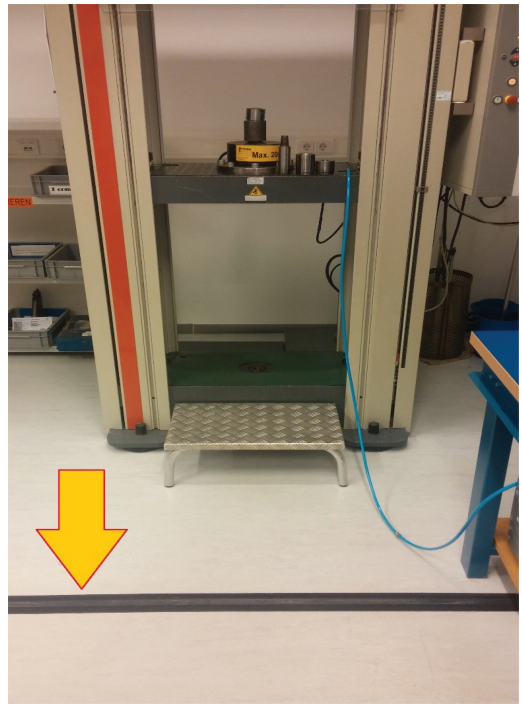

Figure 6. Reference sensor for axial force and detail of floor isolation (rubber joint).

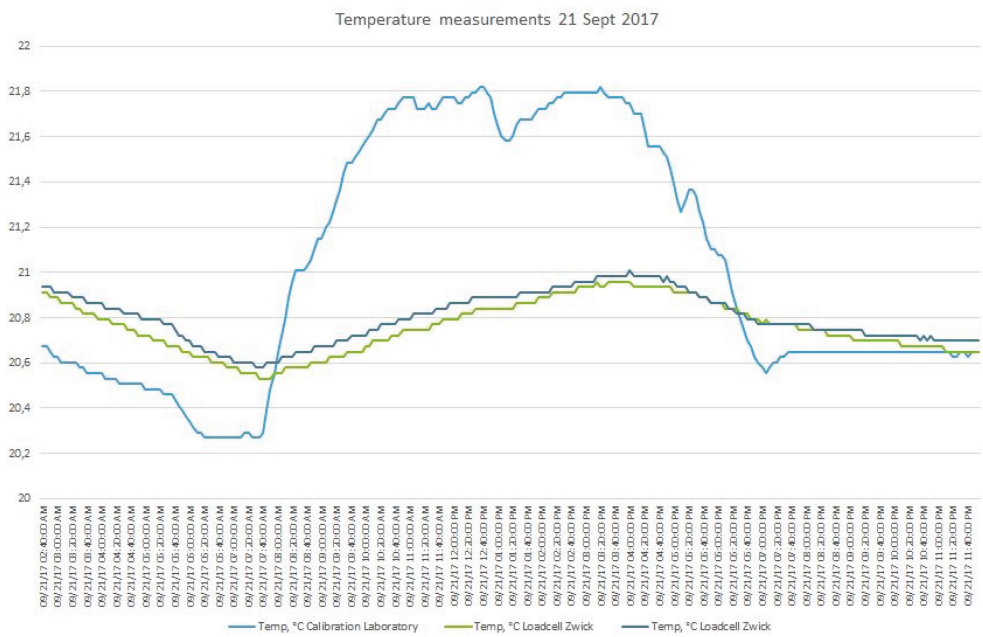

Figure 5. Example records of monitoring temperature for one day in calibration laboratory; vertical scale is in °C.

tion of the cone penetrometer "as is", i.e. no parts are replaced and the penetrometer is not cleaned. Consistent tracking of PFW information provides input for managing calibration intervals and continuous improvement. The calibration process also includes routine electrical checks performed before and after calibration. If the checks fail, then the cone penetrometer is repaired and re-calibrated.

For a subtraction-type cone penetrometer (ISO, 2012), a compression machine applies axial force to the two load cells for q_c and f_s, concurrently. The reference force sensor and its digital output on the read-out computer have full traceability, with calibrations performed every 12 months by a European accredited company.

Calibration of the pressure sensor for pore pressure is done by means of a pressure vessel. The pressure calibration procedure is similar to force calibration, i.e. the cone penetrometer is subjected to water pressure in the pressure vessel. The reference pressure sensor is calibrated using a dead weight tester that is calibrated by an accredited company. Pressure calibration occurs last, as it includes determination of net area ratio.

Calibration of the inclinometer includes mounting of the cone penetrometer in an accredited reference inclination measuring device. The output from the reference inclination device is verified by measuring the lengths of the sides and the triangle formed under various angles and computing the arc tangents with an accredited caliper.

The dimensions (geometry) of the outer surfaces of a cone penetrometer are subject to wear. The dimensions of the cone penetrometer are checked to meet the tolerances prescribed by ASTM (2012) and ISO (2012). The dimensions are measured with an accredited caliper or a rejection jig. Reference calipers have full traceability.

4 CONCLUSIONS

Calibration of a penetrometer is an important step in the metrological confirmation of cone penetration testing. This paper summarises experience of Fugro's calibration laboratory based in The Netherlands. This laboratory performs calibrations for about 3000 cone penetrometers used worldwide. The calibration laboratory is accredited to ISO/IEC 17025:2005 "general requirements for the competence of testing and calibration laboratories". This accreditation status implies rigorous quality standards and complies with most, if not all, standards for cone penetration testing, worldwide. The accreditation status is unique for cone penetration test equipment. It also applies to tools such as the ball penetrometer and T-bar penetrometer, which include sensors calibrated within the range of accredited measurement capabilities.

REFERENCES

ASTM International 2012. Standard practice for minimum requirements for agencies engaged in testing and/or inspection of soil and rock as used in engineering design and construction, ASTM D3740-12. West Conshohocken: ASTM International.

ASTM International 2012. Standard test method for electronic friction cone and piezocone penetration testing of soils, ASTM D5778-12. West Conshohocken: ASTM International.

ISO 2003. Measurement management systems – requirements for measurement processes and measuring equipment, International Standard ISO 10012:2003. Geneva: International Organization of Standardization.

ISO 2012. Geotechnical investigation and testing – Field testing – Part 1: Electrical cone and piezocone penetration test, International Standard ISO 22476-1:2012. Geneva: International Organization of Standardization.

ISO 2014. Petroleum and gas industries – Specific requirements for offshore structures – Part 8: Marine soil investigations, International Standard ISO 19901-8:2014. Geneva: International Organization of Standardization.

ISO/IEC 2005. General requirements for the competence of testing and calibration laboratories, International Standard ISO/IEC 17025:2005. Geneva: International Organization for Standardization & International Electrotechnical Commission.

Peuchen, J. & Terwindt, J. 2014. Introduction to CPT accuracy, *Keynote in 3rd International Symposium on Cone Penetration Testing CPT'14*. May 12–14, 2014 – Las Vegas, Nevada, 45 p.

Randolph, M.F. 2016. New tools and directions in offshore site investigation, *Australian Geomechanics* 51(4): 81–92.

Taylor & Francis
Taylor & Francis Group
http://taylorandfrancis.com

Cone Penetration Testing 2018 – Hicks, Pisanò & Peuchen (Eds)
© 2018 Delft University of Technology, The Netherlands, ISBN 978-1-138-58449-5

Defining geotechnical parameters for surface-laid subsea pipe-soil interaction

J. Peuchen
Fugro, Nootdorp, The Netherlands

Z. Westgate
Fugro, Houston, USA

ABSTRACT: The interaction between surface-laid pipelines and the seabed typically takes place within the upper 0.5 m of the seabed. The key geotechnical parameters for assessing pipe-soil interaction are intact and remoulded undrained shear strength, interface shear resistance, submerged soil unit weight, and coefficient of consolidation. This paper summarises experience deriving design geotechnical parameters for various shallow stratigraphy conditions characteristic of different geographic regions. It is shown that characterisation of the upper 0.5 m of the seabed can require site-specific evaluations and ranking of geotechnical investigation tools. This is illustrated for (1) stratigraphic definition and (2) geotechnical parameterisation. The ranking includes cone penetration tests, T-bar/ball penetrometers, free fall penetrometers, box core sampling and in-box miniature T-bar or ball penetration testing, piston core sampling, push sampling and laboratory testing.

1 INTRODUCTION

Design of surface-laid subsea pipelines is typically done according to API RP 1111 (2015), ISO 13623 (2009), DNVGL-RP-F114 (2017), or equivalent. Axial expansion, lateral buckling, hydrodynamic and route curve stability, and free-spans are the typical design situations requiring geotechnical input. The key geotechnical parameters are intact undrained shear strength (s_u), remoulded undrained shear strength ($s_{u,r}$), pipe-soil interface shear resistance—expressed as an undrained strength ratio ($s_{u,res}/\sigma'_{v0}$) or a drained interface friction angle (δ_{res}), effective soil unit weight (γ'), and coefficient of consolidation (c_v). Soil erodibility is another key consideration, which affects the seabed around the pipeline.

The geotechnical parameters of the seabed are important for the zone between the seabed surface (seafloor) and to a depth below seafloor on the order of 0.5 m, depending on pipeline diameter and its embedment. Frequently, this part of the seabed is also the zone with active or recent geological processes and associated high degree of soil variability. Accurate characterisation of this surficial zone represents a major challenge to pipeline design.

The objective of this paper is to provide guidance for development of a site investigation programme for surface-laid pipelines. Section 2 discusses pipeline route characterisation, including cost-effective selection of investigation tools. Section 3 presents supplementary discussion about the state of practice, with focus on in-situ penetration testing.

2 INTEGRATED SITE INVESTIGATION

2.1 *Investigation tools*

Defining geotechnical parameters for surface-laid subsea pipe-soil interaction (PSI) typically requires specialist integration of data acquired by means of tools in the following categories (Table 1): (a) marine geophysical investigation, (b) in-situ testing, (c) sampling and (d) laboratory testing. As evident from the large number of listed tools and their associated applicability in Table 1, no single tool on its own has complete capability of providing the desired information for design.

The column *Use* in Table 1 should be read as relative use of a geophysical technique for seafloor mapping and sub-seafloor mapping, but should be read in terms of deployments of combined in-situ test tools and sampling tools for in-situ testing sampling. The *Applicability* columns of Table 1 show multiple site conditions ranging from uniform, extremely low (EL) strength, hemipelagic clays to hard ground conditions. The *Applicability* ranking of a particularly laboratory test should

Table 1. Comparison of site investigation tools for design of surface-laid subsea pipelines.

Tool	Use	Geotechnical Parameter	Applicability: EL Clay SP	EL Clay GP	Layered Clay and Sand SP	Layered Clay and Sand GP	VL to M Clay SP	VL to M Clay GP	>M Clay SP	>M Clay GP
Marine geophysical investigation										
Seafloor and sub-seafloor mapping	****		+/–	–	+/–	–	+/–	–	+/–	–
In-situ testing										
Cone penetration test (CPT)	****	s_u ($s_{u,r}$, γ')	+	++	+	+	++	++	+	+
T-bar/ ball penetration test (TPT/BPT)	**	s_u	+/–	++	+/–	+/–	+/–	++	–	–
Cyclic T-bar/ ball penetration test (TPT, BPT)	*	$s_{u,r}$	+/–	++	+/–	+/–	+/–	++	–	–
Piezocone pore pressure dissipation test	*	c_v (s_u)	++	++	++	+	++	++	+	+/–
Piezoprobe/ piezo-ball pore pressure dissipation test	*	c_v (s_u)	–	++	+/–	+/–	+/–	++	–	–
In-situ vane shear test	*	s_u, $s_{u,r}$	–	++	–	–	–	++	–	–
Free fall penetration test—CPT penetrometer	*	s_u	+	+	+/–	+/–	++	++	+/–	+/–
Free fall penetration test—accelerometers	*	s_u	–	–	+/–	+/–	+	+	+/–	+/–
Pipeline section test—self-weight	*	s_u	+/–	++	–	–	+/–	+/–	–	–
Pipeline section test—SMARTPIPE®	*	s_u, $s_{u,r}$, c_v	+/–	++	–	+/–	+/–	++	–	–
Sampling (+ laboratory testing)										
Piston sampler—SMARTSURF® incl. CPT or (miniature) TPT/ BPT	*	s_u, $s_{u,r}$, $s_{u,res}/\sigma'_{v0}$, δ_{res}, γ', c_v	++	+	+	+	++	++	+/–	+/–
Box corer + MTPT/ MBPT	***	s_u, $s_{u,r}$, $s_{u,res}/\sigma'_{v0}$, δ_{res}, γ', c_v	++	+	+/–	+	+/–	++	–	–
Free fall piston corer/ gravity corer	***	s_u, $s_{u,r}$, $s_{u,res}/\sigma'_{v0}$, δ_{res}, γ', c_v	–	–	+/–	+/–	+	+	–	–
Vibrocorer	**	s_u, $s_{u,r}$, $s_{u,res}/\sigma'_{v0}$, δ_{res}, γ', c_v	–	–	–	–	+/–	+/–	+/–	+/–
Rotary core sampler	*	s_u, $s_{u,res}/\sigma'_{v0}$, δ_{res}, γ'	–	–	–	–	–	–	+	+
Laboratory testing										
Laboratory miniature vane test (MV)	****	s_u, $s_{u,r}$	–	+	–	+	–	++	–	–
Low stress interface shear box test	**	$s_{u,res}/\sigma'_{v0}$, δ_{res}, c_v	–	++	–	+	–	++	–	+
Incremental oedometer or CRS test	**	c_v	–	+	–	+	–	++	–	+/–

SP = stratigraphic profiling; GP = geotechnical parameter values; EL = extremely low strength (s_u 10 kPa); VL = very low strength (10 kPa s_u 20 kPa); M = medium strength (40 kPa s_u 75 kPa); Parameters between brackets have possible applicability; they are not considered for the GP applicability rating; ++ = high applicability; + = medium applicability; +/– = possible applicability; – = no applicability; * = less than 0.1% of tool deployments; ** = between 0.1% and 1%; *** = between 1% and 10%; **** = more than 10%.

consider the ranking of the sampling tool. The lower of the two rankings applies.

Note that Table 1 includes rarely-used tools, yet does not cover all possible tools or potential future tools. For example, magnetometer survey and borehole drilling and sampling are omitted, while possible future tools include the in-situ toroid penetrometer and the in-situ hemi-ball penetrometer (White et al. 2017).

2.2 *Soil provinces and data coverage*

Limited general guidance on integrated site investigation is included in the standards for pipeline design listed in Section 1. In practice, integrated site investigation leads to development of a ground model and, often, multiple soil provinces. A soil province is an area in which geotechnical conditions are assessed as similar. The vertical range of expected geotechnical conditions is described and summarised in a predicted soil profile associated with a soil province.

The delineation of soil provinces takes account of data coverage by the techniques and tools listed in Table 1. Seafloor mapping typically provides full data coverage for the seafloor area of interest. Data accuracy and data resolution primarily depend on the tool or technique and deployment method. Sub-seafloor mapping can provide linear, 2D data coverage along selected survey track lines. Section 3 provides further information on technology limitations on data coverage for sub-seafloor mapping.

In-situ testing represents intrusive investigation, i.e. tools penetrate the seabed at selected locations.

This implies acquisition of point data, generally compiled in vertical profiles. Associated sampling and laboratory testing provides complementary data coverage to verify and calibrate in-situ test results.

Effects of geotechnical uncertainty and spatial variability in pipeline design are discussed in, e.g. White et al. (2015). Inevitably, data integration requires experienced geo-professionals for assessing uncertainties and developing fit-for-purpose ground models and geotechnical parameter selection.

2.3 *Geotechnical parameter values*

A predicted soil profile typically considers uncertainty using low estimate LE, best estimate BE and high estimate HE values for the geotechnical parameters listed in Section 1 and Table 1. Accurate measurement of shallow soil properties is critical for assessing PSI response. For soft fine-grained soil (common to most moderate to deep-water hydrocarbon-producing basins), the critical parameters are s_u and $s_{u,r}$. Not only do s_u and $s_{u,r}$ affect axial and lateral undrained resistance, but they dominate the initial, or as-laid, pipeline embedment. For EL strength soil, γ' can be just as important as strength due to buoyancy effects. In coarse-grained materials, δ_{res} is often the critical parameter, but γ' is also important, and s_u can be important for assessing as-laid embedment, due to the high frequency cyclic loading of the soil during the lay process, which is seastate-driven (Westgate et al. 2010). Consolidation coefficient c_v is the main parameter that determines the drainage response of the soil, and therefore which resistance parameters require quantification.

Figure 1 illustrates challenges in assessing accurate s_u and $s_{u,r}$ values for an EL Clay scenario of Table 1. The presented (point) data are for a single investigated location cluster that serves as one of multiple location inputs for a predicted soil profile of a soil province. The in-situ test methods represented by Figure 1 are the (piezo)cone penetration test (CPT) and the T-bar penetration test (TPT). The presented laboratory test methods are the miniature T-bar penetration test (MTPT) in a box core sample, and the laboratory miniature vane test (MV) and the torvane test (TV) performed in box core and piston core samples. The presented test results are according to ISO (2014). The scale of the upper horizontal axis of the diagram applies to CPT, TPT and MTPT penetration resistance values. The scale of the lower horizontal axis applies to CPT sleeve friction, undrained shear strength and remoulded undrained shear strength $s_{u,rMV}$ according to Method c) of ISO (2014), i.e. after 5 to 10 rotations for the vane. The cyclic portion of the TPT and the two MTPTs were started in the penetration phase.

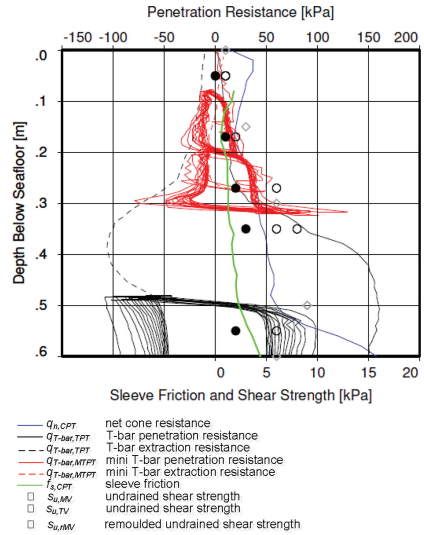

Figure 1. Project example of challenges in assessing s_u and $s_{u,r}$ values for deepwater low strength clays.

Figure 1 shows more (high quality) project data than usually available in practice for a single location. This allows the evaluation of scenarios with less data, e.g. which criteria to apply for selection of s_u and $s_{u,r}$ values if only CPT data or only MV data were available. Similarly, which criteria should be applied for LE, BE and HE values for a soil province investigated at multiple profiling locations. A further consideration for the example of Figure 1 is the estimation of combined uncertainty values applicable to (a) the data points in terms of depth below seafloor and test values such as $q_{n,CPT}$, and (b) the derivation of fit-for-purpose sets of s_u and $s_{u,r}$ values (including any intermediate values for partially remoulded conditions) for a particular PSI calculation model. Section 3 includes some guidance on estimation of uncertainty values for some of the tools of Table 1. The selected piecewise linear LE, BE and HE profiles should aim to capture the subtleties of strength variation with depth, including (a) extremely low or negligible strength at seafloor, (b) any surficial crust layers, and (c) the potential for water entrainment effects from surficial cycling. Overconservative bounding of the data, particularly the strength at seafloor, can have a significant widening effect on the range of PSI outputs such as pipe embedment and lateral or axial resistance parameters.

3 SITE INVESTIGATION PRACTICE

3.1 *Marine geophysical investigation*

Seafloor mapping provides information about soil conditions at seafloor and about the general

geomorphological setting. The common tools are multi-beam echo sounder (MBES) and the side-scan sonar (SSS). MBES backscatter data can often be processed to determine whether the surface materials are predominantly fine-grained or coarse-grained (e.g. IOGP 2017).

Sub-seafloor mapping typically provides no direct information about site conditions immediately below seafloor (BSF) within the zone of influence for surface-laid pipelines. Particularly, commonly available seismic reflection survey tools provide no stratigraphic resolution for this part of the seabed (e.g. DNVGL 2017).

3.2 *Cone penetration testing*

Table 1 shows the *Use* for cone penetration tests (CPTs) as **** (>10% for all deployments), higher than for any other tool in the in-situ testing and sampling categories. Their current dominance in pipeline practice relates to a combination of data value versus cost of data acquisition. Piezocone penetrometers lead this trend with more than 95% use, mostly with a filter positioned in the cylindrical section of the cone tip (u_2 position).

CPT data generally allow stratigraphic profiling to about 40 mm resolution, generating data points every 0.02 m of penetration. CPTs cannot accurately distinguish loose sand from low strength clay between seafloor and about 0.1 m BSF. This is because of a combination of initial embedment effects applicable to the cone penetrometer and the friction sleeve of the cone penetrometer achieving full embedment below about 0.15 m BSF. In this case, it is noted that the example of Figure 1 shows f_s data starting below about 0.1 m BSF.

The Medium Applicability (Table 1) assigned to stratigraphic profiling for EL Clay relates to accuracy of CPT parameter values. For the CPT results presented in Figure 1, the uncertainty values for $q_{n,CPT}$ and $f_{s,CPT}$ are about ± 5 kPa and ± 3 kPa respectively (Peuchen & Terwindt 2015). Uncertainty values for precision are significantly better. The depth accuracy class is estimated as Z1 according to ISO (2014), i.e. data point depth uncertainty of better than ± 0.1 m.

Deriving s_u from CPTs is generally based on $s_u = q_{n,CPT}/N_{kt}$, where N_{kt} is an empirical cone factor. Values of N_{kt} typically consider a reference method for s_u derived from a process of sampling and laboratory testing. EL clays, common at deepwater locations, present challenges to this practice. The following comments are offered:

- N_{kt} factors for EL clays are commonly taken from published correlations (e.g. Mayne et al. 2015) with laboratory test data at strength and stress levels higher than EL clays close to seafloor, i.e. outside the published correlations. Also, overconsolidation mechanisms (e.g. Kuo et al. 2010) and associated apparent overconsolidation ratios for EL clays (e.g. Fig. 1) close to seafloor typically differ from published correlations.
- In practice, the effects of limited embedment of a cone penetrometer are ignored for selection of N_{kt} values. This practice can underestimate s_u for the upper 0.2 m BSF, possibly by up to about 30%.
- CPT parameter values for EL clays, especially near seafloor, are close to their measuring limits.
- Site-specific spot checks for N_{kt} can be made in case of undisturbed, non-pressure, soil sampling at the same location cluster. The checks typically comprise index strength testing conducted on soil retained in the sampler, i.e. before removal of the sample from the sampler. Common index strength tests are the TV and MV as shown on Figure 1. The number of data points from these index tests is, at best, a small fraction of those derived from CPTs, and include at least the same level of uncertainty in the derived values. EL clays are typically outside the applicability range of undrained triaxial tests and direct simple shear tests. These laboratory test types generally provide no added value compared to index strength tests on undisturbed EL clay retained in a sampler.
- MTPTs and miniature ball penetration tests (MBPTs) performed in box cores and large-diameter samples can be used to support derivation of N_{kt}. However, any errors in selection of N_{Tbar} and N_{ball} values will show high correlation with the errors for N_{kt}.
- In case of sparse data, approximate laboratory checks for N_{kt} can be obtained from disturbed samples, by deriving $s_{u,r}$ and estimating a strength sensitivity factor S_t.

Table 1 shows that values for $s_{u,r}$ and γ' can be broadly derived from CPT parameters. Particularly, $s_{u,r}$ can be correlated to $f_{s,CPT}$ (e.g. Quiros & Young 1988), at high precision but limited accuracy. Figure 1 shows reasonable correlation for $s_{u,rMV} \sim 1.0\, f_{s,CPT}$. Correlations between $f_{s,CPT}$ and $s_{u,r}$ should consider: (a) cone penetrometer type, (b) a reference test method for $s_{u,r}$, and (c) soil behaviour type including range of soil strength or overconsolidation ratio *OCR*. It is noted that $f_{s,CPT}$ is probably more related to residual strength than remoulded strength. Furthermore $f_{s,CPT}$ can be dominated by soil-soil shear resistance at low *OCR* values and by soil-steel resistance at high *OCR* values.

CPTs require a robust seafloor-based template providing self-weight resistance to the push-in system and the heave-compensated tensioning of the lifting/ communication cable(s). The template can affect CPT measurements from seafloor to 0.5 m BSF (Peuchen et al. 2005), if all the following conditions are met:

- Penetration of the template into the seabed > ~0.2 m, i.e. typically soil consisting of EL clay or similar.

– Template bearing pressure > ~ 10 kPa.
– Lateral distance between the edge of the template and the axis of the cone penetrometer is < 0.5 m.

Some systems allow estimation of the magnitude of template penetration into the seabed by means of a mechanical settlement gauge with about 0.5 m measuring range. The SMARTSURF® system (Randolph 2016) is an example of a specific site investigation tool for combined in-situ testing and piston sampling for surface-laid pipelines and cables. It is equipped with retractable mudmats and seafloor detection tools for deployment on extremely soft seabed.

3.3 *T-bar/Ball Penetration Testing*

As indicated by Table 1, the T-bar and ball penetrometer capabilities for soil profiling and, therefore, geotechnical parameter values are limited to relatively uniform fine-grained soils. For the TPT results presented in Figure 1, the uncertainty value for $q_{T\text{-}bar,TBT}$ is about ± 3 kPa for the penetration phase (Peuchen and Terwindt 2016) compared to ± 5 kPa for the CPT. Slightly higher uncertainty applies to the extraction phase and any cyclic phases. As for the CPT, uncertainty values for precision are significantly better, and the depth accuracy class is estimated as Z1.

A consideration for TPT and BPT interpretation is presumed soil closure around the penetrometer except for the push rod/ shaft. However, a slot in soil can apply close to seafloor, occasionally in combination with a detached lump of soil on top of the T-bar or ball. The depth of slotting depends on properties such as s_u, OCR and γ. It can exceed several T-bar or ball diameters, as illustrated with finite element analysis (e.g. Tho et al. 2012). Slotting can also change in-situ soil properties by water entrainment. As entrainment can take place during pipeline installation, cyclic penetration testing can be used for assessing changes in undrained shear strength during pipe laying and therefore assessment of as-laid embedment. Comparisons between surface-breaking cycles and deep cycles can be used to assess a soil's susceptibility to water entrainment-driven strength degradation.

3.4 *Free-fall Penetration Testing—Cone Penetrometer*

Future frequency of use of CPTs may reduce, as equipment capabilities and interpretive capabilities are evolving for the free-fall penetration test equipped with a CPT penetrometer. Peuchen et al. (2017) provide a summary for this type of free-fall tool, particularly considering extremely low strength soils at and close to seafloor.

3.5 *Sampling*

A SMARTSURF® system, or equivalent, is preferred for shallow seabed sampling (Table 1). The box corer is a secondary tool. Box core sampling and associated laboratory testing are often used and occasionally misunderstood. This is further discussed below. The other samplers listed in Table 1 typically have Possible Applicability and No Applicability. These classifications relate to reliability of complete sample recovery for the upper 0.5 m BSF. ISO (2014) provides background information about such sample recovery limitations. The penetration capabilities of the box corer limit the effective use of the tool to clays of extremely low and very low strength (Table 1). For these types of soil, the box corer has continuous sample recovery to penetration depth, typically up to 0.5 m BSF. This allows for accurate characterisation of the layering of the upper seabed (Fig. 2). Nevertheless, it is possible that the top material, particularly loose non-cohesive material, is washed out of the sampler when the box corer is retrieved to the vessel. As for all types of non-pressure sampling, total stress conditions inevitably change upon extraction of a sample from the soil. This can lead to soil swelling, loss of saturation and formation of free gas in the sample where gas was previously in solution in the pore water.

To minimize this effect, MTPTs or MBPTs are commonly performed in box cores or large diameter sub-samples of a box core, immediately after sample recovery. Figure 1 presents example results for conventional displacement-controlled test procedures. Conventional deep cyclic phases (Figure 1) can be compared to surface-breaking cyclic phases, as for the TPT and BPT. Load-controlled cycles can also be employed to assess the self-burial of the penetrometer under a fixed or variable combination of cyclic loading. This can be useful for riser or pipeline embedment assessments and to derive seabed stiffness values for riser fatigue design.

3.6 *Laboratory testing*

The usual limitations apply to laboratory tests on intact samples. Laboratory testing typically

Figure 2. Examples of seabed stratigraphy from box core sampling: (left) upper EL clay (slurry) layer and (right) upper shelly layer (from White et al. 2015).

includes characterisation testing (water content, Atterberg limits, density of solid particles, unit weight, carbonate content, particle size analysis) and index strength testing (intact and remoulded MV and TV, direct shear) relevant to the soil type. Testing to quantify the pipe-soil interface shear resistance is generally performed on remoulded and reconstituted samples to simulate the soil disturbance due to pipeline laying. This type of specialist testing typically covers low normal stress loading conditions, variations in shearing rates, pre-consolidation level, interface surface roughness, and cyclic loading (Boukpeti & White 2017).

4 MAIN POINTS

Design of surface-laid pipelines requires characterisation of the (approximately) upper 0.5 m of the seabed for (1) stratigraphic definition and (2) accuracy of geotechnical parameter values. This is linked to critical ranking of site investigation systems. The ranking includes sub-seafloor mapping, cone penetration tests, T-bar/ball penetration tests and box core sampling combined with in-box miniature T-bar or ball penetration testing. Experience from practice provides opportunities for significant data enhancement and avoidance of pitfalls through careful selection of sampling and testing equipment, procedures and interpretation.

REFERENCES

American Petroleum Institute, 2015. API RP 1111 Design, Construction, Operation, and Maintenance of Offshore Hydrocarbon Pipelines (Limit State Design. Washington, D.C.: API), 5th Edition.

Boukpeti, N. & White, D.J., 2017. Interface shear box tests for assessing axial pipe-soil resistance, *Géotechnique, Vol. 67, No. 1*, 18–30.

DNVGL, 2017. DNVGL-RP-114: Recommended Practice F114: Pipe-soil interaction for submarine pipelines, May.

International Association of Oil & Gas Producers IOGP, 2017. Report 373-18-1 Guidelines for the Conduct of Offshore Drilling Hazard Site Surveys. 46p.

International Organization for Standardization, 2009. ISO 13623:2009 Petroleum and Natural Gas Industries - Pipeline Transportation Systems. Geneva: ISO.

International Organization for Standardization, 2014. ISO 19901-8:2014 Petroleum and Natural Gas Industries - Specific Requirements for Offshore Structures – Part 8: Marine Soil Investigations. Geneva: ISO.

Kuo, M.Y.H., Bolton, M.D., Hill, A.J. & Rattley, M.J., 2010. New evidence for the origin and behaviour of deep ocean 'crusts'. In Gourvenec, S. and White, D. Eds. *Frontiers in Offshore Geotechnics II: Proceedings of the 2nd International Symposium on Frontiers in Offshore Geotechnics, Perth, Australia, 8-10 November 2010*. Boca Raton: CRC Press, 365–370.

Mayne, P.W., Peuchen, J. & Baltoukas, D.B., 2015. Piezocone evaluation of undrained strength in soft to firm offshore clays. In Meyer, V. ed. *Frontiers in Offshore Geotechnics III: proceedings of the Third International Symposium on Frontiers in Offshore Geotechnics ISFOG 2015), Oslo, Norway, 10–12 June 2015*, Boca Raton: CRC Press, 1091–1096.

Peuchen, J., Looijen, P. & Stark, N., 2017. Offshore characterisation of extremely soft sediments by free fall penetrometer, Society for Underwater Technology: Offshore Site Investigation and Geotechnics Committee, ed. Offshore Site Investigation and Geotechnics: Smarter Solutions for Future Offshore Developments: Proceedings of the 8th International Conference 12–14 September 2017. Royal Geographical Society, London, UK: Volume 1. London: Society for Underwater Technology, 370–377.

Peuchen, J. & Terwindt, J. 2016. Critical appraisal of T-bar penetration tests. Lehane, B.M., Acosta-Martinez, H.E. and Kelly, R.B. Eds. *Geotechnical and Geophysical Site Characterization 5: Proceedings of the Fifth International Conference on Geotechnical and Geophysical Site Characterization (ISSMGE TC-102—ISC'5), Gold Coast, Queensland, Australia, 5–9 September 2016*. Sydney: Australian Geomechanics Society, 351–356.

Peuchen, J. & Terwindt, J., 2015. Measurement uncertainty of offshore cone penetration tests. In Meyer, V. ed. Frontiers in Offshore Geotechnics III: proceedings of the Third International Symposium on Frontiers in Offshore Geotechnics ISFOG 2015), Oslo, Norway, 10–12 June 2015, Boca Raton: CRC Press, 1209–1214.

Peuchen, J., Adrichem, J. & Hefer, P.A., 2005. Practice notes on push-in penetrometers for offshore geotechnical investigation. In Gourvenec, S. and Cassidy, M. Eds., *Frontiers in Offshore Geotechnics ISFOG 2005: Proceedings of the First International Symposium on Frontiers in Offshore Geotechnics, University of Western Australia, Perth, 19–21 September 2005,* London: Taylor & Francis, 973–979.

Randolph, M.F., 2016. New tools and directions in offshore site investigation, *Australian Geomechanics, Vol. 51, No. 4*, December, 81–92.

Quiros, G.W. & Young, A.G. 1988. Comparison of Field Vane, CPT, and Laboratory Strength Data at Santa Barbara Channel Site. Richards, A.F. Ed. *Vane shear strength testing in soils: field and laboratory studies*. Philadelphia: American Society for Testing and Materials, ASTM STP 1014, 306–317.

Tho, K.K., Leung, C.F., Chow, Y.K., & Palmer, A.C., 2012. Deep cavity flow mechanism of pipe penetration in clay, *Canadian Geotechnical Journal, Vol. 49*, 59–69.

Westgate, Z.J., Randolph, M.F., White D.J. & Li, S., 2010. The influence of seastate on as-laid pipeline embedment: a case study, *Applied Ocean Research, 32, (3):* 321–331.

White, D.J., Westgate, Z.J., Ballard J-C. & Bransby M.F., 2015. Best practice geotechnical characterization and pipe-soil interaction analysis for PHPT pipeline design, *Proc. Offshore Technology Conference, Houston, OTC 26026-MS.*

White, D.J., Stanier, S.A., O'Loughlin, C.D., Chow, S.H., Randolph, M.F., Draper, S.D., Mohr, H., Morton, J.P., Peuchen, J., Fearon, R. Roux, A. & Chow, F.C., 2017. Remote intelligent geotechnical seabed surveys – technology emerging from the RIGSS JIP, *Society for Underwater Technology: Offshore Site Investigation and Geotechnics Committee*, *ed. Offshore Site Investigation and Geotechnics: Smarter Solutions for Future Offshore Developments: Proceedings of the 8th International Conference 12–14 September 2017.* Royal Geographical Society, London, UK: Volume 2. London: Society for Underwater Technology, 1214–1222.

Cone Penetration Testing 2018 – Hicks, Pisanò & Peuchen (Eds)
© 2018 Delft University of Technology, The Netherlands, ISBN 978-1-138-58449-5

Shallow depth characterisation and stress history assessment of an over-consolidated sand in Cuxhaven, Germany

V.S. Quinteros & T. Lunne
Norwegian Geotechnical Institute, NGI, Oslo, Norway

L. Krogh & R. Bøgelund-Pedersen
Ørsted Wind Power (formerly DONG Energy Wind Power), Copenhagen, Denmark

J. Brink Clausen
Geo, Copenhagen, Denmark

ABSTRACT: A comprehensive field campaign was carried out on an aged, dense, over-consolidated sand in Cuxhaven, Germany. CPTs along with a suite of additional in-situ tests, including DMTs, PLTs, shear wave velocity measurements (SDMT and MASW), nuclear densometer, manual drive-in cylinder, temperature, suction and volumetric water content testing were performed on a clean sand to a depth of about four meters. Aim of this field-testing program was to characterize *in-situ* a clean North-Sea sand and by doing so overcome calibration chamber effects (like reconstitution, ageing, and imposed boundary conditions). The field campaign forms part of an effort for the determination of *in-situ* stress history as well as engineering strength and stiffness properties within the 'low' stress regime (< 50 kPa vertical effective stresses). Details of the field results together with an assessment of OCR and K_0 values are introductory presented in this paper. The background of this study is the soil characterisation at 'shallow depths' for subsea structures such as suction buckets, cables, pipelines, satellites and light gravity base structures.

1 INTRODUCTION

Interpretation of CPT results on dense-very dense marine sands at shallow depths in terms of relative density, D_r, is commonly done using either empirical or semi-empirical methods developed based on calibration chamber testing, CC, and/or centrifuge tests involving measurements on freshly reconstituted sand. Hence, some important features like layering, fabric, ageing, cementation, bonding and over-consolidation, OC, effects resulting from glaciation and potential wave loading cannot be replicated in the laboratory. Obviously, CPT profiles obtained in CC may differ significantly from field CPT profiles.

In order to overcome the issues of analysing CPTs from laboratory testing conditions, and with the long-term purpose of creating a field database of shallow CPTs on over-consolidated dense sands, Ørsted Wind Power, Geo and NGI joined efforts to characterise the upper sand layer of a research site in Cuxhaven, Germany. The site was chosen because of its relatively homogeneous sand unit of dense over-consolidated state, and since the deposition conditions resemble offshore sands around the North Sea. The characterization of Cuxhaven sand is part of an R&D project with the aim of developing a framework for interpretation of OCR, K_0 and ultimately relative density, strength and stiffness properties of over-consolidated marine sands.

2 THE SITE

2.1 *Description and general location*

The test field is located around 5 km south of Cuxhaven, Germany, approximately 6 km east of the North Sea coast (see Fig. 1). The test site is part of a sand/gravel pit, which is owned by Plambeck Erd- und Tiefbau GmbH. The pit started operations in1980 and soil has been excavated from the area since then. Approximately 16 m to 20 m of sand has been excavated at site within the last ca. 35 years. The exact overburden height is uncertain, but based on the information provided by Plambeck, about 18 m can be assumed as representative. Moreover, the Cuxhaven test field has also been used for research studies related to monopile installations and thus, several monopiles of 4.3 m diameter and 21 m buried length placed with 26 m distance in between (see Fig. 2) are located in the vicinity of the testing area. The specific field location chosen for testing is expected to be influenced

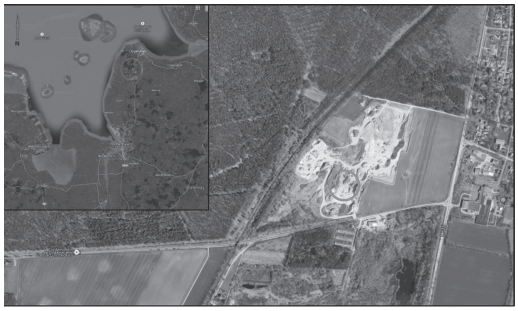

Figure 1. Location of Cuxhaven research site (google\ maps).

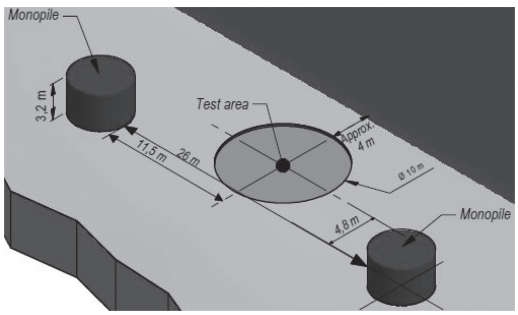

Figure 2. Schematic overview of field tests locations.

by the monopile installations to a minor degree. An adjacent 7 m high embankment lies approximately 4 meters west of the testing area. Testing near the embankment was avoided. As seen in Figure 2, the testing area tested was circular with a diameter of 10 m. Several tests were carried out, including: CPTs, dilatometer tests, DMTs, seismic dilatometer, SDMTs, plate load tests, PLTs, nuclear densometer, ND, manual drive-in cylinder density tests, MD, as well as sampling, suction, volumetric water content and temperature. Multichannel analysis of surface waves, MASW, were performed right outside the circular testing area. The upper soil at the site is characterized by a 4.7 m thick marine fine to medium sand, overlying clay. The ground water table, GWT, was measured at 3.1 m.

2.2 *Depositional environment and material source*

Before the glaciations, thick layers of sands were deposited by ancient rivers in large parts of the North Sea area. During the earlier glaciations (Saale and Elster) the area closest to present day shore line was ice-covered, whereas in the latest glaciation thick fluvial or deltaic sediments were deposited in a cold environment without vegetation. Deposition, erosion and re-deposition during the glaciations sorted and packed the sediments but also contributed with silt and clay sediments. Deltaic deposits formed along the ancient shorelines and fluvial deposits continued in braided streams with numerous channels. The different cycles of sand deposits are difficult to distinguish when looking at isolated samples.

The clean upper sand unit of Cuxhaven was observed in the field to be homogeneous (similar grain size), but the unit weight of the layers varied significantly. This variation is believed to be a consequence of the depositional environment and impact of wave loading.

3 FIELD TESTING PROGRAM

3.1 *Overview of results*

A summary of the field tests performed are given in Table 1, together with information about the number of tests and respective depths. During testing, the site was carefully dug in 0.5 m intervals using an excavator for the first 0.4 m, whereas the remaining 0.1 m was cautiously manually excavated. Measurements were carried out at each excavated depth, on a levelled surface, to obtain a dissected profile of index parameters.

3.2 *Excavation log*

Shallow surface stratigraphy of the site, measurements of water content, wc, unit weight,γ, and dry unit weight, γ_d, are presented in Figure 3. As seen in Figure 3a, the sand thickness is about 4.7 m, and GWT lies at about 3.1 m depth and the zone saturated by capillarity (above GWT) was about 0.3 m.

Table 1. Summary of field tests in Cuxhaven sand.

Test type	No.	Depth (m)
CPT*	7	0 to 5.5
DMT†	2	0 to 5.5
SDMT‡	2	0 to 5.5, V_s from 1 to 5
MASW§	4	0 (from the surface)
Plate load test (PLT)	5	0; 0.5; 1; 2; 3
Nuclear densom. (ND)	34	0; 0.5; 1; 1.5; 2; 2.5; 3; 3.5; 3.67
Manual densom. (MD)	40	0; 0.5; 1; 1.5; 2; 2.5; 3; 3.5; 3.67
Sampling (–)	6	0; 0.5; 1; 1.5; 2; 2.5; 3; 3.5; 4
Temperature (t)	5	0; 0.5; 1; 2; 3
Suction (ψ)	5	0; 0.5; 1; 2; 3
Vol. water content (θ)	5	0; 0.5; 1; 2; 3

* Cone Penetration Test, † Dilatometer, ‡ Seismic Dilatometer, § Multichannel Analysis of Surface Waves.

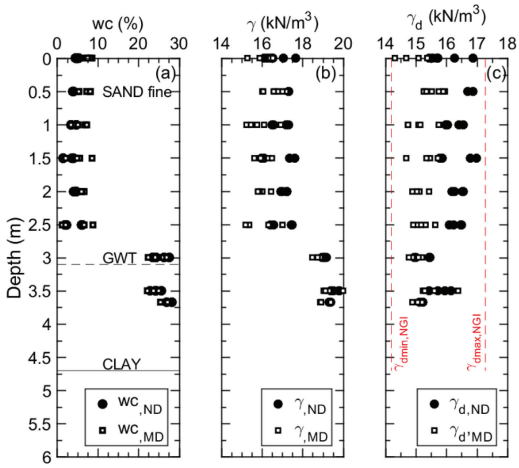

Figure 3. Excavation log: (a) stratigraphy, (b) water content, (c) unit weight, and (d) dry unit weight.

Water content was determined from samples sent to the NGI laboratory in Oslo, Norway, while values of γ and γ_d were obtained manually, with great care, using the drive-in cylinder technique, MD, and nuclear densometer, ND. MD measurements were performed using cylinders of 70.4 mm diameter and two different heights, namely 50 mm and 100 mm, following ASTM D-2937-10 recommendations. Significant scatter of results was observed during MD tests despite the great care exerted during sampling. ND measurements were done in parallel using a calibrated nuclear density gauge (model Troxler 3440). Measurements were complying with ASTM D-2922, using the 'direct transmission mode' by inserting the nuclear source into the ground. Less scatter of ND results was observed. Given the fact, that MD measurements are more susceptible to errors (dilation or contraction of sand while pushing the cylinder) and systematically lower than the ND measurements, they are considered less trustworthy.

Decagon 5TM soil moisture and temperature probes were used to estimate the volumetric water content, θ, which was about 0.1 m^3/m^3 from 0 m to 2 m depth and 0.2 m^3/m^3 at 3.0 m depth. Suction was measured using MP-6 calibrated ceramic disks. A suction of about 10 ± 2 kPa was measured.

4 OVERVIEW OF TEST RESULTS

4.1 *CPT results*

CPT tests were performed using Geo's CPT-truck and a standard AP van den Berg 10 cm^2 cone. Profiles of cone resistance, q_c, sleeve friction, f_s, and pore water pressure, u_2, vary considerable with depth inferring layering within the sand unit (see Fig. 4). Scatter of the CPT measurements was observed within the relatively small circular testing area of 10 m. A distinctive "S" shape of u_2 is observed in Figure 4c, which is attributed to the unsaturated soil conditions as well as uncertainties while measuring small values of u_2. Two dissipation tests were performed at about 4 m depth, the results verified GWT level.

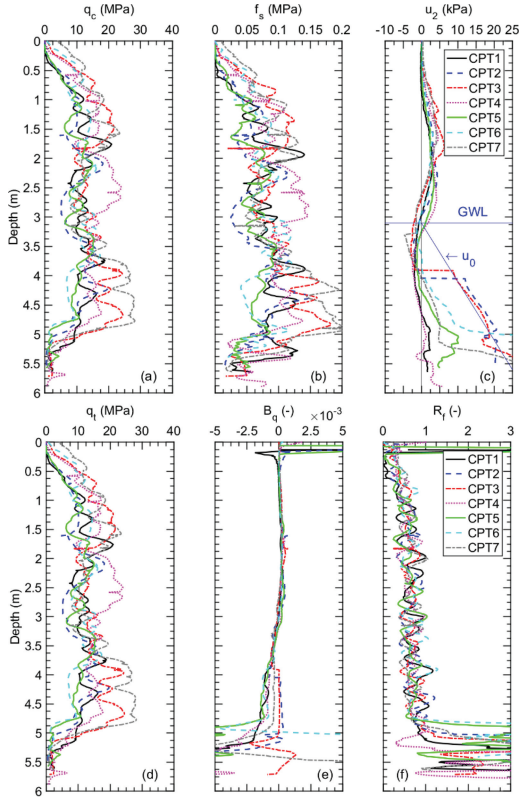

Figure 4. CPT: (a) q_c, (b) f_s, (c) u_2, (d) q_t, (e) B_q, (f) R_f.

For Cuxhaven sand, q_c reached its full value (also called quasi stationary value q_{st}), at about 0.7 m (see Fig. 4a) indicating the sand being OC, since NC sand usually reaches q_{st} much deeper at values of > 1.0 m, depending on sand density and its characteristics. As seen in Figure 4d q_t is equal to q_c, as expected for a clean sand. R_f shown in Figure 4e is 0.5, in average for the entire sand layer, though significant scatter is observed due to soil layering. B_q, shown in Figure 4f, is almost constant in the unsaturated zone above GWL, with small variations as expected from the u_2 measurements. B_q values decrease as soon as the CPT reaches ground water.

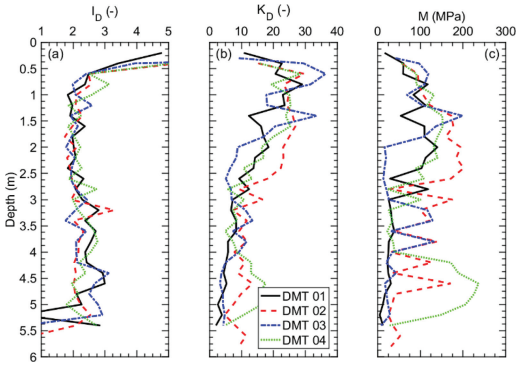

Figure 5. DMT: (a) I_D, (b) K_D, and (c) M.

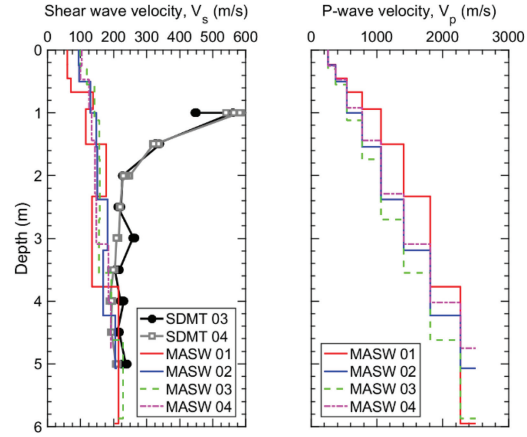

Figure 6. (a) V_s from SDMT and MASW, (b) V_p from MASW.

4.2 *DMT results*

DMT tests were performed following ASTM D6635–01 (2007) procedures. Results are presented in terms of Material index, I_D, Horizontal stress index, K_D, and Dilatometer modulus, M, (see Fig. 5). Almost constant I_D values were obtained from 0.5 m to ca. 4.7 m depth. However, K_D and E_D results were affected by soil layering, especially because these parameters are not normalized as I_D.

4.3 *Shear and P-wave velocities*

Shear wave velocities, V_s, were obtained using SDMT and MASW equipment. Two test pairs were performed on top of each other, while two additional MASW were performed outside the tested perimeter. The SDMT probe consisted of two sensors spaced 0.5 m, and a falling hammer system with a wooden beam mounted on the CPT truck was used to generate shear waves. The beam and the SDMT probe distance was 0.95 m. The hammer weight was 18.8 kg and four falling heights, namely 40, 80, 160 and 360 mm, were used to determine the energy giving the best signal. Results are given in Figure 6a. From MASW readings, V_s and P-wave velocities, V_p, were derived (see Figs. 6a and 6b).

High resolution 1D MASW were performed using a 24 channel Geode digital seismograph, 48 no. 10HZ vertical geophones. Details of the MASW technique are found in Park et al. 1999. Data processing was performed using NGI *in-house* software.

V_s values from SDMT are deemed unreliable at depths between 0 m to ca. 3.5 m depth, even though a geometrical depth correction was applied. Hence, $V_{s,MASW}$ values were considered more credible than $V_{s,SDMT}$. Note though that $V_{s,SDMT}$ and $V_{s,MASW}$ cannot be directly compared since they differ in terms of travel path and polarisation. $V_{s,SDMT}$ is an invasive method where the tool is deployed in downhole mode, and $V_{s,MASW}$ is non-invasive surficial method.

4.4 *PLT results*

Plate loading tests, PLTs, were performed at the same location at meter-intervals using a 0.3 m diameter plate. Figure 7 shows the average load measured, P, relative to plate settlement. The ultimate bearing capacity, P_{ult}, varied between 35 kN and 70 kN. At first glance, the variation of P_{ult} seems to be quite high, but the variation is reasonable given the layering of the soil. P_{ult} compares quite well with the corresponding distributions of q_c and K_D from CPT and DMT respectively. Nevertheless, note that P_{ult} at 3 m depth was affected by the GWL and a lower P_{ult} value was expected.

4.5 *Material composition and index tests*

Grain size distribution curves, GSD, were determined at each excavated depth (see Fig. 8). Because of the homogeneity of the GSDs, the sand was mixed to a batch. Hence, almost all index and advanced tests (except wc) were performed on the batched sand. Results of triaxial testing are presented in Quinteros et al. (2017). Values of d_{10} and d_{60} are given in Figure 8; C_U and C_C are 2.3 and 1.1 respectively. The fines content was less than 3%. Unit weight of solid particles, γ_s, is 26.2 kN/m^3. Maximum and minimum dry unit weights, $\gamma_{d,max}$ = 17.27 kN/m^3 and $\gamma_{d,min}$ = 14.19 kN/m^3, were obtained using NGI *in-house* methods.

A scanning electro-micrograph, SEM, is shown also in Figure 8. From the SEM, particle roundness, R = 0.75, sphericity, S = 0.90, and regularity,

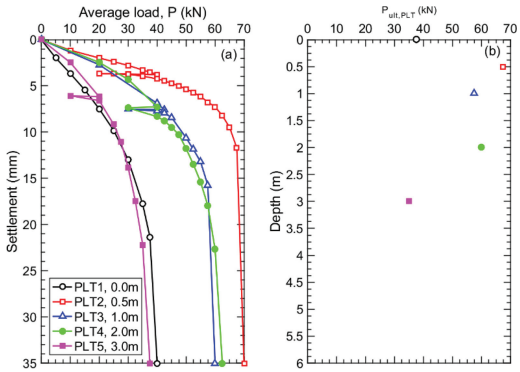

Figure 7. PLT: (a) Load vs. settlements, (b) P_{ult} vs. depth.

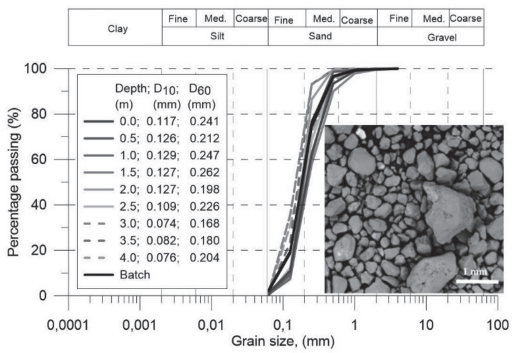

Figure 8. GSDs and SEM image of Cuxhaven sand.

ρ = 0.82, were obtained. Grains angularity was determined on a selected 500 g batched sample resulting in 0.4% angular, 12.4% sub-angular, 59.6% sub-rounded, 26.4% rounded and 1.2% rounded particles. Mineralogy of grains was assessed using the X-ray diffraction method, XRD. The main minerals being quartz (93%), alkali-feldspar (4%) and plagioclase (3%).

5 ASSESSMENT OF STRESS HISTORY

5.1 *Estimation of OCR*

The mechanically over-consolidation ratio, OCR, is defined as the maximum past effective consolidation stress, σ'_p, over the present effective overburden stress, σ'_{vo}, as:

$$OCR = \sigma'_p / \sigma'_{vo} \quad (1)$$

As discussed in Chapter 2, the Cuxhaven site has been excavated by around 18 m ± 2 m. Hence OCR can be calculated using Equation 1 (see Fig. 9).

Mayne et al. (2009) presented a so-called unified-approach, for a first-order estimation of the yield stress from CPT results:

$$\sigma'_p = 0.33\,(q_t - \sigma_{vo})^{m'} \quad (2)$$

where q_t = corrected cone resistance ($q_t = q_c + u_2(1 - a)$) in kPa, σ_{vo} = vertical total stress in kPa, and m' is a fitting exponent ($m' \approx 0.72$ for clean quartz to silica sand).

Using Equations 1 and 2, OCR profiles were estimated reasonably well from CPT results (see Fig. 9a).

Monaco et al. (2014) proposed a multi-parameter approach in terms of the empirical equation for homogeneous soils:

$$OCR = 0.0344\,(M_{DMT}/q_c)^2 - 0.4174\,(M_{DMT}/q_c) + 2.2914 \quad (3)$$

Figure 9b shows calculated OCR profiles using Equation 3 from combined close-by CPTs and DMTs. Note that Equation 3 does not predict OCR from CPT-DMT at shallow depths. OCR estimation based on DMT alone (Marchetti, 1980) was also tried, but unreliable estimates were obtained here as well.

5.2 *Estimation of K_0*

The coefficient of lateral earth pressure at rest is defined as the ratio of effective horizontal stress over the effective vertical stress, $K_0 = \sigma'_{h0}/\sigma'_{vo}$. Typical values of K_0 reported in the literature are 0.4 for loose and 0.6 for dense NC sands. For wave-densified OC sands a constant $K_0 = 1$ is often assumed. Jaky (1944) proposed the well-known formula

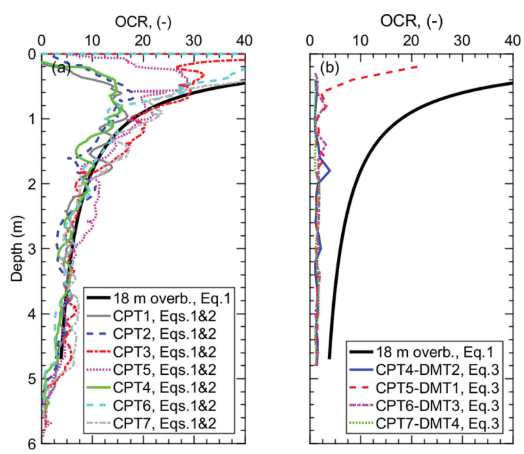

Figure 9. OCR based on: (a) CPT after Mayne et al. (2009), and (b) CPT-DMT after Monaco et al. (2014).

$K_0 = (1 - \sin\phi')$. Wroth (1973) stated that K_0 of OC sand is higher than K_0 of NC sand; hence, reflecting the effect of OCR on K_0, Kulhawy & Mayne (1990) proposed an equation based on the effective friction angle of soil ϕ' and OCR:

$$K_0 = (1 - \sin\phi')\cdot(OCR)^{\sin\phi'} \quad (4)$$

Using Equation 4, K_0 was estimated using $\phi'_{cv} \approx 32°$ (from triaxial tests) as recommended by Lee et al. (2013) for dense sands, while OCR was obtained from Equation 1, see Figure 10. As seen in this figure, K_0 changes significantly with depth and is obviously not constant as often assumed in practice. Hence, standard K_0 equations (derived for clayey soils) seem to be applicable for estimating K_0 in the case of the unloaded OC Cuxhaven sand site. In Figure 10a, K_0 is calculated using Equations 4, 1 and 2 for CPT tests.

A CPT-DMT multi-parameter approach, as proposed by Marchetti (1985), was also used to estimate K_0, namely:

$$K_0 = 0.376 + 0.095\, K_D - D_3 \cdot (q_c/\sigma'_v) \quad (5)$$

where: D_3 = fitting parameter equal to 0.0017 for CC data, 0.0046 for Po river sand, or 0.005 for seasoned sand and 0.002 for freshly deposited sand after Baldi et al. (1986). Given the range of possible values of D_3, the multi-parameter approach will return rough estimations of K_0 only. For Cuxhaven sand D_3 = 0.005 was used. Figure 10b shows the K_0 assessment based also on CPT-DMT Equation 5. As seen in this figure, the multi-parameter approach seems to follow the theoretical K_0 calculated after Kulhawy & Mayne (1990) as per Equation 4, but significant scatter is observed.

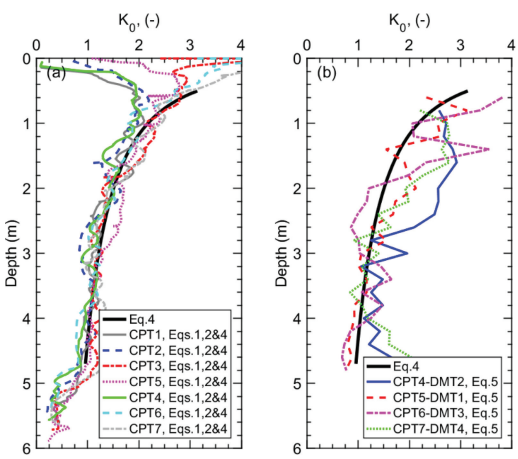

Figure 10. Assessment of K_0 from CPT after Kulhawy & Mayne (1990) and from CPT-DMT after Marchetti (1985).

6 CONCLUSIONS

A comprehensive site characterization program carried out on Cuxhaven sand has been presented. The clean, quartzitic, aged, dense sand of Cuxhaven is a typical North Sea sand. Aim of the field campaign was to obtain data from a natural OC sand in contrast to calibration chamber test results on freshly deposited sand. This research is part of an overall study to develop appropriate correlations for estimating OCR, K_0 and ultimately D_r in an OC sand at shallow depths. Based on the field results and subsequent site stress history assessment, the following initial conclusions were drawn:

- Nuclear density measurements of unit weights are higher than manual density measurements using the drive-in cylinders. Large scatter is related to the results in spite of the great care exerted during sampling with drive-in cylinders.
- From CPT, DMT and PLT results significant variability is observed as a result of the geological depositional history of the site. However, the sand unit is quite homogeneous in terms of grain sizes.
- CPT gives a more detailed profile than DMT. However, due to the rate of change of q_c, local peaks of q_c may be underestimated, since q_c may not be fully developed to a quasi-stationary value.
- V_s results from SCPT are unreliable at shallow depths (< 3.5 m). Hence, MASW is considered to give more realistic results at shallow depths.
- OCR was reasonably estimated from CPT readings using Mayne et al. (2009) method. While the multi-parameter approach (CPT-DMT combined) as proposed by Monaco et al. (2014) did not provide reliable estimations at shallow depth.
- K_0 was estimated using Kulhawy & Mayne (1990) approach as well as the multi-parameter approach after Marchetti (1985). Both methods returned similar results.

ACKNOWLEDGEMENTS

The research presented herein was performed as a Joint Industry Project carried out between: Ørsted Wind Power, Geo and NGI. The efforts of all parties are highly appreciated. The support of other involved companies during the fieldwork, such as GEO-Engineering, Plambeck Gmbh and Apex Geoservices is gratefully acknowledged.

REFERENCES

ASTM D2922–05. 2005. Standard Test Methods for Density of Soil and Soil-Aggregate in Place by Nuclear Methods (Shallow Depth). *ASTM International*. West Conshohocken, PA.

ASTM D2937–10. 2010. Standard Test Method for Density of Soil in Place by the Drive-Cylinder Method. *ASTM International*. West Conshohocken, PA.

ASTM D6635–01. 2007. Standard Test Method for Performing the Flat Plate Dilatometer. *ASTM International*. West Conshohocken, PA.

Baldi, G., Bellotti, R., Ghionna, V., Jamiolkowski, M., & Pasqualini, E. 1986. Interpretation of CPTs and CPTUs; 2nd part: drained penetration of sands. *Proc. 4th Int. Geotech. Seminar*, Singapore, pp 143–156.

Jaky, J. 1944. The coefficient of earth pressure at rest. In Hungarian (A nyugalmi nyomas tenyezoje). *Journal of the Society of Hungarian Architects and Engineering*, 355–358.

Kulhawy, F.H. & Mayne, P.W. 1990. Manual on estimating soil properties for foundation design. Report EPRI EL-6800, *Electric Power Research Institute*, Palo Alto, 306 p.

Marchetti, S. 1985. On the Field Determination of K_0 in Sand. *Proc. 11th Int. Conf. Soil Mech. Found. Eng.* S. Francisco, Vol. 5: 2667–2672.

Mayne, P.W., Coop, M.R., Springman, S., Huang, A-B., & Zornberg, J. 2009. State-of-the-Art Paper (SOA-1): GeoMaterial Behavior and Testing. *Proc. 17th Intl. Conf. Soil Mech. Geotech. Eng.*, Vol. 4. Alexandria, Egypt, Millpress/IOS Press Rotterdam: 2777–2872.

Monaco P.; Amoroso S.; Marchetti S.; Marchetti D.; Totani. G. Cola, S. & Simonini, P. 2014. Overconsolidation and Stiffness of Venice Lagoon Sands and Silts from SDMT and CPTU. *J. Geotech. Geoenviron. Eng.* ASCE, v. 140:1, p. 215–227.

Lee, J., Park, D. Kyung, D. and Lee, D. 2013. Effect of Particle characteristics on K0 Behavior for Granular Materials. *Proc. 18th Int. Conf. Soil Mech. & Geotech. Eng.*, Paris 2013. pp 337–380.

Park, C.B., Miller, R.D., & Xia, J. 1999. Multi-channel analysis of surface waves (MASW): *Geophysics*, May-June issue.

Quinteros, V.S., Lunne, T., Dyvik, R., Krogh, L., Bøgelund-Pedersen, R., & Bøtker-Rasmussen, S. 2017. Influence of Pre-Shearing on the Drained Strength and Stiffness of a Marine North Sea Sand. *Proc. 8th Int. Offshore Site Invest. Geotech. Conf*. Sep. 12–14. London.

Wroth, C.P. 1973. General theories of earth pressure and deformation. *Proc. 5th Eur. Conf. Soil Mech. Found. Eng.* Vol. 2, Madrid, Spain, 33–52.

Taylor & Francis
Taylor & Francis Group
http://taylorandfrancis.com

Cone Penetration Testing 2018 – Hicks, Pisanò & Peuchen (Eds)
© 2018 Delft University of Technology, The Netherlands, ISBN 978-1-138-58449-5

Assessment of pile bearing capacity and load-settlement behavior, based on Cone Loading Test (CLT) results

Ph. Reiffsteck
IFSTTAR, Paris, France

H. van de Graaf
Lankelma, Oirschot, The Netherlands

C. Jacquard
Fondasol, Avignon, France

ABSTRACT: The Cone Loading Test (CLT) consists of stopping the static penetration at a desired level and carrying out a loading of the cone by successive steps. This test is carried out with a standard static penetrometer, equipped with some extra features. The test principle is that at selected depths an electric CPT cone tip is submitted to incremental loading while measuring the settlement of the cone. The test result is a load-displacement curve for both friction sleeve and cone tip. Considering that the cone of the penetrometer is like a reduced model pile, the CLT test is a suitable tool for foundation design. In this paper, a direct method is proposed for using the cone resistance and limit sleeve friction of the CLT test to calculate the bearing capacity and to predict the settlement of a pile at different loads. This paper presents a new approach for transforming a CLT-load-displacement curve into load-displacement curves of a pile (t-z curves). A direct and clear distinction of the bearing capacity of the pile tip and the pile shaft mobilized at different loads becomes possible.

1 PILE DESIGN

Determining the working load on a pile close to its real bearing capacity is still very difficult. In direct design method the bearing capacity R_c of a pile is computed from (CEN, 2005):

$$R_c = R_b + R_s \tag{1}$$

where:
R_b is the base resistance and
R_s the shaft resistance.

This separation of the pile capacity into two terms is a common feature of all the design methods used in practice: i.e. ϕ'–c', CPT, standard penetration test (SPT), Ménard pressuremeter test (MPT). The base and shaft resistance are computed from:

$$R_b = A_b \times q_b \tag{2}$$

$$R_s = \Sigma P_i \times h_i \times q_{s;i} \tag{3}$$

where:
A_b: pile base (+other details for open-ended piles, driven H piles, etc.);
q_b: base pressure;
h_i: width of the ground layer i;
P_i: pile perimeter in the ground layer i;
$q_{s;i}$: unit shaft friction in the ground layer i.

The tip capacity R_b is related to a mean value of the shear strength derived from these tests (in situ and lab) multiplied by a factor related to the failure mechanism and adjusted for the soil type and for the remoulding effect of the technique.

The shaft term R_s accounts for the change of soil properties in the vicinity of the pile after it has been installed, for the soil variability (vertically but not only) and for the (complex) pile-soil interaction. Figure 1 shows an example of the loading sequence of an instrumented pile. Hence, for every segment of the shaft, shaft resistance q_s has to be computed from the shear strength times a factor depending of the influences above.

The computation of the pile settlement is based on the notion of transfer functions of the t-z curves (laws establishing the relation between the

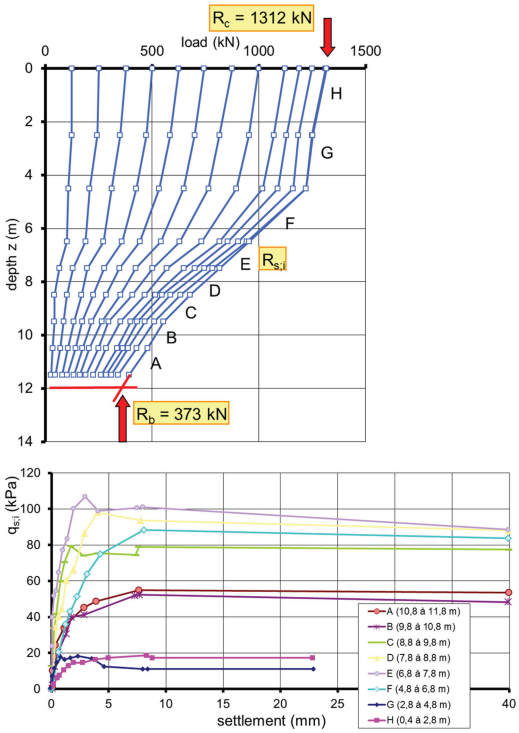

Figure 1. (a) Evolution of load in pile segments (b) Measured shaft friction (Merville, France).

lateral friction and the displacement of the pile on one hand, and on the other hand the stress and the displacement at toe level). The concept of transfer function was originally presented by Coyle and Reese (ASCE, 1966). Calculations are usually carried out in the strain range of 10^{-2} and 10^{-3}.

The most commonly used technique for defining these curves is the determination of curvatures from a compilation of pile load test results (NEN, 1991). An alternative method consists in defining the characteristic points of the curves from the parameters obtained from the determination of the bearing capacity resulting from semi-empirical methods related to in situ tests (AFNOR, 2012; Burlon et al., 2014).

2 CONE LOADING TEST

Attempts have been made by several authors to develop a test method using a penetrometer test, based on either the plate bearing test or static pile loading test procedures in order to reach a stress strain relationship (Haefeli and Fehlmann, 1957; Ladanyi, 1976; Sanglerat, 1974). Reiffsteck et al. (2009) proposed a procedure which may lead to improvement of direct design method. This test, called Cone Loading Test (CLT), can be carried out during a Cone Penetration Test (CPT) as a complementary, fast and economic test.

After a several zero measurements performed with the rods unclamped, the cone tip is loaded by a minimum of ten successive steps each lasting 60 seconds. An alternative way is a constant very slow speed until the cone resistance of the soil is reached (Faugeras et al, 1983; Arbaoui et al., 2006; Reiffsteck et al., 2009). The stress-settlement curve relates the pressure applied on the cone to the settlement of the top of the push rods at the end of each loading stage (Figure 2). The curves consist of a linear part at small strain level, then a curved part at the onset of plasticity and a linear part at higher strain level.

This test can be performed with a standardized electrical cone penetrometer (CEN/ISO, 2005). Moreover accurate displacement of rods and push force must be measured. When a piezocone is used, both increase of pore pressure and shear resistance on the friction sleeve are measured.

The cone loading test requires several corrections, resulting from the push rods compression effect or from the initial conditions of the test. Comparison of correction methods of the measured displacement shows that the use of a friction reducer imposes a accurate measurement of the thrust force applied at the top of the rods (Q_t). Generally a 15 cm^2 cone is used. This minimizes the friction on the 10 cm^2 string of rods. Reliable correction is to estimate a mean friction value obtained from the difference between the force measured at the top and at the cone level (Ali et al., 2008). At shallow depth deviation of rods is neglected but if deeper tests are planned use of inclinometer is suggested (CEN/ISO, 2005). Figure 3 shows two examples of CPT profiles obtained on sites listed in Table 1 were CLT have been performed at several depths. Although loading tests were carried out at different depths (approximately every 1.5 m) no disturbance of the CPT profiles due to CLT tests was observed.

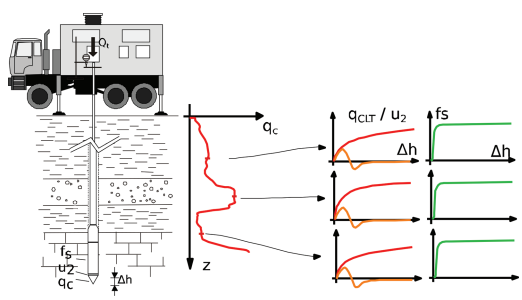

Figure 2. Cone loading test principles (Reiffsteck et al., 2009).

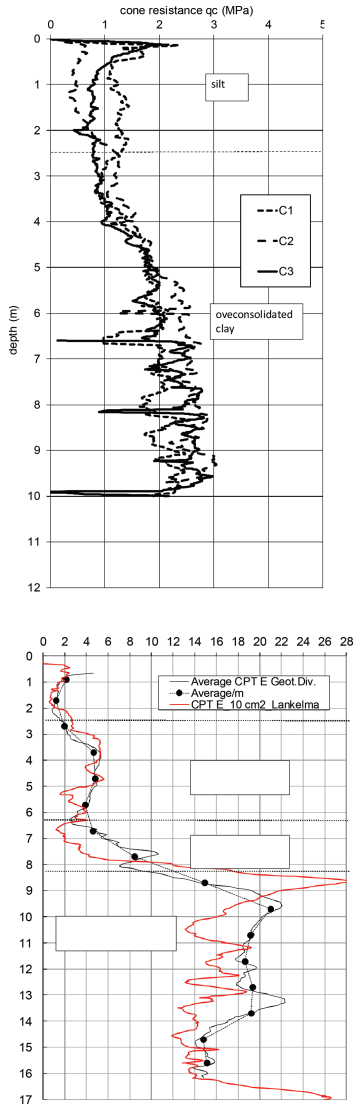

Figure 3. CPT tests profiles for (a) Merville, France and (b) Limelette (Belgium).

3 CONE LOADING TEST DIRECT DESIGN METHOD

Considering that the cone penetrometer is a reduced pile model, and that the deformation of the soil around a cone gives effects similar to the soil deformation observed around a full-scale pile during loading, then, the cone loading test curves reflect the interaction between a slim pile and the surrounding soil. A very useful and interesting consequence of this statement is the potential of the cone loading test to be a foundations design tool. As in a pile loading test, during a cone loading test, the applied cone pressure is recorded according to displacement in each loading stage. In the same manner, the curve of sleeve friction mobilization law can be drawn as shown on Figures 4 and 5.

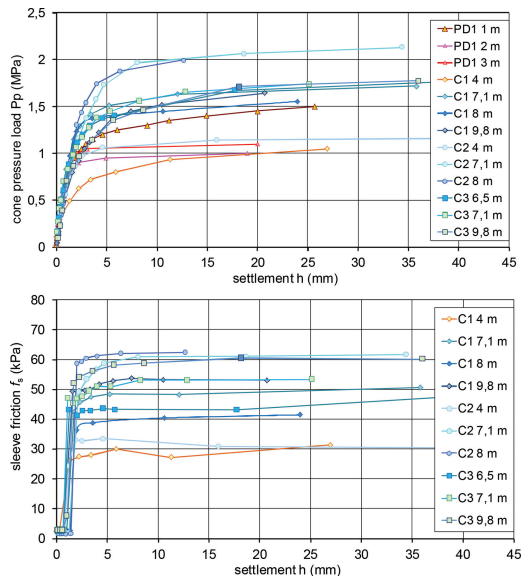

Figure 4. (a) cone loading tests curves (b) Measured sleeve friction in clay (Merville, France).

Table 1. Test sites where CPT and CLT test have been performed.

Location	Country	Soil profile	Depth	Cone type	Driving unit
Jossigny	France	Plateau silt	3	Mech.	Lw DPT
Orleans	France	sand	4	Mech.	Lw DPT
Merville	France	Ypresian clay	4/9.8	Mech.-piezocone	Lw DPT/Crawler
Choisy-au-bac	France	Silty sand/chalk	12	Piezocone	Crawler
Oirshot	Netherland	clay	8	Piezocone	Crawler
Limelette	Belgium	Silt/sand	18	Piezocone	Crawler
StMichielsgestel	Netherland	sand	13	Piezocone	Crawler
Les Moulineaux	France	Sandy soil/chalk	23	Piezocone	Truck

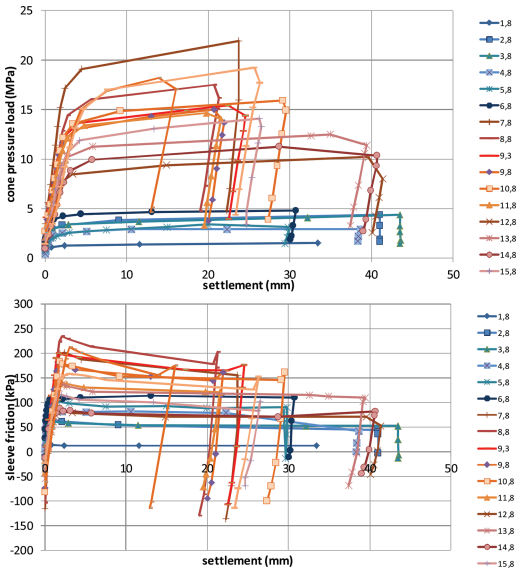

Figure 5. (a) cone loading tests curves (b) Measured sleeve friction in sand (Limelette, Belgium).

Values of the measured force acting on the friction sleeve divided by the area of the sleeve can be identified to the unit skin friction resistance q_s determined during a pile loading test with extensometer or vibrating wire transducers (Figure 1).

Then in the general case of a layered ground for which the distribution of penetrometer limit cone resistance q_{CLT} with depth are known, each term of equation 1 will be computed from the following equations:

$$R_b = [q_o + k_p \times (q_{CLT})] \times \pi \times B^2/4 \quad (4)$$

$$R_s = \Sigma_i^n k_s \times f_s \times \pi \times B \times l_i \quad (5)$$

where:

q_o is the total vertical pressure,
k_p is the bearing factor,
k_s is the pile soil interaction factor,
B is the diameter of the pile,
f_s is the limit unit shaft friction of the ith layer,
l_i the thickness of the ith layer.
q_{CLT} the limit cone resistance obtained near the tip of the pile.

The comparison and the correlation between the mobilization curve obtained from the cone loading test and that of the static pile loading test, for the same site and same ground type, give access to influence factors. However, there are some factors which depend on the size and geometry of the tip used in the cone loading test (in order to limit the friction and thus limit the corrections on the measurement a 15 cm^2 cone is used), as well as the friction sleeve influence (steel used for friction sleeve is particularly smooth compared to some piles shafts). It must be noted that values derived from CLT test differ drastically from the one used for example in the very interesting keynote of De Cock (2008).

As a matter of fact, it is necessary to integrate a correction factor which takes account of the scale factor between the friction sleeve and the pile shaft k_s and cone and pile tip k_p. The ratio of the estimated load mobilized by the shaft and the pile tip is very close to the ratio observed on the tests collected during this work. As a result, no particular factor was applied. However, the predicted total load remains less than the total bearing capacity observed. A model factor equal to 2 has to be applied to correct the calculated values.

Figure 7a shows a regression curve obtained for 20 piles in various soils (clay, silt, sand and chalk) and of different kind (screw, bored, driven piles). The pile-soil interaction factor is given by NF P94-262 standard (AFNOR, 2012; Burlon et al., 2014). A good prediction is observed with a mean value close to unity at 50% of the distribution curve. Further fitting of model factors is needed. It should be noted that usual French CPT direct design method used q_c and not f_s to derive the shaft friction.

4 DERIVING T-Z CURVES FROM CLT TESTS RESULTS

The goal of this research was to develop a method that would give a prediction of a complete load settlement curve for pile, based on the analysis of the friction mobilization curves (t-z curves) at different levels of the cone loading test. The approach consists of transforming the CLT sleeve friction and cone resistance curves representative of the soil along the shaft and below the tip into a settlement (or t-z) curve (Figure 6). To plot these curves, the forces (q_c and f_s) are normalized by their maximum observed value and the displacement h is normalized by the diameter of the cone. Then, exponential curves similar to those used in the NF P94-262 standard are calibrated on scattered plots (AFNOR, 2012; Burlon at al., 2014).The way this new method has been developed is very close to one described by Briaud for shallow foundations and also used in NEN6743 (Briaud, 2007; Larsson and Bengtsson, 2008; NEN, 1991).

The settlement at the top of the foundation w_{found} can be determined as a function of the pile load as the sum of the value of the settlement of the top of the pile w_{skin} and the settlement due to compression

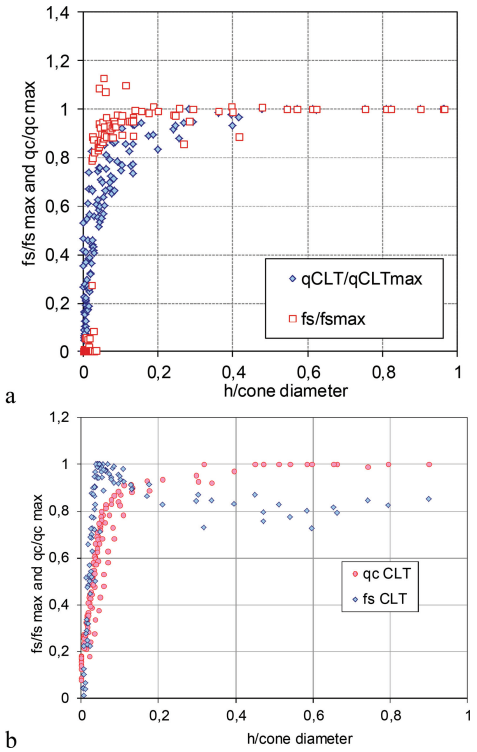

Figure 6. Normalized t-z curves for tip and shaft for (a) clay and (b) sand.

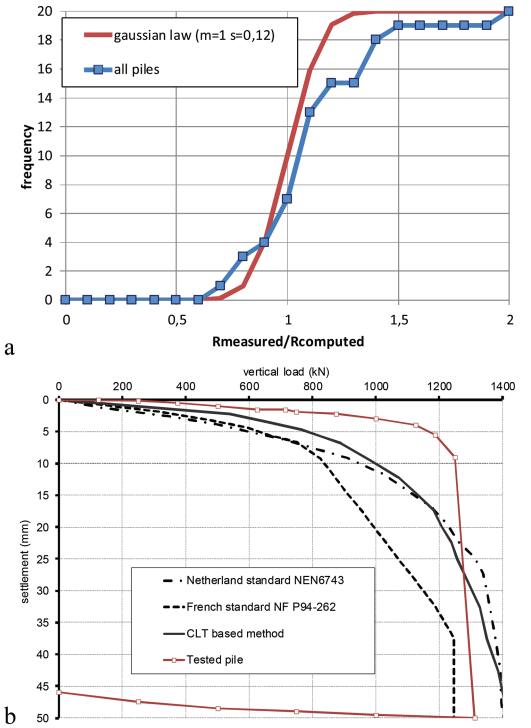

Figure 7. Bearing capacity and settlement prediction for 20 piles; example of predicted load settlement curve in clay (Merville).

of the soil layers situated below the pile tip level w_{tip}. The settlement of the top of the pile includes the settlement w_{el} relative to the pile point due to elasticity of the pile (elastic shortening).

$$w_{found} = w_{skin} + w_{tip} + w_{el} \quad (5)$$

where

- w_{tip} and w_{skin} are obtained from relative load settlement curve constructed with the average cone resistance and sleeve friction versus the relative settlement s/B,
- w_{el} is function of the assumed linear variation of the vertical effort in the pile (Figure 7b).

Figure 7b shows a comparison of the load settlement curve predicted with the CLT direct method obtained with a simple spreadsheet or the PIVER software, in comparison with the actual curve of the pile loading test.

The example given in Figure 7b corresponds to a pile with a depth of 12 m and a diameter of 0.5 m, drilled in the Flanders clay at Merville. The CLT dimensioning approach is fit well and gives a very similar result to the methods based on the results of Ménard pressuremeter and cone penetration tests on which French (Frank & Zhao method used in AFNOR, 2012) and Dutch (NEN, 1991) standards are based.

5 CONCLUSIONS

In the present paper a new direct design method based on the cone loading test is described, taking advantage of the intrinsic quality of the CPT test: reproducibility, precision and furthermore giving access to strength but also stiffness. Application to a database of 20 pile loading test results shows the quality of prediction of the bearing capacity and of the load settlement curves. Further research needs to include more case studies on different sites and soils: loam and sand to define the adapted rheological factors. This new design method offers high potential application to spread footing design. This is a new field of research to explore.

ACKNOWLEDGMENTS

The authors thank Fondasol, Lankelma Geotechniek Zuid, IFSTTAR, Blaise Pascal University of

Clermont-Ferrand for the support they were able to provide during this study.

REFERENCES

AFNOR (2012) Justification des ouvrages géotechniques, Normes d'application nationale de l'Eurocode 7, Fondations profondes, NF P94-262, 204 pages.

Ali H., Reiffsteck P., Bacconnet C., Gourves R., Baguelin F., Van De Graaf H. (2008) Facteurs d'influence de l'essai de chargement de pointe, *Journées Nationales de Géotechnique et de Géologie de l'Ingénieur*, Nantes, pp. 467–474.

Arbaoui H., Gourvès R., Bressolette Ph., Bodé L. (2006), Mesure de la déformabilité des sols in situ à l'aide d'un essai de chargement statique d'une pointe pénétrométrique, Can. Geotech. J. 43(4) 355–369.

Briaud J.-L., (2007), Spread Footings in Sand: Load Settlement Curve Approach, J. of Geotech. and Geoenv. Engrg, ASCE, 133(8) 805–920.

Burlon S., Frank R., Baguelin F., Habert J., Legrand S. (2014) Model factor for the bearing capacity of piles from pressuremeter test results—Eurocode 7 approach, Géotechnique, 64 (7), pp. 513–525.

CEN/ISO (2005) Geotechnical investigation and testing - Field testing—Part 1: Electrical cone and piezocone penetration tests, EN/ISO 22476-1, 41 p.

CEN (2005) Eurocode 7: geotechnical design - Part 1: general rules NF EN 1997-1, 175 p.

Coyle H M,Reese L C. (1966) Load transfer for axially loaded piles in clay. Journal of Soil Mechanics and Foundations Division, 92(Suppl 2): 1—26.

De Cock F.A., (2008), Sense and sensitivity of pile load-deformation behaviour. BAP V: *5th Int. Symp. on Deep Foundations on Bored and Auger Piles*, pp. 23–46.

Faugeras, J.C., Fortuna, G., Gourvès, R., (1983). Mesure de la compressibilité des sols à l'aide du pénétromètre statique. *Int. Symp. In situ testing*, Paris, 2: 269–274.

Haefeli R., Fehlmann H.B. (1957) Measurement of soil compressibility in situ by means of the model pile test, Proc. 4th *Int. Conf. SMFE*, London, (1) 225–230.

Ladanyi B. (1976) Use of the static penetration tests in frozen soils, Canadian Geotechnical Journal, Vol. 13, No. 2, pp. 95–110.

Larsson, R., Bengtsson, P.-E. (2008) Field determination of stress-strain relations of clay till, *4th Int. Symp. on Def. Char. of Geomaterials (IS-Atlanta 2008)*, pp. 875–882.

NEN (1991). Calculation method for bearing capacity of pile foundation, compression pile, Dutch Standard NEN 6743, 31 p.

Reiffsteck Ph., (2009) ISP5 Pile Prediction Revisited, ASCE Geotechnical Special Publication N° 185, Contemporary topics in in situ testing, analysis and reliability of foundations, IFCEE Orlando, pp. 50–57.

Reiffsteck Ph., Bacconnet C., Gourvès R., van de Graaf H.C., Thorel L. (2009) Measurements of soil compressibility by means of cone penetrometer, Soils and Foundations, 49(3) 397–408.

Sanglerat G. (1974) The state of the Art in France, *ESOPT*, Stockholm, pp. 47–58.

Cone Penetration Testing 2018 – Hicks, Pisanò & Peuchen (Eds)
© 2018 Delft University of Technology, The Netherlands, ISBN 978-1-138-58449-5

CPT based settlement prediction of shallow footings on granular soils

J. Rindertsma & W.J. Karreman
Van Oord Dredging and Marine Contractors, Rotterdam, The Netherlands

S.P.J. Engels
Arcadis Nederland BV, Arnhem, The Netherlands

K.G. Gavin
Delft University of Technology, Delft, The Netherlands

ABSTRACT: Van Oord DMC executed a large land reclamation project, where requirements had to be met concerning the settlement of shallow foundations to be placed on the sand fill. CPT based settlement predictions performed in the design phase had to be verified with zone load testing. After completing the project, all measurement data were analysed to gain insight into the accuracy of existing correlations between CPT data and settlement of a sand fill. The correlations by De Beer & Martens (1957), Schmertmann (1978), Peck et al. (1996) and Robertson (1990) were considered. From the total number of zone load tests, 43 test were selected which allowed for comparison of the results with the predictions using the mentioned correlations. It was concluded that the CPT to stiffness correlation of Robertson combined with the analytical model of Schmertmann corresponds very well with the measurements, consistently showing only small deviations from the measured settlement.

1 INTRODUCTION

Large land reclamation projects commonly have requirements for the settlement of shallow foundations to be placed on the sand fill. The standard method of verification of these requirements for hydraulic fill is estimating the settlement using CPT's. Because of the large variation in the results of the existing correlations between foundation stiffness and cone resistance found in literature, it is often necessary to verify the quality of the predictions by means of costly zone load testing.

2 PROJECT DESCRIPTION

2.1 *General description*

Van Oord DMC have executed a large land reclamation project in Kuwait. Purpose of the project was to construct an approximately 12 km^2 sand platform to function as a foundation for future construction. The thickness of the platform was on average 4 m, with a maximum of 6.5 m. The platform was constructed partly on an existing layer of silty clay (sabkha) and partly on existing sandy deposits. One of the performance requirements for the platform was to limit the maximum settlement of shallow footings placed directly on the sand fill. To achieve this requirement, several techniques of ground improvement were executed: dynamic replacement of the existing sabkha and dynamic compaction complemented by high energy impact compaction of the fill material throughout the site. The dynamic replacement resulted in the creation of sand columns through the sabkha layer to the bearing strata below. The purpose of these columns, with the reclamation as load spreading platform, was to limit the deformations of the sabkha layer by transferring the majority of the reclamation and future foundations loads to the bearing strata.

2.2 *Ground improvement quality control*

One of the quality control methods for the ground improvement works was the execution of CPT's. The site was divided into large sub-areas, which in turn where subdivided in control boxes of 50 m by 50 m. In each of these control boxes CPT's were performed. The purpose of the CPT's was to identify the control boxes with the largest expected settlement under the design foundation load. In those boxes zone load tests (ZLT's) where then performed to verify that the actual foundation settlement would not exceed the required maximum value.

To determine the locations for the ZLT's, the CPT to soil stiffness correlation according to Rob-

ertson (1990) combined with the settlement prediction method of Schmertmann et al. (1978) was applied. Using this method the settlement of the shallow footing was predicted for each control box and used as a basis for selecting the ZLT location for each sub-area. Due to the size of the site thousands of CPT's and dozens of ZLT's were executed over the course of the project providing a large amount of data.

The ground water level at the site was elevated due to the hydraulic filling method. The phreatic water level at the moment of executing the CPT's and ZLT's was typically 1 m to 2 m below the surface level of the fill.

2.3 *Fill material*

A limited amount of particle size distribution tests was performed at the fill area. The sand of the fill is coarse to very coarse (average D50 of 0.40 mm), poorly graded and contains a fine content of approximately 3% after placement. Field density tests showed that the material of the top layer was compacted to a dry density of on average 1720 mT/m^3, a relative density D_r of 75% to 80% (relative compaction 95.5%).

Several other parameters of the fill material used for the construction of the platform were investigated. In Figure 1 a soil behaviour types (SBTn) chart (Robertson 1990) shows the distribution of the individual CPT measurement of normalized cone resistance and sleeve friction.

As is common in the Middle-East, the fill material consists partly of calcareous sand. The carbonate content of the material was investigated and found to vary over the site. On average a carbonate content of 20% was found. At specific locations it was measured to be 70% to 80%. The sandy material in the original ground profile of the site is not calcareous. The carbonate content is of importance for the analyses as the results of high stress testing methods like cone penetration testing are influenced by crushing of the particles.

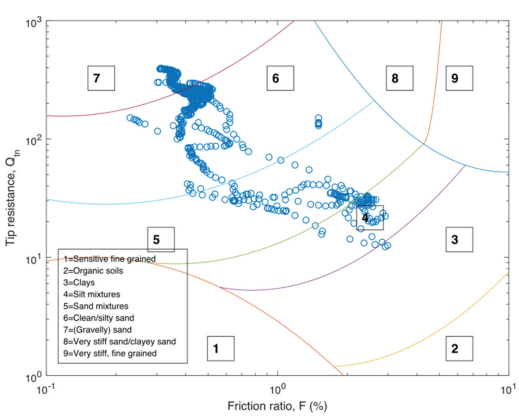

Figure 1. SBTn chart ZLT DD145.

3 CPT BASED SETTLEMENT PREDICTION

Execution of CPT's is a cost effective way to gather information on the present soil type and behaviour. Besides a good insight into the strength of the soil, CPT results also give indications of the material stiffness. For granular soils, various analytical and empirical correlations exist between CPT measurements, stiffness properties and the expected settlement of a shallow foundation on the soil. A selection of these correlations is mentioned below.

3.1 *Analytical and empirical models*

De Beer & Martens (1957) developed an expression to predict settlement of a shallow footing based on the stress increase due to loading and the stiffness of distinguished soil layers based on a linear relation with the cone resistance. The method was intended to provide a safe upper limit of the expected settlement. Equations (1) and (2) were derived.

$$s = 2.3 \cdot \frac{H}{C} \cdot \log_{10}\left(\frac{\sigma'_0 + \Delta\sigma}{\sigma'_0}\right) \tag{1}$$

$$C = 1.5 \cdot \frac{q_c}{\sigma'_0} \tag{2}$$

where s = settlement; H = thickness of the layer considered; C = compressibility coefficient; s'_0 = effective vertical stress at considered depth; Δs = pressure increase due to loading; and q_c = cone resistance.

The improved Schmertmann (1978) method uses the strain influence factor I_z, which can be derived from the strain influence diagram and depends on the geometry of the footing. The stiffness of the soil is modelled using the secant Young's modulus, obtained from a linear relation with the cone resistance. The expected settlement can be obtained with equations 3–5.

$$s = q_b \cdot B \cdot \int_0^z \frac{I_z}{E_s} dz \tag{3}$$

$$E_{s,i} = 2.5 \cdot \overline{q_{c,i}} \quad \text{for circular/square foundation} \tag{4}$$

$$E_{s,i} = 3.5 \cdot \overline{q_{c,i}} \quad \text{for strip foundation} \tag{5}$$

where s = settlement; q_b = unit load acting on the base; B = footing width; I_z = strain influence factor

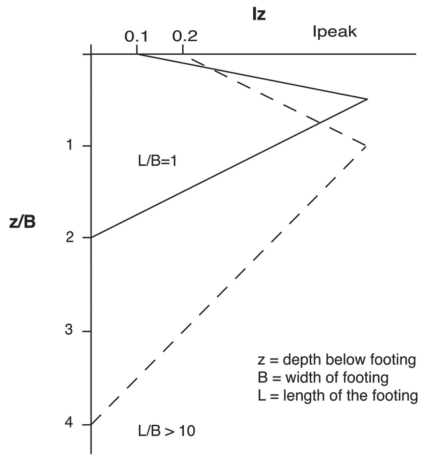

Figure 2a. Influence diagram Schmertmann (1978).

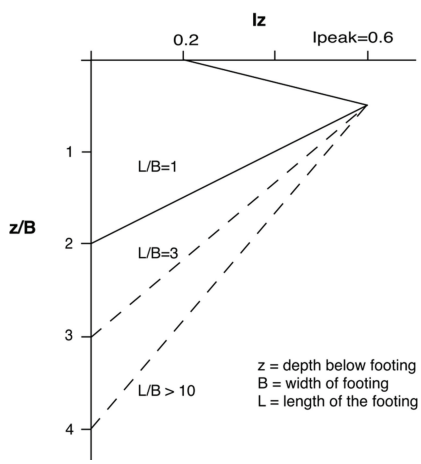

Figure 2b. Influence diagram Peck et al. (1996).

at depth z; E_s = secant Young's modulus at depth z; and q_c = cone resistance. The strain influence diagram is shown in Figure 2a.

Both De Beer and Martens and Schmertmann based their stress distribution calculation on the equation of Boussinesq (1883) and Newmark (1942).

Peck et al. (1996) proposed a modification of the Schmertmann method. They presented a different influence diagram where the depth and size of the peak of the influence I_{peak} is independent of the foundation geometry, in combination with adjusted expressions for the Young's modulus as a function of the cone resistance. Also a distinction is made between direct elastic settlement and time dependent deformation (creep). The equations 6–8 proposed for settlement calculations are slightly different from those by Schmertmann (1978).

$$s = q_b \cdot \sum_{i=1}^{n} \frac{I_z \cdot \Delta z}{E_{s,i}} \tag{6}$$

$$E_{s,i} = 3.5 \cdot q_c \tag{7}$$

$$E_{s,i} = 3.5 \cdot q_c \cdot \left(1 + \log_{10} \frac{L}{B}\right) \leq 3.5 \cdot q_c \cdot 1.4 \quad \text{for rectangular foundation} \tag{8}$$

where q_c = weighted average cone resistance; L = is the length of the footing; and B = width of the footing. The strain influence diagram is shown in Figure 2b.

Several more recent publications are available presenting an adjusted strain influence diagram with a more general formulation to suit all footing geometries (Mayne & Poulos 1999) or multiple interacting footings (Lee et al. 2007). Das & Sivakugan (2007) give an overview of the existing methods for settlement calculation based on CPT's and SPT's.

3.2 *CPT to stiffness correlation*

The above mentioned methods for prediction of footing settlement include a rough estimation of the material stiffness. Robertson (1990) suggested a more inclusive method making use of normalized and dimensionless CPT parameters. Based on this a distinction can be made between soil behaviour types using the SBTn chart. Equation 9 was proposed for the stiffness modulus based on the soil behaviour type index, the cone resistance and the stress state.

$$E' = 0.015 \cdot 10^{(0.55 I_c + 1.68)} \cdot \left(q_t - \sigma_{v0}\right) \tag{9}$$

where E' = Young's modulus; I_c = soil behaviour type index; q_t = corrected net cone resistance; and s_{v0} = in situ total vertical stress. This stiffness is based on combination with the aforementioned strain influence diagram of Schmertmann (1978).

The methods and correlations mentioned are generally only suitable for uncemented normally consolidated cohesionless sandy soils. Stress state parameters like consolidation state and reloading stiffness are not explicitly incorporated.

From experience it is know that the settlement that results from these correlations can vary, also depending on the specific site conditions. Because of the extensive amount of measurement data generated at the project, an evaluation of the CPT based settlement prediction methods can be performed.

4 ZONE LOAD TESTS

4.1 *General*

Van Oord DMC executed a large number of zone load tests to verify the settlement predictions.

A zone load test comprised the incremental loading of a square concrete footing of 3 m by 3 m by 0.6 m up to a load of 250 kPa. A test took three days and the settlements of the footing were measured as a function of time and load.

4.2 *Set up*

The set up of a ZLT is illustrated in Figures 3 and 4 and is designed after the experiences in current practice (Briaud & Gibbens 1999). The load on the footing is transferred from the concrete support blocks to the footing in between by extending a hydraulic jack. Reference beams with measurement devices were installed and supported at reasonable distance from the loading zone. On the footing, four measurement locations were evenly distributed over the surface and the average measured settlement was used as input for the verification of the maximum settlement.

Each load step comprised 20% of the maximum load of 250 kPa and was held for 2 hours. The maximum load was maintained for 48 hours.

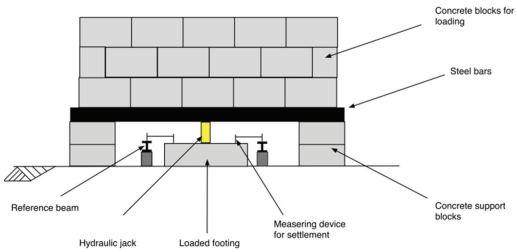

Figure 3. Schematic ZLT set up.

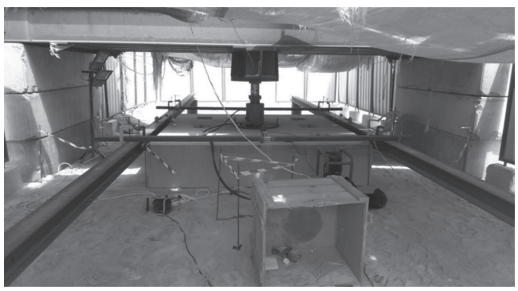

Figure 4. Close up photograph ZLT.

4.3 *Results*

An example of the resulting time displacement curve is presented in Figure 5. In the measured settlements a time dependent behaviour is observed.

5 ACCURACY OF EXISTING CORRELATIONS

To gain more insight in the accuracy of the existing correlations between CPT data and settlement of the sand fill under loading, all the measurement data were analysed after completing the project. From the total number of zone load test results, 43 zone load tests were selected which allowed for comparison of the predictions. In these tests, the sand body had a minimum thickness of 5 m above existing soft soil layers of silt or sabkha. The presence of silt or sabkha at the lower part of the foundation influence depth is expected to have minor impact on the foundation settlement, considering these layers were already treated by dynamic replacement (see section 2.1) and are relatively stiff.

5.1 *Processing of the CPT data*

At the location of every ZLT five CPT's were performed prior to testing. Unless significant variation was observed in the measurements indicating

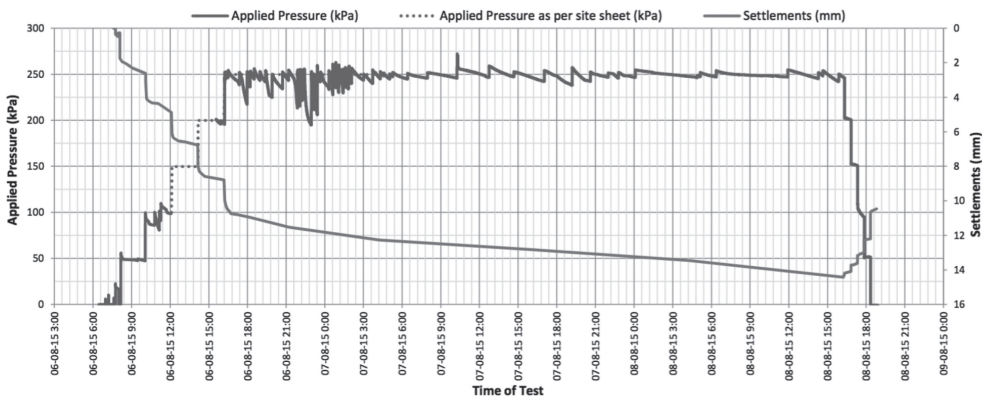

Figure 5. Output ZLT DD145.

high soil variability, the average resulting cone resistance and friction ratio were used for processing. The cone resistance and friction ratio were normalized and introduced in the SBTn chart of Robertson. Based on the resulting soil types, the soil layers were automatically defined, with a minimum soil layer thickness of 0.25 m. The process is illustrated in Figures 6 and 7. With this soil profile and corresponding CPT data the settlement calculations were performed using the available correlations.

5.2 *Comparison of results*

The predicted settlement based on the CPT data via the correlations and the actually measured settlement were compared to establish the error that occurs when using the correlations for settlement prediction. Only the measured direct settlement is used for comparison. The long term part of the measurements was excluded as the correlations in principle concern direct elastic deformation.

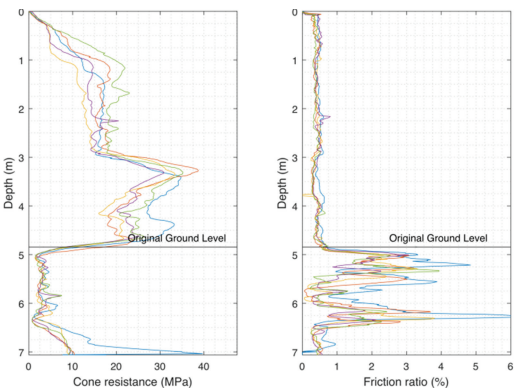

Figure 6. CPT data at ZLT DD145.

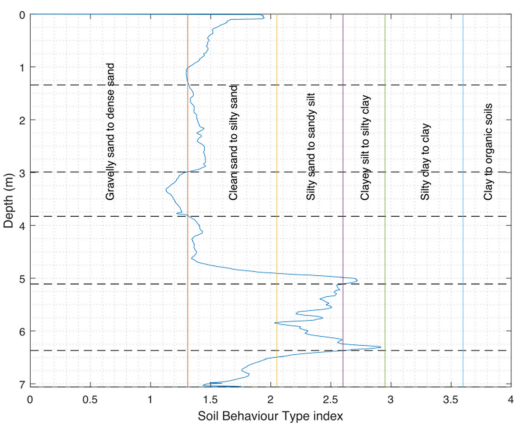

Figure 7. Layering based on CPT's at DD145.

At first, a distinction is made between locations with (1) only sand, (2) sand and silt, and (3) sand, silt and sabkha. The results per group are compared with the overall results. Another distinction in location concerns the thickness of the fill layer. At locations where the thickness of the applied fill is small, the in-situ sand determines a large part of the stiffness to be measured instead of the calcareous sand fill. From the data available no difference was observed between the errors encountered for the distinct situations. Based on these conclusions, the 43 zone load tests are treated as a uniform group.

It was investigated if the encountered error could be described as normally distributed. This was generally the case. The resulting means and standard deviations of the error per prediction method are given in Table 1.

5.3 *Conclusions*

After combining the zone load test measurements with the predictions based on the corresponding CPT's, it was evaluated which existing correlation best fitted the measurements. It was concluded that from the considered methods the CPT to stiffness correlation of Robertson, based on the analytical model of Schmertmann for stress distribution, corresponds very well with the measurements, consistently showing only small deviations from the measured settlement.

5.4 *Uncertainties and imperfections*

The ZLT's showed an increasing settlement while the load was kept constant. Such time dependent behaviour of the material can be caused by consolidation effects or by creep.

The permeability of the fill material is expected to be such that no or very little excess pore water pressure will occur during loading. Therefore it is not expected that consolidation of the sand is an important factor. In the cases that a silt or sabkha layer was present underneath the fill layer, loading can cause consolidation of these layers. However,

Table 1. Error in settlement calculated with analytical methods compared to ZLT measurements.

	Error	
Method	Mean (%)	Standard deviation (%)
De Beer and Martens	28	16
Schmertmann	42	13
Peck et al.	–2	23
Robertson	0	20

the compression of this layer is very limited due to the executed dynamic replacement and would not explain the fact that also at locations without such layers the time dependent behaviour was observed.

The time dependent behaviour can be caused by creep of the calcareous sand. Although no relation was found between the carbonate content present at specific ZLT's locations and the error between the predictions methods and the actual settlement measurements, this cannot be disregarded because of the limited amount of related soil investigation. The behaviour of crushable particles can be of significant influence on the CPT data. In the analyses for this project no shell correction factor was applied.

To verify the uncertainties mentioned above, additional testing is advised for future loading tests, execution of plate load test with variable plate dimensions, concerning the pore water pressures, and measurements of the distribution of the occurring strain over depth.

Finally, it is mentioned that the set up of the ZLT's is of influence on the test results. Although the tests were executed as carefully as possible, the environmental and practical limitations of the situation can affect the measurements. For example, the distance between the supports and the actual footing was relatively small; 1.5 m. Consequently, a stress increase was created in the influence zone of the footing before loading and measurement was started. As the sand will not behave fully elastic, the measured response of the footing can be stiffer during loading than generally to be expected and the total settlement of the footing at maximum load is reduced. The difference is calculated to be in the order of 10% to 15%.

6 CONCLUSIONS

For a specific project, the comparison of CPT based settlement prediction methods with the measurement results of zone load tests (ZLT's) showed that the CPT to stiffness correlation of Robertson combined with the analytical model of Schmertmann corresponds very well with the settlements taking place during zone load testing. The predicted settlement consistently shows only small deviations from the measured settlement. As the correlations give a reasonably reliable estimation of the expected settlement, the number of ZLT's to be performed in future projects to verify settlement requirements can be reduced.

Distinction is made between three types of soil layering at the site and also test locations with predominantly original silica sand deposits and locations with a thick calcareous sand fill with variable carbonate content. No abnormality between the errors of the predictions for the several situations is observed.

The fact that the fill material was calcareous sand does not appear to have influenced the accuracy of the predictions. No correction factor is applied on the CPT results to correct for the presence of the carbonate content in this project. In other cases this is probably necessary.

In the considered models long term deformation is not included. During the ZLT's time dependent settlements were observed. These settlements most likely result from creep of the sand and might be influenced by the carbonate content. To gain more insight in the cause of long term deformation for similar projects additional testing is advised including investigation of the carbonate content that is present and pore water pressure measurements occurring during loading.

REFERENCES

Boussinesq, J. 1883. Application des potentials a l'etude de l' equilibre et du mouvement des solides elastiques. Paris: Gauthier-Villars.

Briaud, J.L. & Gibbens, R. 1999. Behaviour of five large spread footings in sand. Journal of geotechnical and geoenvironmental engineering 125(9): 787–796.

Das, B. & Sivakugan, N. 2007. Settlement of shallow foundations on granular soil – an overview. *International journal of geotechnical engineering* 1(1): 19–29.

De Beer, A. & Martens, E. 1957. Method of computation an upper limit for the influence of heterogeneity of sand layers on the settlement of bridges. *4th International conference on soil mechanics and foundation engineering; Proceedings*: 275–282.

Lee, J. et al. 2007. Strain influence diagrams for settlement estimation of both isolated and multiple footings in sand. *Journal of geotechnical and geoenvironmental engineering* 134(4): 417–427.

Mayne, P. & Poulos, H.G. 1999. Approximate displacement influence factors for elastic shallow foundations. *Journal of geotechnical and geoenvironmental engineering* 125(6): 453–460.

Newmark, N.M. 1942. *Influence charts for computation of stresses in elastic foundations*. Technical report; University of Illinois Bull.

Peck, R.B. et al. 1996. *Soil Mechanics in Engineering Practice*; *3rd edition*. New York: John Wiley and sons.

Robertson, P.K. 1990. Soil classification using the cone penetration test. *Canadian geotechnical journal* 27(1): 151–158.

Robertson, P.K. 2009. Interpretation of cone penetration tests - a unified approach. *Canadian geotechnical journal* 46(11): 1337–1355.

Schmertmann, J.H. et al. 1978. Improved strain influence factor diagrams. *Journal of geotechnical engineering division* 104(8): 1131–1135.

Cone Penetration Testing 2018 – Hicks, Pisanò & Peuchen (Eds)
© 2018 Delft University of Technology, The Netherlands, ISBN 978-1-138-58449-5

Analysis of acceleration and excess pore pressure data of laboratory impact penetrometer tests in remolded overconsolidated cohesive soils

R. Roskoden, A. Kopf, T. Mörz & S. Kreiter
Centre of Marine Environmental Science (MARUM), University Bremen, Bremen, Germany

ABSTRACT: Free fall *CPTu* measurements have two data acquisition approaches: direct measurement of sleeve friction (f_s) and tip resistance (q_c) or estimation of these via acceleration data. However, enhanced impact velocities cause strain rate effects on the sediment, which requires to correct q_c, and f_s for these rate effects. The pore pressure (u_2), an important parameter for evaluating soil properties, is not corrected for the penetration rate effects yet. Hence, a laboratory free fall calibration test, with a miniature cone penetration lance, which measures u_2 and acceleration, was designed. The objective was to investigate responses of the acceleration—data to calculate kinematic f_s and q_c. Additionally, we studied dynamic u_2-responses for their penetration rate effect. We also investigated existing penetration rate-corrections for remolded, overconsolidated cohesive soils. In total six experiments were conducted, each of which consisted of four penetrations with impact velocities of 0.02 to 2 m/s. We estimated f_s and q_c from acceleration-data for a remolded, overconsolidated cohesive soil. New rate correction values have been found for this soil, which show a dependency on consolidation histories. Moreover, we identified possible rate effects on u_2-responses as increases in the modulus excess pore pressure. This will help to analyze existing and future u_2-measurements.

1 INTRODUCTION

Most Cone Penetration Tests (*CPTu*) are pushed with a constant penetration velocity of 0.02 m/s, termed standard. *CPTu* measures the soil's sleeve friction (f_s), tip resistance (q_c) and pore pressure (u_2). Free fall or dynamic *CPTu* measurements, standardized from the ASTM 1982 for borehole free fall CPT (Riggs, 1982), have two data acquisition approaches: direct measurements of the dynamic q_c and f_s, or estimation of soil strength parameters via acceleration-data (Dayal and Allen, 1973; Stoll et al., 2007). Dynamic *CPTu* have financial benefits and are more time efficient. However, dynamic *CPTu* measurements systematically overestimate q_c and f_s if compared to standard *CPTu*-data. This is called penetration rate effect (Dayal and Allen, 1973; Dayal and Allen, 1975). Attempts have been made to correct q_c, and f_s for penetration rate effects. For example EQ 1:

$$\frac{q_c}{q_{c,st}} = \mu \log_{10}\left(\frac{V}{V_{st}}\right) + 1 \qquad (1)$$

With $q_{c,st}$ = standard tip resistance, μ = penetration rate factor V = penetration velocity, V_{st} = standard velocity, (Dayal and Allen, 1975). Furthermore, higher penetration velocities might result in increased undrained shear stresses which can cause dilatancy in overconsolidated clays (Burns and Mayne, 1998). This may cause negative u_2 during penetration (Paniagua et al., 2016). Additionally, dynamic u_2-measurements can show exaggerated u_2-responces (Seifert et al., 2008), independent from its sign. Although, u_2 is an important parameter for evaluating soil properties and stability, so far it is not corrected for penetration rate effects. However, Chow et al. (2014) evaluated free fall dissipation tests in centrifuge modelling and concluded that, besides an atypical rise of the pore pressure, the dissipation behavior is identical to standard *CPTu*. Furthermore, Lucking et al. (2017) utilized short term rates of excess pore pressure dissipation to identify sediment types. Nevertheless, the initial atypical u_2-response reduces the engineering applicability for high impact *CPTu*. Soil behavior charts, based on u_2 or f_s, are especially not applicable for kinematic *CPTu* (Robertson, 1990; Roskoden, 2016). Chow et al. (2017) mention a possible back-calculation of the pore pressure ratio, allowing u_2-estimation even without a pressure transducer. However, Lucking et al. (2017) and Albatal and Stark (2017) emphasize the need of free fall calibration chamber tests to investigate u_2-behaviour. Hence, we implemented an experimental setting similar to a calibration chamber test, called 'calibration free fall test'. The objective

of the calibration free fall test is to evaluate rate effects and sensor performances for acceleration—and u_2-equipment. The scientific goals are to investigate: (1) kinematic f_s and q_c in remolded overconsolidated cohesive soils. (2) Penetration rate corrections for the given soil. (3) u_2-response for different penetration rates and consolidation pressures and (4) to evaluate polyethylene porous filter stone clogging for pogo-style deployments.

2 METHODOLOGY

The grain size distribution of a natural cohesive soil from the 'Hemelinger Marsch', south of Bremen, Germany, was altered to fit a coefficient of consolidation smaller than 2×10^{-7} m/s. Alterations were done via admixing commercially available micro silt (d_{50} = 30 µm) and sand (d_{50} = 0.210 mm) from *Euroquarz GmbH*. Both soils were tested for geotechnical index values such as liquid limit (*LL*), plastic limit (*PL*) and shrinking limit (*SL*), plasticity index (I_p) and shrinking index (I_S) (DIN 18122), coefficient of consolidation (c_v), compression index (C_C), recompression index (C_R) and swelling index (C_S) (DIN 18135), Table 1.

The artificially prepared soil was remolded. Its water content was increased to 55% while mixing it constantly until the soil was homogenized to a slurry. The slurry was transferred into a self-designed container. The slurry was then consolidated to an effective normal stress of 64 or 32 kPa. Water content after consolidation was between 35 to 40% (tested at different depths). Vertical homogeneity was visually verified via push cores. Consolidation pressure was removed before testing. The measurements were done via a custom-built miniature cone penetration lance, recording u_2- and acceleration-data. Acceleration was used to calculate the total resistance force (F_T), EQ 2:

$$F_T = m(g - a) \tag{2}$$

with m = *CPTu* mass in kg, g = gravitational acceleration and a = measured acceleration in m/s², respectively. Six experiments, each with four penetrations with different penetration velocities (0.02–2 m/s) per batch, were conducted. For reference purposes, each batch starts with a pushed test (V_{st}). Dynamic tests are guided via a sled (attached to vertical guides, Figure 1).

Repeatability was tested in each batch, by using either impact velocities 1 m/s or 2 m/s twice per batch. Sampling frequency was 500 Hz. Designed container (81 liters, ~0.176 m²) from bottom to top: (1) 10 mm vertical drainage socket. (2) 20 mm gravel layer. (3) Metal grid to separate slurry and gravel. (4) 5 vertical drains (filters candles) ~250 mm long, filled with gravel (to reduce consolidation time). (5) ~465 mm soil (after consolidation). (6) 5 mm polyethylene porous filter plate (porosity ~35%). (7) 100 mm pressure plate (~12 kg). (8) 1 cm water layer to keep current saturation. Schematic design of the experimental setup is shown in Figure 1. The size of the container was

Table 1. Soil classification of original 'Hemelinger Marsch' soil and the synthetically altered soil.

Soil	Hemelinger Marsch	Synthetically altered
Clay	16.8%	8.3%
Silt	73.6%	84.8%
Sand	9.6%	6.9%
LL	60.6%	37.8%
PL	19.0%	13.26%
SL	8.1%	5.9%
I_p	41.6	24.6
I_s	52.5	32.5
c_v [m²/s]	9.5E-7	1,24E-06
C_C	0.4	0.26
C_R	4.3E-2	3.0E-3
C_S	6.52E-2	2.3E-2

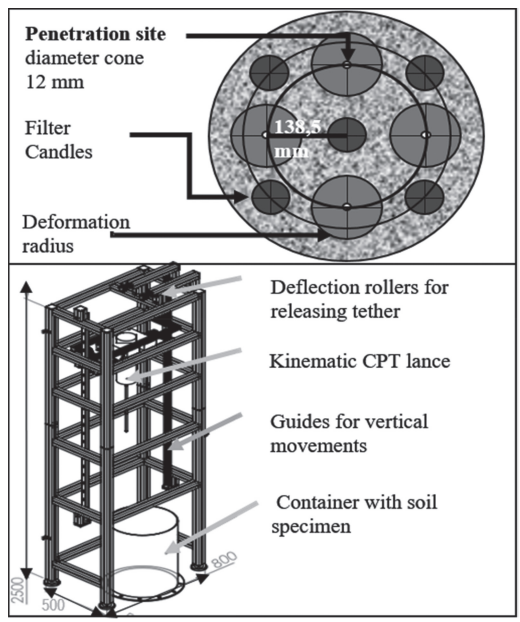

Figure 1. Upper: Top angle showing plastic defamation radius of penetration sites and drainage/filter-candle sites. Lower: Free fall tower with vertical guidance system and deflection rollers, dimensions in mm (altered after Stephan (2015)).

designed to fulfil the boundary conditions for the plastic deformation radius, EQ 3 (Lu et al., 2004):

$$R_p = 1.5\sqrt{I_r}\, R_c \tag{3}$$

with R_p = plastic deformation radius, I_r = rigidity index (~50, after Keaveny (1985) solution chart), and R_c = cone radius (6 mm). Hence, no geometric overlap of plastic deformation radius between different penetrations is expected (Figure 1). Vertical drains are below penetration depth and are not expected to interfere with resistance or u_2-behaviour. For dividing the total resistance into f_s and q_c an additional experiment was carried out. A miniature penetration lance, which can measure q_c and the total resistance force directly, was pushed into the specimen with four different constant velocities (Table 2, Ex. 0). Before each free fall experiment, the pore pressure assembly (tubing, u_2-sensor and filter stone) was saturated. In-between batches, the filter stone was treated differently to evaluate clogging effects of the filter media. Treatment options were: (1) cleaning by swiping, (2) cleaning by flushing and (3) no cleaning, also called pogo-style (common deployment method for impact penetrometer (Stegmann et al., 2006)). After finishing one experiment the soil was recycled for further experiments and if needed the volume increased by adding more artificial soil-mass. Furthemore, the pore pressure filter stone (same material as the pore pressure plate) was cleaned via pressure washing (initial porosity ~35%).

Table 2. Experimental setting and cleaning option for each penetration per experiment (Pen I to IV).

Experiment:	0~	3	4	5	6	7
Title	VE*	S	F	F	P	P
Cons.[kPa]	64	64	32	32	32	32
Pen I						
static (u2 & FT)	0.02°		0.02	0.02	0.02	
Pen II						
static (u2 & FT)	0.15	x^				
dynamic					1	
pore pressure					x	
acceleration					x	
Pen III						
static (u2 & FT)	0.2					
dynamic		1	1	2	1	1
pore pressure		x	x	x	x	x
acceleration		x		x	x	x
Pen IV						
static (u2 & FT)	0.23					
dynamic		2	1	2	2	2
pore pressure		x	x	x	x	x
acceleration		x		x	x	x

~ Missing numbers in-between experiments-sequence represent failed tests (e.g. data logger failure).* VE = Velocity Experiment, S = Swiping, F = Flushing, P = Pogo Style.° Numbers represent impact velocity in m/s. ^ × = collected data.

3 RESULTS

3.1 *Estimation of q_c and f_s via acceleration data*

Due to the homogenization of the soil, and negligible total over burden stress (max 1.2% of total penetration resistance with a max penetration depth of 20 cm) one can assume a constant q_c over depth. Hence, an average q_c-value for experiment 0 is found, which is then subtracted from the total resistance force. This will result in f_s, EQ 4:

$$F_T = F_q + F_f + F_d + F_b \tag{4}$$

With the force at the tip $F_q = A_c\, q_c$ and the force at the sides $F_f = A_s f_s$ (A_c, the q_c-area and A_s, the f_s-area). Albatal and Stark (2017) argue that the force at the sides, F_f, the drag force, F_d, and the buoyancy force, F_b, can be neglected due to limited cone dimensions and penetration depth. However, Figure 2a shows the total force, normalized to q_c-area, called apparent tip resistance ($q_{c,a}$), and q_c over depth.

Q_c remains around an average of 114 kPa. Whereas, apparent q_c is increasing with depth

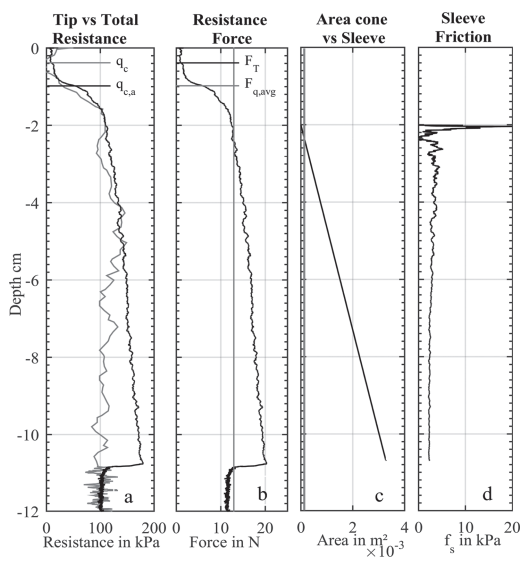

Figure 2. a: Differences in apparent tip resistance ($q_{c,a}$) and q_c in kPa. b: Resistance force vs average-force at tip. c: Advancing area of the sleeve. d: Deducted sleeve friction in kPa. Execution with standard penetration velocity.

(~7.33 kPa/cm). Here, the maximum difference between q_c and apparent q_c is 66 kPa, which is 36% of the apparent q_c, but would increase for higher depths. At depth 2 cm (3.3 times cone radius) surficial boarder effects on the q_c and apparent q_c stabilize (Chow et al., 2014). Therefore, this depth was taken as reference depth for the estimation of the dynamic q_c ($q_{c,dy}$). Figure 2b shows total force in N over depth with an average tip force as reference (~13 N, grey line). The difference of these forces equals the sleeve force. Figure 2c shows the calculated increasing f_s-area of the advancing lance over depth (black line) vs the constant q_c-area (~ 0.113×10^{-3} m², grey line). The resulting f_s is shown in Figure 2d. f_s is constant over depth where the f_s-area is bigger than the q_c-area with a value of ~3 kPa.

3.2 *Velocity dependency on tip resistance*

Figure 3 shows all calculated or measured and averaged q_c-data. Estimations of static q_c, where not directly measured, were done via the reference depths 2 cm, where f_s is supposed to equal ~0 and the q_c-area is bigger than the f_s-area. The dynamic tip resistance ($q_{c,dy}$) was calculated via the acceleration-data, EQ 5:

$$q_{c,dy} = \frac{m(g - a(s^*))}{A_c} \tag{5}$$

With $a(s^*)$ = acceleration data between 2–2.5 cm (~3.3–4.16 times cone radius), where the q_c-area is bigger than the f_s-area. The correlation of the normalized tip resistance ($Q_c = q_c/q_{c,st}$) vs the logarithmic normalized penetration velocity gives two regression lines which follow the expression of EQ 1 (Figure 3). This provides two new penetration rate factors: 0.74 and 0.31 for 32 and 64 kPa effective consolidation stress, respectively.

3.3 *Pore pressure data and clogging effect*

Measured u_2 over time (t) is shown in Figure 4. Figure 4a displays u_2 for constant velocities (0.02 m/s), while Figure 4b displays dynamic u_2-data for falling heights of 5 cm (impact velocity 1 m/s) and Figure 4c for falling heights of 20 cm (impact velocity 2 m/s), respectively. Please note different time scales. Additionally Figure 4b and c include free fall time through the air while Figure 4a shows only the penetration time. Hence, Figure 4b and c are divided into 3 time sequences: (1) the jerk, the initial 0.02 s of the acceleration,

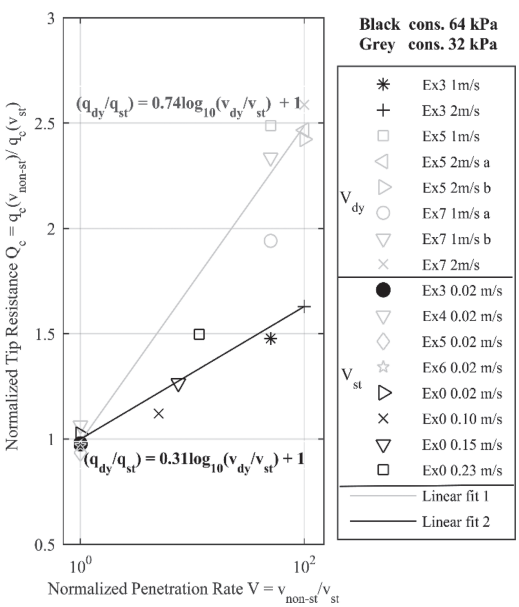

Figure 3. $Q_c = q_c/q_{c,st}$ versus the logarithmic penetration velocity normalized to standard penetration velocity. Legend divided into static (V_{st}) and dynamic tests (V_{dy}). Black symbols: experiments with a consolidation history of 64 kPa. Grey symbols stand for 32 kPa.

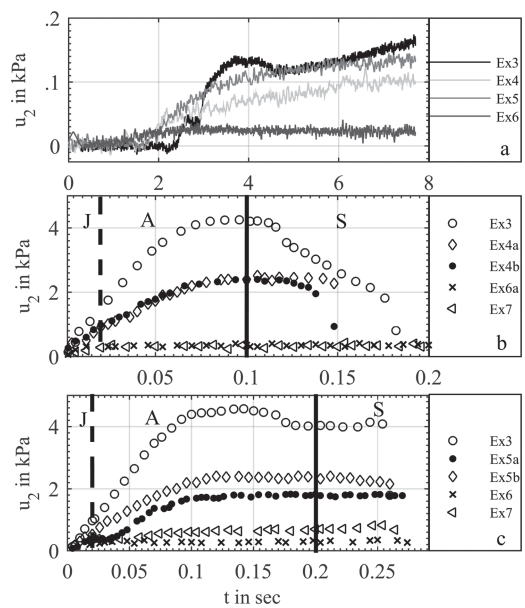

Figure 4. a: Static u_2 over time for experiment 3 to 6. b: Dynamic u_2 (falling height = 5 cm, impact velocity = 1 m/s) over time for experiment 3, 4, 6 and 7. 6b is not shown (due to reasons of clarity and comprehensibility) but behaves like 6a. c: Dynamic u_2 (falling height = 20 cm, impact velocity = 2 m/s) over time for experiment 3, 5, 6 and 7. Description in text.

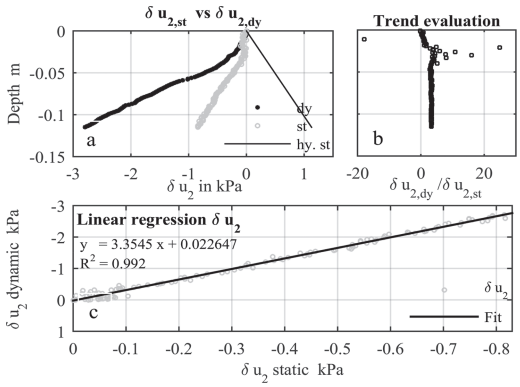

Figure 5. Excess pore pressure analysis. a: δu_2 static vs dynamic over depth. b: Ratio of dynamic and static showing trend evolution. c: Linear regression between δu_2 static vs dynamic.

where $\delta a/\delta t \neq 0$ (m/s³), (2) acceleration in the air and (3) acceleration in the sediment. The effectiveness of each cleaning option can be evaluated with Figure 4. Swiping cleans less than 50% porous filter stones contamination (Figure 4b and c experiment 3). Flushing does clean current contamination by ~80% (Figure 4b and c, experiment 4a, 4b, 5a and 5b, respectively). Pogo-deployment hinders u_2-acquisition immensely (Figure 4b and c, experiment 7 and 6). Moreover, the effectiveness of the filter stone is reduced by around 35% per penetration experiment (Figure 4a).

3.4 *Qualitative evaluation of dynamic u_2*

Figure 5 shows a qualitative evaluation of excess pore pressure (δu_2) for experiment 3. The modulus of the dynamic excess pore pressure ($|\delta u_{2,dy}|$) have higher values then the modulus of the static data ($|\delta u_{2,st}|$, Figure 5a). The trend evaluation indicates a constant or slightly increasing trend after the first 2 cm ($\delta u_{2,dy}/\delta u_{2,st} = 3.3$, Figure 5b). A linear fit of static and dynamic excess pore pressure gives a goodness of fit of $R^2 = 0.992$ (Figure 5c).

4 DISCUSSION

4.1 *Estimation of q_c and f_s via acceleration data*

In contrast to Stark (2011) and the later publication of Stark (Albatal and Stark, 2017; Lucking et al., 2017), this experiment shows a clear dependency of the total force on sleeve friction (~36%), which increases for greater penetration depth (Figure 2). However, the estimation of the dragging force and buoyancy force (EQ 4, cumulative effect < 5% of the total force) was found negligible for these free fall calibration tests. Figure 1 at depth 2 to 2.5 cm shows f_s-instabilities, which is a result of the q_c-area being bigger than the f_s-area. Therefore, we recommend calculating f_s only for depth where the f_s-area is bigger than the q_c-area. Nevertheless, the obtained constant f_s-values after a depth of 2.5 cm indicates success in deducting kinematic f_s via acceleration-data. The derived values of ~3 kPa are in range for cohesive sediments with a clay content of ~8% (Lunne et al., 1997).

4.2 *Velocity dependency on tip resistance*

Penetration rate factors of this study go well with literature values (Dayal and Allen, 1975; Steiner, 2013). Furthermore, the penetration rate factor for fit one (32 kPa consolidation stress) is almost twice as high as for fit two (64 kPa consolidation test). This suggests the lower the maximum consolidation the higher the penetration rate factor. The consolidation is a reflection of the dissipated pore water in the sediment. Lower stages of consolidation can have a higher pore water volume, which can increase excess pore pressure in cohesive soils, especially with penetration velocities bigger than standard penetration velocity. Hence, the effective stress decreases and q_c increases due to undrained conditions (Salgado et al., 2013).

4.3 *Pore pressure data*

Figure 4a shows a clear decrease in u_2 over all experiments, suggesting a lifespan of the filter stone of 1 to 2 experiments. Static u_2-data for experiment 3 and 4 seem similar, because of the different consolidation stresses. Flushing the filter stone in-between penetrations can enhance the performance of the filter stone (Figure 4b and c experiment 4a to b and 5a to b). Figure 4b and c (experiment 3, 6 and 7) show that the options of swiping and pogo-mode are insufficient for laboratory experiments due to lack of ambient pressure which might re-saturate the filter stone (Lucking et al., 2017). Furthermore, the dynamic data indicate a direct influence of the acceleration on the u_2-data, shown in Figure 4b and c. The jerk and acceleration in the air clearly overprints u_2-data. This can be dealt with if u_2-is set to zero upon impact. Nevertheless, the acceleration-influences on u_2 might suggest that if the acceleration changes abruptly, another jerk might appear, distorting the true soil u_2-signals. Moreover, there seems to be an artificial bias (visible in Figure 4c experiment 3, as a sin function), indicating a friction effect from the guiding system and deflection rollers of the free fall tower, on the measurements (Figure 1). However, no frequency analysis has been done yet.

4.4 *Qualitative evaluation of dynamic u_2*

Figure 5 shows a direct correlation between penetration velocities and modulus excess pore pressure. The relation for mono-layered cases may be estimated via trend evaluations. Layered-systems might not be as simple due to different pore pressure distribution and boundary conditions.

5 CONCLUSION

We investigated kinematic *CPTu* parameters on a descriptive basis. No generalisations are made about kinematic testing yet, but we regard our experimental efforts to implement calibration free fall tests as successful. In respect to the goals introduced above, we conclude that: (1) we successfully deployed a method to derive kinematic total force, and divide it into kinematic q_c and f_s for a known geometrical-setup. The deduction of kinematic f_s opens the possibility for further analyzes like the soil classification charts of Robertson (1990) and shall be investigated in a field study in the estuary Firth of Thames, New Zealand, with the impact penetrometer '*Nimrod*' (Stark, 2011). (2) We derived two consolidation-history dependent penetration rate factors for remolded overconsolidated, cohesive soils. (3) Modulus excess pore pressure increases with enhanced penetration velocity if equal experimental conditions are used. (4) Pogo-deployments are insufficient for laboratory tests.

ACKNOWLEDGEMENTS

We thank the Deutsche Forschungsgemeinschaft (*DFG*) for funding this project through the international graduate school INTERCOAST at MARUM, University of Bremen. Furthermore, we would like to thank C. Zoellner, T. Fleischman and M. Huhndorf for their technical support, A. Saeed for student assistance, J. Titschack for grain size analysis, M. Kluger, A. Roesner, W. Menapace and E. Horstman for helpful comments.

REFERENCES

18122, D., 2000. *DIN Deutsche Institut für Normung e. V., Zustandsgrenzen (Konsitenzgrenzen)*. Beuth, Berlin.

18135, D., 2012. *DIN Deutsche Institut für Normung e. V. Eindimensionaler Kompressionsversuch.* Beuth, Berlin.

Albatal, A., Stark, N., 2017. Rapid sediment mapping and in situ geotechnical characterization in challenging aquatic areas. *Limnology and Oceanography: Methods* 15, 690–705.

Burns, S., Mayne, P., 1998. Monotonic and dilatory pore-pressure decay during piezocone tests in clay. *Canadian Geotechnical Journal* 35, 1063–1073.

Chow, S., O'Loughlin, C., Randolph, M., 2014. Soil strength estimation and pore pressure dissipation for free-fall piezocone in soft clay. *Géotechnique* 64, 817–827.

Chow, S., O'Loughlin, C., White, D., Randolph, M., 2017. An extended interpretation of the free-fall piezocone test in clay. *Géotechnique*, 1–14.

Dayal, U., Allen, J.H., 1973. Instrumented impact cone penetrometer. *Canadian Geotechnical Journal* 10, 397–409.

Dayal, U., Allen, J.H., 1975. The Effect of Penetration Rate on the Strength of Remolded Clay and Sand Samples. *Canadian Geotechnical Journal* 12, 336–348.

Keaveny, J., 1985. In-Situ Determination of Drained and Undrained. University of California, Berkeley.

Lu, Q., Randolph, M., Hu, Y., Bugarski, I., 2004. A numerical study of cone penetration in clay. *Géotechnique* 54, 257–267.

Lucking, G., Stark, N., Lippmann, T., Smyth, S., 2017. Variability of in situ sediment strength and pore pressure behavior of tidal estuary surface sediments. *Geo-Marine Letters*, 1–16.

Lunne, T., Powell, J.J.M., Robertson, P.K., 1997. *Cone Penetration Testing in Geotechnical Practice*. Taylor & Francis.

Paniagua, P., Carroll, R., L'Heureux, J.-S., Nordal, S., 2016. Monotonic and dilatory excess pore water dissipations in silt following CPTU at variable penetration rate, 5th International Conference On Geotechnical And Geophysical Site Characterisation (ISC5), Queensland, Australia.

Riggs, C., 1982. A Proposed Standard Test Method for a Free Fall Penetration Test. *Geotechnical Testing Journal* 5, 89–92.

Robertson, P.K., 1990. Soil classification using the cone penetration test. *Canadian Geotechnical Journal* 27, 151–158.

Roskoden, R., 2016. Cone Penetration Tests The soil classification and analytic assessments of dynamic and static penetrometer test data. Universität Bremen, Master Thesis, 2016, Bremen.

Salgado, R., Prezzi, M., Kim, K., Lee, W., 2013. Penetration rate effects on cone resistance measured in a calibration chamber, 4th International Conference on Site Characterization, ISC'4.

Seifert, A., Stegmann, S., Mörz, T., Lange, M., Wever, T., Kopf, A., 2008. In situ pore-pressure evolution during dynamic CPT measurements in soft sediments of the western Baltic Sea. *Geo-Marine Letters* 28, 213–227.

Stark, N., 2011. Geotechnical investigation of sediment remobilization processes using dynamic penetrometers. Universität Bremen, Bremen.

Stegmann, S., Mörz, T., Kopf, A., 2006. Initial Results of a new Free Fall-Cone Penetrometer (FF-CPT) for geotechnical in situ characterisation of soft marine sediments. *Norwegian Journal of Geology/Norsk Geologisk Forening* 86.

Steiner, A., 2013. Sub-Seafloor Characterization and Stability of Submarine Slope Sediments using Dynamic and Static Piezocone Penetrometers. Bremen, Universität Bremen, Diss., 2013.

Stephan, S., 2015. A rugged marine impact penetrometer for sea floor assessment. Bremen, Universität Bremen, Diss., 2015.

Stoll, R.D., Sun, Y.F., Bitte, I., 2007. Seafloor properties from penetrometer tests. *IEEE Journal of Oceanic Engineering* 32, 57–63.

Cone Penetration Testing 2018 – Hicks, Pisanò & Peuchen (Eds)
© 2018 Delft University of Technology, The Netherlands, ISBN 978-1-138-58449-5

CPT-based parameters of pile lengths in Russia

I.B. Ryzhkov
BGAU, Ufa, Russia

O.N. Isaev
Gersevanov NIIOSP, Moscow, Russia

ABSTRACT: In Russia, Cone Penetration Testing (CPT) is developing towards the use of heavy cone penetration rigs to evaluate soil conditions and in particular, calculate the bearing capacity of driven piles. This trend was formed in the former USSR as early as fifty years ago, when mass construction was reoriented toward wide application of precast reinforced concrete and driven piles. The parameters of pile foundations were developed based on the CPT data. In subsequent decades, the range of tasks to be solved by means of CPT significantly expanded, calculations were more reliable and CPT procedures improved.

1 INTRODUCTION

At present, CPT in Russia is developing in the way that was formed during reorientation of construction toward mass application of driven piles. In the second half of the 20th century, Russia's technical policy was oriented toward "industrialization of construction", i.e. wide application of precast reinforced concrete and pile foundations made of short driven piles (6…10 m). Thus, CPT of soils, which did not attract special attention in the USSR earlier, was being greatly developed. This method helped solve the problem of choosing the pile lengths for mass construction when the speed and reliability of assessing the load-bearing capacity of piles became particularly important. Exceptionally favourable conditions made it possible to carry out research in this field: the annual volume of pile application in the country reached 10 million m^3, hundreds of static tests of piles were done annually, scientific institutions worked on the new effective CPT rigs, the research was regularly funded, etc. High-performance CPT rigs were developed and widely used (C-832 and others); methods for calculating the pile bearing capacity and the technological parameters of pile foundations were developed based on the CPT data. The principal features of these developments were as follows:

- extensive use of self-propelled CPT rigs equipped with electrical probes incorporating friction sleeves - 310 mm in length
- calculation of soil resistances on the pile side surface by means of sleeve friction resistances f_s (ignoring q_c)
- approach to technological procedures of piling (avoidance of the piles underdriven up to the designed depth, etc.).

2 CPT APPLICATION IN DESIGNING PILE FOUNDATIONS IN RUSSIA

At present, pile foundation engineering in Russia is developing in the same direction, but after the crisis of the 1990s, the volumes of pile application slightly decreased, the share of driven piles also decreased. However, the pile lengths used in urban construction increased and the bored piles of large diameters and lengths (20 ... 40 m) were used more widely. The role of CPT decreased to some extent, since the existing CPT equipment was not adapted for such deep depths. More powerful CPT rigs are still needed for survey work in Russia. The problem was not challenging in the former USSR, since piles up to 12 m in length were mainly used in mass construction, and the possibilities of CPT met the requirements of the time. Nevertheless, the range of techniques of the time proved to be very effective and has not lost its significance to the present time.

First, this refers to heterogeneity of soils at the investigated site. Due to its simplicity and low price, CPT makes it possible to determine pile resistances at different points of the site, allowing the site to be divided into separate sections where certain pile bearing capacities can be obtained. This allows the optimal pile lengths to be chosen for each section of the site; this cannot be done by means of any

other method used to determine the pile bearing capacity. In practice, CPT-based division of the site is possible in almost any conditions where piles are expected to be used. It helps choose the most economical parameters of pile foundations.

The following characteristics of pile resistance are used in current Russian Standards (Building Code SP 24.13330.2011; Building Code SP 25.13330.2012):

- particular values of the ultimate pile resistance (resistances at the specific site points)
- generalized values, i.e. the characteristic strength and pile bearing capacity within a specific section (or the whole) of the site.

The mean values of such resistances at the selected section (after the CPT data) are the characteristic (most probable) strength of a pile of any given length. Pile bearing capacity is the ratio of the characteristic strength and the reliability coefficient of soil γ_g determined by statistical processing of the particular values of pile resistances at the section (most often - γ_g = 1.05...1.15). Pile foundations are designed with regard to the generalized values of pile resistance, i.e. pile bearing capacity, but an additional "reserve" is introduced as the reliability coefficient γ_k, which takes into account the test method for the ultimate pile resistances (after the CPT data γ_k = 1.25).

The pile characteristic strength can be determined either by averaging the particular values of the maximum pile resistances calculated at different points of the site or by averaging the original data, i.e. cone resistance q_c and sleeve friction resistance f_s (for each depth). As is seen from numerous calculations, both approaches give almost identical results (Ryzhkov & Isaev 2016). However, the first approach (assuming preliminary calculations of the ultimate pile resistances) has an important advantage: it makes it possible to identify the "strong" and "weak" sections of pile resistances and draw up the relevant cartograms of such resistances.

The points to determine the ultimate pile resistances ("CPT points") are located more or less evenly within the site. The ultimate resistances of piles incorporating a particular profile are calculated for each point for the depths of 3 m, 4 m, 5 m, ... h m, where h is the highest (reached) CPT depth. If the soils are heterogeneous, the site is divided into sections where the standard value of pile resistances and pile bearing capacity are established.

In contrast to the approaches adopted in most countries of the world, Russian Standards require the ultimate pile resistances to be calculated using both cone resistance q_c and sleeve friction resistance f_s. The value of f_s determines the pile side resistance. Soil resistance under the pile footing is determined by the mean value of cone resistance (q_c) at a section within one diameter above and four diameters below the end mark of the designed pile. Pile end/pile side resistances are determined if multiply q_c and f_s by the relevant "transition coefficients" from the probe to the pile. The coefficients for thawed (Building Code SP 24.13330.2011) and frozen (Building Code SP 25.13330.2012) soils are given in the tables of Russian Standards. Unlike a number of foreign methods of calculation, the whole of these dependencies are single-valued, i.e. each value of q_c and f_s correspond to the values of pile end/pile side resistances (R and f respectively) strictly defined at a given depth, but not the intervals.

Calculations for piles made of monolithic concrete (bored, drilled with/without enlarged bases, etc.) have been paid much less attention in Russia (due to small volumes of their use) than calculations for driven piles. Prior to 2000, such calculations were absent in Russian Standards, and when they appeared, they were largely based on foreign ideas (only cone resistances q_c were used). Just in the second decade of the 21st century there appeared test methods for resistances of thawed and frozen soils on the pile side surface by means of the sleeve friction resistance (Gotman & Glazachev 2014; Standard STO 36554501-049-2016). However, calculations were more reliable for driven piles, as compared to the foreign methods. Figure 1 shows a dissipation diagram of the CPT-based calculations made for the driven pile resist-

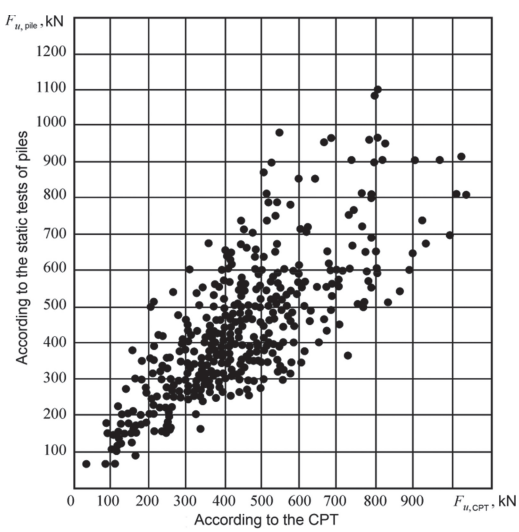

Figure 1. Schematic illustration of the ultimate pile resistances evaluated by CPT data (in accordance with SP 24.13330.2011) $F_{u,CPT}$ compared to the ultimate resistances evaluated by static tests of the full-sized piles $F_{u,pile}$.

ances versus the values determined after static tests of the given piles.

The results shown refer to the driven piles immersed into thawed soils; the piles ranged from 0.2×0.2 m to 0.4×0.4 m in section and from 3 m to 18 m in immersion depth (503 piles). The CPT rig was equipped with an electrical probe incorporating a friction sleeve (C-832).

Calculations were carried out in accordance with Russian Standards using the formula, which did not almost change for the last 3...4 decades. If it applies to thawed and frozen soils, as well as to electrical probes equipped with a friction sleeve, the formula for the specific pile resistance F_{ui} at a CPT point can be represented in its universal form as follows:

$$F_{ui} = k\left(R_{pc}A + \gamma_{af} u \sum R_{la} h_i\right) \quad (1)$$

Where k = coefficient considering the difference in permafrost soil conditions during CPT procedure (given the original soil temperature) and life cycle of the designed structure (given the specified soil temperature), for thawed soils – k = 1; $R_{pc} = \beta_1 q_c$ = unit ultimate soil resistance under the pile end obtained at the specified point after CPT; R_{la} = unit ultimate soil resistance along the pile side surface obtained at the specified point after CPT; for thawed soils - $R_{la} = \beta_2 f_s$, for frozen soils – $R_{la} = \beta_2 f_{si}$; = transition coefficients are determined by the tables: for driven piles and thawed soils given in (Building Code SP 24.13330.2011) (β_1 = 0.20…0.90; β_2 = 0.30…1.00), for driven piles and frozen soils—in (Building Code SP 25.13330.2012) (β_1 = 0.22…0.42; β_2 = 0.18…0.38); q_c = cone resistance; f_s = unit sleeve friction resistance of thawed soil in probe pusing; f_{si} = unit sleeve friction resistance of frozen soil at the beginning of pushing, after freezing of the probe in the soil (relaxation-creep CPT) (Ryzhkov & Isaev 2016; Building Code SP 25.13330.2012); h_i = thickness of i-layer of soil; γ_{af} = coefficient dependent upon the soil conditions (thawed or frozen) and pile material (for driven piles and thawed soils γ_{af} = 1); A, u = pile area and cross-sectional perimeter respectively.

According to the data presented at the CPT'10 and CPT'14 symposiums (Viana da Fonseca 2010; Flinn et al. 2014), foreign CPT-based methods used to calculate the bearing capacity of driven piles are less reliable than those used for monolithic piles (bored, drilled, etc.). Foreign specialists often use the percentage of cases as a criterion for reliable calculations when the disagreements between the calculated and "accurate" (determined by static tests) results are within ±20%, i.e. $F_{u,CPT}$ / $F_{u,pile}$ = 0.8…1.2. According to (Viana da Fonseca 2010), this percentage is 20% for driven piles, 34% for bored piles, 44% for drilled piles (CFA), and this share is 50% for the results presented in Figure 1. At CPT'14 (Flinn et al. 2014) presented an analysis of the CPT-based reliable calculations of the bearing capacity of an in-situ pile with an extracted casing (DCIS). The mean value of the ratio between the calculated pile resistances and the measured ones (obtained by static tests) varied within 0.81...1.2 in eight considered methods, coefficient of variation - 0.26...0.44. The mean value of the ratios between the calculated resistances $F_{u,CPT}$ and certain static tests $F_{u,pile}$ was 1.02, the coefficient of variation - 0.31, for the data shown in Figure 1.

The information given shows that, despite the acceptable accuracy of CPT-based calculations for pile resistances, the errors in assessment of pile resistances ("errors of calculation models") towards the "dangerous side" may exceed 20...25% at some points of the site. However, buildings and structures possess sufficient stiffness necessary for redistribution (balance) of loads imposed on piles. Some of the loads imposed on the piles with poor resisitivity are redistributed to the neighboring piles with an excessive resistivity.

In these cases it is necessary that the acting loads do not exceed the mean values of the pile resistances (taking into account the relevant random factors). The "errors" in assessment of the mean values are always less than the "errors" of the particular values. In the normal law of distribution, the "errors" of the mean values will be $\sqrt{n}$ times less than the "errors" of the particular values (n - the number of CPT points). In general, "errors" in calculating the average pile resistances are approximately 2...3 times less than the "errors" of their particular values. For this reason, Russian Standards (Building Code SP 24.13330.2011; Building Code SP 25.13330.2012) are oriented to the pile lengths which are to be chosen with regard to the mean values of pile resistances which are subject to additional correction (relevant "reserves" of the strength are introduced). The reliability coefficient γ_k, which takes into account the test method for pile bearing capacity (for CPT γ_k = 1.25), compensates the entire range of possible "errors" when calculating the pile bearing capacity after the CPT data.

3 CPT FOR MEETING CHALLENGES IN PILE FOUNDATION ENGINEERING

To immerse the driven piles strictly to the designed depth is challenging in pile foundation engineering. Due to the great variety of engineering and geological conditions, it is not always possible to select a hammer of suitable power and provide the necessary pile strength, so that the whole 100% piles reach the

designed depth. Some of the piles cannot be completely immersed to such a depth and they have to be cut down. In the former USSR the volume of cut reinforced concrete reached 0.5 million m^3 per year due to the underdriven piles. The bearing capacity of the underdriven piles may appear to be lower than the designed one and the foundation will need to be strengthened. Additional material resources and time are always required to meet the challenges.

A method was developed to select the pile lengths in order to overcome such an irregular situation for thawed soils (Ryzhkov & Isaev 2016), and then for frozen ones (Standard STO 36554501-049-2016); here, underdriven piles and wastes of reinforced concrete were minimized. The principle of this method is that the pile length (depth of immersion) is defined by both the necessary bearing capacity and processing capability of immersing them to the designed depth. Two requirements are necessary to be taken into account:

- energy of a pile driving hammer should make it possible to immerse the pile to a given depth in 10...15 minutes
- pile strength should be sufficient to withstand the expected number of hammer blows.

CPT proved to be the most effective for meeting these requirements. This is because CPT helps determine the pile resistances at each meter of piling, i.e. for depths of 1 m, 2 m, 3 m, 4 m ... etc. With respect to these resistances, it is not problematic to determine the average value of set per blow at each meter of piling using the known formulas relating the failure to the ultimate pile resistance. The reciprocal of such value of set per blow (in meters) is nothing more than the number of blows per meter of immersion. Summing up the whole of the blows, one gets the expected total number of hammer blows needed to immerse the pile to a given depth. Obviously the whole calculations must be made using software, since they are too time-consuming to perform "manually".

The resulting number of hammer blows makes it possible to evaluate both technological parameters mentioned above. First, it determines the duration of piling: the work speed of diesel hammers is approximately one blow per second. Secondly, it allows assessing the risk of pile breaking-up during the procedure and to select piles incorporating blow resistance sufficient to withstand the expected number of blows.

Special tables have been developed (Ryzhkov & Isaev 2016) to assess the dynamic stability of piles (the allowable number of blows with the specified hammer). For example, prismatic piles with unstressed transverse bar reinforcement made of class B20 concrete crack at 210 blows (pile "C" according to Russian Standards) if one uses a 2.5 m rod hammer, 0.15 m thick oak layer and 2.2 m blow drop, complete breaking-up of the pile head occurs at 380 blows. Piling during 3.5 and 6.3 minutes corresponds to this number of blows, i.e. cracks appear in the pile in 3.5 minutes, and complete breaking-up of the pile head occurs in 6.3 minutes of piling.

If one uses 0.20 m oak layer and class B25 concrete piles incorporating the same equipment, cracking occurs at 410 blows, complete breaking-up—at 800 blows. When using tubular hammers, probability of pile breaking-up increases. If one uses a tubular hammer (instead of a rod hammer) with 1.8 *t* striking mass and 2.8 m blow drop, the number of blows which cause cracking will decrease to 50 blows in the first case (class B20 concrete and 0.15 m layer) and to 90 - in the second case. Complete breaking-up of the pile head should be expected at 200 and 370 blows respectively.

Thus, a designer is able to choose the pile lengths and number of piles; in here, not only the expected operational loads are taken, but also technological effectiveness of erecting the pile foundation is ensured: the piles are immersed to the specified depth within an acceptable time. For this purpose, the designer chooses an appropriate diesel hammer and the relevant strength (impact resistance) of the pile material in addition to the pile dimensions. If such a choice is difficult or impossible for any reason, the piles of shorter lengths are chosen, but in larger quantities. In here, material consumption of the foundation may either decrease or increase. Developed is the technique for the simplified CPT-based assessment of material consumption of two schematized pile foundations which take the same load (Ryzhkov & Isaev 2016). The first option involves the piles to be immersed to a given depth regardless of the "failures", the second one anticipates that they are immersed up to the specified insignificant "failure" regardless of the achieved depths. The depths are the same in the first option and pile trimming is not needed, but the number of piles is greater than in the second option. The pile bearing capacity is greater in the second option, the number of piles is smaller, and the immersion depths vary for each pile. The pile heads are cut down if the heads are above the designed ones.

The studies have shown that the material consumption of these schematized options depends on the rate of increase in pile resistances with depth; this is easily estimated by CPT data. If the rate of increase in pile resistances is over 100...150 kN/m (e.g., in availability of a strongly marked bearing stratum), decrease in the pile lengths with increase in their number is not economical, i.e. their material consumption will increase. On the contrary, piling to a given depth is more economical at a lower rate. No wonder that the ideal options have been consid-

ered, but numerous random factors, structural features of the buildings, texture of the bed, etc. can significantly affect the procedure in reality. Nevertheless, understanding of the situation at the schematic level always simplifies solution to the practical problems and helps optimal decisions to be made.

4 CONCLUSION

In Russia CPT aims at obtaining data for pile foundation engineering. CPT makes it possible to take into account the real heterogeneity of the soils at the investigated site, which, if necessary, is divided into sections and the pile bearing capacity is differentiated for each section. The ultimate resistances of driven piles are well-calculated, which is due to the use of sleeve friction resistance when calculating the resistance of soil on the pile side surface. When choosing the pile length and other parameters, the technological requirements for piling to the designed depth are to be taken into account.

REFERENCES:

Building Code SP 24.13330.2011 2011. Pile foundations. Moscow, 85 p.

Building Code SP 25.13330.2012 2012. Soil bases and foundations on permafrost soils. – Moscow, 117 p.

Flinn, C.N., McCabe and Egan D. 2014. Driven cast-in-situ piles in granular soils: applicability of CPT methods for pile capacity. In Proc. 3rd Int. Symposium on CPT. Las Vegas, Nevada, USA–2014. pp. 789–796.

Gotman, A.L. & Glazachev, A.O. 2014. Study on vertically loaded bored piles in clays and their calculation after CPT data // Bases, foundations and soil mechanics. №2. pp. 70–78.

Ryzhkov, I.B. & Isaev, O.N. 2016. Cone penetration testing of soils in geotechnics. Stockholm, Sweden: ASV Construction. 408 p.

Standard STO 36554501-049-2016 2016. “CPT Application for Soil Foundation Control on Permafrost. General guidelines”. NIIOSP. Moscow. 54 p.

Viana da Fonseca, A. 2010. Regional Report for Southern Europe. In Proc. 2nd Int. Symposium on CPT. Huntington Beach, CA, USA, May, pp.

Taylor & Francis
Taylor & Francis Group
http://taylorandfrancis.com

Cone Penetration Testing 2018 – Hicks, Pisanò & Peuchen (Eds)
© 2018 Delft University of Technology, The Netherlands, ISBN 978-1-138-58449-5

Comparison of settlements obtained from zone load tests and those calculated from CPT and PMT results

A. Sbitnev
Menard Middle East, Dubai, UAE

B. Quandalle
Menard, Rueil-Malmaison, France

J.D. Redgers
Consultant, UK

ABSTRACT: This paper presents a comparison of settlement results for a construction site where soil improvement by compaction methods was undertaken. A direct comparison of the settlements obtained during the execution of several Zone Load Tests (ZLT) with the settlements estimated based on the results of Cone Penetration (CPT) and Pressuremeter Testing (PMT) for the improved soil is shown. The post treatment PMT and CPT were carried out beyond the depth of the soil treatment. The associated calculations were necessary to predict the settlement of the zone load test adjacent to the test positions. The study addresses an important difference in the results often obtained from ZLT and the calculations performed prior to the execution of the ground improvement work. It also presents the actual site test results and compares them with the calculated settlement based on the comprehensive post treatment testing regime and shows the range of differences in predicted and actual settlements.

1 INTRODUCTION

A comparison of settlement results is presented for a construction site where soil improvement was undertaken by dynamic compaction and vibro compaction. However, due to the fact that vibro compaction was implemented within limited area of the treated site, only the area of the site improved by dynamic compaction is considered in this assessment.

Within the dynamically compacted area, the required bearing capacity for isolated footings varies from 200 kPa to 250 kPa as specified by the client for no more than 25 mm settlement. The energy input for the compaction alters according to the required bearing capacity. This is accomplished by using two different grids of (triangular or rectangular) compaction points. Based on the predesign the grids implemented for construction were 6.0 m by 6.0 m for the bearing capacity of 200 kPa and 4.25 m by 4.25 m for where the bearing capacity requirement is greater than 200 kPa. Based on the preliminary tests, an average depth of improvement to 8.0 m was necessary with the maximum depth of 10.0 m from the working platform.

In terms of testing, three number ZLT, four number PMT and twenty-four number CPT with pore pressure measurement were undertaken in line with the project specification. Please refer to Figure 1 for the general project layout.

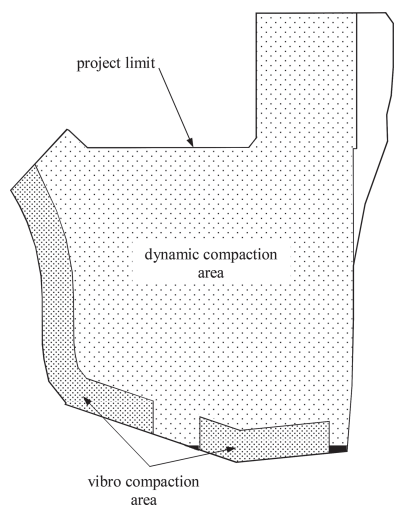

Figure 1. General project layout including areas improved by dynamic compaction (considered in the paper) and vibro compaction techniques.

2 SOIL CONDITIONS

The project site is located approximately 1 km north of Seeb International Airport, Muscat, Oman. The ground surface is generally flat and covered with fill material consisting of a silty sand. The site is located on the Batinah coast and can be divided into five geological units. The sub-surface materials consist of variably cemented deposits of Quaternary age underlain by Tertiary sedimentary rock:

1. Beach sands—a strip of beach sand along the coast consists of slightly silty fine to medium sand with shell fragments.
2. Recent near shore deposits—these sediments are composed of reworked alluvium and marine sediments extending from coastal plain.
3. Sub-recent alluvium—sands and gravels have been primarily deposited during storms and display a wide range of grain size decreasing from piedmont to coast. This alluvium is better graded and bedded, locally cemented.
4. Ancient alluvium—this alluvium comprises poorly graded, reddish brown and yellow variably cemented sandy gravels, with cobbles originating from Hawasina and Samail nappes.
5. Tertiary sedimentary Rock—this unit consists of variably weathered, pinkish yellow, mottled red calcareous Conglomerate containing rounded Chert, Quartzite and limestone in a matrix of calcareous silt. This unit underlies the entire project site.

However, only the upper 8 to 10 metres of the site are of interest due to their initial loose state and the subsequent application of soil treatment to increase their stiffness within the envisaged thickness in order to achieve the project specification by means of the available bearing capacity, limitation of absolute and differential settlements as well as mitigation of the risk of liquefaction for the design level seismic event.

The general soil conditions are anticipated to be as follows:

- Ground water was encountered during the investigation period: from +1.50 m CD to +2.50 m CD;
- Final ground level: +6.10 m CD;
- Working platform level for execution of soil improvement works: +3.75 m CD;
- Foundation base elevation: +2.20 m CD;
- Particle size distribution curves for boreholes for the depth of improvement (from +3.75 m CD to −6.25 m CD) represent the natural sandy material.

All of the tests carried out (pre and post treatment) demonstrate that the site is generally represented by homogeneous reclaimed fill material with low fines content of less than 10% passing the 63 micron sieve. Figures 2 and 3 present the averaged profiles prepared from the post CPT and PMT test results within the area subjected to dynamic compaction.

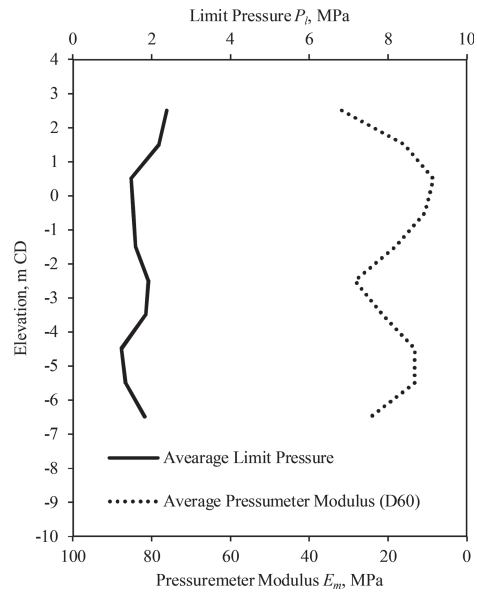

Figure 2. Average PMT profile.

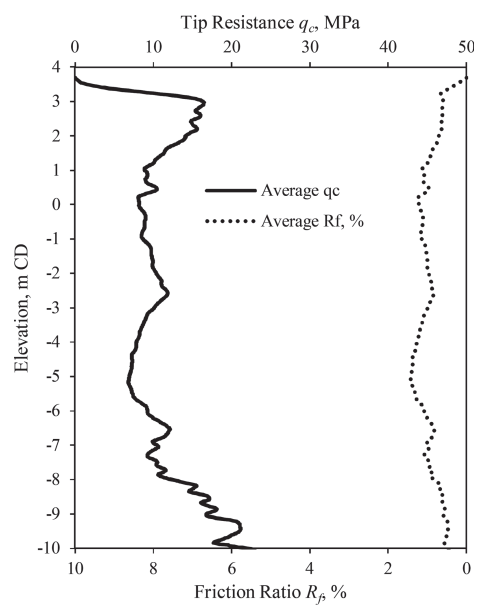

Figure 3. Average CPT profile.

After completion of the soil improvement works, the soil stiffness shows only minor variations in the test profiles, both horizontally and vertically indicating the improved homogeneity of the site. The achieved stiffness of the soil meets the project requirements, as shown by post treatment testing. Despite post compaction tests providing satisfactory results, an important difference between the settlements obtained from ZLT and those calculated from the PMT and CPT is noticed and warranted further investigation and is presented here.

3 ZONE LOAD TEST (ZLT) RESULTS

As part of the quality control three zone load tests were performed within the area improved by the dynamic compaction.

A zone load test program was completed employing a kentledge system in accordance with ASTM D1196/D1196M-12 by a third party. The test load is produced by a hydraulic jack activated by a pump. The pressure, as registered by means of a pressure gauge, is used to determine the magnitude of the applied load. The size of the plate utilized for the ZLTs is 2.5 m by 2.5 m; the plate is situated on the top of the levelled and compacted working platform.

A platform carrying concrete blocks provides the reaction to the hydraulic jack. An array of secondary steel beams and main test beam supports the platform. As the load is incrementally applied, the deflections (settlements of the plate) are measured relative to the fixed reference beams using dial gauges. Such deflections are monitored for each loading increment using four dial gauges with a scale value of 0.01 mm up to a range of 50.0 mm. The loading and deflection of the plate is measured against time.

The loading procedure is summarized in Table 1.

Table 1. ZLTs loading cycle.

Load (% of design load)	Load holding time hours	Stage
15%	0.5	Preloading
0%	1	Loading
25%	2	Loading
50%	2	Loading
75%	2	Loading
100%	6	Loading
125%	6	Loading
150%	12	Loading
100%	2	Unloading
50%	2	Unloading
0%	2	Unloading

Table 2. Actual applied pressures and obtained during ZLTs settlements.

% of design load	ZLT-01		ZLT-02		ZLT-03	
	p kPa	Δ mm	p kPa	Δ mm	p kPa	Δ mm
0%	0.0	0.0	0.0	0.0	0.0	0.0
25%	56.5	0.42	62.8	0.27	50.2	0.46
50%	113.0	1.02	125.6	0.84	100.5	1.11
75%	169.5	1.48	186.8	1.67	150.7	1.53
100%	224.5	2.33	249.6	2.78	199.3	2.08
125%	281.0	2.76	312.4	3.75	249.6	2.78
150%	337.5	4.80	375.1	4.98	299.8	4.39

The actual applied pressure along with the recorded corresponding settlements for each test during the loading phase are given in the Table 2.

Generally, the settlements represent a similar behaviour as expected from the resembling soil profile, and show only minor variations under the design pressures as well as under the maximum applied stress of 150% of the design load with settlements not exceeding 5 mm of the planned and calculated 25 mm.

4 PRESSUREMETER TEST (PMT) RESULTS

As part of the quality control four PMT were carried out within the area improved by dynamic compaction. However, only the three tests located in the vicinity of the zone load tests are considered in this study and are therefore used for the settlement calculation comparisons, as being the most representative of the soil conditions in relation to the location of ZLT.

The following PMT tests are used for comparison with the corresponding ZLT tests:

- ZLT-01 and PMT-01 (project ref. PMT-KH-201)
- ZLT-02 and PMT-02 (project ref. PMT-KH-202)
- ZLT-03 and PMT-03 (project ref. PMT-KH-206)

Based on the results of the PMT data, and the pressuremeter modulus in particular, the settlements are calculated for the same pressures being applied during execution of the zone load tests. The calculation model used is as per Paragraph 4 of the French Standard, D60 AN "Interpretation and Application of Pressuremeter Tests Results to Foundation Design". In this document, the settlement is given by Equation 1 below:

$$s = \frac{1.33}{3E_B} p R_0 \left(\lambda_2 \frac{B}{2R_0} \right)^{\alpha} + \frac{\alpha p \lambda_2 B}{9E_A} \quad (1)$$

where E_A = equivalent pressuremeter modulus corresponding to the zone of volumetric influence, E_B = equivalent pressuremeter modulus corresponding to the zone of deviatoric influence, p = contact pressure added to the soil by the footing, R_0 = reference length equal to 0.30 m, α = structure coefficient variable according to the nature of the soil and the ratio E/P_L, λ_1 & λ_2 = shape coefficients, which are function of the length to width ratio of the foundation; and B = width of footing.

When comparing PMT calculations to the more known or conventional methods of settlement calculations such as the commonly used Schmertmann method, differences become apparent. The main feature and distinction of the design scheme used for settlement prediction based on pressuremeter testing is the definition of the effective depth, which is equal to 8B below the foundation base level, where B is a width of footing, as opposed to the Schmertmann where a depth equal to 2B is considered for square footings.

The results of the calculations performed for each PMT and for each step of loading of the corresponding zone load test are summarized in the Table 3 below.

The estimation of the settlements is based on the methodology provided in the D60 standard and includes both immediate (spherical) and maximum (deviatoric) components, i.e. computed values are corresponding to the total settlements of the soil beneath the footing, not just the immediate deformations. Furthermore, it is shown in Table 3 that the calculated settlement values are generally 150% to 300% higher than those obtained during zone load tests. It is noted that the difference decreases with the increase of load. This relation between applied pressure and obtained settlements could be explained by the loading schedule during ZLT's increases from 2 hours for low pressures up to 12 hours for the maximum load, thus higher settlements occur under the higher pressure, perhaps when held for a longer duration being more representative.

Table 3. Considered pressures and calculated settlements based on PMT results.

% of design load	PMT-01		PMT-02		PMT-03	
	p kPa	Δ mm	p kPa	Δ mm	p kPa	Δ mm
0%	0.0	0.0	0.0	0.0	0.0	0.0
25%	56.5	1.42	62.8	1.22	50.2	1.30
50%	113.0	2.49	125.6	2.45	100.5	2.59
75%	169.5	3.73	186.8	3.64	150.7	3.89
100%	224.5	4.94	249.6	4.86	199.3	5.14
125%	281.0	6.19	312.4	6.09	249.6	6.44
150%	337.5	7.43	375.1	7.31	299.8	7.74

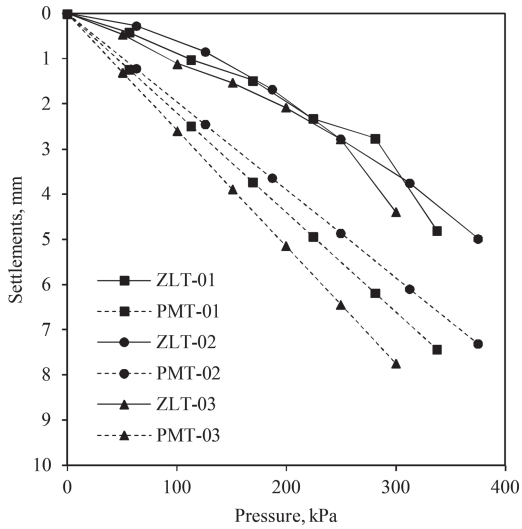

Figure 4. Obtained (continuous lines—ZLT) and calculated (dotted lines—PMT) of settlement vs pressure.

5 CONE PENETRATION TEST (CPT) RESULTS

In total 32 CPTs were carried out within the area subjected to soil improvement but only 24 tests are located in the part of the site improved by dynamic compaction. Out of these 24 tests, only the three closest to the related zone load tests are considered and used for the settlement calculations.

The following CPTs are used for comparison with the corresponding ZLTs:

- ZLT-01 and CPT-01 (project ref. CPT-KH-202)
- ZLT-02 and CPT-02 (project ref. CPT-KH-212)
- ZLT-03 and CPT-03 (project ref. CPT-KH-222)

Based on the tip resistance of the soil obtained from the CPTs, the immediate settlements are calculated for the same pressures as those applied during the execution of the zone load tests. The immediate foundation static settlements are calculated based on the semi-empirical method of Schmertmann (1970).

Since the load for the zone load tests was applied during a limited period of time (only 34 hours), the creep correction factor C_2 is taken to be equal to 1.0 for the current study. Moreover, two different approaches are considered for the definition of the Young's modulus based on the tip resistance:

- The approach introduced by Schmertmann (1978) where the ratio between the Young's

modulus and the tip resistance is fixed and equal to 2.5.

– The approach introduced by Robertson (2015), where the ratio α between the Young's modulus and tip resistance depends on the soil behavior type index I_c:

$$E = \alpha \cdot \left(q_t - \sigma_{V0}\right) \tag{2}$$

where α = alpha factor, q_t = cone penetration resistance corrected for pore water effects; and σ_{V0} = total vertical stresses.

$$\alpha = 0.015 \cdot \left[10^{0.55 \cdot I_c + 1.68}\right] \tag{3}$$

where I_c = soil behaviour type index.

The results of the settlement calculations performed for each CPT based on the pressure increments and the two methods of alpha determination are summarized in Tables 4 & 5 respectively.

The settlements calculated from the CPT tip resistance and alpha ratio of 2.5 are 500–900% greater than those obtained during zone load tests. Meanwhile, the settlements calculated by considering Robertson's approach are 300% to 500% greater

Table 4. Considered pressures and settlements estimated based on CPT with consideration of $\alpha = 2.5$.

% of design load	CPT-01		CPT-02		CPT-03	
	p kPa	Δ mm	p kPa	Δ mm	p kPa	Δ mm
0%	0.0	0.0	0.0	0.0	0.0	0.0
25%	56.5	3.41	62.8	3.36	50.2	3.15
50%	113.0	7.67	125.6	7.52	100.5	7.04
75%	169.5	12.36	186.8	12.00	150.7	11.31
100%	224.5	17.28	249.6	16.95	199.3	15.73
125%	281.0	22.64	312.4	22.19	249.6	20.57
150%	337.5	28.28	375.1	27.70	299.8	25.63

Table 5. Considered pressures and settlements estimated based on CPT with consideration of α as per Robertson (2015).

% of design load	CPT-01		CPT-02		CPT-03	
	p kPa	Δ mm	p kPa	Δ mm	p kPa	Δ mm
25%	56.5	1.14	62.8	1.12	50.2	1.05
50%	113.0	2.56	125.6	2.51	100.5	2.35
75%	169.5	4.12	186.8	4.00	150.7	3.77
100%	224.5	5.76	249.6	5.65	199.3	5.24
125%	281.0	7.55	312.4	7.40	249.6	6.86
150%	337.5	9.43	375.1	9.23	299.8	8.54

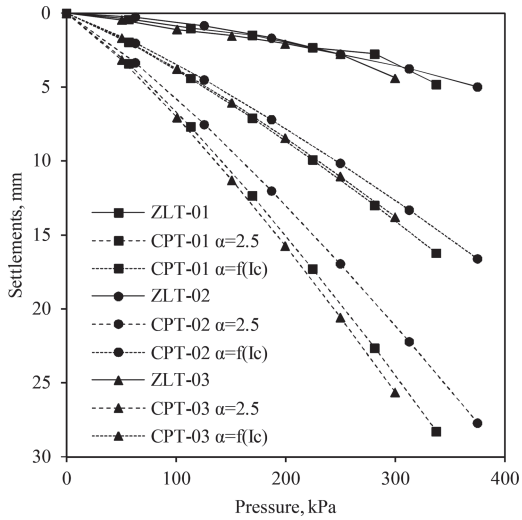

Figure 5. Obtained (continuous lines) and calculated based on CPT results (dotted lines with α as per Robertson (2015) and dotted lines with α of 2.5) settlements against pressure applied during ZLTs.

than the actual obtained values. These are notable differences between estimated and actual deformations. This can lead us to revisit our assumptions and, where we can, apply engineering judgement or other learned sources for greater accuracy and hence time and cost savings from the more suitable application of knowledge. Presented nonconformity could be due to the use of the actual measured cone penetration resistance as is, with no application of a carbonate correction factor accounting for the crushability of shell fragments or high compressibility of the carbonate sands, present on site, which would have led to an increased stiffness and hence lower calculated settlements as reported by Al-Homoud and Wher (2006). Notwithstanding the above, the influence of the presence of carbonate sand with shell fragments is not addressed in the current paper, as no appropriate testing allowing assessment of the influence of such material is available for the concerned project.

The same trend of a decrease in ratio with the CPT as for PMT testing is noticed, i.e. the difference is decreasing with the increase of load. Although, the decrease is lower than that achieved by the PMT testing.

However, to align the settlement values calculated from CPT testing to those calculated from PMT testing, the ratio between the tip resistance and the Young's modulus has to be approximately equal to 7.5. According to Bowles (1997), this value corresponds to the lower bound of the typical ratios for overconsolidated sands, considered

as appropriate after dynamic compaction or other such soil improvement where the soils under treatment are exposed to greater stresses. Thus, after treatment they exhibit an overconsolidation ratio OCR greatly in excess of 1 after the application treatment that increases the horizontal and vertical stresses from the action of pounders as outlined by Fellenius (2002) or vibrators as reported by Massarsch (2002).

6 CONCLUSIONS

The paper presents a case study of a direct comparison of the settlements obtained during the execution of several zone load tests (ZLT) with the settlements estimated based on the results of cone penetration (CPT) and pressuremeter (PMT) testing for the soil improved by dynamic compaction. The following key points can be summarized.

1. The use of the pressuremeter testing for settlement predictions provides good convergence with the actual settlements obtained in the field during the performance of the zone load test in coarse-grained soil.
2. The initial methodology of settlement calculations based on the outcome of cone penetration tests provided by Schmertmann is resulting in higher values of settlements when compared to the actual observed deflections of the zone load tests performed over improved coarse-grained reclamation fill, and that of the pressuremeter.
3. The ratio of 2.5 between the Young's modulus and the cone penetration resistance is at lower limit and could be applicable for normally consolidated soils in natural state but not for sandy soils being treated with the use of one of the soil improvement techniques. Therefore, ratios typical for overconsolidated sands such as 7.5 can be recommended as appropriate after dynamic compaction and/or vibro compaction, when the site stress/strain state has been changed by the treatment.
4. Robertson's approach to define the actual ratio between the Young's modulus and the tip resistance provides more relevant and accurate settlement predictions of isolated footings placed over material with low fines content, since it is based not only on soil stiffness but also on the behavior of the soil.
5. Nevertheless, the methodology of estimation of Young's modulus from CPT results proposed by Robertson (2015) results in conservative values of predicted settlement when comparing to the settlements calculated based on PMT results.
6. Further case histories and studies of the direct comparison of the settlement estimation based on CPT and ZLT results should be completed and analyzed in order to specify and refine the ratio between cone penetration resistance and Young's modulus as the currently used approach is generally conservative. Especially in carbonate sands containing high percentage of shell fragments and those with a changed stress regime.

REFERENCES

Al-Homoud, A. & Wehr, W. 2006. Experience of vibro-compaction in calcareous sand of UAE. *Geotechnical and Geological Engineering*, 24 (3), 757–774.

Bowles, J.E. 1997. *Foundation Analysis and Design*, International Edition.

Fellenius, B. & Massarsch, K. 2001. Dynamic compaction of coarse grained soils—a case history. *The 54th Annual Canadian Geotechnical Conference*

Massarsch, K.M. & Fellenius, B.H. 2002. *Dynamic compaction of granular soils*, Canadian Geotechnical Journal, Vol. 39 (3), 695–709.

Massarsch, K.M. 2002. *Ground vibrations caused by soil compaction*. Wave 2002. Proceedings International Workshop, Okayama, Japan, 25–37.

Robertson, P.K. 1990. Soil classification using the cone penetration test. *Canadian Geotechnical Journal*, 27 (1), 151–158.

Robertson, P.K. & Cabal, K.L. 2015. *Guide to Cone Penetration Testing for Geotechnical Engineering*, 6th Edition, Signal Hill, California, Gregg Drilling & Testing, Inc.

Schmertmann, J.H. 1970. Static cone to compute static settlement over sand. *ASCE Journal of Soil Mechanics & Foundations Division*, 96 (3), 1011–1043.

Schmertmann, J.H., Hartmann, J.P. & Brown, P.R. 1978. Improved strain influence factor diagrams, *ASCE Journal of the Geotechnical Engineering Division*, 104 (GT8), 1131–1135.

Cone Penetration Testing 2018 – Hicks, Pisanò & Peuchen (Eds)
© 2018 Delft University of Technology, The Netherlands, ISBN 978-1-138-58449-5

Direct use of CPT data for numerical analysis of VHM loading of shallow foundations

J.A. Schneider
USACE, St. Paul, MN, USA

J.P. Doherty
The University of Western Australia, Crawley, WA, Australia

M.F. Randolph
Centre for Offshore Foundation Systems, The University of Western Australia, Crawley, WA, Australia

K. Krabbenhøft
University of Liverpool and Optum CE, Liverpool, England, UK

ABSTRACT: CPT data are often used directly for geotechnical analyses, such as for pile capacity. Advances in automated mesh generating strategies now allow for direct use of CPT data within finite element analyses. This paper presents the results of finite element analyses of shallow foundations with widths varying between 0.5 m and 30 m resting on an offshore soft clay having strength linearly increasing with depth below a crust. Results based on a soil profile using CPT data directly input into the finite element soil model at depth increments of 25 mm are compared with results based on a soil profile with strength linearly increasing with depth below a crust with constant strength. The effects of mesh density and use of remeshing strategies on model run time and results are discussed. Results indicate that numerical analyses based on direct incorporation of a CPT profile may allow for identification of failure surfaces that result in lower optimized capacities than those that try to fit strength using simpler soil profiles.

1 INTRODUCTION

Undrained shallow foundations resistance under vertical (V), horizontal (H), moment (M), and combined (VHM) loading is proportional to undrained strength (s_u). Strength increasing with depth and shallow crusts will influence the size of the bearing capacity mechanisms, operational undrained strength, and ultimate resistance (e.g. Davis & Booker 1973, Gourvenec & Randolph 2003, Feng et al. 2015). To account for these effects, undrained strength (s_u) can be modeled as linearly increasing with depth (z) from a surface value ($s_{u,0}$):

$$s_u = s_{u,0} + kz \tag{1}$$

For clays with a uniform strength crust (of $s_{u,0}$) over strength increasing proportionally with depth below mudline, an expression for undrained strength is:

$$s_u = \max(s_{u,0}, kz) \tag{2}$$

Soil profiles in this paper take the form of Eq. 2.

There will be some variability around an idealized design profile in natural soils which can effect bearing capacity (e.g., Griffiths & Fenton 2001). This paper explores whether averaging out of such variability over the relevant vertical range results in little effect on the computed foundation capacity, or whether the presence of variability, as indicated by a CPT profile, may allow for lower resistance shallow foundation mechanisms to form.

Undrained strength estimated from two cone penetration profiles are used to compare numerical analysis of shallow foundation response under vertical (V) and combined (VHM) loading. Linear fits to s_u estimated from net cone tip resistance ($q_n = q_t - \sigma_{v0}$), as well as s_u estimated from CPT data directly, were used for numerical analysis of shallow foundation capacity.

The questions this paper aims to address are:

- Do results of shallow foundation bearing capacity analyses based on linear strength profiles differ from those based on CPT data input directly?
- If results differ, is the difference due to the meshing inaccuracies or due to the formation of a lower resistance mechanism?

- Do analyses based directly on CPT data take significantly longer to run for the same mesh density?
- Are finer meshes required for bearing capacity analyses based directly on CPT data to achieve comparable numerical accuracy?

Most of these questions are addressed by comparing numerical analysis results to results obtained using plastic limit analysis, specifically the normalized strength factors presented for a crust overlying strength increasing proportionally with depth (see Figure 12 in Davis & Booker 1973). The method assessment is followed by an example of VHM loading analysis of a tidal turbine foundation on soft clay.

2 SOIL PROFILES

Two profiles of s_u estimated from q_n from an offshore soft clay site (GOG 6, Low et al. 2010) are shown in Figure 1 and 2. The data were converted

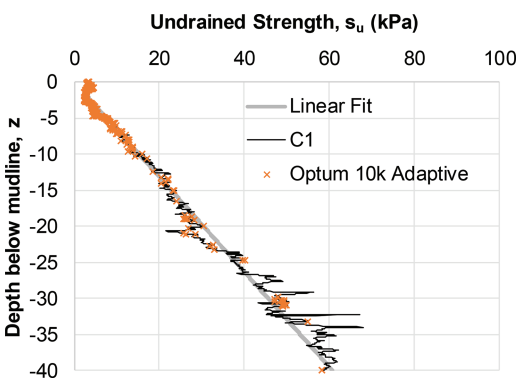

Figure 1. Comparison of CPT-1 profile to crust over k linear fit.

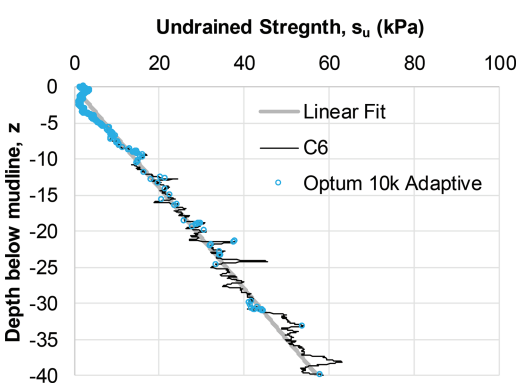

Figure 2. Comparison of CPT-6 profile to crust over k linear fit.

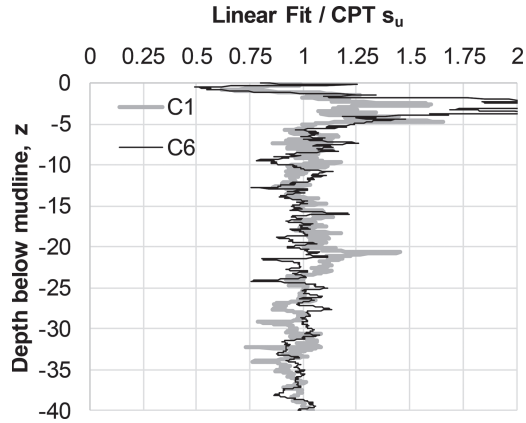

Figure 3. Ratio of linear fit of q_n to measured CPT q_n profile.

Table 1. Summary of linear strength parameters fit to CPT data.

CPT	$s_{u,0}$ (kPa)	Crust thickness (m)	k (kPa/m)	COVs_u Upper 5 m	COVs_u 40 m profile
CPT-1	2.9	1.9	1.52	0.21	0.12
CPT-6	1.9	1.325	1.43	0.40	0.27

to undrained strength using $s_u = q_{net}/N_{kt}$ and an N_{kt} factor of 13.5. A constant ratio of G/s_u of 75 was used in elastoplastic analyses. The data indicate a shallow crust with strength increasing with depth (from an intercept of 0) below the crust.

Linear trends were fit by first determining the crust strength as the median cone tip resistance in the upper 3 m of the profile. The slope of cone penetration tip resistance increasing with depth was adjusted until the median ratio of the linearly fitted s_u to that measured from cone tip resistance was unity for the entire 40-meter profile. Linear profiles are underlain in gray in Figures 1 and 2, and the ratios of calculated to measured net cone tip resistance are shown in Figure 3. There is greater variability in CPT-6 compared to CPT-1, in particular in the upper 5 m of both profiles compared with the variability at greater depths. Combined crust and linear fits to the CPT data are summarized in Table 1.

3 MODEL SETUP AND ANALYSIS METHODS

Finite element analysis (FEA) and Finite element limit analysis (FELA) were performed using the

computer software Optum G2 (Optum CE 2017). Footings were modeled in plane strain as weightless rigid plates of width *B*, centered in a domain 15*B* wide, and 2.5*B* deep. Two types of meshing were used in analysis; (i) a uniform distribution of elements; and (ii) adaptive meshing. Adaptive meshing used standard parameters (Optum CE 2017) which updates the mesh three times during the analysis, increasing the number of elements in locations of, in this case, high shear dissipation (shear stress times shear strain rate at failure).

Within Optum G2, strength profiles for a layer can be input as (i) constant; (ii) linearly increasing with depth; (iii) varying with depth from a tabular input; and (iv) varying laterally and vertically from a tabular input. Undrained strength based on CPT data was input in 0.025 m increments using option (iii). Crusts were modeled using option (i), and the underlying strength increasing with depth was modeled using option (ii). The points in Figures 1 and 2 indicate strength values interpolated by the software for one of the cases in this study; a 16 m wide footing analyzed with 10,000 elements using adaptive remeshing.

Initially, four types of analysis were performed, with detailed descriptions of each analysis type in Optum CE (2017):

1. Lower bound (LB) FELA
2. Upper bound (UB) FELA
3. Strength reduction (SR) FEA using 6-node Gauss elements (Krabbenhoft and Lyamin 2015)
4. Multiplier elastoplastic (MEP) FEA using 6-node Gauss elements (Krabbenhoft et al 2007)

When analyses were performed for an isolated loading condition (V, H, or M), plate boundary conditions were selected to restrict movement in non-loaded directions. For example, when vertical capacity was assessed, the plate was not allowed to translate horizontally or rotate. When combined loading was investigated, no structural restraints were used.

Figures 4 and 5 illustrate aspects of analysis type. The four analysis methods were applied to CPT and linear strength profiles based on CPT-1, using 10,000 elements, once with adaptive meshing, and once without, and resulting in four groups of the analyses. Main observations include:

- SR and MEP results lie between LB and UB FELA results.
- The range of results is small when adaptive meshing is used.
- Analyses were performed on a laptop with 16 GB of RAM, and a 2.8 GHz Intel i7–7700HQ four core processor with hyperthreading. FELA analyses tended to take about 15 seconds. The multiple iterations involved with a strength reduction analysis increased the average duration by about 5 times to 75 seconds. MEP analyses involved 10 elastic and 10 plastic stages, and increased duration by 30 times over FELA to about 450 seconds.
- There is no apparent difference in run time for soil profiles based on tabulated CPT data as compared to linear profiles.

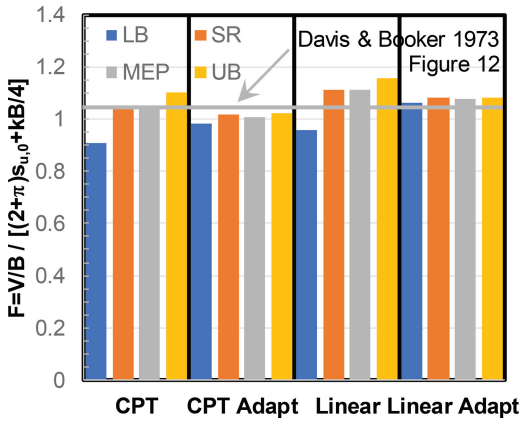

Figure 4. Comparison of results for four types of analysis, two types of strength profile (CPT & linear) and two types of meshing (uniform and adaptive).

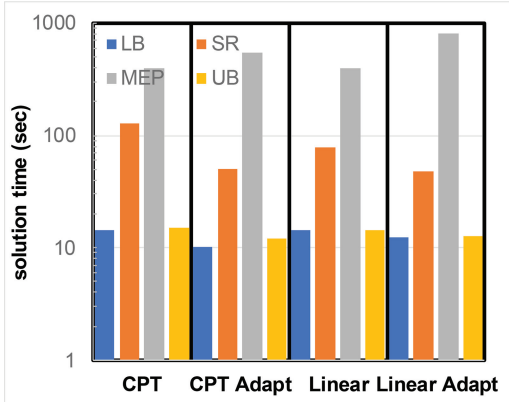

Figure 5. Time to reach solution for method, meshes and profiles in Figure 4.

Due to shorter runs times and ability of UB and LB FELA analysis to narrowly bound the problem, results from these two types of FELA are the focus of the remainder of the paper.

4 MESH DENSITY

The influence of mesh density on collapse load can be inferred from Figures 6 and 7 for linear and

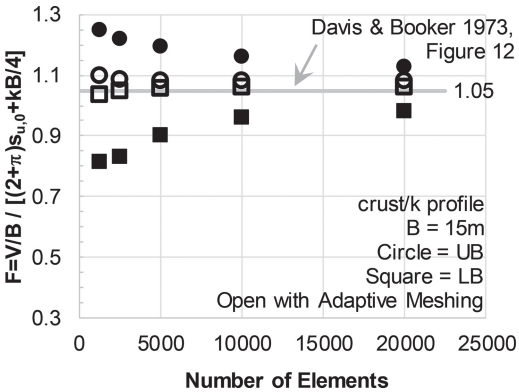

Figure 6. Influence of number of elements used in analysis on upper bound and lower bound FELA results for 15 m wide footing and crust over k linear fit profile.

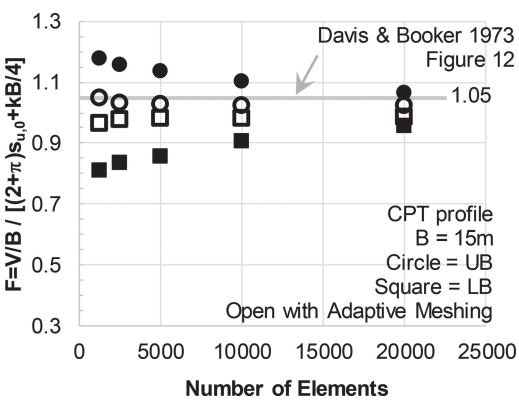

Figure 7. Influence of number of elements used in analysis on upper bound and lower bound FELA results for 15 m wide footing and CPT based profile.

CPT profiles, respectively. A 15 m wide footing with strength profiles based on CPT-1 was used for this comparison. It is noted that:

- Adaptive meshing more rapidly converges to a smaller difference between LB and UB results as compared to a uniform mesh.
- LB results are > 98% of UB results when using adaptive meshing and for linear strength profile cases with more than 10,000 elements. This reduces slightly for CPT based profiles, with LB results > 96% of UB results when using adaptive meshing and more than 10,000 elements.

The range between UB and LB results is essentially constant in this case for more than 5,000 elements when using adaptive meshing. The analyses reported in the rest of the paper are based on 10,000 elements with adaptive meshing.

5 WIDTH EFFECTS

Davis & Booker (1973) indicated normalized vertical capacity (F) increased with $kB/s_{u,0}$, up to a value of about 20, reducing with further increases. For values of k in Table 1, $kB/s_{u,0}$ of 20 corresponds to footings up to 38 m in width. Differences in normalized vertical capacity are shown for footing widths between 0.5 and 36 m for linear and CPT based profiles in Figures 8 and 9, for CPT-1 and CPT-6, respectively. The linear profiles match well with the results from Davis & Booker (1973), but normalized vertical resistance factor, F, based on the CPT profile are up to 15%

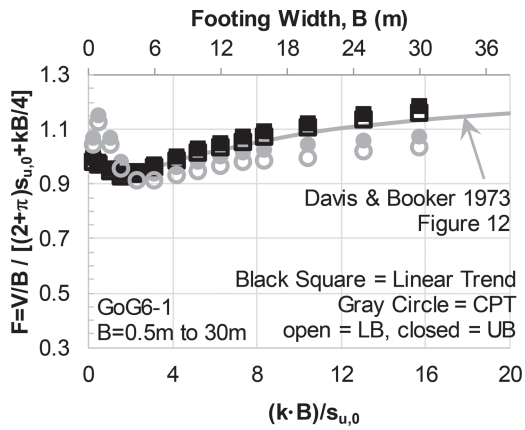

Figure 8. Influence of width on normalized bearing capacity for CPT-1 directly using CPT profile and using linear crust above proportional strength profile.

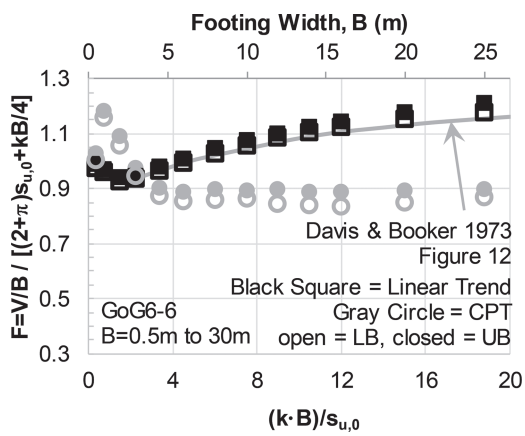

Figure 9. Influence of width on normalized bearing capacity for CPT-6 directly using CPT profile and using linear crust above proportional strength profile.

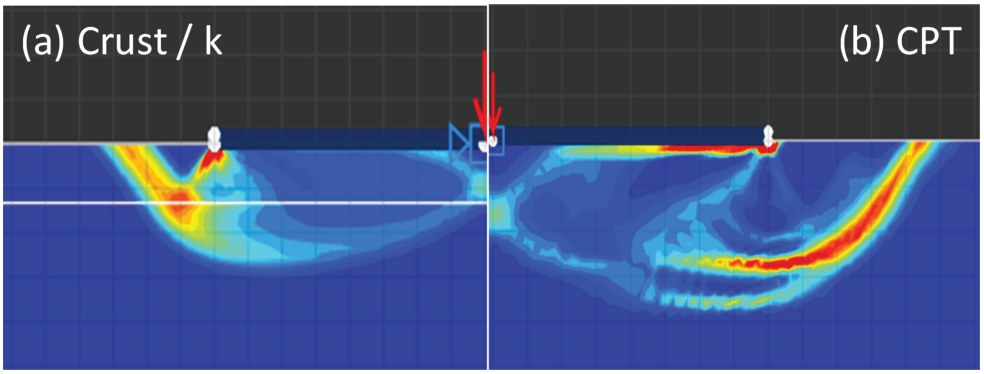

Figure 10. Shear strain contours for upper bound analysis of a footing width of 16 m for profile CPT-6 using (a) a crust over strength increasing proportionally with depth model; and (b) CPT based s_u profile.

higher for footing widths less than about 3 to 4 m, and lower by a similar amount thereafter. These differences are consistent with the differences between the linear and CPT based s_u profiles in Figures 1–3, highlighting difficulties in simplifying strength profiles.

The F values for CPT-6 tend to be lower than those for CPT-1. This can largely be attributed to the weak layer between 3 and 5 m depth in the CPT-6 based profile. Contours of shear strain are shown in Figure 10, which indicate a deeper failure mechanism passing through the underlying weak soil for the CPT based analysis as compared to the linear profile.

6 COMBINED LOADING

A comparison of yield envelopes for VHM loading of CPT based strength profile, and the crust above proportionally increasing strength profile is made using the loading and geometry for a tidal turbine system, discussed by Maynard et al. (2013). The strength profile based on CPT-6 was used in this comparison, as it showed the largest difference for the vertical loading case with wide footings. The foundations system was modeled as a conjoined skirted system (e.g., Gourvenec & Steinepepreis 2007, Gourvenec & Jensen 2009) with (B) 3.5 m wide suction (plane strain) 'caissons' at the two edges; (d) 1.75 m long skirts; and (s') 18.5 m wide center to center footing spacing. Full interface friction (of $s_{u,0}$) and no breakaway conditions were assumed on the soil-skirt interfaces.

The submerged weight of the structure was estimated at 70 kN/m (Maynard et al. 2013). For this example, the maximum horizontal load was assessed for pure horizontal loading (e = 0 m), as well as loading heights of e = 5, 10, 15 (shown in Figure 11) and 20 m. Pure moment loading was also considered.

Results are summarized in Table 2 for the crust over strength increasing proportionally with depth profile, and Table 3 for the CPT based s_u profile. Figure 11 shows contours of shear strain within a deformed mesh after approximately 1 m of displacement. The failure patterns indicate an essentially isolated footing sliding response, with downstream rotation and plunging.

The simplified linear strength profile results in 60% higher vertical resistance than the CPT based profile. Once again, this is attributed to the soft layer from 3 to 5 m depth in CPT-6. For low moments (e·H), horizontal load for the two cases is similar, because average strength in the crust is similar for the two cases. For the CPT case, the weak layer dominates at higher moments resulting in much lower calculations of horizontal loads that can be resisted.

Normalized combined HM response is plotted in Figure 12, with the isolated footings normalized to width in terms of sliding, and width added to the spacing for moment resistance of the rigidly connected pair. The linear strength profile case tends to match well with results in Gourvenec & Barnett (2011) in terms of normalized moment near 1.15 to 1.3, but tends to be higher in terms of normalized horizontal resistance at 4 instead of approximately 3 for d/B of 0.5. The much lower moment resistance for the CPT based analysis is in part due to the higher fraction of vertical capacity mobilized by the 70 kN/m submerged weight of the structure, but more due to the concentration of the failure surface within a weak zone underlying a strong zone that is typically not accounted for in generalized methods.

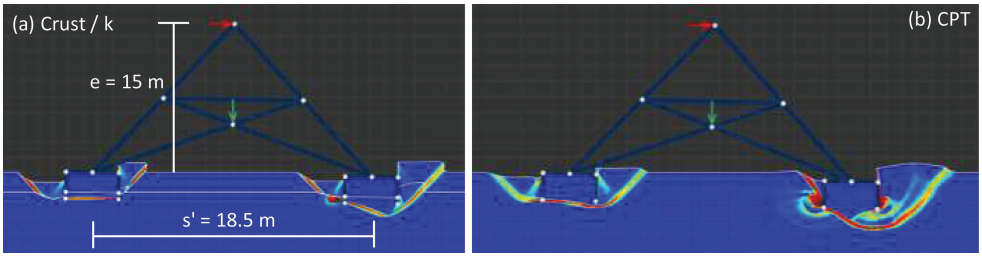

Figure 11. Shear strain contours for upper bound analysis of a conjoined pair of 3.5 m wide skirted foundations with a 1.75 m skirt length spaced by 18.5 m and an eccentricity (e) of 15 m for profile C6 using (a) a crust over strength increasing proportionally with depth model; and (b) CPT based s_u profile.

Table 2. Results from combined analysis using linear strength profile.

Analysis	e (m)	V (kN/m)	UB H (kN/m)	LB H (kN/m)
V	–	184.6	–	–
VH	0	70	54.6	53.3
VHM1	5	70	52.3	51.0
VHM2	10	70	48.8	47.4
VHM3	15	70	44.5	43.2
VHM4	20	70	40.2	38.9
Analysis	**e (m)**	**V (kN/m)**	**UB M (kNm/m)**	**LB M (kNm/m)**
M	–	70	1096	1053

Table 3. Results from combined analysis using CPT based strength profile.

Analysis	e (m)	V (kN/m)	UB H (kN/m)	LB H (kN/m)
V	–	115.7	–	–
VH	0	70	54.5	52.2
VHM1	5	70	40.1	36.9
VHM2	10	70	34.3	31.2
VHM3	15	70	27.4	24.5
VHM4	20	70	21.5	19.1
Analysis	**e (m)**	**V (kN/m)**	**UB M (kNm/m)**	**LB M (kNm/m)**
M	–	70	456.3	401.9

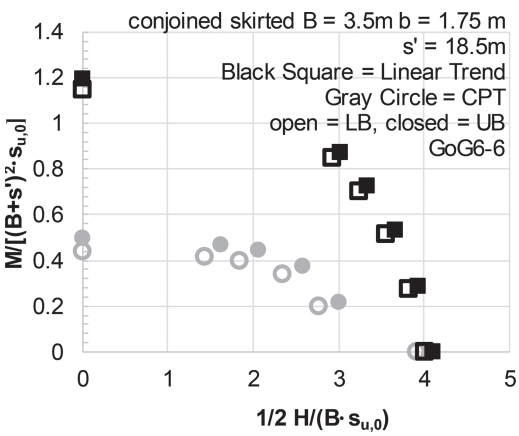

Figure 12. Influence of width on normalized bearing capacity for CPT-6 directly using CPT profile and using linear crust over k profile.

7 SUMMARY AND CONCLUSIONS

This paper summarized results from FEA and FELA of undrained loading of shallow foundations on a soft clay profile with strength increasing proportionally with depth below a uniform strength crust to assess whether analysis based on a detailed strength profile from CPT data produced results that differed significantly from simplified linear strength profiles. It is concluded that:

1. Analysis with strength profiles based directly on CPT data were more likely to be influenced by weak layers within nominally uniform material. These features do not necessarily average out in analysis.
2. When using adaptive meshing, the differences in results do not appear to be due to meshing issues, but the potential for more complex mechanisms to develop, taking advantage of weaker soils.
3. Solution times for models with strength based on detailed CPT profiles were of similar duration compared to analyses based on linear strength profiles.
4. It is arguable that a finer mesh may be needed when using CPT based strength profiles. However, when using 10,000 elements and adaptive meshing, the differences between upper bound and lower bound solutions was less than 5%.

It is acknowledged that similar results can be obtained using a CPT based profile or an idealized

linear profile that includes soft layers. However, the selection of the soil strength profiles can be subjective and may differ significantly between analysts. The ability to perform analyses rapidly with strength profiles that are based directly on high (vertical) resolution digital CPT data provides a rational approach for assessing potential failure modes and a step towards more consistent foundation design in practice.

REFERENCES

Davis, E.H., and Booker, J.R. (1973). "The effect of increasing strength with depth on the bearing capacity of clays." Géotechnique, 23(4): 551–563.

Feng, X., Gourvenec, S., Randolph, M.F., Wallerand, R., and Dimmock, P. (2015). "Effect of a surficial crust on mudmat capacity under fully three-dimensional loading." Géotechnique, 65(7): 590–603.

Gourvenec, S. and Randolph, M.F. (2003). "Effect of strength non-homogeneity on the shape of failure envelopes for combined loading of strip and circular foundations on clay." Géotechnique, 53(6): 575–586.

Gourvenec, S. and Steinepreis, M (2007). Undrained limit state of shallow foundations acting in consort." International Journal of Geomechanics, 7(3): 194–205.

Gourvenec, S., and Jensen, K. (2009). "Effect of embedment and spacing of conjoined skirted foundations on undrained limit states under general loading." International Journal of Geomechanics, 9(6): 267–279.

Gourvenec, S., and Barnett, S. (2011). "Undrained failure envelope for skirted foundations under general loading." Géotechnique, 61(3): 263–270.

Griffiths, D.V., and Fenton, G.A. (2001). "Bearing capacity of spatially random soil: the undrained clay Prandtl problem revisited." Géotechnique, 51(4): 351–359.

Krabbenhoft, K., Lyamin, A.V. and Sloan (2007). "Formulation and solution of some plasticity problems as conic programs." International Journal of Solids and Structures, 44(5): 1533–1549.

Krabbenhoft, K. and Lyamin, A.V. (2015). "Strength reduction finite element limit analysis." Géotechnique Letters, 5: 250–253.

Low, H.E., Lunne, T., Andersen, K.H., Sjursen, M.A., Li, X., and Randolph, M.F. (2010). "Estimation of intact and remoulded undrained shear strengths from penetration tests in soft clays." Géotechnique, 60(11): 843–859.

Maynard, M.L., Schneider, J.A., McEntee, J., and Newberg, E. (2013). "Suction caissons for cross-flow tidal power systems," Proceedings of the Institute of Civil Engineers—Geotechnical Engineering, 166(2): 99–110.

Optum CE (2017). Optum G2: Theory, Optum Computational Engineering: 85.

Taylor & Francis
Taylor & Francis Group
http://taylorandfrancis.com

Cone Penetration Testing 2018 – Hicks, Pisanò & Peuchen (Eds)
© 2018 Delft University of Technology, The Netherlands, ISBN 978-1-138-58449-5

Evaluation of existing CPTu-based correlations for the undrained shear strength of soft Finnish clays

J. Selänpää, B. Di Buò, M. Haikola & T. Länsivaara
Tampere University of Technology, Tampere, Finland

M. D'Ignazio
Norwegian Geotechnical Institute, Oslo, Norway

ABSTRACT: The Tampere University of Technology has been carrying out an extensive research program on soil testing in Finland. The aim of this research project is to collect data from high-quality in situ and laboratory tests and derive correlations for strength and deformation properties specific to Finnish clays. Correlation models for the undrained shear strength of soft clays based on CPTu measurements have been proposed in the literature by several authors. However, such models are often calibrated from a specific site or soil type. Thus, validation of these models is required before applying them to different soil conditions. In this paper, the existing correlations for the undrained shear strength of soft clays based on CPTu data are compared to test the results from different sites in Finland. The validity of the existing models is assessed for Finnish clays by evaluating their bias and uncertainties.

1 INTRODUCTION

The scope of this paper involves assessing the validity of existing correlations for (s_u) in Finnish soils based on the piezocone (CPTu) parameters. Data collected by the Tampere University of Technology (TUT) from seven clay sites in Finland are exploited to evaluate the correlations that are commonly used in Sweden and Norway. Specifically, the validity of the CPTu correlations for s_u from the triaxial compression (TXC; s_{uC}) and direct simple shear (DSS; s_{uDSS}) tests is checked against TXC and DSS tests on high-quality samples of soft clays. The CPTu correlations for s_{uDSS} are also compared with down-hole field vane (FV; $s_{ucorrFV}$) test results from the different sites. Finally, the bias and uncertainties of the examined correlations are evaluated with respect to the presented dataset of Finnish clays.

2 SOIL INVESTIGATION

2.1 *Test sites*

Table 1 summarizes the basic properties of the seven clay sites considered in this study. The investigated clays were slightly overconsolidated (overconsolidation ratio, OCR < 3), and they covered a wide range of water contents (w = 66–127%) and sensitivities (S_t = 16–98). The natural water content was above the liquid limit (w_L) in all the sites, and the remolded undrained shear strength (s_u^{re}) was generally lower than 2 kPa. Some of the sites have been presented and discussed in Di Buò et al. (2016) and Selänpää et al. (2017).

Table 1. Basic Soil Properties of the Investigated Sites.

Site	OCR (–)	w (%)	w_L (%)	I_P (%)	S_t (–)
Lempäälä	1.1–1.4	68–127	42–69	16–26	24–54
Perniö	1.2–2.5	70–110	44–75	19–47	37–72
Murro	1.2–1.9	66–95	58–97	28–53	20–23
Masku	1.4–1.8	80–117	66–95	39–59	18–21
Paimio	1.3–1.9	67–109	40–66	16–36	66–98
Sipoo	1.2–2.0	79–116	66–89	36–63	16–45
Joensuu	1.2–2.8	72–109	65–95	39	20–35

Where: OCR = overconsolidation ratio from oedometer test with constant-rate-of-strain (CRS) of 0.001–0.0025 mm/min depending on clay type; w = water content; w_L = liquid limit; I_p = plasticity index; and S_t = sensitivity from the fall cone test

The maximum penetration depths reached were 9 m at Lempäälä and Perniö, 23 m at Murro, 15 m at Masku, 11 m at Paimio and Sipoo, and 16 m at Joensuu. The depths for sampling were chosen by observing the most homogenous layers from the CPTu data. The deepest sampling depths were 7 m at Lempäälä, 8 m at Perniö and Masku, 5 m at Murro and Joensuu, and 9 m at Paimio and Sipoo.

2.2 *In situ tests and sampling*

Pairs of sampling and in situ tests were performed within 2 meters of each other. The in situ tests performed consisted of the CPTu and FV tests. Seismic and resistivity measurements were also gathered. However, the evaluation of soil properties from such measurements is beyond the scope of this study. Therefore, these data are not presented.

The CPTu tests were carried out using a low-capacity (0.75t) and high-sensitivity probe, which is expected to provide high accuracy in soft, homogenous soils (Sandven, 2010). The tests fulfil the requirements of application class 1 according to ISO (2012). The excess pore pressure during penetration (u_2) was measured right above the cone tip.

To verify the test repeatability and perform resistivity and seismic measurements, a minimum of three tests were conducted at each site. In general, the repeatability was good, as discussed in Di Buò et al. (2016). Therefore, the piezocone data used to evaluate the correlations in this study were based on a single CPTu sounding for each site.

FV measurements were obtained using a downhole vane device equipped with a casing. This setup has been shown to provide high accuracy in both torque and rotation measurements (Selänpää et al., 2017). However, the pushing of the vane into the soil always causes some disturbance. Thus, repeatability was also checked for the vane tests by performing a minimum of three tests for each depth. It was assumed that differences in the measured torques—and therefore, s_u—were mainly due to disturbance, and the highest of the measured values was taken as the most representative.

FV measurements must be corrected to account for anisotropy and rate effects (Bjerrum, 1973). In Finland, this is done by means of a reduction factor that depends on the liquid limit (Ratahallintokeskus, 2005). Only corrected FV results are discussed in this study.

2.3 *Laboratory tests*

Soil sampling was mainly performed using an open-drive tube sampler with a diameter of 132 mm designed at TUT (Di Buò et al., 2016). The sampler is a small-scale reproduction of the SGI-type Laval open-drive block sampler (Larsson, 2011). The main difference with the SGI sampler is that the soil is stored in the sampling steel tube and extruded only before testing. This feature was designed to avoid possible damaging of the sample during handling and lateral stress reduction during storage. The sampler is also equipped with a cutting wire system that separates the sample from the ground prior to sampler withdrawal. An air feeding system was also implemented to prevent suction at the cutting end (Di Buò et al., 2016).

The Perniö test site included some high-quality samples taken by a Sherbrooke-type mini block sampler (Emdal et al., 2016). For two out of eight of these high-quality samples, a considerably higher s_{uC} was measured, in comparison with the other test results. These two tests are samples that have been prepared and trimmed for testing within 24 h of sampling. The effect of storage time was studied by Amundsen et al. (2017) and the short swelling time resulting in smaller disturbance may partly explain the superior results. In Figures 5–8, the two tests can be easily identified, as they had the highest measured s_{uC} among the tests ($s_{uC} > 25$ kPa).

The laboratory tests on the tube samples included consolidated isotropic undrained compression (CIUC) and extension (CIUE) tests, consolidated anisotropic undrained compression (CAUC) tests and extension (CAUE) tests, DSS tests, CRS oedometer and index tests. This study focuses only on the test results from the CIUC, CAUC, and DSS tests. The laboratory tests were conducted in a climatized room with a constant temperature of 20°C.

The cell pressure (σ'_{cell}) in the CIUC tests was chosen as the smallest value between [$0.73 \cdot \sigma'_1$; $0.6 \cdot \sigma'_p$], where σ'_1 is the effective vertical stress and σ'_p is the preconsolidation stress. The basic principles for selecting between these values were as follows: *a)* to consolidate close to the in situ hydrostatic stress level, and *b)* to ensure that the yield surface did not expand during consolidation. The consolidation pressure was kept constant for 24 h, while the end of consolidation was verified by the measured volumetric strain. The preconsolidation stress σ'_p was inferred from the CRS oedometer tests on samples from the same tube as the triaxial specimens.

The CAUC test results seemed in line with those of the CIUC tests, with differences in terms of the measured peak s_{uC} in the order of ±3%. Therefore, the CAUC and CIUC tests are analyzed and presented together.

In the DSS tests, the samples were first consolidated to a stress level close to the preconsolidation stress. They were then unloaded to the in situ stress state before shearing.

The average failure times in the CIUC and DSS tests were 2.5 h and 1.25 h, respectively. In this study, no strain-rate correction was applied to the test results.

The sample quality of the triaxial specimens was evaluated according to Lunne et al.'s (1997) criteria, which are based on the volume change during reconsolidation to the effective in situ stress. According to the sample quality classification by Lunne et al. (1997), 7 out of 37 triaxial test results

could be classified as "Good," while the remaining 30 were "Very good to excellent."

3 INTERPRETATION OF THE UNDRAINED SHEAR STRENGTH

The net cone resistance q_{net} ($= q_T - \sigma_{v0}$) is related to s_u by means of the cone factor N_{kt}, as

$$s_u = \frac{q_T - \sigma_{v0}}{N_{kt}} = \frac{q_{net}}{N_{kt}}, \quad (1)$$

where q_T = corrected cone resistance; σ_{v0} = vertical total stress.

The effective cone resistance q_e ($= q_T - u_2$) is related to s_u by means of the cone factor N_{ke}, as

$$s_u = \frac{q_T - u_2}{N_{ke}} = \frac{q_e}{N_{ke}}, \quad (2)$$

where u_2 = measured pore pressure.

The excess pore water pressure Δu ($= u_2 - u_0$) is related to s_u by means of the cone factor $N_{\Delta u}$, as

$$s_u = \frac{u_2 - u_0}{N_{\Delta u}} = \frac{\Delta u}{N_{\Delta u}}, \quad (3)$$

where u_0 = initial pore pressure in situ.

Numerous correlations for cone factors have been presented to evaluate s_u for local soil conditions. In this study, the cone factors that are generally used in Scandinavia were evaluated for Finnish soil conditions. The correlations of the cone factors evaluated in this study are presented in Table 2.

Correlations 1, 2, and 3 were proposed by Larsson and Mulabdic (1991) for Swedish clays. Larsson and Mulabdic (1991) suggested that N_{kt} and $N_{\Delta u}$ depend on the liquid limit (w_L). Correlations 1 and 3 can be used in soils with *OCR* values higher than 1.3 by multiplying the equation by $(OCR/1.3)^{b-1}$, where b can be taken as equal to 0.8 (Larsson & Åhnberg, 2003). This is accounted for in the interpretation.

Correlation 2 is only valid for slightly overconsolidated clays. Therefore, it is used in this study only when *OCR* is lower than 2—which is taken as the upper boundary of the "low" *OCR* data points.

Correlations 4–9 were established by Karlsrud et al. (2005) for Norwegian clays, including one site from the United Kingdom. These correlations are divided into two groups based on their sensitivity as $S_t < 15$ and $S_t > 15$. The lowest S_t value in the dataset in Table 1 is 16. However, correlations 4, 6, and 8 for $S_t < 15$ are also evaluated in this study. The cone factors N_{kt} and $N_{\Delta u}$ were observed to be functions of *OCR* by Karlsrud et al. (2005), while N_{ke} was observed to depend on the pore pressure ratio B_q. The correlations are based on the high-quality samples taken by the Sherbrooke block sampler. No reduction was applied to the measured peak s_{uC}.

Table 2. Correlations for cone factors for s_{uC} and s_{uDSS}.

n.	s_u	Correlation	Note
1	s_{uDSS}	$N_{kt} = 13.4 + 6.65 \cdot w_L$	OCR ≈ 1.3
2	s_{uDSS}	$N_{\Delta u} = 14.1 – 2.8 \cdot w_L$	*OCR ≈ 1.3
3	s_{uC}	$N_{kt} = 3.6 + 13.2 \cdot w_L$	OCR ≈ 1.3
4	s_{uC}	$N_{kt} = 7.8 + 2.5 \cdot \log(OCR) + 0.082 \cdot I_p$	$S_t < 15$
5	s_{uC}	$N_{kt} = 8.5 + 2.5 \cdot \log(OCR)$	$S_t > 15$
6	s_{uC}	$N_{ke} = 11.5 – 9.05 \cdot B_q$	$S_t < 15$
7	s_{uC}	$N_{ke} = 12.5 – 11.0 \cdot B_q$	$S_t > 15$
8	s_{uC}	$N_{\Delta u} = 6.9 – 4.0 \cdot \log(OCR) + 0.07 \cdot I_p$	S_t 15
9	s_{uC}	$N_{\Delta u} = 9.8 – 4.5 \cdot \log(OCR)$	$S_t > 15$

Where: B_q = pore pressure ratio = $(u_2 - u_0)/(q_T - \sigma_{v0})$;
*Valid only for slightly overconsolidated clayey soils.

4 EVALUATION OF THE CORRELATIONS

When comparing the CPTu measurements and s_u values, an average CPTu value taken from a ±5-cm distance from the middle of either the triaxial or DSS samples or FV was used. Index properties were taken within a ±10-cm distance with respect to the comparison level.

In Figures 1 and 2, the undrained shear strength is calculated using the average N_{kt}, $N_{\Delta u}$, and N_{ke} values for the dataset. The calculated mean values were N_{kt} = 16.8 and $N_{\Delta u}$ = 10.7 for s_{uDSS}; N_{kt} = 17.5 and $N_{\Delta u}$ = 9.3 for $s_{ucorrFV}$; and N_{kt} = 10.7, $N_{\Delta u}$ = 7.0, and N_{ke} = 5.6 for s_{uC}. These reference values are used for comparison with the correlations in Table 2. The results generally showed good agree-

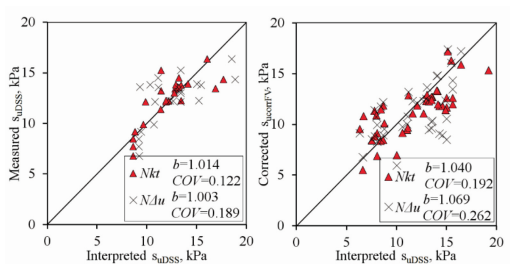

Figure 1. Comparison between the interpreted and measured s_{uDSS} and $s_{ucorrFV}$ values using the average N_{kt} and $N_{\Delta u}$.

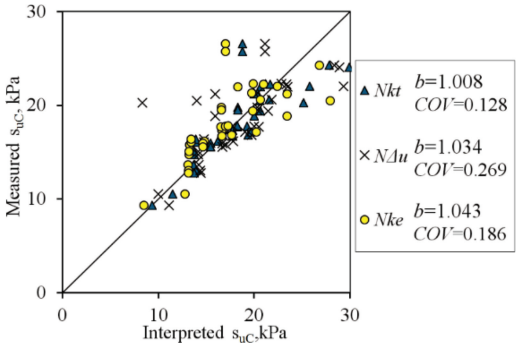

Figure 2. Comparison between the interpreted and measured s_{uC} values using the average N_{kt}, $N_{\Delta u}$, and N_{ke}.

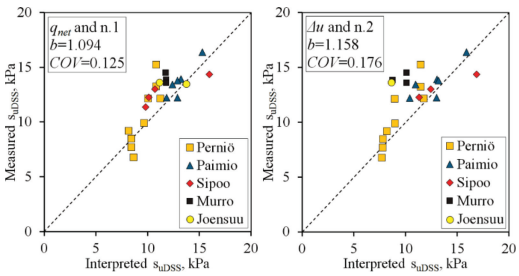

Figure 3. Interpretation of s_{uDSS} using correlations 1 and 2.

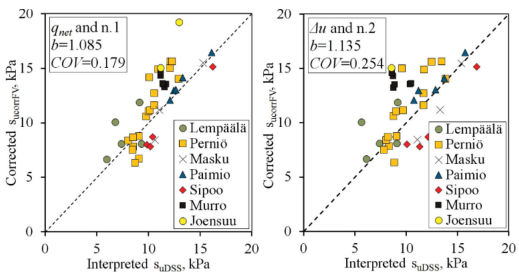

Figure 4. Interpretation of s_{uDSS} using correlations 1 and 2.

ment between the measured and calculated s_{uC} and s_{uDSS}, especially when using Equation 1. Higher scatter could be observed when using Equations 2 and 3, and in general, for $s_{ucorrFV}$.

In Figures 3–8, the s_u values calculated from the cone factor models in Table 2 are compared with the measured s_u values. The goodness of each correlation model was evaluated through the calculation of the bias factor (b) and coefficient of variation (COV), following Ching and Phoon (2014). The bias factor b is defined as the mean value of the ratio (measured s_u)/(calculated s_u).

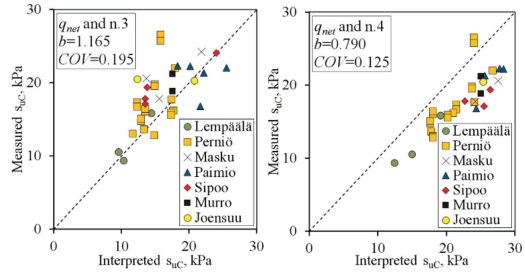

Figure 5. Interpretation of s_{uC} using correlations 3 and 4.

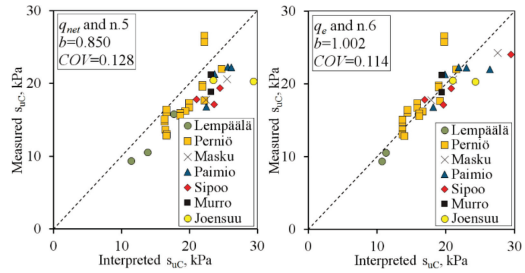

Figure 6. Interpretation of s_{uC} using correlation 5 for q_{net} and correlation 6 for q_e

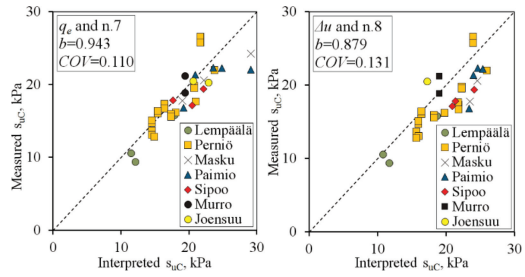

Figure 7. Interpretation of s_{uC} using correlation 7 for q_e and correlation 8 for Δu.

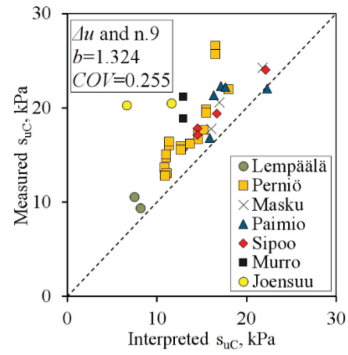

Figure 8. Interpretation of s_{uC} using correlation 9 for Δu.

If $b = 1$, the prediction is unbiased. The COV is calculated as the ratio of the standard deviation of the (measured s_u) / (calculated s_u) ratio and the bias factor. These values are summarized in Tables 3–6.

In Figure 1, the interpretation of s_{uDSS} and $s_{ucorrFV}$ using constant cone factors resulted in the following: *i)* nearly unbiased predictions, and *ii)* lower calculated $COVs$ when using N_{kt} compared with $N_{\Delta u}$. However, the COV values relative to $s_{ucorrFV}$ were consistently higher than those for s_{uDSS}, indicating a higher variability of FV measurements compared with DSS.

In Figure 2, the calculated b values suggest an almost unbiased prediction ($b = 1.01$–1.05) when using constant N_{kt}, N_{ke}, and $N_{\Delta u}$ factors in each site. The lowest variability was observed when using Equation 1, resulting in a $COV = 0.13$. The higher observable scatter associated with Equations 2 and 3 resulted in higher calculated COV values (>0.18).

As shown in Figure 3, correlations 1 and 2 underestimated the s_{uDSS} of Finnish clays by 9% and 16%, respectively, and gave $COVs$ of 0.12 and 0.17.

When comparing the measured $s_{ucorrFV}$ and s_{uDSS} from correlation 1 in Figure 4, a similar b value was obtained as that for the measured s_{uDSS}. However, the COV was larger (0.18 vs. 0.12). In contrast, s_{uDSS} from correlation 2 underestimated $s_{ucorrFV}$ by 14%. The scatter was also larger compared with correlation 1 ($COV = 0.26$).

In Figure 5, measured s_{uC} is compared with s_{uC} interpreted based on correlations 3 and 4 in Table 2. Correlation 3 underestimates the measured values by 17% ($b = 1.17$) with a $COV = 0.20$. On the contrary, correlation 4 overestimates s_{uC} ($b = 0.79$), even though the calculated COV (0.125) is lower than the COV from correlation 3.

According to Figure 6, correlation 5 overestimates by 15% ($b = 0.85$), while correlation 6 provides an almost unbiased prediction. In both cases, relatively low variability around the mean trend is observed ($COV = 0.114$–0.128).

As shown in Figure 7, correlations 7 and 8 slightly overestimate s_{uC} by 6–12% with COV of 0.11–0.13. The COV of correlation 8 is notably improved in comparison to the reference value ($COV = 0.26$ vs $COV = 0.13$).

Correlation 9 in Figure 8 underestimates s_{uC} by 32% ($b = 1.324$). The COV is significantly higher than for correlation 8 (0.26 vs 0.13).

Tables 3–6 summarize the evaluated b and COV for the correlations in Table 2. Correlations 4, 6, and 8 are for $S_t < 15$, while correlations 5, 7, and 9 are for $S_t > 15$.

Table 3. Summarized Results of the Interpreted s_{uDSS}.

	N_{kt} aver.	n.1 ($w_L \cdot OCR$)	$N_{\Delta u}$ aver.	n.2 ($w_L \cdot OCR$)
b	1.014	1.094	1.003	1.158
COV	0.122	0.125	0.189	0.176

Table 4. Summarized Results of the Interpreted $s_{ucorrFV}$.

	N_{kt} aver.	n.1 ($w_L \cdot OCR$)	$N_{\Delta u}$ aver.	n.2 ($w_L \cdot OCR$)
b	1.040	1.085	1.069	1.135
COV	0.192	0.179	0.262	0.254

Table 5. Summarized Results of the Interpreted s_{uC} with N_{kt}.

	N_{kt} aver.	n.3 ($w_L \cdot OCR$)	n.4 (I_P OCR)	n.5 (OCR)
b	1.008	1.165	0.790	0.850
COV	0.128	0.195	0.125	0.128

Table 6. Summarized Results of the Interpreted s_{uC} with $N_{\Delta u}$ and N_{ke}.

	N_{ke} aver.	n.6 (B_q)	n.7 (B_q)	$N_{\Delta u}$ aver.	n.8 (I_P OCR)	n.9 (OCR)
b	1.043	1.002	0.943	1.034	0.879	1.324
COV	0.186	0.114	0.110	0.269	0.131	0.255

5 DISCUSSION AND CONCLUSIONS

The main challenge in verifying CPTu-based correlations is to gather a reliable dataset of test results for the comparison. For the dataset used in this study, the comparison between the existing correlations and undrained shear strength from FV resulted in the highest variability (Table 4). For the DSS, the variability was slightly lower (Table 3), while the smallest variability (lowest $COVs$) was found for the triaxial compression test results (Tables 5–6). This may indicate that, for practical applications, the use of triaxial compression data will result in a more reliable estimate of cone factors compared with other test types. This is primarily reflected in Figure 2, and confirmed in Tables 5–6. Particularly, the best correlation was found between the triaxial compression test values and the interpretation based on correlations 6 and 7 for N_{ke}.

The higher variability in the DSS tests compared with the triaxial tests may have been partly due to the lack of experience with DSS testing at TUT. The DSS equipment was taken into use for the first time at TUT during this research project.

Under—or overestimation of s_u observed by the bias factor can result from differences in sample qualities in datasets, even if samples are classified with the same quality. Another reason for this could be the properties of the clays. For instance, Norwegian clays are siltier than clays in Sweden and Finland are, whereas in Finland, the organic content of the clays is often higher than that in Sweden, as summarized by Broms (1974). Clays at the Murro, Joensuu, and upper layer in the Lempäälä testing sites consist of higher organic content than 2%; the other sites exhibit lower organic content. It could be reasonable to leave these sites out of the dataset in future analyses.

Another aspect is that even though the accuracy of CPTu probes, especially in terms of the capacity to measure low values, has improved, the results can vary among the different manufacturers (Sandven, 2010); this can affect the correlation results.

Based on the change in the *COV* values from the reference values (based on mean cone factors), it seems that it may be beneficial to include *OCR* or B_q in the interpretation of s_{uC}. This can be observed in Table 6. In interpretations based on N_{kt}, such a benefit is, however, not too clear (Table 5). The B_q parameter was observed to correlate with the *OCR*, as reported by Lunne et al. (1997) and Karlsrud et al. (2005). Moreover, D'Ignazio et al. (2016) discussed, based on a large soil database, how the undrained shear strength of Finnish clays is predominantly dependent on the *OCR*. In addition, the plasticity index seems also to improve the evaluation, especially when $N_{\Delta u}$ is used to assess s_{uC} (Table 6).

Dividing correlations 4–9 into two groups by sensitivity does not seem appropriate for Finnish clays, although the Finnish dataset did not include samples with S_t lower than 15. As shown in Table 6, the interpretation based on N_{ke} and $N_{\Delta u}$ intended for low-sensitive Norwegian soils seems valid for Finnish clays. Even though the Norwegian data consists of high-quality block samples, the evaluation of s_{uC} seems to work well, especially when using N_{ke}. The evaluations based on N_{kt} seemed to give too-high values compared to the measurements (Table 5). Interpretations using $N_{\Delta u}$ showed over—and underestimated s_{uC} values, depending on which sensitivity group was considered (Table 6). It must be pointed out that a disadvantage of the N_{ke} method is that it is sensitive to the accuracy of both the measurements of cone resistance, and especially, pore pressure in soft, sensitive soils. Moreover, the use of the B_q parameter is not suitable for heavily overconsolidated clays, as the value could be very small or even negative (Powell et al., 1988).

As shown in Tables 3–5, the interpretation of s_u from average N_{kt} works relatively well. The use of parameters such as liquid limit and *OCR* (correlations 1–3) gives also satisfactory results. Nevertheless, one of the difficulties in evaluating the goodness of the correlations 1–3 for the Finnish dataset is that there is already high scatter in the original correlation results from the Swedish dataset, as mentioned by Larsson et al. (2007). Furthermore, Larsson et al. (2007) suggested that s_u anisotropy depends on the liquid limit. Therefore, for practical applications the interpreted s_{uC} could be scaled using factors that are functions of w_L, in order to use anisotropic strength in calculations.

In Sweden, FV test results are corrected based on the liquid limit and *OCR* (Larsson et al., 2007). This method was developed to provide a good fit with the DSS strength. A thorough study on the applicability of this method to Finnish clays is recommended in the future, as it could decrease the scatter in the interpreted vane test results.

The dataset was relatively narrow in terms of strength and *OCR* ranges, as the authors' main interest was to focus on very soft soils. Combining the present database with other databases could increase the reliability of the evaluation of s_u.

REFERENCES

Amundsen, H.A., Jønland, J., Emdal, A., & Thakur, V. 2017. An attempt to monitor pore pressure changes in a block sample during and after sampling. *Geotechnique Letters.* vol. 7 (2).

Ching, J., and Phoon, K.-K. 2014. Transformations and correlations among some clay parameters—the global database. *Canadian Geotechnical Journal*, 51(6), 663–685.

Bjerrum, L. 1973. Problems of Soil Mechanics and Construction on Soft Clays. *State-of-the-art report. Proceedings of the 8th ICSMFE,* Moscow, 3, pp 111–159

Broms, B.B., 1974. Scandinavia. *General report. European symposium on penetration testing, ESOPT,* Stockholm, June 5–7 1974. Proceedings. Vol. 2. pp 14–23.

Di Buò, B., D'Ignazio, M., Selänpää, J. & Länsivaara, T. 2016. Preliminary results from a study aiming to improve ground investigation data. *Proceedings of the 17th Nordic Geotechnical Meeting,* Reykjavik, 25–28 May 2016, 1, pp 187–197

D'Ignazio, M., Phoon, K.K., Tan, S.A., & Länsivaara, T.T. 2016. Correlations for undrained shear strength of Finnish soft clays. *Canadian Geotechnical Journal*, *53*(10), 1628–1645.

Emdal, A., Gylland, A., Amundsen, H.A., Kåsin, K. & Long, M. 2016. Mini-block sampler. *Canadian Geotechnical Journal,* 53(8), 1235–1245.

ISO. 2012. Geotechnical investigation and testing—Field testing—Part 1: Electrical cone and piezocone penetration tests, *International Standard ISO 22476–1:2012*

Karslrud, K., Lunne, T., Kort, D.A. & Strandvik S. 2005. CPTU correlations for clays. *Proc. of the XVI-th International Conference on Soil Mechanics and Geotechnical Engineering.* Osaka 2005, 693–702

Larsson, R. & Mulabdic, M. 1991. Piezocone Tests in Clay. *Swedish Geotechnical Institute, SGI,* Linköping, Report 42, 240 pp.

Larsson, R. & Åhnberg, H., 2003. Long-term effects of excavations at crests of slopes. *Swedish geotechnical institute.* Linköping 2003. Report 61. 130p

Larsson, R., Sällfors, G., Bengtsson, P.-E., Alén, C., Bergdahl, U. & Eriksson, L. 2007. Skjuvhållfasthet: utvärdering i kohesionsjord. *Swedish geotechnical institute.* Linköping 2007, Information 3.

Larsson, R. 2011. Metodbeskrivning för SGI:s 200 mm diameter 'blockprovtagare'-Ostörd provtagning i finkornig jord (In Swedish) *Swedish Geotechnical Institute, SGI.* Göta River Commission. GÄU. Subreport 33. Linköping.

Lunne, T., Berre, T. & Strandvik, S. 1997. Sample disturbance effects in soft low plasticity Norwegian clay. *Proc. of Conference on Recent Developments in Soil and Pavement Mechanics,* Rio de Janeiro, 1997, 81–102

Lunne, T., Robertson, P.K. & Powell, J.J.M. 1997. Cone penetration testing in geotechnical practice. London, Spon Press. 312p

Powell, J.J.M., Quarterman, R.S.T. & Lunne, T. 1988. Interpretation and use of the piezocone test in UK clays. *Penetration Testing in the UK:* 151–156. London: Thomas Telford.

Ratahallintokeskus 2005. Radan stabiliteetin laskenta, olemassa olevat penkereet. *Ratahallintokeskuksen julkaisuja B15,* Ratahallintokeskus, Helsinki. (In Finnish. In English: Guidelines for embankments stability calculation by the Finnish Transport Agency, publication B15).

Sandven, R. 2010. Influence of test equipment and procedures on obtained accuracy in CPTU. *In Proceedings of the 2nd International Symposium on Cone Penetration Testing (CPT'10),* Huntington Beach, Calif. Edited by Mitchell et al.

Selänpää, J., Di Buò, B., Länsivaara, T. & D'Ignazio, M. 2017. Problems related to field vane testing in soft soil conditions and improved reliability of measurements using an innovative field vane device. *In Landslides in Sensitive Clays.* pp. 109–119. Springer International Publishing.

Taylor & Francis
Taylor & Francis Group
http://taylorandfrancis.com

Cone Penetration Testing 2018 – Hicks, Pisanò & Peuchen (Eds)
© 2018 Delft University of Technology, The Netherlands, ISBN 978-1-138-58449-5

Applications of RCPTU and SCPTU with other geophysical test methods in geotechnical practice

Z. Skutnik, M. Bajda & M. Lech
Warsaw University of Life Sciences, Poland

ABSTRACT: The resistivity cone penetration test (RCPTU) and seismic cone penetration test (SCPTU) results may be used as well for quantitative and for qualitative analysis of the subsoil on tested sites. Electrical resistivity tomography (ERT) with RCPTU and SCPTU procedures are capable of detecting discrete horizons that would normally be missed using other tests at specific depth intervals. In the first tested site the RCPTU and SCPTU results have been used to define sub-surface stratigraphy and the soil porosity of the Pliocene clay deposits, while in the other site to identify the layers of organic subsoil and deformation parameters of subsoil. In the third tested site geotechnical in situ investigations were carried out using of 10 cm^2 CPTU cone and 15 cm^2 RCPTU cone. All these tests may be carried out in the preliminary investigation phase of ground conditions as well as supplementary studies and are most effective when are combined.

1 INTRODUCTION

The recent years have shown dynamic developments of the Warsaw City, involving the construction of many high-rise buildings, roads, extension of subway lines and other geoenvironmental engineering projects. This is why enhancement in the site characterization techniques is required. A geoenvironmental site characterization requires an evaluation of stratigraphy, as well as geotechnical, hydrogeological and environmental parameters. Combining geophysical and geotechnical *in situ* techniques is the best way to achieve all of the required information (Campanella et al., 1994).

Seismic tests provide the advantage of an evaluation of the mechanical response of the medium, although only at very small strain levels, with the possibility of testing geomaterials in their undisturbed state on site. Interpretation of wave propagation in different frameworks can provide information at several levels of details (Jamiolkowski et al., 1985, Stokoe et al., 2005).

Electrical techniques, can be used to study different environmental characteristics that are important during the site characterization for waste disposal and monitoring migration of contamination plumes (Elis et al. 2004, Fukue et al. 2001). The detection and delineation of the shape of the plume is an important component of geoenvironmental site characterization.

2 GEOLOGICAL CHARACTERISTICS OF TESTED SITES

The study area lies within a regional geomorphologic unit called the Warsaw Basin. It was formed during the central-Polish and Baltic glaciations. The test sites are located in Warsaw in the Vistula River valley (Fig. 1).

The first tested site called Stegny is located in Stegny district. It is the place where for the last few years a wide research program has been executed by the Warsaw University of Life Sciences

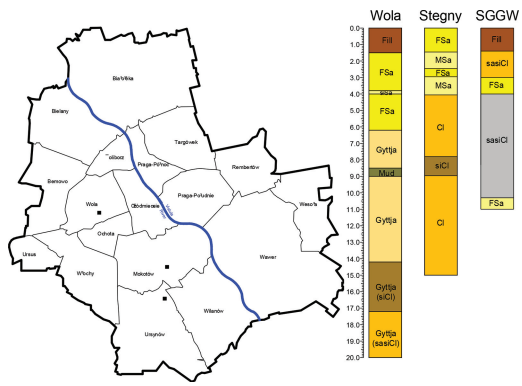

Figure 1. The map of Warsaw—location of tested sites and typical borehole profiles.

and other research institutions (Barański, 2004). The Stegny site is located in the southern part of Warsaw. The stratigraphy consists of Quaternary deposits developed as fine and medium dense sand layers of thickness not exceeding 4,5 m, underlain by Pliocene clays. The clay beds reveal a clear layered structure characterized by different color of the particular layers. The free groundwater table is at a depth of 3.2 m.

The second tested site called Wola is located within the geomorphologic structure called the "Żoliborz channel" and denuded post-glacial plateau in the east.

Partly fluvial deposits of the Vistula Glaciation (Ql_4), are represented by dense fine and medium sands, locally with interbeddings of silts and dense clayey sands.

The sands cover the continuous layer of silty muds of thickness from 1 m to approximately 3.5 m, underlain by peats with gyttja interbeddings, 2.5–5 m thick.

The thin-out of this layer has been observed at tested site. The a/m complex overlies a series of lacustrine gyttja prevailing in volume in the "Żoliborz channel". The top of gyttja has been observed from the depth of approximately 6 m to 13.5 m under the ground surface, the bottom level decreases to the east. The grain-size distribution of gyttja relates to silts, silty clays and more plastic silty clays, stiff and very stiff, with organic matter content from 10% to over 30%, locally even to 50% and calcium carbonate content in the range of 3–5% and over 5%.

The third site called SGGW, covers areas the margin of the denudated moraine plateau in the border zone of the Vistula river valley. The discussed research site is located in the marginal zone of the south part of Warsaw moraine upland in Ursynów. In the Ursynów region these sediments form a continuous, distinct layer, consisting mostly of fine sands. Above the fluvioglacial sediments lies a layer of melt-out sediments from the Odranian Glaciation, represented by grey boulder clay. The thickness of the clay layer (gQpO) is from several to tens of meters. In some places, the Odranian boulder clay is covered by fluvioglacial sands and gravel or/and ice-dammed silts. Above them or directly on the boulder clay, occurs the melt out till from the Wartanian Glaciation (the last glaciation in this area) (gQpW) (Sarnacka 1992).

Typical borehole profiles from Stegny, Wola and SGGW sites are shown in Figure 1.

3 IN SITU TESTING

The in-situ testing program was very extensive and depended on the site. It consisted of both piezocone penetrometer tests (RCPTU and SCPTU), and electrical resistivity tomography (ERT). The CPTU data requires a good estimation of correlation coefficients to determine geotechnical parameters (Lunne et al. 1997). These coefficients depend on the geologic formation and can be site-specific.

There are several kinds of geophysical tests that can be used for the delineation of stratigraphy and determination of soil parameters. Recently, techniques, which are the combination of standard geotechnical tests with the geophysical module, have been used in the field. The combination of seismic measurements and static cone penetration tests parameters has made a significant improvement to the CPTU test. The measurement of shear wave velocity allows to obtain the initial shear modulus of soil at a very low strain level. Knowledge about the G-modulus is important in practical geotechnical solutions, particularly in the prediction of soil structure interaction (LoPresti et al. 1999, Stokoe et al. 2005).

Geophysical methods have been used for many years in exploration of industrial and energy mineral beds, geological and engineering surveys, as well as geotechnical surveys (Campanella 2008). The less known and commonly used instrument is the RCPT (RCPTU) resistivity cone (Fig. 2), a combination of a static CPTU probe and the measurement of soil resistivity. The probe consists of two main elements: first for measuring parameters determined in standard CPTU test, the second is a module measuring the electrical resistivity. It includes two or four annular electrodes with insulating plastic elements between the electrodes.

The standard CPTU tests showed high variability of strength parameters due to the numerous sand and silt lenses. Moreover, the previous surveys showed high diversity of the geological structures, in particular the depth of the top of undisturbed Pliocene deposits. The properties of those deposits determine the geotechnical design the most of both of above ground and the underground structures in Warsaw.

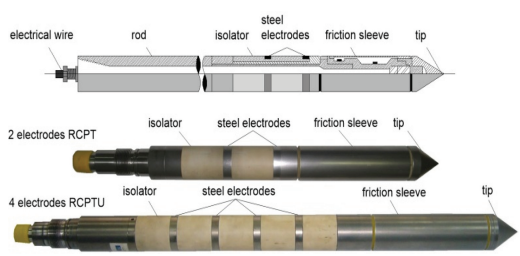

Figure 2. Schematic diagram of two- and four-electrodes RCPT cones.

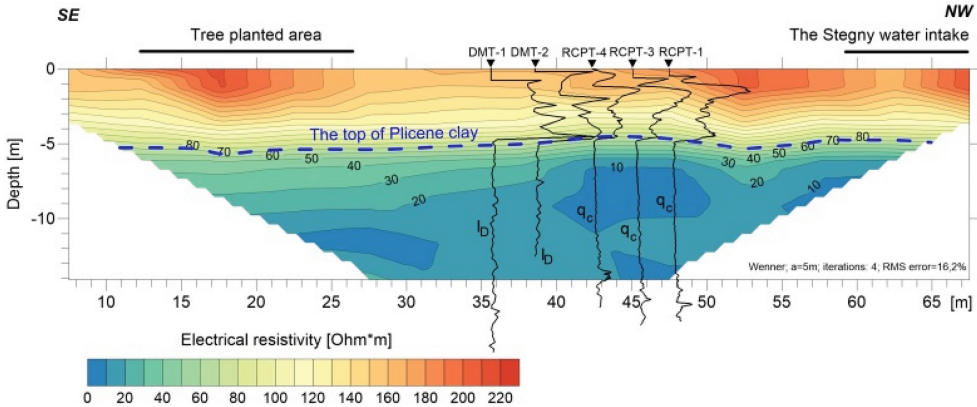

Figure 3. The electrical resistivity cross-section showing the top of clay layer—Stegny site.

The geotechnical and geophysical test results using RCPT probe have been applied to the determination of a much-diversified geological structure in Warsaw. Figure 3 shows the electrical resistivity cross-section of the subsoil in Stegny site obtained using electrical resistivity tomography (ERT).

The graph shows changes in the electrical resistivity in the structure's subbase to the depth of approx. 15 m below ground level. The profile analysis shows that non-cohesive soils with electrical resistivity of up to 200 Ωm exist at the depth of approx. 6 m. However, in the testing transect (in the middle of the profile), the base of the non-cohesive formations is at the depth of approx. 4.5 m, and in the areas planted with trees it was determined, based on the changes in electrical resistivity, at the depth of approx. 6 m. In this area, the layer of soils showing higher electrical resistivity reaches slightly deeper.

It may be due to the lower moisture content of the soils in the rhizosphere, and thus the determined sand base position in this area may be erroneous. The position of the upper surface of clay deposits in this area must be validated by boreholes or probing. The soils characterized by the resistivity of several to several dozen Ωm can be observed below the non-cohesive formations. The cross-section also shows the cone resistance values (q_c) obtained during RCPT tests, indicating the transition in the soil type in the tested area at the depth of 4.0÷4.2 m below ground level.

The detailed analysis of RCPT tests (Fig. 4) shows a boundary between the sands and the clays in this area at the depth of approx. 4 m below ground level. According to RCPT tests the electrical conductivity for sands is between 1.5 to 10 mS/m (respectively, the resistivity is between 100 to several hundred Ωm), and for clays is between 80 and 250 mS/m (respectively, the resistivity is between 4 and 12 Ωm). Further analysis of Figure 4 shows the correlation between the friction ratio and the measured electrical conductivity in this study. These parameters respond in a similar manner to changing the type of soil. The coefficient of friction in sands up to a depth of 4.2 m below the ground level does not exceed 1.6% and rapidly increases in clay.

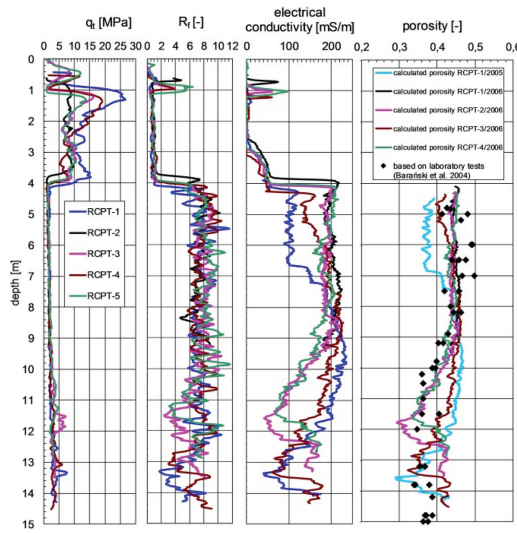

Figure 4. The RCPT test results and predicted porosity in clays—Stegny site.

The electrical conductivity behaves in the same way—in sands reaches very small values (1.5 mS/m), and is the greater, the soil is more cohesive (even 250 mS/m in this study).

By comparing the two measured parameters—friction ratio and electrical conductivity at the same time it is also easy to determine the changes

of humidity or the presence of soil contamination. The results of the RCPT tests on the Stegny site clearly showed that between the second and fourth meter of probing, the friction ratio R_f does not change, while the electrical conductivity of the soil increases.

The gradual increase in electrical conductivity starts at a depth of 2.7 meter below ground level which is caused by the presence of a groundwater table, which, due to capillary fringe or fluctuations, results in an increase in the humidity of the sand at this depth. The reading stabilized at an average of 3.4 m to the value of 50 mS/m, which indicates that this is the depth of the water table.

Moreover, the electrical resistivity tests using RCPT probe and electrical resistivity measurements of soil and the ground water have allowed to determine a relationship between the porosity and the formation factor F. For most rocks and soils, an empirical relationship formulated by Archie (1942), expressed as a ratio of saturated soil resistivity and fluid in the soil pores is called a formation factor. Assuming that the degree of saturation the Pliocene clays is close to one (Kaczyński 2007), the following relationship was used to determine the porosity:

$$n = 0{,}39 \cdot \left(\frac{\rho_{bSAT}}{\rho_f} \right)^{-0{,}27} \tag{1}$$

where n = porosity [-]; ρ_{bSAT} = electrical resistivity of soil in fully saturated conditions [Ωm]; ρ_f = electrical resistivity of pore fluid (from laboratory tests; ρ_f = 8.3 Ωm).

Measurement of electrical conductivity in Pliocene clays at Stegny site indicates a higher sensitivity of this parameter compared to shear wave velocity determined by SCPT. Measurement of electrical conductivity allowed to highlight in the subsurface very thin layers of silts or fine sands within Pliocene clay deposits (Fig. 5). Sands showed lower conductivity (higher resistivity) values than clays. Also in Figure 5 there is a significant difference between values of shear wave velocity at the depth of about 4 m due to effect of soil type changes and influence of ground water table. Values of shear wave velocity in sands exceed 500 m/s while in Pliocene deposits is equal to 200 m/s. The shear modulus G_0 calculated directly from shear wave velocity measured during SCPT test gives values in range of about 70 to 85 MPa for clays and from 450 to 1000 MPa for sands. G_0 modulus was also estimated from q_c measurements from formulas given by Rix and Stokoe (1991) (Skutnik et al., 2011).

In the Wola site the RCPTU and SCPTU were carried out. Example of the typical test results are presented in Figure 6. Measurement of electrical conductivity in organic subsoil (dominated by gyttja) indicates higher sensitivity of this parameter compared then shear wave velocity determined by SCPT.

Electrical conductivity allowed to distinguish in the subsurface layers of gyttja and peat. Gyttja showed very low conductivity (higher resistivity) values, lower than peat or even silt. A significant difference values of shear wave velocity from the surface to the depth of about 6 m is observed. Values of shear wave velocity in this zone varies since 150 m/s to 700 m/s.

In the SGGW site soundings were carried out using two cone penetrometers sizes, standard 10 cm² CPTU cone and 15 cm² RCPTU cone. The test results, values of q_c and f_s obtained from

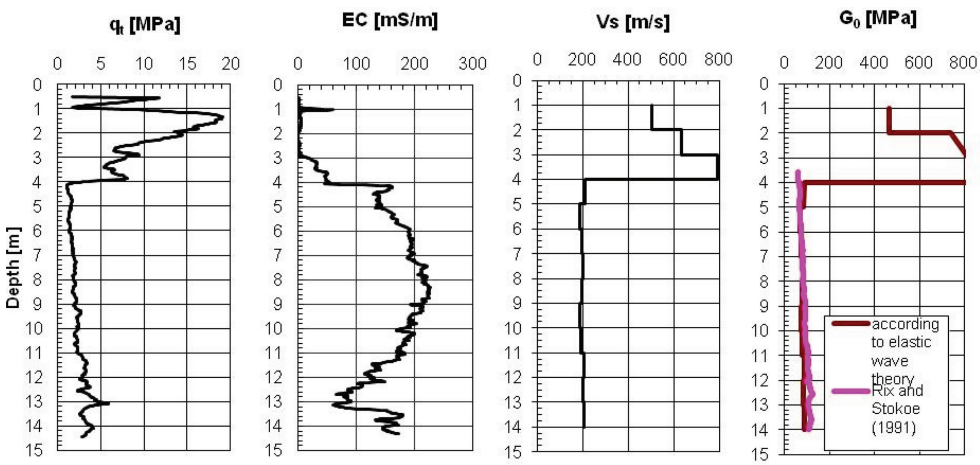

Figure 5. The RCPTU and SCPTU results—Stegny site.

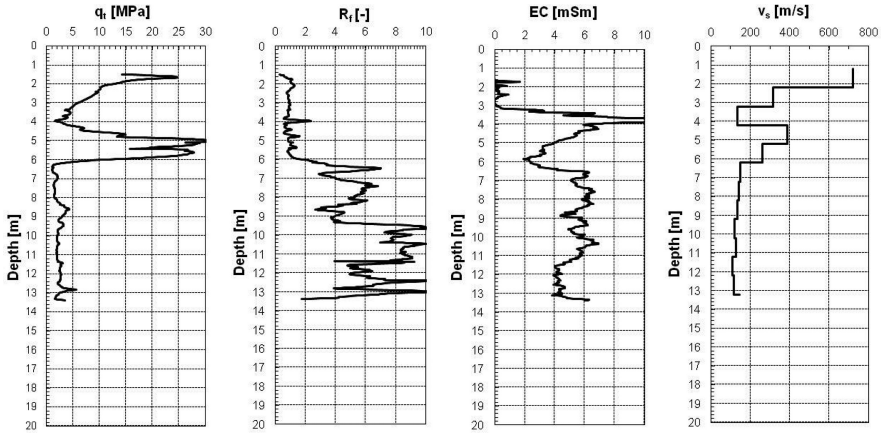

Figure 6. RCPTU and SCPTU results—Wola site.

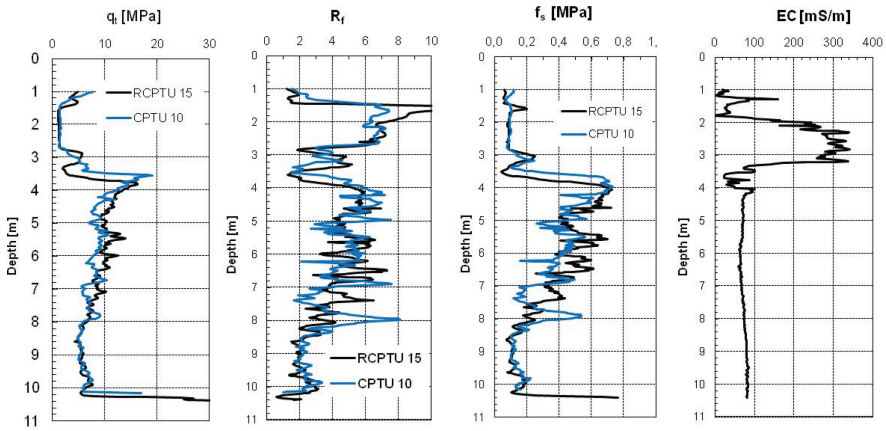

Figure 7. RCPTU and CPTU results—SGGW site.

both types of cones are near the same and are presented in Figure 7, while cones types in Figure 8. The electrical conductivity values obtained from RCPTU soundings and the ERT method in the analyzed SGGW site were presented by Bajda et al., 2015. In the case of RCPTU, this is a continuous measurement in the profile, whereas in the case of ERT tests the obtained values of the electrical conductivity were averaged. Nevertheless, in both cases it has been shown that in the depth range from 2 m to 4 m there is a zone with a changeable conductivity resulting from changes in humidity as well as the type of soil.

4 CONCLUSIONS

In situ tests like CPTU supplemented with additionally measured parameters like resistivity from

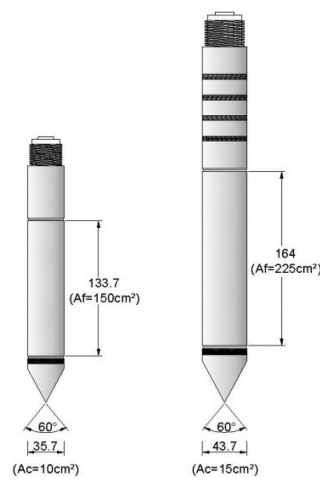

Figure 8. CPTU 10 cm^2 and RCPTU 15 cm^2 - SGGW site.

RCPTU, shear wave velocity from SCPT or SDMT is probably the best way to estimate geotechnical parameters, especially for soils from which collecting a good quality undisturbed soil sample for laboratory tests is impossible or problematic.

Generally it can be said that seismic or electrical resistivity methods always provide parameters for the soil in its natural and undisturbed state. The research confirmed that resistivity depends mostly on the type of the soil, presence of water and the concentration of ions in pore water. Based on geoelectrical research, it is impossible to unquestionably indicate all factors responsible for resistivity changes.

The observed relations between the decrease in resistivity and the content of organic matter for organic sediments from the Wola site allow to distinguish gyttja or peat layers. The accuracy of measurements of the electrical cone allows to mark even the thinnest interlayers in a profile, like in the SGGW site.

REFERENCES

Archie, G.E. 1942. The electrical resistivity log as an aid in determining some reservoir characteristics. *Transactions of the American Institute of Mining and Metallurgical Engineers* 146, 54–61.

Bajda, M., Lech M., Skutnik Z. 2015. Wykorzystanie czteroelektrodowego stożka CPTU 15 cm^2 do oceny wybranych parametrów podłoża gruntowego. *Inżynieria Morska i Geotechnika - XVII KKMGiIG,* 296–300 (In Polish).

Barański M. 2004. Analysis of Pliocene clay behaviour in effective stress conditions from the Stegny site. *Research Project KBN No. 5 T12B 04122.* Warsaw University, Faculty of Geology, Institute of Hydrogeology and Engineering Geology (In Polish).

Campanella, R.G. 2008. Geo-environmental site characterization. [W:] Huang A. i Mayne P. W. *Geotechnical and Geophysical Site Characterization.* Taipei, 1–4 April 2008. London: Taylor and Francis Group. 3–15.

Campanella, R.G., Davies, M.P., Boyd, T.J. & Everard, J.L. 1994. In-situ testing methods for groundwater contamination Studies. *Symposium on Developments in Geotechnical Engineering, From Harvard to New Delhi.* Balkema. 1936–1994.

Elis, V.R., Mondelli, G., Giacheti, H.L., Peixoto A.S.P., Hamada J. 2004. The use of electrical resistivity for detection of leacheate plumes in waste disposal sites. *Proceedings ISC-2 on Geotechnical and Geophysical Site Characterization,* Viana da Fonseca & Mayne (eds.), Millpress, Rotterdam. 467–474.

Fukue, M., Minato, T., Matsumoto, M., Horibe, H., Taya N. 2001. Use of resistivity cone for detecting contaminated soil layers. *Engineering Geology. 60.* 361–369.

Jamiolkowski, M., Ladd, C.C., Germaine, J.T. & Lancellotta, R. 1985. New developments in field and laboratory testing of soils. Theme Lecture, Proc. 11th ICSMFE, San Francisco, 1: 57–152.

Kaczyński, R. 2007. Geologiczno–inżynierskie zachowanie się iłów londyńskich i warszawskich. *Geologos 11.* 481–490 (In Polish).

LoPresti, D.C.F., Pallara, O., Jamiolkowski, M., Cavallaro, A. 1999. Anisotropy of small stiffness of undisturbed and reconstituted clays. *Pre-failure Deformation of Geomaterials, Jamiolkowski, Lancellotta&LoPresti (eds).* Balkema, Rotterdam: 3–10.

Lunne, T.; Robertson, P.K. & Powell, J.J.M. Cone penetration testing in geotechnical practice. *Blackie Academic & Professional*, 311 p.

Rix, G.J & Stokoe, K.H. 1991. Correlation of initial tangent modulus and cone resistance, *Calibration Chamber Testing.* Elsevier. New York. 351–362,

Sarnacka Z. 1992: Stratigraphy of quaternary sediments of Warsaw and its vicinity. *Pr. Państw. Inst. Geol.* 138, 1–36.

Skutnik, Z., Bajda, M., & Lech, M. 2011. Stiffness of the soil determined from in situ testing, Proceedings of the 15th European Conference on Soil Mechanics and Geotechnical Engineering: Geotechnics of Hard Soils - Weak Rocks. Part 1 / ed. by Andreas Anagnostopoulos, Michael Pachakis, Christos Tsatsanifos. 465–470.

Stokoe, K.H.II, Rathje, E.M., Axtell, P.J. 2005. Development of an in situ method to measure the nonlinear shear modulus of soil. *Proceedings of the 16th International Conference on Soil Mechnics and Geotechnical Engineering,* Osaka. Millpress. Rotterdam. 751–754.

Cone Penetration Testing 2018 – Hicks, Pisanò & Peuchen (Eds)
© 2018 Delft University of Technology, The Netherlands, ISBN 978-1-138-58449-5

CPT in a tropical collapsible soil

C.S.M. Soares, F.A.B. Danziger, G.M.F. Jannuzzi & I.S.M. Martins
Federal University of Rio de Janeiro, Brazil

M.E.S. Andrade
Technological Federal University of Paraná, Brazil

ABSTRACT: A test site was established in Primavera do Leste, a city 200 km east of Cuiabá, Central-West region of Brazil, one of the main Brazilian areas of soya and corn production. The research aimed at improvement of the knowledge of soil characteristics in that region, where serious problems related to foundations of silos are frequent. The present paper presents cone penetration tests performed in dry and rainy seasons. One block sample and tube samples have been collected, and characterization, determination of clay minerals and oedometer tests in specimens in natural water content and on soaked specimens have been performed. Soil collapsibility of the upper layer was verified. CPT results indicated three soil behaviour types, however for one of those layers the soil behaviour type was not properly indicated by the CPT. The CPTs performed in dry and rainy seasons allowed the conclusion that the variation of the water content is limited to 2.0–2.5 m depth.

1 INTRODUCTION

As the second largest producer of soybeans worldwide, Brazil accounts for 30 percent of the global production of the crop. The country had in 2015 over 29 million hectares of land available and used for farming soybean. Brazil is also the third largest producer of corn worldwide (Worldatlas 2017).

The Mato Grosso state, Central-West region of Brazil (Fig. 1), is the largest producer of soybean, corn, cotton and meat among all Brazilian states. Primavera do Leste, a city 200 km east of Cuiabá (Fig. 2), the capital of the state, is the second largest producer of soybean and corn in the state (IMEA 2010).

The huge production demands a significant number of silos. Since most of the soils in the state are unsaturated, collapsible soils, large settlements are frequent in the rainy season, both in cases of shallow and deep foundations, with significant losses.

Figure 1. Mato Grosso state, Central-West region of Brazil (adapted from Google Maps).

Figure 2. Primavera do Leste and Cuiabá, Mato Grosso State (Google Maps).

In order to contribute to the understanding of the soil behaviour, a test site was established in Primavera do Leste, and a number of in situ and laboratory tests have been performed, which are described below.

2 SOME GEOTHECNICAL PROBLEMS IN THE AREA

2.1 *General*

Soils in the region of Cuiabá and Primavera do Leste are unsaturated, with a meta-stable structure and high void ratio, with a critical value of approximately 0.8 (Conciani & Soares 1996). The collapse occurs when the suction reduces in the rainy season and there is an increase in the state of stress due to external loads. In some cases the sole suction reduction is enough to provoke the collapse, and the soil is then designated as truly collapsible (e.g., Reginatto & Ferreira 1973). It will be seen later in the paper that the upper soil in the test area may be included in this category.

2.2 *Some case histories*

A settlement of approximately 70 cm was recorded at the middle of a raft (40 cm at the border) in a silo close to the city of Campo Novo do Parecis, some 400 km Northwest of Cuiabá, indicating that the collapsibility issue affects a very large area in Mato Grosso state.

Figure 3. Settlement of 14 cm at the border of a raft of a silo in the surroundings of Primavera do Leste city.

Conciani & Soares (1996) reported another case in the same region where settlements of 25 cm to 40 cm have been recorded in a raft foundation for a silo. The raft was simply levelled and additional settlements occurred, causing the interruption of the system of transportation of the soybean, with significant losses.

Not only silos are affected by soil collapse, buildings are subjected to the same problem as well, even when pile foundations are used (e.g., Barbosa & Conciani 2000, Barbosa 2002).

The authors of the research herein reported visited two silos with foundation problems in the surroundings of Primavera do Leste, one of which shown in Fig. 3. The recorded settlement of approximately 14 cm at the border of the raft prevents the soybean to be collected in the area of the bottom of the raft due to the limitation of the collection system, therefore causing an important operational problem.

3 TEST SITE

3.1 *General*

A test site was established at the city of Primavera do Leste, mostly because of the support provided by a foundation company which has offered part of his deposit to be used as a test site. The coordinates of the test site are 15°34'52.6"S and 54°20'00.0"W.

3.2 *Tests performed*

Although SPT is the regular test performed in Brazil for soil investigation, the research reported herein aimed also at introducing the CPT as a regular tool for that purpose. Therefore, four CPTs have been performed, as indicated in Table 1. Two tests have been carried out in the rainy season, in February, and two in the dry season, in July.

A 10 cm^2 regular piezocone penetrometer and a 200 kN rig capacity were used, produced by COPPE/UFRJ and Grom Eng., in a partnership which started in 1984 (Fig. 4). The cone and friction load capacities are 50 kN and 7.5 kN, respectively. The penetrometer has been calibrated in the

Table 1. CPT tests performed.

Test	Date	Max. depth (m)	Season
1	04/02/2015	8.84	Rainy
2	05/02/2015	5.97	Rainy
3	13/07/2015	9.04	Dry
4	14/07/2015	8.25	Dry

ranges expected in the field, before and after each series of tests. The standard rate of 20 mm/s was used in all tests. Since the water table is much below the maximum depth tested, pore pressure has not been recorded. A friction reducer was used in all tests performed.

Tube samples, 100 mm in diameter, have been collected at 1, 2 and 5 m nominal depths, in the rainy season. One cubic block sample (side of 300 mm) has been collected at 1.85 m depth, also in the rainy season. The maximum distance between CPT deployments and samples is around 9 m.

A number of index tests, determination of mineralogy and collapsibility tests have been performed, which results are presented below.

Figure 4. CPT performed in the rainy season.

4 TEST RESULTS

Fig. 5, where all CPTs are plotted together, presents a summary of the main test results. Three layers can be easily identified: the top of the deposit, with no more than 0.5 m, a second layer between 0.5 m and 2.5 m approximately and the third one, from 2.5 m depth to the maximum depth tested. The first layer, extremely resistant, probably due to desiccation, has been identified only by the very high values of cone resistance q_c and friction sleeve f_s, since no samples have been collected from this layer.

The second layer is identified by very low values of f_s, whereas showing a high void ratio value (around 1.2) and low total unit weight (less than 14 kN/m^3). The third layer presents f_s mostly in the range 120–200 kPa, having a smaller void ratio (around 0.9) and higher total unit weight (around 17 kN/m^3). The second layer shows a plasticity index I_p of 27%, whereas the third layer is more plastic, with $I_p = 45\%$.

An interesting feature of this material is the significant difference in soil type when the dispersing agent (sodium hexametaphosphate solution) is used or not, as illustrated in Fig. 6. In fact, when the dispersing agent was used, a significant amount of clay was shown, whereas the soil is a silty sand or sandy silt when it was not used. This

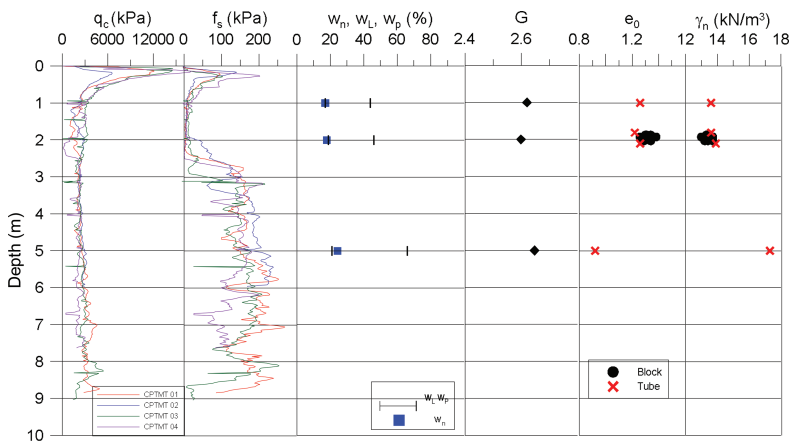

Figure 5. Cone resistance (q_c); friction sleeve (f_s); liquid limit (w_L), plastic limit (w_P) and natural water content (w_n); (b) specific gravity (G); initial void ratio (e_0); total unit weight (γ_n).

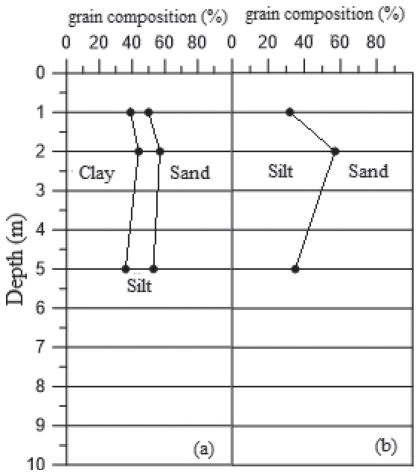

Figure 6. Grain size distribution versus depth (a) with dispersing agent; (b) without dispersing agent.

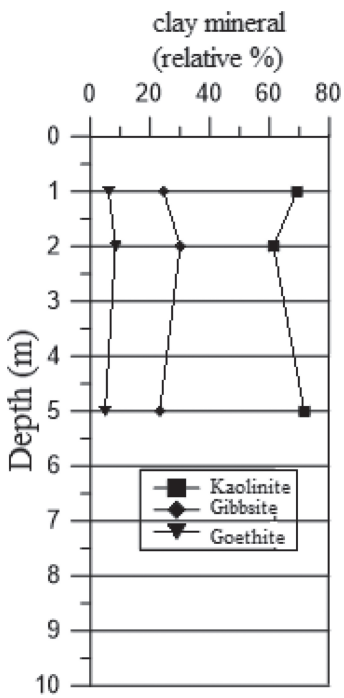

Figure 7. Clay minerals versus depth.

is a typical behaviour of a lateritic soil, as reported by e.g., Nogami and Vilibor (1981).

Mineralogical analysis was performed with X-ray diffraction at the Clay Mineralogy Laboratory, Geology Department, Federal University of Rio de Janeiro, and the obtained results are presented in Fig. 7. Kaolinite is the clay mineral predominant in the profile, which is consistent with other collapsible soils from the same area (e.g., Conciani 1997). None of the minerals present in the soil is related to soil expansion, which is also consistent with other lateritic collapsible soils.

Collapsibility tests performed in specimens trimmed from the block sample revealed 18% of collapse when the soil was soaked at 200 kPa, indicating serious problems according to the classification suggested by Jennings & Knight (1975).

5 DISCUSSION

5.1 *Differences in dry and rainy seasons*

A comparison is now undertaken between tests performed in the dry and the rainy seasons. For the sake of clarity, CPT results are magnified with respect to Fig. 5 in Figs. 8a and 8b. It must also be pointed out that despite both tests, CPT-01 and

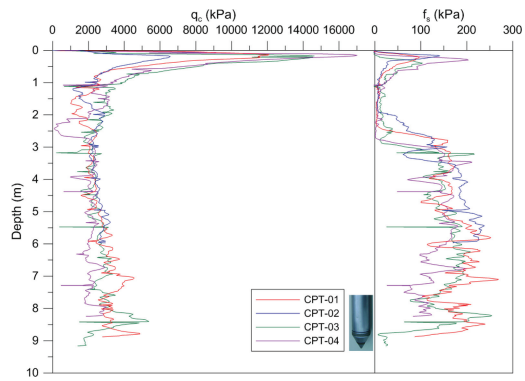

Figure 8a. CPTs performed in rainy season (CPT-01 and CPT-02) and dry season (CPT-03 and CPT-04).

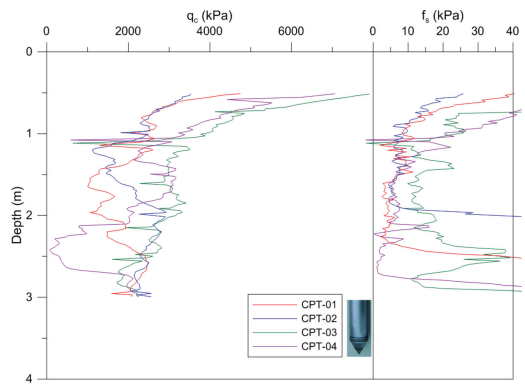

Figure 8b. Magnification of data from Fig. 8a, 0.5–3.0 m depth.

CPT-02 have been performed in the rainy season, CPT-02 was conducted just after heavy raining, and q_c (unexpectedly not f_s) recorded a difference close to ground level.

It can be observed that q_c values are higher for the CPTs performed in the dry season than in the rainy season to 2.0–2.5 m depth. Also, the same observation is valid for f_s only to approximately 1.3 m depth in the case of CPT-04 and the whole layer (2.5 m) in the case of CPT-03. The reason for the difference, as mentioned in section 2.1, is the suction reduction in the rainy season due to the increase in water content, which reached approximately 2.5 m depth.

It must be pointed out that the differences verified in the depth range 6 m–9 m may be attributed to heterogeneity of this layer, as well as to some extent to rod inclination. In fact, all tests presented an inclination increasing with depth, and CPT-04 showed the highest values, especially from 4.2 m depth, reaching 12° at the end of the test.

5.2 *Soil behaviour type*

Soil behaviour type (Robertson 2010) for CPT-01 is presented in Figs. 9 and 10, respectively the SBT chart and the SBT versus depth. It can be observed that the upper 2.5 m of the profile has been classified in general as a granular material (silty sand and sandy silt), whereas below 2.5 m depth was classified as clay. In fact, since the purpose of this classification is to provide the soil behaviour type, it can be said that it was not efficient to catch the soil behaviour type of the layer below 2.5 m, since the whole profile is constituted by lateritic soils, which behave like silty sands or sandy silts, i.e., like the soil tested without dispersing agent. An amendment of this chart is recommended to properly identify this type of soil.

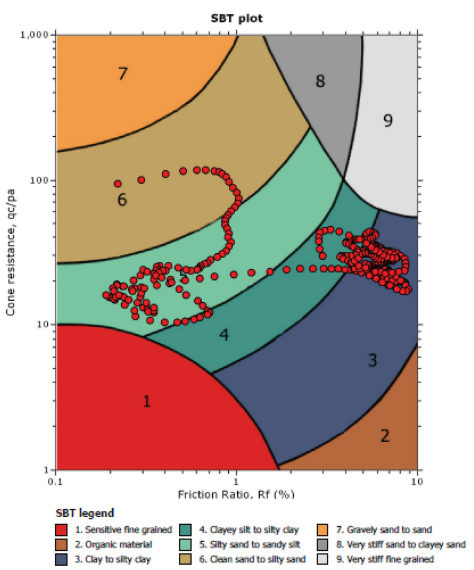

Figure 9. Test results (based on CPT-01) in the SBT chart from Robertson (2010).

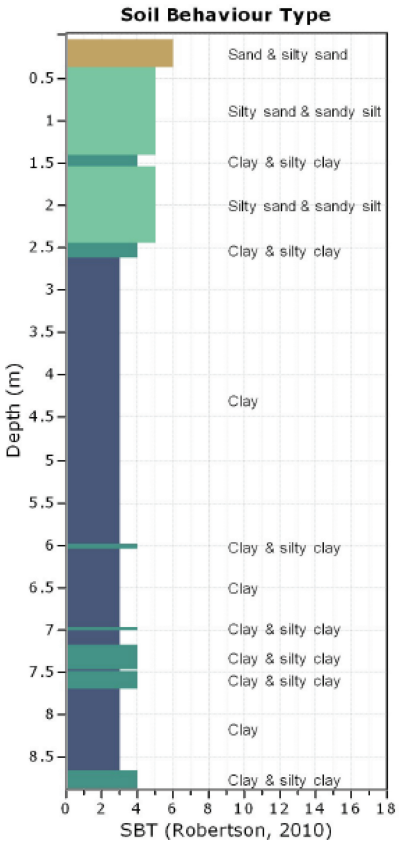

Figure 10. Test results (based on CPT-01), SBT versus depth, (Robertson 2010).

Since the test results indicate quite different results between the second and the third layers, some explanation must be provided. In fact, the cone resistance is very much influenced by the soil stiffness (e.g., Douglas & Olsen 1981), and thus the measured values seem to indicate small variation of stiffness with depth. On the other hand, it is generally assumed that the friction sleeve is related to the re moulded soil, or to the sensitivity in the case of soft (saturated) clays. The test results therefore seem to indicate a meta-stable behaviour of the upper 2.5 m of the profile, as suggested by Douglas & Olsen (1981), although those authors have not referred to unsaturated soils. Thus it seems that soil collapsibility may be indicated from

the CPT by very low friction ratio values, around 0.3% in the present case.

6 CONCLUSIONS

A test site was established in Primavera do Leste, a city 200 km east of Cuiabá, Central-West region of Brazil, one of the main Brazilian areas of soya and corn production. The research aimed at improvement of the knowledge of soil characteristics in that region, where serious problems related to foundations of silos are frequent.

CPT results indicated three soil layers: the first from the surface to 0.5 m depth; the second from 0.5 m to 2.5 m depth; the third one from 2.5 m to the tested depth, around 9 m.

Laboratory tests conducted in samples collected in the second and third layers have confirmed the qualitative difference verified in the CPT tests. In fact, the second layer is identified by very low values of f_s, whereas showing a high void ratio value (higher than 1.2) and low total unit weight (less than 14 kN/m^3). The third layer presents f_s mostly in the range 120–200 kPa, having a smaller void ratio (around 0.9) and higher total unit weight (around 17 kN/m^3). The second layer shows a plasticity index I_p of 27%, whereas the third layer is more plastic, with $I_p = 45\%$.

A significant difference in grain size distribution has been observed when the dispersing agent was used or not. When the dispersing agent was used, a significant amount of clay was shown, whereas the soil is a silty sand or sandy silt when it was not used. This is a typical behaviour of a lateritic soil, as reported by e.g. Nogami and Vilibor (1981), representing the real soil behaviour.

Mineralogical analysis indicated that kaolinite is the clay mineral predominant in the profile, which is consistent with other collapsible soils from the same area (e.g., Conciani 1997). None of the minerals present in the soil is related to soil expansion, which is also consistent with other lateritic collapsible soils.

Collapsibility tests performed in specimens trimmed from the block sample revealed 18% of collapse when the soil was soaked at 200 kPa, indicating serious problems according to the classification suggested by Jennings & Knight (1975).

Despite CPT results have indicated two soil behaviour types, the deepest layer was identified as clay by the SBT classification, which is not consistent with the real soil behaviour, better indicated by a sandy silt or silty sand, as the whole profile.

It seems that soil collapsibility may be indicated from the CPT by very low friction ratio values, around 0.3% in the present case.

The CPTs performed in dry and rainy seasons allowed the conclusion that the variation of the water content is limited to 2.0–2.5 m depth.

ACKNOWLEDGEMENTS

The authors would like to thank Luiz Carlos de Oliveira, for his help in performing most of the index tests; Edgard Luis dos Santos Bispo and Luiz Roberto da Rocha Marinho for assisting in the field testing and sampling; Prof. Helena Polivanov for performing the X-ray diffraction mineralogical analyses at the Clay Mineralogy Laboratory, Geology Department, Federal University of Rio de Janeiro.

REFERENCES

Barbosa, F.M.D.R. 2002. Monitoramento de recalque de um edifício construído sobre solo colapsível. Dissertação de Mestrado, Universidade Federal de Campina Grande, Campina Grande, PB, Braisl.

Barbosa, F.M.D.R. & Conciani, W. 2000. Estudo de caso de um pequeno edifício com fundações em solo colapsível. In: IV Seminário de Engenharia de Fundações Especiais e Geotécnica, Vol. 2, pp. 202–209, São Paulo.

Conciani, W. 1997. Estudo do colapso do solo através de ensaios de placa monitorados com tensiômetros e tomografia computadorizada. Tese de Doutorado, Universidade de São Paulo, São Carlos, SP, Brasil.

Conciani, W. & Soares, M.M. 1996. Colapso do solo de fundação de um silo – estudo de caso. In: II Seminário de Engenharia de Fundações Especiais e Geotecnia, Vol. II, pp. 287–298, São Paulo.

Douglas, B.J. & Olsen, R.S. 1981. Soil classification using electric cone penetrometer. In: Cone Penetration Testing and Experience, American Society of Civil Engineering, pp. 209–227, New York, USA.

Instituto Matogrossense de Economia Agropecuária, IMEA. 2010. available in http://www.imea.com.br/upload/publicacoes/arquivos/justificativamapa.pdf. Visited in 17/02/2016.

Jennings, J.E. & Knight, K. 1975. A guide to construction on or with materials exhibiting additional settlement due to a collapse of grain structure. In: Proceedings of the 6th Regional Conference for Africa on Soil Mechanics and Foundation Engineering, pp. 99–105.

Nogami, J.S. & Villibor, D.F. 1981. Uma nova classificação de solos para finalidades rodoviárias. In: Simpósio Brasileiro de Solos Tropicais em Engenharia, pp. 30–41, Rio de Janeiro.

Reginatto, A.R. & Ferrero, J.C. 1973. Colapse potencial of soils and soil-water chemistry. In: Proceedings VIII Int. Conf. on Soil Mechanics and Foundation Engineering, Vol. 2.2, pp. 177–183, Moscow.

Robertson, P.K. 2010. Soil behaviour type from the CPT: na update. 2º International Symposium on Cone Penetration Testing, CPT'10, Huntington Beach, CA, EUA. www.cpt10.com

WorldAtlas. 2017. available in www.worldatlas.com. Visited in 08/12/2017.

Cone Penetration Testing 2018 – Hicks, Pisanò & Peuchen (Eds)
© 2018 Delft University of Technology, The Netherlands, ISBN 978-1-138-58449-5

Liquefaction resistance by static and vibratory cone penetration tests

F.T. Stähler, S. Kreiter, M. Goodarzi, D. Al-Sammarraie & T. Mörz
MARUM-Center for Marine Environmental Sciences, University of Bremen, Bremen, Germany

ABSTRACT: Soil liquefaction is an important hazard and one of the causes of earthquake-related disasters. The prediction of soil liquefaction is a major issue in geotechnical engineering and the soil liquefaction resistance is often determined in-situ by static Cone Penetration Tests (CPT). The determination of the soil liquefaction resistance relies on empirical correlations and one way to increase accuracy might be the use of vibratory CPT. We report on displacement-controlled vibratory and static CPT performed in a calibration chamber under a simulated field boundary condition, known as BC5. Vibratory CPT led to a reduction in cone resistance for medium- to very-dense Ticino sand. The reduction ratio increased at high vibrational frequencies and was independent of the relative density for the specific stress state and type of soil. A correlation between the liquefaction resistance and static or vibratory CPT is proposed.

1 INTRODUCTION

Earthquakes are natural hazards and endanger human life by structural damage or ground failure. Soil liquefaction is one type of ground failure and the determination of the soil liquefaction resistance is an important issue in geotechnical earthquake engineering (Lo et al., 1996).

Various in-situ investigation methods have been proposed for determining the soil liquefaction resistance, including static cone penetration tests (CPT), flat dilatometer tests or shear wave velocity measurements (Ndoj et al., 2015). Static CPT are widely used and provide repeatable, continuous and cost efficient profiles (Sadrekarimi, 2016).

The determination of soil liquefaction resistance by static CPT relies on empirical correlations from comprehensive datasets (Sadrekarimi, 2016, Jorat et al., 2015). Those correlations have different target parameters and focus on the cyclic resistance ratio, the critical cone resistance, the factor of safety or the liquefaction probability (Robertsen & Wride, 1998, Shibata & Teparaksa, 1988, Idriss & Boulanger, 2006, Lai et al., 2006).

The use of empirical correlations and the quasi-static style of standard CPT lead to uncertainties in the determination of the soil liquefaction resistance (Jorat et al., 2015, McGillivary et al., 2000). One way to increase accuracy might be vibratory CPT, which imposes cyclic loading on the soil during penetration (Sasaki & Koga, 1983). This loading causes a local increase in pore pressure and a reduction in the cone resistance of liquefiable soils (Wise et al., 1999). The reduction in the cone resistance is used as a measure of the soil liquefaction resistance and is quantified by the reduction ratio *RR*:

$$RR = 1 - \left(\frac{q_{cv}}{q_{cs}} \right) \tag{1}$$

where q_{cv} = vibratory cone resistance; and q_{cs} = static cone resistance (Sasaki & Koga, 1983).

Different vibratory CPT-methods have been proposed for the determination of the *RR* and the vibration may be either horizontal or vertical and may be applied downhole or uphole (Jorat et al., 2015, Sasaki & Koga, 1983, McGillivary et al., 2000, Samui & Sitharam, 2010). Additionally, different vibrational frequencies have been utilized for field and laboratory CPT, which increase the *RR* if the first natural frequency of the soil sample is exceeded in a calibration chamber (Bonita et al., 2004). Other studies by Koga et al. (1987), Tokimatsu (1988) and Bonita et al. (2004) showed an increase in the *RR* as a function of decreasing relative density, overburden stress or critical shear strength.

The in-situ stress state and sediment material properties are difficult to determine during field investigations. This study therefore utilizes static and vibratory CPT in a calibration chamber to determine: (1) the dependence of *RR* on vibrational frequency and relative density under laboratory conditions, and (2) the feasibility of vibratory CPT for the determination of the soil liquefaction resistance.

2 METHODOLOGY

2.1 *Sample material properties*

We use Ticino sand from Northern Italy, a uniform coarse to medium sand which consists of angular to subrounded particles (Fioravante & Giretti, 2015, Fig.1). Ticino sand has been used in numerous studies and its geotechnical properties are well known (Table 1). The main mineral constituents are Feldspar (65%), Quartz (30%) and Mica (~5%) (Jamiolkowski et al., 2001).

2.2 *Calibration chamber*

The *RR* is determined by static and vibratory CPT in the MARUM calibration chamber (MARCC). This laboratory chamber is described by Fleischer et al. (2016) and is similar to a large triaxial cell with a sample of 30 cm diameter and 54.5 cm height. The sample is laterally enclosed by a flexible latex membrane and surrounded by three circumferential Linear Variable Displacement Transducers (LVDT). These sensors are placed at vertical distances of 15, 25 and 35 cm from the top of the sample. The horizontal stress on the sample is applied by water pressure in the cell and the vertical stress is controlled by a water-filled rubber cushion at the bottom of the sample. The upper boundary of the sample is a rigid sinter metal filter and syringe pumps are utilized for pore-pressure, backpressure and pore fluid volume control (Fleischer et al., 2016).

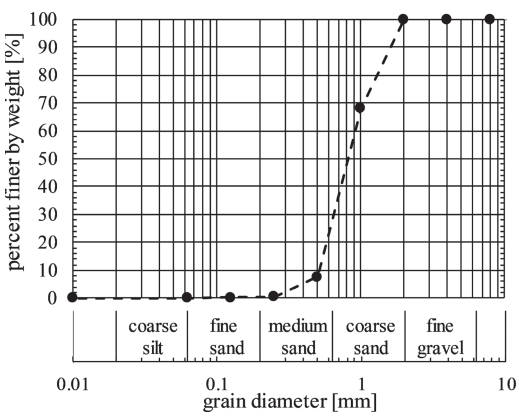

Figure 1. Grain-size distribution of Ticino sand according to DIN 18123 (2011).

Table 1. Geotechnical properties of Ticino sand, where e_{min} = minimum void ratio; e_{max} = maximum void ratio; Gs = specific gravity; D_{50} = median cumulative grain size; and U_c = unconformity index.

Reference	e_{min} [–]	e_{max} [–]	G_S [–]	D_{50} [mm]	U_c [–]
This study*	0.579	0.927	2.683	0.81	1.78
[1]	0.574	0.923	2.68	0.53	1.3
[2]	0.578	0.924	–	0.53	1.61
[3]	0.568	0.915	2.67	0.50	1.58

* Determination according to DIN 18126 (1996), DIN 18124 (2011) and DIN EN ISO 14688–2 (2013), [1] Fioravante & Giretti (2015), [2] Butlanska et al. (2014), [3] Kulhawy & Mayne (1990).

2.3 *Sample preparation*

Sixteen Ticino sand samples were prepared by air pluviation to have relative densities between 50 and 100%. All medium-dense to very-dense samples were vacuum-saturated in the MARCC. A full vacuum was applied on the sample and de-aired and demineralized water was allowed to slowly percolate from the bottom to the top of the sample (ASTM D7181, 2011). A backpressure of 100 kPa was applied after saturation and a Skempton' B-value of at least 0.95 was reached. The mean effective stress was subsequently increased to 126.67 kPa by applying a vertical effective stress of 200 kPa and a horizontal effective stress of 90 kPa. These conditions represent a burial depth of 18 to 20 m, which is important for off- and onshore monopile foundations. The consolidation lasted for 90 minutes and all volume changes were measured during consolidation (DIN 18137–2, 2011).

2.4 *Testing conditions*

Five boundary conditions are defined for calibration chamber testing (Table 2). BC5 is the most advanced boundary condition with a quasi-constant lateral stiffness and a constant vertical stress on the sample boundary (Balachowski, 2006). The quasi-constant lateral stiffness simulates infinite surrounding soil and reduces boundary artefacts

Table 2. Boundary conditions for calibration chambers (Huang & Hsu, 2005, Balachowski, 2006).

Boundary condition	Top & bottom boundary		Lateral boundary	
	Stress	Strain	Stress	Strain
BC1	Constant	-	Constant	–
BC2	–	0	–	0
BC3	Constant	-	–	0
BC4	–	0	Constant	–
BC5	Constant	–	Constant stiffness	

in the calibration chamber (Huang & Hsu, 2005). These artefacts are expected to be significant for all samples in the MARCC not under BC5 conditions, because the sample to cone diameter ratio of $R_d = 25$ is less than the recommended value of $R_d \geq 33$ or $R_d \geq 100$ for loose or very dense sand, respectively (Ahmadi & Robertson, 2008).

The lateral stiffness control for BC5 in the MARCC is based on the cylindrical cavity expansion model by Ladanyi (1972). This model utilizes the equilibrium equation in cylindrical coordinates for zero body forces and no vertical stress variations:

$$\frac{d\sigma_r}{dr} + \frac{\sigma_r - \sigma_\theta}{r} = 0 \tag{3}$$

where r = sample radius; σ_r = total principal stress in the radial direction; and σ_θ = total principal stress in the tangential direction.

This equilibrium equation is integrated for an incremental change in the radius from r_i to r_{i+1} of the cavity expansion:

$$\sigma_r^{i+1} = -q_{i,i+1}(\ln(1+\varepsilon_r^{i+1}) - \ln(1+\varepsilon_r^{i})) + \sigma_r^{i} \tag{4}$$

where $q_{i,i+1}$ = deviatoric stress at increment i to $i + 1$; ε_r = radial strain; and σ_r = radial stress at the increment indicated by the superscript.

The initial radial stress σ_r^i of 190 kPa and the initial radial strain ε_r^i of 0 are known before the CPT-cavity expansion and the induced radial strain ε_r^{i+1} is derived by three LVDT sensors during cone penetration. The deviatoric stress $q_{i,i+1}$ depends on the stress level, the distance from the center of cavity expansion and the soil properties and is determined by a lateral compression test on each sample before the CPT (Huang & Hsu, 2005). This compression test is performed by increasing the horizontal stress by 10 kPa/min until a maximum radial strain of 0.08% is reached (Huang & Hsu, 2005). The deviatoric stress between i and $i + 1$ varies systematically for each strain increment, following:

$$q_{i,i+1} = \left| \frac{\Delta\sigma_h}{\Delta \ln(1+\varepsilon_r^{i,i+1})} \right| \tag{5}$$

The lateral compression test determines a relation between ε_r and $q_{i,i+1}$. This function is assumed to be valid during CPT-cavity expansion as well and is used, together with Equation 4, to control the horizontal stress at the sample boundary as a unique function of ε_r. After lateral compression, all samples were reconsolidated to a horizontal stress of 190 kPa following the procedure proposed by Huang & Hsu (2005). The apparent tangent Young's modulus is derived from the gradient of the stress-strain curve at a lateral strain of 0.07% for further evaluation.

Table 3. Test scheme for static and vibratory CPT.

f [Hz]			ε_A [mm]	D_R [%]
Static			–	50–100
10	20	30	±0.5	50–75
10	20	30	±0.5	75–90
10	20	30	±0.5	90–100

2.5 *Cone penetration*

All CPT are performed drained, utilizing a small cone with a diameter of 12 mm. The test scheme includes 7 static CPT and 9 vibratory CPT at three different vibrational frequencies f of 10, 20 and 30 Hz and the same displacement amplitude ε_A of ± 0.5 mm (Table 3). Each static and vibratory CPT series includes different relative densities. The vibration is oriented in the penetration direction and is induced by a highly dynamic hydraulic piston with a 2 kHz real-time controller. The penetration rate of 20 ± 0.3 mm/s was constant for all CPT following DIN EN ISO 22476-1 (2013), and the steady-state cone resistance is determined for each CPT at a penetration depth of usually 100 to 300 mm. The vibratory and static cone resistances are then used to determine RR for different relative densities and vibrational frequencies using Equation 1.

3 RESULTS

3.1 *The static cone resistance*

The steady state cone resistance of static CPT increases exponentially with an increase in the relative density (Fig. 2):

$$q_{cs} = 2.86 \cdot 10^6 e^{2.61 D_R},\ R^2 = 0.99 \tag{6}$$

where D_R = relative density; and R^2 = coefficient of determination.

The state of soil, in terms of relative density and stress level, is expressed by the state parameter Ψ (Been & Jeffries, 1985). The state parameter was determined by Fioravante & Giretti (2015) for Ticino sand and is utilized for a mean effective stress of 126.67 kPa. A linear correlation is found between the static cone resistance and the state parameter:

$$q_{cs} = (-180.26\psi - 16.16) \cdot 10^6,\ R^2 = 0.99 \tag{7}$$

3.2 *The reduction ratio RR*

The difference between the static and vibratory cone resistance Δq_c is determined for each vibratory CPT and takes the measured vibratory and the calculated static cone resistance for exactly the same relative density into account (Fig. 2). Δq_c increases as a function of either increasing vibrational frequency or increasing relative density and allows a calculation of the reduction ratio *RR*.

In contrary to expectations, *RR* is independent of relative density (Fig. 3). This is related to nearly parallel trends of static and vibratory cone resistances and similar Δq_c for all density ranges. Increases in Δq_c and *RR* are therefore mainly related to increases in the vibrational frequency (Fig. 3):

$$\Delta q_c = q_{cs} - q_{cv} = 4 \cdot 10^5 f,\ R^2 = 0.86 \text{ and} \quad (8)$$

$$RR = \Delta q_c / q_{cs} = 0.016 f,\ R^2 = 0.99 \quad (9)$$

3.3 *The liquefaction resistance*

The liquefaction resistance, in terms of the cyclic resistance ratio *CRR,* is defined by Fioravante & Giretti (2015) for Ticino sand and for an earthquake magnitude of 7.5. The *CRR* depends on the state para- meter and is related to the static and vibratory cone resistance in Equation 7 and 8:

$$CRR_{7.5} = 6.4 \cdot 10^{-9} (q_{cs}) + 0.041, R\boxtimes = 0.99 \text{ and} \quad (10)$$

$$CRR_{7.5} = 6.4 \cdot 10^{-9} (q_{cv} + 4 \cdot 10^5 f) + 0.041 \quad (11)$$

where $CRR_{7.5}$ = cyclic resistance ratio for an earthquake magnitude of 7.5.

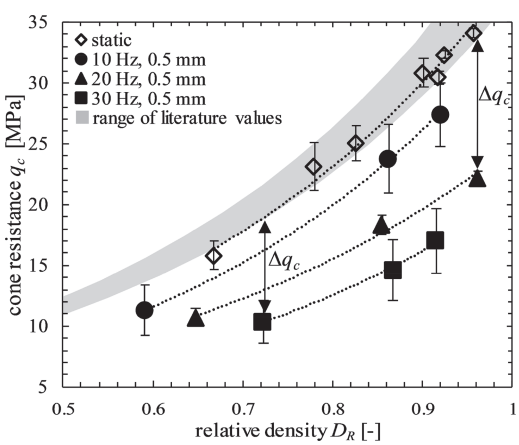

Figure 2. Static and vibratory cone resistance q_c as a function of the relative density D_R for different vibrational frequencies and a constant amplitude of $\varepsilon_a = \pm$ 0.5 mm.

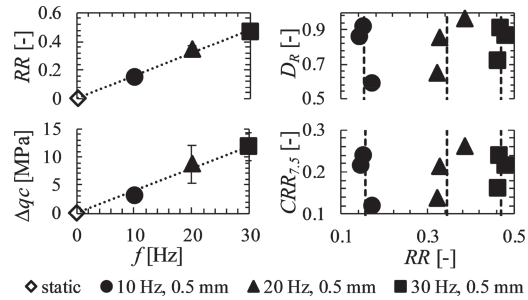

Figure 3. Reduction ratio *RR* and the difference in the cone resistance Δq_c as a function of the vibrational frequency *f* as well as the relative density D_R and the cyclic resistance ratio *CRR* as a function of the reduction ratio *RR*.

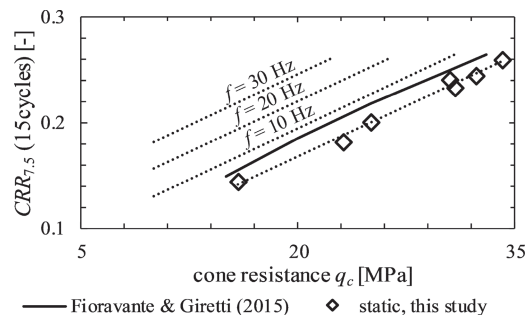

Figure 4. Measured static and calculated vibratory cone resistance q_c as a function of the cyclic resistance ratio *CRR* and the vibrational frequency *f*.

All correlations of *CRR* are illustrated in Figure 4 and a linear increase in *CRR* is observed as a function of either increasing static or increasing vibratory cone resistance for a specific frequency.

The *CRR* is independent of *RR* (Fig. 3). This indicates that the *RR* cannot be used to determine soil liquefaction resistance for our specific stress state and range of relative density.

4 DISCUSSION

4.1 *The static cone resistance*

The static cone resistance in Equations 6 and 7 is compared with CPT correlations from Fioravante & Giretti (2015), Jamiolkowski et al. (2001) and Baldi et al. (1986) on Ticino sand at the same stress state (Fig. 2). This comparison indicates that our data fall within the range defined by previous studies.

4.2 *Static and vibratory CPT under BC5*

The theory of CPT-cavity expansion suggests an increase in the radial zone of influence for an increase in the relative density or soil stiffness

(Bonita et al., 2004). Such an increase in the radial zone causes a higher radial strain at the sample boundary during CPT and a higher maximum horizontal stress under boundary condition BC5 (Huang & Hsu, 2005).

An increase in the maximum horizontal stress is observed in our study and is related to an increase in the relative density or the apparent tangent Young's modulus (Fig. 5). This relation is independent of the mode of penetration and indicates that differences in the static and vibratory cone resistance are not related to differences in the horizontal stress.

4.3 *The reduction ratio RR*

Contractive or dilative soil behavior causes water to flow in or out of the sample during drained CPT. This water volume is measured and the total outflow is plotted against the relative density for all modes of penetration (Fig. 6).

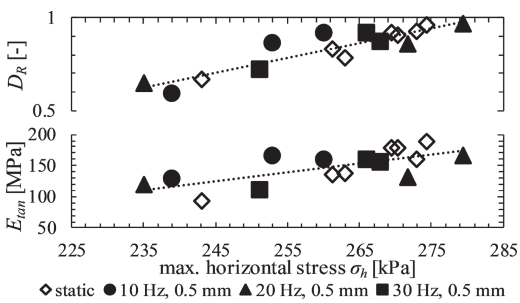

Figure 5. Relative density D_R and apparent tangent Young's modulus E_{tan} as a function of the maximum horizontal stress σ_h.

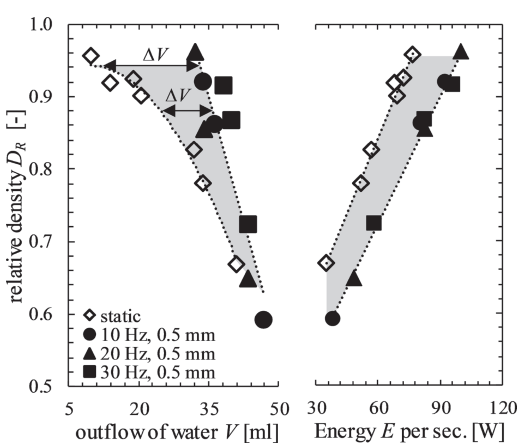

Figure 6. Relative density D_R as a function of the total outflow of pore water V and the mean energy E per second.

The vibratory outflow is distinctly higher than the static outflow, although both decrease with an increase in the relative density. During vibratory cone penetration the sediment immediately surrounding the cone might not be fully drained and an increase in the total outflow might indicate an increase in the pore pressure due to vibratory CPT. Such increase would lead to a reduction in soil strength and might explain a reduction in the cone resistance of vibratory CPT.

The difference ΔV between the static and vibratory outflows increases with an increase in relative density, which indicates that the zone of vibrational influence in the soil mass is larger at higher densities, probably due to a higher stiffness of the soil. A larger zone of influence leads to an increase in the outflow for the same contractive change of pore space, but possibly to less effective drainage and to a higher pore pressure. The influence of pore pressure may explain the negligible changes in the *RR* for different relative densities or zones of influence.

This observation differs from previous studies by Bonita et al. (2004), Tokimatsu (1988) and Sasaki & Koga (1983) who consistently observed a decrease in the *RR* with an increase in the relative density. This different observation may be related to differences in the soil type, the stress state or the vibrational method, because these studies all utilized vibratory CPT with a defined energy for all densities.

In this study, the mean energy imparted to the soil increases with an increase in the relative density and is a function of the frequency and force of penetration (Fig. 6). The energy of vibratory CPT is higher than for static CPT but is similar for all modes of vibratory cone penetration. The similarity of vibratory CPT may be caused by energy dependent changes of the grain skeleton, possibly combined with an increase in the pore pressure. This leads to a lower cone resistance and penetration force with an increase in the vibrational movement. Different energies of static and vibratory CPT suggest a complex relation and require further testing.

The effect of different frequencies on the *RR* was studied by Bonita et al. (2004), who observed an abrupt increase in the *RR* after exceeding the first natural frequency of ~25 Hz. This abrupt increase is not observed in our study (Fig. 3), probably due to smaller dimensions of the MARCC with a higher natural frequency of the system. An increase in the *RR* might be explained by a decrease in the drainage capability of the soil and by an increase in pore pressure around the cone.

4.4 *The liquefaction resistance*

An increase in *CRR* is related to an increase in the static cone resistance, which is consistent with

previous studies on Ticino sand by Fioravante & Giretti (2015) (Fig. 4). Because the *RR* is mainly dependent on vibrational frequency and not on relative density, *RR* is insufficient for determining the *CRR* for this specific state and type of soil. This observation is in contrast to previous studies by Tokimatsu (1988) and Koga et al. (1987) who determined the liquefaction potential or the cyclic soil strength on the basis of the *RR*. Such differences in observations may be related to differences in the vibrational frequency of 200 Hz, the technical realization of vibratory CPT, the stress state or material properties.

5 CONCLUSION

Static and vibratory CPT were performed in a small-volume calibration chamber under BC5 boundary conditions. Vibratory CPT reduced the cone resistance in medium- to very-dense Ticino sand. The reduction ratio increased with an increase in the vibrational frequency and was independent of the relative density. A scheme for the determination of soil liquefaction resistance is proposed, based on the static or vibratory cone resistance for a defined frequency. A reduction of the cone resistance might be related to an increase in pore pressure and to changes in the drainage capability.

ACKNOWLEDGEMENTS

This project was supported by the Federal Ministry for Economic Affairs and Energy (BMWi), Project: Vibro Drucksondierungen, FKZ: 0325906 A and the MARUM—Center for Marine Environmental Sciences, University of Bremen. We thank Marc Huhndorf, Joann Schmid, Wolfgang Schunn, Amr Elshafei and Tim Stanski for invaluable technical assistance. We acknowledge Daniel A. Hepp, Matt J. Ikari and Max O. Kluger for helpful discussions on the paper.

REFERENCES

Ahmadi, M.M. & Robertson, P.K. 2008. A numerical study of chamber size and boundary effects on CPT tip resis-tance in NC Sand. *Scientia Iranica* 15(5): 541–553.

ASTM D7181 2011. Standard Test Method for Consolidated Drained Triaxial Compression Test for Soils. ASTM International, West Conshohocken, USA.

Balachowski, L. 2006. Penetration Resistance of Lubiatowo Sand in Calibration Chamber Tests. *Archives of Hydro-Engineering and Environmental Mechanics* 53(4): 311–329.

Baldi, G., Bellotti, R., Ghionna, V., Jamiolkowski, M. & Pasqualini, E. 1986. Interpretation of CPTs and CPTUs - part II: drained penetration in sands. *Fourth International Geotechnical Seminar on Field Instrumentation and in Situ Measurements; Proc.*, Singapore.

Been, K., Jefferies, M.G. (1985). A state parameter for sands. *Géotechnique* 35(2): 99–112.

Bonita, J., Mitchell, J.K. & Brandon, T.L. 2004. The effect of vibration on the penetration resistance and pore water pressure. In Mayne, V. d. F. (ed.), *Geotechnical and Geophysical Site Characterization; Proc. ISC–2*. Porto, 19–22 September 2004, Rotterdam: Millpress.

Butlanska, J., Arroyo, M., Gens, A. & O'Sullivan, C. 2014. Multi-scale analysis of cone penetration test (CPT) in a virtual calibration chamber. *Canadian Geotechnical Journal* 51(1): 51–66.

DIN 18123, 2011. Soil, investigation and testing – Deter-mination of grain-size distribution. German Standards.

DIN 18124, 2011. Soil, investigation and testing – Determination of density of solid particles – Capillary pycnometer, wide mouth pycnometer, gas pycnometer. German Standards.

DIN 18126, 1996. Soil, investigation and testing – Determination of density of non-cohesive soils for maxi-mum and minimum compactness. German Standards.

DIN 18137–2, 2011. Soil, investigation and testing – Determination of shear strength – Part 2: Triaxial test. German Standards.

DIN EN ISO 14688–2, 2013. Geotechnical investigation and testing – Identification and classification of soil – Part 2: Principles for a classification. German Standard.

DIN EN ISO 22476–1, 2013. Geotechnical investigation and testing – Field testing – Part 1: Electrical cone and piezocone penetration test. German Standards.

Fioravante, V. & Giretti, V. 2015. Unidirectional cyclic resistance of Ticino and Toyoura sands from centrifuge cone penetration tests. *Acta Geotechnica* 11(4): 953–968.

Fleischer, M., Kreiter, S., Mörz, T. & Huhndorf, M. 2016. A Small Volume Calibration Chamber for Cone Penetration Testing (CPT) on Submarine Soils. In Lamarche, G., et al. (eds.), *Submarine Mass Movements and their Consequences*: 181–189, Springer.

Huang, A.-B. & Hsu, H.-H. 2005. Cone penetration tests under simulated field conditions. *Géotechnique* 55(5): 345–354.

Idriss, I.M. & Boulanger, R.W. 2006. Semi-empirical procedures for evaluating liquefaction potential during earthquakes. *Soil Dynamics and Earthquake Engineering* 26(2–4): 115–130.

Jamiolkowski, M., Lo Presti, D.C.F. & Manassero, M. 2001. Evaluation of relative density and shear strength of sands from CPT and DMT. *Soil Behavior and Soft Ground Construction*: 201–238.

Jorat, M.E., Mörz, T., Moon, V., Kreiter, S. & de Lange, W. 2015. Utilizing piezovibrocone in marine soils at Touranga Harbor, New Zealand. *Geomechanics and Engineering* 9(1): 1–14.

Koga, Y., Sasaki, Y., Itoh, Y. & Matsuo, O. 1987. Field investigation of seismically damaged sites by use of vibratory cone penetrometer. In Raufaste, N.J. (Ed.

18th Joint Meeting of the U.S.-Japan Cooperative Program in Natural Resources Panel on Wind and Seismic Effects, Proc.

Kulhawy, F.H. & Mayne, P.W. 1990. Manual on estimating soil properties for foundation design. Cornell University, Ithaca, New York.

Ladanyi, B. 1972. In-situ Determination of Undrained Stress-strain Behavior of Sensitive Clays with the Pressuremeter. *Canadian Geotechnical Journal* 9(3): 313–319.

Lai, S.-Y., Chang, W.-J. & Lin, P.-S. 2006. Logistic Regression Model for Evaluating Soil Liquefaction Probability Using CPT Data. *Journal of Geotechnical and Geoenvironmental Engineering* 132(6): 694–704.

Lo, R.C., Henderson, P.W., Morrison, K.I. & Finn, W.D.L. 1996. Seismic geotechnical considerations - An overview (No 1853). *Eleventh World Conference on Earthquake Engineering;* Acapulco, 23–28 June 1996, Elsevier Science.

McGillivary, A., Casey, T., Mayne, P.W. & Schneider, J.A. 2000. An Electro-Vibrocone for site-specific evaluation of soil liquefaction potential. In Mayne & Hryciw (eds.), *Innovations and Applications in Geotechnical Site Characterization; Proc. Geodenver.*

Ndoj, A., Shkodrani, N. & Hajdari, V. 2015. Evaluation of liquefaction potential of soil using CPT and SPT. *Proceedings of International Conference on Architecture, Structure and Civil Engineering.* Antalya, Turkey.

Robertsen, P.K. & Wride, C.E. 1998. Evaluation of cyclic liquefaction potential using the cone penetration test. *Canadian Geotechnical Journal* 35: 442–459.

Sadrekarimi, A. 2016. Evaluation of CPT-based characterization methods for loose and medium-dense sands. *Soils and Foundations* 56(3): 460–472.

Samui, P. & Sitharam, T.G. 2010. Design of a piezovibrocone and calibration chamber. *Geomechanics and Engineering* 2(3): 177–190.

Sasaki, Y. & Koga, Y. 1983. Vibratory cone penetrometer to assess the liquefaction potential of the ground. In Chung, R.M., Lew, H.S., Kovacs, W.D. (ed.), *14th Joint Panel Conference of the U.S.-Japan Cooperative Program in Natural Resources; Proc.*

Shibata, T. & Teparaksa, W. 1988. Evaluation of liquefaction potentials of soils using cone penetration tests. *Soils and Foundations* 28(2): 49–60.

Tokimatsu, K. 1988. Penetration tests for dynamic problems. *First International Symposium on Penetration Testing ISOPT-1; Proc. Orlando, 20–24 March 1988*. Rotterdam, Brookfield: Balkema.

Wise, C.M., Mayne, P.W. & Schneider, J.A. 1999. Prototype piezovibrocone for evaluating soil liquefaction susceptibility. *Earthquake Geotechnical Engineering*: 537–542.

Taylor & Francis
Taylor & Francis Group
http://taylorandfrancis.com

Cone Penetration Testing 2018 – Hicks, Pisanò & Peuchen (Eds)
© 2018 Delft University of Technology, The Netherlands, ISBN 978-1-138-58449-5

In situ characterisation of gas hydrate-bearing clayey sediments in the Gulf of Guinea

F. Taleb, S. Garziglia & N. Sultan
IFREMER, Département REM, Unité des Géosciences Marines, Plouzané, France

ABSTRACT: Increasing needs for energy resources have moved deep offshore developments and research efforts towards regions where high pressure and low temperature conditions allow gas and water to form Gas Hydrates (GH). However, owing to difficulties in sampling and preserving GH under in-situ stability conditions, GH-bearing sediments remain particularly challenging to characterise using conventional laboratory methods. This paper presents the experience gained in the use acoustic and piezocone soundings in characterising gas-hydrate bearing clayey sediments offshore Nigeria. Acoustic measurements of compressional wave velocity are shown to be an expedient means of both detecting and quantifying GH in sediments. Piezocone data and their location in normalised soil classification charts highlight trends in response suggesting that GH-bearing clayey sediments are predominately contractive at large strains. The observed trend of increasing cone resistance combined with increasing pore pressure suggests that the sensitivity of GH-bearing sediments tend to increase with their stiffness and strength.

1 INTRODUCTION AND GEOLOGICAL SETTING

Gas hydrates (GH) are ice-like solid compounds formed of gas molecules, which are trapped within a crystalline structure of water molecules (Sloan, 2003). Due to their wide geographical distribution and potential as a future energy resource but moreover as a geotechnical hazard for various offshore operations, GH have stimulated significant industrial and academic interests. They mainly occur in continental margins and polar permafrost layers (Kvenvolden, 1993). The presence of these metastable geo-compounds requires: (a) low temperature, (b) high pressure and (c) sufficient amount of gas with a concentration exceeding the solubility limit in water. Despite significant advances made to characterise the fabric and structure of GH bearing sediments, considerable uncertainty remains regarding their mechanical behaviour and response to external forcing. This is particularly true for GH-bearing fine-grained sediments, which remain challenging to preserve or synthesise prior to laboratory testing. Hence, in this work, their detection and characterisation has been inferred via in-situ acoustic and geotechnical measurements in the Gulf of Guinea.

The Gulf of Guinea is one area where dense accumulation of shallow GH has been confirmed based on various coring and geophysical data and in-situ measurements (Sultan et al., 2007 & 2010).

In certain cases, solid GH and free gas were observed to coexist due to the presence of free gas voids within the hydrates nodules; hence, resulting in a material with a spongy texture. The latter studies have also shown that piezocone sounding allows the detection of GH, based on simultaneous increases in cone tip resistance, sleeve friction and pore water pressure. However, as discussed by several authors, it is complicated to distinguish a GH rich layer from a heavily cemented clay one (Lunne et al., 1997).

The present work is built upon these findings with the aim of understanding the effect of the concentration and distribution of GH on the mechanical behaviour of their host sediment. This mainly requires the detection, quantification and characterisation of GH, which was possible by correlating in situ- acoustic and geotechnical measurements. This investigation was carried out by comparing the similarities and the differences between a reference site without GH and three GH-bearing sites. Finally, different classification charts were used conjointly in order to highlight trends in mechanical response of GH-bearing clayey sediments.

2 TOOLS AND METHODS

2.1 *In-situ measuring tools*

In-situ measurements were carried out using the Penfeld seabed rig developed by Ifremer to ensure

Table 1. Investigated sites.

CPT site	Depth (m)	Nearby Vp site
GMPFM06-01	1140	GMPFV07-01
ERCPT02-05	1180	GMPFV07-05
GMPFM06-10	1141	GMPFV07-08
ERCPT02-08	1177	GMPFV03-03

continuous penetration of a rod down to 30 m below seabed with a thrust of 40 kN at a standard rate of 2 cm/s (Sultan et al., 2007). The rod can push two types of probes into the sediment to alternatively carry out piezocone or acoustic soundings. Pressure compensated sensors in the piezocone include two different load cells to measure the tip resistance and the sleeve friction along with a differential pore pressure sensor located immediately behind the cone (u_2 position).

The ultrasonic fork allows carrying out acoustic soundings by measuring on the fly the velocity of compressional waves (Vp) up to 2200 m/s. This unique 'direct-insertion' device utilises pulse transmission in which a compressional wave of 1-MHZ is produced at one branch of the fork and recorded at the opposite one located 7 cm apart. Four sites are presented in this paper (Table 1): one reference site (GMPFM06–01) and three GH-bearing sites (ERCPT02–05, GMPFV07–08 and ERCPT02–08). GH were detected at all of these sites using direct (Sultan et al., 20007) and indirect methods (Wei et al., 2015).

2.2 *Effective medium modelling*

In this work, the effective medium model developed by Helgerud et al. (1999) has been used to estimate GH concentration in the sediment by relating the stiffness of the dry frame to porosity, mineralogy and effective stress (Figure 1). The model allows accounting for the effect of hydrate habit in the pore space by alternatively assuming that: a) hydrate alters only the pore fluid elastic properties; b) hydrate contributes stiffness to the sediment by becoming part of the load-bearing framework.

The use of Helgerud et al. (1999) model together with the in-situ Vp measurement leads to the detection and the quantification of an upper bound (S_{hmax}) and a lower bound (S_{hmin}) for gas hydrates and free gas contents in the sediment. Based on studies performed by Ghosh et al. (2010), only S_{hmin} will be shown in this paper, since it is more reliable than S_{hmax}.

The porosity along with the clay, calcite and quartz fractions required as input parameters to the model were determined from a sediment core representative of the study area. Following Helgerud et al (1999), the elastic properties and

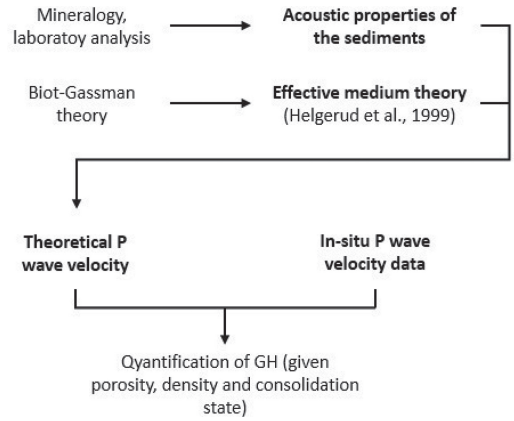

Figure 1. Effective medium theory (Helgerud et al., 1999).

Table 2. Properties of sediment constituents (Helgerud et al., 1991).

Constituent	Bulk modulus (GPa)	Shear modulus (GPa)	Density (g/cm^3)
Clay	20.9	6.85	2.58
Calcite	76.8	32.0	2.71
Quartz	36.6	45.0	2.65
GH	7.9	3.3	0.90
Methane Gas	0.10–0.12	0	0.23

densities used in this study for the different minerals are shown in Table 2.

3 RESULTS

The GMPFM06–01 and GMPFV07–01 are CPTu and Vp reference sites at which neither GH nor free gas were detected. These sites serving as a basis to compare with GH bearing sites are characterised by compressional velocities varying between 1450 m/s and 1510 m/s and a linear increase with depth of the cone tip resistance, sleeve friction and pore water pressure. Figure 2 shows the Vp profiles at sites GMPFV07–05, GMPFV07–08 and GMPFV03–03 and the CPTu results at sites ERCPT02–05, GMPFM06–10 and ERCPT02–08. The presence of GH can clearly be observed by sudden increases in the Vp profiles combined with strong variations in q_t, f_s and Δu_2. It is noteworthy that in some cases GH-bearing sediments were too stiff to allow piezocone penetration down to 30 m depth. This eventually leads to an early refusal as can be seen on Figure (2-a) and (2-b) for sites ERCPT02–05 and GMPFM06–10. At site

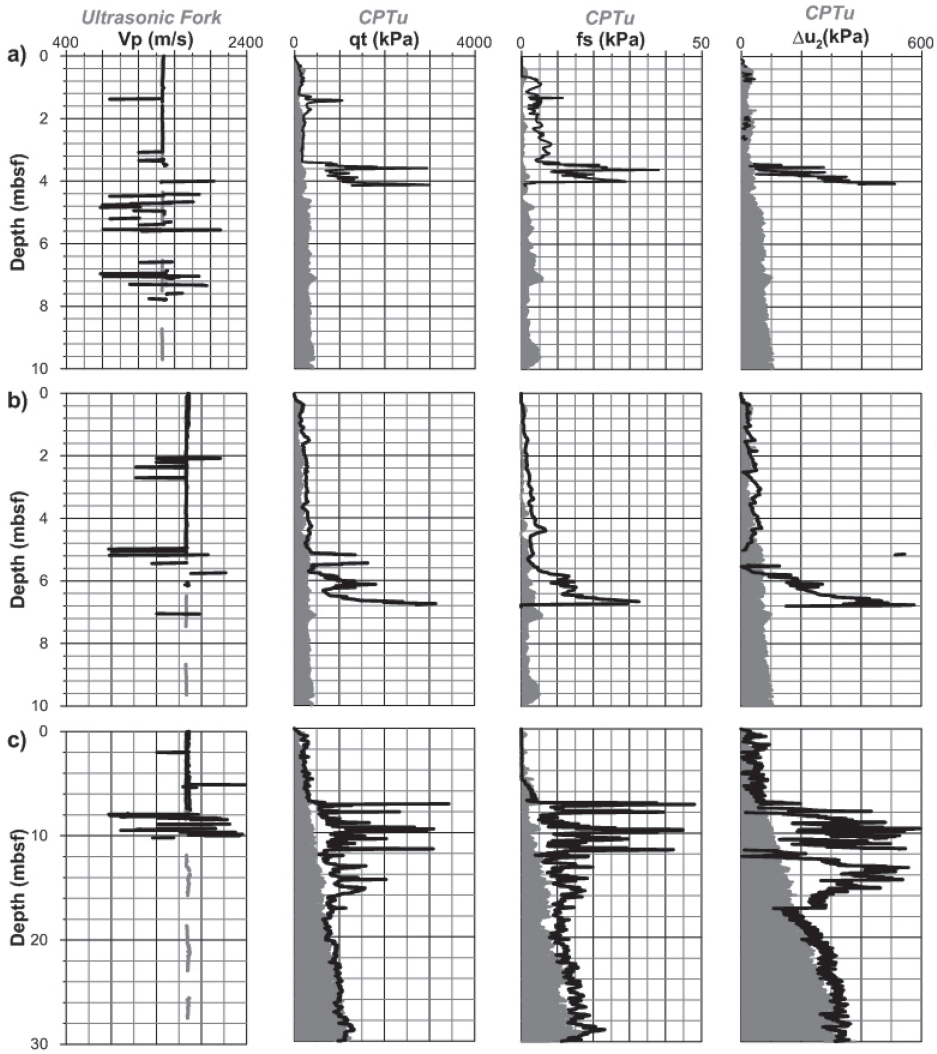

Figure 2. In-situ Vp and CPTu measurements at GH- bearing sites (black continuous lines) (a) GMPFV07–05- and ERCPT02–05 (black continuous lines, (b) GMPFV07–08 and GMPFM06–10 and (c) GMPFV03–03 and ERCPT02–08-. Reference sites GMPFV07–01 and GMPFM_06–01 are shown as dashed grey lines and grey shaded areas respectively.

ERCPT02–05, an early refusal at around 4.2 mbsf is noticed for the Penfeld CPTu and at 8.5 mbsf for the Penfeld Vp. An increase in Vp can be observed at 4 mbsf where it was possible to calculate a value of 28% for S_{hmin}. These observations correlates with high q_t values up to 3000 kPa, which is nearly 6 times higher than that of the reference site at the same depth. Further increases noticed in f_s and Δu_2 that are also 5 to 6 times higher than that of the reference highlight the strong presence of GH.

The GMPFM06–10 profiles suggest that GH were met at around 5 mbsf with a Vp value rising up to 1700 m/s, where a value of 26% for S_{hmin} was calculated.

For the ERCPT_02–08, simultaneous increase in q_t, f_s and Δu_2 readings are observed at around 7 mbsf. The q_t profile suggests the presence of two distinct GH rich layers. In the first one extending from 7 mbsf to 11.5 mbsf, q_t reaches values as high as 3153 kPa to 4913 kPa. The second one extends from 12.5 mbsf to 17.5 mbsf with q_t values in the range of 1062 kPa to 2004 kPa. These observations correlate with strong variations in the Vp profile. It is to note that at this site, at 8.2 mbsf, 8.4 mbsf

and 8.6 mbsf, GH concentrations of 45%, 55% and 40% correlate with q_t values as different as 2946 kPa, 1285 kPa and 1483 kPa, respectively.

It is noteworthy that in situ acoustic measurements can also be used to identify the presence of free gas that significantly decreases the compressional wave velocity below 1500 m/s.

In order to further compare and highlight features of GH-bearing clayey sediments during in-situ testing, piezocone data were plotted in different classification charts. Figure 3 shows the soil behaviour classification charts proposed by Schneider et al., (2008 and 2012). Overall, piezocone data from GH-bearing sites (ERCPT02–05, GMPFM06–10 and ERCPT02–08) can be clearly distinguished from that of reference site (GMPFM06–01) by showing a more pronounced trend of increasing $\Delta u_2 / \sigma'_{v0}$ values with increasing Q_t values. Most of the data from GH-bearing sites plot in zone 1b of chart (a) indicating a clay behaviour. While thirty-one percent of these data fall in the region of Taranto cemented clays (after Jamiolkowski et al., 1986), the rest tend to plot towards the region of ice lenses (after Fortier and Yu, 2012). Some points are scattered in zone 1a/3 but none were detected in zone 2. This indicates that piezocone penetration occurred fully undrained in GH-bearing sediments. Based on the Q_t-R_f chart (Figure 3-b), the majority of data plots in zone 1c for GH-bearing sites, which by comparison with the reference site suggests that the presence of GH tends to increase the sensitivity of the host sediment.

For site GMPFM06–10, some data plot in the drained sand mixtures zone (zone 2). On the other hand, some data from site ERCPT02-08 plot in zone 2 and even left of it with friction ratios (F_r) lower than 0.1% as reported by Fortier & Yu (2012) for ice lenses.

In order to investigate why some GH-bearing sediments from site GMPFM06-10 have different classification between the two charts, piezocone data have been plotted in charts updated by Robertson (2016) as bubbles whose size is proportional to the GH content (Figure 4). The majority of the piezocone data for the GH-bearing sites plot in the clay-like contractive (CC) and sensitive (CCS) regions on the $Q_{tn} - \Delta u_2 / \sigma'_{v0}$ chart (Figure 4) with one point in the transitional contractive region (TC). However, no points were observed in the sand-like dilative region (SD), which is in accordance with chart (a) in Figure 3. On the other hand, for sites ERCPT02-05 and GMPFM06-10, the Q_{tn}-F_r chart (Figure 4) suggests a tendancy towards a dilative behaviour. This is not the case for the ERCPT02-08, where the behaviour was shown to be varying between sand-like contractive (SC) and transitional contractive (TC), with some points left of the classification zones owing to values of (F_r) lower than 0.1%. The low (F_r) values can be attributed to the fact that the friction heat caused by the penetration of the piezocone altered the stability conditions of GH and therefore led to their dissociation. This response can be ascribed to the low GH concentrations in sediment as shown in Figure 4. Such behaviour can be compared to that

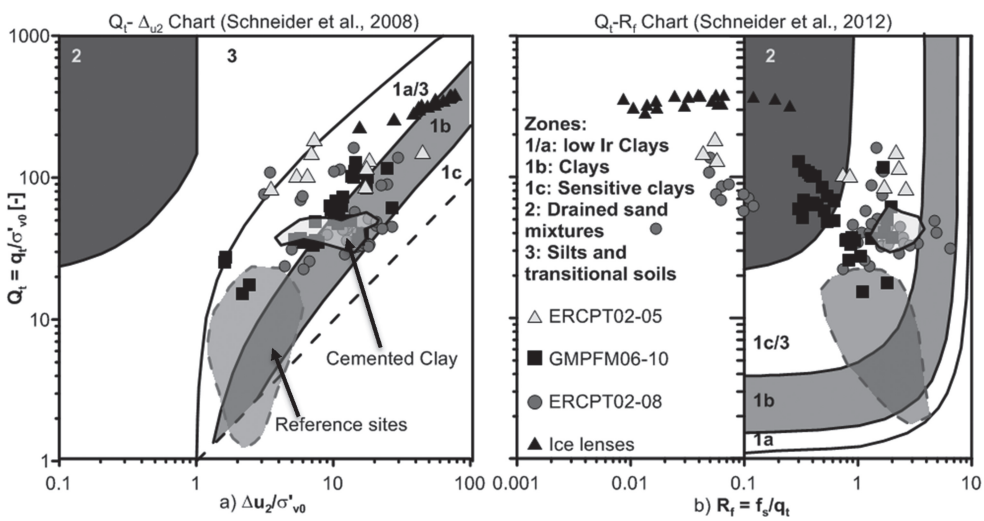

Figure 3. Reference site GMPFM06–01 (without GH), GH-bearing sites, Taranto cemented clays (after Jamiolkowski et al., 1986) and ice lenses (after Fortier & Yu, 2012) data plotted in: (a) Q_t-Δu_2 chart (Schneider et al., 2008) and (b) $Q - Rf$ chart (Schneider et al., 2012).

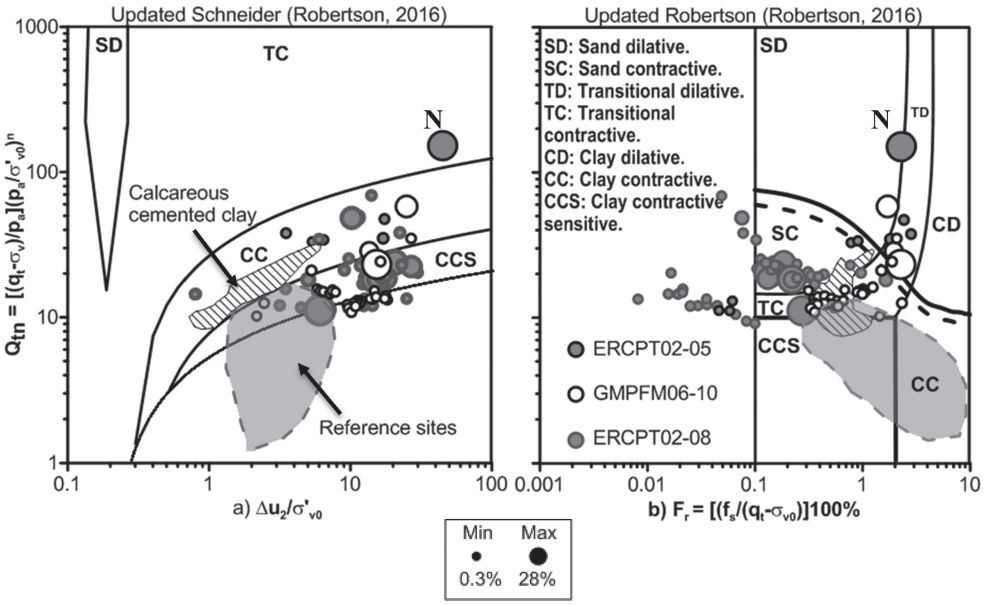

Figure 4. Reference site GMPFM06–01 (without GH), GH content (S_{hmin}) shown as bubble plots and calcareous cemented clay (after Robertson, 2016) data plotted in: (a) Updated Schneider CPTu chart (b) Updated SBTn chart (Robertson, 2016).

of ice lenses discussed by Fortier & Yu (2012) in terms of low F_r values.

4 DISCUSSION

In this work, it was possible to detect the presence of GH based on in-situ geotechnical and acoustic measurements. The presence of GH was confirmed whenever positive velocity anomalies were accompanied by a simultaneous increase in all of the CPTu parameters. Using an effective medium model, the concentration of GH could have been derived from Vp measurements and found to vary from 0.3% to 28%.

Based on soil classification charts using normalized piezocone tip resistance and pore pressure parameters (Figures, 3a and 4a), GH-bearing sediments show a contractive behaviour. This finding contrasts with results from triaxial tests suggesting that the presence of GH in sandy sediment tends to enhance dilation by filling the pore space (Hyodo et al., 2013). Triaxial test results have also shown that the stiffness and strength of GH-bearing sands tend to increase with GH saturation. By contrast, while in the present study the highest value of Q_{tn} and $\Delta u_2 / \sigma'_{v0}$ correlates with the highest estimated GH concentration (N in Figure 4), the rest of the normalised piezocone data does not bear a proportional relationship with hydrate content.

There is however a general trend of increasing Q_{tn} values with increasing $\Delta u_2 / \sigma'_{v0}$ values (Figures 3a and 4a) which can be taken to indicate that the sensitivity of GH-bearing clayey sediments tend to increase with their stiffness and strength. Robertson (2016) suggested that such a trend might reflect the gradual influence of increasing microstructure of in-situ soils. Alternatively, piezocone data can be here discussed with reference to the variety of GH morphologies observed in clayey sediments. Based on visual observations reported by Sultan et al. (2010) from a core collected nearby ERCPT0205, these morphologies vary from millimetre thick veins to pebble-sized nodules. Correlation of these observations with piezocone data reveals that sediment intervals containing groups of hydrate veins consistently plot in the contractive region of the different classification charts as observed by Schneider et al. (2012) and Robertson (2016) for Taranto and Copper Marl calcareous cemented clays (Figures 3a, 4a). On the other end of the spectrum, the behaviour of a sediment interval containing a hydrate nodule (N in Figure 4) plots in the contractive region of the Q_{tn}- $\Delta u_2 / \sigma'_{v0}$ chart and the dilative region of the Q_{tn}-F_r chart. Given the size of this nodule is larger than the diameter of the piezocone, such a difference can hardly be explained by strong bonding between hydrate and sediment particles as noted for heavily cemented soils by Robertson (2016). It is considered more likely that the difference in

classification between charts relates predominantly to the microstructure of the hydrate nodule itself. Should this suspicion be confirmed by experimental studies, identification of similarities and differences between charts may prove to be helpful in distinguishing sediment containing hydrate veins from those containing nodules.

5 CONCLUSION

The main objective of this work was to detect GH-bearing sediments using acoustic and piezocone sounding before determining trends in mechanical behaviour as a function of GH concentration. Analysis of compressional wave velocities (Vp), CPTu readings and classification charts have shown the following:

- Positive Vp anomalies accompanied by simultaneous increase in CPTu readings are indicative of the presence GH.
- The piezocone penetration occurred fully undrained in GH-bearing clayey sediments.
- Unlike GH-bearing sandy sediments, GH-bearing clayey sediments are generally characterised by a contractive behaviour.
- The identification of a general trend of increasing cone piezocone resistance combined with increasing pore pressure suggests that the sensitivity of GH-bearing clayey sediments tend to increase with their stiffness and strength.
- Results have shown that there is not a unique trend between the piezocone resistance and GH content, suggesting that probably the morphology of GH has a significant effect on the overall mechanical properties of the host sediment.
- Identification of similarities and differences between charts was proposed as a means of distinguishing the presence of different GH morphologies.
- Sediment intervals containing groups of hydrate veins tend to consistently plot in the contractive region of different normalised classification charts.
- Stiffer, stronger and more sensitive sediments containing GH nodules appear to be differently classified as contractive or dilative depending on the chart.
- Further investigations supported by experimental data would be helpful in substantiating the influence of various forms and amount of GH on trends in piezocone response.

REFERENCES

Fortier, R. and Yu, W. (2012). Penetration Rate-Controlled Electrical Resistivity and Temperature Piezocone Penetration Tests in Warm Ice-Rich Permafrost in Northern Quebec, Canada. Sustainable Infrastructure Development in a Changing Cold Environment ASCE 2012.

Ghosh, Ranjana, Kalachand Sain, and Maheswar Ojha. "Effective Medium Modeling Of Gas Hydrate-Filled Fractures Using The Sonic Log In The Krishna-Godavari Basin, Offshore Eastern India". Journal of Geophysical Research 115.B6 (2010).

Helgerud, M., Dvorkin, J., Nur, A., Sakai, A. and Collett, T. (1999). Elastic-wave velocity in marine sediments with gas hydrates: Effective medium modeling. Geophysical Research Letters, 26(13), pp. 2021–2024.

Hyodo, M., Yoneda, J., Yoshimoto, N. and Nakata, Y. (2013). Mechanical and dissociation properties of methane hydrate-bearing sand in deep seabed. Soils and Foundations, 53(2), pp. 299–314.

Jamiolkowski, M., Ladd, C.C., Germaine, J.T., Lancelotta, R., (1985). New developments in field and laboratory testing of soils. In: Proceedings of the 11th International Conference on Soil Mechanics and Foundation Engineering, A.A. Balkema, San Fransisco, CA, pp. 57–153.

Kvenvolden, K. (1993). Gas hydrates-geological perspective and global change. Reviews of Geophysics, 31(2), pp. 173–187.

Lunne, T., Robertson, P.K. and Powell J.J.M. 1997. Cone penetration testing in geotechnical practice. Taylor and Francis Group. London and New York.

Robertson, P. (2012). Interpretation of in-situ tests – some insights. In: ISC'4.

Schneider, J., Randolph, M., Mayne, P. and Ramsey, N. (2008). Analysis of Factors Influencing Soil Classification Using Normalized Piezocone Tip Resistance and Pore Pressure Parameters. Journal of Geotechnical and Geoenvironmental Engineering, 134(11), pp. 1569–1586.

Schneider, J., Hotstream, J., Mayne, P. and Randolph, M. (2012). Comparing CPTUQ-F and $Q - \Delta u_2/\sigma'_{v0}$ soil classification charts. Géotechnique Letters, 2(4), pp. 209–215.

Sultan, N., Voisset, M., Marsset, T., Vernant, A., Cauquil, E., Colliat, J. and Curinier, V. (2007). Detection of free gas and gas hydrate based on 3D seismic data and cone penetration testing: An example from the Nigerian Continental Slope. Marine Geology, 240(1–4), pp. 235–255.

Sultan, N., Marsset, B., Ker, S., Marsset, T., Voisset, M., Vernant, A., Bayon, G., Cauquil, E., Adamy, J., Colliat, J. and Drapeau, D. (2010). Hydrate dissolution as a potential mechanism for pockmark formation in the Niger delta. Journal of Geophysical Research, 115(B8).

Wei, J., Pape, T., Sultan, N., Colliat, J., Himmler, T., Ruffine, L., de Prunelé, A., Dennielou, B., Garziglia, S., Marsset, T., Peters, C., Rabiu, A. and Bohrmann, G. (2015). Gas hydrate distributions in sediments of pockmarks from the Nigerian margin – Results and interpretation from shallow drilling. Marine and Petroleum Geology, 59, pp. 359–373.

Cone Penetration Testing 2018 – Hicks, Pisanò & Peuchen (Eds)
© 2018 Delft University of Technology, The Netherlands, *ISBN 978-1-138-58449-5*

Gas effect on CPTu and dissipation test carried out on natural soft-soil of Barcelona Port

D. Tarragó & A. Gens
Universitat Politècnica de Catalunya, Barcelona, Spain

ABSTRACT: There is abundant evidence that gas is present in the sediments of the prodelta of the Llobregat River in the area of the Barcelona Port. The presence of gas has been directly observed by gas releases and deflagrations occurring during a site investigation campaign involving boreholes and CPTu tests. Methane has been identified by means of BAT permeameter tests. The record of a CPTu test performed in an area where gas is known to be present has been examined in detail. In spite that there are several features that could be related to the gas presence, it is challenging to identify unambiguously the presence of the gas from the CPTu record alone.

1 INTRODUCTION

An extensive enlargement of Barcelona Port that includes breakwaters and quays was constructed on the prodelta of the Llobregat River. Several geotechnical and geophysics studies were performed in the zone of breakwater and quay to investigate and control soil behaviour before and during construction.

The prodelta comprises young soils deposited during the Holocene. The principal layers that compose this prodelta are illustrated in Figure 1. The main layer, about forty meters thick, is composed of soft silty clay interbedded with thin silty sand layers a few centimetres thick. Canals (pers. comm.) observed gas bubbles coming from the seabed during the first geophysical study along prodelta arising from organic matter present in these soils.

As a soft soil, geotechnical parameters of prodelta could be well characterized by cone penetration tests with pore pressure measurements (CPTu), as well by piezometer recordings and soil sampling. However, inconsistent results were obtained on some instances and, on several occasions, gas escapes hampered boring. In response, BAT permeameter tests were performed to evaluate gas properties, Torstensson (1984).

2 EVIDENCE OF GAS PRESENCE IN THE LLOBREGAT PRODELTA

Geophysical studies performed in the Llobregat river prodelta detected pockmarks and acoustic shadow zones that indicated the existence of biogenic gas, as reported by Urgeles et al. (2007), Urgeles et al. (2011), and Liquete et al. (2008).

Also, the Barcelona Port Authority had performed a geophysical study inside the enlargement zone. This study showed an acoustic shadow zone, apparently due to the presence of gas (Figure 2). It affected the main part of the new South breakwater and the alignment of quay (Alonso et al. 1995).

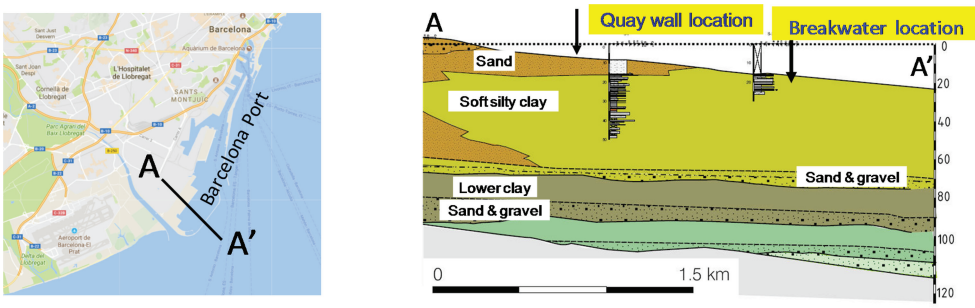

Figure 1. (left) location map and (right) geologic cross section profile of Llobregat river prodelta, Gamez (2007).

Figure 2. Acoustic shadow zone from geophysical seismic investigation and current map of the zone, modified from Alonso et al. (1995).

During construction, in order to control settlements and excess pore pressure, vibrating wire piezometers were emplaced under South breakwater and the Prat quay. These piezometers measured the variation of water pressure due to changes in sea level and the pore water pressure generated by construction.

Unusual results were obtained from the piezometers records in the shadow zone: (i) abrupt changes of excess pore pressure and (ii) phase difference between piezometers and attenuation of pore water pressure generated by tides.

Regarding abrupt changes, an anomalous unexpected change of a closed piezometer installed inside the shadow zone of the Prat quay is depicted in Figure 3. This behaviour is not related to the construction process. It is similar to behaviour reported by Riboulot et al. (2013) in a submarine landslide in Nigeria.

Phase difference and attenuation phenomena can be observed in Figure 4. It shows that the original tidal pore pressure is lower than pore pressure water response of soil, and wave crests do not occur at the same time. Similar results were described by Wheeler (1988), Okusa (1985) and Brandes (1999) in gassy soils. Hence, this behaviour would indicate the existence of gas at different soil depths of the silty-clay layer of the prodelta.

In addition, an extensive site investigation was carried out in the Prat quay location during 2007. The drilling of several boreholes failed due to the presence of gas -. In some cases, gas escapes from the boreholes continued for to 40 hours. Also, deflagrations occurred during borehole drilling and CPTu penetration. In total, eighteen different instances of gas escapes and deflagrations were reported.

Soil specimens recovered from boreholes were largely silty-clay interbedded with sands, both con-

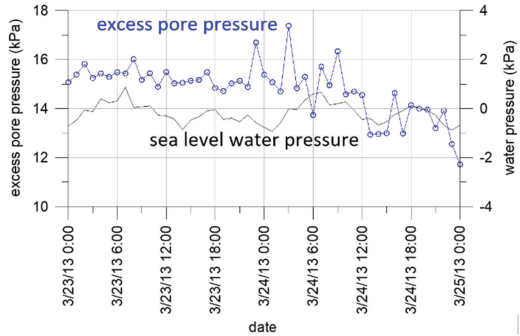

Figure 3. Anomalous records of excess pore pressure from a piezometer installed in silty clay in the Llobregat prodelta.

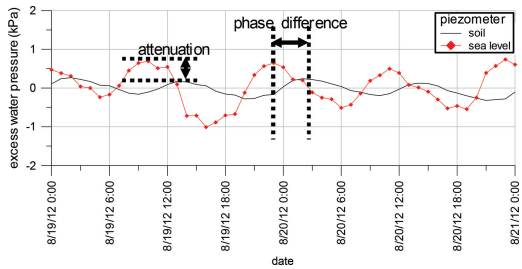

Figure 4. Recorded results of pore pressure behaviour in silty clays of Llobregat prodelta.

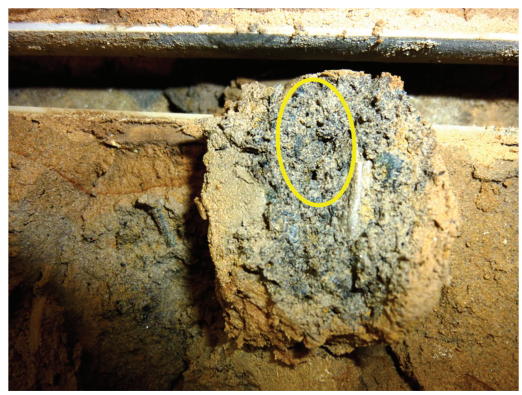

Figure 5. Rounded voids in sandy soil sample from zone with anomalous behaviour.

taining some organic matter. The organic matter is composed mainly by carbon in gives the silty clay a blackish colour and a bad smell. Even so, organic matter content in soil does not reach 3%. The structure of these type of soils is characterized by interconnected voids in which free gas can be located, see Figure 5.

In order to evaluate dissolved gas concentration close to anomalous boreholes and CPTu tests, BAT permeameter tests were carried out. Methane (CH_4) was found in eleven cases. The percentage of dissolved methane lies in the range of less than 1% to 72%. Only two samples had 100% of dissolved gas, indicating the presence of free gas.

3 BEHAVIOUR OF CPTU AND DISSIPATION TESTS IN GASSY SOILS

Piezocone tests sometimes encounter gassy soils see, for instance, Sultan et al. (2007), Sultan et al. (2010) and Steiner et al. (2013). They found that gas results in the following features of CPTu results: (i) existence of additional water pore pressures (u_2), higher than the expected excess pore pressure of cohesive soil and (ii) lower cone penetration resistance (q_c) than expected resulting in low values of undrained shear strength (c_u).

There is also some limited literature on dissipation tests performed on gassy soils. Seifert et al. (2008) reported a dissipation path of dilatant soil with free gas. Also, pore water pressure at the end of the test was higher than hydrostatic water pressure. However, unusual dissipation test results can also be due to the complex interaction of soils and piezocone. For instance, free gas presence may cause the desaturation of the pore pressure sensor but, unfortunately, other soil behaviour such as a highly dilatant soil can produce similar effects.

4 CPTU AND DISSIPATION TESTS RESULTS

Although gas escape and deflagration happened during cone sounding, a number of CPTu and dissipation tests could be completed and examined. Unfortunately, only one CPTu test was performed in the vicinity of an area where gas presence was clearly established (Fig. 6).

The soil profile comprises a shallow recent hydraulic fill from seabed to about -13 m, underlain by sands and silts to -18 m that, in turn, overlies a layer of silty clay with fine sand and organic matter lenses that extends to at least the end depth of the sounding at –41.5 m. The sand layers are spaced in a range of about 1 m to 0.5 m, and lateral continuity is not wholly preserved. Pore water pressure development is not particularly strong in either of the upper two layers of hydraulic fill and it in the sands and silts, but it is more significant in the lower interlayered silty clay unit.

To check the existence of free gas, the records of q_c, u_2 and f_s (sleeve friction) were examined.

Figure 7 shows the piezocone results from -20 m to -23 m; free gas was found at elevation -21.8 m. In this zone, the CPTu profile suggests that free gas is located in the interlayered soil.

As shown in Figure 7, free gas is located at the upper part of a 0.35 m thick sandy soil layer. At that point, it an abrupt reduction of u_2 with values lower than the hydrostatic pressure is observed An unusual u_2 behaviour is also observed at the lower

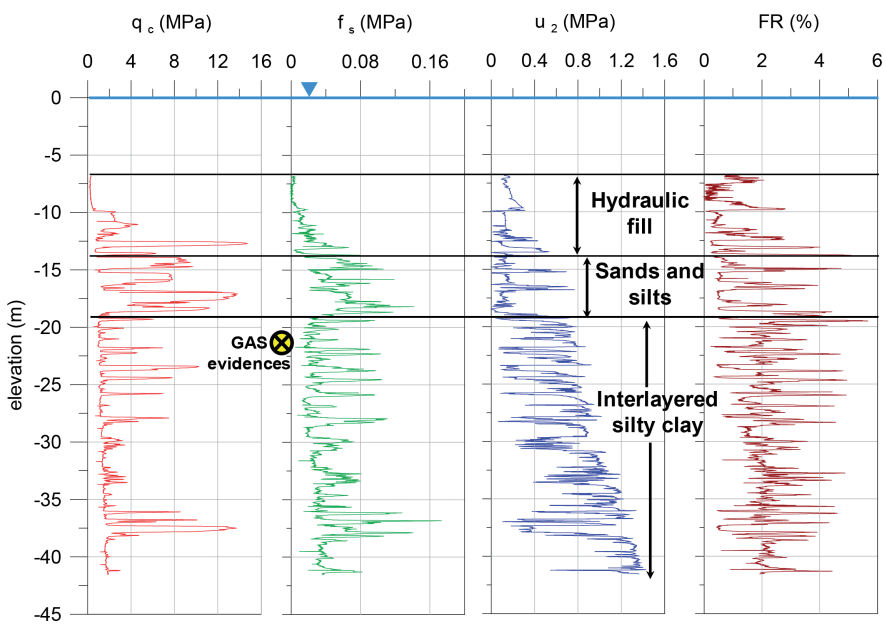

Figure 6. Profile of CPTu results in the quay.

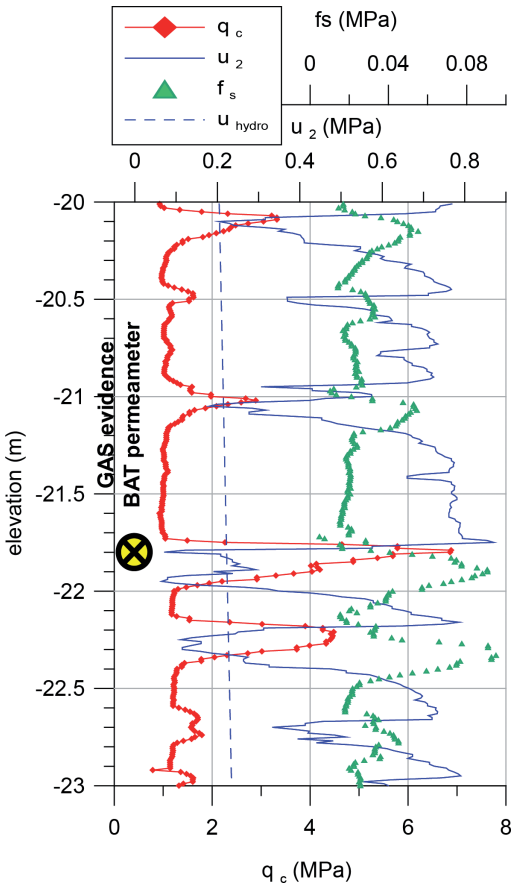

Figure 7. Results of q_c, u_2 and f_s in CPTu sounding with free gas presence in the quay.

part of the upper silty clay layer (–21.2 to –21.7), where a large u_2 development was recorded just before the reduction mentioned above.

Next to the CPTu test of Figure 6, another CPTu test was performed without problems. Undrained shear strength and pore water pressure distribution with depth have been plotted in Figures 8 and 9. It is not possible to tell whether the high water pressures are the normal response in cohesive soil or whether the presence of gas also plays a role. In contrast, gas presence in the sandy layers could account for some of the abrupt u_2 reductions, down to values near to zero, such as occurs in u_2 plot of Figure 6.

Also, only a reduction of the c_u/σ'_v ratio drop was detected to a value of 0.22, at elevation of about –35 m at the end of the sounding. This behaviour was not detected in the previous CPTu and previous investigations, it was known that c_u was around 0.25 vertical effective stress.

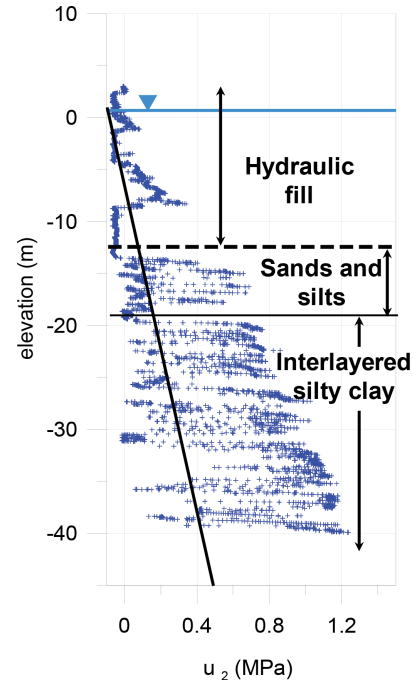

Figure 8. c_u values from CPTu carried out in the quay.

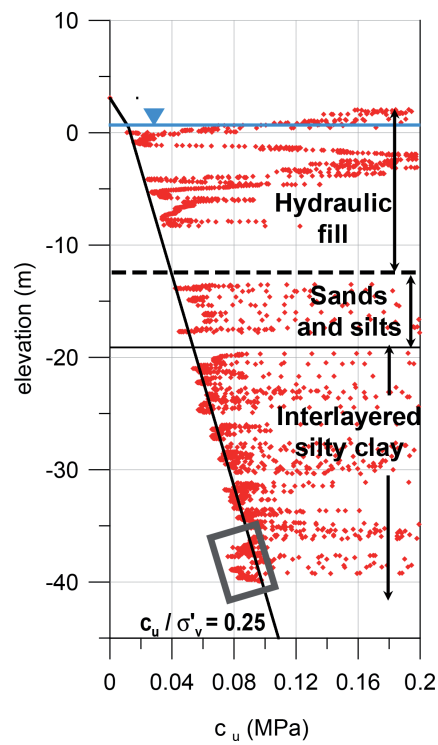

Figure 9. u_2 values from CPTu carried out in the quay.

5 CONCLUDING REMARKS

There are numerous evidences of the presence of gas in the Llobregat prodelta that have emerged in different site investigations carried out over the last two decades for the enlargement of the Barcelona Port.

A CPTu sounding, where free methane was detected, shows a behaviour that may be related to the presence of gas. It involves an abrupt reduction of u_2 in sandy soil at the point where gas was detected and an unexpected rise of u_2 in adjacent cohesive soil.

It has also c_u ratios, somewhat lower than 0.25 in several piezocone test. It is hypothesized that this reduction may be due to gas migration upwards.

However, it must be accepted that, even in locations where the gas is known to be present, it is challenging to confirm its presence form the CPTu records alone.

ACKNOWLEDGEMENTS

Authors are grateful to R. Griell from the Autoritat Portuària de Barcelona for the technical and financial support for the work reported here.

REFRENCES

Alonso, B., Baraza, J., Ercilla, G., Estrada, F., Farrán, M. and Palanques, A. 1995. Estudio Geofísico y sedimentológico en el área de ampliación del Puerto de Barcelona. CSIC report to Internal document Barcelona Port Authority.

Brandes, H. 1999. Predicted and measured geotechnical properties of gas-charged sediments. International Journal of Offshore and Polar Engineering 9, 219–225.

Canals, M. 2007. Personal communication.

Gàmez, D. 2007. Sequence Stratigraphy as a tool for water resources management in alluvial coastal aquifers: application to the Llobregat delta (Barcelona, Spain). Thesis. Technical University of Catalunya.

Liquete, C., Canals, M., De Mol, B., De Batist, M. and Trincardi, F. 2008. Quaternary stratal architecture of the Barcelona prodeltaic continental shelf (NW Mediterranean). Marine Geology, 250, 234–250.

Okusa, S. 1985. Wave induced stresses in unsaturated submarine sediments. Geotechnique, Vol. 35 (No. 4) (1985), pp. 517–532.

Riboulot, V., Cattaneoa, A., Sultana, N., Garzigliaa, S., Kera, S., Imbertc, P., and Voisseta, M. 2013. Sea-level change and free gas occurrence influencing a submarine landslide and pockmark formation and distribution in deepwater Nigeria. Earth and Planetary Science Letters, Volume 375, 1 August 2013, Pages 78–91

Robertson, P.K. 2013. CPTu dissipation tests – theory to practice (Webminar). Gregg Drilling & Testing, Inc.

Seifert, A., Stegmann, S., Morz, T., Lange, M., Wever, T. & Kopf, A. 2008. In situ pore-pressure evolution during dynamic CPT measurements in soft sediments of the western Baltic Sea. GeoMar. Lett. 28, No. 4, 213–227.

Steiner, A., L'Heureux, J.-S., Kopf, A., Vanneste, M., Longva, O., Lange, M. & Haflidason, H. 2012. An in-situ free-fall piezocone penetrometer for characterizing soft and sensitive clays at Finneidfjord (Northern Norway). In Submarine mass movements and their consequences (eds Y. Yamada, K. Kawamura, K. Ikehara, Y. Ogawa, R. Urgeles, D. Mosher, J. Chaytor and M. Strasser), pp. 99–109. Dordrecht, the Netherlands: Springer.

Urgeles, R., De Mol, B., Liquete, C., Canals, M., De Batist, M., Hughes-Clarke, J.E., Amblàs, D., Arnau, P.A., Calafat, A.M., Casamor, J.L., Centella, V., De Rycker, K., Fabrés, J., Frigola, J., Lafuerza, S., Lastras, G., Sànchez, A., Zuñiga, D., Versteeg, W. and Willmott, V. 2007. Sediment undulations on the Llobregat prodelta: Signs of early slope instability or sedimentary bedforms. Journal of Geophysical Research, 112, B5, 102.

Urgeles, R., Cattaneo, A., Puig, P., Liquete, C., De Mol, B., Amblàs, D., Sultan, N. and Tincardi, F. 2011. A review of undulated sediment features on Mediterranean prodeltas: distinguishing sediment transport structures from sediment deformation. Marine Geophysical Research, 32, 49–69.

Sultan, N., Voisset, M., Marsset, T., Vernant, A.M., Cauquil, E., Colliat, J.L. and Curinier, V. 2007. Detection of free gas and gas hydrate based on 3D seismic data and cone penetration testing: An example from the Nigerian Continental Slope. Marine Geology 240 (2007) 235–255.

Sultan, N., Savoye, B., Jouet, G., Leynaud, D., Cochonat, P., Henry, P., Stegmann, S. and Kopf, A. 2010. NOTE - Investigation of a possible submarine landslide at the Var delta front (Nice continental slope, southeast France). Canadian Geotechnical Journal, 47 (2010), pp. 486–496.

Torstensson, B.A. 1984. A new system for ground water monitoring. Ground Water Monit. Rev., 4 (4) (1984), pp. 131–138

Wheeler, S.J. 1988. A conceptual model for soils containing large gas bubbles. Geotechnique, 38 (3) (1988), pp. 389–397.

Taylor & Francis
Taylor & Francis Group
http://taylorandfrancis.com

Cone Penetration Testing 2018 – Hicks, Pisanò & Peuchen (Eds)
© 2018 Delft University of Technology, The Netherlands, ISBN 978-1-138-58449-5

Comparison of cavity expansion and material point method for simulation of cone penetration in sand

Faraz S. Tehrani & Vahid Galavi
Department of Geo-Engineering, Deltares, Delft, The Netherlands

ABSTRACT: Over the years, many attempts have been made to simulate the cone penetration process in coarse-grained and fine-grained soils. The simulation methods range from pure analytical methods to complicated numerical approaches. Among the analytical methods, cavity expansion analysis has gained more attractions due to its relative simplicity and robust theoretical background. Analytical cavity expansion analysis is limited to rather simplistic soil constitutive models. As a result, numerical cavity expansion analyses have been attempted to cover this limitation. Another method that has gained much attention in the past decade is the Material Point Method (MPM) whose promising capabilities in simulating large deformation problems can be used for simulating the cone penetration. In this paper, we model the cone penetration in loose, medium dense and dense sands using numerical spherical cavity expansion method and axisymmetric MPM. In all the analyses, soil behavior is modelled using Mohr-Coulomb constitutive model. The soil is assumed to be dry in all analyses. Results are compared with a cylindrical cavity expansion solution.

1 INTRODUCTION

1.1 *Cone penetration in sand*

The cone penetration test (CPT) is a key method for site characterization. This is partly because of its simplicity and partly as a result of the development of cone resistance-based correlations for design of shallow (e.g. Schmertmann, 1970; Mayne & Poulos, 1999; Lee et al., 2008; O'Loughlin & Lehane, 2010) and deep (e.g. Lee & Salgado, 1999; Xu et al., 2008) foundations, soil parameter estimation (e.g. Lune et al. 1997), and liquefaction resistance estimation (e.g. Seed & De Alba, 1986; Idriss & Boulanger, 2006). The apparent simplicity of the CPT, however, hides considerably complex mechanics (Arshad et al. 2014, Tehrani et al. 2017). These include possible partial drainage during penetration; particle size effects; the large displacements, rotations, shear deformations and mean stresses that develop around the cone; and the particle crushing that takes place near the cone. This complexity leads to significant challenges in theoretical modelling of cone penetration.

1.2 *Cavity expansion method*

The most applicable methods for simulation of cone penetration in sand have been based on cavity expansion analysis (Salgado & Randolph, 2001; Salgado & Prezzi, 2007). Cavity expansion is based on inflating a zero or finite radius (with initial radius of r_0) axisymmetric cavity (cylinder or sphere) in the depth of interest. As the pressure inside the cavity increases, the cavity expands radially. At a certain radial displacement, the expanding pressure will not increase with further radial expansion and reach a steady state value, referred to as the limit pressure (p_{limit}), which can be used to calculate the cone tip resistance. In this paper, spherical cavity expansion will be used to calculate cone penetration resistance. The cone resistance q_c can be obtained from the limit pressure by solving the vertical equilibrium of the stresses assumed around the cone as shown in Figure 1.

In Figure 1, ϕ' represents the friction angle of the material (sand in our study). The following relationship between q_c and p_{limit} can be obtained:

$$q_c = p_{\text{limit}}(1 + \tan\alpha \cdot \tan\phi') \tag{1}$$

where α is 60 degrees in CPT. Following Randolph et al. (1994), ϕ' is calculated based on the friction of cone-soil interface.

1.3 *Material point method*

The Material Point Method (MPM), first introduced by Suslkey et al. (1994), has also gained attentions in simulating cone/pile penetration in recent years (Tehrani et al. 2016; Galavi et al. 2017). The MPM can be considered as an extension of the Updated Lagrangian Finite Element

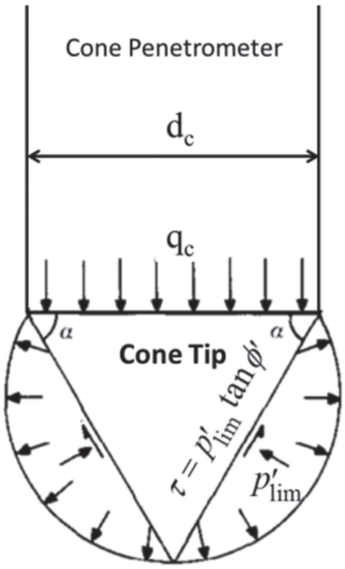

Figure 1. Spherical cavity expansion (modified after Randolph et al. 1994).

Method (UL-FEM). The method uses Lagrangian material points (or mesh) that is defined over the material of the body and a background (Eulerian) mesh that is defined on the computational domain. The Lagrangian material points carry all computational data including stresses and state variables. In the beginning of each calculation step, the computational data are projected from the material points to the background mesh. The governing equations are solved on the background mesh similar to the UL-FEM. In order to prevent mesh distortion, associated with the Lagrangian method, the computational data are mapped back from the background mesh to the material points at the end of each computational step and the mesh is reset before the next computation step. In this way, the method benefits from the advantages of both Lagrangian and Eulerian methods, without having disadvantages of those methods, namely the mesh distortion in the Lagrangian method and the numerical dissipation in the Eulerian method.

Extra calculation steps introduced in the MPM, compared to the UL-FEM, make the method computationally expensive. The numerical simulation of large deformation problems, such as the cone penetration can be carried out less expensively, if the effect of rotational symmetry of the penetrometer and the surrounding soil is taken into consideration in the formulation of the material point method. This results in a new formulation which is based on a two dimensional axisymmetric formulation developed by Sulsky & Schreyer (1996). This formulation of the MPM can significantly reduce number of elements and material points compared to the three dimensional formulation. The detailed formulation of axisymmetric MPM used in this paper can be found in Galavi et al. (2018).

2 NUMERICAL ANALYSES

2.1 *Geometry*

Figure 2 shows the discretized geometry of the finite element model for cavity expansion analysis. The initial cavity of radius 8 mm was embedded at the depth of 1 m below the soil surface. The

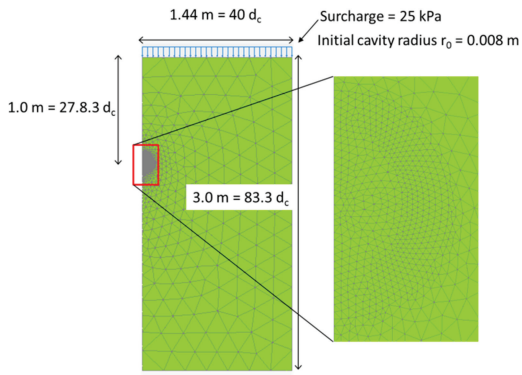

Figure 2. Geometry and mesh used for CEM analyses.

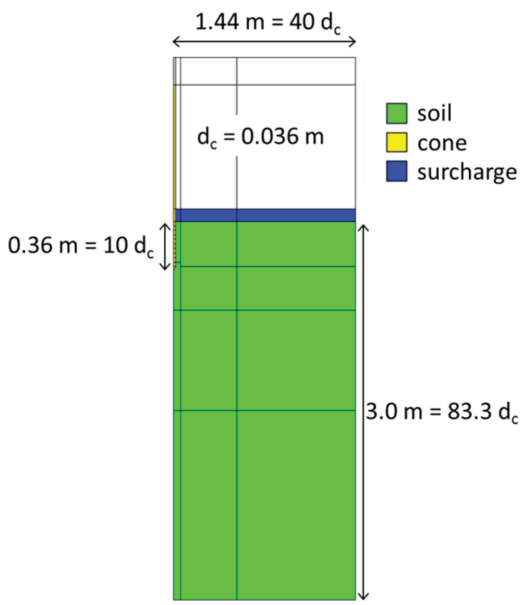

Figure 3. Geometry used for MPM analyses.

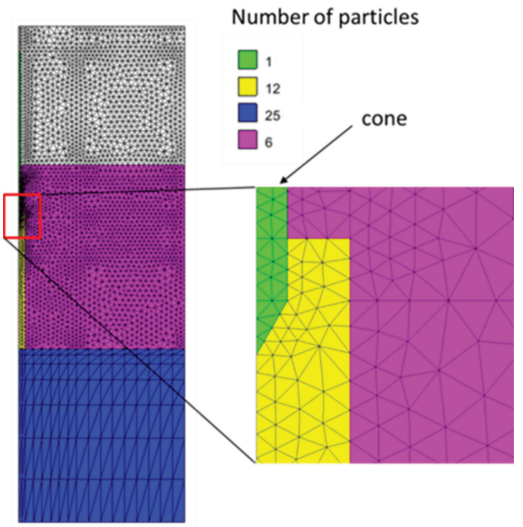

Figure 4. Mesh and number of particles used for MPM analyses.

domain is discretized with 1865 axisymmetric 15-noded triangular elements.

Figure 3 and Figure 4 show the dimensions as well as mesh & particle specifications of the MPM model, respectively. As shown in these figures, in the MPM calculations, the penetrometer is initially embedded $10d_c$ below the soil surface. The diameter of the cone in the numerical analyses is taken as $d_c = 36$ mm.

The MPM model consists of 5950 linear triangular elements and 28782 material points.

2.2 *Soil model parameters*

Baskarp sand is chosen for the numerical analyses. To simplify numerical simulations, Mohr-Coulomb soil constitutive model is adopted. The model parameters and basic characteristics of Baskarp sand are presented in Table 1.

The dry unit weight of 16 kN/m^3 was used for all cases in order to maintain the same initial stress condition. The Young's modulus is calculated for the reference depth of 1 m below the ground level. Following formulas were used to calculate the Young's moduli:

$$q_c = 1.64 p_A \exp(A) B \quad \text{(Salgado \& Prezzi 2007)} \tag{2}$$

$$A = 0.1041\phi_c + (0.0264 - 0.0002\phi_c) D_R \tag{3}$$

$$B = (\sigma'_h / p_A)^{(0.841 - 0.0047 D_R)} \tag{4}$$

where σ'_h is the horizontal effective stress and reference stress $p_A = 100$ kPa.

Table 1. Model parameters and basic properties of Baskarp sand.

Property	ID and Unit	Loose	Medium dense	Dense
Specific unit weight	G_s (–)	2.65		
Maximum void ratio	e_{max} (–)	1.018		
Minimum void ratio	e_{min} (–)	0.542		
Relative density	D_R [%]	30	50	90
Young's modulus	E [kN/m^2]	7894	14000	43659
Poisson's ratio	ν [–]	0.2	0.2	0.2
Cohesion	c′ [kPa]	1	1	1
Peak Friction angle	ϕ'_p [°]	32.8	36.5	43.4
Dilation angle	ψ [°]	2.8	6.5	13.4
Critical state friction angle	ϕ'_c [°]	30	30	30
Coefficient of lateral earth pressure at rest	K_0 [–]	0.5	0.5	0.5

$$E_{oed} = 4q_c \tag{5}$$

$$E = E_{oed} \frac{(1-2\nu)(1+\nu)}{1-\nu} \tag{6}$$

Peak friction angles were derived for the reference depth of 1 m under surcharge load of 25 kPa. Correlations presented by Bolton (1986) for the Triaxial condition were used to derive the peak frictions angles, iteratively.

2.3 *Results and discussion*

Cavity expansion analyses were performed using Plaxis 2D 2016.01. In order to well capture the large deformation of elements around the cavity, finite element analyses were performed with updating mesh. Figure 5 shows the limit pressure from cavity expansion analyses along with the corresponding q_c values from spherical cavity expansion analyses.

Figure 6 shows the profile of cone tip resistance with depth obtained from the MPM analysis of cone penetration in loose, medium dense and dense sand models. The q_c values calculated from eq. (2), corresponding to z = 1 m ~$28d_c$, are also shown on Figure 6. The cone penetration resistance calculated using eq. (2) at depth z = 1.0 m ~ $28d_c$, is equal to 2265 kPa for the loose sand, 3954 kPa for the medium dense sand, and 12045 kPa for the dense sand. Figure 6 shows that there is a good agreement between MPM results and q_c values from Salgado & Prezzi (2007).

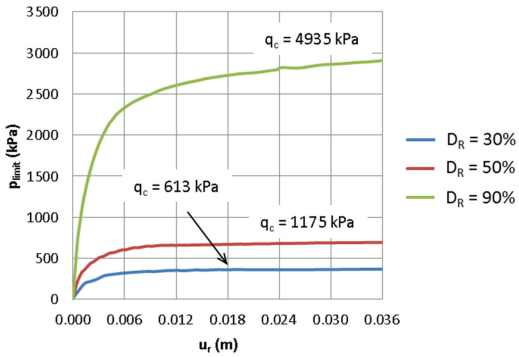

Figure 5. Limit pressure resulting from expansion of spherical cavity along with the corresponding cone tip resistances.

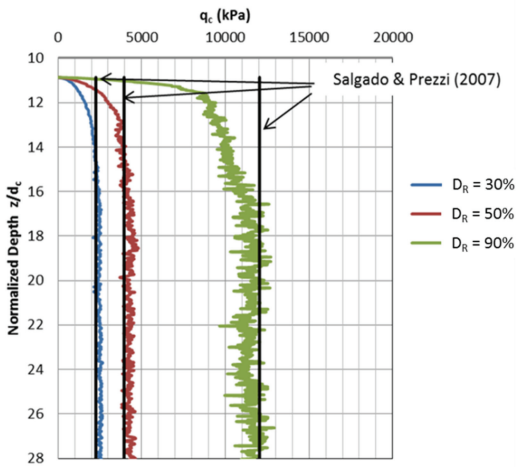

Figure 6. Cone penetration resistance profile from MPM analyses.

Comparison of results obtained from the numerical cavity expansion analyses with those of axisymmetric MPM, suggests that the q_c value calculated using spherical cavity expansion analysis is remarkably lower than those of MPM and values derived from Salgado & Prezzi (2007). It is worth mentioning that that eq. (2) is based on regression analyses that Salgado & Prezzi (2007) performed on cone penetration resistances derived from cylindrical cavity expansion analyses, whereas the numerical cavity expansion analyses presented in this study is based on spherical cavity expansion method. Review of literature reveals that spherical and cylindrical cavity expansion analyses both perform well for certain class of problems. For instance, Satapathy (1997) argues that the spherical cavity expansion solution is preferable for applications that involve high velocity penetration, whereas for cases where the penetrator is in contact with the target, e.g., in static punching, the cylindrical cavity expansion solution is preferable. Despite this argument, to derive the final conclusion on the accuracy of the axisymmetric MPM, it is necessary to compare the results with experimental evidences.

3 CONCLUSION

In this study, cone penetration in Baskarp sand was simulated numerically using spherical cavity expansion method and axisymmetric Material Point Method. Cone penetration was simulated in loose (D_R = 30%), medium dense (D_R = 50%) and dense (D_R = 90%) sands under the effect of 25 kPa surface surcharge. Elastic-perfectly plastic soil model with Mohr-Coulomb failure criterion was used to model the behavior of soil. The results showed that numerical spherical cavity expansion resulted in remarkably lower cone resistance compared to the axisymmetric MPM. Further comparison suggested that the cone penetration resistance values derived from the axisymmetric MPM were in a very good agreement with the cylindrical cavity expansion solution of Salgado & Prezzi (2007). However, to derive a definitive conclusion, comparison with experimental analysis data is necessary.

REFERENCES

Arshad, M.I., Tehrani, F.S., Prezzi, M., & Salgado, R. (2014). Experimental study of cone penetration in silica sand using digital image correlation. Géotechnique, 64(7), 551–569.

Galavi, V., Beuth, L., Coelho, B.Z., Tehrani, F.S., Hölscher, P., & Van Tol, F. (2017). Numerical simulation of pile installation in saturated sand using material point method. Procedia Engineering, 175, 72–79.

Galavi, V., Tehrani, F.S., Martinelli, M., Elkadi, A. & Luger, D. (2018). Axisymmetric formulation of the material point method for geotechnical engineering applications. NUMGE 2018, Submitted.

Idriss, I.M. & Boulanger, R.W. (2006). Semi-empirical procedures for evaluating liquefaction potential during earthquakes. Soil Dynam. Earthquake Engng 26, No. 2–4, 115–130.

Lee, J. & Salgado, R. (1999). Determination of pile base resistance in sands. J. Geotech. Geoenviron. Engng 125, No. 8, 673–683.

Lee, J., Eun, J., Prezzi, M. & Salgado, R. (2008). Strain influence diagrams for settlement estimation of both isolated and multiple footings in sand. J. Geotech. Geoenviron. Engng 134, No. 4, 417–427.

Lune, P.K. Robertson, J.J.M. Powell., "Cone Penetration Testing in Geotechnical Practice". Blackie Academic & Profesional, London 1997.

Mayne, P.W. & Poulos, H.G. (1999). Approximate displacement influence factors for elastic shallow foundations. J. Geotech.Geoenviron. Engng 125, No. 6, 453–460.

O'Loughlin, C.D. & Lehane, B.M. (2010). Nonlinear cone penetration test-based method for predicting footing settlements on sand. J. Geotech. Geoenviron. Engng 136, No. 3, 409–416.

Randolph, M.F., Dolwin, R., & Beck, R. (1994). Design of driven piles in sand. Geotechnique, 44(3), 427–448.

Salgado, R. & Randolph, M.F. (2001). Analysis of cavity expansion in sand. Int. J. Geomech. 1, No. 2, 175–192.

Salgado, R. & Prezzi, M. (2007). Computation of cavity expansion pressure and penetration resistance in sands. Int. J. Geomech. 7, No. 4, 251–265.

Satapathy, S. (1997). Application of Cavity Expansion Analysis to Penetration Problems (No. IAT. R-0136). Texas Univ at Austin Inst for Advanced Technology.

Schmertmann, J.H. (1970). Static cone to compute static settlement over sand. J. Soil Mech. Found. Div. 96, No. 3, 1011–1043.

Seed, H.B. & De Alba, P. (1986). Use of SPT and CPT tests for evaluating the liquefaction resistance of sands. In Use of in situ tests in geotechnical engineering, Geotechnical Special Publication No. 6. New York, NY, USA: American Society of Civil Engineers.

Sulsky D, Chen Z, Schreyer HL. A particle method for history-dependent materials. Comput Methods Appl Mech Eng 1994; 118:179–96.

Sulsky, D. & Schreyer, H.L.1996. Axisymmetric form of the material point method with applications to upsetting and Taylor impact problems. Computer Methods in Applied Mechanics and Engineering, Journal of Applied Mechanics, Vol. 139, 409–429.

Tehrani, F.S., Nguyen, P., Brinkgreve, R.B., & van Tol, A.F. (2016). Comparison of Press-Replace Method and Material Point Method for analysis of jacked piles. Computers and Geotechnics, 78, 38–53.

Tehrani, F.S., Arshad, M.I., Prezzi, M., & Salgado, R. (2017). Physical Modeling of Cone Penetration in Layered Sand. Journal of Geotechnical and Geoenvironmental Engineering, 144(1), 04017101.

Xu, X., Schneider, J.A. & Lehane, B.M. (2008). Cone penetration test (CPT) methods for end-bearing assessment of open—and closed-ended driven piles in siliceous sand. Can. Geotech. J. 45, No. 8, 1130–1141.

Taylor & Francis
Taylor & Francis Group
http://taylorandfrancis.com

Cone Penetration Testing 2018 – Hicks, Pisanò & Peuchen (Eds)
© 2018 Delft University of Technology, The Netherlands, ISBN 978-1-138-58449-5

Soil behavior and pile design: Lesson learned from some prediction events—part 1: Aged and residual soils

G. Togliani
Geologist, Massagno, Switzerland

ABSTRACT: Pile design methods generally do not consider phenomena such as aging, cementation and weathering, responsible for the presence of microstructures in the soil surrounding the piles and affecting their performance. Some prediction events involving known structured soils are analyzed taking as a reference the CPT-based SBT classification system recently updated by P.K. Robertson (2016). It is shown that the normalized small-strain rigidity index K^*_G can be useful to assess the impact of soil microstructure on pile capacity.

1 INTRODUCTION

The prediction events chosen are Merville (2003) and Porto (2004), locations where at the time of prediction, it was known that soils were aged and residual, respectively, and therefore micro-structured.

Tables summarizing soils and piles characteristics are provided below, while some CPTu plots (Page 2) complete the information as illustration of all the data used for piles design (axial capacity and load-movement curves).

For both sites it is sufficient to observe the CPT SBT I_c and fine contents (FC) curves (Figures 2 and 5) to see how their trend has been influenced by the soil microstructure. In fact, despite the lithological difference, the corresponding I_c curves are quite similar, proving that the Merville Flanders clays show a behaviour at the border to "sand like" soils, whereas, due to very high f_s values, the Porto silty sands are close to behave as "clay like".

Pairs of measured values should be used to calculate K^*_G; however, being too few those of V_s, it is reasonable to refer to derived values since the measured and predicted V_s curves are close enough one to the other (Figures 1 and 4).

To clarify the meaning of the parameters appearing in the graphs on Page 2, a specific glos-

Table 1. Merville: Soil and pile details.

Pile type and length:	Driven (IHC S70), 9.4 m
Material and Diameter:	Steel Pipe (open ended), 0.508/0.487 m
Driving Date:	04.08.2003
Soil Plug Height:	7.27 m
SLT Date:	05.19.2003
Deposit:	Marine (Ypresian)
Lithology:	Clays (50% Smectit, CF = 93%)
Soil structure from	Aging, Mechanical OC
GWT, w_n, γ	(–1.5/–1.9 m), 32.3%, 18.5 (kN/m^3)
Atterberg Limits:	LL = 69.2%, IP = 40.5%

Table 2. Porto: Soil details.

Deposit:	Residual (Saprolite)
Lithology:	Silty clayey sand with some gravel
Soil structure from	Incomplete granite weathering
GWT, w_n, γ	–10/–12 m, 16/22.5%, 16.6/20 kN/m^3
CF	3.3/9.5%
Atterberg Limits:	LL = 32/44%, IP = 5/17%

Table 3. Porto: Pile details.

Pile type:	Driven (C1) precast	Bored (E9) cased	Bored (T1) CFA
Material:	Concrete	Concrete	Concrete
Shape:	Square	Round	Round
Diameter (m):	0.35	0.60	0.60
Length (m):	6.0	6.0	6.0
Driving Date:	Sept.2003	-.-	-.-
Cast in situ Date:	-.-	Aug.2003	Aug.2003
SLT Date:	Jan.2004	Jan.2004	Jan.2004

sary is reported in §9 with symbols, definition and reference equations, mainly derived from the CPT Guide (P.K. Robertson, 2015), the Manual of Subsurface Investigation (P.W. Mayne, 2001) and the CPT State of Practice Report (P.W. Mayne, 2007).

2 PILE CAPACITY DESIGN METHODS

Some CPT based, direct design methods (LCPC, Eslami&Fellenius, KTRI and Togliani), described by Niazi and Mayne (2013), were used to verify their sensitivity to the presence of a soil structure.

The latest version (Santa Cruz Prediction Event, 2017) of the mentioned Author's method, is the following:

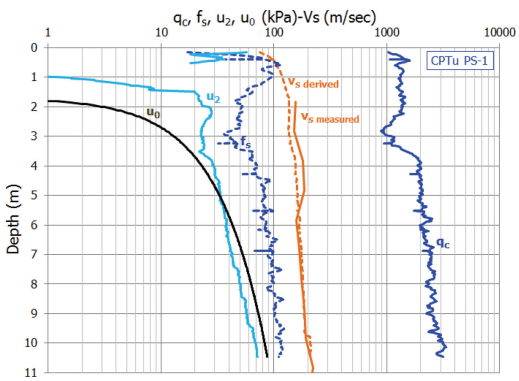

Figure 1. Merville: Guide plot.

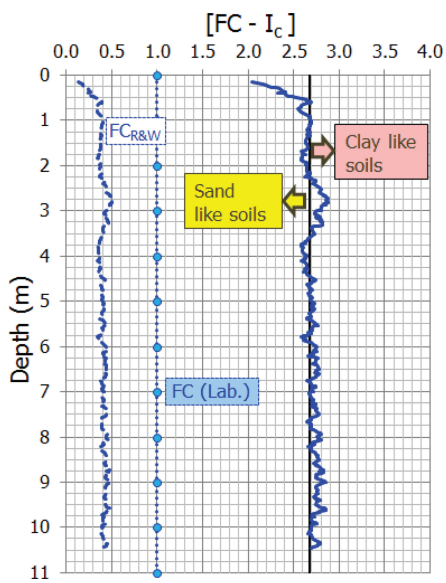

Figure 2. Merville: Soil behaviour plots.

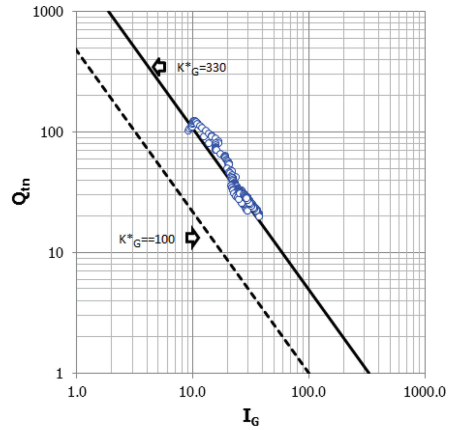

Figure 3. Merville K*G plots.

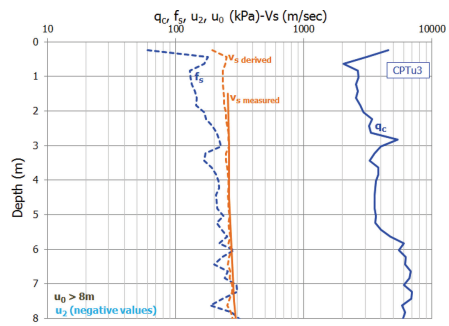

Figure 4. Porto: Guide plots.

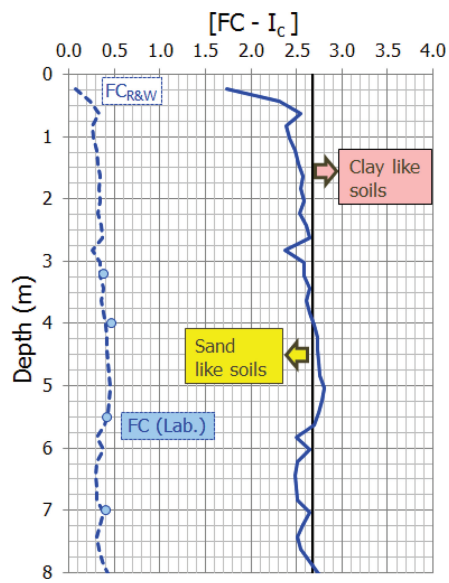

Figure 5. Pile capacities comparison.

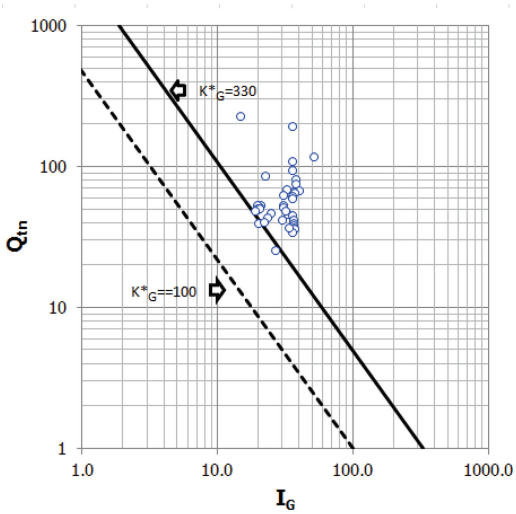

Figure 6. Porto K*G plots.

Table 4. β and λ coefficients.

Pile Type	β	λ
Driven (precast/jacked)	1.00	0.30
Drill.Displacement.	0.90	0.25
Pipe (Open End)	0.70	0.20
CFA, Bored (cased-cohesionless, bentonite)	0.60	0.15
Bored (bentonite-upper bound)	0.60	0.10
Bored (cased—cohesive)	0.50	0.10
Bored (bentonite-lower bound)	0.40	0.05

2.1 *Unit Friction (q_s)*

$$q_s = \beta\, q_c^{0.4} \quad \text{if } f_s \le 20 \qquad (1)$$
$$q_s = \beta\{q_c^{0.52}[\,(0.4 + LN(R_f)]\} \quad \text{if } R_f \ge 1.5 \qquad (2)$$
$$q_s = \beta\{q_c^{0.51}[0.8 + (1 - R_f)/8]\} \quad \text{if } 1 \le R_f < 1.5 \qquad (3)$$
$$q_s = \beta\{q_c^{0.53}[0.8 + (1.1 - Rf)/8]\} \quad \text{if } R_f < 1 \qquad (4)$$

2.2 *Unit Base (q_b)*

$$q_b = q_{c\ toe}[\lambda + (0.005\ Lpile/Dpile)] \qquad (5)$$

where $q_{c\ toe}$ goes from + 8 dtoe to –4dtoe.

Table 4 summarizes the corresponding Pile Type coefficients:

The capacities derived from the four quoted methods were then compared with the ones calculated from the approach specified below, including the normalized rigidity index K^*_G.

2.3 *Unit friction (q_s)*

$$q_s = \beta q_c^{[0.3 + x]} \qquad (6)$$

where $x = LOG(K^{*\alpha}_G)$

2.4 *Unit base (q_b): the same of § 2.2*

3 LOAD-MOVEMENT PREDICTION

The Chen & Kulhawy criterion (2002), shown in Figure 4, has been used to estimate the force-movement correlation for each pile and then the corresponding predicted curve, set via the Ratio Function.

According to this Function, the equation for unit resistance at a given movement in relation to the target resistance and target movement, is expressed by the following equation (B.Fellenius-Red Book):

$$r = r_{trg}\,(\delta/\delta_{trg})^{\theta} \qquad (7)$$

where r = variable force r_{trg} = target resistance
δ = var. movement δ_{trg} = movement at r_{trg}
θ = function coefficient ($0 < \theta < 1$)

The resistances derived with the new design method were considered as the target ones while the corresponding movement was set at s/d = 10% to obtain a complete load-movement curve.

For Merville piles, the cohesive soil curve was taken as reference, while for Porto, the cohesionless soil curve was used (Figure 4).

The superposition between measured and predicted load-movement diagrams is obtained by adjusting the value of the ϑ coefficient within

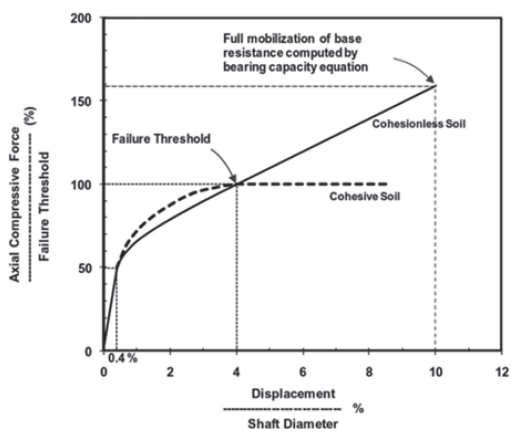

Figure 7. Chen & Kulhawy Criteria.

reasonable limits until a satisfying agreement was obtained; hence the theoretically evaluated curves are of Class C.

4 MERVILLE PILE DESIGN

The capacities obtained with the several design methods considered are presented in Figure 5; Figure 6 shows the predicted load-movement curve, modeled using a function coefficient equal to 0.04.

Histograms in Figure 5 show the credible shaft resistance obtained with all the methods except for LCPC that, being only based on q_c, is unable to appreciate the improvement of subsoil characteristics due to the presence of microstructure.

The trend of the load-movement curves suggests that the toe capacity evaluated both with LCPC and Eslami&Fellenius methods could be overestimated.

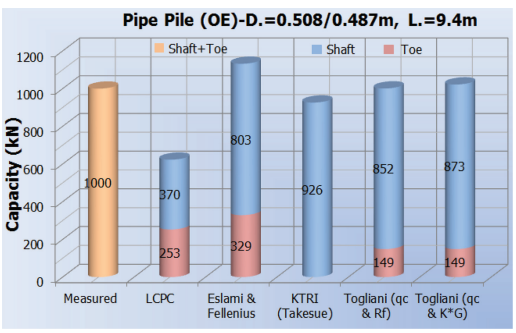

Figure 8. Pile capacities comparison.

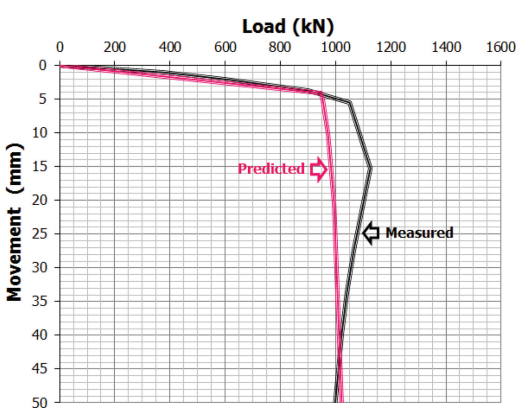

Figure 9. Load-movement comparison.

5 PORTO PILES DESIGN

In this experimental site, the toe resistance was measured via strain gauges at a movement equal to s/d = 10%, for pile E9 only, as represented in Figure 7.

The predicted load-movement curve (Figure 8) was assembled using function coefficients equal to 0.12 for shaft and 0.4 for toe resistance, respectively.

As previously noted, the LCPC shaft resistance is clearly inadequate as well as, in the opposite direction, the one obtained by KTRI (there is no difference between bored and driven piles!), while Eslami&Fellenius method was not considered, as more appropriate for driven piles

The design related to CFA Pile (T1) is summarized below and the notes concerning shaft resistance (Figure 9) are similar to the previous ones.

The function coefficient used for the predicted load-movement curve (Figure 10), this time has been set equal to 0.15.

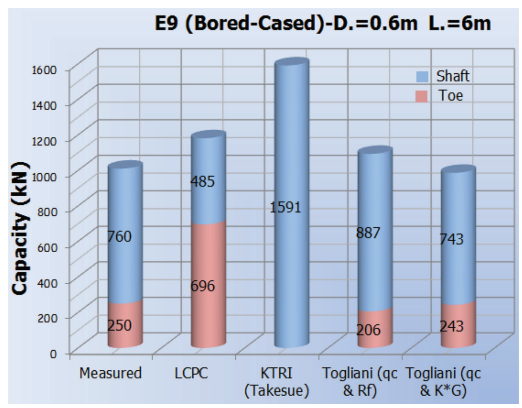

Figure 10. E9: Pile capacities comparison.

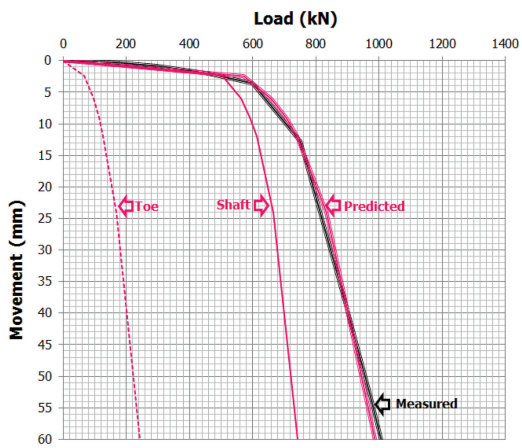

Figure 11. E9: Load-movement comparison.

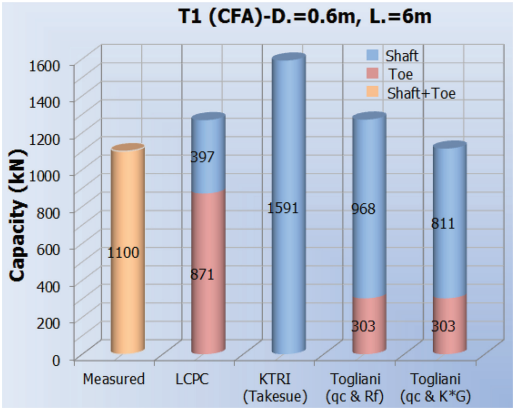

Figure 12. T1: Pile capacities comparison.

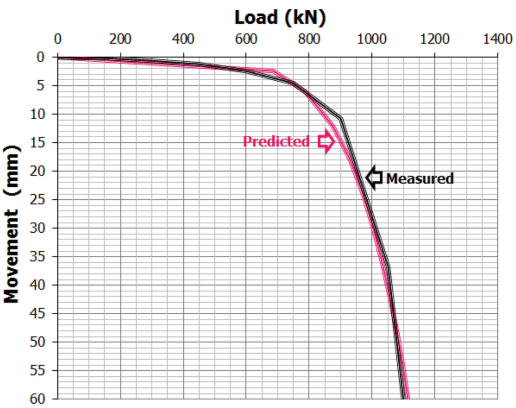

Figure 13. T1: Load-movement comparisons.

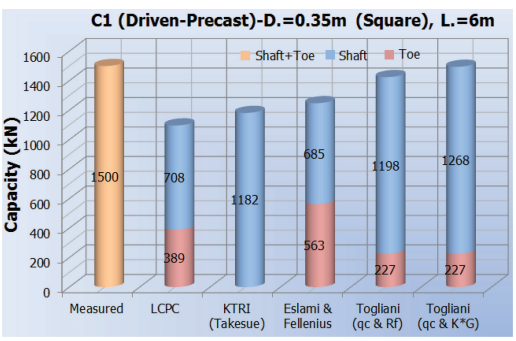

Figure 14. C1: Pile capacities comparison.

Figure 11 shows the capacities of the driven precast pile (C1) and Figure 12, the load-movement curves.

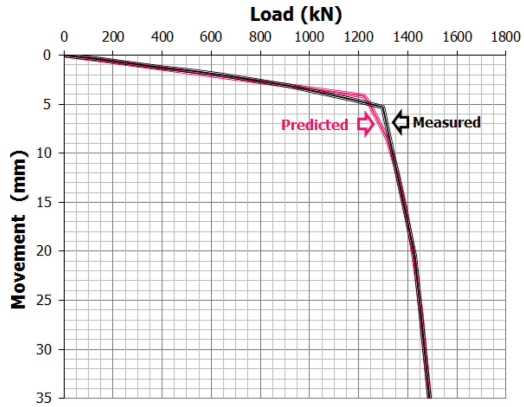

Figure 15. C1: Load-movement comparison.

To close on the predicted one, a function coefficient equal to 0.08 was used in this case, proving that shaft resistance is totally dominant.

Once again the LCPC shaft resistance is inadequate as well as the one derived from Eslami &Fellenius as the high f_s values are not balanced by consistent q_c values, in spite of the choice of unit frictions falling in the field with rather high shaft correlation coefficient (silty clay, silt).

The KTRI method, that for bored cased (E9) and CFA piles (T1) showed largely overestimated results, this time provides a consistent shaft resistance (clearly, now the non-difference between drilled and driven piles is reasonable).

About the new design method, it should be stressed that the prefabricated piles of both experimental sites seem, as expected, less performing ($\alpha = 0.11$) than those cast in place ($\alpha = 0.10$).

6 CONCLUSIONS

Cone resistance values are the most reliable among the measured CPTu parameters; however, as mentioned above, the sole consideration of q_c does not allow to understand the possible dilatant behaviour of the micro-structured soil. Hence, at least in these instances, the LCPC method becomes unreliable.

The design methods giving greater weight to f_s (KTRI and Eslami & Fellenius) provide good result in Merville because q_c and f_s values are mutually consistent.

On the contrary, this is not the case for Porto where very high f_s values (the silty sand soil retains a residual part of the parent rock structure), are unbalanced in comparison to q_c values.

While the shaft capacity predicted for the driven pile C1 with Eslami & Fellenius method is then inap-

propriate, for the same pile the one predicted using KTRI method, is adequate because its aforementioned ambivalence, at least in this case, is winning.

The Togliani method (2008/2017) that uses, jointly with q_c, also the friction ratio R_f, is less affected by the fluctuations in the f_s values; this is the reason why it provides very accurate pile capacity for Merville, remaining excellent (-5%) for pile C1 in Porto, good for pile E9 (+8%) and again sufficiently approximated for pile T1 (+ 16%) still located on the same site.

Finally, the newly proposed design method based on q_c and K^*_G values can be considered as self-adjusting with a good approximation to soils of different lithology and microstructural origin and proves to be promising; obviously, further confirmations are needed.

7 GLOSSARY

z	= depth
γ_n	= natural unit weight
q_c	= cone resistance
f_s	= sleeve friction
u_2	= pore pressure measured behind the cone
q_t	= corrected cone resistance = $q_c + u_2(1-a)$
R_f	= friction ratio = $(f_s/q_t)100$
σ_v	= vertical stress = $z\gamma n$
u_0	= hydrostatic pore pressure
σ'_v	= effective vertical stress = $\sigma_v - u_0$
σ'_p	= effective max. past vertical stress
OCR	= overconsolidation ratio = σ'_p/σ'_v
q_{tn}	= net corrected cone resistance = $q_t - \sigma_v$
Q_{tn}	= normalized cone resistance = $[(q_t - \sigma_v)/P_a][P_a/\sigma'_v]^n$
I_c	= classification index (P.K. Robertson)
$FC_{R\&W}$	= Fine content (Robertson & Wride)
$I_c > 3.5$ FC	= 1, $1.31 < I_c < 3.5$ FC = $1.75I_c^{3.25} - 3.7$, $I_c < 1.31$ FC = 0
CF	= Clay Fraction
Vs	= shear wave velocity
V_s derived (Porto)	= 118.8 LOG(f_s) – 18.5 (P.W. Mayne)
V_s derived	(Merville)-Baldi (1992) mod. Togliani = $277q_c^{0.12}\sigma'^{0.18}_v$ if $\sigma'_v < 100$ kPa otherwise = $277\ qc^{0.13}\sigma'^{0.22}_v$
G_0	= maximum.shear modulus = ρV_s^2
I_G	= small-strain rigidity index = (G_0/q_{tn})
K^*_G	= normalized small-strain rigidity index = $Q_{tn}^{0.75}I_G$

ACKNOWLEDGMENT

Many thanks are addressed to Prof. P.K. Robertson, and to Dr. L. Albert for their critical review and suggestions.

REFERENCES

Chen, Y.J. and Kulhawy, F.H.2002. *Evaluation of drained axial capacity for drilled shafts*. Conference: International Deep Foundations Congress 2002.

Fellenius B.H.2017. *Basic of foundation design.* Red Book, Electronic Edition, January 2017.

Fellenius B.H, Terceros H.M.and Massarsch K.R.2017. *Bolivian experimental site for testing*. Proceedings 3rd International Conference on Deep Foundations. Santa Cruz 2017.

Mayne P.W. 2001. *Manual on subsurface investigation*. FWHA, Washington DC.

Mayne, P.W.2007.NHRCP Project 20–05; Task 37–14: *Cone Penetration Testing—State-of Practice*.TRB.

Niazi F.S.and Mayne P.W.2013.*Cone penetration test based direct methods for evaluating axial capacity of single piles.*

Springer Science + Business Media Dordrecht 2013 P.K.Robertson.2015. *CPT Guide.* Electronic Edition.

P.K.Robertson.2016. *Cone penetration test (CPT)- based soil behaviour type (SBT) classification system—an update.*

Canadian Geotechnical Journal, 53(12)1910–1927.

Togliani, G. 2008. *Pile capacity prediction for in situ tests*. Proceedings ISC-3 April 1–4, 2008. 1187–1192. Taylor & Francis Group, London, UK.

Cone Penetration Testing 2018 – Hicks, Pisanò & Peuchen (Eds)
© 2018 Delft University of Technology, The Netherlands, ISBN 978-1-138-58449-5

Soil behavior and pile design: Lesson learned from recent prediction events—part 2: Unusual NC soils

G. Togliani
Geologist, Massagno, Switzerland

ABSTRACT: Pile design methods generally do not consider that the presence in the soil surrounding the piles of a microstructure related to phenomena such as aging, cementation and weathering, could significantly affect their performance. Analyzing soils classified as NC with reference to the CPT-based SBT classification system recently updated by P.K. Robertson, it is possible to highlight, via the normalized small-strain rigidity index K^*_G, the presence of a microstructure and to define his impact on piles design.

1 INTRODUCTION

Tables summarizing soils and piles characteristics of Santa Cruz (2017), the prediction event chosen for the part 2 of the paper, are provided below. The following CPTu plots contain the data used for the piles design.

At first glance the Santa Cruz alluvial layers appear, as stated, normally consolidated (e.g. see the u_2 curve and compatibility between derived and lab. FC values in Figures 1 and 2); however, their K^*_G values run around the upper limit of sedimentary soils, demonstrating that, even if of recent deposition, these mainly sand-like soils have been influenced by some phenomenon that has increased their stiffness (Figure 3).

Pairs of measured values should be used to calculate K^*_G, but being too few those of V_s, it is

Table 1. Santa Cruz: Soil details.

Deposit:	Alluvial (Holocene)
Lithology	Layers of sand, silt and clay
Soil structure from	Chemical Diagenesis?
GWT	–2.2 m
FC	12/53%

Table 2. Santa Cruz: Pile details.

Pile Type:	Driven (C2) Drill Disp.	Bored (A3) Bentonite	Bored (B2) CFA
Material:	Concrete	Concrete	Concrete
Shape:	Round	Round	Round
Diameter (m):	0.45	0.62	0.45
Length (m):	9.5	9.5	9.5
Cast in situ Date:	March 07	March 08	March 11
SLT Date:	March 25	March 20	March 23

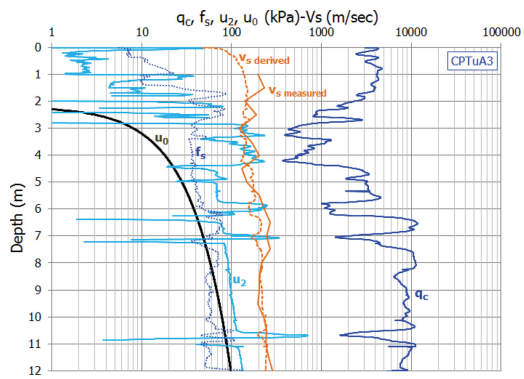

Figure 1. CPTu basic plots.

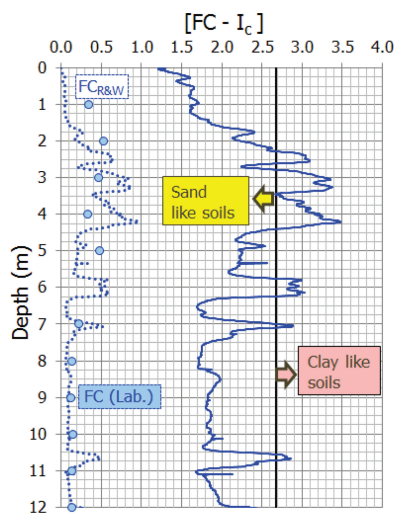

Figure 2. Soil behaviour.

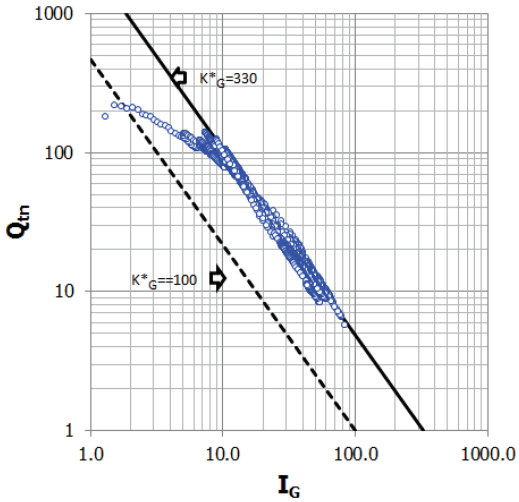

Figure 3. K*G plot.

reasonable to employ derived values since the V_s curves (measured/predicted), are close enough to each other (Figure 1).

Meaning of parameters appearing in the previous figures is provided in the glossary reported at §8.

2 PILE CAPACITY DESIGN METHODS

To verify their sensivity to the presence of a soil structure, the CPT based direct design methods (LCPC, Eslami & Fellenius, KTRI and Togliani) described by Niazi and Mayne (2013) have been used.

The Author's method, updated just before the prediction, now focuses on the following equations:

2.1 *Unit Friction (q_s)*

$$qs = \beta q_c 0.4 \text{ if } fs < 20 \quad (1)$$

$$q_s = \beta\{q_c^{0.52}[(0.4 + LN(Rf)]\} \text{ if } Rf > 1.5 \quad (2)$$

$$q_s = \beta\{q_c^{0.51}[0.8 + (1–R\ f)/8]\} \text{ if } 1 < Rf < 1.5 \quad (3)$$

$$q_s = \beta\{q_c^{0.53}[0.8 + (1.1–Rf)/8]\} \text{ if } Rf < 1 \quad (4)$$

2.2 *Unit Base (q_b)*

$$q_b = q_{c\ toe}[\lambda + (0.005\ Lpile/Dpile)] \quad (5)$$

where $q_{c\ toe}$ goes from +8 dtoe to –4dtoe.

Table 3 summarizes the corresponding Pile Type coefficients:

Capacities derived from the four quoted methods were then compared with the ones derived from the method specified below, including the normalized rigidity index K^*_G.

Table 3. β and λ coefficients.

Pile type	β	λ
Driven (precast/jacked)	1.00	0.30
Drill.Displacement.	0.90	0.25
Pipe (Open End)	0.70	0.20
CFA, Bored (cased-cohesionless, bentonite)	0.60	0.15
Bored (bentonite-upper bound)	0.60	0.10
Bored (cased—cohesive)	0.50	0.10
Bored (bentonite lower bound)	0.40	0.05

Table 4. α, β, λ coefficients.

Pile Type	α	β	λ
Drill Displacement—Santa Cruz (C2)	0.10	0.90	0.60
CFA—Santa Cruz (B2)	0.10	0.70	0.40
Bored (Bentonite) - Santa Cruz (A3)	0.10	0.40	0.15

2.3 *Unit friction (q_s)*

$$Q_s = \beta q_c^{[0.3 + x]}$$

where $x = LOG(K^*_G{}^{\alpha})$

2.4 *Unit base (q_b): same of § 2.2*

The following table shows the Pile Types coefficients developed for the new method (Class C Predictions), significantly different from the previous ones; specifically for λ, values from two (B2 an C2) to three times (A3) higher are obtained.

A reasonable explanation is the fact that in Santa Cruz the embedment into the bearing layer for the estimate of the toe resistance (from + 8d to –4d), is entirely (C2 and B2 piles) or almost entirely (A3 Pile) occurring in a medium dense to dense sand characterized by fair values of the cone resistance.

3 LOAD-MOVEMENT PREDICTION

The Chen & Kulhawy criterion (2002), shown in Figure 4, has been used to choose the force/movement distribution for every pile; subsequently the corresponding predicted curve was set via the Ratio Function.

According to this Function, the equation for unit resistance at a given movement in relation to the target resistance and target movement, is expressed by the following equation (B.Fellenius-Red Book):

$$r = r_{trg}\ (\delta/\delta_{trg})^{\theta} \quad (7)$$

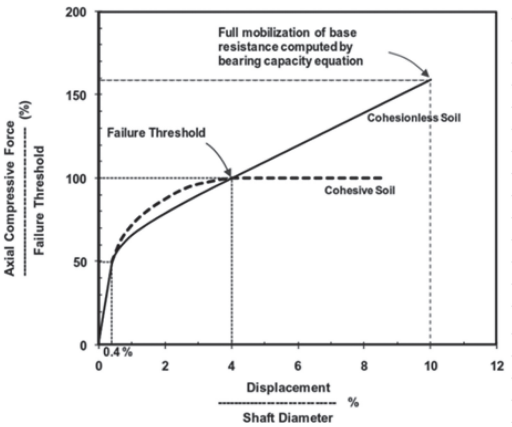

Figure 4. Chen & Kulhawy criteria.

where r = variable force; r_{trg} = target resistance; δ = var. movement δ_{trg} = movement at r_{trg}; θ = function coefficient ($0 < \theta < 1$).

The resistances derived with the new design method were considered as the target ones while the corresponding movement was set at s/d = 10% to obtain a complete load-movement curve. For Santa Cruz, the cohesionless soil curve of Figure 4 was adopted.

The superposition between measured and predicted load movement diagrams is obtained by adjusting the value of the ϑ coefficient within reasonable limits until a satisfying agreement was obtained; hence the theoretically evaluated curves are of Class C.

4 SANTA CRUZ PILES DESIGN

The incomplete elimination of the "bentonite cake" during concreting has lowered the shaft resistance of A3 pile (Figure 5); this is why the new method used a β coefficient equal to 0.40 (Table 3 & 4).

In Figure 5, the LCPC capacity is too high, while the Togliani method (2008/2017) with β and λ coefficients averaged among upper and lower bound (Table 3), shows a reduced toe resistance for the reason given at §2; the same, obviously occurs for B2 and C2 piles.

The function coefficient used for the predicted load-movement curve of A3 pile (Figure 6) is equal to 0.4, also in relation to a very likely imperfect toe cleaning.

For B2 and C2 piles (Figure 8 and Figure 10), the ϑ coefficient is equal to 0.32 and 0.25, respectively, showing an increasingly rigid response of the soil may be due to the progressive increase in

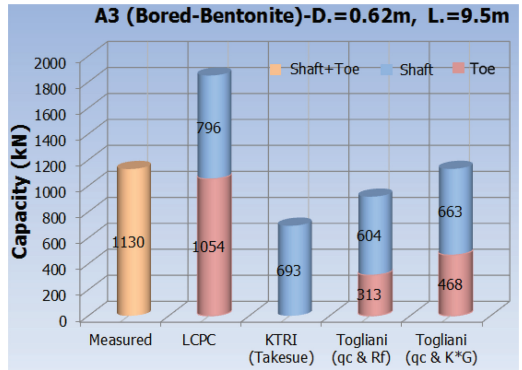

Figure 5. A3: Pile capacities comparison.

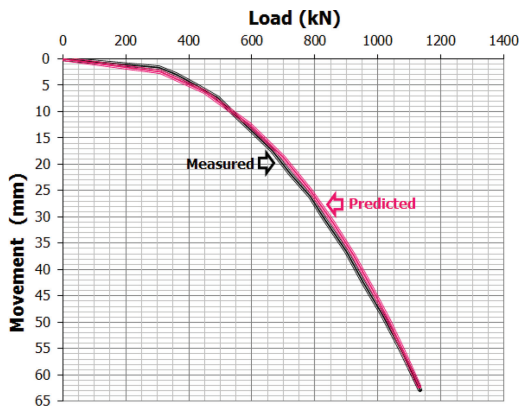

Figure 6. A3: Load-movement comparison.

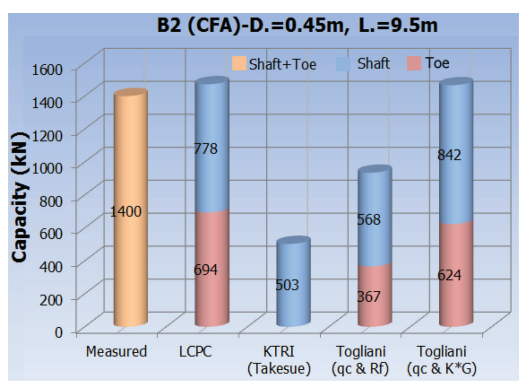

Figure 7. B2: Pile capacities comparison.

the soil displacement caused by the different technique of execution.

Surprisingly, for the CFA pile (B2 in Figure 7), the LCPC method provides satisfactory results

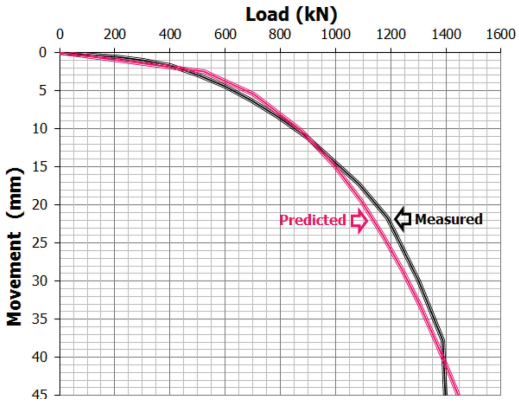

Figure 8. B2: Load-movement comparison.

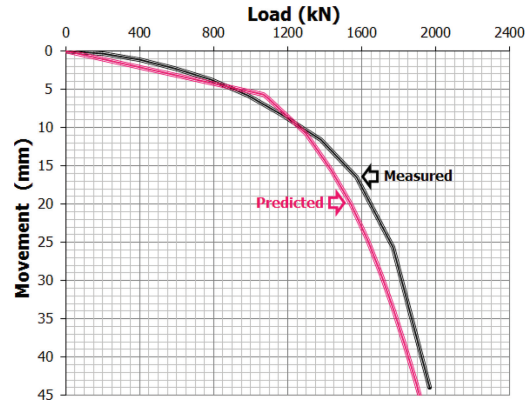

Figure 10. C2: Load-movement comparison.

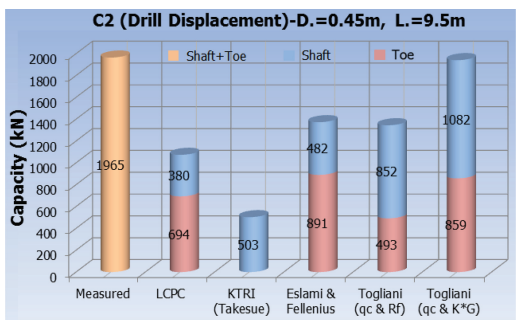

Figure 9. C2: Pile capacities comparison.

for both components (cast screwed piles was the choice), while this time both KTRI and Togliani methods lead to a totally inadequate shaft resistance. Very likely, in this case, their design is affected by weak values of f_s due to a structure rearrangement occurred during the CPTu execution.

For the drill displacement pile (C2 in Figure 9), the LCPC method provides a shaft resistance unexpectedly half the one of pile B2 and a third of the actual one, in spite of having chosen, as a guideline, the driven cast pile type effectively carried out.

Also shaft resistances provided by KTRI and Eslami&Fellenius methods are severely inadequate, once again due to reduced f_s values; the same problem affects, albeit less, the Togliani method.

As a last note, related to the load-movement curves, it has to be stressed that the choice of pile capacity at s/d = 10%, is purely conventional.

In fact this choice should be made, regardless of the pile diameter at a standard movement of, for example, 30 mm as suggested by Fellenius et al. (2017).

5 CONCLUSIONS

The sole cone resistance, despite being the most reliable among the measured CPTu parameters, does not allow to understand the possible dilatant behaviour of a micro-structured soil; consequently, at least in these instances, the LCPC method, providing random results, appears not completely reliable.

Design methods giving higher priority to f_s values (KTRI and Eslami& Fellenius), in this case are negatively affected and therefore not suitable, by f_s values often reduced probably as a result of the break/loosening of interparticle bonds caused by the cone being located in front of the friction sleeve.

The Togliani method (2008/2017), using the coefficients of Table 3 (Class A Prediction), provides too low pile capacities [respectively –24% (A3), –33% (B2) and –32% (C2)] being the most likely reason an inadequate choice of λ values.

Replacing them with the "consistent" values of Table 4 and, accordingly, using toe resistances obtained from the new method the approximation would be much better [–5% (A3), –15% (B2) and –13% (C2), see Figures 5, 7 and 9].

One could then argue that the Togliani method (2008/2017), updated for the λ values and with the proposed q_c and R_f combinations, is able to characterize in a reasonable, balanced way the mechanical behaviour of NC, micro-structured soils.

Finally, the q_c, K^*_G pair, as proposed in the new design method, provides appropriate and promising results, however to be confirmed with additional, future analyses.

GLOSSARY

z = depth
γ_n = natural unit weight

q_c = cone resistance
f_s = sleeve friction
u_2 = pore pressure measured behind the cone
q_t = corrected cone resistance = $q_c + u_2(1 - a)$
R_f = friction ratio = $(f_s/q_t)100$
σ_v = vertical stress = $z\gamma n$
u_0 = hydrostatic pore pressure
σ'_v = effective vertical stress = $\sigma_v - u_0$
σ'_p = effective max. past vertical stress
OCR = overconsolidation ratio = σ'_p / σ'_v
q_{tn} = net corrected cone resistance = $q_t - \sigma_v$
Q_{tn} = normalized cone resistance = $[(q_t - \sigma_v)/P_a][P_a/\sigma'_v]^n$
I_c = classification index (P.K. Robertson)
$FC_{R\&W}$ = Fine content (Robertson & Wride)
$I_c > 3.5$ FC = 1, $1.31 < I_c < 3.5$ FC = $1.75I_c^{3.25} - 3.7$, $I_c < 1.31$ FC = 0
CF = Clay Fraction
Vs = shear wave velocity
V_s = derived-Baldi (1992) mod. Togliani = $277q_c^{0.12}\sigma'^{0.18}_v$ if $\sigma'_v < 100$ kPa otherwise = $277\ qc^{0.13}\sigma'^{0.22}_v$
G_0 = maximum.shear modulus = ρV_s^2
I_G = small-strain rigidity index = (G_0/q_{tn})
K^*_G = normalized small-strain rigidity index = $Q_{tn}^{0.75}I_G$

Ed.: Symbols, definition and reference equations are mainly derived from the CPT Guide (P.K. Robertson, 2015), the Manual of Subsurface Investigation (P.W. Mayne, 2001) and the CPT State of Practice Report (P.W. Mayne, 2007).

ACKNOWLEDGMENT

Many thanks are addressed to Prof. P.K. Robertson, and to Dr. L. Albert for their critical review and suggestions.

REFERENCES

Canadian Geotechnical Journal, 53(12)1910–1927.

Chen, Y. J. and Kulhawy, F. H.2002. *Evaluation of drained axial capacity for drilled shafts*. Conference: International Deep Foundations Congress 2002.

Fellenius B.H.2017. *Basic of foundation design.* Red Book, Electronic Edition, January 2017.

Fellenius B.H,Terceros H.M.and Massarsch K.R.2017. *Bolivian experimental site for testing*. Proceedings 3rd International Conference on Deep Foundations. Santa Cruz 2017.

Mayne P.W. 2001. *Manual on subsurface investigation*. FWHA, Washington DC.

Mayne, P.W.2007.NHRCP Project 20–05; Task 37–14: *Cone Penetration Testing State-of Practice*. TRB.

Niazi F.S.and Mayne P.W.2013.*Cone penetration test based direct methods for evaluating axial capacity of single piles*.

Springer Science + Business Media Dordrecht 2013 P.K.Robertson.2015. *CPT Guide.* Electronic Edition P.K.Robertson.2016. *Cone penetration test (CPT)-based soil behaviour type (SBT) classification system—an update*.

Togliani, G. 2008. *Pile capacity prediction for in situ tests*. Proceedings ISC-3 April 1–4, 2008. 1187–1192. Taylor & Francis Group, London, UK.

Taylor & Francis
Taylor & Francis Group
http://taylorandfrancis.com

Cone Penetration Testing 2018 – Hicks, Pisanò & Peuchen (Eds)
© 2018 Delft University of Technology, The Netherlands, ISBN 978-1-138-58449-5

A probabilistic approach to CPTU interpretation for regional-scale geotechnical modelling

L. Tonni & M.F. García Martínez
Department of DICAM, University of Bologna, Italy

I. Rocchi
Department of Civil Engineering, Technical University of Denmark, Denmark

S. Zheng & Z.J. Cao
State Key Laboratory of Water Resources and Hydropower Engineering Science, Wuhan University, China

L. Martelli & L. Calabrese
Servizio Geologico, Sismico e dei Suoli, Regione Emilia-Romagna, Italy

ABSTRACT: The paper describes part of a study carried out to develop the geotechnical model of a coastal area on the Adriatic Sea, between the municipalities of Cesenatico and Bellaria-Igea Marina in the Emilia-Romagna region (Italy). A large experimental database, provided by the Geological, Seismic and Soil Survey of the Emilia-Romagna Authority, was used to develop a stratigraphic model of the upper 30 m subsoil of this coastal area, together with estimates of the mechanical parameters of the different soil units. A Bayesian approach was used to identify the most probable number of soil layers and their thicknesses, based on the Soil Behaviour Type Index obtained from CPTU results. This tool has already been used for small scale areas and its implementation in large datasets could eventually provide a preliminary estimate of the expected soil conditions at a site, taking into account statistically the inherent spatial variability in a rational and transparent way.

1 INTRODUCTION

A joint study focusing on the coastal plain facing the Adriatic Sea, in the southeastern part of the Emilia-Romagna Region, was carried out in cooperation with the Geological, Seismic and Soil Survey (GSSS) of the Emilia-Romagna Authority (RER), leading to a preliminary geotechnical model of this area (Tonni et al. 2016). The investigated territory, approximately 12 km long and 10 km wide, includes the municipalities of Cesenatico, Gatteo, San Mauro Pascoli, Savignano sul Rubicone and Bellaria-Igea Marina, which are well-known touristic sites and generally highly populated areas. This paper uses a dataset of borehole (BH) logs and piezocone (CPTU) measurements provided by the GSSS in order to develop a geotechnical model at a regional scale, also accounting for the depositional environment of the different soil units detected in the area. In particular, a Bayesian approach has been applied to cone penetration data for stratigraphic profiling purposes.

It is worth observing that Bayesian approaches have been successfully adopted for probabilistic geotechnical characterization in a number of contributions (e.g. Wang & Cao 2013, Wang et al. 2016, Cao et al. 2016) and a variety of applications, dealing with the evaluation of geotechnical model uncertainty (e.g. Zhang et al. 2012) or back analysis of soil parameters (e.g. Juang et al. 2013, Chiu et al. 2012), can be found in the literature.

As for geotechnical site investigations, most of these studies focused on quantifying uncertainty in the geotechnical parameters, seldom paying attention to soil stratification except for a few contributions, such as those proposed by Cao and Wang (2013), Wang et al. (2013, 2014), Houlsby and Houlsby (2013).

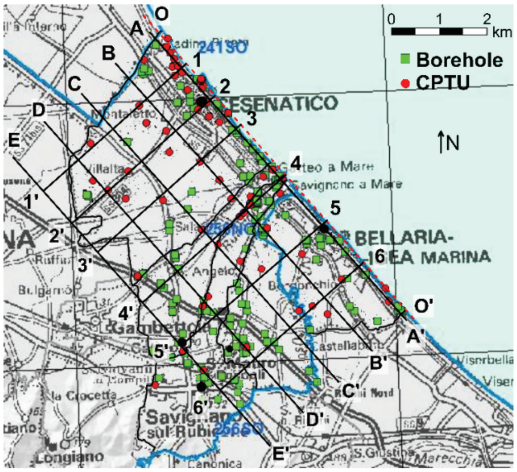

Figure 1. Area of study showing the location of site investigations and the alignments chosen for the cross sections.

2 GEOLOGICAL SETTINGS

Figure 1 shows the geographical boundaries of the study area and the location of the site investigations which form the main part of the available database. The alignments selected for the stratigraphic sections are also reported in the figure.

The local geology consists of the so-called Emilia Romagna Supersynthem (Supersintema Emiliano-Romagnolo, in Italian) which is an alternation of alluvial, deltaic, coastal and marine deposits arranged into different sedimentary cycles driven by transgression-regression of the sea. The thickness of the Emilia Romagna Supersynthem is maximum near the coast and progressively diminishes towards the Apennines. The Supersynthem is subdivided into two lower-rank hierarchic units, namely the Lower Emilia-Romagna Synthem (AEI) and the more recent Upper Emilia-Romagna Synthem (AES), dating back to Middle Pleistocene. The AES is further subdivided into a number of subsynthems, with AES8, AES7 and AES6 being those of interest on the study area. Due to transgressive-regressive depositional sequences, these units are typically characterized by marine and paralic deposits in the lower part and alluvial sediments in the upper part.

In particular, the Ravenna Subsynthem (AES8), outcropping in this area, was deposited after the last glaciation. Its lower boundary dates back to the beginning of the Holocene (10,000 years ago). This geological unit mainly consists of littoral sands and fine-grained alluvial sediments which were deposited by Apennine rivers. The AES8 does not present here any depositional nor erosional gap, except close to the coastline, where the littoral sands are separated from alluvial sediments by an erosional marine scarp formed during the last sea regression. Such littoral belt is 0.5 to 1 km wide, 4 to 12 m thick. In the following, such sandy unit will be indicated as Unit A.

The alluvial formations can be in turn distinguished between deposits characterized by a dense alternation of fine to very fine sands, sandy silts, silts to clayey silts, with a maximum thickness of 3–4 m (fluvial channel deposit, Unit B1), and floodplain deposits. These latter, composed of fine-grained sediments, form a maximum 20 m thick wedge, with locally interbedded clays containing undecomposed organic material. In the following, these sediments will be labelled as Unit B2, when predominantly clayey, and Unit B3, when predominantly silty.

Finally, sand-silt-clay mixtures, arranged in 1 to 6 m thick layers and referable to levee and crevasse deposits, form Unit B4.

3 METHODOLOGY

The experimental database provided by the GSSS includes 140 BH logs, 52 CPTU and 5 seismic piezocone tests (SCPTU), pushed to a depth of 15 to 30 m. In addition, laboratory tests were carried out on approximately 15% of the BHs available, providing soil classification and basic mechanical characterisation. The cross sections were selected to be approximately equally spaced (1.5–2 km), compatibly with the location of the available data. Five longitudinal sections (A-A' to E-E') were taken parallel to a straight reference line running along the coast whilst six cross sections (1–1' to 6–6') were selected in the orthogonal direction, as shown in Figure 1.

The probabilistic soil stratification, i.e. the determination of the number of layers (N) and their thickness (HN = [H1, H2, …, HN]) under a probabilistic framework, was based on the Soil Behaviour Type index, Icn, which is calculated iteratively from the dimensionless normalized cone resistance Qtn and the friction ratio Fr, according to the procedure described in Robertson (2009). The soil classes were then defined in terms of the Soil Behaviour Type (SBTn), corresponding to a well defined interval of values assumed by Icn. To keep the computational time at a minimum, one in five data points were used for the analysis (i.e. every 0.1 m), since this sampling frequency was found to basically guarantee the same reliability in the identification of N and HN obtained with higher rates, despite the risk of including rogue data points. On the other hand, running averaging of the data to

remove spurious data had an adverse effect on the standard deviation associated with the identification of boundaries.

Due to spatial variability of soils, Icn fluctuates with depth and this poses a profound challenge in identifying soil stratigraphy (i.e., N and HN) from a single Icn profile with a certain reliability. Under the Bayesian framework, the uncertainty in N and HN estimated from the Icn profile is explicitly quantified using their posterior distributions, reflecting the degrees-of-belief in their estimates. For a given profile of Icn denoted by ξ, the identification of soil stratigraphy can be divided into two steps (Cao et al. 2017):

1. Comparison of the soil stratification models with different numbers of soil layers based on the conditional probability $P(N|\xi)$ and determination of the most probable N* among a number of possible N values. Using Bayes' Theorem, $P(N|\xi)$ is written as:

$$P(N|\xi) = P(\xi|N)P(N)/P(\xi) \quad (1)$$

Where P(N) is the prior probability of N reflecting the prior knowledge on N in the absence of CPTU data, $P(\xi)$ is the probability density function of ξ, assumed as constant and independent from N, while $P(\xi|N)$ is the conditional probability of ξ given the soil stratification models with N layers, also frequently referred to as the "evidence" for soil stratification models with N layers provided by ξ.

Based on Eq. (1), $P(N|\xi)$ is proportional to the evidence $P(\xi|N)$, which means that maximizing $P(\xi|N)$ with respect to N leads to the maximum value of $P(N|\xi)$ and hence N*. Calculation of $P(\xi|N)$ is pivotal to evaluating Eq. (1) for quantifying uncertainty in N based on ξ and thus determining the most probable number of layers N*.

2. Evaluation of $P(HN|\xi, N)$ for quantification of uncertainty in layer thickness HN based on ξ for a given soil stratification model with N soil layers and determination of their most probable thicknesses H*N and boundaries D*N. Within a Bayesian framework, $P(HN|\xi, N)$ is referred to as the posterior distribution of HN based on ξ, and it is expressed as:

$$P(HN|\xi, N) = P(\xi|HN, N)P(HN|N)/P(\xi|N) \quad (2)$$

Where $P(\xi|HN, N)$ is the likelihood function quantifying information on HN of the soil stratification model with N soil layers provided by ξ, $P(HN|N)$ is the prior distribution of thicknesses and $P(\xi|N)$ is the evidence for the soil stratification model with N layers, used as a normalizing constant, as it is independent from HN for a given N value. Determination of N* and its corresponding most probable thickness HN* requires the formulation of the likelihood function $P(\xi|HN, N)$ and prior distribution $P(HN|N)$ as well as calculation of the model evidence $P(\xi|N)$. Details on the method can be found in Cao et al. (2017).

Figure 2 shows an example of piezocone logs from a test carried out along the cross section 2–2', together with soil classification results in terms of Icn and SBTn and the soil stratigraphy from an adjacent BH. The SBTn profile reveals a pronounced prevalence of clay-like sediments

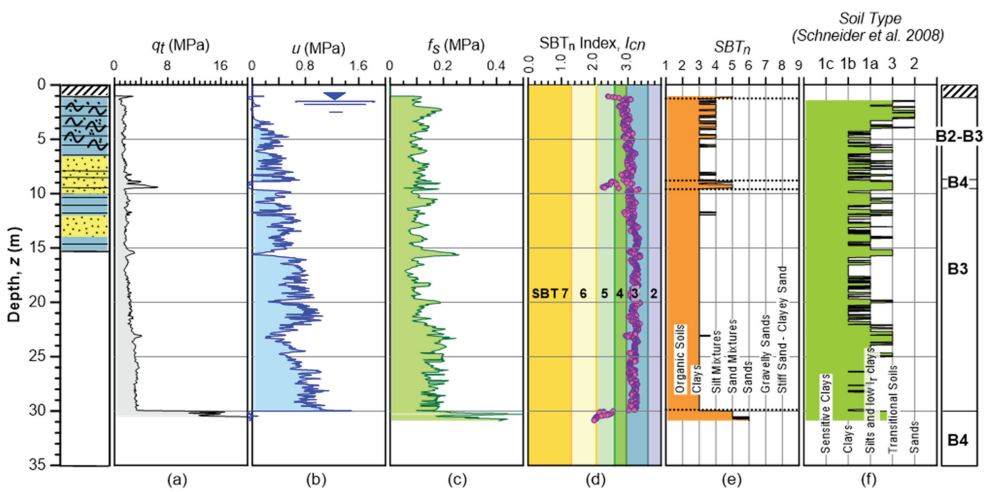

Figure 2. Example of piezocone data and comparison of CPTU-based soil classification results with BH log (CPTU22–4 from cross section 2–2').

(SBTn = 3) from 6 to approximately 30 m in depth, whilst an alternation of silts (4) and clays (3) is observed in the upper 6 meters. Based on the Icn profile depicted in column (d), the figure shows the most probable boundaries of soil layers (horizontal dashed lines in column (e)) provided by the Bayesian analysis. Such boundaries have been identified at 1.22, 8.78, 9.47 and 29.88 m from ground surface, with standard deviations equal to 0.027, 0.107, 0.097 and 0.036 m respectively.

For useful comparison, results from the application of the classification method developed by Schneider et al. (2008) have been reported in Figure 2 as well. This latter approach, which relies on the normalized tip resistance Qt and pore pressure ratio ($\Delta u2/\sigma'v$) for soil classification, has been especially devised to correctly identify intermediate sediments, where partial consolidation is very likely to occur during cone penetration. According to the computed soil type profile (f), a pronounced intermediate nature of fine sediments is observed, with a significant amount of experimental points falling in the domain of silts (1a) and transitional soils (3), these latter including a wide variety of soil mixtures (i.e. clayey sands, silty sands, silty sands with clay, clayey sands with silt).

4 GEOTECHNICAL MODEL

The following analyses focus on the cross section 2–2′, orthogonal to the coast and thus including both Units A and B previously mentioned. Besides, due to gentle sloping of the ground surface, such alignment allows a rather straightforward cross-correlation of in situ test logs.

Four CPTU tests (CPTU22-1 to CPTU22-4 from right to left) and two boreholes (BH22-1 and BH22-2 from right to left) were available for interpretation and are presented as "raw data" in Figure 3(a). Figure 3(b) presents the profiles of the computed Icn and the corresponding SBTn for the whole set of CPTU, together with the indication of the most probable boundaries of soil layers. The associated geological Units, as commented in Section 2, are also reported.

The SBTn profiles generally appear rather uniform in Unit B2, whilst a certain heterogeneity is observed in the other soil layers. A few interbedded coarse-grained layers have been identified in CPTU22-2 and CPTU22-4, which might indicate proximity to abandoned streams.

In this preliminary attempt to apply a Bayesian approach to the available data, the probabilistic identification of soil stratification has been carried out separately for each sounding, in order to have a more robust interpretation. According to results, it generally appears that there is no correspondence across the tests in N and HN, i.e. number and boundaries of layers identified along each vertical. It is worth mentioning here that the proposed soil stratification is coupled with rather low values of the standard deviation, typically in the range 0.001–0.1 m and only exceeding such interval (0.33 m) for the boundary detected at a depth of 21.76 m in CPTU22-2. A combined analysis of the tests would be undoubtedly crucial for the development of a comprehensive 2D and 3D stratigraphic model of the area and is currently in progress.

As a final remark on stratigraphic conditions, it must be observed that the application of the method of Schneider et al. (2008) to the whole set of CPTU confirms the outcome previously commented for CPTU 22-4, i.e. a prevalence of silts and intermediate sediments (1a and 3) rather than clay-like soils (SBTn = 3). In such case, partial drainage may occur during a standard rate CPTU (Tonni and Gottardi 2009, 2010, García Martínez et al. 2016) and this may have a significant effect on the derived soil parameters. Schnaid et al. (2004) have amply discussed the consequences of partial drainage on the undrained strength su, with reference to piezocone data in a natural silty deposit and a tailings deposit from a gold mine, and values of the undrained strength ratio $su/\sigma'v0$ have been interpreted in terms of the most likely drainage conditions. It was observed that this effect can result in an overestimation of su values, thus leading to unsafe design.

In what follows, estimates of the undrained shear resistance su in fine-grained soils, as determined from CPTU22-4, are presented. Assuming normally-consolidated or slightly overconsolidated sediments, a cone factor Nkt = 14 has been adopted to convert the CPTU net cone resistance to undrained strength. Figure 4 shows the undrained shear strength calculated in pronounced fine grained sediments (clays, clayey silts, silty clays) located below the water table, thus excluding intermediate soils. Three separate trends can be observed for su within the soil layer from 10 to 30 m in depth (labelled as Layer 4). In particular, when the whole data points are analysed, the computed estimates shows a bimodal frequency distribution (Figure 5). When distinguishing between Unit B2 and Unit B3, clays present a log-normal distribution, while silts/clayey silts follow a bimodal distribution, with significantly high values of su. In this latter case, the computed su must be considered with a great deal of uncertainty, due to potential partial drainage. It is interesting to note how the changes in trend are separated by thin soil layers, classified as transitional, indicating a change in depositional environment.

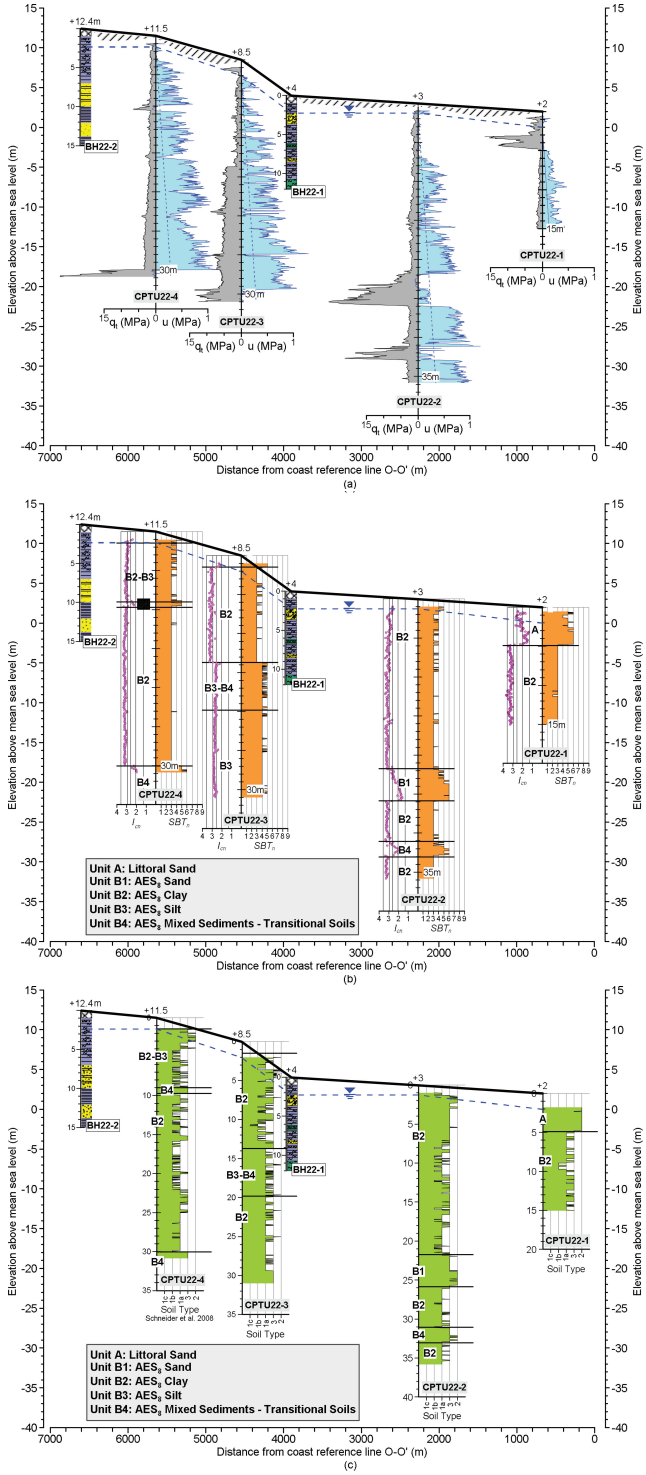

Figure 3. Cross section 2–2': (a) CPTU test results; (b) Icn and SBTn profiles in conjunction with Unit subdivision; (c) CPTU-based classification results according to Schneider et al. (2008).

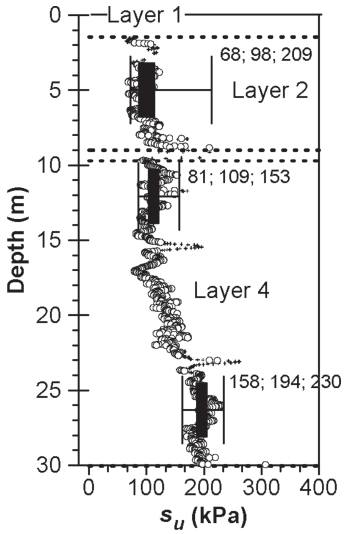

Figure 4. Undrained shear strength for CPTU22.

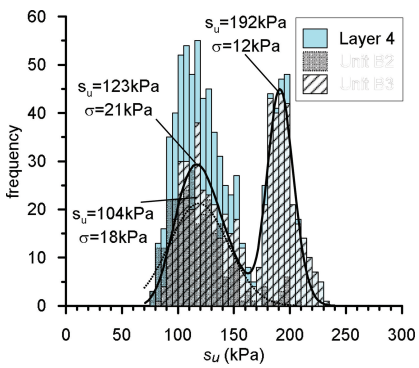

Figure 5. Frequency distribution of undrained shear strength within different soil sub-units.

5 CONCLUSIONS

The paper describes part of a study carried out to develop a regional geotechnical model of the coastal area of the Emilia-Romagna region. A Bayesian approach has been adopted to identify soil stratification from CPTU. Geological information have been also taken into account to help in identifying soil stratigraphy. A few issues on the estimate of undrained shear strength in fine-grained soils from CPTU data are briefly discussed, especially with reference to predominantly silty sediments.

The development of a regional-scale geotechnical model of this area aims at providing guidance on the selection of appropriate tests and correct data interpretation.

REFERENCES

Cao, Z.J. & Wang, Y. 2013. Bayesian approach for probabilistic site characterization using cone penetration tests. J. Geotech. Geoenviron. Eng., 139: 267–276.

Cao, Z.J., Wang, Y. & Li, D.Q. 2016. Quantification of prior knowledge in geotechnical site characterization. Engineering Geology. 203: 107–116.

Cao Z.J., Zheng S., Li D.Q. & Phoon K.K. 2017. Bayesian Identification of Soil Stratigraphy based on Soil Behavior Type Index. Submitted to Journal of Engineering Mechanics.

Chiu, C.F., Yan, W.M. & Yuen, K.V. 2012. Reliability analysis of soil-water characteristics curve and its application to slope stability analysis. Engineering Geology. 135–136: 83–91.

Garcia Martinez, M.F., Tonni, L., Gottardi, G., Rocchi, I. 2016. Influence of penetration rate on CPTU measurements in saturated silty soils. Proc. 5th Int. Conf. on Geotechnical and Geophysical Site Characterisation (ISC'5), Gold Coast (Australia), Vol. 1, pp. 473–478.

Houlsby, N.M.T. & Houlsby, G.T. 2013. Statistical fitting of undrained strength data. Géotechnique, 63(14): 1253–1263.

Juang, C.H., Luo, Z., Atamturktur, S. & Huang, H.W. 2013. Bayesian updating of soil parameters for braced excavations using field observations. Journal of Geotechnical and Geoenvironmental Engineering. 139(3): 395–406.

Robertson, P.K., 2009. Interpretation of cone penetration tests—a unified approach. Can. Geotech. J., 46(11): 1337–1355

Schnaid, F., Lehane, B.M., Fahey, M., 2004. Characterisation of unusual geomaterials. Proc. ISC-2, Vol.1, pp. 49 −73.

Schneider, J.A., Randolph, M.F., Mayne, P.W., Ramsey, N.R. 2008. Analysis of factors influencing soil classification using normalized piezocone tip resistance and pore pressure parameters. J. Geotech. Geoenviron. Eng., 134(11), 1569–1586

Tonni, L., Gottardi, G.,2009. Partial drainage effects in the interpretation of piezo-cone tests in Venetian silty soils. In: Proc.17th ICSMGE, IOSPress, Vol.2, pp.1004–1007.

Tonni, L., Rocchi, I., Cruciano, N.P., Garcia-Martinez, M.F., Martelli, L., Calabrese, L. 2016. A multidisciplinary tool for the development of a regional-scale geotechnical model: a case study in the North-Western Adriatic coastal area. Procedia Engineering, 158, 546–551.

Wang, Y. & Cao, Z.J, 2013. Probabilistic characterization of Young's modulus of soil using equivalent samples. Engineering Geology. 159: 106–118.

Wang, Y., Cao, Z.J. & Li, D.Q. 2016. Bayesian perspective on geotechnical variability and site characterization. Engineering Geology. 203: 117–125.

Wang, Y., Huang, K. & Cao, Z.J. 2013. Probabilistic identification of underground soil stratification using cone penetration tests. Canadian Geotechnical Journal, 50(7): 766–776.

Wang, Y., Huang, K. & Cao, Z.J. 2014. Bayesian identification of soil strata in London clay. Géotechnique, 64(3): 239–246.

Zhang, J., Tang, W.H., Zhang, L.M. & Huang, H.W. 2012. Characterizing geotechnical model uncertainty by hybrid Markov Chain Monte Carlo simulation. Comp. Geotech., 43: 26–36.

Cone Penetration Testing 2018 – Hicks, Pisanò & Peuchen (Eds)
© 2018 Delft University of Technology, The Netherlands, ISBN 978-1-138-58449-5

CPTu-based soil behaviour type of low plasticity silts

L.A. Torres-Cruz
University of the Witwatersrand, Johannesburg, South Africa

N. Vermeulen
Jones & Wagener, Johannesburg, South Africa

ABSTRACT: The application to low plasticity silts of two CPTu-based soil behaviour type charts proposed by Schneider and co-workers during the last decade is explored. One chart is based on tip resistance and sleeve friction (*Q-F*), and the other is based on tip resistance and dynamic pore water pressure (*Q-U2*). CPTu soundings made at two mine tailings deposits with a predominance of silt-sized particles were considered. The results indicate that the mechanical response of the CPT in these low plasticity silts can be indistinguishable from that of sands. As such, it is argued that the potential for misleading classifications can be reduced if the name of the 'sands' zone of the charts includes low-plasticity soils in general, regardless of fines content. Additionally, a new boundary for the drained zone of the *Q-U2* chart is proposed to enhance the classification of loose or very compressible low-plasticity soils in which largely drained penetration is possible at low values of Q.

1 INTRODUCTION

The cone penetration test (CPT) and more specifically the piezocone (CPTu) has proven itself to be one of the most valuable site characterisation tools available to the geotechnical engineer, where ground conditions permit its use. The CPTu in its most basic configuration provides virtually continuous measurement with depth of cone tip resistance (q_c), shaft friction (f_s), and dynamic pore water pressure behind the cone shoulder (u_2). Additionally, pore pressure dissipation data can be obtained during pauses for rod changes. These measurements, with appropriate calibration and correction, may be used to derive many geotechnical design parameters, or can directly be converted into design solutions (e.g. Lunne et al. 1997). The CPTu has found particular application in characterising hydraulic fills including tailings from mining processes, ash from thermal power plants and land reclamation or dredge fills.

One of the first and primary interpretations of CPTu data is that of delineating the ground profile into layers of similar soil type. In contrast to laboratory soil type classification, based on physical parameters such as particle size distribution (PSD) and Atterberg limits, CPTu classification relies on measured mechanical response to identify soil behaviour type (SBT). Nonetheless, CPTu SBT charts typically classify soils using conventional physical descriptors such as SAND, SILT & CLAY together with state or behavioural descriptors relating to drainage, dilation, overconsolidation and sensitivity. In particular, CPTu SBT charts typically make a primary separation of the profile into (i) drained, SAND-like soils and (ii) undrained CLAY-like soils. Such a separation is useful given that the approaches to interpret CPTu data differ in sands and clays. However, this combined physical-behavioural classification can yield misleading results in low plasticity soils such as coal ash and several types of mineral tailings. Although such soils are predominantly silt-sized, their mechanical behaviour can be indistinguishable from that of sands. Importantly, this does not occur in tailings with significant plasticity such as those derived from kimberlite ores.

Two SBT charts, which adopt a physical-behavioural classification scheme and are based on normalised CPTu parameters, were proposed by Schneider et al. (2008, 2012). The normalised parameters used in these charts are:

$$Q = \frac{q_t - \sigma_{v0}}{\sigma'_{v0}} = \frac{q_n}{\sigma'_{v0}} \tag{1}$$

$$F(\%) = \frac{f_s}{q_n} 100 \tag{2}$$

$$U2 = \frac{u_2 - u_0}{\sigma'_{v0}} = \frac{\Delta u_2}{\sigma'_{v0}} \tag{3}$$

where q_t is the total tip resistance corrected for unequal area (Lunne et al. 1997), σ_{v0} is the total

Table 1. SBT Zones of the Schneider et al. (2008, 2012) classification charts.

Zone	Simplified SBT description*
1a	Clays with low rigidity index (I_R)
1b	Clays
1c	Sensitive clays
3	Silts and transitional soils
2	Essentially drained sands and sand mixtures

* See Schneider et al. (2008) for full descriptions.

vertical stress, q_n is the net cone tip resistance, σ'_{v0} is the effective vertical stress, u_0 is the in-situ pore water pressure, and Δu_2 is the excess penetration pore water pressure.

Whereas Q and F are almost universally used by most SBT charts, in the Schneider charts $U2$ replaces the more common B_q ($= \Delta u_2/q_n$) as the normalised pore pressure parameter. Schneider et al. (2008) show that although Q-$U2$ and Q-B_q spaces are equivalent (since $U2 = B_q \cdot Q$), plotting data in Q-$U2$ space has the advantage of facilitating the distinction between the effects of overconsolidation and partial consolidation. Schneider et al. (2012) extended into Q-F space the framework proposed by Schneider et al. (2008) and updated the interpretation of some of the zones of the Q-$U2$ chart.

The Schneider charts delineate clay zones based on trends from simple models of undrained penetration and delineate a sand zone based on actual CPTu data. To a large extent the charts aim at identifying whether cone penetration takes place under drained, undrained, or partially drained conditions (see zones in Table 1).

Given the theoretical grounding of the Schneider charts and their agreement with the physical characteristics of soils across a variety of deposits, they are an interesting alternative for further development. Accordingly, the current paper explores the performance of the charts in low plasticity silts by considering CPTu soundings conducted at a thermal power coal ash dam and at a gold tailings dam. The results presented are expected to be useful to practitioners implementing the charts in similar soil types.

2 SITE INFORMATION

2.1 *Thermal power coal ash dam*

The thermal power coal ash dam considered herein is an upstream construction that employs hydraulic deposition. Fly ash from the precipitators and coarse bottom ash from the boilers are pumped separately in slurry form to the ash dam. The outer walls are constructed using only fly ash whereas the central area accepts both fly ash and bottom ash.

Laboratory classification tests conducted on 12 samples obtained from boreholes at different depths from different locations of the outer wall show that fines content (FC), taken as percentage of particles smaller than 75 µm, varies from 51% to 93%, with an average of 75% and that the remainder of the particles are almost entirely sand-sized (< 4.25 mm) (Figure 1). All specimens are non-plastic, and classify as low plasticity silts (ML) according to the Unified Soil Classification System (USCS). Although predominantly a sandy silt, borehole profiles from different locations of the outer wall indicate that bands of silty sand are present in the deposit. The consistency of the ash, assessed from Shelby tube samples recovered during sonic drilling and from standard penetration testing, varies from stiff to very stiff throughout the entire depth of the outer wall.

Two CPTu soundings (CPT3 and S02/2) conducted at the mid-height of the outer wall were selected for analysis. Profiles of u_0 and of the time required to achieve 50% dissipation of Δu_2 (t_{50}) were determined from dissipation tests conducted at approximately 2 m intervals. Table 2 presents some of the main features of the CPTu soundings. It is worth noting that the low (< 100 s) t_{50} values suggest that some degree of consolidation took place during cone penetration (DeJong & Randolph 2012).

Since the Q-$U2$ chart relies on readings of Δu_2 to determine SBT, its use is only possible in saturated soils. For the purposes of the current analysis, capillary effects were disregarded and only soil below

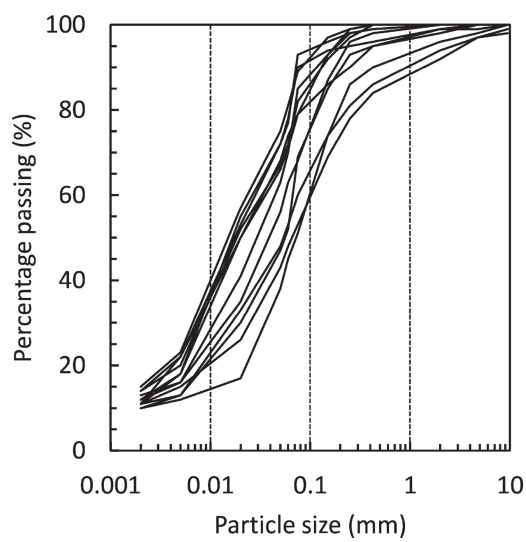

Figure 1. PSD curves of 12 samples from the coal ash dam.

Table 2. Characteristics of CPTu soundings.

Sounding no.:	CPT3	S02/2	WNNR1	J&WWEST1
Distance considered (m):	18.1	24.8	14	3
Quantity of dissipation tests	13	11	7	1
t_{50} (s)				
Minimum	8	1	4	20
Maximum	76	4	32	20
Average	25	2	16	20

the water table was assumed to be saturated. Furthermore, in order to compare the performance of the *Q-U2* and *Q-F* charts, the latter was also only employed for depths below the water table.

2.2 *Merriespruit gold tailings dam*

The second site considered herein is the Merriespruit gold tailings dam in South Africa which failed catastrophically on 22 February 1994. This case history has been documented in a variety of sources as reflected by the references in Papageorgiou (2004).

Laboratory classification tests conducted on 41 samples collected from different locations on the dam and on the breached tailings showed that *FC* varied from 42% to 99%, with an average of 77%, and that the remainder of the particles are sand-sized (< 4.25 mm). Plasticity index (PI) varied from 0 to 9, and the resulting USCS classifications were ML (predominant) and SM. As discussed by Papageorgiou (2004), it is likely that a significant portion of the contained tailings was in a loose contractive condition.

Two CPTu soundings (WNNR1 and J&WWEST1) conducted on the beach of the dam approximately one month after the failure were selected for analysis. As per the South African geotechnical practice of the time, the soundings did not include f_s readings. Profiles of u_0 and t_{50} were determined from dissipation tests conducted at approximately 2 m intervals. Table 2 presents some of the main features of the CPTu soundings. As in the coal ash dam, the low t_{50} values suggest that consolidation took place during the soundings (DeJong & Randolph 2012). Only measurements made below the water table were considered in the current work.

3 PERFORMANCE OF THE CHARTS

A summary of the classifications yielded by the *Q-F* and *Q-U2* charts is presented in Tables 3 and 4, respectively. The level of agreement between the two charts is also reported in Table 3 for the soundings conducted at the coal ash dam. A data point was considered to be classified equally by the charts if they yielded at least one common SBT description. For instance, a data point in zone 1c/3 of the *Q-F* chart was considered equally classified by the *Q-U2* chart if the latter yielded zone 1a/3, 3, or 1c.

Table 3. Fraction of data classified into the different zones of the Q-F chart.

Zone	CPT3	S02/2
1a	0.0	0.08
1b	0.03	0.46
1c/3	0.75	0.46
2	0.22	0.0
Agreement with Q-U2 chart	0.35	0.29

Table 4. Fraction of data classified into the different zones of the Q-U2 chart.

Zone	CPT3	S02/2	WNNR1	J&WWEST1
1a/3	0.0	0.19	0.35	0.0
1b	0.0	0.01	0.11	0.0
1c	0.0	0.0	0.0	0.0
2	0.85	0.26	0.07	0.50
3	0.15	0.54	0.47	0.50

3.1 *Soundings at the coal ash dam*

Results from sounding CPT3 are shown in Figure 2. On the *Q-F* chart the data plots predominantly in zone 1c/3. Conversely, on the *Q-U2* chart the data plots predominantly in zone 2. Although the charts yield different results, in a sense both classifications can be considered correct. The predominantly 'silt' classification by the *Q-F* chart is in agreement with the USCS classification of the ash. And although the ash is mostly a silt, as opposed to a sand, the "drained" descriptor of zone 2 yielded by the *Q-U2* chart is in agreement with the low values of t_{50} and *U2*. It thus seems appropriate to conclude that chart *Q-F* yielded the correct physical descriptor but wrong behaviour, whereas the opposite situation resulted in chart *Q-U2*. Since it is the mechanical behaviour of the soil that is of interest in geotechnical applications, the results from chart *Q-U2* can be regarded as more appropriate for this case.

Different classifications are also yielded by the charts when considering sounding S02/2 (Figure 3). The data on the *Q-F* chart plots mostly

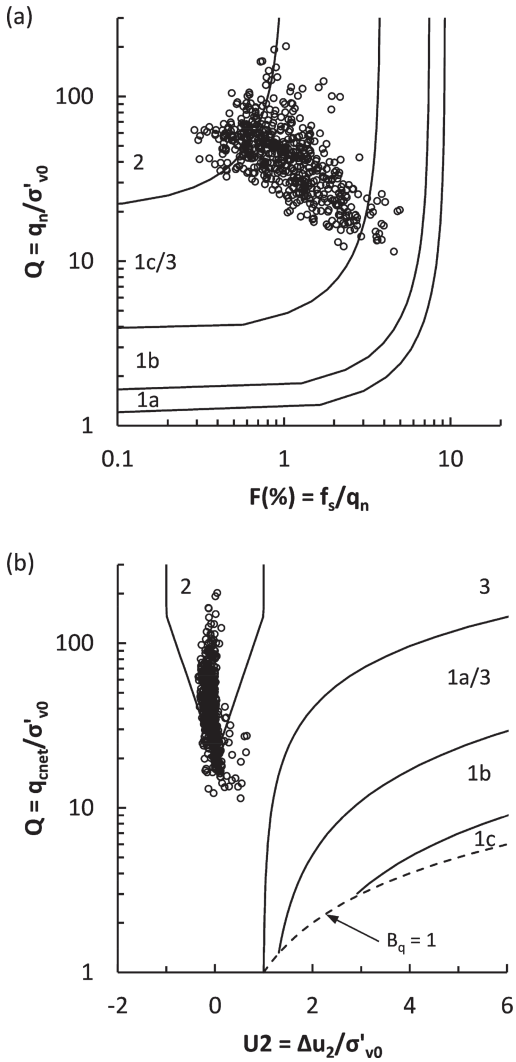

Figure 2. Sounding CPT3 through ash material.

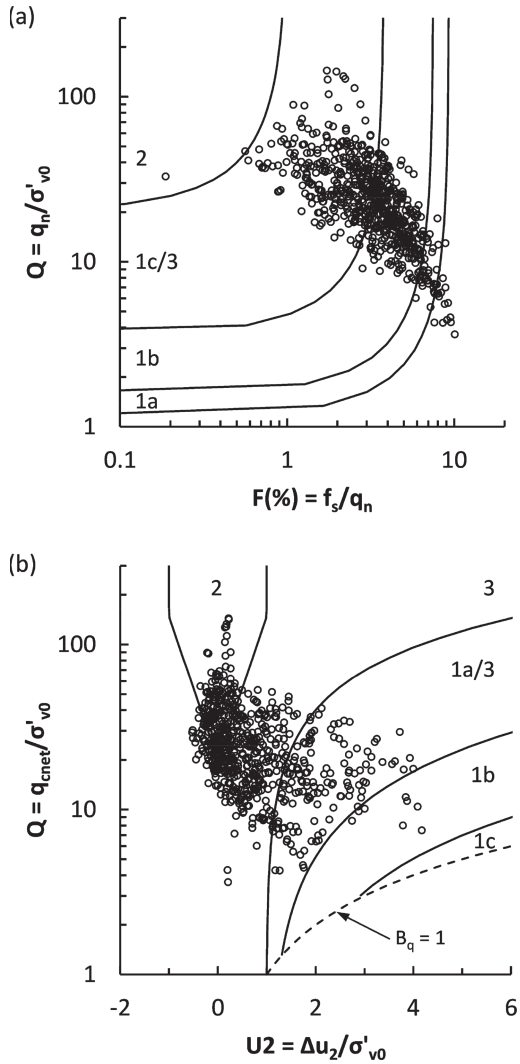

Figure 3. Sounding S02/2 through ash material.

in zones 1b and 1c/3 with virtually no data points in the drained region. In the *Q-U2* chart, the data plots mostly in zones 1a/3, 2, and 3, with only very few data points in the clay zone. Given that there are no clays present in the ash deposit, it is again clear that the results of

The *Q-U2* chart are in better agreement with the nature of the soil profile.

3.2 *Soundings at the Merriespruit tailings dam*

Figure 4 shows the results of sounding WNNR1 on the *Q-U2* chart. Most of the data falls in zones 1a/3 and 3, which is consistent with the predominantly ML classification of the tailings. It is also noted that despite the scatter, the overall trend of the data is in very good agreement with one of the premises of the *Q-U2* chart: As penetration becomes drained ($U2 \approx 0$) Q approaches 20. This =suggests that the lower bound of $Q \approx 20$ for zone 2 is a good fit for this particular sounding.

A different trend is observed in the results of sounding J&WWEST1 (Figure 5). In this case the data points are split in equal proportions over zones 2 and 3. Again, this is in agreement with the predominantly ML classification of the tailings and the low t_{50} and $U2$ values. However, for this sounding drained ($U2 \approx 0$) penetration persists at

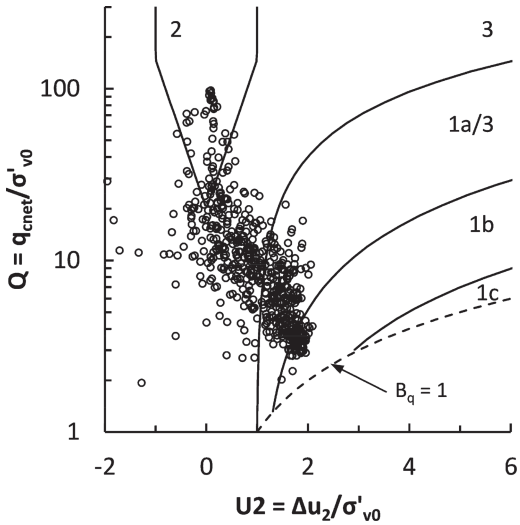

Figure 4. Sounding WNNR1.

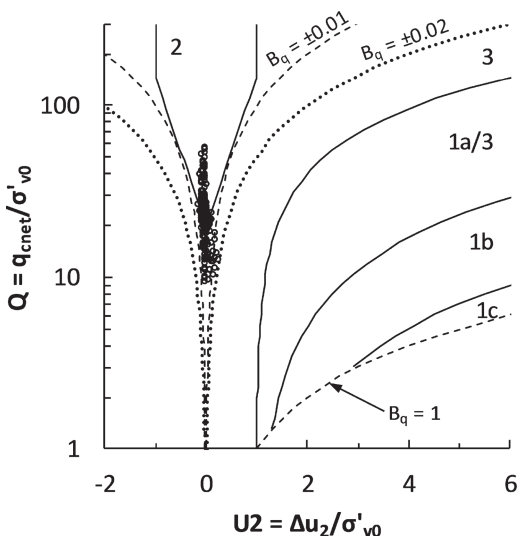

Figure 5. Sounding J&WWEST1.

Q values as low as 10. This is likely a consequence of the loose in-situ condition of the Merriespruit tailings.

4 DISCUSSION

Table 3 indicates that the level of agreement between the two charts was rather low (35% and 29%) at the coal ash dam. Specifically, the data plots closer to the undrained region in the *Q-F* chart than in the *Q-U2* chart. In this case, it is known that the *Q-U2* chart is yielding more realistic results because clays are absent from the coal ash dam and because *U2* is a more direct indicator than *F* of the level of drainage during penetration. It is thus apparent that the *Q-F* chart is underestimating the extent of drained penetration and overestimating the presence of clays (i.e. undrained penetration). A site-specific adjustment to overcome these shortcomings of the *Q-F* chart would require that its boundary lines be shifted downwards and to the right. This would result in a greater portion of ash data being classified in the drained region, which would be consistent with the low *U2* and t_{50} values, and would reduce the portion of ash classified as clay, in agreement with the non-plastic nature of the material. It is worth noting that such shift of the boundary lines is in general agreement with the SBT zones in *Q-F* space recently proposed by Saye et al. (2017).

Although overall, the *Q-U2* chart yielded results that are in good agreement with the nature of the ash and tailings deposits, two instances have been noted in which the resulting classification is somewhat misleading.

The first instance is that soundings CPT3 and J&WWEST1 indicate that important portions of the ash and gold tailings, which are predominantly low-plasticity silts, plot in zone 2 which corresponds to drained sands and sand mixtures (Table 4, Figures. 2b and 5). As noted above, this classification yields the correct behavioural descriptor (i.e. drained) but the incorrect physical descriptor (i.e. sand). The reason for this partial misclassification lies in two assumptions implicit in the name of zone 2 and its boundaries in the *Q-U2* chart. The first assumption implied by the name of the zone (Table 1) is that cone penetration is only likely to be drained ($U2 \approx 0$) in sand or sand mixtures ($FC < 50\%$). However, the data presented herein indicates that largely drained penetration can also occur in low plasticity silts with *FC* well above 50%. The second assumption implied by the name and boundaries of zone 2 is that at low absolute values of *U2*, $Q > 20$ is only likely if $FC < 50\%$. The lower bound of $Q = 20$ for zone 2 was chosen by Schneider et al. (2008) based on empirical data and numerical simulations. As such, the lower bound is a reasonable estimate for many situations as also confirmed by the results of sounding WNNR1 (Fig. 4). Nonetheless, it is convenient to explore the validity of the underlying assumption that for drained penetration conditions *FC* is inversely correlated to *Q*.

As a starting point one can consider the trends reported by Jefferies & Been (2015) which indicate that, for drained penetration, the magnitude of the normalised tip resistance is predominantly

a function of the state parameter (ψ) and of soil compressibility which can be represented by the slope (λ) of the steady state line (SSL). *FC* is independent from stress level and density and is therefore not correlated to ψ. It follows that if *FC* has an effect on *Q*, a correlation should be expected between *FC* and λ.

Schofield & Wroth (1968) presented results indicating a direct correlation between PI and λ in clays, providing a rational justification for an *FC*-λ correlation in plastic soils. Conversely, data for non-plastic soils collated from different sources does not support an *FC*-λ correlation. This is illustrated in Figure 6 where data from low plasticity soils of different origin fail to reveal a systematic correlation between *FC* and λ. The λ values in Figure 6 were extracted from Torres-Cruz (2016) and assume a straight line idealisation of the SSL in e-$log_{10}(p')$ space, where e is the void ratio and p' is the mean effective stress. The lack of correlation observed in Figure 6 is in agreement with Been et al. (2012), who noted that it is a "dubious assumption that fines content is a good proxy for material behaviour".

Seeing that drained behaviour and $Q > 20$ are possible regardless of *FC*, it seems warranted to reconsider the name of zone 2 to "essentially drained low plasticity soils". This would result in a decoupling of

FC and mechanical response which, as supported by the experimental data presented herein, is justified in low plasticity soils.

The second instance in which there is a deviation between the results of the *Q*-*U2* chart and the observed mechanical response is in the occurrence

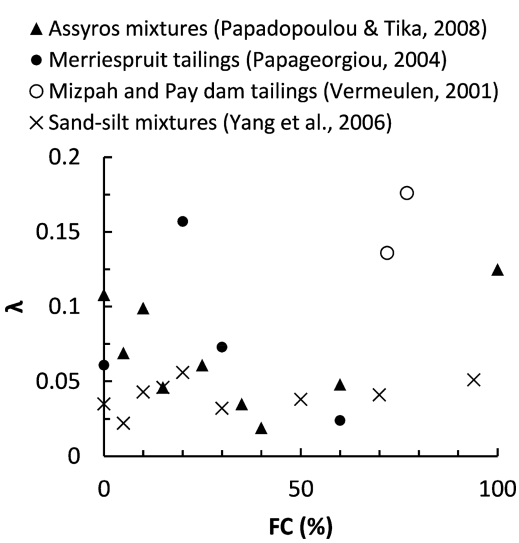

Figure 6. λ vs *FC* data for low plasticity soils.

of drained behaviour at $Q < 20$ (Figure 5). Schneider et al. (2008) pointed out that drained penetration at $Q < 20$ was possible in loose compressible sands, and the data for sounding J&WWEST1 indicates that the same is also possible in low plasticity silts. To reduce the possibility of misclassifying drained soils into zone 3, it is suggested that the boundaries of zone 2 are reconsidered by taking account of the parameter B_q. Given that one of the main effects of partial drainage on CPTu results is to influence tip resistance, it seems convenient to distinguish between drained and undrained conditions by considering Δu_2 normalised by q_n, i.e. B_q.

The exact value of B_q that should be used to identify drained conditions is still an unresolved issue. However, useful guidelines can be found in the literature. For example, Figure 5 shows that the original zone 2 proposed by Schneider et al. (2008) implies that the maximum absolute B_q value that can be regarded as drained is approximately 0.01. Similarly, Jefferies & Been (2015) suggested that a maximum absolute B_q value of 0.02 should be used to identify drained conditions. Regardless of the B_q value adopted to identify drained penetration, it is suggested herein that a contour of an adequate B_q value be adopted as a boundary for zone 2. As illustrated in Figure 5, such boundary would eliminate the need for a lower limit of *Q* and enable the correct identification of drained behaviour even in loose or compressible deposits of low plasticity soils were $Q < 20$ is possible.

5 CONCLUDING REMARKS

The current paper has explored the framework proposed by Schneider et al. (2008, 2012) to estimate SBT from CPTu data. The framework was chosen for study because its rational basis and agreement with empirical data make it an attractive option for further development.

The CPTu soundings considered herein were made at a coal ash disposal facility and a gold tailings dam as examples of low plasticity silts with FC ≥ 50%. Overall, the results of the *Q*-*U2* chart were more realistic than those of the *Q*-*F* chart. The site-specific modifications that would have to be made to the *Q*-*F* chart in order to obtain better results are in general agreement with the findings of Saye et al. (2017).

Significant portions of the ash and gold tailings deposit were classified in zone 2 of the *Q*-*U2* chart which corresponds to drained sand and sand mixtures. Accordingly, it is suggested that the name of zone 2 be changed to "essentially drained low plasticity soils" so that it accommodates both silty SANDS as well as sandy SILTS of low plasticity. The suggestion is supported by CPTu results

indicating that drained penetration is possible in low plasticity silts and by laboratory results that show that there is no systematic correlation between the FC and λ for low plasticity soils. It has also been suggested that the boundary for drained behaviour (zone 2) be defined in terms of a B_q contour (e.g. ± 0.01 or ± 0.02). The proposed boundary enables the identification of drained behaviour in loose or compressible deposits of low plasticity soils without imposing a lower bound on Q.

REFERENCES

Been, K., Romero, S., Obermeyer, J., & Hebeler, G. 2012. Determining in situ state of sand and silt tailings from the Cpt. In *Proceedings of the 16th international conference on tailings and mine waste 2012*. Keystone, Colorado, USA.

DeJong, J.T. & Randolph, M. 2012. Influence of partial consolidation during cone penetration on estimated soil behaviour type and pore pressure dissipation measurements. *J. Geotech. Geoenviron. Eng.* 138(7): 777–788.

Jefferies, M. & Been, K. 2015. *Soil liquefaction: a critical state approach*. Boca Raton, USA: CRC Press.

Lunne, T., Robertson, P.K., & Powell, J.J.M. 1997. *Cone penetration testing in geotechnical practice.* New York: Blackie Academic and Professional.

Papadopoulou, A. & Tika, T. 2008. The effect of fines on critical state and liquefaction resistance characteristics of non-plastic silty sands. *Soils and Foundations* 48(5): 713–725.

Papageorgiou, G. 2004. *Liquefaction assessment and flume modelling of the Merriespruit gold and Bafokeng platinum tailings.* PhD Thesis. University of the Witwatersrand. South Africa.

Saye, S.R., Santos, J., Olson, S.M. & Leigh, R.D. 2017. Linear trendlines to assess soil classification from cone penetration test data. *J. Geotech. Geoenviron. Eng.* 143(9): 04017060.

Schneider, J.A., Randolph, M.F., Mayne, P.W. & N.R. Ramsey 2008. Analysis of factors influencing soil classification using normalized piezocone tip resistance and pore pressure parameters. *J. Geotech. Geoenviron. Eng.* 134(11): 1569–1586.

Schneider, J.A., Hotstream, J.N., Mayne, P.W. & Randolph, M.F. 2012. Comparing CPTU Q-F and Q-Δu2/σ'_{v0} soil classification charts. *Géotechnique Letters* 2: 209–215.

Schofield, A.N. & Wroth, P. 1968. *Critical state soil mechanics.* London: McGraw-Hill.

Torres-Cruz, L.A. 2016. *Use of the cone penetration test to assess the liquefaction potential of tailings storage facilities.* PhD Thesis. University of the Witwatersrand. South Africa.

Vermeulen, N.J. 2001. *The composition and state of gold tailings.* PhD Thesis. University of Pretoria. South Africa.

Yang, S.L., Sandven, R. & Grande, L. 2006. Steady-state lines of sand-silt mixtures. *Canadian Geotechnical J.* 43(11): 1213–1219.

Taylor & Francis
Taylor & Francis Group
http://taylorandfrancis.com

Cone Penetration Testing 2018 – Hicks, Pisanò & Peuchen (Eds)
© 2018 Delft University of Technology, The Netherlands, ISBN 978-1-138-58449-5

Interpretation of soil stratigraphy and geotechnical parameters from CPTu at Bhola, Bangladesh

Zinan A. Urmi & M.A. Ansary
Bangladesh University of Engineering and Technology, Dhaka, Bangladesh

ABSTRACT: Soils are very complex materials and characterization of soil behavior requires interpretation of many geotechnical parameters, such as soil stratigraphy, stress history and index properties. Piezocone Penetration Test (CPTu) is a proven tool for effective and reliable subsoil exploration and for evaluation of near continuous soil stratigraphy and interpretation of many geotechnical parameters. The CPTu measurements (q_c, f_s and u_2) can be interpreted by using theoretical, analytical, and statistical methods; or by using other in-situ tests techniques or laboratory investigations to evaluate suitable geotechnical parameters that can be used in engineering practice. This paper presents interpretation of soil stratigraphy and evaluation of geotechnical parameters from CPTu measurements using laboratory investigations and in-situ Standard Penetration Test (SPT). Three pairs of CPTu and SPT tests were performed on the coastal embankment located in southern part of Bangladesh. The assessed geotechnical parameters include Soil Behavior Type, Mean Grain Size and Fines content. It is expected that this paper will provide valuable insight of CPTu data interpretation of the studied geologic setting, at Bhola, Bangladesh.

1 INTRODUCTION

Soil Investigations has evolved to improve understanding of soil type, stratigraphy and its strength and sustainability as a structural element or a resisting element in facing erosion. The Standard Penetration Test (SPT) is widely employed in-situ test. Even though there have been many attempts to standardize the SPT process, it is still a problem for geotechnical engineers to gather reliable and repeatable SPT results. A significant experience related to the design methods from the local SPT correlation has been built. However, in future, it is expected that more CPT will be performed thus improving local experience and the reliability of site investigation data. However, until a reliable CPT database has been created, it is necessary to be able to correlate between SPT and CPT in order to use SPT-based data that already exist.

The Cone Penetration Test (CPT) has become a significantly popular in-situ test to do site investigation and do geotechnical design. It is useful for stratigraphy delineation and continuous fast record of parameters such as cone tip resistance (q_c) and sleeve friction (f_s). The merits of the CPT are the repeatability, continuous measurement, and simplicity (Robertson et al, 1983).

In this study an approach has been taken to obtain soil profile based on cone tip resistance(q_c), friction ratio (R_f), Soil behavior index (I_c) and pore water pressure (u) to depths up to 30 m. SPTs tests have been done in the same location (within 2 m to 3 m of CPT locations) to interpret Geotechnical parameters such as grain size, fines content and behavior index from available CPT-SPT based correlations. Also, an approach has been taken to interpret SPT blow count (N_{60}) from CPT cone tip resistance (q_c). Interpreted results have been compared with laboratory obtained results and new correlations have been proposed where laboratory obtained data deviated from existing correlations.

2 FIELD INVESTIGATIONS

2.1 *General*

Field investigations were carried out mainly through the application of Cone Penetration Testing (CPT) and Standard Penetration Testing (SPT). A total of three pairs of CPT and SPT were performed in different locations within the study area and each pair of CPT and SPT was carried out as close as possible (SPT were performed within 2 m to 3 m of CPT locations), maximum horizontal distance between each CPT locations was not greater than 500 m. In this research, field investigations were carried out in Charfasson, Bhola, Bangladesh as shown in Figure 1.

The geologic formations of the research site are loamy to clayey, calcareous and poorly drained. Calcareousness decreases from west toward east of the Meghna confluence while the silt content in

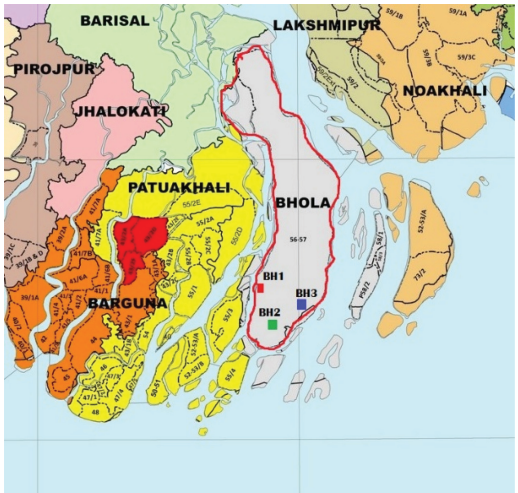

Figure 1. Study location.

soil decreases both toward the east and the west of Bhola district.

2.2 *Cone Penetration Test*

CPT soundings were advanced using a Hogentogler type piezocone penetrometer with a cross sectional area of 10 cm^2 and which can measure the pore water pressure (u_2), as well as the cone tip resistance (q_c) and sleeve friction(fs). To perform the test, the cone was pushed vertically into the ground at a constant rate of approximately 20 mm/sec. During the advancement, measurements of dynamic pore water pressure, tip resistance and sleeve friction were recorded continuously at 10 mm depth increments. The typical penetration depth for this study was approximately 28–32 m below from ground surface.

2.3 *Standard Penetration Test*

SPT were conducted according to ASTM D1586. Boreholes for the SPT were advanced by wash boring. The split spoon sampling method was used to obtain soil samples from boreholes and disturbed representative samples were collected. Samples recovered from boreholes were stored in plastic bags which were used for laboratory testing. Potential source of uncertainty which may affect SPT N-value has been carefully taken into account. Borehole drilling, soil sampling and SPT N-value recording procedures were observed by experienced geologist during the entire test program and this individual provided visual descriptions of the collected samples. SPT N-value and a sample were taken at every 0.45 m intervals. Rope and cathead SPT hammer-release was used and the efficiency of hammer was estimated to be 60%.

3 SOIL STRATIGRAPHY

Based on the results of the subsurface explorations, the subsoil profile at study area can be divided into three strata. The soil within the test area is primarily comprised of grey medium stiff to stiff clayey silt of medium plasticity with traces of fine sand and loose to medium dense fine sand with trace of silt and mica. The soil strata of borehole 1 and 3 are interbedded with the aforementioned two types of soil whereas borehole 2 is single layered comprising only grey medium stiff to stiff clayey silt. The ground-water table is located 4.5 m below from EGL in all the boreholes. Note that, there was considerable variability in the measured SPT N-value between boreholes, at different depths ranging from 3 to 16 and maximum corrected cone tip resistance (q_{c1}) was close to 12 MPa.

3.1 *CPT-SPT profile*

Cone Tip resistance q_{c1} (normalized) and SPT blow count N_{60} and $N_{1,60}$ (normalized) have been plotted along with depth for all three bore holes. It observed that q_{c1} varies from 0.5 to 12 MPa and peak values are reached below 15 m depth. SPT blow count N_{60} varies from 3 to 16. On Figure 2, it may be observed that CPT and SPT values seems to be proportional in most of the cases.

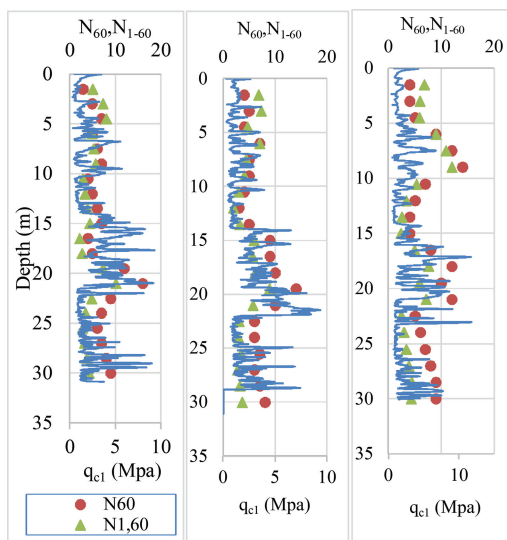

Figure 2. CPT-SPT profile of Borehole 1, 2 and 3 respectively.

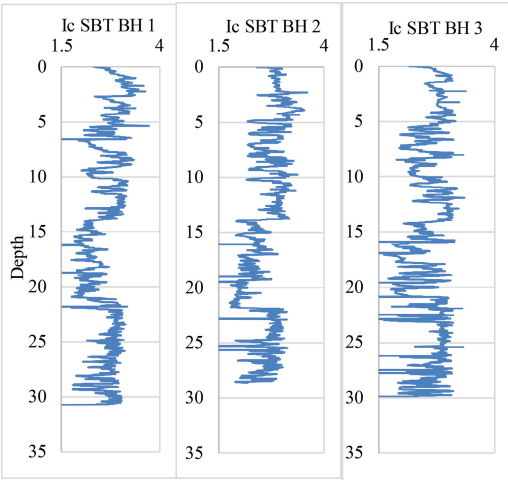

Figure 3. SBT profile for all the bore holes.

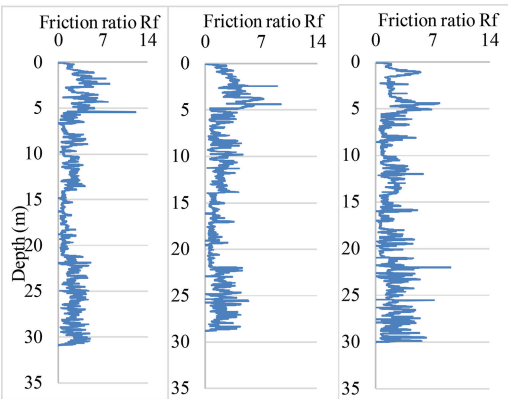

Figure 4. Variation of friction ratio with respect to depth.

3.2 *SBT profile*

Soil Behavior index I_c was determined for all the boreholes using the equation provided by Robertson (1990).

$$I_{SBT} = [(3.47 - \log(qc/pa))^2 + (\log Rf + 1.22)2]^{0.5}$$

All the boreholes have similar trends of variation in behavior index(I_c) and varying from 0 to about 3.5 for all the boreholes.

3.3 *Variation of friction ratio*

Friction ratio (Rf or f_r) is defined as the ratio of sleeve friction (fs) to cone tip resistance (q_c)

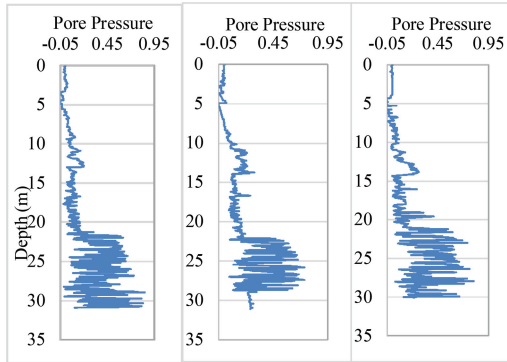

Figure 5. Variation of pore pressure with respect to depth for all three bore holes.

$$Rf\% = 100*f_s/q_c$$

Friction ratio of all three boreholes has similar pattern and most cases it varies between 0 to 5. The peak value of friction ratio for all three bore holes varies from 9 to 12.

3.4 *Variation of pore pressure*

Pore pressure varies from 0 to 0.4 MPa bellow 20 m depth and suddenly increases up to 0.85 MPa after 20 m. All three boreholes show similar variation.

4 LABORATORY INVESTIGATION

4.1 *Sieve analysis*

Soil sampled recovered from the three boreholes were individually assessed and classified based on dry sieve analysis. Sieve analysis was performed according to ASTM C136 on 20 disturbed soil sample from 3 boreholes. These soils contain reasonable amounts of fines (fc) ranging from 5 to 26%, fineness modulus ranging from 0.49 to 1.36 and mean grain size (d_{50}) ranging from 0.14 to 0.25.

5 ANALYSIS AND RESULTS

5.1 *Interpretation of mean grain size from the ratio of Cone Tip Resistance (q_c) to SPT blow count (N_{60})*

A range for Mean grain size (d_{50}) was determined based on correlations presented by Robertson et al. for North American soil (1983), Burland and Burbidge for London soils (1985), Kulhawy & Mayne for soils of California (1990), Canadian foundation engineering manual (Canadian Geotechnical Society 1992) and Anagnostopoulos

Table 1. Soil Gradation chart.

	Bore hole 1		Bore hole 2		Bore hole 3	
Depth	d_{50}	f_c	d_{50}	f_c	d_{50}	f_c
1.50	0.18	8.90	0.25	10.00	0.19	15.56
4.50	0.14	15.62	ND	ND	ND	ND
9.00	ND	ND	0.16	15.00	0.14	7.90
12.00	0.17	11.12	ND	ND	0.16	15.00
15.00	0.18	6.34	0.17	9.30	ND	ND
16.50	ND	ND	ND	ND	0.22	2.77
18.00	0.18	4.77	0.19	6.62	ND	ND
21.00	0.14	8.50	ND	ND	0.18	10.21
24.00	ND	ND	0.19	26.00	ND	ND
25.50	0.18	10.52	ND	ND	0.22	4.29
28.50	ND	ND	0.20	6.72	ND	ND
30.00	0.20	5.00	ND	ND	ND	ND

ND = Not Determined

for Greek soils (2003) and are shown in Figure 6. The laboratory obtained results are plotted on the same figure to compare the interpreted results to the actual results. The qc/N_{60} ratio of selected data set are less scattered and vary from about 2–12 for a variation of d_{50} from 0.14–0.25 mm whereas the available correlations give a range of d_{50} from 0.06 to 0.5 for the same variation of qc/N_{60} ratio.

5.2 *Interpretation of fines content size from the ratio of Cone Tip Resistance (q_c) to SPT blow count (N_{60})*

The fines content based correlations proposed by Chin et al. (1988) and Kulhawy & Mayne (1990) are presented in Figure 7 along with collected data sets of this study. Laboratory obtained data are a little scattered but appeared to be a logarithmic relationship unlike the interpreted values from available linear correlations. But the trend line of plotted data set shows that with increasing qc/N ratio, fines content decreases as indicated by previous researchers. The determination factor (R^2) based on 20 data points is 0.344 > 0.3 which although relatively poor, considered to provide a starting point for the CPT database.

5.3 *Interpretation of behavior index from the ratio of Cone Tip Resistance (qc) to SPT blow count (N60)*

Calculated CPT based Ic was plotted against the ratio of CPT cone resistance q_c to SPT blow count N_{60} and compared to the existing correlation between q_c/N and Ic provided by Jefferies & Davies (1993) which was modified by Robertson and Wride in (1998) and Robertson (2012). Fig. 8 shows that

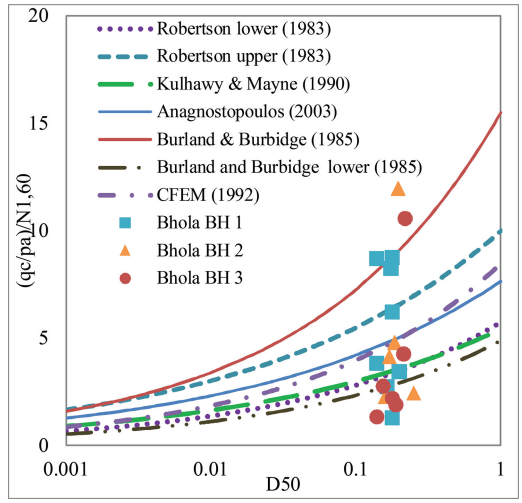

Figure 6. Variation of ratio $(q_c/pa)/N_{60}$ with mean grain size, d_{50} comparison.

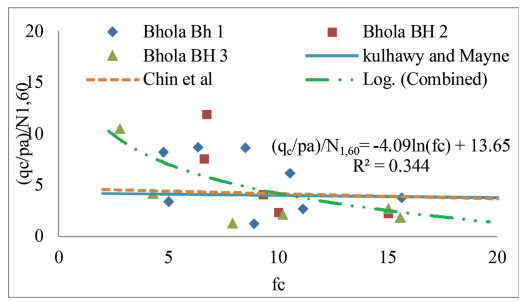

Figure 7. Variation of ratio $(q_c/pa)/N_{60}$ with fines content, f_c comparison.

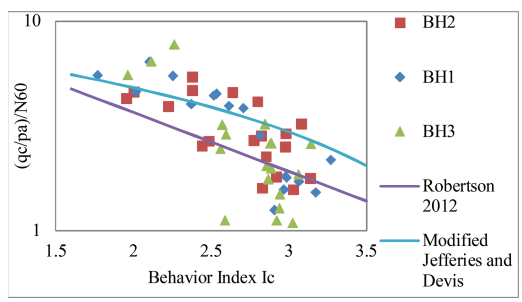

Figure 8. $(q_c/pa)/N_{60}$ Vs CPT-based SBT index Ic comparison.

q_c/N ratio for 54 study data points show the same pattern as existing correlations. q_c/N ratio for selected data points varies from 1 to 7 with a variation of SBT index from 1.8 to 3.3 whereas existing

correlations suggest that with similar variation of SBT index q_c/N has a range of 1.5 to 5.

5.4 *Interpretation of SPT blow count (N_{60}) from CPT cone tip resistance*

Elbana et al (2011) proposed a linear relationship between SPT blow count and CPT cone tip resistance which is $q_{c1} = 0.45*N_{1,60}$. To establish a linear relationship between qc and N60, normalized cone tip resistance was plotted against SPT blow count for 55 data points. On Figure 9 we observe that, although the data points are scattered, the linear average trend line gives a relationship between CPT and SPT close to Elbana et al which is $q_{c1} = 0.42 * N_{1,60}$ with a coefficient of determination (R^2) = 0.1327.

5.5 *Interpretation of Shear Strength Parameter (ϕ) from SPT and CPT*

Drained friction angle obtained from direct shear test was compared with SPT based friction angle provided by Wolff (1989), Kulhawy and Mayne (1990) and Hatanaka and Uchida (1996) respectively and CPT based friction angle provided by Robertson and Campenella (1983), Kulhawy and Mayne (1990) and Minmura (2003), these values are shown in Table 2.

From above table we observe that for a variation of SPT from 4.5 to 6, the interpreted drained friction angle of internal friction remains within the range of 25–30° whereas results obtained from direct shear test shows a variation of ϕ of 30–31°. For a variation of cone resistance from 1.1–1.8 MPa existing correlations provides a range of 23–31° whereas drained friction angle from direct shear test varies from 30 to 31°. Hatanaka & Uchida 1996 and Mimura 2003 are in best agreement with the laboratory test results.

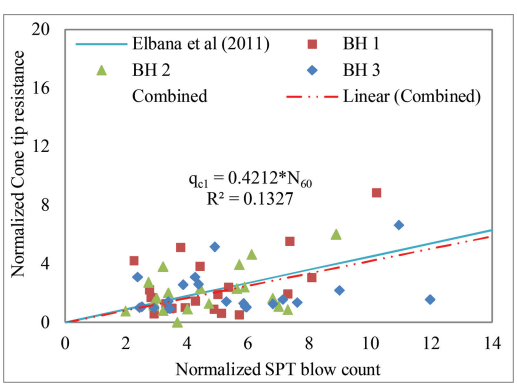

Figure 9. Variation of normalized cone tip resistance (q_{c1}) with normalized SPT blow count $N_{1,60}$ comparisons.

Table 2. Comparison of drained friction angle from direct shear test results with SPT & CPT based friction angle.

	Sample	Bhola 1	Bhola 2	Bhola 3
From SPT	Direct shear test	31	30.5	30
	SPT N60	6	4.5	4.5
	Kulhawy & Mayne 1990	27.3	25.08	25.08
	Hatanaka & Uchida 1996	29.95	28.62	28.62
	Wolff 1989	28.88	28.44	28.44
From CPT	CPT qc	1.8	1.1	1.17
	Robertson & Campanella 1983	27.47	23.65	24.22
	Kulhawy & Mayne 1990	25.08	22.71	23.04
	Mimura 2003	30.59	28.21	28.54

6 CONCLUSIONS

This study was intended to assess the best way possible to evaluate the use of correlations between laboratory and field investigation data so that it serves in various ways from saving time to saving money.

This study suggests that CPT data can be utilized to obtain high quality soil stratigraphy. Interpreted mean grain size and fines content from available correlations deviate from actual values. But better fines content values can be interpreted for local soil using $(q_c/pa)/N_{1,60} = -4.09\ln(fc) + 13.65$. On the other hand, behavior index based correlations gives values close to the real values. Also, interrelation between CPT and SPT proposed by Elbana et al (2011) may prove to be very useful for the local soil types. Drained friction angles interpreted from both CPT and SPT give values reasonably close to laboratory investigations, with more recent correlations giving better agreement.

Very little researches have been conducted with CPT-SPT data interpretation in our country, this study was a small part of an extensive research to profile, characterize and analyze soils from the northern-most riverine embankment to the southern-most coastal embankment.

ACKNOWLEDGEMENT

The authors would like to acknowledge the JST-JICA for the fund to undertake *Research on Disaster Prevention/Mitigation Measures against Floods and Storm Surges in Bangladesh* (Component C2) which provided data for this paper

REFERENCES

Alam et al, J.W. 1990. Geological Map of Bangladesh. Dhaka: Geological Survey of Bangladesh.

Ameratunga et al, C. 2016. *Correlations of Soil and Rock Properties in Geotechnical Engineering*. P.144.

Chin et al, T.C. 1988. SPT-CPT correlations for granular soils. *Proc. 1st international symposium on cone penetration testing. Orlando, USA*. (1): 335–339.

Elbanna et al, S. 2011. SPT–CPT correlations for oil sands tailings sand. *Proc. Tailings and Mine Waste, Vancouver, BC, 6–9 November 2011*.

Elkateb, T.M. & Ali H.E. 2010. CPT-SPT correlations for calcareous sand in the Persian Gulf Area. *2nd international symposium on cone penetration testing, CPT'10, California, USA*, Paper N0. 2–13.

Jamiolkowski, M. Baldi, G. Bellotti, R. Ghionna, V. & Pasqualini, E. 1985. Penetration resistance and liquefaction of sands. *Proc. 11th international conference on soil mechanics and foundation engineering, San Francisco*, (4): 1891–1896.

Kasim et al, C. 1986. Field Correlation of Cone and Standard Penetration Tests. *Journal of Geotechnical Engineering*., P.112(3):368–372.

Kulhawy et al, P.W. 1990. *Manual on estimating soil properties for foundation design*. NewYork: Electric PowerResearch Inst., Geotechnical Engineering Group, (EPRI-EL-6800): 2 36 to 2–28.

McNulty, G. & Harney, M.D. 2010. Comparison of CPT-and DMT-correlated effective friction angle in clayey and siltysands. *2nd international symposium on cone penetration testing, CPT'10, California, USA*, Paper ID 2-53.

Meyerhof, G.G. 1956. Penetration tests and bearing capacity of cohesion less soils. *Proc. SM1*, (82): 1–19.

Muromachi, T. 1981. Cone penetration testing in Japan, cone penetration testing and experience, *G.M. Norris and R.D.Holtz (eds), ASCE, New York*, 49–75.

Robertson et al, A. 1983. SPT-CPT Correlations. *Journal of Geotechnical Engineering*, 109(11): 1449–1459.

Robertson et al. 1985. Liquefaction Potential of Sands Using the CPT. *Journal of Geotechnical Engineering*., 111(3):384–403.

Robertson et al. 1983. Interpretation of cone penetration tests. Part I: Sand. *Canadian Geotechnical Journal*. 20(4): 718–733.

Robertson P.K. & Cabal K.L.2010, *"Guide to Cone Penetration Testing for Geotechnical Engineering"*.

Robertson. P.K. 2012. *Cone penetration test (CPT)-based soil behavior type (SBT) classification system an update*.

Schmertmann, J.H. 1975. Measurement of in-situ shear strength. *ASCE Specialty Conference on In-Situ Measurement of Soil Properties*, (2): 57–138.

Cone Penetration Testing 2018 – Hicks, Pisanò & Peuchen (Eds)
© 2018 Delft University of Technology, The Netherlands, ISBN 978-1-138-58449-5

Thermal Cone Penetration Test (T-CPT)

P.J. Vardon
Geo-Engineering Section, Delft University of Technology, The Netherlands

D. Baltoukas & J. Peuchen
Fugro, The Netherlands

ABSTRACT: The Thermal Cone Penetration Test (T-CPT) records temperature dissipation during an interruption of the Cone Penetration Test (CPT) to determine the thermal properties of the ground, taking advantage of heat generated in the cone penetrometer during normal operation. This paper compares two interpretation models for thermal conductivity. It is found that the thermal conductivity can be accurately determined. Care must be taken of the initial heat distribution and sensor location within the temperature cone to achieve accurate results. Furthermore, laboratory test data are presented that show that the full-displacement push of a penetrometer into sandy strata has limited influence on thermal conductivity values.

1 INTRODUCTION

Heat flow through the ground is of importance for applications from power cables, (shallow) geothermal energy and the storage of certain types of waste. There are currently few methods of determining the in-situ thermal properties, and those which exist either take a considerable amount of time or suffer from poor reliability or robustness.

The Thermal Cone Penetration Test (T-CPT) records temperature dissipation during an interruption of the Cone Penetration Test (CPT) to determine the thermal properties of the ground, taking advantage of heat generated in the cone penetrometer during normal operation. The T-CPT can be used over a large range of depths, unlike a needle probe, and can be taken during a CPT, thereby greatly reducing operation time. T-CPT measurements can be interpreted according to an empirically determined interpretation method (Akrouch et al., 2016) and a physics-based interpretation method (Vardon et al. 2017; the authors of this paper). This paper compares these methods.

2 THERMAL CONE PENETRATION TEST

The T-CPT uses a standard cone penetrometer with the addition of a temperature sensor, for example in the centre of the cone tip, as shown in Figure 1.

The T-CPT protocol is the same as for a CPT where cone tip resistance, sleeve friction and sometimes pore-pressures at various locations in the

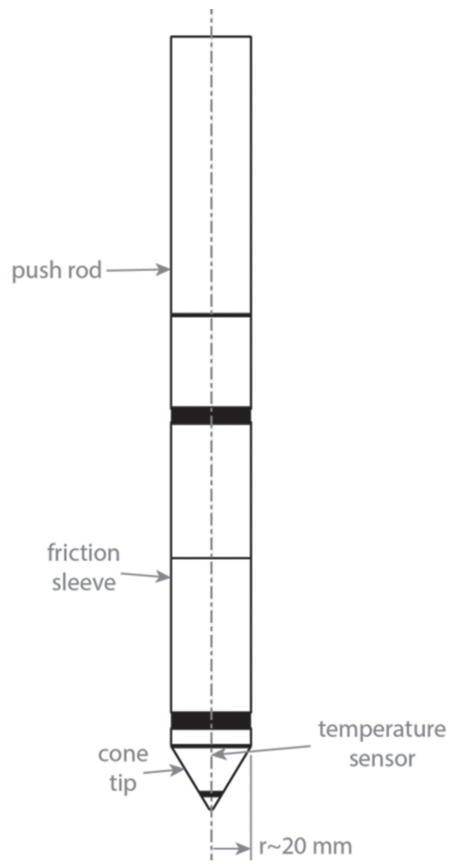

Figure 1. T-CPT cone penetrometer.

cone are measured (e.g. ISO, 2012). At the location where the thermal conductivity is required, the test is interrupted (stopped) and the temperature decay is recorded. The test is continued until the thermal conductivity converges to a good solution or until no further thermal decay is observed.

No heat source is required in the cone penetrometer and a minimum temperature difference between the ground and the cone penetrometer is required of approximately 3°C.

3 INTERPRETATION METHODS

3.1 *Physics-based interpretation method*

3.1.1 *Principles*

This method uses a 1D axisymmetric heat conduction equation. Therefore, this method should be used in situations which are dominated by conduction, as is typical in soils. Vardon et al. (2017) gave three different approximate solutions all of which gave the same final solution to determine the thermal conductivity. The simplest of these is a solution for an instantaneous heat release along a line inside a finite medium, which is given by Carslaw and Jaeger (1959) as:

$$T(r,t) = T_0 + \frac{H_0 / L}{4\pi kt} \exp\left(-\frac{c_p \rho r^2}{4kt}\right) \tag{1}$$

where T is the temperature, r is the radial coordinate, t is time, T_0 is the initial temperature, H_0/L is the heat release per unit length, k is the thermal conductivity, c_p is the specific heat capacity and ρ is the density.

Taking the natural logarithm and rearranging gives:

$$\ln(T - T_0) = \ln\left(\frac{H_0 / L}{4\pi k}\right) - \ln(t) - \frac{c_p \rho r^2}{4kt} \tag{2}$$

and recognising that the last term is insignificant at small r and large t, leads to an expression for the thermal conductivity:

$$k = f_{TC} \frac{H_0 / L}{4\pi\left(t\left(T - T_0\right)\right)} \tag{3}$$

where f_{TC} is a factor included for calibration of the T-CPT cone, mainly relating to the location of the temperature sensor.

The heat content per length, H_0/L, can be calculated by:

$$H_0 / L = (T_{max} - T_0) c_{p,steel} \rho_{steel} A_{cone} \tag{4}$$

where A_{cone} is the cross sectional area of the T-CPT cone and T_{max} is the maximum recorded temperature.

It can be observed that the gradient of Equation 2 with respect to ln (t) is -1, and exploiting this leads to an expression for the initial in-situ temperature as:

$$T_0 = \frac{t_1 T_1 - t_2 T_2}{t_1 - t_2} \tag{5}$$

where the subscript 1 relates to the earlier time and 2 the later.

For all of these equations, sufficient time is required to yield a converged answer. For a typical soil this time has been seen to be between 500 and 1000 seconds. For very early times in the test the assumption of an infinite line does not hold.

Alternatively a graphical method can be used, based on Equation 2. Again recognising that at long times the last term is insignificant and that the gradient of ln $(T - T_0)$ – ln (t) is –1 allows the intercept of a linear extrapolation of a ln $(T - T_0)$ – ln (t) from the linear portion to the y-axis to be used in the following:

$$k = f_{TC} \frac{S(T_{max} - T_0)}{4\pi \exp(i_T)} \tag{6}$$

where i_T is the intercept. An example is shown in Figure 2, where the recorded data is shown as a curved line and the linear extrapolation is shown by the straight line.

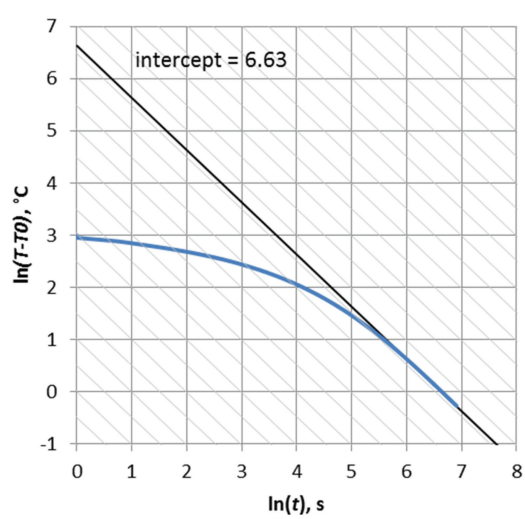

Figure 2. Example graphical method (Vardon et al. 2017).

3.1.2 *Calibration factor*

A numerical modelling study was carried out to determine the f_{TC} calibration factor. The factor corrects for two aspects: (i) the cavities in the cone penetrometer; and (ii) the location of the sensor. 1D modelling was carried out to test the working of the method, eliminating the above two effects (see Vardon et al., 2017 for details).

The model was simulated using COMSOL v5.2 using heat conduction. The geometry was 2D axisymmetric and includes a realistic geometry moderately simplified to reduce the complexity of the mesh and interior air-filled voids of the cone were removed. The mesh is presented in Figure 3.

The simulations were run in two stages, (i) a heat generation phase to represent pushing the cone through soil, and (ii) a heat dissipation stage to simulate the T-CPT. In the first stage, only the cone penetrometer was modelled (not the soil), with a heat flux boundary on the cone tip (500 W/m^2). In the second stage, the soil is included in the simulation and the model had a fixed temperature boundary condition of T_0 at the far field and zero flux conditions at all other boundaries. Both stages simulated 1000 seconds. The initial temperature for all materials was 20°C. A range of thermal conductivities of the soil were simulated. The other material properties of the soil were: specific heat capacity, c_p = 800 J/kgK and density, ρ = 2000 kg/m^3. For the steel of the cone penetrometer they were: specific heat capacity c_p = 475 J/kgK, density, ρ = 7850 kg/m^3 and the thermal conductivity, k = 44.5 W/mK.

The results of a typical simulation are shown in Figure 4. The temperature dissipation after 500 seconds of the heat dissipation part of the test is shown. The temperature distribution is uneven, with higher temperatures close to the cone tip. The heat flow can be observed to be largely radial, albeit with some strong 2D effects.

The calibration factor, calculated considering only the average area of steel in the cross section

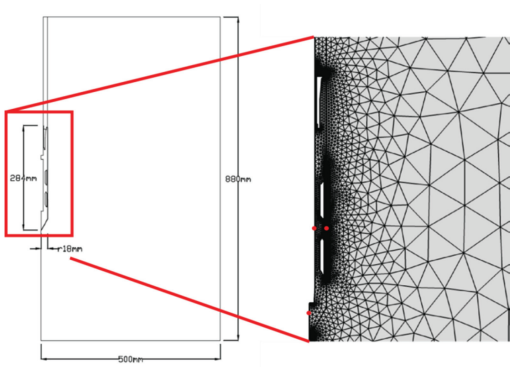

Figure 3. Domain and mesh details (Vardon et al., 2017).

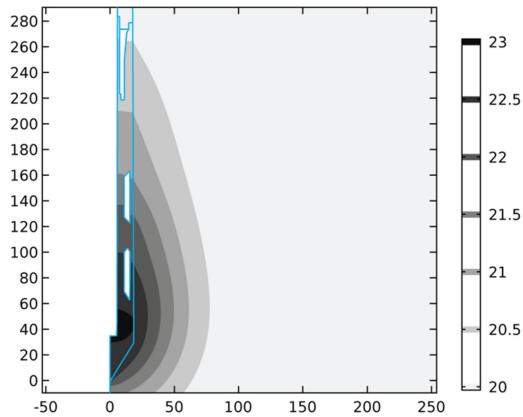

Figure 4. Contour plot of temperature (in °C) at 500 seconds, after the dissipation part of the test has begun (Vardon et al., 2017). Axes are in mm.

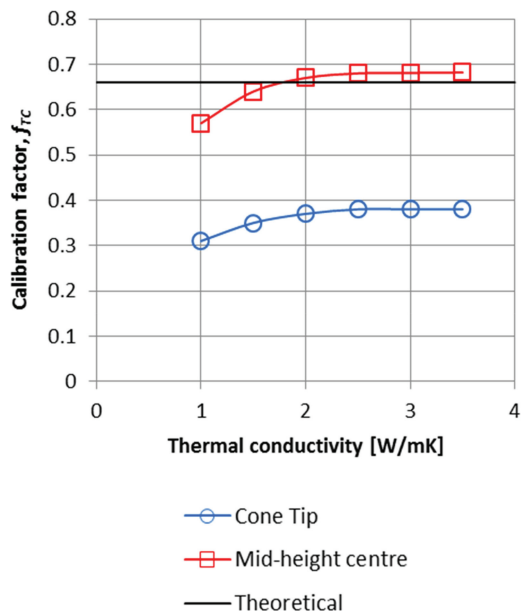

Figure 5. Calibration factor for the cone with sensor at the cone tip and mid-height (Vardon et al., 2017).

of the cone penetrometer, is 0.66. For the simulation presented here, with the temperature sensor in the cone tip, the calibration factor ranged from 0.3 to 0.38 with the thermal conductivity ranging from 1 to 3.5 W/mK, as shown in Figure 5. Between thermal conductivities of 2 to 3.5 W/mK the calibration factor is seen to be virtually constant. As shown, if the temperature sensor was moved to the mid-height of the cone, the calibration factor

would be close to the value correcting only for the cross sectional area.

3.2 *Empirical interpretation method*

Akrouch et al. (2016) recognised that the heat conduction and hydraulic flow equations are mathematically equivalent. They therefore proposed adopting the form of an empirical equation used to estimate the hydraulic conductivity for pore water pressure dissipation in CPTs to estimate the thermal conductivity from T-CPTs.

A numerical parametric study was carried out to calibrate the empirical equation leading to the following equation:

$$k = \frac{77}{(t_{50})^{0.968}} \tag{7}$$

where t_{50} is the time (s) for dissipation of half the initial increase in temperature and k is expressed in W/mK.

After comparing Equation 7 to experimental results the equation was modified to:

$$k = \frac{125}{t_{50}} \tag{8}$$

It is noted that both Equation 3 and 8 are inversely proportional to time, and both require knowledge of a maximum and minimum temperature. However, the empirical method requires a fictional maximum temperature, derived from a post data collection hyperbolic fit whereas the physics-based method requires simply the maximum recorded temperature.

4 COMPARISON OF INTERPRETATION METHODS

The two methods have been tested against the field (T-CPT) and comparative laboratory data provided by Akrouch et al. (2016) with a cone diameter of 44 mm, Data Set 1, and Vardon et al. (2017) with a cone diameter of 36 mm, Data Set 2.

4.1 *Data set 1*

Figure 6 compares the interpretation methods for the 3 sites of Data Set 1: Fugro, NGES and LA. The data was used for the calibration of the empirical method, therefore this method was expected to perform well. It is noted that the cone is a different cone than used to calculate the calibration factor for the physics-based method (Section 3.1.2), but this factor has also been used here.

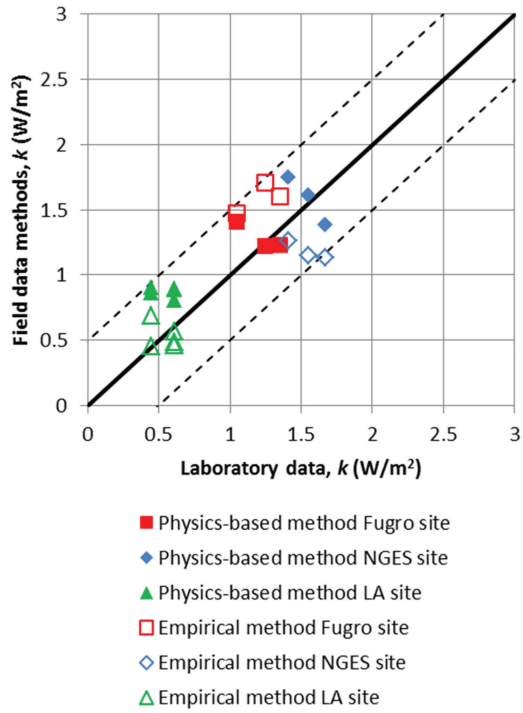

Figure 6. Comparison of interpretation methods.

It is seen that both methods can show the trends in the thermal conductivity behaviour. However, the physics-based method (shown with the solid data points) more accurately determines the difference between the Fugro and NGES sites. In general, the physics-based method slightly overpredicts the values (they are above the black line), which suggests that this cone has a marginally lower calibration factor, although it is thought likely that sampled material may have slightly desaturated.

The observed inability of the empirical method to demonstrate the difference between the Fugro and NGES sites is attributed to a higher heat capacity of the soil at the Fugro site, of about 10 to15%. The empirical method utilises a t_{50} value (the time taken for the elevated cone temperature to dissipate to half its value) and, as illustrated in Equation 2, the heat capacity plays an important role early in the test. The heat capacity was considered in the empirical model, but only in the calculation of the constants in Equations 7 and 8, and therefore does not distinguish between soils with different heat capacities.

Further differences between the two methods are that the empirical method requires a hyperbolic curve fitting procedure to determine T_{max} and

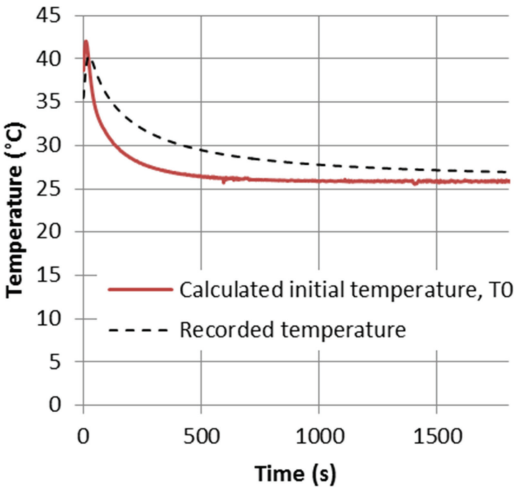

Figure 7. T_0 determination for Fugro site, 8.6 m depth.

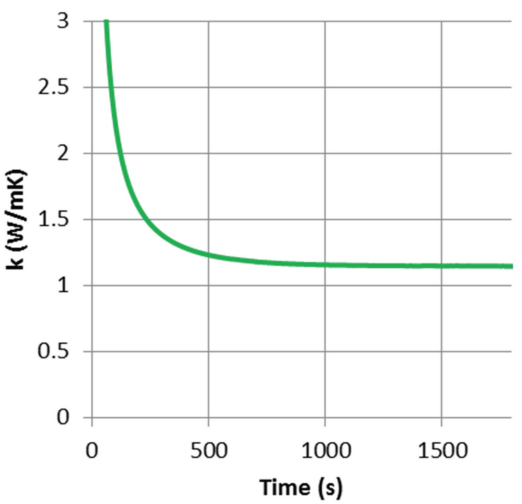

Figure 8. k determination for Fugro site, 8.6 m depth.

T_0. T_{max} in this case is not the maximum recorded temperature as defined in Section 3.1.1, but a fictional maximum from the hyperbolic fit. The hyperbolic fit utilises all of the data taken in this test to gain a good fit, i.e. 1800 seconds, whereas Equation 5 is seen to determine this same value in around 600 seconds (25.90°C), as shown in Figure 7, in contrast to the recorded temperature which does not reach this in-situ temperature even at 1800 seconds.

The calculated value of thermal conductivity for the physics-based method is also seen to converge in the same time as T_0 (around 600 seconds), as shown in Figure 8, indicating that the test could be reduced in time, by up to a factor of 3 for both methods.

4.2 *Data Set 2*

Data Set 2 covers four different methods: (i) T-CPT, (ii) in-situ thermal needle probe, (iii) thermal needle probe on sampled material, tested immediately after sampling, and (iv) thermal needle probe on sampled material in the laboratory, including undisturbed, reconstituted and multiple density tests. The T-CPTs were undertaken as CPTU according to ISO (2012), stopped at the selected test depths, and the temperatures recorded. The thermal needle probe tests were performed according to the ASTM (2014) D 5334-14 standard. The soil profiles at the test locations were mainly sand, but at some locations clay is located close to the ground surface. The calibration factor f_{TC} = 0.35 was used in all cases, matching a thermal conductivity of 2 W/mK, as an a priori best estimate of thermal conductivity.

Only select results from in-situ tests are presented here for clarity and brevity. Four different locations are shown in Figures 8 to 10 with a range of depths from 5 m to 35 m. The thermal needle probe tests and the T-CPTs were generally a few metres apart horizontally at each location, and in Figure 10 the sub-locations were up to 10 m apart. It was not always possible to do tests at the same depth, as in deeper locations where the T-CPT could easily take tests the in-situ needle probe proved fragile and in shallower depths a sufficient temperature increase in the cone was not always achieved. At location 4a, to compensate for the lack of comparable results at depth, a borehole was drilled and an in-situ needle probe was taken below the bottom of the borehole at about 34 m depth.

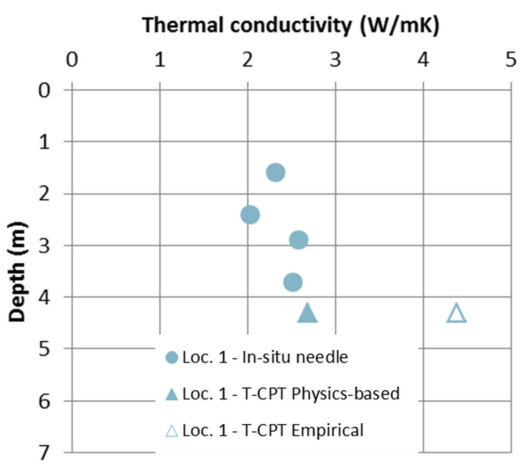

Figure 8. Thermal conductivity results at location 1.

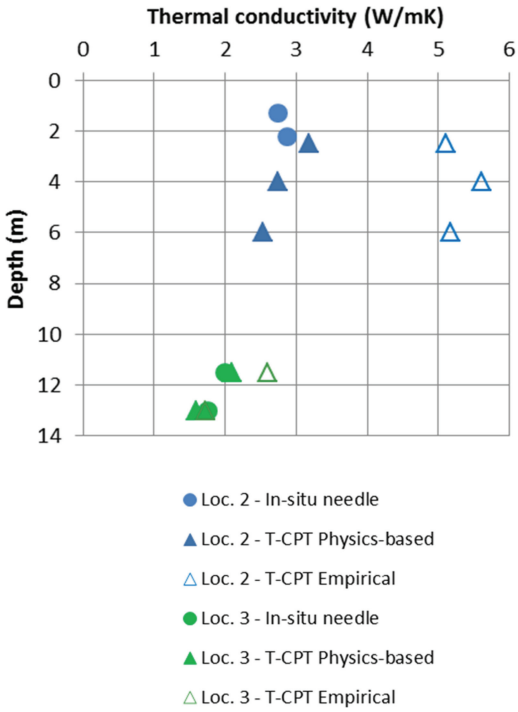

Figure 9. Thermal conductivity results at locations 2 and 3.

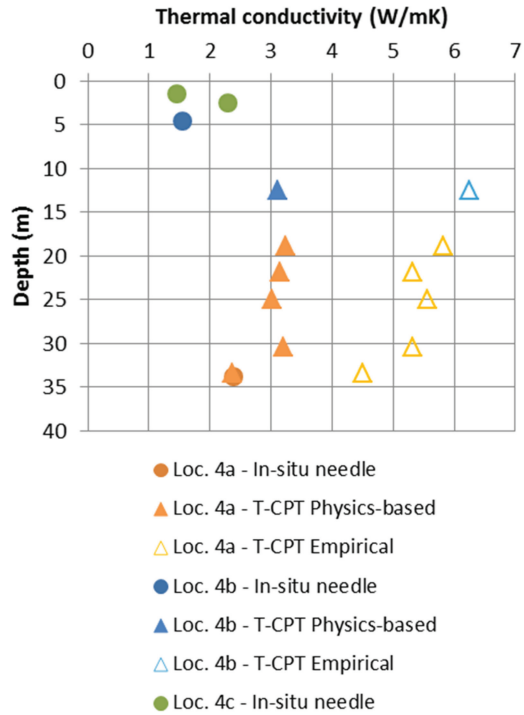

Figure 10. Thermal conductivity results at location 4.

All figures show excellent agreement between the physics-based method and the in-situ needle probe tests, with a range of depths and thermal conductivities. The empirical method generally significantly overestimates the thermal conductivities, with the exception of location 3. However, it is observed that between tests at the same location a reasonable comparative trend is observed, see Figure 10 (location 4). It is thought that the overestimates are due to a number of factors, including the reduced cone radius (a lower initial heat content) and the wider range of thermal conductivities. In all cases the t_{50} values for Data Set 2 were significantly lower than for Data Set 1, due mainly to lower amount of heat contained in the smaller diameter cone. It is thought that while the empirical method proposed a single equation, each cone would have different parameters.

In all cases the thermal conductivity changes over the soil depth profile. This is consistent with changes in density (generally increasing, due to increasing overburden stresses), and with a variation due to soil material changes. In particular, CPTU interpretation shows clay near surface and sand at greater depths for locations 1, 2 and 4, and in location 3 a small clay layer was observed at 13 m giving a lower thermal conductivity.

5 INFLUENCE OF SAND DENSITY

In comparison to a needle probe, a cone penetrometer has a large diameter, therefore increased soil disturbance applies. The rate of penetrometer insertion is typically 20 mm/s (ISO, 2012), which, in fine grained soils, results in undrained deformations, i.e. largely without volume change. However, for sandy soils, drained conditions may apply. It is noted that heat moves through both the fluid and solid parts of soil and therefore the structure is of a lesser importance.

The zone of influence of a CPT in sandy soil depends on particle size distribution, in-situ stress conditions and drainage. It has been estimated to be up to 8 cone diameters horizontally (Mel'nikov & Boldyrev, 2015). Even in dry sand volumetric strains are small, with both contractive and expansive strains being less than 2% outside ~0.2 cone diameters (Mel'nikov & Boldyrev, 2015).

The thermal zone of influence (Figure 5) is approximately 2 cone diameters within the part of the test needed to calculate the thermal conductivity.

Figure 11 presents example results of laboratory tests undertaken to investigate the sand density aspect. The thermal conductivity tests were

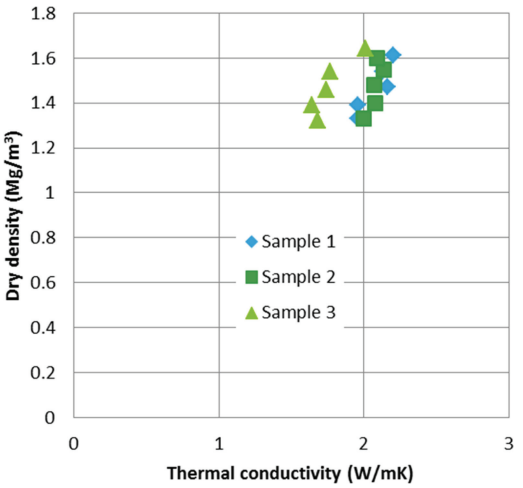

Figure 11. Thermal conductivity against density for 3 samples.

performed using a KD2 Pro Thermal Properties Analyzer (Decagon Devices, Inc.) with a TR-1 thermal needle probe (100 mm length, 2.4 mm diameter), according to ASTM (2014). The samples had dry densities from ~1.3 to ~1.6 Mg/m^3, so representing about a ± 10% volumetric strain from the mean. The initially moist samples were flooded with water and subjected to increasing densification by means of a vibrating table. The thermal conductivities for each sample have an average range of 0.24 W/mK and therefore for a 2% volumetric strain the approximate difference would be approximately 0.02 W/mK, which is within the measurement error.

While using a cone penetrometer to take in-situ measurements may have a limited error due to density changes, this is thought to be significantly less than that of taking samples, which were found, in general, to exhibit slightly lower thermal conductivity values than the field tests, attributed mainly to total stress relief upon sampling and de-saturation.

6 CONCLUSIONS

This paper compares two interpretation methods for deriving in-situ thermal conductivity of soil from a cone penetrometer equipped with a temperature sensor. The test method (T-CPT) relies on a temperature rise in the steel of the penetrometer during a cone penetration test and subsequent measurement of temperature decay during a pause in penetration. The test equipment is more robust than needle probe type tests and therefore allows thermal conductivity to be measured at depth, without tools being swapped. The physics-based method is shown to reliably measure the thermal conductivity over a wide range of conditions and requires only spreadsheet-type analysis to be undertaken. A method of predicting the initial in-situ temperature is also shown allowing the test to be undertaken in a significantly reduced time.

REFERENCES

Akrouch, G.A., Briaud, J.-L., Sanchez, M. & Yilmaz, R. 2016. Thermal cone test to determine soil thermal properties, *Journal of Geotechnical and Geoenvironmental Engineering*, 142(3): 04015085.

ASTM 2014. D 5334-14 *Standard test method for determination of thermal conductivity of soil and soft rock by thermal needle probe procedure.* ASTM.

Carslaw, H.S. & Jaeger, J.C. 1959. *Conduction of heat in solids*, 2nd Edition, Oxford University Press, pp. 509.

ISO 2012. *EN ISO 22476-1:2012 Geotechnical investigation and testing. Field testing. Electrical cone and piezocone penetration test.* ISO.

Mel'nikov, A.V. & Boldyrev, G.G. 2015. Deformation Pattern of Sand Subject to Static Penetration, *Soil Mechanics and Foundation Engineering*, 51(6): 292–298.

Vardon, P.J., Baltoukas, D. & Peuchen, J. 2017. Interpreting and validating the Thermal Cone Penetration Test (T-CPT). *Submitted to Géotechnique*.

Taylor & Francis
Taylor & Francis Group
http://taylorandfrancis.com

Cone Penetration Testing 2018 – Hicks, Pisanò & Peuchen (Eds)
© 2018 Delft University of Technology, The Netherlands, ISBN 978-1-138-58449-5

Development of numerical method for pile design to EC7 using CPT results

J.O. Vasconcelos, J. O'Donovan & P. Doherty
Gavin and Doherty Geosolutions Ltd., Dublin, Ireland

S. Donohue
University College Dublin, Dublin, Ireland

ABSTRACT: In the UK and Ireland bearing pile design is generally based on the "design by calculation" methodology where soil strength parameters are obtained from in-situ data or through empirical correlation with ground test results. Direct ground test results from Cone Penetration Tests (CPT's) are seldom used to complete ultimate limit state designs to satisfy EC7. This paper discusses the development of a numerical method where direct results from CPTs are used to design bearing piles. The method was verified through a case study where a large amount of CPT data was available. The resulting pile designs were compared to the more commonly used "design by calculation" approach and "design by pile load test". The numerical method was incorporated into the AllPile (Axially and Laterally Loaded Pile) software which supports single pile design according to EC7.

1 INTRODUCTION

1.1 *Pile design to EC7*

Eurocode 7 offers a number of methodologies for completing pile design to satisfy Ultimate Limit State (ULS) requirements. Typically, the Serviceability Limit State (SLS) requirements for pile design are satisfied once ULS requirements are met. This paper does not consider SLS design in detail and focusses on ULS design.

The three ULS design verification methods offered by EC 7 are: design by calculation, design by load test and design by ground test. "Design by calculation" is satisfied by determining characteristic parameters for the strata encountered. These parameters are typically arrived at through correlation with the results of field tests and through direct measurement using laboratory testing. The characteristic parameters are used to calculate characteristic pile base and shaft resistance. Partial factors are applied to these characteristic resistance values to determine design resistance values. The ULS design is verified provided that these resistance values are greater than the applied design loads. One of the drawbacks of this method is that the correlation between field test results and geotechnical parameters is typically conservative and this adds an implicit factor of safety to the design on top of the stated partial factors used in the calculation. The methods of calculating resistance from characteristic parameters rely on a number of empirical factors that will also contain an implicit conservatism in their determination. This conservatism is then transferred to the resistance calculation reducing the efficiency of the design.

Design by load test is satisfied by completing static load tests on piles and back calculating pile resistance from the stress-strain curves generated during the test. Correlation factors are applied to the measured pile resistance. These correlation factors decrease as the number of tests carried out increase allowing for more efficient designs to be obtained provided a sufficient number of tests is carried out. The advantage of this method is that the pile resistance is directly measured in the form of the stress-strain relationship for the pile removing implicit conservatism that can develop in the design by calculation method. The disadvantage of this method is that pile load tests are typically expensive to carry out and to achieve the full benefit of this method the pile testing is ideally done prior to the installation of working piles on sacrificial preliminary piles. This further increases the cost associated with this method making it an unattractive option for most clients.

Design by ground test is a design method that offers the efficiency advantages of the design by load test without the large additional cost of the preliminary pile load tests. This method directly correlates the results of field tests with pile resistance. This essentially skips a stage in the design by calculation method where the characteristic

parameters are first calculated before pile resistance. Skipping this stage removes the potential for an implicit conservatism to be introduced to the design. A partial factor is applied to the correlated resistances based on the number of field tests completed. This factor reduces as the number of tests completed increases. This method utilises field tests that are likely to be completed as part of a ground investigation prior to the design process and so no additional cost is incurred. The field tests that are typically used for this method are the Standard Penetration Test (SPT) and Cone Penetration Test (CPT). The correlations between CPT field tests and pile resistance is discussed in the next section.

1.2 *Pile capacity using CPT results*

Previous Research (Robertson & Cabal, 2010; Briaud and Tucker, 1988; Tand and Funegard, 1989) has demonstrated that CPT methods generally give less conservative predictions of axial pile capacity compared to other methods. This has been attributed to the continuous profile of soil response that the CPT provides. Generally, CPT methods use correlation factors applied to measured CPT values. The correlation factors consider a combination of influences such as scale effects, rate of loading effects, difference of insertion techniques, position of the CPT friction sleeve and differences in horizontal soil displacements.

The LCPC Method proposed by Bustamante & Gianeselli (1982) provides guidance that is relevant to many different pile installation methods and provides good estimates of the axial capacity of single piles. The method is empirical and is based upon pile load tests. The pile unit end bearing, q_b, is calculated from the calculated equivalent average cone resistance, q_c, multiplied by an end bearing coefficient, k_c, that depends on pile type and ground conditions. The pile unit side friction, q_s, is calculated from measured q_c values divided by a friction coefficient, α_{LCPC}, which is also dependent on ground conditions and pile type. The advantage of this method is that only the measured cone resistance, q_c, is used for the calculation of both side friction and pile end bearing resistance.

The methodology recommended by EC 7 follows the rationale presented in the LCPC method. The correlations between pile resistance and field test values are based solely upon the cone penetration resistance, q_c. The unit base resistance, q_b, and unit shaft resistance, q_s, are obtained through correlations based on the upon the q_c values and the permitted settlement of the piles. EC7 recommended values of q_b and q_s are given in Table 1 and 2 respectively.

For ULS design, the values correlated at the ultimate settlement of the pile head, s_g, should be used. The values of q_b and q_s are multiplied by the pile base and shaft area respectively to obtain the resistance values as a force.

Table 1. Relationship between unit base resistance, pb, and average cone penetration resistance, qc, as a function of normalised settlement proposed by EC7.

Normalised settlement s/D_s; s/D_b	Unit base resistance q_b, in MPa, at average cone penetration resistance qc (CPT) in MPa.			
	$q_c = 10$	$q_c = 15$	$q_c = 20$	$q_c = 25$
0.02	0.7	1.05	1.40	1.75
0.03	0.9	1.35	1.80	2.25
0.10 (= s_g)	2.00	3.00	3.50	4.00

Note: Intermediate values may be interpolated linearly.
In the case of cast in-situ piles with pile base enlargement, the values shall be multiplied by 0.75.
s is the normalised pile head settlement,
D_s is the diameter of the pile shaft,
D_b is the diameter of the pile base,
s_g is the ultimate settlement of the pile head.

Table 2. Relationship between unit shaft resistance, q_s, and average cone penetration resistance, q_c, proposed by EC7.

Average cone penetration resistance q_c (CPT) in MPa	Unit shaft resistance q_s in MPa
0	0
5	0.040
10	0.080
≥15	0.120

Note: Intermediate values may be interpolated linearly.

The values provided above are for coarse granular material and may vary depending on the relevant country's National Annex. Unit base and shaft resistance can also be obtained by multiplying the q_c values by an empirical coefficient c_s and $c_{b,0.1}$ respectively which can vary depending of the pile type and the soil type (Equation 1 and 2) (BS8004:2015).

$$q_{b,0.1} = c_{b,0.1} \times q_{c,b} \tag{1}$$

$$q_{s,j} = c_{s,j} \times q_{c,j} \tag{2}$$

where $q_{c,j}$ is the measured cone resistance in layer j and $q_{c,b}$ is the average cone resistance measured over a distance ±1.5 pile diameters below the pile base.

BS8004:2015 recommends values of empirical coefficients that are provided in Table 3 which are correlated for an ultimate resistance at a settlement equal to 10% of pile diameter, s_g.

Table 3. Recommended values for empirical coefficients c_s and $c_{b,0.1}$ from BS8004:2015.

	c_s			$c_{b,0.1}$		
Soil type	High displacement piles	Low displacement piles	Replacement piles	High displacement	Low displacement	Replacement piles
Sand	0.0004–0.009	0.0015–0.004	0.003–0.006	0.3–0.5	0.15–0.25	0.15–0.25
Silt	0.006–0.01		0.003–0.006	Data not available		
Medium to high strength/ over consolidated Clay	0.007–0.017		0.008–0.012	0.8–1.3	0.4–0.65	0.34–0.66
Low strength/ normally consolidated to lightly over-consolidated Clay	0.007–0.017		0.008–0.012	0.9–1.0		0.9–1.0

The ultimate resistance is calculated for each CPT test and is used to calculate a characteristic resistance that is a function of the number of tests that were carried out. The characteristic resistance, R_{ck}, is selected as the lowest of either the minimum resistance calculated, $R_{cal,min}$, or mean resistance calculated, $R_{cal,mea}$, from the CPT method (Equation 3).

$$R_{ck} = min\left(\frac{R_{cal,mean}}{\xi_3}, \frac{R_{cal,min}}{\xi_4}\right) \tag{3}$$

The values of ξ_3 and ξ_4 depend on the number of CPT's that were completed and reduce as the number of tests increases. They also depend on the relevant country's National Annex. For example, if one CPT was completed in the UK, $\xi_3 = \xi_4 = 1.4$. These correlation values may be divided by 1.1 where the pile loads can be redistributed i.e. the structure has sufficient stiffness and strength to transfer loads from "weak" to "strong" piles. Following determination of the characteristic resistance, the design resistance, R_d, is determined using the relevant partial factors, γ_{total}, in the National Annexes to EC7 (Equation 4).

$$R_d = \frac{R_{ck}}{\gamma_{total}} \tag{4}$$

2 ALLPILE SOFTWARE

2.1 *Numerical model*

A drawback to the design by ground test methodology is that it is time-consuming to iterate when a large number of CPT tests are available. A numerical method was developed following the advice of EC7 and relevant standards including British Standards and the UK and Irish National annexes and incorporated in the ALLPile (Axially and Laterally Loaded Pile) software.

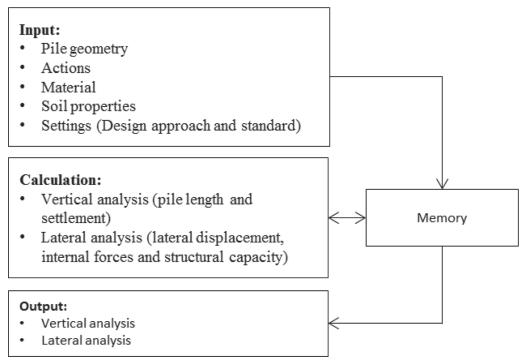

Figure 1. AllPile framework.

The software enables the rapid re-calculation of the pile capacity for different load combinations.

The software is used to complete pile designs to the three methodologies in EC7. Figure 1 illustrates the ALLPile framework. A ground model is entered into the software along with characteristic properties to complete pile design by calculation. The derivation of the characteristic properties is left to the user. The results from static pile load tests can be entered into the software to complete the design by load test methodology. In addition, CPT results may be entered into the programme to complete design by ground test. The pile design can be completed by any number of these methods depending on the availability of information.

2.2 *Algorithm framework*

The design by ground test algorithm (Figure 2) is discussed in more detail in this section. This method relies on field test results over the full pile length and to 1.5 times the pile diameter below the base. Only CPT's that have reached this depth should be included. To estimate this depth, it is recommended that an initial pile design is completed

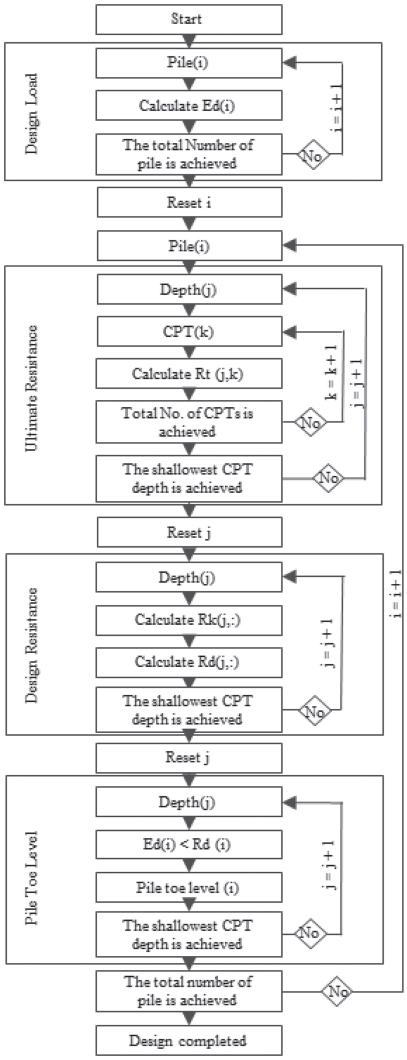

Figure 2. Algorithm framework as flowchart.

using characteristic properties. The depth from this calculation is used to determine which CPT's are included to design by ground test. The first stage is to discount any CPT's that are too shallow.

The ALLPile algorithm increments depth until pile resistance exceeds the applied load. At each depth interval the pile base and shaft resistance are calculated for each CPT using the results of cone resistance and the empirical correlations between that and pile resistance. This procedure is completed for each depth interval until the shallowest CPT depth is reached. The total resistance at each depth interval and from each CPT is used to create a two-dimensional array. The characteristic total pile resistance is determined at each depth interval using Equation 3 and design total pile resistance is determined using Equation 4.

Dead loads, G_k, and live loads, Q_k, are combined applying the correspondent action partial factors (e.g. γ_G, the action partial factor of dead loads and γ_Q, the action partial factor of live loads) as recommended by EC7 (Equation 5). Design load, E_d, and design resistance, R_d, are compared at each interval of depth. Pile toe level is achieved when the applied load is lower than the design resistance. The flowchart in Figure 2 summarises the calculation steps.

$$E_d = G_k \quad \gamma_G + Q_k \quad \gamma_Q \tag{5}$$

3 CASE STUDY

The model was verified using a number of case studies where several CPTs were completed. One of those case studies is presented here. The piles were designed by applying EC7 design by ground test and coefficients suggested by BS8004:2015. The accuracy of the results was evaluated by comparison with results found by the design by calculation and design by pile load test methodology. The case study is located in the Belfast Harbour area of Belfast city. The Belfast Harbour region is underlain by relatively thick deposits of Belfast Sleech.

The sleech is a Quaternary deposit that was deposited in post Glacial times. It is described as a soft, sensitive estuarine clay in Gregory & Bell (1991) and was formed by deposition from the River Lagan. The sleech is lightly over consolidated due to variations in groundwater level and secondary compression. Due to the soft nature of the sleech and low cobble content it is well suited for investigation using CPT technique. The CPT results allow for a more accurate and less conservative design to be completed using the design by ground test method as cone penetration resistance is obtained over the full pile length. In addition, due to the risk associated with the sleech deposit, it is more common to test piles in the Belfast Harbour area.

3.1 *Case study: bearing piles driven to fine to medium sand material*

The case study comprises the analysis of a 380 mm diameter driven pile. Eight CPTs were completed on site to depths of between 14 and 16 m below existing ground level (bgl), Figure 3. Piles were driven to a depth of 14.1 m below existing ground level (bgl).

Ground investigation carried out on site shows that the stratigraphy of the area comprised between 1.2 m and 3.5 m of Made Ground or Fill material. It consisted of concrete, hardcore fill and medium dense black silty sand, fine to medium gravel with

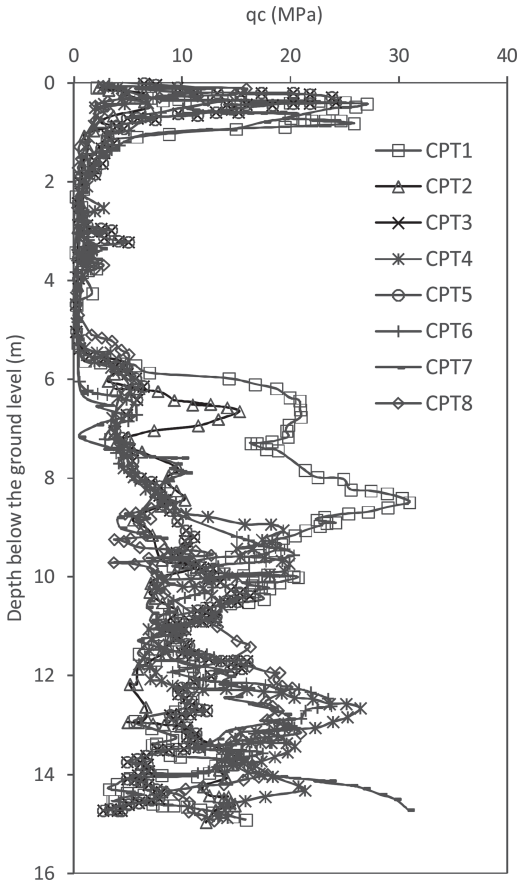

Figure 3. CPT's used in the ground test design approach for the case study.

bricks and concrete and very soft black sandy silty organic clay. Belfast Sleech was encountered beneath the Made Ground with a thickness that ranged from 2.1 m to 4.8 m. The sleech consisted of very soft pale bluish grey slightly sandy silty organic clay and medium dense grey silty fine to medium sand. Fluvial Glacial deposits comprised loose to medium dense grey to organic brown silty fine to medium sand containing occasional thin layers of reddish brown silty clay. These deposits occurred from 6.25 m to 20.0 m below existing ground level. Glacial Till deposits were encountered below the sands and consisted of stiff to very stiff reddish brown slightly sandy silty clay containing occasional lenses of silty fine to medium sand. The lower Glacial Till deposits comprised very stiff gravelly sandy silty clay with smooth sub-rounded cobbles and boulders. These deposits were present from 18 m below existing ground level to a maximum depth of 36.5 m below existing ground level (bgl). The c_s and $c_{b,0.1}$ factor used for the analysis are summarized in Table 4. The resistance was calculated for intervals of depth of 0.1 m.

The calculation was carried out applying partial factors for resistance of driven piles with verification of SLS as per the UK National Annex to EC7. Partial factors of total resistance equal to 1 and 1.5, for DA1C1 and DA1C2 respectively, were applied.

Values of $\xi_3 = 1.33$ and $\xi_4 = 1.2$ for 8 CPTs were adopted.

The proposed toe level is 14.1 m below existing ground level (bgl). The design resistance was calculated as 1048 kN and 699 kN for combination DA1C1 and DA1C2 respectively.

Three working pile load tests were completed on site (Figure 4). The pile resistance was estimated by extrapolating the load *vs* settlement curve. The pile ultimate resistance is assumed to occur when the pile settlement reached 10% of pile diameter. The design resistances calculated for DA1C1 and DA1C2 are summarized in Table 5.

"Design by calculation" was also completed using the beta method. A value of N_q was determined to be 43.50 at the pile base from the SPT and CPT results.

The resulting characteristic base resistance was calculated to be 418 kN. A value of $\beta = 1.0$ was used for the shaft resistance calculation in the Fluvial Glacial deposits while the contribution of the Made Ground and Belfast Sleech was ignored. The characteristic shaft resistance was 539 kN.

Table 4. Empirical coefficients, c_s and $c_{b,0.1}$, used for the strata in the case study.

Stratum	c_s	$c_{b,0.1}$
Made Ground	0.002	0.3
Belfast Sleech	0.01	0.9
Fluvial Glacial	0.009	0.5

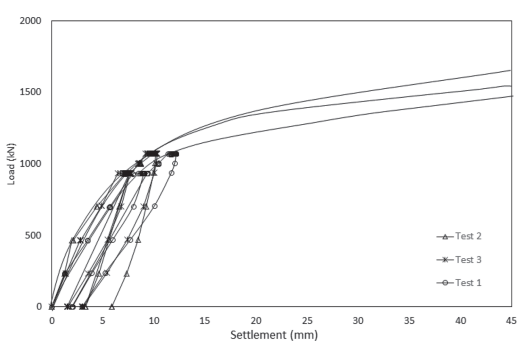

Figure 4. Static load test results from working pile tests completed during the case study.

Table 5. Total design resistance according to EC7 for the case study.

Methodology	Combination	Design resistance, (R_d kN)
Design by ground test	DA1C1	1048
	DA1C2	699
Design by pile load test	DA1C1	1057
	DA1C2	705
Design by calculation	DA1C1	957
	DA1C2	693

The design resistances calculated for DA1C1 and DA1C2 are summarized in Table 5.

4 DISCUSSION OF RESULTS

A case study was presented where CPT field tests and pile load tests were available. Piles were designed using the calculation, pile load test and ground test approaches. A number of developments are made to the design by ground test framework to enable a numerical implementation of the methodology proposed in EC7. The software enabled the end user to switch between all three EC7 design methodologies allowing the end user to easily compare the results from one design methodology to another.

The case study showed that the resulting design using ground test results was less conservative than the more commonly used design by calculation. The least conservative design was obtained using design by load test, which is to be expected as it is using the pile resistance as a direct input.

An advantage of completing design by ground test is that the CPT results are directly correlated with pile resistance using empirical factors. In agreement with previous research this method was found to be less conservative than design by calculation where characteristic properties must be inferred from the field tests before pile resistance is calculated. A further advantage is that both minimum and mean pile resistance from the available CPT results is used in the determination of characteristic resistance, which increases confidence that variability across the site has been accounted for. Finally, the ξ factors used to reduce both the mean and minimum total resistance are reduced as the number of available tests increases. This provides incentive to complete a suite of CPT results to achieve a less conservative design. It is more likely that variation across the site will be accounted for due to this.

If there was a particular portion of the site where early refusal of CPT's consistently occurred, then it would not be possible to complete design by ground test in this location and design by calculation or design by load test would have to be used.

5 CONCLUSIONS

The recommendations in EC7 for completing single pile design by ground test were interpreted to enable a software algorithm to be written in order to carry out the design calculations. The software allows piles to be designed using direct ground test information efficiently and for a number of different load cases. The software can also complete pile design by calculation and by load test allowing direct comparison. The algorithm framework is presented as implemented in the pile design software, ALLPile (Axially and Laterally Loaded Pile).

A case study is outlined where pile designs completed by all three methodologies could be compared. The case study is located in the Belfast Harbour area where the presence of Belfast Sleech means that CPT's and pile load tests are commonly included in design specifications. The results are discussed as well as their implications for each test methodology.

REFERENCES

Briaud, J.L. and Tucker, L.M., 1988. Measured and predicted axial response of 98 piles. Journal of Geotechnical Engineering, 114(9), pp.984–1001.

BS 8004:2015 Code of practice for foundations.

BS EN 1997–1:2004+A1:2013 Eurocode 7. Geotechnical design. General rules.

Bustamante, M. and Gianeselli, L., 1982, May. Pile bearing capacity prediction by means of static penetrometer CPT. In Proceedings of the 2-nd European Symposium on Penetration Testing (pp. 493–500).

Gregory, B.J. and Bell, A.L., 1991. Geotechnical properties of Quaternary deposits in the Belfast area. Geological Society, London, Engineering Geology Special Publications, 7(1), pp.219–228.

NA+A1:2014 to BS EN 1997–1:2004+A1:2013. UK National Annex to Eurocode 7. Geotechnical design. General rules.

Robertson, P.K. and Cabal, K.L., 2010. Guide to cone penetration testing for geotechnical engineering. Gregg Drilling and Testing Inc., USA, pp.6–15.

Tand, K.E. and Funegard, E.G., 1989. Pile capacity in stiff clays—CPT method. In Proceedings of Twelfth International Conference on Soil Mechanics and Foundation Engineering. Rio de Janeiro (Vol. 1, pp. 349–352).

Cone Penetration Testing 2018 – Hicks, Pisanò & Peuchen (Eds)
© 2018 Delft University of Technology, The Netherlands, *ISBN 978-1-138-58449-5*

Prehistoric landscape mapping along the Scheldt by camera- and conductivity CPT-E

J. Verhegge & Ph. Crombé
Department of Aarchaeology-Prehistory Research Unit, Ghent University, Gent, Belgium

M. van den Wijngaert
Geosonda Environment nv, Sint-Denijs-Westrem, Belgium

ABSTRACT: Over the past decade, paleolandscape reconstruction was introduced as part of a preventive archaeological evaluation strategy along the Scheldt river, due to the unexpected discovery of well-preserved prehistoric landscapes and sites during construction works in the Antwerp harbor area. Hereby, CPT is an important tool in combination with coring and/or near surface geophysical survey. Applications of CPT range from desktop studies, which determine evaluation strategies, to actual paleolandscape mapping by sedimentological data interpretation. CPT-Es (with added camera and/or electrical conductivity sensors) calibrate and validate geophysical subsurface modelling and soil behavior types are interpreted. Particularly, (electrical conductivity) CPT-C disentangles sedimentological and hydrological variations in electrical conductivity values. On the other hand, camera CPT improves differentiation of organic rich sediments and detection of thin organic soil horizons within homogenous (cover)sands. The usability of CPT is illustrated through recent prehistoric landscape evaluation studies along the Scheldt river.

1 INTRODUCTION

1.1 *Archaeological background*

Over the past decades, well-preserved Late Glacial to Middle Holocene paleolandscapes and prehistoric archaeological sites dating back to the Final Paleolithic to Early Neolithic period have been discovered during harbor infrastructure works to expand the port of Antwerp in the Waasland Scheldt polder region (Crombé, 2005). These remnants of former hunter-gatherer and early farmer-herder habitation were encountered by accident and triggered prompt rescue excavations, which were uncomfortable to both archaeologists and developers. The unexpected nature of these finds was partially caused by the covering sediment sequence, which both protects the sites and impedes detection using traditional archaeological prospection methods, such as test pitting or remote sensing (De Clercq et al., 2012).

Therefore, buried paleolandscape mapping strategies have been developed to reduce costs for subsequent archaeological site detection *sensu stricto* through intensive core sampling (Crombé and Verhegge, 2015). At first, paleolandscape mapping relied primarily on coring (Bats, 2007, De Clercq et al., 2011). However, due to the labor intensity of deep manual coring and the financial burden of mechanical coring, recent research has focused on exploring alternative techniques, such as CPT (Missiaen et al., 2015), in combination with electrical resistance imaging and electromagnetic induction survey (Verhegge et al., 2016a).

1.2 *Geological background*

The prehistoric sites were mainly found on Weichselian Late Pleniglacial and Late Glacial cover sand ridges, river dunes, natural levees and point bars within the fossil Pleistocene floodplain and were gradually buried due to ground water and sea level rise (Figure 1) (Crombé et al., 2011, Crombé et al., 2015).

As such, a primary aim of the prehistoric landscape evaluation is a reconstruction of the topography of the top of the Pleistocene sedimentary sequence. Secondly, it has to be determined to what degree later sedimentation has protected this paleosurface or if erosion has destroyed it as well as the prehistoric sites this paleosurface might contain. Due to sea level rise and surfacing local ground water levels, depressions in the landscape were first covered by Late Atlantic alder carr peat. Peat development was interrupted by a short period of organic rich and clayey supratidal freshwater floodplain sedimentation, after which a sedge fen and birch carr formed. Further acidification resulted in an oligotrophic peat layer (Deforce et al., 2014). From the middle ages onwards, the increased influ-

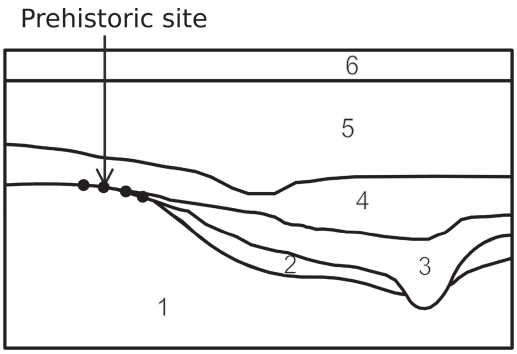

Figure 1. Schematic section of the regional lithostratigraphy and stratigraphic position of Early Mesolithic to Early Neolithic sites in the Waasland Scheldt polders. 1. Weichselian (cover) sand 2. Basal peat layer 3. Organic rich clay intercalation 4. Upper peat layer 5. Clayey to sandy estuarine sediments 6. Top soil.

ence of the sea caused erosion of the prehistoric landscape and covered it with varying sandy to clayey estuarine floodplain sediments as successive embankment attempts gradually claimed the land from the sea (Missiaen et al., 2016 and references therein).

2 METHODOLOGY

2.1 *Lithological and stratigraphic interpretation of CPT-E*

Although CPTs are primarily developed for geotechnical purposes (Robertson and Cabal, 2012), the correlation of the recorded soil mechanical data to the sedimentological variables, such as grain size, makes them suitable for lithostratigraphic mapping of soft alluvial plain deposits (e.g. Amorosi and Marchi, 1999). Particularly electric (piezo-)CPTs allow an easy identification of peat layers by the greater friction ratio- (R_f), often >5% and negative pore pressure values (Lunne et al., 1997). Due to the high vertical data density, even thin peat layers down to about 20 cm are mapped correctly (Lunne et al., 1997). However, the added value of pore pressure data is rather limited in our study region (Missiaen et al., 2015) in contrast to studies in surfacing peat bogs (Long and Boylan, 2012, Long, 2005). Therefore, only CPT-Es are employed and piezocones are not used in this study.

Rapid interpretation of the CPT data in desktop studies is done through comparison with lithostratigraphic knowledge of the region. Furthermore, soil behavior types (SBT) are determined by a Robertson (1990) chart adapted by Fugro GeoServices to the subsoils of the Netherlands with consolidated Holocene peats using an approximated normalization (Koster, 2016). High quality cores (e.g. Begemann core) are used to validate these interpretations and to adjust the SBT chart to the local situation, if necessary. The cores are also used to determine the organic soil types more accurately or to assess if paleosols are present on top of or within the sediments below. Further subsurface modeling and visualization are facilitated through a three dimensional geographic information system using ESRI ArcGIS and Rockware Rockworks software.

2.2 *CPT(-C) and near surface geophysical paleolandscape mapping*

Electrical resistivity imaging (ERI)- and electromagnetic induction (EMI) survey provides a horizontally dense dataset in addition to the vertically dense CPT data. These near surface geophysical data are interpreted, calibrated or validated using two possible CPT applications. On the one hand, regular electric CPTs provide depths of lithological data of layers and depths of their transitions. On the other hand, electrical conductivity (EC) sensors are added to the conus and continuous EC is recorded continuously during penetration to determine if CPT-E and EC variations correlate.

2.3 *Camera-CPT*

A first test was performed with a camera CPT recording images every 1.5 cm during penetration. Subsequently the images were processed to correct the illumination and collated into an image log. This test was aimed as distinguishing similar soil behavior types with differing lithologies by their color. Furthermore, it was aimed at mapping small remnants of eroded or reworked peat layers and organic rich soil horizons with a thickness below the SBT identification limit of regular CPT-E.

2.4 *Study area*

Three possible uses of CPT in prehistoric paleolandscape mapping will be illustrated based on paleolandscape reconstruction results (Figure 2) from the sites of 'Prosperpolder Zuid' (PPZ) (51°19'15"N 4°13'08"E) (Saey et al., 2016) and 'Doelpolder Noord' (DPN) (51°19'57"N 4°14'58"E) (Verhegge et al., 2016a, Missiaen et al., 2015). The adjacent sites are located on the left bank of the Scheldt river, between the port of Antwerp and the national border (Figure 2-inset map).

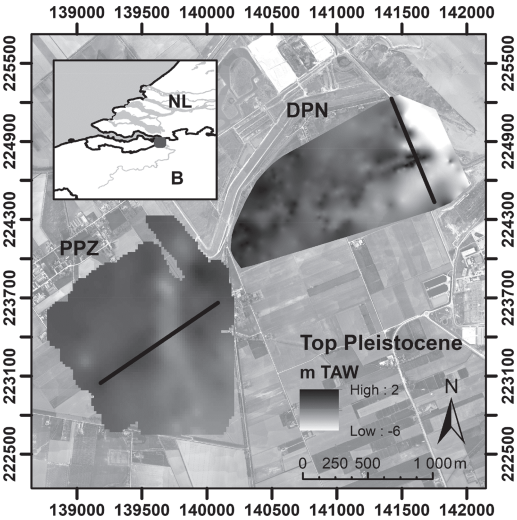

Figure 2. Map of the study areas of PPZ and DPN with an interpolated elevation model of the top of the Pleistocene sediment sequence and locations of the transects on Figure 4 Figure 2and Figure 5. Inset map: the location of the study region close to the border between Belgium and The Netherlands. (Belgian Lambert '72 coordinate system, Belgian reference level-Tweede Algemene Waterpassing).

3 RESULTS

3.1 *CPT in archaeological desktop studies*

Often, CPTs are available from geotechnical studies or from national repositories by the time an archaeological evaluation of a planned construction site is started. During a desk based assessment of the archaeological potential of a study area, CPTs are rarely considered as helpful data. Even if the number of CPTs or their depth is insufficient to map the paleolandscape topography, they provide valuable information to develop a mapping strategy.

A publicly available CPT at PPZ (https://www.dov.vlaanderen.be/data/sondering/2006–046736) indicated a possible burial depth of the Pleistocene sands of 4 and possibly up to 7 m, which excluded efficient manual coring. Furthermore, the presence of clays and shallow groundwater implies the use of electrical near surface geophysical methods instead of ground penetrating radar. A relatively thick peat layer suggests the use of CPT-E is possible but the presence of small and thin variations (e.g. Rf peak at 7 m) warns that high quality cores are necessary for CPT interpretation.

3.2 *CPT as primary paleolandscape mapping tool*

After the desk top study, extensive coring was considered not cost-efficient at PPZ. Therefore, CPT-E was used as principal survey technique in combination with EMI. Figure 3 illustrates that qc and Rf accurately map the main lithostratigraphic variations. However, the SBT interpretation is not able to differentiate between the peat layer and organic rich clayey tidal mudflat sediments.

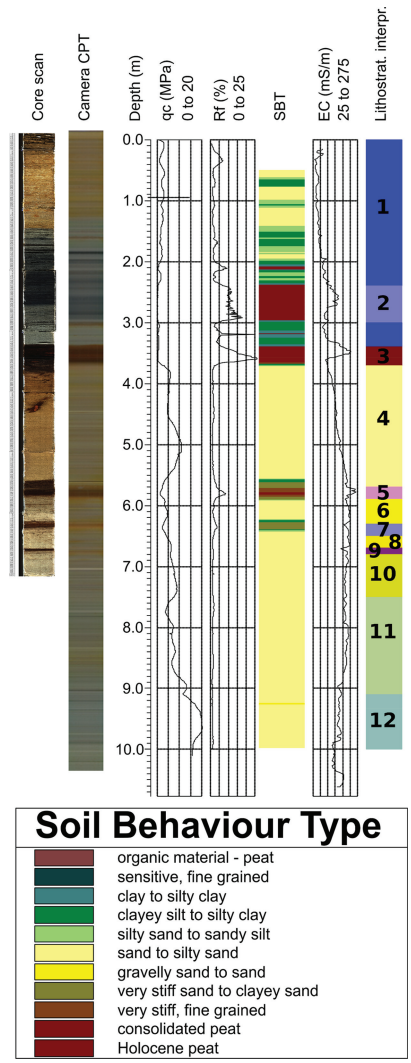

Figure 3. From left to right: Begemann core scan, Camera CPT, CPT-E (qc, Rf, SBT), EC log, Lithostratigraphic interpretation (1. Clayey to sandy estuarine sediments 2. Organic rich clayey tidal mudflat sediments 3. Peat layer 4. Younger Dryas cover sand 5. Upper Allerød soil horizon 6. Upper Allerød cover sand 7. Middle Allerød soil horizon 8. Lower Allerød cover sand 9. Lower Allerød soil horizon 10. Late Pleniglacial/Older Dryas cover sand 11. Weichselian fluvial sediments 12 (Reworked) Tertiary sand with shells.

Furthermore, thin organic horizons are identified as very stiff sand to clayey sand and can not be correctly interpreted without validation through coring (Figure 3-left).

Figure 4 shows that transects (or grids) of interpreted CPTs were capable of mapping the post-Pleistocene topography as well as the varying presence of its peat cover. Indeed, even a series of organic Allerød soil horizons within homogeneous sandy sediments, identified in cores, could be mapped through the dropping qc.

The camera CPT log has decreased the interpretative reliance on coring as it differentiated between consolidated peat (Figure 3, layer 3) and unconsolidated and highly organic fine grained saltmarsh deposits (Figure 3, layer 2), which often contain pieces of reworked peat. Secondly, even the relatively thin remnants of largely eroded peat layers can be mapped (Figure 4, layer 3). Furthermore, the camera CPT log increased the capability to map more subtle organic rich sandy Allerød horizons, which do not show qc or Rf variations (e.g. Figure 3, layer 9). In particular, the upper Allerød soil horizon (Figure 4, layer 5) could not be differentiated at the right side of the transect. This horizon consists of leached organic rich sand with a darker color in the cores. Therefore, it could be detected using a camera CPT log.

3.3 *CPT and near surface geophysical paleolandscape mapping*

Figure 5 shows ERI and CPT data at DPN and illustrates that the Rf and EC both increase due to the peat layer. However, the EC also increases above and below the peat layer at the end of the transect, located closer to the dike which embanks the Scheldt estuary. Here, a brackish groundwater lens intrudes into the subsoil via the peat layer.

The high EC due to this saltwater intrusion also renders the low induction number approximation to derive apparent $EC_{(a)}$ from the quadrature phase signal of the receiving coil invalid (McNeill, 1980). As such, the EC_a values above about 100 mS/m in Figure 6 deviate from the actual EC, in addition to not correlating to the prehistoric paleolandscape variability (Verhegge et al., 2016a). Nevertheless, the brackish water zone is accurately

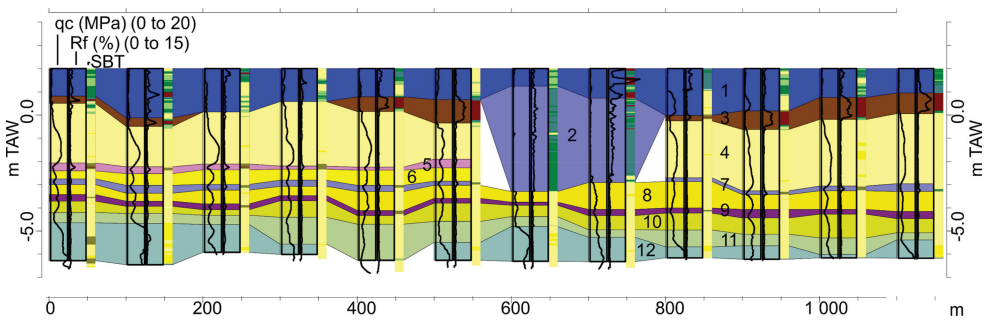

Figure 4. Transect at PPZ with interpreted CPT-Es (qc, Rf, SBT with legend in Figure 3) and interpreted lithostratigraphy Figure 3) (Belgian reference level-Tweede Algemene Waterpassing).

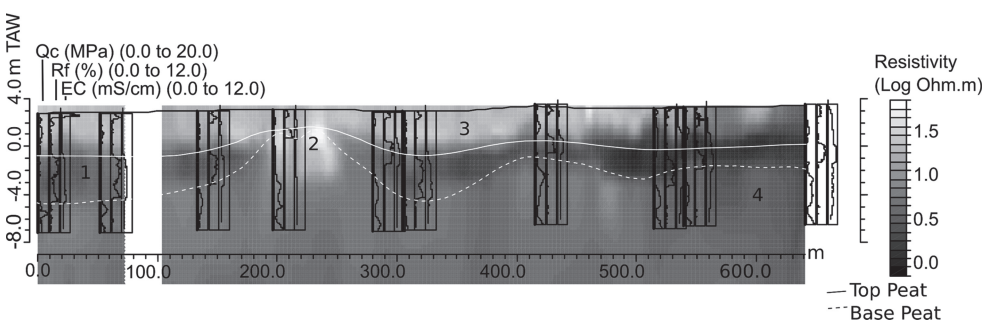

Figure 5. CPT-C transect and electrical resistivity section at DPN, which was inverted using a CPT derived forward model for the top and base of the peat layer. 1. Middle Holocene peat in depression 2. Late Weichselian dune 3. (Post-) Medieval estuarine floodplain sediments 4. Increased EC outside peat layer, due to brackish groundwater lens from the Scheldt river (after Verhegge et al., 2016a figure 2) (Belgian reference level-Tweede Algemene Waterpassing.

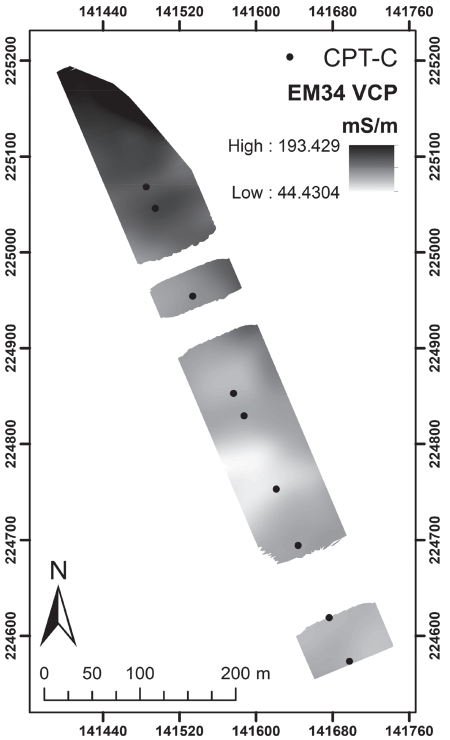

Figure 6. Interpolated EM34 VCP survey data with locations of CPT-Cs in Figure 5 (after Verhegge et al., 2016a Figure 4a) (Belgian Lambert '72 coordinate system).

delineated by the EMI data. Therefore, CPTs are preferred to ERI or EMI for paleolandscape mapping in brackish or saltwater environments (Verhegge et al., 2016a).

However, if no brackish groundwater is present, a geophysical modelling approach using EMI survey with multiple coil pairs and CPTs as calibration data has proven successful to reconstruct the basis of the Holocene peat layer (Saey et al., 2016, Verhegge et al., 2016b).

The EC log on Figure 3 shows that the upper Allerød peaty soil horizon causes a small EC peak. However, the middle and lower Allerød soil horizons consist of organic rich sand and cause a small EC drop. Unfortunately, these variations are too small for near surface geophysical detection using ERI or EMI.

4 DISCUSSION AND CONCLUSION

This paper has demonstrated the value of CPT for archaeological prospection of prehistoric landscapes buried below peat layers and embanked estuarine floodplain sediments. As such, CPT has started to be included in archaeological practice in the study region.

The conversion of CPT-E data to SBTs is particularly useful for ease of communication with archaeologists but possible errors have to be checked using coring. The visualization of CPTs in sections and on maps with lithostratigraphic interpretation is also important to this purpose. Nevertheless, some important limitations of CPT-E were observed, such as the interpretation of horizons <20 cm or the similarity between organic rich unconsolidated clays and peat.

The first camera CPT results provide a solution for these issues. Importantly, the camera CPT log is acquired, processed and visually interpreted straightforwardly. However, further research is necessary to improve the camera CPT results. This should focus on color calibration and analysis to fulfill the additional quantitative potential of colors for SBT interpretation.

While the EC depth log records both lithological as hydrological EC variations (e.g. salt- or freshwater), the CPT-E data can be used to distinguish soil texture from saltwater variations. As such, combined CPT-E and EC logging provides an important tool to interpret and model the major lithological and hydrological variations in both ERI and EMI near surface geophysical data in (embanked) estuarine floodplains. An actual integration of the *in situ* measured EC values in the modelling procedure of the near surface ERI and EMI data could improve results even further. The causes for the differentiation between the EC responses of the Allerød soil horizons require further research as well.

ACKNOWLEDGEMENTS

The IWT (HBC.2016.0549) and FWO (G024911 N) funded this research. The Renard center for marine geology-Ghent university is acknowledged for the use of the core scanner. Geoprobe Environmental Technologies n.v. is thanked for the demo with the camera CPT.

REFERENCES

Amorosi, A. & Marchi, N. (1999) High-resolution sequence stratigraphy from piezocone tests: an example from the Late Quaternary deposits of the southeastern Po Plain. *Sedimentary Geology,* 128, 67–81.

Bats, M. (2007) The Flemish wetlands. An archaeological survey of the valley of the River Scheldt. IN Barber, J., Clark, C., Cressy, M., Crone, A., Hale, A., Henderson, J., Housley, R., Sands, R. & Sheridan, A. (Eds.) *Archaeology from the wetlands. Recent perspectives.*

Proceedings of the 11th WARP conference. Edinburgh, Society of Antiquaries.

Crombé, P. (2005) The last hunter-gatherer-fishermen in Sandy Flanders (NW Belgium). The Verrebroek and Doel excavation Projects. Vol.1, Gent, UGent.

Crombé, P., Sergant, J., Robinson, E. & De Reu, J. (2011) Hunter-gatherer responses to environmental change during the Pleistocene-Holocene transition in the southern North Sea basin: Final Palaeolithic-Final Mesolithic land use in northwest Belgium. *Journal of Anthropological Archaeology,* 30, 454–471.

Crombé, P. & Verhegge, J. (2015) In search of sealed Palaeolithic and Mesolithic sites using core sampling: The impact of grid size, meshes and auger diameter on discovery probability. *Journal of Archaeological Science,* 53, 445–458.

Crombé, P., Verhegge, J., Deforce, K., Meylemans, E. & Robinson, E. (2015) Wetland landscape dynamics, Swifterbant land use systems, and the Mesolithic-Neolithic transition in the southern North Sea basin. *Quaternary International,* 378, 119–133.

De Clercq, W., Bats, M., Bourgeois, J., Crombé, P., De Mulder, G., De Reu, J., Herremans, D., Laloo, P., Lombaert, L., Plets, G., Sergant, J. & Stichelbaut, B. (2012) Development-led archaeology in Flanders: an overview of practives and results in the period 1990–2010. In Webley, L., Vander Linden, M., Haselgrove, C. & Bradley, R. (Eds.) *Development-led archaeology in Northwest Europe.* Oxford and Oakville, Oxbow Books.

De Clercq, W., Bats, M., Laloo, P., Sergant, J. & Crombé, P. (2011) Beware of the known. Methodological issues in the detection of low density rural occupation in large surface archaeological landscape assessment in Northern-Flanders (Belgium). In Blancquaert, G., Malrain, F., Stäuble, H. & Vanmoerkerke, J. (Eds.) *Understanding the Past: A Matter of Surface-Area. Acts of the XIIIth Session of the EAA Congress, Zadar 2007.* Oxford, Archeaopress.

Deforce, K., Storme, A., Bastiaens, J., Debruyne, S., Denys, L., Ervynck, A., Meylemans, E., Stieperaere, H., Van Neer, W. & Crombé, P. (2014) Middle-Holocene alluvial forests and associated fluvial environments: A multi-proxy reconstruction from the lower Scheldt, N Belgium. *The Holocene,* 24, 1550–1564.

Koster, K. (2016) Cone Penetration Testing: A Sound Method for Urban Archaeological Prospection. *Archaeological Prospection,* 23, 55–69.

Long, M. (2005) Review of peat strength, peat characterisation and constitutive modelling of peat with reference to landslides.

Long, M. & Boylan, N. (2012) In situ testing of peat–a review and update on recent developments. *Geotechnical Engineering Journal of the SEAGS & AGSSEA,* 43, 41–55.

Lunne, T., Robertson, P.K. & Powell, J.J.M. (1997) *Cone penetration testing in Geotechnical Practice*, Spon Press Taylor & Francis Group.

MCNEILL, J.D. (1980) Electromagnetic terrain conductivity measurement at low induction numbers. Geonics Limited Ontario, Canada.

Missiaen, T., Jongepier, I., Heirman, K., Soens, T., Gelorini, V., Verniers, J., Verhegge, J. & Crombé, P. (2016) Holocene landscape evolution of an estuarine wetland in relation to its human occupation and exploitation: Waasland Scheldt polders, northern Belgium. *Geologie en Mijnbouw/Netherlands Journal of Geosciences*, 1–28.

Missiaen, T., Verhegge, J., Heirman, K. & Crombé, P. (2015) Potential of cone penetrating testing for mapping deeply buried palaeolandscapes in the context of archaeological surveys in polder areas. *Journal of Archaeological Science,* 55, 174–187.

Robertson, P.K. (1990) Soil classification using the cone penetration test. *Canadian Geotechnical Journal,* 27, 151–158.

Robertson, P.K. & Cabal, K.L. (2012) *Guide to Cone Penetration Testing for Geotechnical Engineering (5th edition),* Signal Hill, California, USA, Gregg Drilling & Testing, Inc.

Saey, T., Verhegge, J., De Smedt, P., Smetryns, M., Note, N., Van De Vijver, E., Laloo, P., VAN Meirvenne, M. & Delefortrie, S. (2016) Integrating cone penetration testing into the 1D inversion of multi-receiver EMI data to reconstruct a complex stratigraphic landscape. *Catena,* 147, 356–371.

Verhegge, J., Missiaen, T. & Crombé, P. (2016a) Exploring Integrated Geophysics and Geotechnics as a Paleolandscape Reconstruction Tool: Archaeological Prospection of (Prehistoric) Sites Buried Deeply below the Scheldt Polders (NW Belgium). *Archaeological Prospection,* 23, 125–145.

Verhegge, J., Saey, T., Van Meirvenne, M., Missiaen, T. & Crombé, P. (2016b) Reconstructing Early Neolithic Paleogeography: EMI-Based Subsurface Modeling and Chronological Modeling of Holocene Peat below the Lower Scheldt Floodplain in NW Belgium. *Geoarchaeology,* 32, 159–176.

Cone Penetration Testing 2018 – Hicks, Pisanò & Peuchen (Eds)
© 2018 Delft University of Technology, The Netherlands, ISBN 978-1-138-58449-5

Comparative analysis of liquefaction susceptibility assessment by CPTu and SPT tests

A. Viana da Fonseca, C. Ferreira, A.S. Saldanha & C. Ramos
CONSTRUCT-GEO, Faculty of Engineering, University of Porto, Porto, Portugal

C. Rodrigues
Polytechnic Institute of Guarda, Guarda, Portugal

ABSTRACT: The assessment of liquefaction susceptibility from field tests is conventionally based on the Factor of Safety (FS_{liq}) against liquefaction, relating the Cyclic Resistance Ratio (CRR) with the Cyclic Stress Ratio (CSR). The calculation of CSR is relatively straightforward, whereas CRR strongly depends on the in situ technique from which it is derived. Distinct approaches have been proposed based on quantitative liquefaction risk indexes, namely the Liquefaction Potential Index (LPI) and the Liquefaction Severity Number (LSN). In Portugal, a pilot site for liquefaction assessment has been set up in the Lower Tagus Valley, near Lisbon, within the European H2020 LIQUEFACT project. In this paper, the geotechnical field data from SPT and CPTu is integrated in the three approaches to liquefaction assessment. A comparative analysis of the results is presented and discussed, highlighting the differences and limitations of these in situ tests in the assessment of liquefaction susceptibility in loose granular soils.

1 INTRODUCTION

Portugal's mainland and its Atlantic coast are located on the western and southern margins of the Iberian Peninsula. The seismicity of the Portuguese territory is heterogeneous and is classified according to regions with distinct seismic behavior, as in the Portuguese National Annex of Eurocode 8 (EC8-NA) (CEN, 2010). Seismicity increases in intensity from North to South and is concentrated in the South and the Atlantic margins. According to existing records, earthquake epicentres are mostly located in the Lisbon region, in the Lower Tagus River Valley (LTV) region, and along the Algarve coast (Ferrão et al. 2016). The greater Lisbon area is probably the zone with greater seismic risk, and it is affected by the occurrence of large magnitude (>8) distant earthquakes and of medium magnitude (>6) near earthquakes (Azevedo et al. 2010). An example of a distant event is the 1755 Lisbon earthquake ($M > 8.5$) generated in the Eurasian-Nubia plate boundary zone, and local intraplate ($M \approx 6$–7) earthquakes occurred more frequently, namely in 1344, 1531 and 1909.

Earthquake-Induced Liquefaction Disasters (EILDs) are responsible for significant additional structural damage and casualties, particularly in zones where specific geologic, geomorphological, hydrological and geotechnical characteristics indicate liquefaction potential of soils. The presence of thick profiles of recent alluvial sand deposits in a high seismicity area is a good example of the combination of the necessary liquefaction triggering conditions (LIQUEFACT, 2017). Information regarding liquefaction in Portugal has been collected and analyzed by Jorge (1993). Subsequently, Jorge & Vieira (1997) identified the locations of historical liquefaction events coupled with a reliability classification. A liquefaction potential zonation map of Continental Portugal was developed by Jorge (1993) and further discussed by Jorge & Vieira (1997). This zonation map was derived from the superposition and generalization of two basic maps: the liquefaction opportunity map and the liquefaction susceptibility map. For the greater Lisbon area, the authors produced a detailed representation, which identified high to very-high liquefaction susceptibility areas, mostly along the NE region of Lisbon, in the Lower Tagus Valley (LTV).

Based on this map, the region for the pilot site was selected and later refined from the analysis of existing geotechnical data, mainly covering the municipalities of Vila Franca de Xira, Benavente, Montijo and Barreiro.

2 APPROACHES TO THE ASSESSMENT OF LIQUEFACTION SUSCEPTIBILITY

2.1 *Factor of safety*

The most common approach to the assessment of the liquefaction suscetibility is the "Simplified Procedure", originally introduced by Seed & Idriss (1971), also recommended by Eurocode 8. This procedure consists on the computation of the factor of safety to liquefaction, as the ratio between the cyclic resistance ratio (CRR) and the cyclic stress ratio (CSR), expressed in Equation 1. The CRR is a measure of the capacity of the soil at a given point in depth to resist to liquefaction and the CSR refers to the expected seismic action on the soil at a specific location.

$$FS_{liq} = \frac{CRR}{CSR} \tag{1}$$

The expression for calculating CSR, according to the proposal of Seed and Idriss (1967), is as follows:

$$CSR = \frac{\tau_{cyc}}{\sigma'_{v0}} = 0.65 \cdot \frac{a_{\max}}{g} \cdot \frac{\sigma_{v0}}{\sigma'_{v0}} \cdot r_d \tag{2}$$

where a_{max} is the peak ground acceleration at the site, g is the acceleration of gravity, σ_{v0} and σ'_{v0} are the total and effective vertical stresses at the specific depth and r_d is a shear stress reduction coefficient.

The local peak ground acceleration (PGA or a_{max}) at the site was defined based on the National Annex of Eurocode 8 (EC8-NA) (CEN, 2010), as summarised in Table 1. For a return period of 475 years and a corresponding building importance class of II, the importance factor, γ_I, for the seismic zone of Vila Franca de Xira/Benavente is equal to 1.0. The corresponding magnitudes of Seismic Type 1 and Type 2 are 7.5 and 5.2, respectively, and a_{max} are equal to 1.0 and 1.7, respectively. These reference a_{max} must then be corrected to the local ground type, typically type D, corresponding to 'deposits of loose-to-medium cohesionless soil, or of predominantly soft-to-firm cohesive soil' (CEN, 2010) using the parameter *S*.

Table 1. Calculation of a_{max} for Vila Franca de Xira and Benavente, according to EC8-NA (CEN, 2010).

Parameter	Seismic action Type 1	Seismic action Type 2
Seismic zone	'1.4'	'2.3'
M_w	7.5	5.2
a_{gR} (m/s^2)	1.0	1.7
γ_I	1	1
Soil type	D	D
S	2.00	1.77
$a_{máx}$ (m/s^2)	2.00	3.00

The parameter r_d is a stress reduction coefficient, can be computed as proposed by Liao & Whitman (1986), also recommended by Youd et al. (2001), as a function of depth. However, other authors included the earthquake magnitude in its computation, namely Idriss (1999), also suggested by Boulanger & Idriss (2014) and adopted in this work, as follows:

$$r_d = e^{[\alpha(z)+\beta(z)\cdot M]} \tag{3}$$

$$\text{with} \quad \alpha(z) = -1.012 - 1.126\sin\left(\frac{z}{11.73} + 5.133\right) \tag{4}$$

$$\text{and} \quad \beta(z) = 0.106 + 0.118\sin\left(\frac{z}{11.28} + 5.142\right) \tag{5}$$

where z = depth (m) and M = earthquake magnitude.

The capacity of the soil to resist liquefaction is provided by the CRR, which can be evaluated from in situ test and lab results. The standard penetration tests (SPT) and cone penetration test (CPT) are particularly convenient, given the extensive worldwide database and past experience. The most recent approaches to the assessment of liquefaction potential, following the proposals of Idriss & Boulanger (2010) and Boulanger & Idriss (2014), for SPT and CPT, respectively were adopted. These approaches consider the computation of the cyclic resistance ratio (CRR) from the normalized penetration resistance, adjusted to an equivalent clean sand (cs), as indicated below:

$$CRR_{7.5} = \exp\left(\frac{(N_1)_{60cs}}{14.1} + \left(\frac{(N_1)_{60cs}}{126}\right)^2 - \left(\frac{(N_1)_{60cs}}{23.6}\right)^3 + \left(\frac{(N_1)_{60cs}}{25.4}\right)^4 - 2.8\right) \tag{6}$$

$$CRR_{7.5} = \exp\left(\frac{q_{c1Ncs}}{113} + \left(\frac{q_{c1Ncs}}{1000}\right)^2 - \left(\frac{q_{c1Ncs}}{140}\right)^3 + \left(\frac{q_{c1Ncs}}{137}\right)^4 - 2.8\right) \tag{7}$$

where $(N_1)_{60cs}$ is the normalized equivalent clean sand SPT penetration resistance, and q_{c1Ncs} corresponds to the normalized equivalent clean sand cone resistance. A clean sand is considered to have a fines content (FC) below 5%, as suggested by

Idriss & Boulanger (2004). The introduction of the percentage of fines in these approaches reflects its importance in the liquefaction susceptibility of the soil. However, it should be noted an estimate of the FC, especially below 25%, may be inaccurate if based solely in the lithological descriptions of the SPT logs, in the absence of grain size distribution of those soils.

Details of the calculations based on SPT and CPT are provided in Boulanger & Idriss (2014). For ease of computation, all CPTu analyses were made using CLiq® software (v.2.0.6.92, GeoLogismiki, 2017).

For earthquake magnitudes other than 7.5, the cyclic stress ratio needs to be corrected by a magnitude scaling factor *MSF*. In this work, the calculation of *MSF* was made according to Idriss and Boulanger (2010) taking into account the type of soil, as follows:

$$MSF = 6.9\exp\left(-\frac{M_w}{4}\right) - 0.058 \leq 1.8, \quad \text{for sandy soils} \tag{8}$$

$$MSF = 1.12\exp\left(-\frac{M_w}{4}\right) + 0.828 \leq 1.13, \quad \text{for clayey soils} \tag{9}$$

2.2 *Liquefaction potential index*

An alternative approach to liquefaction assessment is based on Liquefaction Potential Index (LPI). This index, originally developed by Iwasaki et al. (1978), combines the safety factor with depth, z, to 20 m:

$$LPI = \int_0^{20m} F \cdot W(z)dz \tag{10}$$

$$\text{where } W(z) = 10 - 0.5z \tag{11}$$

$$\text{and } F = 1 - FS_{liq}, \text{ if } FS_{liq} \leq 1 \text{ and } F = 0, \text{ if } FS_{liq} > 1 \tag{12}$$

where FS_{liq} is the factor of safety previously defined in Equation 1. Based on correlations between computed LPI values and observations of liquefaction events from Japanese earthquakes, surficial liquefaction damages were classified. Table 2 shows the classification proposed by Sonmez (2003).

2.3 *Liquefaction severity number*

The Liquefaction Severity Number (LSN) is a quantitative indicator of the consequences of liquefaction, developed by Tonkin & Taylor (2013), and represents the expected damage effects of shallow liquefaction on direct foundations, based on post-liquefaction reconsolidation settlements and is defined as:

$$LSN = 1000 \cdot \int \frac{\varepsilon_v}{z} dz \tag{13}$$

where ε_v is the volumetric densification strain due to post-liquefaction consolidation of soil layer i, calculated from Zhang et al. (2002), and z is the depth of the soil layer in metres, below the ground surface, referring only to the top 10 m of the soil profile. Liquefaction severity can be classified in terms of expected damage, as follows:

Table 2. Classification of liquefaction potential based on LPI (Sonmez, 2003).

LPI	Liquefaction potential
0	Very low
0 LPI 5*	Low
5* LPI 15**	High
15**> LPI	Very high

Table 3. Liquefaction severity and damage based on LSN (Tonkin & Taylor, 2013).

LSN range	Typical performance
0–10	Little to no expression of liquefaction
10–20	Minor expression of liquefaction, some sand boils
20–30	Moderate expression of liquefaction, sand boils and some structural damage
30–40	Moderate to severe liquefaction, settlement can cause structural damage
40–50	Major expression of liquefaction, damage ground surface, severe total and differential settlements
>50	Severe damage, extensive evidence of liquefaction at surface, severe total and differential settlements affecting structures, damage to services

3 SELECTION AND CHARACTERISATION OF THE PILOT SITE

3.1 *Collection and analysis of existing information*

The selection of the location of the pilot site was based on the analysis of existing geological and geotechnical information in the metropolitan region of Lisbon along the Lower Tagus Valley. With the collaboration of public institutions,

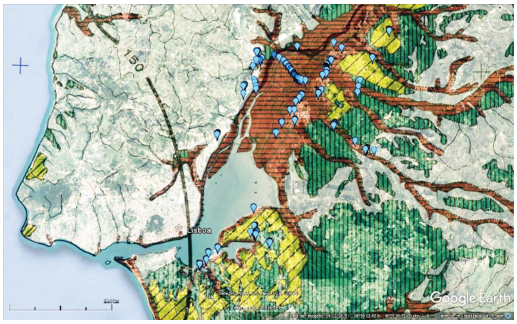

Figure 1. Location of the geotechnical reports collected in the greater Lisbon area, superimposed on the liquefaction zonation map (from Jorge, 1993). Red, yellow and green correspond to high to very high, moderate, and low liquefaction susceptibility zones, respectively; markers indicate geotechnical information.

governmental agencies, private companies, contractors and design offices, 95 geotechnical reports were selected, summing up to more than 350 test results. The analysis of the collected reports was carried out according to the type of geotechnical data, and the classification of the liquefaction susceptibility of each soil profile was made. A minimum factor of safety of 1.00 was considered, associated with a minimum thickness of the liquefiable soil layer of 3 m. For ease of visualization and interpretation, each data point was geographically located and color-coded according to its liquefaction susceptibility, preliminarily on Google Earth®.

3.2 *Location of the pilot site*

The municipality of Vila Franca de Xira is adjacent to Benavente where the 1909 earthquake occurred. Important works associated to the construction of a major highway (A10), including a 12 km bridge and viaduct, provided a wealth of information from extensive geological and geotechnical site characterization. The area in the agricultural plains of the 'Lezíria Grande de Vila Franca de Xira' was found to have the ideal geological, hydrogeological and geotechnical, as well as operational conditions, for setting up a research pilot site on liquefiable soils. The area of the pilot site was divided into zones, named Site Investigation (SI) points, identified by the respective number. The geotechnical tests consists of 2 SPT at SI1 and SI7, 8 CPTu at SI1 to SI7 and SI10, as well as 3 SDMT and a wide range of geophysical tests (seismic refraction, SASW and HVSR) (not discussed in this paper). Figure 2 indicates the testing locations, including the geophysical measuring points.

Figure 2. Location of site investigation points for in situ characterisation at the pilot site.

3.3 *Liquefaction susceptibility assessment at the pilot site*

For the purpose of comparison, two specific testing locations have been selected, where a greater number of tests has been performed, namely SI1 and SI7. Figure 3 illustrates the SPT results obtained in these two locations, in terms of simplified soil profiles and the normalized penetration resistance $(N_1)_{60cs}$ relevant for liquefaction studies. The soil profiles are significantly different, but it is worth noting that the values of the normalized penetration resistance do not exceed 15 blows in the first 30 m at both locations.

Figures 4 and 5 show the CPTu tests results in terms of cone resistance, sleeve friction ratio, pore pressure and soil behavior type index (according to Robertson and Wride, 1997) for testing locations SI1 and SI7, respectively. Again, the comparison between the two soil profiles evidences considerable differences, not only in terms of the nature of the soil in depth, but also in terms of strength.

Comparing the soil profiles in Figure 3 with the soil behavior profiles in Figs. 4 and 5, the distinction is clear. While SPT results lead to the interpretation of homogenous soil layers, CPTu results reveals the existence of thin interbedded layers of clay/silt in the sandy deposits, which are clearly identified in the CPTu by means of the pore pressure measurements above the hydrostatic line. This fact will necessarily have an impact in the response of the soil in the context of liquefaction.

From these results, the assessment of liquefaction susceptibility was made. The factors of safety against liquefaction have been computed in depth for the two locations based on SPT and CPTu results in Figures 6 and 7. The low values of the factors of safety obtained in depth suggest the existence of thick layers of highly susceptible soils to liquefaction at both locations. The differences

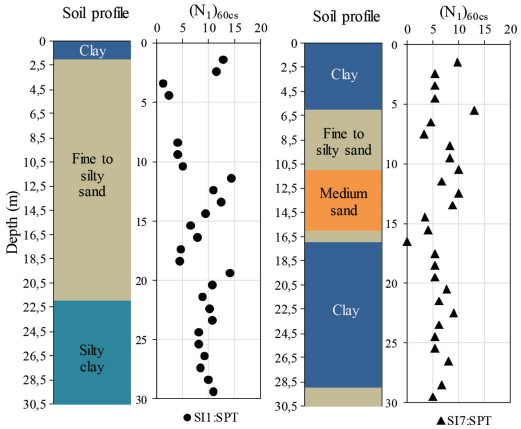

Figure 3. SPT results at the pilot site (SI1 and SI7).

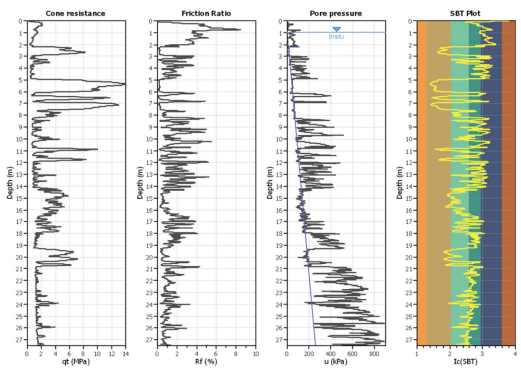

Figure 4. CPTu results: q_t; R_f; u; I_c for SI1.

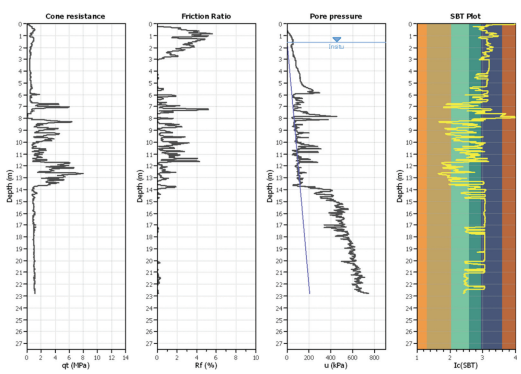

Figure 5. CPTu results: q_t; R_f; u; I_c for SI7.

between the absolute values of FS_{liq} obtained from SPT and CPTu are not significant. It is however interesting to note the variability of the CPTu-based FS_{liq}, associated with the presence of inter-bedded layers of fine and granular soils.

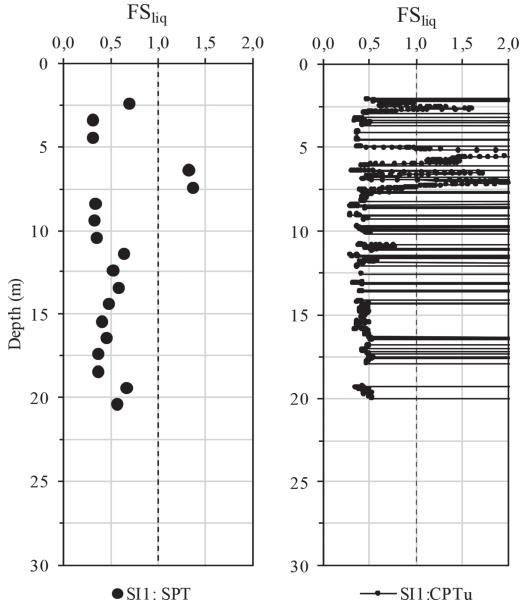

Figure 6. Comparison of SPT and CPTu assessment of liquefaction potential via FS_{liq} at SI1.

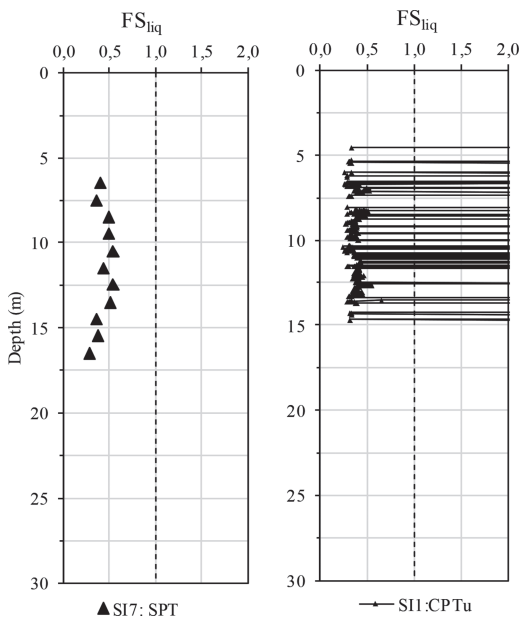

Figure 7. Comparison of SPT and CPTu assessment of liquefaction potential via FS_{liq} at SI7.

The quantitative liquefaction indexes LPI and LSN have also been computed from these test results. A summary is provided in Table 4.

Table 4. LPI and LSN indexes computed from SPT and CPT results (for seismic action Type 1).

	LPI		LSN	
Test location	SPT	CPTu	SPT	CPTu
SI1	31.7	15.9	85.6	26.7
SI7	26.5	12.5	51.8	12.2

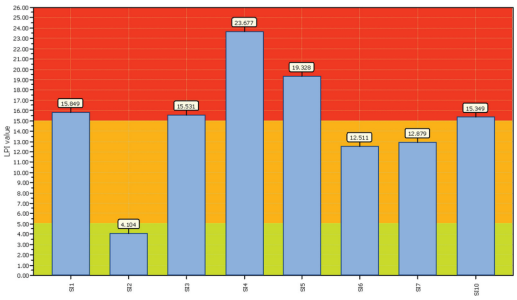

Figure 8. LPI values for CPT tests.

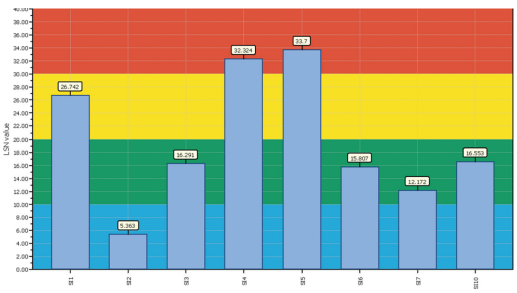

Figure 9. LSN values for CPT tests.

Comparing the values of LPI and LSN obtained from SPT and CPT tests, significant differences can be observed, especially at SI1. Given the presence of interbedded layers in the soil profiles, which were only identified by the CPTu test, the discrepancies in the quantitative indices are expected. In these soils, SPT-based liquefaction risk indices fail to accurately assess soil behavior with regard to liquefaction, providing considerably higher values that those estimated from CPTu results.

For assessing the variability of these indices across the pilot site, the overall results obtained in the 8 CPTu tests in terms of LPI and LSN are presented in Figures 8 and 9, respectively.

The results exhibit considerable variation of the LPI and LSN values across the pilot site, with only one location with low liquefaction potential (SI2). The test locations with higher LPI also have high LSN, although the expected damage associated with liquefaction should not be severe in any location (LSN lower than 40).

4 CONCLUSIONS

Different methodologies for the assessment of liquefaction susceptibility by means of in situ penetration tests have been applied in a pilot site in liquefiable soils. The comparison of these methodologies provided an additional level of information and enabled to highlight the limitations of some of the approaches. In fact, the comparison between the derived values of the liquefaction risk indexes based on SPT and CPTu tests evidenced considerable discrepancies, which are a reflection of the level of detail of the characterization offered by each testing method.

For the case study of this paper, which involved profiles with interbedded layers of clay and silt in sand deposits, the results obtained using SPT data were satisfactory in terms of the factor of safety, but unrepresentative in terms of LPI and LSN. The combination of different approaches for liquefaction susceptibility assessment enabled to define and identify the most affected zones, to be subsequently applied for microzonation of the site.

ACKNOWLEDGEMENTS

LIQUEFACT project ("Assessment and mitigation of liquefaction potential across Europe: a holistic approach to protect structures/infrastructures for improved resilience to earthquake-induced liquefaction disasters") has received funding from the European Union's Horizon 2020 research and innovation programme under grant agreement No GAP-700748.

Acknowledgements are due to the Portuguese stakeholders of LIQUEFACT, namely Teixeira Duarte, LNEG, ENMC, CMMontijo, CMBenavente, ABLGVFX, BRISA, CENOR, GEOCONTROLE and COBA, as well as to Dr. Sara Amoroso, Dr. Luca Minarelli and Dr. Rui Carrilho Gomes.

REFERENCES

Azevedo, J., Guerreiro, L., Bento, R., Lopes, M. & Proença, J. 2010. Seismic vulnerability of lifelines in the greater Lisbon area. Bull Earthquake Eng (2010) 8: 157.

Boulanger, R.W. & Idriss, I.M. 2014. CPT and SPT based liquefaction triggering procedures. Report No. UCD/CGM-14/01. Center for Geotechnical Modeling, University of California, Davis. 134 pp.

CEN, 2010. Eurocode 8: Design of structures for earthquake resistance.

Ferrão C., Bezzeghoud M., Caldeira B. & Borges J.F. 2016. The Seismicity of Portugal and Its Adjacent Atlantic Region from 1300 to 2014: Maximum Observed Intensity (MOI) Map. Seismological Research Letters 87(3): 743/750. doi: 10.1785/0220150217.

GeoLogismiki, 2017. https://geologismiki.gr/products/cliq/ (accessed in November 2017)

Idriss, I.M. 1999. An update to the Seed-Idriss simplified procedure for evaluating liquefaction potential. Proc. of the TRB Workshop on New Approaches to Liquefaction, Federal Highway Administration.

Idriss, I.M. & Boulanger, R.W. 2004. Semi-empirical procedures for evaluating liquefaction potential during earthquakes, in Proceedings, 11th International Conference on Soil Dynamics and Earthquake Engineering, and 3rd International Conference on Earthquake Geotechnical Engineering, D. Doolin et al., eds., Stallion Press, Vol. 1, pp. 32–56

Idriss, I.M. & Boulanger, R.W. 2010. SPT-Based Liquefaction Triggering Procedures. Report No. UCD/CGM-10–02. Center for Geotechnical Modeling, Department of Civil and Environmental Engineering, University of California, Davis. 259 pp.

Iwasaki, T., Tatsuoka, F., Tokida, K. & Yasuda, S. 1978. A practical method for assessing soil liquefaction potential based on case studies at various sites in Japan. Proceedings of the 2nd International Conference on Microzonation. San Francisco, CA, USA, pp. 885–896.

Jorge, C. & Vieira, A. 1997. Liquefaction Potential Assessment - Application to the Portuguese Territory and to the Town of Setúbal. Seismic Behaviour of Ground and Geotechnical Structures, Sêco e Pinto (ed), Balkema: 33–43.

Jorge, C. 1993. Zonation of Liquefaction Potential. Application Attempt to the Portuguese Territory. MSc in Sciences in Engineering Geology, New University of Lisbon.

Liao, S.S.C. & Whitman, R.V. 1986. A Catalog of Liquefaction and Non-Liquefaction Occurrences during Earthquakes. Research Report. Cambridge: Department of Civil Engineering, Massachusetts Institute of Technology.

LIQUEFACT, 2017. Available at http://www.liquefact.eu. (accessed in November 2017).

Robertson, P.K., and Wride, C.E. 1997. Cyclic liquefaction and its evaluation based on SPT and CPT. Proceedings, NCEER Workshop on Evaluation of Liquefaction Resistance of Soils.

Saldanha, A.S. 2017. Microzonation of liquefaction susceptibility. Application to a case study in the Greater Lisbon area. Master Thesis, Univ. Porto (in Portuguese).

Seed, H.B. & Idriss, I.M. 1971. Simplified procedure for evaluating soil liquefaction potential. J. Geotech. Engrg. Div., ASCE, 97(9):1249–1273.

Sonmez, H. 2003. Modification of the liquefaction potential index and liquefaction susceptibility mapping for a liquefaction-prone area (Inegol, Turkey), Environmental Geology, 44 (2003), pp. 862–871

Tonkin & Taylor, 2013. Canterbury earthquakes 2010 and 2011. Land Report as at 29 February 2012. Earthquake Commission (108 pp., http://www.tonkin.co.nz/canterbury- land-information/docs/downloads2592013/T&T-Stage-3-Report.pdf).

Youd, T.L., Idriss, I.M., Andrus, R.D., Arango, I., Castro, G., Christian, J.T., ... & Ishihara, K. 2001. Liquefaction resistance of soils: summary report from the 1996 NCEER and 1998 NCEER/NSF workshops on evaluation of liquefaction resistance of soils. Journal of Geotechnical and Geoenvironmental Engineering, 127(10), 817–833.

Zhang, G., Robertson, P.K. & Brachman, R.W. 2002. Estimating liquefaction-induced ground settlements from CPT for level ground. Canadian Geotechnical Journal, 39(5), pp.1168–1180.

Taylor & Francis
Taylor & Francis Group
http://taylorandfrancis.com

Cone Penetration Testing 2018 – Hicks, Pisanò & Peuchen (Eds)
© 2018 Delft University of Technology, The Netherlands, ISBN 978-1-138-58449-5

Application of CPT testing in permafrost

N.G. Volkov & I.S. Sokolov
GEOINGSERVICE (Fugro Group), Moscow, Russia

R.A. Jewell
Fugro GeoConsulting, Brussels, Belgium

ABSTRACT: This paper introduces some of the physical processes influencing the mechanical properties of permafrost and the effect of temperature change in the range 0°C to –10°C. The critical role of saline concentration in the pore fluid is described. Examples of recent CPT investigations at different permafrost sites in Russia are given to highlight the type of data that can be obtained and the interpretation for foundation engineering. Some of the investigations were completed in extremely cold conditions.

1 INTRODUCTION

The properties of frozen soil depend critically on ground temperature which impacts the performance of piled and shallow foundations in permafrost. Relatively small change in the sub-zero ground temperature of permafrost can cause significant change in the properties of the frozen soil. The mechanical properties of saline permafrost, as found in the Arctic (low lying areas, nearshore and offshore), are particularly sensitive to temperature and salinity. Indeed, saline permafrost generally contains pore fluid (with high salt concentration) at temperatures well below freezing. The mechanical behaviour of saline permafrost is a major challenge for the design of foundations for buildings, infrastructure and gas projects under development in the Arctic.

The temperature sensitivity of saline permafrost increases the challenge to recover and test undisturbed samples in the laboratory. To minimize disturbance, the sample temperature should be maintained as close to the original in situ temperature as possible. Any significant deviation in sample temperature during handling, storage or transportation may cause irreversible disturbance from thaw-refreezing. In situ testing of permafrost is highly advantageous, given the additional complexity of temperature control to obtain undisturbed samples for laboratory testing.

Thermosyphons are commonly used to extract heat from the ground that is transmitted to the atmosphere during winter, to maintain the ground at low temperature. The heat transfer mechanism works in one direction and does not introduce heat to the ground in summer. CPT can measure directly the ground properties and temperature at a controlled distance from installed thermosyphons, to monitor performance. The small hole formed by execution of the CPT may then be used to house a plastic tube containing thermistors for permanent temperature monitoring of the thermosyphons.

Piezocone tests (CPTu) with a temperature sensor provide valuable data on permafrost. The pore pressure sensor helps highlight boundaries between frozen and unfrozen layers. Other types of sensor permit measurement of resistivity for data on ice content; the presence of volatile organic materials such as methane may be measured with membrane interface (MIP) technology, all in the same test.

2 SALINE PERMAFROST

2.1 *General information*

Saline permafrost is widespread in the Arctic region along the coast, in low lying areas, nearshore and offshore. The source of salinity is the sea water. Salinity varies significantly depending on soil type, location with respect to the sea, and geological history of the soil strata. High salinity in permafrost soils was caused by the Quaternary transgression and regressions of the Polar Ocean. Cyclic temperature fluctuations inside saline permafrost, usually marine sediments, induce the formation of overcooled water brine lenses (cryopegs). Cryopegs are defined as a layer of unfrozen ground that is perennially cryotic (forming part of the permafrost), in which freezing is prevented by depression of the freezing-point due to the pore solution (Fotiev, 1999).

Saline frozen soil is a highly complex geotechnical material (Table 1). The soil behavior changes dramatically with only a small change in

Table 1. Frozen soil criteria.

Soil condition	Unfrozen	Plastic frozen	Solid frozen
Ice	Ice-free	Ice-bearing	Ice-bonded
Mechanics	Soil properties	Plastic properties	Elastic properties
Compression Index, a		a < 0.01 MPa^{-1}	a > 0.01 MPa^{-1}
Sand	>0°C	0 to −0.1°C	−0.1°C
Clay	>−0.2°C	−0.2 to −1.0°C	−1.0°C
Saline Clay*	>−1.0°C	−1.0 to −4.0°C	−4.0°C

*Saline Clay case for w = 33% Ds = 0.5% Cps = 15‰.

temperature. General soil mechanics applies when the soil temperature is above 0°C. Once the temperature is below freezing and the first crystals of ice start forming, the soil is considered as plastic frozen or ice bearing. Further reduction of temperature causes more ice crystals to form in the soil pore medium; when a critical volume of ice crystals is formed these start to bond together and the frozen soil is considered as solid frozen or ice-bonded. Russian standards (GOST 25100) provide the specific criterion named Compression Index (a) to classify plastic frozen and solid frozen soils.

Temperature boundaries between unfrozen/plastic-frozen/solid-frozen soils are determined specifically for each permafrost soil by field or laboratory testing. Several examples are provided in Table 1.

2.2 *Unfrozen water content*

The amount of unfrozen water has a controlling influence on the strength and deformation behavior of permafrost (Yershov, 1997). The amount of unfrozen water is determined by several factors, most critically temperature, salinity and mineral composition.

An example of temperature dependence of unfrozen water content on salinity (Ds) in frozen clay is shown in Figure 1 (Yershov, 1997). The total water content is 48% when the clay temperature is above 0°C. Cooling the clay causes some portion of pore water to freeze gradually as the temperature decreases. Thus at −1°C the total water content is shared between ice content (28%) and unfrozen water content (20%). Further cooling down to −5°C increases ice content to 38% and decreases unfrozen water content to 10%.

The influence of salinity is also highlighted, Figure 1. The amount of unfrozen water increases as salinity increases under otherwise equal conditions, including total water content. For instance, the proportion of ice and unfrozen water 28% and 20% occurs at −1°C for the saline frozen clay Ds = 0.1% but at −8°C for the saline clay Ds = 1.5%.

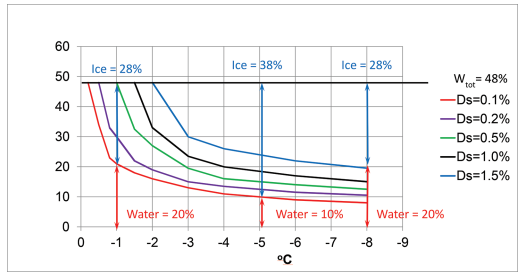

Figure 1. Unfrozen water content in frozen saline clay as a function of salinity (Ds) and temperature (Yershov, 1997).

Table 2. Preliminary design values for shear strength of adfreezing for saline frozen soils (clays).

Soil salinity, D_{sal},%	Design values for shear resistance R_{af}, kPa				
	−1°C	−2°C	−3°C	−4°C	−6°C
0.05	100	150	200	250	300
0.10	75	130	180	230	290
0.20	40	95	150	210	270
0.30	25	60	110	170	245
0.50	10	30	60	100	150

*SP 25.13330.2012 (former SNiP 2.02.04-88) provides these numbers for estimation purposes.

This impact of salinity influences the mechanical properties of the clay in a similar way.

2.3 *Mechanical properties and pile bearing capacity*

Mechanical properties of saline frozen soils depend strongly on temperature and salinity due to the unfrozen water content. For example, parameters for the shear resistance due to adfreezing, R_{af}, for saline frozen soils as a function of temperature and salinity are shown in Table 2. These parameters are from the Russian Standard "Soil bases and foundations on permafrost soils" (SP 25.13330.2012), taken from Table B.9 at page 66.

These parameters illustrate the dramatic effect of temperature and salinity on the mechanical properties of saline frozen soils. Changing temperature by 5°C, from −6°C to −1°C, would decrease soil shear resistance by 3 times for relatively pure water (D_s = 0.05%) or 15 times for more saline soil (D_s = 0.50%). An increase in soil salinity (perhaps misjudged by site investigation) from D_s = 0.05% to D_s = 0.50% would decrease soil shear resistance by a factor 2 (at −6°C) to10 (at −1°C).

Similar changes in magnitude due to salinity are observed for other mechanical properties of soil including deformation modulus.

3 EXAMPLES OF CPT TESTING IN PERMAFROST

3.1 *Salekhard and Labytnangy*

In 2014, Fugro performed geotechnical investigation of permafrost at several sites located in Salekhard and Labytnangy, Western Siberia, Russia. Permafrost was detected at 22 locations with the CPT temperature sensor. There was no refusal due to cone resistance and no "pre-drilling" was needed to conduct the tests; all predetermined depths for testing were achieved and the maximum depth was 34 m. The soil temperature was between 0°C and –1.2°C and the average cone resistance between 8 and 40 MPa, depending on the soil type.

3.2 *Vorkuta railway*

In 2015 Fugro performed a pilot project for Russian Railway to diagnose the condition of a railway embankment, located on permafrost near Vorkuta city, Russia (Sokolov et al. 2016). The CPT was performed directly from a railway flat-car within a 3 hours period. Total penetration was reached at a depth of 12 m. Two soil layers were identified, which correlated to the borehole data obtained several years previously, and the mechanical properties were estimated for each layer according to SP 25.13330.2012; E_f = 42 MPa (deformation modulus) and C_{eq} = 480 kPa (equivalent cohesion) for the first soil layer, and E_f = 22 MPa and C_{eq} = 84 kPa for the second soil layer. CPT results showed permafrost between 4 m and 12 m depth. Six detailed measurements of temperature with thermal equilibration (analogy with pore water pressure measurement) were performed that showed subzero values between –0.1°C and –0.7°C.

3.3 *Thermosyphon monitoring at Salekhard College*

CPT testing was applied in December, 2016 to diagnose the condition of piled foundations at the Salekhard College, Western Siberia, Russia. The frozen soil under Salekhard College was maintained by thermosyphons that were exposed in the crawl space below the building. CPT tests were completed from within the crawl space to measure cone resistance q_c [MPa], sleeve friction f_s [kPa] and temperature T [°C] at several locations relative to the thermosyphons and piles. Data was obtained both within the zone of influence of the thermosyphons and at sufficient distance from thermosyphons and piles to provide "baseline" measurements. Based on this data: 1) the cooling effect of the thermosyphons was directly measured (soil temperature decrease), 2) the pile bearing capacity could be estimated, and 3) pile capacity compared at different locations beneath the building (Volkov et al. 2017).

As a result of this investigation, it was determined that all the soils in the foundation are in a frozen state and that there is no permafrost thawing to a depth of 8 m, as had been implied by a previous investigation using conventional methods. The measured temperature values in the reference CPT locations were between –0.4°C to –1.3°C. Based on the code calculation, the bearing capacity of a single driven pile 300 mm × 300 mm and 8 m long is about 53 tons without taking into account the active layer; this significantly exceeds the design load of 20 tons. The thermosyphons had a cooling effect on the frozen soil. During the first winter season the soil temperature decreased by –0.5°C to –0.8°C (to –1.0°C to –2.1°C absolute values), resulting in an increased pile bearing capacity up to 77 tons, 42% higher than the reference pile capacity in the natural ground.

3.4 *Ob Bay*

Fugro performed geotechnical site investigation in 2017 on the Gydan peninsula near Ob Bay, Western Siberia, Russia. The soil conditions on the site were characterized by continuous permafrost with solid frozen sand at a mean annual ground temperature about –6°C. Such soil conditions are often stated to be unsuited for CPT investigation. Since there was no published data to substantiate that belief, Fugro performed a CPT trial to confirm applicability of the method in such soil conditions. The cone used for this test included sensors for temperature, pore pressure and electrical conductivity. The result of the CPT test is shown in Figure 2.

The cone resistance values for the sand varied between 20 MPa and 55 MPa. The sleeve friction ranged between 100 kPa and 600 kPa. Such numbers are high and correspond to very dense sand.

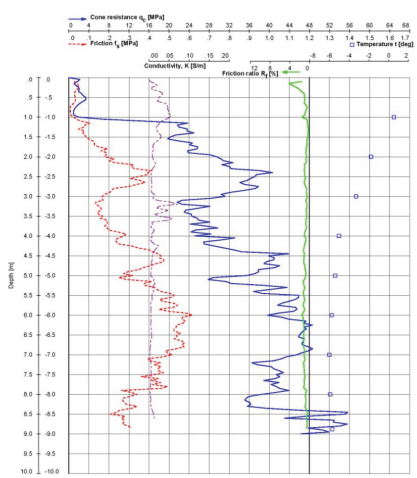

Figure 2. CPT profile in frozen sand at Ob Bay.

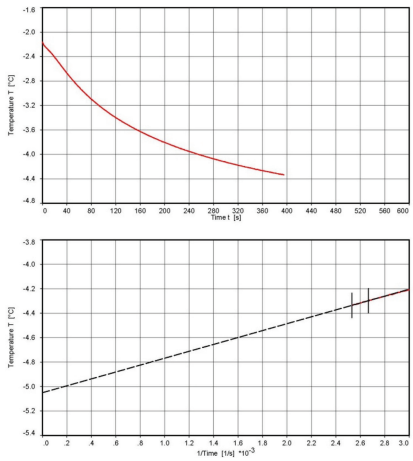

Figure 3. CPT temperature measurement at 4 m in frozen sand.

The electrical conductivity (resistivity) was also measured and the values varied between 0.0023 S/m (440 Ohm*m) and 0.0705 S/m (14 Ohm*m). It should be noted that between 3.0 m and 3.7 m the electrical conductivity is relatively high which is likely due to an increase in salinity. The average electrical conductivity equals 0.03 S/m (electrical resistivity 45 Ohm*m) in this depth interval. This is high (low) compared with the electrical conductivity for sand situated below 0.0037 to 0.0093 S/m (273 to 120 Ohm*m). This presumed increase in salinity corresponds with a marked reduction in cone resistance for the sand compared with the sand below; q_c = 22 to 28 MPa in the (presumed) saline sand interval and q_c = 36 to 48 MPa in the (presumed) non-saline sand interval below. All these correlations correspond qualitatively with the ratios of recommended values in SP 25.13330.2012 (Table 2).

An example of temperature measurement in frozen sand is provided in Figure 3. The time spent for temperature measurement is about 400 seconds. Other temperature measurements in this test were between 300 and 600 seconds. The accuracy of temperature measurement is 0.05°C. The resolution of the temperature sensor is 0.001°C.

The cone becomes heated due to friction between the cone surface area and the ground during cone penetration. In frozen sand the heat is absorbed by the surrounding media and the resulting temperature change is not as large as is in non-frozen soils. The tremendous advantage of CPT testing in permafrost soils, compared to non-frozen soils, is that the time required for temperature measurement is significantly shorter. While it would take several hours to stabilize cone temperature equal to that of the surrounding non-frozen soil where q_c = 20 to 40 MPa, in frozen soil with similar cone resistance values it takes about 10 minutes to complete temperature measurement.

The CPT data from Ob Bay (Figure 2) shows the depth of the active layer as about 1 m. This is shown by the temperature measurement at 1 m equal to 0°C. The cone resistance q_c also jumps significantly from 1 MPa to 24 MPa at this depth.

The minimum measured soil temperature was −6.0°C at 7 m depth. Below this depth the soil temperature starts gradually to increase reaching −5.7°C at a depth 9 m. It should be noted that the observed pattern of temperature variation with depth fully corresponds with the theoretical insights into the temperature regime of permafrost in the layer of annual temperature fluctuation.

4 GEOTECHNICAL MONITORING

4.1 *Existing practice*

Geotechnical monitoring of structures built on permafrost is very important. As described earlier, permafrost is very sensitive to temperature and salinity change, and these may be induced by climate change and man-made impact. There is a strong need for monitoring technology to provide sufficient data on frozen soil conditions below a structure.

The majority of structures on permafrost are built on piled foundations. An illustrative analysis for the condition of pile foundations is given below.

The frozen soil condition in relation to pile foundations can be classified in four stages (see Table 3).

1. Normal condition of frozen soil is when the designed pile bearing capacity corresponds (equals) to the actual pile bearing, and exceeds the load transferred to the pile. The soil tem-

Table 3. Frozen soil condition classification with reference to pile load and pile bearing capacity.

Foundation condition	Description
1. Normal	No visible problem detected Pile Load Actual PBC ≈ Design PBC Soil Temperature ≤ Design Value
2. Weakened	No visible problem detected Pile Load ≤ Actual PBC ≤ Design PBC Soil Temperature > Design Value
3. Poor	Visible deformations/displacements of pile are detected. Actual PBC ≤ Pile Load Soil Temperature > Design Value
4. Critical	Critical deformations/displacements of pile are observed. Actual PBC ≪ Pile Load Soil Temperature > Design Value

perature regime corresponds to that assumed in design, which is usually equal to the natural ground temperature "as it was" before the construction started, or colder (if thermosyphons are applied). Based on general practice, it is assumed that if the temperature of frozen soil is maintained at a certain level, no problems caused by permafrost should be faced.

2. Weakened condition is when due to an increase of the soil temperature, or other reason, the frozen soil becomes weaker. Actual pile bearing capacity is then less than designed, but it still exceeds the load transferred to the piles.
3. Poor condition is when the weakening of frozen soil continued and reached the point when the actual pile bearing capacity is close to the pile load. At this stage the pile load starts to redistribute between the piles which are typically installed in pile groups. The load on a weak pile equals its actual pile bearing capacity and the rest of load transfers to a neighboring pile. This redistribution of load prevents the structure from failure. However, minor deformation and damage may occur and be visible.
4. Critical condition is when the weakening of frozen soil reaches the point when actual pile bearing capacity is less than the load applied to the pile. In this case, settlement of the structure occurs and significant deformation and damage causes the operation of the supported structure to be suspended and often complete closure of the structure follows.

Based on the classification in Table 3, measures and solutions for engineering protection of a structure and foundation can be identified as follows:

Normal condition—no additional engineering measures for protection are required.

Weakened condition usually requires low-cost measures and solutions, which are aimed at indirectly improving the soil foundation, but not the structure itself, such as:

- application of thermal insulation,
- readjustment of existing thermosyphon operation,
- control on surface water flow,
- change of snow removal procedures,
- finding and fixing water leaks from surrounding civil infrastructure.

Poor condition requires high-cost measures and solutions, aimed at directly improving the soil foundation and support for the structure, such as:

- application of additional thermosyphons,
- reinforcement of the structure by installation of anchors, reinforcement supports, etc,
- reinforcement of foundation framework,
- installation of additional piles.

Critical condition—no engineering measures for protection are considered. Complete shutdown of a structure is enforced. Engineering design of the structure demolition is required.

4.2 *Existing methods for geotechnical monitoring on permafrost*

Current geotechnical monitoring methods for structures located on permafrost can be classified into three groups: 1) geodetic, 2) structural and 3) temperature.

The geodetic group includes various methods such as 3D Laser Scanning, Total Station Theodolite, HydroLevel, etc. All these methods measure distances, angles, coordinates, etc. of reference points on a structure in a certain period of time. Comparison of positions of the reference points provides information on whether the structure has been displaced or not and by how much. These methods only detect the deformation of a structure, which happens when a structure foundation is in Poor or Critical condition. The geodetic methods are not capable to predict whether deformation may occur or not, i.e. are not applicable for Normal or Weakened condition, as zero displacement is detected.

The structural group includes methods which use strain gauges and/or load cells, installed in structural elements for geotechnical purpose inside piles or near the contact between pile head and the structure itself. The strain gauges provide the strain which the pile is experiencing. Load cells provide the load transferred from structure to pile. Analysis of stress-strain behavior of the structure and distribution of loads on piles allows identification of critical strains or pile-load redistribution, which correlates to Poor and Critical conditions of the soil foundation. However, as for the geodetic approach, these methods are not capable to identify Normal or Weakened condition or to predict future deformation before it occurs.

The temperature monitoring methods are usually limited to temperature monitoring wells installed near piles and/or thermosyphons. This method is the most widespread for monitoring foundations in permafrost. Temperature monitoring detects the temperature regime of foundation soils. If the soil temperature stays within design values, the condition of the soil foundation is assumed to be good. If the temperature rises, then based on subjective opinions of experts, special engineering measures and solutions are developed. It should be noted, that usually no additional investigation is performed and often wrong/inappropriate measures are applied, sometimes causing harmful side effects and needless expense. If no engineering measures are applied, then the soil foundation may reach the critical condition causing loss of the structure. Temperature monitoring is necessary for geotechnical monitoring, however, it is not enough to diagnose the soil foundation

condition and develop proper solutions for engineering protection.

4.3 *CPT application for geotechnical monitoring*

A new standard STO 36554501-049-2016 was released by Russian design institute NIIOSP in 2016. The standard rules and guides CPT application on permafrost to monitor, diagnose and control soil foundations. For saline permafrost it is suggested to use CPT equipment that measures the following parameters in one push:

- q_c [MPa] – cone resistance, or soil resistivity under the cone tip
- f_s [kPa] – sleeve friction, or soil resistivity along the cone sleeve
- T [°C] – soil temperature
- u_2 [kPa] – pore pressure
- K [S/m] – electrical conductivity of soil.

Based on the data obtained by the cone, the following parameters can be calculated:

- Pile Bearing Capacity (PBC) estimated according to STO 36554501-049-2016,
- Soil temperature as a direct measurement,
- Soil salinity estimated from electrical conductivity, and
- Deformation modulus and soil strength calculated according to STO 36554501-049-2016.

For geotechnical monitoring purposes, CPT testing should be performed at the same key locations periodically (annually or every three/five years) depending on the site conditions. The results of CPT from one location should be compared to the corresponding results measured previously to evaluate the trend in parameters and foundation properties (PBC, Temperature and Salinity). If one parameter is gradually changing, then the trend should be analyzed and engineering measures considered.

An example of PBC analysis is provided in Table 4 where based on the relation between the interpreted PBC, Pile Load (PL) and designed PBC, the permafrost foundation condition can be derived.

Table 4. CPT monitoring.

Foundation condition	CPT
1. Normal	Measured PBC is equal or greater than the design PBC.
2. Weakened	Measured PBC is less than the design PBC, but higher than the design PL. The difference is not significant.
3. Poor	Measured PBC is less than the design PBC and equals the design PL.
4. Critical	Measured PBC is less than the design PL.

The CPT technology is the only method today, which can detect permafrost soil foundation degradation at an early stage. This degradation may be caused by a rise in either temperature and/or salinity in frozen soils. Other methods are not capable to determine when soil foundation start weakening. Also the data from CPT testing can forecast when and under which conditions the poor condition may occur, since it measures not only soil temperature, but also salinity and mechanical properties of the permafrost soils, together with the interpreted PBC.

Application of CPT technology can solve the problem of geotechnical monitoring for foundations in permafrost.

5 CONCLUSIONS

Several big infrastructure projects have been developed in recent years in the Arctic region, where saline permafrost is widespread. Permafrost degradation is a significant challenge for Arctic infrastructure which may be impacted by climate change or more direct man-made causes. Even a small increase in ground temperature and/or salinity of saline frozen soil can significantly decrease the mechanical properties of the soil and hence the bearing capacity of piles. The CPT is a powerful method to monitor and diagnose the condition of soil foundations on permafrost. Correct knowledge of soil foundation conditions permits properly designed engineering solutions and remedial measures to be derived, avoiding high costs or loss of monitored structures.

REFERENCES

GOST 25100-95. Soils. Classification. (in Russian).

Fotiev, S.M. 1999. Patterns in the formation of ion-salt composition in natural water of Yamal peninsula. *Earth Cryosphere*: 40–65 (in Russian).

Sokolov, I.S., Volkov, N.G. & Isaev, V.S. 2016. Cone Penetration Testing for Railways on Permafrost. *Proc. of the XI International Conference on Permafrost*, Potsdam, Germany.

SP 25.13330.2012 Soil bases and foundations on permafrost soils. (in Russian).

STO 36554501-049-2016 "CPT Application for Soil Foundation Control on Permafrost". Moscow: AO NIC "Stroitelstvo", 2016, 53 p. (in Russian).

Volkov, N., Sokolov, I. & Jewell, R. Investigation by Cone Penetration Tests of Piled Foundations in Frozen Soil Maintained by Thermosyphons. // *ISSN 2313–4410, American Scientific Research Journal for Engineering, Technology, and Sciences*, 2017, Volume 31, No. 1, pp. 40–58.

Yershov, E.D. 1998. *General Geocryology.* Cambridge: Cambridge University Press.

Cone Penetration Testing 2018 – Hicks, Pisanò & Peuchen (Eds)
© 2018 Delft University of Technology, The Netherlands, ISBN 978-1-138-58449-5

Comparison of mini CPT cone (2 cm^2) vs. normal CPT cone (10 cm^2 or 15 cm^2) data, 2 case studies

G.T. de Vries, C. Laban & E. Bliekendaal
Marine Sampling Holland, Velsen Noord, The Netherlands

ABSTRACT: For decades, the standard for CPT testing has pre-scribed use of a cone with a surface area of 10 cm^2. For cones with a projected surface area smaller than 5 cm^2, standards appear to question and suggest the application of a correction factor.

This paper discusses results of CPT tests performed with a Mini CPT system, in which cones with a nominal surface area of 2 cm^2 were used, compared to CPT results obtained with a standard 10 cm^2 or 15 cm^2 CPT cone. Two cases are presented. In case 1, project objective was validation of mini cone results for further use of the mini CPT system during construction works at the Dutch Maasvlakte 2 port extension. In the other case, the mini CPT system was used to proof soil deterioration along a newly built quay in a Dutch port. Finally, some suggestions are made regarding improvements to- and application of Mini CPT systems.

1 INTRODUCTION

CPT cones with a projected surface area smaller than 5 cm^2 have been around for decades. Whether or not results of such cones can be used, either with- or without correction factors applied, has been a matter of much research and debate. Some initial comparative testing by Tumay & Kurup (Tumay & Kurup, 1997) suggested, that for a cone with a nominal surface area of 1.27 cm^2, a correction factor of 0.85 should be applied as compared with results of a 10 cm^2 cone. Later research by Tumay & Kurup (Tumay & Kurup, 1999) seemed to indicate, for a 2 cm^2 cone the average q_c found would be 11% higher and average f_s would be 11% lower in comparison with a 10 cm^2 cone. A paper by (Peuchen et al.,2005) concluded, that for CPT tests in sands, differences between 2 cm^2 and 10 cm^2 cones depended on relative density. Later research by (Tufenkjian & Yee, 2010), where different cone sizes were tested in a test chamber filled with sand, compacted to various relative densities, showed that at low relative densities, tip resistance of a mini cone generally was lower than with a larger cone, whereas at high relative densities, tip resistance of a mini cone was mostly higher than in tests with a larger cone equivalent. In a study by (Powell & Lunne, 2005) no systematic differences between tests with different cone sizes in British clays were found. In a field study by (Yoon et al. 2013), differences between a 2 cm^2 cone and a 10 cm^2 cone appeared to be minimal.

Various studies show, that differences between CPT results are not exclusively found in CPTs made with different cone size, but are can be caused by cone operator (Tiggelman & Beukema, 2006, Kardan et al., 2016) found differences in q_c up to 10% and differences in f_s that were even larger) or cone manufacture. (Powell & Lunne, 2005) stated, that the resulting friction ratio R_f could differ as much as 1–4%.

In this paper, 2 cases are presented in which CPTs were made with a 2 cm^2 cone and a 15 cm^2 cone (case 1) or a 10 cm^2 cone (case 2). An attempt is made to quantify and interpret differences between different cone sizes.

2 MINI CPT SYSTEM

The miniature CPT equipment spread as proposed by (Tumay & Kurup, 2001) includes the following (see Figure 1):

- Hydraulic power unit
- Thrust machine/drive assembly, apparatus providing thrust to the push rods so that the required constant rate of penetration is controlled. In the mini CPT system, a downward force is accomplished through continuous chain-driven traction blocks.
- Coiled push rod: thick-walled cylindrical stainless steel tube (diameter 12 mm) used for advancing the penetrometer to the required test depth (maximum 10 m)

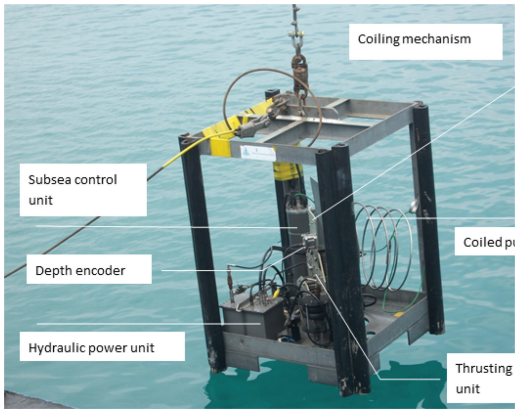

Figure 1. Mini CPT system.

- Coiling mechanism: while pushing, the coiled push rod is straightened by a set of two fixed- and two movable rollers. These rollers provide the mechanism which coils the rod for storage and straightens it again as it is pushed into the soil. The rod is plastically deformed (approx. 2%) as it is coiled and straightened.
- Friction-cone penetrometer (CPT): mounted on the lower end of the push rods, including a cone, a friction sleeve and internal sensing devices for the measurement of cone resistance and sleeve friction, having the following characteristics:

Tip cross sectional area	:	2 cm^2
Sleeve area	:	30 cm^2
Sleeve offset	:	5.0 cm
Probe length	:	14.2 cm
Probe diameter	:	1.59 cm
Cone area ratio	:	0.676

  Cones are of the subtraction type. The mini-cone has the same tip area/friction sleeve area ratio as a standard 10 cm^2 cone and hence is a down-sized version of a standard cone.
- Data acquisition and system control are both accomplished using a PC compatible computer running software written for this purpose. The analogue signals from the cone sensors are converted into digital data and transmitted to the data collection/control computer. Important parts of the data acquisition system are:

Depth Encoder—Penetration is measured using an optical shaft encoder attached to the lower fixed roller of the coiling mechanism (so, friction coupled to the push-rod). The roller diameter and encoder are sized and selected so that the output of the encoder is one pulse per millimeter.

Base frame inclinometer—inclination of the seabed frame can be monitored by an inclinometer, built into the subsea controls housing. The seabed frame inclinometer gives seabed frame inclination in x- and y direction.

3 PROJECT CASE 1

3.1 *Land reclamation Maasvlakte 2 port extension*

A first opportunity to compare 15 cm^2 cone results vs. 2 cm^2 cone results presented itself in 2009. At that time, construction of the new Maasvlakte 2 port extension was in full swing. The port extension comprises a land reclamation, made by initial dumping- and later hydraulic filling with medium- to coarse grained sand. To check compaction of sand in the offshore part of the reclamation, the objective was to make use of a mini cone SPT system. Prior to the actual offshore compaction testing, a project was initiated to validate mini CPT results. In early august 2009 (from 13–08 till 18–08), prior to quay construction, 140 CPT tests were made with a 15 cm^2 cone till maximum 40 m depth, along ca. 1800 m. of future quay, using standard land CPT equipment. For validation of mini CPT results, 3 sub-locations several hundreds of m. apart, each containing 3 CPT locations, were selected.

CPT tests (on land) with the mini CPT (seabed-) system till target depth of 10 m were made in 2 phases;

On 27–08, CPTs were made at location L III (CPT locations 45, 46 and 47). At CPT location 45, 4 attempts till 0.65 m, 0.64 m, 2.12 m and 3.35 m depth were made, after which further attempts at this location were aborted. At CPT locations 46 and 47, CPTs could be made till target depth.

On 19–10, CPTs were made at locations L II (CPT locations 57, 59 and 61) and L I (CPT locations 83, 85 and 87). At location 83, 2 attempts were needed (CPT 83 till 6.7 m. and CPT83–2 till 10 m.). CPT 87 was stopped at 7.2 m depth. Other CPTs could be made till target depth without re-attempts.

3.2 *Interpretation of results*

At all locations, a general good correspondence is found between the shapes of CPT curves resulting from tests with a 15 cm^2 cone vs. results with a 2 cm^2 cone. Some example CPTs are given in Figures 2–5.

CPTs made with the 2 cm^2 cone generally look more "spikey", with peaks (both in q_c and Rf) often showing higher values than the larger cone, and troughs showing lower values than the larger cone. Both these characteristics may be caused by the small cones being more responsive to vertical variation in sediment as suggested by (Hird et al., 2001).

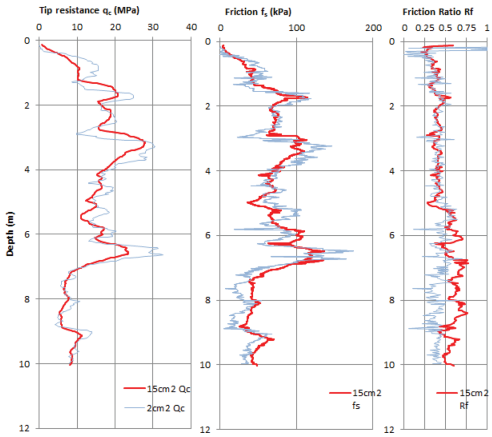

Figure 2. CPT results at location 46.

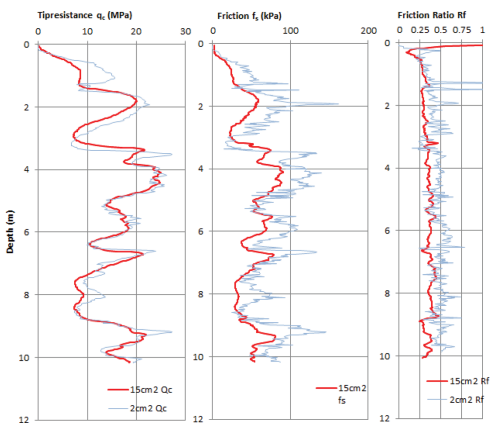

Figure 3. CPT results at location 47.

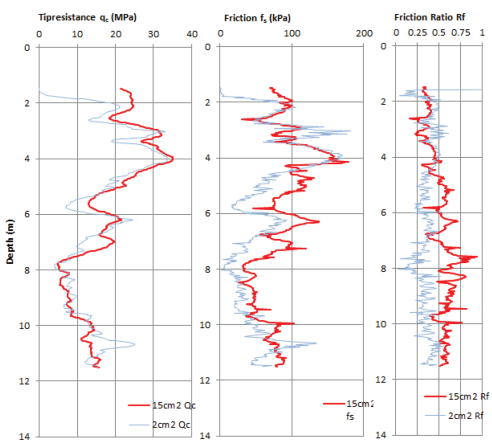

Figure 4. CPT results at location 59.

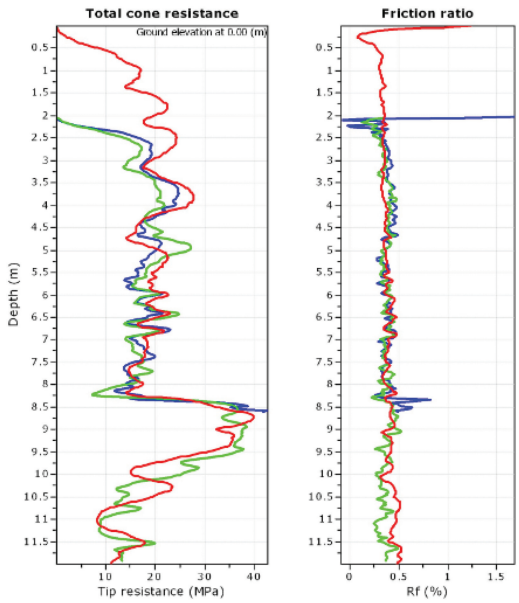

Figure 5. overlay plot of CPTs made at location 83.

A concise analyses of CPT results has been made by comparing average q_c and average f_s values of both cone dimensions. Results can be found in Table 1.

Average q_c varies between –14% to +12.8%, average f_s varies between –44% to +42.1%. In most cases where average q_c for a 2 cm² cone is higher, f_s is higher as well. Where average q_c is lower, average f_s tends to be lower. Differences seem rather random. When all CPT results are summarised, average q_c difference is only 1.5% and average f_s difference is 9.9%.

At one location, a check could be made to see if repeatability might be an issue. At location 83 (see Figure 5), 2 CPT attempts with a 2 cm² cone were made. A comparison between these 2 CPTs is given in Table 2.

The comparison shows, even CPTs made only minutes apart with only one cone size may result in a q_c difference of –3.5% and an f_s difference of –8.7%

It is not clear, whether or not differences observed between CPTs made with 2 cm² and 10 cm² cones can all be attributed to cone size.

Besides cone size, several other factors could have influenced CPT results. CPTs with different cone sizes at locations L I and L II were made several months apart. During this time, construction works continued. Surface level elevation during this period was lowered from reference +6 m to reference +4 to reference +5 m CPTs with the mini cone hence started at a level up to 2 m. below the

Table 1. Comparison of average q_c and f_s values of CPTs made with a 2 cm^2 cone vs. 15 cm^2 cone.

Location	avg q_c2 cm^2 (MPa)	avg f_s 2 cm^2 (kPa)	avg q_c 10 cm^4 (MPa)	avg f_s 10 cm^2 (kPa)	avg q_c difference (MPa)	avg q_c difference (%)	avg f_s difference (kPa)	Avg f_s difference (%)
46	14.72	61.10	13.52	63.30	–1.20	–8.9	2.20	3.5
47	15.14	69.35	14.03	48.12	–1.11	–7.9	–21.23	–44.1
57	15.87	65.86	15.30	72.81	–0.57	–3.7	6.95	9.5
59	15.39	60.83	17.50	82.25	2.11	12.1	21.42	26.0
61	15.289	63.05	18.23	108.94	2.34	12.8	45.89	42.1
83	19.00	71.09	20.66	80.29	1.66	8.0	9.20	11.5
85	19.03	71.21	16.70	61.43	–2.33	–14.0	–978	–15.9
87	21.01	84.98	22.15	90.26	1.14	5.1	5.28	5.8
Average all locations	17.01	68.43	17.26	75.93	0.26	1.5	7.49	9.9

Table 2. Comparison of average q_c and f_s values of 2 CPTs made with a 2 cm^2 cone.

Location	avg q_c 83	avg f_s 83	avg q_c 83–2	avg f_s 83–2	avg q_c diff. (mpa)	avg q_c diff. (%)	avg f_s diff. (kpa)	avg f_s diff. (%)
83	18.20	71.42	17.59	65.68	–0.61	–3.5	–5.74	–8.7

original level of the CPTs made with a 15 cm^2 cone. (see Figures 4 and 5). The top part of the CPTs was located in the unsaturated soil zone. Tidal variations (high tide ca. reference level + 1.5 m, low tide ca. reference level –0.5 m) may have influenced groundwater level. Soil saturation may also have varied due to variations in precipitation and evaporation. Zawadzki & Bajda (Zawadzki & Bajda, 2016) already observed, saturation levels might cause variation in both q_c an Fr up to 50%. The zone in the CPTs that might be affected by saturation differences between both project stages stretches till surface level –6.5 m.

4 PROJECT CASE 2

4.1 *Haringhaven Ijmuiden*

A second project enabling comparison of 10 cm2 cone CPT results with results of CPTs made with a 2 cm^2 cone took place in April 2012. Sometime after the Visserijhaven had been deepened and a new quay wall was constructed in IJmuiden port in 2011, the port authority wanted to check general condition- and possible deterioration of the seabed due to shipping movement and ships propeller action. For this purpose, 48 CPTs using a Mini CPT Seabed system with 2 cm^2 cones were made till target depth of 10 m -seabed. The CPT system was deployed from a barge suitable for inland waters. Position keeping was done using spud-poles. Hoisting took place using a crawler crane, with a GPS mounted in the crane boom. During the time of testing with the mini CPT, the seabed was located at ca. 10–12 m—reference level. Mini CPT test results could be compared to CPTs made prior to quay wall renewal with a 10 cm^2 cone (on 23–10–2009). 12 CPTs made with the larger cone (till target depth ca. 22 m—seabed) were available for comparison. CPTs were evenly spread along the quayside which has a length of ca. 500 m. CPTs with a 10 cm^2 cone were made from a survey barge, kept on position with spud poles. For CPT pushing, use was made of a 20-ton nominal pushing force set of CPT rams, located on deck, through a moon pool. A casing was lowered ca. 1–2 m into seabed prior to CPT deployment. During testing with the larger diameter cone, seabed was located between 4.5–9 m minus reference level.

An original typical soil profile at the interval of interest would look as follows:

–10 m till –13 m: medium dense to dense silty sand
–13 m till –15 m: thinly interbedded silty sand and sand
–15 m till –18 m: thinly interbedded sandy silt, silt and clay
> –18 m: sand, dense

During testing with the mini cone, penetration achieved varied between 4.4 m and 10 m. Ultimate penetration depended on where the lower dense sand layer was located, in no mini CPT attempt a penetration of more than 2 m into this layer was achieved.

4.2 *Interpretation of results*

Prior to further processing, all mini CPT depths were corrected for slope, based on the inclination values of the inclinometers built in to the seabed frame. In 6 of the 12 mini CPTs, an unrealistically high Fr was observed in the top 4 m. The reason for this is not exactly clear, as further down friction tends to return to normal values. Maybe this was caused by a malfunctioning or damaged cone, (though not observed by the field crew), or by earlier construction activities. q_c results for these CPTs could still be used. In order to make curves of mini CPT tests match the 10 cm2 CPT results as closely as possible, adjustments to depth were made to 8 of the 10 cm^2 cone CPT results, apparently there had been some inaccuracies in vertically referencing these CPTs. The largest vertical shift needed was 0.7 m for CPT 100. For CPTs 101 and 103 shifts of 0.4 m and 0.3 m were needed respectively. For CPTs 102, 109, 112 116 and 118 shifts of less than +/– 0.2 m were applied. After all adjustments had been made, the mini CPT results were used to prove, that after quay construction, dredging and consecutive vessel movement a disturbed zone with loosened soil of 1–2 m thickness existed, where CPTs showed a considerably lower tip resistance q_c and a relatively high skin friction. Below this disturbed zone, for all CPTs, q_c results of 10 cm^2 CPT and 2 cm^2 CPT seemed to correspond well. (see Figures 6 and 7)

As in case 1, CPT results with a 2 cm^2 cone appear to be more spikey than CPT results made with a 10 cm^2 cone. It also seems apparent from Figures 5 and 6, that the envelope encompassing q_c and Rf values of a 2 cm^2 cone is larger, i.e. the mini CPT results tend to exhibit higher extreme values. This may again be attributed to the mini cone being more responsive to thin layers.

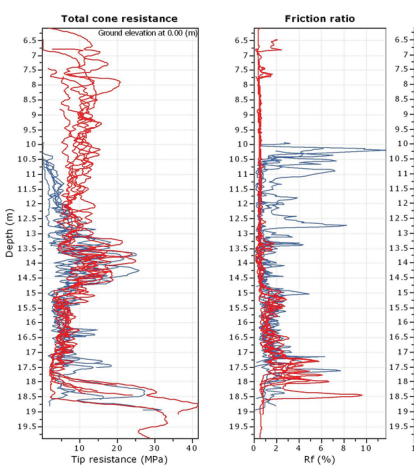

Figure 6. Overlay plot of 6 succesfull CPT test locations. 2 cm^2 results in blue, 10 cm^2 results in red. Both q_c and Fr / Rf match well, as does the derived SBT (Soil behaviour type) in the non-disturbed zone, located below reference –13 m..

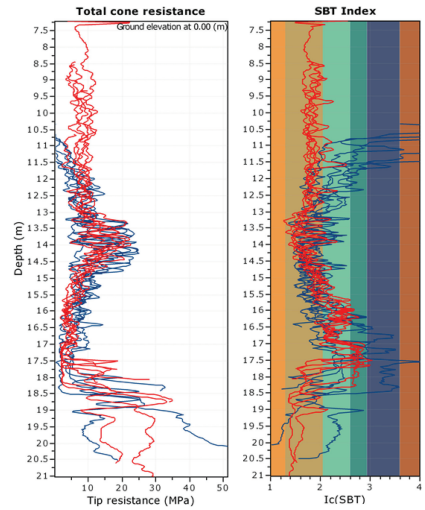

Figure 7. Overlay plot, comparing CPT tests at 6 remaining locations. 2 cm^2 results (with unrealisticaly high Fr in the top few m) in blue, 10 cm^2 results in red. q_c results still match well, as does the derived SBT (Soil behaviour type)in the non disturbed zone located below reference –12.5 m.

In order to quantify differences between CPTs made with various cone sizes, a comparison was made between average q_c and average f_s values. In this analysis, the "disturbed" zone above reference –13 m was disregarded. Only 2 cm^2 CPT results with valid friction values were used. Results can be found in Table 3 below

The average q_c values of 2 cm^2 CPT results as compared to 10 cm^2 CPT results vary between –14% to + 25%, the f_s results vary between –20.4% to + 9.2%. As in case 1, when the average q_c for a 2 cm^2 cone is lower than for a 10 cm^2 cone, the difference in f_s values tends to be negative as well (and vise versa).

If averages of all CPTs are calculated, the difference in q_c is only 3.4% and the difference in f_s only –2.98%.

It is again not sure if all differences between CPTs made with different cone sizes at the same location are caused by cone size only. CPTs with different cone sizes were made 2.5 years apart, during which time the harbour was deepened and a new quay wall was constructed in the direct vicinity of the CPT locations. This might have a profound effect on q_c and f_s values observed.

Table 3. Comparison of average q_c and f_s values of CPTs made with a 2 cm^2 cone vs. 10 cm^2 cone.

Summary		2 cm^2		10 cm^2					
2 cm^2 CPT no.	10 cm^2 CPT no	avg q_c (MPa)	avg f_s (kPa)	avg q_c (MPa)	avg f_s (kPa)	avg q_c difference (MPa)	avg q_c difference (%)	avg f_s difference (kPa)	avg f_s difference (%)
1	100	10.80	51.05	10.32	43.48	–0.48	–4.67	–7.56	–17.39
3	101	7.47	68.88	8.31	75.52	0.84	10.14	6.65	8.80
7	102	8.35	78.82	8.70	79.40	0.34	3.96	0.58	0.73
11	103	7.51	84.56	6.58	70.25	–0.93	–14.09	–14.32	–20.38
13	104	9.20	91.60	8.36	83.10	–0.84	–10.10	–8.50	–10.23
15	105	8.62	94.59	11.500	104.17	2.88	25.04	9.57	9.19
avg all CPTs		8.66	78.25	8.96	75.99	0.30	3.37	–2.26	–2.98

5 CONCLUSION AND RECOMMENDATIONS

In both presented cases, circumstances for a comparative test between cones of different sizes were not ideal. CPTs with large- (10 cm^2 and 15 cm^2) and small (2 cm^2) nominal surface areas were in both cases made several months or even years apart, under changing circumstances. Despite all these influences unaccounted for, differences between CPT results obtained with various sizes of cones seem rather random and non-systematic. Average differences over multiple CPTs seem to fall well within bounds that are to be expected for CPTs made by different operators made with equal-size cones of different manufacturers.

There is no scientific basis for any expectation that the response of the miniature cone should be significantly different from those of a standard cone, except for resolution. From a theoretical (continuum mechanics) standpoint, the response should be exactly the same except that the smaller cone should have higher resolution; i.e., it should respond more sharply to stratigraphic changes and it should be able to resolve thinner layers.

Numerical analysis to address the question of comparability of CPT results acquired with different cone sizes is quite feasible, but such has not yet been published.

Further research into the matter seems in place. In the mean time, there should be no objections to use cones with smaller dimensions on a variety of projects. Especially not, when CPT results and derived CPT parameters can be calibrated against borehole data and laboratory results. Various succesfull projects with miniature cone systems have already proven this.

REFERENCES

Hird, C.C., Johnson, P. and Sangtian, N., 2001. Performance of miniature piezocone in profiling thinly layered soil. Proc. XVth ICSMGE, Istanbul, August 2001.

Kardan, C., Viking, K., Nik, L., Larsson, S., 2016, Influence of operator performance on quality of CPTu results, Proceedings of the 17th Nordic Geotechnical Meeting, NGM 2016 Reykjavik.

Lunne, T., Robertson, P.K. and Powell, J.J.M. 1997. Cone penetration testing in geotechnical practice. Blackie Academic & Professional. London.

Peuchen, J., Adrichem, J., & Hefer, P.A., 2005. Practice notes on push-in penetrometers for offshore geotechnical investigation. Proceedings of the Frontiers in Offshore Geotechnics, London, United Kingdom. 973–979.

Powell, J.J.M., Lunne, T., 2005, *A comparison of different sized piezocones in UK clays*, Proc. XVI ICSMGE, Osaka, June 2005.

Powell, J.J.M., Lunne, T., 2005, Use of CPTU data in clays / fine grained soils, Studia Geotechnica et Mechanica, Vol. XXVII, No. 3–4, 2005.

Robertson, P.K., 1990. Soil classification using the cone penetration test. Canadian Geotechnical Journal, Vol. 27 (1), pp. 151–158.

Tiggelman, L., Beukema, H.J., 2006, Ringonderzoek sonderen, Geotechniek, januari 2006.

Tufenkjian, M R, Yee, E, Thompson, D.J., 2010. Comparison of cone and minicone penetration resistance for sand at shallow depth, 2nd International Symposium on Cone Penetration Testing, Huntington Beach, CA, USA. Volume 2&3: Technical Papers, Session 2: Interpretation, Paper No. 22.

Tumay, M.T. and Kurup, P.U., 1997. Calibration and implementation of miniature electroniccone penetrometers for road and highway design and construction, Louisiana.

Transportation Research Center, Project No.88–1GT Final Report, 71p.

Tumay, M.T. and Kurup, P.U., 1999. *A Continuous intrusion miniature cone penetration test system for transportation applications*, Louisiana Transportation Research Center, Project No.96–3GTX Final Report, 60p.

Tumay, M.T. and Kurup, P.U., 2001. Development of a continuous intrusion miniature cone penetration test system for subsurface explorations, Soils and Foundations, 41 (6), 129–138.

Yoon, S, Kim, K, Lee, J H, Shin, D., 2013. Scale Effects and Field Applications for Continuous Intrusion Miniature Cone Penetrometer, Journal of the Korean Society of Civil Engineers, Volume 33, Issue 6, 2013, pp. 2359–2368.

Zawadzki, L., Bajda, M., 2016. Impact of the moisture content in medium sands on CPTU test results, Annals of Warsaw University of Life Sciences – SGGW, Land reclamation no 48 (3), 2016: 221–231.

Cone Penetration Testing 2018 – Hicks, Pisanò & Peuchen (Eds)
© 2018 Delft University of Technology, The Netherlands, ISBN 978-1-138-58449-5

The development of "Push-heat", a combined CPT-testing/thermal conductivity measurement system

G.T. de Vries
Marine Sampling Holland, Velsen Noord, The Netherlands

R. Usbeck
Fielax, Bremerhaven, Germany

ABSTRACT: In design of offshore powercables, thermal characteristics of the soil in which the future cable will be located are needed to calculate and predict cable capacity and lifetime. Traditionally, thermal characteristics were measured in the laboratory, on samples obtained with various drilling and coring techniques. Unfortunately, for various reasons, results of laboratory testing are not always consistent. This necessitated the design of a reliable system to measure thermal characteristics, both in the laboratory and in-situ. Older in-situ measurement techniques have mainly focussed on deployment in soft soil and deep water. For use in coastal environments, with complicated soil profiles and soil types more resilient to penetration, these older systems have only limited practical use. Early development of a system combining vibrocoring with in situ thermal conductivity measurement has proved reasonably succesfull but in some soil types still rendered anomalous results. This paper discusses the development of a new measurement system which combines traditional CPT pushing- and measurement technology with an existing well established in-situ thermal measurement technique. Some initial measurement results are presented.

Keywords: CPT testing, thermal conductivity, in-situ testing, equipment, testing and procedures

1 INTRODUCTION

In a number of engineering applications, measurement of heatflow / thermal conductivity and thermal capacity is important. Common applications where thermal conductivity is measured are heat exchange systems for energy storage (mostly onshore), geothermal energy projects (mostly onshore), basin- and basin maturity studies in oil and gas industry (mostly offshore), design of offshore oil- and gas flowlines and pipelines, design of offshore HVDC / AC electricity cables. The offshore market has seen a recent rise in the amount of windfarms (each having their own infield- and export high voltage electricity cables) planned and under construction or already constructed. Furthermore, there is a joint European effort to create a European electricity grid, for considerable parts accommodated by offshore high voltage cables and divider stations.

All these offshore activities have given rise to a recently increased demand for assessing thermal conductivity values in shallow-water regions, which are important for estimating the dissipation mechanisms of thermal energy and the environmental impact of power cables. Penetration depths of more than 3 meters are essential for optimal cable burial and obtaining geothermal gradient estimations independent of seasonally influenced sediment layers.

2 MEASURING THERMAL CONDUCTIVITY

Considered best practise for determining thermal conductivity was, until very recently, taking offshore soil samples for consecutive thermal resistivity testing in a geotechnical laboratory, typically by using a thermal needle probe as in Figure 1. The main drawback of testing thermal conductivity in the laboratory is, that test conditions are often ill controlled, particularly watercontent, which has a major impact on test results. In addition, boundary effects (due to limited sample size) and limited test volume of soil are not well accounted for.

For these reasons, there is an increasing tendency in the market to ask for in-situ testing of thermal conductivity.

Several systems for in situ thermal conductivity measurement have been developed, in the past each having their own drawbacks:

Figure 1. Thermal needle probes.

- In-situ borehole tests, utilising a "thermal loop" - borehole required and takes a long time to set up and test—less suitable for shallow offshore testing)
- Push-in systems based on needle probes (Fugro a.o.) - limited penetration capacity due to vulnerability of the probe. Can be used in very soft (far offshore) soils only.
- Push- in systems based on larger size CPT cones (Neptune) – measurements are done consecutively at discrete depths which is very time consuming
- Heat-flow probes (TDI Brooks, Fielax)

Heat flow probes are designed to study thermal properties of the sediment and consist of a sensor string (typically1 cm diameter) with a series of thermistors and heater elements, attached to the side of a strength element, generally 3–5 m long (see Figure 2). The strength element is a steel tube with an added instrumentation package near the top for sensor data acquisition and control storage. Measurements include monitoring heat gradients as a result of the probe insertion into soil as well as heat dissipation with time produced by an impulse of the heater elements, which are fired after temperature has reached a stable level and heats up the probe and surrounding sediment. The probe then measures (and records) the thermal decay of heat, by which depth-dependent thermal conductivity and diffusivity can be calculated (Evenset et al, 2016, Hyndman et al, 1979). Main parameters of interest include geothermal gradients and thermal conductivities of the surficial 3- to 5-m portion of the seafloor sediment. These data are used for both engineering design of structures under thermal load, such as wellbores and pipelines, as well as sedimentary basin hydrocarbon maturation studies for exploration purposes.

A major advantage of this technology is, that measurements are taken simultaneously over the full penetration depth of the sensor into seabed, which makes measuring efficient. Until recently, the only deployment mode for a heatflow probe

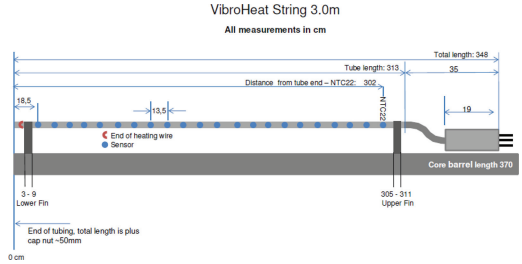

Figure 2. Heat flow probe, containing 22 thermistors, attached to a strength element. Data connections to a data acquisition unit can be made from the connection pod displayed on the right.

Figure 3. Vibrocorer, with combined vibroheat measurement string and core barrel attached.

was to drop it with a gravity-corer type setup. This deployment mode is only suitable in very soft sediment. A development by Fugro Gmbh, Fielax and Schmidt (Germany) (Dillon et al, 2012) has lead to a deployment mode using a vibrocorer, which makes the probe suitable for deployment nearshore, in tougher sediment. Deployment depth currently is limited to 3.5 m. depth (or 5 m. ultimately using a long 6 m. core barrel). See Figure 3.

Thermal conductivity measurement systems combined with CPT-push technology were not commercially available until recently.

Aim of the development of a HeatFlow Push Probe (HF-PP) / "push-heat" was, to develop a thermal conductivity measurement system that would incorporate measurement of standard CPT test parameters (tip resistance, skin friction, optionally cone inclination, porewater pressure) and is suitable to measure thermal conductivity to a greater depth then 5 m.

Development was planned to take place in 2 stages, which are further discussed below.

3 DEVELOPMENT STAGE 1: PROOF OF CONCEPT—HF PUSH PROBE

3.1 *Experience with VibroHeat*

Prior to starting any development, some initial experience was gained with the VibroHeat device. Although being a fully functional and fairly efficient system, it displayed the following disadvantages during deployment;

- having an extra probe attached ca. 5 cm away from a coring tube makes the tube asymetric and total effective diameter of the coring tube larger. This causes maximum penetration of the combi-coring tube to be less than for a conventional coring tube
- especially in "difficult" sediment like e.g. gravelly soils or very dense fine sand, penetration may take considerable time and force. This causes (also dependent on vibratory force and weight of the vibrocorer uses) a lot of soil disturbance around the vibrocorer, which in turn may influence thermal characteristics of the soil. (Evemset et al, 2016)
- On one of the initial projects, due to unequal seabed, the vibrocorer, which has a high centre of gravity, toppled over frequently, causing core barrels to bend and the HF probe attached to be damaged. On 20 stations, 5 probes were used.

Above flaws prompted the combination of Heat flow measurements with a Mini CPT machine.

3.2 *Adapting the HF probe system for use with a miniature CPT system*

The "normal" HF probe consists of a hollow tube with an external diameter of 14 mm, Wall thickness 3.5 mm, Internal diameter 7 mm. The normal probe contains 22 temperature sensors and up to 5 heating wires. The total amount of wire strands inside hence is 54. As the normal coiled rod for a mini CPT system (see Figure 4) is not so much different in size (having an external diameter of 12.7 mm., wall thickness 3.5 mm., internal diameter 5.7 mm.) inspired the idea to build a heatflow measurement string directly into a CPT coiled rod, initially as a dummy without the possibility to perform simultaneous CPT measurements. Having a slightly smaller diameter available and reserving some space already for the CPT cone wiring, this meant the amount of thermistors had to be reduced to 13 instead of 22. Only 1 heating wire was used. The length of the CPT coil was limited to 6 m, sensor spacing was 0.4375 m. The measurement principle (see Figure 5) for thermal conductivity measurements remained comparable to the earlier vibroheat device. In september 2013, initial measurements with the now "push-in probe" were done at the cable route for OWP Gemini. At 21stations, a cpt was performed first and a thermal conductivity measurement afterwards, using different CPT machines. Results obtained were of excellent quality, no liquefaction phenomena around the measuring device were observed and no probes were damaged.

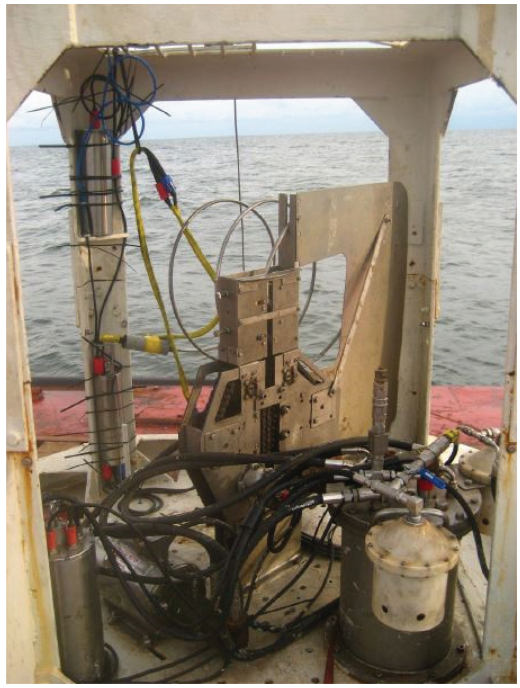

Figure 4. CPT frame with coiled tube modified for thermal measurements and titanium pressure housings containing data acquisition and power supply.

Since this initial conception, the "dummy" push probe (so without CPT cone attached) has been succesfully deployed on various projects all around Europe. An interesting spin-off for use in shallow (land- or offshore boreholes) has in the mean time been developed as well.

After validation had taken place, the decission was taken to proceed with stage 2 of the development.

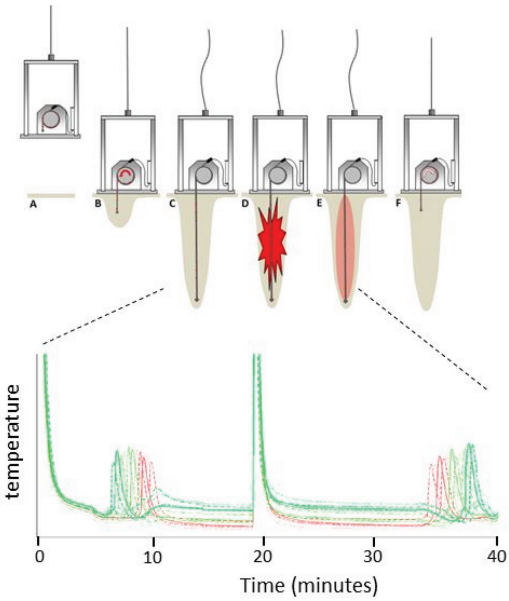

Figure 5. Principle of a heat flow measurement. A: Heat flow probe lowering to the seabed. B: Penetrating into seabed. C: Recording temperatures of thermal decay of frictional heat (approx. 20 minutes). D: Artificial heat pulse. E: Recording temperatures of thermal decay of heat pulse (approx. 20 minutes). F: Retrieval to surface. Clearly, temperature rises during the penetration and retrieval processes inside the CPT apparatus as successive peaks can be seen.

4 DEVELOPMENT STAGE 2: COMBINATION CPT / HF PUSHPROBE

This stage comprised the design of a heatflow push-probe with a 2 cm2 subtraction type of CPT cone, as normally used in the Mini CPT system. Cones used were analogue cones, allowing measurement of tip resistance, skin friction and porewater pressure. Cone inclination was not incorporated to the design yet. The cone has the following dimensions;

Tip cross sectional area	:	2 cm^2
Sleeve area	:	30 cm^2
Sleeve offset	:	5.0 cm
Probe length	:	14.2 cm
Probe diameter	:	1.59 cm
Cone area ratio	:	0.676

With the cone, a maximum tip resistance of 45 MPa is feasible. Connecting the cone to the heatflow pushprobe was not altogether easy, as the pushprobe is normally filled with oil. Connection to the cone had to be made watertight. 10 extra wires were inserted into the pushprobe, to allow passing of cone power supply and signals. (see Figure 6). Actual connection to the cone could be made by installing an extra steel transfer piece at the end of the push probe, fitted with a 10-pin mini lemo-type (E-type) connector. At the other end, a split out was made with 2 subconn connectors for the HF part of the device and 1 impuls connector to go to the CPT data acquisition system. Since the system was implemented, it has been tested at various locations with varrying degrees of succes. On a project at OWP Fécamp, weathered bedrock was present very near surface. Due to this, no significant penetration into seabed could be achieved. On a project in the Gulf of Biscaye, coarse material was present near surface. Although the CPT cones functioned well initially, they bent or became damaged otherwise early on in the lifetimes of probes. The HF part of the system continued to function flawlessly. Changing of cones in the field proved unpractical, due to the very minute size of the Lemo connectors. In practise, this meant whenever a cone was damaged, for the combination to continue functioning, a new probe with undamaged cone had to be installed.

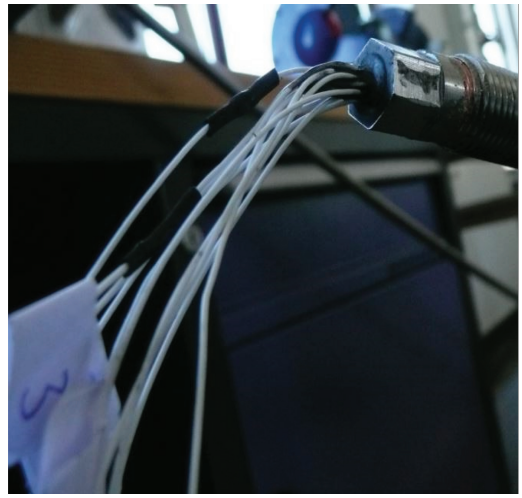

Figure 6. Connections of HF push-probe to CPT cone under construction. Wiring of the CPT cone is visible here.

Some initial probes have been developed with a length of up to 10 m. Since the probes proved quite vulnerable, cycletime as a combiprobe (i.e. without maintenance) is hence for the time being limited and construction of a 10 m. probe is quite tedious, the decision was made to limit probe length to 6 m. until some further developments making the set-up more robust have been implemented.

5 FURTHER DEVELOPMENTS, CONCLUSIONS AND RECOMMENDATIONS

Development of a push probe to measure thermal characteristics of the seabed has proven succesfull and overcomes some of the problems with earlier systems. Data quality of the Heat Flow equipment is, almost without exception, very high. The dummy version with no CPT cone attached is quite robust and hence is a very usefull and efficient tool to measure thermal characteristics of soil in the top 6 m. of sediment om varrying stratigraphies. Although the current set-up with analogue cones is functioning, it is relatively vulnerable. Application of a dummy- or a combi probe should therefore be decided upon based on expected stratigraphy. In "soft" soil, the combi probe can well be used. In profiles with abundant gravel or very dense sand, the dummy probe is preferred. Further development of the HF-CPT probe encompasses implementation of a digital cone (with tip/skin friction / porewater pressure and cone inclination measuring capability) is underway. This will make replacement of CPT cones in the field much easier, as a different type of connector can be used (a type that can rotate freely without causing wiring to damage). Additionally, this will reduce the number of wires needed to transfer power to- and signals from the cone to 4 only. This in turn will make construction of the combi probe somewhat easier.

On the interpretation side of things, it is interesting to notice that an abundant amount of combined measurements or coinciding measurements of CPT data and thermal conductivity data is becoming available. It might prove a usefull exercise, to see if a relation can be found between soil thermal characteristics and other physical parameters (often derived from CPT data).

REFERENCES

Dillon, M., Müller, C., Usbeck, R., 2012, Acquiring thermal conductivity data from shear-resistant sediments, Sea Technology, 53(2), 57–61.

Evenset, G., Kiaer, L.E., Kingman, K., Daniela, D, Thillart, R.v.d., de Vries, G.T., Dillon, M., 2016, Thermal characterization of seabed along the NordLink cable route – results and comparison of measurement methods, Cigre 2016, B1-313.

Hartmann, A. & Villinger H., 2002, Inversion of marine heat flow measurements by expansion of the temperature decay function. Geophys. J. Int., 148(3): 628–636.

Hyndman, R., Davis, E. & Wright, J., 1979. The measurement of marine geothermal heat flow by a multipenetration probe with digital acoustic telemetry and insitu thermal conductivity, Mar. Geophys. Res., 4, 181–205.

Taylor & Francis
Taylor & Francis Group
http://taylorandfrancis.com

Cone Penetration Testing 2018 – Hicks, Pisanò & Peuchen (Eds)
© 2018 Delft University of Technology, The Netherlands, ISBN 978-1-138-58449-5

Free fall penetrometer tests in sand: Determining the equivalent static resistance

D.J. White
University of Southampton, UK

C.D. O'Loughlin
University of Western Australia, Australia

N. Stark
Virginia Tech, USA

S.H. Chow
University of Western Australia, Australia

ABSTRACT: Free Fall Penetrometer (FFP) tests provide an efficient way to determine the penetration resistance at shallow depths in sandy soils, and are being used increasingly in geotechnical, geomorphological and coastal engineering applications. A limitation of free fall penetrometers is the effect of their high velocity on the penetration resistance. This affects the drainage condition, creates a viscous-type enhancement of the mobilised strength, and also introduces inertial drag forces. It is useful if the measured FFP resistance can be adjusted back to the resistance that would be expected in a standard Cone Penetrometer Test (CPT) at the same location. With this adjustment, the resistance can be used in the same correlations and design methods as standard CPT data. Adjustments for viscous-type rate effects and inertial drag have been proposed and explored in detail for clay soils. The contribution of this paper is to outline a correction scheme for drainage condition, which is more relevant for sandy soils. This correction utilizes the dissipation response at the end of the FFP test, in combination with the measured or derived FFP tip resistance. Relationships for penetration resistance in drained and undrained conditions based on density state are developed. It is shown that the high velocity FFP resistance can be uniquely mapped to a resistance from a standard CPT, when combined with the dissipation response. With development and validation, this new framework could enhance the value of FFPs as a complementary or alternative technology alongside conventional static penetration testing.

1 INTRODUCTION

1.1 *Free fall penetrometry*

Free-fall penetrometers (FFPs) are devices that are dropped from above the seafloor and self-penetrate into the seabed. Data gathered during the deceleration, such as tip and shaft resistance, are interpreted to determine the seabed properties.

Conventional push-in penetrometers are commonly deployed using a seabed reaction frame lowered from a survey vessel. FFPs can be deployed from smaller and less expensive vessels. Also, because they allow coverage of a large seabed area in a relatively short time frame, they have particular potential in supplementing data from push-in penetrometer tests that are undertaken at large spatial intervals, reducing the uncertainty associated with spatial variability.

Most free-fall penetrometers have geometries that resemble their 'push-in' counterparts. However, the velocity at impact with the seabed is typically up to 10 m/s depending on geometry and drop height. which is almost three orders of magnitude higher than push-in penetrometers, inserted at a standard rate of 0.02 m/s.

1.2 *Interpretation in clay soils*

In soft clay seabeds, FFPs travel at undrained rates of penetration. The measured data must be interpreted in a framework that accounts for the effect of strain rate on the mobilized soil strength, within the undrained range, to determine a soil strength that is equivalent to a constant (and much lower) velocity push-in test.

Recent studies have established frameworks for making this type of correction, which include

allowance for the apparent different effects of strain rate on shaft friction and tip bearing (Steiner et al. 2014; Chow et al. 2014, Chow et al. 2017).

It has also been demonstrated that these devices can measure the coefficient of consolidation if the penetrometer remains in the seabed after installation to record the dissipation of excess pore pressure (Mulukutla 2009, Chow et al. 2014). As a result, there is now a complete framework for interpretation of an FFP in soft clay to determine the same strength and consolidation parameters as a conventional piezocone test.

1.3 *Interpretation in sandy soils*

FFPs have also been tested in sandy soils, and have proven capable of identifying subtle stratigraphic layering within the upper tens of centimetres of the seabed (Stark et al. 2009), providing a powerful tool for wide area surveys of shallow seabed geomorphology. However, to date there is no equivalent interpretation method for sands to determine a soil strength parameter from the FFP tip resistance. Instead, the tip resistance is sometimes altered for strain rate effects to determine a corrected quasi-static penetration resistance, using the same type of approach as for tests in clay.

To establish a rigorous interpretation of FFPs in sandy soils, it is necessary to introduce an additional element to the interpretation process, to allow for drainage conditions. In clay soils, both FFP tests and conventional push-in CPTs involve undrained penetration, so allowance need only be made for viscous-type strain rate effects in estimating the appropriate undrained shear strength. In contrast, FFP tests in sand generally involve undrained penetration, whereas push-in tests are generally fully drained.

To illustrate this point, the boundaries for undrained and drained penetration are shown in Figure 1 using the dimensionless velocity, $V = vD/c_h$, where v is the penetrometer velocity, D is the diameter of the penetrating object and c_h is the consolidation coefficient. For $V < 0.1$, drained conditions apply but for $V > 30$ undrained conditions apply, based on both theoretical and numerical modelling (e.g. Colreavy et al. 2015, Chatterjee et al. 2013). These criteria lead to combinations of soil type – defined by c_h – and penetrometer velocity that fall in each drainage regime.

The domain of FFP tests is illustrated as $v > 0.1$ m/s, with a reasonable upper limit being of the order of 10 m/s, whereas conventional tests adopt a standard velocity of 0.02 m/s. For sandy soils, the consolidation coefficient may lie in the range 10^4–10^6 m^2/year, which leads to undrained or partially-drained conditions during FFP penetration.

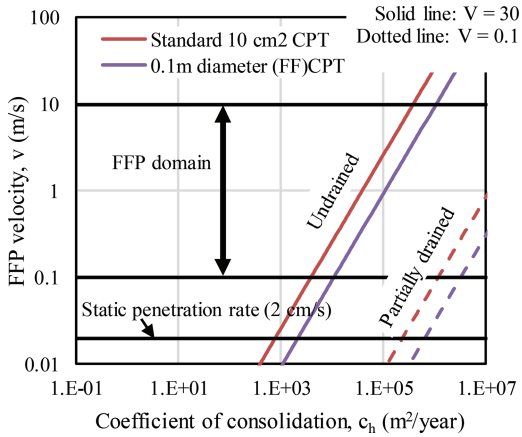

Figure 1. Drainage during penetrometer tests.

A conventional static push-in test is fully drained in sandy conditions. The u_2 pore pressure measurement provides an indication of the drainage regime, and the Robertson (1990) classification charts indicate that in sands and silty sands the normalized u_2 pore pressure ($B_q = (u_2-u_0)/q_{net}$) will not exceed ~0.2.

An FFP penetrating at a velocity that is two orders of magnitude higher, will show the pore pressure response equivalent to a much lower permeability soil, with a more significant value of B_q, that could be positive or negative, depending on whether the soils is dilatant or contractile.

1.4 *Interpretation for drainage in sandy FFP tests*

This paper outlines a new approach to allow for the effect of drainage in the interpretation of FFPs. It operates on the following basis:

1. A generic model is established for penetration resistance of the same soil in both drained and undrained conditions.
2. The model is tied to two soil parameters: relative density, I_d, and consolidation coefficient, c_h.
3. Relative density controls the penetration resistance in both drained and undrained conditions, and therefore also sets the ratio between drained and undrained resistance.
4. Consolidation coefficient controls the velocity thresholds between fully undrained, partially-drained and fully drained penetration.

Since the model has two soil parameters, they can only be uniquely defined from two FFP test measurements, and so the interpretation relies on both the dynamic penetration resistance, q_{dyn}, and also a dissipation stage immediately after the FFP comes to rest from which c_h can be determined. The

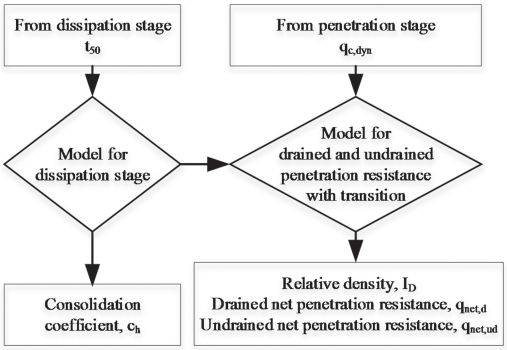

Figure 2. Interpretation scheme to allow for drainage condition.

model scheme is outlined in Figure 2. The following sections describe each element of the model.

The model is applied via example scenarios of soil that has uniform relative density with depth.

2 COEFFICIENT OF CONSOLIDATION

For a free fall cone penetrometer, the dissipation of excess pore pressure around the tip can be approximated by the following approximation to the time for 50% of the excess pore pressure to dissipate, t_{50}:

$$T_{50} = \frac{c_h t_{50}}{D^2} \rightarrow c_h = \frac{D^2 T_{50}}{t_{50}} \tag{1}$$

where T_{50} can be taken as 0.6, which is appropriate for typical values of rigidity ratio based on numerical analysis, and assumes that the prior penetration is fully undrained (Mahmoodzadeh et al. 2015).

The value of c_h determined from the dissipation data can be used to convert the velocity profile of the FFP deceleration into a profile of dimensionless velocity, V (assuming that the consolidation coefficient derived for the end of the drop also applies throughout the profile). As for static penetration tests, this idealized dissipation response can be applied to the dissipation seen in dilatant soil where an initial rise in pore pressure is often observed (Sully et al. 1999).

The penetration resistance between the undrained and drained regions can be defined using a 'backbone' curve of the form:

$$q_{net,dyn} = q_{net,ud} + \left(q_{net,d} - q_{net,ud}\right)\left(\frac{1}{1+\left(\frac{V}{V_{50}}\right)}\right) \tag{2}$$

where $V_{50} \sim 1$ (Randolph & Hope 2004).

Field studies show FFPs can provide consistent pore pressure data, despite the high velocity impact (Albatal et al. 2017), with a Bernoulli-type correction at the u_2 positon during free fall (Mumtaz et al. 2018).

3 DRAINED RESISTANCE

The drained penetration resistance, $q_{c,d}$, can be linked to the relative density via conventional correlations derived for clean sands, which are widely used in engineering practice for all sands. Many such correlations are available, which vary in their detail. The approach by Jamiolkowski et al. (2003) is adopted here:

$$I_D = \frac{1}{C_2}\ln\left(\frac{q_{net,d}}{C_0 p'^{C_1}_0}\right) \tag{3}$$

where $q_{c,d}$ and p'_0 are in kPa, and the coefficients are $C_0 = 300$ (dimensional), $C_1 = 0.46$, $C_2 = 2.96$. In our analysis, we have assumed for illustrative purposes an earth pressure coefficient of 0.5 and an in situ effective unit weight of 8 kN/m^3, meaning that $p'_0 = 5.3z$ where z is the depth below the seabed in metres.

If information on the soil mineralogy is available, the more sophisticated correlations of Mayne (2014) could be used, and other alternatives to Equation 3 exist, particularly at lower stress level and low embedment depth (e.g. Emerson et al. 2008), and may be preferred.

4 UNDRAINED RESISTANCE

The undrained penetration resistance, $q_{c,ud}$, is linked to relative density via Bolton's correlations, which provide a connection between density and angles of friction and dilation, varying with effective stress level (Bolton 1986). These correlations can be applied to determine the undrained strength of sands, by recognizing that in undrained failure the dilation angle must be zero. In Bolton's terminology, this requires a relative dilatancy, I_R, of zero, so that:

$$\begin{aligned} &I_R = I_D(Q - \ln p') - 1 \\ &\text{Undrained failure}: I_R = 0 \text{ so } p'_f = e^{Q - \frac{1}{I_D}} \end{aligned} \tag{4}$$

In silica sands, Q, referred to as the crushing strength parameter, is commonly taken as 10 (where p′ is defined in kPa) (Randolph et al. 2004). If mineralogical information is available, the value

of Q could be refined. Using the mean stress at failure, p'_f, the undrained strength can be calculated as:

$$s_u = \frac{1}{2} p'_f \left(\frac{6 \sin \phi_{cv}}{3 - \sin \phi_{cv}} \right) \tag{5}$$

adopting here the compressive failure criterion, and using the constant volume or critical state friction angle, ϕ_{cv}. Bolton (1986) shows this is relatively invariant for siliceous soils (31–33° with 32° adopted in this paper). For other mineralogies, alternative values are recommended (e.g. Randolph et al. 2004).

The undrained strength could also be augmented by a viscous adjustment for strain rate, following Randolph (2004) and Chow et al. (2017). Also, a cavitation criterion, dependent on the back pressure (i.e. water depth) could be used to set an upper limit on p'_f. For simplicity these additional elements have not been included in the model in the present paper.

The undrained strength can be converted to undrained penetration resistance, $q_{c,ud}$ via a conventional bearing factor, N_{kt}. We have adopted a value of $N_{kt} = 12$ which is the mean value from studies of clay soils reported by Lunne et al. (2011). However, this value is subject to the same uncertainties as for static CPTs, particularly at shallow embedment where a lower value of N_{kt} could be utilized instead (e.g. Aubeny & Shi 2006).

$$q_{net,u} = N_{kt} s_u \tag{6}$$

5 COMBINED MODEL

The analysis steps described above lead to backbone curves shown in Figure 3, which correspond to a depth of z = 2 m and use the parameters given previously.

It is notable that the backbone curves show divergent shapes at low and high relative density: in loose materials the undrained resistance is less than the drained resistance, whereas in dense materials the opposite is true. This is consistent with the effect of dilatancy, with the dense material dilating, causing a rise in effective stress and an increase in penetration resistance in undrained conditions.

The backbone curves do not cross, meaning that for any combination of q_c and V, there is a unique density state, which in turn has a pair of unique drained and undrained penetration resistances.

The transition between fully drained and fully undrained takes place over two orders of magnitude of V. Typical uncertainty in consolidation coefficient could be a factor of five, which gives

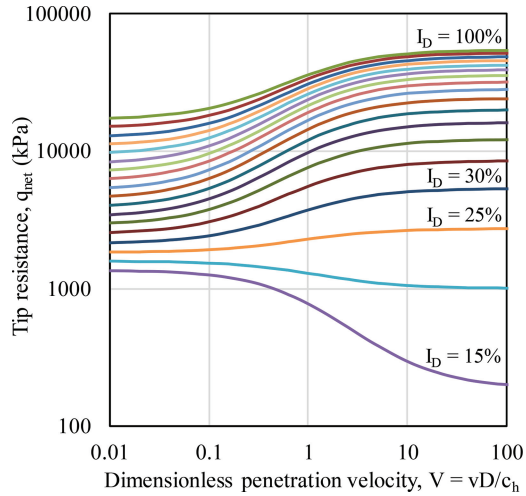

Figure 3. Example backbone curves linking dynamic penetration resistance to relative density and penetration speed.

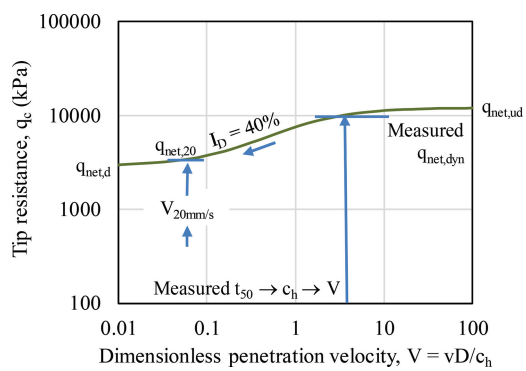

Figure 4. Illustration of interpretation scheme.

only a minor variation in the penetration resistance or the inferred relative density. For this reason, minor refinements in the adopted dissipation solution have only minimal effect on the model.

The log scale hides the significant range in penetration resistance: a change in relative density of 5% typically leads to a change in penetration resistance of ~15% in drained conditions. In undrained conditions, a 5% change in I_D doubles the undrained penetration resistance at low relative density, but has only a 10% effect close to $I_D = 1$.

The practical approach for using this models to interpret FFP results is shown in Figure 4. At all depths within the deceleration response, the measured q_c can be combined with the current V that is inferred using the c_h derived from the final dissipation test. This (q_c,V) pair identifies a relative den-

sity line, which can then be used to determine the drained limit, $q_{c,d}$ (or $q_{c,20}$, the penetration resistance at the standard rate of 20 mm/s) as well as the undrained limit, $q_{c,ud}$.

6 SYNTHETIC FFP ANALYSES

To illustrate the behavior of the model, a set of synthetic FFP penetration responses have been generated for uniform sand, with the parameters given earlier in this paper, and assuming a consolidation coefficient of $c_h = 10^6$ m²/year. The penetrometer is idealized as a 0.1 m diameter cone with a 60° tip, one metre in length, of solid steel. Shaft resistance is neglected.

Firstly, the responses in uniform loose and medium dense sand are compared for a range of impact velocities from 2.5–10 m/s, which are typical for FFPs (Young et al. 2011, Stark et al 2009). The assumption that relative density is constant with depth is adopted here, but may not apply in real sediments.

In loose sand (Figure 5), the synthetic dynamic resistance, $q_{c,dyn}$, is initially close to the undrained limit, $q_{c,u}$, but as the penetrometer decelerates the resistance converges to the drained limit, $q_{c,d}$.

In this soil, the conventional CPT profile (marked $q_{c,0.02}$) is fully drained. Below the initial few centimetres, the loose sand is contractile, so slowing of the probe is accompanied by an increase in resistance. A conventional rate effect correction that reduces the resistance with strain rate (or velocity) would not be appropriate in a contractile soil since it would adjust the measured resistance downwards instead of upwards. A viscous rate effect could be added into this model, but would have a minor effect relative to drainage.

Having determined these equivalent values of penetration resistance, any interpretation that is conventionally applied to the push-in cone tip resistance can also be applied. Where relative density is required, it is already known directly from the interpretation process.

The medium dense sand (Figure 6) is dilatant, so the opposite trend is evident. The rate effect due to drainage is much stronger than a conventional viscous-type rate effect. A four-fold increase in velocity causes an approximate doubling of resistance.

The effect of relative density is highlighted in Figure 7. The fully drained and fully undrained profiles of tip resistance are shown for a range of relative densities, along with FFP responses for an impact velocity of 10 m/s.

These profiles highlight the stronger effect of density on undrained tip resistance compared to drained tip resistance. This suggests that the penetration resistance in an FFP test could be a more sensitive measure of density variations than a conventional cone (although such detection of density gradations in an FFP test requires the drainage-based interpretation in this paper). Figure 7 also highlights the rapidity of the deceleration in dense sands, emphasizing the need for rapid data logging. For I_D = 0.75, the full deceleration takes <0.01 seconds.

A limitation of the analyses presented, which also applies to static CPTs, is that they rely on Equations 3 and 6 for penetration resistance, which

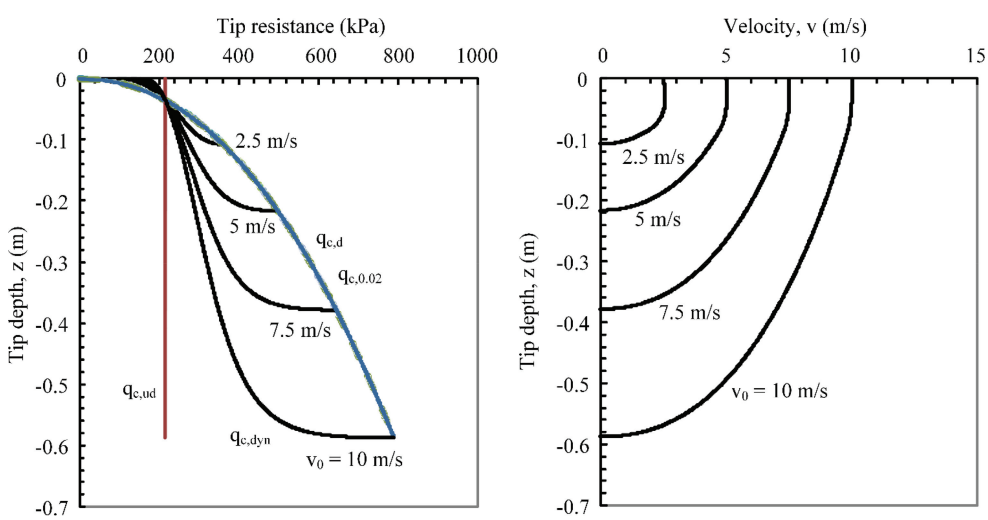

Figure 5. Synthetic responses in loose sand (I_D = 0.15) for varying impact velocity.

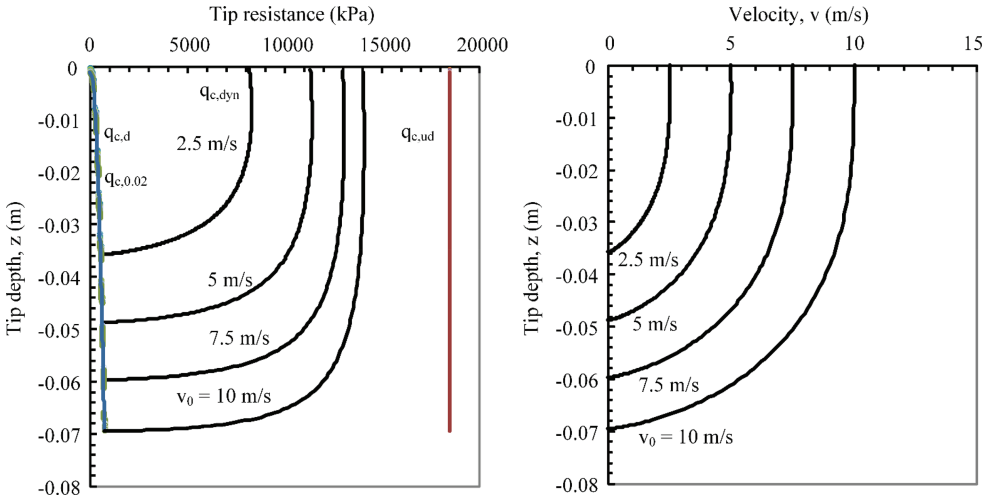

Figure 6. Synthetic responses in medium dense sand ($I_D = 0.45$) for varying impact velocity.

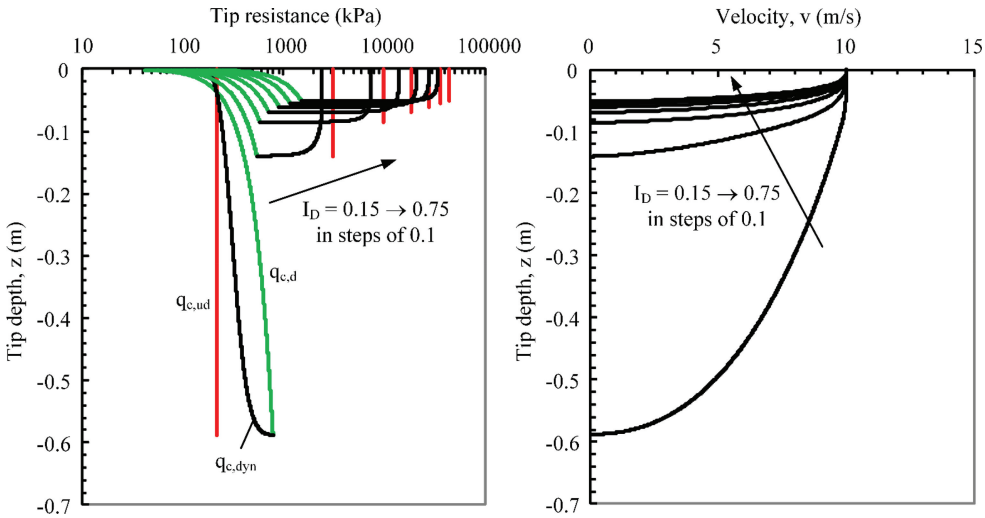

Figure 7. Synthetic responses for varying relative density.

are strictly for deep penetration, whereas lower bearing factors apply at shallow embedment.

7 CONCLUSIONS

A simple new procedure to interpret free fall penetration tests in sandy soils has been outlined. The method extends existing approaches that consider only viscous-type rate effects. The method introduces a simple approach to the effect of drainage on penetration resistance using a model for sand that captures the effect of relative density on both the drained and undrained penetration resistance. This model uses Bolton's correlations to define the undrained strength of sand at a given density, and conventional correlations to link (drained) cone resistance to relative density.

Using this model, the FFP resistance during deceleration in undrained or partially drained conditions can be uniquely mapped to a resistance from a standard CPT, when combined with a consolidation coefficient derived from the dissipation response.

With development and validation, this new framework could enhance the value of FFPs as a complementary or alternative technology alongside conventional static penetration testing.

REFERENCES

Albatal A. & Stark N. 2017. Rapid sediment mapping and in situ geotechnical characterization in challenging aquatic areas. Limnol. Oceanogr.: Methods 15, 2017, 690–705.

Aubeny, C.P. & Shi H. 2006.Interpretation of impact penetration measurements in soft clays: ASCE Journal of Geotechnical and Geoenvironmental Engineering, 132:770–777.

Bolton M.D. 1986. The strength and dilatancy of sands. Geotechnique, 36(1), 65–78.

Chatterjee, S. Gourvenec, S.M & White D.J. 2014. Assessment of the consolidated breakout response of partially embedded seabed pipelines. Géotechnique 64(5): 391–399.

Chow, S.H., O'Loughlin, C.D. & Randolph, M.F. 2014. Soil strength estimation and pore pressure dissipation for free-fall piezocones in soft clay. Geotechnique 64(10):817–827.

Chow S.H., O'Loughlin C.D., White D.J. & Randolph M.F. 2017. An extended interpretation of the free-fall piezocone test in clay. Géotechnique. 67(12):1090–1103.

Colreavy, C, O'Loughlin, C & Randolph, M (2016). Estimating consolidation parameters from field piezoball tests Géotechnique, 66(4): 333–343.

Emerson. M., Foray, P., Puech, A. & Palix, E. 2008. A global model for accurately interpreting CPT data in sands from shallow to greater depth. Int. Conf. Geotechnical and Geophysical Site Characterization. 687–694 Taylor & Francis.

Jamiolkowski, M.B., Lo Presti, D.C.F. & Manassero, M. 2003. Evaluation of relative density and shear strength of sands from cone penetration test (CPT) and flat dilatometer (DMT), Soil Behaviour and Soft Ground Construction, ASCE, GSP 119, 201–238.

Lunne, T., Andersen, K.H., Low, H.E., & Randolph, M.F. 2011. Guidelines for offshore in situ testing and interpretation in deepwater soft clays. Can. Geotech. J. 48,543–556.

Mahmoodzadeh, H., Wang, D. and Randolph, M.F. 2015. Interpretation of piezoball dissipation testing in clay. Géotechnique, 65(10): 831–842.

Mayne, P.W. 2014. Keynote: Interpretation of geotechnical parameters from seismic piezocone tests. Proc. 3rd Int. Symp. Cone Penetration Testing, CPT'14, 47–73.

Mumtaz, M.B., Stark N. & Brizzolara S. 2018. Pore pressure measurements using a portable free fall penetrometer. Proc. CPT '18, Delft (this proceedings).

Mulukutla, G.K. 2009. Determination of geotechnical properties of seafloor sediment. PhD thesis, U. New Hamp., USA.

Randolph, M.F. & Hope, S. 2004. Effect of cone velocity on cone resistance and excess pore pressures. Proc. Int. Symp. Deformation Characteristics of geo- materials, 147–152.

Randolph, M.F. 2004 Characterisation of soft sediments for offshore applications. 2nd International Site Character-ization Conference, Porto, Portugal, Vol. 1, pp. 209–232.

Randolph M.F., Jamiolkowski M.B. & Zdravkovic L. 2004. Load carrying capacity of foundations. Proc. Skempton Memorial Conference. 207–240.

Robertson P.K. 1990. Soil classification using the cone penetration test. Canadian Geotechnical Journal, 27(1): 151–158.

Stark,N., Hanff, H. & Kopf A. 2009. Nimrod: a tool for rapid geotechnical characterization of surface sediments. Sea Technology 50 (4), 10–14.

Steiner, A., Kopf, A.J., L'Heureux, J.-S., Kreiter, S., Stegmann, S., Haflidason, H. & Moerz, T. 2014. In situ dynamic piezocone penetrometer tests in natural clayey soils–a reappraisal of strain-rate corrections. Can. Geotech. J. 51, 272–288.

Sully, J.P., Robertson, P.K., Campanella, R.G. & Woeller, D.J. (1999). An approach to evaluation of field CPTU dissipation data in overconsolidated fine-grained soils. Canadian Geotechnical Journal 36, No. 2, 369–381.

Young, A.G., Bernard, B.B., Remmes, B.D., Babb, L. & Brooks, J.M. (2011). CPT Stinger - an innovative method to obtain CPT data for integrated geoscience studies. Offshore Technology Conf.. Houston, Texas, United States.

Taylor & Francis
Taylor & Francis Group
http://taylorandfrancis.com

Cone Penetration Testing 2018 – Hicks, Pisanò & Peuchen (Eds)
© 2018 Delft University of Technology, The Netherlands, ISBN 978-1-138-58449-5

The variability of CPTU results on the AMU-Morasko soft clay test site

J. Wierzbicki & R. Radaszewski
Institute of Geology, Adam Mickiewicz University, Poznan, Poland

M. Waliński
Geoprojekt-Poznan S.C., Poland

ABSTRACT: The paper presents results of tests conducted on a test site at Adam Mickiewicz University (AMU) in Poznań, Poland. The test site is located in the area of distribution of normally consolidated postglacial clayey silty sands and sandy clays. These soils are characterized by high porosity and are fully saturated, therefore, from a geotechnical point of view they can be defined as soft clays. There were 9 CPTU tests conducted along with research drillings and taking samples for laboratory analyses in the area of 8 ha. This paper focuses on the analysis of the uniformity of the soft clay layer found on the test site and on the analysis of variability of the CPTU tests conducted there. The results obtained enabled to separate a statistically homogeneous batch of soil in the subsoil and to form a reference set of CPTU results characteristic of the soft clay layer.

1 INTRODUCTION

The foundation design on soft clay has been always a big challenge for geotechnical engineers. It regards both the choice of proper method of foundation and the appropriate derivation of geotechnical parameters of subsoil. In the case of soft clays the problem of evaluation geotechnical parameters is particularly important, because of well-known difficulties in obtaining the high quality samples for laboratory tests. It should be also stated, that in the term of clay deposits we can describe very wide range of soil of various origin. For example the very well-known clay sites concerns marine clay, varved clay, expansive clay and many of them were subjected to the detailed geological and geotechnical analysis and treated as a reference test site (e.g. L'Heureux et al. 2017).

At this background, the special case of soft clayey deposits is the late Pleistocene glacial sediment, which can be treated as an intermediate or transition soil (Kezdi et al. 1971, Lunne et al. 1997). Due to geological history of last 15 thousands years, a large areas of northern Poland are covered by glacial and postglacial sediments, and most of them are the mixture of clay, silt and sand. This deposits are very often normally consolidated and has relatively high porosity. The average contains of clay particles of 13%, make this low plasticity soil quite stiff if it is dry. Whether, a high porosity and large amount of sand particles (very often over 50%), makes probable the strongly change of geotechnical parameters because of saturation. Because of a clay and silt content it behaves under the load as a fine-grained and undrained soil, and simultaneously, because of high sand and water content, the obtaining of high quality sample is almost so difficult as in the case of saturated sand (Borowczak 2008). Unfortunately for urbanists, this kind of soil is very common in the close vicinities of many cities in Poland, and also because of its thickness, reaches dozen meters of depth, states a real problem for the developing the infrastructure.

In this case a need of well investigated reference test site becomes obvious. One of the most awaited features of reference test site is the uniformity of soil, both vertical and horizontal, on the possible large area. For the purpose of checking the natural variability of soil, the results of several CPTU located on a relatively large area can be used. In this paper such investigations on newly developed test site in Poznan, Poland, were presented.

2 AMU—MORASKO TEST SITE

The test site is located within the Adam Mickiewicz University campus next to the northern border of Poznań. Because it is adjacent to Morasko Meteorite Nature Reserve (where large parts of Morasko meteorite were found), the site was called "AMU-Morasko test site".

The analyzed test site does not have strictly defined boarders, however, previous studies including: 14 CPTU tests, 2 flat dilatometer DMT tests, 26 drillings, 4 FVT tests tests focused on the area of approx. 8 ha within a 250-meter wide and 700-meter long longitudinally oriented grid. (Fig. 1). Umownie opisują go współrzędne geograficzne: 16°54'55'' ÷ 16°55'06'' E and 52°27'56'' ÷ 52°28'17'' N.

In the next 2 years the southwestern part of the test site will become a foundation to a planned student dormitory. During and after its construction one will provide the monitoring of soil subsidence to correlate the results of in situ and laboratory tests with an actual subsoil deformation.

Morphology of the analyzed area was formed by glacial and fluvioglacial processes of the Vistulian glaciation (Karczewski 1976; Stankowski 2008). It lies on the contact of the marginal zone of the sandur of Naramowice-Umultowo and on an adjacent outwash plain of an upland (Krygowski 1961, Chmal 1997). To the North of the test site there is a latitudinally oriented arc of hills, which forms a terminal moraine with its accumulation at the top of Mount Moraska (154 m a.s.l.). These hills are composed of glacitectonically deformed glacial tills and Quaternary sandy-gravel sediments along with torn loose xenoliths of Mio-Pliocene clays of the so-called Poznan series (Chmal 1997). The test site area is situated on the ordinates ranging between 93–105 m a.s.l. and gently falls to the South in the direction of the left tributary of the Warta River, i.e. Różany Strumień.

The Quaternary sediment thickness in the above described area reaches c. 40 m. These deposits represent the thick glacial till of the Riss glaciation (Oder and Warta) and glacial till of the Weichselian glaciation (Vistula). Deposits of the above mentioned glacial tills (within the meaning of geological cartography) separate fluvioglacial sandy sediments (the so-called lower) from the Leszno Phase of the Vistulian glaciation. The complex of glacial sediments is covered with fine and medium sands with single grains of gravel of the so-called first sandur level from the youngest Poznan glaciation. A sample geological profile from drilling no w1 conducted on the test site in 2014 documenting the layer of the sandur sands and silty clayey sediments of the Vistulian glaciation were presented in Figure 2.

The test site was created to conduct research on silty clayey sands and sandy silty clay of the Vistulian glaciation. In the southern part of the test site they are under a layer of c. 3-meter thick sandur

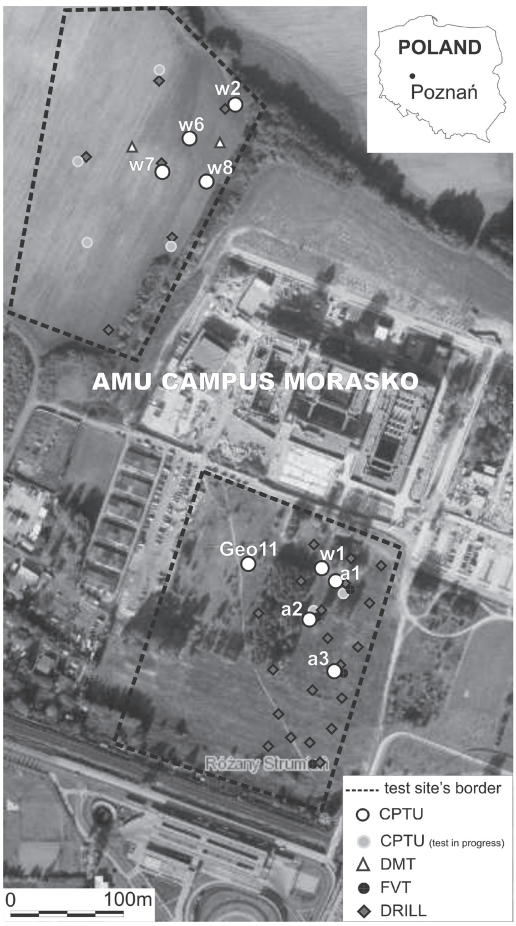

Figure 1. Research location on the AMU-Morasko test site.

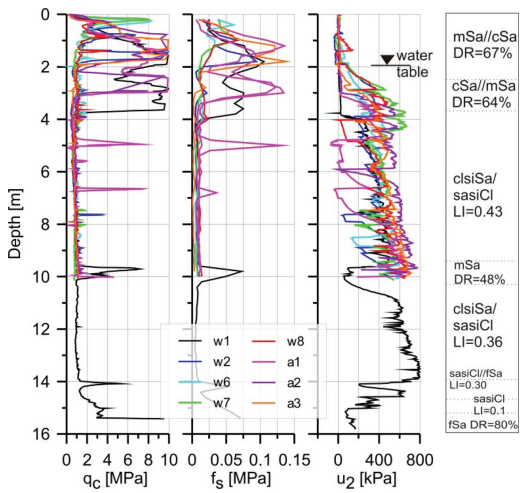

Figure 2. Basic CPTU parameters measured at 8 testing points and drilling profile at w1.

sands and in its northern part they are on the surface. The bottom of the layer was documented by the CPTU results at depths of: 12.5 m b.g.l. (in the northern part of the site) and 15.5 m b.g.l. (southern part). Thus, this is a thick deposit of sediments with a distinct lateral spread and specific, repetitive physical characteristics. Cartographic classification of these sediments as glacial till does not take into account their facies characteristics or genetic types which were described by Morawski (1984) or Liszkowski (1996). The existing analysis of the collected results of grain size and structural characteristics, as well as literature data on the analyzed area (Karczewski 1974, Stankowski 2000 and 2008), allow to initially assume a watermorainic genesis for these soils. They could be formed at the end of the Pleistocene as a result of a simultaneous sedimentation of the material melted from ice and the material transported by thawing waters on the foreland of the ice sheet. In the geotechnical sense, these soils should be treated as the so-called intermediate soils (Kezdi 1971, Radaszewski & Stefaniak 2017) with the content of silt fraction of c. 10%. According to the classification of PN-EN ISO 14688, most often these are soils of the following types: saSi, siSa, less often clsaSi (see Fig. 3).

The above mentioned soils are typically of soft or very soft consistency which can be contributed to the water conditions of the soil within the test site. It often results from a close proximity to a watercourse, the direction of flow of groundwaters and structural features. These are soils showing a relatively narrow range of plasticity and contain 3–5% $CaCO_3$ at the same time. Their basic physical parameters are summarized in Table 1.

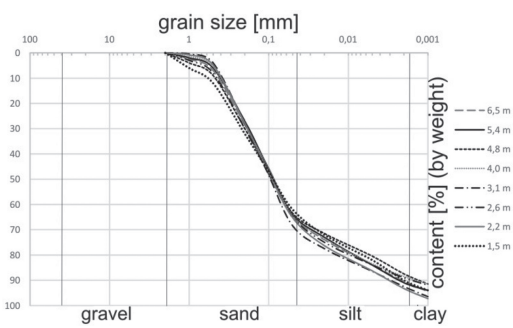

Figure 3. Grain size distribution curves of intermediate soils from the AMU-Morasko test site.

Table 1. Basic physical parameters of the analyzed intermediate soils.

	Natural moisture [%]	Plasticity limit [%]	Liquidity limit [%]	Plasticity index [%]	Liquidity index [–]	$CaCO_3$ [%]
Interval	13,25 ÷ 17,35	9,07 ÷ 12,67	15,39 ÷ 23,90	4,44 ÷ 10,96	0,35 ÷ 0,75	3 ÷ 5
Average	16,67	10,88	17,01	6,13	0,66	-

3 CPTU RESULTS

The analyses carried out within the framework of this paper are based on 9 CPTU tests conducted with two Pagani devices, which belonged to two different geotechnical companies. The tests were performed between April and June with a high level of groundwaters at a depth of approx. 2 m b.g.l. CPTU tests were located so that they would cover the entire area of the test site to allow their correlation with the results of geological drilling.

Figure 2 shows CPTU results from a selected research point characterized by a distinct layer of fluvioglacial sediments in the near-surface part. In this profile on can also notice sandy interbeddings sometimes occurring in the soft clays profile. One of them, at depth of c. 10 m, clearly separates a series of soft clay into two parts different in terms of properties (lower values of R_f and I_c and higher values of B_q were simultaneously registered).

4 ANALYSIS OF REPEATABILITY OF CPTU RESULTS

The collected data have been divided into two groups. The first one included 8 probe tests performed on the test site with one probe. The second one included 1 probe test conducted with a different probe, but from the same manufacturer. The first group of data was used for the analysis of natural variability of the subsoil within the site, the separation of a homogeneous part of the profile and statistical determination of the result pattern in this layer. The second group was a test attempt of homogeneity of the test site.

4.1 *Variability of CPTU results on individual measurement depths*

Within the group of 8 probe tests we conducted an analysis of basic statistical parameters of the distribution of the results obtained for each measurement depth, every 1 cm. The analysis included the following parameters: corrected cone resistance – q_t, sleeve friction – f_s, pore pressure behind cone – u_2, friction ratio – R_f, soil behavior index – I_c, pore pressure parameter – B_q, normalized cone resistance – Q_t (Lunne et al. 1997, Robertson 2009). It was found that the parameters related

to cone resistance and sleeve friction are characterized by high variability within the surface fluvioglacial layers and very low variability within the soft clay layer (especially below the depth of 5 meters) (Fig. 4). The coefficient of variation in this layer only locally exceeds 0.15. It is against this background that one can also notice a presence of larger sand interbeddings in the soft clay layer.

The variability of pressure measurements u_2 and calculated B_q parameter, wich is characterized by significant differences at the same depth within the test site, is somewhat different (Fig. 4). This is probably due to slight fluctuations in the content of the clay fraction in these strongly sandy sediments, which affects the water permeability of the soil and was recorded by the pore pressure measurement system. This hypothesis is also confirmed by the currently conducted CPTU testing at a four times lower penetration speed. The presence of less cohesive laminates affecting the plasticity of the soil was also recorded during drillings and sampling. At the same time, it should be noted that despite the coefficient of variation reaching 0.35 in this layer, a steady trend of changes u_2 is evident in a nearly whole sediment profile. It is unambiguously related to the effect of vertical stress and hydrostatic pressure. From the depth of approx. 8 m the trend slightly changes, which is reflected by an increase in the average value of B_q from 0.36 to 0.41 (Fig. 5).

The homogeneity of the subsoil in the analyzed layer may also be an evidence of the fact that the averaging of the CPTU data in 20-centimeter fragments of probe tests does not significantly affect the values of the coefficient of variation of the probe tests results, as compared to its value determined for measurements performed every 1 cm (Fig. 6).

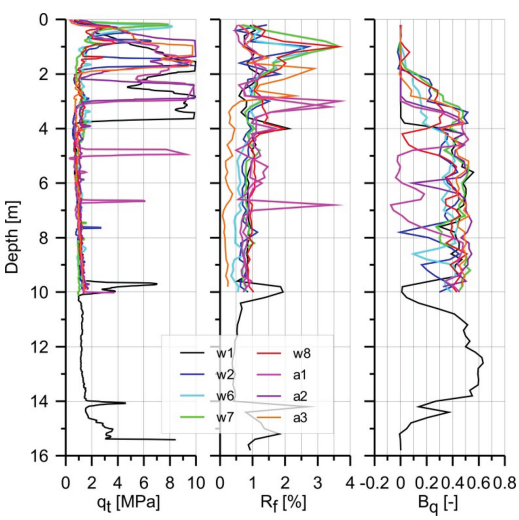

Figure 4. q_t, R_f and B_q values for 8 reference CPTUs.

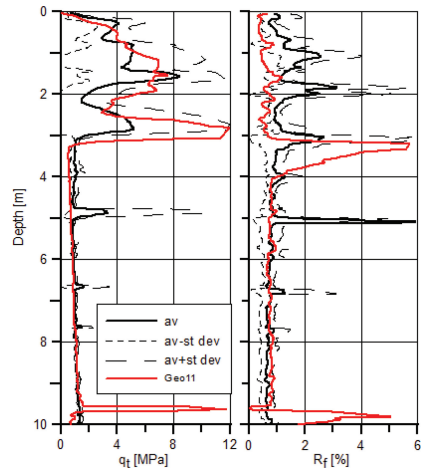

Figure 5. q_t and R_f values at testing point Geo11 on the background of average values and standard deviation intervals calculated for 8 reference CPTUs.

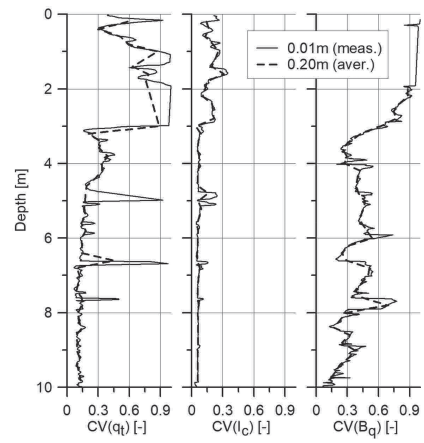

Figure 6. Comparison of the coefficient of variation *CV* of the q_t, I_C, B_q parameters in the group of 8 CPTU in the case of actual measurements conducted every 0.01 m and averaged in 0.2 m intervals.

4.2 *Cluster analysis, separation of homogeneous groups*

In order to select the most statistically homogeneous part of the profile within the AMU-test site, a cluster analysis of all collected data was performed. The analysis was performed using the *k*-means method, according to the methodology presented by Młynarek and others (2007). For this purpose, the CPTU data was standardized and averaged in 0.2-meter thick intervals, resulting in a slight smoothening effect, as shown in Figure 6. Based on the observations of Młynarek and others (2004), the analysis used only dimensionless parameters

characterized by normalization in terms of vertical stress: Q_t, F_r, I_c, B_q. All variables from 9 probe test were treated as one set of data for analysis. The analysis was carried out for 9 solutions, which allowed to obtain from 2 to 10 homogeneous groups within the test site. To choose the most advantageous solution the weighted mean of the coefficient of variation was used (Wierzbicki 2007) (1).

$$CV_{av} = \frac{\sum_1^n (l_n CV_n)}{m} \tag{1}$$

where: CV_{av} – weighted average coefficient of variation of CPTU parameter, n – number of cluster, m – number of data in all clusters, l_n – number of data in n-th cluster, CV_n - coefficient of variation in n-th cluster.

The most optimal division into groups, with the smallest coefficient of variation of individual parameters (mainly B_q) in the largest possible layer, was obtained for 4 or 9 divisions on the whole test site (Fig. 7). In the case of adopting the division into 4 clusters, the soft clay layer between the 3rd and 10th meter of depth is almost entirely represented by cluster 1 (Fig. 8). Division into 9 clusters splits this layer into 3 clusters. However, as the analysis of variability shows, dividing additional clusters causes slight changes in the values of the coefficient of variation within this layer (Table 2). It seems reasonable to accept the hypothesis of considering soft clay as a homogeneous geotechnical layer.

Statistical repeatability of CPTU results in the soft clay layer was analyzed also by determining the significance of differences between two sets of data. One of these sets included 8 probe tests previously used in the cluster analysis, the other one included the results of 1 additional probe test conducted with a different probe by an independent company. In this case the Student's t-test of statistical significance between the means was applied. The values of the measured CPTU parameters were analyzed. Test results confirm, although to various degrees, statistical resemblance of the results of the additional probing to the results of the other tests (Table 3). It is worth noting that statistical resemblance of the results did not change despite the use of a different measuring device.

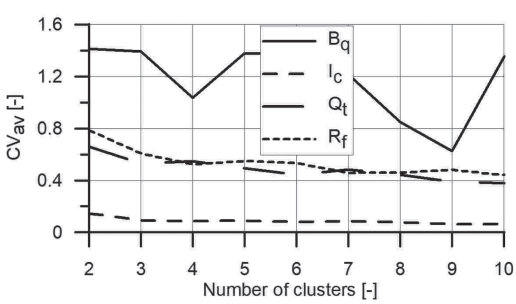

Figure 7. Dependence of the value of average coefficient of variation CV on the number of divisions on the test site.

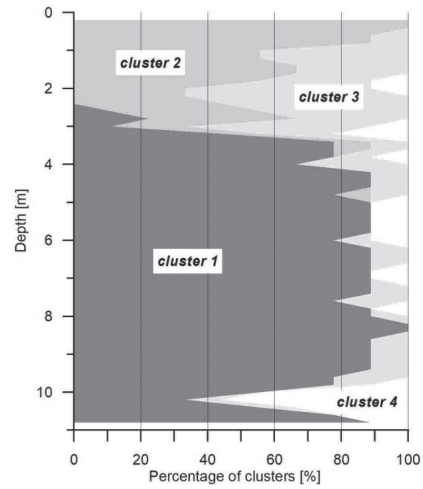

Figure 8. The role of individual clusters in the analyzed soils depending on the depth.

Table 2. The value of the coefficient of variation CV in the soft clay layer with a division into 1 or 3 clusters.

	4 clusters solution	9 clusters solution		
	Cluster 1	Cluster 1a	Cluster 1b	Cluster 1c
N	287	78	144	87
CV of R_f	0.51	0.69	0.49	0.34
CV of I_c	0.07	0.06	0.05	0.05
CV of B_q	0.17	0.09	0.11	0.18
CV of Q_t	0.37	0.22	0.28	0.39

4.3 *Statistical parameters of a homogenous group of soft clay*

Having considered the previously identified homogeneity of the soft clay layer and normality of the distribution of the probe test parameters, basic statistical characteristics of this layer were also determined, including 95% confidence intervals for the mean (Table 4). Analyzing the values of the determined parameters one needs to note that they apply to the layer from the depth range of 3.5 to 9.2 m. In the case of not normalized parameters, the results of this analysis do not take into account the trend with which their values changes with the depth.

Table 3. The results of the statistical significance Student's t-test in the soft clay layer between a group of 8 probe tests and an additional CPTU (the differences are statistically insignificant for $p > 0.05$ according to the Kolmogorov-Smirnov test).

CPTU parameter	p-value for normal distribution (group of 8 CPTU's)	p-value for normal distribution (additional CPTU)	p-value for two groups
q_t	0.41	0.83	0.06
f_s	0.38	0.22	0.10
u_2	0.12	0.10	0.95

Table 4. Descriptive statistics of CPTU parameters determined in the soft clay layer for 8 probe tests.

	Descriptive statistics					
CPTU parameter	N	Mean	–95% con. interv.	+95% con. interv.	Median	St. dev.
q_t [MPa]	198	1.90	1.49	2.30	1.13	2.87
f_s [MPa]	198	0.02	0.01	0.02	0.01	0.03
u_2 [kPa]	198	429.53	402.76	456.30	468.25	191.01
R_f [%]	198	0.81	0.74	0.88	0.83	0.50
I_c [–]	198	2.37	2.32	2.42	2.46	0.35
q_n [MPa]	198	1.79	1.39	2.19	1.01	2.87
B_q [–]	198	0.39	0.37	0.41	0.45	0.17
Q_t [–]	198	50.24	36.28	64.21	20.27	99.62

5 SUMMARY

Test results presented in this paper suggest that the AMU-Morasko test site is an interesting example of a homogenous layer of significantly thick soil found in a large area. Therefore, the soil itself, both intermediate and soft soil, is an interesting and important study subject in practical terms. In addition, many years of opportunities to use this area in the future and planned foundation of buildings in a part of the test site mean that the AMU-Morasko test site should be considered in a long-term perspective.

Currently there are additional DMT, FVT and CPTU tests being conducted at different test speeds and with the use of different devices (Radaszewski & Stefaniak 2017). There are planned down-hole seismic studies, as well as taking high quality undisturbed samples for laboratory testing. The statistical analysis of the analyzed soils will also be expanded with the results of a functional cluster and trend analysis and with the use of Baysian probability in the analysis of data.

REFERENCES

Borowczak P. 2008. O właściwościach gruntów mało spoistych zmieniających się w procesie konsolidacji na podstawie badań pasty gruntowej. Geologia, 34, 4: 594–602.

Chmal R. 1997. Objaśnienia do Szczegółowej Mapy Geologicznej Polski w skali 1:50000 ark. Poznań: 1–31. PIG Warszawa.

Karczewski A. 1976. Morphology and lithology of closen depression area lockated on the north slope of Morasko Hill near Poznań. In Hieronim Hurnik (ed.), *Meteorite Morasko and region of its fall:* 7–19. Wydawnictwo Naukowe UAM Poznań.

Kezdi A., Ladanyi J., Kabai J. 1971. Compaction of transition soils. *Proc. of 4th Int. Conf. on Soil Mechanics, Budapest 1971:* 177–185.

Krygowski B. 1961. Geografia fizyczna Niziny Wielkopolskiej: 1–204. PWN Warszawa.

L'Heureux J.S., Lunne T., Lacasse S., Carroll R., Strandvik S.O. & Ozkul Z. 2017. Norway's National GeoTest Site Research Infrastructure (NGTS). *Proc.of the 19th Int. Conf. on Soil Mechanics and Geotechnical Engineering*, Seoul 2017: 611–614.

Liszkowski J. 1996. Cechy diagnostyczne oraz typowe sekwencje subfacji glin morenowych vistulianu środkowej Wielkopolski. *Geologos, vol. 1:* 159–174. Wydawnictwo Naukowe UAM Poznań.

Lunne, T., Robertson, P.K., and Powell, J.J.M. 1997. Cone penetration testing in geotechnical practice. New York: Blackie Academic, EF Spon/Routledge Publ.

Młynarek, Z., Wierzbicki, J. & Wołyński, W. 2005. Use of cluster method for in situ tests. *Stud. Geotech. Mech*, 27, 3/4: 16–27.

Morawski W. 1984. Osady wodnomorenowe. *Prace Instytutu Geologicznego, vol. 108:* 1–74. Wydawnictwa Geologiczne Warszawa.

PN-EN-ISO 14688 (parts: 1 & 2). 2006. European standard *Geotechnical investigation and testing – Identification and classification of soil (Identification and description – part 1; Principles for a classification – part 2)*. PKN Warszawa.

Radaszewski R., Stefaniak K. 2017. The problem of determining shear strength of intermediate soils. *Przegląd Geologiczny, vol. 65 no. 10/2:* 864–872.

Robertson, P.K. 2009. Interpretation of Cone Penetration Test-ing – a unified approach, Canadian Geotechnical Journal, 46 (11), 1337–1355.

Stankowski W. 2000. Budowa geologiczna i morfologia Rezerwatu Meteoryt Morasko. In J. Biernacka & J. Skoczylas (eds.) *Przewodnik LXXI zjazdu Polskiego Towarzystwa Geologicznego,* Poznań 2000: 394–398. Bogucki Wydawnictwo Naukowe S.C. Poznań.

Stankowski W. 2008. Morasko Meteorite. A curiosity of the Poznań region: 1–94. Wydawnictwo Naukowe UAM Poznań.

TC-16 (1999) ISSMGE International Reference Test Procedure for Cone Penetration Test (CPT) and Cone Penetration Test with Pore Pressure (CPTU).

Wierzbicki, J. 2007. Determination of homogenous geotechnical layers in strongly laminated soil by means of CPTU and cluster analysis. In V. Cuellar et al. (eds.) *Geotechnical Engineering in Urban Enviornment,*. Vol. 5, 575–579. Millpress, Rotterdam.

Cone Penetration Testing 2018 – Hicks, Pisanò & Peuchen (Eds)
© 2018 Delft University of Technology, The Netherlands, ISBN 978-1-138-58449-5

Shear strengths determined for soil stability analysis using the digital Icone Vane

M. Woollard & O. Storteboom
A.P. van den Berg, Heerenveen, The Netherlands

A.S. Damasco Penna
Damasco Penna, São Paulo, Brazil

É.S.V. Makyama
Damasco Penna, São Paulo, Brazil

ABSTRACT: At locations where the soil is exposed to high and varying forces, for example at a dike or around a mining area, additional parameters for stability analysis should often be measured. Determination of the undrained shear strength is a commonly used method to define soil stability. The Field Vane Test (FVT) can be used for in-situ measurement and evaluation of the shear strength. It can be deployed in soft soils, but also in fine-grained soils such as silts, organic peat, tailings and other geomaterials where a prediction of the undrained and remolded shear strength is required. This paper describes a FVT system called Icone Vane, which is part of the Icone® data acquisition concept that is based on fully digital data transfer and meets the requirements of ASTM D2573/ D2573M and other FVT standards. Specific details of fieldwork with the Icone Vane performed at tailings dams are presented.

1 INTRODUCTION

Geotechnical engineers often want to estimate the shear strength and bearing capacity of soils as part of the characterization process. The shear strength of soils determines the maximum load that can be applied on it. The undrained shear strength is commonly used as soil stability parameter and there are different ways to obtain it.

This paper focuses on the comparison between the undrained shear strengths of three Brazilian tailings dams' soils measured using the piezocone penetration test (CPTU) and the field vane test (FVT).

2 PIEZOCONE PENETRATION TEST

The piezocone penetration test is an in-situ method used for determining the geotechnical soil characterization, measuring tip resistance, dynamic pore pressure and sleeve friction during penetration.

The electrical cone is pushed into the soil with a constant rate and produces a continuous profile of soil data. During a pause in penetration, any existing excess pore pressure around the cone will dissipate. The rate of dissipation depends on the compressibility and permeability of the soil. The analogic cone signals are subject to disturbances during transfer to the data logger.

The paper describes a particular digital cone (Icone®) manufactured by A.P. van den Berg, which has been available since 2006. The digital cone, differs from the analog cone by its system in which the analog signals are digitized already inside the cone.

Digitizing means that the analog signals are sampled with frequency and converted into a digital data stream. This digital data stream is more robust and less sensitive to distortion and loss of accuracy in comparison with the analog signals.

Additionally, the Icone is stronger compared to its analog predecessor.

3 ICONE AND CLICK-ON MODULES

In the past five years several click-on modules for the Icone were developed. In this chapter the following three are described: the seismic module (Fig. 1), the conductivity module (Fig. 2) and the magnetometer module (Fig. 3). A fourth application for vane testing is described in chapter 4. All modules except the Icone Vane can be used with a 10 cm^2 and a 15 cm^2 Icone®. When CPT-data is not required, the click-on modules can also be used with a dummy tip instead.

Figure 1. Seismic module with 10 cm² Icone.

Figure 2. Conductivity module with 10 cm² Icone.

Figure 3. Magneto module with 10 cm² Icone.

3.1 *Seismic module*

Seismic tests are performed to investigate the elastic properties of the soil. For this purpose a shear wave (S) or a compression wave (P) is guided into the soil. Elastic soil properties are essential input for prediction of ground-surface motions related to earthquake excitation and for assessment of: foundation design for vibrating equipment, offshore structure behavior during wave loading and deformations around exca-vations.

3.2 *Conductivity module*

The measurement of electrical conductivity in the subsoil is a function of both the conductivity of the pore water and the soil particles, the first being the dominant factor. With the Conductivity module changes in the concentration of (dissolved) electrolytes are determined without specifying the exact nature of these electrolytes. Therefore the module facilitates separation of zones with differentiated water content, including determining the water table depth and the thickness of the capillary zone or separation of fresh and salt water carrying soil layers. Another very important application of the conductivity module is detection of (the degree of) contamination in a soil body. Further soil investigation should provide details on the actual contaminants.

3.3 *Magneto module*

Unknown structures and obstacles, like unexploded ordnance (UXO), are a risk factor in the execution of earthworks. To avoid risks of damage and interruptions of work, these underground elements must be identified and mapped. Most underground structures contain metal such as sheet-piles, ground anchors and pipe lines or a combination of metal and concrete, such as reinforced foundation piles. Power supply cables and above structures have in common that they affect the earth's magnetic field.

Using the Magneto module, metal objects in the underground can be detected by interpreting anomalies of the earth's magnetic field.

4 ICONE VANE

The vane shear test is primarily used to determine the undrained shear strength s_u of saturated clay layers. The test can also be used in fine-grained soils such as silts, organic peat, tailings and other geomaterials where a prediction of the undrained shear strength is required. The Icone Vane meets the requirements of ASTM D2573/ D2573M.

4.1 *Principles*

The FVT consists of four rectangular blades fixed at 90° angles to each other, that are pushed into the ground to the desired depth. This is followed by the measurement of the torque required to produce rotation of the blades and hence the shearing of the soil. The chosen blade size depends on the strength of the soil and the torque capability of the tool; the stronger the soil, the smaller the blades of the vane. So, the vane is being rotated by the drive unit with a constant speed and a maximum torque of 100 Nm. The torque applied to the vane is measured continuously. Both parameters are visualized in a torque vs. rotation graph as shown in Figure 9.

The Icone® Vane has many features that facilitate an accurate vane test. The actuator is integrated in the same compact housing, enabling easier, faster and more accurate operation. The vane is pushed out of its protection tube and retracted again after the test. This advantage

Figure 4. Icone Vane (without protection tube).

allows more vane tests at different depths without the need of retrieving the tool to surface level. The vane rotation speed is adjustable from 0.1 °/s to 12 °/s for fast remoulding.

The vane tool is pushed into the soil by means of standard casing tubes and CPT-rods. Depth is measured on the pushing device and added to the field data by the Icontrol data logger. The Icone Vane can be used for onshore as well as offshore applications.

4.2 *Data processing and visualizing*

During a vane test, the vane is being rotated with a constant speed of 0.1°/s, while the required torque is measured with respect to the angle of rotation. This measured torque is analytically converted to the shearing resistance of the cylindrical failure surface of the vane used, and expressed in kPa. A typical shear curve is shown in Figure 9. The highest value of this curve is a measure for the undrained shear strength of the soil material that is being investigated. A repetition of this test, after thorough remoulding of the soil, provides a uniform curve of which the highest value is a measure of the remoulded shear strength.

5 PRACTICAL EXPERIENCES ICONE VANE

5.1 *Aim of the study*

In November 2015 the greatest environmental disaster in the Brazilian history happened, when a tailings dam in the city of Mariana /MG collapsed and generated a tidal wave of 32 to 40 million cubic meters of mining waste. This washed across villages and farmlands until reaching the shore, several kilometers away.

This happening made other mining companies study their tailings dams, using geophysics, CPTU and FVT. The aim of this study is to present the peak and remolded undrained shear strength of tailings dams' soils by means of CPTU and in three different tailings dams located in the Brazilian state of Minas Gerais.

Figure 5. Pagani TG63 & CME-550X.

5.2 *Equipment used*

The soil investigations were performed using the Icone®) pushed into the soil by a Pagani TG63 rig and the Icone Vane penetrated by a CME-550X. These systems achieve a maximum pushing force of 100 kN, allowing depths of up to 40 m to be reached.

5.3 *Test results*

CPTU has been used in soil exploration and in estimations of the undrained shear strength of soft soils.

The cone responds to in-situ mechanical behavior of the soil and not directly to soil classification criteria based on distribution and soil plasticity. It offers the possibility to classify soil by the type of behavior.

The standard formula used for determination of the undrained shear strength (s_u) using the tip resistance (q_t) values corrected for the pore pressure effect can be written as:

$$s_u = \frac{q_t - \sigma_V}{N_{kt}} \tag{1}$$

where σ_V = total overburden stress and N_{kt} = empirical cone factor.

Typically N_{kt} varies from 10 to 18, with 14 as an average. This value (N_{kt} = 14) was used to estimate the peak shear strength using CPTU.

The remolded undrained shear strength ($s_{u\,(Rem)}$) can be assumed equal to the sleeve resistance (f_S).

The torque of the FVT can be converted to peak shear strength with the following equation:

$$s_u = \frac{0.86M}{\pi D^3} \tag{2}$$

where M = maximum measured torque and D = diameter of the vane.

Similarly, the remolded shear strength is derived using the torque values for the remolded condition.

Figure 6 shows on the left the cone resistance q_t in MPa and the pore water pressure u in kPa, obtained by CPTU in soils of tailings dam no. 1. The cone resistance varies from 3 to 15 MPa. The short peak values of the pore water pressure indicate small non-permeable soil layers.

Figure 6 shows on the right the soil behaviour type SBT obtained by CPTU and the undrained shear strength s_u derived and measured by using CPTU and the FVT respectively, performed in soils of tailings dam no. 1. The SBT-index indicating soil of type silty sand to sandy silt with small layers of clean sand to silty sand and clayey silt to silty clay. The FVT results indicate apparent shear strengths of 100 to 250 kPa. The CPTU and vane tests were carried out at a horizontal spacing of less than 10 m.

Figure 7 shows on the left the cone resistance q_t and pore water pressure u obtained by CPTu in soils of tailings dam no. 2. Again cone resistance varies from approximately 3 to 15 MPa. The pore water pressure is most of the time below the hydraulic pressure, indicating permeable soil layers.

Figure 7 shows on the right the soil behaviour type SBT obtained by CPTu and the undrained shear strength s_u derived and measured using CPTu and the vane tester respectively, performed in soils of tailings dam no. 2. The SBT-index indicating more layers of clean sand to silty sand in comparison with tailings dam no. 1.

Figure 8 shows the cone resistance q_t and pore water pressure u obtained by CPTu in soils of tailings dam no. 3. Also for this tailings dam cone resistance varies from approximately 3 to 15 MPa and at greater depths values go up to 20 MPa. The pore water pressure indicates non-permeable layers at a depth from 20 up to 24 m.

Figure 8 shows on the right the soil behaviour type BST obtained by CPTu and the undrained shear strength s_u derived and measured using CPTu and the vane tester respectively, performed in soils of tailings dam no. 3. The SBT-index indicating soil of type silty sand to sandy silt and at greater depths mostly clayey silt to silty clay.

The vane tests in the tailings dams were performed with a faster rotation rate than usual, in an attempt to achieve undrained conditions.

Figure 9 shows the graph torque vs. rotation in natural and remolded condition at a depth of 12 meters from the ground surface of tailings dam nº3.

The soils tested in tailings dams are composed of very heterogeneous materials and the tip resistances are measured every 1 centimeter in CPTU, which results in a graph with a large range of resistance values along the depth. Different from CPTU, in the vane test the shear strengths are measured at specific pre-determined depths by means of a vane tool of 10 centimeters of height, resulting in one average measurement of the soil layer.

Figure 10 shows the lower limit line of the peak undrained shear strengths range derived from the CPTU data, and derived s_u values for the FVT in soils of tailings dams nº 01, nº 02 and nº 03.

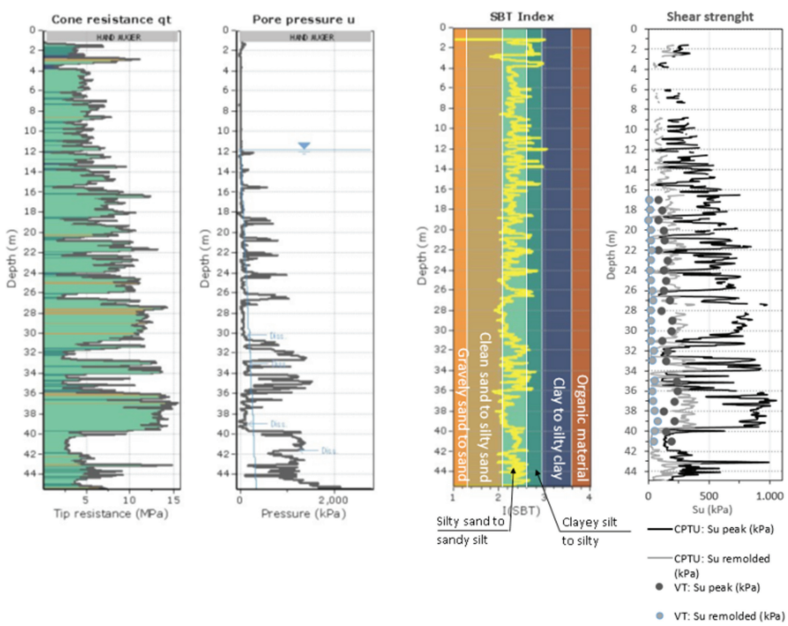

Figure 6. Parameters q_t and u measured along the depth using CPTU (figure left) + Parameters SBT and s_u measured and estimated along the depth using CPTU and vane test (figure right)– Tailings dam nº1.

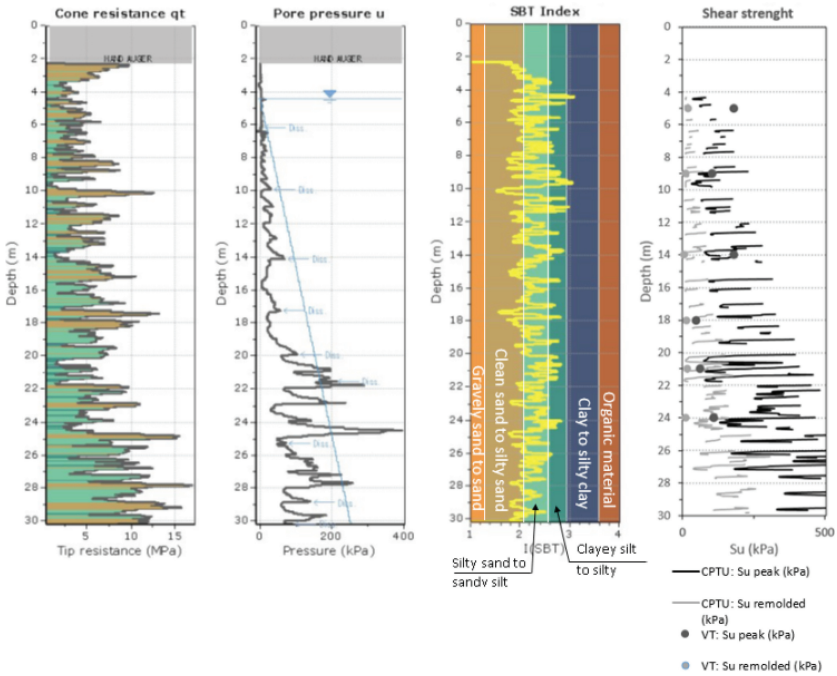

Figure 7. Parameters q_t and u measured along the depth using CPTU (figure left) + Parameters SBT and s_u measured and estimated along the depth using CPTU and vane test (figure right)– Tailings dam nº2.

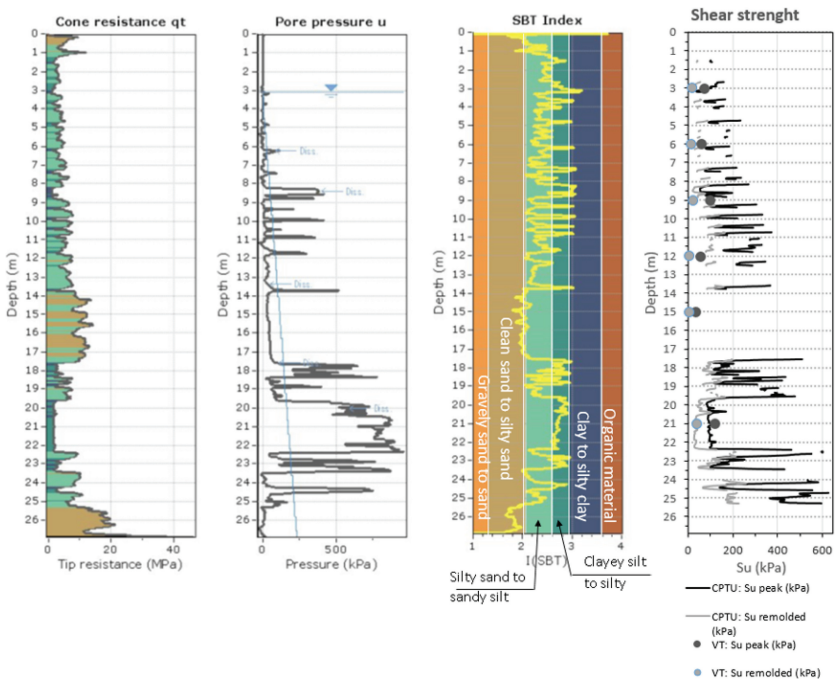

Figure 8. Parameters q_t and u measured along the depth using CPTU (figure above) + parameters SBT and s_u measured and estimated along the depth using CPTU and vane test (figure right)– Tailings dam nº3.

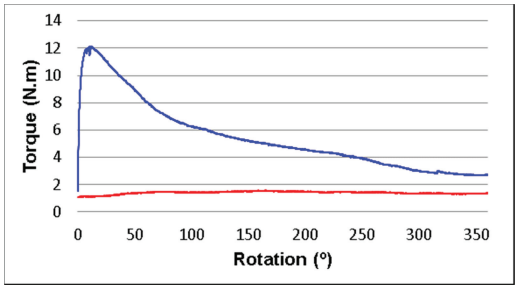

Figure 9. Graph torque vs. rotation in natural and remolded conditions—Depth 12 m—Tailings dam nº3.

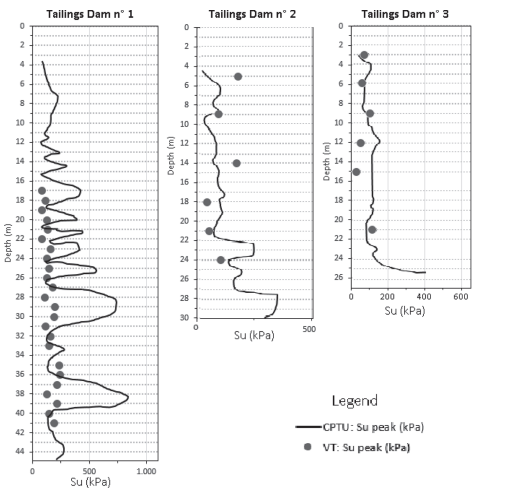

Figure 10. Lower limit line of derived s_u estimated in CPTU and s_u derived using the vane test in soils of tailings dams nº 01, nº 02 and nº 03.

The derived values of undrained shear strength for the CPTU and the FVT show local correlation for some of the zones with low CPTU q_t values.

As shown in the above graphics, the tests were made in soils of predominately silty and sandy nature, where undrained conditions may not have been achieved during the test phases of the CPTU and FVT. If undrained conditions were not achieved, then the equations for deriving undrained shear strength do not apply.

6 CONCLUSIONS

The torque obtained in the Icone® Vane is precise, as the rotation and torque measurement is right above the vane tool.

Figure 10 indicates challenges in characterising the undrained shear strength of three Brazilian tailings dams, primarily because of the silty and sandy nature of the tailings and the associated drainage conditions during CPTU and FVT.

REFERENCES

ASTM International, 2015. ASTM D2573/D2573M-15 Standard Test Method for Field Vane Shear Test in Saturated Fine-Grained Soils. West Conshohocken: ASTM International.

Woollard, M.; Storteboom, O.; Länsivaara, T.; Selänpää, J. 2016.Additional parameters measured in a single CPT, Click-on modules for the digital cone. 6 pages.

Woollard, M.; Storteboom, O.; Loria, M.C. 2014.Additional parameters measured in a single CPT, Click-on modules for the digital cone. 10 pages.

Robertson, P.K.; Cabal, K.L. 2015. Guide to Cone Penetration Testing for Geotechnical Engineering. 6th Edition. 143 pages.

Cone Penetration Testing 2018 – Hicks, Pisanò & Peuchen (Eds)
© 2018 Delft University of Technology, The Netherlands, ISBN 978-1-138-58449-5

Metal objects detected and standard parameters measured in a single CPT using the Icone with Magneto click-on module

M. Woollard & O. Storteboom
A.P. van den Berg, Heerenveen, The Netherlands

L. Gosnell & P. Baptie
1st Line Defence Ltd, Hoddesdon Herts, UK

ABSTRACT: The paper describes a digital CPT system called Icone®. This system is easily extendable by click-on modules to measure additional parameters and any module is automatically recognized by a digital data logger, thus creating a true plug & play system. By moving to smart digital communication, sufficient bandwidth over a thin flexible measuring cable was created to accommodate additional parameters, without the need for changing cones, cables or data loggers. The following click-on modules are described: seismic, conductivity, magneto and vane. Feedback from fieldwork with the Icone and the magnetometer module (Magneto) highlights the user experience with this approach.

Using the magnetometer module, metal objects in the underground can be detected by interpreting anomalies of the earth's magnetic field. The application of this module is illustrated by two unexploded ordnance (UXO) survey projects for clearance ahead of piling.

1 INTRODUCTION

Due to its benefits, digital technology is used in many applications and is now also available to support efficient soil investigation. The possibilities of this technology have led to the development of the digital cone, the digital data logger and digital click-on modules.

2 DIGITAL CONE

The paper describes a particular digital cone (Icone®) manufactured by A.P. van den Berg, which has been available since 2006. The integration of intelligent electronics provides a range of possibilities in order to make further improvements to the electrical cone and to simplify its use. In addition, the Icone was made stronger compared to its analog predecessor.

The Icone basically uses the same measuring sensors as applied in the analog cone. The difference however is that the analog signals are being digitized and multiplexed already inside the cone.

Digitizing means that the analog signals are being sampled with a certain frequency and converted into a digital data stream. This digital data stream is more robust, and therefore less sensitive to distortion and loss of accuracy in comparison with the analog signals.

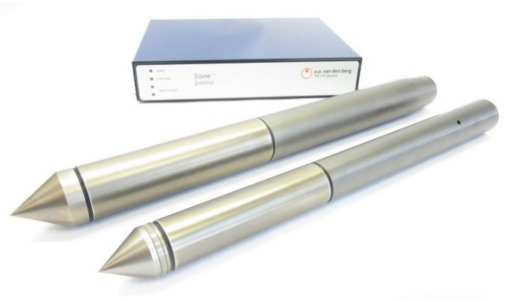

Figure 1. Icone 10 cm^2 and 15 cm^2 area with Icontrol data logger.

By multiplexing, an almost unlimited amount of sensor signals can be combined into one digital data stream and transmitted through a simple 4-wired cable.

A built-in memory capacity increases the user friendliness of the Icone system. For example:

- the Icone number and calibration data are stored inside and are exchanged automatically with the Icontrol data logger.
- Extreme sensor values are stored in memory and can be read for evaluation purposes.
- The memory capacity allows the data storage of a full working day.

The Icontrol data logger provides power to the Icone and synchronizes the Icone signals with the depth signal, recorded from the pushing device. The Icontrol transmits the signals to a computer system, where the CPT-parameters are shown on real time graphs.

The use of smart electronics for the Icone system has provided the following benefits:

- The accuracy of the total data acquisition system is determined only by the accuracy of the Icone and the depth sensor.
- Interchangeable click-on modules with specific sensors can be easily added to the Icone without the need of changing cables and data loggers. These modules are automatically recognized by the Icontrol and the corresponding display is automatically shown on the screen.
- An Icone can be combined with one or more (different) modules.

3 ICONE AND CLICK-ON MODULES

In the past five years several click-on modules for the Icone were developed. In this chapter the following three are described: the seismic module, the conductivity module and the application for vane testing. A fourth application, a magnetometer module, is described in Chapter 4. All modules, except the Icone Vane, can be used in combination with a 10 cm^2 and a 15 cm^2 Icone®. When CPT-data is not required, the click-on modules can also be used with a dummy tip instead.

3.1 *Seismic module*

Seismic tests are performed to investigate the elastic properties of the soil. For this purpose a shear wave (S) or a compression wave (P) is guided into the soil. Elastic soil properties are essential input for prediction of ground-surface motions related to earthquake excitation and for assessment of: foundation design for vibrating equipment, offshore structure behavior during wave loading and deformations around excavations.

Figure 2. Seismic module with 10 cm^2 Icone.

3.2 *Conductivity module*

The measurement of electrical conductivity in the subsoil is a function of both the conductivity of the pore water and the soil particles, the first being the dominant factor. With the Conductivity module changes in the concentration of (dissolved) electrolytes are determined without specifying the exact nature of these electrolytes. Therefore the module facilitates separation of zones with differentiated water content, including determining the water table depth and the thickness of the capillary zone or separation of fresh and salt water carrying soil layers. Another very important application of the conductivity module is detection of (the degree of) contamination in a soil body. Further soil investigation should provide details on the actual contaminants.

3.3 *Vane module*

The vane test is primarily used to determine the undrained shear strength s_u of saturated clay layers. The test can also be used in fine-grained soils such as silts, organic peat, tailings and other geomaterials where a prediction of the undrained shear strength is required. The Icone Vane has many features that facilitate an accurate vane test. The actuator is integrated in the same compact housing, enabling easier, faster and more accurate

Figure 3. Conductivity module with 10 cm^2 Icone.

Figure 4. Icone Vane (without protection tube).

operation. The vane is pushed out of its protection tube and retracted again after the test.

4 MAGNETO MODULE

Unknown structures, obstacles like unexploded ordnance (UXO), and high voltage cables are a risk factor in the execution of earthworks. To avoid risks of damage and interruptions of work, these underground elements must be identified and mapped. Most underground structures are built out of metal such as sheet-piles, ground anchors and pipe lines or a combination of metal and concrete, such as reinforced foundation piles. Power supply cables and above structures have in common that they affect the earth's magnetic field.

Using a magnetometer (Magneto module, Figure 5), metal objects in the underground can be detected by interpreting anomalies of the earth's magnetic field. In addition, the standard CPT-parameters can also be measured if the Icone is mounted in front of the Magneto module.

4.1 *Principles*

The earth's magnetic field consists of power lines that run from North to South. Ferro metallic objects have the property to be influenced by the earth's magnetic field, causing them to act as a magnet themselves. This local magnetic field disturbs the earth's magnetic field in such a way, that the object can be detected and localized with a magnetometer.

The magnetometer sensor used is able to measure magnetic field anomalies in three orthogonal directions with a sensitivity of 0.5 µT. Anomalies can be detected at a distance of 2 meter depending on the size of the object and the position relative to the natural North-South field lines. In practice it is not interesting to know the exact value of the magnetic field, but rather the difference in value at a particular location.

When the Magneto module is used without the CPT-functionality of the Icone, the pushing rate can be increased from 2 cm/s to 20 cm/s. To accurately respond to changes in the measured value, in particular when detecting UXO's, also the gradients of the orthogonal measured anomalies are determined. With the Ifield processing software, alarm values can be set to stop pushing when one of these gradients is exceeded.

Figure 5. Magneto module with 10 cm^2 Icone.

4.2 *Technical specifications*

The technical specifications of the Magneto module are shown in Table 1. The module has a total weight of 4.8 kg.

4.3 *Data processing and visualizing*

The parameters measured by the magneto module are the anomaly of the earth's magnetic field in three orthogonal directions and the inclination relative to the vertical Z-axis. The gradients of the anomalies are determined for analysis and assessment purposes during measurement. The position of the magneto module in the Z-plane at the actual depth is calculated in order to know more precisely the position of the measured object.

The above mentioned parameters and gradients are shown in real time graphs. An example of these graphs is shown in Figure 6.

Table 1. Magneto module technical specifications.

Item	Specification
Length	600 mm without Icone
Diameter	44 mm
Weight	4.8 kg without Icone
Sensors	Magneto: – measuring range 0–100 µT – sensitivity: 0.5 µT Inclination: – measuring range 0°–20° – sensitivity: 0.5°

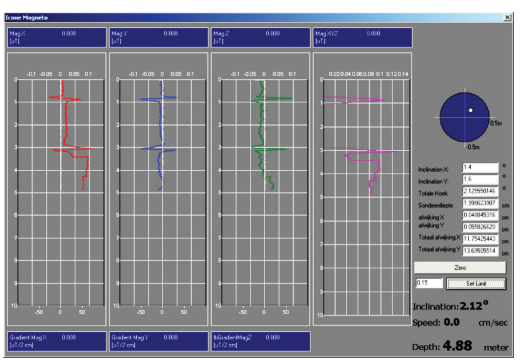

Figure 6. Results of a magneto test.

5 PRACTICAL EXPERIENCES MAGNETO MODULE

5.1 *Background and aim*

The discovery of suspected UXO during construction works and development projects can cause considerable disruption to operations as well as cause unwanted delays and expense. Unexploded ordnance in the UK can originate from three principal sources, including munitions deposited as a result of military training and exercises, munitions lost, burnt, buried or otherwise discarded either deliberately, accidentally or ineffectively, or munitions resulting from wartime activities including bombing in WWI and WWII, long range shelling and defence activities.

The magneto module can be used for UXO Intrusive Survey for clearance ahead of piling. This method permits survey at depths not achievable by non-intrusive survey methods. Anomalies identified during the survey having similar characteristics of an unexploded bomb are then avoided or investigated.

The two notable cases below are an investigation in Sheerness Bridge and Royal Wharf, both located in London and deemed to be medium UXO risk.

5.2 *Methodology & equipment used*

The program of the UXO Intrusive Survey is created based on an assessment of the scope of works for each project. Based on a drawing of the proposed pile layout, the minimum number of probe pushes with the Magneto module is then calculated to determine the length of time required. Each survey can provide a column of clearance with often more than one pile being covered by each survey reducing the overall number of surveys required.

The UXO Intrusive Survey is conducted with a CPT unit which can vary in size from 3.5–20 ton machines. For both case studies, a 20 ton Steyr CPT truck with the Magneto module was used. The CPT truck is positioned at a selected location and the Magneto module is inserted into the ground using hydraulic pressure applied to push rods (Fig. 7).

The sensor is checked and tested at the beginning of each day and the results recorded. During each survey, magnetic field data is recorded real-time on a computer mounted inside the truck. During the survey the computer plots continuous graphical records of magnetic field data. The survey is terminated when the bomb penetration depth for the site is achieved.

On completion of the penetration phase of the test the probe and rods are retracted. As the rods re-enter the test vehicle they are cleaned of soil and fluid by using rubber scrapers fitted in the vehicle's casing hanging beneath the vehicle. Similarly during penetration the rods pass through the cleaning system preventing contaminants present on the rods entering the ground.

Figure 7. Magneto pushed into the soil.

The data is interpreted within the entire nT amplitude capability from Magneto (1 to 100,000 nT). The program defaults the nT amplitude to the largest positive/negative nT value recorded on the survey currently on screen, with the view adjusted. In very clean ground with little ferrous influence, the nT amplitude usually defaults to about 10,000 to 20,000 nT. In ground with a lot of ferrous influence the nT amplitude usually defaults to anywhere between 60,000 and 100,000 nT.

Considerations must be in place when carrying out each survey test, including ground conditions, tonnage, inclination, speed of test, and any magnetic influence. Each test is carried out at a speed of 10 cm/s depending on the considerations above. The test is stopped once 5–6 tons of consistent pressure is applied, but this can also vary based on the density and conditions of the surround strata.

If an anomaly is identified during the survey works, additional data may be required as a confirmatory measure. This will require additional survey positions to the agreed works. This process is referred to as 'triangulation', a procedure to collect additional data in order to pinpoint the anomaly. Once the location has been identified, further investigation can be carried out in order to determine the identity of the object.

5.3 *Case study 1: Sheerness bridge*

5.3.1 *Purpose of investigation*

In February of 2017, a UXO magnetometer survey was carried out ahead of construction piling locations. A detailed UXO risk assessment was carried out earlier, which showed a risk that the site may have been contaminated with items of both Ger-

man and British unexploded ordnance. The aim of the intrusive survey was to minimize the risk that magnetic anomalies, which may have indicated the presence of unexploded ordnance, were located at proposed pile positions.

5.3.2 *Test method*

The positions were set out by a site engineer using the GPS coordinates obtained from the drawing as indicated in Figure 8.

Each test was carried out by pushing to the maximum bomb penetration depth (specific to each location depending on the strata). The live data was first quality assurance checked by the on-site Explosive Ordnance Disposal Engineer in attendance, with the interpretation carried out by geophysicists.

5.3.3 *Test results*

One investigation at position 372 presented a ferrous anomaly that covered two individual pile locations, see Figure 8 (pile locations not indicated). The Magneto test as given in Figure 9 shows an anomaly between 5.2 and 6.2 m depth. Additional testing was requested in order to collect more data; position 172A and 172B were investigated directly where the piles should be positioned. These tests resulted in the anomaly being present on position 172A as indicated in Figure 10.

Due to the depth of the object at approximately 6.5 m, a series of temporary works were carried out. Shoring was used, which allows excavations to be completed in a controlled safe manner. This allowed Explosive Ordnance Disposal engineers to locate the anomaly at staged intervals with hand-held magnetometers.

The item in turn was identified to be part of a pre-existing old pile location as shown in Figure 11. The item was deemed safe and allowed the customer to carry on with works and proceed with building the bridge.

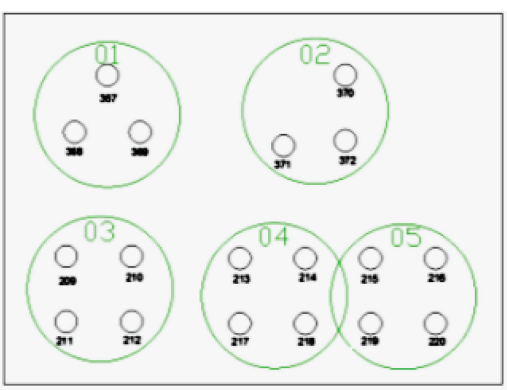

Figure 8. Drawing to set test positions.

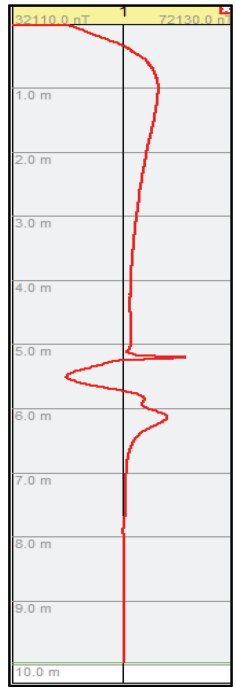

Figure 9. Magneto test position 172.

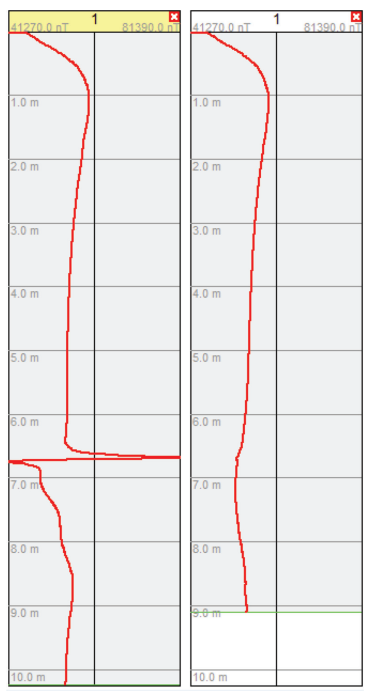

Figure 10. Additional test positions 172A & 172B.

5.4 *Case study 2 – Royal Wharf*

5.4.1 *Purpose of investigation*

Royal Wharf, an area in London was assessed as medium UXO risk. Again, the aim of the survey was to minimize the risk that magnetic anomalies were located at proposed pile positions.

5.4.2 *Test method*

The same test method as in Case Study 1 was applied.

Figure 11. Item located at 5.2–6.2 m depth position 172A.

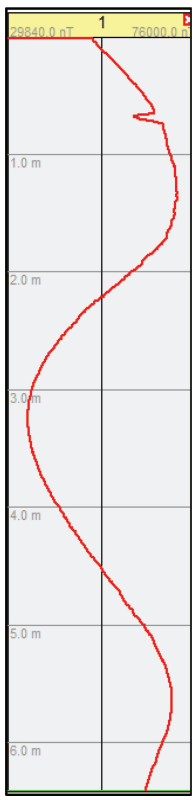

Figure 12. Data trace of 2.5 m ferrous anomaly.

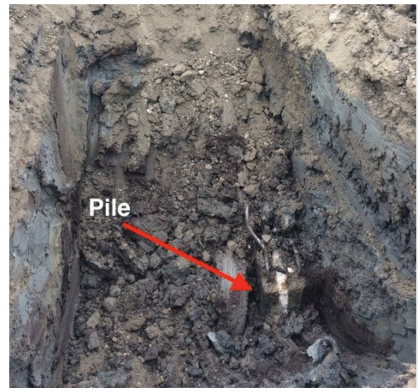

Figure 13. Item causing ferrous influence at Royal Wharf.

5.4.3 *Test results*

An anomaly was detected during the push of the (Icone®) Magneto module starting at a depth of 2.5 m which spanned the entire depth of survey, see Figure 12.

This particular object presented bomb like characteristics and was required to be investigated to make a visual identification of the object.

The position was investigated using a series of 200 mm staged excavations in order to determine the cause of the influence. This was overseen by an Explosive Ordnance Disposal Engineer, who exposed the item at 2.5 m which was identified as an existing steel-reinforced concrete pile as shown in Figure 13. This allowed 1st Line Defence and the customer to confirm the ferrous anomaly was not unexploded ordnance and to carry on with the deep intrusive works.

6 CONCLUSIONS

CPT systems are in the course of time continuously improved by the effective use of the latest state of the art. Developments include the application of digital electronics inside the cone, offer a range of new features and benefits. One of these is the ability to easily extend CPTs by click-on modules to measure additional parameters. This paper describes a particular system that allows any click-on module is to be automatically recognized by a data logger, creating a true plug & play system. Case studies for a magnetometer click-on module called " Icone® Magneto", which can directly detect metal objects in the underground by interpreting anomalies of the earth's magnetic field. In addition, the standard CPT-parameters can also be measured if a CPT penetrometer is mounted in front of the Magneto module. The risk of UXO asks for extra

precautions and a controlled and precise way of working, whereby alarm values incorporated in the data acquisition software allow to stop pushing when one of specific variables is exceeded. When an anomaly is detected additional investigation is necessary to determine the exact location.

UXO survey with the (Icone) Magneto module has proven to give reliable results. In both case studies an anomaly was detected at a particular position. By additional investigation, the exact location could be stated and the item could be unearthed and identified, after which the customer could carry on with the deep intrusive works.

REFERENCES

Brouwer, J.J.M. 2007. In-situ soil testing. HIS BRE Press.

Lunne, T, Robertson P.K. & Powell J.J.M. 2004. Cone Penetration Testing. Sponn press.

Schnaid, F. 2009. In situ testing in Geomechanics, the main tests. Taylor & Francis.

La Rochelle, P., Zebdi, P.M., Leroueil, S., Tavenas, F. & Virely, D. 1988. Piezocone Tests in Sensitive Clays of Eastern Canada. *Proceedings of the International Symposium on Penetration Testing*, ISOPT-1, Orlando, 2, Balkema Pub., Rotterdam., 831–841.

Randolph, M.F. & Wroth, C.P. 1979. An analytical solution for the consolidation around a driven pile. *Int. Journal for Num. and Anal. Methods in Geomech.* Vol. 3, pp. 217–229.

Wroth, C.P. 1984. The interpretation of in situ soil tests. *Geotechnique*, 34(4) 449–488.

Vesic. A.S. 1972. Expansion of cavities in infinite soil mass. Journal of the Soil Mechanics and Foundation Division, *Proc. of the ASCE,* Vol. 98, No. SM3., 265–290.

Woollard, M., Storteboom, O. & M. Coto Loria 2013. Additional Parameters Measured in a Single CPT, Click-on Modules for the Digital Cone. *Proc., Geotechnics for sustainable developments: Geotec Hanoi 2013*, Hanoi, Vietnam, 899–908.

Taylor & Francis
Taylor & Francis Group
http://taylorandfrancis.com

Cone Penetration Testing 2018 – Hicks, Pisanò & Peuchen (Eds)
© 2018 Delft University of Technology, The Netherlands, ISBN 978-1-138-58449-5

Simulation of liquefaction and consequences of interbedded soil deposits using CPT data

Fred Yi
Terracon Consultants, Inc., Colton, CA, USA

ABSTRACT: Several corrections have been proposed since 1990s for the interpretation of liquefaction potential and analysis of the consequences of liquefaction based on cone penetration test (CPT) measurements. However, few publications address how these factors affect the calculation results. In this study, extensive studies of soil liquefaction and its consequences were performed using selected CPT data from two sites located within 7 km of the fault rupture of the 1999 Kocaeli, Turkey earthquake ($M_w = 7.5$). The effects of thickness of interval for averaging, thin layer correction and transition zone were examined in detail.

1 INTRODUCTION

Although simplified procedures of liquefaction evaluations have proved to be effective tools for sandy soils (Youd & Idriss, 2001; Idriss & Boulanger, 2008; Yi, 2010), at sites dominated by clayey and sandy silt layers, several cases have been reported where the ground surface settlement observed was substantially smaller than the settlement predicted by currently used methods (Lew & Tran, 2012). It has also been reported that the engineering procedures currently used to evaluate liquefaction consequences appear to have a tendency to over-predict liquefaction effects in interbedded sand, silt, and clay deposits (Youd et al., 2009; Boulanger et al., 2016).

In this paper, extensive studies of soil liquefaction and its consequences were performed using selected CPT data from two sites composed of interbedded sand, silt, and clay deposits and located within 7 km of the fault rupture of the 1999 Kocaeli, Turkey earthquake. At these sites, liquefaction should have occurred but and no discernible movements were observed (Youd et al., 2009). Due to their simplicity, ease of application and cost effectiveness to field engineers, traditional simplified procedures were used in this study. Various issues, such as calculating layer thickness, correcting for thin layers, and correcting for transition zones, were examined in detail. The intent was to provide guidance to engineers in the use of simplified procedures for various site conditions encountered in their projects. Based on the current simplified procedures, suggestions and recommendations were made to engineers in the use of computer-based liquefaction calculation software for CPT data. This paper will also discuss future research needs and improvements to the evaluation of the consequences of liquefaction of interbedded soil deposits.

2 STUDIES RELATED TO INTERBEDDED DEPOSITS

One of the main advantages of CPT is the continuous nature of the test results, usually in 2 cm or 5 cm intervals in USA, which provide excellent profiles of soil type, detailed stratigraphy, and in situ mechanical properties of the ground (Robertson, 2011). This allows geotechnical engineers to characterize very thin interbedded soil layers. However, for thin interlayered soil profiles, the continuous nature of CPT data can present challenges in interpretation and liquefaction analysis. Various corrections have been proposed since the 1990s (Vreugdenhil et al., 1994; Robertson & Fear, 1995; Idriss & Boulanger, 2008; Robertson, 2011).

The first correction is for cone penetration resistance in thin soil layers. Studies show that cone resistance is influenced by the soil ahead of and behind the penetrating cone. Robertson & Fear (1995) pointed out that thin sand layers embedded in soft clay deposits are often incorrectly classified as silty sands based on CPT soil behavior type (SBT) charts. Correcting for tip resistance could improve soil classification. Figure 1 shows the correction of CPT tip resistance based on studies originated by Vreugdenhil et al. (1994) and further improved by Robertson & Fear (1995), Youd et al. (2001), and Idriss & Boulanger (2008).

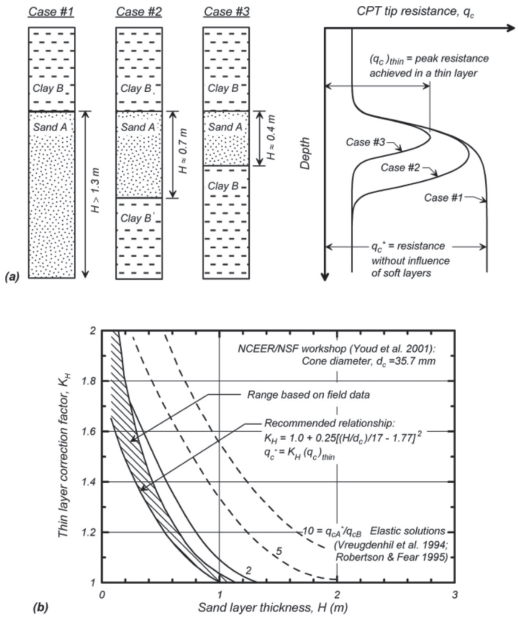

Figure 1. Thin-layer correction factor (K_H) for determining equivalent thick-layer CPT tip resistance: (a) a schematic of thin-layer effects and (b) the relationship recommended in Youd et al. (2001) (after Idriss & Boulanger 2008).

In a thin interbedded soil layer profile, the change of soil type from one soil layer to another (e.g., from a sand to a clay) is called a *transition zone*. In liquefaction analysis, CPT data within the thin transition zone can result in misinterpretation of soil type, which may, in turn, suggest that the soil in the transition zone has the potential to liquefy, resulting in conservative additional calculated post-earthquake deformations (Robertson, 2011). The transition zone can be automatically detected and removed with computer-based CPT analysis software using following criteria:

$$Transition\ zone = \frac{\left|(I_c)_j - (I_c)_i\right|}{\left|Z_j - Z_i\right|} > \left(\frac{\Delta I_c}{\Delta T}\right)_{cri} \qquad (1)$$

where $(I_c)_i$ and $(I_c)_j$ are SBT Index at layer i and j; Z_i and Z_j are corresponding depths. ΔI_c is the I_c change in given thickness ΔT, both defined by user. Figure 2 illustrates transition zones (sections in red color) automatically detected, where $(\Delta I_c/\Delta T)_{cri}$ = 0.30/0.12 m.

In CPT calculations, the calculation layer thickness is usually larger than the CPT data interval. Boulanger et al. (1995 & 1997) used a "*critical* $q_{c\text{-}1}$," which is the averaged tip resistance within the

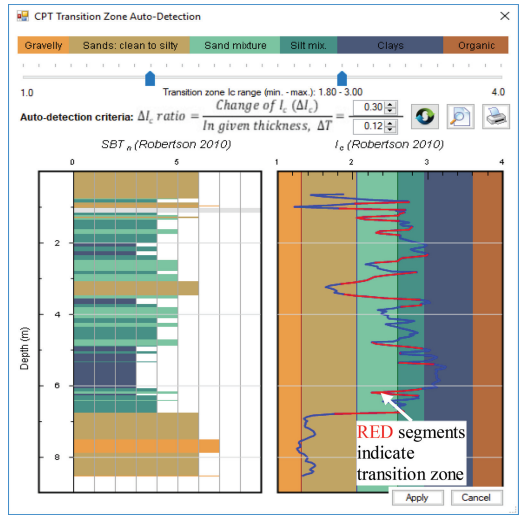

Figure 2. Illustration of automatically identified transition zone (red line segments of I_c profile) of interlayered soil profile by computer software.

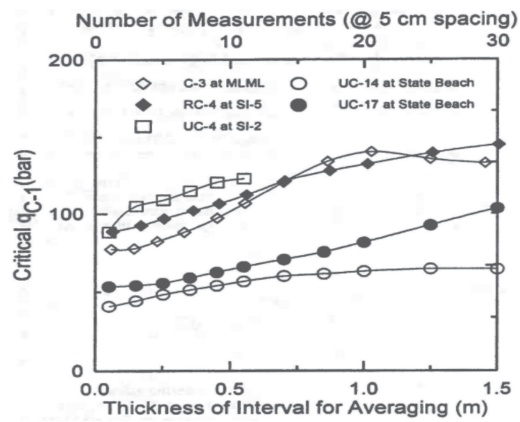

Figure 3. Critical CPT tip resistance vs. thickness of interval used for averaging (after Boulanger et al., 1997).

"*thickness of interval for averaging.*" Figure 3 shows the critical q_c versus the thickness of interval for averaging from five CPT profiles.

Boulanger et al. (1997) stated that "a reasonable averaging interval is probably about 0.6 m because continuous layers of this thickness can be a source of significant deformations." They selected 0.6 m as the guideline for determining critical q_c. This guideline is probably correct for relatively thick sandy layer soil profiles. However, for thin interlayered soil deposits, a smaller thickness of interval for averaging should be used.

Although these corrections and considerations have been carried out by researchers for decades, little literature is available for how these factors quantitatively affect the CPT calculation results, for example, liquefaction-induced settlement and lateral spreading. In this study, the author intended to examine the effects of these factors in detail by simulating various sites that consist of interbedded soil deposits and experienced strong shaking during 1999 Kocaeli, Turkey, earthquake.

3 1999 KOCAELI, TURKEY, EARTHQUAKE

On August 17, 1999, a magnitude 7.5 earthquake struck Kocaeli, Turkey. It was one of the most destructive earthquakes in Turkey. According to Barka et al. (2002), more than 10,000 km^2 of land, an area stretching from Duzce to Istanbul and home to 15 million people and about 40 percent of Turkish industry, experienced forcible shaking. The earthquake generated a 126-km-long fault rupture that extended across four segments of the North Anatolian Fault. The surface rupture was generally characterized by right-lateral strike slip with a maximum displacement of 5.5 m and average displacement greater than 1 m. Peak ground accelerations recorded on rock and stiff soil within 20 km of the fault rupture ranged from 0.2 to 0.4 g (Youd et al., 2009).

Detailed research into the damages and the consequences of this earthquake was performed and documented by the Pacific Earthquake Engineering Research Center (PEER) (http://peer.berkeley.edu/ publications/turkey/adapazari/). In this earthquake, three sites located within 7 km of the fault rupture exhibited negligible displacement. Youd et al. (2009) performed detailed studies for those sites. Two of the sites, Çark Canal and Cumhuriyet Avenue in Adapazari, which were underlain by fine-grained sediment, were analyzed in this study. The details of the damage can be found from Youd et al. (2009). According to Youd et al. (2009), several buildings near Çark Canal penetrated as much as 100 mm into the underlying fine-grained sediment, and several four-story buildings along Cumhuriyet Avenue penetrated as much as 170 mm into softened or liquefied sediment(Bray et al., 2001), indicating that liquefaction or cyclic ground softening occurred. No other surface manifestations were observed during post-earthquake investigations. Both standard penetration test (SPT) boreholes and CPT soundings were performed by the research group. The CPT sounding data used in this study were downloaded from http://peer.berkeley.edu/publications/turkey/ adapazari/phase4/cark/ index.html.

4 SIMULATION OF INTERLAYERED SOIL DEPOSIT

Data from CPT 1–22 and CTP 1–24 from Çark Canal and CPT 4–24 from Cumhuriyet Avenue were studied in detail. All CPT data obtained during PEER post-earthquake investigations had been recorded every 2 cm during penetration. Figure 4 shows the typical non-normalized SBT of CPT 4–24. In USA, CPT readings are typically taken at 2 cm or 5 cm (Mayne, 2007). In order to confirm the effect of the recording interval, data from one CPT sounding (CPT-1) from a Southern California site (SoCal) that recorded at every 5 cm during penetration, were also analyzed.

Liquefaction-induced settlement and lateral spreading were selected as the quantitative parameters for examining affecting factors. In order to maintain the consistency of the methods, liquefaction potential was calculated in accordance with Robertson & Wride (1998); the liquefaction-induced settlement calculation and lateral spreading calculation were based on Zhang et al. (2002 and 2004, respectively).

4.1 *Averaging thickness of calculation*

The effect of averaging thickness in the calculation was studied first. In order to accommodate different CPT recording intervals, a *CPT recording interval multiplier (RIM)*, *n*, was introduced:

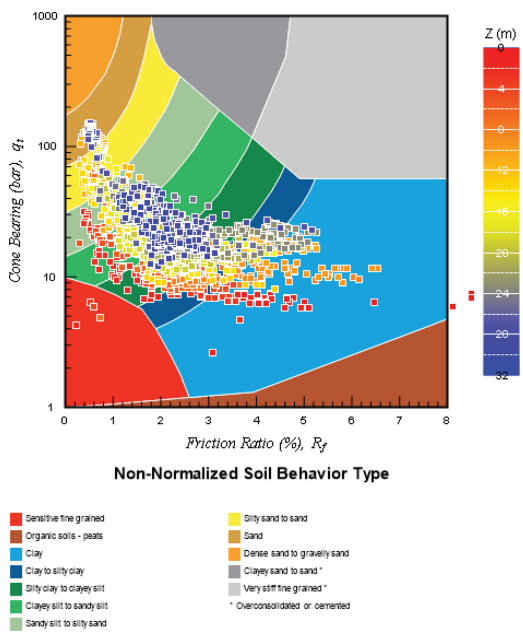

Figure 4. Non-normalized Soil Behavior Type of CPT 4–24.

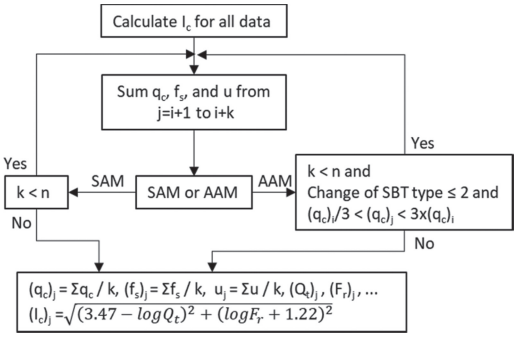

Figure 5. Flowchart indicating SAM and AAM methods.

$$n = \Delta T / \Delta t \tag{2}$$

where, ΔT is the calculation averaging thickness and Δt is the recorded CPT data interval.

Two calculation sublayer averaging methods were utilized: 1) simple averaging method (SAM) and 2) advanced averaging method (AAM). Figure 5 shows the algorithm of the methods.

Calculations were performed for the four CPT profiles. For all four profiles, the results indicate that, when *RIM n* is less than 4, both methods basically average the same number of measurements. As *n* increases, AAM catches some of the thin layers. However, no significant difference is exhibited within the calculated liquefaction-induced settlement or lateral spreading. The differences are generally within ±10 percent for Δt of 2 cm and within ±20 percent for Δt of 5 cm when *n* varies from 1 to 12. The calculations discussed hereafter are all based on AAM.

The comparison of the typical CPT profile (normalized SBT_n, q_c, sleeve friction f_s, and SBT Index I_c) for n = 1 and 12 is shown in Figure 6 for CPT 1–24 profile from Çark Canal with Δt of 2 cm. It is clear that with a large value for *n*, the thin layers measured are eliminated. *RIM n* of 12 corresponds to ΔT of 0.24 m and 0.60 m for Δt of 2 cm and 5 cm, respectively. Boulanger et al. (1997) suggest that ΔT of 0.6 m (based on Δt = 5 cm data) is the most reasonable averaging interval. It seems that ΔT of 0.6 m overly eliminated the thin layers, the most important advantage of the CPT sounding method. These results also indicate that the *thin layer elimination* in averaging seems independent of Δt.

The effects of *RIM* are shown in Figure 7 in calculated liquefaction-induced settlement normalized to that at *n=1* versus *n* value. Generally speaking, the liquefaction-induced settlement is not significantly affected by averaging for *n* up to

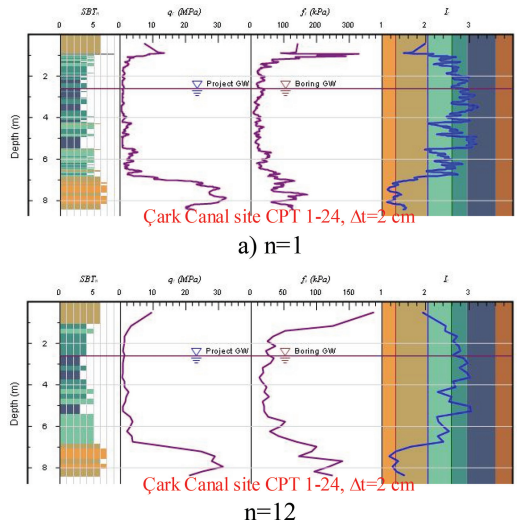

Figure 6. Comparison of CPT profiles for a) n = 1 and b) n = 12.

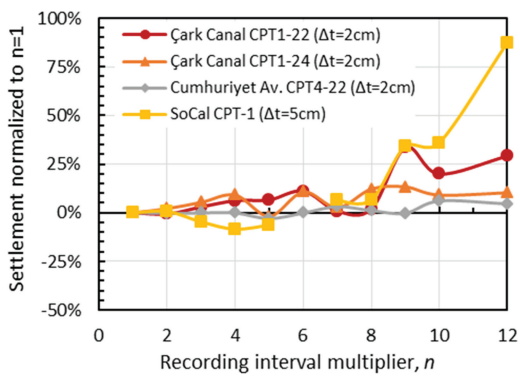

Figure 7. Liquefaction-induced settlements versus *RIM, n*.

8 and is significantly affected when *n* is larger than 8. This tendency is independent of Δt. An extreme value was encountered in CPT-1 results at *n=6* and was removed in Figure 7 in order to generalize the effects.

Based on these results, a *RIM* value of larger than 8 should not be used in the averaging calculations. This author recommends *n* be between 2 and 5.

4.2 *Thin layer correction*

The penetration resistance from CPT is influenced by the strength and stiffness of the soils around the actual penetration interval. The zone of influence may be about 20–50 cm for a CPT (Idriss & Boulanger, 2008). Thin layer correction is proposed to

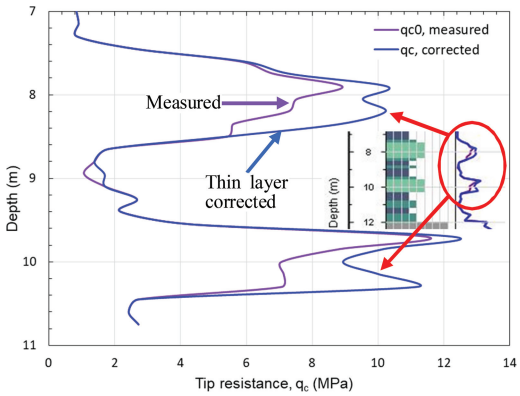

Figure 8. Illustration of thin layer correction.

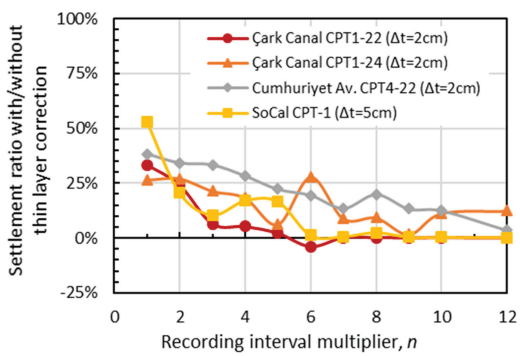

Figure 9. Effect of thin layer correction expressed in percent of change of liquefaction-induced settlement relevant to value without correction as a function of *RIM*.

correct the influence of the weaker layer ahead of the CPT cone. Figure 8 illustrates typical thin layer correction results based on the algorithm shown in Figure 1.

The influence of thin layer correction on liquefaction-induced settlement is shown in Figure 9, expressed in percent of change of liquefaction-induced settlement due to thin layer correction relevant to the value without correction as a function of *RIM*. It can be seen that thin layer correction generally increases the liquefaction-induced settlement within 20 percent for most cases. This effect decreases with the increase in *RIM* value because at larger *n* values, the thin layers are eliminated.

The increase of liquefaction-induced settlement after thin layer correction can be explained as follows.

Due to the zone of influence during cone penetration, the discrete measurements taken near the interface between soils of significantly different strengths and stiffness may not be representative of either soil. As such, the transition layer above a clay layer may be classified as clay when calculated based on the original measurements as shown in the upper portion of Table 1. After thin layer correction, tip resistance increases. The SBT zone changes from non-liquefiable clayey soil ($I_c \geq 2.6$) to liquefiable silty soil ($I_c < 2.6$). This is shown in the lower portion of Table 1.

4.3 *Transition zone correction*

The transition zone correction is simply for automatically detecting the thin transition zone (e.g., from a sand to a clay or from a clay to a sand) by removing it from calculations of liquefaction

Table 1. Changes of SBT after thin layer correction.

Calculation based on measured tip resistance										
Z_b(m)	q_c	*SBT*	I_c	$(SBT)_{1c}$	$CSR_{7.5}$	$CRR_{7.5}$	*FS*	γ_{max}(%)	ε_v(%)	ΔS_I (*cm*)
5.03	898.5	5	2.87	4	0.24	0.70	2.00			0.0000
5.05	898.5	5	2.86	4	0.24	0.70	2.00			0.0000
5.07	898.5	5	2.87	4	0.24	0.74	2.00			0.0000
5.09	898.5	5	2.88	4	0.24	0.70	2.00			0.0000
5.11	951.3	5	2.88	4	0.24	0.70	2.00			0.0000
Calculation based on thin layer corrected tip resistance										
Z_b(m)	q_c	*SBT*	I_c	$(SBT)_{1c}$	$CSR_{7.5}$	$CRR_{7.5}$	*FS*	γ_{max}(%)	ε_v(%)	ΔS_I (*cm*)
5.03	1,477.3	5	2.57	5	0.22	0.10	0.46	32.752	3.48	0.0695
5.05	1,501.3	5	2.59	5	0.22	0.10	0.45	35.267	3.64	0.0728
5.07	1,525.8	5	2.59	5	0.22	0.10	0.45	34.353	3.58	0.0716
5.09	1,550.8	5	2.59	5	0.22	0.10	0.45	33.516	3.53	0.0705
5.11	1,668.9	5	2.58	5	0.22	0.10	0.47	31.511	3.39	0.0679

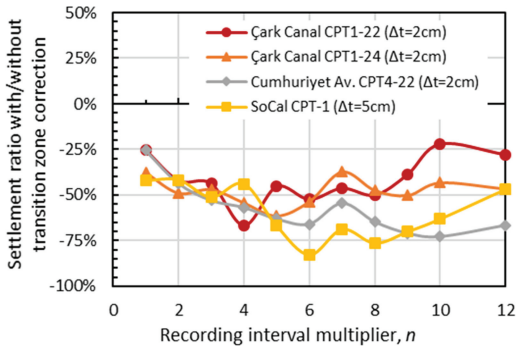

Figure 10. Effect of transition zone removal expressed in percent of change of liquefaction-induced settlement relevant to value without transition zone removal as a function of *RIM*.

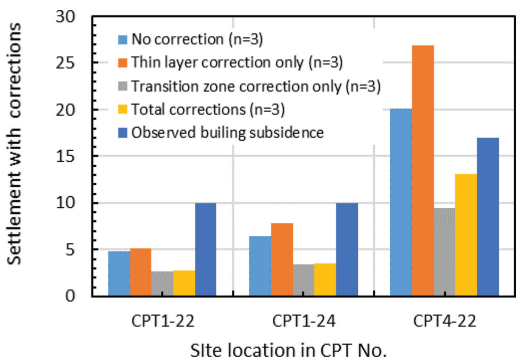

Figure 11. Estimated liquefaction-induced settlements compared to observed building subsidence.

potential and its consequences. Figure 2 illustrates the "CPT Transition Zone Auto-Detection" tool in computer software. The transition zones detected are shown in red line segments on the I_c profile. The user can confirm the transition zones graphically by changing the ΔI_c and ΔT and refreshing the calculations.

Figure 10 shows the effect of transition zone correction, expressed in percent of change of liquefaction-induced settlement relevant to value without transition zone removal. Obviously, liquefaction-induced settlement decreases with transition zone correction. The results shown in Figure 10 indicate that this decrease ranges from approximately 40 percent to 75 percent depending on *RIM*, *n*. For the recommended *n=2* to *5*, the average decrease is about 50 percent. In other words, estimated liquefaction-induced settlement will be reduced to half after transition zone correction.

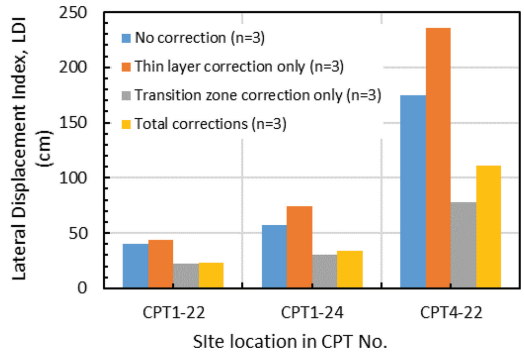

Figure 12. Estimated lateral displacement index.

4.4 *Estimated liquefaction-induced settlement*

The estimated liquefaction-induced settlements are compared with observed building subsidence in Figure 11. At the Çark Canal site, the estimated liquefaction-induced settlement is 2.8 cm at CPT 1–22 (35 m from the channel) and 3.5 cm at CPT 1–24 (9 m from the channel). These values are approximately 30 percent of the observed building subsidence. These results seem reasonable because the estimated settlement is for free field while the observed building subsidence included settlement caused by building load and ground softening. The calculated liquefaction severity numbers (LSN) (Tonkin & Taylor Ltd, 2013) indicate "little to no expression of liquefaction, minor effects" for both CPT locations. This accords with the fact that no sand boils were observed.

The calculated liquefaction-induced settlement is 13.1 cm at CPT 4–22, the Cumhuriyet Avenue site, about two-thirds of the observed building subsidence. The LSN number indicates "moderate expression of liquefaction." The calculated settlement seems reasonable, but other surface manifestation does not agree with field observation except the building subsidence.

4.5 *Estimated lateral spreading*

Lateral spreading was also analyzed, expressed as *lateral displacement index* (*LDI*). Figure 12 shows the *LDI* results and the effects of corrections. The calculated *LDI* ranges from 23 to 34 cm for the Çark Canal site and 110 cm at Cumhuriyet Avenue. These results do not agree with field observations.

5 CONCLUDING REMARKS

Detailed simulations were performed for CPT profiles underlying interbedded sand, silt and clay

deposits using current liquefaction evaluation procedures and the consequence calculation methods. Effects of averaging thickness, thin layer correction and transition zone correction were examined in detail. The effect of averaging thickness was discovered to be independent of the CPT data recording interval. A *RIM* (*n*) value larger than 8 should not be used, and *n=2* to *5* is recommended.

Thin layer correction tends to increase liquefaction-induced settlement predictions and *LDI* and may result in over-prediction. The simulation results indicate that liquefaction-induced settlement of interbedded soil deposits can be reasonably predicted using current procedures and methods, provided both thin layer and transition zone corrections are made. However, lateral spreading results do not agree with field observations for interbedded soil deposits. Further research is needed for this topic.

REFERENCES

Barka, A., et al. (2002) "The surface rupture and slip distribution of the 17 August 1999 İzmit Earthquake (M 7.4), North Anatolian Fault." Bull. Seismol. Soc. Am., 92(1), 43–60.

Boulanger, R.W., et al. (2016) "Evaluating liquefaction and lateral spreading in interbedded sand, silt, and clay deposits using the cone penetrometer." 5th Int. Conf. on Geotechnical and Geophysical Site Characterisation, Gold Coast, Australia.

Boulanger, R.W., Idriss, I.M., and Mejia, L.H. (1995) "Investigation and Evaluation of Liquefaction Related Ground Displacements at Moss Landing during the 1989 Loma Prieta Earthquake." Report No. UCD/CGM-95/02, UC Davis.

Boulanger, R.W., Mejia, L.H., and Idriss, I.M. (1997) "Liquefaction at Moss Landing During Loma Prieta Earthquake." J. Gotech. Geoenviron. Eng., 1997, 123(5): 453–467.

Bray, J.D., et al. (2001) "Documenting incidents of ground failure resulting from the August 17, 1999 Kcaeli, Turkey Earthquake." PEER Center, http://peer.berkeley.edu/ publications/turkey/adapazari/index.html April 28, 2003.

Idriss, I.M., and Boulanger, R.W. (2008) "Soil Liquefaction During Earthquake", Earthquake Engineering Research Institute, EERI Publication MNO-12.

Lew, M., and Tran, L. (2012) "Case History of Observed Liquefaction-Induced Settlement versus Predicted Settlement", Proc., 15th World Conference on Earthquake Engineering, Lisbon, Portugal, 2012.

Mayne, P. (2007) "Cone Penetration Testing", NCHRP Synthesis 368, Transportation Research Board, Washington, D.C.

Robertson, P.K., and Fear, C.E. (1995) "Liquefaction of sands and its evaluation." Proc., 1st Int. Conf. on Earthquake Geotech. Engrg.

Robertson, P.K., and Wride, C.E. (1998) "Evaluating cyclic liquefaction potential using the cone penetration test", Canadian Geotechnical Journal, 35: 442–459.

Robertson, P.K. (2011) "Automatic software detection of CPT transition zones." Geotechnical News, June, 2011.

Tonkin & Taylor Ltd. (2013) "Liquefaction vulnerability study", Report prepared for Earthquake Commission, New Zealand.

Vreugdenhil, R., Davis, R., and Berrill, J. (1994) "Interpretation of cone penetration results in multilayered soils." Int. J. Numer. and Analytical Methods in Geomech., 18, 585–599.

Yi, F. (2010) "Procedure to Evaluate Liquefaction-Induced Settlement Based on Shear Wave Velocity", The 9th U.S. National and 10th Canadian Conference on Earthquake Engineering (9USN/10CCEE), Toronto, Canada.

Youd, T.L., et al. (2009) "Zero-Displacement Lateral Spreads, 1999 Kocaeli, Turkey, Earthquake", J. Gotech. Geoenviron. Eng., 2009, 135(1): 46–61.

Youd, T.L., and Idriss, I.M. (2001) "Liquefaction Resistance of Soil: Summary Report from the 1996 NCEER and 1998 NCEER/NSF Workshops on Evaluation of Liquefaction Resistance of Soils", J. Gotech. Geoenviron. Eng., Vol 127(4), April 2001, pp. 297–313.

Zhang, G., Robertson, P.K., and Brachman, R.W.I. (2002) "Estimating liquefaction-induced ground settlements from CPT for level ground." Canadian Geotechnical Journal, Ottawa, 39: 1168–1180.

Zhang, G., Robertson, P.K. and Brachman, R.W.I. (2004) "Estimating Liquefaction-Induced Lateral Displacements Using the Standard Penetration Test or Cone Penetration Test." J. Gotech. Geoenviron. Eng., 2004, 130(8), 861–871.

Taylor & Francis
Taylor & Francis Group
http://taylorandfrancis.com

Cone Penetration Testing 2018 – Hicks, Pisanò & Peuchen (Eds)
© 2018 Delft University of Technology, The Netherlands, ISBN 978-1-138-58449-5

Correlations among SCPTU parameters of Jiangsu normally consolidated silty clays

H. Zou, S. Liu & G. Cai
Southeast University, Nanjing, China

A.J. Puppala
University of Texas at Arlington, Texas, USA

ABSTRACT: The enhanced seismic piezocone penetration testing (SCPTU) provides a convenient method to measure V_s together with other three indices including the cone tip resistance, sleeve frictional resistance and pore water pressure in a close proximity. In this study, a database containing 117 sets of data points is compiled for the stress-normalized SCPTU parameters of the Jiangsu normally consolidated silty clays. An approach based on the multivariate distribution method is utilized to develop the multivariate correlations among the normalized shear wave velocity (V_{s1}) and other three indices. It is shown that the correlations are reliable to describe the dependence of the V_{s1} on other three indices for the Jiangsu normally consolidated silty clays. Moreover, the uncertainties within V_{s1} can be reduced by incorporating more than one index in the prediction.

1 INTRODUCTION

The shear wave velocity, V_s, describes the soil stiffness at the small strain and can be used to evaluate the soil behavior type and ground motion (Long & Donohue 2010). The seismic piezocone penetration test (SCPTU) provides the reliable V_s measurement together with other three indices including the cone tip resistance (q_t), sleeve frictional resistance (f_s) and pore water pressure (u_2). The correlations among these four parameters have been studied for different clayey soils based on the regression analysis (Long & Donohue 2010, Cai et al. 2014, L'Heureux et al. 2017).

The correlations developed using the regression analysis, to a large extent, depend on a subjective selection of the formula model when more than one testing index is involved in the curve-fitting. The determination of an accurate model to improve the accuracy of prediction by including more testing indices is of particular interest to geotechnical engineers.

A recent approach to establish the multivariate correlations among soil parameters is using the multivariate distribution model. This approach involves four main steps including: (1) a data transformation to convert each non-Gaussian soil parameter to a standard normal variable; (2) a correlation analysis to estimate the product-moment (Pearson) correlation coefficients among the transformed variables; (3) a Bayesian updating to derive the mathematical correlations of one transformed variable conditional on other transformed variables; and (4) a back transformation to convert the statistics such as the median value of a transformed variable to the corresponding physical soil parameter. This method has been demonstrated to be an effective tool to capture the multivariate correlations among the soil parameters and thus improve the accuracy of the predictions by including multiple testing indices (Ching et al. 2014, Liu et al. 2016, Zou et al. 2017). A simple way to establish the correlations among the transformed variables would be using the multiple regression analysis and thus the steps (2) and (3) can be condensed (e.g., Kootahi & Mayne 2016). In this study, the correlation analysis and Bayesian updating are still used as they provide a systematic way to evaluate the correlation characteristics among the soil parameters and quantify the uncertainties within the predictions.

In this study, the multivariate distribution model is used to derive the multivariate correlations among V_s and the other three SCPTU parameters for the Jiangsu normally consolidated (NC) silty clays. To achieve this objective, a database including the four SCPTU parameters for the Jiangsu silty clays is presented. The statistics of the soil parameters in the database are introduced. Detailed procedures to implement the multivariate distribution model are then conducted. The correlations for the V_s conditional on the

other three SCPTU parameters are developed and validated. The feasibility of the multivariate distribution model in describing the correlations of the SCPTU parameters for the Jiangsu silty clays is therefore demonstrated.

2 SCPTU DATABASE FOR JIANGSU NC SILTY CLAYS

2.1 *Site conditions and SCPTU tests*

A comprehensive geotechnical investigation has been conducted on the Quaternary soils of 29 sites in the Jiangsu province, China. The geologic formations and site conditions of the testing sites are available in the literature (Cai et al. 2014, Zou et al. 2017). More than two hundred SCPTU soundings have been performed over these testing sites with the soils ranging from soft clay, clay, silty clay, silt, silty sand and sand. This study only focuses on the behavior of the normally consolidated to slightly over consolidated silty clays with the overconsolidation ratio (OCR) between 1.0 and 2.5.

The schematic of the SCPTU probe used in this study is available in the literature and its geometry is in accordance with the international standard (Cai et al. 2014). The cross-correlation method is utilized to assess the times between successive intervals to estimate V_s (Campanella & Stewart 1991). A representative SCPTU profile for the Jiangsu silty clay is given in Figure 1. The soil strata mainly contain two silty clay units with the upper silty clay ranging from 0 to approximately 15.0 m beneath the ground surface and the lower silty clay lying under 15.0 m.

Figure 1 indicates that the shear wave velocity V_s may be well correlated to q_t, f_s and u_2. The V_s seems to increase with q_t and f_s, whereas it may decrease with u_2 for the silty clay. For example, several peak values of q_t and f_s are observed at a depth interval of 14.0 to 15.0 m, and the corresponding V_s value in this depth interval is larger than those

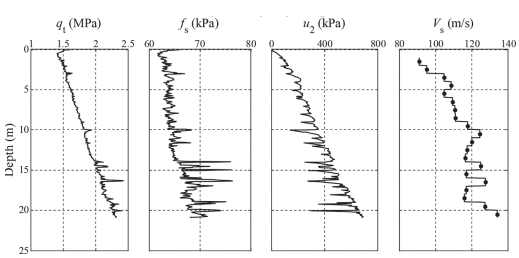

Figure 1. Representative SCPTU profile for Jiangsu silty clays.

in the adjacent vicinity. On the contrary, the measured u_2 values in this interval are low. A potential explanation is that these four parameters are all a function of the silt contents. A high silt content may contribute to the increase of soil stiffness and thus lead to the high measurements of q_t, f_s and V_s. However, as the silt content increases, the dissipation rate of the excess pore water pressure during the cone penetration may increase and thus lead to the decrease of u_2. Therefore, it is reasonable to assume that all the q_t, f_s and u_2 data are useful to describe V_s.

Besides, Figure 1 shows that the four SCPTU indices tend to increase with the increase of depth (or vertical stress). Therefore, in this study all these four parameters are normalized with respect to the vertical stress, as follows:

$$Y_1 = q_{t1} = \frac{q_t}{p_a} \cdot C_N \quad \text{where} \quad C_N = \left(\frac{p_a}{\sigma'_{v0}}\right)^{\alpha} \le 1.70$$

$$\alpha = 1.338 - 0.249\left(\frac{q_{t1}}{p_a}\right)^{0.264}$$

$$Y_2 = f_s / \sigma'_{v0}$$

$$Y_3 = \Delta u_2 / \sigma'_{v0} = (u_2 - u_0)/\sigma'_{v0}$$

$$Y_4 = V_{s1} = V_s (p_a / \sigma'_{v0})^{0.25}$$

where $Y_1 = q_{t1}$ is the normalized cone tip resistance, $Y_2 = f_s/\sigma'_{v0}$ is the normalized sleeve frictional resistance, $Y_3 = \Delta u_2/\sigma'_{v0}$ is the normalized excess pore pressure, $Y_4 = V_{s1}$ is the normalized shear wave velocity in m/s, C_N is the overburden correction factor, σ_{v0} is the vertical total stress in kPa, σ'_{v0} is the vertical effective stress in kPa, u_0 is the hydrostatic pressure in kPa, and p_a is the atmospheric pressure.

The definition for the normalized cone tip resistance q_{t1} follows that given by Idriss and Boulanger (2004). The main benefit of this definition, instead of the more common expression that $Q_t = (q_t - \sigma_{v0})/\sigma'_{v0}$, is that it seems to consider the impact of σ'_{v0} better for the shallow soils. For instance, in Figure 1 at a depth of 3.0 m with a ground water table of 0.1 m, the vertical total and effective stresses are estimated to be σ_{v0} = 54 kPa and σ'_{v0} = 25.6 kPa using γ_s = 18 kN/m^3. At this location the q_t is measured to be 1.55 MPa. Then, $q_{t1} = q_t C_N/p_a$ is estimated to be 9.63, corresponding to an acceptable value for the silty clay. However, using $Q_t = (q_t - \sigma_{v0})/\sigma'_{v0}$, Q_t is estimated to be 58.5, corresponding to an unreasonably high value for the cohesive soils. The usage of f_s/σ'_{v0} and $\Delta u_2/\sigma'_{v0}$, instead of the more widely used $F_r = f_s/(q_t - \sigma_{v0})$ and $B_q = \Delta u_2/(q_t - \sigma_{v0})$, is to ensure that the selected four parameters are measured independently. The definition of V_{s1} follows that suggested by Lunne et al. (1997).

Using the above formulas, a database containing 117 sets of $\{Y_1, Y_2, Y_3, Y_4\}$ is compiled for the Jiangsu NC silty clays. The V_{s1} evaluates the averaged seismic behavior of soil every one meter. Therefore, all the q_{t1}, f_s/σ'_{v0}, and $\Delta u_2/\sigma'_{v0}$ are also averaged every one meter to ensure the consistency of the database. These averaged indices are then used in the subsequent statistical analysis. The validation of the constructed multivariate distribution model is crucial to ensure the reliability of the developed correlations. Therefore, one SCPTU sounding is extracted from each site to form a validation dataset to evaluate the performance of the developed multivariate correlations. The rest of the data are used in the construction of the multivariate distribution model and named calibration dataset. The sample sizes of the calibration and validation datasets are 93 and 24, respectively. The statistics of these two datasets are summarized in the next section.

2.2 *Basic statistics of SCPTU parameters*

Basic statistics including the mean, coefficient of variation (COV), maximum value (Max), and minimum value (Min) of the four normalized parameters are summarized in Table 1. Among the four parameters, $Y_2 = f_s/\sigma'_{v0}$ shows the highest variability with COV = 0.52. On the contrary, $Y_4 = V_{s1}$ is associated with the lowest variability with COV = 0.16. The variability of $Y_3 = \Delta u_2/\sigma'_{v0}$ is 0.32, less than Y_2. A potential implication is that the u_2 may be a more reliable measurement for the silty clays. Besides, it is shown in Table 1 that the statistics of the calibration and validation datasets are similar, except that the scatters of the validation data seem to be slightly less significant than those of the calibration data.

The soil behavior types of the Jiangsu NC silty clays are examined by plotting the q_{t1}, F_r and B_q data within the two SCPTU datasets in the Robertson (1990) soil classification chart, as shown in Figure 2. Most data points are identified as clays and silty clays. Therefore, these data are deemed representative for the Jiangsu NC silty clays.

Table 1. Statistics of the calibration and validation datasets.

	Calibration dataset				Validation dataset			
Variable	Y_1	Y_2	Y_3	Y_4	Y_1	Y_2	Y_3	Y_4
Mean	9.44	0.17	3.47	133.51	9.94	0.18	3.28	138.69
COV	0.28	0.52	0.32	0.16	0.23	0.44	0.29	0.15
Min	5.07	0.04	0.90	88.95	6.20	0.11	1.92	105.02
Max	17.79	0.42	6.31	198.71	13.80	0.37	4.96	183.38

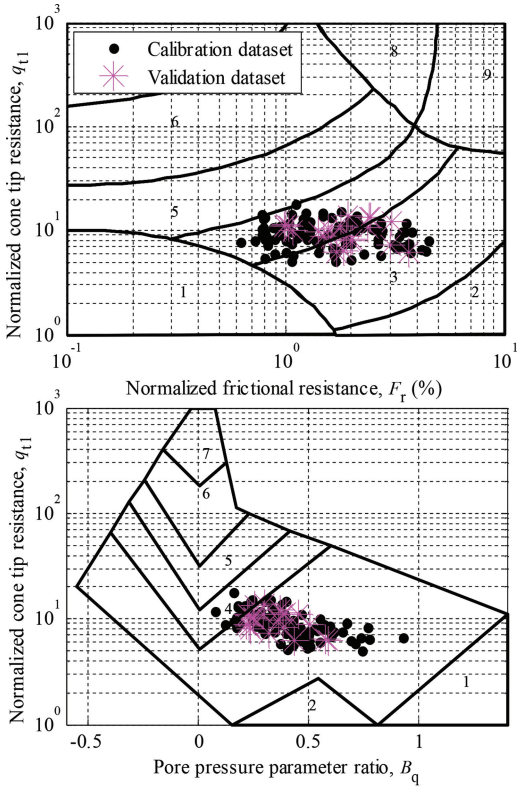

Figure 2. Soil behavior types identified using the Robertson (1990) chart.

3 MULTIVARIATE CORRELATION ANALYSES

The application of a multivariate distribution model in developing multivariate correlations includes the data transformation, correlation analysis, Bayesian updating, and back transformation (Ching et al. 2014, Zou et al. 2017). These procedures are implemented in this section.

3.1 *Transformation of soil parameters*

The primary step to construct a multivariate distribution model is to individually convert the soil parameters to normal variables (Zou et al. 2017). The Box-Cox transformation has been demonstrated to be a simple and effective tool to achieve this goal (Jaksa 2007). In this approach, three transformation parameters including a transformation power (λ) and two standardization parameter (a and b) are involved, as follows:

$$X = \frac{\frac{Y^{\lambda}-1}{\lambda} - a}{b} = \frac{Y^{\lambda}-1-\lambda a}{\lambda b} \quad (1)$$

where Y is the soil parameter and X is the corresponding transformed variable.

The key problem is to find an appropriate transformation power (λ) to achieve the normality of Y^{λ}. This is obtained by using the MATLAB library function *boxcox*. Table 2 summarizes the estimated λ values for the four SCPTU parameters. The standardization parameters, a and b, are then the mean and standard deviation of $(Y^{\lambda} - 1)/\lambda$, respectively.

To check the normality of each transformed variable, the histogram and formal normality test method, the Kolmogorov-Smirnov (KS) test, are used. The KS-p value quantitatively evaluates the probability of the evidence that the variable follows a standard normal distribution. The results of the KS test are shown in the last column of Table 2. The histograms and fitted normal distribution functions (smooth curves) of the transformed X variables are illustrated in Figure 3. It is evident that the fitted normal distribution curves match the histograms well for the transformed q_{t1}, and $\Delta u_2/\sigma'_{v0}$. It seems that the fitted normal distribution curves do not match well for the transformed f_s/σ'_{v0} and V_{s1}, as illustrated in Figure 3. These two histograms show a bimodal behavior.

Table 2. Statistics of the calibration and validation datasets.

Variable	λ	a	b	KS-p
Y_1	0.013	2.238	0.290	0.99
Y_2	0.133	–1.689	0.421	0.44
Y_3	0.678	1.913	0.758	0.94
Y_4	–0.053	4.301	0.123	0.69

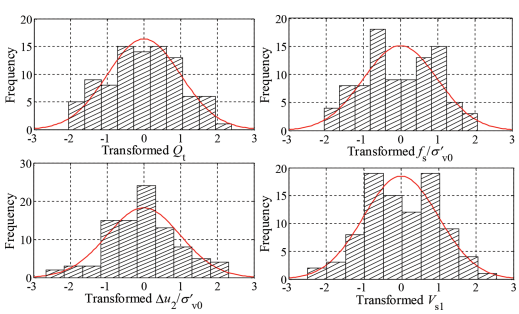

Figure 3. Transformation parameters and histograms of the transformed variables.

However, the KS-p values for these four variables are 0.99, 0.94, 0.44 and 0.69. All these four probability values are larger than the small probability of 0.05. Therefore, the event that each transformed variable individually follows a standard normal distribution is not a small probability event. Thus, these four transformed variables can be viewed as normal variables.

It is worth emphasizing that even if each Y variable individually follows a normal distribution, the four transformed variables do not have to jointly follow a multivariate normal distribution. This conclusion has been highlighted in the literature. Nevertheless, it has been revealed that meaningful results can still be derived in the case that the transformed variables do not strictly follow a multivariate normal distribution (Ching et al. 2014). Therefore, a rigorous test on the multivariate normality of the four transformed variables is not conducted here. Instead, this study focuses on developing the multivariate correlations for V_{s1} since it is of main interest for geotechnical engineers.

3.2 *Correlations among transformed variables*

Once the soil parameters are individually converted to normal variables, the linear correlations among these variables can be estimated to produce a correlation matrix and then establish a multivariate distribution model with the hypothesis that they jointly follow a multivariate normal distribution. The linear correlation between any pair of the X variables is quantitatively assessed using the product-moment (Pearson) correlation coefficient and can be obtained using the MATLAB library function *corr*. The estimated correlation matrix for the calibration dataset of X variables is given in Table 3.

Table 3 shows that the correlation between X_4 and X_1 is relatively strong with the correlation coefficient close to 0.70. However, the correlations between X_4 and other two variables (X_2 and X_3) are weak with the absolute correlation coefficients less than 0.50. This is reasonable since both V_{s1} and q_{t1} evaluates the soil stiffness and their correlations have been widely studied, whereas strong

Table 3. Estimated Pearson correlation coefficients among X variables.

Variable	X_1	X_2	X_3	X_4
X_1	1.000	0.374	0.031	0.691
X_2	0.374	1.000	0.151	0.382
X_3	0.031	0.151	1.000	–0.463
X_4	0.691	0.382	–0.463	1.000

correlations among V_{s1}, f_s/σ'_{v0} and $\Delta u_2/\sigma'_{v0}$ have been insufficiently reported. It will be shown in this study that f_s/σ'_{v0} and $\Delta u_2/\sigma'_{v0}$ are still useful to provide valuable information to improve the accuracy of the predicted V_{s1} although they are weakly correlated.

4 MULTIVARIATE CORRELATIONS

4.1 *Bayesian updating and back transformation*

For a set of X variables following a multivariate normal distribution, the mean value and variance of one variable conditional on other variables can be derived using a Bayesian updating technique, as follows (Ching et al. 2014):

$$E[X_i] = \begin{bmatrix} \delta_{ij} & \delta_{ik} & \cdots & \delta_{is} \end{bmatrix} \begin{bmatrix} 1 & \delta_{jk} & \cdots & \delta_{js} \\ \delta_{kj} & 1 & \cdots & \delta_{km} \\ \vdots & \vdots & \ddots & \vdots \\ \delta_{mj} & \delta_{mk} & \cdots & 1 \end{bmatrix}^{-1} \begin{bmatrix} X_j \\ X_k \\ \vdots \\ X_s \end{bmatrix} \tag{2}$$

$$\mathrm{var}[X_i] = 1 - \begin{bmatrix} \delta_{ij} & \delta_{ik} & \cdots & \delta_{is} \end{bmatrix} \begin{bmatrix} 1 & \delta_{jk} & \cdots & \delta_{js} \\ \delta_{kj} & 1 & \cdots & \delta_{km} \\ \vdots & \vdots & \ddots & \vdots \\ \delta_{mj} & \delta_{mk} & \cdots & 1 \end{bmatrix}^{-1} \begin{bmatrix} \delta_{ij} \\ \delta_{ik} \\ \vdots \\ \delta_{is} \end{bmatrix} \tag{3}$$

where δ_{ij} is the product-moment correlation coefficient between X_i and X_j and it is the (i, j)th entry in Table 3, $E[X_i]$ and $\mathrm{var}[X_i]$ are the mean and variance of X_i, respectively.

Based on these two statistics, the percentiles of the Y variables can be obtained using the back transformation, as follows (Liu et al. 2016):

$$Y_\eta = \left(b\lambda X_\eta + a\lambda + 1\right)^{1/\lambda} \tag{4}$$

where X_η and Y_η are the ηth percentile of X and Y, respectively.

In this study, the median and 95% confidence interval (CI), corresponding to $\eta = 0.50$, 0.025 and 0.975, for the predicted V_{s1} are studied. The 95% CI describes the interval within which we are 95% sure that the actual V_{s1} value is located, and therefore it is useful to evaluate the uncertainties within the predictions. However, only the mathematical equations for the median values are presented as they are suggested to be used in deterministic analysis. The performances of these correlations are also discussed.

4.2 *Bivariate correlations*

The median-based bivariate V_{s1}-q_{t1}, V_{s1}-f_s/σ'_{v0}, and V_{s1}-$\Delta u_2/\sigma'_{v0}$ correlations derived from the developed multivariate distribution model are given as follows:

$$V_{s1} = \left(-1.177 q_{t1}^{0.0132} + 1.984\right)^{-18.9} \tag{5a}$$

$$V_{s1} = \left[-0.0444\left(f_s/\sigma'_{v0}\right)^{0.133} + 0.807\right]^{-18.9} \tag{5b}$$

$$V_{s1} = \left[0.0059\left(\Delta u_2/\sigma'_{v0}\right)^{0.678} + 0.759\right]^{-18.9} \tag{5c}$$

Figure 4 presents the median values (smooth curves) of V_{s1} predicted using Equation (5). The calibration dataset, validation dataset and the predicted 95% CIs are also shown in Figure 4. It is evident that the predicted median values of V_{s1} agree with the calibration and validation data well,

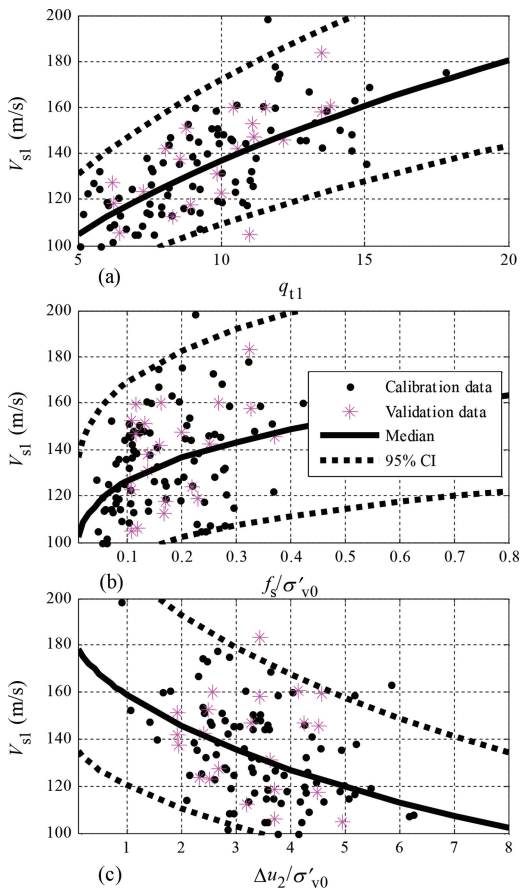

Figure 4. V_{s1} predicted using: (a) q_{t1}; (b) f_s/σ'_{v0}; (c) $\Delta u_2/\sigma'_{v0}$.

and the predicted 95% CIs are also in accordance with the scatter of these two datasets. Therefore, the constructed multivariate distribution model is deemed reasonable to describe the V_{s1}-related bivariate correlations for the Jiangsu NC silty clays.

Although these bivariate correlations agree well with the calibration and validation data, the predicted V_{s1} values are significantly scattered with respective to the actual measurements. The calculated coefficients of determination (R^2) for the above three correlations are 0.49, 0.15 and 0.22, respectively. These low R^2 values indicate the unsatisfactory performances of the bivariate correlations.

4.3 *Multivariate correlations*

It is of interest to predict V_{s1} using more than one testing index. Since the V_{s1}-q_{t1} correlation shows the best performance, it is of interest to investigate how this correlation can be enhanced by including the other two indices. Based on the constructed multivariate distribution model, the multivariate correlations for the median of V_{s1} conditional on $\{q_{t1}, f_s/\sigma'_{v0}\}$, $\{q_{t1}, \Delta u_2/\sigma'_{v0}\}$, and $\{q_{t1}, f_s/\sigma'_{v0}, \Delta u_2/\sigma'_{v0}\}$ are obtained, as follows:

$$V_{s1} = \left(-1.085 q_{t1}^{0.0132} - 0.0167 (f_s/\sigma'_{v0})^{0.133} + 1.902\right)^{-18.9} \tag{6a}$$

$$V_{s1} = \left[-1.202 q_{t1}^{0.0132} + 0.0061 \left(\Delta u_2/\sigma'_{v0}\right)^{0.678} + 1.996\right]^{-18.9} \tag{6b}$$

$$V_{s1} = \left[\begin{array}{l} -1.059 q_{t1}^{0.0132} - 0.0264 \left(f_s/\sigma'_{v0}\right)^{0.133} + \\ 0.0065 \left(\Delta u_2/\sigma'_{v0}\right)^{0.678} + 1.868 \end{array}\right]^{-18.9} \tag{6c}$$

The medians of V_{s1} predicted using Equation (6) are plotted against the actual measurements for the calibration and validation datasets in Figure 5. The R^2 values of the above three equations are calculated to be 0.50, 0.72 and 0.76, respectively. It is evident that the uncertainties associated with the predicted V_{s1} can be reduced by incorporating more than one testing index since the R^2 values are increased.

4.4 *Model errors of correlations*

A more rational evaluation of the performances of the correlations is to use the model error (ε), defined as the ratio of measured V_{s1} over predicted V_{s1}. The two main benefits of this model error include that: (1) it provides a better description on the prediction performance; and (2) it can be used in reliability-based analysis (e.g., Phoon 2015). The mean value of ε, $E[\varepsilon]$, describes the central posi-

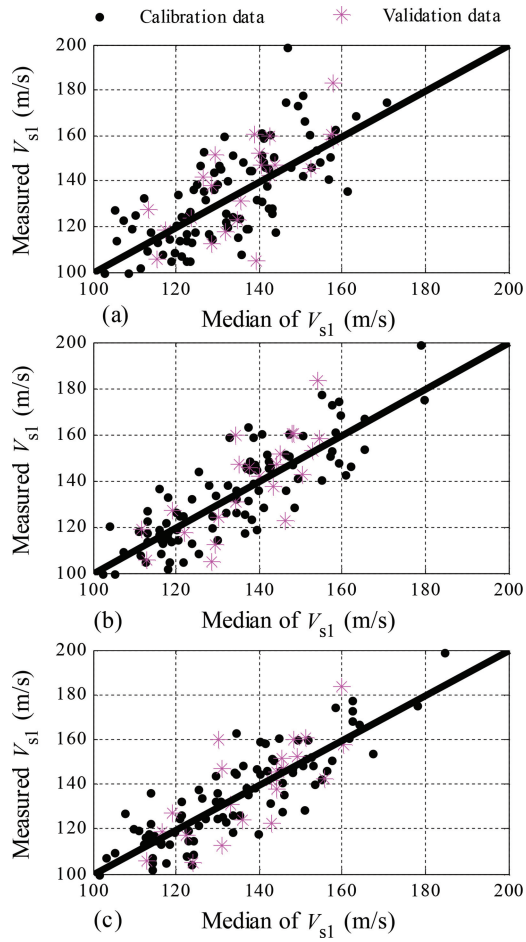

Figure 5. Predicted median of V_{s1} conditional on: (a) $\{q_{t1}, f_s/\sigma'_{v0}\}$; (b) $\{q_{t1}, \Delta u_2/\sigma'_{v0}\}$; (c) $\{q_{t1}, f_s/\sigma'_{v0}, \Delta u_2/\sigma'_{v0}\}$.

tion (i.e., systematic bias) of the predictions with respect to the actual measurements, whereas the coefficient of variation of ε, COV_ε, describes the magnitude of scatter of the predictions around the measurements.

Figure 6 shows the histograms and fitted normal distribution functions of the ε values for the V_{s1}-q_{t1}, V_{s1}-$\{q_{t1}, f_s/\sigma'_{v0}\}$, V_{s1}-$\{q_{t1}, \Delta u_2/\sigma'_{v0}\}$, and V_{s1}-$\{q_{t1}, f_s/\sigma'_{v0}, \Delta u_2/\sigma'_{v0}\}$ correlations. It seems that each ε can be approximated using a normal variable as the fitted curves match well with the histograms. All the $E[\varepsilon]$ values are around 1.00, indicating that these correlations are unbiased. This is reasonable since Figure 5 shows that all the data points are relatively uniformly scattered around the reference line. Moreover, when more testing indices are involved, the predicted V_{s1} values become closer to the actual measurements as the $E[\varepsilon]$ values are

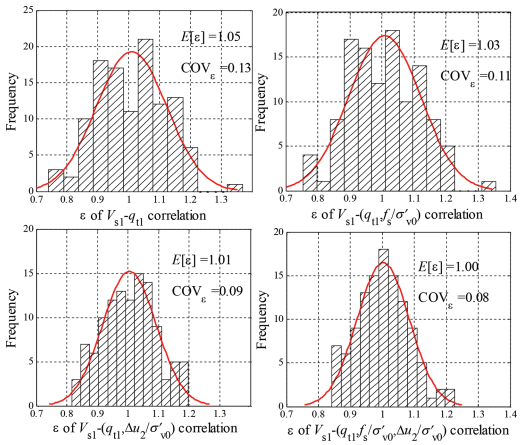

Figure 6. Model errors for V_{s1} correlations.

closer to 1.00 and the COV_ε values consistently decrease from 0.13 to 0.08. The reduction of COV_ε is clear in Fig. 6 since the histograms are more concentrated around the $E[\varepsilon]$ values when more testing indices are included.

Based on the above analyses, it is safe to conclude that the V_{s1}-related equations are suitable for the SCPTU parameters of the Jiangsu NC silty clays. The multivariate distribution model provides a useful way to establish the multivariate correlations among the soils parameters. However, it is worth emphasizing that the model and correlations developed in this study are suggested for the Jiangsu NC silty clays. Caution shall be exercising when these equations are used in the other soils as site-specific effect plays an important role in geotechnical correlations (e.g., Zou et al. 2017). A primary validation using new local data shall be necessary.

5 CONCLUSIONS

In this study, a multivariate distribution model is used to describe the multi-dependency within four SCPTU parameters of Jiangsu normally consolidated (NC) silty clays. A database containing 117 data points of $\{q_{t1}, f_s/\sigma'_{v0}, \Delta u_2/\sigma'_{v0}, V_{s1}\}$ is compiled and portioned into a calibration dataset for developing the multivariate distribution model and a validation dataset for the validation. Based on the constructed model, multivariate correlations for V_{s1} are developed for the Jiangsu NC silty clays. It is shown that the model is capable of the multivariate correlations among the four SCPTU parameters, and the uncertainties associated with the V_{s1} can be consistently reduced by incorporating more than one testing.

ACKNOWLEDGEMENTS

Majority of the work presented in this paper was funded by the National Key R&D Program of China (2016YFC0800200) and the National Natural Science Foundation of China (Grant No. 41672294). These financial supports are gratefully acknowledged.

REFERENCES

Cai, G., Puppala, A. J., & Liu, S. 2014. Characterization on the correlation between shear wave velocity and piezocone tip resistance of Jiangsu clays. *Engineering Geology* 171: 96–103.

Campanella, R.G. & Stewart, W.P. 1991. Downhole seismic cone analysis using digital signal processing. In Proceedings of Second International Conference on Recent Advances in Geotechnical Earthquake Engineering and Soil Dynamics, St. Louis, Missouri, 77–82, 11–15 March.

Ching, J.Y., Phoon, K.K. & Chen, C.H. 2014. Modeling piezocone cone penetration (CPTU) parameters of clays as a multivariate normal distribution. *Canadian Geotechnical Journal* 51(1): 77–91.

Idriss, I.M. & Boulanger, R.W. 2004. Semi-empirical procedures for evaluating liquefaction potential during earthquakes. Proc., Joint Conf., 11th Int. Conf. on Soil Dynamics and Earthquake Engineering (SDEE), and The 3rd Int. Conf. on Earthquake Geotechnical Engineering (ICEGE), 32–56, Berkeley, Calif..

Kootahi, K. & Mayne, P.W. 2016. Index test method for estimating the effective preconsolidation stress in clay deposits. *Journal of Geotechnical and Geoenvironmental Engineering* 142(10).

L'Heureux, J. & Long, M. 2017. Relationship between shear-wave velocity and geotechnical parameters for Norwegian clays. *Journal of Geotechnical and Geoenvironmental Engineering,* 04017013.

Liu, S., Zou, H., Cai, G., Bheemasetti, T., Puppala, A. J., Lin, J. 2016. Multivariate correlation among resilient modulus and cone penetration test parameters of cohesive subgrade soils. *Engineering Geology* 209: 128–142.

Long, M. & Donohue, S. 2010. Characterization of Norwegian marine clays with combined shear wave velocity and piezocone cone penetration test (CPTU) data. *Canadian Geotechnical Journal* 47 (7): 709–718.

Phoon, K.K. Reliability of geotechnical structures. 2015. In proceedings of the 15th Asian Regional Conference on Soil Mechanics and Geotechnical Engineering, 2(1): 1–9, Fukuoka, November, 2015.

Robertson, P.K. 1990. Soil classification using the cone penetration test. *Canadian Geotechnical Journal* 27 (1): 151–158.

Zou, H., Liu, S., Cai, G., Puppala, A.J. & Bheemasetti, T. 2017. Multivariate correlation analysis of seismic piezocone penetration (SCPTU) parameters and design properties of Jiangsu quaternary cohesive soils. *Engineering Geology* 228: 11–38.

Taylor & Francis
Taylor & Francis Group
http://taylorandfrancis.com

Cone Penetration Testing 2018 – Hicks, Pisanò & Peuchen (Eds)
© 2018 Delft University of Technology, The Netherlands, ISBN 978-1-138-58449-5

Author index

Agaiby, S.S. 65
Al-Baghdadi, T. 255
Albatal, A. 151
Alderlieste, E.A. 411
Allievi, L. 73
Al-Sammarraie, D. 79, 591
Amoroso, S. 85, 241
Anamali, E. 93
Andrade, M.E.S. 249, 585
Ansary, M.A. 643
Arroyo, M. 221, 329, 455
Augarde, C. 255

Bagińska, I. 109
Bajda, M. 579
Bałachowski, L. 117, 371
Ball, J. 255
Baltoukas, D. 649
Baptie, P. 715
Barbosa, H.T. 227
Barounis, N. 123, 129
Bates, L. 351
Baziw, E. 137
Bienen, B. 3, 213
Bihs, A. 143
Bilici, C. 151
Blake, A. 255
Bliekendaal, E. 683
Bøgelund-Pedersen, R. 525
Boone, M.D. 157
Boulanger, R.W. 25
Bray, J.D. 165
Brennan, A. 255
Brik, A. 173, 179
Brink Clausen, J. 525
Brizzolara, S. 461
Brown, M. 255

Cai, G. 731
Calabrese, L. 629
Calvello, M. 295
Camacho, C.B. 193
Camacho, M.A. 193
Cao, Z.J. 629
Cardoso, A. 199
Carlson, M. 417
Carroll, R. 205
Chow, S.H. 3, 213, 695
Christopher, N. 303
Chung, S.G. 469
Collico, S. 221
Coombs, W. 255
Coutinho, R.Q. 227, 235
Crombé, Ph. 663
Cruz, J. 241
Cruz, M. 241
Cruz, N. 241
Cubrinovski, M. 165
Cuomo, S. 295
Curran, T. 73

Damasco Penna, A.S. 709
Danziger, F.A.B. 249, 585
Davidson, C. 255
Davidson, J. 199
de Gast, T. 289
de Greef, J. 317, 389
de la Torre, C. 165
de Lange, D.A. 383
De Nijs, G.A. 101
De Nijs, G.J.J. 101
de Vries, G.T. 683, 689
Deakin, R. 73
DeJong, J.T. 25
Devincenzi, M. 221
Dhimitri, L. 93
Di Buò, B. 185, 571
D'Ignazio, M. 185, 395, 571
Dmitriev, G.Y. 359
Doan, L.V. 263, 269, 275
Doherty, J.P. 3, 563
Doherty, P. 657
Donohue, S. 657
Duffy, W.P. 157

Engels, S.P.J. 539

Ferreira, C. 669
Fityus, S. 351
Flores-Eslava, R. 347

Galavi, V. 295, 611
García Martínez, M.F. 281, 629
Garziglia, S. 599
Gavin, K.G. 45, 377, 539
Gens, A. 455, 605
Gerken, D.E. 157
Ghasemi, P. 295
Gibbs, P. 303
Goodarzi, M. 79, 309, 591
Gosnell, L. 715
Gottardi, G. 281
Gundersen, A.S. 323, 395
Gusmão, A.D. 227
Gylland, A. 143

Haikola, M. 571
Haugen, E. 417
Hauser, L. 329
Hayashi, H. 335
Helle, T.E. 339
Heredia, W. 193
Hermann, S. 395
Hicks, M.A. 289

Ibarra-Razo, E. 347
Imre, E. 351
Isaev, O.N. 359, 365, 551

Jacquard, C. 533
Janecki, W. 109
Jannuzzi, G.M.F. 249, 585
Jewell, R.A. 677
Joosten, S. 389

Kaltsas, D. 513
Karabacak, D. 407
Karlsrud, K. 395
Karreman, W.J. 539
Kåsin, K. 417
Kassner, M. 417
Kawa, M. 109
Kleven, A. 395
Kluger, M.O. 309
Knappett, J. 255
Konkol, J. 117, 371
Kopf, A. 401, 545
Kovacevic, M.S. 377
Krabbenhøft, K. 563
Krall, T. 165

Kreiter, S. 79, 309, 545, 591
Krogh, L. 303, 525

Laban, C. 683
Länsivaara, T. 185, 571
Lech, M. 579
Lehane, B.M. 263, 269, 275
Lengkeek, H.J. 317, 389
Lewis, M.R. 157
L'Heureux, J.S. 323, 395, 401, 417
Libric, L. 377
Liu, S. 731
Lo Presti, D.C. 435
Long, M. 143, 339, 401
Looijen, P. 407
Lundberg, A.B. 411
Lunne, T. 249, 323, 417, 525

Makyama, É.S.V. 709
Mantaras, F.M.B. 477
Marchetti, D. 85
Martelli, L. 629
Martinelli, M. 295
Martins, I.S.M. 585
Mayne, P.W. 65, 423, 491
McCallum, A.B. 431
McNinch, J.E. 151
Meisina, C. 435
Meissl, S. 199
Mejia, J. 193
Mellia, F.C. 235
Międlarz, K. 117
Minarelli, L. 85
Minkin, M.A. 359
Młynarek, Z. 441
Mo, P.Q. 447
Mohr, H. 3
Monaco, P. 85
Monforte, L. 329, 455
Mörz, T. 79, 309, 545, 591
Mumtaz, M.B. 461

Nguyen, T.D. 469
Nielsen, S.W. 303
Nordal, S. 143, 339

Odebrecht, E. 477
O'Donovan, J. 657
O'Loughlin, C.D. 3, 695
Orazalin, Z.Y. 483
Ouyang, Z. 491

Paniagua, P. 143, 205, 395
Papamichael, S. 499
Parasie, N. 407
Parolini, C. 455
Parra, J.G. 505
Pedersen, R.B. 303
Perez, N. 221
Peuchen, J. 407, 423, 513, 519, 649
Philpot, J. 123, 129
Pinheiro, A.V.S. 249
Powell, J.J.M. 93
Puppala, A.J. 731

Quandalle, B. 557
Quinteros, S. 323
Quinteros, V.S. 525

Radaszewski, R. 703
Ragni, R. 3
Ramos, C. 669
Randolph, M.F. 3, 213, 563
Rangel-Núñez, J.L. 347
Raymackers, S. 199
Reale, C. 377
Redgers, J.D. 557
Reiffsteck, Ph. 533
Rica, S. 101
Richards, D. 255
Riemens, H.J. 101
Rindertsma, J. 539
Rivera-Cruz, I. 347
Robertson, P.K. 157, 173
Rocchi, I. 281, 629
Rodrigues, C. 241, 669
Rømoen, M. 395
Roskoden, R. 545
Rouainia, M. 309
Ryzhkov, I.B. 359, 551

Saldanha, A.S. 669
Salinas, L.M. 193
Sampurno, B. 303
Sbitnev, A. 557
Schanz, T. 351
Schnaid, F. 477
Schneider, J.A. 3, 563
Schneider, M.A. 3
Schweiger, H.F. 329
Selänpää, J. 185, 571
Sharafutdinov, R.F. 359, 365
Sinjorgo, G. 513
Skutnik, Z. 579
Smaavik, T. 395
Soares, C.S.M. 585
Sokolov, I.S. 677
Stacul, S. 435
Stähler, F.T. 79, 309, 591
Stanier, S.A. 3
Stark, N. 151, 461, 695
Stefani, M. 85
Stefaniak, K. 441
Stocks, E. 165
Storteboom, O. 709, 715
Strandvik, S. 417
Sultan, N. 599

Taleb, F. 599
Tarragó, D. 605
Tehrani, F.S. 611
Terwindt, J. 383
Togliani, G. 617, 623
Tonks, D. 179
Tonni, L. 281, 629
Torres-Cruz, L.A. 635
Tyldsley, C. 73

Urmi, Z.A. 643
Uruci, E. 417
Usbeck, R. 689

Van Baars, S. 101
van de Graaf, H. 533
van den Wijngaert, M. 663
van der Linden, T.I. 383
Vanneste, M. 401
Vardon, P.J. 289, 649
Vasconcelos, J.O. 657
Veldhuijzen, A. 417
Veracoechea, A. 505
Verbeek, G. 137
Verhegge, J. 663
Vermeulen, N. 635
Viana da Fonseca, A. 669
Vieira, N. 505
Volkov, N.G. 359, 677
Vrettos, C. 499

Wadman, H. 151
Waliński, M. 703
Wang, L. 255
Ward, D. 93
Westgate, Z. 519
White, D.J. 3, 695
Whittle, A.J. 483
Wierzbicki, J. 441, 703
Woollard, M. 709, 715

Yamanashi, T. 335
Yi, F. 723
Yu, H.S. 447

Zakatov, D.S. 365
Zheng, S. 629
Zou, H. 731